UNIVERSITY OF BELGRADE
Technical Faculty in Bor

PROCEEDINGS

32nd International Conference

Ecological Truth & Environmental Research

24-26 June 2026

Editor
Prof. Dr Ana Radojević

EcoTER'26

Hotel Sunce, Sokobanja, Serbia

UNIVERSITY OF BELGRADE
Technical Faculty in Bor

PROCEEDINGS

32nd International Conference

Ecological Truth & Environmental Research

24-26 June 2026

Editor
Prof. Dr Ana Radojević

EcoTER'26

Hotel Sunce, Sokobanja, Serbia

PROCEEDINGS

32nd INTERNATIONAL CONFERENCE

ECOLOGICAL TRUTH & ENVIRONMENTAL RESEARCH – EcoTER'26

Editor of the Proceedings:

Prof. Dr Ana Radojević, University of Belgrade – Technical Faculty in Bor

Technical Editors of the Proceedings:

Prof. Dr Tanja Kalinović, University of Belgrade – Technical Faculty in Bor

Ass. Prof. Dr Jelena Kalinović, University of Belgrade – Technical Faculty in Bor

Sonja Stanković, MSc, University of Belgrade – Technical Faculty in Bor

Editor of the 7th Student Section:

Prof. Dr Žaklina Tasić, University of Belgrade – Technical Faculty in Bor

Technical Editor of the 7th Student Section:

Anđelija Bogdanović, MSc, University of Belgrade – Technical Faculty in Bor

Publisher: University of Belgrade – Technical Faculty in Bor, Bor

For the publisher: Prof. Dr Dejan Tanikić, Dean

Printed: University of Belgrade – Technical Faculty in Bor, Bor, 100 copies, electronic edition

Year of publication: 2026

This work is available under the Creative Commons Attribution-Non-commercial-NoDerivs licence (CC BY-NC-ND)

CIP - Каталогизација у публикацији Народна библиотека Србије, Београд

502/504(082)(0.034.2)
574(082)(0.034.2)

INTERNATIONAL Conference Ecological Truth & Environmental Research (32 ; 2026 ; Sokobanja)

Proceedings [Elektronski izvor] / 32nd International conference Ecological Truth & Environmental Research - EcoTER'26, Sokobanja, Serbia, 24-26 June 2026 ;
[organized by] University of Belgrade, Technical faculty in Bor (Serbia) ; [co-organizers University of Banja Luka, Faculty of Technology – Banja Luka (B&H) ... [et al.]] ; [editor Ana Radojević]. - electronic ed. - Bor : University of Belgrade, Technical faculty in Bor, 2026 (Bor : University of Belgrade, Technical faculty in Bor). - 1 USB fleš memorija ; 1 x 2 x 4 cm

Sistemski zahtevi: Nisu navedeni. - Nasl. sa naslovne strane dokumenta. - Preface / Ana Radojević. - Tiraž 100. - Bibliografija uz svaki rad.

ISBN 978-86-6305-171-3

a) Животна средина -- Зборници b) Екологија -- Зборници

COBISS.SR-ID 197972745

The 32nd International Conference
Ecological Truth & Environmental Research – EcoTER'26

is organized by:

UNIVERSITY OF BELGRADE
TECHNICAL FACULTY IN BOR
(SERBIA)

Co-organizers of the conference:

University of Banja Luka, Faculty of Technology, Banja Luka
(B&H)

University of Montenegro, Faculty of Technology, Podgorica
(Montenegro)

University of Zagreb, Faculty of Metallurgy, Sisak
(Croatia)

University of Pristina, Faculty of Technical Sciences, Kosovska Mitrovica
(Serbia)

Association of Young Researchers – Bor
(Serbia)

The EcoTER'26 conference is financially supported by

Republic of Serbia
MINISTRY OF SCIENCE,
TECHNOLOGICAL DEVELOPMENT AND INNOVATION

Platinum Donors of the EcoTER'26 conference

ZiJin
SERBIA ZIJIN MINING

ZiJin
SERBIA ZIJIN COPPER DOO

Gold Donors of the EcoTER'26 conference

HBIS SERBIA

ИНЖЕЊЕРСКА
КОМОРА
СРБИЈЕ

ElixirPrahovo

Silver Donor of the EcoTER'26 conference

EKSPLOZIVI
rudex

Sponsor of Best Poster Awards

processes
an Open Access Journal by MDPI

Media Partnership with

applied sciences
an Open Access Journal by MDPI

SCIENTIFIC COMMITTEE

Prof. Dr Snežana Šerbula, University of Belgrade, Technical Faculty in Bor, Bor (Serbia), *President*

Prof. Dr Dejan Tanikić, University of Belgrade, Technical Faculty in Bor, Bor (Serbia)

Prof. Dr Milan Radovanović, University of Belgrade, Technical Faculty in Bor, Bor (Serbia)

Prof. Dr Snežana Milić, University of Belgrade, Technical Faculty in Bor, Bor (Serbia)

Prof. Dr Jovica Sokolović, University of Belgrade, Technical Faculty in Bor, Bor (Serbia)

Prof. Dr Đorđe Nikolić, University of Belgrade, Technical Faculty in Bor, Bor (Serbia)

Prof. Dr Yasumasa Ogawa, Faculty of International Resource Sciences, Akita University, Akita (Japan)

Prof. Dr Alok Mittal, Maulana Azad National Institute of Technology Bhopal, Bhopal (India)

Prof. Dr Markoli Boštjan, University of Ljubljana, Ljubljana (Slovenia)

Prof. Dr Jay Wadhawan, University of Hull, Hull (United Kingdom)

Prof. Dr Martin Brtnický, Mendelova univerzita v Brně, Brno (Czech Republic)

Prof. Dr Jan Bogaert, Liège Université (Gembloux Agro-Bio Tech), Liège (Belgium)

Prof. Dr Isabel Maria De Oliveira Abrantes, University of Coimbra (Portugal)

Prof. Dr Natalija Dolić, University of Zagreb, Faculty of Metallurgy, Sisak (Croatia)

Prof. Dr Shengguo Xue, Central South University, Changsha (China)

Dr Lidija Mančić, Institute of Technical Sciences of the Serbian Academy of Sciences and Arts, Belgrade (Serbia) / Pontifical Catholic University of Rio de Janeiro, Rio de Janeiro (Brasil)

Prof. Dr Aleksandra Nadgórska-Socha, University of Silesia, Katowice (Poland)

Prof. Dr Bojan Marinković, Pontifical Catholic University of Rio de Janeiro, Rio de Janeiro (Brasil)

Prof. Dr Milan D. Antonijević, University of Surrey, School of Chemistry & Chemical Engineering, Guildford (United Kingdom)

Prof. Dr Maurice Millet, Maison Interuniversitaire des Sci., Strasbourg (France)

Prof. Dr Murray T. Brown, University of Otago, Dunedin (New Zealand)

Prof. Dr Darko Vuksanović, University of Montenegro, Faculty of Metallurgy and Technology, Podgorica (Montenegro)

Prof. Dr Xiaosan Luo, Nanjing University of Information Science & Technology, Nanjing (China)

Prof. Dr Irena Nikolić, University of Montenegro, Faculty of Metallurgy and Technology, Podgorica (Montenegro)

Prof. Dr Daniel J. Bain, University of Pittsburgh, Pittsburgh (United States of America)

Dr Stefan Đorđievski, Mining and Metallurgy Institute Bor, Bor (Serbia)

Prof. Dr Tamara Rakić, University of Belgrade, Faculty of Biology, Belgrade (Serbia)

Prof. Dr Fernando Carrillo-Navarrete, Universitat Politècnica de Catalunya, Barcelona (Spain)

Prof. Dr Hyusein Yemendzhiev, "Prof. Dr. Assen Zlatarov" University, Burgas (Bulgaria)

Prof. Dr Polonca Trebše, University of Ljubljana, Faculty of Health Sciences, Ljubljana (Slovenia)

Dr Alena Bartonova, The Climate and Environmental Research Institute NILU, Kjeller (Norway)

Prof. Dr Adrian Eugen Cioablă, Politehnica University Timisoara, Faculty of Mechanical Engineering, Timisoara (Romania)

Prof. Dr George Z. Kyzas, International Hellenic University, Thermi (Greece)

Prof. Dr Nenad Stavretović, University of Belgrade, Faculty of Forestry, Belgrade (Serbia)

Prof. Dr Mustafa Imamoğlu, Sakarya Üniversitesi, Serdivan (Turkey)

Prof. Dr Milutin Milosavljević, Faculty of Technical Sciences, Kosovska Mitrovica (Serbia)

Prof. Dr Šefket Goletić, University of Zenica, Faculty of Mechanical Engineering, Zenica (B&H)

Dr Tanja Brdarić, University of Belgrade, Vinča Institute of Nuclear Sciences – National Institute of the Republic of Serbia, Belgrade (Serbia)

Prof. Dr Milovan Vuković, University of Belgrade, Technical Faculty in Bor, Bor (Serbia)

Prof. Dr Nada Blagojević, University of Montenegro, Faculty of Metallurgy and Technology, Podgorica (Montenegro)
Prof. Dr Džafer Dautbegović, University of Zenica, Faculty of Mechanical Engineering, Zenica (B&H)
Dr Jasmina Stevanović, University of Belgrade, Institute of Chemistry, Technology and Metallurgy, Belgrade (Serbia)
Dr Mirjana Marković, University of Belgrade, Vinča Institute of Nuclear Sciences – National Institute of the Republic of Serbia, Belgrade (Serbia)
Dr Ljiljana Avramović, Mining and Metallurgy Institute Bor, Bor (Serbia)
Prof. Dr Slavica Sladojević, University of Banja Luka, Faculty of Technology, Banja Luka (B&H)
Prof. Dr Popescu Francisc, Politehnica University Timisoara, Faculty of Mechanical Engineering, Timisoara (Romania)
Dr Dragana Ranđelović, Institute for Technology of Nuclear and Other Mineral Raw Materials, Belgrade (Serbia)
Prof. Dr Nada Šumatić, University of Banja Luka, Faculty of Forestry, Banja Luka (B&H)
Dr Viša Tasić, Mining and Metallurgy Institute Bor, Bor (Serbia)
Prof. Dr Milan Trumić, University of Belgrade, Technical Faculty in Bor, Bor (Serbia)
Prof. Dr Borislav Malinović, University of Banja Luka, Faculty of Technology, Banja Luka (B&H)
Prof. Dr Branimir Jovančićević, University of Belgrade, Faculty of Chemistry, Belgrade (Serbia)
Prof. Dr Tatjana Anđelković, University of Niš, Faculty of Sciences and Mathematics, Niš (Serbia)
Prof. Dr Jelena Mitrović, University of Niš, Faculty of Sciences and Mathematics, Niš (Serbia)

HONORARY COMMITTEE

Dr. Petar Paunović
(Zaječar, Serbia)

Prof. Dr Zvonimir Stanković
(Bor, Serbia)

Prof. Dr Velizar Stanković
(Bor, Serbia)

Prof. Dr Milan M. Antonijević
(Bor, Serbia)

Prof. Dr Ladislav Lazić
(Sisak, Croatia)

Dragan Ranđelović, Society of Young Researchers – Bor
(Bor, Serbia)

Toplica Marjanović, Society of Young Researchers – Bor
(Bor, Serbia)

Mihajlo Stanković, Special Nature Reserve of Zasavica
(Sremska Mitrovica, Serbia)

ORGANIZING COMMITTEE

Prof. Dr Ana Radojević, University of Belgrade, Technical Faculty in Bor, Bor (Serbia), *President*

Prof. Dr Tanja Kalinović, University of Belgrade, Technical Faculty in Bor, Bor (Serbia), *Vice President*

Prof. Dr Marija Petrović Mihajlović, University of Belgrade, Technical Faculty in Bor, Bor (Serbia), *Vice President*

Prof. Dr Maja Nujkić, University of Belgrade, Technical Faculty in Bor, Bor (Serbia)

Prof. Dr Žaklina Tasić, University of Belgrade, Technical Faculty in Bor, Bor (Serbia)

Prof. Dr Milica Veličković, University of Belgrade, Technical Faculty in Bor, Bor (Serbia)

Prof. Dr Ljubiša Balanović, University of Belgrade, Technical Faculty in Bor, Bor (Serbia)

Prof. Dr Milan Gorgievski, University of Belgrade, Technical Faculty in Bor, Bor (Serbia)

Prof. Dr Jelena Šćepanović, University of Montenegro, Faculty of Metallurgy and Technology, Podgorica (Montenegro)

Prof. Dr Dejan Petrović, University of Belgrade, Technical Faculty in Bor, Bor (Serbia)

Asst. Prof. Dr Jelena Kalinović, University of Belgrade, Technical Faculty in Bor, Bor (Serbia)

Enisa Nikolić, English language teacher, University of Belgrade, Technical Faculty in Bor, Bor (Serbia)

Sonja Stanković, MSc, University of Belgrade, Technical Faculty in Bor, Bor (Serbia)

Anđelija Bogdanović, MSc, University of Belgrade, Technical Faculty in Bor, Bor (Serbia)

Vladan Nedelkovski, MSc, University of Belgrade, Technical Faculty in Bor, Bor (Serbia)

Aleksandar Cvetković, MSc, University of Belgrade, Technical Faculty in Bor, Bor (Serbia)

Miljan Marković, MSc, University of Belgrade, Technical Faculty in Bor, Bor (Serbia)

Oliver Marković, MSc, Tech Support, University of Belgrade, Technical Faculty in Bor, Bor (Serbia)

Dragan Milenković, MSc, Tech Support, University of Belgrade, Technical Faculty in Bor, Bor (Serbia)

THE LIST OF REVIEWERS OF EcoTER'26

Dr Lidija Mančić, Institute of Technical Sciences of the Serbian Academy of Sciences and Arts, Belgrade (Serbia)/Pontifical Catholic University of Rio de Janeiro, Rio de Janeiro (Brasil)

Dr Tanja Brdarić, University of Belgrade, Vinča Institute of Nuclear Sciences – National Institute of the Republic of Serbia, Belgrade (Serbia)

Prof. Dr Matej Fike, University of Maribor, Faculty of Energy Technology, Krško (Slovenia)

Dr Dragana Ranđelović, Institute for Technology of Nuclear and Other Mineral Raw Materials, Belgrade (Serbia)

Prof. Dr Grozdanka Bogdanović, University of Belgrade, Technical Faculty in Bor, Bor (Serbia)

Prof. Dr Snežana Milić, University of Belgrade, Technical Faculty in Bor, Bor (Serbia)

Prof. Dr Tamara Rakić, University of Belgrade, Faculty of Biology, Belgrade (Serbia)

Dr Dragana Adamović, Mining and Metallurgy Institute Bor, Bor (Serbia)

Prof. Dr Ivana Savić Gajić, University of Niš, Faculty of Technology, Leskovac (Serbia)

Dr Ljiljana Avramović, Mining and Metallurgy Institute Bor, Bor (Serbia)

Dr Mirjana Marković, University of Belgrade, Vinča Institute of Nuclear Sciences – National Institute of the Republic of Serbia, Belgrade (Serbia)

Dr Viša Tasić, Mining and Metallurgy Institute Bor, Bor (Serbia)

Dr Stefan Đorđievski, Mining and Metallurgy Institute Bor, Bor (Serbia)

Dr Dragana Božić, Mining and Metallurgy Institute Bor, Bor (Serbia)

Prof. Dr Jelena Mitrović, University of Niš, Faculty of Sciences and Mathematics, Niš (Serbia)

Prof. Dr Miloš Ilić, University of Novi Sad, Faculty of Sciences, Novi Sad (Serbia)

Prof. Dr Vesna Grekulović, University of Belgrade, Technical Faculty in Bor, Bor (Serbia)

Prof. Dr Ivana Marković, University of Belgrade, Technical Faculty in Bor, Bor (Serbia)

Prof. Dr Ana Radojević, University of Belgrade, Technical Faculty in Bor, Bor (Serbia)

Prof. Dr Tanja Kalinović, University of Belgrade, Technical Faculty in Bor, Bor (Serbia)

Prof. Dr Žaklina Tasić, University of Belgrade, Technical Faculty in Bor, Bor (Serbia)

Prof. Dr Slađana Alagić, University of Belgrade, Technical Faculty in Bor, Bor (Serbia)

Prof. Dr Ana Simonović, University of Belgrade, Technical Faculty in Bor, Bor (Serbia)

Prof. Dr Milica Veličković, University of Belgrade, Technical Faculty in Bor, Bor (Serbia)

Prof. Dr Maja Nujkić, University of Belgrade, Technical Faculty in Bor, Bor (Serbia)

Prof. Dr Milan Gorgievski, University of Belgrade, Technical Faculty in Bor, Bor (Serbia)

Prof. Dr Ljubiša Balanović, University of Belgrade, Technical Faculty in Bor, Bor (Serbia)

Asst. Prof. Dr Jelena Kalinović, University of Belgrade, Technical Faculty in Bor, Bor (Serbia)

Asst. Prof. Dr Jelena Jordanović, University of Belgrade, Technical Faculty in Bor, Bor (Serbia)

Asst. Prof. Dr Vladimir Nikolić, University of Belgrade, Technical Faculty in Bor, Bor (Serbia)

PREFACE

The 32nd International Conference *Ecological Truth & Environmental Research – EcoTER'26* has been dedicated for more than three decades to presenting the latest scientific achievements, research findings, and innovative approaches in the fields of ecology, environmental protection, and sustainable development. In 2026, the conference was held in Sokobanja, Serbia, at Hotel Sunce, from 24 to 26 June.

The primary aim of the conference is to bring together leading experts, researchers, professionals, and young scientists from diverse fields in order to foster the exchange of knowledge, strengthen scientific collaboration, and promote innovative solutions to contemporary environmental challenges. By connecting science, education, industry, and society, EcoTER'26 seeks to inspire the transformation of attitudes and practices in everyday life, as well as within economic and industrial systems, contributing to a more sustainable future.

The 32nd International Conference *Ecological Truth & Environmental Research – EcoTER'26* is organized by the University of Belgrade, the Technical Faculty in Bor, with the co-organization of the University of Banja Luka, the Faculty of Technology; the University of Montenegro, the Faculty of Technology – Podgorica; the University of Zagreb, the Faculty of Metallurgy – Sisak; the University of Pristina, the Faculty of Technical Sciences – Kosovska Mitrovica; and the Association of Young Researchers – Bor (Serbia).

The Proceedings of EcoTER'26 include 98 scientific papers authored by researchers, academics, and industry representatives from universities, research institutions, and organizations across the following countries: Bosnia and Herzegovina, Bulgaria, the Czech Republic, Finland, Italy, Montenegro, North Macedonia, Pakistan, Romania, Slovenia, the Netherlands, the United Kingdom, the United States of America, Uzbekistan, and Serbia. It is our great honour and pleasure to welcome all participants and contributors and to express our sincere appreciation for their valuable scientific contributions.

Within this year's conference programme, the 7th Student Section – EcoTERS'26 was also organized. We highly value the contribution of students and their mentors, whose enthusiasm, creativity, and dedication represent an important foundation for the advancement of scientific knowledge. We encourage young researchers to continue exploring, questioning, and expanding the boundaries of knowledge, recognizing that education and scientific discovery are lifelong processes.

The support of our donors, together with their commitment, trust, and willingness to cooperate, has significantly contributed to the successful organization of the conference. The Organizing Committee expresses its deepest gratitude to the Platinum donors of the conference – Serbia Zijin Mining DOO Bor and Serbia Zijin Copper DOO Bor; the Gold donors – HBIS SERBIA, the Serbian Chamber of Engineers, and Elixir Prahovo; and the Silver donor – Rudex Explosives.

We extend our sincere appreciation to all authors who contributed to these Proceedings. Special recognition is given to the members of the Scientific, Organizing, and Honorary Committees, reviewers, invited speakers, session chairs, and all participants whose dedication and support have contributed to the success and continuity of EcoTER.

Our sincere gratitude goes to everyone who has contributed to the organization and delivery of this conference. Your efforts and collaboration continue to strengthen the mission of EcoTER and its role in promoting scientific excellence, environmental responsibility, and sustainable development.

Ana Radojević

Prof. Dr Ana Radojević

President of the Organizing Committee

TABLE OF CONTENTS

Plenary Lectures

Jay Wadhawan
DROPLET ELECTROCHEMISTRY: FROM LABORATORY TO INDUSTRIAL APPLICATIONS 1

Grozdanka Bogdanović
FROM WASTE TO RESOURCE: A SUSTAINABLE APPROACH TO LEACHING OF SULFIDIC TAILINGS 2

Invited Lectures

Vesna Vučurović
BIOETHANOL AS A RENEWABLE ENERGY SOURCE: EFFICIENCY, SUSTAINABILITY, AND ENVIRONMENTAL IMPACT 5

Bojana Bajić, D. Vučurović, S. Dodić
BIOPROCESS ENGINEERING FOR CIRCULAR BIOECONOMY: MODELLING, OPTIMIZATION AND VALORISATION OF AGRO-INDUSTRIAL RESIDUES AND WASTES 12

Ana Simonović
APPLICATION OF ENVIRONMENTALLY SAFE INHIBITORS FOR METAL CORROSION PROTECTION 18

Ivan Savić, I. Savić Gajić, T. Palanački Malešević, I. Mihalj Lubaščik, Z. Svirčev, J. Meriluoto
PAN-LIFE-CARPET CONCEPT: INTEGRATING WASTE VALORIZATION AND BIOCRUST ENGINEERING 22

Jovana Bezdan, A. Bezdan
NATURE-BASED SOLUTIONS UNDER CLIMATE CHANGE: AN OVERVIEW OF KEY FINDINGS FROM THE UNSFA PILOT SITE WITHIN THE DALIA AND SWIM PROJECTS 29

Conference Papers

Žarko Radović, N. Tadić
EFFECT OF AIR OXYGEN ENRICHMENT AND EXCESS AIR RATIO ON SOLID FUELS COMBUSTION 40

Nebojša Tadić, I. Nikolić, N. Jovović, A. Drakulović, V. Radmilović
STRENGTH AND MICROSTRUCTURE OF FLY ASH BASED GEOPOLYMERS CONTAINING WASTE PLASTIC 46

Aleksandra Papludis, S. Alagić, S. Milić, D. Medić, J. Nikolić, V. Stankov Jovanović, G. Stojanović
AN ASSESSMENT OF THE PRESENCE OF DIBENZ(a,h)ANTHRACENE, A PROBABLE HUMAN CARCINOGEN, IN THE BOR REGION, ON THE BASIS OF ITS CONTENT IN STEMS AND LEAVES OF COMMON IVY, LILAC, AND FIG 51

Aleksandar Cvetković, Ž. Tasić, M. Petrović Mihajlović, A. Simonović, M. Radovanović, A. Bogdanović, M. Antonijević, S. Stanković
ELECTROCHEMICAL SENSING OF CAFFEINE 57

Milutin Stojadinović, V. Marjanović, I. Svrkota
FUNDAMENTALS OF WASTE CHARACTERISATION SAMPLING ACCORDING TO CEN/TR 15310 63

Boris Novaković, N. Paskaš, Z. Stojanović, V. Lakušić, I. Živić
ENVIRONMENTAL VARIABLES AFFECT DISTRIBUTIONAL PATTERNS OF THE RIFFLE BEETLE (Coleoptera: Elmidae) SPECIES IN THE SERBIAN STREAMS AND RIVERS 71

Boris Novaković, J. Đuknić, N. Paskaš, M. Raković, V. Lakušić, I. Živić
RIFFLE BEETLE *Elmis maugetii* Latreille, 1802 (Coleoptera: Elmidae): NOTES ON THE SPECIES' MORPHOLOGICAL PLASTICITY IN THE BALKAN PENINSULA 78

Radenka Kolarov, Dj. Petrov, N. Galečić, D. Skočajić, J. Čukanović, S. Đorđević, M. Ocokoljić
CHALLENGES, LIMITATIONS AND KNOWLEDGE GAPS CONCERNING ALLOCHTHONOUS TREES IN URBAN ENVIRONMENTS: WINGED ELM 83

Radenka Kolarov, Dj. Petrov, N. Galečić, D. Skočajić, J. Čukanović, S. Đorđević, M. Ocokoljić
THE INFLUENCE OF THE URBAN HEAT ISLAND ON *Abelia* × *grandiflora* (ROVELLI EX ANDRÉ) REHDER TAXA 85

Radenka Kolarov, Dj. Petrov, N. Galečić, D. Skočajić, J. Čukanović, S. Đorđević, M. Ocokoljić
Pyracantha angustifolia (Franch.) C.K.SCHNEID. A NEW EXOTIC SPECIES IN THE DENDROFLORA OF BELGRADE 93

Milena Nikolić, A. Zdravković, D. Marković Nikolić, D. Stojadinović, T. Nikolić
EVALUATION OF ECOLOGICAL POTENTIAL OF VETERNICA RIVER BASED ON CHEMICAL QUALITY PARAMETERS 100

Vesna Obradović, M. Perović, T. Vučković
MICROBIOLOGICAL QUALITY OF THE VELIKA MORAVA RIVER: ECOLOGICAL AND PUBLIC HEALTH ASPECTS 106

Milan Đorđević, B. Stojanović, A. Zdravković, D. Stojadinović, T. Nikolić, Đ. Miltenović

ANALYSIS OF PHYSICAL HAZARDS IN THE ENVIRONMENT AND THEIR IMPACT ON HUMAN HEALTH: CASE STUDY OF THE CITY OF NIŠ, REPUBLIC OF SERBIA 112

Milan Đorđević, B. Stojanović, A. Zdravković, D. Stojadinović, T. Nikolić, M. Nikolić

IDENTIFICATION AND ANALYSIS OF NON-IONIZING ELECTROMAGNETIC RADIATION IN THE ENVIRONMENT: CASE STUDY OF LESKOVAC CITY, REPUBLIC OF SERBIA 119

Sanja Pavlović

COMBINED METEOROLOGICAL MEASUREMENTS OF URBAN AND RURAL THERMAL ENVIRONMENTS IN BELGRADE 126

Jovana Galjak, M. Krstić, S. Milojević, G. Milentijević

HEAVY METAL DISTRIBUTION AND CHEMICAL SPECIATION IN SOILS NEAR THE GORNJE POLJE FLOTATION TAILINGS 135

Ivana Kostić Kokić, D. Bogdanović, N. Stanković, T. Anđelković

AMMONIUM HYDROXIDE AND MILK FAT CONTENT EFFECT ON BENZYL BUTYL PHTHALATE EXTRACTION 142

Viša Tasić, V. Kamenović, B. Radović, R. Kovačević, N. Ristić, Z. Damnjanović, M. Cocić

INDOOR PM_{10} AND $PM_{2.5}$ IN RESIDENTIAL APARTMENTS IN BOR, SERBIA: NON-HEATING SEASON ANALYSIS 146

Biljana Budzakoska Gjoreska, S. Trajanovski, S. Trajanovska

INFLUENCE OF LITTORAL HABITAT CHARACTERISTICS ON MACROINVERTEBRATE COMMUNITIES IN LAKE OHRID 153

Vesna Marjanović, Z. Štirbanović, R. Marković

PLANNING AND IMPLEMENTATION OF MINING WASTE SAMPLING: STANDARDS AND LEGAL REGULATIONS 162

Miljan Vilimonović, J. Vesković, A. Okolišan, M. Vesković, M. Lučić, A. Onjia

MULTIVARIATE ASSESSMENT OF HEAVY METALS IN RIVER WATER FROM NOVI PAZAR AREA 169

Branislava Matić, V. Vukmanović, S. Živković Perišić

URBAN AIR QUALITY MEASURED CLOSE TO SCHOOLS AND KINDERGARTENS WITHIN THE LOCAL MONITORING NETWORK IN SERBIA 175

Tamara Mitić, A. Marić, K. Jovičić, V. Đikanović, N. Marinković, S. Anđus, J. Čanak Atlagić

UNCOVERING HIDDEN DIVERSITY OF *Sabanejewia balcanica* IN SERBIA: THE DISCOVERY OF NOVEL HAPLOTYPES 181

Olga Jakovljević, S. Popović, M. Pećić, D. Jerinkić
DIATOMS FROM LUDAŠ LAKE AND THEIR APPLICATION IN BIOINDICATION 187

Predrag Pajic, Ž. Rudic, N. Rakonjac
ASSESSMENT OF GROUNDWATER SUITABILITY FOR IRRIGATING URBAN GREEN SPACES IN ALLUVIAL AQUIFERS 194

Predrag Pajic, Ž. Rudic, N. Rakonjac
LONG-TERM PERSISTENCE OF FLUORIDE CONTAMINATION IN ALLUVIAL GROUNDWATER: A CASE STUDY OF THE CARINA WELLFIELD IN KLADOVO (SERBIA) 201

Željko Ćirović, D. Kleut, D. B. Stojanović, M. Jovašević-Stojanović
COMPARISON OF SATELLITE DATA WITH LOW-COST SENSOR NETWORK PM DATA IN FOUR CITIES IN SERBIA 210

Madalina Zot, F. Popescu
ASSESMENT OF SEDIMENTABLE PARTICULATE MATTER IN TIMISOARA 217

Ivana Kostić Kokić, N. Stanković, D. Bogdanović, T. Petronijević, M. Dudić, T. Anđelković
IMPACT OF DIMETHYL PHTHALATE ON THE GROWTH AND STRUCTURE OF CYANOBACTERIA (*Microcystis* sp.) 222

Ivana Kostić Kokić, N. Stanković, D. Bogdanović, T. Petronijević, M. Dudić, T. Anđelković
IMPACT OF DIMETHYL PHTHALATE ON THE GROWTH AND STRUCTURE OF GREEN ALGAE (*Chlorella* sp.) 228

Anđelija Bogdanović, Ž. Tasić, M. Petrović Mihajlović, A. Simonović, M. Radovanović, M. Antonijević, A. Cvetković
ELECTROCHEMICAL DETERMINATION OF CEFTRIAXONE USING A GRAPHITE ROD ELECTRODE 233

Milan Gorgievski, M. Marković, V. Grekulović, N. Štrbac, M. Marković, M. Zdravković, K. Božinović
SEM-EDS AND DTA-TGA ANALYSIS OF CORN STALKS USED FOR THE BIOSORPTION OF COPPER IONS FROM SYNTHETIC SOLUTIONS 239

Dubravka Nikolovski, S. Đurić, D. Mićić, G. Trajkovska, Lj. Lazić, T. Stajić, D. Stošić, K. Kralj, J. Zec
LONG-TERM TRENDS OF AIRBORNE POLLEN IN PANČEVO 243

Milena Nikolić, A. Zdravković, D. Marković Nikolić, G. Petković, T. Nikolić
REMOVAL OF SYNTHETIC DYE FROM AQAEOUS SOLUTIONS USING *Qercus cerris* ACORN CUPS 250

Milena Nikolić, A. Zdravković, D. Marković Nikolić, N. Ristić, I. Ristić
KINETIC AND THERMODYNAMIC ASPECTS OF PESTICIDE SORPTION ONTO HORSE CHESTNUT SEED SORBENT 256

Jovana Perendija, V. Ljubić, D. Milošević, S. Cvetković, M. Đuriš, Ž. Milovanović

COMPARATIVE KINETIC ANALYSIS OF CATIONIC DYES ADSORPTION ONTO SUSTAINABLE LIGNOCELLULOSIC BIOSORBENTS 261

Verica Ljubić, J. Perendija, D. Milošević, Ž. Milovanović, S. Cvetković, K. Trivunac

MECHANISMS AND FACTORS INFLUENCING Ni(II) BIOSORPTION BY BACTERIAL EXOPOLYSACCHARIDES: A REVIEW 266

Dunja Banđur, R. Prodanović, M. Spasojević Savković, M. Stanković, D. Bartolić, O. Prodanović, N. Surudžić

ENZYMATIC DEGRADATION OF PHENOL VIA HRP PERIODATELY IMMOBILIZED ONTO GMA-CO-EGDMA MACROPOROUS CARRIERS 273

Nena Velinov Georgiev, M. Radović Vučić, M. Petrović, M. Kostić, M. Momčilović, J. Mitrović, A. Bojić

SORPTION OF TEXTILE DYES ONTO BISMUTH-MODIFIED WOOD WASTE SORBENT: KINETIC AND EQUILIBRIUM ANALYSIS 279

Saša Rančev, M. Petrović, S. Najdanović, N. Velinov Georgiev, J. Mitrović, M. Radović Vučić, A. Bojić

SELF-MADE PULSATING ATMOSPHERIC PRESSURE CORONA PLASMA REACTOR FOR DEGRADATION OF A TEXTILE DYE IN SYNTHETIC TEXTILE EFFLUENT 284

Jelena Mitrović, N. Velinov Georgiev, M. Momčilović, M. Petrović, M. Kostić, S. Najdanović, A. Bojić

THERMALLY ACTIVATED PEROXYDISULFATE DEGRADATION OF REACTIVE TEXTILE DYES 290

Darko Anđelković, M. Branković

DIRECT INFUSION MS AS A PROMISING TOOL FOR PESTICIDES QUALITATIVE SCREENING IN APPLES 297

Darko Anđelković, M. Branković

CALIBRATION PERFORMANCES OF A MULTIRESIDUE PESTICIDES ANALYSIS IN LEMON AND LETTUCE ON QqQ AND ION TRAP MASS SPECTROMETERS 304

Darko Anđelković, M. Branković

THE NATURE OF THE MATRIX EFFECT IN GC/MS PESTICIDES ANALYSIS IN APPLES AND ITS RELATION TO EXTRACT DILUTION 310

Isidora Santrač, F. Sekereš, M. Živković, J. Korać Jačić, M. Milenković, J. Danilović Luković

DEGRADATION OF PONCEAU S DYE BY ADVANCED OXIDATION PROCESSES: COMPARATIVE ANALYSIS AND TOXICITY OF TRANSFORMATION PRODUCTS 316

Isidora Santrač, F. Sekereš, M. Živković, J. Korać Jačić, M. Milenković, J. Danilović Luković

BIOLOGICAL EFFECTS OF EVANS BLUE AND ITS DEGRADATION PRODUCTS ON GROWTH AND VIABILITY OF THE GREEN MICROALGA *Chlamydomonas ccidophila* PM01 324

Irina Vasić, I. Čeliković, A. Samolov, T. Milanović, A. Kandić, M. Đurašević

ANNUAL EFFECTIVE DOSE DUE TO INGESTION OF HERBAL INFUSIONS FROM ASTERACEAE MEDICINAL PLANTS 330

Dušan Nikolić, S. Marjanović, M. Dimitrijević, Z. Marković, A. Dobričić, M. Stanković, B. Rašković

CONCENTRATIONS OF METALS AND METALLOIDS IN MEAT OF THE COMMON CARP (*Cyprinus carpio*) FARMED USING FEED BASED ON INVERTEBRATE ANIMAL PROTEIN ORIGIN 336

Dunja Banđur, D. Bartolić, M. Stanković, M. Prokopijević, N. Surudžić, S. Stanković, M. Mićić

LABEL-FREE FLUORESCENCE-BASED OPTICAL BIOSENSOR FOR RAPID DETECTION OF FUNGAL PATHOGENS 343

Katarina Jovičić, V. Đikanović, J. S. Vranković

REDOX BIOMARKERS IN SEMINAL PLASMA OF CULTURED RAINBOW TROUT: TOS, TAS, AND OSI 348

Petar Petrov

UTILIZATION OF A PRODUCT FROM SULFURIC ACID PRODUCTION, POLLUTING THE ENVIRONMENT, WITH APPLICATION IN FERROUS METALLURGY 353

Despina Kostadinova Jankovski, M. Arizanova, B. Ristovski, E. Velickova, D. Doneva-Shapcheska

VALORIZATION OF BREWERY SPENT GRAIN INTO BIOPLASTIC FILMS: INFLUENCE OF BIOMASS LOADING ON BARRIER AND ANTIOXIDANT PROPERTIES 360

Boris Novaković, M. Raković

SOUTHEASTERN EUROPEAN BLACKBIRD *Turdus merula aterrimus* (MADARÁSZ, 1903) IN THE BALKAN PENINSULA 368

Pasquale Napoletano, E. Vitale, A. De Marco, C. Arena

PROPERTIES OF PLANT AND SOIL SHAPING FRUIT AND OIL TRAITS IN DIFFERENT CULTIVARS OF *Olea europaea* L. 374

Dragana Ranđelović, S. Valiyev, M. Nasirov, J. Amirov

GERMINATION OF *Artemisia diffusa* Krasch. ex. Poljakov SEEDS ORIGINATED FROM RANGELAND SITES OF DIFFERENT GRAZING INTENSITIES 381

Mihajlo Stanković, N. Beslac, D. Romčević

NEW FINDING SPECIES ABLEPHARUS KITAIBELII BIBRON & BORY, 1833 (*Reptilia: Squamata: Scincidae*) IN BOSNIA AND HERZEGOVINA 386

Mihajlo Stanković

CONTRIBUTION OF THE DISTRIBUTION OF THE SPECIES *Ricciocarpos natans* (L.) CORDA 1829 IN THE SNR ZASAVICA AND MAČVA WITH THE ANALYSIS OF THE HABITAT 394

Sonja Stanković, M. Radovanović, A. Simonović, Ž. Tasić, A. Cvetković, V. Nedelkovski, D. Medić

PROCESS OPTIMIZATION OF ZnO-ASSISTED PHOTOCATALYTIC DEGRADATION OF METHYL ORANGE USING RESPONSE SURFACE METHODOLOGY 403

Uroš Stamenković, I. Marković, D. Manasijević, K. Božinović, M. Nedeljković, A. Kovačević

CHARACTERIZATION OF THE Sn78Bi22 ALLOY AS AN ENVIRONMENTALLY FRIENDLY LEAD-FREE SOLDER 410

Miljan Marković, M. Gorgievski, V. Grekulović, N. Štrbac, M. Marković, K. Božinović, M. Zdravković

CHANGE IN METAL REMOVAL DEGREE DURING COPPER ION BIOSORPTION ONTO RAW AND CALCINED CHICKEN EGGSHELLS 417

Ivana Marković, U. Stamenković, M. Nedeljković, D. Manasijević, Lj. Balanović

ENVIRONMENTAL ASPECTS AND EXPERIMENTAL INVESTIGATION OF SAC/GNS COMPOSITE LEAD-FREE SOLDER 422

Katarina Stojanović, M. Simić, D. Aćimović, B. Savić Rosić, M. Ječmenica Dučić, T. Brdarić

THERMAL TRANSFORMATION OF NSAID-DERIVED MATERIALS: MORPHOLOGICAL AND COMPOSITIONAL INSIGHTS 427

Katarina Stojanović, M. Simić, D. Aćimović, B. Savić Rosić, M. Ječmenica Dučić, T. Brdarić

PRODUCTION COST ASSESSMENT OF SnO_2-MWCNT@SS ELECTRODE FOR WASTEWATER TREATMENT 432

Natalija Nedić, S. Bulatović, T. Tadić, B. Marković, A. Nastasović

AMBROSIA-BASED BIOSORBENTS FOR REMOVAL OF RHODAMINE B FROM AQUATIC SOLUTION 438

Ljubiša Balanović, U. Stamenković, I. Marković, K. Božinović, M. Gorgievski, V. Grekulović, T. Jogrić

EFFECT OF Ni AND Si ADDITIONS ON FUNCTIONAL PROPERTIES OF Cu-30Zn BRASS 443

Katarina Stojanović, M. Simić, D. Aćimović, B. Savić Rosić, M. Ječmenica Dučić, D. Maksin, T. Brdarić (SERBIA)

SYNERGISTIC INTERACTION BETWEEN Sb AND RARE-EARTH OXIDES IN SnO_2 ELECTROCATALYSTS 452

Milan Đorđević, B. Stojanović, A. Zdravković, D. Stojadinović, T. Nikolić, S. Stojanović
QUANTITATIVE DETERMINATION OF ESSENTIAL AND TOXIC ELEMENTS CONTENT IN PEACH FRUITS BY ICP-OES METHOD 456

Sofija Banković, M. Lj. Petrović, A. Janković, M. Rakin, M. Vukašinović Sekulić
ANTIOXIDANT ACTIVITY OF CLOVE ESSENTIAL OIL 463

Dragana Randjelović, V. Savić, V. Topalović, M. Koprivica, J. Nikolić
GROWTH PARAMETERS RESPONSE OF *Ocimum basilicum* 'Genovese' TO PHOSPHATE GLASS AS AN ALTERNATIVE FERTILIZER 471

Milan Grozdanović, M. Mančić, J. Đoković, D. Tanikić, A. Đorđević
INTEGRATED HYBRID SYSTEMS FOR RESIDENTIAL ENERGY AUTONOMY: A LITERATURE REVIEW 478

Milan Nedeljković, S. Mladenović, V. Ćosović, I. Marković, J. Petrović, U. Stamenković
GREEN ENGINEERING APPROACH TO Sn-0.7Cu/xGNS COMPOSITES PRODUCED BY POWDER METALLURGY: MICROSTRUCTURAL AND MECHANICAL PROPERTIES FOR SUSTAINABLE ELECTRONICS 485

Snežana Urošević, M. Vuković
TEXTILE WASTE MANAGEMENT IN THE CONTEXT OF THE CIRCULAR ECONOMY AND ITS SOCIOECONOMIC EFFECTS 490

Danijela Voza, M. Veličković, M. Panić, A. Fedajev, S. Arsić, D. Mladenović
GREEN PURCHASING DETERMINANTS AMONG GENERATION Z: AN EXPLORATORY FACTOR ANALYSIS 497

Marija Ivanović, S. Knežević, Lj. Kljajević, N. Mladenović Nikolić, I. Maksimović, K. Cmiljanović, S. Nenadović
GREEN METAKAOLIN GEOPOLYMERS: SYNTHESIS AND CHARACTERIZATION DURING AGEING 503

Dragi Peltechki
DIAGNOSING CRITICAL RAW MATERIALS SECTOR READINESS IN CANDIDATE COUNTRIES: A PESTLE-BASED ASSESSMENT OF NORTH MACEDONIA 509

Marija Stojanoska, V. Atanasova
SUSTAINABLE TRANSPORT AND FIGHT AGAINST POLLUTION, CASE STUDY 516

Luka Grbović, O. Jakovljević, J. Krizmanić, B. Tubić, M. Kračun Kolarević, S. Anđus, B. Vasiljević
ADDITIONAL RECORDS ON BENTHIC DIATOM *Encyonema Bonapartei* Heudre, C.E. Wetzel & Ector (Cymbellales, Bacillariophyceae) IN WATER BODIES OF THE UVAC SPECIAL NATURE RESERVE (SERBIA) 523

Bojana Tubić, J. Đuknić, N. Marinković, N. Popović, L. Grbović, M. Raković, M. Paunović

AQUATIC MACROINVERTEBRATE FAUNA AT SELECTED SAMPLING SITES IN THE GRADAC RIVER 530

Olga Jakovljević, A. Božić, S. Popović

DIATOM ASSEMBLAGES IN BIOFILMS OF FRUŠKA GORA WATERFALLS (SERBIA) 536

Slađana Popović, Z. Krantić, O. Jakovljević, A. Anđelković, A. Milićević

pH-DEPENDENT GROWTH RESPONSES OF *Chlorella* STRAINS IN BG11 MEDIUM 541

Nataša Kojadinović, S. Đuretanović, M. Radenković, A. Milošković, T. Veličković, M. Jakovljević, V. Simić

ASSESSMENT OF THE LENGTH–WEIGHT RELATIONSHIP AND RELATIVE CONDITION FACTOR OF SCADAR BLEAK IN THREE WESTERN BALKAN LAKES 546

Vesna Obradović, M. Perović, T. Vučković

QUANTIFYING SAMPLING CONTRIBUTION TO MEASUREMENT UNCERTAINTY IN MICROBIOLOGICAL GROUNDWATER ANALYSIS 551

Vesna Obradović, M. Perović, J. Lekić

MEASUREMENT UNCERTAINTY OF WASTEWATER SAMPLING FOR MICROBIOLOGICAL ANALYSIS USING DUPLICATE SAMPLING AND ANOVA APPROACH 556

Maja Nujkić, Ž. Tasić, T. Kalinović, D. Medić, A. Radojević, J. Kalinović, J. Jordanović, S. Đorđievski, N. Apostolov

PREPARATION AND APPLICATION OF MODIFIED ZEOLITE FROM INDUSTRIAL WASTE 561

Vanja Trifunović, S. Milić, Lj. Avramović, S. Vasiljević, D. Medić, V. Nedelkovski, D. Božić

TRANSFORMATION OF WASTE FROM HAZARDOUS TO NON-HAZARDOUS: STABILIZATION OF SOLID RESIDUE OBTAINED AFTER TWO-STEP HYDROMETALLURGICAL TREATMENT OF EAF DUST 568

Isidora Santrač, J. Korać Jačić, M. Milenković, M. Živković

HOW STRUCTURAL MODIFICATIONS INFLUENCE ENVIRONMENTAL RISK: A CASE STUDY OF STEROIDAL DERIVATIVES 576

Jelena Janjić, M. Ćurić

IMPACT OF FOG DISPERSION ON AVIATION AND ENVIRONMENTAL SAFETY 582

Vesna Djikanović, J. Vranković, K. Jovičić

MICRO AND MESOPLASTIC PARTICLES IN WATER AND SEDIMENT IN SPECIAL NATURE RESERVE “OBEDSKA BARA” 590

Marko Pezdevšek, A. Roger, M. Fike, K. Sredenšek
NUMERICAL ASSESSMENT OF THE IMPACT OF FLOATING PHOTOVOLTAIC SYSTEMS ON LAKE THERMAL REGIME 595

Bojana Petrović, M. Jovanović, B. Radović, R. Kovačević, M. Jovašević-Stojanović
SOURCE-ASSOCIATED HEALTH RISKS RELATED TO METALLIC AND CARBONACEOUS PM_{10} FRACTION AT TWO URBAN SITES IN SERBIA 602

Usama Bin Moazzam, H. Nawab, K. Nasir, I. Batool
CLIMATE-INDUCED PROJECT SCOPE CREEP AND COST OVERRUNS IN LONG-HORIZON INFRASTRUCTURE PROJECTS: THE MEDIATING ROLE OF ADAPTIVE RISK RE-ASSESSMENT 610

Student Section – EcoTERS'26

Student: Dragana Kerkez
Mentors: Svetlana Nešović, Kristina Filipović, Jovana Krstić
HEALTH IMPACTS AND PREVENTION STRATEGIES OF URBAN AIR POLLUTION 620

Student: Jelena Zec
Mentors: Milena Rikalović, Dubravka Nikolovski
ASSESSMENT OF THE IMPACT OF FINE SUSPENDED PARTICLES PM_{10} AND LEAD ABSORBED ONTO THEM IN AMBIENT AIR OF PANČEVO ON PUBLIC HEALTH 622

Student: Minja Stojadinović
Mentor: Maja Nujkić
PRESENCE AND INFLUENCE OF PHARMACEUTICAL POLLUTANTS IN THE ENVIRONMENT 624

Student: Nataša Janjić
Mentor: Žaklina Tasić
COPPER CORROSION INHIBITORS IN CHLORIDE ENVIRONMENTS 626

Student: Saška Dumitrašković
Mentors: Milan Gorgievski, Vesna Grekulović
ADSORPTION ISOTHERMS FOR COPPER IONS BIOSORPTION ONTO GRAPE STALKS 628

Student: Veljko Jovanović
Mentor: Maja Nujkić
THE IMPACT OF BIODEGRADABLE PLASTICS ON THE ENVIRONMENT 630

Student: Marina Karabašević
Mentors: Vesna Grekulović, Milan Gorgievski
ELECTROCHEMICAL BEHAVIOR OF COPPER IN PRESENCE OF OAK BARK MACERATE 632

Student: Snežana Nikolić
Mentor: Maja Nujkić

PHOTOCATALYTIC NANOMATERIAL FOR HEAVY METAL REMEDIATION 634

Student: Nataša Apostolov
Mentor: Maja Nujkić

MECHANISMS AND CHALLENGES OF PHOTOCATALYTIC NANOMATERIALS IN HEAVY METAL REMOVAL 636

Students: Nebojša Radović, Aleksa Vizi, Željka Nikolić
Mentors: Ivan Kojić, Ksenija Stojanović

BIODIESEL PRODUCTION FROM SUNFLOWER OIL USING CALCINED CIGARETTE ASH AS A WASTE-DERIVED CATALYST 638

Student: Marija Vesković
Mentor: Antonije Onjia

IDENTIFICATION OF HEAVY METAL SOURCES IN RIVER SEDIMENT IN THE KRUPANJ AREA 640

Student: Aleksandra Jović
Mentor: Maja Nujkić

RECYCLING OF ERDITE AND $KFES_2$ FROM WASTE SLUDGE AS FUNCTIONAL MATERIALS FOR ENVIRONMENTAL PROTECTION 642

Student: Teodora Jogrić
Mentor: Ljubiša Balanović

INFLUENCE OF Ni AND Si ADDITIONS ON THE MICROSTRUCTURE, MECHANICAL PROPERTIES AND CONDUCTIVITY OF CuZn30 ALLOY 644

Student: Jovana Levkić
Mentors: Tanja Kalinović, Jelena Kalinović

ENVIRONMENTAL IMPACT AND EMISSION CONTROL IN PYROMETALLURGICAL COPPER PRODUCTION 646

Student: Mladen Radić
Mentors: Jelena Kalinović, Ana Radojević

IMPACT OF ARTIFICIAL INTELLIGENCE USE ON AIR POLLUTION 648

Student: Nataša Đorđević
Mentors: Jelena Kalinović, Tanja Kalinović

PLANTS AS BIOINDICATORS OF AIR POLLUTION 650

Author index 652

Plenary Lectures

Abstract

DROPLET ELECTROCHEMISTRY: FROM LABORATORY TO INDUSTRIAL APPLICATIONS

DOI: 10.5937/EcoTER26001W

Jay Wadhawan[1,a*]

[1] Chemical Engineering, School of Engineering & Technology, Faculty of Science & Engineering, The University of Hull, Cottingham Road, Kingston-upon-Hull HU6 7RX, UNITED KINGDOM

[a] https://orcid.org/0000-0002-1691-7169

Abstract

Electron transfer reactions in droplets on a surface is a fascinating platform that can be used for the study of chemistry in confined volumes ranging over 18 orders of magnitude: from yoctolitres to microlitres. However, they also provide a methodology to enable the coupling between biochemical, geochemical and electrochemical systems, which enables opportunities in the redox recovery of strategic and growth minerals, and empowering communities of living organisms in relatively anoxic environments. One of the problems in the study of micro-organisms attached to redox surfaces is the occurrence of non-uniform material flux, which results from the singularity at the basal contact.

In this lecture, the chemistry at triple-phase boundaries will first be examined through understanding the role played by the non-uniform electric field that exists. Although this work might appear somewhat specialised and adventurous, it enables the showcasing of the challenges in the continual translation of chemistry in the laboratory to the applied settings of the manufacturing and analytical process industries, where research directions are purposely constrained to drive economic growth. Accordingly, droplet electrochemistry commercialisation journeys and successes will be highlighted through applications in environmentally and socially responsible technologies for (1) new concept pH sensors for oceanology and biomedical point-of-care settings; (2) offshore oil and gas wastewater remediation; (3) green chemistry for jet fuels and mass transportation products; and (4) strategic metal extraction.

ACKNOWLEDGEMENT

This work has been funded by, amongst others, EPSRC, Innovate UK, The Leverhulme Trust and The University of Hull.

[*] *j.wadhawan@hull.ac.uk*

Abstract

FROM WASTE TO RESOURCE: A SUSTAINABLE APPROACH TO LEACHING OF SULFIDIC TAILINGS

DOI: 10.5937/EcoTER26002B

Grozdanka Bogdanović[1,a*]

[1] University of Belgrade, Technical Faculty in Bor, Vojske Jugoslavije 12, 19210 Bor, SERBIA

[a] https://orcid.org/0000-0002-1013-4075

Abstract

The mining industry plays a key role in a country's development, contributing significantly to both economic and technological progress. However, mining activities often cause considerable environmental impacts. Sulfide-rich tailings are commonly associated with acid mine drainage (AMD), heavy metal mobilization, and long-term environmental contamination. These tailings are residues from the mineral concentration stage, and are therefore predominantly composed of gangue minerals, such as quartz (SiO_2), carbonates ($CaCO_3$), various oxides (Al_2O_3, MgO, Fe_2O_3, Fe_3O_4), as well as pyrite (FeS_2). Additionally, these tailings contain sulfide minerals such as chalcopyrite ($CuFeS_2$), sphalerite (ZnS), galena (PbS), and pyrrhotite ($Fe_{1-x}S$), which remain after the extraction of economically valuable metals from ores. Meanwhile, advances in resource recovery technologies have shown that many historical and active tailings deposits still contain significant concentrations of critical and valuable metals, including cobalt, nickel, zinc, copper, rare earth elements, and precious metals. In recent years, rising global demand for critical raw materials, driven by the energy transition, electrification, and low-carbon technologies, has intensified interest in tailings reprocessing as a secondary resource strategy. Sustainable leaching technologies have emerged as promising methods for recovering residual metals from sulfidic tailings while simultaneously reducing the environmental liabilities associated with long-term tailings storage. Traditional acidic leaching systems based on sulfuric acid remain widely used due to their high extraction efficiency; however, these processes often involve substantial chemical consumption and generate secondary waste streams. Consequently, current research increasingly focuses on sustainable alternatives such as bioleaching, glycine leaching, ionic liquids, deep eutectic solvents (DES), chloride systems, and oxidative alkaline leaching. Among these approaches, bioleaching has attracted considerable attention because of its low energy requirements and reduced environmental impact. This review examines recent advances in sustainable leaching technologies for processing sulfide tailings and highlights some of the challenges and opportunities for future research. It focuses on their role in circular economy strategies, the recovery of critical metals, and the sustainable management of mining waste

Keywords: *sulfidic tailings, metal recovery, leaching, mining waste valorization, circular economy.*

[*] *gbogdanovic@tfbor.bg.ac.rs*

ACKNOWLEDGEMENT

The author is grateful to the Ministry of Science, Technological Development and Innovation of the Republic of Serbia for financial support according to the contract with registration No. 451-03-34/2026-03/200131.

REFERENCES

[1] Zou, K., Zhang, Y., Shen, L., *et al*. Chem. Eng. J. 2025, 503, 158198.

[2] Nakhaei, F., Corchado-Albelo, J., Alagha, L., *et al*. Sep. Purif. Technol. 2025, 354 (4), 128973.

[3] Marilović, D., Bogdanović, G., Stevanović, Z., *et al*. Min. Metall. Explor. 2026, 43 (1), 657–672.

[4] Petrović, S., Bogdanović, G., Antonijević, M. Trans. Nonferrous Met. Soc. China. 2018, 28 (7), 1444–1455.

[5] Stanković, V., Milošević, V., Miličević, D., *et al*. Chem. Ind. Chem. Eng. Q. 2018, 24 (4), 333–344.

[6] Petrović, S.J., Bogdanović, G.D., Antonijević, M.M., *et al*. Min. Metall. Explor. 2026, 43(2), 1935–1949.

[7] Petrović, S.J., Bogdanović, G.D., Antonijević, M.M., *et al*. Metals. 2023, 13 (11) 1818.

[8] Kinnunen, P., Karhu, M., Yli-Rantala, E., *et al*. Clean Eng. Technol. 2022, (8), 100499.

[9] Behnajady, B., Najafi, M., Saeid Karimi, S.J. Taiwan Inst. Chem. Eng. 2025, (172), 106118.

[10] Kursunoglu, S. J. Sustain. Metall. 2025, 11, 2023–2050.

[11] Araujo, F.S.M., Taborda-Llano, I., Nunes, E.B., *et al*. Geosciences. 2022, 12, 319.

[12] Schueler, T.A., de Aguiar, P.F., Vera, Y.M., *et al*. J. Sustain. Metall. 2021, 7, 1523–1536.

[13] Maltrana, V., Morales, J. Metals. 2023, 13, 1862.

[14] Wang, D., Liu, Q. Hydrometallurgy. 2026, 243, 106723.

[15] Crane, R.A., Mohammad, A., Jin, F., *et al*. Hydrometallurgy. 2025, 236, 106506.

[16] Jamett, I., Carrasco, P., Olmos, M., Hernández, P. Minerals. 2023, 13, 22.

[17] Zante, G., Yu Boltoeva, M. Sustain. Chem. 2020, 1, 238–255.

[18] Tezyapar Kara, I., Kremser, K., Wagland, S.T., *et al*. Environ. Chem. Lett. 2023, 21, 3329–3350.

[19] Watling, H.R., Watkin E.L.J., Ralph, D.E. Environ. Technol. 2010, 31 (8–9), 915–933.

[20] Antonijević, M.M., Dimitrijević, M., Stevanović, Z.O., *et al*. Hazard. Mater. 2008, 158 (1), 23–34.

[21] Stevanović, Z.O., Antonijević, M.M., Bogdanović, G.D., *et al*. Chem. Ecol. 2011, 27 (5), 401–414.

Invited Lectures

Review

BIOETHANOL AS A RENEWABLE ENERGY SOURCE: EFFICIENCY, SUSTAINABILITY, AND ENVIRONMENTAL IMPACT

DOI: 10.5937/EcoTER26005V

Vesna Vučurović[1,a*]

[1] Faculty of Technology Novi Sad, University of Novi Sad, Boulevard cara Lazara 1, 21000 Novi Sad, SERBIA

[a] https://orcid.org/0000-0002-2923-552X

Abstract

Bioethanol is one of the most widely used renewable liquid biofuels and a viable alternative to fossil fuels. Its use instead of fossil fuels can significantly reduce greenhouse gas emissions, contributing to climate change mitigation and improved energy sustainability. Beyond its role as a fuel, bioethanol is extensively used as a solvent, disinfectant, and basic chemical for a broad range of products in the chemical, food, and pharmaceutical industries. Industrial bioethanol production is primarily based on microbial alcoholic fermentation by the yeast Saccharomyces cerevisiae, which converts sugars derived from carbohydrate-rich biomass into ethanol. Traditionally, production relies on first-generation feedstocks, including sugar- and starch-based plant materials such as sugarcane, sugar beet, molasses, cereal grains, potatoes, cassava, etc. However, concerns regarding food security and land use have encouraged the development of second-generation lignocellulosic biomass and third-generation algal biomass as alternative feedstocks. Despite its well-recognized advantages, large-scale bioethanol production from non-food feedstocks continues to face important challenges related to energy efficiency, process optimization, long-term sustainability, and overall environmental performance. This paper therefore provides a comprehensive and critical assessment of bioethanol production efficiency, sustainability considerations, and environmental impacts across different feedstock generations, highlighting both technological progress and remaining limitations.

Keywords: bioethanol, renewable energy, sustainability, efficiency, environmental impact.

INTRODUCTION

Bioethanol is an ethanol (C_2H_5OH) produced via microbial alcoholic fermentation by yeast, usually *Saccharomyces cerevisiae*, from carbohydrate-rich biomass. It is one of the most widely utilized renewable liquid biofuels and is recognized as an environmentally friendly alternative to fossil fuels [1]. Over the past few decades, global bioethanol production has increased several-fold, primarily driven by its use as a fuel-grade biofuel, reaching approximately 31.3 billion gallons in 2024, with a trend of continued growth [2]. Its use instead of fossil fuels enables a substantial reduction in greenhouse gas emissions up to 75%, while simultaneously addressing pressing environmental and energy challenges [3,4]. Bioethanol is extensively applied in the transport sector, either blended with gasoline at concentrations of 5, 10, or 85% (E5-E85) or as a component in octane enhancers such as ethyl

* *vvvesna@uns.ac.rs*

tertiary butyl ether (ETBE). While low-percentage blends can be used in conventional engines without modification, high-percentage blends such as E85 require flexible fuel vehicles (FFVs) [4].

Industrial bioethanol production primarily relies on microbial alcoholic fermentation, in which sugars derived from carbohydrate-rich biomass are converted into ethanol by yeast [1,5]. Globally, first-generation (1G) feedstocks, such as sugar-containing (sugarcane, sugar beet, molasses, etc.), and starch-containing raw materials (corn, wheat, cassava, sweet sorghum, and potatoes), dominate commercial bioethanol production [1,5,6]. Starch-based feedstocks contribute approximately 60% of the worldwide bioethanol supply, whereas sugar-based feedstocks account for nearly 40% [6]. The prevalence of starchy and sugary biomass is attributed to its high conversion efficiency, ethanol yield, and cost-effectiveness, making it a preferred choice in industrial applications [5–7]. Globally, first-generation (1G) feedstocks are characterized by high quality, minimal pretreatment requirements, established conversion technologies, and large production volumes, resulting in efficient processing and relatively high ethanol yields that underpin the economic viability of bioethanol worldwide [8].

Despite the continued global reliance on first-generation (1G) feedstocks, increasing concerns about food security, land availability, and long-term sustainability have accelerated the transition toward the use of non-food biomass resources. Lignocellulosic biomass, classified as second-generation (2G), and algal biomass, representing third-generation (3G) feedstocks, are increasingly recognized as promising options for decoupling bioethanol production from competition with the food supply [2,8–10]. At the same time, advances in pretreatment strategies, enzymatic hydrolysis, and fermentation technologies have enabled the utilization of a broader spectrum of feedstocks, marking the progressive evolution of bioethanol production pathways. Nevertheless, achieving improved sustainability, enhanced energy efficiency, and economic viability, particularly for 2G and 3G bioethanol, remains a significant challenge that continues to shape current research and technological development efforts [5–11].

Fourth-generation (4G) biofuels rely on genetically engineered microalgae and designed microorganisms to enhance carbon capture and directly improve bioethanol productivity through advanced synthetic biology. Fifth-generation (5G) biofuels focus on genome-edited and metabolically engineered crops with modified cell wall structures to increase sugar yields and reduce processing costs. However, both approaches remain at an early research stage and are not yet commercially viable, while also raising important technical, environmental, and societal considerations [2].

METHODOLOGY

This review is based on a systematic analysis of scientific literature and analytical data related to bioethanol production, bioconversion processes, and analytical techniques. Publications were retrieved from electronic databases, including Google Scholar, Scopus, ScienceDirect, and PubMed, using predefined keywords related to bioethanol production, fermentation, sustainability, and life cycle assessment. The selected publications were published from 2018 to 2024, ensuring that the information is up-to-date and relevant.

THE CURRENT STATUS AND TRENDS OF BIOETHANOL PRODUCTION

Over the past few decades, global bioethanol production has expanded significantly as countries increasingly adopt renewable fuel strategies. As presented in Figure 1, according to the Renewable Fuels Association (RFA), worldwide fuel bioethanol output reached approximately 31.31 billion gallons in 2024, marking a new high in annual production driven by sustained demand for cleaner transport fuels. The United States remains the dominant producer, accounting for about 52% of global output, with production primarily based on corn, which benefits from well-established industrial infrastructure and high conversion efficiency. Brazil follows as the second-largest producer with roughly 28% of total global ethanol output, predominantly from sugarcane, while India contributes around 6%. EU countries contribute roughly 5% of global bioethanol production, primarily using sugar beet, corn, and wheat as feedstocks. According to the second revision of the EU Renewable Energy Directive (RED III, 2018/2001), the EU aims to achieve a minimum 45% share of renewable energy in overall consumption by 2030, with bioethanol playing an important role in meeting these targets [3].

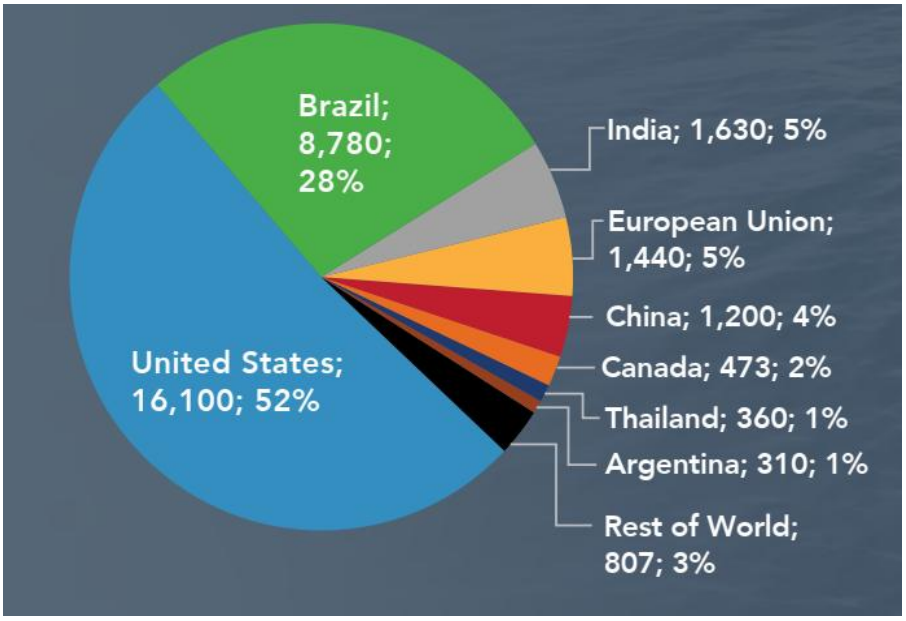

Figure 1 *Global fuel ethanol production by country in 2024 [3]*

Continued expansion of bioethanol production over recent decades (Figure 2) reflects policy support, technological progress, and industrial scaling to reduce transport-sector greenhouse gas emissions globally.

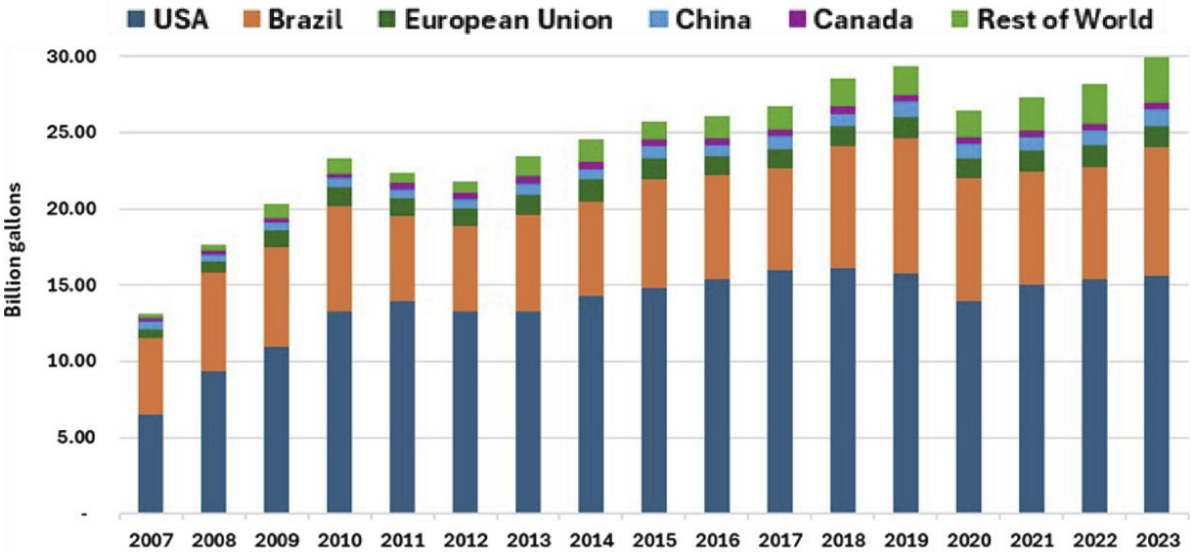

Figure 2 *Historical overview of global ethanol production by leading countries in 2024 [2]*

TECHNOLOGY READINESS LEVELS (TRLS) OF BIOETHANOL GENERATIONS

Bioethanol production technologies are generally classified into five generations based on feedstock type and level of technological maturity, as presented in Table 1.

First-generation (1G) bioethanol, obtained from sugar- and starch-rich crops such as corn, wheat, barley, potatoes, rice, sugarcane, and sugar beet, still dominates global production, accounting for approximately 99% of the total output. On a global scale, around 60% of bioethanol is produced from corn, 25% from sugarcane, 3% from wheat, and 2% from molasses, with the remainder derived from other cereals, cassava, and sugar beet [9]. Due to well-established processing infrastructure and optimized fermentation technologies, 1G bioethanol has achieved full commercial worldwide deployment (TRL 9).

Second-generation (2G) bioethanol is based on lignocellulosic biomass, including agricultural residues, grasses, wood, forestry by-products, and waste paper. Although extensive research and pilot-scale development have been conducted, large-scale commercialization remains limited because of high pretreatment costs, energy requirements, and techno-economic constraints [4,8]. Within the EU, lignocellulosic ethanol represented only about 1% of total bioethanol production in 2021 [13], and current technological readiness is estimated at TRL 7–8, with only a few early commercial facilities in operation [14].

Third-generation (3G) bioethanol, produced from microalgae, macroalgae, and cyanobacteria, remains largely at proof-of-concept and laboratory scale (TRL 3–4). Fourth-generation (4G) concepts involve genetically engineered microorganisms, such as modified algae and cyanobacteria, designed to enhance carbon fixation and biofuel yields, but these approaches are still confined to scientific research [2,10]. The emerging fifth generation (5G) builds upon genome editing, metabolic engineering, and synthetic biology to develop optimized energy crops with altered cell wall composition and improved biomass

characteristics; however, these strategies remain at an early experimental stage and face technical as well as environmental and societal considerations [2].

Table 1 *Technological readiness level (TRL) of five bioethanol generations [2,10,12]*

Generation	Feedstocks	Advantages	Limitations	TRL
1G	Edible biomass: corn, sugarcane, sugar beet, wheat, barley, potatoes, cassava	• Technologically developed • Established industrial infrastructure • High conversion efficiency • Up to ~75% GHG reduction vs. fossil fuels • Valorized by products and waste streams	• Competition with food and feed supply • Intensive use of arable land and water • Indirect land use change (ILUC) concerns	**TRL 9**
2G	Lignocellulosic biomass: straw, agricultural residues, wood, forestry waste, paper waste, grasses	• Utilization of non-edible biomass • Reduced food-fuel competition • High resource availability • Valorization of waste streams	• Complex pretreatment required • High energy demand • Formation of fermentation inhibitors • Higher production costs	**TRL 7–8**
3G	Algal biomass: microalgae, macroalgae, cyanobacteria	• High photosynthetic efficiency • No competition for arable land • Potential CO_2 sequestration • Can be integrated with wastewater treatment	• Early-stage development • High cultivation and harvesting costs • Energy-intensive processing • Scale-up challenges	**TRL 3–4**
4G	Genetically engineered microorganisms (modified microalgae, cyanobacteria, yeast)	• Enhanced carbon capture • Improved photosynthesis and biomass productivity • Potential direct CO_2-to-fuel conversion	• Experimental stage • Biosafety and ecological concerns • Regulatory and public acceptance issues	**TRL 1**
5G	Genome-edited and metabolically engineered energy crops	• Optimized cell wall composition • Reduced pretreatment requirements • Higher sugar yields • Improved biomass quality	• Research phase • Ethical and societal considerations • Regulatory uncertainty • Long-term environmental impact not fully assessed	**TRL 1**

Across all generations, bioethanol development aims to strengthen sustainability by reducing greenhouse gas emissions, enhancing carbon sequestration, supporting rural economies, and improving energy security through the use of renewable biomass resources.

EFFICIENCY, SUSTAINABILITY, AND LIFE CYCLE ASSESSMENT

Assessing the sustainability of bioethanol production requires an integrated evaluation of greenhouse gas (GHG) emissions, energy efficiency, life cycle performance, and economic viability across feedstock types and process pathways. Life cycle assessment (LCA) studies widely confirm that replacing fossil fuels with bioethanol can significantly reduce GHG emissions, though the degree of reduction depends strongly on the type of feedstock and system boundaries used in the analysis [14,15]. For example, first-generation (1G) ethanol

from corn or sugarcane typically shows moderate reductions in life cycle GHG emissions relative to conventional gasoline, depending on assumptions regarding land-use change and energy inputs [16]. In contrast, lignocellulosic (2G) bioethanol has been shown to deliver much greater emission reductions through the use of agricultural residues and biomass energy recovery, with GHG savings often exceeding 80–90% compared to gasoline in optimized scenarios [2,17,18].

Recent LCA modelling based on operational cellulosic ethanol data demonstrates that advanced waste valorization strategies, such as combined electricity generation from lignin and biogas recovery, can reduce primary energy consumption by over 60% and cut life-cycle GHG emissions by up to 95% compared with baseline fossil-intensive systems [17,18]. However, third-generation (3G) pathways, including algal biomass, can sometimes exhibit relatively higher GHG emissions per unit energy due to high electricity and processing demands, underscoring the need for improved cultivation and conversion technologies [16,18]. Methodological choices in LCA (such as system boundaries, functional units, and coproduct allocation) also significantly influence reported outcomes, which highlights the importance of harmonized assessment frameworks for reliable comparisons [14,15].

Overall, the efficiency and long-term sustainability of bioethanol production are determined not only by the physicochemical properties of the feedstock but also by the integration and optimization of key processing stages, including carbohydrate hydrolysis, alcoholic fermentation, and downstream ethanol recovery operations such as distillation, rectification, and dehydration (absolutization) [19–21]. The selection of an appropriate bioconversion configuration directly affects energy demand, enzyme consumption, process economics, and environmental performance. Conventional strategies such as separate hydrolysis and fermentation (SHF) and simutaneous saccharification and fermentation (SSF) differ in operational complexity and resource utilization, while the development of simultaneous saccharification and co-fermentation (SSCF) enables the efficient co-utilization of sugar, improving carbon conversion efficiency and overall ethanol productivity [2,19–21].

CONCLUSION

Bioethanol plays a strategic role in achieving climate neutrality and renewable energy targets, particularly within policy frameworks such as the EU Renewable Energy Directive. Although first-generation bioethanol remains economically dominant, sustainable long-term expansion requires accelerated deployment of advanced lignocellulosic and algal technologies. Strengthening policy support, harmonizing life cycle assessment methodologies, and fostering investment in innovative processing technologies will be essential to ensure that bioethanol contributes effectively to decarbonization, energy security, and the development of a circular bioeconomy.

ACKNOWLEDGEMENT

The author is grateful to the Ministry of Science, Technological Development and Innovation of the Republic of Serbia for financial support according to the contract with registration No. 451-03-34/2026-03/ 200134.

REFERENCES

[1] Li, J., Zhao, T., Xu, Y., *et al*. Renew. Energy. 2022, 188, 223–239.

[2] Ghazali, M.F.S.M., Mustafa, M. Energy Convers. Manag. X. 2025, 26, 100933.

[3] Renewable Fuels Association. Annual world fuel ethanol production, 2024. Available from: https://ethanolrfa.org/resources/annual-industry-outlook

[4] Bušić, M., Marđetko, N., Kundas, S., *et al*. Food Technol. Biotechnol. 2018, 56(3), 289–311.

[5] Tse, T.J., Wiens, D.J., Reaney, M.J.T. Fermentation. 2021, 7(4), 268.

[6] Assaf, J.C., Mortada, Z., Rezzoug, S.A., *et al*. Processes. 2024, 12(5), 1001.

[7] Hans, M., Lugani, Y., Chandel, A.K., *et al*. Biomass Convers. Biorefin. 2023, 13, 7423–7440.

[8] Moonsamy, T.A., Mandegari, M., Farzad, S., *et al*. Ind Crops Prod. 2022, 188, 115675.

[9] Hoang, T.D., Nghiem, N. Fermentation. 2021, 7, 314.

[10] Zuliani, L., Serpico, A., De Simone, M., *et al*. Processes. 2021, 9(9), 1583.

[11] Jain, S., Kumar, S. Energy. 2024, 296, 131130.

[12] Kowalski, Z., Kulczycka, J., Verhé, R., *et al*. Front Energy Res. 2022, 10, 919415.

[13] Flach, B., Lieberz, S., Bolla, S. Biofuels Annual 2021, European Union. Washington (DC): USDA Foreign Agricultural Service, 2021.

[14] Vasilakou, K., Nimmegeers, P., Thomassen, G., *et al*. Appl Energy. 2023, 344, 121263.

[15] Soleymani, A.T, Grzesik, K., Rödl, A., *et al*. Energies. 2021, 14(10), 2939.

[16] Elliot, P.E. Int J Energy Environ Sci. 2025, 5(2), 1–6.

[17] Patel, K., Singh, S.K. Clean Technol Environ Policy. 2023, 25(8), 2489–2510.

[18] Zhai, J., Liu, P., Xiong, Q., *et al*. Bioresour Technol. 2026, XXX, 133506.

[19] Vučurović, D., Bajić., B, Vučurović, V., *et al*. Fermentation. 2022, 8(3), 114.

[20] Katanski, A., Vučurović, V., Vučurović, D., *et al*. Fermentation. 2024, 10(3), 144.

[21] Vučurović, V., Katanski, A., Vučurović, D., *et al*. Fermentation. 2025, 11(2), 80.

EcoTER'26
eco.tfbor.bg.ac.rs
32nd International Conference
Ecological Truth & Environmental Research
24–26 June 2026, Hotel Sunce,
Sokobanja, Serbia

Review

BIOPROCESS ENGINEERING FOR CIRCULAR BIOECONOMY: MODELLING, OPTIMIZATION AND VALORISATION OF AGRO-INDUSTRIAL RESIDUES AND WASTES

DOI: 10.5937/EcoTER26012B

Bojana Bajić[1,a*], Damjan Vučurović[1,b], Siniša Dodić[1,c]

[1] Department of Biotechnology, Faculty of Technology Novi Sad, University of Novi Sad, Boulevard cara Lazara 1, 21 000 Novi Sad, SERBIA

[a] https://orcid.org/0000-0001-9786-2376
[b] https://orcid.org/0000-0002-0555-6089
[c] https://orcid.org/0000-0002-3072-0549

Abstract

Having in mind current environmental challenges and depletion of resources, the sustainable development of bioprocesses represents an important strategy for advancing a circular, bio-based economy. The integration of biological systems and engineering principles enables the creation of production processes aligned with the principles of the circular economy. While optimizing bioprocess parameters at early stages of bioprocess development significantly enhances product yield and minimizes by-products, it also reduces waste. Optimization of process parameters, such as temperature, pH value, aeration and agitation rate, medium composition, etc., in accordance with the complex needs of the biocatalysts leads to environmentally sustainable and economically feasible production. Moreover, subsequent modelling and simulation of optimized bioprocesses enable scientists to observe and examine system behaviour through different scenarios and conditions. Bioprocess modelling and simulation serve as key tools for accelerating the transition from laboratory studies to pilot-scale and industry. The generated models follow the development of the bioprocess from its inception in the laboratory until the industrial plant start-up and validation, supplemented by data that become available as the scale increases. The integration of optimization, modelling and simulation techniques contributes to faster, more efficient bioprocess development while meeting modern sustainability and circular-economy requirements.

Keywords: bioprocess, optimization, modelling, simulation, circular bioeconomy.

INTRODUCTION

Current generation of substantial quantities of agro-industrial residues, by-products, and waste materials is the result of increasing industrialization, continuous population increase, and intensive agricultural production. Traditionally, these streams have been considered waste requiring treatment and disposal. However, contemporary concepts based on the principles of circular bioeconomy view these materials as valuable renewable resources that can be valorised into biofuels, biopolymers, enzymes, microbial proteins, biosurfactants, and other value-added bioproducts [1,2].

* *baj@uns.ac.rs*

Large volumes of agro-industrial residues and by-products are produced annually in agriculture and food-processing industries. When inadequately managed or discharged into the environment without safe disposal, these materials might lead to the degradation of the environment and pose risk to both human and animal health. However, considering their composition and characteristics, as well as vast amounts, they have an enormous potential to generate sustainable bioproducts. For waste material to be a useful substrate, it should be abundant, non-toxic, cheap, and able to support rapid growth and multiplication of selected microorganism [1,3,4].

The development of sustainable bioprocesses based on renewable raw materials is an important prerequisite for realizing the principles of the circular bioeconomy. In this context, modelling, optimization, simulation, process scale-up, and techno-economic analysis have a key role in improving process performance and their industrial implementation. The aim of the paper is to analyse and emphasize the significance of the optimization, modelling, and simulation of bioprocesses in the development of sustainable, efficient bioprocesses for the utilization of agro-industrial residues, by-products and wastes for production of microbial biomass, biopolymers, biofuels, and high-value bioactive products.

AGRO-INDUSTRIAL RESIDUES, BY-PRODUCTS AND WASTES AS RAW MATERIAL IN BIOTECHNOLOGICAL PRODUCTION

A considerable amount of agro-industrial waste is generated from post-harvest activities and industrial processing operations. The constant, rapid population growth has transformed food production and agro-industrial systems, and, consequently, increasing productivity and, in turn, generating vast quantities of agro-industrial residues, by-products and waste. Unless treated properly, agro-industrial waste can generate significant greenhouse gas emissions, and as a result, intensify climate change through various mechanisms. Therefore, identifying efficient and sustainable management strategies for agro-industrial residues has become a key priority in the agricultural sector, emerging as one of the most urgent environmental challenges of the 21st century [5].

Due to their biodegradable nature and composition, agro-industrial residues and byproducts, represent adequate raw materials for biotechnological production, provided they fulfil all mandatory and most supplementary requirements. As with any biotechnological production process, the producing microorganism requires balanced cultivation media to grow and produce the desired product. Many agro-industrial residues are rich in carbohydrates, proteins, lipids, minerals, and other compounds suitable for microbial growth and biotechnological production. Their utilization contributes to waste reduction, environmental protection, resource efficiency, and supports the development of sustainable bioprocesses [1,2].

In recent decades, scientists around the world have been devoted to finding solutions to reduce generated agro-industrial residues and wastes through the improvement and development of the biotechnological production of various high-value products. Numerous types of agro-industrial residues, wastes, and by-products have been successfully used to produce a variety of bioproducts.

For example, soybean molasses, spent sugar beet pulp, wheat starch intermediates, and organic municipal waste have been used as substrates for bioethanol production [6–10]. Waste glycerol, vegetable oil industry wastewaters, confectionery industry wastewaters, and winery wastewaters have been utilized for biopolymer xanthan biosynthesis [11–14]. Wheat chaff has been used as a lignocellulosic substrate for cellulase and xylanase production [15].

In order to select the appropriate raw material for biotechnological production at an industrial scale it is necessary to consider several criteria, presented on Figure 1. The key criteria for assessing suitability of agro-industrial residues, by-products and wastes as biotechnological raw materials, are including carbon content, biological availability, consistency, seasonal availability, the possibility of alternative application, local technological potential and geographical location. Additionally, figure 1 shows the classification of agro-industrial residues and by-products that can serve as raw materials for biotechnological production. The agro-industrial residues and wastes are divided into four basic groups: agricultural residues from the field (stalks and straw), residues generated during agricultural processing (corn cobs, chaff and husks), industrial residues (fruit and vegetable peels, pomace, waste oils and waste water from the food industry) and industrial by-products (molasses, whey, raw glycerol, bagasse) [2,16].

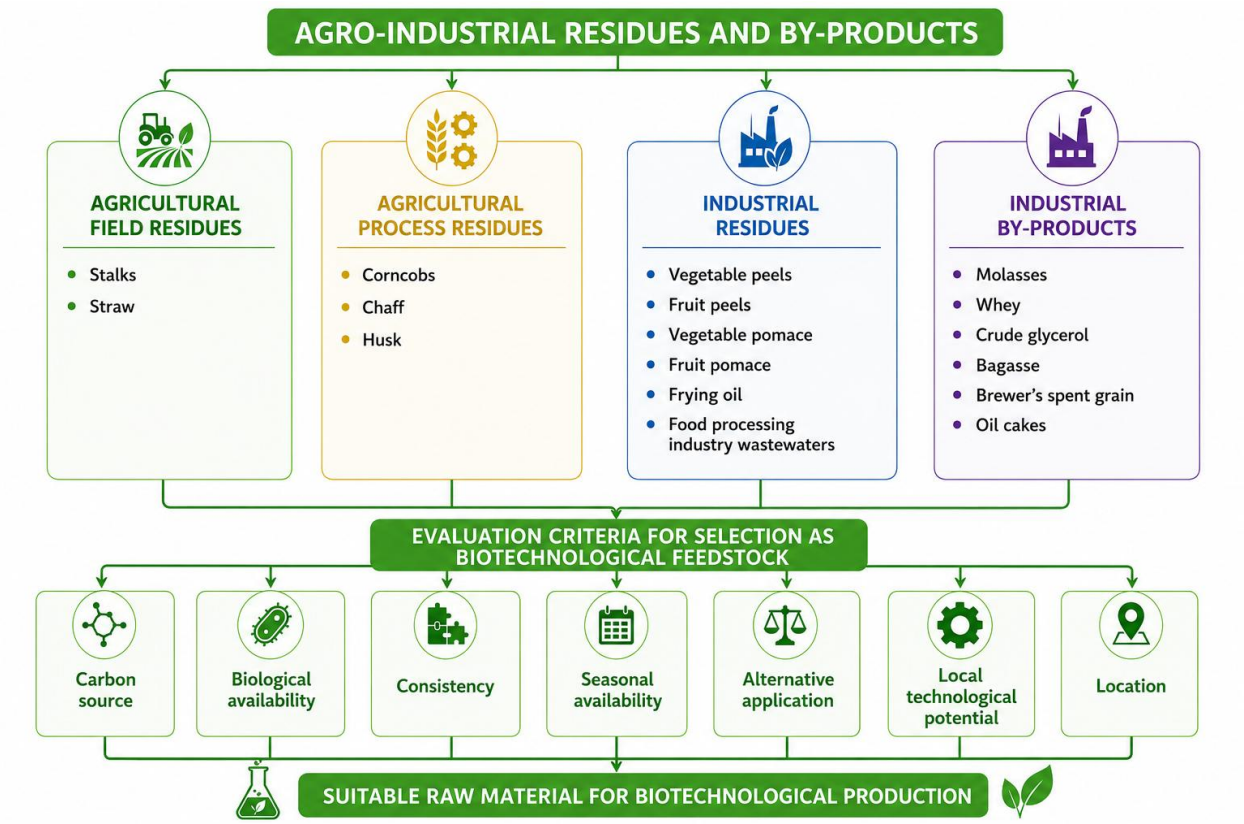

Figure 1 *Classification of agro-industrial residues and by-products and criteria for their selection as raw materials for biotechnological production*

OPTIMIZATION OF BIOPROCESSES FOR UTILIZATION OF AGRO-INDUSTRIAL RESIDUES, BY-PRODUCTS AND WASTES

The response surface methodology (RSM) is one of the most popular techniques for designing an experimental plan and modelling and describing interactions among many factors, which makes it particularly suitable for solving optimization problems. RSM is a statistical technique based on fundamental principles of statistics that aims to plan experiments, build empirical models, and evaluate the effects of independent variables on the desired response variable. Choosing the appropriate experimental design is a key step in applying the response surface methodology. When examining the influence of three factors on the observed bioprocess, the Box-Behnken design is most often used because it is much more efficient than other experimental designs [17–19].

Optimization of bioethanol production from soybean molasses showed that adjustment of initial sugar concentration and fermentation time significantly increased bioethanol concentration while reducing residual sugar levels [6]. In xanthan production studies, optimization of nutrient composition enabled increased xanthan yield and more efficient nutrient utilization, demonstrating the importance of medium formulation for bioprocess performance [11,13]. Agricultural residues can also serve as substrates for enzyme production. Wheat chaff was successfully utilized for simultaneous cellulase and xylanase production by *Trichoderma reesei*, while optimization of cultivation temperature, pH value, and cultivation time enhanced enzyme activities and overall process efficiency [15]. Complete bioprocess development of *Trichoderma harzianum* bioagent production included medium optimization, kinetic analysis, and economic assessment, demonstrating how optimization contributes to bioprocess development [20].

PROCESS MODELLING AND SIMULATION OF BIOPROCESSES FOR UTILIZATION OF AGRO-INDUSTRIAL RESIDUES, BY-PRODUCTS AND WASTES

When it comes to the use of modelling and simulation, they play a crucial role in the design and development of bioprocesses. They enable prediction of process performance, optimization of operational parameters, economic feasibility, and bioprocess scale-up. Additionally, modelling and simulation allow the prediction of different scenarios, and substitute experiments during the bioprocess design and development while facilitating the transition of lab- and pilot-scale systems to industrial level. Modelling involves defining a bioprocess with mathematical equations, whereas simulation refers to the solution of these mathematical equations to predict process behaviour, both improve the bioprocess understanding and help identify critical parameters in the bioprocess. SuperPro Designer is a process simulator that facilitates modelling, evaluation, and optimization of bioprocesses, and is applied for techno-economic analysis of different bioprocesses and with different raw materials. Furthermore, bioprocess simulation is a valuable tool for engineers and scientists, as it allows for the interpretation of results, analysis of the entire bioprocess, prioritization of issues, and guidance for research efforts. It also assists in identifying the most important areas for improvement as well as elimination of alternatives with little cost-effective potential [9,21–25].

Mathematical and simulation models provide detailed information regarding process performance, material flows, economic indicators, and production costs [7,9,12]. The importance of these approaches has been demonstrated in numerous studies. An example is the development of an integrated process for bioethanol and biogas production from organic municipal waste. Simulation studies showed that modelling can be used to evaluate different process scenarios, identify critical parameters, and assess economic feasibility [9]. Similarly, process and cost models developed for bioethanol production from spent sugar beet pulp enabled comprehensive analysis of capital investment, operating costs, process efficiency, and overall economic viability [7]. In research focused on bioethanol production from wheat-processing intermediates, process modelling supported evaluation of different starch hydrolysis procedures and assessment of the economic performance [8]. In addition, process modelling was successfully applied to the development of a process and economic model of xanthan gum production from confectionery industry wastewaters, demonstrating that waste-derived substrates can be successfully incorporated into economically feasible bioprocesses [12].

CONCLUSION

Bioprocess modelling and optimization plays a crucial role in the development of bioprocesses for sustainable valorisation of agro-industrial residues and wastes. Different agro-industrial residues, by-products, wastes and wastewaters, can be used as renewable raw materials for production of microbial biomass, biopolymers, biofuels, biosurfactants, enzymes, antimicrobial compounds, and other valuable bioproducts. Process modelling, optimization, and techno-economic analysis are essential tools for improving process efficiency, reducing production costs, and enabling industrial implementation of biotechnological processes. The application of statistical optimization methods and bioprocess modelling and simulation significantly contributes to development of sustainable and economically viable bioprocesses.

ACKNOWLEDGEMENT

The author is grateful to the Ministry of Science, Technological Development and Innovation of the Republic of Serbia for financial support according to the contract with registration No. 451-03-34/2026-03/ 200134.

REFERENCES

[1] Bajić, B., Vučurović, D., Vasić, Đ., *et al*. Foods. 2023, 12(1), 107.
[2] Vučurović, D., Bajić, B., Trivunović, Z., *et al.* Foods. 2024, 13(5), 711.
[3] Sadh, P.K., Duhan, S., Duhan, J.S. Bioresour Bioprocess. 2018, 5, 1.
[4] Ukaegbu-Obi, K.M. J Microbiol Microb Technol. 2016, 1(1), 5.
[5] Vigneswari, S., Noor, M.S.M., Ariffin, F., *et al.* J Renew Mater. 2026, 14(3), 6.
[6] Rončević, Z., Bajić, B., Dodić, S., *et al.* Hem Ind. 2019, 73(1), 1–12.
[7] Vučurović, D., Bajić, B., Vučurović, V., *et al.* Fermentation. 2022, 8(3), 114.
[8] Katanski, A., Vučurović, V., Vučurović, D., *et al.* Fermentation. 2024, 10(3), 144.
[9] Gegić, B., Vučurović, D., Dodić, S., *et al.* Energies. 2024, 17, 4286.

[10] Vučurović, V., Katanski, A., Vučurović, D., *et al.* Fermentation. 2025, 11(2), 80.
[11] Bajić, B., Vučurović, D., Dodić, S., *et al.* Chem Ind Chem Eng Q. 2017, 23(3), 329–339.
[12] Bajić, B., Vučurović, D., Dodić, S., *et al.* J Clean Prod. 2017, 168,169–180.
[13] Rončević, Z., Bajić, B., Vlajkov, V., *et al.* Braz J Chem Eng. 2020, 37, 617–627.
[14] Trivunović, Z., Mitrović, I., Puškaš, V., *et al.* J Food Process Preserv. 2021, 45, e15849.
[15] Jovanović, M., Vučurović, D., Bajić, B., *et al.* J Serb Chem Soc. 2020, 85(2), 177–189.
[16] Smith, J.E. Biotechnology. 4th ed. Cambridge, UK: Cambridge University Press; 2004.
[17] Ferreira, S.L.C., Bruns, R.E., Ferreira, H.S., *et al.* Anal Chim Acta. 2007, 597(2), 179–186.
[18] Madamba, P.S. LWT Food Sci Technol. 2002, 35, 584–592.
[19] Esfahanian, M., Nikzad, M., Najafpour, G., *et al.* Chem Ind Chem Eng Q. 2013, 19, 241–252.
[20] Mitrović, I., Vučurović, D., Al-Ani, L.K.T., *et al.* J Appl Microbiol. 2023, 134, lxad115.
[21] Petrides, D., Cooney, C.L., Evans, L.B., *et al.* Comput Chem Eng. 1989, 13, 553–561.
[22] Heinzle, E., Biwer, A.P., Cooney, C.L. Development of sustainable bioprocesses: Modeling and assessment. Hoboken (NJ): John Wiley & Sons; 2006.
[23] Harrison, R.G., Todd, P.W., Rudge, S.R., *et al.* Bioseparations science and engineering. 2nd ed. Oxford, UK: Oxford University Press; 2015.
[24] Canizales, L., Rojas, F., Pizzaro, C.A., *et al.* Processes. 2020, 8, 1180.
[25] Ortiz, I., Valdez-Vazquez, I., Hernandez-Vazquez, A., *et al.* Energy Convers Manag. 2024, 306, 118319.

Review

APPLICATION OF ENVIRONMENTALLY SAFE INHIBITORS FOR METAL CORROSION PROTECTION

DOI: 10.5937/EcoTER26018S

Ana Simonović[1,a*]

[1] University of Belgrade, Technical Faculty in Bor, Vojske Jugoslavije 12, 19210 Bor, SERBIA

[a] https://orcid.org/0000-0003-2392-0048

Abstract

Corrosion is the gradual destruction of metals caused by reactions with their environment. As metals are a large group of elements with numerous industrial uses in various settings, protecting their surfaces from aggressive ions is essential. Metal corrosion can lead to environmental pollution through the release of metal ions via dissolution, and leakage of chemicals stored in tanks or transported through pipes. Thus, metal corrosion poses threats in three main areas: economics, safety, and environmental protection. Corrosion should be reduced by applying appropriate methods, such as the use of suitable corrosion inhibitors. Recently, new corrosion inhibitors with minimal or zero negative environmental impact, known as eco-friendly or green inhibitors, have been researched and developed. Corrosion inhibitors adsorb onto metallic surfaces and protect them from deterioration. Pharmaceutical compounds, amino acids, purines, plant extracts, and similar substances have attracted special attention from researchers as environmentally safe inhibitors. These organic compounds contain heteroatoms, making them suitable as metal corrosion inhibitors in many aggressive environments, as confirmed by numerous studies. Over the last few decades, drugs have proven to be a good alternative to conventional corrosion inhibitors due to their non-toxicity and minimal environmental impact.

Keywords: corrosion inhibitors, environmentally safe, metals.

INTRODUCTION

Metals used in various branches of industry, construction, and as electrical conductors are subject to corrosion in their environments. The presence of ions such as chlorides and sulphates contributes to corrosion and leads to the deterioration of metal. Corrosion is recognised as a technical, economic, and environmental problem. To reduce the corrosion of metals and their alloys, corrosion inhibitors play a significant role. In order to protect the surface of metals from corrosion, overcome risky and hazardous corrosion effect, and thus reduce damage and losses due to dissolution, corrosion inhibitors have found significant application. Corrosion inhibitors can be organic [1,2] and inorganic compounds [3,4]. The most effective corrosion inhibitors are organic compounds [5,6]. The most representative compounds were from following groups: tetrazole compounds, triazole compounds, benzotriazole and benzotriazole derivates [7–10]. Literature on this subject suggests that these

* *asimonovic@tfbor.bg.ac.rs*

compounds contain heteroatoms (S, N, O) and aromatic rings in their structures, and/or p bonds, which enable them to be adsorbed onto the metal surface. However, due to the numerous harmful effects of these compounds on the environment, their use is being questioned, and organic compounds that do not affect the environment with their action are gaining increasing importance. Thus, drugs [11,12], amino acids [13,14], plant extracts [15], purines [16] etc. have been particularly distinguished as effective, non-toxic, inexpensive corrosion inhibitors in various solutions.

DISCUSSION

Scientists have recently focused their research on the use of unused or expired drugs as environmentally safe corrosion inhibitors for metals and alloys. The drugs have shown good inhibitory properties in various environments, especially in acidic solutions.

Alsairi *et al.* [17] researched corrosion of Cu metal in 0.5M HCl and the inhibition of the expired drug Cefazolin. The study confirmed that Cefazolin is an effective inhibitor of copper corrosion, with the highest efficiency (87%) observed at the highest inhibitor concentration, namely 300 ppm of Cefazolin. It has been shown that temperature changes reduce the inhibition efficiency. Electrochemical measurements showed that the expired drug functioned as a mixed–type inhibitor. The adsorption of the drug on the copper surface followed Temkin's adsorption model. The estimated values of ΔG_{oads} range from −12.81 to −16.68 $kJmol^{-1}$, indicating that the drug is physically adsorbed on copper at the temperatures used. The formation of a protective antibiotic film on the electrode surface was confirmed using SEM techniques, and EDX studies confirmed the presence of drug molecules on the copper surface, which are observed as C, N and O peaks in the EDX pattern. Ceftazidime [18] also showed good inhibitory properties in an acidic chloride environment, i.e. in a 0.1 M HCl solution. The inhibition efficiency increased with increasing concentration and the highest inhibition value of 94.2% was achieved at a concentration of 300 ppm in a corrosive environment. As in the previous study, this antibiotic was shown to belong to the group of mixed inhibitors by the use of electrochemical methods.

In the absence of the antibiotic, copper metal dissociates and forms cuprous ions, which react with chloride ions in the solution to form CuCl. The latter does not provide sufficient protection for the copper metal, as it transforms into a soluble $CuCl_2$ complex through reaction with chloride ions [19].

$$Cu \rightarrow Cu^{+} + e^{-} \text{ (fast)} \quad (1)$$

$$Cu^{+} + Cl^{-} \rightarrow CuCl \quad (2)$$

$$CuCl + Cl^{-} \rightarrow CuCl_2^{-} \quad (3)$$

The formed $CuCl_2^-$ is adsorbed on the copper surface and it can be dissolved according to the following equation [19]:

$$CuCl_2^{-} \text{ (surface)} \rightarrow CuCl_2^{-} \text{ (solution)} \quad (4)$$

The formed $CuCl_2^-$ might further oxidize to Cu^{2+} ions according to the reaction:

$$CuCl_2^{-} \text{ (surface)} \rightarrow Cu^{2+} + 2Cl^{-} + e \quad (5)$$

While the cathodic reaction proceeds as follows:

$$2H^+ \; 2e^- \rightarrow H_2\uparrow \quad (6)$$

On the contrary, the presence of the Ceftazidime antibiotic within the solution, because the adsorption of the antibiotic molecules on the copper surface restricts the dissolution of copper and so, minimizing the corrosion rate. The adsorption of the antibiotic on the Cu surface belongs to Temkin's model and the estimated values of ΔG^o_{ads} are around 20 $kJmol^{-1}$, referring that the adsorption of investigated inhibitor at copper is physisorption. The interaction of the expired antibiotic with the copper surface could be assigned to the existence of N, O atoms, and p-electrons in the structure of the expired antibiotic.

The antibiotics linezolid and piperacillin with expired shelf lives were tested as possible inhibitors of copper corrosion in a 1 M HNO_3 solution. It was also shown that increasing the concentration of the inhibitor in the solution increases corrosion inhibition and for the highest tested concentration of linezolid of 450 ppm was 91.73%, and for the piperacillin was 95.66%, while increasing the temperature decreases it. Potentiodynamic polarization confirmed that these drugs operate as mixed inhibitors [20]. The examined expired linezolid and piperacillin drugs inhibit the Cu from corroding in 1.0 M HNO_3 solution by adsorping to its surface. The adsorption of both inhibitors follows the Langmuir isotherm. It is evident from the inhibitory efficiency and corrosion parameters obtained from different methodologies that the IE of the piperacillin drug is higher than that of the linezolid drug because piperacillin has a larger molar mass than linezolid. Therefore, the piperacillin drug will form a thicker adsorbed layer on the surface than linezolid, resulting in a higher IE. However, the molecular composition of the drugs under examination contains many heteroatoms, including O, N, and F in linezolid, and O, N, and S in piperacillin. These heteroatoms contribute to the adsorption process on the surface of copper through their lone pairs of electrons, which serve as chelating centres distributed along the molecule.

Tasić *et al*. [12] confirmed in their research the effective inhibitory properties of cephradine in preventing copper corrosion in a 0.9% NaCl solution. In the presence of cephradine, the corrosion current density decreased compared to the inhibitor-free solution. These changes in corrosion current density result from the adsorption of inhibitor molecules on the copper surface and the formation of a protective film which was approved by applying of the scanning electron microscopy (SEM) and energy dispersive analysis of X-rays (EDS). The highest inhibition efficiency, 92.4%, was achieved at a concentration of $5\cdot10^{-3}$ M, based on data from potentiodynamic polarization measurements. the adsorption of cephradine on the copper surface obeys Langmuir adsorption isotherm. It is known that the ionisation of organic compounds depends on the pH value of the aqueous solution. In the pH range from 2.5 to 7.3, cephradine exists as a zwitterion. After the adsorption of chloride ions, the metal surface becomes negatively charged, which facilitates the adsorption of the zwitterion.

CONCLUSION

All presented researches confirm that the use of drugs as potential eco-friendly inhibitors demonstrates good inhibitory properties in aggressive environments, leading to reduced maintenance costs and environmental protection. The results of the studies confirm the

spontaneous adsorption of drug molecules on the electrode surface via the lone electron pairs of heteroatoms.

ACKNOWLEDGEMENT

The authors are grateful to the Ministry of Education, Science and Technological Development of the Republic of Serbia, within the funding of the scientific research work at the University of Belgrade, Technical Faculty in Bor, according to the contract with registration number 451-03-34/2026-03/200131.

REFERENCES

[1] Bilgiç, S. Int. J. Corros. Scale Inhib. 2023,12, 1224–1260.

[2] Hamadi, L., Mansouri, S. Oulmi, K. *et al*. Egypt. J. Pet. 2018, 27, 1157–1165.

[3] Edwards, M., Hidmi, L. Corros. Sci. 2002, 44, 1057–1071.

[4] Munoz, A. I., Antón, J.G., Guiñón, J.L. *et al*. Electrochim. Acta 2004, 50, 957–966.

[5] Simonović, A.T., Tasić, Ž.Z., Rdovanović, M.B., *et al*. ACS Omega 2020, 5 12832−12841.

[6] Antonijević, M.M. Milić, S.M., *et al*. Int. J. Electrochem. Sci. 2009, 4, 1719–1734.

[7] Antonijeivc, M.M., Milic, S.M., Petrovic, M.B. Corros. Sci. 2009, 51, 1228.

[8] Quraishi, M.A., Farooqi I.H., Saini, P.A. Brit Corros J. 2000, 35, 78.

[9] Qafsaoui, W., Blanc, C., Pébère, N., *et al*. Electrochim. Acta 2002, 47, 4339.

[10] Antonijevic, M.M., Milic, S.M., Dimitrijevic, M.D., *et al*. Int. J. Electrochem. Sci. 2009, 4, 962.

[11] Tasić, Ž.Z., Petrović Mihajlović, M.B., Simonović, A.T., *et al*. Sci. Rep. 2019, 9, 14710.

[12] Tasić, Ž.Z., Petrović Mihajlović, M.B., Radovanović M.B., *et al*. J. Mol. Struct. 2018, 1159, 46–54.

[13] Radovanović, M.B., Petrović, M.B., Simonović, A.T., *et al*. Environ. Sci. Pollut. Res. 2013, 20, 4370–4381.

[14] Simonović, A.T., Petrović, M.B., Radovanović, M.B., *et al*. Chem. Pap. 2014, 68, 362–371.

[15] Murungi, P.I., Sulaimon, A.A. Corros. Rev. 2022, 40, 127–136.

[16] Petrović Mihajlović, M.B., Tasić, Ž.Z., Radovanović, M.B., *et al*. Metals 2022, 12, 1150.

[17] Alsairi, R.A., Kamel, M.M., Mohamed, M.M. Molecules 2024, 29, 1157.

[18] Kamel, M.M., Mohsen, Q., Anwar, Z.M., *et al*. J. Mater. Res. Technol. 2021, 11, 875–886.

[19] Sherif, E.M. Int. Electrochem. Sci. 2012, 7, 1884–97.

[20] Abdallah, M., Alfakeer, M., El Guesmi, N., *et al*. Green Chem. Lett. Rev. 2025, 18 2474131.

Original Research

PAN-LIFE-CARPET CONCEPT: INTEGRATING WASTE VALORIZATION AND BIOCRUST ENGINEERING

DOI: 10.5937/EcoTER26022S

Ivan Savić[1,a*], Ivana Savić Gajić[1,b], Tamara Palanački Malešević[2,c], Ivana Mihalj Lubaščik[2,d], Zorica Svirčev[2,3,e], Jussi Meriluoto[2,3,f]

[1] University of Niš, Faculty of Technology, Bulevar oslobođenja 124, 16000 Leskovac, SERBIA

[2] University of Novi Sad, Faculty of Sciences, Department of Biology and Ecology, UNS, Trg Dositeja Obradovića 2, 21000 Novi Sad, SERBIA

[3] Abo Akademi University, Faculty of Science and Engineering, Biochemistry, Tykistokatu 6A, 20520 Turku, FINLAND

[a] https://orcid.org/0000-0002-9638-5413 [b] https://orcid.org/0000-0001-5019-3806

[c] https://orcid.org/0000-0003-2044-8470 [d] https://orcid.org/0000-0003-4493-7295

[e] https://orcid.org/0000-0001-8355-7661 [f] https://orcid.org/0000-0002-6300-301X

Abstract

Land degradation in arid and semi-arid regions poses a major global threat to ecological stability, food security, and socio-economic resilience. Cyanobacteria-dominated biological soil crusts (biocrusts) play a critical role in soil stabilization and nutrient enrichment, but their early establishment and persistence are frequently limited by severe climatic conditions. This study combines cyanobacterial inoculation (Tolypothrix sp.) with bio-based polysaccharide matrices derived from agro-industrial and marine waste to accelerate biocrust development on loess sediment. Alginate (29.34% yield) and fucoidan (5.18% yield) were successfully isolated from the brown seaweed Laminaria digitata, while native cellulose (30.58% yield) was extracted from plum shells (Prunus domestica). Structural integrity was confirmed via FTIR spectroscopy, followed by an evaluation of their water-holding capacity (WHC) and water swelling capacity (WSC). Alginate exhibited superior hydrocolloid properties, achieving the highest WHC (0.8 g/g) and WSC (2.1 mL/g). During a 30-day laboratory cultivation, the addition of all isolated polysaccharides significantly enhanced biological crust development and biomass accumulation compared to the cyanobacteria-only treatment. The most pronounced stimulatory effect was achieved with 0.3% (m/v) alginate, which induced a ninefold increase in chlorophyll a content (352.46 µg/g) compared to the cyanobacteria control (38.33 µg/g). Fucoidan and cellulose also promoted biocrust growth, yielding significantly higher chlorophyll a value (94.82 µg/g and 77.90 µg/g, respectively) than the polysaccharide-free control. These findings validate the Pan-Life-Carpet framework, demonstrating that valorizing renewable biomass waste into eco-friendly support matrices provides a highly effective, cost-efficient, and scalable strategy for accelerated dryland restoration and soil erosion control.

Keywords: land degradation, biocrusts, cyanobacteria, waste valorization, polysaccharides, soil restoration.

[*] *savicivan@tf.ni.ac.rs*

INTRODUCTION

Arid and semi-arid ecosystems are highly vulnerable to erosion, nutrient loss, and biodiversity decline under climate change, requiring scalable and cost-effective restoration strategies [1,2]. Biological soil crusts (biocrusts), particularly cyanobacteria-dominated early successional stages, are critical for soil stabilization, nutrient enrichment, and water regulation [3]. While artificial inoculation can accelerate crust development, extreme temperatures, irregular precipitation, and poor soil structure often limit establishment and persistence, especially during early colonization [4]. Agro-industrial and marine biomass residues represent promising bio-based supports [5].

In this study, the Pan-Life-Carpet concept is presented: a circular restoration approach in which agro-industrial residues serve as bio-based matrices for cyanobacterial inoculation, combined with physical carriers to enhance soil adhesion, moisture retention, and inoculum stability. The effectiveness of this approach for early-stage soil stabilization under simulated dryland conditions is evaluated, providing insights into scalable and resource-efficient restoration strategies.

MATERIALS AND METHODS

Chemicals and reagents

In this study, 96% (*v/v*) ethanol, concentrated hydrochloric acid, and sodium hydroxide (Zorka Pharma, Šabac, Serbia), as well as potassium bromide (purity ≥98%) (Sigma-Aldrich, St. Louis, MO, USA) were used.

Plant material

Laminaria digitata biomass was purchased from Ozon Way (Belgrade, Serbia), and shells of *Prunus domestica* from Southeastern Serbia (42°53′19″N, 22°01′35″E). The raw materials were air-dried at ambient temperature for seven days. After that, the plant materials were milled and sieved before further use. A 0.5 mm fraction of brown seaweed biomass was used for the isolation of alginate and fucoidan, while a 0.7 mm fraction of plum shells was used for cellulose isolation. The moisture content was found to be 10.6% (*w/w*) for the brown seaweed biomass and 8.17% (*w/w*) for the plum shells.

Extraction of polysaccharides from plant material

Brown seaweed biomass (500 g) was depigmented using 70% (*v/v*) ethanol (5 L) at room temperature (22 ± 2 °C) for 24 h. Subsequently, the pretreated biomass was subjected to ultrasound-assisted extraction using 0.1 mol/L hydrochloric acid at 50 °C and the liquid-to-solid ratio of 15 mL/g for 6 min. Ultrasonic bath (Sonic, Niš, Serbia) operating at a frequency of 40 kHz and a total power of 300 W was used. Alginate was selectively precipitated from the filtrate by adding 2% (*w/v*) calcium chloride ($CaCl_2$) in a 1:1 (*v/v*) ratio. The obtained alginate was bleached twice with 20 mL of acetone at 18 °C. Fucoidan was precipitated from the supernatant remaining after alginate removal by the addition of 96% (*v/v*) ethanol in a 4:1 (*v/v*) ratio. The precipitated alginate and fucoidan were dried, ground in an electric mill, and stored at room temperature.

Plum shell powder (50 g) was suspended in 500 mL of 18% (*w/v*) NaOH and subjected to alkaline extraction at 70 °C for 90 min. The solid residue was washed with distilled water to pH neutral. The obtained material was then bleached with 500 mL of 30% (*v/v*) H_2O_2 until complete whitening was achieved. The isolated native cellulose was air-dried and stored in a sealed glass container at 25 ± 2 °C.

Fourier transform infrared spectroscopy

Fourier Transform Infrared Spectroscopy (FTIR) was used for structural characterization of isolated polysaccharides. Spectra of KBr pellets were recorded in the wavenumber range of 4000–400 cm^{-1} at a resolution of 2 cm^{-1} on a BOMEM Hartmann & Braun MB-series spectrophotometer (Quebec, Canada). The recorded spectra were processed using Win-BOMEM Easy software (Galactic Industries, Salem, New Hampshire, USA).

Hydration properties of isolated polysaccharides

To measure water-holding capacity (*WHC*) and water swelling capacity (*WSC*), 0.5 g of the polysaccharide was added to 20 mL of distilled water at room temperature. After centrifuging the hydrated samples at 6000 rpm for 10 min, the *WHC* was calculated according to Eq. 1. The *WSC* determination involved dispersing the samples for 24 h at room temperature. After measuring the volume of the swollen polysaccharide, the *WSC* was calculated using Eq. 2.

$$WHC\left(\frac{g}{g}\right) = \frac{m_2 - m_1}{m_1} \tag{1}$$

where, m_1 is a dry sample mass, m_2 is a sample mass after immersion in water and centrifugation.

$$WSC\left(\frac{mL}{g}\right) = \frac{V_1 - V_0}{m_1} \tag{2}$$

where, V_1 is a volume of swollen sample (mL), V_0 is a volume of dry sample (mL), and m_1 is a mass of dry sample (g).

Biocrust development and growth assessment

The potential of isolated polysaccharides, including alginate, fucoidan, and cellulose, to promote cyanobacterial biocrust establishment was evaluated on loess sediment under controlled laboratory conditions. Cyanobacterial inocula (*Tolypothrix* sp.) obtained from the Novi Sad Cyanobacterial Culture Collection (NSCCC, Serbia) were cultivated in nitrogen-free BG11 medium at 25 ± 2 °C under daylight conditions. Experiments were conducted in Petri dishes filled with homogenized loess sediment. Cyanobacterial inoculum (0.494 mg DW cm^{-2}) was applied alone and combined with isolated polysaccharides, namely alginate, fucoidan, and cellulose at concentrations of 0.3%, 0.5% and 1% (*m/v*), respectively. Non-inoculated sediment treated only with water served as the control. Application of cyanobacterial inoculum was performed manually using a Pasteur pipette. Biocrust were cultivated under daylight at room temperature (25 ± 2 °C) for 30 days, while irrigation was carried out on weekdays using about 30–50 mL of water per container. Following cultivation, developed biocrust material was collected, homogenized, and prepared for chlorophyll *a* analyses. Chlorophyll *a* extraction and quantification were performed according to Park et al. [6] and Chamizo *et al*. [7]. Homogenized biocrust material was extracted in 96% ethanol,

vortexed and incubated at 80 °C for 5 min, after which the incubation was continued at 4 °C for 24 h. The samples were vortexed, sonicated for 10 min, and centrifuged at 3000 rpm for 10 min (Beckman Coulter Avanti J-15). The obtained supernatants were analyzed spectrophotometrically at 665 and 750 nm using a SPECTROstar Nano spectrophotometer (BMG LABTECH, Germany), while absorbance at 665 nm (A_{665}) was corrected by subtracting the absorbance measured at 750 nm. Chlorophyll *a* concentration, expressed in µg/g, were calculated according to Ritchie [8] and Castle *et al*. [9] (Eq. 3):

$$\text{Clorophyll } a\left(\frac{\mu g}{g}\right) = \frac{11.9035 \times A_{665} \times V}{m \times L} \quad (3)$$

where, V is the solvent volume (mL), m is the dry mass of the sample (g), and L is the cuvette path length (cm).

Statistical analysis

All experiments were performed in triplicate, and the results were expressed as mean ± standard deviation. Statistical analysis was conducted using GraphPad Prism 9 (San Diego, CA, USA). Statistical differences between groups and treatments were evaluated via one-way ANOVA (Tukey's and Dunnett's post hoc tests) and Student's t-test at a 95% confidence level ($p < 0.05$).

RESULTS AND DISCUSSION

In the present study, brown seaweed biomass was utilized as a sustainable source of alginate and fucoidan. Plum shells were selected as an alternative lignocellulosic material for cellulose isolation. The valorization of these by-products is significant from both environmental and economic perspectives. The obtained alginate yield (29.34 ± 0.45%) falls within the range commonly reported for brown seaweeds (15%–40%) [10]. In contrast, the fucoidan yield (5.18 ± 0.09%) is consistent with previously reported values (1%–10%) [11]. Cellulose was isolated from plum shell, which matches the high cellulose content of 30.58 ± 0.79% typically reported for lignocellulosic materials [12].

Structural characterization of isolated polysaccharides

FTIR spectra confirmed the structural integrity and successful isolation of all three polysaccharides (Figure 1). In the spectrum of alginate (Figure 1a), characteristic bands of a uronic acid-rich structures were identified through O–H and C–H stretching at 3385 cm^{-1} and 2930 cm^{-1}, carboxylate ($–COO^-$) asymmetric and symmetric stretching at 1617 cm^{-1} and 1417 cm^{-1}, and glycosidic bond and C–O–C ring vibrations between 1046 cm^{-1} and 1130 cm^{-1}. For fucoidan (Figure 1b), successful isolation of the sulfated polysaccharide was validated by characteristic O–H and C–H bands (3360 cm^{-1} and 2927 cm^{-1}), alongside prominent sulfate group indicators at 1240 cm^{-1} (S=O) and 851 cm^{-1} (C–O–S), reflecting equatorial substitution at the C-4 position in accordance with literature reports [13]. The cellulose spectrum (Figure 1c) displayed a broad O–H band at 3307 cm^{-1} indicating extensive hydrogen bonding, a C–H stretching band at 2886 cm^{-1}, and an absorbed water bending peak at 1652 cm^{-1} [14]. Crystalline cellulose features were evident from peaks at 1425 cm^{-1} and 1374 cm^{-1}, while the absorption at 896 cm^{-1} confirmed the presence of β-glycosidic linkages. Ultimately, these differing chemical functionalities suggest complementary mechanisms that

could be exploited to enhance cyanobacterial growth and productivity within the cultivation systems.

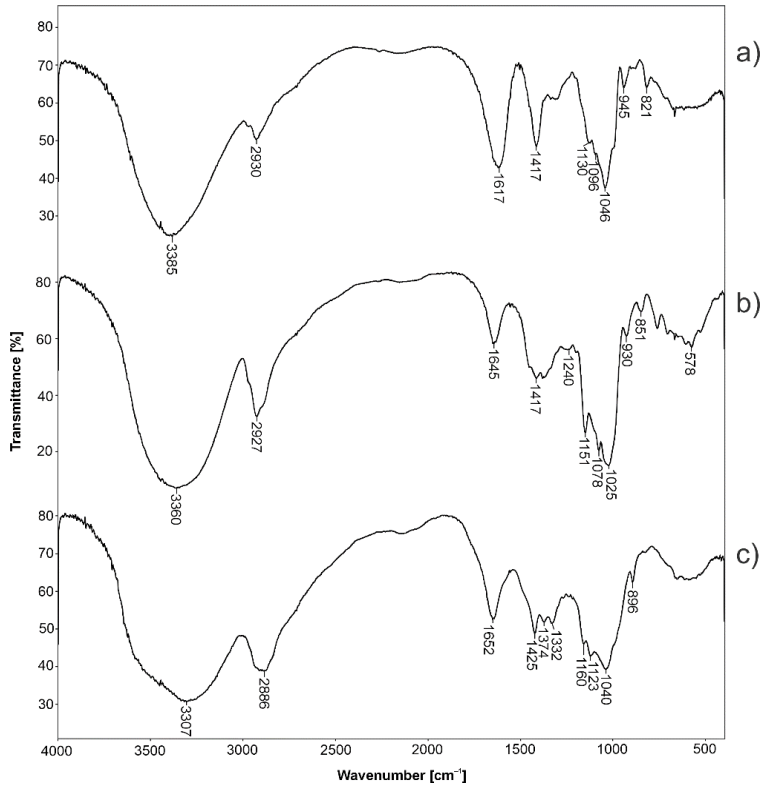

Figure 1 *FTIR spectra of isolated: a) alginate; b) fucoidan; and (c) cellulose*

Hydration properties of isolated polysaccharides

The *WHC* and *WSC* are key functional parameters that reflect the hydration behavior and structural organization of polysaccharides. They depend on the molecular architecture, crystallinity, and porosity, as well as the availability and accessibility of hydrophilic functional groups capable of forming hydrogen bonds with water [15]. The obtained results indicate different hydration properties among the analyzed polysaccharides (Table 1).

Table 1 *Water-holding capacity (WHC) and water swelling capacity (WSC) of analyzed polysaccharides*

Sample	*WHC* (g/g)	*WSC* (mL/g)
Alginate	0.8 ± 0.02^{c}	2.1 ± 0.12^{c}
Fucoidan	0.2 ± 0.01^{a}	0.46 ± 0.08^{a}
Cellulose	0.4 ± 0.01^{b}	0.84 ± 0.02^{b}

Different lowercase letters (a, b, c) in the same column indicate statistically significant differences between groups, as determined by Tukey's post hoc test at the 95% confidence level ($p < 0.05$).

Alginate exhibited the highest hydration values, confirming its superior ability to hold and absorb water, which is consistent with literature describing alginate as a highly tunable hydrocolloid [16]. The linear structure of alginate, composed of uronic acid residues, provides a high density of carboxyl groups that strongly interact with water molecules. Ca^{2+}-mediated junction zones enable the formation of a network capable of significant swelling without

structural collapse. Such systems achieve optimal water holding only when a balance is maintained between the crosslinking density and the available free volume within the gel network. The moderate WHC and lower WSC of cellulose can be attributed to its highly ordered and semi-crystalline structure, where extensive intra- and intermolecular hydrogen bonds within cellulose microfibrils limit the accessibility of hydroxyl groups and restrict water diffusion pathways [17]. In contrast, fucoidan exhibited the lowest hydration capacity despite the presence of highly hydrophilic sulfate groups. The hydration behavior of fucoidan is highly dependent on the degree of branching, sulfate distribution, and molecular weight heterogeneity [18]. The observed low swelling implies that strong intramolecular interactions and possible aggregation effects dominate over simple hydrophilicity. Specifically, electrostatic repulsion between sulfate groups can cause conformational packing under aqueous conditions, thus reducing the available hydration volume.

Biocrust development

Chlorophyll *a* content is commonly used as an indicator of biocrust development [6,19,20]. Cyanobacterial inoculation with *Tolypothrix* sp. successfully initiated biocrust formation on loess sediment (Table 2). The addition of isolated polysaccharides further stimulated biocrust development and biomass accumulation. Among the tested polysaccharides, alginate showed the most pronounced enhancement, which is likely related to its high-water retention capacity, supporting the importance of moisture availability [21]. Other studies also showed that natural polysaccharides significantly promote biocrust growth [22,23]. However, the chlorophyll *a* concentrations obtained here were multiple times higher, supporting the applicability of the Pan-Life-Carpet concept for ecosystem restoration [24].

Table 2 *Chlorophyll a content of developed crusts on loess sediment*

Sample	Chlorophyll *a* (μg/g)
Uninoculated sediment	0.18 ± 0.06^{a}
Cyanobacteria	$38.33 \pm 5.10^{*, b}$
Cyanobacteria + Alginate (0.3%)	$352.46 \pm 28.67^{*, c}$
Cyanobacteria + Fucoidan (0.5%)	$94.82 \pm 6.44^{*, d}$
Cyanobacteria + Cellulose (1%)	$77.90 \pm 4.38^{*, e}$

Asterisks indicate statistically significant differences compared to the control according to Dunnett's post hoc test at the 95% confidence level ($p < 0.05$). Different letters (a, b, c, d, e) indicate statistically significant pairwise differences among treatments according to the unpaired t-test at the 95% confidence level ($p < 0.05$).

CONCLUSION

This study successfully demonstrates the potential of utilizing natural polysaccharides isolated from marine biomass and agro-industrial by-products as sustainable bio-matrices to accelerate the establishment of cyanobacterial biocrusts. Alginate stood out with the highest water-holding and swelling capacities, which proved to be the critical driving factor for inoculum survival and proliferation. Biological assays on loess sediment confirmed that the application of all tested polysaccharides significantly enhances early-stage biocrust development, with the 0.3% (*m/v*) alginate treatment inducing the highest biomass accumulation and a more than ninefold increase in chlorophyll a concentration. The proposed Pan-Life-Carpet concept provides an innovative, ecologically safe, and resource-efficient

strategy capable of broad application in combating land degradation, enhancing sand stabilization, and restoring degraded dryland ecosystems worldwide.

ACKNOWLEDGEMENT

This research was supported by the Ministry of Science, Technological Development and Innovation of the Republic of Serbia (Grant No. 451-03-34/2026-03/200133, 451-03-33/2026-03/ 200125, and 451-03-34/2026-03/ 200125) and the Science Fund of the Republic of Serbia, #17807, The Loess Plateau Margins: Towards Innovative Sustainable Conservation – LAMINATION.

References

[1] Nandi, S., Das, S., Gorain, S., *et al.* Discover Soil. 2025, 2 (1), 48.

[2] Alkandari A, Alsayegh MA, Abdulraheem AA. In: Fostering Arid Lands Agriculture in the Face of Climate Change: Mitigation and Adaptation Synergy. Cham: Springer Nature Switzerland; 2026. p. 339–367.

[3] Gufwan, L.A., Peng, L., Gufwan, N.M., *et al.* Microb. Ecol. 2025, 88 (1), 8.

[4] Yadav, P., Singh, R.P., Hashem, A., *et al.* Microorganisms. 2023, 11 (10), 2507.

[5] Lamponi, S., Barletta, R., Santucci, A., Life. 2025, 15 (12), 1908.

[6] Park, C.H., Li, X.R., Jia, R.L., *et al.* Arid Land Res. Manage. 2016, 31 (1), 81–93.

[7] Chamizo, S., Adessi, A., Mugnai, G., *et al*. Microb. Ecol. 2019, 78 (2), 482–493.

[8] Ritchie, J.R. Photosynth. Res. 2006, 89, 27–41.

[9] Castle, S.C., Morrison, C.D., Barger, N.N. Soil Biol. Biochem. 2011, 43 (4), 853–856.

[10] Mendes, J.C., Valente, J.F., Sousa, F., *et al.* Mar. Drugs. 2026, 24 (2), 60.

[11] Sinurat, E., Marraskuranto, E., Artanti, N., *et al.* Int. J. Biol. Macromol. 2025, 311, 143592.

[12] Susi, S., Ainuri, M., Wagiman, W., *et al.* Int. J. Biomater. 2023, 2023 (1), 9169431.

[13] Zayed, A., Finkelmeier, D., Hahn, T., *et al.* Mar. Drugs. 2023, 21 (1), 48.

[14] He, H., An, F., Wang, Y., *et al.* Int. J. Biol. Macromol. 2021, 190, 810–818.

[15] Karim, A., Raji, Z., Habibi, Y., *et al.* Crit. Rev. Food Sci. Nutr. 2024, 64 (32), 11722–11756.

[16] Chen, M., Long, A., Zhang, W., *et al.* Sep. Purif. Technol. 2025, 353, 128265.

[17] Zhang, T., Hu, Y., Dong, Y., *et al.* Polymers. 2025, 17 (15), 2064.

[18] Zhang, X., Wei, Z., Xue, C. Crit. Rev. Food Sci. Nutr. 2022, 62 (32), 8935–8953.

[19] Rozenstein, O., Zaady, E., Katra, I., *et al.* Aeolian Res. 2014, 15, 217–226.

[20] Zhao, Y., Wang, N., Zhang, Z., *et al.* Land Degrad. Dev. 2021, 32, 285–295.

[21] Bu, C., Wu, S., Yang, Y., *et al.* PLoS ONE. 2014, 9 (3), e90049.

[22] Peng, C., Zheng, J., Huang, S., *et al.* J. Appl. Phycol. 2017, 29, 1421–1428.

[23] Fick, S.E., Barger, N.N., Duniway, M.C. Ecohydrology. 2019, 12, e2089.

[24] Palanački Malešević, T., Meriluoto, J., Mihalj, I., *et al.* Catena. 2024, 244, 108265.

Original Research

NATURE-BASED SOLUTIONS UNDER CLIMATE CHANGE: AN OVERVIEW OF KEY FINDINGS FROM THE UNSFA PILOT SITE WITHIN THE DALIA AND SWIM PROJECTS

DOI: 10.5937/EcoTER26029B

Jovana Bezdan[1,a*], Atila Bezdan[1,b]

[1] University of Novi Sad, Faculty of Agriculture, Department of Water Management,
Trg D. Obradovica 8, 21000 Novi Sad, SERBIA
[a] https://orcid.org/0009-0000-5620-2048
[b] https://orcid.org/0000-0003-3713-3002

Abstract

Constructed wetlands (CWs) are nature-based solutions increasingly applied for domestic wastewater treatment, yet their performance is sensitive to climatic conditions. This study presents an overview of key findings from the Gložan CW pilot site in Vojvodina, Serbia, assessed within the framework of the DALIA and SWIM Horizon Europe projects. Long-term treatment performance analysis demonstrated high and stable removal efficiency for organic matter, with average BOD_5 removal exceeding 90%, while phosphorus and suspended solids exhibited greater variability. Seasonal analysis indicated significantly lower BOD_5 removal during summer. Future climate projections were analysed using an ensemble of eight bias-corrected EURO-CORDEX regional climate models under the RCP8.5 scenario. Results indicate a progressive increase in thermal stress, with tropical days nearly doubling by 2071–2100, alongside a 49% reduction in frost days, a 21% increase in maximum one-day precipitation, and a modest decline in the Seljaninov Hydrothermal Coefficient. These changes present both opportunities — through extended frost-free operational seasons — and challenges, including increased hydraulic loading from extreme rainfall and moisture deficits during the growing season. Integrating climate adaptation into the long-term management of nature-based wastewater treatment systems is strongly recommended.

Keywords: constructed wetlands, nature-based solutions, wastewater treatment, climate change, treatment performance.

INTRODUCTION

Constructed wetlands are increasingly recognized as cost-effective nature-based solutions for the treatment of domestic wastewater, industrial effluents, and urban runoff [1]. These systems utilize natural biogeochemical and physical processes to remove organic matter and nutrients, while simultaneously providing additional environmental and social benefits [2]. As constructed wetlands represent nature-based solutions that utilize natural processes for pollutant removal, their performance may be influenced by changes in weather conditions caused by climate change. Numerous studies worldwide have investigated the impacts of climatic conditions, seasonal variability, and climate extremes on the pollutant removal efficiency of constructed wetlands [3–9].

* *jovana.bezdan@polj.edu.rs*

This study focused on a constructed wetland system that has been used for wastewater treatment in the settlement of Gložan, located in the Vojvodina region of Serbia, through previously published studies [6,8,9] and new analyses conducted within this paper. Research activities related to the Gložan constructed wetland system started within the Horizon Europe project DALIA as part of the demo site activities at "Begečka Jama", whose activities were completed in 2025, and are continuing through newly initiated activities within the Horizon Europe project SWIM.

MATERIALS AND METHODS

Study Area

The study was conducted in relation to a constructed wetland (CW) system for wastewater treatment located in Gložan, a settlement in the Vojvodina region, northern Serbia (approximately 45.27°N, 19.57°E) (Figure 1). The region is characterised by a continental climate with warm summers and cold winters. Given that temperature and moisture conditions directly govern microbial community dynamics, plant productivity, and biogeochemical cycling within CW systems, detailed climate analysis is essential for contextualising both current treatment performance and long-term system sustainability.

Figure 1 *Location of the constructed wetland in Gložan and an aerial view of the site*

Treatment Performance of the Gložan Constructed Wetland

In addition to the climate change analysis, the long-term treatment performance of the Gložan constructed wetland (CW) was evaluated using previously published monitoring results [6]. The analysis included pollutant removal efficiency for biochemical oxygen demand (BOD5), chemical oxygen demand (COD), suspended solids (SS), ammonium nitrogen (NH4-N), total nitrogen (TN), and total phosphorus (TP). Descriptive statistical analysis, seasonal comparison, and trend analysis were performed in order to assess treatment stability and long-term operational behaviour of the CW system. Seasonal differences were evaluated using analysis of variance (ANOVA), while temporal trends were analysed through regression analysis and significance testing.

Climate Data and Model Ensemble

Historical reference and projected future climate conditions were analysed using an ensemble of eight [10] bias-corrected Regional Climate Models (RCMs) from the EURO-CORDEX project database, at a spatial resolution of 0.1° (~11 km). The historical

period was used as a model-based reference baseline to ensure methodological consistency with future climate projections. The selection of this specific ensemble was based on the recommendations of the Digital Climate and Climate Change Atlas of the Republic of Serbia, developed within the framework of the project "Advancing Medium and Long-Term Adaptation Planning in the Republic of Serbia," funded by the Green Climate Fund in collaboration with the Ministry of Agriculture, Forestry and Water Management and the Ministry of Environmental Protection of the Republic of Serbia [10]. This ensemble has undergone verification of climate simulations over the territory of Serbia and is considered an appropriate multi-model configuration for national and regional climate assessments [10].

The eight ensemble members comprised combinations of three Global Climate Models (GCMs) — ICHEC-EC-EARTH, MOHC-HadGEM2-ES, and MPI-M-MPI-ESM-LR — dynamically downscaled by four regional models: CLMcom-CCLM4-8-17, DMI-HIRHAM5, KNMI-RACMO22E, and MPI-CSC-REMO2009. The full list of ensemble members is provided in Table 1.

Table 1 *EURO-CORDEX regional climate model ensemble used in this study [10]*

Ensemble Member Acronym	Regional Model	Global Model
gcm-ICHEC-EC-EARTH-rcm-CLMcom-CCLM4-8-17	CLMcom-CCLM4-8-17	ICHEC-EC-EARTH
gcm-ICHEC-EC-EARTH-rcm-DMI-HIRHAM5	DMI-HIRHAM5	ICHEC-EC-EARTH
gcm-ICHEC-EC-EARTH-rcm-KNMI-RACMO22E	KNMI-RACMO22E	ICHEC-EC-EARTH
gcm-MOHC-HadGEM2-ES-rcm-CLMcom-CCLM4-8-17	CLMcom-CCLM4-8-17	MOHC-HadGEM2-ES
gcm-MOHC-HadGEM2-ES-rcm-KNMI-RACMO22E	KNMI-RACMO22E	MOHC-HadGEM2-ES
gcm-MPI-M-MPI-ESM-LR-rcm-CLMcom-CCLM4-8-17	CLMcom-CCLM4-8-17	MPI-M-MPI-ESM-LR
gcm-MPI-M-MPI-ESM-LR-rcm-MPI-CSC-REMO20091	MPI-CSC-REMO2009	MPI-M-MPI-ESM-LR (r1i1p1)
gcm-MPI-M-MPI-ESM-LR-rcm-MPI-CSC-REMO20092	MPI-CSC-REMO2009	MPI-M-MPI-ESM-LR (r2i1p1)

For each ensemble member, median values across the eight models were calculated for each climate index and time period, following standard practice for ensemble-based climate projections. The use of the ensemble median rather than the mean reduces sensitivity to outlier model realisations and provides a robust central estimate of projected change.

All future climate projections were conducted using the Representative Concentration Pathway 8.5 (RCP8.5) scenario, which describes a high greenhouse gas emission trajectory characterized by continuously increasing emissions throughout the 21st century. The RCP8.5 scenario from the IPCC Fifth Assessment Report (AR5) was selected because recent climate trends in Serbia already correspond to temperature changes projected under this scenario for the coming decades, making the application of lower-emission scenarios less representative for the study area [11,12].

Climate Indices

Five climate indices were selected to characterise conditions relevant to the hydrological and thermal functioning of the constructed wetland system. These indices were computed for three time periods: a historical/reference period (1996–2025), which covers the operational period of the constructed wetland since 2004, and two future periods (2041–2070 and 2071–2100). The indices are described below:

a) Seljaninov Hydrothermal Coefficient (SHC)

The Seljaninov Hydrothermal Coefficient (SHC) is a compound agro-climatic index defined as:

$$SHC = \frac{10 \cdot P_{sum}}{T_{sum}}, \quad (1)$$

where P_{sum} is the sum of daily precipitation (mm) and T_{sum} is the temperature sum (°C), both calculated over the period when monthly mean air temperature exceeds 10°C [13].

The SHC reflects the balance between moisture availability and thermal energy during the biologically active growing season, making it a useful proxy for wetland productivity and treatment efficiency.

b) Consecutive Dry Days Index (CDD)

The Consecutive Dry Days Index (CDD) represents the maximum number of consecutive days within a year with daily precipitation below 1 mm. This index characterises the severity and duration of dry spells, which may reduce water levels in the wetland, increase pollutant concentrations, and stress vegetation and microbial communities involved in wastewater treatment processes.

c) Highest One-Day Precipitation Amount (Rx1d)

The Highest One-Day Precipitation Amount (Rx1d) represents the annual maximum 24-hour precipitation amount (mm). This index captures extreme precipitation events that may cause hydraulic overloading of constructed wetland (CW) systems, mobilise accumulated sediments, and temporarily impair treatment performance through reduced hydraulic retention time, influent dilution, or bypass flows that result in incomplete treatment [14].

d) Frost Days Index (FD)

The Frost Days Index (FD) represents the annual number of days with minimum temperatures below 0°C. Frost conditions are critical for CW operation, as near-zero temperatures suppress microbial metabolic activity, reduce nitrification and denitrification rates, and may cause surface freezing that alters hydraulic pathways [15].

e) Tropical Days Index (TD)

The Tropical Days Index (TD) represents the annual number of days with maximum temperatures exceeding 30°C. Elevated temperatures accelerate evapotranspiration, reduce dissolved oxygen levels, and may favour specific microbial degradation pathways within the wetland [16,17].

RESULTS AND DISCUSSION

Treatment Performance and Operational Stability of the Gložan Constructed Wetland

The previously published assessment of treatment performance at the Gložan CW indicated generally high and stable pollutant removal efficiency, particularly for organic matter [6] (Table 2, Figure 2). Average BOD5 removal efficiency exceeded 90%, with relatively low variability, suggesting stable biological treatment performance over the analysed period. COD and TN removal efficiencies were also comparatively high, averaging approximately 78% and 79%, respectively, while NH4-N and suspended solids showed moderate variability. In contrast, TP removal exhibited the highest variability, indicating less stable phosphorus retention processes. Seasonal analysis showed significantly lower BOD5 removal efficiency during summer periods, likely associated with elevated temperatures, altered oxygen dynamics, and hydrological variability. Trend analysis indicated statistically significant long-term increases in TP, NH4-N, and TN removal efficiency, while suspended solids removal showed a slight decreasing trend. These findings provide important context for the climate change analysis, as future increases in thermal stress, drought occurrence, and precipitation extremes may further influence the biological and hydraulic functioning of the CW system.

Table 2 *Long-term pollutant removal efficiency and variability of the Gložan constructed wetland*

Parameter	Mean Removal Efficiency (%)	Standard Deviation	CV (%)
BOD_5	90.6	7.6	8.3
COD	78.5	15.1	19.2
Suspended solids	69.6	31.5	45.2
NH4-N	71.3	29.0	40.7
TN	79.1	18.4	23.2
TP	58.7	36.4	61.9

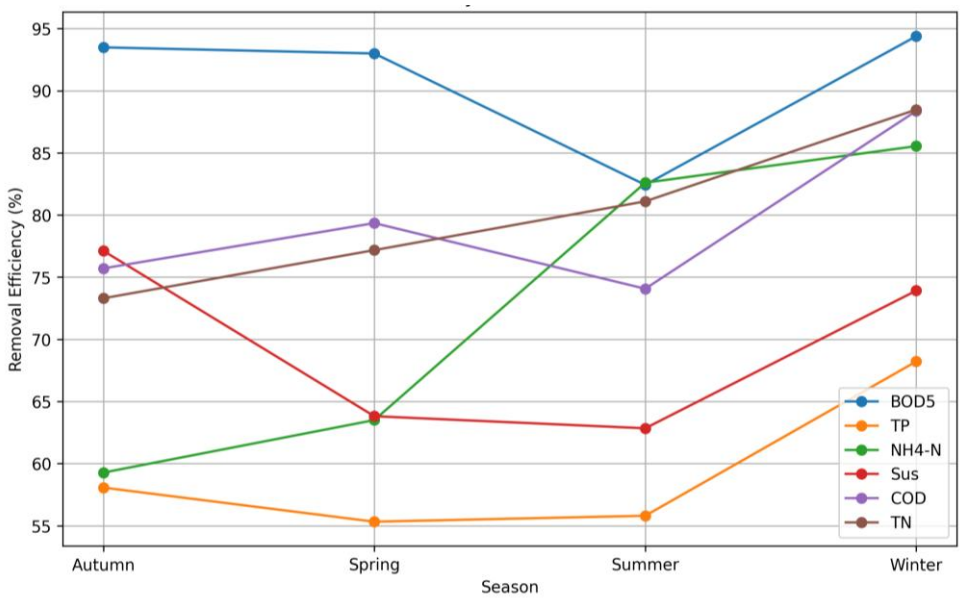

Figure 2 *Seasonal removal efficiency of the Gložan constructed wetland*

Overview of Projected Climate Change

The results of the multi-model ensemble analysis reveal a clear and consistent pattern of climate change at the Gložan site over the 21st century under the RCP8.5 scenario. The projected changes encompass warming-driven shifts in both temperature-related and precipitation-related indices, with implications for the seasonal functioning, treatment capacity, and ecological stability of the constructed wetland. Median values of all five climate indices across the three time periods are summarised in Table 3.

Table 3 *Median values of selected climate indices for the baseline and future periods under RCP8.5*

Climate Index	Unit	1996–2025	2041–2070	2071–2100	Trend
Seljaninov Hydrothermal Coefficient (SHC)	–	1.08	1.06	0.98	Decreasing
Consecutive Dry Days (CDD)	days	26	26	28	Slightly increasing
Max 1-day Precipitation (Rx1d)	mm	40.4	44.3	48.9	Increasing
Frost Days (FD)	days	79	62	40	Strongly decreasing
Tropical Days (TD)	days	36	51	79	Strongly increasing

Seljaninov Hydrothermal Coefficient (SHC)

The Seljaninov Hydrothermal Coefficient (SHC) showed a modest but progressive decline from 1.08 in the baseline period (1996–2025) to 1.06 in the mid-century period (2041–2070), and further to 0.98 by the end of the century (2071–2100). Although SHC values across all analysed periods generally correspond to humid growing-season conditions, the projected late-century value approaches the threshold of insufficient moisture supply relative to increasing thermal demand. According to commonly used classifications, SHC values between 1.0 and 1.4 indicate slightly to moderately humid conditions, while values between 0.8 and 1.0 are considered slightly dry [10].

In the context of constructed wetlands, the SHC reflects the balance between water availability and biological activity during the warm season. A declining SHC indicates that future growing seasons are likely to become warmer and/or drier, potentially reducing water availability in surface-flow or free-water systems and increasing evapotranspiration losses from vegetated beds. In subsurface-flow CW systems, reduced precipitation during active treatment periods may alter hydraulic retention times and affect pollutant removal processes. Although the absolute change is relatively modest, the observed trend towards reduced moisture availability should be taken into account in the long-term design and operational planning of the facility.

Consecutive Dry Days

The Consecutive Dry Days (CDD) index remained stable at 26 days in both the baseline and mid-century periods, with a moderate increase to 28 days projected by 2071–2100. Although this change is numerically small, the persistence and gradual extension of dry spells during the second half of the century is consistent with broader regional projections for the Western Balkans, which anticipate more pronounced summer dryness under high-emission scenarios [13].

For constructed wetland operation, extended dry periods without significant rainfall can reduce influent dilution, and increase the concentration of incoming wastewater loads [14]. The projected increase in maximum dry spell duration, while modest under the current ensemble, should be considered when planning for resilience against drought-induced hydraulic stress, particularly in combination with increasing temperatures and evapotranspiration demand.

Extreme Precipitation: Maximum One-Day Rainfall

In contrast to the general tendency toward drying, the maximum one-day precipitation (Rx1d) showed a clear increasing trend across all periods: from 40.4 mm in the baseline to 44.3 mm by mid-century (+9.7%) and 48.9 mm by end-of-century (+21.0%). This finding is consistent with the well-established thermodynamic relationship between atmospheric warming and the intensification of extreme precipitation events, whereby a warmer atmosphere can hold and subsequently release more moisture.

The intensification of extreme rainfall events presents a significant operational challenge for CW systems. Events exceeding the hydraulic design capacity of the wetland can cause surface overflow, bypass of the treatment zone, and the mobilisation of previously deposited organic matter and sediment-bound nutrients. A 21% increase in maximum single-day rainfall by the end of the century suggests the need to revise stormwater management infrastructure and inlet/outlet engineering at the Gložan facility. Buffer storage capacity and overflow contingency design may need to be upgraded to accommodate more intense peak inflows without compromising treatment quality. Additionally, frequent intense rainfall events may periodically accelerate water transfer through the system, shortening effective hydraulic retention times and transiently reducing pollutant removal efficiency [18].

Frost Days

One of the most striking projected changes is the substantial reduction in frost days (FD), declining from 79 days per year in the baseline period to 62 days by mid-century and just 40 days by 2071–2100. This represents a reduction of approximately 49% in annual frost days over the course of the century, reflecting the strong warming signal embedded in the RCP8.5 scenario.

Frost conditions represent one of the primary operational constraints for constructed wetlands in continental climates. At temperatures near or below 0°C, microbial metabolic rates — including those driving nitrification, denitrification, BOD removal, and phosphorus cycling — are markedly reduced. The projected reduction in frost days by nearly 40 days per year by the end of the century therefore represents a potentially significant improvement in year-round treatment performance. Longer frost-free operating periods would extend the season of optimal biological activity, and improve the reliability of treatment during the winter months [4]. This finding suggests that the long-term efficacy of CW-based wastewater treatment in the region is likely to improve in terms of cold-season constraints, even as warm-season challenges intensify.

Tropical Days

The tropical days (TD) index, representing days with maximum temperature exceeding 30°C, showed the most dramatic increase of all indices analysed: from 36 days in the baseline to 51 days by mid-century (+42%) and 79 days by the end of the century (+119%). This more

than doubling of tropical day frequency by 2071–2100 underscores the severity of the projected warming and its potential consequences for warm-season CW operation.

High temperatures have a complex and often opposing set of effects on constructed wetland treatment processes [19]. On one hand, elevated temperatures accelerate microbial metabolic rates, potentially enhancing organic matter degradation and nitrogen transformation during warm periods. On the other hand, increasing temperatures reduce oxygen solubility in water, which may compromise aerobic treatment processes and promote the development of anaerobic zones in saturated substrates. Increased evapotranspiration during tropical days can further reduce the system water balance, increase pollutant concentrations in the effluent, and stress macrophytes commonly used in CW systems. Furthermore, very high temperatures can shift microbial community composition towards thermophilic or heat-tolerant species, potentially altering biological treatment dynamics and affecting the efficiency and stability of pollutant removal processes [20]. The projected near-doubling of tropical day frequency over the century suggests that summer operational management of the Gložan CW will need to evolve substantially, potentially including water level adjustments and more frequent monitoring of dissolved oxygen and nutrient effluent concentrations.

CONCLUSION

Overall, the analysis of long-term treatment performance demonstrated that the Gložan CW currently provides relatively high and stable removal efficiency for several key wastewater quality parameters, particularly BOD5, COD, and TN. Nevertheless, higher variability observed for phosphorus, suspended solids, and ammonium removal suggests that some treatment processes may be more sensitive to external environmental and hydrological fluctuations.

The projected climate changes further indicate increasing climatic variability and thermal stress for the Gložan constructed wetland over the 21st century. The emerging pattern under RCP8.5 is characterised by warmer, drier growing seasons (declining SHC), longer dry spells (increasing CDD), more intense individual precipitation events (increasing Rx1d), substantially shorter frost seasons (decreasing FD), and significantly more frequent extreme heat days (increasing TD).

These changes have varying implications for CW treatment performance. The reduction in frost days is likely to have a net positive effect on year-round treatment efficiency, reducing the duration of cold-season performance suppression. However, the increasing frequency of extreme heat events, intensified peak rainfall, and growing moisture deficit during the growing season collectively represent new operational challenges that could progressively offset these gains if not proactively managed.

The obtained findings indicate that climate adaptation strategies should become an integral part of the long-term management, monitoring, and operational planning of nature-based wastewater treatment systems.

ACKNOWLEDGEMENT

This work was supported by the European Union's Horizon Europe innovation action program under grant agreement No. 101094070, project DALIA (Danube Region Water Lighthouse Action); European Union's Horizon Europe innovation action program under grant agreement No.

101215230, project SWIM (Sustainable Water and Integrated Management of Fish Migration and their Habitats in the Danube River Basin and NW Black Sea); the Ministry of Science, Technological Development, and Innovation of Serbia (Grant No. 451-03-34/2026-03/200117 dated 05 February 2026).

REFERENCES

[1] Calheiros CS, Pereira SI, Castro PM. Constructed wetlands as nature-based solutions. In: Vymazal J, editor. An Introduction to Constructed Wetlands. New York: Nova Science Publishers; 2020. p. 97–142.

[2] Wu, H., Wang, R., Yan, P., *et al*. Nat Rev Earth Environ. 2023, 4 (4), 218–234.

[3] Werker, A.G., Dougherty, J.M., McHenry, J.L., *et al*. Ecol Eng. 2002, 19 (1), 1–11.

[4] Yan, Y., Xu, J., Wetlands. 2014, 34 (2), 243–253.

[5] Dykes, C., Pearson, J., Bending, G., *et al*. J Water Process Eng. 2025, 72, 107350.

[6] Bezdan, J., Long-Term Treatment Efficiency of Constructed Wetlands as Nature-Based Solutions for Wastewater Treatment. In: Proceedings of COAST 2026; 9–13 Jun 2026; Herceg Novi, Montenegro. 2026.

[7] Akratos, C.S., Tsihrintzis, V.A. Ecol Eng. 2007, 29 (2), 173–191.

[8] Bezdan J, Bezdan A. Analysis of the Impact of Climate Change on Constructed Wetlands in the Danube River Basin: A Case Study of the Gložan Settlement Region. In: Proceedings of the 3rd International 16th National Congress of Agricultural Structures and Irrigation – ICASI 2025; 24–27 Jun 2025; Ankara, Türkiye. 2025. p. 85.

[9] Bezdan J, Bezdan A, Blagojević B, et al. Assessment of Climate Change Impact on the Constructed Wetlands – Nature-Based Solutions for Sustainable Wastewater Management. In: Proceedings of the 1st RethinkBlue Conference Organized by COST Action CA22122; 23–25 Apr 2024; Zadar, Croatia. 2024. p. 37–38.

[10] Ministry of Environmental Protection of the Republic of Serbia (MEPRS). Digital Climate and Climate Change Atlas of the Republic of Serbia. 2022. Available from: https://atlas-klime.eko.gov.rs

[11] Vujadinovic Mandic M, Vuković Vimić A, Ranković-Vasić Z, *et al*. Climate change risks in agricultural plant production of Serbia. In: Proceedings of the EGU General Assembly; May 2022; Vienna, Austria. 2022. p. EGU22-10522.

[12] Vujadinović Mandić M, Ranković-Vasić Z, Ćosić M, *et al*. Report on the Impact of Climate Change on the Agriculture Sector, with Proposed Adaptation Measures. Activity 1: Risk and Vulnerability Assessment – Observed Occurrences, Impacts, and Levels of Affectedness. 2023. Available from: https://adaptacije.klimatskepromene.rs/wp-content/uploads/2022/03/Agriculture-1.-Risk-and-Vulnerability-assessment.pdf

[13] Vuković A, Vujadinović Mandić M. Study on Climate Change in the Western Balkans Region. Sarajevo: Regional Cooperation Council Secretariat; 2018.

[14] Davis L. A Handbook of Constructed Wetlands: A Guide to Creating Wetlands for Agricultural Wastewater, Domestic Wastewater, Coal Mine Drainage, Stormwater in the Mid-Atlantic Region. Volume 1: General Considerations. Washington, DC: USDA-Natural Resources Conservation Service; 1995.

[15] Ji, B., Zhao, Y., Vymazal, J., *et al*. Ecol Eng. 2020, 157, 105992.

[16] Kadlec, R.H. Ecol Eng. 2006, 26 (4), 328–340.

[17] Jayswal N, Rodríguez J. Effect of Temperature and Loading Frequency on the Performance of Vertical Subsurface Flow Constructed Wetlands: Modelling Study Using HYDRUS. bioRxiv. 2021. Available from: https://doi.org/10.1101/2021.03.25.436912
[18] Silva, G., da Silva Júnior, É.D. Water Environ Res. 2026, 98 (3), e70324.
[19] Kadlec, R.H., Reddy, K.R. Water Environ Res. 2001, 73 (5), 543–557.
[20] Wang, H., Xu, D., Han, J., *et al*. Sci Total Environ. 2021, 781, 146798.

Conference Papers

EcoTER'26
eco.tfbor.bg.ac.rs
32nd International Conference
Ecological Truth & Environmental Research
24–26 June 2026, Hotel Sunce,
Sokobanja, Serbia

Original Research

EFFECT OF AIR OXYGEN ENRICHMENT AND EXCESS AIR RATIO ON SOLID FUELS COMBUSTION

DOI: 10.5937/EcoTER26040R

Žarko Radović[1,a*], Nebojša Tadić[1,b]

[1] University of Montenegro, Faculty of Metallurgy and Technology,
Cetinjski put, bb, 81000 Podgorica, MONTENEGRO

[a] https://orcid.org/0009-0005-3699-9869

[b] https://orcid.org/0009-0007-5458-8232

Abstract

The subject of this article is an analysis of the influence of air oxygen enrichment and excess air on the solid fuel combustion and the GHG emission. Combustion conditions for three different chemical compositions and heating values of solid fuels are defined by changes in values of O_2 (21–30%) and λ (1.2–1.4). GHG emission is defined as the sum of CO_2 and NO_x. For all analyzed solid fuels, the correlation of $\%O_2$, excess air ratio, flame temperature, volume of combustion products and GHG emissions was calculated. The results were obtained using analytical method. The flame temperature increase with increasing values of $\%O_2$ and as a results of this, emission of NO_x increases. This can be explained by statement that at higher combustion temperature, volume of thermal NO_x increase. On the other hand the combustion temperature decreases for all fuel types.

Keywords: flame temperature, combustion, excess air ratio, NO_x.

INTRODUCTION

Improvements in the overall energy efficiency of an industrial plant are primarily achieved by reducing the energy input values and also the energy losses on the output side of a process step [1]. The changes in combustion conditions, especially fuel of lower heating value, causes a change in combustion temperature and volume of gaseous products. The changes in air excess in furnaces mainly affect the extent of NOx (formed from nitrogen contained in the volatile matter) emission[2,3].

Air excess ratio determines some combustion characteristics and affects NO_x emissions [4,5]. Oxygen-enriched combustion technology is accomplished by raising the oxygen content in the intake air, enabling combustion to be mainly governed by the mass ratio of oxygen to fuel instead of the conventional air-fuel ratio [6]. The fuel-combustion process is significantly affected by the heating value of fuel, the amount of combustion air, the air-preheating temperature, the oxygen enrichment in the air and waste gas temperature.

One of the key objectives of thermal engineering calculations for fossil fuel combustion is to define the conditions and determine the quantities that influence heat exchange

* *zarkor@ucg.ac.me*

intensification, reduce specific fuel consumption, and minimize the harmful impact of exhaust gases on the environment.

MATERIALS AND METHODS

The central hypothesis of this paper is that an analytical correlation exists between the chemical composition of the fuel mixture, the air enrichment, excess air ratio and the emission of primary combustion byproducts (CO_2, NO_x), which have a dominant impact on air pollution.

One of the key objectives of thermal engineering calculations for fossil fuel combustion is to define the conditions and determine the quantities that influence heat exchange intensification, reduce specific fuel consumption, and minimize the harmful impact of exhaust gases on the environment.

For these calculation the varying composition of solid fuels (S1,S2,S3) are used as shown in the Table 1.

Table 1 *The chemical composition of solid fuels (%)*

	C	H	O	N	S	W	A
S1	70	5.5	4.2	1.5	4.8	3.0	11.0
S2	75	4.2	3.0	2.1	4.2	2.5	9.0
S3	79	2.5	2.5	2.5	3.0	2.5	8.0

The values of the oxygen content in combustion air for each analyzed fuel were selected from a range 21÷30%, and values of excess air ratio: λ=1.2÷1.4, (Table 2). The heating values (Qd) are calculated on the base of fuel chemical composition.

Table 2 *The content of the oxygen in combustion air, Qd, and λ for analyzed fuels*

	S1	S2	S3
λ	1.2÷1.4	1.2÷1.4	1.2÷1.4
Qd (MJ/kg)	29.41	29.91	29.12
% O_2	21÷30	21÷30	21÷30

Combustion products (V_c) primarily determined by combustion temperature (t_c) significantly impacts greenhouse gas emissions, its dependence on the excess air coefficient (λ) was determined analytically.

RESULTS AND DISCUSSION

Analysis of the calculation results reveals two opposing trends in the influence of an increasing coefficient λ. As the value of λ increases, the volume of combustion products rises linearly, while the combustion temperature decreases for all fuel types (Figure 1).

The difference is reflected in the absolute values of these quantities, which result from the different chemical composition as well as the value of the excess air coefficient (λ) itself.

When these dependencies are viewed from the perspective of thermal efficiency in the combustion process, it is evident that any reduction in combustion temperature decreases the thermal effect, which is undesirable.

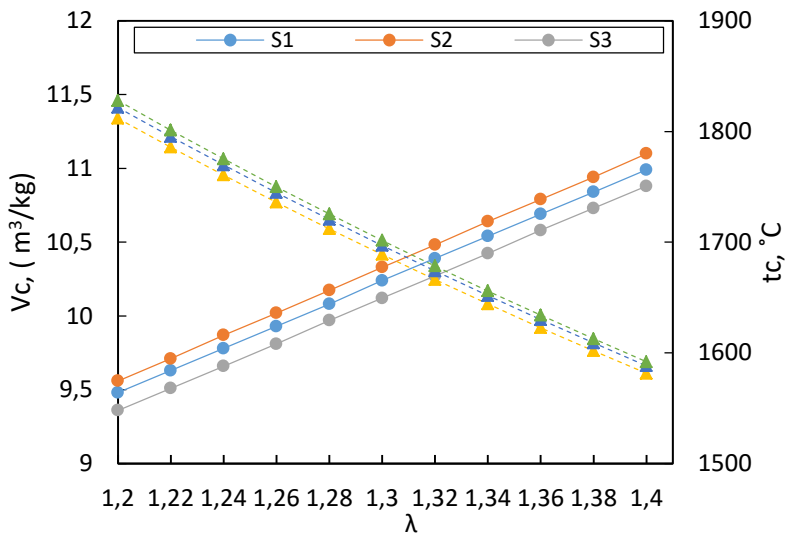

Figure 1 *Combustion temperature of solid fuels and products volume as a functions of λ*

On the other hand, if the primary focus is environmental protection, any increase in Vc generally leads to higher emissions of gaseous pollutants, unless it is predominantly influenced by combustion temperature. Both of these seemingly negative effects are, in fact, a "compromise" with the necessary process parameters, which require a certain excess of air.

The Figure 2 illustrates the dependence of CO_2 emissions per unit mass of solid fuels, as well as the relative % of CO_2 in the total volume of gaseous products. Excess air, which is a technological prerequisite for stable combustion, does not participate in the reaction itself and, therefore, does not contribute to an increase in CO_2 emissions.

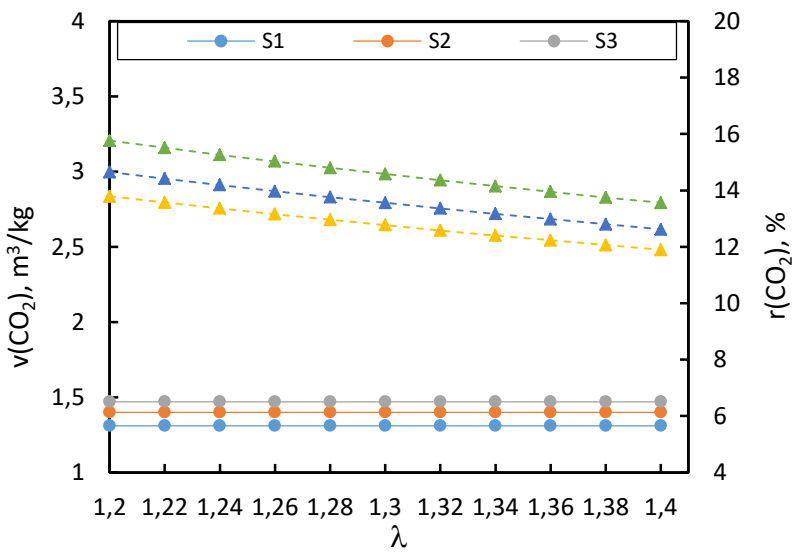

Figure 2 *Volume of CO_2 as a functions of λ*

Based on the discussed mechanisms of NO_x formation during the combustion of different fuel types, the influence of the excess air coefficient (λ) on NO_x emissions and their volume share in the total combustion products is defined (Figure 3).

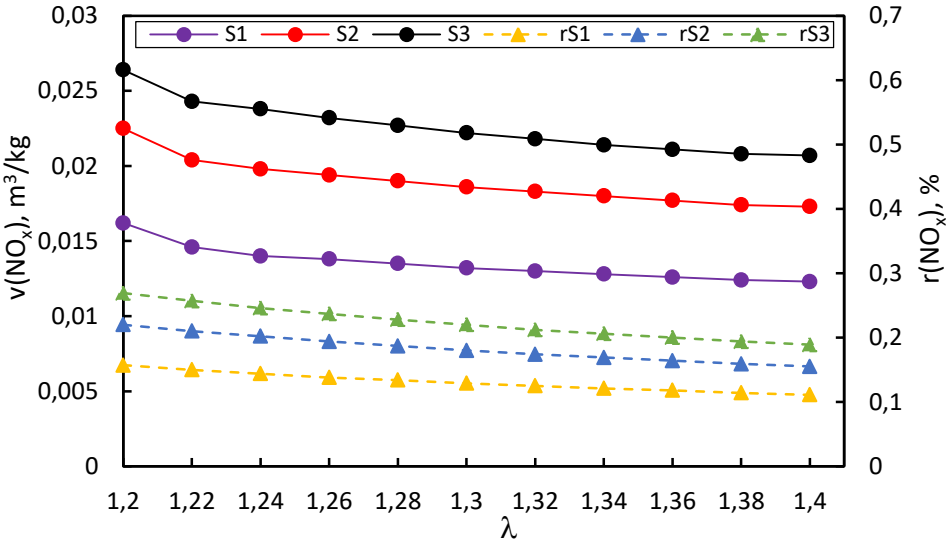

Figure 3 *Volume of NO_x as a functions of λ*

As the excess air coefficient (λ) increases, the specific NO_x volume per unit of fuel decreases following a slightly exponential relationship. Because to compare different fuels in terms of greenhouse gas emissions, emission coefficient $K(NO_x)$ is often used the influence of excess air on this coefficient is defined (Figure 4).

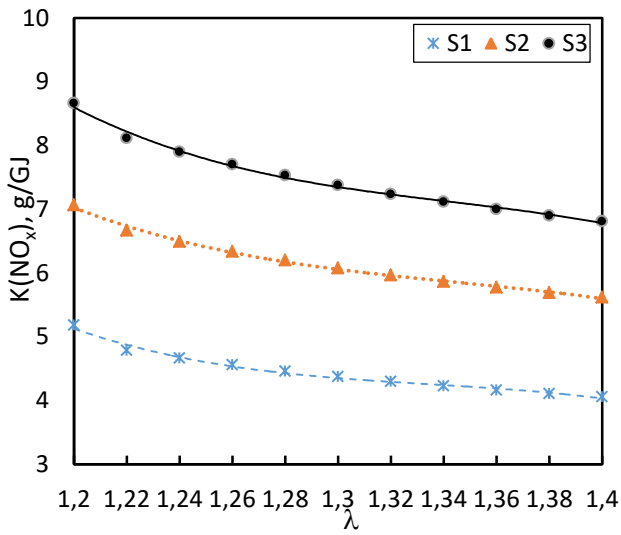

Figure 4 *The coefficient of NO_x emission as a functions of λ*

In all analysed cases, for all solid fuel types, the NO_x emission coefficient decreases as λ increases, following a slightly exponential trend, which is a consequence of the reduction in combustion temperature.

As a consequence of the intensification of the combustion process, there is a change in the flame temperature and the volume of the combustion products formed. As typical, representative examples of the interdependence of the mentioned parameters, graphs related to the average value of the coefficient λ=1,3 from the analyzed range for all solid fuel, are presented (Figure 5).

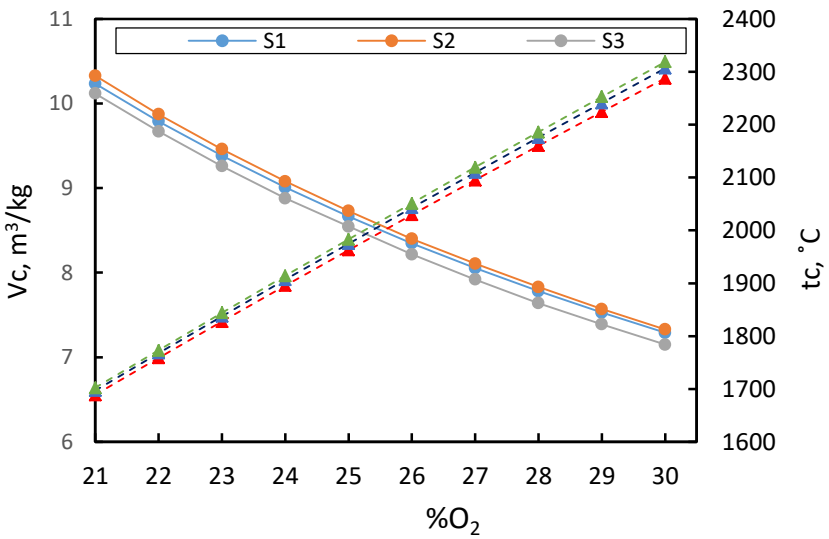

Figure 5 *The influence of oxygen enrichment on the temperature and combustion products volume*

Graphical presentations of the derived calculations show that with the enrichment of air for combustion, i.e., with the increase in the percentage of oxygen in it, the volume of combustion products decreases, and the flame temperature increases.

The influence of the O_2 content in enriched air on the volumetric emission of NO_x and the emission coefficient $K(NO_x)$ is shown in the Figure 6.

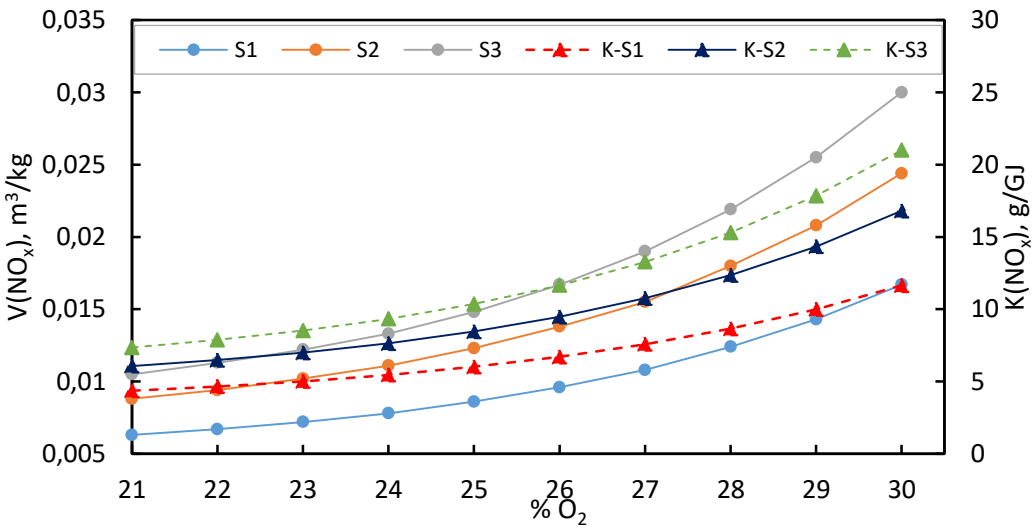

Figure 6 *The influence of % O_2 on the volume and the emission coefficient $K(NO_x)$*

Analytical calculations were performed for all types of fuel and all values of the excess air coefficient, but only the graphical dependencies for the average value of λ=1,30 are shown. For all analyzed solid fuels, it is observed that NO_x emissions increase with air enrichment, i.e., with the increase in % O_2, more or less according to an approximately exponential law.

CONCLUSION

An increase in the value of λ leads to a linear rise in the volume of combustion products and a decrease in combustion temperature for all analysed solid fuels. The excess air coefficient does not influence CO_2 emissions, which primarily depend on the chemical composition of the fuel but it does reduce CO_2's relative share in the combustion products due to the increased total volume.

Increase in λ generally results in a reduction in the unit volume emission $V(NO_x)$ and the emission coefficient $K(NO_x)$. For all analyzed fuels, with the increase in % O_2, the volume of combustion products decreases, and the flame temperature increases. Considering this, the most favorable heat technology indicators are achieved at an enrichment of 30% O_2, but the environmental effects must also be taken into account.

With the increase in O_2 content, the combustion temperature significantly increases, which is the basic precondition for the formation of “thermal” NO_x, so that enriching the air with oxygen leads to an increase in NO_x emissions.

REFERENCES

[1] Lalović, M., Radović, Ž., Jauković, N. Materiali in Tehnologie 2006, 40 (3), 89–92.

[2] Gil, S., Fossil Fuel and the Environment, Dr. Shahriar Khan (Ed.), 2012, p. 37–61.

[3] Song, W., Defu, C., Zhiguo, W., *et al*. Energies 2020, 13(14), 3557.

[4] Ding, H. Ziqu, O., Xiaoyang, C., *et al*. Journal of Thermal Science 2023, 32, 1263–1277.

[5] Abbassi, M., Domenico, L. Cornelis, V. Processes 2021, 9, 1723.

[6] Wang, H.Y. Processes 2024, 12, 2282–2288.

EcoTER'26
eco.tfbor.bg.ac.rs
32nd International Conference
Ecological Truth & Environmental Research
24–26 June 2026, Hotel Sunce,
Sokobanja, Serbia

Original Research

STRENGTH AND MICROSTRUCTURE OF FLY ASH BASED GEOPOLYMERS CONTAINING WASTE PLASTIC

DOI: 10.5937/EcoTER26046T

Nebojša Tadić[1,a*], Irena Nikolić[1,b], Nina Jovović[1,c], Aleksandar Drakulović[1,d], Vuk Radmilović[2,e]

[1] Faculty of Technology, University of Montengro, Džordža Vašingtona bb, 81000 Podgorica, MONTENEGRO

[2] Faculty of Technology and Metallurgy, University of Belgrade, Karnegijeva 4, 11000 Belgrade, SERBIA

[a] https://orcid.org/0009-0007-5458-8232

[b] https://orcid.org/0000-0001-6781-3485

[c] https://orcid.org/0009-0000-5154-2465

[d] https://orcid.org/0009-0002-8730-9467

[e] https://orcid.org/0000-0002-1035-7068

Abstract

This paper investigated the properties of fly ash based geopolymers containing waste plastic (high-density polyethylene (HDPE)). Influence of fly ash substitution with a 30% of plastic waste on the compressive and flexural strength unit weight and microstructure of geopolymers was investigated. The results have shown that plastic dosage led to the wakening geopolymer structure, i.e. impairs mechanical properties. The positive effect of plastic waste addition is reflected in the decrease of unit weight which is beneficial with respect of the structure load. Microstructural investigations have shown the particle of plastic waste embedded into the reaction product of geopolymerisation i.e. into the alumino-silicate gel.

Keywords: fly ash, high-density polyethylene, (HDPE) geopolymer, unit weight, strength.

INTRODUCTION

Publicly accessible information from Montenegro indicates that the thermal power station in Pljevlja disposed of around 360 metric tonnes of fly ash in 2020, with an estimated 12 million tonnes of fly ash already deposited at the Maljevac landfill in Pljevlja [1]. Thus, the valorisation of this waste material is of great importance from the standpoint of environment protection. Currently, extensive research is caring out into the field of fly ash valorisation in a new environmentally friendly building material.

Moreover, plastic pollution has become one of the most pressing ecological issues, as rapidly increasing production of disposable plastic products overwhelms the world's ability to deal with them. Data from 2021 indicate that in Montenegro, plastic waste constitutes 15.3%

* *nebojsa@ucg.ac.me*

of the total solid municipal waste and that 75.65 kg of plastic waste is generated per capita in Montenegro [2]. It represents a serious hazard for the ecosystem which also need to be solved.

Valorisation of fly ash using geopolymerization technology is widely investigated in a pass decade. Geopolymerization is a relatively new technology that can transform natural or waste aluminosilicate materials (fly ash or metakaolin), with alkali activation, into an amorphous to semi-crystalline inorganic polymer – the geopolymer [3–5]. The process includes several steps: dissolution of the starting material in a highly alkaline silicate solution and formation of aluminate and silicate monomeric species, formation of Si and/or Si-Al oligomers in an aqueous solution, condensation of oligomeric species in an aluminosilicate network - geopolymer, and hardening. Sodium silica solution is mainly used as activator in the geopolymerization process.

The aim of this paper was to investigate simultaneous valorisation of fly ash and plastic waste (high-density polyethylene (HDPE)) through geopolymerisation process into the new materials with a possible application in the civil engineering. This approach is of great importance from the standpoint of environment protection which will contribute to reintroducing waste into the production cycle instead of disposing of it in landfills.

MATERIALS AND METHODS

Fly ash was supplied form coal fired power station in Pljevlja (Figure 1a)) and plastic waste (HDPE) from the MONTWAY LLC Podgorica (Figure 1b)).

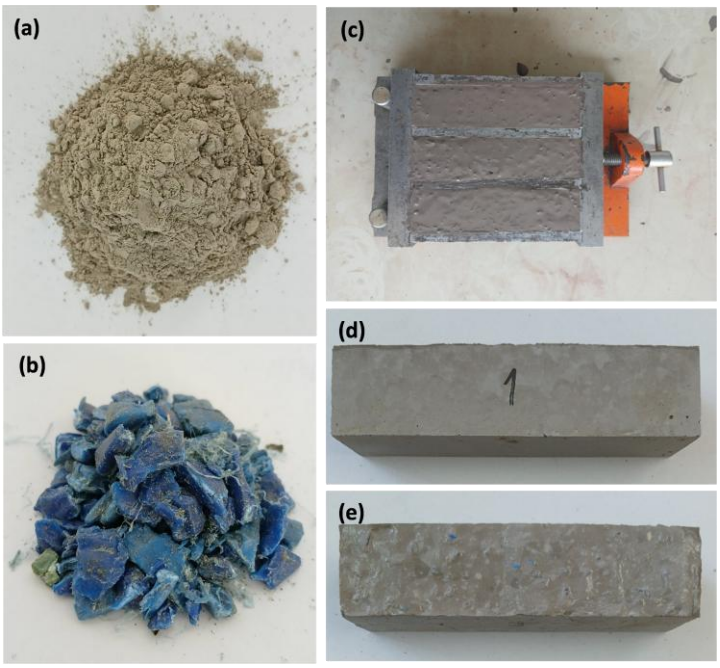

Figure 1 *a) Flay ash; b) Waste plastic HDPE; c) Casted fly ash based geopolymer; d) the hardened fly ash based geopolymer without and e) with waste HDPE*

Fly ash based geopolymer were prepared by mixing of fly ash with alkali activator at solid to liquid (S/L) ratios of 1.4. Alkali activator was prepared by mixing of 7M NaOH solution

and Na_2SiO_3 solution (commercial water glass) in a mass ratio of 1. Prepared geopolymers were casted in mould (40 × 40 × 160 mm) (Figure 1c)), covered with a nylon and cured in the oven at the temperature of 65°C for a period of 48 h. After 7 days, the samples were removed from mould, and rest at the room condition for additional 2 weeks and conducted for mechanical testing (testing for compressive and flexural strength). Before mechanical testing, the samples were weighted and unit weight (kg/m^3) was calculated.

Fly ash based geopolymer containing HDPE was prepared by adding HDPE to the starting mixture by fly ash replacement with 30% to the total solid content fooling the same procedure. The fragments remained after the testing of mechanical properties were used for a microstructural analysis.

Microstructural investigations were carried out using the FEI Helios NanoLab 660 SEM/FIB dual beam system, equipped with the EDAX energy dispersive X-ray spectrometer (EDS).

RESULTS AND DISCUSSION

Sample of fly ash based geopolymers without HDPE addition is given in Figure 1d) and the figure of geopolymer sample synthesized with 30 % of waste HDPE is given in Figure 1e). The results of mechanical testing were given in the Figure 2.

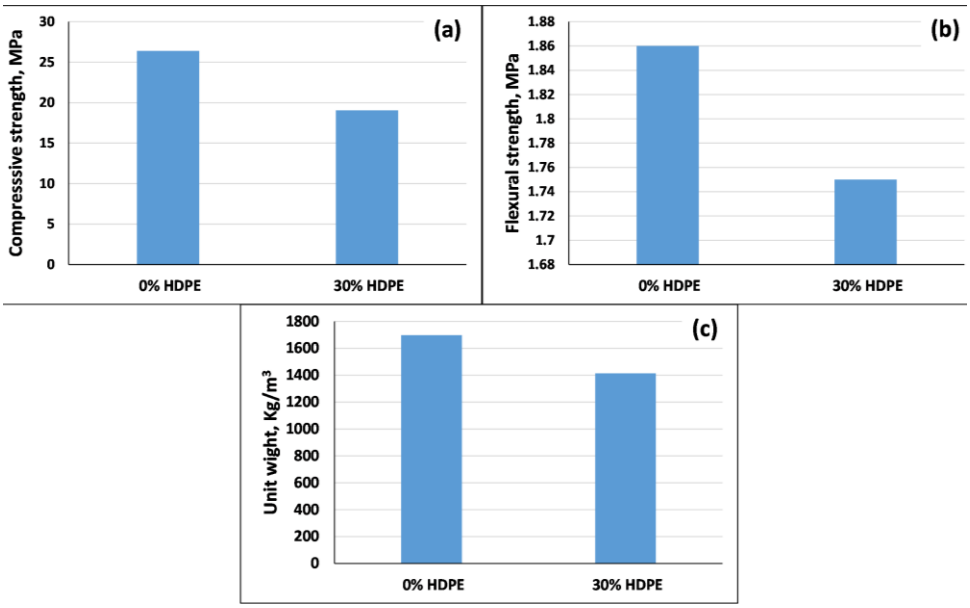

Figure 2 *Influence of plastic waste addition on the a) compressive strength; b) flexural strength and c) unit weight of geopolymer*

It is evident that, addition of waste plastic led to the weakening of fly ash based geopolymers. Fly ash based geopolymer synthesized without waste plastic, reach the compressive strength of 26.41 MPa while fly ash substitution with 30% of waste HDPE led to the decrease of compressive strength to the 19.06 MPa (Figure 2a)). Likewise, flexural strength of geopolymers with 30% waste HDPE also decreases from 1.87 MPa to 1.75 MPa (Figure 2b)). The benefit of HDPE addition is reflected in a decrease of unit weight of fly ash

geopolymers from 1698 kg/m^3 to 1414 kg/m^3 (Figure 2c)) which is important from the standpoint of application of these materials in the practice. Reduction of the unit weight of building materials is important because it reduces the self-weight of the structure and the load on the construction and foundations.

The results of SEM/EDS analysis are given in the Figure 3 and Table 1. The SEM photography clearly show the particle of plastic waste embedded in a geopolymer binder. The results of EDS analysis taken from the geopolymer binder area denoted with a red cross indicate the high content of silicon, aluminium and oxygen (Table 1) *i.e.* the presence of alumina-silicate gel, as the major binding phase generated due to the geopolymerisation reaction [6].

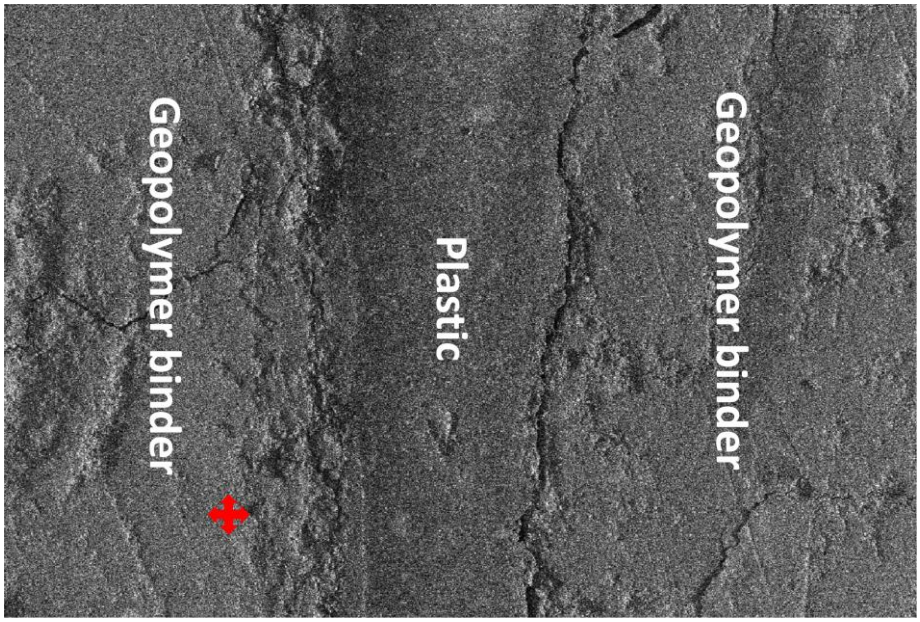

Figure 3 *SEM photography of fly ash based geopolymer containing plastic (HDPE) waste*

Table 1 *The results of EDS analysis taken from the geopolymer are in Figure 3, denoted with red cross*

Element	wt.%
Oxygen	38.83
Aluminium	10.78
Silicon	23.70
Iron	3.10
Calcium	8.90
Chromium	0.08
Potassium	2.81
Phosphorous	4.58
Sulphur	1.12
Magnesium	0.8
Sodium	4.94
Titanium	0.25
Vanadium	0.11

CONCLUSION

The results have shown that fly ash based geopolymers can be synthesized with 30% of waste (HDPE) plastic. Although, substitution of fly ash with 30% of HDPE lead to the decrease of compressive and flexural strength of fly ash based geopolymers for a 7.4% and 5.9%, respectively, they can be used in a civil engineering. The benefit of substituting ash with 30% plastic is reflected in a decrease of unit weight of fly ash based geopolymers. Microstructure of fly ash based geopolymer containing the plastic waste is consisting of plastic embedded in a geopolymer binder. Existence of geopolymer binder is confirmed by EDS analysis which indicated presence of alumina-silicate gel.

ACKNOWLEDGEMENT

The authors are grateful to the Innovation Fund of Montenegro for financial support according to the contract with registration No. CGI-004-24.

REFERENCES

[1] Local action plan for environmental protection of the municipality of Pljevlja 2022–2026.

[2] State management waste plan in Montenegro for a period of 2024–2028. Available from: https://www.gov.me/dokumenta/1b9a9af3-c1c1-43c2-a10b-48388084af11

[3] Luhar, I., Luhar, S. J. Compos. Sci. 2022, 6(8), 219.

[4] Kalombe, R.M., Ojumu, V.T, Eze C.P. *et al*. Materials 2020, 13(24), 5699.

[5] Prasad, B.V., Daniel, A.P., Anand N. *et al*. J. Eng. Design Technol., 2022, 20(2), 436–454.

[6] Tian, Q., Sun, S., Sui, Y. *et al*. Ceramics-Silikaty, 2021, 65(1), 9–23.

Original Research

AN ASSESSMENT OF THE PRESENCE OF DIBENZ(a,h)ANTHRACENE, A PROBABLE HUMAN CARCINOGEN, IN THE BOR REGION, ON THE BASIS OF ITS CONTENT IN STEMS AND LEAVES OF COMMON IVY, LILAC, AND FIG

DOI: 10.5937/EcoTER26051P

Aleksandra Papludis[1,a*], Slađana Alagić[1,b], Snežana Milić[1,c], Dragana Medić[1,d], Jelena Nikolić[2,e], Vesna Stankov Jovanović[2,f], Gordana Stojanović[2,g]

[1] University of Belgrade, Technical Faculty in Bor, Vojske Jugoslavije 12, 19210 Bor, SERBIA

[2] University of Nis, Faculty of Sciences and Mathematics, Department of Chemistry, Višegradska 33, 18000 Niš, SERBIA

[a] https://orcid.org/0000-0002-5388-2428

[b] https://orcid.org/0000-0002-2893-9285

[c] https://orcid.org/0000-0002-5000-9156

[d] https://orcid.org/0000-0001-9980-5949

[e] https://orcid.org/0000-0002-9351-331X

[f] https://orcid.org/0000-0001-7885-0476

[g] https://orcid.org/0000-0002-3128-6510

Abstract

In this work, the capacity of unwashed aerial parts of plant species: common ivy (CI), lilac (CL), and fig (CF), for DhA detection in biomonitoring purposes was investigated, using GC/MS, and the Pearson's correlation analysis. Additionally, the detected DhA concentrations were compared with the interrelated lawmaking. GC/MS detected many considerable DhA quantities and documented different capacity of the investigated species for DhA deposition/bioaccumulation, where CI, and CF, showed a better ability for the atmospheric dust retention than CL. However, the highest DhA concentrations were detected in CL parts: 1200.9 µg/kg for stems, and 174.5 µg/kg for leaves, which is even higher than the related USEPA limit values (LVs) for residential soils. Simultaneously, for CL parts, the highest number of locations lacking in DhA was found. Other species showed that almost all selected locations had measurable DhA concentrations, often at the levels that surpassed mentioned USEPA LVs. This means that all locations with such levels may signify possible dermal risks from direct contacts with aerial parts. The results of the Pearson's analysis confirmed that the industrial center in Bor, with the heating plant and the mining-metallurgical complex, can be one of significant but not the main source of DhA.

Keywords: Dibenz(a,h)anthracene, common ivy, lilac, fig, biomonitoring.

INTRODUCTION

Dibenz(a,h)anthracene (DhA) is a polycyclic aromatic hydrocarbon (PAH) consisting of five aromatic rings. It is mainly used for research purposes. In the environment, it occurs as a

* *apapludis@tfbor.bg.ac.rs*

result of the incomplete combustion of organic materials [1], and DhA it is primarily present in emissions produced during the combustion of gasoline, wood, and coal [2].

Some of the most important chemical and physical properties of DhA are as follows: form (at the room temperature) – solid, colorless, with a "bay-region" structure (Figure 1), formula – $C_{22}H_{14}$ [3], molecular weight - 278.35, solubility - 0.5 µg/L, vapor pressure - $1.0 \cdot 10^{-10}$ mm Hg, Henry's Law Constant - $7.30 \cdot 10^{-08}$ atm m^3/mol, Log K_{ow} - 6.84, and Log K_{oc} - 6.52 [4]. The reported values proves high lipofility of this compound, which normally enables an easy infiltration through biological membranes of various living organisms.

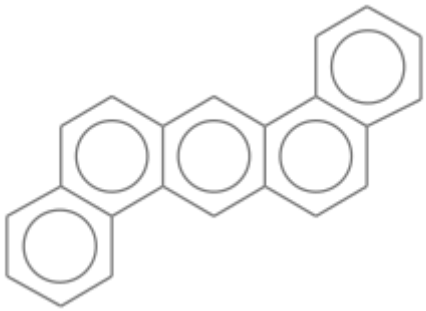

Figure 1 *Molecular structure of DhA [3]*

This compound can enter the human body through skin absorption or inhalation lung, after which it is dissolved in blood and distributed further to various target organs. In the body of experimental animals, more precisely, in their liver, it is metabolized by mixed-function oxidase enzymes, forming and transformed into dihydrodiols. Further epoxidation of the intermediate: 3,4-dihydrodiol, can lead to the formation of a diol-epoxide, which is considered the ultimate carcinogenic metabolite of dibenz(a,h)anthracene DhA [1]. Studies showed that the exposure to DhA has been closely linked to a higher risk of various respiratory illnesses, including asthma, obstructive lung diseases, and respiratory infections [2]. However, there are no studies evaluating its toxicity in humans. Based on confirmed evidence of carcinogenicity in animals, the United States Environmental Protection Agency (USEPA) has classified dibenz(a,h)anthracene this PAH compound as a B2 substance, meaning it is which means that it can be considered a probable human carcinogen [1].

From this reason, USEPA included DhA into the list of 16 priority PAHs that are the most dangerous for all living organisms [4–6]. They all can be found in USEPA Risk-Based Screening Tables, which contain the defined limit values (LVs) for each of 16 PAHs in tap water as well as in residential and industrial soil. A particular attention of this Agency was paid to the soil because it represents a very slowly renewable natural resource [7], which serves as a main environmental sink for PAHs [8]. In the case of this environmental sphere, when concentrations of PAHs are equal to or surpass the related LVs, further evaluations are required for the potential remediation. USEPA LVs are calculated on the basis of the target cancer risk (TR) of $1 \cdot 10^{-6}$ and 2 standards of the target hazard quotients (THQ): 1.0 and 0.1. The defined LVs for both standards for DhA in residential and industrial soils are: 0.11 and 2.1 mg/kg, respectively [5,6,9].

Unfortunately, there are still no defined toxicity LVs for DhA in plants, and also, in the scientific literature data, there are no any suggestions regarding this issue.

In this paper, the content of DhA is detected to establish, for the very first time, its concentrations in the above ground parts of the selected plants from the Bor region, as a well known highly polluted region but chiefly by heavy metals. The selected plants were: common ivy (CI), lilac (CL), and fig (CF) var. crna Petrovača, due to the fact that these plants were not investigated earlier with regard to PAH biomonitoring. Also, there was a hope that the detected DhA concentrations in the above ground parts of these plants can point to the environmental quality of the investigated region, primarily considering DhA pollution that comes from the atmosphere, and perhaps from the emissions of the city heating plant and the mining-metallurgical complex, as possible main sources.

MATERIALS AND METHODS

The contents of DhA were evaluated in the unwashed stems and leaves of CI, CL, and CF assembled at 9 locations from urban-industrial (UI), rural (R) and 1 touristic (T) zone from the Bor region. Touristic zone was a location next to the Borsko jezero (BJ), (eng. Bor Lake), while the locations from R zone were settlements: Oštrelj (O), Slatina (S), Krivelj (K), and Gornjane (G); sites from UI zone were: Flotacijsko jalovište (FJ), Bolničko naselje (BN), Slatinsko naselje (SN), and Naselje Sunce (NS). The distances of the mentioned sites from the city heating plant and the copper smelter in the industrial zone of the town of Bor are as follows: 0.7 km for FJ – flotation tailings pond out of use, 1.3 km for the site BN, near the city hospital, then for the two sites at the periphery of the town - 3.2 km for SN, and 3.6 km for NS. The sites in R zone are located as follows: 4.5 km for O, 6.5 km for S, 8 km for K, and 19 km for G. The distance for BJ site is 7 km.

The samples of the chosen plant parts were taken at the selected sites in September 2020, and analyzed as dried, unwashed material, in the same way as explained in Papludis *et al.* [5], and Papludis *et al*. [10] for (washed) roots and the corresponding soils of the same plant species. Leaves and stems of CI, CL, and CF, were used as unwashed, given that in this way they can reflect an actual state of seasonal pollution in the Bor region. Namely, unwashed aerial parts reflect the sum of an atmospheric deposition, and bioaccumulation of contaminants in these parts. Most importantly, for DhA isolation, the partially modified QuEChERS (Quick, Effective, Cheap, Easy, Rugged, Safe) technique was used [5,8], while for its identification and quantification, gas chromatographic-mass spectrometric (GC/MS) method was performed. The results are given in µg/kg DW (dry weight).

Additionally, the results of chemical analysis were subjected to the Pearson correlation analysis as a statistical method that may help in biomonitoring procedures, pointing to main sources of the pollutant, i.e., DhA, on the basis of correlations between the detected DhA contents and the parameter: distance (D). In the concrete study, this parameter denotes the distance of the sampling sites from the industrial center in the town of Bor as the possible main source of DhA pollution.

RESULTS AND DISCUSSION

The results of GC/MS analysis for DhA contents in leaves and stems of CI, CL, and CF are given in Table 1.

Table 1 *The content of DhA (µg/kg, dw) in the leaf and stem samples of CL, CF, and CI*

Location / Plant species and their parts	CL		CF		CI	
	Leaf	Stem	Leaf	Stem	Leaf	Stem
FJ	nd	nd	128 ± 0.5	161 ± 8	130.7 ± 3.5	170.6 ± 2.5
BN	nd	1200.9 ± 88.5	87 ± 3	230 ± 0.5	112 ± 4	87 ± 4
SN	nd	nd	72.7± 3.5	190 ± 5	59.96 ± 3.66	nd
NS	174.5 ± 6.8	nd	89.4 ± 2.6	73.4 ± 1.6	110 ± 7	72.7 ± 7.1
O	nd	nd	96.2 ± 1.5	149.2 ± 4.5	111 ± 3.8	117 ± 18
S	nd	nd	27.46 ± 2.15	98 ± 9	28 ± 2.3	95.11 ± 4.27
BJ	47.3 ± 3.6	950.3 ± 41.7	40.3 ± 3.5	142.56 ± 2.39	58 ± 10	69 ± 4
K	84 ± 1	nd	53.2 ± 3.5	nd	45.4 ± 1.7	124 ± 1.9
G	35.7 ± 3.5	nd	13.8 ± 0.8	nd	76 ± 2	99 ± 7

Based on the obtained results, it can be said that the concentrations of DhA varied among plant species but also among plant parts, as well as among locations and there were no any rules that can be defined. The highest DhA concentration was detected in the case of CL stems, at the U/I site BN: 1200.9 µg/kg. The highest DhA concentration for leaves was found in the same plant species, at the site NS: 174.5 µg/kg (also in U/I zone). However, at the same time, this plant species had the highest number of locations with DhA level: nd (in comparison with CF, and CI). In the case of CF, and CI above ground parts, DhA was detected at almost all locations, mostly in significant concentrations (Table 1), which may suggests a better tendency of their aerial organs for atmospheric dust capturing. This situation, namely, the variability in DhA presence and its quantities in plant parts at the selected locations may also represent a first signal of the existence of different sources of DhA in the investigated region.

Interestingly, in many cases, the obtained DhA values were higher than the corresponding USEPA LVs for residential soil, considering both defined standards for THQ [6]. This further indicates that, similarly to the case with soil, a direct contact with the stems and leaves of the investigated plants at some locations could pose a risk from DhA, primarily regarding the human skin (at points of direct contacts). These locations (given in bold in the Table 1) are as follows:

1) site NS for CL leaves, and sites BN, and BJ, for CL stems:
2) site FJ for CF leaves, and sites FJ, BN, SN, O, and BJ for CF stems, and
3) sites FJ, BN, NS, O, and K for CI leaves, and sites FJ, O, and K for CI stems.

Almost all other DhA values for its deposition/bioaccumulation in the investigated plant parts were below the detection limits (marked as: nd) and only at few locations, some measurable values were recorded.

As explained, in terms of obtaining safe information on plants' parts usability in the detection of assumable DhA major sources, the Pearson correlation analysis was applied to the detected concentrations and the parameter D. The results showed that the Pearson's

correlation coefficients mostly had negative character, which points that the concentrations of DhA decreased with D increasing. This is normally to expect in the case of point sources, which may signalize that DhA had an origin that can be connected with the industrial center in Bor. However, given that the computed values were very low, it can be concluded that the supposed connection was at the very low level, too, and finally that - the city heating plant and mining-metallurgical complex cannot be considered as the main and sources of DhA. Only the detected concentrations in stems and leaves of CF were in statistically significant correlations with D (p = -0,755*, and p = -0,804**, respectively). These facts represent one more proof that the industrial center can be one of significant but not the main source of DhA. Its other sources can be: traffic, heating in individual households based on wood and coal, controlled combustions in agricultural fields in autumn, spontaneous forest fires, as well as spontaneous ignitions in the city landfill, etc.

CONCLUSION

The results of chemical analysis in this work provided evidence of many cases with considerable DhA concentrations, and revealed different capacity of the investigated plant species for DhA deposition/biaccumulation, where CF, and CI, showed a better capability for the atmospheric dust retention in comparison with CL. However, the highest DhA concentrations were detected in CL aerial parts: 1200.9 μg/kg for stems (at the site BN), and 174.5 μg/kg for leaves (at the site NS), which are higher values than the proscribed USEPA LVs for residential soils. At the same time, this plant species showed the highest number of locations, which were without the detected DhA. The other plant species showed that almost all selected locations had measurable DhA concentrations, in many cases even at the levels that surpassed the related USEPA LVs. It can be concluded that all locations with these levels may represent a signal on possible dermal risks from a direct contact with plant parts considering all investigated species.

The results of statistical analysis pointed that the industrial center in Bor, with the heating plant and the mining-metallurgical complex, can be one of significant but not the main source of DhA. The other sources can be: traffic, domestic heating, controlled combustions in rural zone, spontaneous forest combustions, as well as spontaneous ignitions in the city landfill, etc.

ACKNOWLEDGEMENTS

The authors are grateful to the Ministry of Science, Technological Development and Innovation of the Republic of Serbia, for all the financial support of this work, within the funding of the scientific research work at the University of Belgrade, Technical Faculty in Bor (contract number 451-03-34/2026-03/200131), and at the University of Niš, Faculty of Science and Mathematics in Niš (451-03-34/2026-03/200124).

REFERENCES

[1] Bhattacharya, S., Chakraborty, P., Roy, S. Dibenz[a,h]anthracene, Editor: Philip Wexler, Encyclopedia of Toxicology (Third Edition), 2014, p. 62–66.

[2] Xie, Y., Guo, Z., Liu, J. *et al.* Environ. Hlth. Adv. 2025, 13, 100120, 1–8.

[3] Available from: https://webbook.nist.gov/cgi/cbook.cgi?ID=53-70-3

[4] Alagić, S., Maluckov, B., Radojičić, V. Clean Technol. Environ. Res. 2015, 17, 597–614.

[5] Papludis, A., Alagić, S., Milić, S. *et al.* Environments 12(8), 256.

[6] USEPA, 2024. United States Environmental Protection Agency (2024): Risk-Based Screening Tables — Generic Tables; Regional Screening Levels, RSLs, Summary Tables (TR=$1x10^{-6}$ and THQ=1.0, and THQ=0.1) May 2024. Available from: https://www.epa.gov/risk/regional-screening-levels-rsls-generic-tables

[7] Petruzzelli, G., Pezzarossa, B. Pedron, F. Environments 2025, 12, 183.

[8] Cvetkovic, J., Mitic, V., Stankov-Jovanovic, V. *et al.* Anal. Methods. 2016, 8, 1711–1720.

[9] Alagić, S., Stankov-Jovanović, V., Mitić V. *et al.* Sci. Total Environ. 2016, 562, 561–570.

[10] Papludis, A., Alagić, S., Milić, S. *et al.* Materials protection 2023, 64(1), 13–21.

EcoTER'26
eco.tfbor.bg.ac.rs
32nd International Conference
Ecological Truth & Environmental Research
24–26 June 2026, Hotel Sunce,
Sokobanja, Serbia

Original Research

ELECTROCHEMICAL SENSING OF CAFFEINE

DOI: 10.5937/EcoTER26057C

Aleksandar Cvetković[1,a*], Žaklina Tasić[1,b], Marija Petrović Mihajlović[1,c], Ana Simonović[1,d], Milan Radovanović[1,e], Anđelija Bogdanović[1,f], Milan Antonijević[1,g], Sonja Stanković[1,h]

[1] University of Belgrade, Technical Faculty in Bor, Vojske Jugoslavije 12, 19210 Bor, SERBIA

[a] https://orcid.org/0009-0003-5184-6874 [b] https://orcid.org/0000-0001-6544-1980

[c] https://orcid.org/0000-0001-5486-3870 [d] https://orcid.org/0000-0003-2392-0048

[e] https://orcid.org/0000-0002-5175-6022 [f] https://orcid.org/0009-0008-9984-4970

[g] https://orcid.org/0000-0002-2201-066X [h] https://orcid.org/0000-0003-0745-5422

Abstract

Caffeine is one of the most widely consumed psychoactive compounds and has gained increasing attention as an environmental and anthropogenic marker due to its frequent occurrence in wastewater and aquatic systems. Electrochemical methods have recently emerged as attractive alternatives for caffeine determination because of their simplicity, low cost, rapid response, and sensitivity. In this work, graphite pencil electrodes were investigated as renewable and economically accessible carbon-based electrodes for caffeine analysis in Britton–Robinson buffer using cyclic voltammetry. The electrochemical behavior of caffeine was investigated at different scan rates in order to evaluate the anodic response and oxidation characteristics of the system. In addition, Python-based data processing was applied for visualization, regression analysis, and automated interpretation of cyclic voltammetry data. The obtained results indicate predominantly irreversible electrochemical behavior of caffeine on graphite pencil electrodes with a significant dependence of anodic peak current on scan rate. The proposed approach demonstrates the potential of combining low-cost electrochemical sensing with open-source computational tools for electrochemical data analysis.

Keywords: caffeine, cyclic voltammetry, graphite pencil electrode, electrochemical analysis, Python.

INTRODUCTION

Caffeine (CAF) is a naturally occurring purine alkaloid widely present in coffee, tea, energy drinks, pharmaceuticals, and numerous consumer products. Due to its high consumption and continuous release into wastewater systems, caffeine has attracted significant attention as a biomarker and anthropogenic indicator of human activity and domestic wastewater contamination. Its presence in aquatic environments is frequently associated with urban pollution, wastewater discharge, and environmental monitoring studies, making caffeine an important target compound in analytical chemistry and environmental assessment [1–3].

*acvetkovic@tfbor.bg.ac.rs

The increasing demand for rapid and accessible monitoring methods has stimulated the development of alternative analytical approaches for caffeine determination. Conventional methods such as chromatography and spectroscopic analysis provide high sensitivity and accuracy but often require expensive instrumentation, complex sample preparation, and specialized laboratory conditions. In recent years, electrochemical methods have become increasingly attractive due to their simplicity, rapid response, low operational cost, and suitability for real-time analysis [4–6].

Among various electrochemical sensing materials, carbon-based electrodes have gained particular importance because of their favorable electrochemical properties, chemical stability, and economic accessibility. Graphite pencil electrodes (PGE) represent a low-cost and renewable alternative to conventional solid electrodes, by removing the need for surface renewal and making the preparation process trivial in comparison with other electrodes, while being widely available [7–11].

In this work, cyclic voltammetry was employed for the investigation of caffeine oxidation behavior on graphite pencil electrodes in Britton–Robinson (BR) buffer at different scan rates. Furthermore, Python-based scientific computing and data processing tools were utilized for automated visualization, regression analysis, and interpretation of electrochemical data. The integration of low-cost electrochemical sensors with open-source computational methods represents a promising approach for reproducible and accessible electrochemical analysis [10–15].

MATERIALS AND METHODS

A caffeine solution with a concentration of $1 \cdot 10^{-3}$ M was prepared in Britton–Robinson (BR) buffer. Electrochemical measurements were performed using cyclic voltammetry (CV) in a three-electrode electrochemical system consisting of a graphite pencil electrode (PGE) as the working electrode (WE), a platinum wire as the counter electrode (CE), and a calomel electrode as the reference electrode (RE). HB graphite leads for mechanical pencils were used as graphite pencil electrodes. The electrochemical response of caffeine was investigated at scan rates of 20, 50, and 100 mV/s.

Graphite pencil electrodes (PGE) were selected due to their low cost and wide availability. Cyclic voltammetry measurements were carried out in order to evaluate the electrochemical behavior of caffeine and the influence of scan rate on the anodic response of the system.

Electrochemical data obtained from the IVIUM electrochemical workstation were exported in ASCII format and processed using Python-based scientific computing tools. A custom Python-based workflow was developed for electrochemical data interpretation and visualization of cyclic voltammetry measurements. Numerical processing and structured data handling were performed using NumPy and Pandas libraries, while SciPy was applied for regression analysis and peak-related data processing. Visualization of cyclic voltammetry curves and regression plots was performed using Matplotlib and PyQtGraph libraries. The complete experimental and computational workflow used in this study is presented in Figure 1 [4–6,8,9,12–15].

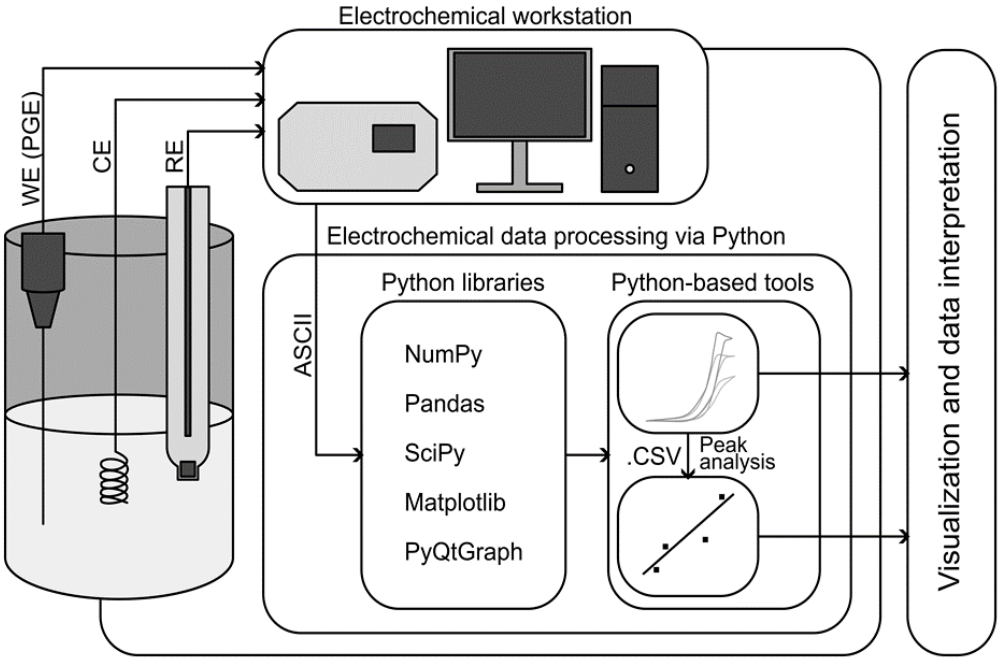

Figure 1 *Schematic representation of the electrochemical and Python-assisted workflow used for cyclic voltammetry data acquisition, processing, regression analysis, and interpretation*

RESULTS AND DISCUSSION

Figure 2 presents cyclic voltammograms obtained for $1 \cdot 10^{-3}$ M caffeine solution in BR buffer using a graphite pencil electrode at scan rates of 20, 50, and 100 mV/s, which are represented by blue, red, and green curves, respectively.

The obtained voltammograms show a pronounced anodic response in the high potential region, while no clearly defined cathodic counterpart was observed during the reverse scan, indicating predominantly irreversible electrochemical behavior of caffeine on the graphite pencil electrode surface. Similar electrochemical behavior of caffeine oxidation on carbon-based electrodes has been previously reported in the literature [10,16]. The observed oxidation region and voltammetric profile are also in agreement with previously described anodic oxidation mechanisms of caffeine in aqueous media [16]. The applicability of graphite pencil electrodes for caffeine oxidation in the high potential region may also be associated with the relatively wide anodic potential window and favorable electrochemical properties of graphite-based materials [11].

The anodic peak potential (Ep) was observed in the high potential region between approximately 1.58 and 1.62 V, while the anodic peak current (*Ip*) increased with increasing scan rate. The shift of Ep toward more positive potentials together with the increase of *Ip* at higher scan rates is characteristic of irreversible electrochemical oxidation processes and agrees with previously reported electrochemical behavior of caffeine on carbon-based electrodes [10,16]. According to the obtained results, the anodic peak current increased from 0.0275 mA at 20 mV/s to 0.1083 mA at 100 mV/s, while *Ep* shifted from 1.5860 to 1.6207 V. An increase in scan rate resulted in a significant increase in anodic current intensity together with noticeable changes in voltammetric profile and peak shape. At higher scan rates, the

existing anodic features became more pronounced, which is consistent with the oxidation of caffeine on heterogeneous graphite-based electrode surfaces [5,10,11].

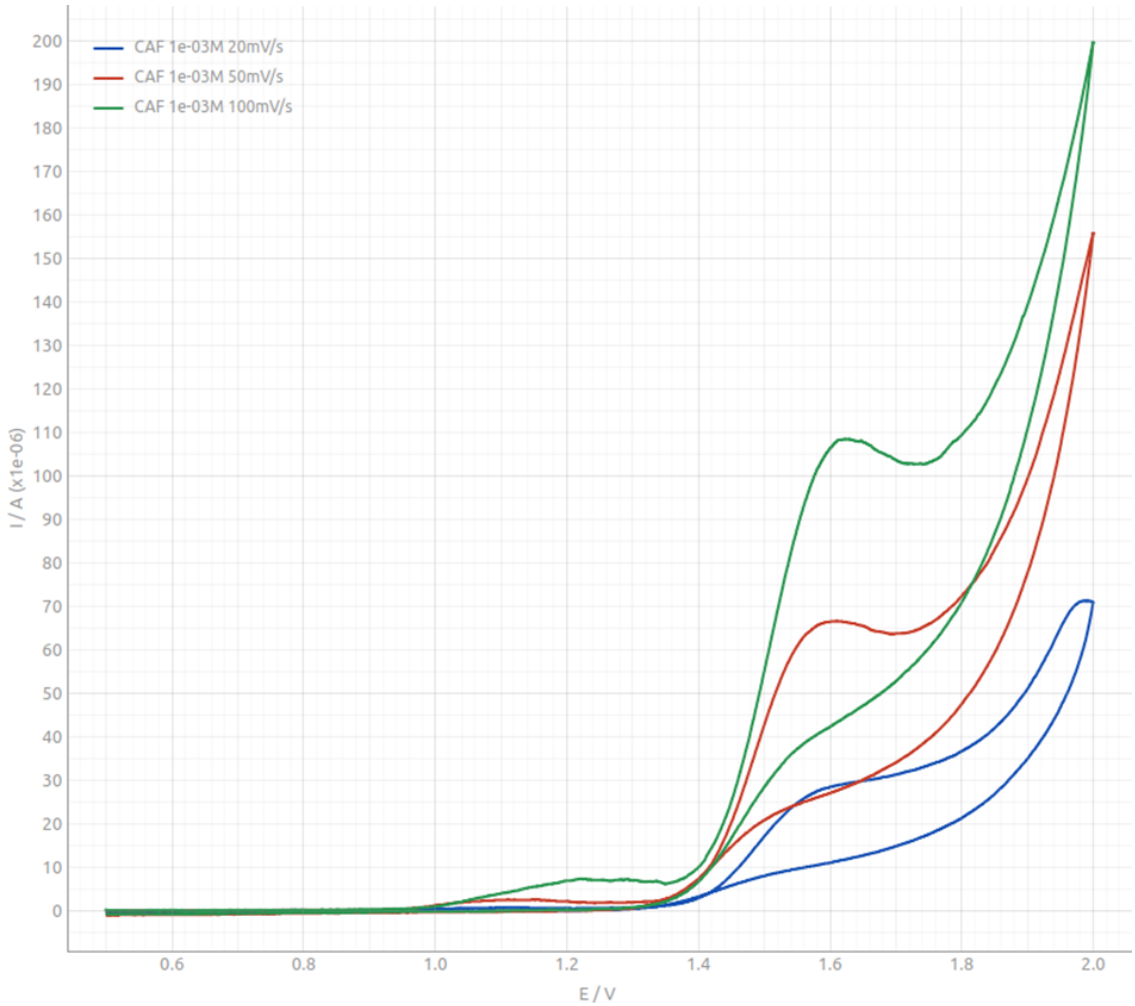

Figure 2 *Cyclic voltammograms obtained for $1 \cdot 10^{-3}$ M caffeine solution in Britton–Robinson buffer using a graphite pencil electrode (PGE) at scan rates of 20, 50, and 100 mV/s*

a) *b)* *c)*

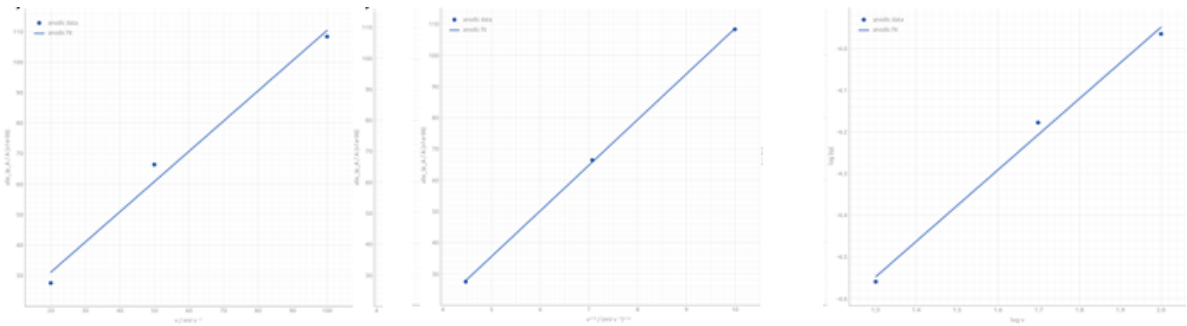

Figure 3 *Regression relationships obtained for anodic peaks, current dependence on scan rate: a) Ip vs v; b) Ip vs $v^{1/2}$; and c) log(Ip) vs log(v)*

Table 1 *Regression parameters and anodic peaks obtained for caffeine oxidation at different scan rates using a graphite pencil electrode (PGE)*

Concentration	Peak	Scan rate (mV/s)	*Ep* (V)	*I* (mA)	Regression	Slope *b*	Intercept	R^2	R
$1 \cdot 10^{-3}$ M	Anodic	20	1.5860	0.0275	*Ip vs v*	~ 0	~ 0	0.9851	0.9925
	Anodic	50	1.6002	0.0664	*Ip vs √v*	~ 0	~ 0	0.9998	0.9999
	Anodic	100	1.6207	0.1083	*log(Ip) vs log(v)*	0.8566	-5.6620	0.9930	0.9965

Figure 3 presents regression relationships obtained for anodic peak current dependence on scan rate, including *Ip vs v*, *Ip vs √v*, and *log(Ip) vs log(v)*. Table 1 summarizes the corresponding regression parameters. The obtained regression coefficients indicate a strong dependence between anodic peak current and scan rate. The Ip vs √v relationship exhibited the highest correlation coefficient (R^2 = 0.9998), suggesting a significant diffusion contribution to the oxidation process of caffeine on the graphite pencil electrode surface.

The slope obtained from the log(Ip) vs log(v) regression analysis was 0.8566, indicating a mixed-controlled electrochemical process involving both diffusion and surface-related adsorption effects. Such behavior is consistent with previously reported electrochemical responses of caffeine on carbon-based electrodes and may also be influenced by the heterogeneous structure and electroactive surface variability of graphite pencil electrodes. The obtained results demonstrate that graphite pencil electrodes combined with Python-assisted electrochemical data analysis represent a suitable low-cost approach for electrochemical characterization of caffeine [5,8–11].

CONCLUSION

The obtained results demonstrate that PGEs can be successfully applied for the electrochemical characterization of caffeine in BR buffer using cyclic voltammetry. The investigated system exhibited predominantly irreversible electrochemical behavior with a clear dependence of anodic peak current and peak potential on scan rate. Regression analysis indicated a significant diffusion contribution together with surface-related effects during the oxidation process of caffeine on the graphite pencil electrode surface.

The developed Python-assisted workflow enabled systematic visualization, regression analysis, and interpretation of cyclic voltammetry data using open-source computational tools. The combination of low-cost graphite pencil electrodes and accessible Python-based data processing represents a promising approach for simple and reproducible electrochemical analysis.

ACKNOWLEDGEMENT

The research presented in this paper was done with the financial support of the Ministry of Science, Technological Development and Innovation of the Republic of Serbia, within the funding of the scientific research work at the University of Belgrade, Technical Faculty in Bor, according to the contract with registration number 451-03-134/2026-03/200131.

REFERENCES

[1] Gonçalves, E.S., Rodrigues, S.V., Silva-Filho E.V. Rev. Ambient. Água 2017, 12(2), 192–202.

[2] Kurissery, S., Kanavillil, N., Verenitch, S., *et al*. Ecol. Indic. 2012, 23, 501–508.

[3] Wu, J., Yue, J., Hu, R., *et al*. Int. J. Civ. Environ. Eng. 2010, 2, 98–102.

[4] Yenealem, D., Michu, F., Pilli, S.R., *et al*. S. Afr. J. Chem. Eng. 2025, 51, 225–231.

[5] Teshome, T., Gure, A., Kitte, S.A., *et al*. Int. J. Electrochem. Sci. 2024, 19, 100698.

[6] Sun, J.Y., Huang, K.J., Wei, S.Y., *et al*. Colloids Surf. B Biointerfaces 2011, 84, 421–426.

[7] Navratil, R., Kotzianova, A., Halouzka, V., *et al*. J. Electroanal. Chem. 2016, 783, 152–160.

[8] Coelho, R.M., Silva, A.R.M., Dias, G.F., *et al*. Chemosensors 2025, 13(3), 84.

[9] David, I.G., Popa, D.E., Buleandra, M. J. Anal. Methods Chem. 2017, 1, 1905968.

[10] Tasić, Ž., Petrović Mihajlović, M., Simonović, A., *et al*. Sensors 2022, 22, 9185.

[11] Tasić, Ž., Petrović Mihajlović, M., Simonović, A., *et al*. Results Phys. 2021, 22, 103911.

[12] Rodríguez, O., Pence, M., Rodríguez-López, J. Anal. Chem. 2023, 95, 4840−4845.

[13] Zheng, W. ECS Advance 2023, 2, 040502.

[14] Vishart, J.L., Castillo-León, J., Svendsen, W. SoftwareX 2021, 15, 100720.

[15] Rodríguez-Valenzuela, F.J., González-Meza, O.A., Gutiérrez, A.G.G., *et al*. ECS Transactions 2022, 106(1), 195–202.

[16] Tadesse, Y., Tadese, A., Saini, R.C., *et al*. Int. J. Electrochem. 2013, 849327.

EcoTER'26
eco.tfbor.bg.ac.rs
32nd International Conference
Ecological Truth & Environmental Research
24–26 June 2026, Hotel Sunce,
Sokobanja, Serbia

Review

FUNDAMENTALS OF WASTE CHARACTERISATION SAMPLING ACCORDING TO CEN/TR 15310

DOI: 10.5937/EcoTER26063S

Milutin Stojadinović [1,2,a*], Vesna Marjanović [1,b], Ivan Svrkota [1,c]

[1] Mining and Metallurgy Institute Bor, Alberta Ajnštajna 1, 19210 Bor, SERBIA

[2] University of Belgrade, Technical Faculty in Bor, Vojske Jugoslavije 12, 19210 Bor, SERBIA

[a] https://orcid.org/0009-0005-7760-216X

[b] https://orcid.org/0000-0001-8005-5244

[c] https://orcid.org/0000-0002-1105-1554

Abstract

Waste characterization is a fundamental prerequisite for making informed decisions regarding waste treatment, recovery, and disposal. Because waste materials are generally heterogeneous and it is impractical to analyse an entire waste population, representative sampling is essential for obtaining reliable analytical results. This paper presents a review of the main principles and requirements for waste sampling based on the CEN/TR 15310 series of technical reports and other relevant literature. Particular attention is given to the process of developing a sampling plan, including the definition of testing objectives, identification of the population to be sampled, assessment of spatial and temporal variability, selection of appropriate sampling approaches, determination of statistical parameters, and specification of practical sampling instructions. Different sampling patterns and considerations related to increment size, sample size, and the use of composite or individual samples are also discussed. The review highlights the importance of understanding waste heterogeneity and applying statistically sound sampling strategies to ensure representative results. Properly designed sampling plans contribute significantly to the reliability of waste characterization data and support compliance with regulatory and technical requirements.

Keywords: CEN/TR 15310:1-5, Variability, Sampling plan, Waste characterisation.

INTRODUCTION

According to the Law on Waste Management of the Republic of Serbia, waste represents "any matter or object that the holder discards, intends or is required to discard". Waste is created as a consequence of various human activities, including industrial production, construction works, agricultural activities and everyday activities of the population [1].

Reliable data on the characterization of the waste is needed to enable a decision to be made on the appropriate way in which it should be treated, recycled or disposed of. However, for practical and economic reasons, it is impossible to analyse the entire series of wastes to be managed. That is why it is necessary to carry out sampling of waste material. A waste sample represents a certain amount of waste separated from a larger mass of waste in a way that

* *milutin.stojadinovic@irmbor.co.rs*

ensures that its properties faithfully represent the characteristics of the entire amount of waste from which it was taken. Therefore, smaller parts, also known as samples, must be collected and brought to the laboratory for further analysis [2–3].

Such materials are generally heterogeneous; therefore, the test program should specify the amount of material for which the characteristics of interest will be determined. There are three main steps in the process of sampling waste materials: preparation of the sampling plan, sampling in the field in accordance with the sampling plan and transport of samples to the laboratory for testing [4–9].

DEFINING THE SAMPLING PLAN

The objective of sampling is to collect representative samples that accurately reflect the composition of the waste. The preparation of a sampling plan includes defining the objectives of the investigation, determining the parameters and scope of testing, gathering information about the waste, establishing safety measures, and selecting the appropriate sampling method and technique [4–9]. The main statistical steps in defining a sampling plan are given in Table 1.

Table 1 *Main statistical steps in defining a sampling plan for a testing programme*

Step	Subject
	Specify the objective of the Testing Programme
1	Specify the objective of the Testing Programme
	Develop the Technical Goals from the objective
2	Define the population to be sampled
3	Assess variability
4	Select the sampling approach
5	Identify the scale
6	Choose the required statistical approach
7	Choose the desired reliability
	Determine the practical instructions
8	Choose the sampling pattern
9	Determine the increment/ sample size
10	Determine the use of composite or individual samples
11	Determine the required number of samples
	Define the Sampling Plan
12	Define the Sampling Plan

Specify the objective of the Testing Programme is a general statement of its overall purpose. The objective must be clearly defined before selecting a sampling strategy, as it is the primary step in determining the type and quality of information to be obtained from sampling. Some examples of test objectives are:

- basic characterisation, which consists of a thorough determination of the behaviour and characteristics of the required material;

- compliance testing, which consists of periodic testing to determine compliance with specific requirements or reference conditions (legal or contractual);

- on-site verification, which consists of a “quick check” method to determine consistency with other tests or other formulated documentation.

In most cases, test objectives are too general to provide detailed instructions for designing a sampling plan, so it is necessary to develop technical objectives from the objective [4–9].

Developing technical goals for the objective translates the general objectives of a testing programme into specific sampling and data analysis requirements. They provide the basis for selecting statistical tools and defining practical sampling instructions, including the material to be sampled, the scope of testing and the required confidence level [4–9].

Defining the population to be sampled - The term "population" is a statistical term used to define the total amount of material from which information is sought through sampling. Defining the population should be one of the first steps in developing a sampling plan.

Overall population and population - It is usually impractical to sample the total population, especially if it is an overall population that represents the entire production of an industrial plant over its entire existence. Therefore, it is common to define the “population” as a convenient subset of the total population – e.g., a month’s ash production may represent the typical production performance of a waste incineration plant. It is important to emphasise that the correct selection of the population depends on the experience and judgment of the interested parties and that this is not a statistical task. It is also important to define the population explicitly in time and/or space. If this is not done, it is impossible to predict that the sampling will be completed in a representative manner.

Sub-population - A problem may arise if it is difficult or impossible to access certain parts of the population during sampling. In such circumstances, it is useful to define a subset of the population – a “sub-population” – which limits the sampling to a more convenient area. A sub-population is therefore a specific part of the population that is intended to be sampled and is considered to sufficiently characterise the population. It is important to understand that the resulting samples may be representative of the defined sub-population. [4–9].

Assessing variability - A key element in the design of a testing program is the requirement to understand the major components of variability in the population to be sampled. In general, variability is a characteristic of waste that cannot be changed without extensive waste manipulation. Variability may be **spatial**, arising from heterogeneity within the material, or **temporal,** resulting from changes in the production over time. Spatial variability may occur within or between layers of a waste body, while temporal variability may be cyclic, driven by known factors, or random (mostly unknown) [4–9].

Selecting the sampling approach - There are two primary approaches to sampling: Probabilistic sampling and judgmental sampling. The use of a probabilistic sampling approach is always recommended where a quantifiable level of reliability is required for the population being tested. The basis of the probabilistic sampling approach is that each element within the population has an equal chance of being selected by the sampling process. This implies that the entire population is available for sampling, even if, for example, there is a large amount of material. In contrast, in the case of the judgmental sampling approach, samples are taken at best on a partially probabilistic basis and at worst on a non-probabilistic basis. The most common reason for choosing this approach is when it is impossible to sample

the entire population for whatever reason. Judgmental sampling can also be used when a specific location or subject is being targeted. Judgmental sampling results in sampling of a sub-population. However, within that sub-population, it may be possible to achieve a probabilistic approach, which is always advised, as at least the results will be representative of that sub-population [4–9].

Identifying the scale - The „scale" is a crucial element that defines a sampling program. It defines the minimum amount (mass or volume) of material below which variations are considered insignificant. For example, if the scale is defined as a barrel of waste, then variations in any characteristic of the waste within the barrel are not of concern. The amount of spatial variability in a population cannot be quantified without defining the scale at which that variability occurs. For example, the variability at the gram level of material in a sub-population is greater than the variation at the kilogram level. Depending on the object of the testing program, the sampling scale may be equal to the size of individual particles (for granular materials), or the size of the sub-population or population. The scale may be defined in terms of time frames - daily, annual, etc [4–9].

Choosing the required statistical parameter - A statistical parameter is any numerical characteristic of a population - a mean or standard deviation, percentile, etc. A key step in planning a testing program is to specify the statistical parameter to be estimated. The choice also affects the type of sampling and the number of samples required. When testing is aimed at basic characterisation, the examination will most likely require measures of variability and extreme behaviour of key constituents. Sometimes a large number of samples is needed to meet these requirements. When the objective is compliance testing, the choice of statistical parameter is usually predetermined by the compliance regulation, as is the size of the scope that the material must meet. Mean values and percentiles are usually used. In the case of on-site verification, the investigation will focus either on measured values in relation to a compliance level that must not be exceeded, or simply "present-absent" measurement of the attribute.

Choosing the desired reliability - The reliability of a testing program is a general term that encompasses three statistical concepts - "bias", "precision" and "confidence interval". The objective of the testing program will influence the degree of confidence that is considered acceptable, but the final selection of confidence criteria is almost always a compromise between expectations and cost.

Given the important decisions that are based on the findings of the basic characterisation test, it is suggested that the confidence should be as high as possible. In contrast, for the "quick check" method of on-site verification, the achieved confidence will in many cases be low. A unique feature of probabilistic sampling is that it allows a range of deviation, also known as a confidence interval, to be placed around the estimate of any parameter. The semi-width of the confidence interval is usually known as the 'precision'. This depends on:

- the desired level of confidence;
- the variability in the population or subpopulation
- the sampling scheme;
- the number of samples chosen;

- the assumed statistical probability distribution in the population; [4–9].

Determining the Practical Instructions - From the objective of the sampling plan, technical objectives are developed that are more detailed. The technical objectives must be translated into practical instructions that are given to the sampler before sampling [4].

Choosing the sampling pattern - The sampling pattern defines where, when and how the required samples are selected from the population. Figure 1 illustrates sampling patterns of probabilistic and judgmental sampling.

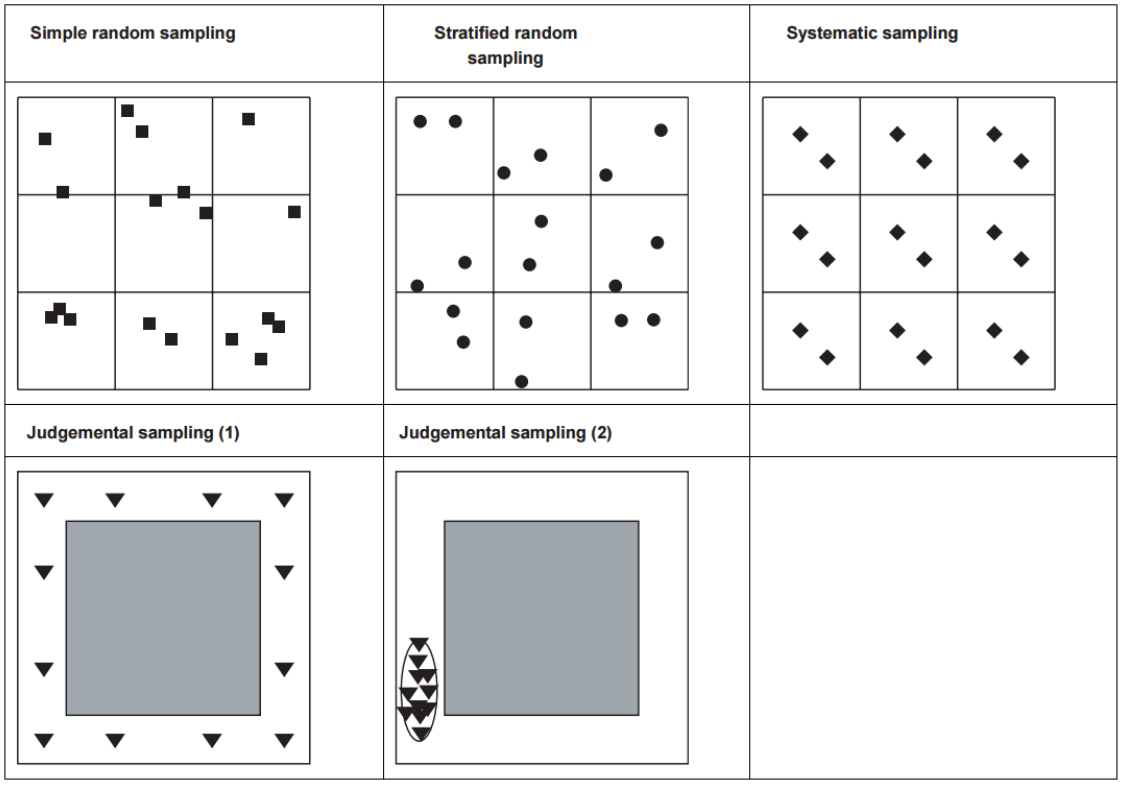

Figure 1 *Sampling patterns of probabilistic and judgmental sampling [4]*

With simple random sampling, every portion of the population has the same (small) chance of being selected as a sample. However, the resulting samples will not necessarily be very evenly spread across the population. In stratified random sampling, a predetermined number of samples are uniformly distributed across a predefined number of parts of the population.

With systematic sampling, samples are distributed evenly throughout the population, starting from a randomly selected starting point (to meet the requirements of probability sampling - that each element of the population has an equal chance of being sampled).

Judgemental sampling encompasses various sampling patterns that generally differ in the extent to which they deviate from a probabilistic sampling approach. Option (1) in Figure 1 represents a type of judgemental sampling that is based on a probabilistic approach, but only for a portion of the population. In contrast, the pattern for option (2) is completely biased. It provides no information about the waste, except in the immediate vicinity of the samples, and nothing can be concluded about the quality of the selected portion of the population [4].

Determination of the increment and sample size - An increment is the amount of material (mass or volume) that is obtained through one single sampling action. It is not analysed as a separate unit, but is combined with other individual samples to form a composite sample.

The degree to which we have to take account of the increment and sample size will very much depend on the type of waste material sampled. The minimum increment size of an individual sample is governed by the need for the sampling device to accommodate all particle sizes. In contrast, there is no practical need for a minimum size when sampling liquids, as the particle size is at the molecular level [4].

The minimum increment and sample size are not relevant for creating a sampling plan for **liquid materials**, as the potential differences are at the molecular level compared to the sample size. When forming composite samples, the sample size will be determined by the number of individual samples and their size, which in turn depends on the dimensions of the sampling equipment [4]. **Powdery materials and sludges** have small particle sizes, while sludges also have a certain amount of liquid. Provided that the sampling equipment allows the entry of all particles contained in the material, then there are no additional requirements for the minimum size of individual samples. Similarly, considering the small particle size in this type of material, differences between individual particles will not have a major effect on the characteristics of the sample, because in practice, the sample consists of a very large number of particles, and there are no additional requirements for the minimum size of individual samples. With this in mind, the sample size will be determined by the amount of material the laboratory requires to perform the test, while the dimensions of the sampling equipment will determine the size of the individual samples. As with liquids, when forming composite samples, the sample size will be determined by the number of individual samples and their size [4].

When sampling particulate or granular material, the minimum size of the individual sample must be taken into account. The size of the sampling equipment opening must be large enough to allow entry of all particles present in the material. In practice, the opening of the sampling equipment must be at least three times the diameter of the largest particle. For practical reasons, the diameter of the largest particles can be substituted by the size of the (estimated) 95-percentile of the particle size distribution.

The actual size of the samples and individual samples depends not only on the minimum size of the samples and individual samples, but also on:

- The amount of material required by the laboratory to perform the analysis;
- The number of increments in the composite sample (when increments are taken);
- the relation between the mass of the minimum increment size and the minimum sample size (in relation to the number of increments in a composite sample) [4].

The use of composite versus individual samples - The objective of the testing program, and in particular the choice of statistical parameter, dictates the choice between composite and individual samples, i.e. which type of sample will generate more relevant data.

Note that there is a difference in meaning between an increment sample that forms a composite sample and the sample that is obtained from a single sampling operation.

When an approximate indication of the quality of the material is sufficient to meet the objective of the test, as in e.g. on-site verification, where one or at most a few samples would suffice, then the cost of analysis and sampling is low. Conversely, a significant number of individual samples need to be taken if a reliable estimate of the mean quality value for one or more composite samples is required. Such an approach may be acceptable for compliance testing (where compliance is relative to the mean concentration). In this case, the cost of sampling may be high, but the cost of analysis would be low. When a significant number of samples are taken to give a realistic estimate of the quality of the material and to provide information on the degree of heterogeneity of the material, as in the case of basic characterisation, the cost of both sampling and analysis will be high. [4–9]

Defining the Sampling Plan - The previous chapters of this paper were intended to contribute to the definition of a sampling plan. The various choices and decisions made are brought together in a single document that is called a sampling plan and represents the initial step in the sampling process in a broader sense.

CONCLUSION

Representative sampling is essential for obtaining reliable waste characterisation data. Due to the inherent heterogeneity of waste materials, the preparation of a well-defined sampling plan is necessary to ensure sample representativeness and reduce uncertainty. The CEN/TR 15310 series provides a systematic framework for defining sampling objectives, assessing variability and selecting appropriate sampling strategies. Proper implementation of these principles improves the quality of analytical results and supports regulatory compliance and informed waste management decisions.

ACKNOWLEDGEMENT

The authors are grateful to the Ministry of Science, Technological Development and Innovation of the Republic of Serbia, Agreement on the implementation and financing of scientific research work of the National Research Institute in 2026, No. 451-03-33/2026-03/ 200052

REFERENCES

[1] Law on Waste Management, "Official Gazette of the Republic of Serbia", no. 109/2025, Article 5, Item 28.

[2] SRPS EN 14899: Characterization of waste - Framework for the preparation and implementation of a sampling plan. Institute for Standardization of Serbia, Belgrade.

[3] Pierre Hennebert, Giovanni Beggio. Sampling and sub-sampling of granular waste: size of a representative sample in terms of number of particles. Detritus, 2021, 17, pp.30–41. ⟨10.31025/2611-4135/2021.15139⟩. ⟨ineris-04034933⟩

[4] CEN/TR 15310-1: 2006, Characterization of waste - Sampling of waste materials - Part 1: Guidance on selection and application of criteria for sampling under various conditions.

[5] CEN/TR 15310-2: 2006, Characterization of waste - Sampling of waste materials - Part 2: Guidance on sampling techniques.

[6] CEN/TR 15310-3: 2006, Characterization of waste - Sampling of waste materials - Part 3: Guidance on procedures for sub-sampling in the field.

[7] CEN/TR 15310-4: 2006, Characterization of waste - Sampling of waste materials - Part 4: Guidance on procedures for sample packaging, storage, preservation, transport and delivery.

[8] CEN/TR 15310-5: 2006, Characterization of waste - Sampling of waste materials - Part 5: Guidance on the process of defining the sampling plan.

[9] RCRA Waste Sampling - Draft Technical Guidance - Planning, Implementation, and Assessment, August 2002.

EcoTER'26
eco.tfbor.bg.ac.rs
32nd International Conference
Ecological Truth & Environmental Research
24–26 June 2026, Hotel Sunce,
Sokobanja, Serbia

Original Research

ENVIRONMENTAL VARIABLES AFFECT DISTRIBUTIONAL PATTERNS OF THE RIFFLE BEETLE (Coleoptera: Elmidae) SPECIES IN THE SERBIAN STREAMS AND RIVERS

DOI: 10.5937/EcoTER26071N

Boris Novaković[1,a*], Nikola Paskaš[1], Zoran Stojanović[1], Vidak Lakušić[2,b], Ivana Živić[2,c]

[1] Serbian Environmental Protection Agency, Ministry of Environmental Protection of the Republic of Serbia, Žabljačka 10A, 11160 Belgrade, SERBIA

[2] University of Belgrade, Faculty of Biology, Studentski trg 16, 11000 Belgrade, SERBIA

[a] https://orcid.org/0000-0003-4846-6371

[b] https://orcid.org/0000-0002-0768-0382

[c] https://orcid.org/0000-0002-4397-9904

Abstract

This study examined the impact of environmental variables on distributional patterns of 12 riffle beetle species (Coleoptera: Elmidae) in the Serbian streams and rivers. During six–year period (2019–2024), a total of 68 waterbodies of the Serbian streams and rivers from that riffle beetles were included (of total 226 running waterbodies covered by water status monitoring). During Regular National Annual Water Monitoring Programmes of the SEPA (Serbian Environmental Protection Agency), riffle beetle sampling was carried out simultaneously with aquatic macroinvertebrate samples in line with the AQEM protocol (multi-habitat sampling). Among all environmental variables analyzed, a total of 16 variables most important for aquatic macroinvertebrate community in general, and species' stream/river longitudinal distribution, were selected. Canonical Correspondence Analysis (CCA) revealed that the most significant parameters for each riffle beetle species depending on the species-specific ecological preference, and on the other hand, with regard to aquatic beetle species longitudinal distribution, the species' distributional patterns only corresponded with the RCC (River Continuum Concept) principle in larger Serbian rivers. It is concluded that limited riffle beetle species distribution in small and medium submountain and mountain streams/rivers is primarily affected by local water quality conditions and species-specific microhabitat preference rather the principle proposed by the RCC.

Keywords: riffle beetle, abiotic factors, distributional pattern, streams, rivers, Serbia.

INTRODUCTION

The longitudinal distribution of aquatic beetles in streams and rivers is mainly affected by environmental gradients that change from upstream to downstream. Principally, important variables include water temperature, flow velocity, dissolved oxygen, substrate type, vegetation cover, nutrient levels, and stream size. Upstream sections are typically cold, fast-flowing, and oxygen-rich, supporting specialized rheophilic species, while downstream

* *boris.novakovic@sepa.gov.rs*

reaches are warmer, slower, and richer in fine sediments and vegetation, favoring lentic-associated beetles. Human impacts such as pollution, dams, and land-use change can also modify these natural distribution patterns.

The River Continuum Concept (RCC) was first introduced by [1]. The concept asserts that the biological community in a stream system is largely regulated by geomorphological factors, and it was unique in that it proposed that streams were continua of both geomorphologic and biological factors: a new idea in ecosystemology at that time. The concept divides a river system into three major groups based on stream position order and comprising headwater streams, medium-sized streams, and large rivers. The transport, use, and storage of organic matter along the continuum take place in a symbiotic relationship with the distribution of macroconsumer groups. Also, this concept asserts that the macroinvertebrate community will exist in a fashion that optimally exploits its nutritive source of organic matter [2]. The present study also analyze did the riffle beetle species' distributional patterns correlated with the River Continuum Concept (RCC) principle.

Riffle beetles (order Coleoptera, family Elmidae), both larvae and adults, do not come to the surface to breathe. Instead, they rely on a specialized physical gill called a plastron – a dense, water–repellent layer of fine hairs that traps a thin film of air against their bodies. The longitudinal distribution of riffle beetles is strongly influenced by changes in water chemistry along the river continuum. Upstream reaches usually have cold, well–oxygenated water, low conductivity, low nutrient concentrations, and neutral to slightly acidic pH, which favor sensitive riffle beetle species adapted to fast-flowing habitats. Midstream sections often contain moderate nutrient and organic matter levels that can support higher species diversity. Downstream reaches generally show warmer water, higher conductivity, increased nutrients, and lower dissolved oxygen, conditions that reduce the abundance of many riffle beetles because most species require clean, oxygen-rich water. Plastron, permanent air film functions as a physical gill, allowing oxygen to diffuse from the surrounding water into the plastron while carbon dioxide diffuses out. Because of this mechanism, riffle beetles can remain submerged for long periods without surfacing. Also, riffle beetles provide excellent indicators of water quality and perhaps also climate change [3].

The main goal of this study is to provide the data on significance of different environmental variables in a six-year period (2019–2024) to riffle beetle species' distribution in the Serbian streams and rivers.

MATERIALS AND METHODS

Riffle beetle samples were taken using a hand net (25x25 cm, 500 µm mesh size) or specimens were manually collected using a tweezer. The samples were collected in the period 2019–2024 (six years, July–November). The majority of aquatic beetle specimens were collected with other aquatic macroinvertebrate samples during the Regular Annual Water Monitoring programmes conducted by the Serbian Environmental Protection Agency (SEPA). The multi-habitat sampling procedure [4] and AQEM protocol [5] were applied. The samples were preserved using 70–90% ethyl-alcohol. Containers were labelled with all necessary information, and transported to the laboratory for sorting, counting, and identification. For

identification, the stereomicroscope Carl Zeiss StereoDiscovery V.8 with Axio Cam ICc5 and ZEN2 imaging software and appropriate taxonomic aquatic beetle keys were used.

A total of 12 riffle beetle species, sampled in the Serbian streams and rivers in a six-year period (2019–2024) period at 68 watercourses (of total 226 running waterbodies covered by water status monitoring), were studied with regard to the selected environmental variables: *Elmis cf. aenea, Elmis cf. maugetii, Elmis cf. rioloides, Limnius volckmari, Limnius opacus, Limnius intermedius, Oulimnius tuberculatus, Riolus cupreus, Macronychus quadrituberculatus, Potamophilus acuminatus, Esolus angustatus* and *Esolus parallelepipedus.* Among all riffle beetle species recorded, some are common (e.g. *Elmis cf. maugetii, Limnius opacus*), but some, such as *Macronychus quadrituberculatus* and *Potamophilus acuminatus*, are scarcely found in Serbia. Regarding species' abundance per sampling site, a total abundance of beetle specimens is included. Due to well-known larval identification problem for this family, only imago specimens were considered, except three species for which larval stages were identified: *Riolus cupreus, Macronychus quadrituberculatus* and *Potamophilus acuminatus.*

Among all environmental variables measured, a total of 16 variables most important for aquatic macroinvertebrate assemblages in general, and species' distribution along stream/river, were selected, based on general ecological requirements of aquatic macroinvertebrate community – Physico–chemical parameters: pH, water temperature, water conductivity, dissolved oxygen (DO), oxygen saturation (%), ortophosphate (PO_4^{3-}), total phosphorus (TP), ammonium (NH_4^+), nitrates (NO_3^-), total nitrogen (TN), total organic carbon (TOC); Abiotic parameters: air temperature, water flow, sampling site elevation, canopy and riparian vegetation coverage. Water chemistry parameters were analyzed according to standardized analytical methods proposed for each parameter measured for the purposes of Regular Annual Monitoring Programmes conducted by the Serbian Environmental Protection Agency (SEPA), and the mean annual values of each parameter were included with regard to significance to riffle beetle species distribution. Also some additional parameters, not measured in regular water monitoring programmes, and found to be as important for benthic invertebrate fauna, were measured in the field, such as: sampling site elevation, water flow (preliminary rapid field estimation), and canopy and riparian vegetation coverage at sampling site (visual observation).

To get more precise data on effect of measured environmental variables to riffle beetle assemblages as well as species' distribution in the investigated Serbian streams and rivers (2019–2024 period), as well as correlations referred to composition of populations and environmental variables, Canonical Correspondence Analysis (CCA) was used [6–8]. Length of the vector represents its significance in the mean gradient. The analysis of the relationship between the structure of populations of elmid species and environmental variables was carried out on the same selected set of samples within all 226 sampling stations (2019–2024 period). The selection of the most significant influencing factors was conducted out using the previous (*forward*) selection, using the Pearson correlation test within the CCA framework analysis. Applying prior selection, based on Pearson's correlation test ($p \leq 0.05$), the gradient impact of environmental variables on each riffle beetle species populations was determined, and the most indicative parameters for riffle beetles were selected. Monte Carlo permutation test

(1000 permutations, $p \leq 0.05$) was used for confirming a statistical significance of the sum of all eigenvalues of individual factors. Canonical Correspondence Analysis (CCA) was performed in the statistical software Flora [8].

RESULTS AND DISCUSSION

Based on the Canonical Correspondence Analysis (Figure 1), by observing the relationship between parameters and riffle beetle species in the middle gradients, it was determined that there is a separation by the studied riffle beetle species, and also by the measured environmental variables. By using Monte Carlo permutation test (1000 permutations), a statistical significance of the sum of all individual eigenvalues was proven ($p \leq 0.05$).

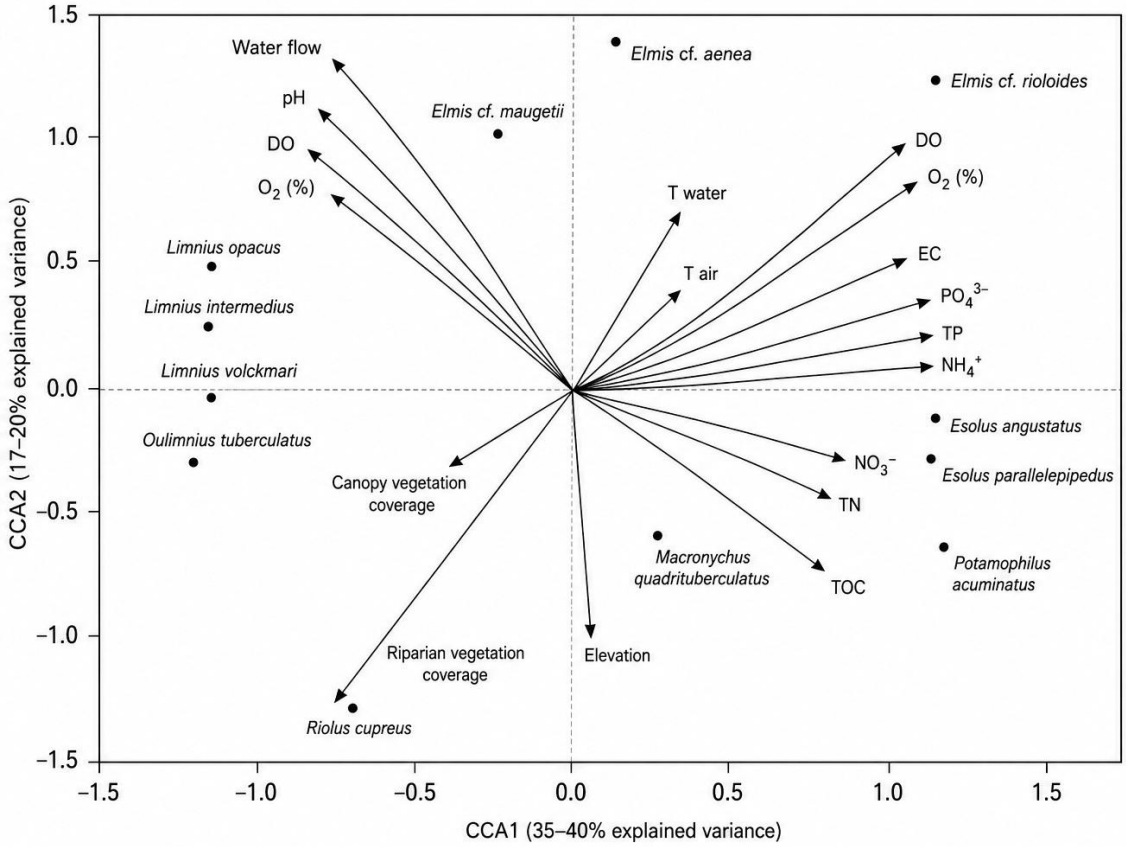

Figure 1 *Canonical Correspondence Analysis (CCA) – Riffle beetle species and environmental variables*

Canonical Correspondence Analysis (CCA) explained the relationship between species distribution and environmental variables across the studied stream/rivers in Serbia. The first axis, CCA1 (35–40% explained variance), mainly represents a gradient from clean, fast-flowing, oxygen-rich habitats on the negative side to warmer, nutrient-enriched, and more disturbed habitats on the positive side. The second axis, CCA2 (17–20% explained variance), reflects variation associated with temperature, elevation, and vegetation coverage. Species positioned close to environmental vectors are positively associated with those variables, while species located opposite to the vectors are negatively associated.

Species such as *Limnius opacus*, *Limnius intermedius*, *Limnius volckmari*, and *Oulimnius tuberculatus* are distributed on the negative side of CCA1, indicating strong associations with high water flow, elevated dissolved oxygen (DO), higher oxygen saturation (%), and relatively high pH. These species are therefore characteristic of clean, well-oxygenated, and fast–flowing stream environments with low nutrient concentrations. Among them, *Limnius opacus* and *Limnius intermedius* appear particularly sensitive to pollution and nutrient enrichment, making them good indicators of healthy stream ecosystems. *Limnius volckmari* occupies a more central position, suggesting moderate ecological tolerance, whereas *Oulimnius tuberculatus* is additionally associated with canopy and riparian vegetation, indicating the species' preference for shaded habitats.

Riolus cupreus is strongly associated with riparian vegetation coverage, canopy vegetation, and higher elevation, while being negatively related to nutrient variables. Its CCA position in suggests that this species prefers cold, forested, minimally disturbed submountain and mountain streams with dense vegetation cover and low anthropogenic influence.

Elmis cf. maugetii and *Elmis cf. aenea* CCA positions indicated relationship with oxygen-rich and flowing water conditions. *Elmis cf. maugetii* is closely associated with water flow and high oxygen availability, reflecting preference for relatively clean running waters. *Elmis cf. aenea* shows a stronger association with the upper part of CCA2, suggesting tolerance for slightly warmer waters while still requiring good oxygen conditions.

Elmis cf. rioloides is positioned on the positive side of both axes and is positively associated with dissolved oxygen, oxygen saturation, conductivity (EC), and ortophosphate (PO_4^{3-}). This indicates that the species can tolerate moderate nutrient enrichment while still favoring oxygenated habitats. Its ecological position suggests adaptability to intermediate environmental conditions.

Species located on the positive side of CCA1, including *Esolus angustatus*, *Esolus parallelepipedus*, *Macronychus quadrituberculatus* and *Potamophilus acuminatus* are associated with higher nutrient concentrations, warmer temperatures, increased conductivity, and increased organic matter. *Esolus angustatus* and *Esolus parallelepipedus* are closely related to nitrate (NO_3^-), ammonium (NH_4^+), and electrical conductivity (EC), indicating tolerance to nutrient-enriched and potentially disturbed habitats. *Macronychus quadrituberculatus* is associated with total organic carbon (TOC) and total nitrogen (TN), suggesting preference for organic-rich stream environments. *Potamophilus acuminatus*, positioned furthest toward the enriched conditions, is strongly associated with TOC, TN, nitrate (NO_3^-), and higher water temperatures, indicating the highest tolerance to organic pollution and eutrophication among the recorded taxa.

Overall, the CCA showed a distinct ecological separation between sensitive riffle beetle species inhabiting clean, oxygen-rich, forested streams, and on the other hand, low-tolerant riffle beetle species adapted to nutrient-enriched, warmer, and more disturbed aquatic environments.

CONCLUSION

Riffle beetles are strongly associated with clean, fast-flowing freshwater habitats, and species distribution is mainly affected by environmental conditions related to water chemistry and habitat structure. Dissolved oxygen is one of the most important factors for riffle beetles in general, due to both larvae and adults depend on highly oxygenated water for respiration. Current velocity also plays a major role, as riffle beetles are specially adapted to live in riffles and flowing sections of streams and rivers. The efficiency of the plastron depends on high dissolved oxygen concentrations in the water. In polluted rivers, especially where organic pollution and eutrophication occur, dissolved oxygen levels decrease due to increased microbial decomposition and nutrient enrichment. Fine sediments and contaminants can also interfere with the plastron surface and reduce gas exchange efficiency. Therefore, many riffle beetle species are highly sensitive to pollution and are usually absent from degraded or oxygen–poor habitats, which is corroborated by the data obtained from the present study.

Water temperature influences species composition, with most riffle beetles preferring cool and stable thermal conditions commonly found in upstream and midstream stretches of stream/rivers. Substrate type is another key variable, since coarse materials such as gravel, cobbles, and stones provide surfaces for attachment, feeding, and shelter, but not considered in our study due to complexity. Measured water chemistry variable values, including low conductivity, low nutrient concentrations, and neutral to slightly acidic pH, are generally associated with higher riffle beetle diversity and abundance.

Organic pollution, eutrophication, and excessive sedimentation are negatively affect riffle beetle communities by reducing oxygen availability and covering coarse substrates with fine sediments.

The distribution of riffle beetle species in running waters of Serbia could not be explained by the River Continuum Concept (RCC), except in case of larger rivers. According to the RCC, upstream and midstream river stretches are characterized by low temperatures, fast currents, coarse substrates, and high dissolved oxygen concentrations. These conditions favor riffle beetles because their plastron respiration requires oxygen–rich flowing water. In these sections, riffle beetles can attach to stones and gravel and efficiently exchange gases through the plastron.

This River Continuum Concept (RCC) principle stated that physical and chemical conditions change gradually from upstream to downstream, leading to predictable changes in aquatic macroinvertebrate assemblages. In larger rivers downstream stretches are characterized by warmer water, slower, and richer in fine sediments and organic matter, while dissolved oxygen often decreases. Based on our results, longitudinal distribution of riffle beetles follows the environmental gradients predicted by the RCC only in case of larger Serbian rivers where riffle beetle species are distributed, but not supported the RCC priniciple for small and medium submountain and mountain streams/rivers, where local water microhabitat conditions and species-specific microhabitat preference shaped riffle beetle species distributional patterns.

REFERENCES

[1] Vannote, R.L., Minshall, G.W., Cummins, K.W., *et al*. Can. J. Fish. Aquat. Sci. 1980, 37 (1), 130–137.

[2] Carpenter, D.A. Testing the river continuum concept: Exploring ecological processes in the Wheeling Creek watershed. Graduate Theses, Dissertations, and Problem Reports. West Virginia University 2001; p. 82.

[3] Elliott, J. M. Freshw. Rev. 2008, 1(2), 189–203.

[4] Hering, D., Verdonschot, P.F.M., Moog O., *et al.* Hydrobiologia 2004, 516, 1–20.

[5] AQEM Consortium Manual for the application of the AQEM system, Version 1.0. 2002; p. 202.

[6] Ter Braak, C. Ecology 1986, 67, 1167–1179.

[7] Ter Braak, C., Verdonschot, P. Aquat. Sci. 1995, 57, 255–289.

[8] Karadžić, B. Water Res. Manag. 2013, 3 (1), 45–54.

Original Research

RIFFLE BEETLE *Elmis maugetii* Latreille, 1802 (COLEOPTERA: ELMIDAE): NOTES ON THE SPECIES' MORPHOLOGICAL PLASTICITY IN THE BALKAN PENINSULA

DOI: 10.5937/EcoTER26078N

Boris Novaković[1,a*], Jelena Đuknić[2,b], Nikola Paskaš[1], Marko Raković[3,c], Vidak Lakušić[4,d], Ivana Živić[4,e]

[1] Department of National Laboratory, Serbian Environmental Protection Agency, Ministry of Environmental Protection of the Republic of Serbia, Žabljačka 10A, 11160 Belgrade, SERBIA

[2] Department for Hydroecology and Water Protection, Institute for Biological Research "Siniša Stanković", National Institute of the Republic of Serbia, University of Belgrade, Despota Stefana Blvd. 142, 11060 Belgrade, SERBIA

[3] Department of Biodiversity and Environmental Research, University of Belgrade-Institute for Multidisciplinary Research, Despota Stefana Blvd. 142, 11060 Belgrade, SERBIA

[4] Department of Invertebrate Zoology and Entomology, University of Belgrade, Faculty of Biology, Studentski trg 16, 11000 Belgrade, SERBIA

[a] https://orcid.org/0000-0003-4846-6371 [b] https://orcid.org/0000-0003-3635-5463

[c] https://orcid.org/0000-0002-3658-3362 [d] https://orcid.org/0000-0002-0768-0382

[e] https://orcid.org/0000-0002-4397-9904

Abstract

The study present data on morphological plasticity of the riffle beetle species, Elmis maugetii (Coleoptera: Elmidae) in the Balkan Peninsula. In general, morphological plasticity of the riffle beetles explains that identification of imagoes is difficult due to many species expressed high morphological variability influenced by environmental conditions. For the purposes of this study, riffle beetle samples were sampled in 2014-2017 period from four Balkans' countries: Serbia, Bosnia and Herzegovina, North Macedonia and Greece. Species morphological variability are related to body shape, pronotum structure, abdomen length/width and size, and it can vary considerably among beetle populations. Determining morphological plasticity, shaped by genetically-based species characters as well as ability of organism to alter its physical structure in response to environmental conditions, is inherently complex. Such complexity stems from distinguishing species' ecological responses from genetic variation in the light of spatio-temporal and environmental context. The present study specifically discussed ecophenotypic and morphometric plasticity of Elmis maugetii among investigated localities (different population ecophenotypes) assumpting that water discharge, water temperature, dissolved oxygen concentration in water, HYMO (hydromorphological) characteristics, are strongly associated with the riffle beetle species morphological plasticity.

Keywords: aquatic beetle, ecophenotype, morphological plasticity, abiotic factors, the Balkans.

* *boris.novakovic@sepa.gov.rs*

INTRODUCTION

Morphological plasticity in aquatic beetles arises through complex interactions among ontogenetic processes, genetic and ecological factors. Altogether, these factors shape variation in body size, coloration, appendage structure, respiration-related adaptations, dispersal ability, and reproductive traits among aquatic beetle populations. Though each factor might be minor on its own, their cumulative effects often could result in a considerably higher, disproportionate impact on organisms. Aquatic beetles are excellent model organisms for studying ecophenotypic variability due to species occurred in diverse freshwater habitats and respond strongly to environmental gradients.

Among aquatic macroinvertebrates, morphological plasticity is known from caddisfly study from lakes and streams. Caddisflies like *Limnephilus externus* display remarkable phenotypic plasticity when inhabiting both lakes (lentic) and streams (lotic) [1].

Morphological plasticity in Ephemeroptera (mayflies) refers to the remarkable ability of their aquatic nymphs to alter physical traits-such as gill size, ionocyte cell counts, and body size at metamorphosis-in response to environmental stressors like poor water quality, predation pressure, and temperature fluctuations, such as *Baetis rhodani* species [2]. Also, a single study regarding stress and response: a systematic review of epigenetic pathways underlying gene expression and phenotypic plasticity in aquatic invertebrates is recently published [3].

Evidence of phenotypic plasticity along an altitudinal gradient is know from a single study the dung beetle *Onthophagus proteus* [4], but there are no studies related to morphological plasticity of aquatic beetles in general. Morphological plasticity of aquatic beetles is poorly known in general. A single, related study of influence on hydraulic pressure on morphometric variability of same species from the present study (*Elmis maugetii)* is known [5].

The main objective of the study is to predict factors affect morphological plasticity of the riffle beetle species *(Elmis maugetii)* in the Balkans as well as to estimate which factors predominantly triggered this species morphological plasticity.

MATERIALS AND METHODS

Riffle beetle specimens of *Elmis maugetii* (only imagoes, not larval individuals) were collected using Surber net (300 cm^2, 250 μm mesh size) and hand net (25x25 cm, 500 μm mesh size), and manually by tweezer. Samples were preserved using 70% ethanol solution, and further analysed in the laboratory with selecting characteristic riffle beetle specimens for the purposes of this study. Riffle beetle samples were taken in the 2014–2017 period covering four Balkans' countries: Serbia, Bosnia and Herzegovina, North Macedonia and Greece. Identification of the organisms was performed on Leica MS5 and Carl Zeiss SteREO Discovery.V8 stereomicroscopes by using appropriate taxonomic keys.

RESULTS AND DISCUSSION

The riffle beetle *Elmis maugetii* showed morphological plasticity mainly in response to abiotic conditions associated with running-water habitats. As a rheophilic representative of the elmids, we assumed its morphology is strongly influenced by hydrodynamics, water flow-driven factors, oxygen availability, temperature, riverbed substrate size and composition, and the amount of available food (resource). Our prediction is the most important abiotic factor for riffle beetle morphological variability is current discharge, which is corroborated by the data from previous study of same riffle beetle species [5]. According to this study, a larger riffle beetle specimens were found in streams characterized by higher flow velocity, and on other hand, water level and sampling depth is not significant in terms of the species' body size. Populations inhabiting fast-flowing streams and torrents often develop more flattened and streamlined body forms, stronger claws, and more compact appendages that improve resistance against hydraulic stress and help maintain attachment to stones or submerged wood. In slower running waters, specimens may appear slightly broader or less dorsoventrally flattened (one of possible "scenarios" is the existence of different species' ecophenotypes as adaptive forms, provided in Figure 1).

Elmis maugetii ecophenotypical variability is primarily related to body shape, pronotum structure, pronotum/abdomen length/width and size, and it could vary considerably among different populations.

Morphological plasticity in riffle beetles is strongly linked to current flow velocity because these insects live in fast-flowing stream habitats where hydrodynamic stress shapes survival, attachment, respiration, and feeding behavior. Also, water temperature is important factor for morphological plasticity. In cold, highly oxygenated mountain streams, cuticular microstructures and body surface features associated with gas exchange may differ from those in warmer or less oxygen-rich waters. Temperature itself can influence body size and developmental timing; cooler habitats often produce slower development and sometimes larger, more heavily sclerotized adults, whereas warmer streams may favor smaller body size and faster life cycles. Dissolved oxygen concentration in water and HYMO (hydromorphological) characteristics, are important in terms of aquatic beetle morphological plasticity. Oxygen concentration is important factor because elmids rely heavily on plastron respiration. We assumed that food amount and its availability (resource) could also affect the species' morphological variability.

In the light of evolutionary processes, morphological plasticity of riffle beetles is also closely related to reproductive isolation in geographically fragmented freshwater habitats such as canyons, gorges, and isolated mountain streams. Because riffle beetles are highly dependent on fast-flowing, oxygen-rich lotic environments and generally possess limited dispersal ability, populations separated by deep valleys, waterfalls, gorges, or canyon systems may experience reduced gene flow over time. In terms of the species' dispersal ability, it is important that two riffle beetle *Elmis maugetii* species forms exist, brachypterous (non-flying) and macropterous (ability to fly), and potentially, could be occurred in a same population. Differences in current discharge, substrate composition, water chemistry, and microhabitat structure among isolated stream systems can drive local morphological adaptations, including variation in body shape, attachment structures, and size. As these populations remain isolated,

ecological specialization and hydrodynamic adaptation may gradually contribute to genetic divergence and reproductive isolation through allopatric speciation. In canyon and gorge systems, physical barriers and habitat discontinuity can prevent interbreeding between populations, allowing independent evolutionary trajectories shaped by local hydraulic conditions. Consequently, morphological plasticity associated with flow velocity may not only reflect short-term ecological responses but may also play an important role in long-term diversification and speciation processes in riffle beetles, particularly for species inhabiting fragmented freshwater habitats.

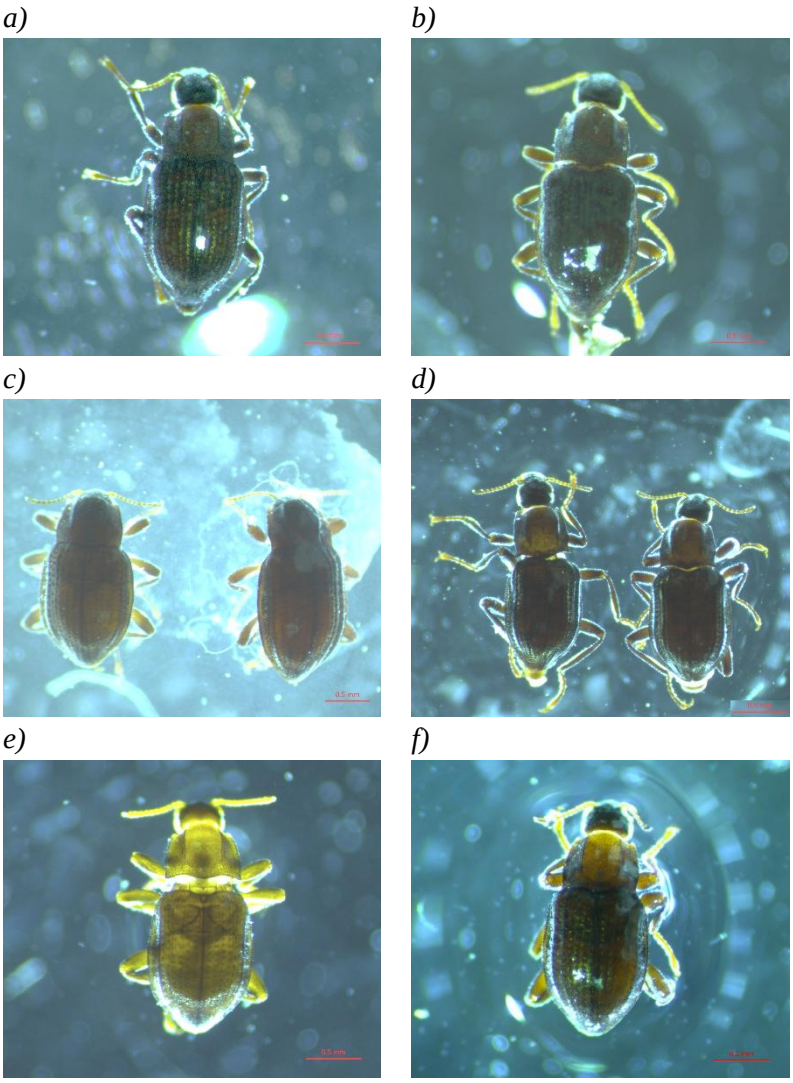

Figure 1 *Different ecophenotypes of the riffle beetle Elmis maugetii Latreille, 1802 from the Balkan Peninsula, localities of findings: a) Boturići-Rasina (central Serbia); b) Niš-Kutinska Reka (SE Serbia); c) Krepoljinska Reka (E Serbia); d) Čapljina/Buna River (Bosnia and Herzegovina); e) Pčinja River upstream the Kumanovo (North Macedonia); f) Ano Kefalari/Zygaktes (Greece)*

CONCLUSION

Hydraulic stress strongly influenced riffle beetle *(Elmis maugetii)* body shape, flattening, claw development, and attachment structures needed for survival in fast-flowing streams.

Specimens from torrential habitats are usually more streamlined and dorsoventrally flattened than those from slower running waters reducing drag and help them remain attached to stones and submerged wood improving adhesion in turbulent water.

Besides hydrodynamic conditions, morphological plasticity of the riffle beetle *(Elmis maugetii)* is closely associated with water temperature, and consequently, dissolved oxygen concentration in water (due to its plastron respiration), and HYMO (hydromorphological) characteristics, primarily riverbed substrate type and composition, and food amount (resource) and its availability.

Overall, genetic variation, phylogeographic patterns, phenotypic plasticity, and inter- and intrapopulation variability in riffle beetle describe how geography and environmental conditions influence the genetic and physical differences of these aquatic insects. Phylogeography examines how populations from different streams or regions are genetically related and how historical isolation or dispersal shaped their distribution. Ecophenotypes (visually distinguishable types exclusively linked to phenotypic plasticity) refer to variations in morphology affected by environmental factors such as water flow, water temperature, dissolved oxygen concentration in water, HYMO (hydromorphological) characteristics of stream/river, and not associated with the species' genetic variability.

Our assumptions are there are two major riffle *Elmis maugetii* ecophenotypes: rheophilic (slim and long occurred in fast current) and rheophobic (wide and round-shaped occurred in slower current), with many "intermediate" ecophenotypes varied depend on triggering morphological plasticity factors, predominantly water discharge and its intensity (an ecophenotype is a form or an organism that developed due to environmental influences rather than genetic differences). In fact, ecophenoptype is regarded as some kind of adaptive form to local water conditions, i.e. species adaptation.

Also, the present study pointed out that phenotypic plasticity complicates riffle beetle classical taxonomy problems underlining the need for combining morphological (with identification based on species *aedeagus* characteristics) and molecular (DNA-compliant) approach such as DNA barcoding for precise species identification. Determining morphological plasticity, shaped by genetically-based species characters as well as ability of organism to alter its physical structure in response to environmental conditions, is inherently complex. Such complexity stems from distinguishing species' ecological responses from genetic variation in the light of spatio-temporal and environmental context.

REFERENCES

[1] Parisek, C.A., Marchetti, M.P., Cover, M.R. Fresh. Sci. 2023, 42 (2), 161–175.

[2] McKenzie, M., Scott, J., Wood, P.J., *et al*. Ecol. Entomol. 2024, 49 (4), 500–507.

[3] Johnson, E., Wong, J. Front. Mar. Sci. 2026, 13. 10.3389/fmars.2026.1767697.

[4] Stanbrook, R.A., Harris, W.E., Wheater, C.P., *et al.* PeerJ 2021, 9, e10798.

[5] Novaković, B. Tehnika 2020, 75, 105–109.

Abstract

CHALLENGES, LIMITATIONS AND KNOWLEDGE GAPS CONCERNING ALLOCHTHONOUS TREES IN URBAN ENVIRONMENTS: WINGED ELM

DOI: 10.5937/EcoTER26083K

Radenka Kolarov[1,a], Djurdja Petrov[2,b*], Nevenka Galečić[2,c], Dejan Skočajić[2,d], Jelena Čukanović[1,e], Sara Đorđević[1,f], Mirjana Ocokoljić[2,g]

[1] University of Novi Sad, Faculty of Agriculture, Trg Dositeja 8, 21000 Novi Sad, SERBIA

[2] University of Belgrade, Faculty of Forestry, Kneza Višeslava 1, 11030 Belgrade, SERBIA

[a] https://orcid.org/0000-0003-1976-7618 [b] https://orcid.org/0000-0001-5207-2741

[c] https://orcid.org/0000-0003-2771-4583 [d] https://orcid.org/0000-0002-2679-3278

[e] https://orcid.org/0000-0003-3327-5484 [f] https://orcid.org/0000-0002-4096-8433

[g] https://orcid.org/0000-0002-9171-2833

Abstract

Variable ecosystem conditions and diverse socio-economic developments over the centuries have contributed to the uncontrolled transatlantic introduction of allochthonous trees, leading to their presence in cultivated European landscapes. For this reason, a systematic reconnaissance approach was applied in the municipality of Novi Beograd during 2024, when the species Ulmus alata Michx. was identified. According to the authors' knowledge, this is the only recorded finding of the species in Serbia; consequently, local space users were interviewed. Considering the need for holistic perspectives in sustainable urban development, as well as the integration of urban, suburban and rural spatial concepts at both local and regional levels, all phenological changes of Winged elm were recorded during 2025. An evaluation of phenological events and a morphometric analysis of leaves were carried out. A mass occurrence of leaf aphid galls was documented, together with the absence of flowering and fruiting phenophases. The results indicate that, alongside formal, technical and conceptual requirements, it is essential to take into account the potential benefits and risks arising from ecological challenges.

Keywords: Ulmus alata *Michx.*, assisted migration, database, Eriosoma ulmi, landscape-suitable elms.

ACKNOWLEDGEMENT

The authors are grateful to the Ministry of Science, Technological Development and Innovation of the Republic of Serbia for financial support according to the contract with registration No. 451-03-34/2026-03/200169, 451-03-34/2026-03/200117 and 451-03-33/2026-03/200117.

REFERENCES

[1] Alpert, P., Bone, E., Holzapfel, C. Plant Ecol. Evol. 2000, 3, 52–66.

* *djurdja.stojicic@sfb.bg.ac.rs*

[2] Nyssen B, Den Ouden J, Verheyen K, *et al.* Integrating black cherry in forest management in the Netherlands and Belgium," In: Krumm F, Vitkova L, editor. Introduced Tree Species in European Forests. Joensuu: European Forest Institute; 2016. p.362.

[3] Pötzelsberger, E., Spiecker, H., Neophytou, C., *et al*. Curr. For. Rep. 2020, 6, 339–353.

[4] Pančić, J. Šumsko drveće i šiblje. Belgrade: Glas Srp. učenog društva; 1871. Knj. XXX.

[5] Pančić J, Flora Kneževine Srbije, Beograd. 1874. p.798.

[6] Pančić J, Dodatak flori Kneževine Srbije. Glas Srp. učenog društva; 1884. Knj. XXX.

[7] Vukićević E, Dekorativna dendrologija. ICS: Beograd, 1974. p.379

[8] Mratinić E, Kojić M, Samonikle vrste voćaka u Srbiji. Belgrade: Institut za poljoprivredna istraživanja Srbije, 1998.

[9] Tucović A, Ocokoljić, M. In: Proceadings of 6th Symposium on the Flora of Southeastern Serbia; (4–7 July); Sokobanja, Serbia. 2000. p. 227–239.

[10] Petrov Dj, Ocokoljić M, Galečić N, *et al*. In: Proceedings of the 30th International Symposium Conference Ecological Truth and Environmental Research; (20–23 June); Bor, Serbia. 2023. p. 210–215.

[11] Čukanović, J., Đorđević, S., Petrov, Dj., *et al*. Horticulturae 2025, 11, 684.

[12] Đorđević, S., Tóth, A., Kuczman, G., *et al*. Sustainability 2025, 17, 9865.

[13] Anastasijević N. Podizanje i negovanje zelenih površina. Belgrade: Šumarski fakultet; 2011.

[14] Bartula M. Flora donjeg toka reke Save. Belgtrade: Univerzitet u Beogradu, 2001.

[15] Škorić A, Filipovski G, Ćirić M. Klasifikacija zemljišta Jugoslavije. Sarajevo: Akademije nauka i umjetnosti Bosne i Hercegovine; 1985. Posebna izdanja knjiga LXXVIII.

[16] Cosmulescu, S., Ionescu, M. Int. J. Biometeorol. 2018, 62(11), 2007–2013.

[17] Meier U. BBCH-Monograph. Growth Stages of Plants. Berlin: Blackwell Wissenschafts-Verla; 1997. p.622.

[18] Ruiz, D., Campoy, J.A., Egea, J. Environ. Exp. Bot. 2007, 61, 254–263.

[19] Pl@ntNet data at GBIF. Available from: https://identify.plantnet.org/k-world-flora/species/Ulmus%20alata%20Michx./data

[20] Urban, J. J. For. Sci., 2003, 49(8), 359–379.

[21] Samardžić I, Filipović D, Anđelković G. In: Proceadings of the 8th Symposium Lokalna samouprava u planiranju i uređenju prostora i naselja; (23–25 April); Herceg Novi, Crna Gora. 2020. p. 419–426.

[22] Barczak, T., Bennewicz, J., Korczynski, M., *et al.* Insects 2021, 12, 173.

[23] Coeurdacier AN, Perez Hidalgo I, Petrović-Obradović O, In: Abstract Proceedings of the 8th International Symposium on Aphids: 8-12 June: Catania, Italy. 2009. p. 84.

[24] Linex, R. The Elms of Texas. Available from: https://txmn.org/centraltexas/files/2020/06/Texas-Elms.pdf

EcoTER'26
eco.tfbor.bg.ac.rs
32nd International Conference
Ecological Truth & Environmental Research
24–26 June 2026, Hotel Sunce,
Sokobanja, Serbia

Original Research

THE INFLUENCE OF THE URBAN HEAT ISLAND ON *Abelia × grandiflora* (ROVELLI EX ANDRÉ) REHDER TAXA

DOI: 10.5937/EcoTER26085K

Radenka Kolarov[1,a], Djurdja Petrov[2,b*], Nevenka Galečić[2,c], Dejan Skočajić[2,d], Jelena Čukanović[1,e], Sara Đorđević[1,f], Mirjana Ocokoljić[2,g]

[1] University of Novi Sad, Faculty of Agriculture, Trg Dositeja 8, 21000 Novi Sad, SERBIA

[2] University of Belgrade, Faculty of Forestry, Kneza Višeslava 1, 11030 Belgrade, SERBIA

[a] https://orcid.org/0000-0003-1976-7618 [b] https://orcid.org/0000-0001-5207-2741

[c] https://orcid.org/0000-0003-2771-4583 [d] https://orcid.org/0000-0002-2679-3278

[e] https://orcid.org/0000-0003-3327-5484 [f] https://orcid.org/0000-0002-4096-8433

[g] https://orcid.org/0000-0002-9171-2833

Abstract

The effects of urban heat islands (UHIs) are an increasing challenge for urban environments, with many studies focusing on trees, yet there is a lack of explanations regarding how urbanization and UHIs affect shrub species. This study addresses that gap by investigating the cultivars 'Little Richard' and 'Sunrise' of the North American hybrid Abelia × grandiflora (Rovelli ex André) Rehder. *The research was conducted using a cascading design approach at the Skyline mixed-use development within the UHI zone of the Savski Venac municipality in Belgrade, over the period 2023–2025. The effects of UHI on the temporal consistency of phenological pattern elements and flowering abundance were analysed through interactions between air temperature and flowering abundance using Spearman rank correlations and linear regression. The results indicate that flowering varied and correlated with daily maximum and minimum temperatures, as well as day length, which influences plant phenophases. The findings highlight Glossy Abelia as suitable for biodiversity conservation and ecosystem services under UHI conditions, implying the optimisation of urban management, restoration, planning, and design strategies.*

Keywords: urban expansion, outdoor ornamental plants, air temperatures, resilience, ecosystem services.

INTRODUCTION

Urban heat islands (UHIs) are caused by urban structures, such as heat-absorbing materials, anthropogenic heat emissions, and increased infrared radiation, which result in higher air temperatures in urban areas compared to neighboring peri-urban and rural regions [1,2]. The UHI phenomenon is also closely linked to climate change and rapid urban development, leading to negative impacts on air quality due to pollutant accumulation, as well as rapid fluctuations in temperature and precipitation patterns, thereby increasing the risk of extreme weather events [3]. These interconnected effects highlight the need for

* *djurdja.stojicic@sfb.bg.ac.rs*

comprehensive research aimed at mitigating the negative consequences of urban microclimates and preserving ecosystem services. To this end, the European Green Deal, the EU Biodiversity Strategy for 2030, and European guidelines on tree planting have been introduced, supporting biodiversity as well as the role of urban greenery, which also includes shrubs [4,5].

Therefore, this study analyses the impact of the UHI, within a challenging urban context, on the flowering of the shrub taxa *Abelia* × *grandiflora* (Rovelli ex André) Rehder (common name Glossy Abelia), cultivars 'Little Richard' and 'Sunrise'. As the boundaries between *Abelia* R.Br. cultivars are often blurred and generally difficult to determine [6], cultivar identification was taken from the work contractors and confirmed through three consecutive years of monitoring. The cultivar 'Little Richard' is a compact plant with green leaves that acquire vivid bronze-red hues in autumn [7,8]. The cultivar 'Sunrise' is a cascading, finely textured plant with variegated green-yellow leaves that turn orange to deep red-burgundy in autumn. Its leaves remain variegated throughout the year, whereas other cultivars have green leaves during summer [7,8]. Both cultivars produce fragrant, ornamental white flowers in summer that attract pollinators, including bees and butterflies. They are also evergreen, although in colder climates they lose around 50% of their foliage in autumn, with the remaining leaves adopting a more intense red colour [6,8]. In light of the above, this study analyses the flowering of two *A.* × *grandiflora* cultivars, as introduced shrub taxa, under the complex influence of the UHI in a moderately continental climate characterised by hot summers without a pronounced dry period and minimal precipitation during the winter half of the year (RHMZ). The specific objectives are to determine the relationships between phenological patterns and flowering abundance with maximum and minimum air temperatures, as well as their contributions to aesthetics and ecosystem services. The purpose of the study is to optimise cultivation conditions through the prediction of phenological sustainability and flowering abundance, and to incorporate the benefits of ornamental shrub taxa into strategies for conserving urban dendroflora.

MATERIALS AND METHODS

The study area is part of a cascading design approach to the access of the Skyline mixed-use development within an urban heat island (UHI) zone in Belgrade, Serbia. Within the built planters, three individuals of *A.* × *grandiflora* 'Little Richard' and one individual of *A.* × *grandiflora* 'Sunrise' were identified. A description of the locations is presented in Table 1.

Each day over three consecutive years (2023–2025), at the individual level, phenological descriptors from the extended BBCH scale [9] were used for *A.* × *grandiflora* 'Little Richard' and 'Sunrise': 60 (day when the first flower opened), beginning of flowering – 61 (day when more than 10% of flowers were open), full flowering – 65 (day when more than 50% of flowers were open), and end of flowering – 69 (day when more than 80% of flowers had finished flowering). Recorded dates were automatically converted into DOY (day of year), where 1 January = DOY 1, 10 January = DOY 10, etc. Phenological patterns were analysed through graphical comparison of temporal overlap and statistically. Flowering duration was expressed as the number of days during which plants bore flowers, while flowering

abundance was assessed using the scale [10]: 0 – no flowers (0% of branches with flowers); 1 – very low (<20%); 2 – low (>20–<40%); 3 – moderate (>40–<60%); 4 – abundant (>60–<90%); and 5 – maximum (>90%).

Table 1 *Description of the research area*

Individua	Latitude φ	Longitude λ	Altitude H (m)	Taxa	Aspect	Slope*
1.	44º47'58.39"N	20º27'06.54"E	90	'Little Richard'	W	4.22°
2.	44º47'58.62"N	20º27'06.78"E	91	'Little Richard'	NW	4.60°
3.	44º47'58.52"N	20º27'06.91"E	91	'Little Richard'	NW	4.60°
4.	44º47'58.30"N	20º27'06.69"E	91	'Sunrise'	W	4.22°

*Slope angle: 3–5° (inclined terrain)

The effects of urban heat island influence on the temporal consistency of flowering abundance were analysed using interactions between air temperature and flowering abundance through Spearman rank (ρ) correlations and linear regression. The strength and direction of correlations were determined by the value and sign of the coefficient (−1 to 1) according to Gilbert [11]. Daily data on maximum and minimum air temperatures were obtained from the Republic Hydrometeorological Service of Serbia (RHMS) [12,13] from the Main Meteorological Station (MMS) Belgrade (44°47′54.44″N and 20°27′53.35″E; altitude 132 m), as it is located within an urban heat island zone at a distance of 1033.56 m from the study area. Data processing was performed at the population level, based on mean values for both cultivars and all individuals due to their established similarity, using XLSTAT 2022, PAST 4.11, and Google Earth Pro.

RESULTS AND DISCUSSION

In our study, within the phenological patterns, the absolute differences between the earliest and latest DOY values were 44 (BBCH 60), 25 (BBCH 61), 50 (BBCH 65), and 23 days for BBCH 69 (Figure 1). All key phenological phases occurred earliest in 2025, while the latest occurrences for the first two phases were recorded in 2023; full flowering and the end of flowering occurred latest in 2024, identified as the warmest year globally according to the Republic Hydrometeorological Service of Serbia. The patterns observed in our study differ from those reported by Casey [7] and the University of Delaware [8], according to which both cultivars flower during summer. In Belgrade (Serbia), flowering extended from early summer to early winter, with an average duration of 161.67 days over three consecutive years (140 days in 2023, 178 days in 2024, and 167 days in 2025). However, the results partially correspond with the GBIF database [14] for the Northern Hemisphere, where flowering phenological patterns are reported for the period June–November at altitudes up to 200 m. The phenological flowering patterns can be characterised by temporal consistency across the years in which observations were conducted (Figure 1).

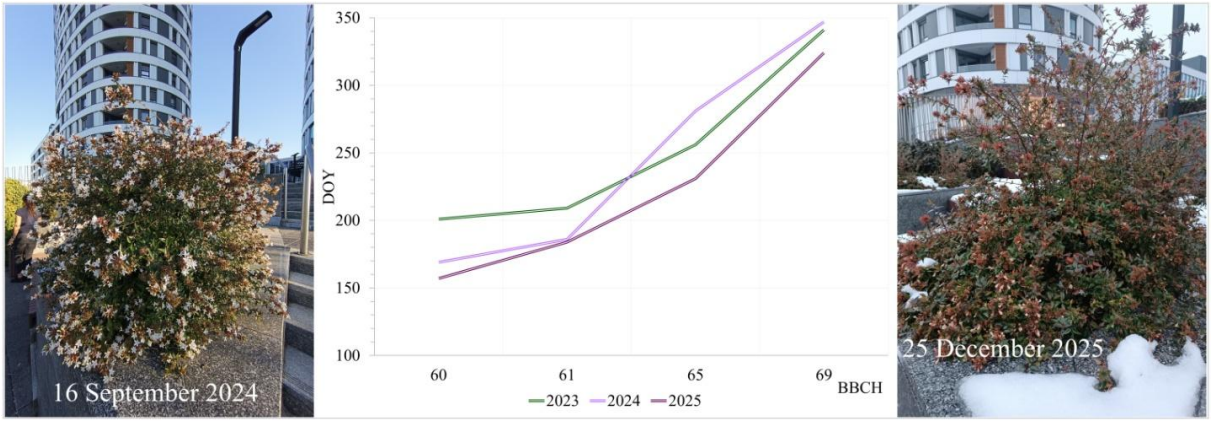

Figure 1 *Phenological flowering patterns of Glossy Abelia in Belgrade based on in situ observations during the study years (2023–2025), and visual aspects at the full flowering stage (left) and at the beginning of the climatological winter (right).*

The results indicate that flower formation varied throughout the study period and that it correlates with climatic parameters across the research years, while the day of year (DOY) was not a significant factor for the elements of the flowering phenophase. The validity of these conclusions is supported by the results of descriptive statistics (Table 2). This is further confirmed by the obtained values of the Spearman rank (ρ) coefficient, for the days when the first flower opened (60), the beginning of flowering (61), full flowering (65), and the end of flowering (69) of Glossy Abelia, which were not statistically significant.

Table 2 *Descriptive statistics for BBCH 60 (first open flower), BBCH 61 (beginning of flowering), BBCH 65 (full flowering), and BBCH 69 (end of flowering) as key elements of the phenological flowering patterns of Glossy Abelia in Belgrade during the period 2023–2025.*

Parameters	60BBCH	61BBCH	65BBCH	69BBCH
Standard deviation	18.571	11.343	20.412	9.741
Variation coefficient	0.106	0.059	0.080	0.029
Variance	344.889	128.667	416.667	94.889
Standard err. of the variance	517.333	193.000	625.000	142.333

Given that, to the authors' knowledge, this is the first study addressing flowering abundance and temperature ranges, values for the five-level scale ratings were separated into two periods: up to 30 September (i.e. until the end of the growing season) and from 1 October (end of the growing season) to the end of flowering. Ranges of daily temperatures corresponding to flowering abundance ratings were determined in accordance with Lalić *et al.* [15], who emphasized that at different geographical latitudes the length of the growing season is closely related to temperature and duration of sunlight, and Zaytseva *et al.* [16], who highlighted that under given climatic conditions and day-length regimes in Europe, both temperature and photoperiod must be considered. A comparative analysis identified the ranges of daily maximum and minimum temperatures for the flowering abundance of Glossy Abelia (Table 3).

Table 3 *Ranges of daily maximum (T_{max}) and minimum (T_{min}) air temperatures (based on RHMS data) corresponding to flowering abundance ratings (1–5) of Glossy Abelia (own in situ recorded data)*

Flowering Abundance	T_{max} (°C)	T_{min} (°C)	T_{max} (°C)	T_{min} (°C)
	Up to 30 September		From 1st October to the end of flowering	
		2023		
1	30.0–37.2	15.4–25.3	3.6–22.7	0.0–10.9
2	24.2–35.4	15.4–24.8	7.6–23.0	3.5–9.3
3	23.7–34.0	13.5–18.9	16.2–26.9	5.3–14.4
4	26.4–33.3	18.4–20.7	14.0–30.2	5.3–19.6
5	21.2–32.6	13.1–20.8	22.2–28.1	9.7–16.0
		2024		
1	39.7–28.6	17.1–27.5	1.1–9.7	-1.0–4.9
2	20.1–33.7	14..9–23.0	3.9–13.5	0.2–5.2
3	16.4–28.7	11.3–8.6	4.8–19.7	-0.1–9.4
4	15.6–32.2	7.0–15.6	3.9–25.9	-1.0–16.3
5	-	-	9.1–29.2	0.4–17.6
		2025		
1	23.2–38.6	14.3–26.2	2.2–16.1	-0.5–8.9
2	21.4–35.4	14.0–23.7	4.7–25.9	1.9–14.0
3	21.4–35.4	14.0–23.7	8.2–25.6	5.6–15.3
4	19.5–36.5	12.9–23.6	-	-
5	22.0–35.8	11.5–22.4	-	-

Spearman correlation coefficients, with a significance level of $p < 0.05$, confirmed strong positive correlations between Tmax and Tmin for all three years (0.918 in 2023, 0.938 in 2024, and 0.921 in 2025), and significant moderate negative correlations of Tmax and Tmin with flowering abundance only for 2024 (−0.599 for Tmax and −0.633 for Tmin). Therefore, regression analyses were performed based on daily maximum and minimum air temperatures, separated by periods, to determine their influence on flowering abundance (Figures 2 and 3).

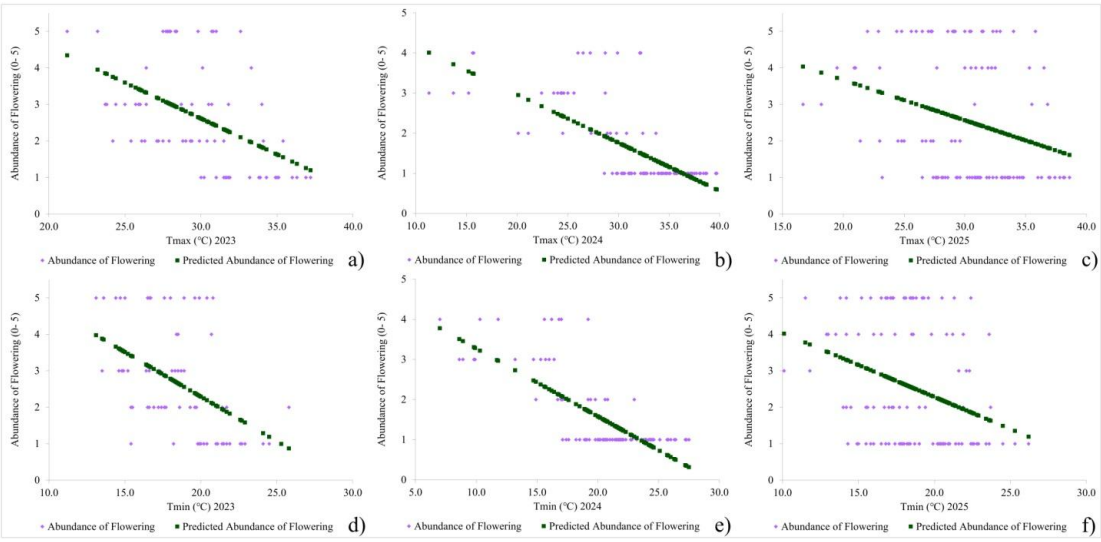

Figure 2 *Scatterplots and predicted effects of daily maximum (a, b, c) and minimum (d, e, f) air temperatures on flowering abundance up to the end of the growing season (30 September)*

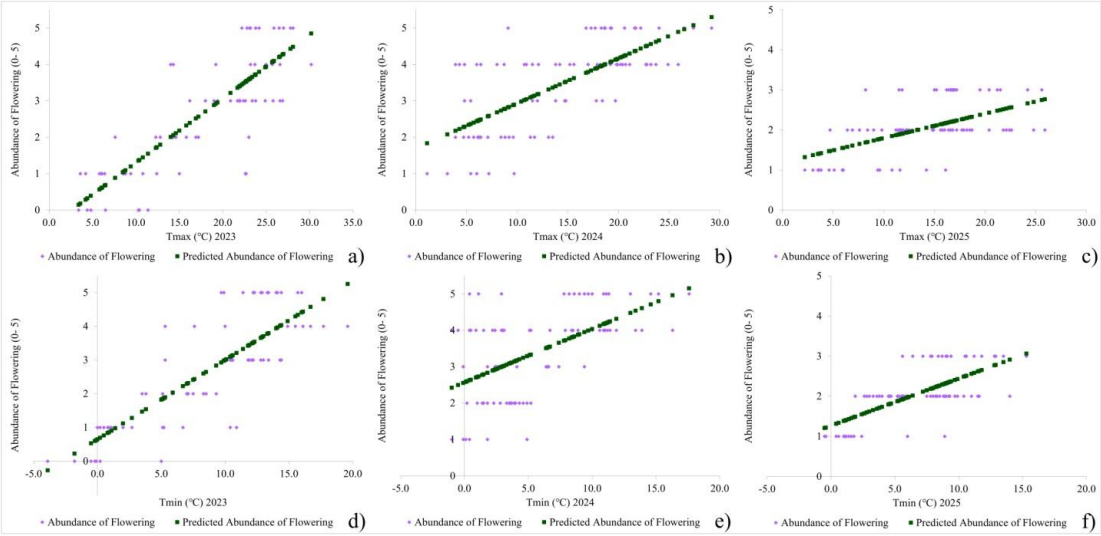

Figure 3 *Scatterplots and predicted effects of daily maximum (a, b, c) and minimum (d, e, f) air temperatures on flowering abundance 1 October to the end of flowering.*

Variable trends are noticeable after approximating the extracted data and determining the regression lines. The statistical significance of the conclusions, at $p < 0.05$, is confirmed by the results of regression ANOVA. Up to 30th September, for Tmax the values were $F = 12.533$, $p < 0.0005$ (2023); $F = 97.284$, $p < 0.0000$ (2024); and $F = 11.573$, $p < 0.0009$ (2025), while for Tmin they were $F = 22.595$, $p < 0.0000$ (2023); $F = 140.025$, $p < 0.0000$ (2024); and $F = 14.144$, $p < 0.0002$ (2025). From 1st October to the end of flowering, for Tmax the values were $F = 135.865$, $p < 0.0000$ (2023); $F = 76.765$, $p < 0.0000$ (2024); and $F = 31.353$, $p < 0.0000$ (2025), while for Tmin they were $F = 135.654$, $p < 0.0000$ (2023); $F = 35.782$, $p < 0.0000$ (2024); and $F = 67.281$, $p < 0.0000$ (2025).

The results of the regression analysis for flowering abundance indicate that daily maximum and minimum air temperatures, analysed by periods, were key factors influencing flowering abundance, along with day length, which affects phenophases of temperate zone plants [17]. Furthermore, the relationship between flowering and air temperatures suggests that long sunny days with high temperatures—particularly when plants are grown in stone planters that absorb heat [1], led to a reduction in flowering abundance. Conversely, shorter day lengths combined with rising temperatures contributed to increased flowering abundance. These findings are important for supplementing the list of suitable plants for landscape design in urban heat island (UHI) zones and rapidly developing urban areas, such as the municipality of Savski Venac, with an urbanisation rate of 91.89% [18], which attract organisms crucial for ecosystem services, including bees, butterflies, and birds, many of which have been displaced over the last decade due to anthropogenic pressures [2].

CONCLUSION

The findings of this intensive, pioneering case study conducted in Belgrade during 2023, 2024, and 2025 stand out for their contribution to knowledge on the acclimatization and sustainability of Glossy Abelia taxa in urban heat island (UHI) zones. The analysed taxa are recommended for achieving structural “layering” across all open urban spaces to support biodiversity conservation and ecological sustainability. The study highlights key events in

flowering patterns to emphasise the influence of air temperatures on shifts in urban phenology of Glossy Abelia, providing a basis for operationalizing urban planning and design. Continued phenological monitoring is necessary to further clarify the causes and consequences of shifts in flowering phenophases and abundance, as well as questions related to the spatial and temporal organisation of ecological communities.

ACKNOWLEDGEMENT

The authors are grateful to the Ministry of Science, Technological Development and Innovation of the Republic of Serbia for financial support according to the contract with registration No. 451-03-34/2026-03/200169, 451-03-34/2026-03/200117 and 451-03-33/2026-03/200117.

REFERENCES

[1] Santamouris, M. Renew. Sustain. Energy Rev. 2013, 26, 224–240.

[2] Ocokoljić, M., Petrov, Dj., Vujičić, D. In: Proceedings of International scientific and professional conference Politehnika; 15.12.2023; Belgrade, Serbia. 2023. p. 106–111.

[3] Cuce, P.M., Cuce, E., Santamouris, M. Sustainability. 2025, 17, 1303.

[4] EU Biodiversity Strategy for 2030 Bringing Nature Back into Our Lives. In: Communication from the European Parliament; EC. Brussels, Belgium. 2020.

[5] Guidelines on Biodiversity-Friendly Afforestation, Reforestation and Tree Planting. In: Commission Staff Working Document; EC. Brussels, Belgium. 2023.

[6] Landrein, S., Buerki, S. Wang, H.F., *et al*. Ann. Bot. 2016, 1–13

[7] Casey, C.R. Abelia: A Beautiful and Fragrant addition to Your Garden. 2021. Available from: https://www.fairfaxgardening.org/wp-content/webdocs/pdf/Abelia.pdf

[8] University of Delaware. Botanic gardens. 2023 Spring Plant Sale Catalog. Available from: https://canr.udel.edu/udbg/wp-content/uploads/sites/16/2023/04/shrubs.pdf

[9] Meier U. BBCH-Monograph. Growth Stages of Plants. Berlin, Vienna: Blackwell Wissenschafts-Verlag; 1997. p. 622.

[10] Stilinović, S. *Semenarstvo šumskog i ukrasnog drveća i žbunja*. Belgrade, Serbia: Šumarski fakultet; 1985.

[11] Gilbert, R.O., Statistical methods for environmental pollution monitoring. New York: Van Nostrand Reinhold; 1987. p. 336.

[12] Republic Hydrometeorological Service of Serbia. Available from: https://www.hidmet.gov.rs/ciril/meteorologija/klimatologija_godisnjaci.php

[13] Ogimet Weather Information Service. Available from: https://www.ogimet.com/synopsc.phtml.en

[14] Pl@ntNet data at GBIF. 2026. Available from: https://identify.plantnet.org/k-world-flora/species/Abelia%20%C3%97%20grandiflora%20(Rovelli%20ex%20Andr%C3%A9)%20Rehder/data

[15] Lalić, B., Ejcinger, J., Dalamarta, A., *et al*. Meteorologija i klimatologija za agronome. Novi Sad, Srbija: Univerzitet u Novom Sadu-Poljoprivredni fakultet; 2021.219 pp

[16] Zaytseva, O., Terrel Gutierrez, M., Graeff-Hönninger, S. Int. J. Plant Biol. 2022, 13, 71–81.

[17] Heide, O. M. New Phytol. 1994, 128, 347–362.

[18] Copernicus Earth observation program.
Available from: https://land.copernicus.eu/local/urban-atlas/urban-atlas-2018

EcoTER'26
eco.tfbor.bg.ac.rs
32nd International Conference
Ecological Truth & Environmental Research
24–26 June 2026, Hotel Sunce,
Sokobanja, Serbia

Original Research

Pyracantha angustifolia (Franch.) C.K.SCHNEID. A NEW EXOTIC SPECIES IN THE DENDROFLORA OF BELGRADE

DOI: 10.5937/EcoTER26093K

Radenka Kolarov[1,a], Djurdja Petrov[2,b*], Nevenka Galečić[2,c], Dejan Skočajić[2,d], Jelena Čukanović[1,e], Sara Đorđević[1,f], Mirjana Ocokoljić[2,g]

[1] University of Novi Sad, Faculty of Agriculture, Trg Dositeja 8, 21000 Novi Sad, SERBIA

[2] University of Belgrade, Faculty of Forestry, Kneza Višeslava 1, 11030 Belgrade, SERBIA

[a] https://orcid.org/0000-0003-1976-7618 [b] https://orcid.org/0000-0001-5207-2741

[c] https://orcid.org/0000-0003-2771-4583 [d] https://orcid.org/0000-0002-2679-3278

[e] https://orcid.org/0000-0003-3327-5484 [f] https://orcid.org/0000-0002-4096-8433

[g] https://orcid.org/0000-0002-9171-2833

Abstract

The study examines the condition and visual characteristics of Pyracantha angustifolia (Franch.) C.K. Schneid., a newly recorded taxon in the dendroflora of Belgrade. The recorded taxon has been present at the study site for 10 years, demonstrating remarkable resilience as well as excellent aesthetic qualities. Morphometric traits of the evergreen leaves, flowers, and fruits were analysed, along with flowering and fruiting abundance, which contribute to the attractiveness of green spaces in the urban landscape, where this taxon plays an important role as a border element in landscape architectural compositions. The dimensions of the analysed morphological characteristics of *P. angustifolia fell within the range reported in the literature for its natural habitat. These results are important for the continued monitoring of P. angustifolia, as the species has shown invasive tendencies in some countries, which could threaten local biodiversity if left unmanaged. Moreover, the study highlights the significance of this taxon for bird feeding and habitat provision, particularly for house sparrows, whose populations are negatively affected by excessive urbanisation.*

Keywords: narrowleaf firethorn, introduction, morphology, visual characteristics, landscape design.

INTRODUCTION

The plant world is highly diverse, and in design there is often a focus on using new and more attractive taxa. As a result, urban dendroflora is very dynamic and rich in introduced species. Green spaces are designed to fulfil various ecosystem functions, but the visual aspect is often decisive, leading to the introduction of exotic species into urban landscapes for their aesthetic benefits as well as benefits to the human population [1]. Historically, in landscape architecture, ornamental plants with pronounced decorative traits were the most common choice for designing and greening urban areas [2,3]. Exotic species were once a symbol of prestige, with evergreen taxa dominating due to their year-round visual impact [3]. The

* *djurdja.stojicic@sfb.bg.ac.rs*

aesthetic quality of green spaces and landscape attractiveness draws more user attention, encourages longer visitor stays, and contributes positively to mental well-being. In this context, the morphological appearance of plants is a key element in design [4], as aesthetics evoke positive impressions and influence human psyche and well-being. Plant diversity, habit, ornamental features, colours, and seasonal changes create striking visual effects [5]. Human vision is particularly stimulated by the use of varied colours, which evoke different emotions [6]. Regarding ornamental plant elements, the most prominent features are rich colours, diverse forms, and distinct textures [5].

Due to the significant role of exotic ornamental plants in landscape design, the aim of this study is to investigate the newly recorded taxon *Pyracantha angustifolia* (Franch.) C.K. Schneid. in Belgrade, providing new insights into the morphological traits and adaptability of this introduced shrub.

MATERIALS AND METHODS

In this study, a newly recorded taxon for the dendroflora of Belgrade, *Pyracantha angustifolia* (Franch.) C.K. Schneid. (narrowleaf firethorn), was analysed at Bežanijska Kosa, Samarska Street No. 8, where a border formed by five individuals of narrowleaf firethorn was documented. The location was georeferenced at coordinates 44°49′30.18″ N and 20°23′1.04″ E, at an altitude of 95 m. The border has a height of 118 cm and a length of 5.8 m (Figure 1).

Figure 1 *Analysed border formed by P. angustifolia: a) and its visual aspects during; b) full flowering; and c) full fruit ripeness*

The individuals are 10 years old, planted in spring 2015 during the reconstruction of the green area (data obtained from an interview with the property owner, on whose land the border is located). The study included measurements of height and length (using a tape measure). Flowering and fruiting abundance were assessed following Stilinović [7], along with decorative value and vitality. These parameters were evaluated on a scale of 1 to 5, where 1 represents <20% abundance, low aesthetic value, or poor vitality, and 5 represents

>90% abundance, high aesthetic quality, or strong vitality. In May 2025, during full flowering, inflorescences and fully mature leaves were collected and measured, while fruits were harvested at ripening at the end of summer in September. For morphometric analyses, 30 samples of each element were collected from the southern part of the canopy. Leaf length and width, two diameters of the inflorescence, number of flowers per inflorescence, largest diameter of individual flowers, number of stamens, and fruit diameter were measured. All measurements were taken using high-precision electronic calipers (±0.001 mm). The number of fruits per cluster and the number of seeds per fruit were also recorded. Leaf, flower, and fruit colours were defined using the RGB (Red/Green/Blue) colour system.

Quantitative morphological data were analysed using descriptive statistics in XLSTAT 2020, while the Spearman rank test was performed using the SRplot statistical program [8].

RESULTS AND DISCUSSION

The family *Rosaceae* Juss. comprises 104 genera, including the genus *Pyracantha* M. Roem. Within the genus *Pyracantha*, which belongs to the subfamily *Amygdaloideae* Arn., tribe *Maleae* Small, and subtribe *Malinae* Reveal, there are six accepted species [9]. One of these is *Pyracantha angustifolia* (Franch.) C.K. Schneid. *P. angustifolia* is an evergreen shrub (rarely a small tree) that reaches a height of 2 to 4 (5) m and a spread of up to 5 m [10]. The branches are vertically oriented; when young they are densely covered with greyish-white hairs, later becoming dark grey or reddish-brown. Sharp thorns up to 2 cm long are present on the branches. The plant tolerates pruning well and is therefore suitable for forming hedges and borders. The leaves are simple, arranged spirally or in clusters. They are 2–7 cm long and 5–13 mm wide. The leaf margin is entire and recurved. The upper surface is dark green and glossy, while the underside is densely covered with white hairs. The leaves are borne on petioles 1–3 mm long [11,12]. The flowers are white, with around 30 flowers grouped in inflorescences. Individual flowers are 8–12 mm in diameter, with five sepals and approximately 20 stamens [13]. The flowering period lasts from April to June. The fruits are pome-type, round to slightly flattened, and small, measuring 5–9 mm in diameter. At maturity, they turn yellow or orange. Each fruit contains 3–6 seeds. The fruits are not edible for humans, as they contain hydrogen cyanide [12,14–17].

The mean scores for vitality and ornamental value were 4.8 and 4.6, respectively. Leaf length ranged from 44 mm to 62 mm, while leaf width ranged from 7 mm to 11 mm (Figure 2a). The maximum recorded leaf length was 10 mm greater than that reported in the literature (10–50 mm), whereas the leaf width fell within the reported range of 4–12 mm [13]. The diameter of the inflorescences ranged from 15 to 35 mm. The number of flowers per inflorescence varied between 5 and 22, while the diameter of individual flowers ranged from 5 to 10 mm (Figure 2b). The number of stamens ranged from 12 to 20 (Table 1). According to the literature, inflorescences contain up to 30 flowers, measure 20–40 mm in diameter, individual flowers are 5–12 mm in diameter, and flowers contain up to 20 stamens [12,13], which is consistent with our findings. Fruit diameter ranged from 3 to 7 mm (Figure 2c), which is also in agreement with the data reported by Chari *et al.* [13].

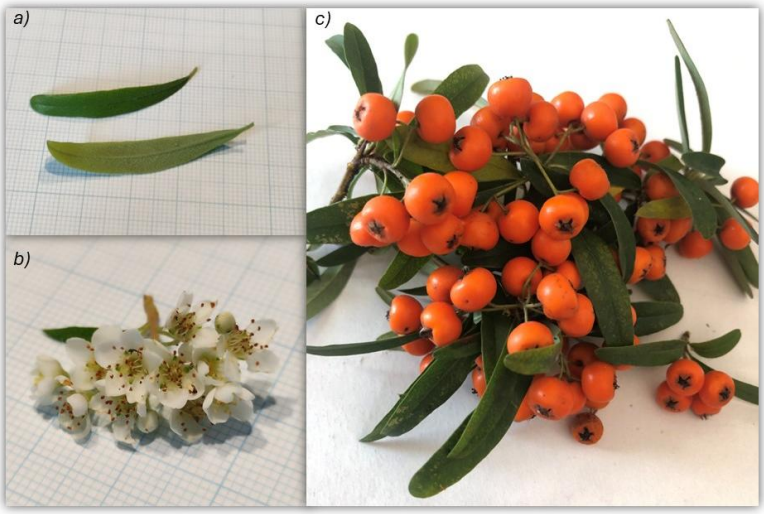

Figure 2 *Analysed morphological parameters of P. angustifolia: (a) leaves, (b) flowers and inflorescences, and (c) fruits*

By applying descriptive statistics, ranges as well as standard deviations and coefficients of variation were determined (Table 1).

Table 1 *Descriptive statistics of morphological parameters of the taxon P. angustifolia*

Character	N	Mean	Min	Max	Std	CV
Leaf length (cm)	30	5.54	44	62	0.520	9.385
Leaf width (cm)	30	0.89	7	11	0.122	13.808
No of flowers	30	12.8	5	22	3.969	31.007
Corymb radius (mm)	30	27	15	35	5.031	18.633
Flower radius (mm)	30	7.90	5	10	1.446	18.294
No of stamens	30	15.23	12	20	2.112	13.865
Fruit group radius 1	30	29.57	23	41	5.65	19.13
Fruit group radius 2	30	24.17	16	33	4.84	20.01
No of pomes	30	16.57	9	28	4.99	30.147
Pome radius	30	4.73	3	7	0.91	19.17
Seed	30	5	5	5	0	0

The standard deviations for leaf length and width were low (0.520 and 0.122), while the coefficients of variation (9.385 and 13.808) indicate low variability in leaf size. Spearman's rank correlation coefficient, at a significance level of $p < 0.05$, between leaflet length and width confirmed a negative correlation (−0.44), indicating that leaflet width decreases as its length increases (Figure 3a). The adaxial leaf surface was determined to be dark green (RGB 90/130/93), while the abaxial surface was grey-green (RGB 120/126/56). The appearance, colour, and size of flowers are highly important for design and aesthetics in landscape architecture; therefore, the visual characteristics of both inflorescences and flowers were also assessed. The colour of the petals was estimated as waxy white (RGB 222/212/200). Flowering abundance was rated as maximal (5). Moderate variability is indicated by the mean coefficients of variation (18.633, 18.294, and 13.865) for inflorescence diameter, flower

diameter, and number of stamens, respectively, whereas variability was high for the number of flowers per inflorescence, with a coefficient of variation of 31.007. Spearman's rank correlation coefficient, at $p < 0.05$, between inflorescence diameter and number of flowers (0.37), as well as between flower diameter within the inflorescence and number of stamens (0.81), indicates positive correlations (Figures 3b and 3c), while other correlations were not significant.

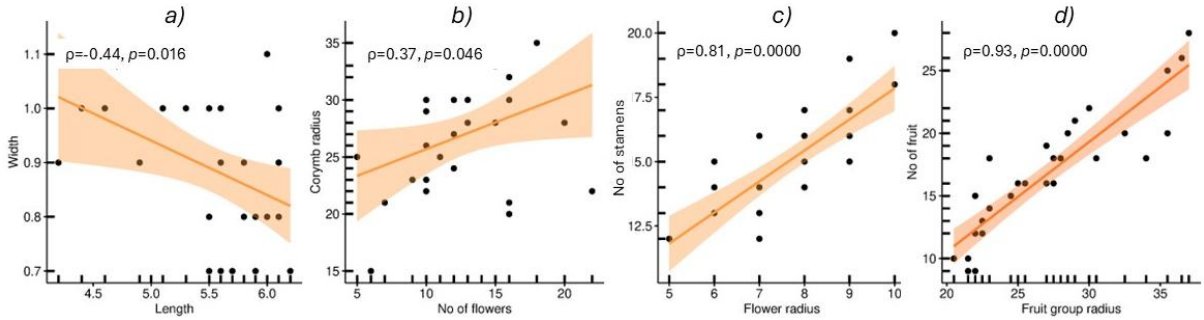

Figure 3 *Scatter plots for Spearman's rank correlation: a) leaf length and width; b) number of flowers and corymb radius; c) flower radius and number of stamens; and d) fruit group radius group and the number of fruits. The shaded area represents the 95% confidence interval*

Fruit yield was maximal (score 5). Each fruit contained five seeds, as also reported by Adams *et al.* [12], indicating high seed production. The pomes were described as round to slightly flattened, in orange-red to orange-yellow shades ranging from RGB 213/92/52 to 252/149/80. A standard deviation of 4.99 and a high coefficient of variation (30.147) for the number of fruits per cluster indicate greater variability, consistent with the analysis of the number of flowers per inflorescence. Spearman's rank correlation coefficients, at a significance level of $p < 0.05$, were statistically significant only for the mean diameter of the fruit cluster and the number of fruits (0.93), whereas no significant correlations were found for the other analysed fruit parameters (Figure 3d).

The results of this study indicate good adaptability and excellent condition of the analysed taxon, as also noted by Adams *et al.* [12], who highlight *P. angustifolia* as highly resilient. The taxon tolerates both high and low temperatures, as well as humid and dry conditions, partial shade, wind, soil salinity, and nutrient-poor soils [10–12]. Indicators of successful acclimatisation include all analysed morphological parameters, as well as maximal flowering abundance and excellent fruit production. In Europe, the species has become naturalised in Russia, Italy, Portugal, and Germany; however, it is classified as an invasive species and its use is prohibited in Australia [18]. During the study, the presence of *Passer domesticus* L. (house sparrow) was recorded within the analysed border, indicating that narrowleaf firethorn serves both as a habitat and a food source for this urban bird species, which inhabits densely branched shrubs that are becoming increasingly scarce due to urbanization [19]. The house sparrow plays an important role in maintaining biodiversity and controlling insect populations through urban food chains [20]. However, since *P. angustifolia* is easily dispersed and spread by birds [21] and exhibits invasive characteristics, it is necessary to continue monitoring its dispersal and potential further spread. Monitoring of this taxon is particularly important given

the presence of large areas of unmanaged land in the vicinity of the site where narrowleaf firethorn was recorded.

CONCLUSION

Our study provides important data in the form of a quantitative overview of the morphological characteristics of a newly recorded taxon in Belgrade. The highly ornamental evergreen taxon *P. angustifolia*, characterised by dark green leaves with a distinctive grey-green hue, abundant ornamental white inflorescences, and bright orange pome fruits, may represent a valuable new element in plant design within the urban landscape, particularly for borders and hedges. In addition to ornamental value, recent trends increasingly favour the cultivation of taxa that are resistant to climate change and exhibit rapid growth. The studied taxon, besides its morphometric characteristics, has also demonstrated excellent vitality, qualifying it as a highly resilient shrub suitable for use in the design of green spaces under urban environmental conditions.

ACKNOWLEDGEMENT

The authors are grateful to the Ministry of Science, Technological Development and Innovation of the Republic of Serbia for financial support according to the contract with registration No. 451-03-34/2026-03/200169, 451-03-34/2026-03/200117 and 451-03-33/2026-03/200117.

REFERENCES

[1] Schlaepfer, M.A., Sax, D.F., Olden, J.D. Conserv. Biol. 2011, 25, 428–437.

[2] Clouston B., Zixin C., Ci'an X. Landscape Garden Plant Configuration; Beijing: China Construction Industry Press; 1992.

[3] Fekete, A., Sárospataki, M., Takács, K. Acta Univ. Sapientiae Agric. Environ. 2014, 6, 57–68.

[4] Ahern, J. Landsc. Ecol. 2013, *28*, 1203–1212.

[5] Yuan, J., Zhang, L., Kim, C.S. Plants. 2023, 12, 1431.

[6] Angelini, L., Caon, M., Caparrotta, S. et al. In Proceedings of ACM International Joint Conference on Pervasive and Ubiquitous Computing; 12–16 September 2016; Heidelberg, Germany. 2016. P. 1001–1009.

[7] Stilinović S. Semenarstvo šumskog i ukrasnog drveća i žbunja. Belgrade: Šumarski fakultet; 1985.

[8] Tang, D., Chen, M., Huang, X., et al. PLoS ONE. 2023, e0294236.

[9] POWO, 2026. Plants of the World Online. Facilitated by the Royal Botanic Gardens, Kew. Available from: https://powo.science.kew.org

[10] Adams LD. Reproductive Ecology of Pyracantha angustifolia in Afromontane Grasslands of the Eastern Free State. MSc dissertation. Phuthaditjhaba, South Africa: University of the Free State; 2020. p. 103.

[11] Nesom, G.L. 2010. Phytoneuron. 2010, 2, 1–6.

[12] Adams, L.D., Giovannoni, D., Clark, V.R. et al. Plants. 2023, 12, 1308.

[13] Chari LD, Martin GD, Steenhuisen S-L, et al. Invasive Plant Sci. Manag. 2020, 13, 120–142.

[14] Zechmeister, L., Schroeder, W. A. Journal of Biological Chemistry. 1942, 144, 315–320.

[15] Wang Y., *et al*. IOP Conf. Ser.: Earth Environ. Sci. 2018, 199, 05201.

[16] Kaviani, B., Deltalab, B., Kulus, D. et al. Horticulturae. 2022, 8, 964.

[17] Song, S., Li, J., Liu, H., *et al*. Food Frontiers. 2023, 4(4), 1720–1736.

[18] *Pyracantha angustifolia* (Franch.) C.K.Schneid. in GBIF Secretariat (2023). GBIF Backbone Taxonomy. Checklist dataset https://doi.org/10.15468/39omei

[19] Guallar, S., Cai, X., Quesada, J. Revista Catalana d'Ornitologia, núm. 2025, 41, 9–20.

[20] Summers-Smith, D. The Sparrows: A Study of the Genus Passer. Berkhamsted: T & AD Poyser; 1988. p. 342.

[21] Adams, L.D., Martin, G.D., Downs, C.T. *et al*. Biol. Invasions. 2022, 24, 2809–2819.

Original Research

EVALUATION OF ECOLOGICAL POTENTIAL OF VETERNICA RIVER BASED ON CHEMICAL QUALITY PARAMETERS

DOI: 10.5937/EcoTER26100N

Milena Nikolić[1,a*], Aleksandar Zdravković[1,b], Dragana Marković Nikolić[1,c], Danijela Stojadinović[1,d], Tanja Nikolić[1,e]

[1]Academy of Applied Studies of Southern Serbia, Department of Higher Technology and Art School, Vilema Pušmana 17, 16000 Leskovac, SERBIA

[a] https://orcid.org/0000-0002-6631-936X

[b] https://orcid.org/0000-0001-9906-3543

[c] https://orcid.org/0000-0003-3171-9838

[d] https://orcid.org/0000-0002-6335-8101

[e] https://orcid.org/0009-0007-8932-6128

Abstract

This study aimed to assess the ecological potential of the Veternica River based on chemical parameters in the part of its course through the city of Leskovac. Before entering the city, the Veternica River flows through rural areas of intensive agricultural production and is therefore susceptible to pollution from runoff of mineral fertilizers and pesticides. A significant problem is also the accumulation of waste on certain parts of riverbanks, where construction debris, household and plastic waste can be found. Based on chemical indicators, the ecological status of the Veternica River ranged from III (moderate) at the sampling locations 1, 2, and 3 to IV (bad) at sampling location 4.

Keywords: ecological potential, Veternica River, biological oxygen demand, chemical oxygen demand.

INTRODUCTION

The exceptional properties of water and its crucial importance for existence of life formed a very specific relationship of individuals and human societies towards this unique resource. Water is the most valuable fluid with a great capacity to receive and transport various pollutants. The intensive industrial development is primarily characterized by a constant increase in the consumption of water which is sent back after usage to watercourses but qualitatively altered [1].

In order to assess the impact of pollution on aquatic ecosystems, it is necessary to be familiar with the nature and the amount of pollution, as well as the capacity of receivers to accept pollution [2]. The river water pollution is associated with the type of wastewater originating from urban, industrial and agricultural activities that reaches surface and underground waters [3].

* *milenai.chem@gmail.com*

Human activities affect aquatic ecosystems through deforestation, urbanization, and agricultural development, soil drainage, discharge of pollutants and regulation of watercourses. Water quality can vary greatly depending on morphological characteristics, vegetation and activity in the river basin [4]. Furthermore, water conveyed by rivers and the heterogeneous materials they transport to coastal seas, can provide a significant information on the processes occurring within their drainage basins [5].

The Veternica River is a left tributary of the South Morava River. The length of the river is 73 km and the area of the river basin up to the confluence with South Morava is 515 km^2. Given that it passes by numerous settlements, of which the largest is the city of Leskovac, the pollution of the Veternica River is pronounced. The inhabitants often dispose different types of solid waste, next to the river or into the river itself. The undermining of the bottom, due to the frequent and illegal extraction of gravel in certain places, led to a change in the substrate and the creation of "convenient" places for waste disposal. Since it flows through the area with significant agricultural production, the river is also susceptible to pollution from runoff of mineral fertilizers and pesticides.

Therefore, the aim of this research was to conduct a detailed analysis of parameters and assess water quality, so some further actions could be taken to improve the current state in the field.

MATERIALS AND METHODS

River water sampling was carried out in April 2025, approximately 20 cm below the surface, at four locations: 1) after the estuary of Sušica into Veternica (42° 55' 19" N, 21° 55' 39" E), 2) the entrance into Leskovac - south suburb (42° 58' 35" N, 21° 56' 41" E), 3) the centre of Leskovac (43° 00' 12" N, 21° 56' 35" E) and 4) the northern exit from Leskovac (43° 1' 24" N, 21° 56' 54" E). The samples were collected in polyethylene bottles, preserved by adding chloroform, stored at 4 ºC and analysed as soon as possible. Numerous parameters were determined.

Water temperature (^oC) and pH were measured *in situ*.

Total suspended solids (TSS) were determined via standard SM 2540 D gravimetric method which implies filtering certain volume of river water through a pre-weighed glass-fiber filter and drying the residue to a constant weight at 105 ºC [6].

The concentration of dissolved oxygen (DO) was determined according to well-known Winkler titration method [7]. Total water hardness (TWH) was measured by complexometric titration using EDTA and the indicator Eriochrome black T to determine the total concentration of Ca^{2+} and Mg^{2+} ions [8]. Chloride concentration (Cl^-) was determined by using Mohr's titration method with $AgNO_3$. Potassium chromate was used as an indicator.

A rapid and simple spectrophotometric method was applied for nitrate analysis (NO_3-N). Nitrates absorb UV light, and the first recording was performed on 220 nm. The second recording on 275 nm was used as correction for organic dissolved matter. Furthermore, for ammonia nitrogen content (NH_4-N), Nessler method was applied, and the absorbance was recorded at 425 nm [9].

The content of orthophosphates (PO_4^{3-}) was also determined spectrophotometrically at 690 nm. The method relies on reaction of orthophosphates with molybdate in acidic conditions to form phosphomolybdic acid, which is then reduced to an intense blue compound, proportional to the orthophosphate concentration [10].

Chemical Oxygen Demand (COD) was applied to determine water pollution levels by quantifying the consumption of $K_2Cr_2O_7$, which is a strong oxidant for both organic and inorganic substances. Biochemical Oxygen Demand over 5 days period (BOD_5) was measured in order to determine the amount of dissolved oxygen required by aerobic microorganisms to decompose organic matter in river water samples.

Analysis of river water was also carried out on an inductively coupled plasma-optical emission spectroscopy (ICP-OES) instrument (ARCOS FHE12, SPECTRO, Germany), and the concentrations of trace elements (Cr, Fe, and Mn) were determined. ICP-OES parameters were as follows: RF strength 1500 W, flush pump rate 30 rpm, analysis pump rate 30 rpm, nebulizer gas flow rate 0.95 dm^3/min, coolant gas flow rate 13 dm^3/min, auxiliary gas flow rate 0.8 dm^3/min, and axial viewed plasma mode.

RESULTS AND DISCUSSION

The results of the analysis are presented in the Table 1.

Table 1 *The results of examined parameters of Veternica River water according to sampling locations*

Parameter	Sampling location			
	1	2	3	4
T (^oC)	11.5	11.8	12.0	11.8
TWH (mg $CaCO_3/dm^3$)	133	126	138	144
pH	7.94	7.87	7.98	8.12
DO (mg O_2/dm^3)	7.12	7.16	7.19	6.93
Cl^- (mg/dm^3)	9.94	10.21	10.34	10.65
NO_3-N (mg/dm^3)	2.8	2.8	3.9	3.8
NH_4-N (mg/dm^3)	0.27	0.43	0.39	0.32
PO_4^- (mg/dm^3)	0.12	0.13	0.13	0.12
BOD_5 (mg O_2/dm^3)	4.21	4.53	5.32	6.77
TSS (mg/dm^3)	13.62	12.41	15.75	17.48
COD (mg O_2/dm^3)	12.55	13.84	12.11	14.84
Cr (µg/dm^3)	11	13	13	19
Mn (µg /dm^3)	16	12	18	12
Fe (µg /dm^3)	315	353	345	376

According to the Rulebook on determination of surface and underground waters [11] Veternica River was defined as a watercourse significantly altered by human activity, due to utilization or protection. Furthermore, according to the Rulebook on the parameters of the ecological and chemical status of surface waters and the parameters of the chemical and quantitative status of groundwater [12], Veternica River was classified as type 3 - small and medium-sized watercourses, altitude up to 500 m, with a coarse substrate predominance in the riverbed. Based on water quality, five classes of ecological potential were defined as follows: class I – high, class II – good, class III – moderate, class IV – poor and class V – bad. For

type 3 watercourse, parameters were defined as well as limits for each class and given in the Table 2.

Table 2 *Chemical parameters and limits among classes of ecological potential*

Parameter	Limits among classes of ecological potential			
	I-II	II-III	III-IV	IV-V
pH	6.5-8.5	6.5-8.5	6.5-8.5	<6.5, >8.5
DO (mg O_2/dm^3)	8.5	7.0	5.0	4.0
Cl^- (mg/dm^3)	50	100		
NO_3-N (mg/dm^3)	1.5	3.0	6.0	15.0
NH_4-N (mg/dm^3)	0.05	0.1	0.8	1.0
PO_4^- (mg/dm^3)	0.02	0.1	0.2	0.5
BOD_5 (mg O_2/dm^3)	1.5	5.0	6.0	20.0

In addition, Regulation on limit values of pollutants in surface and groundwater and sediment and deadlines for their achievement [13], defined closer the levels of other parameters for assessing the class of ecological potential of surface water, as given in Table 3.

Table 3 *Classes of ecological potential of surface water according to the limit values of pollutants*

Parameter	Limit values of pollutants in surface waters				
	I class	II class	III class	IV class	V class
TSS (mg/dm^3)	25	25			
COD (mg O_2/dm^3)	10	15	30	125	>125
Fe (µg /dm^3)	200	500	1000	2000	>2000
Mn (µg /dm^3)	50	100	300	1000	>1000
Cr (µg /dm^3)	25	50	100	250	>250

When the value of the ecological status or ecological potential parameter corresponded to the value at the boundary between the classes, the surface water body was classified in a worse class. If one or more ecological status or ecological potential parameters exceed the threshold values of good status, the ecological status or ecological potential of the surface water may be classified at most as moderate [12]. Summary ecological potential of river water on each of the sampling locations was estimated after comparing the obtained data via numerous analysis (Table 2) with the lawfully regulations (Tables 3 and 4) and presented in the Table 4.

The temperature and pH of the river water were fairly uniform at all locations. The contents of chlorides, Cr and Mn did not exceed the limits defined for the I class. The Fe content and TSS did not exceed the limits defined for the II class.

Considering the content of DO, NO_3-N, NH_4-N and PO_4^-, the water quality corresponded to the III class, therefore described as moderate. Although nitrates and phosphates are growth supporting, essential plant nutrients, increased amounts of these anions contribute to eutrophication of aquatic systems, which consequently leads to higher consumption of dissolved oxygen in water. Excess amounts of nitrates and phosphates in watercourses can be caused by several factors: agricultural runoffs (mineral fertilizers and animal manure), septic drainage, industrial wastewater discharge or household garbage dumps [14].

Table 4 *Ecological potential of Veternica River water on each of the sampling locations*

Parameter	Sampling location			
	1	2	3	4
pH	II	II	II	II
DO (mg O_2/dm^3)	III	III	III	III
Cl^- (mg/dm^3)	I	I	I	I
NO_3-N (mg/dm^3)	III	III	III	III
NH_4-N (mg/dm^3)	III	III	III	III
PO_4^- (mg/dm^3)	III	III	III	III
BOD_5 (mg O_2/dm^3)	III	III	III	IV
TSS (mg/dm^3)	II	II	II	II
COD (mg O_2/dm^3)	II	II	II	II
Cr ($\mu g/dm^3$)	I	I	I	I
Mn ($\mu g/dm^3$)	I	I	I	I
Fe ($\mu g/dm^3$)	II	II	II	II
Summary ecological potential	III	III	III	IV

Regarding BOD_5, the water samples collected at sampling points 1, 2 and 3 corresponded to class III, but the sample collected at sampling location 4 corresponded to class IV. BOD_5 is correlated to microbiological contamination and is used to assess pollution levels of freshwater bodies. Higher BOD_5 values indicate more organic pollutants, which also results in lower oxygen availability for aquatic life. It is considered a reliable indicator of anthropogenic pollution [15].

Based on obtained results, summary ecological potentials for water samples at locations 1, 2 and 3 are categorized as moderate (III class), while the ecological potential at location 4 is categorized as bad (IV class). Evidently, the Veternica River water quality is deteriorating as it flows towards the estuary.

CONCLUSION

Given that the sampling of Veternica River water was carried out in the spring, application of fertilizers and pesticides and their runoff could be one of the causes of increase in NO_3-N, NH_4-N and PO_4^- loadings. However, the existence of illegal landfills on the riverbanks and in some cases domestic drainage, would be impossible to ignore. Therefore, it is necessary to put more effort in training and educating farmers and raising of ecological awareness of people living by the river about the preservation of natural resources. Even the slight deterioration in river water quality may cause very serious consequences–not just disturbance in aquatic biota but pose a risk to human health when rivers are used for irrigation or to obtain drinking water. Also, strict legal regulations and significant penalties for reckless waste disposal should be implemented in practice.

REFERENCES

[1] Moretti, A., Ivan H., Skvaril, J.J. Water Process Eng. 2024, 60, 105061.

[2] Bashir I, Lone F, Bhat R, *et al*. Concerns and Threats of Contamination on Aquatic Ecosystems. In: Hakeem, K, Bhat, R, Qadri, H. editors. Bioremediation and Biotechnology. Springer; 2020. p. 1–26.

[3] Vittori Antisari, L., Trivisano, C., Gessa, C. Water Qual. Expo. Health. 2010, 2 (1), 1–13.

[4] Pisinaras, V., Petalas, C., Gemitzi, A. Glob. Nest. J. 2007, 9 (3) 259–268.

[5] Depetris, P. J. Front. Water. 2021, 3, 745912.

[6] Method 2540 of Standard Methods for the Examination of Water and Wastewater, 24th Edition

[7] Carpenter J. Limnol. Oceanogr. 1965, 10 (1), 135–140.

[8] Method 2340 C of Standard Methods for the Examination of Water and Wastewater, 22nd Edition

[9] Guo, Y., Liu, C., Ye R., *et al*. Appl. Sci. 2020, 10, 6874.

[10] Crouch, S., Malmstadt, H. Anal. Chem. 1967, 39 (10), 1084–1089.

[11] Rulebook on determination of surface and underground waters, Official Gazette of the Republic of Serbia, No. 96/2010.

[12] Rulebook on the parameters of the ecological and chemical status of surface waters and the parameters of the chemical and quantitative status of groundwater, Official Gazette of the Republic of Serbia, No. 74/2011.

[13] Regulation on limit values of pollutants in surface and groundwater and sediment and deadlines for their achievement, Official Gazette of the Republic of Serbia, No. 50/2012.

[14] Li, J., Jin, Q., Liang, Y., *et al*. Int. J. Environ. Res. Public Health. 2022, 19 (3), 1890.

[15] Vigiak, O., Grizzetti, B., Udias-Moinelo, A., *et al*. Sci. Total Environ. 2019, 666, 1089–1105.

Original Research

MICROBIOLOGICAL QUALITY OF THE VELIKA MORAVA RIVER: ECOLOGICAL AND PUBLIC HEALTH ASPECTS

DOI: 10.5937/EcoTER26106O

Vesna Obradović[1,a], Marija Perović[1,b*], Tanja Vučković[1]

[1] Jaroslav Černi Water Institute, Jaroslava Černog 80,11 226 Belgrade, SERBIA

[a] https://orcid.org/0009-0008-2157-0615 [b] https://orcid.org/0000-0003-2045-001X

Abstract

Microbiological parameters represent important indicators of water quality and ecological status in river systems. This study evaluates the microbiological quality of the Velika Morava River (Serbia) at its confluence with the Danube during the period 2015–2020, with particular emphasis on seasonal variability. Key parameters included heterotrophic bacteria, aerobic mesophilic bacteria, total and fecal coliforms, Escherichia coli, and Enterococcus spp., analyzed according to ISO and standard microbiological methods. The results indicate that the river predominantly exhibits moderate ecological status (Class III), observed in 67% of samples, while poor status (Class IV) was recorded in 17% of cases. Elevated levels of fecal indicators, particularly E. coli, confirm continuous anthropogenic pressure from untreated wastewater and diffuse sources. Seasonal analysis shows that higher variability and maximum values of microbiological parameters occur during the spring period, primarily due to surface runoff and increased pollutant transport, while during low-flow conditions in late summer, reduced variability but sustained elevated values reflect the dominant influence of temperature and limited dilution capacity. Despite significant organic and fecal pollution, the dominance of oligotrophic bacteria (FO/H > 1) indicates a moderate self-purification potential of the river system.

Keywords: microbiological indicators, Velika Morava, seasonal variability, fecal pollution, self-purification.

INTRODUCTION

Surface waters in intensively used catchments are increasingly exposed to microbiological contamination, primarily originating from untreated wastewater and diffuse agricultural sources. Unlike physicochemical parameters, microbiological indicators provide direct insight into the origin, intensity, and dynamics of pollution, particularly in relation to organic and fecal contamination. The presence of indicator organisms such as *Escherichia coli* and intestinal *enterococci* is widely used to detect recent fecal pollution and to assess potential health risks associated with water use. Their occurrence implies the possible presence of pathogenic microorganisms, including bacteria, viruses, and parasites, and therefore represents an important component in evaluating the suitability of surface waters for drinking water supply, irrigation, and recreational purposes. In addition to fecal indicators, heterotrophic and mesophilic bacteria provide valuable information on organic pollution and

* *marija.perovic@jcerni.rs*

ecosystem functioning [1]. Their abundance is closely controlled by nutrient availability, temperature, and hydrological conditions, reflecting both external pollution pressures and internal biogeochemical processes. The relationship between heterotrophic and oligotrophic bacterial populations, often expressed through indices such as FO/H, enables the assessment of the self-purification capacity and mineralization potential of aquatic systems [2]. The Velika Morava River represents one of the most important river systems in central Serbia, with significant ecological, agricultural, and socio-economic importance. However, it is continuously exposed to anthropogenic pressures that influence the level and seasonal dynamics of microbiological contamination.

The Velika Morava is formed by the confluence of the West and South Morava near Stalać and flows into the Danube between Smederevo and Kostolac. The catchment area of the Velika Morava is approximately 6,126 km², while the entire Morava river system exceeds 37,000 km², covering more than 40% of the territory of Serbia. Hydromorphologically, the river is classified as a lowland river (Type 1), characterized by fine sediment dominance, pronounced meandering, and high hydrological variability. Its flow regime includes frequent spring floods and reduced discharge during summer low-flow periods, which directly influence water quality through dilution during high-flow events and increased contaminant concentrations during low-flow conditions.

The basin, located within the fertile Pomoravlje region, is subject to multiple anthropogenic pressures. Although physicochemical parameters generally correspond to Class I–II, the river is sensitive to organic and nutrient pollution, particularly during low-flow periods when dissolved oxygen concentrations may decline. Microbiological contamination is especially pronounced near urban areas such as Jagodina, Ćuprija, and Paraćin, where untreated municipal wastewater represents a dominant pollution source. Additional pressures include agricultural runoff enriched with nutrients, as well as diffuse pollution and solid waste inputs, resulting in pronounced spatial and temporal variability of water quality, which generally deteriorates in the downstream direction.

The aim of this study is to assess the microbiological quality of the Velika Morava River and to evaluate its ecological status based on standard microbiological indicators, with particular emphasis on seasonal variability and the influence of hydrological and temperature-related factors on microbial dynamics.

MATERIALS AND METHODS

Water samples were collected at a monitoring profile located approximately 2 km upstream from the confluence of the Velika Morava River with the Danube (rkm 1103) during the period 2015–2020 (Figure 1). Sampling was conducted twice per year, in early spring (April) and late summer (August–September), to capture seasonal variability under contrasting hydrological conditions. Microbiological analyses were performed in accordance with national regulations (Official Gazette RS 50/2012 and 74/2011) and internationally accepted methods. Heterotrophic bacteria (HPC) were enumerated according to ISO 6222:1999/2024 at two incubation regimes: (i) 22 ± 2°C for 5–7 days (psychrophilic/autochthonous bacterial population), and (ii) 35 ± 2°C for 48 h (aerobic mesophilic bacteria, indicating allochthonous

and potentially anthropogenic input). Total and fecal (thermotolerant) coliforms, as well as *Escherichia coli* and *Enterococcus spp*., were determined using the Most Probable Number (MPN) method based on defined substrate technology (Colilert-18 and Enterolert E/Quanti-Tray®, IDEXX, USA) [3,4]. Additionally, the abundance of facultative oligotrophic bacteria was determined using R2A medium, and their proportion relative to total heterotrophic bacteria was expressed as the FO/H index, representing an indicator of self-purification potential and organic matter mineralization [2]. Water quality classification was performed according to Serbian regulatory criteria (Official Gazette RS 50/2012 and 74/2011), based on the most unfavorable value among the analyzed microbiological parameters [5,6]. For the purposes of this study, the results are presented as seasonally aggregated datasets (spring and late summer periods). Descriptive statistical analysis was applied to evaluate data variability, including median (Q2), lower (Q1) and upper (Q3) quartiles, interquartile range (IQR), and identification of extreme values using standard box-plot criteria (Q1 − 1.5×IQR and Q3 + 1.5×IQR). These statistics were used to illustrate seasonal differences in microbiological water quality

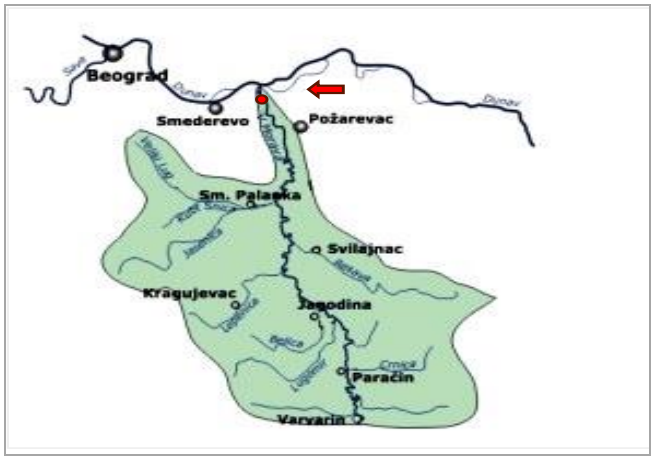

Figure 1 *Location of sampling sites*

RESULTS AND DISCUSSION

The variability and distribution of the analyzed microbiological parameters are presented in Figure 2, showing a wide range between minimum and maximum values for all indicators. The highest variability was observed for heterotrophic bacteria and coliform groups, confirming their sensitivity to changes in environmental conditions and pollution inputs. Elevated average values of these parameters indicate a persistent influence of organic and fecal contamination in the Velika Morava River. Seasonal differences are clearly reflected in the results. As shown in Figure 3, microbiological parameters during the spring period (April–June) exhibit increased variability and generally higher maximum values. This pattern is primarily associated with intensified surface runoff, soil erosion, and resuspension processes, which contribute to the transport of microorganisms and organic matter into the river system. The elevated values of coliform bacteria, *Escherichia coli*, and *enterococc*i further indicate a stronger influence of diffuse pollution sources during high-flow conditions.

In contrast, Figure 4 shows that during the late summer–early autumn period (August–September), the variability of microbiological parameters is reduced, but the values remain

elevated. This reflects more stable hydrological conditions combined with limited dilution capacity. Under low-flow conditions, the influence of temperature becomes more pronounced, enhancing microbial activity and favoring the dominance of mesophilic bacteria.

The comparison between Figures 3 and 4 highlights a clear seasonal shift in controlling factors: hydrological processes dominate during the spring period, while temperature-driven processes become more significant during late summer. These results indicate that microbiological water quality in the Velika Morava River is governed by the combined effects of hydrological variability and thermal conditions, which together control the intensity and dynamics of microbial contamination.

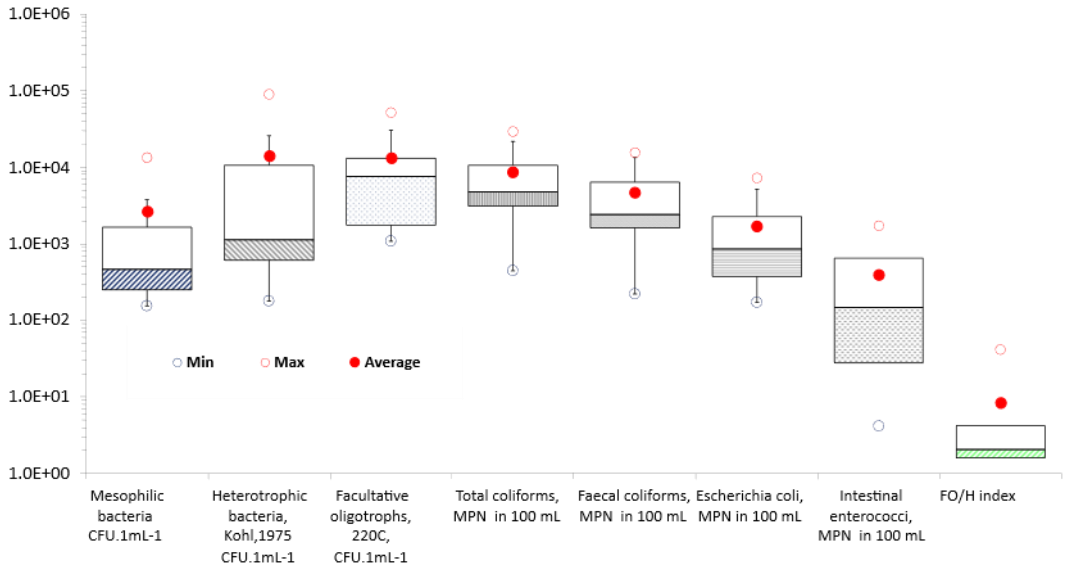

Figure 2 *Distribution of microbiological indicators in the Velika Morava River (2015–2020), presented as minimum, maximum, and mean values*

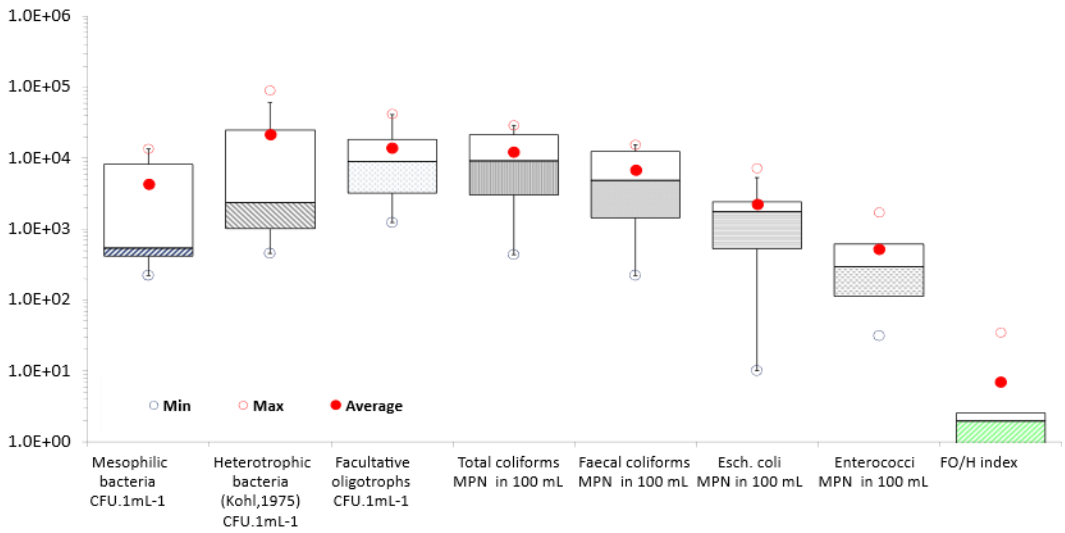

Figure 3 *Seasonal variation of microbiological indicators in the Velika Morava River during the spring period (April–June 2015–2020), presented as minimum, maximum, and mean values*

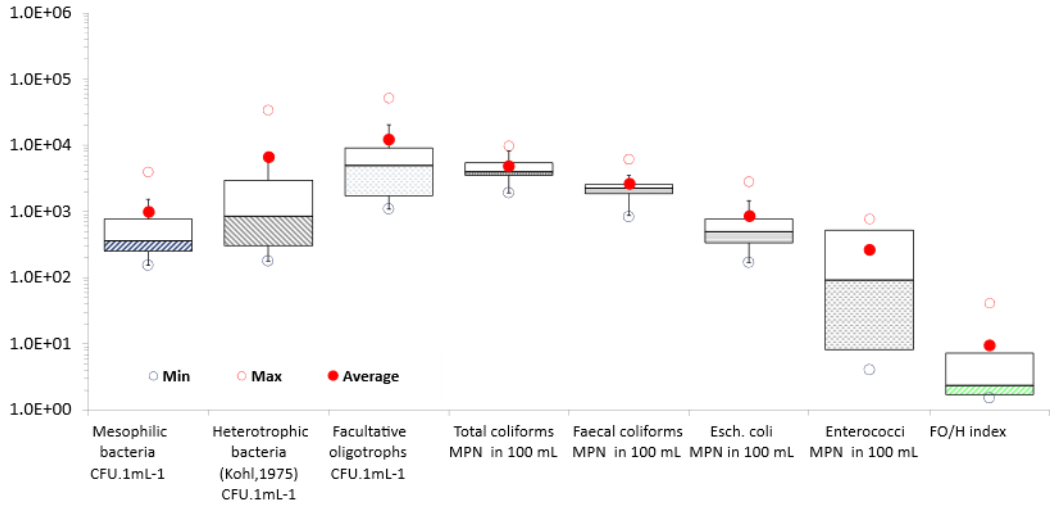

Figure 4 *Seasonal distribution of microbiological indicators in the Velika Morava River during low-flow conditions (August–September 2015–2020), presented as minimum, maximum, and mean values*

CONCLUSION

The results of this study indicate that the Velika Morava River is predominantly characterized by moderate ecological status, accompanied by persistent organic and fecal contamination. Elevated concentrations of indicator bacteria, particularly *Escherichia coli*, confirm continuous anthropogenic pressure and highlight potential sanitary risks associated with water use. The findings further demonstrate that microbiological water quality is strongly influenced by hydrological conditions and seasonal variability. During low-flow periods, increased water temperature and reduced dilution capacity enhance microbial activity, leading to higher abundances of mesophilic bacteria and indicating an elevated risk of the presence of potentially pathogenic microorganisms [1]. Under such conditions, the use of river water for recreational purposes or irrigation of crops consumed without thermal processing may be limited. Although the dominance of oligotrophic bacterial communities suggests a moderate self-purification potential, this natural capacity is insufficient to counterbalance continuous pollutant inputs from both point and diffuse sources. These results emphasize the need for adaptive water management strategies, including the improvement of wastewater treatment infrastructure and the adjustment of treatment processes for drinking water production in accordance with seasonal and hydrological variations. Such measures are essential for achieving a better ecological status and ensuring the safe and sustainable use of water resources in the Velika Morava basin.

REFERENCES

[1] Ćirić SS, Petrović O, Aerobne mezofilne bakterije u monitoringu kvaliteta vode. Lešak (Serbia): University of Priština, Faculty of Agriculture; 2017.

[2] Petrović O, Gajin S, Matavulj M, *et al*. Mikrobiološko ispitivanje kvaliteta površinskih voda. Novi Sad: Institut za biologiju; 1998.

[3] APHA, AWWA, WEF. Standard Methods for the Examination of Water and Wastewater. 24th ed. Washington (DC): American Public Health Association; 2023. Method 9215B.

[4] International Organization for Standardization (ISO). Water quality – Enumeration of culturable microorganisms – Colony count by inoculation in a nutrient agar culture medium (ISO 6222:2024). Geneva: ISO; 2024.

[5] Republic of Serbia. Pravilnik o parametrima ekološkog i hemijskog statusa površinskih voda i parametrima hemijskog i kvantitativnog statusa podzemnih voda [Regulation on parameters of ecological and chemical status of surface waters and chemical and quantitative status of groundwater]. Službeni glasnik RS. 2011; 74.

[6] Republic of Serbia. Regulation on limit values of pollutants in surface and groundwaters and sediments and deadlines for their achievement. Official Gazette of the Republic of Serbia, No. 50/2012.

EcoTER'26
eco.tfbor.bg.ac.rs
32nd International Conference
Ecological Truth & Environmental Research
24–26 June 2026, Hotel Sunce,
Sokobanja, Serbia

Original Research

ANALYSIS OF PHYSICAL HAZARDS IN THE ENVIRONMENT AND THEIR IMPACT ON HUMAN HEALTH: CASE STUDY OF THE CITY OF NIŠ, REPUBLIC OF SERBIA

DOI: 10.5937/EcoTER26112D

Milan Đorđević[1,a*], Branka Stojanović[1,b], Aleksandar Zdravković[1,c], Danijela Stojadinović[1,d], Tanja Nikolić[1,e], Đorđe Miltenović[1,f]

[1] Academy of Professional studies South Serbia, Department of Higher Technology and Art school, Vilema Pušmana 17, 16000 Leskovac, SERBIA

[a] https://orcid.org/0009-0004-4455-4651 [b] https://orcid.org/0009-0002-3748-6422
[c] https://orcid.org/0000-0001-9906-3543 [d] https://orcid.org/0000-0002-6335-8101
[e] https://orcid.org/0009-0007-8932-6128 [f] https://orcid.org/0009-0003-0117-7414

Abstract

The subject of this paper is the identification and analysis of physical hazards (heat, microclimate parameters) transmitted through the area of Niš city. In the paper, 12 measurements of physical hazards were carried out during the day (from 6:00 a.m. to 6:00 p.m.) and in the evening (from 6:00 p.m. to 10:00 p.m.) at 12 selected monitoring places on the territory of the city of Niš from June 2024 until April 2025. Exceedances of measured physical hazards and their potential risk to human health were determined. In June and August 2024, there is a small risk of heat-related disorders for non-acclimatized persons doing heavy work outdoors. The analysis of identified physical hazards in the Niš city indicates the need to monitoring places and the application of personal and collective protective measures for people's work outdoors.

Keywords: heat, microclimate parameters, people's health.

INTRODUCTION

Physical environmental agents, including heat, light intensity, noise, and electromagnetic radiation, can have negative impacts on biological systems, affecting humans, animals, and other living organisms. While the effects of radiation are not visible to the human eye, elevated noise levels are perceived through hearing, and inadequate illumination is detected through the sense of vision [1]. Heat stress as a physical agent affects the working ability of exposed persons in warmer environments. A higher ambient temperature affects humans by causing heat accumulation in the body, which can lead to fatigue, muscle cramps, heat exhaustion, heat rash, and neurological and psychological effects, such as heat stress [2–4]. Wet-bulb globe temperature (WBGT) is an empirical index that considers thermal radiation, temperature, humidity, and airflow velocity. It is used to assess heat stress and can be determined in closed rooms, indoors (equation 1), but also in open spaces, outdoors (equation 2) [2,5–7].

* *milan.djordjevic3093@gmail.com*

$$WBGT_{in} = 0,7\ T_v + 0,3\ T_g \quad (1)$$

$$WBGT_{out} = 0,7\ T_v + 0,2\ T_g + 0,1\ T_a \quad (2)$$

where: T_v - natural ventilation wet bulb temperature (°C); T_g - temperature of the black globe thermometer (°C), and T_a - air temperature (°C).

Temperature of the black globe thermometer is a WBGT index variable used to determine heat stress [8]. Heat stress indices have advantages and disadvantages and have specific applications in various fields, such as industry, military, agriculture, and mining [2–5, 8].

Niš city is characterized by favorable conditions for living and economic development due to its moderate continental climate, advantageous geographical position, and an average altitude from 190–200 m. The mean annual air temperature is approximately 11.5 °C, while average maximum temperatures during the summer months reach from 29–30 °C. The city receives from 580–620 mm of precipitation annually, and average air humidity ranges from 60–65% in summer to 80–85% in winter [9]. In recent years, Niš city has experienced notable economic and infrastructural growth. The turnover of outdoor workers has increased, so it is necessary to identify and analyze heat and microclimate parameters in the urban environment of Niš to determine critical monitoring locations that may compromise environmental quality and the safety of people and workers.

EXPERIMENTAL PART

Description and methodology of measurements and monitoring places

Measurements of physical hazards in the environment on the territory of Niš city were carried out with portable measuring instruments at 12 selected monitoring places (Table 1) every second month from June 2024 to April 2025 (18–19 June 2024, 19–20 August 2024, 20–21 October 2024, 22–23 December 2024, 24–25 February 2025 and 22–23 April 2025).

Locations are in close proximity to gas stations, construction sites for various buildings and facilities and parks.

Table 1 *Monitoring places of physical hazards in the territory of the city of Niš*

Number of monitoring place	Location of the monitoring place	GPS coordinates	
		N	E
1.	Intersection of King Alexander Boulevard and Voždova Street	43°19'53.2"	21°53'11.4"
2.	Intersection of Boulevard Nemanjića and Vojvode Tankosića Street	43°19'35.1"	21°54'05.2"
3.	Čair Park – park in the city center	43°19'44.9"	21°53'52.0"
4.	Pariske komune Street – Elementary School “Dušan Radović”	43°19'30.6"	21°54'12.5"
5.	Factory Leoni (industrial zone)	43°20'28.9"	21°54'44.8"
6.	Roundabout near “Delta Planet”	43°19'20.5"	21°54'30.7"
7.	Aleksandra Medvedeva Street – Trade School	43°20'05.8"	21°53'16.0"
8.	Zetska Street – near Zlatni trag store	43°19'10.3"	21°53'25.3"
9.	Roundabout near University Clinical Center Niš	43°19'26.0"	21°53'40.6"
10.	12th February Boulevard– Technical school zone	43°20'40.2"	21°52'50.5"
11.	Roundabout of Studenička Street and Boulevard St Pantelejmon	43°33'54.3"	21°92'22.2"
12.	Boulevard Medijana – near MOL gas station	43°19'28.5"	21°54'55.0"

Physical hazards were recorded at all monitoring locations during both daytime (6:00 a.m. to 6:00 p.m.) and evening hours (6:00 p.m. to 10:00 p.m.). At each of the 12 selected sites, over the course of the monitored month, two standard 15-minute measurements were conducted-one in the daytime period and one in the evening. The paper analyzes the following physical agents: wet-bulb globe temperature (WBGT, ºC), temperature of the black globe thermometer (T_g, ºC), air temperature (T_a, ºC), relative humidity (%), and airflow velocity (m/s).

Portable devices were used for measurement is HT30 Heat Index WBGT Meter (Extech, China) for measuring heat stress indices (WBGT and T_g), and temperature and relative air humidity, and EN 300 Environmental Meter (Extech, Taiwan) for measuring airflow velocity.

RESULTS AND DISCUSSION

Microclimatic parameters

To assess heat stress several indices have been developed, which including environmental factors (temperature, humidity, and airflow velocity) and/or individual factors (metabolic heat, insulating properties of clothing) [10]. When calculating the WBGT index, metabolic rate, age, body mass index of people, and the influence of worker acclimatization are not considered. This index is included in the International Standard ISO 7243:2017, which was also adopted in the Republic of Serbia, which assesses the impact of heat during an 8-hour working day in a hot working environment [8,11,12]. The measured WBGT values according to the ISO standard are compared with the reference values of the WBGT index, which considers the workers' physical activity (metabolic level) and acclimatization [12,13]. Acclimatization implies a gradual physiological adaptation of the worker, which improves his tolerance to heat stress. This is achieved by subjecting the worker to physical activity for a certain period under heat stress conditions similar to those in his work environment [14]. The classification or determination of the metabolic rate is carried out according to the standard SRPS EN ISO 8996:2022 [12,15]. Higher identified WBGT values than the reference ones indicate a risk of heat-related disorders, and in this case, reducing the worker's heat load is necessary. It is also necessary to perform a better assessment of the thermal stress by the worker using the standard SRPS EN ISO 7933:2023 [12,16]. The clothing worn by workers provides thermal insulation and affects the process of evaporation of sweat from the skin surface, therefore it is necessary to correct the WBGT value (effective WBGT value) when workers do not wear standard clothing (thermal insulation 0.6 clo, cotton and permeable) by the SRPS standard EN ISO 9920:2012 [12,17].

Table 2 provides an overview of the results of measuring wet-bulb globe temperature (WBGT), black bulb temperature (T_g), and air temperature (T_a) during the day and evening for the observed period at 12 monitoring places. Based on the temperature measurements of the heat stress index and air, it is observed that the average WBGT, T_g, and T_a temperatures have high values in June and August 2024. at all monitoring places. In general, temperature values are higher during the day than in the evening in all months of measurement.

Table 2 *Average WBGT, T_g, and T_a values at the monitoring places for day and evening*

Monitoring place	Day						Evening					
	Jun 2024	Aug. 2024	Oct. 2024	Dec. 2024	Feb. 2025	Apr. 2025	Jun. 2024	Aug. 2024	Oct. 2024	Dec 2024	Feb. 2025	Apr. 2025
$WBGT_{av}$ (°C)												
1.	21.1	21.4	13.2	5.9	11.2	18.8	18.3	17.6	10.4	2.9	5.5	19.6
2.	22.8	21.7	12.4	6.4	13.4	18.1	18.2	20.1	11.2	3.7	3.7	17.7
3.	24.4	22.4	12.2	9.6	9.8	18.8	19.7	18.4	10.8	8.3	6.2	18.2
4.	24.6	24.8	10.8	8.8	12.8	16.6	19.8	18.6	13.6	7.1	7.4	17.6
5.	23.2	25.9	10.9	8.2	13.8	18.1	20.2	19.5	14.1	8.1	9.8	16.7
6.	23.2	23.1	10.3	8.4	12.5	18.9	19.9	19.1	13.6	5.7	9.1	16.9
7.	24.2	23.8	11.3	7.2	11.8	19.4	18.7	19.5	12.0	7.3	6.3	17.4
8.	24.5	22.4	12.4	8.8	11.3	20.6	17.7	19.6	11.9	4.6	5.4	17.2
9.	23.6	21.7	12.6	5.4	14.1	20.4	18.7	19.4	10.7	3.5	4.8	18.6
10.	23.4	23.8	13.3	4.9	12.2	21.3	20.4	18.8	11.8	3.4	6.3	18.4
11.	20.8	19.8	11.6	4.8	11.9	19.8	15.9	17.5	9.9	2.8	5.5	17.4
12.	19.3	22.6	12.6	4.9	11.9	18.7	20.9	18.1	11.5	2.5	4.6	17.4
T_{gav} (°C)												
1.	38.1	30.0	16.8	18.4	23.6	24.1	27.0	25.7	17.1	7.9	9.5	27.3
2.	34.6	29.8	17.9	15.4	28.2	25.1	28.8	32.8	17.1	11.3	9.1	23.8
3.	41.2	30.3	20.9	12.9	24.8	25.5	30.4	27.7	16.3	7.9	19.9	23.6
4.	42.7	37.8	22.4	20.1	26.1	26.6	32.0	27.5	14.1	9.8	8.3	23.2
5.	40.5	37.3	23.2	19.7	30.1	27.5	30.7	29.4	14.9	13.1	10.1	21.9
6.	39.6	33.9	25.0	17.9	26.7	26.9	31.8	29.2	15.1	13.4	6.6	22.2
7.	42.4	33.4	25.5	19.4	29.3	27.9	32.9	29.5	17.3	11.7	15.1	22.9
8.	39.2	31.2	22.2	16.2	33.4	26.0	31.7	33.0	16.4	8.1	15.4	22.5
9.	40.2	35.0	18.7	16.3	29.6	25.1	30.4	30.9	18.2	8.4	13.2	23.7
10.	39.1	33.5	19.7	15.5	27.4	24.7	32.3	28.7	16.2	6.4	20.3	25.4
11.	39.6	32.4	20.0	14.9	19.7	23.6	26.7	25.0	17.9	9.6	11.1	24.3
12.	35.1	33.3	22.3	16.1	24.7	25.6	33.4	25.8	16.7	6.9	7.9	24.4
T_{aav} (°C)												
1.	27.3	29.0	17.7	7.0	14.6	24.4	28.6	26.9	11.6	8.0	9.5	19.1
2.	35.3	31.3	17.9	7.3	14.7	24.2	29.6	28.6	13.2	8.9	13.6	20.7
3.	36.3	31.8	16.7	13.8	14.2	24.8	30.9	28.2	12.4	8.4	11.6	21.9
4.	34.1	41.9	15.8	13.4	18.7	22.8	30.7	27.7	17.4	11.1	13.4	21.1
5.	33.5	40.9	14.0	12.3	19.7	22.1	29.2	28.3	17.0	10.1	15.1	21.6
6.	34.4	35.6	16.1	11.6	18.1	22.4	30.9	28.5	17.5	7.9	12.2	22.1
7.	36.6	34.9	14.1	11.3	13.7	22.7	28.6	28.3	11.4	10.7	16.6	19.0
8.	36.3	32.3	15.6	10.1	11.3	23.5	27.8	27.6	13.6	5.4	13.3	22.8
9.	35.3	31.1	16.7	6.6	19.7	24.3	28.7	29.2	13.9	7.3	11.6	20.7
10.	31.9	33.6	19.6	5.7	15.7	24.6	31.9	26.8	15.9	7.2	9.2	23.9
11.	23.4	25.2	16.3	6.7	12.5	22.2	24.3	26.1	9.1	7.1	9.9	19.3
12.	29.4	30.2	16.6	8.4	14.2	21.9	32.1	27.3	11.2	4.0	7.2	19.7

Table 3 shows reference limit WBGT values according to ISO 7243:2017, depending on the metabolic rate and acclimatization or non-acclimatization of persons.

The WBGT index measurements were carried out in the environment, so if we assume that the workers work in acclimatized conditions, there is no risk of heat impact on their bodies, except for the monitoring place 5 (Factory Leoni, industrial zone) for August 2024 in the daytime period measurements and a very high metabolic level of the person, 25.9°C (Table 2) [12]. Non-acclimatized workers with high and very high physical activity, who work outdoors in Niš city, are generally in June and August 2024 at most monitoring places ($WBGT_{av}$ from 19.3 to 25.9°C) subject to probably a small heat stress in the daytime period. The same is the

case for April 2025 at monitoring places 8 ($WBGT_{av}$ = 20.6°C), 9 ($WBGT_{av}$ = 20.4°C) and 10 ($WBGT_{av}$ = 21.3°C). Intense and very intense work to the maximum rhythm of the hands and body; carrying heavy material; working with a shovel and a blacksmith's hammer; intense clutching or digging; climbing stairs or ladders; walking at a speed greater than 5.5 km/h on a flat surface, etc., is characterized by a high and very high metabolic level of workers [15]. In the evening measurement period, the limit reference values exceeded in non-acclimatized persons with a very high metabolic level ($WBGT_{ref}$ = 20.0°C) occur in June 2024. at monitoring places 5, 10, and 12 ($WBGT_{av}$ from 20.2 to 20.9°C) and in August 2024. at monitoring place 2 ($WBGT_{av}$ = 20.1°C), as can be seen from Tables 2 and 3. Heat accumulation in the human body leads to dehydration, rashes, cramps, fainting, exhaustion, and heat stroke [15]. In addition, heat-related disorders of the workers, such as fatigue and sleepiness, can cause distraction and error and thus affect the worker's ability to work and productivity. For the worker to show satisfactory work performance, the heat generated from physical activity must be released by lowering the ambient temperature [18]. When the effective temperature exceeds 25°C, worker productivity decreases, while at temperature values above 33°C, productivity decreases by half [19].

Table 3 *Reference limit WBGT values for acclimated and non-acclimated people for metabolic level classes*

The class (metabolic level)	Metabolic level (W)	Reference limit WBGT values (°C)	
		Acclimatized persons	Unacclimatized persons
0 (resting)	115	33	32
1 (low metabolic level)	180	32	29
2 (moderate metabolic level)	300	28	26
3 (high metabolic level)	415	26	23
4 (very high metabolic level)	520	25	20

The American Conference of Governmental Industrial Hygienists (ACGIH) prescribes a workplace threshold limit value (TLV). The time-weighted average WBGT value, according to ACGIH [14], is used if work and rest are distributed over more than one location. Depending on the percentage of work and regeneration and work intensity, TLV values are defined, with the lowest values for heavy work (50 to 75% work and rest cycle), 27.5°C and very heavy work (25 to 50% work and rest cycle), 28.0°C. The $WBGT_{av}$ values in Table 2 do not exceed the TLV values under conditions where workers are in standard clothing and acclimatized to the heat. Under these conditions (work and rest cycle, workload), the action limit for non-acclimatized healthy and hydrated workers is 24.0 and 24.5°C [14]. Thus, workers who performed work outdoors during the daytime period of June 2024 were exposed to a low risk of heat stress at monitoring places 3, 4, 7, and 8 and in August 2024. at monitoring places 4 and 5 ($WBGT_{av}$ > 24.0°C).

From this analysis, it is concluded that workers during hard and very hard work in non-acclimatized conditions in June and August 2024, primarily in the daytime, can accumulate heat that exceeds the limits according to TLV values [14], which can lead to thermal disorders of the organism. This fact is supported by high T_{gav} and T_{aav} values in June - daytime period: T_{gav} = 34.6 to 42.7°C, T_{aav} = 23.4 to 36.6°C, evening period: T_{gav} = 26.7 to

33.4°C, T_{aav} = 24.3 to 32.1°C, and in August - daytime period: T_{gav} = 29.8 to 37.8°C, T_{aav} = 25.2 to 41.9°C, evening period: T_{gav} = 25.0 to 33.0°C, T_{aav} = 26.1 to 29.2°C.

Monitoring people's exposure to temperature, relative humidity, and airflow velocity can give a realistic picture of the impact of heat stress on them. In the Republic of Serbia, the Rulebook on preventive measures for safe and healthy work at the workplace [20] defines the values of temperature, relative humidity, and airflow velocity that ensure safe and healthy work indoors. Relative humidity has an impact on human health, and the optimal relative humidity for the workplace is in the range of 40 to 60%. The ideal lower limit of relative air humidity is reduced to 30% for heavy and very heavy work and 20% for work in the environment. At high temperatures, the relative humidity of the air should be reduced because a person may feel exhausted. At a relative humidity of over 60%, sweating and heat release become difficult, and the person's body temperature increases [18,19].

In June 2024, values exceeded the relative air humidity of 60% during the daytime at certain monitoring places. The relative humidity of the air in the daytime and evening periods in August 2024, February, and April 2025 falls below 20% relative humidity at all or individual monitoring places. In conditions of less than 40% relative humidity due to dry air, sores in the throat and nose are possible [18, 19]. Airflow velocity was not detected at most monitoring places; it was zero, while in cases where it was detected, it ranged from 0.1 to 1.1 m/s.

The obtained average WBGT, T_g, T_a, reference WBGT limit values, threshold WBGT limit value, and values of relative air humidity in June and August 2024 for high and very high metabolic levels of unacclimatized outdoor workers indicate a low risk of heat stress in the summer period. This is expected because high air temperature and WBGT index values are reached during the summer.

CONCLUSION

Nowadays, the expansion of cities and infrastructure, the growth of traffic, the widespread production of technological devices, along with phenomena such as ozone layer depletion and the greenhouse effect, have significantly increased the presence of potential pollutants and physical hazards in the environment.

The paper identified a small risk of heat impact on humans during the day and evening in the summer months. The measured values are generally within the prescribed limits so outdoor workers can feel comfortable in their working conditions. This, in turn, affects their physical and mental health and prevents the occurrence of accidental situations and serious diseases. Certain microclimate parameters, heat indices, temperature and air humidity clearly show that in June and August 2024, milder symptoms of heat stress may occur in non-acclimatized workers during heavy and very heavy outdoor work. People who work outdoors in the summer for medium- and low-intensity work are not at risk of heat stress.

Depending on the outdoor workplace, people can be protected by appropriate personal protective equipment, reduced exposure to direct sunlight, and increased rest time compared to working time.

Based on the analysis, it can be concluded that the microclimatic parameters (heat, humidity, and airflow velocity) can have a negative effect on the health of the working population of the city of Niš in the summer months.

REFERENCES

[1] Vulević, B., Čedomir, B. Ecologica 2012, 67, 497–500.

[2] Prokeš, B., Mačvanin, N., Simikić, M., *et al*., Savremena poljopr. tehn. 2014, 40 (4), 229–238.

[3] Mazloumi, A., Golbabaei, F., Khani, S.M., *et al*. Health Promot. Perspect. 2014, 4 (2), 240–246.

[4] Monazzam, M.R., Golbabaei, F., Hematjo, R., *et al*. Int. J. Occup. Hyg. 2014, 6 (1), 6–10.

[5] Budd, G.M. J. Sci. Med. Sport. 2008. 11 (1), 20–32.

[6] Dehghan, H., Mortazavi, S.B., Jafari, M.J., *et al*. J. Res. Med. Sci. 2012, 17 (12), 1108–1113.

[7] Golbabaei, F., Hajizadeh, R., Monazzam, M.R., *et al*. Int. J. Occup. Hyg. 2014, 6 (3), 143–148.

[8] Lilić, N.M., Cvjetić, A.S. Tehnika – Rudar. Geol. Metal. 2019, 74 (4), 517–526.

[9] Climate-Data.org, Niš climate data, Available from: https://en.climate-data.org/europe/serbia/nis/nis-1268/

[10] Sharma, M., Alam, S., Suri, N.M., *et al*. J. Therm. Eng. 2021, 7 (14), 2068–2092.

[11] Sharma M., Suri N. M., et al. Int. J. Environ. Sci. Technol. 2022, 19 (11), 11421–11434.

[12] SRPS EN ISO 7243. Ergonomics of the thermal environment – Assessment of heat stress using the WBGT index, 2017.

[13] Gao, C., Kuklane, K., Östergren, P.O., *et al*. Int. J. Biometeorol. 2018, 62 (3), 359–371.

[14] American Conference of Governmental Industrial Hygienists. TLVs for Chemical Substances and Physical Agents and Biological Exposure Indices. Cincinnati: ACGIH; 2022.

[15] SRPS EN ISO 8996. Ergonomics of the thermal environment – Determination of metabolic rate, 2022.

[16] SRPS EN ISO 7933. Ergonomics of the thermal environment – Analytical determination and interpretation of heat stress using predicted heat strain, 2023.

[17] SRPS EN ISO 9920. Ergonomics of the thermal environment – Estimation of thermal insulation and water vapour resistance of clothing, 2012.

[18] Kahya, E., Ulutas, B.H., Ozkan, N.F., J. Eng. Sci. Des. 2018, 6 (1), 38–46.

[19] Babalık F., Ergonomics for Engineers, 5th ed., Dora Publishing, Bursa, 2016.

[20] Official Gazette of the Republic of Serbia, No. 21/2009 and 1/2019. Rulebook on preventive measures for safe and healthy work at the workplace.

EcoTER'26
eco.tfbor.bg.ac.rs
32nd International Conference
Ecological Truth & Environmental Research
24–26 June 2026, Hotel Sunce,
Sokobanja, Serbia

Original Research

IDENTIFICATION AND ANALYSIS OF NON-IONIZING ELECTROMAGNETIC RADIATION IN THE ENVIRONMENT: CASE STUDY OF LESKOVAC CITY, REPUBLIC OF SERBIA

DOI: 10.5937/EcoTER26119D

Milan Đorđević[1,a*], Branka Stojanović[1,b], Aleksandar Zdravković[1,c], Danijela Stojadinović[1,d], Tanja Nikolić[1,e], Milena Nikolić[1,f]

[1]Academy of Professional studies South Serbia, Department of Higher Technology and Art school, Vilema Pušmana 17, 16000 Leskovac, SERBIA

[a] https://orcid.org/0009-0004-4455-4651 [b] https://orcid.org/0009-0002-3748-6422
[c] https://orcid.org/0000-0001-9906-3543 [d] https://orcid.org/0000-0002-6335-8101
[e] https://orcid.org/0009-0007-8932-6128 [f] https://orcid.org/0000-0002-6631-936X

Abstract

The man is daily exposed to radiation and heat while moving through space and carrying out his activities, and these physical hazards adversely affect both people and the environment. The subject of this paper is the identification and analysis of non-ionizing electromagnetic radiation transmitted through the area of Leskovac city. In the paper, 12 measurements of non-ionizing electromagnetic radiation were carried out during the day (from 6:00 a.m. to 6:00 p.m.) and in the evening (from 6:00 p.m. to 10:00 p.m.) at 12 selected monitoring places on the territory of the Leskovac city from June 2024 until April 2025. Monitoring places 1, 3, 7, 9, and 11 can be considered sources of non-ionizing electromagnetic radiation of special interest. The impact of non-ionizing electromagnetic radiation on the population of Leskovac city, as well as workers who work outdoors during the day and evening, has not been identified.

Keywords: monitoring, electromagnetic radiation, people's health.

INTRODUCTION

Physical agents in the environment, such as heat, illuminance, noise, and electromagnetic radiation, have adverse effects on biological systems, people, animals etc. The effects of radiation are invisible to the naked eye, while the impact of increased noise can be felt with the sense of hearing and poor illuminance with the sense of sight [1].

”Invisible pollution” of a physical nature that occurs in the environment is non-ionizing radiation (NIR). These are electromagnetic radiations that do not have sufficient quantum energy to cause ionization of atoms, molecules, or tissues: ultraviolet radiation (UV), visible light, infrared radiation (IC), radiofrequency radiation (RF), extremely low-frequency electromagnetic fields (ELF), and static and stationary electromagnetic fields. The harmful effects of electromagnetic fields or waves on the environment can be monitored by measuring the strength of the electric (*E*) and magnetic fields (*H*), as well as radiation power density-

* *milan.djordjevic3093@gmail.com*

irradiance (*S*) [2–4]. There is some evidence that non-ionizing radiation adversely affects human and animal health. Biological systems exposed to weak electromagnetic fields, even below safety guidelines, show changes in functionality [5]. The International Agency for Research on Cancer (IARC) and the World Health Organization (WHO) have classified ELF magnetic fields produced by electrical devices in group 2B (possibly carcinogenic to humans). These organizations also pointed out that RF radiation can increase the risk of malignant brain tumors in humans [6].

Leskovac city is suitable for living and basic economic activities thanks to its mild temperate-continental climate, favorable altitude (210–240 m), and good location between the highlands and lowlands. In recent years, the city of Leskovac has been developing economically and infrastructurally, which in turn has led to an increase in traffic intensity, communal noise, greater availability of household electrical and wireless devices and appliances, radio and television antennas, mobile phone base stations, and the expansion of electrical and distribution transmission lines. Therefore, the aim of this paper is to identify and analyze the non-ionizing radiation in the urban environment of the city of Leskovac, determine the monitoring places that threaten its quality and the safety of people.

MATERIALS AND METHODS

Description and methodology of measurements and monitoring place

Measurements of electromagnetic radiation in the environment on the territory of Leskovac city were carried out with portable measuring instrument at 12 selected monitoring places (Table 1) bimonthly from June 2024 to April 2025 (16–17 June 2024, 18–19 October 2024, 22–23 February 2025, and 20–21 April 2025). The selected monitoring locations are situated near high-frequency repeaters, mobile phone base stations, and radio and television antennas on the buildings. There are gas stations and construction sites of many facilities near some monitoring places.

Table 1 *Monitoring places of non-ionizing electromagnetic radiation in the city of Leskovac*

Number of monitoring place	Location of the monitoring place	GPS coordinates	
		N	E
1.	The intersection of Bulevar oslobođenja and 28 Marta streets	42°59'47.7"	21°57'20.3"
2.	The intersection of Bulevar oslobođenja and Južnomoravskih Brigada streets	42°59'46.7"	21°56'34.8"
3.	Moše Pijade Street - a park in the city center	42°59'43.2"	21°56'52.7"
4.	Sava Kovačević Street - Elementary School "Vuk Karadžić"	43°00'08.0"	21°56'45.9"
5.	Tekstilna Street - Factory "Falke"	43°00'23.7"	21°56'29.2"
6.	Niška and Nikola Pašića Bulevar Street - roundabout near the "Metla Komerc" store	43°00'12.7"	21°56'10.3"
7.	Dubočica Street - Trade and Hospitality School	42°59'54.8"	21°55'38.4"
8.	Stanoja Glavaša Street near the "Aman" store	42°59'27.9"	21°55'43.9"
9.	Roundabout near the Leskovac City Hospital	42°59'39.3"	21°56'18.7"
10.	Vlajkova Street - Chemical Technology School "Božidar Đorđević Kukar"	42°59'04.3"	21°56'58.4"
11.	The intersection of Njegoševa and Jadranska streets	42°59'50.3"	21°57'42.0"
12.	Kralja Petra Prvog Street - near the "Mol" pump	42°59'30.4"	21°57'38.2"

Physical hazards were detected at each monitoring place during the day (from 6:00 a.m. to 6:00 p.m.) and in the evening (from 6:00 p.m. to 10:00 p.m.). At each of the 12 monitoring places during the observed month in the specified period, two reference 15-minute measurements were performed in the day and evening periods. The paper analyses the following physical agents: electric (*E*, V/m), magnetic field strength (*H*, A/m) and irradiance (*S*, W/m^2).

Portable device was used for measurements is 480836 RF/EMF Strength Meter (Extech, Taiwan) for monitoring high-frequency radiation in the range of 50 MHz to 3.5 GHz characteristic of mobile phone base stations, locating RF access points, detecting RF wireless networks (Wi-Fi) through electric and magnetic field strength and irradiance.

The results obtained in the paper were statistically processed and compared with the prescribed values according to the laws, regulations and standards of the Republic of Serbia and in the world and available safety guidelines.

RESULTS AND DISCUSSION

The regulation in field of non-ionizing electromagnetic radiation in the Republic of Serbia is regulated by: the Law on non-ionizing radiation protection [7], the Rulebook on the limits of exposure to non-ionizing radiation [8], the Rulebook on the sources of non-ionizing radiation of special interest, types, sources, manner, and period of their examination [9], the Rulebook on preventive measures for safe and healthy work when exposed to electromagnetic field [10] and the SRPS EN 50413:2020/A1:2025 standard [11].

The Rulebook on the limits of exposure to non-ionizing radiation prescribes reference limit levels for persons' exposure to electric, magnetic, and electromagnetic fields (Table 2). The adopted basic limits and reference limit levels in the Rulebook are stricter than those recommended by the ICNIRP (International Commission on Non-Ionizing Radiation Protection) guidelines [12]. Reference limit levels are used to assess population exposure and determine the probability of exceeding basic limits. ICNIRP prescribes basic limits and reference limit levels for two exposure scenarios (occupational and general public) depending on the time of exposure to the electromagnetic field of frequencies from 100 kHz to 300 GHz.

Table 2 *Reference limit levels of exposure of the population to the electromagnetic field for the investigated range of radiation frequencies*

Frequencies	Electric field strength, *E* (V/m)	Magnetic field strength, *H* (A/m)	Power density (equivalent plane wave), S_{eq} (W/m^2)
0-400 MHz	11.200	0.0292	0.326
400-2000 MHz	$0.55\ f^{1/2}$	$0.00148\ f^{1/2}$	$f/1250$
2-10 GHz	24.400	0.064	1.600

f - radiation frequencies

The Rulebook on the sources of non-ionizing radiation of special interest, types, sources, manner, and period of their examination [9] defines sources of non-ionizing radiation of special interest. These are sources of electromagnetic radiation that can be harmful to human

health and are defined as stationary and mobile sources whose electromagnetic field in the zone of increased sensitivity reaches at least 10% of the reference limit value prescribed for that frequency. The owners of these sources are obliged to perform periodic measurements.

According to frequency, non-ionizing electromagnetic fields are classified into very low (ELF, up to 300 Hz), intermediate (IF, from 300 Hz to 10 MHz), and radio frequency fields (RF, 10 MHz to 300 GHz). In addition to the mentioned classification, the European Commission divides non-ionizing radiation into one more group static fields, *e.g.*, electric fields of capacitors of certain systems in industry and fields of natural and artificial magnets [3,13]. The sources of the ELF field are devices that transmit electrical energy at a frequency of primarily 50 or 60 Hz, high-voltage transmission lines, distribution networks, and household electrical appliances. Telecommunication systems such as mobile phone base stations, radio and television transmitters, mobile phones and wireless devices, microwave medical devices used in diagnosis and therapy, and microwave link systems produce RF fields [3,14,15].

In countries with modern economies, there is increased concern about the harmful effects of RF radiation from mobile phones and radiation due to the increase in mobile phone base stations and Wi-Fi stations, especially with the introduction of 5G wireless systems operating at higher frequencies [5].

Table 3 shows the average electric (E_{av}) and magnetic field (H_{av}) strength and radiation density (S_{av}) at the observed monitoring places during the day and night periods.

The highest measured average value of the electric field strength is at monitoring place 11 (the intersection of Njegoševa and Jadranska streets), 2.004 V/m (Table 3), which is lower than the reference limit levels in the detection frequency range (50 MHz-3.5 GHz), 11.200–24.400 V/m (Table 2). The exposure factor is determined by calculating the ratio of the average measured electric field value to the reference limit level. If we consider the lower reference limit, the exposure factor is 0.179, which cannot exceed 1 or 100%. All measured values of electric field strength are within the established reference exposure limit level. At the monitoring place 1 (The intersection of Bulevar oslobođenja and Južnomoravskih Brigada streets), 3 (Moše Pijade Street - a park in the city center), 7 (Dubočica Street - Trade and Hospitality School), 9 (Roundabout near the Leskovac City Hospital), in certain months of measurement in the daytime and evening period, the exposure factor for the strength of the electric field is greater than 0.1 and 10%, respectively. This indicates the possibility that the sources of non-ionizing radiation that cause the increased intensity of the electric field at these measuring points are considered sources of special interest. There are two high-frequency repeaters near the intersection of Njegoševa and Jadranska Street, which probably contribute to the increase of non-ionizing radiation at the examined monitoring places. Monitoring place 1 is near measuring point 11, so high-frequency electromagnetic waves from two larger repeaters spread at this place as well. In addition, there is a possibility of the influence of antennas and station devices for telephones and cable television on the tops of surrounding buildings. The roundabout near the city hospital Leskovac (monitoring place 9) has a higher mean electric field strength, which is most likely a consequence of the existence of a large high-frequency radiation repeater on Hisar hill. Monitoring places 3 and 7 are surrounded by residential blocks where there are smaller transmitters of mobile phones, TV stations, and

cable television that contribute to higher values of physical quantities that characterize electromagnetic radiation.

Table 3 *Average values of electric and magnetic field and irradiance at the monitoring places for the day and evening*

Monitoring place	Day						Evening					
	Jun.	Aug.	Oct.	Dec.	Feb.	Apr.	Jun.	Aug.	Oct.	Dec.	Feb.	Apr.
						E_{av} (V/m)						
1.	1.313	1.280	1.525	0.488	0.609	0.661	1.740	1.189	1.196	1.300	0.576	0.638
2.	0.359	0.510	0.459	0.245	0.330	0.386	0.080	0.327	0.755	0.315	0.327	0.240
3.	0.861	0.945	1.625	0.744	0.550	0.461	0.634	0.715	1.167	0.744	0.675	0.312
4.	0.353	0.197	0.182	0.051	0.110	0.057	0.056	0.329	0.501	0.019	0.051	0.026
5.	0.639	0.233	0.485	0.303	0.154	0.301	0.226	0.509	0.565	0.438	0.313	0.312
6.	0.145	0.016	0.010	0.006	0.005	0.007	0.028	0.017	0.060	0.003	0.011	0.011
7.	0.702	0.430	1.147	0.661	0.664	0.275	0.320	0.465	1.378	0.620	0.187	0.205
8.	0.236	0.396	0.350	0.105	0.264	0.257	0.469	0.433	0.358	0.310	0.371	0.043
9.	0.569	0.838	0.193	0.765	0.535	0.428	1.493	1.667	0.654	0.897	0.596	0.356
10.	0.504	0.049	0.017	0.041	0.036	0.023	0.519	0.189	0.023	0.012	0.025	0.019
11.	1.794	1.715	2.004	1.000	0.896	0.858	1.383	1.668	1.826	1.560	0.843	0.617
12.	0.191	0.299	0.124	0.154	0.203	0.303	0.385	0.299	0.261	0.108	0.357	0.228
						H_{av} (mA/m)						
1.	4.001	3.396	4.255	1.217	1.617	1.753	4.618	3.156	3.173	3.448	1.196	1.692
2.	0.889	1.137	1.196	0.650	0.817	1.025	0.212	0.745	1.352	0.835	0.931	0.637
3.	2.138	2.707	4.312	1.974	1.461	1.223	1.627	1.895	3.096	1.974	1.792	0.827
4.	0.938	0.502	0.477	0.135	0.223	0.151	0.150	0.874	1.327	0.052	0.460	0.070
5.	1.612	0.778	1.286	0.625	0.408	0.798	0.610	1.465	1.641	1.163	0.831	0.529
6.	0,391	0.044	0.039	0.015	0.016	0.022	0.079	0.046	0.170	0.008	0.031	0.031
7.	1,894	0.918	2.960	1.753	1.402	0.729	0.890	1.233	3.645	1.617	0.498	0.544
8.	0.633	1.050	0.928	0.144	0.702	0.681	1.137	1.147	0.949	0.846	1.021	0.114
9.	1.511	2.224	0.532	2.030	1.636	1.163	3.962	4.655	2.187	2.380	1.582	0.946
10.	1.204	0.132	0.047	0.129	0.104	0.079	1.376	0.545	0.062	0.033	0.066	0.051
11.	4.761	4.684	5.368	2.653	2.380	2.276	3.671	3.575	4.844	4.138	2.249	1.655
12.	0.543	0.645	0.330	0.408	0.539	0.642	0.623	0.912	0.693	0.287	0.946	0.606
						S_{av} (mW/m^2)						
1.	3.716	4.349	7.110	0.603	0.986	1.056	8.036	3.014	3.720	4.482	0.742	1.080
2.	0.342	0.689	0.560	0.186	0.251	0.396	0.016	0.284	1.513	0.263	0.349	0.153
3.	1.971	2.268	6.938	1.469	0.558	0.564	1.068	1.165	3.613	1.032	1.211	0.258
4.	0.363	0.097	0.085	0.006	0.018	0.008	0.008	0.288	0.664	0.001	0.006	0.002
5.	1.121	0.105	0.624	0.025	0.062	0.240	0.130	0.616	0.812	0.510	0.260	0.135
6.	0.083	0.001	0.001	0.000	0.001	0.000	0.002	0.001	0.001	0.006	0.000	0.000
7.	1.539	0.409	3.303	2.316	0.742	0.200	0.305	0.574	5.037	1.019	0.093	0.111
8.	0.135	0.322	0.325	0.008	0.185	0.131	0.530	0.497	0.168	0.254	0.424	0.004
9.	0.886	1.974	0.117	1.554	1.009	0.510	5.367	8.170	2.100	2.137	0.943	0.337
10.	0.721	0.006	0.001	0.001	0.004	0.002	0.714	0.112	0.001	0.001	0.000	0.001
11.	0.642	8.412	10.860	2.118	2.137	1.954	3.787	6.386	8.849	3.414	1.886	1.056
12.	0.125	0.157	0.042	0.063	0.109	0.155	0.263	0.322	0.181	0.036	0.337	0.155

Also, in monitoring place 11, the maximum average magnetic field strength was identified, 0.005368 A/m. These values also do not exceed the prescribed reference limit levels (H = 0.0292–0.064 A/m). Monitoring at locations 1, 3, 7, 9, and 11 shows that during certain months and both daytime and evening periods, the average magnetic field strength exceeds 10% of the reference limit value when compared to a lower reference limit. In this context, the exposure factor ranges from 0.101 to 0.184. Based on the measured average values of magnetic field strength, the sources contributing to these levels at places 1, 3, 7, 9, and 11 may be classified as sources of non-ionizing radiation of special interest. It is recommended

that the magnetic field strength be measured periodically. In general, in the months of June, August and October, higher mean values of the magnetic field were detected compared to the other months of measurement and for the daytime and evening measurement periods.

From the physical parameters measured in this paper, the Rulebook on the limits of exposure to non-ionizing radiation [8] prescribes a basic limit of population exposure to radiation only for power density in the frequency range of 10-300 GHz (10 W/m^2). The average measured values of physical parameters for the electromagnetic field at the monitoring places in the territory of the city of Leskovac are below the defined limit reference levels in the Republic of Serbia. Residents of the city of Leskovac at the investigated monitoring places are exposed to electromagnetic radiation of 50 MHz-3.5 GHz, without risk to health (insignificant biological tissue response).

RF radiation from high-power telecommunication systems can cause serious damage to the human body if a person is near the RF source and in the direction of the direct beam of radiation. The impact of electromagnetic radiation on a living organism depends on the intensity and frequency of the radiation and the distance of the person from the radiation source. High-frequency radiation with irradiance over 10 mW/cm^2 can cause tissue heating in humans, the so-called thermal effect [2]. According to experimental tests by many authors, in people exposed to RF radiation, the concentration of reactive oxygen species (ROS) increases or decreases, as does the degree of cancer cell growth. This may indicate that a person exposed to RF radiation suffers from oxidative stress and that there is a probability of some form of cancer [5].

From Table 3, it is evident that the mean power density values are significantly lower than the basic limits specified in the rulebook. The mean irradiance values do not exceed the reference limit values; in fact, they are even below 10% of the reference limit, S_{eq} = 0.326–1.600 W/m^2, (indicating an exposure factor of less than 0.1) at all monitoring places during both daytime and evening periods across all months of measurement. The highest mean power density was recorded at monitoring place 11, with a value of 0.010860 W/m^2. Monitoring places 1, 3, 7, 9, and 11 are notable for their elevated mean power density values. Additionally, the measurements taken in June, August, and October show higher power density levels in most places during both daytime and evening periods compared to the other months measured.

CONCLUSION

Today, urbanization and infrastructural development of cities, intensive traffic development, production of technical devices, creation of ozone holes, and the greenhouse effect have increased the number of potential pollutants and physical hazards in the environment.

On the territory of the city of Leskovac, measurements were carried out from June 2024 to April 2025.

Non-ionizing radiation do not endanger the inhabitants of Leskovac. The values of radiation parameters, electric and magnetic field strength, and irradiance are far below the prescribed basic and reference levels.

For the electric and magnetic field strength parameters at monitoring places 1, 3, 7, 9, and 11, the exposure factor ranges from 0.1 to 0.2. During specific months of measurement at these locations, the average values of electric and magnetic field strength were recorded at levels exceeding 10% of the reference limit. The sources contributing to the higher intensity of the electromagnetic field at these monitoring places include high-frequency repeaters, mobile phone base stations, mobile phone transmitters, TV stations, and cable television. These are considered sources of non-ionizing radiation that warrant special attention. It is essential to periodically monitor electromagnetic radiation from these sources by measuring its intensity.

Measured non-ionizing radiation do not affect the mental and physical health of the population of the city of Leskovac.

REFERENCES

[1] Vulević, B., Čedomir, B. Ecologica 2012, 67, 497–500.

[2] Aranđelović, M., Jovanović, J. Medicina rada. Niš: Medicinski fakultet; 2009.

[3] Krstić, I., Krstić, D., Kusalo, A. Inž. Zaštite. 2011, 1 (1), 45–58.

[4] Vulević B, Belić Č In: Proceedings of the Environment to Europe – EnE13; 2013; Belgrade, Serbia.

[5] Barnes, F., Freeman, E.R. Front. Public Health. 2022, 10, 994758.

[6] International Agency for Research on Cancer. *IARC Monogr*. 2013, 102.

[7] Official Gazette of the Republic of Serbia, No. 36/2009. Law on Non-ionizing Radiation Protection.

[8] Official Gazette of the Republic of Serbia, No. 16/2025. Rulebook on the limits of exposure to non-ionizing radiation.

[9] Official Gazette of the Republic of Serbia, No. 104/2009. Rulebook on the sources of non-ionizing radiation of special interest, types, sources, manner, and period of their examination.

[10] Official Gazette of the Republic of Serbia, No. 111/2015 and 130/2021. Rulebook on preventive measures for safe and healthy work when exposed to electromagnetic fields.

[11] SRPS EN 50413:2020/A1:2025. Basic standard on measurement and calculation procedures for human exposure to electric, magnetic and electromagnetic fields (0 Hz - 300 GHz), 2025.

[12] International Commission on Non-Ionizing Radiation Protection. Health Phys. 2020, 118 (5), 483–524.

[13] European Commission. Possible effects of electromagnetic fields (EMF) on human health. 2007.

[14] Lewczuk, B., Redlarski, G., Żak A., *et al.* Biomed Res. Int. 2014, 169459.

[15] Čubonović S, Ranković A, Mijailović V In: Proceedings of the 36th CIGRE Serbia Conference; 2023; Zlatibor, Serbia. p. 1529–1541.

Original Research

COMBINED METEOROLOGICAL MEASUREMENTS OF URBAN AND RURAL THERMAL ENVIRONMENTS IN BELGRADE

DOI: 10.5937/EcoTER26126P

Sanja Pavlović[1,a*]

[1] Academy of Applied Studies Polytechnic, Katarine Ambrozić 3, Belgrade, SERBIA

[a] https://orcid.org/0000-0002-9596-8393

Abstract

Urbanization and climate change jointly intensify local thermal environments, leading to pronounced urban heat island (UHI) effects that impact environmental quality, human health, and energy demand. This study investigates urban microclimate variability through a comparative analysis of urban and rural temperature regimes using a combination of unmanned aerial vehicle (UAV)-based thermal imaging and ground-based meteorological measurement data. The research was conducted in and around Belgrade, where representative urban and rural sites were selected to capture contrasting land surface characteristics. UAV thermal surveys provided high-resolution spatial data on surface temperature distribution. The urban heat island intensity was quantified as the temperature difference between urban and rural environments. Preliminary results indicate a consistent positive temperature anomaly in urban areas, with the strongest UHI intensity observed during summer months and nighttime due to heat retention by built surfaces. Spatial analysis reveals significant heterogeneity within the urban environment, with green spaces exhibiting localized cooling effects. The findings highlight the importance of integrating remote sensing and in situ measurements to improve the understanding of urban climate dynamics under changing climatic conditions. This study contributes to ongoing research on urban climate adaptation by providing a scalable methodological framework and empirical evidence relevant for sustainable urban planning, environmental monitoring and aviation weather forecasting and operational safety.

Keywords: urban heat island (UHI), UAV thermal imaging, land surface temperature (LST), environmental monitoring, aviation safety.

INTRODUCTION

Rapid urbanization and global climate change are increasingly recognized as interacting drivers of environmental transformation, particularly at the local scale [1,2]. Urban areas alter the natural surface energy balance through modifications in land cover, surface albedo, and anthropogenic heat release, leading to the formation of the urban heat island (UHI) effect [3]. This phenomenon, characterized by higher temperatures in urban areas compared to their rural surroundings, has important implications for thermal comfort, air quality, and public health [4]. In recent decades, the interaction between climate change and urbanization has intensified, with rising background temperatures contributing to stronger and more persistent UHI effects [2,5], thereby increasing the frequency and severity of heat extremes in cities.

* *spavlovic@politehnika.edu.rs.*

Understanding urban microclimate variability is therefore essential for developing effective mitigation and adaptation strategies. However, conventional meteorological observations, typically based on sparse ground-based stations, often fail to capture the spatial complexity and fine-scale variability of urban thermal environments [6]. In response to these limitations, remote sensing approaches, particularly those based on unmanned aerial vehicles (UAVs), have emerged as powerful tools for high-resolution monitoring of surface temperature and land-atmosphere interactions [7]. UAV-based thermal imaging enables detailed mapping of spatial temperature patterns, providing valuable insights into intra-urban variability and complementing traditional in situ measurements.

Previous studies conducted in Belgrade have confirmed the presence of a significant urban heat island and highlighted its seasonal variability, as well as its impact on thermal comfort and urban living conditions [8,9]. These findings emphasize the importance of localized studies that integrate advanced measurement techniques with conventional observations.

In this context, the present study aims to investigate urban microclimate variability under climate change conditions by integrating UAV-derived thermal data with ground-based meteorological observations. The specific objectives are: 1) to quantify temperature differences between urban and rural environments, 2) to analyze the temporal variability of UHI intensity, and 3) to assess the spatial distribution of thermal anomalies within urban areas.

By focusing on a representative case study in Belgrade, this research contributes to a better understanding of the local expression of global climate processes and demonstrates the applicability of combined measurement approaches in urban climate analysis.

MATERIALS AND METHODS

Study Area

The study was conducted along urban-rural transect in the vicinity of Belgrade, a metropolitan area characterized by pronounced urban heat island effects. The urban site was located in the New Belgrade municipality, representing a densely built environment with extensive impervious surfaces, high building density, and limited vegetation cover. Such characteristics contribute to increased heat storage and reduced nocturnal cooling. For comparison, the rural site was selected in the Surčin-Dobanovci agricultural zone, approximately 20 km west of the city center. This area is characterized by open land, natural vegetation, and minimal anthropogenic influence, providing a representative reference for background climatic conditions. The selected sites are situated within the same regional climate zone, ensuring comparable synoptic meteorological conditions while preserving distinct differences in land surface properties. This spatial configuration allows for reliable assessment of urban–rural thermal contrasts and urban heat island intensity.

Data Collection

UAV-Based Thermal Measurements

Thermal data were acquired using a UAV platform equipped with a calibrated infrared thermal camera and a high-precision air temperature sensor [10,11] . UAV platform was also equipped with RGB camera for surface classification. The system was configured with GNSS-based positioning (accuracy ~1–2 m) to ensure precise georeferencing of all

measurements, while onboard data logging and real-time telemetry enabled continuous monitoring and synchronization of spatial and thermal data. Flights were conducted under stable weather conditions at three key periods of the day: morning (06:00–09:00), midday (12:00–15:00), and nighttime (18:00–21:00)), from 12 to 19 July 2024. Mission planning was performed using predefined autonomous flight paths to ensure repeatability across all observation periods. Flight altitude ranged between 50 and 120 m above ground level, with speed adjusted according to measurement objectives, allowing both stable hovering and controlled transect sampling. The UAV demonstrated stable flight performance with an average endurance of 25–35 minutes per mission. The sensor payload (~1–1.5 kg) was optimized for energy efficiency and measurement accuracy. Thermal images were processed using photogrammetric techniques to generate georeferenced orthomosaics representing spatial surface temperature distribution. These datasets enabled the identification of localized thermal hotspots and cooling zones, particularly distinguishing between impervious urban surfaces and vegetated areas. The integration of UAV system parameters ensured high spatial and temporal resolution, supporting detailed analysis of urban microclimate variability. The diurnal LST data have been collected in mid-July 2024 (12–19 July) on a clear days and mean land surface temperature values are calculated. UAV-derived Land Surface Temperature (LST) was compared with ground-based air temperature (Ta) observations from the Republic Hydrometeorological Service of Serbia (RHMZ) stations at Belgrade Observatory and Surčin Airport to evaluate urban–rural thermal variability, acknowledging the physical differences between surface and atmospheric temperature measurements (RHMZ, 2024) [12].

Ground-Based Measurements data

Ground-based meteorological measurements data are provided for both the urban and rural sites within the Belgrade transect in Belgrade, ensuring direct comparability under identical synoptic conditions [10,11]. Meteorological data used for the urban–rural temperature comparison were derived from high-resolution gridded climate datasets (e.g., MeteoSerbia1km and ERA5 reanalysis) [12–14]. Urban conditions were represented by grid cells corresponding to the central Belgrade metropolitan area, while rural conditions were defined using surrounding low-density and predominantly vegetated regions with minimal anthropogenic influence. Daily temperature values were aggregated to monthly means in order to reduce short-term variability and ensure climatic representativeness. The urban heat island (UHI) intensity was calculated as the difference between urban and rural mean temperatures (Equation 1):

$$\Delta T = T_{urban} - T_{rural} \quad (1)$$

This methodology ensures spatial consistency and enables comparison under homogeneous synoptic-scale atmospheric conditions. These measurement data were used to validate UAV-derived air temperature profiles and to quantify differences between surface and near-surface atmospheric conditions. Additionally, ground observations provided baseline conditions for assessing urban heat island intensity and for correcting potential radiative and environmental biases in UAV thermal data. The combined use of ground-based and UAV measurements data ensured robust cross-validation of datasets and improved the reliability of spatial temperature mapping across heterogeneous urban and rural environments.

Urban Heat Island Intensity Calculation

Urban Heat Island (UHI) is generally described as a higher average air temperature in cities compared to their less urbanized surrounding areas. Many factors influence the UHI intensity, including local and synoptic weather, season, time of the day, size of the city and its geographical location, urban morphology and anthropogenic heat release. It is well known that the UHI intensity is strong on clear and windless nights and exhibits diurnal and seasonal variations [15]. The examination of UHI can be very important in many fields of climatology and connected scientific disciplines.

Data Analysis

The collected data were analyzed using statistical and spatial methods: Monthly Mean air temperature values in urban and rural environments, independent sample t-tests to evaluate statistical significance between urban and rural temperatures, monthly variation of UHI intensity, diurnal variation of land surface temperature (LST) in urban and rural areas and their difference and UAV-derived thermal maps for visualization of temperature distribution. Temperature (LST) difference is calculated using Equation 2.

$$\Delta LST = LST_{urban} - LST_{rural} \quad (2)$$

RESULTS AND DISCUSSION

The observed urban heat island (UHI) pattern in Belgrade demonstrates a persistent and spatially coherent thermal anomaly characterized by higher temperatures in urban areas compared to surrounding rural environments [12–14]. The magnitude and seasonal variability of the UHI effect are consistent with established findings in urban climatology literature, where built-up environments exhibit enhanced heat storage and reduced nocturnal cooling due to surface material properties and anthropogenic heat emissions [3]. Monthly Mean Temperature in Urban and Rural environment as well as UHI values are presented in Figure 1.

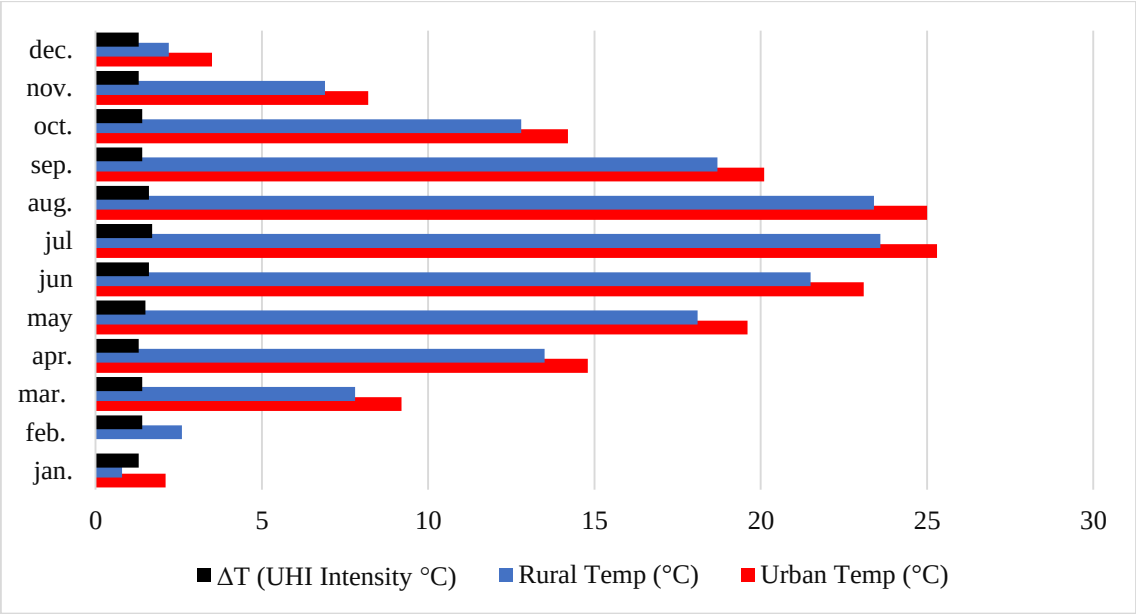

Figure 1 *Monthly Mean Temperature (Urban vs Rural envirnoment)*

The strongest UHI intensity during summer months can be attributed to increased shortwave radiation absorption by impervious surfaces such as asphalt and concrete, combined with reduced vegetation cover and limited evapotranspiration in densely built areas. These factors contribute to higher sensible heat fluxes and reduced latent heat exchange, intensifying urban warming under clear-sky conditions [1]. Similar seasonal amplification of UHI intensity has been reported in other mid-latitude cities, where summer synoptic stability enhances radiative heating contrasts between urban and rural zones [16]. In contrast, the weaker UHI signal observed during winter months is likely the result of reduced incoming solar radiation, increased atmospheric mixing, and more homogeneous surface energy exchanges between urban and rural environments. Additionally, seasonal vegetation loss in rural areas reduces the thermal contrast between land-cover types, partially diminishing the urban–rural temperature gradient . The integration of high-resolution gridded climate data and spatial extraction methods provided a robust framework for quantifying urban–rural thermal differences. The use of datasets such as MeteoSerbia1km and ERA5 reanalysis ensured spatial consistency and allowed for reliable long-term comparison under uniform synoptic conditions [13,14]. However, while gridded datasets offer strong spatial coverage, they may smooth local-scale thermal extremes, particularly in highly heterogeneous urban environments. This limitation highlights the importance of complementing reanalysis data with in situ and UAV-based observations for improved microclimatic representation [7]. Overall, the results confirm that urbanization significantly modifies local thermal regimes in Belgrade, reinforcing the role of land surface transformation in regional climate modification. The findings are consistent with broader global evidence that urban areas are increasingly acting as localized heat amplifiers under contemporary climate change conditions [2]. This has important implications for urban planning, public health, and climate adaptation strategies, particularly in regions experiencing increasing frequency of heatwave events.

The LST obtained results presented in Figure 2 clearly demonstrate a strong diurnal cycle in land surface temperature (LST) for both urban and rural environments.

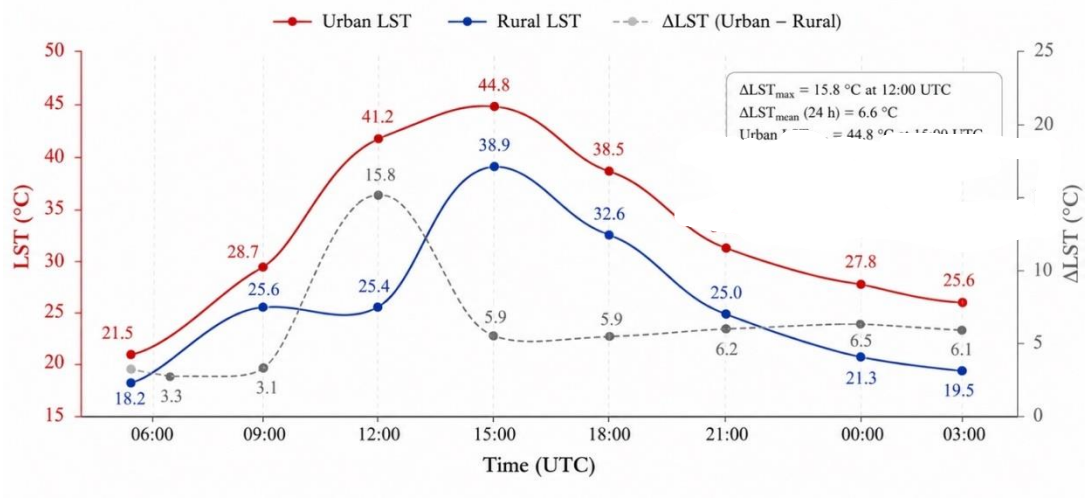

Figure 2 *Diurnal variation of land surface temperature (LST) in urban and rural areas and their difference (ALST = Urban - Rural). Observations were derived from UAV-based thermal infrared imagery on a clear day through interpolation to represent continuous surface temperature variability under clear-sky conditions. All times are Coordinated Universal Time (UTC).*

In both cases, temperatures increase steadily from early morning hours, reaching a pronounced peak in the early afternoon (15:00), followed by a gradual decline toward nighttime. This pattern reflects the expected response of land surfaces to incoming solar radiation and subsequent heat storage and release processes. A key finding is the consistently higher LST observed in the urban area compared to the rural site throughout the entire 24-hour period. The maximum urban LST reached 44.8°C, while the rural maximum was significantly lower at 38.9°C. This persistent temperature difference highlights the presence of a strong Surface Urban Heat Island (SUHI) effect in the study area.The intensity of the urban–rural thermal contrast (ΔLST) increases during the daytime, peaking around the period of maximum solar radiation. This behavior can be attributed to the higher heat capacity and thermal conductivity of urban materials such as asphalt and concrete, which absorb and store large amounts of heat. In contrast, rural surfaces, characterized by vegetation and soil moisture, exhibit greater evaporative cooling, which limits temperature rise. During nighttime and early morning hours, the temperature difference between urban and rural areas decreases but does not disappear entirely. This indicates that urban surfaces release stored heat more slowly than rural environments, contributing to sustained nocturnal warming. Such behavior is a well-documented feature of urban microclimates and is strongly linked to reduced longwave radiation loss and anthropogenic heat retention. Overall, the results confirm a typical urban thermal amplification pattern under clear-sky conditions. The observed diurnal dynamics are consistent with previous studies of SUHI formation, where maximum intensity occurs in the afternoon and is driven by both radiative forcing and surface material properties. These findings emphasize the importance of urban surface composition and land cover in controlling local microclimatic conditions. The results obtained by UAVs LSD temperature maps demonstrate consistently higher surface temperatures within urbanized areas compared to surrounding rural landscapes, particularly during nighttime observations, which is characteristic of urban heat island (UHI) development (Figure 3).

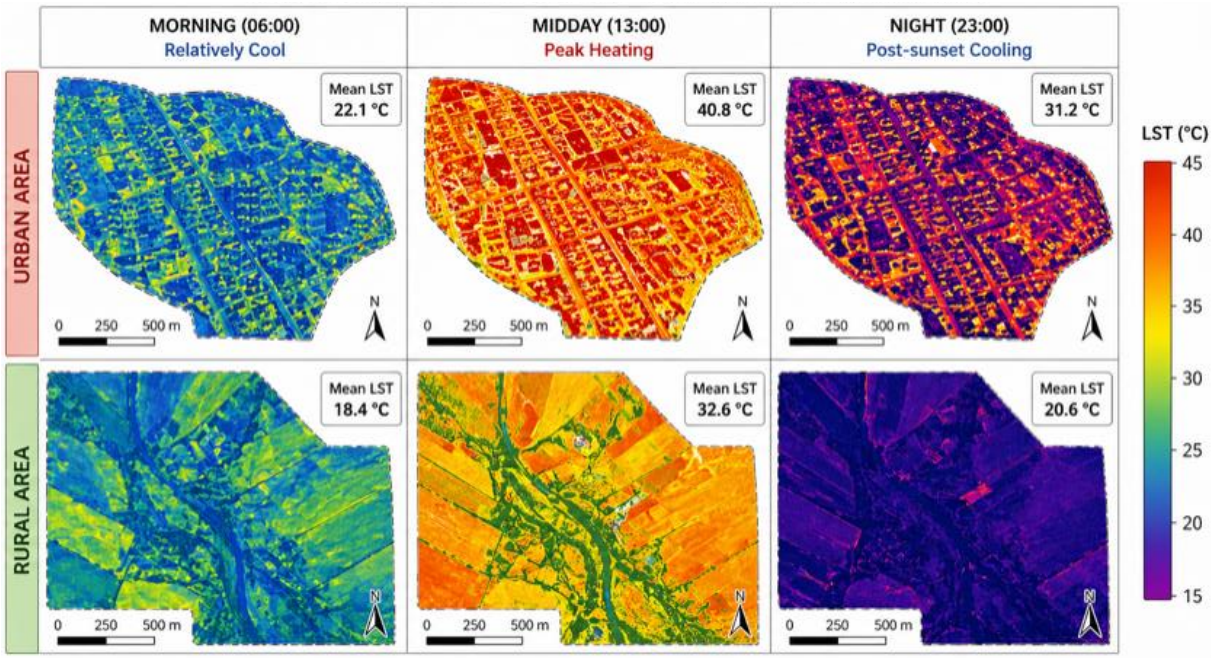

Figure 3 *UAV- derived Land Surface Temperature maps (LST)*

The observed thermal patterns are primarily driven by differences in surface properties and energy balance dynamics. Urban areas, dominated by impervious materials such as asphalt, concrete, and building facades, exhibit high thermal inertia, allowing them to store solar radiation during the day and release it slowly after sunset. This results in elevated nighttime LST values and reduced cooling rates. In contrast, rural areas characterized by vegetation and exposed soil show more efficient radiative cooling and evapotranspiration, leading to lower surface temperatures and stronger diurnal temperature gradients.

The UAV-based LST maps further highlight the influence of micro-scale land cover heterogeneity on local thermal behavior. Within the urban environment, distinct hotspots can be observed in densely built-up zones, transportation corridors, and industrial surfaces, while relatively cooler areas correspond to parks and vegetated patches. This fine-scale variability would not be detectable using coarser satellite imagery, demonstrating the added value of UAV platforms in urban climate studies.

Temporal analysis of UAV-derived thermal imagery indicates that the strongest urban–rural temperature contrasts occur during nighttime conditions. This supports the well-established concept that urban heat islands are primarily nocturnal phenomena, driven by delayed heat release from built surfaces and reduced atmospheric mixing in urban canyons. During daytime, although urban areas still exhibit higher surface temperatures, the contrast with rural zones is generally less pronounced due to the influence of solar heating across both environments.

Despite the strengths of UAV-based thermal mapping, several limitations should be acknowledged. Surface temperature retrieved from thermal imagery represents radiative land surface conditions rather than near-surface air temperature, and therefore direct comparison with meteorological station data should be interpreted cautiously. Additionally, atmospheric conditions, flight timing, and sensor calibration can introduce variability in absolute

temperature values. However, the relative spatial patterns observed in the UAV LST maps remain robust and provide valuable insight into urban thermal dynamics.

Overall, the UAV-derived LST analysis confirms that high-resolution thermal imaging is a powerful tool for detecting urban–rural thermal contrasts and understanding fine-scale heat distribution processes. These findings are consistent with established urban climatology theory and demonstrate the applicability of UAV systems for detailed environmental monitoring in heterogeneous landscapes.

CONCLUSION

This study demonstrates the effectiveness of UAV-derived land surface temperature (LST) mapping for analyzing fine-scale urban–rural thermal variability and its relationship to diurnal surface heating and cooling processes. The results show consistent spatial temperature contrasts between urban and rural environments, with stronger nighttime urban warming and more efficient nocturnal cooling in rural areas. These patterns reflect differences in surface materials, vegetation cover, and heat storage capacity, which govern local energy balance dynamics. When combined with official meteorological observations, UAV thermal imagery provides valuable contextual insight into atmospheric conditions near the surface. Although UAV-derived LST does not directly represent air temperature, the observed spatial and temporal patterns are consistent with established urban climatology and boundary-layer theory. From an aviation meteorology perspective, the findings are particularly relevant for understanding micro-scale thermal processes in the vicinity of airports. Surface temperature heterogeneity influences near-surface air temperature gradients, boundary layer stability, and local turbulence development, all of which are critical factors for flight operations during takeoff, landing, and low-altitude phases. In regions with mixed land cover, such as the urban–suburban–open terrain transition near Belgrade Nikola Tesla Airport, these thermal differences can contribute to localized atmospheric variability that is not fully captured by conventional point-based meteorological observations.

Therefore, UAV-based thermal mapping represents a valuable complementary tool for aviation meteorology by providing high-resolution spatial information on surface heating patterns that affect local atmospheric behavior. This enhances situational awareness of microclimatic conditions relevant to operational safety and supports improved interpretation of near-airport weather variability. Future integration of UAV observations with ground-based measurements and numerical weather prediction models could further strengthen short-range forecasting and risk assessment in aviation environments.

REFERENCES

[1] Grimmond, S. Glob Environ Change. 2007, 17(1), 1–4.

[2] Intergovernmental Panel on Climate Change. Climate Change 2021: The Physical Science Basis. Cambridge: Cambridge University Press; 2021.

[3] Oke, T.R. Q. J. R. Meteorol Soc. 1982, 108, 1–24.

[4] Santamouris, M. Energy Build. 2015, 103, 119–139.

[5] Zhao, L., Lee, X., Smith, R.B., *et al*. Nat. Clim. Change 2014, 4, 109–112.

[6] Hart, M..A, Sailor, D.J. Theor Appl. Climatol. 2009, 95, 397–406.

[7] Manfreda, S., McCabe, M.F., Miller, P.E., *et al*. Remote Sens. 2018, 10(4), 641.

[8] Milovanović, B., Radovanović, M., Schneider, C. J. Geogr. Inst. Jovan. Cvijic SASA 2020, 70(2), 163–170.

[9] Lukić M, Milovanović J. Assessment of outdoor thermal comfort in Belgrade using UTCI. In: Proc. Sinteza Conf.; 2020.

[10] Erasmus+ Programme; Foundation Tempus. Safe drones over safe environment [Internet]. 2023 [cited 2026 Apr 25]. Available from: https://www.ecosafedrones.eu/site/2023/06/20/usage-areas-os-uavs/

[11] Pavlovic S, In: Proceedings of the International Multidisciplinary Conference "Challenges of Contemporary Higher Education" (CCHE 2024); Jan 29–Feb 2; Kopaonik, Serbia. 2024, Vol. 2.

[12] Republic Hydrometeorological Service of Serbia (RHMZ), Meteorological Station Network Data (Belgrade Observatory; Surčin Airport), Belgrade, Serbia, 2024. Available from: https://www.hidmet.gov.rs

[13] Sekulić, A., Kilibarda, M., Protić, D., *et al*. Sci Data. 2021, 8, 123.

[14] Copernicus Climate Change Service. ERA5: fifth generation of ECMWF atmospheric reanalysis of the global climate [Internet]. 2017 [cited 2026 Apr 25]. Available from: https://cds.climate.copernicus.eu/

[15] Kim, Y.H., Baik, J.J. J. Appl. Meteorol. 2005, 44(5), 591–605.

[16] Voogt, J.A., Oke, T.R. Remote Sens. Environ. 2003, 86(3), 370–384.

EcoTER'26
eco.tfbor.bg.ac.rs
32nd International Conference
Ecological Truth & Environmental Research
24–26 June 2026, Hotel Sunce,
Sokobanja, Serbia

Original Research

HEAVY METAL DISTRIBUTION AND CHEMICAL SPECIATION IN SOILS NEAR THE GORNJE POLJE FLOTATION TAILINGS

DOI: 10.5937/EcoTER26135G

Jovana Galjak[1,a*], Miljana Krstić[1,b], Svetomir Milojević[1,c], Gordana Milentijević[1,d]

[1] University of Priština, Faculty of Technical Sciences, Knjaza Miloša 7, 38220 Kosovska Mitrovica, SERBIA

[a] https://orcid.org/0000-0003-3078-9295
[b] https://orcid.org/0000-0002-8280-7689
[c] https://orcid.org/0000-0003-3576-6965
[d] https://orcid.org/0000-0003-2935-100X

Abstract

A modified BCR (Bureau of Community Reference) sequential extraction procedure and the potential ecological risk index method were applied to assess the ecological behavior and potential risks of metals in soil. Inductively coupled plasma optical emission spectrometry (ICP-OES) was used for sample analysis. The mean concentrations of the analyzed metals followed the order: Pb > Cu > As > Ni > Cd. The highest proportions in the mobile fractions were observed for Pb and Cd compared to the other metals. Based on the calculated potential ecological risk index, Cd was identified as having a pronounced impact on the environment due to its high mobility. The order of potential ecological risk was: Cd > As > Pb across all analyzed soil samples, with the highest levels of contamination detected in the immediate vicinity of the tailings dump. The obtained results indicate that the flotation tailings at the Gornje Polje site still contain significant amounts of material that may act as a potential source of heavy metal release into the environment.

Keywords: BCR sequential extraction, heavy metals, bioavailability, potential ecological risk.

INTRODUCTION

The growing demand for metals during industrial development has led to the exploitation of sulfide ores using flotation, a process that separates sulfide minerals from the surrounding material [1]. After the flotation process, material that does not contain economically valuable components is considered tailings and classified as mining waste [2]. The mineralogy of sulfide tailings is highly heterogeneous and specific, and upon exposure to an oxidative environment, it becomes chemically unstable which can lead to the release of harmful metals and environmental contamination if not properly managed [3].

Soil contamination by heavy metals in the vicinity of mining tailings represents a critical environmental challenge [4]. Mining tailings are rich in persistent and potentially toxic elements and are characterized by the presence of organic matter and low pH values, which favor metal mobility [5]. The total metal content is not an adequate indicator of

* *jovana.galjak@pr.ac.rs*

ecotoxicological risk; their behavior in the environment depends not only on total concentration but also on the chemical forms in which they occur [6].

The sequential extraction procedure is widely applied to a large number of potentially toxic elements in various types of samples and represents an important tool for understanding their environmental behavior [4,7]. It primarily defines the distribution of metals within solid matrices, as well as their speciation, mobility, and adsorption capacity [8].

The analytical procedure of sequential chemical extraction was originally developed based on the work of Tessier, Bison, and Campbell in 1979 [6]. In that study, a method for the fractionation of trace metals into five fractions was proposed: exchangeable, carbonate-bound, Fe–Mn oxide-bound, organic matter-bound, and residual. Today, this method is applied to various types of materials, including soils [9], river, lake, and marine sediments [10], atmospheric particles [11], and mining waste [12].

This study investigates the ecological behavior and potential ecological risks of metals in soil located near a flotation tailings pond that is not subject to regular monitoring. For this purpose, a modified BCR sequential extraction procedure was applied, and the potential environmental risk associated with the deposited tailings waste was assessed.

MATERIALS AND METHODS

Sampling, BCR Extraction, and Potential Ecological Risk of Metals

The collected soil samples were air-dried in a closed space at room temperature for one week. After drying to constant weight, the samples were homogenized and sieved to a particle size of < 2 mm. The prepared soil samples (1 g of each sample) were subjected to a BCR sequential extraction procedure, as well as to the determination of pseudototal heavy metal concentrations. For the determination of pseudototal metal content, the ground soil samples were digested with aqua regia (15 mL of 37% HCl and 5 mL of 65% HNO_3) at 80 °C in a water bath for 5–6 hours. Pseudototal concentrations of metals (As, Cd, Cu, Pb, and Ni) in the soil samples were determined using inductively coupled plasma optical emission spectrometry (ICP-OES). The BCR extraction course was as follows:

- Step 1 (exchangeable, water, acid-soluble fraction): 1 g of sample was treated with 0.11 mol/dm³ CH_3COOH and shaken for 16 h to obtain F1;
- Step 2 (reducible fraction): F1 was treated with 0.5 mol/dm³ $NH_2OH{\cdot}HCl$ (adjusted to pH 1.5) and shaken for 16 h to obtain F2;
- Step 3 (oxidizable fraction): F2 was treated with 8.8 mol/dm³ H_2O_2 and 1 mol/dm³ CH_3COONH_2 (adjusted to pH 2) and shaken for 16 h to obtain F3;
- Step 4 (residual fraction): F3 was digested with aqua regia (15 mL of 37% HCl and 5 mL of 65% HNO_3) at 80 °C for 5–6 h to obtain F4.

The contamination factor (C^i_f) for individual metals in sediments was calculated according to the method proposed by Min *et al*. [13]. The contamination factor (C^i_f) for the analyzed sediment samples was determined using the following expression:

$$C^i_f = C^i_{simple} / C^i_{reference} \quad (1)$$

where C^i_f represents the contamination factor for a specific heavy metal, C^i_{simple} denotes the measured concentration of the metal in the analyzed soil sample, and $C^i_{reference}$ represents the reference value used as the basis for the calculation.

The potential ecological risk factor (E^i_f), as defined by Håkanson [14], was used to assess the toxicity of heavy metals and the sensitivity of the environment to their presence. Within this approach, each metal is assigned a specific toxicity coefficient, as follows: Cd = 30, As = 10, Cu = Pb = Ni = 5, and Zn = 1. The potential ecological risk factor for an individual heavy metal was calculated using the following formula:

$$E^i_f = C^i_f \cdot T^i_f \tag{2}$$

where T^i_f represents the toxicity factor for an individual heavy metal. The overall potential ecological risk index (R) for a set of heavy metals is expressed as the sum of the individual risk factors:

$$R = \Sigma E^i_f \tag{3}$$

Accordingly, the potential ecological risk factor (E^i_f) and the overall potential ecological risk index (R) are used to assess the overall environmental impact of heavy metals (Table 1).

Table 1 *Relationship between the potential toxicity index (R), the potential ecological risk index (E^i_f), and pollution level*

Scope of potential ecological risk index (E^i_f)	**Ecological risk of single-factor pollution**	**Scope of potential toxicity index (R)**	**General level of potential ecological risk**
$E^i_f < 40$	Low	$R < 150$	Low grade
$40 \leq E^i_f < 80$	Moderate	$150 \leq R < 300$	Moderate
$80 \leq E^i_f < 160$	Higher	$300 \leq R < 600$	Severe
$160 \leq E^i_f < 320$	High	$600 \leq R$	Serious
$320 \leq E^i_f$	Serious		

RESULTS AND DISCUSSION

Pseudo-total concentrations of heavy metals (Cd, Cu, Pb, Ni, and As) in the studied soil samples indicate a clear enrichment of potentially toxic elements in the investigated area. The observed distribution pattern suggests a significant influence of anthropogenic activities, particularly mining and flotation tailings disposal, on metal accumulation in the soil.

The total concentrations of the analyzed elements in the soil samples ranged from 45 to 263 mg/kg for As, 2.03 to 18.38 mg/kg for Cd, 43.5 to 215.5 mg/kg for Cu, 8.66 to 195.58 mg/kg for Ni, and 611 to 4135 mg/kg for Pb. The concentrations of the examined metals, compared with the maximum allowable concentrations (MAC) prescribed by the national regulation [15], exceeded the permissible limits in almost all samples.

Although pseudo-total concentrations do not directly reflect the mobility or bioavailability of metals, they provide an essential initial indicator of the extent of soil contamination. In this

study, the elevated concentrations suggest that soils near tailings sites are significantly impacted and may pose a potential environmental risk

Table 2 *Chemical composition of soil samples*

Element (mg/kg)	Sample 1	Sample 2	Sample 3	Sample 4	Sample 5	Current limit value*
Cd	10.27	2.03	12.38	18.38	5.58	3
Cu	106.7	43.5	78.6	215.5	73.7	100
Ni	8.66	91.55	64.25	115.86	195.58	50
Pb	4135	611	733	3038	1345	100
As	70.0	45.0	184.0	263.0	124.0	25

*Official Gazette RS 23/94.

The results of the BCR sequential extraction are presented in Figure 1, which shows the distribution of Cd, As, Cu, Ni, and Pb, i.e., their mobility and bioavailability in soils from the investigated area. The distribution between stable and mobile fractions is clearly defined, allowing a more realistic assessment of environmental risk.

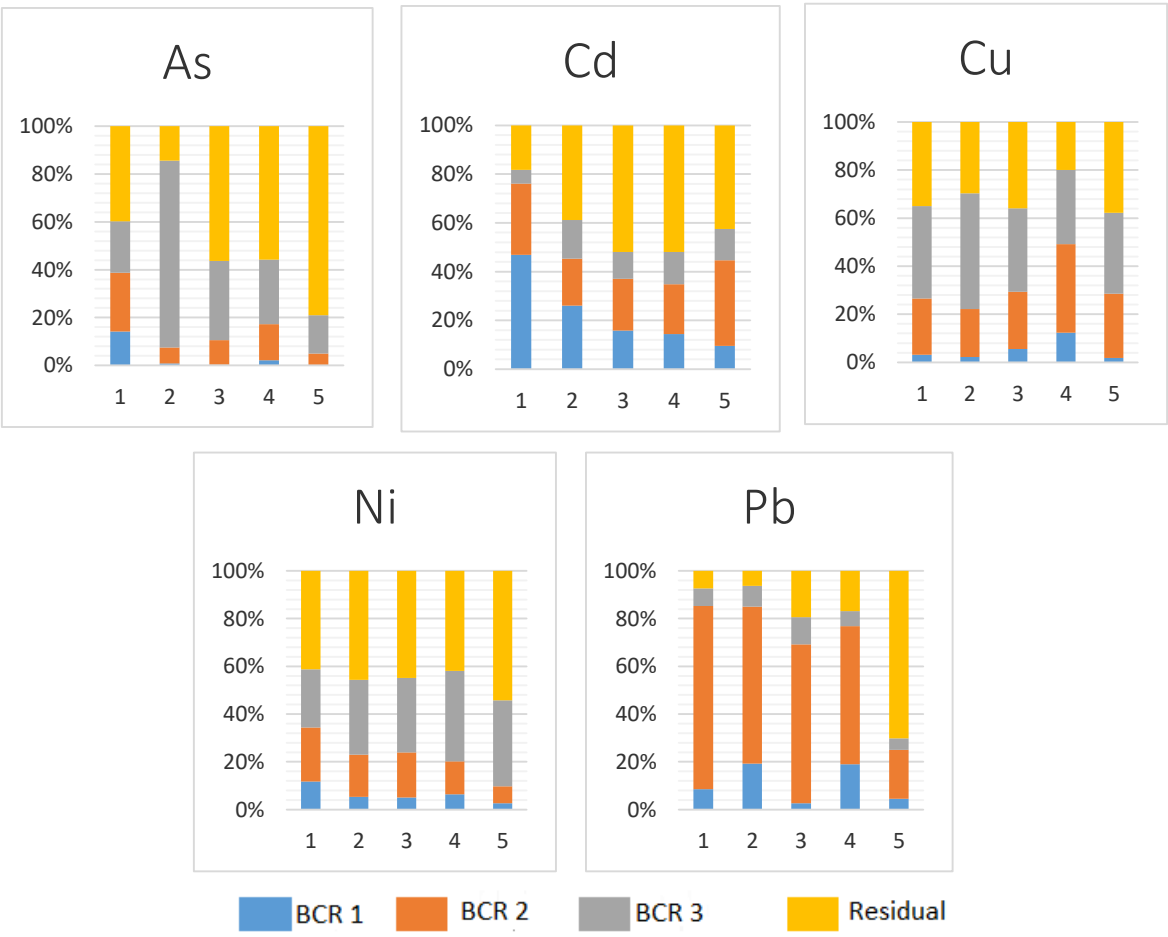

Figure 1 *Distribution of metals in soil samples as determined by modified BCR sequential extraction procedure*

The BCR 1 fraction is considered the most mobile and readily available, as metals in this phase are weakly bound to carbonates and exchangeable sites. Based on Figure 1, Cd appears

as the most mobile metal. Under low pH conditions, carbonates dissolve, leading to the release of Cd into the environment.

The BCR 2 fraction is particularly dominant for Pb and, to a lesser extent, for Cu and Cd, indicating that these metals are associated with Fe–Mn oxides through surface adsorption processes, which largely control their mobility and bioavailability. Under oxidative conditions, characteristic of mining tailings, Fe–Mn oxides and hydroxides play a significant role in the immobilization of metals such as Cd, Ni, As, Cu, and Pb through adsorption. However, the establishment of reducing conditions may destabilize these mineral phases, causing their dissolution and the subsequent release of bound metals into the environment [16].

The third step of the sequential extraction, BCR 3, corresponds to metals bound to organic matter and sulfides. Ni is predominantly associated with this fraction and may therefore be released under oxidizing conditions. Consequently, it shows low abundance in the most mobile fractions (Figure 1). As and Cu are also weakly associated with organic matter.

The residual (BCR IV) fraction represents the most stable form of metal binding, in which metals are associated with silicate minerals and are therefore considered largely unavailable to the environment and living organisms [17]. Based on Figure 1, it can be concluded that all analyzed metals occur in this fraction, with As and Ni showing the highest association with silicate-bound forms.

The main elements representing an environmental hazard are Cd, Pb, and As. The E^i_f values for Pb in samples S1 and S4 indicate a moderate potential ecological risk ($40 \leq E^i_f < 80$). Similar values were observed for As, although in different sampling locations compared to Pb. As exhibited a moderate potential ecological risk in samples S3, S4, and S5.

According to the results presented in Table 3, Cd shows the highest potential ecological risk values. In samples S1, S3, and S4, Cd indicates a higher potential ecological risk level ($80 \leq E^i_f < 160$), while sample S5 shows a moderate potential ecological risk.

The maximum R value was recorded in sample S4. According to the assessment criteria, samples S1, S3, and S5 exhibit a moderate level of ecological risk ($150 < R < 300$), whereas sample S4 indicates a severe level of ecological risk ($300 \leq R < 600$). Therefore, the soils in the investigated area show a significant potential ecological risk due to the presence of Cd, Pb, and As.

Table 3 *Potential ecological risk assessment results of metals in soil samples*

Sample	Element	C^i_{simple} (µg/g)	$C^i_{reference}$ (µg/g)	C^i_f	T^i_f	E^i_f	$R \sum E^i_f$
S1	Cd	10.27	3	3.42	30	102.6	199.2
	Cu	106.7	140	0.76	5	3.8	
	Ni	8.66	75	0.12	5	0.6	
	Pb	4135	300	13.78	5	68.9	
	As	70	30	2.33	10	23.3	
S2	Cd	2.03	3	0.67	30	20.1	52.9
	Cu	43.5	140	0.31	5	1.55	
	Ni	91.55	75	1.22	5	6.1	
	Pb	611	300	2.03	5	10.15	
	As	45	30	1.5	10	15	

***Table 3** continued*

S3	Cd	12.38	3	4.12	30	123.6	204.15
	Cu	78.6	140	0.56	5	2.8	
	Ni	64.25	75	0.85	5	4.25	
	Pb	733	300	2.44	5	12.2	
	As	184	30	6.13	10	61.3	
S4	Cd	18.38	3	6.13	30	183.9	337.65
	Cu	215.5	140	1.54	5	7.7	
	Ni	115.86	75	1.54	5	7.7	
	Pb	3038	300	10.13	5	50.65	
	As	263	30	8.77	10	87.7	
S5	Cd	5.58	3	1.86	30	55.8	135.2
	Cu	73.7	140	0.53	5	2.65	
	Ni	195.58	75	2.61	5	13.05	
	Pb	1345	300	4.48	5	22.4	
	As	124	30	4.13	10	41.3	

CONCLUSION

The aim of this study was to investigate the influence of Gornje Polje flotation tailings on soil contamination with heavy metals. Based on the analysis of pseudo-total concentrations, the presence of As, Cd, Cu, Pb, and Ni was confirmed, with concentrations of the examined metals in most samples significantly exceeding the prescribed limit values.

The results of the sequential extraction indicate that heavy metals in soils adjacent to the flotation tailings are distributed among different geochemical fractions. It was observed that Cd is predominantly present in the mobile fraction, while Pb is mainly associated with the BCR 2 fraction, making it one of the most bioavailable metals after Cd. In contrast, Ni shows a stronger association with the oxidizable fraction, indicating its binding to organic matter and sulfide phases.

To assess the potential environmental risk, the individual ecological risk factor (E^i_f) and the overall risk index (R) were calculated. The results confirm that the mobility of Cd, Pb, and As has a significant influence on environmental risk, with the order of potential risk being Cd > As > Pb. The flotation tailings pond represents a long-term source of contamination, with the potential for metal remobilization under changing physicochemical environmental conditions.

Sequential extraction has proven to be an effective tool for environmental risk assessment and for understanding the behavior of heavy metals in contaminated soils.

ACKNOWLEDGEMENT

The authors are grateful to the Ministry of Science, Technological Development and Innovation of the Republic of Serbia for financial support according to the contract with registration No. OI172037.

REFERENCES

[1] Dold, B. Rev Environ Sci Biotechnol. 2008 7(4), 275–285.

[2] Lottermoser BG. Mine Wastes: Characterization, Treatment and Environmental Impacts, 3rd ed. Springer: Berlin/Heidelberg, 2010.
[3] Rezaie, B., Anderson, A. Sci. Total Environ. 2020, 717, 137211.
[4] Ali, J., Tuzen, M., Shaikh, Q., *et al*. Trends Anal. Chem. 2024, 173, 117639.
[5] Tyagi, A., Haritash, A.K. Acta Geochimica. 2025, 44, 1–24.
[6] Tessier, A., Campbell, P.G.C., Bisson, M. Anal. Chem. 1979, 51(7), 844–851.
[7] Andersen, M.K., Refsgaard, A., Raulund-Rasmussen, K., *et al*. Soil Sci. Soc. Am. J. 2002, 66(6), 1829–1835.
[8] Okoro, H.K., Fatoki, O.S., Adekola, F.A., *et al*. J. Environ. Anal. Toxicol. 2012, 1(S1), 181.
[9] Besser, J.M., Ingersoll, C.G., Brumbaugh, W.G., *et al*. Environ. Toxicol. Chem. 2015, 34(3), 626–639.
[10] Anju, M., Banerjee, D.K. Environ. Monit. Assessment. 2010, 176(1–4), 391–403.
[11] Hughes, J.C., Noble, A.D. Commun. Soil Sci. Plant Anal. 1991, 22(17–18), 1753–1766.
[12] Van der Sloot, H.A. Waste Management. 2003, 23(3), 211–224.
[13] Min, X., Xie, X., Chai, L-Y., *et al*. J. Trans. Nonferrous Met. Soc. China. 2013, 23(1), 208–218.
[14] Hakanson, L. Water Res. 1980, 14(8), 975–1001.
[15] Official Gazette of the Republic of Serbia, No. 23/94.
[16] Palau, J., Benaiges-Fernandez, R., Offeddu, F., *et al*. Sci. Total Environ. 2021, 788(20), 147579.
[17] Rogan, N., Dolenec, T., Serafimovski, T., *et al*. Environ Earth Sci. 2010, 61, 899–907.

EcoTER'26
eco.tfbor.bg.ac.rs
32nd International Conference
Ecological Truth & Environmental Research
24–26 June 2026, Hotel Sunce,
Sokobanja, Serbia

Original Research

AMMONIUM HYDROXIDE AND MILK FAT CONTENT EFFECT ON BENZYL BUTYL PHTHALATE EXTRACTION

DOI: 10.5937/EcoTER26142K

Ivana Kostić Kokić[1,a*], Danica Bogdanović[1,b], Nikola Stanković[2,c], Tatjana Anđelković[1,d]

[1] University of Niš, Faculty of Science and Mathematics, Department of Chemistry, Višegradska 33, 18000 Niš, SERBIA

[2] University of Niš, Faculty of Science and Mathematics, Department of Biology and Ecology, Višegradska 33, 18000 Niš, SERBIA

[a] https://orcid.org/0000-0001-6517-5635
[b] https://orcid.org/0000-0001-5672-9931
[c] https://orcid.org/0000-0002-1604-6543
[d] https://orcid.org/0000-0001-9856-985X

Abstract

In this study, milk fat content and addition of ammonium hydroxide influence on benzyl butyl phthalate (BBP) determination was investigated. Investigated milk samples contained fat in following amounts (%): 0.5, 1.5, and 3.5. Used method included extraction with hexane with and without addition of ammonium hydroxide. The effects of matrix were studied by spiking milk samples with known amount of BBP standard solution in concentration range 50 to 250 µg L^{-1} before extraction steps. Obtained results indicate that the addition of NH_4OH is proved to be an important procedural step, effectively disrupting matrix bonds in milk samples and increasing BBP recoveries up to five times. While untreated samples showed insufficient recoveries (below 50%), the alkaline modification achieved reliable results across all fat levels, even reaching over 100% in specific samples. these results highlight the important role of alkaline conditions in disrupting milk's complex matrix and facilitating the release of hydrophobic phthalates such as BBP.

Keywords: milk, fat content, phthalate, ammonium hydroxide.

INTRODUCTION

Phthalates are chemical substances widely used as additives in production of plastic materials to increase softness and flexibility [1,2]. Bearing in mind a large amount of plastic production, phthalates can be found in many consumer products, such as medical equipment, cosmetics, clothing, as well as food packaging, *etc*. Consequently, humans may be exposed to phthalates through ingestion, dermal absorption, and inhalation, with food ingestion considered the primary route of exposure [3,4]. Phthalates do not form stable bonds with plastics and can release into surrounding media, and food can be contaminated by the contact with food packaging containing phthalates.

Phthalates have lipophilic nature and tend to leak from plastics in oil or fat-containing food [1,5]. In recent years, phthalates have attracted huge public attention and are listed as

*ivana.chem@outlook.com

contaminants of emerging concern because they are recognized as endocrine disruptors or mutagens, which can have adverse effects on human health even at low levels [6].

Milk is a complex matrix consisting of proteins and different amounts of fat, and phthalates can be bound to matrix constituents with different affinity due to their different chain lengths. Milk and milk products can be contaminated during the preparation and packaged processes. The tolerable daily intake (TDI) values established by the European Food Safety Authority (EFSA) panel is 0.5 mg/kg/day for benzyl butyl phthalate (BBP) [6,7].

MATERIALS AND METHODS

Chemicals

BzBP, dibuthyl adipate (DBA) and hexane were purchased from Sigma Aldrich, USA. Hexane was HPLC grade and screened to determine the phthalate background. Stock solution of phthalate and DBA standards were prepared by hexane diluting the amounts that were accurately weighted out by analytical balance with precision at ±0.00001 g (Kern, Germany) and stored at 4 °C. Working standard solutions were at the concentration range from 0.25 to 10 µg mL^{-1}. DBA was used as internal standard at concentration 1 µg mL^{-1}.

All glassware used in this study was soaked and washed with acetone, rinsed with hexane and dried at 120 °C for 4 h to avoid phthalate contamination. After cleaning, glassware was sealed with aluminium foil and stored in a clean environment to avoid adsorption of phthalates from the air.

Samples

Milk samples were purchased from local supermarkets (Niš) and all samples were open at the same time in the same place. Three different types of milk with different milk fat content (0.5, 1.5 and 3.5%) were investigated. The effects of matrix were studied by spiking samples with known amount of phthalates standard solution in concentration range 50 to 250 µg L^{-1} before extraction steps. All spiked samples and blank sample were analysed in three replicates.

A volume of 10 mL spiked milk sample was put in a polypropylene centrifuge tube and 0.5 mL of 3% NH_4OH was added. Mixture was vortexed for 1 min at 1500 rpm (Vortex Genie 2, Scientific Industries, USA) and 30 min at room temperature, to denaturate proteins. After this step, 5 mL of hexane was added, and mixture was vortexed 2 min at 2000 rpm, and centrifuged 10 min at 4000 rpm (Jouan C4i centrifuge, Thermo Scientific). About 5 mL of supernatant was transferred into clean glass tube, evaporated near to dryness at 30 °C, and reconstituted by hexane. Samples were vortexed 1 min at 1000 rpm and transferred to glass vial. DBA was added and samples were analysed by gas chromatography-mass spectrometry. All spiked samples were analysed in three replicates. The same procedure was repeated for spiked milk samples without NH_4OH addition.

Instruments

Analysis was carried out by gas chromatography coupled to mass spectrometer (Hewlett Packard 6890 series GC System with autosampler connected with Agilent 5973 Mass Selective Detector (Electron Ionization MSD-EI, single quadrupole). The separation was achieved with 30 m × 0.25 mm × 0.25 µm a non-polar AGILENT DB-5MS column coated

with 5% phenyl, 95% dimethylpolysiloxane. The MSD was used in the single ion-monitoring (SIM) mode. The identification of target compounds was based on the relative retention time, the presence of target ions and their relative abundance. The most abundant ion m/z 149 was chosen for quantification of BBP. Ion m/z 185 was chosen as representative ion of DBA internal standard. The dwell time was 100 ms.

RESULTS AND DISCUSSION

Calibration curve of BBP standard series was obtained by standard solutions in a concentration range of 0.25 to 10 μgmL^{-1}. Obtained calibration curve was linear with correlation coefficient > 0.9982. Recovery values were calculated for all investigated samples, and their mean values are given in Table 1 and 2.

The obtained data demonstrate a pronounced influence of NH_4OH addition on the extraction efficiency of BBP from milk samples. Without NH_4OH, recoveries were consistently low across all tested concentrations, generally remaining below 50%. This pattern was observed regardless of milk fat content, although samples with 1.5% fat showed slightly higher recoveries compared to 0.5% and 2.5% fat. Such limited extraction efficiency suggests that the native matrix environment of milk—particularly its protein–lipid interactions—restricts the release of BBP during sample preparation.

In contrast, the introduction of NH_4OH significantly enhanced BBP recovery, indicating a strong matrix-modifying effect. Recoveries increased two- to five-fold depending on fat content and spiking level. The most notable improvements were observed in samples with 1.5% fat, where recoveries exceeded 100% at certain concentrations, suggesting both improved extraction and potential matrix-induced signal enhancement. Even in higher-fat samples (2.5%), where analyte entrapment is typically more pronounced, NH_4OH addition resulted in recoveries around 60–123%, representing a substantial improvement over the untreated samples.

Table 1 *Recovery values obtained for BBP extraction from milk samples without NH_4OH addition*

Phthalate	Added concentration (ngg^{-1})	Milk fat content (%)		
		0.5	1.5	2.5
BzBP	5	21.56±0.69	42.97±2.01	24.05±1.00
	15	19.60±0.35	48.45±1.98	45.71±1.15
	25	18.48±0.45	47.61±1.78	44.35±1.08

Table 2 *Recovery values obtained for BBP extraction from milk samples with NH_4OH addition*

Phthalate	Added concentration (ngg^{-1})	Milk fat content (%)		
		0.5	1.5	2.5
BzBP	5	73.26±3.09	104.71±4.28	59.94±1.29
	15	93.24±3.03	125.42±3.05	123.58±2.04
	25	77.45±3.58	63.24±2.12	63.42±1.21

Overall, these results highlight the critical role of alkaline conditions in disrupting milk's complex matrix and facilitating the release of hydrophobic phthalates such as BBP. The comparison clearly demonstrates that NH_4OH addition is essential for achieving reliable and

reproducible extraction performance across varying fat levels. This finding is particularly relevant for analytical workflows targeting phthalates in dairy products, where matrix effects can otherwise compromise quantification accuracy.

CONCLUSION

This study demonstrates that the complex matrix of milk, characterized by strong protein–lipid interactions, significantly disturbs the extraction of benzyl butyl phthalate (BBP). The addition of NH_4OH proved to be an important procedural step, effectively disrupting these matrix bonds and increasing BBP recoveries up to five times. While untreated samples showed insufficient recoveries (below 50%), the alkaline modification achieved reliable results across all fat levels, even reaching over 100% in specific samples. These findings indicate that NH_4OH not only facilitates analyte release but also potentially mitigates matrix-induced signal suppression. This optimized approach provides a robust and reproducible framework for the accurate quantification of hydrophobic phthalates in dairy products. This kind of methodological improvements are essential for ensuring food safety and conducting reliable exposure assessments in complex food matrices.

ACKNOWLEDGEMENT

The authors are grateful to the Ministry of Science, Technological Development and Innovation of the Republic of Serbia for financial support according to the contract with registration No. 451-03-33/2026-03/200124 and 451-03-34/2026-03/200124.

REFERENCES

[1] Tuncel, S.G., Senlik, D. Anal. Lett. 2016, 49, 1334–1343.

[2] Guerranti, C., Sbordoni, I., Fanello, E.L., *et al*. Microchem. J. 2013, 107, 178–181.

[3] Nanni, N., Fiselier, K., Grob, K., *et al*. Food Control 2011, 2, 209–214.

[4] Ge, W.P., Yang, X.J., Wu, X.Y., *et al*. J. Dairy Sci. 2016, 99(10), 7771–7776.

[5] Li, Z., Xue, F., Xu, L., *et al*. J. Chromatogr. Sci. 2011, 49(4), 338–343.

[6] Fasano, E., Cirillo, T., Esposito, F., *et al*. LWT Food Sci. Technol. 2015, 64(2), 1015–1021.

[7] Zhang, D., Liu, H., Liang, Y., *et al*. Front. Earth Sci. China 2009, 3, 73–79.

EcoTER'26
eco.tfbor.bg.ac.rs
32nd International Conference
Ecological Truth & Environmental Research
24–26 June 2026, Hotel Sunce,
Sokobanja, Serbia

Original Research

INDOOR PM_{10} AND $PM_{2.5}$ IN RESIDENTIAL APARTMENTS IN BOR, SERBIA: NON-HEATING SEASON ANALYSIS

DOI: 10.5937/EcoTER26146T

Viša Tasić[1,a*], Vladan Kamenović[1,b], Bojan Radović[1,c], Renata Kovačević[1,d], Nevena Ristić[1,e], Zvonko Damnjanović[2,f], Mira Cocić[3,g]

[1] Mining and Metallurgy Institute Bor, Zeleni bulevar 35, 19210 Bor, SERBIA

[2] Kompjuter centar Bor, Trg Oslobođenja 8, 19210 Bor, SERBIA

[3] University of Belgrade, Technical Faculty in Bor, Vojske Jugoslavije 12, 19210 Bor, SERBIA

[a] https://orcid.org/0000-0001-6710-6529 [b] https://orcid.org/0000-0001-9476-5378

[c] https://orcid.org/0000-0003-4884-1418 [d] https://orcid.org/0000-0003-4108-0855

[e] https://orcid.org/0000-0003-1408-237X [f] https://orcid.org/0000-0002-0600-3988

[g] https://orcid.org/0000-0002-9715-2822

Abstract

This study examines indoor PM_{10} and $PM_{2.5}$ concentrations in residential apartments in Bor, Serbia, during the non-heating season, aiming to assess the relative contributions of indoor and outdoor sources. Measurements were conducted in 30 apartments across two independent campaigns carried out in May–June and August–September. Indoor concentrations were normalized using corresponding outdoor values and expressed as indoor/outdoor (I/O) ratios to enable comparison between the datasets. The results indicate a clear difference between the two periods. During May–June, median I/O ratios were approximately 1.08 for PM_{10} and 1.16 for $PM_{2.5}$, suggesting a dominant influence of indoor sources. In contrast, during August–September, median values decreased to approximately 0.63 for PM_{10} and 0.94 for $PM_{2.5}$, indicating a stronger contribution of outdoor air. These differences were statistically significant ($p < 0.05$) and were further supported by graphical analysis, which revealed broader and right-skewed distributions in May–June compared to more compact distributions in August–September. The findings demonstrate that indoor particulate matter concentrations during the non-heating season are strongly influenced by seasonal changes in ventilation and occupant behavior, with transitional periods showing increased importance of indoor emission processes.

Keywords: indoor air quality, particulate matter, indoor–outdoor relationships, residential exposure.

INTRODUCTION

Particulate matter (PM) is recognized as one of the most significant air pollutants due to its well-established impacts on human health, including respiratory and cardiovascular diseases, lung cancer, and premature mortality [1]. Particulate matter fractions such as PM_{10} and $PM_{2.5}$

* *visa.tasic@irmbor.co.rs*

are particularly important because of their ability to penetrate deeply into the respiratory system and contribute to adverse health outcomes.

Although outdoor air pollution has been extensively studied, indoor air quality has gained increasing attention in recent decades, primarily because people spend the majority of their time indoors [2]. As a result, indoor exposure to particulate matter often represents a substantial portion of total human exposure.

Indoor PM concentrations are governed by a complex interaction between outdoor air infiltration and indoor emission processes. Activities such as cooking, cleaning, and resuspension of settled dust can significantly increase indoor particle levels, sometimes resulting in concentrations that exceed those measured outdoors [3,4]. The relationship between indoor and outdoor concentrations is commonly expressed through the indoor/outdoor (I/O) ratio, which provides insight into the relative importance of infiltration and indoor sources [5].

Bor (Serbia) represents a specific industrial environment influenced by long-term mining and metallurgical activities, which strongly affect ambient air quality [6]. While outdoor particulate matter levels in this region have been widely investigated, indoor environments in residential settings remain less systematically studied.

Recent research has shown that indoor PM concentrations in such environments are strongly influenced by ventilation patterns, building characteristics, and occupant behaviour. In response to this knowledge gap, a citizen science initiative was established, enabling residents to participate directly in indoor air quality monitoring by hosting measurement devices and providing contextual information on their daily activities.

The non-heating season represents a particularly dynamic period, characterized by changes in ventilation regimes and variations in occupant behavior, which may significantly influence indoor PM concentrations. Transitional periods, in particular, may exhibit enhanced variability due to the combined effects of indoor sources and fluctuating air exchange rates.

The aim of this study is to investigate differences in indoor PM_{10} and $PM_{2.5}$ concentrations between two periods of the non-heating season, May–June and August–September, using normalized indoor/outdoor ratios in order to better understand the dominant processes governing indoor air quality in residential environments.

In addition to its scientific objectives, the citizen science framework enabled broader engagement of the local community in environmental monitoring and awareness. By involving residents directly in the measurement process, the study captured real-life indoor exposure conditions that are often difficult to reproduce under controlled experimental settings. Such an approach also allowed for the collection of contextual information on daily activities, which is essential for interpreting short-term variations in indoor particulate matter concentrations. Furthermore, the participatory nature of the project contributed to increasing public understanding of air quality issues in an industrial environment such as Bor, while simultaneously providing a dataset that reflects both environmental conditions and human behaviours. This integration of instrumental measurements and user-reported data represents an important step toward more comprehensive assessments of indoor air quality.

MATERIALS AND METHODS

Indoor particulate matter concentrations were measured in 30 residential apartments in Bor, Serbia, during the non-heating season (Figure 1). The study was designed as two independent sampling campaigns, each including 15 apartments, conducted in May–June (apartments 1–15) and August–September (apartments 16–30). The apartments were selected to represent typical urban residential conditions, with emphasis on non-smoking households and comparable building characteristics.

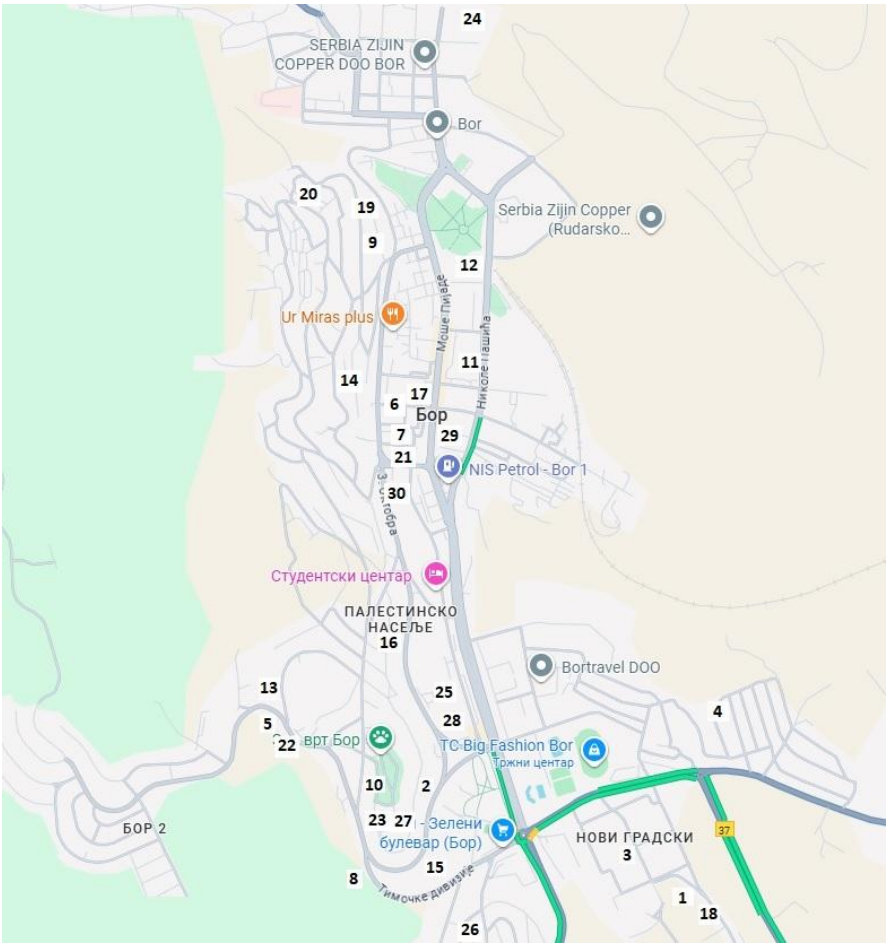

Figure 1 *Spatial distribution of the 30 selected residential apartments in the city of Bor, Serbia*

Indoor PM_{10} and $PM_{2.5}$ concentrations were monitored using compact optical particle sensors (NOVA SDS011 low-cost PM sensor), integrated into automated measuring devices that continuously recorded particulate matter concentrations together with temperature and relative humidity at a temporal resolution of one minute [7]. The performance of this type of sensor has been previously evaluated under different environmental conditions. Prior to deployment, all devices were calibrated under laboratory conditions, and their performance was assessed through comparison with the gravimetric reference method.

Outdoor particulate matter concentrations were obtained from the official automatic monitoring station in Bor (AMS Bor – Town park), where measurements are performed using

a Grimm EDM 180 aerosol spectrometer [8]. Average outdoor concentrations corresponding to each sampling period were used for normalization.

The study was conducted within a citizen science framework, where residents hosted monitoring devices in their homes and recorded their daily activities during the measurement period. This approach enabled a more realistic interpretation of indoor particulate matter variability.

To enable comparison between the two independent datasets, indoor concentrations were normalized with respect to outdoor levels and expressed as indoor/outdoor ratios. Given the relatively small sample size and observed variability, a non-parametric statistical approach was applied. Central tendencies were described using median values, while variability was evaluated through the spread of the data. Extreme values were identified based on their deviation from the main distribution and were examined separately to assess their influence on the results [9]. Differences between the two periods were tested using the Mann–Whitney U test at a significance level of 0.05.

RESULTS AND DISCUSSION

An overview of average indoor and outdoor particulate matter concentrations provides a basis for understanding the observed differences between the two sampling periods and their potential influence on indoor air quality.

Average indoor concentrations were:

- PM_{10}: 21.2 µg/m^3 (May–June) and 17.2 µg/m^3 (August–September)
- $PM_{2.5}$: 12.1 µg/m^3 (May–June) and 9.4 µg/m^3 (August–September)

Average outdoor concentrations were:

- PM_{10}: 20.0 µg/m^3 (May–June) and 26.9 µg/m^3 (August–September)
- $PM_{2.5}$: 9.8 µg/m^3 (May–June) and 10.3 µg/m^3 (August–September)

The normalized indoor particulate matter concentrations showed a clear and systematic difference between the two investigated periods of the non-heating season.

For PM_{10}, the median indoor/outdoor ratio during May–June was approximately 1.08, indicating that indoor concentrations were slightly higher than outdoor levels. In contrast, during August–September, the median decreased to approximately 0.63, suggesting that indoor concentrations were predominantly controlled by outdoor air.

A similar trend was observed for $PM_{2.5}$, where the median value during May–June was approximately 1.16, while in August–September it decreased to approximately 0.94, indicating a reduced influence of indoor sources.

These differences are illustrated in Figure 2, where boxplots show a pronounced shift toward higher values during May–June, along with a wider spread of the data. In contrast, the August–September dataset is more compact, with most values clustered below or around unity.

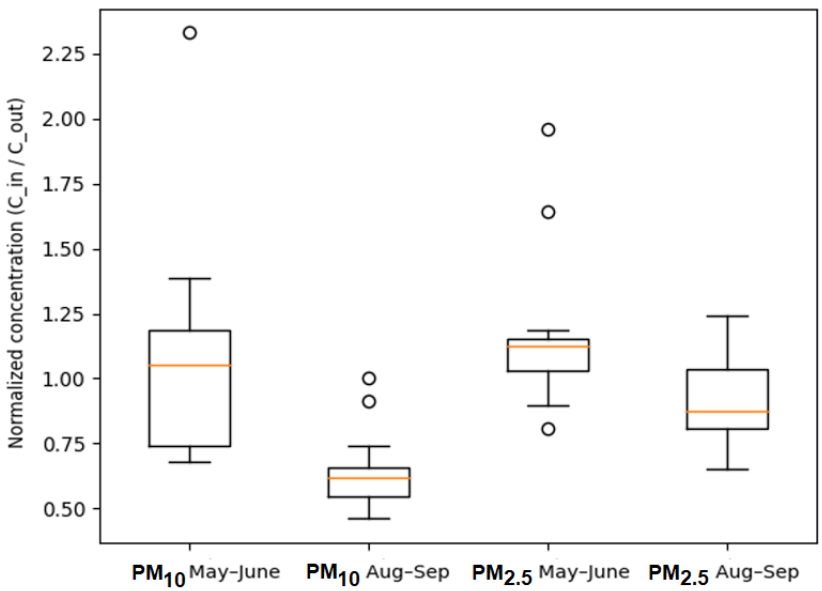

Figure 2 *Boxplots of normalized PM_{10} and $PM_{2.5}$ concentrations (C_in/C_out) for May–June and August–September*

Histogram analysis (Figure 3) further supports these observations. The histogram binning was performed by dividing the range of normalized concentration values into equally spaced intervals. The final number of bins was selected to provide sufficient resolution while maintaining clear visual interpretability of the distributions.

The same binning approach was applied consistently across comparable datasets to enable direct visual comparison. The number of bins was set to k = 7, as this provided a clear compromise between distribution resolution and visual interpretability for the given sample size.

The May–June dataset exhibits a right-skewed distribution, with a noticeable fraction of apartments showing I/O ratios greater than 1.0 and, in some cases, exceeding 2.0 for PM_{10}. The August–September dataset, on the other hand, is centered at lower values and shows reduced variability.

An extreme value observed in the PM_{10} dataset during May–June increased variability but did not significantly affect the central tendency. Its exclusion resulted in only minor changes in the distribution, confirming that the observed differences between the two periods are robust. A similar effect was observed for $PM_{2.5}$, where one elevated value slightly influenced the spread without altering the overall trend.

Statistical testing confirmed that the differences between the two periods were significant ($p < 0.05$), indicating that the datasets represent distinct distributions.

The observed behavior can be explained by seasonal variations in ventilation and occupant activities. The May–June period represents a transitional phase during which ventilation conditions may be less stable and indoor activities such as cleaning and resuspension contribute to elevated concentrations. In contrast, the August–September period is associated with more stable ventilation conditions and higher air exchange rates, leading to stronger coupling between indoor and outdoor air.

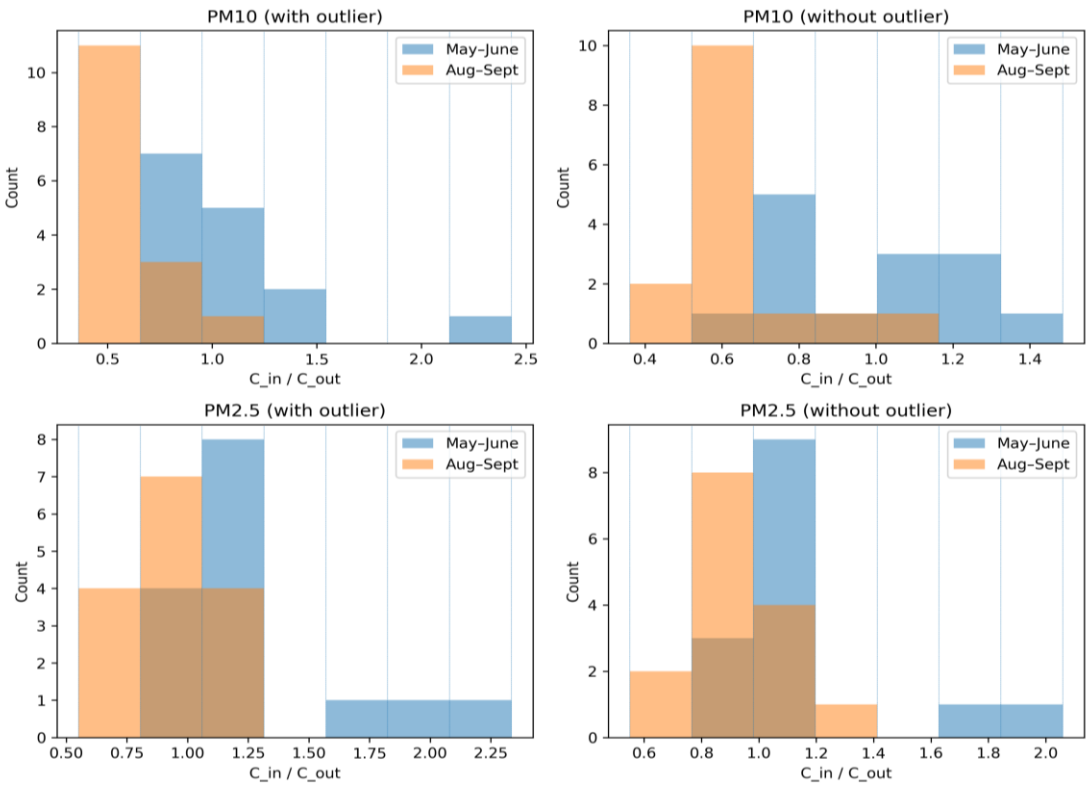

Figure 3 *Histograms of normalized PM_{10} and $PM_{2.5}$ concentrations, illustrating differences in distribution between the two sampling periods*

These findings are consistent with previous studies demonstrating that indoor particulate matter concentrations are controlled by the balance between infiltration and indoor emission processes [3–5].

CONCLUSION

Indoor PM_{10} and $PM_{2.5}$ concentrations in residential apartments in Bor show significant variability during the non-heating season. The May–June period is characterized by a stronger influence of indoor sources, while August–September reflects a greater contribution of outdoor air. The use of normalized indoor/outdoor ratios proved to be an effective approach for comparing independent datasets and identifying dominant processes.

Within the second year of the project, measurements will be extended to an additional 30 apartments, enabling the development of a more comprehensive dataset and allowing direct comparison with results obtained in 2025. This extended dataset will provide a stronger basis for evaluating the temporal stability of indoor air quality patterns in residential environments.

Furthermore, due to space limitations, the present study focuses only on the non-heating season, while the analysis of indoor particulate matter during the heating season will be presented in future publications.

The continuation of measurements within a citizen science framework is expected to contribute to a better understanding of long-term indoor air quality dynamics in industrial urban environments and to support more informed assessment of exposure and associated health risks.

ACKNOWLEDGEMENT

The authors are grateful to the Ministry of Science, Technological Development and Innovation of the Republic of Serbia for financial support according to the contract with registration No. 451-03-33/2026-03/200052.

This work was supported by the Center for the Promotion of Science, Ministry of Science, Technological Development and Innovation of the Republic of Serbia, under Contract No. 1383/24 for the implementation of a citizen science project, dated 18 December 2024.

REFERENCES

[1] World Health Organization. WHO global air quality guidelines: particulate matter ($PM_{2.5}$ and PM_{10}), ozone, nitrogen dioxide, sulfur dioxide and carbon monoxide. Geneva: World Health Organization; 2021.

[2] Morawska, L, Afshari, A, Bae, G.N. *et al*. Indoor Air. 2013, 23(6), 462–487.

[3] Nazaroff, W.W. Indoor Air. 2004, 14 (Suppl. 7), 175–183.

[4] Fromme, H., Twardella, D., Dietrich, S., *et al*. Atmos. Environ. 2007, 41(4), 854–866.

[5] Chen, C., Zhao, B. Atmos. Environ. 2011, 45(2), 275–288.

[6] Tasić, M., Rajšić, S., Novaković, V., *et al*. Facta Univ., Ser. Phys. Chem. Technol. 2006, 4(1), 83–91.

[7] Božilov, A., Tasić, V., Živković, N., *et al*. Environ. Monit. Assess. 2022, 194, 595.

[8] Grimm Aerosol Technik GmbH & Co. KG. EDM 180 environmental dust monitor: operating manual. Ainring: Grimm Aerosol Technik; 2010.

[9] Tukey, J.W. Exploratory data analysis. Reading: Addison-Wesley; 1977.

EcoTER'26
eco.tfbor.bg.ac.rs
32nd International Conference
Ecological Truth & Environmental Research
24–26 June 2026, Hotel Sunce,
Sokobanja, Serbia

Original Research

INFLUENCE OF LITTORAL HABITAT CHARACTERISTICS ON MACROINVERTEBRATE COMMUNITIES IN LAKE OHRID

DOI: 10.5937/EcoTER26153B

Biljana Budzakoska Gjoreska[1,a*], Sasho Trajanovski[1,b], Sonja Trajanovska[2,c]

[1] Department of benthic fauna, PSI Hydrobiological Institute, Naum Ohridski 50, 6000 Ohrid, REPUBLIC OF NORTH MACEDONIA

[2] Department of hydrobotany, PSI Hydrobiological Institute Ohrid, Naum Ohridski 50, 6000 Ohrid, REPUBLIC OF NORTH MACEDONIA

[a] https://orcid.org/0009-0003-3037-2657

[b] https://orcid.org/0000-0002-0682-8568

[c] https://orcid.org/0009-0006-9458-8301

Abstract

Lake Ohrid, one of Europe's oldest and deepest freshwater lakes, represents a unique ecosystem with high biodiversity and numerous endemic species. Its littoral zone comprises a variety of habitats - rocky, sandy and mixed substrates - whose physical and biological characteristics play a crucial role in macroinvertebrate communities. Macroinvertebrates are essential components of littoral ecosystems, contributing to nutrient cycling and food web functioning and are widely used as bioindicators of ecological status. This study analyses the influence of habitat characteristics and structural heterogeneity on the composition, density and diversity of macroinvertebrate fauna. Samples were collected across different substrate types and depth zones, and communities were assessed using the Shannon-Wiener diversity index, Simpson's dominance index and Pielou's evness index, along with complementary ecological indices. Habitat heterogeneity and substrate type were identified as key factors in distribution and community stability. Comparative analysis highlighted local differences: locality Ohrid Bay showed greater ecological stability and endemic species presence, locality River Koselska (Daljan) showed limited diversity and sensitivity to disturbance, while locality HIO–Radozda profile had very good ecological status with sensitive taxa. These findings enhance understanding of habitat–organism interactions in Lake Ohrid and provide valuable data for ecological monitoring, biodiversity conservation and sustainable management of this exceptional lake ecosystem.

Keywords: biodiversity, bioindicators, habitat heterogeneity, ecological monitoring.

INTRODUCTION

Lake Ohrid is characterised by its high biodiversity and a remarkable number of endemic species, making it an important site for scientific research and sustainable resource management [1,2]. Its littoral habitats are highly heterogeneous, including rocky, sandy, habitats with submerged vegetation i.e., macrophytes, and mixed substrates with areas of mud and sand [3,4]. Physical and biological characteristics – such as substrate type, aquatic vegetation, water depth and flow conditions-strongly influence the distribution, abundance

* *biljanab@hio.edu.mk*

and composition of macroinvertebrate communities [5–9]. As integral components of the littoral ecosystem, macroinvertebrates contribute to nutrient cycling, organic matter decomposition and food web dynamics [7,10–12], while their sensitivity to habitat changes makes them reliable bioindicators for assessing the ecological status [13,14] of the habitat of interest. Investigating littoral habitat effects on macroinvertebrates in Lake Ohrid enhances understanding of ecosystem processes and provides essential data for monitoring, conservation and sustainable management of this unique lake [1,3,4,9].

MATERIALS AND METHODS

Field research was conducted at three localities around Lake Ohrid in North Macedonia: Ohrid Bay, River Koselska (Daljan) and profile HIO-Radozda (Figure 1). These sites were selected to represent different levels of anthropogenic pressure, substrate heterogeneity and availability of previous data. Ohrid Bay is located near the urban centre and is influenced by wastewater discharge, air pollution, tourism, and shoreline modification. Daljan, in the transitional zone affected by Koselska River, reflects external inputs of sediments and pollutants. Hydrobiological institute Ohrid-Radozda serves as a reference locality with the longest research history at Lake Ohrid, with extensive datasets for long-term ecological assessment.

1-River Koselska
2-Ohrid Bay
3-Profile: HIO-Radozda

Figure 1 *Location of the sampling localities in Ohrid Lake, Republic of North Macedonia*

Sampling was carried out seasonally during summer and autumn 2025 using the Multihabitat Transect Method for Benthic Material [15], following limnological protocols [10,11,16–20] and the EU Water Framework Directive [21]. Transects were established from the shoreline towards deeper zones, covering littoral, sublittoral and profundal habitats down to 150 m. At the locations Ohrid Bay and Daljan, three depth levels were sampled

corresponding to the lower limit of macrophyte vegetation. At HIO-Radozda profile, littoral sampling points (2 m, 5 m and 10 m) represented three consistent habitat types: sandy-muddy (sand-dominated), muddy-sandy (mud-dominated) with submerge vegetation and muddy substrate.

Macrozoobenthos samples were collected with a van Veen grab sampler (225 cm², 15 × 15 cm). Samples were preserved in 96% ethanol and transported to the laboratory, where they were analyzed under a binocular stereomicroscope. Identification followed standard freshwater invertebrates taxonomic keys [22–29]. Densities were expressed as the number of individuals per square meter (ind/m²).

RESULTS AND DISCUSSION

A total of 49 macrozoobenthos species belonging to eight taxonomic classes were recorded across the studied localities (Table 1). The highest diversity was observed at HBZ–Radozda (37 taxa), while Pristanishte had 24 taxa and Koselska River (Daljan) only 12.

Table 1 *Macrozoobenthos composition at the Ohrid Lake*

Class	Taxa (49)	Profile HIO-Radozda (summer 2025)	Ohrid Bay (autumn 2025)	River Koselska (Daljan) (autumn 2025)
Turbellaria	***Dendrocoelum magnum* Stankovic 1969**	+		
	**Dendrocoelum maculatum* (Stankovic & Komarek, 1927)	+		+
Oligochaeta	*Limnodrilus hoffmeisteri* Claparède, 1862	+		
	Pothamotrix hammoniensis (Michaelsen, 1901)	+		
	Eiseniela tetraedra (Savigny, 1826)	+		
	Tubifex tubifex (Müller, 1774)	+	+	+
	Criodrilus lacuum Hoffmeister, 1845		+	
	**Peloscolex stankovici litoralis* (Hrabě, 1931)		+	
	**Rhynchelmis komareki typical Hr*abě, 1931		+	+
Hirudinea	*Erpobdella octoculata* (Linnaeus, 1758)	+	+	+
	Glossihonia maculosa Sket, 1968	+	+	
	Glossihonia complanata (Linnaeus, 1758)	+	+	
	Glossiphonia pulchella Sket 1968	+	+	
	**Piscicola geometra* Linnaeus, 1761)	+		
	**Dina krilata* Sket 1989	+	+	+
	**Dina lepinja* Sket & Sapkarev, 1986	+		
	**Dina lychnida* (Sket, 1968)	+		
	**Dina profunda* Sket 1989	+		
	**Dina svilesta* Sket 1989	+		
Gastropoda	**Ginaia munda munda* (Sturany, 1894)	+		
	**Xestopyrgula dybowskii* Poliński, 1929	+	+	
	Theodoxus fluviatilis dalmaticus (Linnaeus, 1758)	+		
	**Gyraulus lychnidicus* Hesse, 1928	+		
	**Gyraulus trapezoids* Poliński, 1929	+		
	**Gyraulus albidus* Radoman, 1953		+	
	**Chilopyrgula sturanyi Brusina*, 1896	+	+	
	**Ancylus tapirulus Poliński, 1929*	+		
	**Valvata stenotrema* Poliński, 1929		+	+
	**Ochridopyrgula macedonica macedonica* (Brusina, 1896)		+	
	**Ochridopyrgula macedonica charensis* Radoman, 1978	+	+	
	**Ohridohoratia sturanyi* (Westerlund, 1902)		+	
	**Radix relicta Poliński, 1929*		+	
	**Pyrgohydrobia grochmalickii* (Polinski, 1929)			+
Bivalvia	***Dreissena carinata* (Dunker, 1853)**	+	+	+
	Sphaerium corneum Linnaeus, 1758	+	+	

***Table 1** continued*

Amphipoda	**Gammarus ochridensis abyssalis* Karaman 1931	+		
	**Gammarus ochridensis* (Schäferna, 1926)	+		+
	Gammarus roeselii triacanthus Gervais, 1835	+	+	
	**Gammarus stankokaramani Karaman*, 1976	+		
Isopoda	*Asselus aquaticus* (Linnaeus, 1758)	+	+	
	**Proasselus gjorgjevici f. typicus* (Karaman, 1933)	+		+
	**Proasselus remyi f. Nudus* (Karaman, 1953)	+		
	**Synurella longidactylus* Karaman, 1929	+		
Insecta	*Chironomus plumosus* (Linnaeus, 1758)	+	+	+
	Sialis lutaria (Linnaeus, 1758)	+		
	Baetis sp. Leach, 1815	+		
	Ischura sp. Charpentier, 1840		+	
	Polypedilum pedestre (Meigen, 1830)		+	
	Leptocerus sp. Brewster, 1815			+
Total number of taxa (49)		37	24	12

*The symbol asterisk denotes endemic species

Endemic species (marked with asterisk: *), particularly among Gastropoda, Amphipoda and Hirudinea, highlight the exceptional biological value of Lake Ohrid. Gastropoda were the most species-rich group (14), followed by Hirudinea (10), Oligochaeta (7), Insecta (6), Amphipoda and Isopoda (4 each), while Turbellaria and Bivalvia were represented by two species each.

At HIO-Radozda, the highest total density was observed at 100 m (5475 ind/m²), dominated by *Tubifex tubifex* (3750 ind/m²). Shallow zones (1–5 m) were characterised by lower densities and a greater contribution of Insecta, while deeper zones were dominated by Oligochaeta, Amphipoda and Isopoda (Table 2). At intermediate depths (10–50 m) increased contributions of *Chironomus plumosus* and *Dreissena carinata* were observed in areas with shell accumulations and silted substrates [13]. Profundal zones were dominated by *Tubifex tubifex* and *Synurella longidactylus*, reflecting adaptation to fine, organically enriched sediments with low oxygen availability.

***Table 2** Macrozoobenthos density (ind/m²) by depth and substrate type at the HIO–Radozda profile*

Depth (m)	Bottom facies	Turbellaria	Oligochaeta	Hirudinea	Gastropoda	Bivalvia	Amphipoda	Isopoda	Insecta	Total density (ind m⁻²)	Number of taxa
1	Fine sand with mud and vegetation		100	100			100	0	175	475	5
2	Black sand with mud		275	100			25	0	25	300	5
5	Mud with Chara and ashy shells		50	25	25	375	300		275	0	6
10	Shell zone			75		250			150	1050	4
15	Shell zone	50	425	200	100	450	100	75	475	1875	14
20	Shell zone		125	175	75	500	450	300	75	1700	9

***Table 2** continued*

30	Sand, mud and shells	225	225	50	850	250	400	175	2175	10
50	Mud	300	150	325		375	1000		2150	8
70-80	Mud with sand	825	25			575	25	25	1475	7
100	Mud	4050	50			1250	125		5475	7
150	Mud	75	25			100	125		325	4

Other species with high densities included *Proasellus gjorgjevici f. typicus* (1000 ind/m²), *Dreissena carinata* (800 ind/m²), *Gammarus ochridensis abyssalis* (775 ind/m²) and *Sphaerium corneum* (500 ind/m²). These results point to a stable, resilient benthic community under favourable hydrological conditions, with clear vertical and substrate-related heterogeneity in sustaining Lake Ohrid's benthic biodiversity.

Figure 2 shows a clear change in the composition and density of the benthic fauna with increasing depth and substrate type at the Ohrid Bay locality. The highest total density was observed at 10 m, where Gastropoda and Amphipoda dominated, indicating favorable conditions in mud with shells and *Chara*. The total lowest density was recorded at 20 m, where the simplified fauna is associated with mud and *Dreissena* shells.

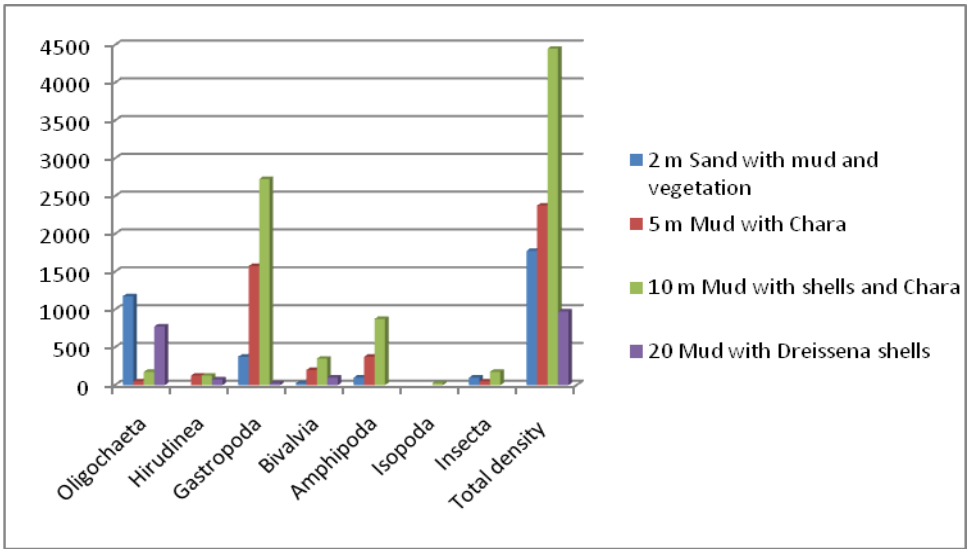

***Figure 2** Density (ind/m²) of macrozoobenthos by depth and substrate type at the Ohrid Bay*

At Ohrid Bay, 24 taxa were registered (Table 3). The highest species richness and density occurred at 5 m on a muddy bottom with *Chara*, where 14 species were identified. Endemic gastropods such as *Ohridohoratia sturanyi* reached 2325 ind/m² at 10 m depth. The community showed clear vertical zonation with diverse assemblages in shallow zones and reduced diversity at 10 m due to unstable sediments. The highest benthic density was observed at 2 m, where a mixed substrate of sand, mud and submerged vegetation supported diverse taxa, mainly Bivalvia and Gastropoda (Figure 2).

Koselska Reka (Daljan) showed only 12 taxa, shaped by detritus-rich substrates and organic enrichment (Figure 3). At 10 m, benthic fauna were absent, reflecting unfavorable conditions, while at 20 m density increased again, dominated by Oligochaeta and Gastropoda typical of muddy habitats with shells with notable contributions from Bivalvia and

Amphipoda. Diversity was low, with sensitive species absent at depth and tolerant forms dominant. In contrast, Ohrid Bay was more stable, supporting higher diversity due to muddy facies, charophytes and endemic gastropods.

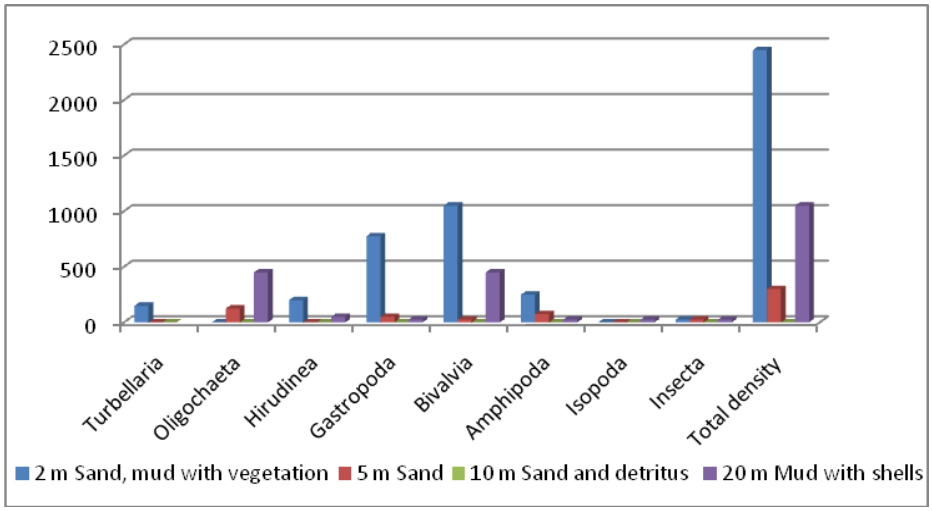

Figure 3 *Density (ind/m²) of macrozoobenthos by depth and substrate type in Daljan*

Table 3 *Ecological status of the localities according to the indices*

2025	Spring	Autumn	
Indices	**HIO-Radozda**	**Ohrid Bay**	**River Koselska (Daljan)**
N (ind/m^2)	17700	9575	3800
Number of species, S	37	24	12
Shannon & Weaver H	5.18	3.93	3.22
Margalef d	19.07	10.05	5.31
Pielou e	0.82	0.73	0.75
Simpson c	0.06	0.11	0.15
ASPT	7.41	4.2	4.6

* Yellow -medium polluted waters; Green-slightly polluted waters; Blue -clean unpolluted waters.
*ASPT (Average Score Per Taxon) Blue - high ecological status; Yellow -moderate ecological status.

Ecological indices confirmed these patterns (Table 3): HBZ–Radozda showed very good ecological status (ASPT 7.41), Ohrid Bay moderate stability with higher diversity (ASPT 4.2), and River Koselska (Daljan) slightly higher tolerance to enrichment (ASPT 4.6). The study demonstrates high structural and functional diversity of macrozoobenthic communities in Lake Ohrid, with clear vertical zonation and strong dependence on substrate type and macrophyte presence. These findings confirm the lake's biological complexity and ecological stability [1–4,14,30].

The highest diversity was recorded within Hirudinea, with significant contributions from Gastropoda and Amphipoda, indicating diverse microhabitats and favorable conditions for organisms with varying ecological requirements. Similar dominance patterns in littoral and sublittoral zones have been reported previously [10], emphasizing the importance of stable substrates and macrophyte communities for benthic fauna development. In contrast, homogeneous and organically enriched facies, such as muddy bottoms or detritus-dominated sediments, support simplified communities dominated by taxa tolerant to low oxygen concentrations and unstable conditions, such as *Tubifex tubifex*. These findings align with

previous studies indicating that substrate structure and vertical zonation are key factors determining the spatial organisation of macrozoobenthos in deep lakes [12,31,32].

The highest biodiversity was observed within *Chara tomentosa* meadows, underscoring the importance of macrophytes as structural engineers of benthic habitats. Charophytes provide shelter, stabilize substrates, and increase surface complexity, thereby enabling the coexistence of diverse taxa. This observation aligns with previous studies emphasizing the central role of macrophytes in maintaining benthic diversity in oligotrophic and mesotrophic lakes [5,6].

The Ohrid Bay locality demonstrates higher diversity and ecological stability, largely due to the presence of muddy facies and macrophytes, as well as the continuous occurrence of endemic gastropods. River Koselska (Daljan) is characterized by organic enrichment and unstable sediments, resulting in reduced diversity and the absence of sensitive taxa at greater depths. This contrast illustrates how substrate instability and anthropogenic pressures can negatively affect benthic macroinvertebrate communities, leading to simplified assemblages dominated by tolerant species [7–9,33]. In littoral zones, moderate densities and the dominance of Oligochaeta, Hirudinea and Amphipoda, together with a lower abundance of Insecta, are consistent with dynamic hydrological conditions and greater exposure to physical disturbance.

Overall, vertical zonation observed in Lake Ohrid's macrozoobenthos underscores the importance of substrate heterogeneity and macrophyte presence in maintaining ecological stability. The high ASPT values at HIO–Radozda confirm a very good ecological status, while the contrasting conditions at Ohrid Bay and River Koselska emphasize the need for continuous monitoring is essential to safeguard the lake's exceptional biodiversity.

CONCLUSION

This study confirmed littoral habitat heterogeneity on the composition, density and diversity of macrozoobenthic communities in Lake Ohrid. Structurally complex habitats, particularly charophytes meadows, supported the highest biodiversity and ecological stability, while homogeneous and organically enriched substrates sustained simplified communities dominated by tolerant taxa such as *Tubifex tubifex*.

Comparative analysis revealed clear differences among localities: Ohrid Bay maintains stable, diverse communities with endemic species; Koselska River (Daljan) is constrained by organic enrichment and unstable sediments; and HIO–Radozda is characterized by very good ecological status with sensitive taxa. These results highlight the exceptional ecological value of Lake Ohrid and emphasize the need for continuous monitoring and adaptive management to safeguard its biodiversity.

ACKNOWLEDGEMENT

The authors express their gratitude to the Ministry of Education and Science for the grant „Limnological investigations of Lake Ohrid (2025-2026)" under Grant Agreement No. 15-6639/17 (24.07.2025).

REFERENCES

[1] Albrecht, C., Wilke, T. Hydrobiologia. 2008, 615, 103–140.

[2] Stanković S. The Balkan Lake Ohrid and its living world. The Hague: Monographie Biol.; 1960. p.357.

[3] Trajanovski, S., Budzakoska Gjoreska, B., Trajanovska, S., *et al*. Hydrobiological Institute Ohrid Rev. 2015, 43(1), 116–130.

[4] Budzakoska-Gjoreska, B., Trajanovski, S., Trajanovska, S. Biologia. 2014, 69(8), 1023–1029.

[5] Blindow, I. Freshw. Biol. 1992, 27(1), 15–27.

[6] Jeppesen E, Søndergaard M, Christoffersen K. The Structuring Role of Submerged Macrophytes in Lakes. Berlin: Springer; 1998.

[7] Allan J.D, Castillo M.M. Stream Ecology: Structure and Function of Running Waters. Dordrecht: Springer; 2007.

[8] Townsend, C.R., Dolédec, S., Scarsbrook, M.R. Freshw. Biol. 1997, 37(2), 367–387.

[9] Trajanovski, S., Budzakoska Gjoreska, B., Trajanovska, S. *et al*. Bot. Serb. 2016, 40(2), 145–151.

[10] Wetzel RG. Limnology: Lake and River Ecosystems. 3rd ed. San Diego: Academic Press; 2001.

[11] Wetzel RG, Likens G. Limnological Analyses. Philadelphia: W. B. Saunders; 1979. p. 263–270.

[12] Cook, D.G. J. Anim. Ecol. 1974, 43, 203–225.

[13] Rosenberg DM, Resh VH. Freshwater Biomonitoring and Benthic Macroinvertebrates. New York: Chapman & Hall; 1993. p. 488.

[14] Armitage, P.D., Moss, D., Wright, J.F., *et al*. Water Res. 1983, 17(3), 333–347.

[15] EN 27828. Water quality - Methods of biological sampling - Guidance on hand net sampling of aquatic benthic macroinvertebrates (ISO 7828:1985). European Committee for Standardization (CEN); 1994.

[16] Dillon RT, Jr. Freshwater Gastropoda. In: Sturm CF, Pearce TA, Valdés A, editors. The Mollusks: A Guide to Their Study, Collection and Preservation. Pittsburgh, PA: American Malacological Society; 2006. p. 251–260.

[17] Lind OT. Handbook of Common Methods in Limnology. St. Louis: Mosby; 1985. p. 199.

[18] Mandaville SM. Benthic Macroinvertebrates in Freshwaters: Taxa Tolerance Values, Metrics, and Protocols. Dartmouth, Canada: Soil & Water Conservation Society of Metro Halifax; 2002. p. 48.

[19] Perez KE, Clark SA, Lydeard C. Freshwater Gastropod Identification Workshop: "Showing Your Shells". A Primer to Freshwater Gastropod Identification. Tuscaloosa, AL: Freshwater Mollusk Conservation Society, University of Alabama; 2004. p. 61.

[20] Rosenberg DM, Davies IJ, Cobb DG, *et al*. Protocols for Measuring Biodiversity: Benthic Macroinvertebrates in Fresh Waters. Winnipeg, Manitoba: Department of Fisheries and Oceans, Freshwater Institute, University of Manitoba; 1997. p. 39.

[21] European Parliament, Council of the European Union. Directive 2000/60/EC of the European Parliament and of the Council of 23 October 2000 establishing a framework for Community action in the field of water policy. Off. J. Eur. Communities. 2000, 327, 1–73.

[22] Barnes RD. Invertebrate Zoology. Philadelphia: Saunders College; 1980. p. 1088.

[23] Karaman, G.S. Poljopr. Šumar. 1976, 22(1), 87–96.

[24] Kerovec M. Guide for the Identification of Invertebrates in Our Streams and Rivers. Zagreb: Sveučilišna naklada Liber; 1986. p. 18–22.
[25] Krstanovski Z. Taxonomy and Ecology of Planaria from Lakes Ohrid, Prespa and Dojran and Adjacent Water-bodies. PhD thesis. Skopje: Sts. Cyril and Methodius University; 1994. 182 p.
[26] Poliński, W. Glas Srp. Kralj. Akad. 1929, 137(65), 131–178.
[27] Radoman P. Hydrobioidea, a Superfamily of Prosobranchia (Gastropoda). II. Origin, Zoogeography, Evolution in the Balkans and Asia Minor. Belgrade: Institute of Zoology, Faculty of Science, Department of Biology; 1985. p. 173.
[28] Radoman P. Hydrobioidea, a superfamily of Prosobranchia (Gastropoda). I. Systematics. Monographs. Belgrade: Serb. Acad. Sci.; 1983. p. 256.
[29] Sapkarev, J. God. Zb. PMF Univ. Skopje. 1964, 15, 5–98.
[30] Trajanovski, S., Budzakoska Gjoreska, B., Trajanovska, S., *et al*. Int. Sci. J. Micro Macro Mezzo Geo Inf. 2016, 6, 108–120.
[31] Hutchinson, G.E. Cold Spring Harb. Symp. Quant. Biol. 1957, 22, 415–427.
[32] Milbrink G. Oligochaeta in freshwater sediments: their ecology and distribution. Dordrecht: Kluwer Academic; 1994.
[33] Budzakoska B, Trajanovski S. In: Proceedings of the 32nd Conference Water Use and Protection "Water 2003"; 2003; Zlatibor, Serbia and Montenegro. 2003. p. 121–126.

EcoTER'26
eco.tfbor.bg.ac.rs
32nd International Conference
Ecological Truth & Environmental Research
24–26 June 2026, Hotel Sunce,
Sokobanja, Serbia

Review

PLANNING AND IMPLEMENTATION OF MINING WASTE SAMPLING: STANDARDS AND LEGAL REGULATIONS

DOI: 10.5937/EcoTER26162M

Vesna M. Marjanović[1,a*], Zoran M. Štirbanović[2,b], Radmila T. Marković[1,c]

[1] Mining and Metallurgy Institute Bor, Alberta Ajnštajna 35, 19210 Bor, SERBIA

[2] University of Belgrade, Technical Faculty in Bor, Vojske Jugoslavije 12, 19210 Bor, SERBIA

[a] https://orcid.org/0000-0001-8005-5244

[b] https://orcid.org/0000-0001-7571-2844

[c] https://orcid.org/0000-0001-9754-1150

Abstract

In this paper, the mining waste sampling process was analyzed with the aim of obtaining a representative sample, which is crucial for reliable laboratory analysis. A special emphasis is placed on drawing up a sampling plan in accordance with relevant standards, such as SRPS EN 14899:2012, SRPS CEN/TR 16365:2013, and the CEN/TR 15310:2009 series, which provide a methodological framework and practical guidelines for sampling in different conditions. Also, the legal regulations in the Republic of Serbia governing the field of mining waste management, including obligations related to classification, testing, disposal, and monitoring of waste, are presented. It was concluded that the proper application of standards and regulations enables efficient management of mining waste, reduction of negative impacts on the environment and contribution to the sustainable development of the mining sector.

Keywords: mining waste, sampling plan, representative sample, standards, legislation, environmental protection.

INTRODUCTION

Mining waste represents a significant source of potential environmental pollution, due to the presence of harmful substances that can negatively affect soil, water resources, and air. In this context, developing sustainable approaches to the management of mining waste is becoming one of the key challenges of the modern mining industry. Sustainable management implies the integration of environmental, economic, and social aspects in order to minimize negative impacts and optimize the use of resources. Management of mining waste involves a series of activities, including its characterization, assessment of potential environmental impacts, and the application of appropriate remediation and control measures [1,2].

The Law on Mining and Geological Research [3] regulates resource exploitation, mining waste management, the construction and use of mining facilities, and the rehabilitation and supervision of these activities. This law stipulates that mining waste must be managed in a way that does not endanger human health and the environment, *i.e.* the law requires that mining

* *vesna.marjanovic@irmbor.co.rs*

waste must be properly classified and recorded, the operator must develop a mining waste management plan, waste disposal must be carried out in a technically and ecologically safe manner, measures to prevent water, soil and air pollution must be applied, mandatory monitoring of landfills and tailings and after the closure of the mine, the operator is obliged to carry out rehabilitation and reclamation of the area.

In the legislation of the Republic of Serbia, the Regulation on the conditions and procedure for issuing a permit for waste management, as well as criteria, characterization, classification, and reporting on mining waste [4] regulates in more detail the conditions and procedure for issuing a permit for waste management, as well as criteria, characterization, classification, and reporting on mining waste. According to this regulation, companies or other legal entities and entrepreneurs that manage waste generated during geological research, exploitation, preparation, and storage of mineral raw materials are obliged to harmonize their operations with the provisions of this regulation.

The Rulebook on Categories, Testing and Classification of Waste [5] prescribes the classification and testing of waste, including the catalogue of waste, categories, and lists of hazardous waste, its characteristics and components, as well as methods of disposal and reuse. It also defines limit values, test parameters and the content of the waste report.

One of the first and basic steps in the characterization of any raw material, including mining waste, is the implementation of the sampling process, in accordance with the basic principles of sampling theory, with the aim of obtaining representative samples. Obtaining a representative sample of mining waste for environmental impact assessment requires a detailed sampling plan. The sampling plan must be done according to standard methods and according to legal regulations. Mandatory standards for drawing up a sampling plan are SRPS EN 14899:2012, which is used as the basic framework for drawing up the plan, followed by the technical report SRPS CEN/TR 16365:2013, the series of standards CEN/TR 15310:2009, and other supporting standards [6–14].

Preparation of a sampling plan according to standard methods

Mining waste represents a significant ecological and technical challenge due to its non-homogeneity and potential impact on the environment. In order to obtain a representative sample, a sampling plan should be prepared according to standard methods and legal regulations. The sampling plan describes the method of collecting the laboratory sample necessary to fulfil the objective of the test program and obtain a representative sample. Mining waste sampling is carried out for the purpose of characterizing the waste, assessing the risk of creating acid rock drainage (ARD), acid mine drainage (AMD), and checking compliance with the limit values for waste disposal.

Standard SRPS EN 14899:2012 (Characterization of waste – Sampling of waste materials – Framework for the preparation and application of a Sampling Plan) determines the procedural steps that need to be taken in the preparation of the sampling plan [6]. This standard is an umbrella European standard that defines the framework for preparing a waste sampling plan. He does not give fixed procedures, but lays down a procedural logic for sampling to be proper and scientifically validated. The key elements of this standard are: defining the sampling objective (Testing Programme). According to him, the sampling plan must be documented and

contain the identification of the population, a sampling strategy that involves determining the number of increments and sampling locations that can be random, systematic or stratified, and a systematic approach that involves determining the required mass of the sample based on grain size. Also, the sampling plan must contain technical instructions (Sampling Operations) that describe in detail which tool is used, which container to use in order to prevent contamination of the sample during transport, and the system for marking the sample taken (date, place, depth of sampling, etc.), Figure 1. According to this standard, sampling is considered complete only when the sampling record is filled out. Any deviation from the plan in the field must be noted, because it directly affects the reliability of the laboratory result.

The principles or basic rules set out in this standard provide a framework that the project manager can use to: develop standardized sampling plans for use in regular or routine circumstances; include specific sampling requirements under European and national legislation; design and develop a sampling plan for case-by-case use. Sometimes more than one sampling plan may be needed to meet all the requirements of the test program. A sampling plan provides the sampler with detailed instructions on how to perform the sampling.

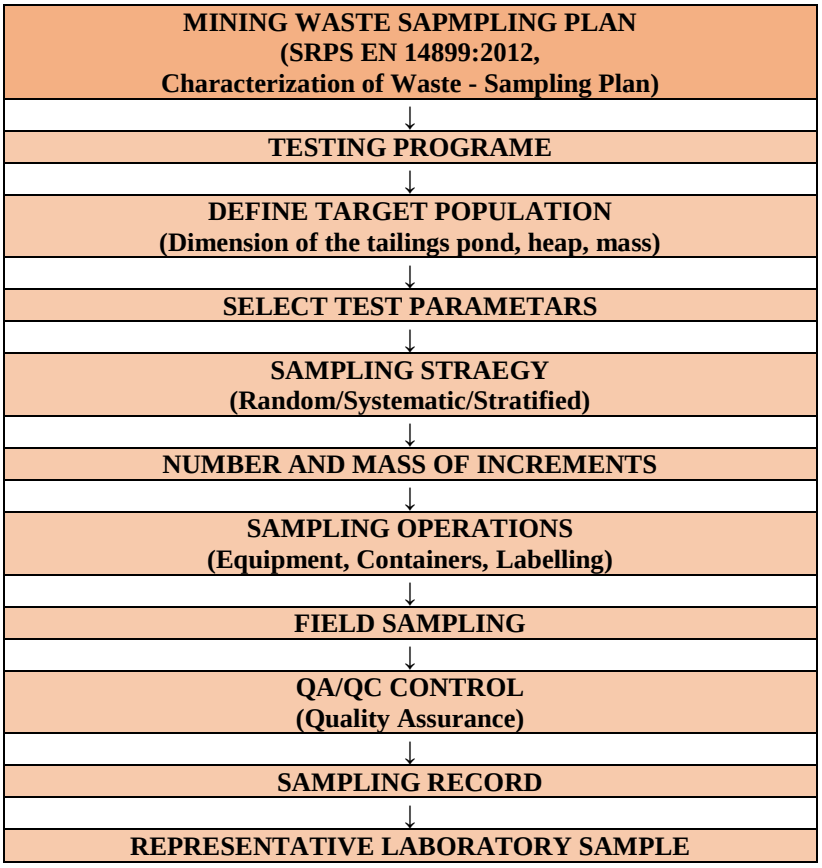

Figure 1 *Mining waste sampling plan*

The sampling plan according to this standard must contain: testing objective, population definition (determining the exact dimensions of the tailings pond (X, Y, Z coordinates) and estimation of total mass), selection of parameters, sampling strategy, mass and number of increments, technical requirements, and quality assurance (QA/QC).

SRPS EN 14899:2012 is used as a basic framework for mining waste sampling, but is rarely used independently. Since mining waste is very specific, a special technical report SRPS CEN/TR 16365:2013, Waste characterization – Sampling of waste from the extractive industry, was developed, which directly follows EN 14899.2012. This technical report provides additional specific information on extractive waste sampling and testing to support the development of suitable sampling plans. This additional guidance for the application of EN 14899:2012 is necessary because extractive waste is significantly different from other types of waste, and the existing sampling scenario given in technical reports CEN/TR 15310-1 to 5. This document should be used together with EN 14899:2012 and CEN/TR 15310-1 to 5 [7].

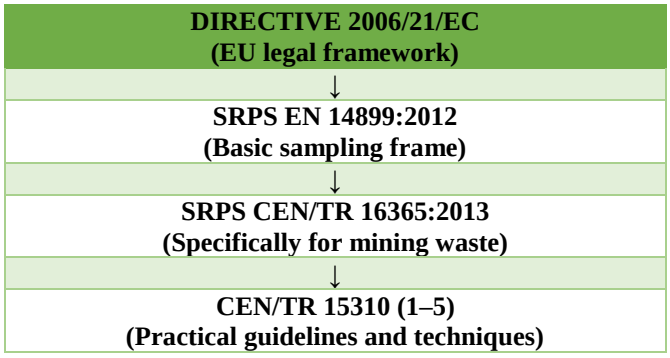

Figure 2 *Hierarchy of standards for creating a mining waste sampling plan*

Preparation of technical reports

The technical report SRPS CEN/TR 16365:2013 uses the logic of EN 14899:2012, but is adapted to challenges such as huge amounts of material and its great heterogeneity. This document provides guidance and specific information for designing and implementing a waste sampling program for mining and quarrying waste. The purpose of this technical notice is to support the development of adequate sampling plans to characterize the waste in accordance with regulatory requirements, operational control, or mine closure plans. The standard focuses on obtaining samples to be representative of the entire mass of waste, which is crucial for assessing potential environmental hazards, such as acid drainage or the presence of heavy metals.

Technical report CEN/TR 16365:2013 does not prescribe one universal method, but offers a framework for creating a Sampling Plan that depends on the phase of the mining project. If the mine is in the exploration phase, then the focus is on cores and analysis of the potential for acid generation (ABA tests). If the mine is in the operational phase, sampling is done directly from strips, from trucks, or from active disposal sites (tailings) to monitor waste variability. If the mine is in the closure phase, methods focus on surface layers and deep drilling to assess long-term stability and reclamation.

According to this technical report, the sample size is determined based on the maximum particle size (granulation) to ensure representativeness, and incremental sampling is recommended, *i.e.*, taking several small "portions" (increments) that are combined into a composite sample.

CEN/TR 16365:2013 is part of a wider package of documents developed for the implementation of Directive 2006/21/EC (known as the Mining Waste Directive) and which represents the key legal act of the EU that regulates the management of waste from the extractive industry [8]. The main objective of the directive is the prevention or reduction of harmful effects on the environment and human health resulting from the management of waste from mining, exploration, extraction, and storage of mineral resources [9].

CEN/TR 15310:2009 is a series of five technical reports (Technical Reports) issued by the European Committee for Standardization (CEN) under the umbrella title "Characterization of waste - Sampling of waste materials". These documents complement SRPS EN 14899:2012 and provide detailed guidance and tools for the practical application of sampling plans in a variety of conditions.

The CEN/TR 15310:2009 series is divided into five specific units:

1. SRPS CEN/TR 15310-1:2009, Waste characterization – Waste sampling – Part 1: Guidelines for the selection and application of sampling criteria under different conditions. This section covers the statistical principles of sampling and helps determine the number and size of samples to achieve the desired precision and reliability. The report shows methods that help in planning sampling in different conditions, but does not provide universal instructions; it provides guidelines for choosing the amount and method of sampling for maximum reliability of the results [10].
2. SRPS CEN/TR 15310-2:2009, Waste characterization – Waste sampling – Part 2: Guidelines for sampling techniques. This section provides practical guidance for sampling different types of waste (solid, liquid, and sludge). This technical report provides information that enables the selection and preparation of equipment and apparatus used for taking samples that can be found in various locations [11].
3. SRPS CEN/TR 15310-3:2009, Waste characterization – Waste sampling – Part 3: Guidelines for field subsampling procedures. It addresses methods for reducing the primary sample to a transportable size while preserving representativeness. It describes procedures in accordance with good practice, with the possibility of applying other appropriate methods [12].
4. SRPS CEN/TR 15310-4:2009, Characterization of waste – Sampling of waste – Part 4: Guidelines for procedures for packaging, storage, protection, transport and delivery of samples. It focuses on preserving sample integrity from sample collection to the laboratory. It describes the procedures for packaging, protection, short-term storage, and transportation of solid and liquid waste samples, with the application of appropriate standards and good practices. When possible and suitable for field application, requirements related to specific storage conditions and protection methods should be selected from the appropriate analytical standard in cooperation with the testing laboratory [13].
5. SRPS CEN/TR 15310-5:2009, Characterization of waste – Sampling of waste – Part 5: Guidelines for drawing up a sampling plan. This technical report contains instructions for documenting the sampling process and developing a sampling plan. It helps with the choice of location and methods, but only provides guidelines based on statistical approaches, in order to achieve reliable results. Due to the variety of waste types, objectives, and sampling techniques, this document does not provide definitive guidance. Only statistical approaches

and statistical methods are given, which are used to determine the sample and the method of collection, to achieve maximum reliability for further testing methods [14].

These reports are of critical importance to laboratories and waste management companies, as they provide a uniform approach necessary for legal compliance and environmental protection. The procedures shown in these documents are in accordance with current good practice.

CONCLUSION

This paper examines the sampling of mining waste as a critical step in its characterization and subsequent management. Due to the pronounced heterogeneity of mining waste, sampling represents a complex process that requires careful planning and the application of appropriate methodologies to ensure sample representativeness. The reliability of laboratory results is directly dependent on the quality of sampling, further emphasizing the importance of a well-designed sampling plan.

Standards such as SRPS EN 14899, SRPS CEN/TR 16365, and the CEN/TR 15310 series provide a comprehensive methodological framework and practical guidance for planning and implementing sampling under various conditions. Their application enables a systematic approach, encompassing the definition of sampling objectives, selection of appropriate strategies, and proper handling, processing, and transport of samples, thereby ensuring the reliability and comparability of results.

In addition to technical considerations, this paper also reviews the legislative framework in the Republic of Serbia governing mining waste management. These regulations clearly define the obligations of operators regarding waste classification, monitoring, safe disposal, and site remediation following the cessation of mining activities. Compliance with these legal requirements, alongside adherence to established standards, forms the foundation of responsible mining waste management.

Based on the presented analysis, it can be concluded that an integrated approach – combining regulatory compliance, standard application, and sound engineering practices – is essential for effective mining waste management. Such an approach contributes to minimizing environmental impacts, conserving natural resources, and supporting the sustainable development of the mining sector.

ACKNOWLEDGEMENT

The authors are grateful to the Ministry of Science, Technological Development and Innovation of the Republic of Serbia for financial support according to the contract with registration No. 451-03-33/2026-03/200052 and 451-03-34/2026-03/ 200131.

REFERENCES

[1] Kalisz, S., Kibort, K., Mioduska, J., *et al*. J. Environ. Manage. 2022, 304, 114239.

[2] Zabaikin, I.V., Lunkin, A.N., Lunkin, D.A. Ecol. Eng. Environ. Technol. 2022, 23(3), 7–14.

[3] Available from: https://www.paragraf.rs/propisi/zakon-o-rudarstvu-i-geoloskim-istrazivanjima.html, *accessed on* 03.04.2026.

[4] Available from: https://www.paragraf.rs/propisi/uredba-o-dozvoli-upravljanje-otpadom-i-rudarskim-otpadom.html, *accessed on* 03.04.2026.

[5] Available from: https://www.paragraf.rs/propisi/pravilnik-kategorijama-ispitivanju-klasifikaciji-otpada.html

[6] SRPS EN 14899:2012, Characterization of waste – Sampling of waste materials – Framework for the preparation and application of a Sampling Plan.

[7] Available from:https://iss.rs/sr_Latn/project/show/iss:proj:41581, *accessed on* 05.04.2026.

[8] Available from: https://www.iea.org/policies/25196-eu-directive-on-the-management-of-waste-from-extractive-industries, *accessed on* 05.04.2026.

[9] Available from: https://eur-lex.europa.eu/EN/legal-content/summary/management-of-waste-from-extractive-industries.html#:~:text=Directive%202006/21/EC%20introduces%20measures%20for%20safe%20management,mineral%20resources%20and%20the.%20It%20must%20be, *accessed on* 05.04.2026.

[10] Available from: https://iss.rs/sr_Cyrl/project/show/iss:proj:21719, *accessed on* 07.04.2026.

[11] Available from: https://iss.rs/sr_Cyrl/project/show/iss:proj:21720, *accessed on* 07.04.2026.

[12] Available from: https://iss.rs/sr_Cyrl/project/show/iss:proj:21721, *accessed on* 07.04.2026.

[13] Available from: https://iss.rs/sr_Cyrl/project/show/iss:proj:21722, *accessed on* 08.04.2026.

[14] Available from: https://iss.rs/sr_Cyrl/project/show/iss:proj:21723, *accessed on* 08.04.2026.

EcoTER'26
eco.tfbor.bg.ac.rs
32nd International Conference
Ecological Truth & Environmental Research
24–26 June 2026, Hotel Sunce,
Sokobanja, Serbia

Original Research

MULTIVARIATE ASSESSMENT OF HEAVY METALS IN RIVER WATER FROM NOVI PAZAR AREA

DOI: 10.5937/EcoTER26169V

Miljan Vilimonović[1], Jelena Vesković[1,a*], Andrijana Okolišan[1,b], Marija Vesković[1], Milica Lučić[2,c], Antonije Onjia[1,d]

[1] University of Belgrade, Faculty of Technology and Metallurgy, Karnegijeva 4, 11120 Belgrade, SERBIA

[2] Innovation Center of the Faculty of Technology and Metallurgy, Karnegijeva 4, 11120 Belgrade, SERBIA

[a] https://orcid.org/0009-0008-4000-7916 [b] https://orcid.org/0000-0002-6310-5235
[c] https://orcid.org/0000-0001-6867-9521 [d] https://orcid.org/0000-0002-5694-7960

Abstract

Surface water pollution has become a serious global problem, particularly pollution caused by heavy metals. This study focused on ten heavy metals (Fe, Cr, Mn, Co, Ni, Cu, Zn, Cd, and Pb) in the water of the Raška River in the vicinity of Novi Pazar city, located in the southwestern part of Serbia, and on the investigation of the processes and activities governing these pollutants in the study area. Three multivariate statistical methods were applied, including principal component analysis supported by Pearson correlation analysis and hierarchical cluster analysis. The results indicated the presence of two principal components, which explained the vast majority of the variance in the dataset, accounting for 93.9%. It was determined that the occurrence of heavy metals in the study area is influenced by both natural processes, such as soil and rock weathering, and anthropogenic activities, including municipal and domestic wastewater discharge and agricultural activities. These results highlight the importance of identifying the main factors controlling heavy metal distribution in surface waters, as this provides a better understanding of water quality and supports more effective monitoring and management.

Keywords: principal component analysis, Pearson correlation, clustering, chemometric analysis, Raška River.

INTRODUCTION

Surface water represents one of the most important natural resources, as it is widely used for drinking water supply, agriculture, industry, and recreation. However, water systems are increasingly exposed to different types of pollution caused by urbanization, industrial development, agricultural activities, and inadequate wastewater management [1]. Among various pollutants, heavy metals are of particular concern because they are persistent in the environment, non-biodegradable, and may accumulate in aquatic ecosystems [2].

Heavy metals can enter surface waters from both natural and anthropogenic sources. Natural inputs are mainly related to the weathering of rocks and soils, while anthropogenic sources include municipal and domestic wastewater discharge, agricultural runoff, industrial

* *jveskovic@tmf.bg.ac.rs*

activities, and traffic-related emissions [3,4]. Once released into aquatic systems, these elements may affect water quality and pose potential risks to aquatic organisms and human health.

Identifying the main processes that control heavy metal distribution in river water is essential for understanding pollution sources and improving water quality management. However, heavy metal concentrations are often influenced by several factors, which makes their interpretation complex. For this reason, multivariate statistical methods are widely used in environmental studies [5]. Pearson correlation analysis, hierarchical cluster analysis, and principal component analysis can help reveal relationships among elements, group pollutants with similar behaviour, and identify possible natural and anthropogenic sources [6].

The Raška River basin, located in the southwestern part of Serbia, is influenced by both natural geological conditions and human activities, including settlements, agriculture, and wastewater discharge. Therefore, this area represents a suitable case study for investigating the factors controlling heavy metal occurrence in surface waters. The aim of this study was to assess the relationships among selected heavy metals in river water from the Novi Pazar area and to identify the main processes affecting their distribution using multivariate statistical methods.

MATERIALS AND METHODS

Study area overview

The study area is located in the southwestern part of Serbia, in southeastern Europe. A total of 18 surface water samples were collected in the vicinity of Novi Pazar city, within the Raška River basin, as shown in Figure 1. The area is predominantly hilly to mountainous, with elevations ranging from approximately 390 to 1800 m above sea level. The climate is temperate continental, with an average annual precipitation of 750–850 mm [7]. The area is mainly covered by forests and pastures, with agricultural land occurring locally.

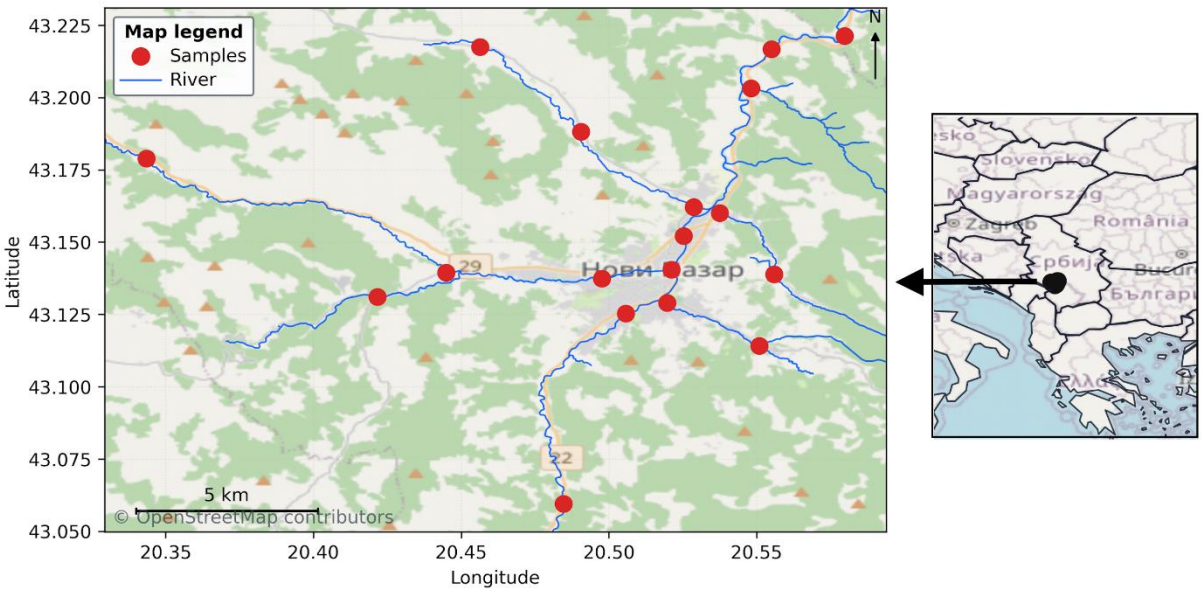

Figure 1 *Overview of the study area with the locations of river water samples*

Surface water sampling and heavy metal analysis

Surface water samples were collected in 1.5 L plastic bottles, which had previously been rinsed with distilled water and then with water from each sampling location. Samples were collected at approximately 20 cm below the water surface, with the bottle opening facing upstream. All samples were acidified on-site to pH < 2 using concentrated HNO_3, in order to ensure that heavy metals remained dissolved in the water and to prevent their precipitation. After sampling, the samples were labelled, stored in a refrigerator, and then transported to the laboratory, where heavy metal concentrations were measured. A total of nine heavy metals were quantified in the surface water samples: Fe, Cr, Mn, Co, Ni, Cu, Zn, Cd, and Pb. The analysis was performed using inductively coupled plasma mass spectrometry (ICP-MS; iCAP TQ, Thermo Fisher Scientific, USA). During the measurements, quality assurance and quality control procedures were followed. The instrument was regularly calibrated, reagent blanks and spiked water samples were analyzed after every six samples, and all analyses were performed in triplicate.

Multivariate statistical analysis

In this study, three multivariate analysis methods were applied. Pearson correlation analysis was used to examine the relationships among heavy metals. The strength of the correlation coefficient r was used to evaluate the degree of association between variables. Correlations were considered weak when $|r| < 0.5$, moderate when $0.5 < |r| < 0.7$, and strong when $|r| > 0.7$ [8,9].

For grouping heavy metals and metalloids according to their similarities, hierarchical cluster analysis was applied. This method is effective for revealing underlying relationships and variations in the dataset [5]. In this study, the analytes were clustered based on similarity using Ward's linkage method and Euclidean distance.

For data dimensionality reduction, principal component analysis was applied. This multivariate statistical method aims to transform a dataset containing correlated variables into a new set of uncorrelated variables. The number of principal components to be retained was determined using the Kaiser criterion, according to which only principal components with an eigenvalue greater than 1 were retained [5,6].

Before conducting multivariate analysis, the dataset was standardized in order to minimize the influence of different concentration ranges. The mentioned methods were used to determine the processes controlling the chemistry of heavy metals in the sampled surface water.

RESULTS AND DISCUSSION

Pearson correlation matrix of surface water samples is presented in Table 1, while dendrogram of heavy metals obtained via hierarchical cluster analysis is shown in Figure 2. It can be seen that a strong positive correlation was characterized for Fe and Mn (r = 0.99) and Fe and Cu (r = 0.93). Additionally, Cu showed a strong positive correlation with Mn (r = 0.92). These findings suggest that similar processes govern Fe, Mn, and Cu behaviour in surface water of the study area. Furthermore, another strong positive correlation was observed between Ni and Zn (r = 0.92) and Ni and Cr (0.77). Also, Cd showed a strong positive correlation with Zn and Pb (r = 0.93), while similar situation was observed for Pb with Co,

Cr, and Ni (r > 0.82). According to Pearson correlation matrix, it can be said that Ni, Zn, Pb, Cd, Cr, and Co share a similar origin. The results of Pearson correlation analysis were further supported by the hierarchical cluster analysis. As shown in Figure 2, all heavy metals were divided into two main clusters. The first cluster included Fe, Mn, and Cu, while the second comprised Ni, Zn, Pb, Cd, Cr, and Co. The grouping of heavy metals within the same cluster suggests that the analytes in each cluster are influenced by similar processes controlling their mobility and concentrations in surface water. In contrast, the analytes grouped in the separate cluster are likely affected by different environmental or anthropogenic processes.

Table 1 *Pearson correlation matrix of surface water samples in the Novi Pazar area*

Analyte	Fe	Cr	Mn	Co	Ni	Cu	Zn	Cd	Pb
Fe	1	0.24	0.99	0.50	0.65	0.93	0.41	0.30	0.41
Cr	0.24	1	0.17	0.81	0.77	0.37	0.82	0.72	0.82
Mn	0.99	0.17	1	0.43	0.60	0.92	0.34	0.23	0.33
Co	0.50	0.81	0.43	1	0.92	0.59	0.97	0.85	0.97
Ni	0.65	0.77	0.60	0.92	1	0.74	0.92	0.87	0.91
Cu	0.93	0.37	0.92	0.59	0.74	1	0.52	0.44	0.52
Zn	0.41	0.82	0.34	0.97	0.92	0.52	1	0.93	1.00
Cd	0.30	0.72	0.23	0.85	0.87	0.44	0.93	1	0.93
Pb	0.41	0.82	0.33	0.97	0.91	0.52	1.00	0.93	1

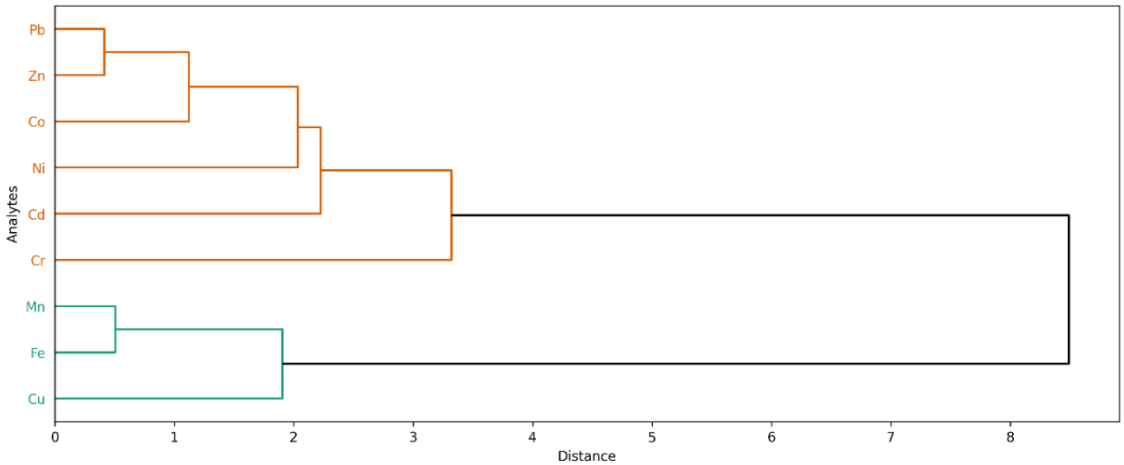

Figure 2 *Dendrogram of surface water samples in the Novi Pazar area*

For a more detailed determination of the processes controlling the behavior of heavy metals in the investigated water, principal component analysis was also performed. The scree plot is shown in Figure 3a, while Figure 3b presents the biplot of the first two principal components with scores and loadings. The loading values for each principal component with an eigenvalue greater than 1, together with the percentage of explained variance, are given in Table 2. The results indicate that two principal components were characterized by eigenvalues greater than 1, and therefore these two components were retained for further analysis. These two principal components explained the vast majority of the variance in the data, amounting to 93.9%.

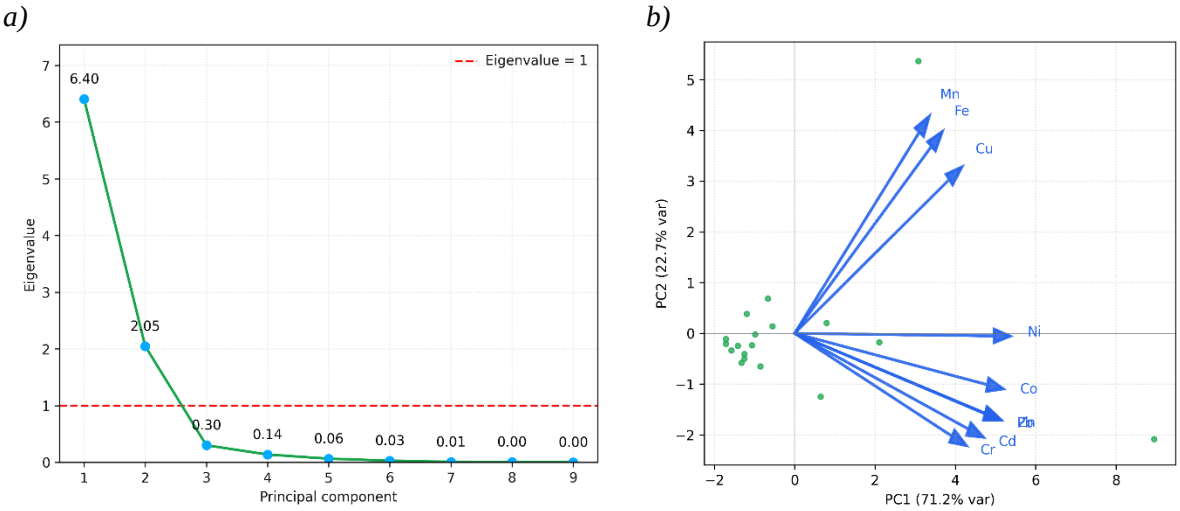

Figure 3 *Scree plot of all principal components (a) and biplot of the first two principal components showing score and loading values*

Table 2 *Loadings of the first two principal components with eigenvalues greater than 1*

Analyte	PC1	PC2
Fe	0.206	0.971
Cr	0.880	0.052
Mn	0.127	0.987
Co	0.920	0.314
Ni	0.850	0.494
Cu	0.348	0.906
Zn	0.969	0.213
Cd	0.932	0.118
Pb	0.966	0.210
Cumulative explained variance (%)	71.2	93.9

The first principal component (PC1) explained 71.2% of the variance and had strong loadings of Cr, Co, Ni, Zn, Cd, and Pb. Nickel, Cd, Pb, and Zn are metals whose presence in the environment is mostly explained as a consequence of anthropogenic activities. Namely, Ni, Cd, Pb, and Zn enter surface waters through the discharge of municipal and domestic wastewater into rivers [10,11]. Since the Raška River, where sampling was conducted, passes through a large number of villages, as well as the town of Novi Pazar, municipal and domestic wastewater can be considered one of the processes controlling the levels of heavy metals in the investigated water. Additionally, Cu, Zn, and Cd are often explained as a result of the excessive use of artificial fertilizers [12]. Therefore, PC1 can be interpreted as an anthropogenic factor.

On the other hand, the second principal component (PC2) explained 22.7% of the variance and was mainly associated with negative loadings of Fe, Mn, and Cu. In the environment, Fe and Mn are considered to be predominantly of geogenic origin, since they are common constituents of the Earth's crust [13]. High loadings of Fe and Mn suggest that these elements may be associated with Fe–Mn oxide/hydroxide phases. Fe and Mn often originate from rocks, soils, and sediments. When river turbidity increases, erosion or sediment resuspension

may occur, allowing these elements to be released into the water [14]. Copper can bind to Fe/Mn oxides and sediments, which may explain why it appears in the same principal component [15]. Hence, PC2 can be explained as natural factor.

CONCLUSION

This study examined the factors controlling heavy metal distribution in the surface water of the Raška River, in the vicinity of Novi Pazar, using Pearson correlation analysis, hierarchical cluster analysis, and principal component analysis. The obtained results indicate that the observed heavy metal concentrations are shaped by several controlling factors, including weathering of soil and rocks, municipal and domestic wastewater discharge, and agricultural practices. These findings highlight the importance of source identification for understanding the processes that influence surface water quality in the Raška River basin.

ACKNOWLEDGEMENT

This work was financially supported by the Ministry of Science, Technological Development and Innovation of the Republic of Serbia (No. 451-03-34/2026-03/ 200135 and 451-03-33/2026-03/200287).

REFERENCES

[1] UNESCO. The United Nations World Water Development Report 2024: Water for Prosperity and Peace. 2024. Available from: https://www.unesco.org/en/articles/united-nations-world-water-development-report-2024-water-prosperity-and-peace

[2] Edo, G.I., Samuel, P.O., Oloni, G.O., *et al*. Chem. Ecol. 2024, 40, 322–349.

[3] Basmacı, A., Akarsu, C., Sivri, N. Int. J. Environ. Sci. Technol. 2023, 20, 5715–5732.

[4] Nieder, R., Benbi, D.K. Rev. Environ. Health 2024, 39, 561–575.

[5] Inobeme, A., Nayak, V., Mathew, T.J., *et al*. J. Environ. Manage. 2022, 309, 114653.

[6] Dupont, M.F., Elbourne, A., Cozzolino, D., *et al*. Anal. Methods 2020, 12, 4597–4620.

[7] Arab Amiri, M., Gocić, M. Environ. Earth Sci. 2021, 80, 777.

[8] Radomirović, M., Ćirović, Ž., Maksin, D., *et al*. Front. Environ. Sci. 2020, 8, 560415.

[9] Pan, X., Wang, W., Liu, T., *et al*. Water 2020, 12, 2869.

[10] Kinuthia, G.K., Ngure, V., Beti, D., *et al*. Sci. Rep. 2020, 10, 8434.

[11] Vesković, J., Bulatović, S., Ražić, S., *et al*. Water Environ. Res. 2024, 96, e11087.

[12] Liao, Z., Chen, Y., Ma, J., *et al*. Int. J. Environ. Res. Public Health 2019, 16, 2805.

[13] Vesković, J., Onjia, A. J. Environ. Sci. 2026, 159, 445–459.

[14] Zhang, J., Wang, K., Yi, Q., *et al*. Environ. Pollut. 2022, 294, 118668.

[15] Dang, D.H., Lenoble, V., Durrieu, G., *et al*. Mar. Pollut. Bull. 2015, 92, 113–124.

EcoTER'26
eco.tfbor.bg.ac.rs
32nd International Conference
Ecological Truth & Environmental Research
24–26 June 2026, Hotel Sunce,
Sokobanja, Serbia

Original Research

URBAN AIR QUALITY MEASURED CLOSE TO SCHOOLS AND KINDERGARTENS WITHIN THE LOCAL MONITORING NETWORK IN SERBIA

DOI: 10.5937/EcoTER26175M

Branislava I. Matić[1,a*], Valentina M. Vukmanović[1,b], Snežana V. Živković Perišić[1,c]

[1] Institute of Public Health of Serbia, Dr Subotića 5, 11000 Belgrade, SERBIA

[a] https://orcid.org/0000-0001-8989-7499

[b] https://orcid.org/0009-0001-5810-0624

[c] https://orcid.org/0000-0001-6435-1190; https://orcid.org/0009-0007-9198-9385

Abstract

Exposing children to environmental pollutants during periods significant for their physiological development can lead to long-lasting health effects, dysfunction, and disease. Aim *of this paper was to focus on a relatively scarce ambient AQ monitoring practice at the locations of preschol and school facilities in Serbia, within the local network of AQ monitoring stations. This was a cross-sectional study covering period 2015 to 2024.*

Measuring points (SO_2, NO_2, soot, PM_{10}) were in front of kindergardens, primary and high *schools in urban settlements. Results originate from the continuous public health programme conducted by the Institute of Public Health of Serbia. In sum, both the absolute number of urban ambient AQ measuring points monitored by the local network of Institutes of Public Health and those in front of the educational facilities have increased in this period: from 73/17 to* 185/29. *Namely, these facilities are chosen more seldom within researched time frame, dropping from 23.29% to 15.12% of all AQ monitoring points. As such facilities are mainly located at important urban intersections, in order to assess the exposure to air pollution of vulnerable population groups (children from preschool to adolescence age), it is recommended to locate more measuring points near them.*

Keywords: preschool and school facilities, ambient air quality, measuring points.

INTRODUCTION

According to their location, schools in the administrative area of large cities can be positioned in the central urban core of the city, in the broader urban area and in rural suburbs, which determines the potential risks from the environment [1]. Given the length of time children spend in school, the school environment represents a significant microclimatic environment, in terms of the impact of air pollution on their respiratory health, above all. According to *International Review of Curriculum and Assessment Frameworks Internet Archive* children in developed countries spend 175 to 220 days a year in school, five to eight hours a day [2].

The aim of this paper was to focus on a relatively scarce ambient AQ monitoring practice at the locations of preschool and school institutions in Serbia, within the local network of AQ monitoring stations.

* *brankicam@batut.org.rs*

MATERIALS AND METHODS

The research tool used in this cross-sectional study is a data base formed and regularly updated by the Institute of Public Health of Serbia (IPHS), as a segment of a continuous AQ monitoring process implemented for the Ministry of Health, through regular reporting of local IPHs from the Network. Sampling, measuring and analyzing level of defined indicators are done by environmental health departments of local / regional IPHs. Data collation, processing and analysis are undertaken by the IPHS, whose assignment is to forward its remarks on possible public health risks to decision-makers. Due to the clear market conditions established in the field of operation of accredited laboratories, the data collected at the IPHS may vary from year to year [3].

Indicators that are monitored are grouped according to the nature of pollution sources, population coverage, traffic density and potential public health risks: SO_2, soot, NO_2, PM_{10} and atmospheric deposition. Together with the key stakeholders at the local level (local self-government, local IPH), each municipality/town produces a Local Action Plan for AQ monitoring, defining the time schedule of monitoring activities and spatial distribution of sampling points, sources of air pollution and choice of pollutants in need of monitoring. Sulphur dioxide and soot are measured daily due to the strong correlation among their ambient air concentrations and fossil fuel combustion, as Serbia‘s key energy source is lignite coal [4]. NO_2 is the most frequently measured specific pollutant, on daily basis. Presence of particulate pollution in ambient air is monitored through sampling of coarse particles of total atmospheric deposition (mg/m^2/day), PM_{10} and $PM_{2.5}$, with different measurement frequency, according to local AQ monitoring plans and specific indication, depending on pollution sources and financial resources of the local administration and the polluter, *per se*.

RESULTS AND DISCUSSION

Table 1 shows precise GIS location of all measuring points: primary schools (PS), kindergartens (KG) and High schools (HS); SOS Children´s Village together with the sellected pollutants monitored. The exception among these educational institutions is the SOS Children's Village (Sremska Kamenica), as the site is not only a teaching, but also a residential space, where complete care is taken of children without parental care in an organized and humane way. The fact that children are going through all of their daily routine at the same spot could be the reason why at this site the most number and type of pollutants are monitored simultaneously.

Although the total number of measuring points in the Local AQ monitoring network for the period 2015–2024 is, actually, increasing, the number of educational facilities used as sampling points is in decline (Figures 1 and 2).

Table 1 *GIS coordinates of educational facilities involved in monitoring*

Facilities (29)		GIS	Pollutants monitored
PRIMARY SCHOOLS (15)			
Rakovica, Beograd	„Nikola Tesla”	44°44´47.55" N 20°26´21.56" E	*SO_2, soot, NO_2, indicative: PM_{10} with heavy metals analysis (As, Cd, Ni, Pb), B(a)P*
Obrenovac, Beograd	“Jefimija”	44°40´06.67" N 20°11´45.50" E	*SO_2, soot, NO_2, PM_{10}, AD*
Višnjica, Beograd	"Pavlović Barili"	44°49´04.88" N 20°32´04.86" E	*SO_2, soot, NO_2, benzene*
Valjevo	"Sestre Ilić"	44°16´09.59" N 19°52´53.01" E	*SO_2, soot, NO_2*
Vranje	„Sv. Marković”	42°32´01.88" N 21°53´53.90" E	*SO_2, soot, NO_2, AD*
	“J.J.Zmaj”	42°54´71" N 21°89´28" E	
Vranjska Banja	„Predrag Devećić”	42°55´58" N 21°89´95" E	*SO_2, soot, NO_2, AD*
Zvečan	„Vuk Karadžić”	42°54´38.81"N 20°50´19.10"E	*SO_2, soot, NO_2*
Kosjerić	“Mito Igumanović”	43°59´40.50" N 19°54´25.85" E	*AD*
Kragujevac	“Stanislav Sremčević”	44°00´39.44" N 20°53´43.49" E	*SO_2, soot, NO_2*
	„M. Jovanović”	44°01´48,66" N 20°54´20,54" E	*SO_2, soot, NO_2, PM_{10} with heavy metals analysis (Pb, Cd, As, Ni)*
Kać	"Đura Jakšić",	45°17´59.45" N 19°56´26.56" E	*SO_2, NO_2, PM_{10} with heavy metals analysis (Pb, Cd, Ni, As), B(a)P, $PM_{2,5}$*
Požarevac	„Kralj Aleksandar I”	44°36´52.2" N 21°10´49.9" E	*SO_2, soot, NO_2, AD with heavy metals analysis (Pb, Cd, Zn)*
Vranovo	“Dositej Obradović”	44°39´50.55" N 20°55´27.08" E	*PM_{10} with heavy metals analysis (Pb, Cd, Ni, As), B(a)P*
Subotica	"S. Marinković" Mala škola	46°05´34" N 19°40´20" E	*PM_{10} with heavy metals analysis (Pb, Cd, Ni, As)*
KINDERGARTENS (11)			
Valjevo	"Bubamara"	44°16´33.64" N 19°52´24.96" E	*SO_2, soot, NO_2*
	„Pčelica”	44°17´01.21" N 19°52´21.99" E	
	„Kolibri”	44°16´56" N 19°55´3" E	
	"Vidra"	44°15´54.16" N 19°53´49.96" E	
Zvečan	Kindergartens	42°54´39.92"N 20°50´12,94"E	*atmospheric deposition (AD)*
Leposavić		43°06´16.98" N 20°48´08.91" E	
Lešak		43°10´09.83" N 20°44´23.68" E	
Zubin Potok		42°55´24.72" N 20°40´22.58" E	
Leskovac	„Kolibri”	42°99´49" N 21°95´63" E	*SO_2, soot, NO_2, AD with heavy metals analysis (Pb, Cd, Zn)*
Kragujevac	Ilićevo, „Čuperak”	44°01´48,22" N 20°57´06,44" E	*SO_2, soot, NO_2*
Sevojno	“Maslačak”	43°50´40.83" N 19°53´45.09" E	*AD with heavy metals analysis (Pb, Cd, Zn, Ni, As, Cu)*
HIGH SCHOOLS (3)			
Kragujevac	Medical	44°01´11,79" N 20°54´33,36" E	*AD with heavy metals analysis (Pb, Cd, Zn)*
Leskovac	Medical	42°99´64" N 21°93´63" E	*SO_2, soot, NO_2, AD with heavy metals analysis (Pb, Cd, Zn)*
Sremska Mitrovica	Economics	42°58´45.61" N 19°35´18.86" E	*SO_2, soot, NO_2*
Sremska* Kamenica	SOS Children´s Village	45°13´31.41" N 19°50´42.69" E	*SO_2, NO_2, NO, NO_X, CO, O_3, BeToXy, PM_{10} with heavy metals analysis (Pb, Cd, Ni, As), B(a)P, $PM_{2,5}$*

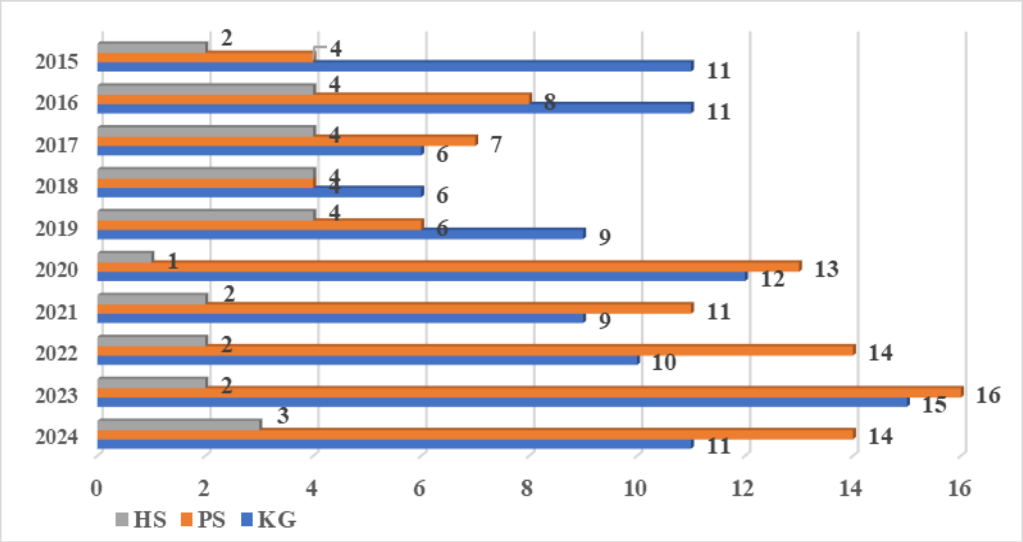

Figure 1 *No. of measuring points in front of educational facilities*

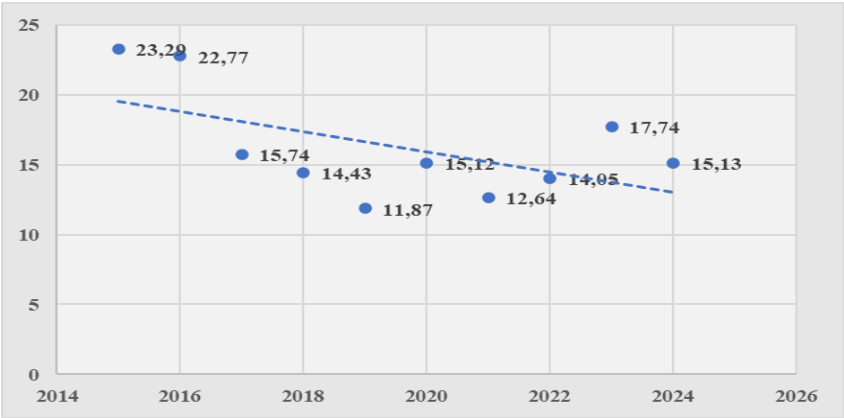

Figure 2 *The declining trend line of coverage of AQ monitoring (%)*

As shown in the following table, pollutants measured in 2024 in front of educational facilities were distributed in the following frequency: SO_2/19, soot/20, NO_2/20, atmospheric deposition/13 and PM_{10}/7. Analyzing values of SO_2, NO_2 and soot, being measured daily, no exceedances of the annual limit value were recorded for any of these parameters at the measuring points close to educational facilities (Table 2).

Measured at 21/185 sampling points, (11.35%) SO_2, soot, NO_2, are monitored mostly on regular basis, in daily measurements, while PM_{10} is often monitored as part of indicative monitoring practice. Atmospheric deposition in front of educational institutions was monitored at 12 out of 185 measuring points in 2024, which is cca 6.5% (6.48%). Only at two points, in Vranje and Vranjska Banja, the mean annual concentration has exceeded the given limit value of 200 mg/m^2/day. At only 6 out of all 185 measuring points in the survey had monitoring of PM_{10} particles in front of educational facilities. In neither of cases did PM_{10} concentration values were beyond the average anual limit value of 40 µg/m^3.

Table 2 *SO_2, soot, NO_2, PM_{10} (μg/m^3) and atmospheric deposition (AD)*

Parameters	**SO_2**	**Soot**	**NO_2**	**PM_{10}**	**AD**
		(μg/m^3)			**mg/m^2/day**
Educational facilities					
Primary schools (15)					
„Nikola Tesla", Rakovica	<10	6.50	21.75		
"Jefimija", Obrenovac	13.50	5.30	12.75	30.83	98.83
"Milena Pavlović Barili", Višnjica	<10	6.10	13,83		
"Sestre Ilić", Valjevo	11.12	11.40	13.90		
„Svetozar Marković", Vranje	25.20	17.30	15.50		**216.52**
"J.Jovanović Zmaj", Vranje	26.80	10.83	16.27		120.17
"P.Devećić", Vranjska Banja	16.38	7.27	7.12		**217.23**
"Vuk Karadzic", Zvečan	4.12	6.05	0.70		
"M. Jovanović", Kragujevac	3.00	36.33	17.33	33.25	
"St.Sremčević", Kragujevac	3.33	28.00	17.92		
Kosjerić					102.20
Vranovo				44,20	
"Sonja Marinković", Subotica				34.90	
"Đura Jakšić", Kać	6.38	13.08	17.70	24.80	
„Kralj Aleksandar I", Požarevac	22.63	8.75	27.74		165.40
Kindergartens (11)					
„Pčelica" Valjevo	11	18.70	13.18		
„Kolibri", Novo Valjevo	11	15.46	14.72		
"Vidra", Valjevo	11	14.63	12.80		
"Bubamara", Podgorska bb, Valjevo	11	14.10	33.63		
"Neven", Vranje	26.97	10.38	23.47		99.42
Zvečan					124.71
Leposavić					113.85
Lešak					122.96
Zubin Potok					111.75
"Kolibri", Leskovac	<5.00	20.70	8.10		
"Kolibri", Kula				23.90	
High schools (3) + 1*					
Medical School, Kragujevac		18.50	27.25		
Medical School, Leskovac	<5.00	27.30	11.80		85.86
Economics HS, Srem.Mitrovica	3.30	15.50	19.06		
SOS Children's village *	8.41		16.52	19.80	
Annual limit values	**50**	**50**	**40**	**40**	**200**

In most cases educational facilities are located at important city intersections, which is justified by choosing traffic-induced pollutants, such as SO_2, NO_2 and soot to be measured on daily basis [5–7]. On the other hand there is a significant disparity between the need to monitor the exposure of children to extremely high values of SO_2 [8,9] and unnecessary monitoring of atmospheric deposition, in which increased values of any parameter are regularly not recorded [4]. Through more rational allocation of resources, some better distribution of measuring stations and determining of parameters to monitor according to continuous air pollution sources, a more valuable assessment of the exposure to air pollution of vulnerable population groups (children from preschool to adolescence age), could be made. For example, the town of Bor and Krivelj village have a long history of environmental pollution due to copper mining and smelting activities, and AQ monitoring is covered with a substantial number of stations and parameters [10,11]. But, besides being an industrial town,

we have children living there, attending institutions of all levels of education (5 primary schools, kindergartens, a high school and University of Technology in Bor) in which they are exposed to pollutans entering from outdoor to indoor space, being well documented through literature [12,13]. Results of the APHEKOM network study indicate that near-road-related pollution may be responsible for a significant portion of the burden of asthma in children, as well as chronic heart diseases, in adults [13,14].

CONCLUSION

After having an insight into the frequency and choice of monitoring air quality at the local level in Serbia, a conclusion is imposed on an existing strong need to make indicator corrections in AQ monitoring in industrially contaminated urban settlements in Serbia and impose continuous monitoring in front of more schools and kindergartens in Bor, Smederevo, Pančevo, Šabac, as well as determining parameters depending on the source of emissions [4, 15–17].

REFERENCES

[1] Wolfe, M.K., McDonald, N.C., Arunachalam, S., *et al*. J Urban Aff. 2020, 7, 43(8):10.1080/07352166.2020.1734013.

[2] INCA (2009). INCA Comparative Tables (Online). International Review of Curriculum and Assessment Framework Internet Archive (INCA), London, UK.

[3] Institute of Public Health of Serbia; Reports, Center of Hygiene and Human Ecology; Available from: https://www.batut.org.rs/index.php?content=1413.

[4] Vujić, B.B., *et al*. Therm. Sci.. 2019, 23(6B), 4055–4065.

[5] World Health Organization. Health effects of transport-related air pollution ISBN 92-890-1373-7; 2005.

[6] Fuller, G., Anderson, R., Atkinson, R., *et al*. Air Qual. Atmos. Health. 2014, 7(4), 459–466.

[7] Simonovski A., Tasić V., Apostolovski-Trijić T., Milikić N., Božilov A. ACTA UNIVERSITATIS Series: Working and Living Environmental Protection, 2020, 17(2), 131–137.

[8] Nikolić, Dj., Milošević, N., Mihajlović, I. *et al*. Water Air Soil Pollut 2010, 206, 369–383.

[9] Stanojević, A.B. Ann Environ Sci Toxicol 2021, 5(1), 023–026.

[10] Tasić, V., Milošević, N., Kovačević, R., *et al*. Chem. Ind. Chem. Eng. Q. 2012, 18(4), 643−652.

[11] Janssen, N.A.H., van Vliet, P.H.N., Aarts, F. *et al*. Atmos. Environ. 2021, 35, 3875–3884.

[12] Perez L., Declercq C., Iňiguez C., Eur Respir J 2013, 42,: 594–605.

[13] Martin R., Dowling K., Pearce D., *et al*. Geosciences 2014, 4, 128–175,

[14] Kovačević R., Jovašević-Stojanović M., Tasić V., *et al*. Chem. Ind. Chem. Eng. Q. 2010, 16(3), 269−279.

[15] Bergstra, A., Brunekreef B., Burdorf, Environ. Health. (2018) 17(30).

[16] Rovira, E., Cuadras, A., Aguilar, X., *et al*., Environ. Res, 2014, 133, 156–163.

[17] Matić, B.I., Rakić, U.D., Dejanović S.M., *et al*. TEHNIKA – KVALITET IMS, STANDARDIZACIJA I METROLOGIJA, 2017, 17(3), 441–447.

EcoTER'26
eco.tfbor.bg.ac.rs
32nd International Conference
Ecological Truth & Environmental Research
24–26 June 2026, Hotel Sunce,
Sokobanja, Serbia

Original Research

UNCOVERING HIDDEN DIVERSITY OF *Sabanejewia balcanica* IN SERBIA: THE DISCOVERY OF NOVEL HAPLOTYPES

DOI: 10.5937/EcoTER26181M

Tamara Mitić[1,a], Ana Marić[2,b], Katarina Jovičić[1,c], Vesna Đikanović[1,d*], Nikola Marinković[1,e], Stefan Anđus[1,f], Jelena Čanak Atlagić[1,g]

[1] Department of Hydroecology and Water Protection, Institute for Biological Research "Siniša Stanković", National Institute of the Republic of Serbia, University of Belgrade, Bulevar despota Stefana, 142, 11108 Belgrade, SERBIA

[2] University of Belgrade, Faculty of Biology, Studentski trg 16, 11000 Belgrade, SERBIA

[a] https://orcid.org/0009-0007-4485-9430 [b] https://orcid.org/0000-0003-1757-3000

[c] https:/orcid.org/0000-0002-5105-1532 [d] https://orcid.org/0000-0002-3876-3420

[e] https://orcid.org/0000-0002-0360-5393 [f] https://orcid.org/0000-0002-1102-7984

[g] https://orcid.org/0000-0002-5330-1558

Abstract

The genus Sabanejewia comprises a diverse group of bottom-dwelling loaches with complex phylogenetic relationships and high morphological and genetic variability across European river systems. This study aimed to determine the phylogenetic position of a western Serbian population of S. balcanica within the broader Danubian–Balkanian framework and assess its genetic distinctiveness. Nine individuals of S. balcanica were sampled from the Ribnica River in Serbia (Kolubara River basin), and mitochondrial cytochrome b (1,140 bp) sequences were used for phylogenetic reconstruction. A total of 240 variable sites and 128 parsimony-informative sites were recovered by analyzing cyt b sequences. Despite the small sample size, two novel mitochondrial haplotypes were identified, which grouped with Serbian sequences of S. balcanica retrieved from GenBank. The phylogenetic tree confirmed high diversity and complex relationships in the Danubian-Balkanian complex. Newly detected haplotypes suggest high genetic complexity of S. balcanica in Serbia, highlighting the importance of continued genetic research to support conservation planning for this protected species in Serbia, as small, localized populations may retain distinct genetic signatures.

Keywords: Balkan spined loach, protected species, cytochrome *b*, phylogeny, freshwater.

INTRODUCTION

The golden loaches of the genus *Sabanejewia* Vladykov, 1929 represent a highly diverse group of rheophilic fish species inhabiting clear, fast-flowing waters. The first comprehensive study on the phylogeny of this genus in Europe by Perdices *et al*. [1] identified six monophyletic mitochondrial lineages, namely, *S. larvata*, *S. aurata*, *S. kubanica*, *S. romanica*, *S. caucasica*, and *S. baltica*. An additional six sublineages comprised a distinct

* *djiki@ibiss.bg.ac.rs*

Danubian-Balkanian complex consisting of *S. balcanica*, *S. bulgarica*, *S. montana*, *S. vallachica*, *S. doiranica*, and *S. thrakica*, with gene flow between sublineages confirmed [2]. Notably, *S. balcanica* was detected across all six sublineages, highlighting its occurrence throughout the various European drainages, high genetic heterogeneity, and lack of the congruence between geographic distribution and phylogeny [2].

The Balkan golden loach, *S. balcanica*, has been recorded in Serbian rivers of the Black Sea and Aegean Sea basins [3], alongside *S. bulgarica* [4]. Both species display a high level of phenotypic plasticity [5]. This results in overlapping diagnostic morphological traits, making morphology-based identification difficult and somewhat unreliable. More recently, a new species of the genus *Sabanejewia* was identified in Serbia, *S. romanica*, a species native and endemic to Romania [6].

According to the IUCN Red List of Threatened Species [7], *S. balcanica* is currently classified as a taxon of Least Concern (LC), but habitat alterations have made local populations endangered [3]. The primary threats to this species include habitat degradation through river regulation, gravel extraction, pollution, and habitat fragmentation caused by damming, all of which reduce the availability of the clean, well-oxygenated, fast-flowing waters this species depends on. Declared as a strictly protected species according to the national legislation, the collection of *S. balcanica* is prohibited without a special permit [8]. As this species is also included in Annex II of the EU Habitats Directive, the establishment of designated conservation areas is required [9–10]. Given the need for this species' protection, its role as a bioindicator of freshwater ecosystem health should be emphasized, making research on its biology, genetic diversity and distribution in Serbian waters necessary. Therefore, the aim of this study is to identify haplotypes present in the sample from the Ribnica River and to infer the phylogenetic position of these individuals within the genus *Sabanejewia*.

MATERIALS AND METHODS

Sampling and DNA extraction

In 2023, nine individuals of the *S. balcanica* were sampled at the Ribnica River (44° 12' 20.916" N, 20° 5' 33.0576" E; Kolubara river basin, Danube watershed) using reversible electronarcosis, and their fin clips were preserved in 96% ethanol until further genetic analyses. Genomic DNA was extracted using the Quick-DNA Miniprep kit (Zymo Research Corporation, USA) following manufacturer's instructions. The mitochondrial gene cytochrome *b* (cyt *b*) has been amplified, as this gene is a commonly used marker in phylogenetic studies [11]. Primers used for amplification of the cyt *b* were P1-F: 5′-GACTTGAAGAACCACCGTTG-3′ and P2-R: 5′-CTCCGATCTTCGGATTACAAGAC-3′. The PCR amplification was performed in 30 µl volume under the following conditions: an initial denaturation step at 94°C for 1 min, followed by 30 amplification cycles consisting of denaturation at 94°C for 15 s, primer annealing at 52°C for 15 s, and extension at 72°C for 1 min. A final extension step was carried out at 72°C for 10 min. Amplified fragments were checked on 1.5% agarose gels stained with SybrGreen (Lonza, CH). PCR products were sent to Macrogen Europe for purification and bidirectional sequencing.

Molecular data analysis

The obtained sequences were manually assembled and compared with existing sequences in the National Center for Biotechnology Information (NCBI) database using the BLAST tool. The cyt *b* sequence of *Sabanejewia larvata* was used as outgroup. To determine the phylogenetic position of sampled *S. balcanica* individuals, 44 sequences of the Danubian-Balkanian complex from the Balkans were retrieved from NCBI and included in the analysis.

The following software was used: Chromas 2.6.6 for visualization of raw chromatograms; Clustal X2 for sequence alignment; IQ-TREE 3.0.1 for selecting the most appropriate model of nucleotide substitution and phylogenetic tree reconstruction; FigTree 1.4.4 for visualization and editing of the phylogenetic tree [12–14]. The best-fitting model of nucleotide substitution was the Tamura-Nei model with empirical base frequencies and gamma-distributed rate variation among sites (TN+F+G4). The phylogenetic tree was constructed using the maximum-likelihood (ML) method with 100,000 bootstrap replicates to assess branch support.

RESULTS AND DISCUSSION

The length of the cyt *b* sequence across all nine samples was 1,140 bp, with 240 variable sites (21.1%) and 128 parsimony-informative sites (11.2%). Utilizing the BLAST tool revealed both previously reported haplotypes (A2105 and 66), as well as two novel haplotypes not present in GenBank. The phylogenetic tree was constructed using sequences of novel haplotypes, as well as 44 sequences obtained from GenBank (Table 1).

Table 1 *Accession numbers of haplotypes used for the reconstruction of the phylogenetic tree. Novel haplotypes from this study are bolded*

Taxon name	Haplotype name	Accession number	Taxon name	Haplotype name	Accession number
S. balcanica	66	AF499192	*S. balcanica*	C90	HQ291824
S. balcanica	RJ57	HQ291787	*S. balcanica*	C92	HQ291825
S. balcanica	RJ58	HQ291788	*S. balcanica*	C358	HQ291831
S. balcanica	IL45	HQ291793	*S. balcanica*	C359	HQ291832
S. balcanica	IL46	HQ291794	*S. balcanica*	C367	HQ291833
S. balcanica	A1219	HQ291795	*S. balcanica*	C824	HQ291834
S. balcanica	A1221	HQ291796	*S. balcanica*	C825	HQ291835
S. balcanica	A2097	HQ291800	*S. balcanica*	C826	HQ291836
S. balcanica	A2105	HQ291803	*S. balcanica*	MNCN 388CRR	AY059361
S. balcanica	A2219	HQ291805	*S. balcanica*	MNCN 354CRA	AY059346
S. balcanica	A2341	HQ291809	*S. balcanica*	MNCN 340CRA	AY059345
S. balcanica	A2342	HQ291810	*S. balcanica*	105	AF499185
S. balcanica	A2793	HQ291813	***S. balcanica***	**RIB1**	**Novel haplotype**
S. balcanica	A2800	HQ291814	***S. balcanica***	**RIB2**	**Novel haplotype**
S. balcanica	A2802	HQ291815	*S. bulgarica*	H41	MN149891

Table 1 *continued*

S. balcanica	1	AF499171	*S. bulgarica*	MNCN 218CRB	AY059353
S. balcanica	2	AF499172	*S. vallachica*	MNCN 127CRU	AY059365
S. balcanica	SR1	ON866527	*S. doiranica*	MNCN 453G	AY059354
S. balcanica	MNCN 213CRO	AY059337	*S. thrakica*	MNCN 1732G	AY059362
S. balcanica	A2457	HQ291818	*S. radnensis*	MNCN 459CRR	AY059357
S. balcanica	A2612	HQ291821	*S. montana*	282	AF499175
S. balcanica	A2613	HQ291822	*S. larvata*	MNCN 243TA	AY059331

According to Perdices *et al*. [1], the most basal branch of the genus is *S. larvata*, which was used as outgroup, followed by the *S. romanica* branch included in this study due to its distribution in the Balkans (Figure 1). The two most diverged lineages originated in the late to middle Miocene, followed by the emergence of the Baltic-Caucasian-Caspian lineages in the Pliocene [1].

The existence of the Danubian-Balkanian complex is strongly supported by high bootstrap values, with *S. vallachica* being the most divergent, also reported by Perdices *et al*. [1]. Some of the internal branches show weaker support, indicating shallower divergence between the sublineages of the complex. This may be linked to the more recent emergence of the complex in the Pleistocene, when cycles of glaciation and interglaciation reshaped the river systems [1].

Sequences of *S. balcanica* within the Danubian-Balkanian complex have been previously reported across multiple sublineages without clear geographic congruence [2], a pattern also reflected in the present study. According to Fedorčák *et al*. [15], *S. balcanica* and *S. bulgarica* comprise two distinct lineages. However, in the current study, their divergence was less pronounced, with sequences of both species nested within the same clade, consistent with the high degree of genetic heterogeneity and shallow divergence characteristic of the Danubian-Balkanian complex. This result should, however, be interpreted with caution, as branch support based on bootstrap values was low to moderate in the central part of the tree. A more comprehensive assessment of the relationship between these two species, incorporating an expanded dataset and morphometric analysis, will be addressed in a subsequent study. The novel haplotypes identified in this study clustered with reference sequences of *S. balcanica* from Serbia, supporting their assignment to this species. This is further supported by morphological identification conducted during sampling. Some of the haplotypes detected in this study had been previously reported for Serbia (A2105) and Romania (66), further highlighting the complex relationships among members of the Danubian-Balkanian complex and the lack of strict geographic structuring.

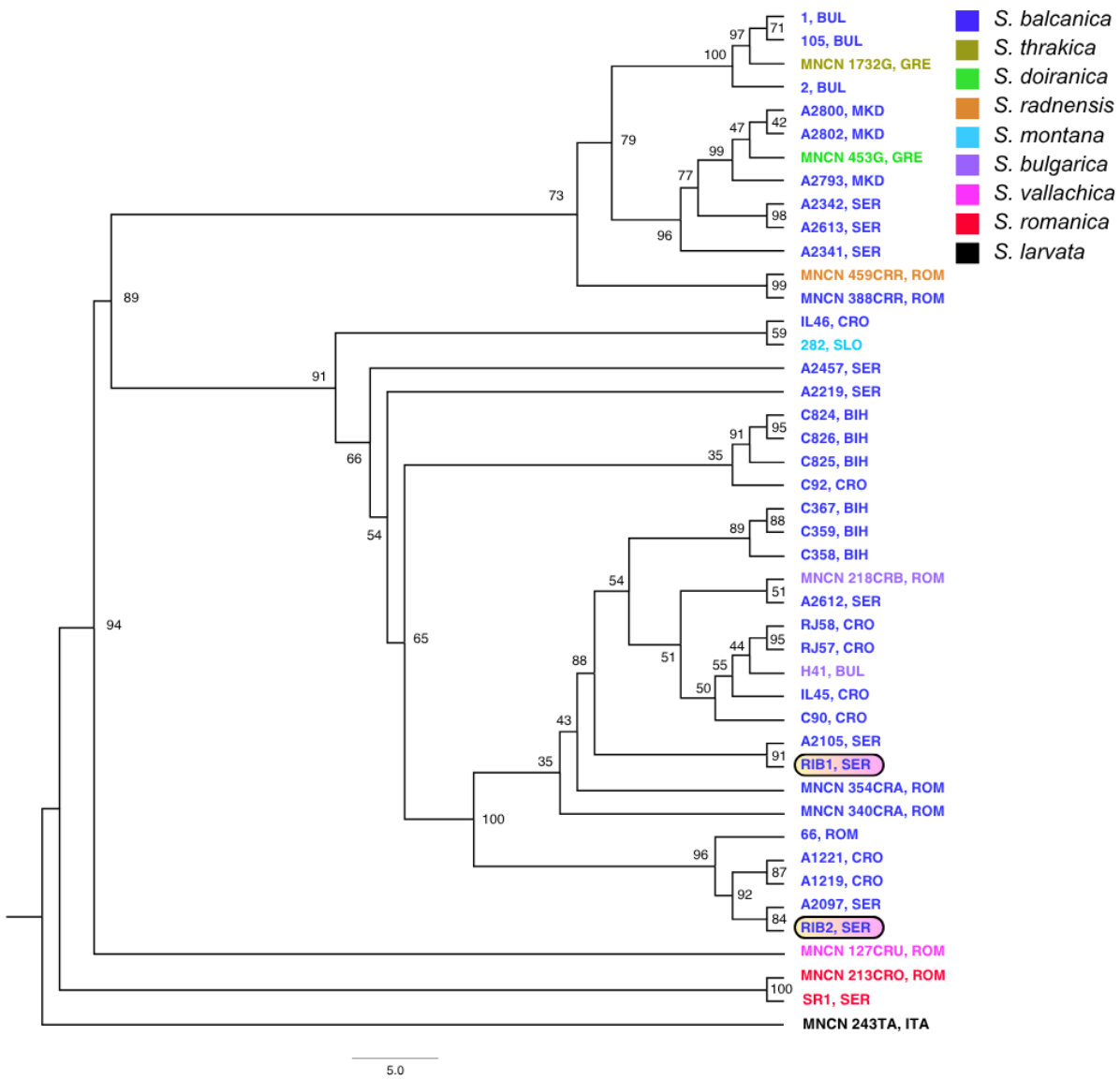

Figure 1 *Phylogenetic tree depicting the position of investigated samples within the genus Sabanejewia. Values at the tree nodes represent boostrap values. Colored taxa names correspond to the species given in the legend. Novel haplotypes from this study are highlighted. Abbreviations of the countries: SER – Serbia, CRO – Croatia, BIH – Bosnia & Hercegovina, ROM – Romania, BUL – Bulgaria, SLO – Slovenia, GR – Greece, ITA – Italy*

These findings support a relatively recent Pleistocene diversification of the Danubian-Balkanian complex, where shallow genetic differences and unresolved internal branching patterns are consistent with a rapid radiation driven by glacial-interglacial cycles that reshaped river connectivity across the Balkans.

CONCLUSION

The novel haplotypes detected in this study emphasize the hidden diversity of *S. balcanica* in Serbia and across broader geographic range. Further genetic research on this species will help uncover its diversity, thereby allowing for better inference of phylogenetic relationships within the genus *Sabanejewia* in Europe, underscoring the need for its protection.

ACKNOWLEDGEMENT

This study was funded by the Ministry of Science, Technological Development and Innovation of the Republic of Serbia, under grant numbers 451-03-33/2026-03/200007 and 451-03-34/2026-03/200178. The study was conducted in accordance with the United Nations Sustainable Development Goals (Agenda 2030), specifically Goal 15 (Life on Land).

REFERENCES

[1] Perdices, A., Doadrio, I., Economidis, P.S., *et al*. Mol. Phylogenet. Evol., 2003, 26(2), 289–299.

[2] Bartonová, E., Papousek, I., Lusková, V., *et al*. Folia Zoologica, 2008, 57(1/2), 60.

[3] Kottelat, M., Freyhof, J. Handbook of European freshwater fishes. Cornol, Switzerland: Publications Kottelat. Vol. 13, 2007.

[4] Pehlivanov A.L., Schabuss, M., Szaloky, Z. *et al*. Chapter 9 Fish. In: Liška I., Wagner, F., Sengl M., Deutsch K. & Slobodnik J. (Ed.): Joint Danube Survey 3 – A Comprehensive Analysis of Danube Water Quality. Vienna: International Commission for the Protection of the Danube River, 2015, pp. 126–139.

[5] Križek, P., Mendel, J., Fedorčák, J., *et al*. In the foothill zone—*Sabanejewia balcanica* (Karaman 1922), in the lowland zone—*Sabanejewia bulgarica* (Drensky, 1928): Myth or reality?. Ecology and Evolution, 2020. 10(14), 7929–7947.

[6] Marić, S.P., Bănăduc, D., Gajić, Đ.D., *et al*. Acta Zool. Bulg. 2022, 74(3), 369–377.

[7] International Union for Conservation of Nature (IUCN). (2024). *Sabanejewia balcanica*. The IUCN Red List of Threatened Species.

[8] Official Gazette of the Republic of Serbia (2016). The Regulation on Proclamation of Strictly Protected and Protected Wild Species of Plants, Animals and Fungi. "Official Gazette RS" No. 98/2016.

[9] Crvena knjiga faune Srbije V – Ribe (2024) Belgrade: Institute for Nature Conservation of Serbia.

[10] EU Habitats Directive 92/43/EEC, Annex II and IV.

[11] Avise, J.C. J. Biol. Sci., 1986, 312(1154), 325–342.

[12] Larkin, M.A., Blackshields, G., Brown, N.P., *et al*. Clustal W and Clustal X version 2.0. bioinformatics, 2007, 23(21), 2947–2948.

[13] Wong, T.K., Ly-Trong, N., Ren, H., *et al*. IQ-TREE 3: phylogenomic inference software using complex evolutionary models.

[14] Rambaut, A. (2018). FigTree v1.4.4. Available from: https://github.com/rambaut/figtree.

[15] Fedorčák, J., Šanda, R., Stefanov, T., *et al*. Fishes, 2023, 8(2), 119.

EcoTER'26
eco.tfbor.bg.ac.rs
32nd International Conference
Ecological Truth & Environmental Research
24–26 June 2026, Hotel Sunce,
Sokobanja, Serbia

Original Research

DIATOMS FROM LUDAŠ LAKE AND THEIR APPLICATION IN BIOINDICATION

DOI: 10.5937/EcoTER26187J

Olga Jakovljević[1,a*], Slađana Popović[1,b], Marija Pećić[1,c], Dragana Jerinkić[1,d]

[1] University of Belgrade, Faculty of Biology, Institute of Botany and Botanical Garden "Jevremovac", Department of Algology and Mycology, Takovska 43, 11000 Belgrade, SERBIA

[a] https://orcid.org/0000-0002-3079-8602
[b] https://orcid.org/0000-0001-7112-5853
[c] https://orcid.org/0000-0003-4477-8976
[d] https://orcid.org/0000-0003-4939-6969

Abstract

The main objectives of this study were to investigate the diversity and composition of the epiphytic diatom community in Ludaš Lake and to assess its ecological status using diatom indices. In total, 57 diatom taxa were recorded across three sampling sites during May and September 2025 (46 taxa in May and 37 in September). The dominant taxa at the studied sites included Fragilaria mesolepta, Halamphora veneta, Nitzschia acidoclinata, Nitzschia amphibia, and Pseudostaurosira brevistriata, with maximum relative abundances ranging from 19.23% to 50.11%. According to Serbian legislation, the ecological status based on phytobenthos was classified as moderate (class III, site L1) and good (class II, sites L2 and L3) in May. In contrast, in September, the status was moderate (class III, sites L1 and L2) and bad (class V, site L3). These findings highlight the need for continuous monitoring that integrates physical, chemical, and biological parameters in order to effectively assess the condition of aquatic ecosystems and detect various forms of pollution.

Keywords: ecological status, phytobenthos, lymnology.

INTRODUCTION

Several groups of organisms are widely used to assess the ecological status of aquatic environments, including fish, macroinvertebrates, macrophytes, phytoplankton and diatoms. Among these, benthic diatoms offer distinct advantages over other groups, making them especially valuable for routine environmental monitoring [1]. Diatoms are recognized as one of the most diverse and informative group of organisms used to assess the ecological status of water bodies under the European Water Framework Directive. Their high species diversity, combined with extensive ecological knowledge, enables their effective use as reliable bioindicators [2]. Diatoms are ubiquitous, easy to sample, and often abundant in different habitats, on hard substrates or in high-velocity rivers where macroinvertebrates, macrophytes, and phytoplankton (typically used in lowland ecosystems) may be absent. In addition, their rapid growth rates enable benthic diatoms to respond quickly to short-term hydrological changes, unlike other bioindicators (for example macroinvertebrates) [1]. However, their morphological and taxonomic identification remains challenging and requires specialized

* *olga.jakovljevic@bio.bg.ac.rs*

expertise [3]. Diatoms have been used less frequently in lake monitoring than in river water quality assessments, although some diatom indices have been developed specifically for lakes [4]. However, several studies have demonstrated the strong potential of epiphytic diatoms for evaluating lakes water quality [5,6].

Ludaš Lake, together with its surrounding complex of wet habitats, represents the only example of shallow, semi-static steppe lakes in our country. It was designated as a Special Nature Reserve in 2006. The protected area covers 846.33 hectares, while its buffer (protective) zone extends over 2,002 hectares. The site is managed under three levels of protection: I, II, and III. In 2008, the “Ludaš” Visitor Center was constructed on the edge of the reserve [7].

The main objectives of this study were: (i) to explore diversity and composition of epiphytic diatom community of Ludaš Lake, and (ii) to estimate the ecological status using diatom indices.

MATERIALS AND METHODS

Sampling

Diatom samples were collected at three sampling points (L1-L3) in Ludaš Lake during May and September 2025. L1 sampling site was located in the southern part of the lake, L2 situated near the Ludaš-Palić canal, and L3 positioned closed to the "Ludaš" Visitor Center. Epiphytic diatoms were sampled by scraping biofilm from older reed stems (*Phragmites australis* (Cav.) Trin. ex Steudel) that had been submerged for an extended period. The collected material was preserved with formaldehyde to a final concentration of approximately 4% [8]. At each sampling event, physicochemical parameters were measured *in situ*. Water temperature, pH, electrical conductivity (EC), and total dissolved solids (TDS) were recorded using Eutech Instruments OaktonR7 probes, while dissolved oxygen concentration and oxygen saturation were determined with an EcoSense ODO200 instrument.

Laboratory work and microscopic analyses

Qualitative and quantitative analysis of diatoms require laboratory processing of samples, including the removal of all cellular organic material, followed by the preparation of permanent slides. Sample processing was carried out using a standard method [8], which involves treatment with hydrochloric acid and potassium permanganate. This procedure yields cleaned material containing the siliceous cell walls (frustules) of diatoms, which were subsequently mounted in Naphrax medium to produce permanent slides. Slides prepared in this manner enable detailed observation of the structures and ornamentation of the silicified cell walls, which represent key taxonomic features for accurate diatom identification and community analysis.

Qualitative analysis was performed using a Zeiss AxioImager M1 light microscope equipped with an AxioCam MRc5 camera and AxioVision 4.9.1 software. Identification was conducted using relevant taxonomic literature [9–11]. Quantitative analysis was carried out on the same microscope by counting 400 valves per slide.

Ecological status assessment based on phytobenthos

Results of the qualitative analysis were used to calculate diatom indices in the OMNIDIA software package [12]. This software provides values for a total of 18 diatom indices which indicate appropriate water quality. According to the scale proposed by Prygiel and Coste [13], diatom index values between 0 and 4.99 correspond to water quality class V (labeled with red color), 5.00–8.99 to class IV (orange), 9.00–12.99 to class III (yellow), 13.00–16.99 to class II (green), and 17.00–20.00 to class I (blue).

In accordance with the *National Rulebook on Parameters of the Ecological and Chemical Status of Surface Waters and Parameters of the Chemical and Quantitative Status of Groundwaters* [14], the first step in assessing water quality is the classification of the water body type. Based on this framework, Ludaš Lake is categorized as a shallow lake situated below 200 m above sea level.

For phytobenthos (epiphytic diatoms), the ecological status of Ludaš Lake is assessed using the IPS diatom index, as prescribed by the National Rulebook.

RESULTS AND DISCUSSION

The values of the measured physicochemical parameters are presented in Table 1. In May, site L1 was characterized by the lowest recorded water temperature, pH, and dissolved oxygen concentration, as well as the highest total dissolved solids (TDS) values. According to Anderson *et al*. [15], seasonal shifts in diatom communities are primarily driven by nutrient availability, while temperature exerts an indirect influence on these changes.

Table 1 *Values of physicochemical parameters measured at the sampling sites of Ludaš Lake (L1-L3) in May and September 2025*

	May			September		
	L1	L2	L3	L1	L2	L3
T (°C)	17.6	19.3	19.4	20.8	19.5	20.8
pH	7.66	8.15	8.55	9.58	7.87	9.27
EC (µS/cm)	1489	916	921	2150	1099	1468
TDS (ppm)	1044	646	646	1503	769	1029
O_2 (mg/l)	6.8	10.8	15.5	17.9	9.6	12.4
O_2 (%)	71	117.2	165.3	199.8	103.9	133.9

A total of 57 diatom taxa were recorded across three sampling sites in Ludaš Lake during May and September 2025 (46 taxa in May and 37 in September). The highest number of taxa (33) was observed at site L1 in September, while the lowest (10) was recorded at site L3 during the same month (Figure 1).

Köster and Pienitz [16] investigated diatom seasonality at a monthly scale in Bates Pond and found that temperature and lake circulation accounted for most of the observed variation in diatom assemblages. In the present study, the genus *Nitzschia* was particularly prominent, with 13 taxa identified.

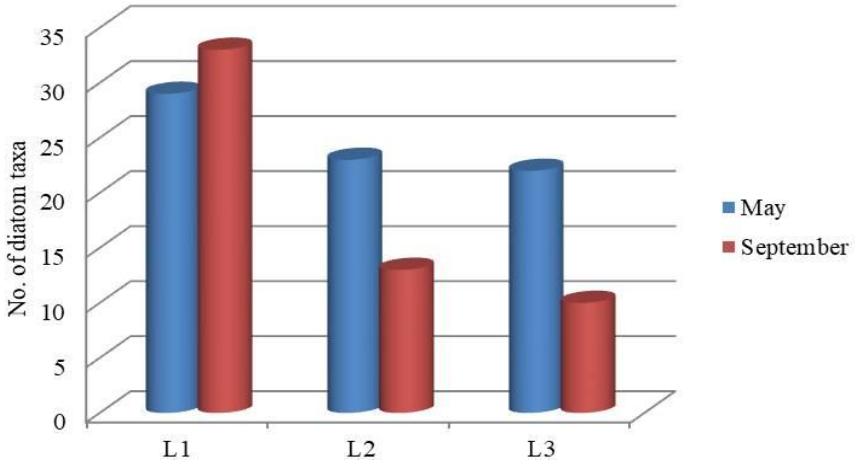

Figure 1 *Number of diatom taxa per site in May and September 2025 at three sampling sites of Ludaš Lake (L1-L3)*

The dominant taxa at the studied sites were *Fragilaria mesolepta* Rabenhorst, *Halamphora veneta* (Kützing) Levkov, *Nitzschia acidoclinata* Lange-Bertalot, *Nitzschia amphibia* Grunow, and *Pseudostaurosira brevistriata* (Grunow in Van Heurck) Williams & Round, with maximum relative abundances ranging from 19.23% to 50.11% (Figure 2). *P. brevistriata* was the dominant taxon at two sites (L1 and L2) in September, whereas the other dominant taxa each prevailed at only one site during a single sampling period. However, several of these taxa (*Halamphora veneta*, *Nitzschia acidoclinata*, and *N. amphibia*) can also be considered common, as they were recorded at all sites in both sampling months. *P. brevistriata* is typically found in calcium-rich lakes and running waters and exhibits a broad trophic tolerance, ranging from oligotrophic to eutrophic conditions, as well as a wide range of electrolyte contents [9]. It is noteworthy that *F. mesolepta* was recorded exclusively at site L2 in May, where it reached a high relative abundance (50.11%) (Figure 2). Although this species is widely distributed in standing and flowing freshwater habitats with moderate to high trophic levels, it is rarely observed in such high abundances [9]. In total, six common species were identified: *Cyclotella meneghiniana* Kützing, *Gomphonema parvulum* (Kützing) Kützing, *Halamphora veneta* (Kützing) Levkov, *Nitzschia acidoclinata* Lange-Bertalot, *Nitzschia amphibia* Grunow, and *Staurosira venter* (Ehrenberg) Cleve & Møller.

Based on Table 2, the ecological status of Ludaš Lake assessed by diatoms ranges from high to bad, depending on the sampling site, sampling month and diatom index. These findings are consistent with previous research conducted in 2022 [17]. A high ecological status was recorded only at a single site during one sampling month and was supported by the values of only two diatom indices. Diatom indices that testify to the presence of nutrients in aquatic ecosystems (Rott TI, TDIL, TDI) indicate a bad ecological status in at least one site, mostly in September (Table 2).

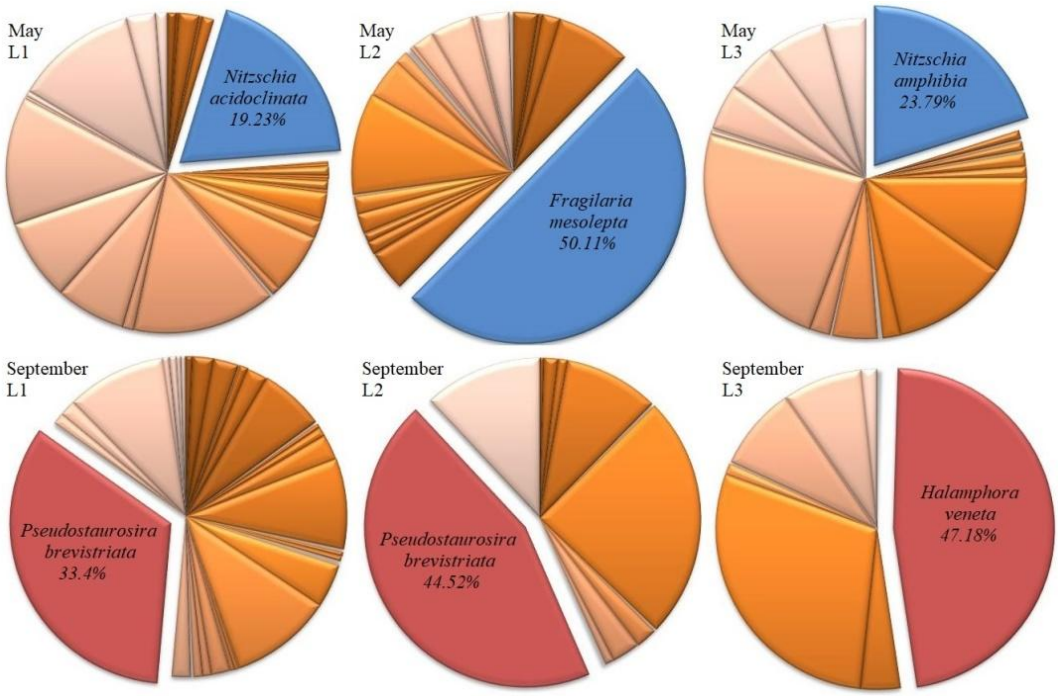

Figure 2 *Percentage representation of dominant diatom taxa at each sampling site of Ludaš Lake (L1-L3) in May and September 2025*

Table 2 *Ecological status of Ludaš Lake based on the diatom indices values at investigated sampling sites (L1-L3) during two sampling seasons (May and September); class boundaries according to Prygiel and Coste [13]. Blue color – high ecological status, green – good, yellow – moderate, orange – poor, red – bad*

	May			September		
	L1	L2	L3	L1	L2	L3
Biological Diatom Index (IBD)	11.3	13.6	13	11.3	11.7	7.5
Specific Pollution Sensitivity Index (IPS)	9.7	13	10.5	8.5	8.2	4.4
Generic Diatom Index (IDG)	6.3	9.8	10.2	8.2	10.6	5
Descy Diatom Index (Descy)	10.5	17.2	9.4	9.9	12.7	6.3
Sládeček Diatom Index (Sla.)	9.5	11.5	12.4	9.6	9.7	9.2
Index of Saprobity-Eutrophication (IDSE)	11.5	12.1	12.5	11.4	10.9	7.2
Artois-Picardie Diatom Index (IDAP)	5	8	9.3	4.8	1.8	2.9
Diatom-based Eutrophication/Pollution Index (EPID)	9.7	14.3	11.5	9.2	8.6	7.1
Lobo Index (Lobo)	12	14.7	17.9	11.9	5.6	11.4
Hürlimann Diatom Index (Hurl.)	7.2	12.2	6.2	8.9	12.7	5
Austrian Trophic Index (Rott TI)	5.7	6.4	4.9	4.7	5	2.3
Rott Saprobic Index (Rott SI)	13.6	15.4	12.9	14.4	13.8	8.1
Trophic Diatom Index for Lakes (TDIL)	9.2	10.7	12	9.4	8.3	4.5
Commission for Economical Community metric (CEE)	7.7	14.6	12.8	7.7	7	8
Watanabe's Index (WAT)	9.4	10.5	14.1	9.8	10.4	10.6
Trophic Diatom Index (TDI)	6.4	12.1	7.9	8.4	10.3	3.3
Pampean Diatom Index (IDP)	8.1	8.2	10.6	6.8	6.4	5.3
Schreiner's Index (SHE)	13.4	15.6	14.9	12.7	11.9	9.6

Considering that the ecological status class boundaries defined in the Serbian legislation [14] differ from those proposed by Prygiel and Coste [13], IPS index values are separated and marked by apropriate color (Table 3), as it is the only index considered relevant for shallow lakes located below 200 m a.s.l., a category that includes Ludaš Lake according to the

national Rulebook. In spring, IPS index values classified the ecological status as moderate (Class III at site L1) and good (Class II at sites L2 and L3) according to the national Rulebook [14]. In September, water quality at site L1 remained unchanged, whereas conditions at sites L2 and L3 deteriorated by one and three quality classes, respectively (Table 3). Compared with the ecological status recorded in 2022, the present results indicate an improvement in water quality at some sites, including improvements of up to two quality classes during spring [17].

Table 3 *Ecological status of Ludaš Lake based on phytobenthos at investigated sampling sites (L1-L3) during two sampling seasons (May and September); class boundaries according to Serbian legislation ("Official Gazette of the RS", no. 74/11). Green color – good ecological status, yellow – moderate, orange – poor, red – bad*

	May			September		
	L1	L2	L3	L1	L2	L3
IPS	9.7	13	10.5	8.5	8.2	4.4

CONCLUSION

This study identified 57 diatom taxa across three sampling sites in Ludaš Lake during May and September 2025, with 46 taxa recorded in May and 37 in September. The results indicate an improvement in water quality at certain sites compared with the ecological status recorded in 2022, highlighting the importance of continuous biomonitoring.

ACKNOWLEDGEMENT

The authors are grateful to the Ministry of Science, Technological Development and Innovation of the Republic of Serbia for financial support according to the contract with registration Nos. 451-03-33/2026-03/200178 and 451-03-34/2026-03/200178.

REFERENCES

[1] Taurozzi, D., Cesarini, G., Scalici, M. Ecol. Indic. 2024, 166, 112309.
[2] Barinova, S., Gabyshev, V., Genkal, S. *et al*. Russian Arctic. Water. 2023, 15, 1533.
[3] Rimet, F., Feret, L., Bouchez, A., *et al*. Hydrobiologia 2019, 839(1), 103–118.
[4] Stenger-Kovács, C, Buczkó, K, Hajnal, É. *et al*. Hydrobiologia 2007, 589, 141–154.
[5] Kelly, M, Urbanic, G, Ács, É. *et al*. Hydrobiologia 2014, 734, 125–141.
[6] Kamberović, J., Stuhli, V., Lukić, Z. *et al*. Turk. J. Bot. 2019, 43(3), 420–430.
[7] Available from: https://www.ekourbapv.vojvodina.gov.rs/rs/надлежности/заштита-природне-баштине-и-биодиверз/заштићена-подручја-у-војводини/срп-лудашко-језеро/
[8] Institute for Standardization of Serbia. Water quality–Guidance standard for the routine sampling and pre-treatment of benthic diatoms from rivers. Belgrade: SRPS EN 13946:2015.
[9] Lange-Bertalot H, Hofmann G, Werum M. *et al*. Freshwater benthic diatoms of Central Europe: over 800 common species used in ecological assessment. Schmitten-Oberreifenberg: Koeltz Botanical Books; 2017. p. 942.

[10] Peeters V, Ector L. Atlas des diatomées des cours d'eau du territoire bourguignon. Volume 1: Centriques, Araphidées. Bourgogne: Service Biodiversité, Eaux et Patrimoine, Pôle Qualité des Eaux, Laboratoire d'hydrobiologie; 2017. p. 310.
[11] Peeters V, Ector L. Atlas des diatomées des cours d'eau du territoire bourguignon. Volume 2: Monoraphidées, Brachyraphidées. Bourgogne: Service Biodiversité, Eaux et Patrimoine, Pôle Qualité des Eaux, Laboratoire d'hydrobiologie; 2018. p. 271.
[12] Lecointe, C., Coste, M., Prygiel J. Hydrobiologia 1993, 269(1), 509–513.
[13] Prygiel J, Coste M. Guide méthodologique pour la mise en œuvre de l'Indice Biologique Diatomées NF T 90-354. Bordeaux: Agences de l'Eau–Cemagref; 2000. p. 134.
[14] Rulebook on parameters of ecological and chemical status of surface waters and parameters of chemical and quantitative status of groundwater. Official Gazette of the RS. 2011; (74/11).
[15] Anderson, N.J. Eur. J. Phycol. 2000, 35, 307–314.
[16] Köster, D., Pienitz, R. J. Paleolimnol. 2006, 35, 395–416.
[17] Jakovljević O, Predojević D. In: The 53rd Annual Conference of the Serbian Water Pollution Control Society WATER 2024; 27–29 May; Palić, Srbija. 2024. p. 143–148. (In Serbian).

EcoTER'26
eco.tfbor.bg.ac.rs
32nd International Conference
Ecological Truth & Environmental Research
24–26 June 2026, Hotel Sunce,
Sokobanja, Serbia

Original Research

ASSESSMENT OF GROUNDWATER SUITABILITY FOR IRRIGATING URBAN GREEN SPACES IN ALLUVIAL AQUIFERS

DOI: 10.5937/EcoTER26194P

Predrag Pajic[1,a], Zeljka Rudic[1,b], Nikola Rakonjac[1,2,c*]

[1] Jaroslav Černi Water Institute, Jaroslava Černog 80, 11000 Belgrade, SERBIA
[2] Soil Physics and Land Management Group, Wageningen University, NETHERLANDS
[a] https://orcid.org/0000-0002-3148-3231
[b] https://orcid.org/0000-0003-4853-8742
[c] https://orcid.org/0000-0002-0206-5233

Abstract

A methodological framework has been developed to assess the suitability of groundwater from alluvial aquifers for the systematic irrigation of urban green spaces. The approach is based on a multi-criteria analysis of the groundwater regime within the alluvial aquifer, systemic long-term monitoring of groundwater quality, and, finally, an evaluation of irrigation suitability that considers national legislation, internationally recognized criteria, and the applicable technical irrigation solution. The proposed approach was verified through monitoring of groundwater regime (quantity and quality) conducted in a section of the right-bank alluvial plain of the Sava River in Belgrade, serving as a representative case of a heterogeneous and anisotropic alluvial environment within an urbanized zone. The results confirm that the developed methodological framework provides a reliable and transferable tool for verifying the reliability of groundwater resources intended for sustainable irrigation in urban areas located on heterogeneous alluvial aquifer systems.

Keywords: alluvial aquifers, groundwater, irrigation, water quality, urban green spaces.

INTRODUCTION

In urbanized areas situated on alluvial plains, groundwater represents a significant and convenient resource for the irrigation of green spaces. The underlying geological layers, composed of heterogeneous and anisotropic sand and gravel, are characterized by high porosity and permeability, which favours the formation of abundant aquifer systems. At the same time, such properties make alluvial aquifers particularly vulnerable to the rapid migration of pollutants, especially under conditions of intensive urbanization and pronounced anthropogenic impact. As a result, changes in groundwater quality may occur, potentially limiting its suitability for irrigation purposes.

Assessing the suitability of groundwater for the irrigation of urban green spaces is a key component of sustainable water resource management in alluvial environments. The quality of these waters directly affects soil properties and the physiological response of plants. An inappropriate chemical composition of irrigation water may lead to e.g., salt accumulation in the soil, soil structure degradation, reduced vitality of green areas, and a range of other

* *nikola.rakonjac@wur.nl*

adverse effects. Consequently, a robust suitability assessment must integrate relevant water quality indicators while accounting for the natural and anthropogenic factors influencing aquifer conditions. Furthermore, given the pronounced spatial and temporal heterogeneity inherent to alluvial aquifers, a systematic and reliable assessment approach is essential.

MATERIALS AND METHODS

The methodological framework presented in this study is based on a multi-criteria analysis encompassing:

- characterization of the groundwater regime within the alluvial aquifer,
- systematic monitoring of groundwater quality over a selected time period, and
- evaluation of groundwater suitability for irrigation in accordance with national criteria, internationally recognized guidelines, and the specific characteristics of the applied irrigation system.

The proposed framework was implemented in the riparian zone along the right bank of the Sava River in Belgrade (Serbia), within an intensively urbanized area [1]. The collected data were analyzed in accordance with current national regulations [2], as well as internationally recognized irrigation water quality guidelines [3,4], while adapting the obtained results to the specific characteristics of urban irrigation systems and green areas. Based on the integration of these criteria, a classification of groundwater quality and an assessment of its suitability for the irrigation were performed. Hence, the outcome of the study is the identification of suitable micro-locations for groundwater exploitation for the irrigation of green spaces in urbanized environments.

RESULTS AND DISCUSSION

Analysis of the groundwater regime

The results of thirty years of continuous monitoring [1], supplemented by data obtained from 10 piezometers installed for the purposes of this study, confirm the dominant influence of the Sava River on the groundwater regime in the riparian alluvial aquifer. The influence of the vertical water balance is of secondary importance. Further inland, groundwater levels are additionally affected by inflows from adjacent higher terrains, and locally by contributions from the underlying limestone formations. Figure 1 presents the results of daily monitoring conducted during the 2025–2026 period.

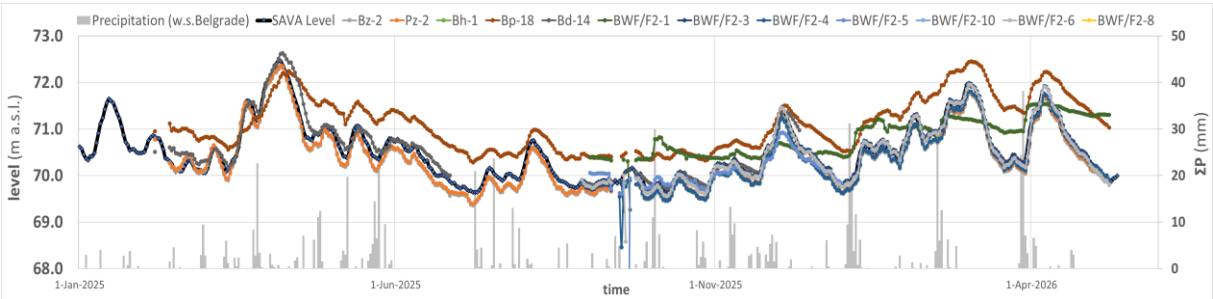

Figure 1 *Variations in groundwater levels within the right-bank alluvial aquifer in relation to the Sava River water levels during the 2025–2026 period*

Furthermore, four parallel sampling campaigns of the Sava River and the adjacent alluvial aquifer conducted during 2025–2026 revealed a similar ionic composition in river and groundwater (Figure 2), indicating the strong hydraulic connection between the two systems. Elevated HCO_3^- concentrations in groundwater likely reflect carbonate mineral dissolution during subsurface flow, while variations in Ca^{2+} concentrations may result from site-specific geochemical processes. The relatively low concentrations of SO_4^{2-}, Cl^-, Na^+, K^+, and Mg^{2+} indicate that carbonate weathering is the principal process controlling groundwater chemistry.

Figure 2 *Changes in the concentrations of ionic species in groundwater and the Sava River*

Groundwater quality monitoring during the selected period

Continuous groundwater quality monitoring has been systematically conducted in the study area for more than 30 years [1]. For the purposes of this study, additional targeted investigations were carried out within the expanded monitoring network during the 2025–2026 through four seasonal sampling campaigns (May, September, and December 2025, and March 2026). A total of 18 groundwater samples collected during this period were subjected to comprehensive chemical analyses.

Groundwater quality at locations identified as potentially suitable for groundwater abstraction for irrigation purposes, primarily within the riparian zone of the alluvial aquifer, was assessed during all four campaigns. Attention was devoted to parameters that may exert long-term impacts on soil properties, vegetation, and the sustainability of irrigation systems. The obtained results were used to evaluate the spatial and seasonal variability of groundwater quality, identify samples exhibiting stable or variable hydrochemical characteristics, detect potentially critical groundwater conditions, and establish a qualitative zoning of the aquifer. The results further served as the basis for verifying the proposed methodology for assessing groundwater suitability and its sustainable use in irrigation systems for urban green areas.

Assessment of groundwater suitability for irrigation

The assessment of groundwater suitability for irrigation purposes is based on the application of valid national regulations and internationally recognized criteria, with the aim of protecting soil, crops, and the environment, as well as ensuring the sustainable use of water over the long term. The following criteria were applied:

- regulations of the Republic of Serbia,
- internationally recognized criteria (FAO, USSL).

Assessment of irrigation water quality according to regulations of the Republic of Serbia

The required quality of irrigation water is defined by the valid bylaw of the Republic of Serbia [2], which prescribes the maximum allowable concentrations (MAC) of hazardous substances (cadmium, lead, mercury, arsenic, chromium, nickel, and fluorine) and harmful substances (copper, zinc, and boron) in irrigation water.

In most samples collected during the four monitoring campaigns conducted in 2025–2026, groundwater exhibited satisfactory quality for irrigation purposes, while the concentrations of the analyzed elements remained within the permissible limits prescribed by the Regulation. Temporary exceedances of mercury concentrations in one sampling series at three locations, as well as arsenic in one sample collected in September 2025, were not observed in the remaining campaigns and may be attributed to short-term, incidental anthropogenic impacts (Table 1).

The results indicate that the groundwater of the alluvial area can be considered suitable for irrigation, whereas the observed deviations were limited in extent and temporary in nature, and therefore do not affect the overall assessment of its usability.

Table 1 *Changes in element concentrations in water*

Sample	Series	Date	Measured concentration in the sample (µg/l)								
			As	Zn	Cd	Ni	B	Cu	Cr	Pb	Hg
Bz-2	I	08.05.25.	<10	14.0	<2	7.3	512.3	<3	<2	<10	<1
Bp-18	I	08.05.25.	<10	16.5	3.1	<5	172.0	<3	<2	<10	<1
Bp-18	IV	09.03.26.	<10	<10	<2	<5	220.3	<3	<2	<10	<0.2
BWF/F2-2	III	11.12.25.	<10	<10	<2	7.3	185.0	<3	3	<10	<0.2
BWF/F2-2	IV	09.03.26.	11.0	<10	<2	<5	158.8	<3	<2	<10	<0.5
BWF/F2-3	II	18.09.25.	<10	<10	<2	<5	<100	<3	<2	<10	9.0*
BWF/F2-3	III	11.12.25.	<10	<10	<2	<5	<100	<3	<2	<10	<0.2
BWF/F2-3	IV	09.03.26.	<10	<10	<2	<5	<100	<3	<2	<10	<0.2
BWF/F2-4	II	18.09.25.	<10	<10	<2	<5	194.8	<3	<2	<10	4.0*
BWF/F2-4	III	11.12.25.	<10	<10	<2	<5	188.6	3.2	<2	<10	<0.2
BWF/F2-4	IV	09.03.26.	<10	<10	<2	<5	163.5	<3	<2	<10	<0.2
BWF/F2-5	III	11.12.25.	<10	<10	<2	<5	340.4	4.9	3.3	<10	<0.2
BWF/F2-5	IV	09.03.26.	<10	<10	<2	<5	378.9	<3	<2	<10	<0.2
BWF/F2-6	II	18.09.25.	<10	<10	<2	<5	223.0	<3	<2	<10	2.0*
BWF/F2-6	III	11.12.25.	23.1	<10	<2	<5	195.5	<3	<2	<10	<0.2
BWF/F2-6	IV	09.03.26.	10.7	<10	<2	<5	257.9	<3	<2	<10	<0.5
BWF/F2-8	III	11.12.25.	<10	<10	<2	<5	770.8	<3	<2	<10	<0.2
BWF/F2-10	II	18.09.25.	70.2*	<10	<2	5.9	701.2	<3	2.1	<10	<0.2
MAC			50	1000	10	100	1000	100	500	100	1

Values marked with (*) deviate from the aforementioned Regulation („OG RS“, 23/94)

Assessment of irrigation water quality according to internationally recognized criteria

Due to the lack of comprehensive national guidelines or bylaws addressing all aspects of irrigation water quality, it is necessary to apply other internationally recognized guidelines, namely those of the Food and Agriculture Organization of the United Nations (FAO, [3]) and the US Salinity Laboratory, United States Department of Agriculture (USSL USDA, [4]). FAO recommends the use of Guidelines for evaluation of water quality for irrigation [3]. These guidelines evaluate common water constituents in all forms of their action as potential causes of problems arising from the use of irrigation water. The USSL proposes a water classification system based solely on the salinity and sodium hazard, according to the values of electrical conductivity (EC) and sodium adsorption ratio (SAR). In addition, parameters that may adversely affect irrigation system components must also be considered, particularly clogging of drippers or sprinklers, as well as the formation of deposits or biofilms in pipes or laterals [3]. These guidelines enable a systematic analysis of key water quality parameters that may potentially have adverse effects on soil quality and on plant growth and development.

A synthesis of the results was performed based on the combined interpretation of electrical conductivity (EC) and sodium adsorption ratio (SAR) values, together with accompanying recommendations in accordance with the aforementioned FAO and USSL criteria. Such a methodological approach provides a framework for assessing groundwater suitability which, in addition to its local significance, is also applicable to other urban areas formed under specific alluvial aquifer conditions**.**

SAR values were low in all samples (<3), indicating a negligible sodium hazard risk and suggesting that, from this aspect, all analyzed waters can be considered safe for the irrigation of various green areas.

From the perspective of salinization risk, most samples exhibited low to moderate EC values, with samples having EC below 0.75 dS/m classified as water of good to very good quality [4]. Samples with elevated EC values (0.9–1.5 dS/m) were classified as waters posing a low risk to plants and can be used for irrigation provided that basic control measures are applied.

Assessment of water quality according to irrigation method and technique

The selection of an irrigation technique represents a key factor influencing water use efficiency, as well as plant growth and development. The choice of irrigation technique depends on the requirements of the cultivated crop, the type and characteristics of the irrigated soil, and the quality of the water available for irrigation [5]. Accordingly, the selection of an irrigation system must be aligned with the assessment of groundwater quality in order to minimize risks and ensure the long-term sustainability of urban green areas.

The interaction between groundwater quality and irrigation techniques was analyzed using the USSL (C–S) classification, which defines salinization and alkalization risks [4]. Water classified as C1–S1 (low salinity – low sodium hazard) can be used for the irrigation of most plant species and soil types and is therefore suitable for all irrigation techniques. Water classified as C2–S1 (moderate salinity – low sodium hazard) can also be used with all irrigation techniques, provided that occasional soil leaching is performed. Water classified as C3–S1 (high salinity – low sodium hazard) cannot be used for the irrigation of soils with poor

filtration characteristics, nor for the irrigation of plants sensitive to salinization. The use of such water requires the implementation of measures for the control or prevention of soil salinization, as well as continuous monitoring of soil electrical conductivity (EC).

Analysis of groundwater suitability for the irrigation of green areas and selection of locations for groundwater source development

Based on the aforementioned criteria, an integrated assessment of groundwater suitability for different irrigation techniques (surface irrigation – flooding, sprinkler irrigation, and drip irrigation) was performed, relying on the USSL classification and identified limiting factors, with a final evaluation of applicability for urban green areas (Table 2).

Table 2 *Assessment of groundwater suitability for different irrigation techniques according to the FAO/USSL classification*

Sample	Series	Date	Surface irrigation	Sprinkling	Drip	USSL	Key limiting factors	General assessment
Bz-2	I	08.05.25.	3	2	2	C3 / S1	EC, bicarbonates	**2**
Bp-18	I	08.05.25.	1	1	1	C2 / S1	nothing significant	**1**
Bp-18	IV	09.03.26.	#N/D	#N/D	#N/D	#N/D	#N/D	#N/D
BWF/F2-2	III	11.12.25.	2	2	2	C2 / S1	EC, bicarbonates	**2**
BWF/F2-2	IV	09.03.26.	2	2	2	C2 / S1	EC, bicarbonates	**2**
BWF/F2-3	II	18.09.25.	1	1	1	C2 / S1	nothing significant	**1**
BWF/F2-3	III	11.12.25.	1	4	4	C1 / S1	Fe, pH, bicarbonates	**4**
BWF/F2-3	IV	09.03.26.	1	1	1	C2 / S1	nothing significant	**1**
BWF/F2-4	II	18.09.25.	2	2	2	C3 / S1	EC, bicarbonates	**2**
BWF/F2-4	III	11.12.25.	2	2	2	C3 / S1	EC, bicarbonates	**2**
BWF/F2-4	IV	09.03.26.	2	2	2	C3 / S1	EC, bicarbonates	**2**
BWF/F2-5	III	11.12.25.	4	4	3	C3 / S1	EC, Cl, bicarbonates	**4**
BWF/F2-5	IV	09.03.26.	4	4	3	C3 / S1	EC, Cl	**4**
BWF/F2-6	II	18.09.25.	2	4	4	C3 / S1	bicarbonates	**4**
BWF/F2-6	III	11.12.25.	2	2	2	C3 / S1	Bicarbonates, pH, Fe	**2**
BWF/F2-6	IV	09.03.26.	2	2	2	C3 / S1	EC, Cl	**2**
BWF/F2-8	III	11.12.25.	4	4	3	C3 / S1	B, bicarbonates	**4**
BWF/F2-10	II	18.09.25.	4	4	4	C2 / S1	EC, bicarbonates, Mn	**4**

GW Suitability: 1- high, 2- moderate, 3- conditional, 4- low; #N/D – no data

Based on the selected criteria, the samples were classified into four groups according to their degree of suitability for the irrigation of urban green areas, together with recommendations for their application:

- water suitable for irrigation (1) – BWF-2-3, Bp-18. Water from these locations represents primary sources for irrigation, with generally favorable characteristics, provided that regular monitoring is established in order to track seasonal variations.
- water moderately suitable for irrigation (2) – BWF-2-2, BWF-2-4, BWF-2-6. Water from these locations is conditionally suitable for irrigation, with mandatory implementation of water, soil, and plant quality monitoring measures, as well as periodic flushing of (parts of) the irrigation system and soil, particularly when cultivating sensitive crops.
- water of low suitability for irrigation (4) – BWF-2-5, BWF-2-8, BWF/F2-10. Water from these locations is not recommended for irrigation without appropriate pretreatment and/or

without mandatory implementation of monitoring measures for water, soil, and plant quality, as well as flushing of (parts of) the irrigation system and soil.

It is assumed that the irrigated soil is properly prepared for crop cultivation, has good filtration characteristics, and/or has an installed drainage system in areas irrigated with water belonging to the C3 category. The integrated analysis of groundwater suitability indicates that seasonal variations in groundwater quality within the alluvial aquifer may significantly affect the possibility of its use for irrigation.

CONCLUSION

The applied multi-criteria methodological framework, based on the integration of groundwater regime analysis, systematic water quality monitoring, and the application of national and international criteria, as well as the requirements of different irrigation techniques, enables a reliable assessment of groundwater suitability and the identification of key risks (salinity, alkalization, technical limitations) and their timely management.

The results obtained for the right-bank alluvium of the Sava River in Belgrade show that groundwater exhibits varying degrees of suitability for irrigation – ranging from fully suitable to conditionally applicable, depending on its natural (hydrogeological and hydrochemical) characteristics and the influence of urban conditions. Accordingly, spatial and temporal mapping of groundwater quality is necessary in order to optimize its use and minimize risks to soil and vegetation.

The practical value of the proposed methodology lies in its ability to identify optimal micro-locations for groundwater abstraction for irrigation purposes, while simultaneously ensuring sustainable resource use and the preservation of the functionality of urban green areas. The proposed framework represents a reliable and transferable approach for assessing groundwater suitability in alluvial aquifers, with direct application in the planning and management of irrigation systems in urban environments.

REFERENCES

[1] Program of observation, measurement and analysis of backwater effect of the Danube River on the shore, caused by the construction and exploitation of HPP "Đerdap 1" and HPP "Đerdap 2". Jaroslav Cerni Water Institute; 2025.

[2] “Regulation on Permissible Quantities of Hazardous and Harmful Substances in Soil and Irrigation Water”. “Official Gazette of the Republic of Serbia”, No. 23, 1994.

[3] Ayers, RS, Westcot, DW. Water quality for agriculture. Irrigation and Drainage Paper 29. Rome: Food and Agriculture Organization of the United Nations; 1985.

[4] USSL USDA. Diagnosis and improvement of saline and alkali soils. Agricultural Handbook 60. (Ed. Richards, L.A.), Washington D.C.: United States Department of Agriculture, United States Salinity Laboratory; 1954.

[5] Fipps, G. Irrigation water quality standards and salinity management strategies (B-1667). Texas Cooperative Extension, Texas A&M University System; 2003.

EcoTER'26
eco.tfbor.bg.ac.rs
32nd International Conference
Ecological Truth & Environmental Research
24–26 June 2026, Hotel Sunce,
Sokobanja, Serbia

Original Research

LONG-TERM PERSISTENCE OF FLUORIDE CONTAMINATION IN ALLUVIAL GROUNDWATER: A CASE STUDY OF THE CARINA WELLFIELD IN KLADOVO (SERBIA)

DOI: 10.5937/EcoTER26201P

Predrag Pajic[1,a], Zeljka Rudic[1,b], Nikola Rakonjac[1,2,c*]

[1] Jaroslav Černi Water Institute, Jaroslava Černog 80, 11000 Belgrade, SERBIA

[2] Soil Physics and Land Management Group, Wageningen University, NETHERLANDS

[a] https://orcid.org/0000-0002-3148-3231

[b] https://orcid.org/0000-0003-4853-8742

[c] https://orcid.org/0000-0002-0206-5233

Abstract

The paper analyzes the long-term persistence of fluoride contamination in the alluvial aquifer of the Carina wellfield in Kladovo, resulting from an accidental release in 1997. The research is based on the analysis of results from thirty years of monitoring of groundwater regime and quality under conditions of abstraction for public water supply purposes. The results show that after the initial contamination event, fluoride concentrations decreased and, after a certain period, stabilized at levels close to the legally permitted maximum values, indicating the establishment of a quasi-stationary state in the aquifer and long-term persistence of pollution. The long-term presence of fluoride in the aquifer represents a significant sanitary and public health issue, especially when groundwater constitutes the only resource for the water supply of the local population. The results of long-term monitoring and comprehensive investigations indicate that the persistence of fluoride contamination in such systems is the result of the interaction between natural and anthropogenic processes, where the management of the abstraction regime plays an important role in controlling groundwater quality.

Keywords: fluoride, groundwater, pollution, long-term monitoring, wellfield.

INTRODUCTION

Fluorine is one of the most reactive chemical elements and occurs in nature in the form of its compounds. Some of them may occur in groundwater originating from natural sources, but it can also be of anthropogenic origin, particularly in areas of intensive industrial activity. For instance, high fluoride (ion of fluorine) concentrations in groundwater represent a significant sanitary and public health issue, especially when contamination enters aquifers used for public water supply. Long-term exposure to concentrations exceeding 1.5 mg/L is considered harmful to human health according to the guidelines of the World Health Organization (2011), while the legislation of the Republic of Serbia prescribes an even stricter maximum allowable concentration of 1.2 mg/L. In heterogeneous and anisotropic alluvial aquifers of high permeability with weak protective cover layers, intensive infiltration, transport, and

* *nikola.rakonjac@wur.nl*

retention processes of contaminants within the porous medium often result in their long-term persistence.

The Carina wellfield in Kladovo depicts a representative example of such a system. The issue of fluoride contamination was first recognized in the mid-1990s, when detailed hydrochemical and geochemical investigations were conducted to determine the origin of contamination, the mechanisms of fluoride migration, and the risk posed to groundwater intended for public water supply. It was established that hydrofluoric acid (HF) and sulfuric acid (H_2SO_4) were used in the production of crystal glass, resulting in the generation of large quantities of waste products rich in fluorides and sulfates. Incomplete neutralization of the waste and its long-term disposal within the wider sanitary protection zone of the wellfield enabled the gradual infiltration of fluorides through a single-layer porous medium and their migration into the aquifer (Figure 1).

The long-term presence of fluoride, occurring at spatially variable concentrations, indicates complex mechanisms governing its distribution and retention. The aim of this paper is to identify the dominant transport and retention processes and to analyze the persistence of fluoride contamination based on the results of long-term monitoring of groundwater balance and quality regime parameters.

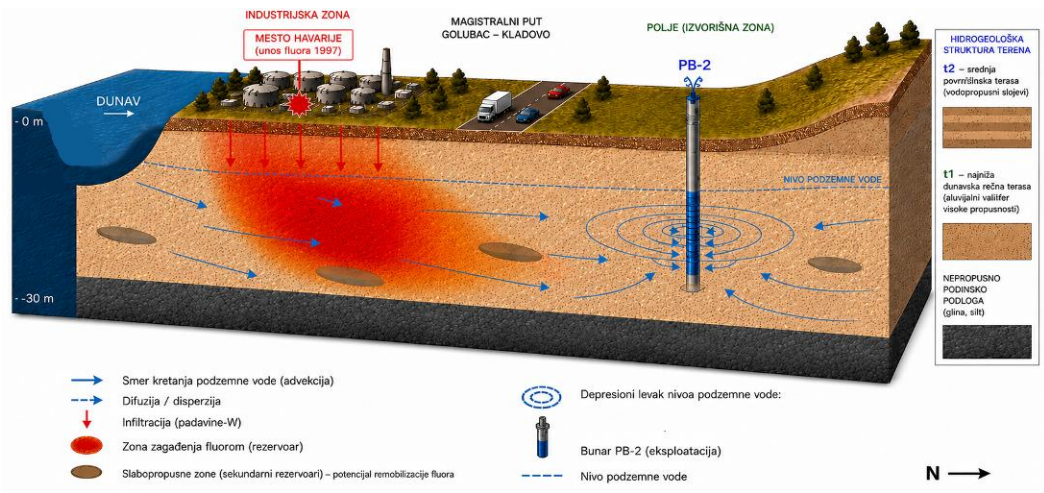

Figure 1 *Conceptual model of fluoride transport in aquifer*

MATERIALS AND METHODS

Methodological approach

The methodological approach applied in this study is based on the integration of two key aspects derived from the results of long-term monitoring:

1. analysis of the groundwater hydrodynamic regime (quantitative approach) and
2. analysis of geochemical processes (qualitative approach).

The first part of the methodological approach involves determining the groundwater regime and water balance, which represents the primary prerequisite for further defining contaminant migration. It is based on the results of continuous long-term monitoring of all influencing regime factors (groundwater and surface water levels, vertical water balance

parameters, groundwater abstraction at the wells of the Carina wellfield, as well as the operation of the groundwater protection system).

The second part of the methodological approach refers to the identification of geochemical processes and governing principles that determine the chemical behavior of fluorine in a porous medium. Particular importance is given to the analysis of the conditions under which fluorine remains dissolved in groundwater or precipitates into the solid phase, since these processes directly control its mobility, migration, and long-term persistence within the aquifer. One of the most important factors affecting dissolved fluoride concentrations is the relationship between calcium and fluoride in groundwater. Under conditions of elevated calcium content, fluoride ions become bound through the formation of sparingly soluble mineral phases, thereby reducing fluoride concentrations in solution and limiting its migration through aquifer layers:

$$CaF_2 \leftrightarrow Ca^{2+} + 2F^-$$

In contrast, in environments with lower calcium content, fluoride remains more mobile and is more easily transported through the aquifer.

Adsorption and desorption processes within fine-grained sediments also play a significant role. Silty and clayey interlayers present within the alluvial aquifer, due to their high content of clay minerals and iron oxides, represent important adsorption surfaces where fluoride can be temporarily retained. Such layers function as secondary contamination reservoirs because changes in hydrochemical conditions may lead to the gradual release of adsorbed fluoride back into the groundwater. This process contributes to the long-term persistence of contamination even after the cessation of active fluoride input into the system.

An important factor in assessing fluoride behavior is the acidity of the environment. Variations in pH values directly affect fluoride mobility, adsorption intensity, and the potential for the formation of complex compounds. The prolonged presence of acidic components may alter the geochemical equilibrium within the aquifer, increase fluoride mobility, and intensify its migration through groundwater.

Long-term monitoring of the groundwater regime

Long-term monitoring represents the basis for understanding the “slow” hydrogeological and geochemical processes that develop over several decades. During the thirty-year period from 1995 to 2025, systematic regime observations [1] were carried out in the zone of the Carina wellfield in Kladovo as illustrated in Table 1.

Table 1 *Monitoring data Gantt chart*

		95	96	97	98	99	00	01	02	03	04	05	06	07	08	09	10	11	12	13	14	15	16	17	18	19	20	21	22	23	24	25
Water Quantity Monitoring																																
Hydrological parameters																																
Climatic parameters																																
Groundwater levels																																
Water source exploitation																																
Water Quality Monitoring																																
Groundwater Quality	Standard																															
	Detailed																															
River Quality																																

RESULTS AND DISCUSSION

Hydrodynamic regime of groundwater at the Carina wellfield

From a hydrogeological perspective, the Carina wellfield is positioned within an aquifer formed in the lowest Danube terrace, composed of sandy–gravelly sediments characterized by high permeability and significant thickness (Figure 2). Currently, this wellfield comprises four production wells (PB-1, PB-2, PB-4, PB-5), with well PB-2 standing out as the most hydrochemically vulnerable due to its immediate proximity to the zone of initial fluoride contamination (illustrated in Figure 1).

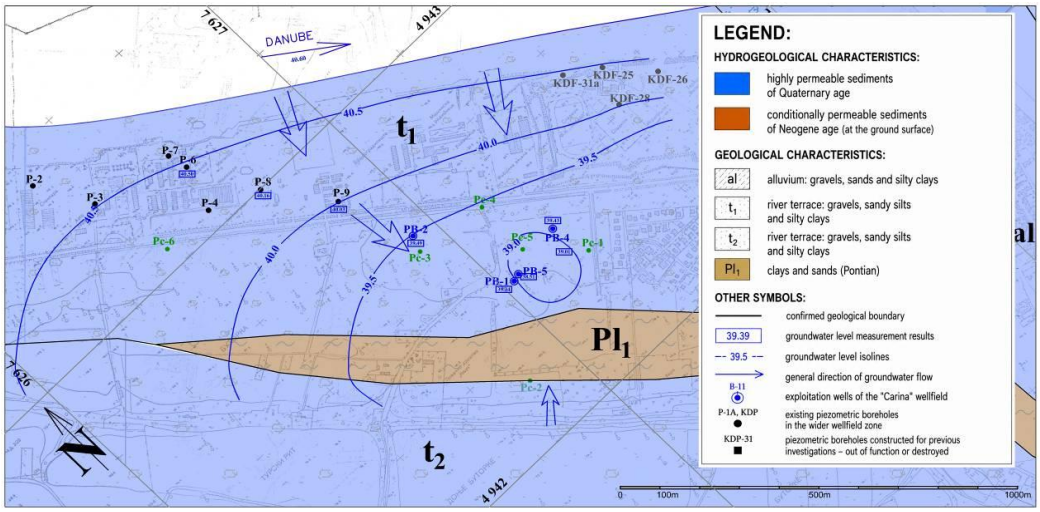

Figure 2 *Hydrogeological map of the Carina well field with piezometric level contour lines*

Active hydraulic connectivity between groundwater and the Danube River is predominantly reflected in groundwater levels, flow directions, and the intensity of aquifer recharge, thereby simultaneously controlling the conditions for fluoride migration through the aquifer. The influence of other parameters is also important, but in the overall water balance it is significantly smaller than the primary inflow of groundwater from the Danube. Groundwater abstraction through the production wells of the wellfield results in drainage of this aquifer (Figure 3).

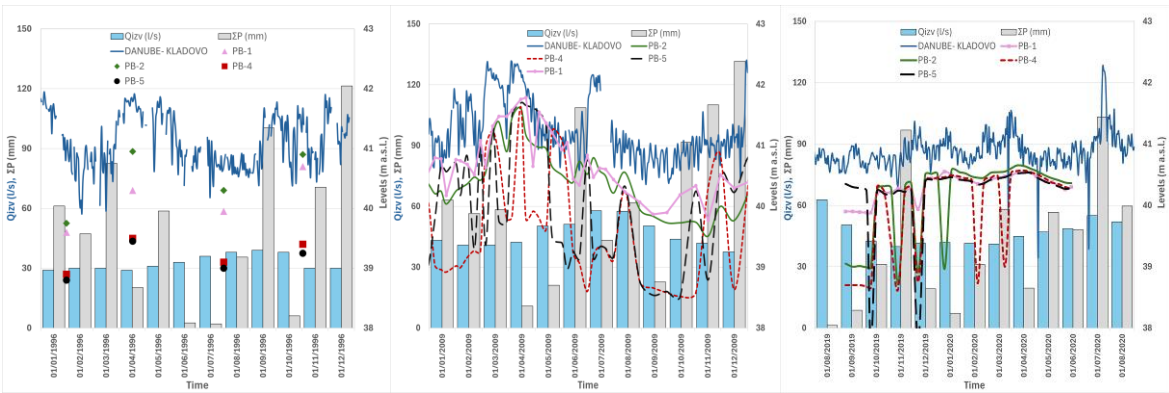

Figure 3 *Dependence of groundwater level fluctuations on the Danube River, precipitation, and groundwater abstraction at the wellfield for representative years (1996, 2009, 2020).*
Note: Continuous monitoring of wells PB-1:4 has been established only after the incident

Contamination of the Carina wellfield with fluorides

Research results have shown that fluoride contamination of the Carina wellfield is directly related to the operation of a crystal glass factory, most likely of the K_2O–PbO–SiO_2 type, in which hydrofluoric and sulfuric acids were used during chemical processing. Under such conditions, fluorine occurs in highly soluble and extremely mobile forms, capable of rapid infiltration through porous sediments and migration through groundwater. In the glass processing industry, fluorine is most applied in the form of hydrofluoric acid or gaseous hydrogen fluoride, where it causes etching of the glass and reacts with SiO_2, forming gaseous silicon fluorides (H_2SiF_6). The solutions used in this process contain various agents such as K_2O, CaO, PbO, or a mixture of HF + H_2SO_4 + H_2O, while after completion of the technological process, neutralization and proper waste storage are required. In the basins of the former glass factory in Kladovo, both soluble waste phases ($KHSO_4$, KHF_2) and insoluble phases ($PbSO_4$, K_2SiF_6) were detected, indicating the presence of fluoride compounds of varying solubility and mobility within industrial waste. Based on this knowledge, in the period 1995–1997, detailed investigations were carried out in the wider zone of the Carina wellfield by the Faculty of Mining and Geology. These studies included hydrochemical analyses of groundwater (from production and dug wells, piezometers, and even deeper artesian wells), geochemical analyses of soils and sediments, and assessment of fluoride migration through soil and aquifer layers. It was determined that the sources of contamination were the old and new crystal glass factories “Kristal,” where the technological process involved the dissolution of silicon dioxide and the formation of soluble fluoride compounds.

Temporal dynamics of fluoride concentration

Long-term monitoring analysis indicates three characteristic phases in the evolution of contamination. The first phase is the “accidental peak” phase (1995–1998), during which maximum fluoride concentrations were recorded immediately after the incident (in the nearest well PB-2, average values exceeded 4.0 mg/L, significantly above the maximum allowable concentration [2] (MAC 1.2 mg/L)). This was followed by an “intensive attenuation” phase, during which, due to natural aquifer flushing and the cessation of the contamination source, fluoride concentrations decreased (in PB-2 to an average of about 2.0 mg/L). Over the last 15 years, a phase of establishment of a “quasi-stationary” state has occurred, in which the decreasing trend has completely stopped. Concentrations have stabilized in the range of 1.0–1.2 mg/L (around the MAC), indicating that the system has reached a dynamic equilibrium. Figure 4 presents the temporal dynamics of fluoride concentration over the monitoring period 1995–2025 (note: complete data series were not available for PB-2 in 2005 and for PB-1 in 2008).

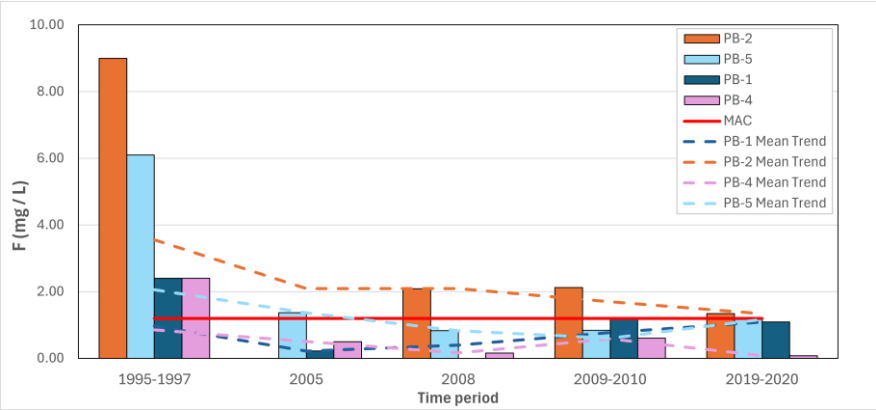

Figure 4 *Temporal dynamics of fluoride concentration during monitoring period 1995–2025*

Spatial migration dynamics of the contamination as a function of groundwater regime

Results of the three-decade monitoring indicate pronounced spatial heterogeneity in fluoride distribution within the aquifer of the Carina wellfield in Kladovo. In addition to geochemical processes, the degree of contamination is primarily influenced by the established groundwater regime, whose parameters were continuously monitored throughout the entire study period (Figure 3). Data analysis shows that contaminant migration within the aquifer is strictly controlled by the dominant hydraulic gradient, which is governed both by natural conditions (influence of the Danube River) and anthropogenic factors (operation of production wells and the peripheral protection system of the settlement).

Figure 5 presents the spatial distribution of average fluoride concentrations for the period 1995–1997 (contamination phase).

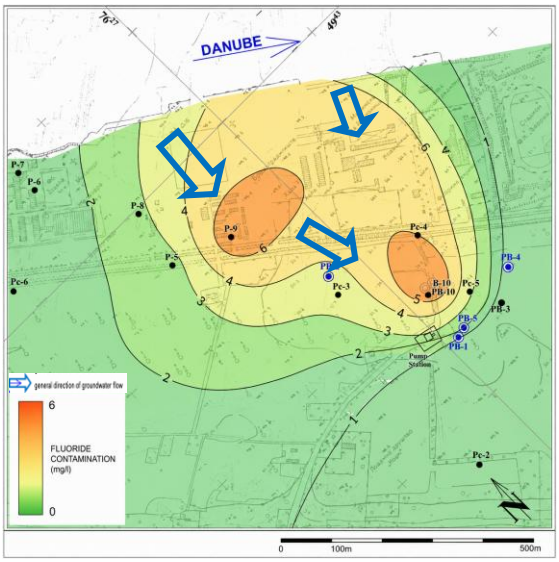

Figure 5 *Fluoride contamination of the Carina groundwater wellfield – spatial distribution*

Within the wellfield, distinct zones can be identified: zones of minimal impact ("clean zones"), which include water facilities located upstream or in close proximity to the Danube River, as well as wells positioned laterally relative to the main contaminant flow path (PB-4),

where fluoride concentrations remain stable and close to natural background levels (< 0.5–1.0 mg/L). In contrast, a zone of maximum impact is also identified, encompassing the immediate vicinity of well PB-2 (formerly PB-10) and the associated piezometer network. The contaminated wells are located along the direct hydraulic flow path from the primary source (the glass factory) and consistently record the highest fluoride concentrations throughout the entire monitoring period (values per period shown at Figure 4). The established groundwater regime, together with intensive abstraction at the wellfield, has created a stable pathway of the contamination front directed toward the most productive part of the wellfield.

Correlation of changes in fluoride concentration with other relevant parameters

For the purpose of interpreting the basic hydrochemical composition of groundwater at the Carina wellfield, the Schoeller diagram was used. This representation indicates that at location the source groundwater is primarily of the bicarbonate-calcium type (Figure 6).

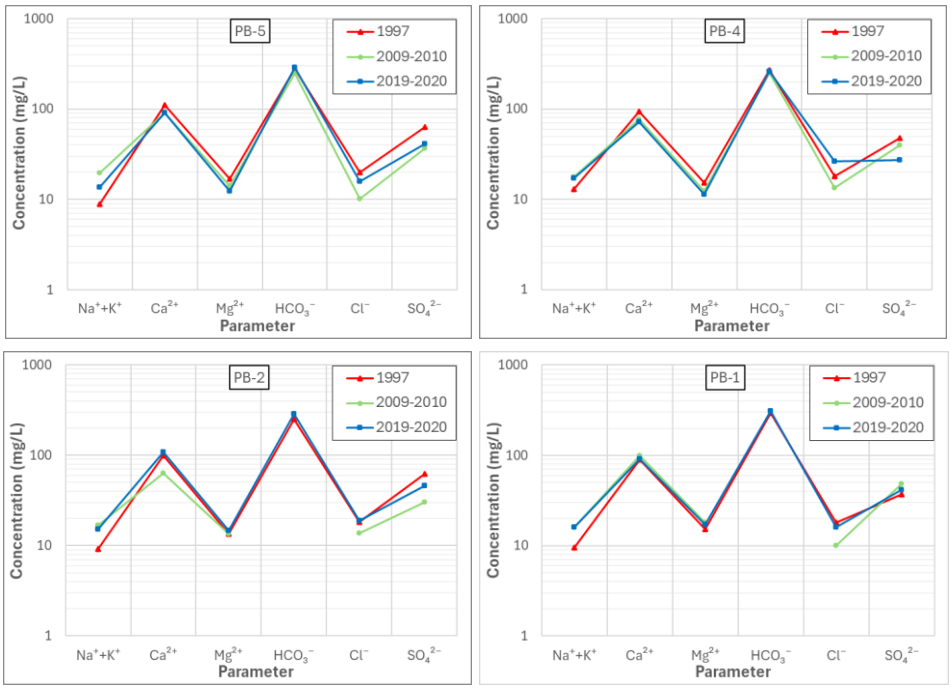

Figure 6 *Schoeller diagram of the basic hydrochemical composition of groundwater*

Statistical data processing and correlation analysis of the investigated parameters enabled the identification of the key correlation factors controlling the distribution and persistence of fluoride in the aquifer. It should be noted that the presented data include all monitoring locations, which are spatially unevenly distributed with respect to the contamination trend, resulting in the nonlinearity of the observed functions.

- Coupled migration of F^- and SO_4^{2} ions:

A pronounced positive correlation was identified, indicating the synchronous migration of these ions and representing a direct indicator of the anthropogenic origin of contamination, i.e., that fluoride originates from the same technological process in which sulfuric acid was used (Figure 7A).

• Thermodynamic control of fluoride saturation (correlation between F^- and Ca^{2+} concentrations):

A moderate inverse correlation was observed, indicating that fluoride concentrations in the aquifer are controlled by equilibrium with the mineral fluorite (CaF_2). Under conditions of elevated calcium content, fluorite precipitation occurs to a certain extent, thereby naturally limiting fluoride mobility. In contrast, a decrease in calcium concentration in groundwater induces an increase in fluoride concentrations. However, the moderate strength of the correlation suggests that additional natural factors also influence aquifer contamination (Figure 7B).

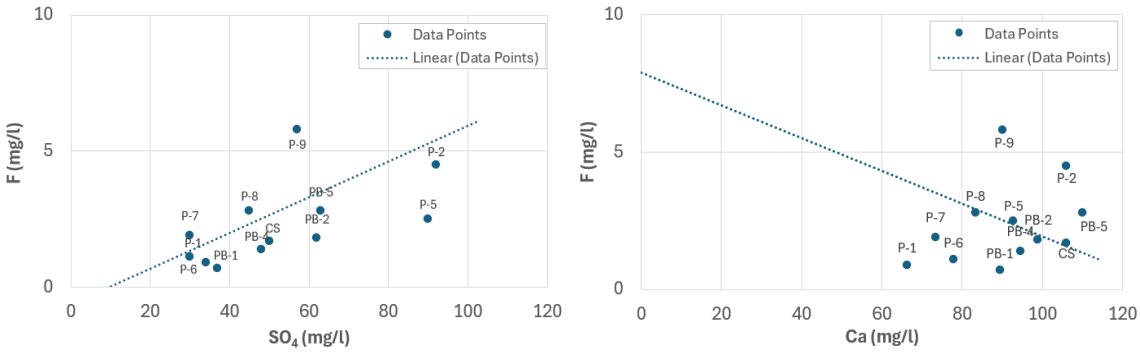

Figure 7 *Correlation of fluoride concentrations with sulfate concentrations (7A) and calcium ion concentrations (7B) during the 1995–2025 period*

• Cation exchange processes:

A negative correlation between sodium (Na^+) and calcium (Ca^{2+}) suggests ion-exchange processes occurring on clay and fine-grained mineral surfaces. Adsorption of Ca^{2+} accompanied by the release of Na^+ further decreases solution saturation with respect to fluoride-bearing minerals, thereby facilitating additional fluoride mobilization into groundwater.

• Desorption mechanisms under alkaline conditions (F^- and HCO_3^-):

The positive correlation indicates that alkaline conditions promote fluoride desorption from the surfaces of iron and aluminum oxides, contributing to its persistence in the aquifer even after the flushing of the primary contamination source.

• Heavy metal mobility and aquifer neutralization capacity:

Despite the confirmed presence of Pb in the waste material, Pb concentrations in groundwater remained below the detection limit throughout three decades of monitoring. This is attributed to the formation of sparingly soluble lead sulfate ($PbSO_4$) within the initial contamination zone, which prevented further migration of this metal toward the pumping wells. Contamination by sulfur, silicon, and other harmful substances was not detected within the wider source area due to their generally limited migration capacity. In addition, analyses showed no significant relationship between pH and fluoride concentrations, indicating that the initially acidic wastewater was largely neutralized along its flow path toward the groundwater abstraction zone.

CONCLUSION

Thirty years of quantitative and qualitative monitoring at the Carina wellfield provided valuable insight into the long-term dynamics of fluoride contamination in an alluvial aquifer, as well as the key factors controlling its persistence. A major contribution of this study is the identification of anthropogenic influences on contamination fate. Intensive groundwater abstraction modifies hydraulic gradients and potentially remobilizes contaminated water from silty and clayey sediments, thereby sustaining contamination long after the primary pollution source was removed. As a result, continuous exploitation reduces the natural flushing capacity of the aquifer and maintains the system in a quasi-stationary state. Hence, groundwater exploitation cannot be seen only as a remediation mechanism, but also as a possible driver of contaminant transport. Therefore, sustainable management of such resources requires integrated (long-term) monitoring and optimized abstraction strategies to effectively control long-term environmental risk.

REFERENCES

[1] Program of observation, measurement and analysis of backwater effect of the Danube River on the shore, caused by the construction and exploitation of HPP "Đerdap 1" and HPP "Đerdap 2". Jaroslav Cerni Water Institute; 2025.

[2] “Regulation on Permissible Quantities of Hazardous and Harmful Substances in Soil and Irrigation Water”. “Official Gazette of the Republic of Serbia”, No. 23, 1994.

EcoTER'26
eco.tfbor.bg.ac.rs
32nd International Conference
Ecological Truth & Environmental Research
24–26 June 2026, Hotel Sunce,
Sokobanja, Serbia

Original Research

COMPARISON OF SATELLITE DATA WITH LOW-COST SENSOR NETWORK PM DATA IN FOUR CITIES IN SERBIA

DOI: 10.5937/EcoTER26210C

Željko Ćirović[1,a*], Duška Kleut[1,b], Danka B. Stojanović[1,c], Milena Jovašević-Stojanović[1,d]

[1] Vinča Institute of Nuclear Sciences-National Institute of the Republic of Serbia, University of Belgrade, Mike Petrovića Alasa 12-14, Belgrade, SERBIA

[a] https://orcid.org/0000-0002-8069-0982 [b] https://orcid.org/0000-0002-5881-6497
[c] https://orcid.org/0000-0002-7178-1970 [d] https://orcid.org/0000-0003-0765-6603

Abstract

Conventional monitoring stations provide reliable measurements of particulate matter (PM) mass concentrations and are valuable for giving information about air quality but due to high costs and operational challenges, only a limited number of such monitors can be deployed. On the other hand, a network of low-cost PM sensors is also a promising approach to increase the measurement density. In addition to the ground-based measurement techniques described earlier, remote sensing can also be used to derive PM concentrations. In this study, we propose an integration of information from multiple measurement approaches. Here, we demonstrate correlations between results obtained by the data from the monitoring stations, low-cost sensors and satellite S-MESH data in western Serbia in the period from April to December 2022. The results indicate good correlations of all low-cost sensor data with S-MESH data with mean correlations around (>70%). Within this study, it is confirmed that the low-cost sensor network and satellite data provide valuable information on PM concentrations at locations which do not have monitoring stations.

Keywords: particulate matter, pollution mapping, satellite data, low-cost sensor network.

INTRODUCTION

Air pollution, especially from fine particulate matter smaller than 2.5 micrometers ($PM_{2.5}$), is a significant public health threat and contributes to millions of premature deaths each year. A large number of epidemiological research has consistently linked high $PM_{2.5}$ levels to serious health issues such as cardiovascular and respiratory diseases [1]. In Europe, air quality management standards are in place to combat elevated $PM_{2.5}$ concentrations. Nevertheless, 94% of the EU's urban population remains exposed to harmful $PM_{2.5}$ levels [2], underscoring the urgent need for accurate, high-resolution monitoring to support effective interventions and evidence-based policymaking.

Traditionally, ground-level $PM_{2.5}$ has been measured using air quality monitoring stations with reference-grade instruments, which yield high-quality local data. However, due to their high installation and maintenance costs, these stations are sparse and unevenly distributed,

* *zeljko.cirovic@vin.bg.ac.rs*

resulting in limited spatial coverage [3]. They often fail to capture inter-urban pollution gradients [4,5]. To address these gaps, various modelling and satellite-based estimation methods have been developed. Yet, each approach has inherent limitations, particularly regarding temporal resolution, spatial representativeness, and accuracy under changing atmospheric conditions.

Satellite-based instruments present an alternative approach by delivering global observations of Aerosol Optical Depth (AOD), which can act as a stand-in for ground-level $PM_{2.5}$ concentrations [6]. Sensors like the Moderate Resolution Imaging Spectroradiometer (MODIS) and the Visible Infrared Imaging Radiometer Suite (VIIRS) have been extensively employed to estimate surface $PM_{2.5}$ using various methods [7]. The S-MESH framework [8] produces high-resolution, bias-corrected daily $PM_{2.5}$ hindcast data for 2021–2022 by downscaling CAMS regional forecasts. It integrates satellite AOD (from VIIRS), CAMS-based $PM_{2.5}$ predictions, meteorological variables, and ground station data (used solely for training) within a stacked machine learning model. In recent years, low-cost sensors have gained traction due to their ability to fill spatial gaps in existing monitoring networks. These devices are small, affordable, and capable of generating highly resolved temporal data, making them especially appealing for urban-scale studies and citizen science initiatives [9–11]. Remote sensing can also help evaluation of the reliability of low-cost sensors [12–14].

In this study, we use the results of a low-cost sensor network that included 12 locations in 4 municipalities in western Serbia in the period from May to December 2022 [15]. We evaluate the correlations between results obtained by the data from the monitoring stations, low-cost sensors and satellite S-MESH data in order to provide more information about air pollution levels. The methods used here are especially important in municipalities in which monitoring of PM within local networks does not exist.

MATERIALS AND METHODS

Low-Cost Sensor Network and Monitoring stations

The low-cost sensor network data was obtained as part of the UNICEF Serbia pilot initiative "Schools for Better Air Quality". Each low-cost sensor was equipped with a PMS7003 air dust sensor to measure particulate matter fractions. The total low-cost sensor network consisted of 129 devices at 43 locations in 15 municipalities in central and western Serbia [15]. Within the study presented here, research was done for four cities including, Čačak, Kosjerić, Novi Pazar and Užice (12 locations in total). These cities are equipped with Serbian Environmental agency monitoring stations [16] and results obtained with low-cost sensors and monitoring stations are compared in our previous publication [15]. Here, we analysed the data set acquired in the period from May to December 2022.

S-MESH approach

The S-MESH framework [8] produces high-resolution, bias-corrected daily hindcasts of $PM_{2.5}$ for 2021–2022 by downscaling CAMS regional forecasts. It employs a stacked machine learning model that integrates satellite AOD (from VIIRS), CAMS $PM_{2.5}$ forecasts, meteorological data, and station observations. The CAMS forecast serves as a predictor to enhance accuracy and fill gaps in AOD data. Rather than aiming to generate real-time

forecasts, S-MESH offers a timely alternative to conventional CAMS reanalysis data. The S-MESH framework used in this study follows a similar structure: a stacked ensemble based on the XGBoost algorithm [17]. It consists of two first-stage beta models, each with slightly different input feature sets, and a second-stage meta model that combines the predictions from the beta models with selected additional predictors.

Data analysis methods

The correlations, corresponding scatter plots and monthly graphs of the $PM_{2.5}$ data obtained from the campaign, from low-cost sensors and monitoring stations, as well as from the S-MESH framework were calculated using *openair* package in R-studio and the plots were created using this tool built for the purpose of analysing air quality data. Land use data shown in Table 1. was derived from CORINE Land Cover 2018 [18] (vector/raster 100 m, Europe, 6-yearly) data which provides pan-European CORINE Land Cover inventory for 44 thematic classes for the 2018 reference year. The dataset has a Minimum Mapping Unit (MMU) of 25 hectares (ha) for areal phenomena and a Minimum Mapping Width (MMW) of 100 m for linear phenomena and is available as vector and as 100 m raster data.

RESULTS AND DISCUSSION

The results presented in Table 1 show a comprehensive overview of the data obtained during the campaign at four locations in each municipality, and their comparison with the data gathered from the S-MESH model database. Figure 1 presents scatter plots and correlation equations for the daily campaign measurements and the S-MESH framework data in the city of Novi Pazar (results for other cities can be seen in the table 1). These were calculated at the GPS coordinates of each of the four locations (one monitoring station and three schools) in the four municipalities, covering the entire campaign period (May–December 2022).

The low-cost sensor network data and the reference stations set in the same municipality show high correlation of >93%, except for one school set in a remote village 13 km away from the reference station location in the town centre (Figure 2). The diversity of the distances and the urban and geographical landscape of the four municipalities indicated the need to examine the relationship between all $PM_{2.5}$ data and the distances of the schools and the reference stations, hence the inclusion of that column in Table 1. As a measurement of the S-MESH estimation for the municipality the correlations of all 4 locations were estimated comparing to the S-MESH data at the reference station location as well as at their own GPS coordinates. In some instances, a few locations were part of the same S-MESH datapoint since the resolution of the data is 1 km (Figure 2). In all municipalities the campaign data shows high correlation with the S-MESH data (>70%) around the central locations with larger concentration of pollution sources. As the distance of the school from the reference station increases the S-MESH data at that location correlate less with the campaign data by 5–10%. Two cases of interest are the ones with unique land use characteristics. First, the remote school in Kosjerić municipality shows an overall low correlation of 25–30% with both the reference data and the S-MESH data. Second, in the school in Novi Pazar municipality, the correlation with its own S-MESH location is 20% lower compared to the correlation between the reference station and its corresponding S-MESH data. This suggests a strong influence

from factors likely not included in the S-MESH framework, probably due to industrial facilities in the vicinity of the latter. Highest overall correlation of 84% of the S-MESH framework data with the campaign measurements was measured at the Novi Pazar reference station location, while the remote school in Kosjerić shows overall lowest correlation to all data.

Table 1 *The correlations of the campaign measurements with the reference station and the distance from it, the correlation with the reference station location S-MESH data, the school's location own S-MESH data and the land use data for that particular (own) location*

Location	SEPA correlation	SEPA Distance	SEPA-SMESH correlation	Own SMESH correlation	Coordinates	Land use
Cacak-SEPA	1	0.00	0.718	**0.73**	43.89333, 20.34553	Sport and leisure facilities
Cacak-CHSch	0.945	1.54 km	0.735	**0.70**	43.88243, 20.33253	Discontinuous urban traffic
Cacak-ElSchSS	0.962	1.50 km	0.748	**0.75**	43.86786, 20.36911	Discontinuous urban traffic
Cacak-ElSchTR	0.959	3.31 km	0.725	**0.65**	43.90631, 20.35658	Discontinuous urban traffic
Kosjeric-SEPA	1	0.00	0.737	**0.74**	44.00294, 19.90518	Discontinuous urban traffic
Kosjeric-ElSchJD	0.262	12.9km	0.301	**0.25**	44.04410, 19.75163	Land principally occupied by vegetation, with significant areas of natural vegetation
Kosjeric-ElSchMI	0.977	0.87km	0.742	**0.71**	43.99370, 19.90793	Discontinuous urban traffic
Kosjeric-TechSch	0.976	1.08km	0.745	**0.72**	43.99262, 19.91031	Discontinuous urban traffic
NoviPazar-SEPA	1	0.00	0.841	**0.84**	43.13928, 20.51617	Discontinuous urban traffic
NoviPazar-ElSchHZ	0.936	4.75km	0.843	**0.76**	43.14105, 20.45814	Discontinuous urban traffic
NoviPazar-ElSchMS	0.977	2.47 km	0.843	**0.66**	43.15987, 20.52680	Complex cultivation patterns
NoviPazar-ElSchRB	0.982	0.87km	0.826	**0.83**	43.13397, 20.51742	Discontinuous urban traffic
Uzice-SEPA	1	0.00	0.764	**0.76**	43.85427, 19.84321	Discontinuous urban traffic
Uzice-ElSchNI	0.973	1.05 km	0.755	**0.65**	43.85404, 19.85919	Discontinuous urban traffic
Uzice-MedSch	0.974	1.00 km	0.753	**0.65**	43.86037, 19.85493	Discontinuous urban traffic
Uzice-TechSch	0.972	0.175km	0.731	**0.73**	43.85581, 19.84585	Discontinuous urban traffic

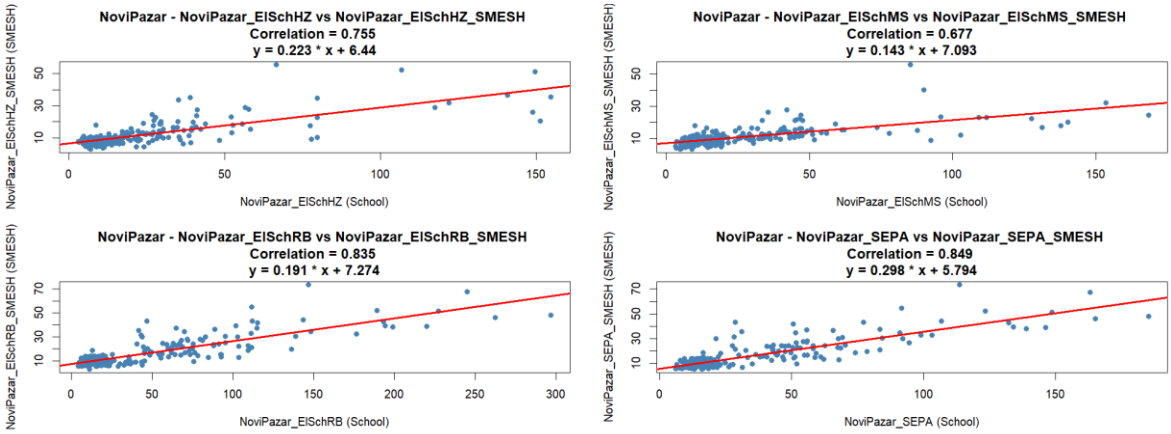

Figure 1 *Scatter plots of daily campaign measurements compared to S-MESH data at locations in Novi Pazar*

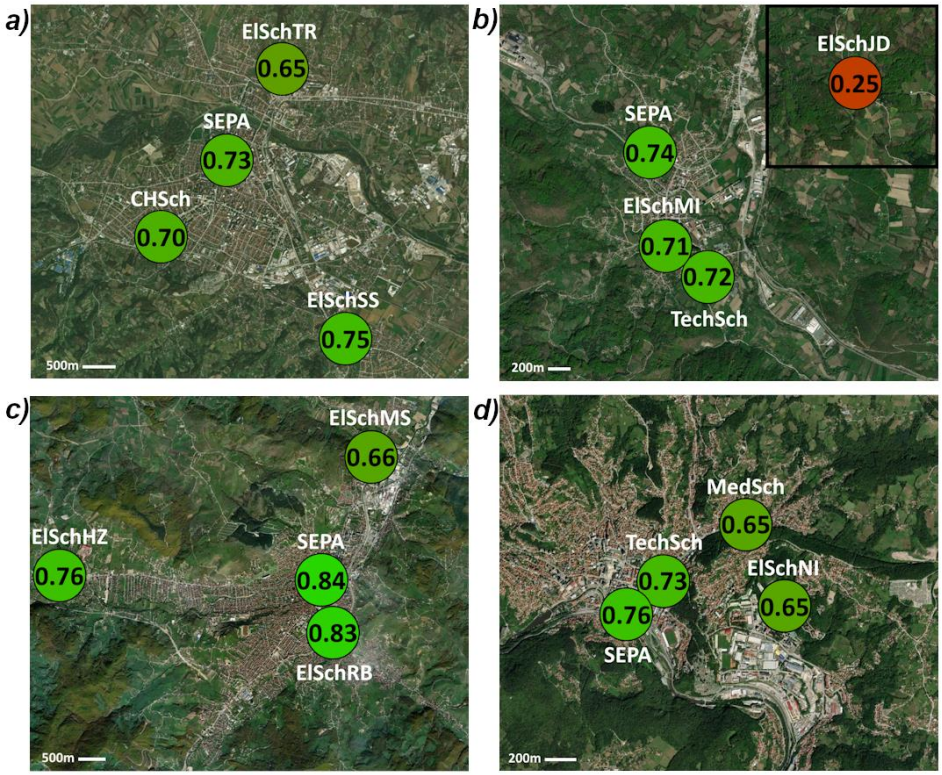

Figure 2 *Maps of the campaign locations with the S-MESH data correlation values*

The correlations of the campaign data with the S-MESH framework data on a monthly level presented in Figure 3 show much higher variance in correlations on a smaller sample of 30–31 days. Monthly correlation values vary mostly between 25–75%. In two schools which are the most remote from their closest monitoring stations the monthly correlations were negative in one summer month in this period. The best monthly correlations overall in all 4 municipalities are measured in July and October of 2022, which is presumably related to the remarkably clear and dry weather, expected in July but surprisingly recorded in weather data history for October 2022 in Serbia. This can be attributed to the better predictions of the S-MESH framework data.

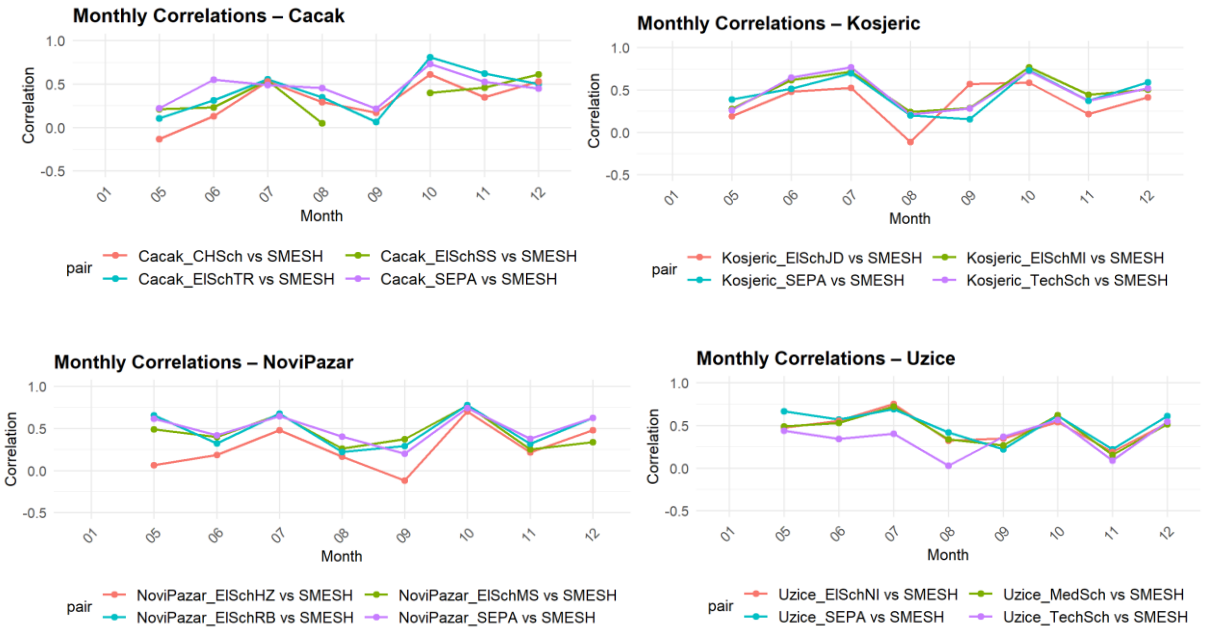

Figure 3 *Changes in the monthly values of correlation between daily data gathered during the campaign and the S-MESH data at the measurement locations*

RMSE (avg. 30.31 µg m^{-3}), MAE (avg. 18.17 µg m^{-3}) and bias (avg. -17.49 µg m^{-3}) values were calculated for all measurement sites. All biases were negative meaning that S-MESH consistently underestimates $PM_{2.5}$ compared to ground sensors. In cities with complex pollution (Novi Pazar, Cacak), SMESH misses peaks which could underestimate exposure risks. Because the model is trained and validated using monitoring stations, it will usually perform best in regions with dense (usually urban), representative monitoring coverage. That is also true with our dataset with the ElSchJD site being a clear outlier. Additionally, while 1 km can be considered high resolution, it still is not street scale and can miss sharp gradients near roads, intersections, street canyons, small heating sources etc.

CONCLUSION

In this study, we show that data from monitoring stations, low-cost sensors, and satellite S-MESH data in western Serbia between April and December 2022 are well correlated. Findings reveal that almost all low-cost sensor data align well with the S-MESH data, with average correlation values of approximately 70%. This study shows that the low-cost sensor networks in combination with satellite derived S-MESH data can provide information on long-term PM concentration trends. This is of particular importance for locations which do not have monitoring stations, but also confirms the usefulness of satellite-derived ground based PM concentrations in general.

ACKNOWLEDGEMENT

This research was funded by the European Union's Horizon Europe Research and Innovation Program under GA 952433, H2020 (VIDIS project) and GA 101060170 (WeBaSOOP project), the Government of Norway and implemented by UNICEF initiative "Schools for Better Air Quality: Citizens-Based Monitoring, STEM Education, and Youth Activism in Serbia" and the Ministry

Science, Technological Development and Innovation of the Republic of Serbia under GA 451-03-33/2026-03/ 20001.

REFERENCES

[1] Pryor, J.T., Lachlan O.C., Stephanie E.S. Front. Public Health. 2022, 10, 882569.

[2] EEA, Air quality status report 2025.

[3] Liu, Y. Atmos. Environ. 2013, 68, 52–53.

[4] Cheeseman, M., Ford, B., Rosen, Z. *et al*. Atmos. Meas. Tech. Discuss., 2021, 1–30.

[5] Just, Allan C., *et al.* Environ. Sci. Technol. 2015, 49.14, 8576–8584.

[6] Handschuh, J., Erbertseder, T., Baier, F. Remote Sens. 2023, 15 (8).

[7] Xu, X., Zhang, C., Liang, Y. Atmos. Environ. 2021, 256, 118302.

[8] Shetty, S., Hamer, P.D., Stebel, K., *et al*. Environ. Res. 2025, 264 (P2), 120363.

[9] Castell, N., Dauge, F.R., Schneider, P., *et al*. Environ. Int. 2017, 99, 293–302.

[10] Hassani, A., Byku´c, S., Schneider, P. *et al*. Atmos. Environ. 2023, 314, 120108.

[11] Lepioufle, J.-M., Schneider, P., Hamer, P.D., *et al.* Environ. Data Sci. 2024, 3, e19.

[12] Li, J., *et al.* Atmos. Environ. 2020, 223, 117293.

[13] Huang, K., Bi, J., Meng, X., Sci. Total Environ. 2019, 697, 134094.

[14] Gupta, P., Doraiswamy, P., Levy, R., *et al.* GeoHealth 2018, 2.6, 172–181.

[15] Stojanović, D.B., *et al.* Sensors 2024, 24.13, 4052.

[16] Serbian Environmental Protection Agency. Serbian Environmental Protection Agency. Belgrade: Ministry of Environmental Protection; 2026. Available from: https://sepa.gov.rs/

[17] Chen, T., Guestrin, C., 2016. Proceedings of the 22nd ACM SIGKDD International Conference on Knowledge Discovery and Data Mining 785–794.

[18] Copernicus Land Monitoring Service. CORINE Land Cover 2018 (vector/raster 100 m), Europe, 6-yearly. 2026. Available from: https://land.copernicus.eu/en/products/corine-land-cover/clc2018

Original Research/Review

ASSESMENT OF SEDIMENTABLE PARTICULATE MATTER IN TIMISOARA

DOI: 10.5937/EcoTER26217Z

Madalina Ileana Zot[1,a*], Francisc Popescu[1,b]

[1] University Politehnica Timisoara, Faculty of Mechanical Engineering, Bv. Mihai Viteazul 1, 100222 Timisoara, ROMANIA

[a] https://orcid.org/0009-0005-7620-3159

[b] https://orcid.org/0000-0001-7736-0758

Abstract

Preliminary proposal work on sedimentable particulate matter (SPM) monitoring in the city of Timisoara (Romania), using passive samplers located in areas with different traffic intensities. The study aims to assess the level of particle deposition and create a database for further research on the chemical composition and pollution sources.

Keywords: SPM, air quality, settleable particulate matter, gravimetric method, environmental monitoring.

INTRODUCTION

Air pollution is one of the most important environmental challenges globally, being associated with significant effects on human health, ecosystems and urban infrastructure. Among the numerous air pollutants, particulate matter (PM) is considered one of the most relevant indicators of air quality, due to its ability to transport toxic compounds and deposit on exposed surfaces in the environment [1]. In urban environments, the main sources of particulate matter are road traffic, industrial activities, construction processes, residential heating and dust resuspension from road surfaces [2]. In addition to the inhalable fractions PM_{10} and $PM_{2.5}$, settleable particulate matter (SPM) is an important component of air pollution, as it reflects the process of gravitational deposition of larger particles on soil, vegetation, buildings and other exposed surfaces. These particles can accumulate heavy metals, polycyclic aromatic hydrocarbons and other contaminants originating from anthropogenic activities, contributing to environmental degradation and contamination of urban soils [3]. Road transport is one of the main sources of particulate emissions in urban environments, both through combustion processes in vehicle engines and through non-exhaust sources, such as tire wear, brake wear and resuspension of particles deposited on the roadway. Recent studies show that, as exhaust emissions are reduced by modern technologies, the contribution of non-exhaust sources is becoming increasingly important in the total balance of particle pollution in cities [4]. Also, traffic intensity and road infrastructure characteristics significantly influence the level of particles present in the atmosphere and the rate of their deposition on urban surfaces [4]. In recent years, the interest of researchers in the study of

* *madalina.zot@upt.ro*

atmospheric deposition processes has increased considerably, as they provide complementary information to the monitoring of suspended particle concentrations. The analysis of settleable particles allows the assessment of the cumulative impact of pollution sources on the environment and the identification of areas with high contamination potential. Recent research has highlighted the fact that particle deposition rates vary significantly depending on traffic density, industrial activities and local meteorological conditions [5,6]. At European level, particulate pollution continues to be a major environmental problem. According to recent reports by the European Commission and the Joint Research Centre (JRC), many European cities still exceed the values recommended by the World Health Organization for atmospheric particulate matter, highlighting the need to expand monitoring programs and studies on atmospheric deposition [2]. In this context, the assessment of sedimentable particulate matter in the city of Timișoara (Romania) represents a first step in the development of a comparative database on atmospheric deposition in the western region of Romania. The study aims to highlight the spatial distribution of sedimentable particulate matter in areas characterized by different intensities of traffic and urban activities, contributing to a better understanding of the influence of anthropogenic sources on environmental quality.

MATERIALS AND METHODS

The study was conducted in the municipality of Timișoara, one of the largest urban centers in western Romania, characterized by intense road traffic, industrial activities, and continuous urban development. The objective of the monitoring paper was to evaluate the spatial distribution of settleable particulate matter (SPM) and to obtain preliminary information regarding atmospheric deposition in areas exposed to different anthropogenic influences.

Six monitoring locations were selected across the city, considering traffic intensity, land use, population density, and proximity to potential pollution sources (Figure 1). A seventh location was set-up in a rural area, with no industrial/road sources. The sampling points included areas located near major road intersections, public transportation stations, educational institutions, residential neighbourhoods, and railway infrastructure. Settleable particulate matter samples were collected using passive deposition samplers, were constructed at University Politehnica laboratory, following the principles described in ASTM D1739-98 (R17), Standard Test Method for Collection and Measurement of Dustfall (Settleable Particulate Matter). The sampling system consists of a glass collecting container, mounted on a steel metal support and protected by an aluminium wind deflector, with the role of reducing the influence of air currents on the particle deposition process. All samplers were installed at a height of approximately 1.7 m above ground level, ensuring uniform collection conditions at all monitoring points.

The sampling container has a diameter of 0.16 m, achieving a collection surface of approximately 0.02 m², which allows for the efficient capture of sedimentable particles deposited gravitationally during the exposure period. Sedimentable particle samples were collected after a variable exposure period. The deposited material was recovered by washing the collection containers with type II distilled water and transported to the laboratory for processing. In the preliminary stage, the samples were passed through a 1 mm stainless steel

sieve to remove impurities and foreign materials. Subsequently, the samples were filtered through glass fiber filters, using a Buchner funnel, to separate the soluble and insoluble fractions of the sedimentable particles. Both fractions were dried at 105 °C until a constant mass was obtained, then cooled in a desiccator to avoid absorption of moisture from the atmosphere. The determination of the amount of sedimentable particles was performed gravimetrically, using an analytical balance with a precision of 0.01 mg.

Figure 1 *Location of SPM monitoring points in Timisoara*

This method is based on the natural gravitational settling of atmospheric particles into collection containers exposed to outdoor conditions over a predefined sampling period. In Figure 2 an example of sampler placed on a sampling site is given.

Figure 2 *SPM sampler in Timisoara, at S6 - Damaro site, with industry, rail & road traffic sources*

A recent study by del Pozo *et al*. [5] on sedimentary particles collected in different urban and industrial areas highlighted the presence of metals such as copper (Cu), lead (Pb), cobalt (Co), cadmium (Cd), chromium (Cr), silver (Ag), arsenic (As) and mercury (Hg). The authors showed that these elements are mainly associated with road traffic, industrial activities and combustion processes, demonstrating the usefulness of sedimentary particles as an indicator of air pollution and the impact of anthropogenic activities on the environment. The application of a standardized sampling methodology ensures the reliability of the collected data and provides a basis for assessing the influence of urban activities and transport-related emissions on atmospheric particle deposition within the study area.

RESULTS AND DISCUSSION

The calculation of SPM deposition rate was done following ASTM-D1739-98(R17) rules:

$$C_{SPM} = \frac{m_{SPM}}{A} \cdot \frac{30}{n} \quad [\frac{g}{m^2} \cdot month] \tag{1}$$

In Equation (1), $\boldsymbol{C_{SPM}}$ represents the concentration of settleable particulate matter, while $\boldsymbol{m_{SPM}}$ denotes the mass of the collected particles. $\boldsymbol{A}$ is the effective collection area of the sampling vessel (m^2), $\boldsymbol{n}$ represents the exposure period expressed in days, and the factor ***30*** is used to normalize the results to a standard monthly deposition rate.

The monitoring study conducted in Timisoara municipality allowed the preliminary assessment of the spatial distribution of sedimentable particulate matter (SPM) in areas characterized by different degrees of anthropogenic influence. The values obtained highlighted variations between monitoring points, suggesting the influence of local factors, such as traffic intensity, density of urban activities and proximity of potential emission sources.

The results obtained for a variable period between 2025–2026 are presented in Table 1.

Table 1 *C_{SPM} concentrations, in [g/m^2·month]*

Period	Days	S1 Brediceanu	S2 Cornesti	S3 Astro	S4 Lenau	S5 Incuboxx	S6 Damaro	S7 Meteo
01/04/2025-31/05/2025	60	16.6975	0.8175	5.6205	17.82	6.6865	6.523	3.24
31/05/2025-01/09/2025	92	16.4918	1.94	6.0324	5.978	4.2831	5.688	3.5157
01/09/2025-31/10/2025	60	12.0625	6.895	4.9175	6.7075	5.9575	5.2875	3.9775
31/10/2025-09/12/2025	39	2.0692	0.2384	0.1038	-	0.957	0.9807	2.2961
09/12/2025-02/03/2026	83	-	-	-	3.7391	5.6439	6.1969	3.1102
02/03/2026-15/05/2026	74	5.1162	-	2.1628	2.2095	2.5662	4.8324	3.5391

As expected, the values recorded for sedimentable particles (SPM) were higher in Timisoara, which can be attributed to the higher degree of urbanization, the intensity of road traffic, the development of industrial activities and the higher population density. These factors contribute to the increase in particle emissions into the atmosphere and, implicitly, to the intensification of their deposition processes. It is to be noted that in Romania the limit

value for C_{SPM} is 17 [g/m^2·month] and that this value refers to environmental assessment of mining industry and not for assessment of air quality in urban areas.

CONCLUSION

The results highlight the influence of local environmental conditions and anthropogenic factors on the distribution of settleable particulate matter within the urban environment. Furthermore, the study demonstrates the usefulness of passive monitoring techniques for evaluating atmospheric deposition and identifying areas potentially affected by increased particulate pollution.

Future investigations will focus on the physical and chemical characterization of the collected particles, particularly the determination of heavy metals associated with traffic and urban activities, with focus on elements specifically identified in EN 14902: Pb, Cd, As and Ni.

ACKNOWLEDGEMENT

This research was partially supported by the cross-border cooperation project AEPS (http://aeps.upt.ro) "Academic Environmental Protection Studies on surface water quality in significant cross-border nature reservations Djerdap/Iron Gate national park and Carska Bara special nature reserve, with population awareness raising workshops", RORS-462, project funded by the INTERREG IPA-CBC Romania-Serbia Programme.

REFERENCES

[1] World Health Organization. (2021). WHO global air quality guidelines: Particulate matter (PM2.5 and PM10), ozone, nitrogen dioxide, sulfur dioxide and carbon monoxide. World Health Organization.

[2] Thunis, P., Pisoni, E., Zauli Sajani, S., *et al*. (2023). Urban PM2.5 atlas air quality in European cities: 2023 report, Publications Office of the European Union. Available from: https://data.europa.eu/doi/10.2760/63641

[3] Machado, M., Santos, J.M., Reisen, V.A., *et al*., Atmos. Environ. 2018, 182, 242–251.

[4] Šarkan, B., Gnap, J., Loman, M., *et al*. Appl. Sci. 2023, 13(3), 1845.

[5] del Pozo, D., Valle, B., Maza, D., *et al*. Environments 2025, 12(9), 304.

[6] Chepkorir, A. (2024). Atmospheric concentrations, dry deposition fluxes and characterization of settleable particulate matter in urban environments (Master's thesis). Jomo Kenyatta University of Agriculture and Technology. Available from: http://ir.jkuat.ac.ke/bitstream/handle/123456789/6296/CHEPKORIR%2C%20A.%20MSc%20Thesis%202024.pdf?sequence=1&isAllowed=y

EcoTER'26
eco.tfbor.bg.ac.rs
32nd International Conference
Ecological Truth & Environmental Research
24–26 June 2026, Hotel Sunce,
Sokobanja, Serbia

Original Research

IMPACT OF DIMETHYL PHTHALATE ON THE GROWTH AND STRUCTURE OF CYANOBACTERIA (*Microcystis* sp.)

DOI: 10.5937/EcoTER26222K

Ivana Kostić Kokić[1,a*], Nikola Stanković[2,b], Danica Bogdanović[1,c], Tamara Petronijević[2,d], Monika Dudić[3,e], Tatjana Anđelković[1,f]

[1] University of Niš, Faculty of Science and Mathematics, Department of Chemistry, Višegradska 33, 18000 Niš, SERBIA

[2] University of Niš, Faculty of Science and Mathematics, Department of Biology and Ecology, Višegradska 33, 18000 Niš, SERBIA

[3] State University of Novi Pazar, Department of Natural Sciences and Mathematics, Vuka Karadžića bb, 36300 Novi Pazar, SERBIA

[a] https://orcid.org/0000-0001-6517-5635 [b] https://orcid.org/0000-0002-1604-6543
[c] https://orcid.org/0000-0001-5672-9931 [d] https://orcid.org/0000-0002-6958-9250
[e] https://orcid.org/0000-0003-3547-4305 [f] https://orcid.org/0000-0001-9856-985X

Abstract

This research was conducted to examine the influence of dimethyl phthalate (DMP) on the growth and physiological response of a cyanobacteria under laboratory conditions. A strain of the cyanobacteria Microcystis sp., isolated from freshwater ecosystems, was used in the experiment. The organisms were cultivated in a standard BG11 medium and its three modifications (nitrate-free BG11-1, phosphate-free BG11-2, and sulphate-free BG11-3) in the presence of three dimethyl phthalate concentrations (250, 500, and 1000 μg/L). Spectrophotometric determination of chlorophyll a was used for monitoring of organism growth and potential morphological changes in cells and contamination were controlled using microscopy. Also, pH value monitoring was done. Results demonstrate that the growth and physiological responses of Microcystis sp. are primarily governed by nutrient availability, while the effect of dimethyl phthalate is secondary and generally weak.

Keywords: dimethyl phthalate, cyanobacteria, chlorophyll *a*.

INTRODUCTION

Aquatic ecosystems are exposed to increasing pressure from anthropogenic activities in the modern era [1]. Industrialization, urbanization, and the extensive use of synthetic materials have led to a significant rise in the input of organic pollutants into the aquatic environment. A particular category is represented by the so-called "new" or emerging contaminants, which are increasingly being detected in surface and groundwater, but whose long-term effects on aquatic organisms and ecosystems are still not fully understood.

Phytoplankton communities are highly sensitive to environmental changes that influence their growth, composition, and dynamics. Therefore, monitoring variations in phytoplankton structure and dynamics is important for predicting future ecological changes. The ecological dynamics of phytoplankton are influenced by various factors: physical (temperature, salinity,

*ivana.chem@outlook.com

light radiation), chemical (availability of nutrients and metals) and biological (predators, viral infections, and toxic effects of bacteria).

Due to these factors, the biomass density of each local phytoplankton population is highly variable and temporally unpredictable. The basic requirements for phytoplankton growth are water, light, and certain inorganic substances. Prokaryotic forms of phytoplankton are referred to cyanobacteria [2].

Cyanobacteria comprise a large, morphologically and ecologically heterogeneous group of phototrophic bacteria. These autotrophic microorganisms have a long evolutionary history, a wide range of metabolic pathways, and numerous adaptive mechanisms. They are photosynthetic prokaryotes that use chlorophyll *a* and phycobiliproteins to harness sunlight as an energy source, and they do not reproduce sexually. Certain species are capable of nitrogen fixation and play important roles in oxygen production, CO_2 fixation, and biomass production [3].

Research shows that representatives of the genus *Microcystis* are sensitive to the presence of various pollutants, including organic micropollutants such as phthalates. These substances can affect growth, photosynthetic activity, and physiological processes, and may also indirectly alter the structure of phytoplankton communities. Due to its frequent dominance, ecological importance, and potential toxicity, the genus *Microcystis* is often used as a model organism in studies examining the impact of pollutants on phytoplankton and the stability of aquatic ecosystems [4].

MATERIALS AND METHODS

Phytoplankton cultivation

The strain *Microcystis* sp. was isolated from a marsh ecosystem. The strain was cultivated under controlled laboratory conditions, using the BG11 nutrient medium for cultivation and maintenance. The chemical composition of the BG11 medium is following (per liter): 1.5 g $NaNO_3$, 0.04 g K_2HPO_4, 0.075 g $MgSO_4 \cdot 7H_2O$, 0.036 g $CaCl_2 \cdot 2H_2O$, 0.006 g $C_6H_8O_7$, 0.006 g ammonium ferric citrate green, 0.001 g $EDTANa_2$, 0.02 g Na_2CO_3, 0.00286 g H_3BO_3, 0.00181 g $MnCl_2 \cdot 4H_2O$, 0.00022 g $ZnSO_4 \cdot 7H_2O$, 0.00039 g $Na_2MoO_4 \cdot 2H_2O$, 0.00008 g $CuSO_4 \cdot 5H_2O$ and 0.00005 g $Co(NO_3)_2 \cdot 6H_2O$.

Experiment

The cyanobacteria strain used in the experiment was inoculated into sterile glass test tubes (a total of 48 test tubes). The impact of three dimethyl phthalate (DMP) concentrations (250 μg/L, 500 μg/L, and 1000 μg/L) on the growth and physiological parameters of the test organism was examined. All phthalate concentrations were tested in triplicate.

Impact of DMP were conducted in four types of nutrient media: standard BG11 medium, nitrate-free BG11 (BG11-1), phosphate-free BG11 (BG11-2), and sulphate-free BG11 (BG11-3).

Following sterilization, 10 mL of the corresponding medium and 1 mL (1000 μL) of the cyanobacterial suspension were added to each test tube and various concentrations of DMP were added. Control tubes did not contain DMP. The pure substance of DMP (CAS Number: 131-11-3, Sigma Aldrich, USA) was used for preparing a stock and working solutions. All DMP solutions used during the experiment were prepared at the laboratory of the Department

of Chemistry, Faculty of Sciences in Niš. The tubes were sealed with medical cotton plugs and placed under laboratory cultivation conditions. After setting up the experiment, the chlorophyll *a* concentration was monitored using the spectrophotometric method by an Agilent BioTek Epoch 2 Microplate Spectrophotometer.

In order to detect potential contamination and prevent irregularities that could affect the accuracy of the results, the test cultures were monitored via microscopic analysis (Leica Microsystems Leica DM1000 and Leica Microsystems DFC295 camera). Also, monitoring of pH value was done SensIon Multimeter (Hach, Germany) during the experiment.

RESULTS AND DISCUSSION

The experiment monitored the production of chlorophyll *a* (Chl *a*) in strains of *Microcystis* sp. during two weeks of exposure to different concentrations of DMP (250, 500 and 1000 µg/L). Measurements were made spectrophotometrically at wavelengths of 678 nm, 720 nm and 750 nm, and the concentration of Chl *a* was calculated according to the formula (1) [2]:

$$Chl\ (\mu g \cdot mL^{-1}) = 14.96 \cdot (OD_{678} - OD_{750}) - 0.616 \cdot (OD_{720} - OD_{750}) \quad (1)$$

The results, presented in Figure 1, show that the response of *Microcystis* sp. varies depending on nutrient conditions and the concentration of dimethyl phthalate, indicating a complex interaction between nutrients and pollutants.

Considering that BG11 is a standard medium for the cultivation of cyanobacteria and microalgae, while BG11-1, BG11-2, and BG11-3 are media with selective deficiencies of nitrate, phosphate, and sulfate, respectively, the obtained results allow for a detailed analysis of the effects of dimethyl phthalate under different nutrient conditions.

In the standard BG11 medium, which provides optimal conditions for growth, *Microcystis* sp. showed a continuous increase in chlorophyll *a* throughout the experiment. The highest values were recorded in the control treatment, while all treatments with dimethyl phthalate (DMP) exhibited slightly lower values. This indicates that under conditions of full nutrient availability, dimethyl phthalate did not have a stimulatory effect but rather acted as a mild growth inhibitor. *Microcystis* sp. did not demonstrate the ability to utilize the presence of the stressor to enhance its growth. Although the differences were not statistically significant ($p > 0.05$), the observed trend suggests that under optimal conditions, the control outperforms the pollutant-treated samples.

Under nitrate-deficient conditions (BG11-1), the overall growth of *Microcystis* sp. was significantly reduced compared to the standard medium, which is expected since nitrogen is essential for the synthesis of proteins, pigments, and nucleic acids. In these conditions, differences between treatments were minimal, and a slight increase in growth was observed at lower concentrations of dimethyl phthalate. However, this effect was not pronounced enough to be considered significant. This suggests that under nitrogen stress, nutrient limitation is the dominant factor, while the influence of dimethyl phthalate is of secondary importance.

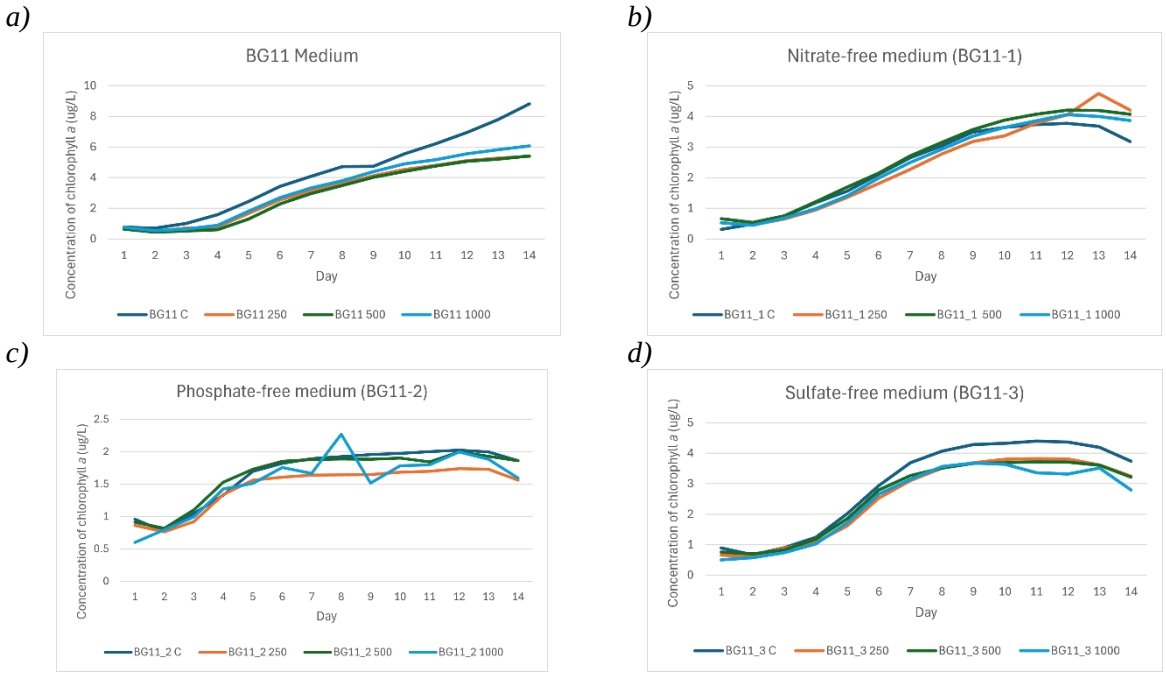

Figure 1 *Chlorophyll a concentration (µg/L) during the Microcystis sp. growth period in different media a) standard BG11 medium; b) nitrate-free medium (BG11-1); c) phosphate-free medium (BG11-2); d) sulphate-free medium (BG11-3)*

In the phosphate-deficient medium (BG11-2), the most pronounced decrease in the growth of *Microcystis* sp. was observed compared to all other conditions. This confirms that phosphorus is critical for energy metabolism, DNA synthesis, and overall cellular function. The treatments showed an uneven response, with some concentrations (e.g., 500 µg/L) yielding values similar to the control, while others were lower. However, no statistically significant differences were found, indicating that phosphate limitation is again the primary factor determining growth, while the effect of dimethyl phthalate is relatively weak and variable.

In the sulfate-deficient medium (BG11-3), the growth of *Microcystis* sp. was higher than under phosphate-deficient conditions but lower than in the standard medium. The highest values were again recorded in the control treatment, while the highest concentration of DMP (1000 µg/L) showed the strongest inhibitory effect. This result is consistent with the role of sulfur in the synthesis of antioxidant molecules such as glutathione. Under sulfate-deficient conditions, the cells likely have a reduced capacity to cope with stress caused by the pollutant. Changes in pH values during the experiment (Table 1) show a clear relationship with the growth dynamics of the cyanobacterium *Microcystis* and its photosynthetic activity. In the standard BG11 medium, where a continuous increase in chlorophyll *a* was recorded, pH values remained high and relatively stable (around 10.4–10.5), which is characteristic of intensive photosynthesis and efficient CO_2 uptake from the medium. Slight variations in the presence of dimethyl phthalate indicate that, under conditions of optimal nutrient availability, this pollutant has a limited effect on photosynthetic activity.

Table 1 *pH values at the end of experiment in all investigated media and DMP concentrations*

Medium	pH	Medium	pH	Medium	pH	Medium	pH
BG11 control	10.54	BG11-1 control	10.18	BG11-2 control	9.73	BG11-3 control	10.51
BG11 250 DMP	10.42	BG11-1 250 DMP	10.33	BG11-2 250 DMP	10.21	BG11-3 250 DMP	10.53
BG11 500 DMP	10.51	BG11-1 500 DMP	10.41	BG11-2 500 DMP	9.44	BG11-3 500 DMP	10.42
BG11 1000 DMP	10.53	BG11-1 1000 DMP	10.30	BG11-2 1000 DMP	9.51	BG11-3 1000 DMP	10.37

Under nitrogen-limited conditions (BG11-1), where growth was significantly reduced, a gradual increase in pH values was observed with increasing concentrations of dimethyl phthalate (from 10.18 to 10.41). This may indicate a reduction in biomass and a shift in metabolic balance, where lower culture density and reduced carbon assimilation lead to variations in the carbonate system. In the phosphate-deficient medium (BG11-2), where growth was most strongly inhibited, pH showed more pronounced oscillations (9.73; 10.21; 9.44; 9.51), reflecting unstable photosynthetic activity and a variable metabolic response of cells under strong nutrient stress, as well as the possible degradation of dimethyl phthalate into phthalic acid in some cases. The initial increase in pH may result from short-term adaptation, while the subsequent decrease indicates the dominance of inhibitory processes and reduced CO_2 fixation.

Under sulfate-limited conditions (BG11-3), a slight decrease in pH values was observed with increasing concentrations of dimethyl phthalate (from 10.51 to 10.37), which is consistent with gradual growth inhibition and reduced photosynthetic activity. This trend may be related to the limited ability of cells to maintain redox balance and efficient carbon fixation under sulfate/sulfur deficiency. Overall, the obtained results indicate that changes in pH values follow the intensity of growth and photosynthesis, with nutrient limitations modifying the response to dimethyl phthalate and leading to stable, variable, or declining pH trends depending on the dominant stress factor.

CONCLUSION

Results demonstrate that the growth and physiological responses of *Microcystis* sp. are primarily governed by nutrient availability, while the effect of dimethyl phthalate is secondary and generally weak. Under optimal conditions, DMP acted as a mild inhibitor of growth and photosynthetic activity, whereas nutrient limitations–particularly of nitrogen and phosphorus–were the dominant factors restricting biomass development and stabilizing or altering the response to the pollutant. Variations in pH further supported these findings, reflecting changes in photosynthetic intensity and carbon assimilation under different nutritional and stress conditions. In general, the study indicates that nutrient stress strongly modulates the response of *Microcystis* sp. to dimethyl phthalate, highlighting the importance of environmental context in assessing the ecological impact of organic pollutants.

ACKNOWLEDGEMENT

The authors are grateful to the Ministry of Science, Technological Development and Innovation of the Republic of Serbia for financial support according to the contract with registration No. 451-03-33/2026-03/200124 and 451-03-34/2026-03/200124.

REFERENCES

[1] Häder, D.P., Banaszak, A.T., Villafañe, V.E., *et al*. Sci. Total. Environ. 2020, 713, 136586.

[2] Stanković NR. Uticaj fitoplanktona na bentosne makrobeskičmenjake slatkovodnih ekosistema u multistres uslovima: laboratorijsko testiranje toksičnog efekta cijanobakterija i zelenih mikroalgi na jedinke vrste *Chironomus riparius* [dissertation]. Niš: Univerzitet u Nišu, Prirodno-matematički fakultet; 2021.

[3] Whitton, B.A., Potts, M., editors. The ecology of cyanobacteria: their diversity in time and space. Berlin: Springer; 2002.

[4] Paerl, H.W., Otten, G. Microb. Ecol. 2013, 65 (4), 995–1010.

EcoTER'26
eco.tfbor.bg.ac.rs
32nd International Conference
Ecological Truth & Environmental Research
24–26 June 2026, Hotel Sunce,
Sokobanja, Serbia

Original Research

IMPACT OF DIMETHYL PHTHALATE ON THE GROWTH AND STRUCTURE OF GREEN ALGAE (*Chlorella* sp.)

DOI: 10.5937/EcoTER26228K

Ivana Kostić Kokić[1,a*], Nikola Stanković[2,b], Danica Bogdanović[1,c], Tamara Petronijević[2,d], Monika Dudić[3,e], Tatjana Anđelković[1,f]

[1] University of Niš, Faculty of Science and Mathematics, Department of Chemistry, Višegradska 33, 18000 Niš, SERBIA

[2] University of Niš, Faculty of Science and Mathematics, Department of Biology and Ecology, Višegradska 33, 18000 Niš, SERBIA

[3] State University of Novi Pazar, Department of Natural Sciences and Mathematics, Vuka Karadžića bb, 36300 Novi Pazar, SERBIA

[a] https://orcid.org/0000-0001-6517-5635 [b] https://orcid.org/0000-0002-1604-6543
[c] https://orcid.org/0000-0001-5672-9931 [d] https://orcid.org/0000-0002-6958-9250
[e] https://orcid.org/0000-0003-3547-4305 [f] https://orcid.org/0000-0001-9856-985X

Abstract

The aim of this research was to examine the influence of dimethyl phthalate (DMP) on the growth and physiological response of a phytoplankton organism under laboratory conditions. A strain of the green alga Chlorella sp., isolated from freshwater ecosystems, was used in the experiment. The organisms were cultivated in a standard BG11 medium and its three modifications (nitrate-free BG11-1, phosphate-free BG11-2, and sulphate-free BG11-3) in the presence of three dimethyl phthalate concentrations (250, 500, and 1000 µg/L). Organism growth was monitored using the spectrophotometric determination of chlorophyll a, while potential morphological changes in cells and contamination were controlled using microscopy. Also, pH value monitoring was done. The results of this study show that the effect of DMP on the growth of the microalgae Chlorella sp. is not only concentration-dependent, but also largely depends on the availability of essential nutrients in the medium.

Keywords: dimethyl phthalate, green algae, chlorophyll *a*.

INTRODUCTION

Phytoplankton represents a diverse community of photosynthetic microorganisms, including prokaryotes and eukaryotes, that are adapted to a wide range of aquatic environments – from freshwater springs and streams, lakes, and lagoons, to coastal marine areas and the open ocean. These organisms play a fundamental role in global biogeochemical cycles and form the base of aquatic food webs [1].

Microalgae exhibit high growth and CO_2 fixation rates, and they are responsible for approximately 32% of global photosynthesis, producing more than 60% of the Earth's oxygen. They contain typical eukaryotic organelles, including plastids with chlorophyll, and inhabit both freshwater and marine ecosystems. Their size ranges from 3 to 30 µm [2].

*ivana.chem@outlook.com

The genus *Chlorella* comprises unicellular green algae from the division Chlorophyta, commonly found in freshwater ecosystems. The cells are small, predominantly spherical, with a single chloroplast containing chlorophylls *a* and *b*, enabling efficient photosynthesis under varying light conditions. Members of this genus lack a motile stage in their life cycle, and reproduction occurs asexually [3].

Chlorella sp. most frequently occurs in mesotrophic and eutrophic aquatic ecosystems. Due to its simple structure, this genus thrives in conditions of limited nutrient availability and fluctuating physicochemical although their growth and metabolic activity remain sensitive to environmental stressors. Consequently, *Chlorella* sp. is widely used as model organisms in ecological and ecotoxicological studies to evaluate the effects of environmental pollutants. Among these, organic contaminants such as phthalates have been shown to influence algal growth, photosynthetic efficiency, and cellular structure, potentially disrupting energy flow and ecosystem stability [3].

MATERIALS AND METHODS

Phytoplankton cultivation

A culture of the green microalga genus *Chlorella*, obtained from the culture collection of the Department of Biology and Ecology, Faculty of Sciences and Mathematics, University of Niš, was used for the experiment. The strain was cultivated under controlled laboratory conditions, using the BG11 nutrient medium for cultivation and maintenance. The chemical composition of the BG11 medium is presented in Table 1.

Table 1 *Composition of standard BG11 medium*

Substance	Concentration (g/L)
$NaNO_3$	1.5
K_2HPO_4	0.04
$MgSO_4 \cdot 7H_2O$	0.075
$CaCl_2 \cdot 2H_2O$	0.036
$C_6H_8O_7$	0.006
Ammonium ferric citrate green	0.006
$EDTANa_2$	0.001
Na_2CO_3	0.02
H_3BO_3	0.00286
$MnCl_2 \cdot 4H_2O$	0.00181
$ZnSO_4 \cdot 7H_2O$	0.00022
$Na_2MoO_4 \cdot 2H_2O$	0.00039
$CuSO_4 \cdot 5H_2O$	0.00008
$Co(NO_3)_2 \cdot 6H_2O$	0.00005

Experiment

The green algal strain used in the experiment was inoculated into sterile glass test tubes. A total of 48 test tubes were used, with 12 tubes per replicate. The impact of three dimethyl phthalate (DMP) concentrations (250 μg/L, 500 μg/L, and 1000 μg/L) on the growth and physiological parameters of the test organism was examined.

Phytoplankton samples, nutrient medium, and DMP were used to conduct the experiment. Four types of nutrient media were prepared: standard BG11 medium, nitrate-free BG11

(BG11-1), phosphate-free BG11 (BG11-2), and sulphate-free BG11 (BG11-3). The dimethyl phthalate (DMP) solution used during the experiment was prepared in the laboratory of the Department of Chemistry, Faculty of Sciences in Niš, by dissolving the pure substance (CAS Number: 131-11-3, Sigma Aldrich, USA).

Following sterilization, 10 mL of the corresponding medium and 1 mL (1000 µL) of the microalgal suspension were added to each test tube. Subsequently, various concentrations of DMP were added. All phthalate concentrations were tested in triplicate. Control tubes did not contain DMP. The tubes were sealed with medical cotton plugs and placed under laboratory cultivation conditions. After setting up the experiment, the chlorophyll *a* concentration was monitored using the spectrophotometric method. An Agilent BioTek Epoch 2 Microplate Spectrophotometer was used.

In addition to spectrophotometric measurements, the test cultures were monitored via microscopic analysis (Leica Microsystems Leica DM1000 and Leica Microsystems DFC295 camera) to detect potential contamination and prevent irregularities that could affect the accuracy of the results.

Monitoring of pH value was done using SensIon Multimeter (Hach, Germany) during the experiment.

RESULTS AND DISCUSSION

Within experiment the production of chlorophyll *a* (Chl *a*) in strains of *Chlorella* sp. during two weeks of exposure to different concentrations of dimethyl phthalate (250, 500 and 1000 µg/L) was monitored. Measurements were made spectrophotometrically at wavelengths of 678 nm, 720 nm and 750 nm, and the concentration of Chl *a* was calculated according to the formula (1) [1]:

$$Chl\ (\mu g \cdot mL^{-1}) = 14.96 \cdot (OD_{678} - OD_{750}) - 0.616 \cdot (OD_{720} - OD_{750}) \quad (1)$$

and presented in Figure 1.

In the first experiment, a typical hormetic response was observed in the standard BG11 medium, where the highest concentration (1000 mg/L) led to growth stimulation, while lower concentrations had an inhibitory effect. This type of response is well documented in the literature and represents an adaptive mechanism of microorganisms to the presence of stressors [4].

However, in the subsequent experiments (BG11-1 and BG11-2) different patterns were observed. In experiment BG11-1, where a modified nitrate-free medium was used as the medium, maximum growth was recorded at the lowest concentration (250 µg/L), while in the phosphate-free medium (BG11-2) the highest growth was observed at the middle concentration (500 µg/L).

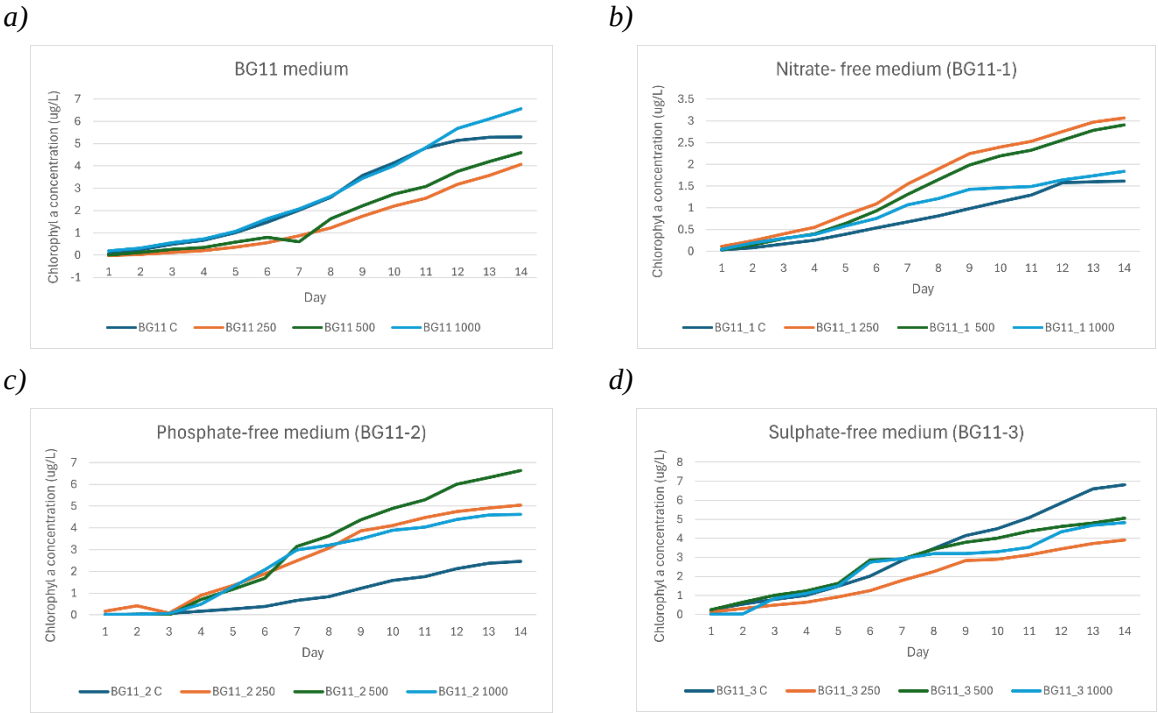

Figure 1 *Chlorophyll a concentration (µg/L) during the growth period of Chlorella sp. in different media: a) standard BG11 medium; b) nitrate-free medium (BG11-1); c) phosphate-free medium (BG11-2); sulphate-free medium (BG11-3)*

These results indicate the existence of an optimal concentration range, within which growth is stimulated, while outside this range there is a decrease in physiological activity.

In the fourth experiment, which was performed in a modified sulphate-free medium (BG11-3), an opposite trend was observed, where the control treatment had the highest chlorophyll *a* value, while increasing the DMP concentration led to a gradual inhibition of growth. Although statistical analysis did not show significant differences, the observed trend indicates a potential toxic effect at higher concentrations.

The results obtained in four experiments show that the effect of dimethyl phthalate on the growth of the microalgae *Chlorella* sp. is not linear, but highly variable and dependent on the experimental conditions. The observed patterns indicate a complex relationship between the concentration of the pollutant and the physiological response of the tested microalgae strain.

Results of pH measurements (Table 2) indicate that in the standard BG11 medium, and in the phosphate-free medium (BG11-2), a gradual decrease in pH values was observed with an increase in the concentration of DMP, which can be associated with growth inhibition and reduced photosynthesis. This effect can be explained by increased respiration, *i.e.*, by a higher production of CO_2, which leads to the formation of carbonic acid and a decrease in pH values.

Also, DMP degradation, *i.e.* the formation of phthalic acid, probably occurred, which also contributes to the decrease in pH value. A similar trend, although less pronounced, was observed in the nitrogen-free medium (BG11-1), where at higher concentrations there is a slight recovery of pH, which may be a consequence of reduced biomass and lower overall metabolic activity.

Table 2 *pH values at the end of experiment in all investigated media and DMP concentrations*

Medium	pH	Medium	pH	Medium	pH	Medium	pH
BG11 control	8.54	BG11-1 control	8.20	BG11-2 control	7.63	BG11-3 control	7.50
BG11 250 DMP	8.34	BG11-1 250 DMP	8.13	BG11-2 250 DMP	7.64	BG11-3 250 DMP	7.62
BG11 500 DMP	8.22	BG11-1 500 DMP	8.04	BG11-2 500 DMP	7.53	BG11-3 500 DMP	7.79
BG11 1000 DMP	8.05	BG11-1 1000 DMP	8.16	BG11-2 1000 DMP	7.48	BG11-3 1000 DMP	7.93

In contrast, in the sulphate-free medium (BG11-3), a continuous increase in pH was recorded with increasing DMP concentration, which is consistent with the pronounced growth inhibition. In this case, the limited availability of sulphate/sulphur further reduces the metabolic and photosynthetic activity of the cells, which leads to reduced gas exchange and a shift in the equilibrium of the carbonate system towards more alkaline environments.

CONCLUSION

The results of this study show that the effect of DMP on the growth of the microalgae *Chlorella* sp. is not only concentration-dependent, but also largely depends on the availability of essential nutrients in the medium. In the standard BG11 medium, a hormetic response was observed, where high concentration stimulates growth. In nitrate-free conditions, the maximum was achieved at the lowest concentration, indicating adaptation to nitrogen stress. Overall, pH variations follow changes in growth and indicate that photosynthetic activity is the main factor controlling the acid-base balance in the medium, with the inhibitory effect of dimethyl phthalate leading to a decrease in CO_2 fixation and pH changes.

ACKNOWLEDGEMENT

The authors are grateful to the Ministry of Science, Technological Development and Innovation of the Republic of Serbia for financial support according to the contract with registration No. 451-03-33/2026-03/200124 and 451-03-34/2026-03/200124.

REFERENCES

[1] Stanković, N.R. Uticaj fitoplanktona na bentosne makrobeskičmenjake slatkovodnih ekosistema u multistres uslovima: laboratorijsko testiranje toksičnog efekta cijanobakterija i zelenih mikroalgi na jedinke vrste *Chironomus riparius* [dissertation]. Niš: Univerzitet u Nišu, Prirodno-matematički fakultet; 2021.

[2] Gimpel, J.A., Henríquez, V., Mayfield S.P. Front Microbiol. 2015, 6, 1376–1390.

[3] Bellinger, EG, Sigee DC. Freshwater algae: identification and use as bioindicators. Oxford: Wiley-Blackwell; 2010.

[4] Calabrese, E.J., Baldwin, L.A. Hum. Exp. Toxicol. 2002, 21 (2), 91–97.

EcoTER'26
eco.tfbor.bg.ac.rs
32nd International Conference
Ecological Truth & Environmental Research
24–26 June 2026, Hotel Sunce,
Sokobanja, Serbia

Original Research

ELECTROCHEMICAL DETERMINATION OF CEFTRIAXONE USING A GRAPHITE ROD ELECTRODE

DOI: 10.5937/EcoTER26233B

Anđelija Bogdanović[1,a*], Žaklina Tasić[1,b], Marija Petrović Mihajlović[1,c], Ana Simonović[1,d], Milan Radovanović[1,e], Milan Antonijević[1,f], Aleksandar Cvetković[1,g]

[1] University of Belgrade, Technical Faculty in Bor, Vojske Jugoslavije 12, 19210 Bor, SERBIA

[a] https://orcid.org/0009-0008-9984-4970 [b] https://orcid.org/0000-0001-6544-1980

[c] https://orcid.org/0000-0001-5486-3870 [d] https://orcid.org/0000-0003-2392-0048

[e] https://orcid.org/0000-0002-5175-6022 [f] https://orcid.org/0000-0002-2201-066X

[g] https://orcid.org/0009-0003-5184-6874

Abstract

Ceftriaxone (CEF) is a widely used third-generation cephalosporin antibiotic frequently detected in environmental samples. In this study, the electrochemical behavior of ceftriaxone was investigated using cyclic voltammetry (CV) and differential pulse voltammetry (DPV) on a graphite rod electrode in Britton–Robinson (BR) buffer at pH 2. CV measurements showed a well- defined irreversible oxidation peak at approximately 1.0 V vs. SCE. Increasing the scan rate resulted in higherin peak current and a movement of the oxidation peak toward higher potentials. DPV measurements revealed that the peak current increased with increasing ceftriaxone concentration from 2 × 10^{-5} to 5 × 10^{-4} mol/L. The graphite rod electrode exhibited good electrochemical response, low cost, and simple preparation.

Keywords: ceftriaxone, electrochemistry, cyclic voltammetry, differential pulse voltammetry, graphite rod electrode.

INTRODUCTION

Antibiotics are an important group of drugs that have been used widely to treat various bacterial infections. They are classified according to different criteria, such as mechanism of action, spectrum of activity, and method of administration. The most common classification is based on their molecular structure. In addition to medical use, antibiotics are also used for food preservation and transport. They can be used to treat sick animals, promote animal growth, improve animal feed quality, and in aquaculture [1].

Cephalosporins

Cephalosporins (Figure 1) are a class of β-lactam antibiotics used to treat various bacterial infections. The β-lactam antibiotic group also includes penicillins, carbapenems, and monobactams. Their β-lactam ring enables binding to bacterial penicillin-binding proteins (PBPs) and inhibits peptidoglycan formation during bacterial cell wall synthesis. The

*abogdanovic@tfbor.bg.ac.rs

differences among these antibiotic groups are related to the structure of the β-lactam ring. Penicillins have a five-membered thiazolidine ring, cephalosporins contain a six-membered dihydrothiazine ring, carbapenems have a modified five-membered ring without a sulfur atom, while monobactams contain only a single β-lactam ring. β-Lactam antibiotics are among the most commonly prescribed antibiotics and have been in clinical use for the longest period, beginning with the production of penicillin in 1945 and continuing to the most recent cephalosporin, cefiderocol, approved in the United States in 2019 and in Europe in 2020. The first cephalosporin, cefazolin, became clinically available in 1974, and since then, six generations of cephalosporins have been developed. Within each generation, differences in chemical structure, particularly in the acyl side chain, result in significant variations in antibacterial spectrum and stability against β-lactamase enzymes [1,2].

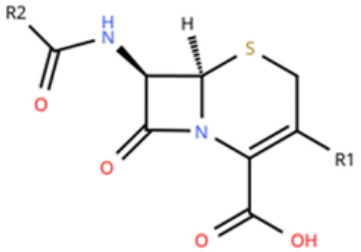

Figure 1 *General chemical structure of cephalosporins [1]*

Ceftriaxone

Ceftriaxone (CEF) (Figure 2) is a well-known antibiotic used to treat infections. It is one of the most widely used antibiotic drugs. Ceftriaxone belongs to the third generation of cephalosporins and acts by inhibiting the formation of mucopeptides in the bacterial cell wall. It is widely used in clinical practice due to its strong antibacterial activity, high resistance to β-lactamase enzymes, proven clinical effectiveness, low toxicity and low risk of allergic reactions. This drug is used to treat of diseases such as urinary tract infections, respiratory tract infections, and sinusitis [3,4]. The strong antibacterial activity of ceftriaxone and other antibiotics in disease treatment has led to their widespread use. Antibiotics are also widely used in veterinary medicine where they are added to animal feed. The uncontrolled use of antibiotics results in the presence of antibiotic residues and their degradation products in the environment. The main sources of antibiotic contamination are the pharmaceutical industry, livestock farming, hospitals, and household wastewater. Some antibiotics exit the body unchanged, while others used in livestock farming and aquaculture can accumulate in food products such as meat, eggs, and milk, which are then eaten by humans. Conventional water treatment methods are often not effective in removing antibiotic residues from water. As a result, these compounds are often found in surface water, groundwater, and drinking water at very low concentrations (ng/L). It is believed that the high use of antibiotics contributes to the development and spread of bacterial resistance. Infections caused by resistant bacteria are more difficult to treat and may cause serious health problems and higher death rates. Therefore, it is important to develop fast, reliable, and low-cost methods for antibiotic detection.

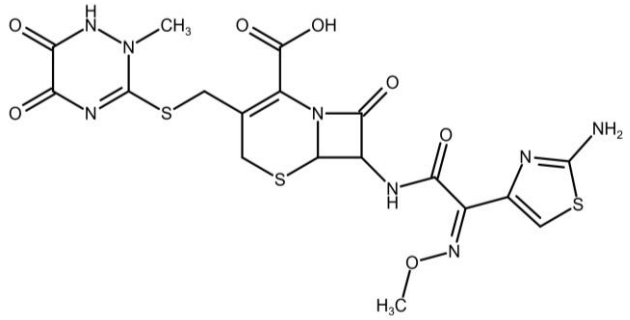

Figure 2 *Molecular structure of ceftriaxone [3]*

For the determination of ceftriaxone (CEF), conventional analytical methods such as high-performance liquid chromatography (HPLC), ultra-performance liquid chromatography (UPLC), UV spectroscopy, IR spectroscopy, and spectrofluorimetry are commonly used. Other methods reported in the literature include spectrophotometric methods, chromatographic methods, and capillary electrophoresis. However, these methods often require expensive instruments, complex procedures, complicated sample preparation, and long analysis times [4–6]. Due to these limitations, there is a need for fast, simple, and low-cost analytical methods [7]. Electrochemical methods are widely used for determining electroactive compounds because they are sensitive, simple, rapid, and inexpensive. Electrochemical methods for ceftriaxone determination also allow *in situ* analysis and usually do not require complicated sample preparation [4,6]. These methods are based on oxidation or reduction processes that occur on the electrode surface. Additionally, electrochemical systems can be miniaturized and used in portable devices [7]. Modern electrochemical techniques include voltammetric, amperometric, and potentiometric methods. Among these, cyclic voltammetry and pulse voltammetry are widely used for studying redox reactions. In cyclic voltammetry, the potential is swept forward and backward over a selected range, while the current is measured simultaneously. This method provides information on redox behavior and reaction kinetics, but it is mainly used for qualitative analysis [8]. Pulse voltammetry techniques, such as differential pulse voltammetry (DPV) and square-wave voltammetry (SWV), use potential pulses instead of continuous scanning. These techniques are highly sensitive and reduce background current effects. They also offer rapid analysis and low detection limits [7,8]. Electrodes are essential components of electrochemical systems and can be made from materials such as glassy carbon, platinum, gold, and modified electrode materials. Carbon-based electrodes are widely used because they are inexpensive, stable, and exhibit good electrochemical performance. Graphite rod electrodes and carbon paste electrodes can also be prepared from waste batteries, making them low-cost and environmentally friendly materials for electrochemical analysis [8].

MATERIALS AND METHODS

Electrochemical measurements were performed using a potentiostat (IVIUM XRE, IVIUM Technologies, Eindhoven, the Netherlands) in a three-electrode system. A graphite rod electrode from waste zinc-carbon batteries was used as the working electrode, a saturated

calomel electrode (SCE) as the reference electrode, and a platinum electrode as the counter electrode. Before each measurement, the graphite rod electrode was mechanically polished with aluminum oxide paste (0.3 μm Al_2O_3), rinsed with distilled water, and dried at room temperature. Britton Robinson (BR) buffer at pH 2 was used as the supporting electrolyte. Cyclic voltammetry (CV) and differential pulse voltammetry (DPV) were used to study the electrochemical behavior of ceftriaxone (CEF) on the graphite rod electrode surface. Solutions with different concentrations of ceftriaxone were prepared in BR buffer for DPV measurements. For CV measurements, a ceftriaxone solution with a concentration of 5×10^{-5} mol/L was used. CV measurements were performed in the potential range from 0.5 V vs. SCE to 1.6 V vs. SCE at different scan rates (10, 25, and 50 mV/s) in BR buffer at pH 2 (Figure 3). The effect of scan rate on ceftriaxone oxidation was studied by observing changes in peak current and peak potential. Differential pulse voltammetry measurements were performed in the potential range from 0.5 V vs. SCE to 1.3 V vs. SCE using a pulse amplitude of 50 mV, pulse time of 20 ms, potential step of 5 mV, and scan rate of 50 mV/s. Measurements were carried out for different CEF concentrations (5×10^{-4}, 8×10^{-5}, 5×10^{-5}, and 2×10^{-5} mol/L) in BR buffer at pH 2 (Figure 4). For comparison, the blank BR buffer solution was measured under the same conditions.

RESULTS AND DISCUSSION

The cyclic voltammetry results showed a pronounced and sharp oxidation peak of ceftriaxone in BR buffer at pH 2 at approximately E ≈ 1.0 V (Figure 3). As the scan rate increased from 10 to 50 mV/s, the peak current also increased, while the peak potential moved toward more positive values. The oxidation peak current increased linearly with scan rate. The corresponding equation could be expressed as follows:

$$Ip(\mu A) = 1.2245 + 0.098v;\ R^2 = 0.959 \quad (1)$$

This behavior indicates an irreversible electrochemical oxidation process of ceftriaxone on the graphite rod electrode surface [3,4]. The blank BR buffer solution showed no electrochemical response in the investigated potential range, confirming that the observed signal originated from ceftriaxone oxidation. Additionally, the absence of a cathodic peak during the reverse scan further confirmed the irreversible nature of the electrochemical process.

The DPV measurements showed that the oxidation peak current of ceftriaxone increased as the concentration increased. As the concentration rose from 2×10^{-5} to 5×10^{-4} mol L^{-1}, the peak current gradually increased, while the peak potential remained nearly constant (Figure 4). All voltammograms displayed a well-defined peak at approximately E ≈ 1.0–1.1 V vs. SCE for all concentrations, indicating a stable oxidation process. The highest peak current was observed at 5×10^{-4} mol L^{-1}. When the concentration decreased (8×10^{-5}, 5×10^{-5} and 2×10^{-5} mol L^{-1}), the peak current also decreased. The linear increase in peak current with concentration confirmed the good sensitivity and analytical performance of the DPV method for quantitative electrochemical determination of ceftriaxone [10,11]. The

corresponding equation, in the examined concentration range of ceftriaxone, can be expressed as follows:

$$Ip(\mu A) = 0.3416 + 0.0074x;\ R^2 = 0.9676 \quad (2)$$

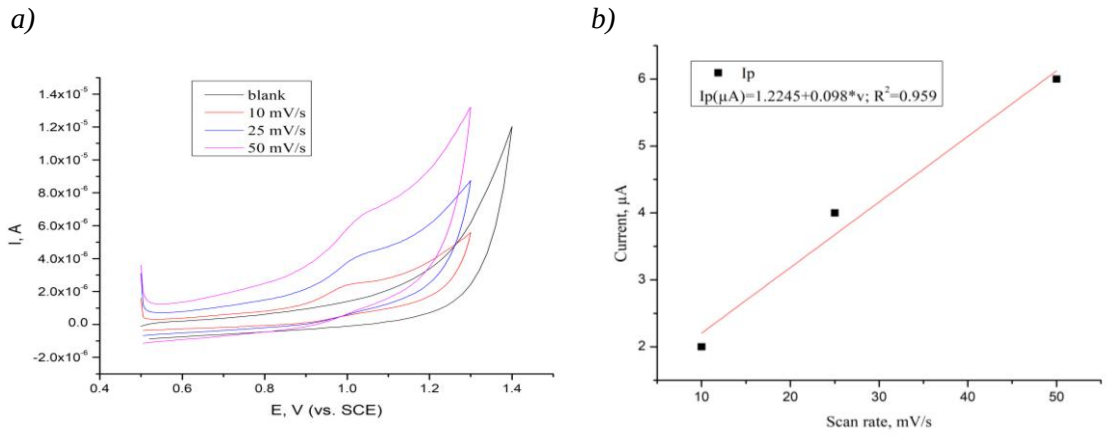

Figure 3 *a) The effect of scan rate on the peak intensity of ceftriaxone; b) Dependence of peak current of 50.0 μM ceftriaxone on the scan rate*

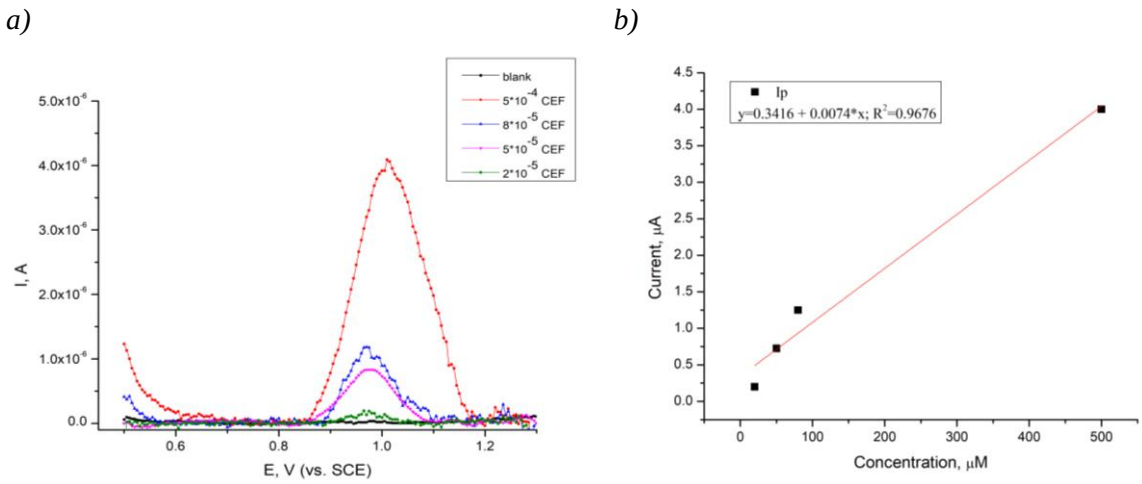

Figure 4 *a) The effect of concentration on the peak intensity of ceftriaxone; b) The dependence of peak current on ceftriaxone concentration (investigated concentration range 20μM –500 μM)*

CONCLUSION

The electrochemical behavior of ceftriaxone was studied using cyclic voltammetry and differential pulse voltammetry on a graphite rod electrode in Britton–Robinson buffer solution at pH 2. Cyclic voltammetry measurements showed a distinct irreversible oxidation peak of ceftriaxone at approximately 1.0 V vs. SCE. Increasing the scan rate resulted in higher peak currents and a shift of the peak potential toward more positive values, indicating irreversible oxidation. Differential pulse voltammetry measurements showed that the oxidation peak current increased with higher ceftriaxone concentrations, while the peak potential remained nearly constant. These results confirmed that DPV is suitable for quantitative determination of ceftriaxone. The graphite rod electrode provided good

electrochemical response and advantages such as low cost, simple preparation, and easy handling. Therefore, this electrochemical method can serve as a simple and reliable alternative for ceftriaxone determination in pharmaceutical and environmental samples.

ACKNOWLEDGEMENT

The research presented in this paper was done with the financial support of the Ministry of Science, Technological Development and Innovation of the Republic of Serbia, within the funding of the scientific research work at the University of Belgrade, Technical Faculty in Bor, according to the contract with registration number 451-03-134/2026-03/200131.

REFERENCES

[1] Partene, D., David, I.G. Cheregi, M-C., *et al*., Noor, H. Chemosensors. 2026, 14 (3), 75.

[2] Boys, M.T.H., Pletzer, D. Int. J. Antimicrob. Agents. 2025, 66 (2), 107527.

[3] Alshahrani, S.M., Alkhammash, A., Alamoudi, A.J., Diam. Relat. Mater. 2025, 155, 112283.

[4] Uddin, M., Kamsong, W., Karuwan, C., *et al*., Chemosphere. 2025, 389,144695.

[5] Bougna, H.H., Dongmo, L., Jiokeng, S., *et al*. ChemElectroChem. 2024, 11 (11), 1–11.

[6] Silvaa, F., Nameb, L., Tibab, D., *et al*. Talanta. 2024, 266, 125075.

[7] Wang, W., Cai, M. Int. J. Electrochem. Sci. 2025, 20, 100903.

[8] Kumar, R., Salwan, S., Kumar, P., *et al*. Analytica. 2022, 10 (3), 472.

[9] Radovanovic, M., Simonovic, A., Petrović Mihajlović, M., *et al*. Chemosensors. 2025, 13 (8), 282.

[10] Bitew, Z., Amare, M. Electrochem. Commun. 2020, 121, 106863.

[11] Tasić, Ž., Petrović Mihajlović, M., Radovanovic, M. Nature. 2022, 12 (1), 5469.

EcoTER'26
eco.tfbor.bg.ac.rs
32nd International Conference
Ecological Truth & Environmental Research
24–26 June 2026, Hotel Sunce,
Sokobanja, Serbia

Original Research

SEM-EDS AND DTA-TGA ANALYSIS OF CORN STALKS USED FOR THE BIOSORPTION OF COPPER IONS FROM SYNTHETIC SOLUTIONS

DOI: 10.5937/EcoTER26239G

Milan Gorgievski[1,a*], Miljan Marković[1,b], Vesna Grekulović[1,c], Nada Štrbac[1,d], Marina Marković[1,e], Milica Zdravković[1,f], Kristina Božinović[1,g]

[1] University of Belgrade, Technical Faculty in Bor, Vojske Jugoslavije 12, 19210 Bor, SERBIA
[a] https://orcid.org/0000-0002-9899-719X [b] https://orcid.org/0000-0002-4734-1481
[c] https://orcid.org/0000-0001-6871-4016 [d] https://orcid.org/0000-0003-4836-1350
[e] https://orcid.org/0009-0007-7553-6423 [f] https://orcid.org/0000-0001-9488-9151
[g] https://orcid.org/0000-0002-9834-448X

Abstract

This paper presents the results of SEM-EDS and DTA-TGA analysis of corn stalks before and after the biosorption of Cu^{2+} ions. Certain differences in the adsorbent structure and in the elemental analysis of the sample surface were observed. In micrographs of raw corn stalks, pores and cavities can be seen, which facilitate the penetration of the aqueous phase into the adsorbent structure, where copper ions are adsorbed at the internal active sites. After the biosorption of Cu^{2+} ions, a distinctly different surface morphology of corn stalks can be observed. The absence of cavities and channels is evident, with a compact and uniformly ordered lamellar structure. The EDS spectra of corn stalks, before and after copper ion biosorption, indicate the possible exchange of potassium, calcium, and magnesium with copper during the biosorption process. Based on the DTA-TGA analysis, the degradation of the corn stalk sample occurs in several stages.

Keywords: copper ions, biosorption, corn stalks, SEM-EDS, DTA-TGA.

INTRODUCTION

Rapid technological development enabled humans to exploit the planet's natural resources more intensively, but it also caused a steady increase in environmental pollution. Major contributors to natural water contamination include wastewater from urban areas, ore deposits, non-ferrous and ferrous metallurgy, the textile and paint industries, and various agricultural activities. Consequently, the increasing discharge of heavy metals into aquatic ecosystems has become a serious threat to both the environment and human health, highlighting the urgent need to develop efficient and sustainable wastewater treatment methods [1].

Agricultural by-products, such as corn stalks, are promising, low-cost, and environmentally friendly adsorbents for removing metal ions from contaminated water. Because of their lignocellulosic structure and numerous functional groups, both modified and unmodified corn stalks can effectively bind heavy metal ions through biosorption [2].

* *mgorgievski@tfbor.bg.ac.rs*

Biosorption is the ability of biomaterials to accumulate and concentrate heavy metals from even very dilute aqueous solutions. The biosorption process involves a solid phase (biological material) and a liquid phase (solvent, usually water) containing the dissolved metal [3].

It is a passive metabolic process, meaning it does not require energy, and the amount of pollutants adsorbed depends on the structure of the biosorbent and kinetic equilibrium [4]. Biosorption is determined by chemical equilibrium and is largely influenced by pH, ion concentration, and interactions between ions of different metals [5].

The main advantages of biosorption over conventional purification technologies, in addition to its efficiency in removing metal ions from aqueous solutions, are the availability and low cost of these adsorbents, which are usually waste products from the wood, agricultural, and food industries. Therefore, biosorption can serve as an alternative to existing conventional wastewater treatment technologies [3].

MATERIALS AND METHODS

Corn stalks collected from agricultural fields near Bor were used as the adsorbent material. Before use, the samples were mechanically ground and sieved, and the particle size fraction of (-1 + 0.4) mm was selected for the biosorption experiments.

RESULTS AND DISCUSSION

The morphology of corn stalks before and after biosorption of Cu^{2+} ions was analyzed using a scanning electron microscope (SEM) (VEGA 3 LMU TESCAN) equipped with an integrated energy-dispersive X-ray detector (X-act SDD 10 mm², Oxford Instruments). Before SEM analysis, the samples were coated with a thin layer of chromium in a sputter coater (QUORUM Q150T ES) to ensure conductivity. The prepared samples were then transferred to the microscope chamber and observed at an accelerating voltage of 8 kV.

SEM-EDS analysis of the corn stalks was performed both before and after Cu^{2+} ion biosorption. Certain differences in the structure of the adsorbent and in the elemental composition of the sample surface were observed. Figure 1 shows the surface morphology of corn stalks before and after copper ion biosorption, along with the corresponding EDS spectra.

Figure 1a shows a micrograph of the surface of corn stalks before copper ion biosorption, where cavities and channels are visible. These features facilitate the movement of the aqueous phase through the structure. It is assumed that copper ions penetrate these cavities and channels into the adsorbent structure, where they are adsorbed onto internal active sites. After copper ion biosorption (Figure 1b), the surface morphology of the stalks changes significantly. Cavities and channels are no longer observed, and the surface of the corn stalks becomes more compact, most likely due to the incorporation of copper ions into the structure.

EDS imaging was performed at several points on the sample surfaces to detect the heterogeneous distribution of elements. In both untreated corn stalks and corn stalks after copper ion biosorption, peaks for Cr are observed in the EDS spectrum. These Cr peaks occur because the adsorbent surface was coated with chromium in the vaporizer before imaging to make it conductive. The EDS spectrum of corn stalks before biosorption (Figure 1c) shows a high content of Ca, C, O, K, Si, Mg, and P. After copper ion biosorption (Figure 1d), the

peaks for K, Mg, Ca, and Si disappear, while peaks for Cu appear. Therefore, it can be assumed that K, Mg, and Ca are most likely exchanged with Cu by an ion exchange mechanism during the biosorption process.

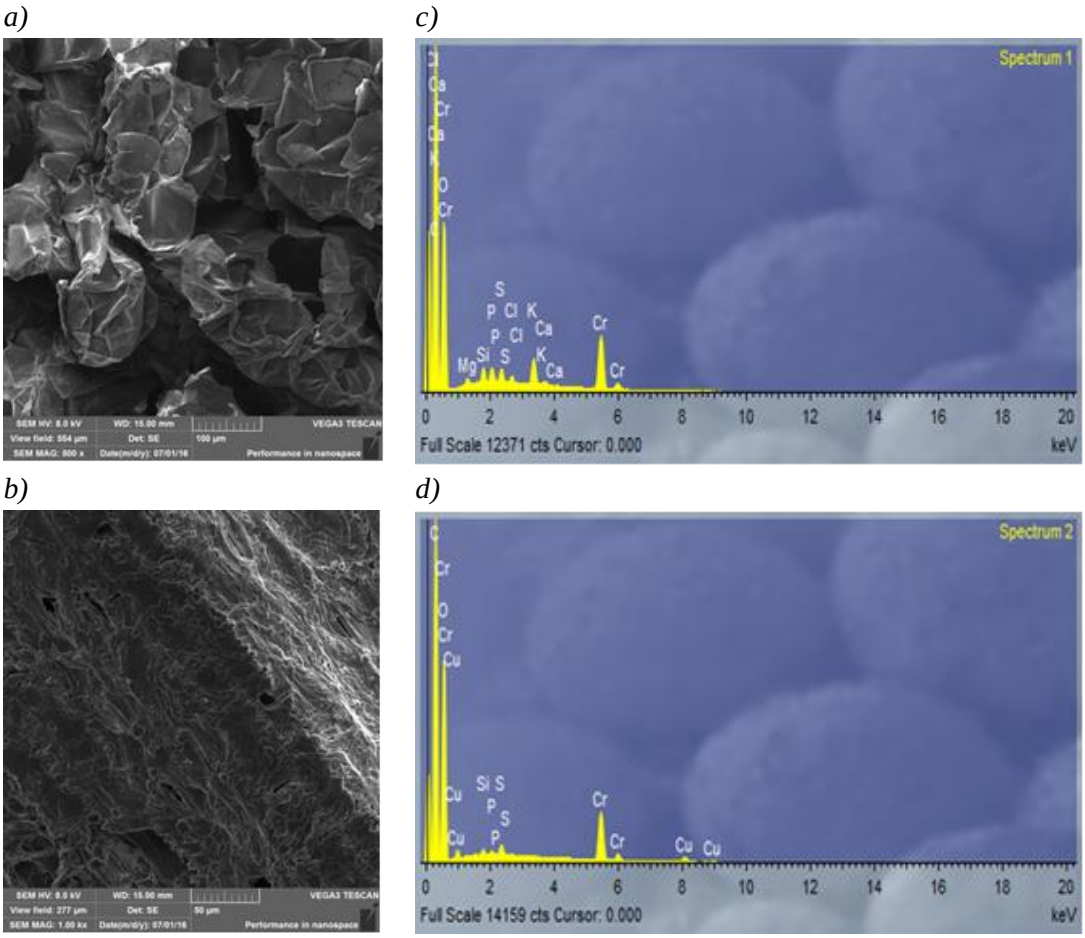

Figure 1 *SEM micrograph of the surface of corn stalks: a) before biosorption of copper ions (magnification 500×); b) after biosorption of copper ions (magnification 1000×); c) EDS spectrum of untreated corn stalks; d) EDS spectrum of corn stalks after biosorption of copper ions*

Thermal analysis provides important information about the thermal stability and degradation of the material. In this paper, DTA-TGA analysis of corn stalks was performed using a simultaneous DSC-TGA device (SDT Q600). A 4 mg sample was heated in an inert nitrogen atmosphere at a constant heating rate of 10 °C/min over a temperature range from 20 °C to 900 °C, and the results are shown in Figure 2.

Examining the TGA curve in Figure 2, a mass loss of about 7.6% is observed between 20 °C and 200 °C, resulting from the loss of physically bound (adsorbed) water from the sample. Additionally, Figure 2 shows that this process is accompanied by an endothermic peak on the DTA curve, with a minimum at 64.39 °C. In the temperature range from 200 °C to 900 °C, a mass loss of 77% is observed on the TGA curve, originating from the decomposition of lignocellulosic components in the adsorbent structure and the formation of volatile products such as CO, CO_2, and others [6]. In the same temperature range, an exothermic peak appears on the DTA curve, with a maximum at 300 °C, which corresponds

to the decomposition temperature of hemicellulose. In summary, the total mass loss in the temperature range from 20 °C to 900 °C was 84.6%.

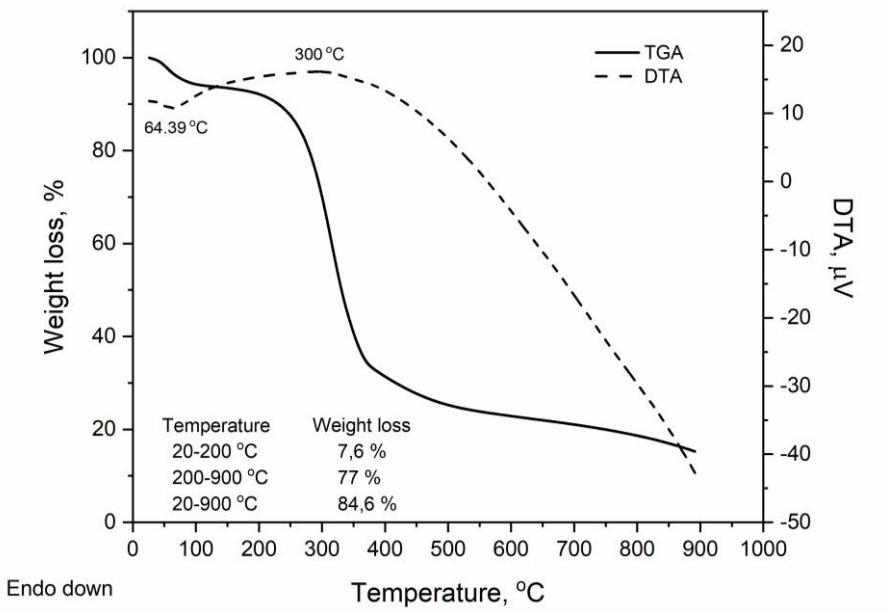

Figure 2 *DTA-TGA analysis of corn stalks*

CONCLUSION

This study presents the findings of SEM-EDS and DTA-TGA analyses conducted on corn stalks before and after the biosorption of Cu^{2+} ions. SEM analysis of corn stalks before and after copper ion biosorption shows that the surface morphology of corn stalks significantly changes after copper ion biosorption. The EDS spectra of corn stalks, before and after copper ion biosorption, indicate the possible exchange of potassium, calcium, and magnesium with copper during the biosorption process.

Based on the DTA-TGA analysis, the degradation of the corn stalk sample occurs in several stages.

ACKNOWLEDGEMENT

The research presented in this paper was done with the financial support of the Ministry of Science, Technological Development and Innovation of the Republic of Serbia, within the funding of the scientific research work at the University of Belgrade – Technical Faculty in Bor, according to the contract with registration number 451-03-34/2026-03/200131.

REFERENCES

[1] Ahluwalia, S.S., Goyal, D. Bioresour. Technol. 2007, 98, 2243–2257.
[2] Zhao, D., Chen, H., Zhao, Q., *et al*. Environ. Technol. Innov. 2025, 38, 104140.
[3] Abbas, H.S.J. Chem. Sci. Technol. 2014, 3 (4), 74–102.
[4] Velásquez, L., Dussan J.J. Hazard. Mater. 2009, 167, 713–716.
[5] Ahalya, N., Ramachandra, T.V., Kanamadi, R.D. Res. J. Chem. Environ. 2003, 7, 71–78.
[6] Yang, H., Yan, R., Chen H., *et al*. Fuel. 2007, 86, 1781–1788.

EcoTER'26
eco.tfbor.bg.ac.rs
32nd International Conference
Ecological Truth & Environmental Research
24–26 June 2026, Hotel Sunce,
Sokobanja, Serbia

Original Research

LONG-TERM TRENDS OF AIRBORNE POLLEN IN PANČEVO

DOI: 10.5937/EcoTER26243N

Dubravka Nikolovski[1,a*], Snežana Đurić[1,b], Danijela Mićić[1,c], Gabrijela Trajkovska[1,d], Ljiljana Lazić[1,e], Tamara Stajić[1,f], Dušan Stošić[1,g], Ksenija Kralj[1,h], Jelena Zec[1,i]

[1]Institute of Public Health Pančevo, Miloša Obrenovića 2, 26000 Pančevo, SERBIA

[a] https://orcid.org/0000-0002-1602-095x [b] https://orcid.org/0009-0001-8540-1596

[c] https://orcid.org/0009-0004-9505-3929 [d] https://orcid.org/0009-0001-7988-8270

[e] https://orcid.org/0009-0009-3241-5079 [f] https://orcid.org/0009-0003-9100-0304

[g] https://orcid.org/0009-0009-8162-2955 [h] https://orcid.org/0009-0003-6609-007x

[i] https://orcid.org/0009-0005-8960-0620

Abstract

This study presents a five-year aerobiological survey (2021–2025) of airborne pollen in Pančevo, Serbia, conducted using continuous volumetric sampling with standardized methodology. The monitoring period extended from February to November each year, encompassing tree, grass, and weed pollination seasons. Daily pollen concentrations were analyzed microscopically, with particular attention to annual maxima, cumulative value, and pollination duration.

Comparative analysis revealed that Cupressaceae/Taxus, Urticaceae, and Ambrosia pollen exhibited the highest average annual values, while Cupressaceae, Salix, and Betula recorded the greatest maximum concentrations. Poaceae, Pinaceae, and Urticaceae demonstrated the longest pollination periods. Increasing multi-year trends were observed for taxa such as Amaranthus, Fraxinus, and Populus, whereas declining trends were noted for Artemisia, Betula, Cannabaceae, and Poaceae.

The rising concentrations of ragweed (Ambrosia), a highly allergenic species, highlight the urgent need for preventive measures in both urban and rural environments. Overall, the findings emphasize the importance of continuous aerobiological surveillance and long-term assessment of pollen dynamics as a foundation for public health planning, allergen exposure reduction, and improvement of quality of life for sensitive populations in Pančevo.

Keywords: airborne pollen, long-term trend.

INTRODUCTION

Airborne pollen has represented a significant etiological factor in allergic reactions over the past century, when in the late 19th and early 20th centuries scientists began linking pollen exposure to alergic conditions. The first organized national airborne pollen survey was conducted in the United States in 1929. From there, techniques for pollen collection and counting were refined, and by the 1950s–1960s in Europe and other parts of the world, standardized methods and pollen counting networks were established. According to the

* *dubravka.nikolovski@gmail.com*

statement of the Environmental Protection Agency of Serbia, one measuring site represents a territory with a diameter of 30 km to 50 km, depending on the orography of the terrain [1]. Depending on meteorological conditions, pollen can be found at altitudes greater than 1 km [2]. Nowadays, systematic aeropollen monitoring provides the basis for clinical and public health purposes: the investigation, prevention, diagnosis, and management of pollen–induced allergies.

In Serbia, the measurement of airborne concentrations of allergenic pollen species is currently carried out by the Environmental Protection Agency, within the framework of the national monitoring network. This monitoring system is aligned with the recommendations of the International Association for Aerobiology, which defines the monitoring period according to climatic conditions. Data from this network are submitted to the European Aeroallergen Network (EAN).

MATERIALS AND METHODS

Study Area

The study was conducted in Pančevo, a city located in the southern part of Vojvodina, Serbia. Pančevo lies approximately 15 km northeast of Belgrade, at the confluence of the Tamiš and Danube rivers. The region is characterized by a continental climate, with cold winters, warm summers, and moderate precipitation. Its geographical position, combined with significant agricultural activity and surrounding forested areas, provides a diverse source of airborne pollen.

Sampling procedure

Aeropollen was collected using the continuous volumetric method [3]. Sampling was performed with a LANZONI VPPS 2000 SAMPLER, located in the building of the City Administration at a height of about 15 m above ground level and operating continuously for a period of seven days. From each seven-day sample, daily subsamples were prepared according to standardized methodology [4] and subsequently analyzed microscopically in the laboratory. The monitoring period was from the beginning of February until the first days of November.

Pollen identification

Microscopic analysis included identification of pollen grains from the following taxa: *Acer* (maple), *Alnus* (alder), *Ambrosia* (ragweed), *Artemisia* (mugwort), *Betula* (birch), *Cannabaceae* (hemp), *Carpinus* (hornbeam), *Chenopodiaceae/Amaranthaceae (*goosefoot/ amaranths), *Corylus* (hazel), *Cupressaceae and Taxus* (cypress and yew), *Fagus* (beech), *Fraxinus* (ash), *Juglans* (walnut), *Moraceae* (mulberry), *Pinaceae* (pine), *Plantago* (plantain), *Platanus* (plane tree), *Poaceae* (grasses), *Populus* (poplar), *Quercus* (oak), *Rumex* (sorrel), *Salix* (willow), *Tilia* (linden), *Ulmaceae* (elm) and *Urticaceae* (nettle).

The following indicators are monitored [5–9]: annual maximum airborne pollen concentrations (grains/m^3 per day), pollination period length (number of days), cumulative airborne pollen concentrations during the pollination period (grains/m^3), and the number of days per year exceeding threshold values of pollen concentrations.

Airborne pollen measurements encompass three distinct pollination seasons. The tree pollination season begins in early February with the flowering of hazel (*Corylus*) and alder (*Alnus*) and continues until early May. The grass pollination season extends from May until the end of July, and in addition to grasses, this period is also marked by the flowering of pine (*Pinus*) and linden (*Tilia*). The weed pollination season lasts from early August until early November, characterized primarily by the flowering of ragweed (*Ambrosia*).

RESULTS AND DISCUSSION

Daily concentrations of pollen in the air of the city of Pančevo were examined in the period from 2021 to 2025. In the five-year comparative analysis of daily pollen concentrations in the air, all available data are presented graphically

Here is presented (Figure 1) a trend of five-year daily pollen concentration for the six species with the highest total annual concentrations. All available data is presented numerically (Tables 2–4).

The comparative analysis of aeropollen examination results in the period from 2021 to 2025 by plant species was carried out for the following parametars: total annual pollen concentrations (Table 2), in the air referring to the monitoring period determined by the Environmental Protection Agency (Table 1), maximum annual pollen concentrations (Table 3), number of pollination days (Table 4), where the minimum, maximum and average values are given for each parameter.

Table 1 *Airborne pollen monitoring periods from 2021 to 2025*

Year	Start Date of Annual Pollen Season	End Date of Annual Pollen Season
2021	February1, 2021	October 31, 2021
2022	January 31, 2022	October 30, 2022
2023	January 30, 2023	November 5, 2023
2024	February 5, 2024	November 3, 2024
2025	February 2, 2025	November 2, 2025

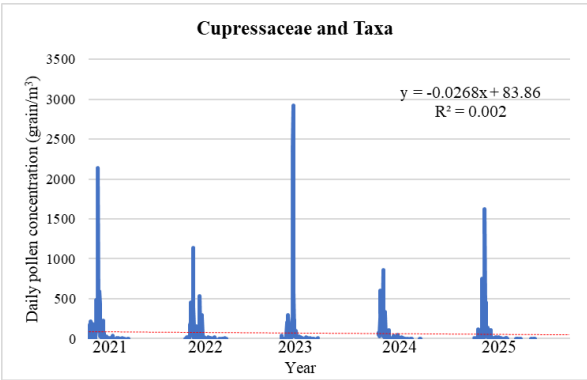

a) Cupressaceae and *Taxa*

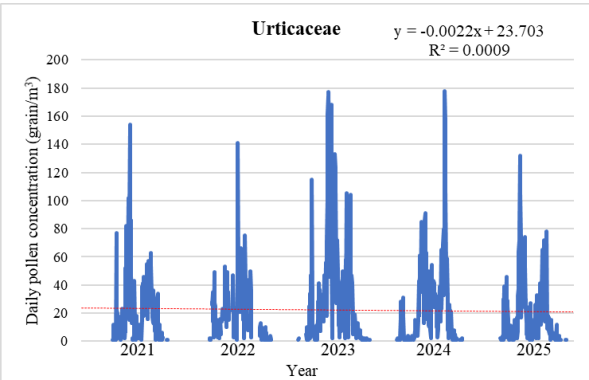

b) Urticaceae

Figure 1 *continued*

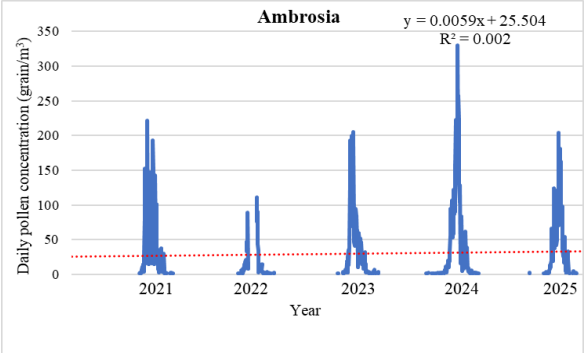

c) Ambrosia

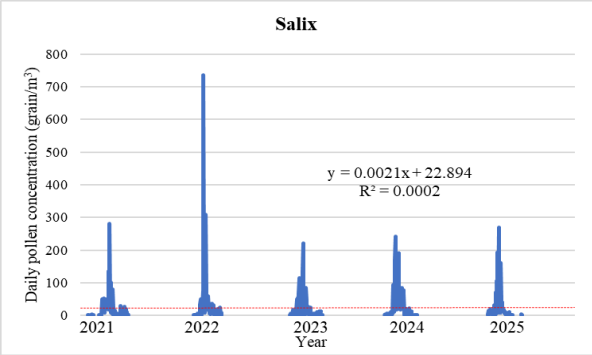

d) Salix

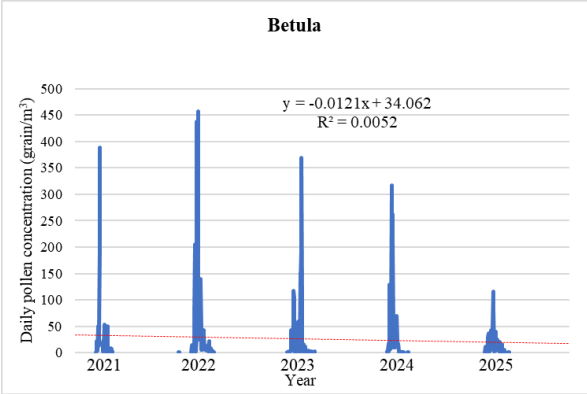

e) Betula

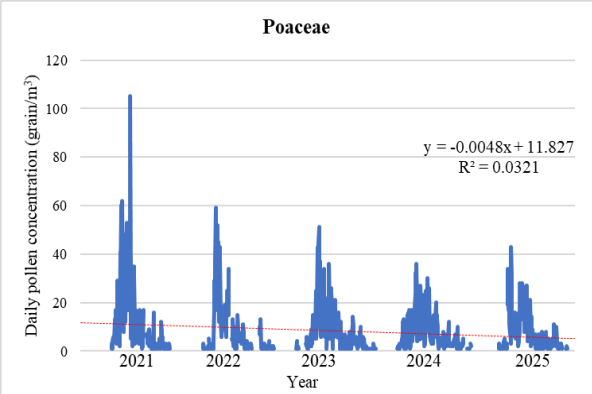

f) Poaceae

Figure 1 *Trend of five-year daily pollen concentration - six species with the highest total annual concentrations: a) Cupressaceae and Taxa; b) Urticaceae; c) Ambrosia; d) Salix; e) Betula; f) Poaceae*

Table 2 *Total concentrations of aeropollen in the air of the city of Pančevo in the period from 2021 to 2025*

Plant species	Total pollen concentration (number of pollen grains / m^3 of air)					Minimum	Maximum	Five-year average value*
	Year							
	2021	2022	2023	2024	2025			
Acer / maple	544	708	964	1144	729	544	1144	818
Alnus / alder	278	963	109	592	446	109	963	478
Ambrosia / ambrosia	2846	880	3302	4489	3130	880	4489	2929
Artemisia / mugwort	134	102	252	178	120	102	252	157
Betula / birch	1120	2598	1729	1722	840	840	2598	1602
Cannabaceae / hemp	287	193	278	408	196	193	408	272
Carpinus / hornbeam	150	1066	181	588	868	150	1066	571
Chenopodiaceae / Amar. / goosfoot/amaranths	212	187	268	553	230	187	553	290
Corylus / hazel	351	660	209	604	420	209	660	449
Cupressaceae / Taxae / cypress and yew	7858	5455	8552	5310	7091	5310	8552	6853
Fagus / beech	246	355	53	239	162	53	355	211
Fraxinus / ash	290	370	487	593	514	290	593	451
Juglans / walnut	454	278	523	446	267	267	523	394
Moraceae / mulberry	383	845	684	1561	202	202	1561	735
Pinaceae / pine	1036	421	353	447	707	353	1036	593

Table 2 *continued*

Plantago / plantain	82	70	231	187	135	70	231	141
Platanus / plane tree	183	71	90	87	144	71	183	115
Poaceae / grasses	1734	1201	1579	1410	1328	1201	1734	1450
Populus / poplar	504	466	700	331	599	331	700	520
Quercus / oak	246	167	224	191	306	167	306	227
Rumex / sorrel	74	45	74	72	67	45	74	66
Salix / willow	1647	2511	1624	2315	1929	1624	2511	2005
Tilia / linden	347	338	251	350	334	251	350	324
Ulmaceae / elm	141	208	150	286	295	141	295	216
Urticaceae / nettle	2737	2495	5628	4015	2841	2495	5628	3543

Among all analyzed taxa, *Cupressaceae* and *Taxa*, *Urticaceae*, and *Ambrosia* pollen demonstrated the highest average five-year value.

Table 3 *Maximum concentrations of airborne pollen in the air of the city of Pančevo in the period from 2021 to 2025*

Plant species	**Maximum concentrations of airborne pollen (number of pollen grains / m^3 of air)**					**Minimum**	**Maximum**	**Five-year average value***
	Year							
	2021	**2022**	**2023**	**2024**	**2025**			
Acer / maple	67	73	90	104	68	67	104	80
Alnus / alder	19	358	16	183	71	16	358	129
Ambrosia / ambrosia	222	111	205	330	204	111	330	214
Artemisia / mugwort	11	11	30	13	10	10	30	15
Betula / birch	389	457	369	317	116	116	457	330
Cannabaceae / hemp	22	16	16	21	21	16	22	19
Carpinus / hornbeam	17	240	18	61	65	17	240	80
Chenopodiaceae / Amar. / goosfoot/amaranths	12	10	17	17	8	8	17	13
Corylus / hazel	105	73	18	97	109	18	109	80
Cupressaceae / Taxae / cypress and yew	2143	1143	2921	859	1625	859	2921	1738
Fagus / beech	78	59	7	42	36	7	78	44
Fraxinus / ash	19	44	38	32	52	19	52	37
Juglans / walnut	74	30	68	57	33	30	74	52
Moraceae / mulberry	62	112	105	273	32	32	273	117
Pinaceae / pine	112	32	25	28	54	25	112	50
Plantago / plantain	7	4	6	10	6	4	10	7
Platanus / plane tree	31	15	9	13	32	9	32	20
Poaceae / grasses	105	59	51	36	43	36	105	59
Populus / poplar	102	78	236	42	93	42	236	110
Quercus / oak	35	24	43	41	44	24	44	37
Rumex / sorrel	6	4	4	3	5	3	6	4
Salix / willow	282	736	221	241	269	221	736	350
Tilia / linden	45	44	31	43	59	31	59	44
Ulmaceae / elm	20	22	24	42	59	20	59	33
Urticaceae / nettle	154	141	177	178	132	132	178	156

The highest average five-year maximum pollen value was recorded for *Cupressaceae*, *Salix*, and *Betula* pollen.

Table 4 *Number of pollination days of airborne pollen in the air of the city of Pančevo in the period from 2021 to 2025*

Plant species	Number of pollination days (n)					Minimum	Maximum	Five-year average value*
	Year							
	2021	2022	2023	2024	2025			
Acer / maple	73	58	77	83	79	58	83	74
Alnus / alder	48	54	31	43	46	31	54	44
Ambrosia / ambrosia	86	67	103	129	98	67	129	97
Artemisia / mugwort	49	39	72	70	47	39	72	55
Betula / birch	49	66	75	55	58	49	75	61
Cannabaceae / hemp	71	57	78	81	73	57	81	72
Carpinus / hornbeam	54	73	57	60	52	52	73	59
Chenopodiaceae / Amar. / goosfoot/amaranths	80	75	98	113	94	75	113	92
Corylus / hazel	49	57	44	38	47	38	57	47
Cupressaceae / Taxae / cypress and yew	97	100	105	94	115	94	115	102
Fagus / beech	33	41	24	31	27	24	41	31
Fraxinus / ash	85	81	93	81	76	76	93	83
Juglans / walnut	38	37	57	45	50	37	57	45
Moraceae / mulberry	31	29	40	38	31	29	40	34
Pinaceae / pine	102	89	96	109	115	89	115	102
Plantago / plantain	60	51	106	86	92	51	106	79
Platanus / plane tree	27	24	36	23	30	23	36	28
Poaceae / grasses	151	146	200	198	187	146	200	176
Populus / poplar	45	58	43	50	40	40	58	47
Quercus / oak	40	36	30	35	49	30	49	38
Rumex / sorrel	47	35	54	59	51	35	59	49
Salix / willow	87	80	86	82	79	79	87	83
Tilia / linden	52	56	62	63	62	52	63	59
Ulmaceae / elm	43	45	34	44	42	34	45	42
Urticaceae / nettle	137	138	177	179	172	137	179	161

Poaceae, *Urticaceae*, *Pinaceae*, and *Cupressaceae* and *Taxa* pollen had the longest pollination in the five-year average period.

CONCLUSION

Analysis of airborne pollen concentrations in Pančevo during the period 2021–2025 revealed distinct temporal trends among major allergenic taxa. Increasing concentrations were documented for *Acer*, *Alnus*, *Ambrosia*, *Carpinus*, *Chenopodiaceae/Amaranthus*, *Corylus*, *Fraxinus*, *Moraceae*, *Plantago*, *Populus*, *Quercus*, *Salix*, *and Ulmaceae*. *Declining trends were observed for Artemisia*, *Betula*, *Cannabaceae*, *Cupressaceae/Taxae*, *Fagus*, *Juglans*, *Pinaceae*, *Platanus*, *Poaceae*, *Rumex*, *Tilia*, and *Urticaceae*.

The taxa showing the most significant multi-year increases were *Amaranthus*, *Fraxinus*, and *Populus*, all of which have moderate allergenic potential. The upward trend in ragweed pollen concentrations highlights the importance of implementing preventive strategies for its control in both urban and rural areas, while promoting the planting of tree species with no allergenic potential to safeguard public health.

Continuous aerobiological surveillance and long-term evaluation of airborne pollen dynamics are critical for developing targeted interventions that reduce allergen exposure, improve the quality of life of sensitive populations, and provide a solid scientific basis for evidence-based public health planning in Pančevo.

ACKNOWLEDGEMENT

Pollen monitoring was financially supported by the City of Pančevo through Contract No. XI-13-404-210/2019 for the procurement of pollen monitoring services, dated December 30, 2019; Contract No. XI-13-404-250/2021, dated January 24, 2022; and Contract No. XI-13-405-129/2023, dated January 3, 2024.

REFERENCES

[1] Environmental Protection Agency of Serbia. Pollen Monitoring Portal. 2026. Available from: https://sepa.gov.rs/polen/ (accessed on March 2, 2026).

[2] Sikoparija, B., Birgermajer, S., Ivosevic, B., *et al*. U. Atmosphere 2025, 16, 1060.

[3] Hirst, J.M. Ann. Appl. Biol. 1952, 39(2), 257–265.

[4] SRPS EN 16868:2019. Ambient Air – Sampling and Analysis of Airborne Pollen Grains and Fungal Spores for Networks Related to Allergy – Volumetric Hirst Method. Serbian Institute for Standardization: Belgrade, Serbia, 2019. Available from: https://iss.rs/en/project/show/iss:proj:64320 (accessed on March 2, 2026).

[5] Institute of Public Health Pančevo. Annual Report on the Measurements of Allergenic Pollen in Ambient Air in the Territory of the City of Pančevo for the Period from February 1, 2021, to October 31, 2021. Pančevo, Serbia, 2022. Available from: https://www.pancevo.rs/?wpfb_dl=4363 (accessed on March 2, 2026).

[6] Institute of Public Health Pančevo. Annual Report on the Measurements of Allergenic Pollen in Ambient Air in the Territory of the City of Pančevo for the Period from January 31, 2022, to October 30, 2022. Pančevo, Serbia, 2023. Available from: https://www.pancevo.rs/?wpfb_dl=4735 (accessed on March 2, 2026).

[7] Institute of Public Health Pančevo. Annual Report on the Measurements of Allergenic Pollen in Ambient Air in the Territory of the City of Pančevo for the Period from January 30, 2023, to November 5, 2023. Pančevo, Serbia, 2024. Available from: https://www.pancevo.rs/?wpfb_dl=5188 (accessed on March 2, 2026).

[8] Institute of Public Health Pančevo. Annual Report on the Measurements of Allergenic Pollen in Ambient Air in the Territory of the City of Pančevo for the Period from February 5, 2024, to November 3, 2024. Pančevo, Serbia, 2025. Available from: https://www.pancevo.rs/?wpfb_dl=5576 (accessed on March 2, 2026).

[9] Institute of Public Health Pančevo. Annual Report on the Measurements of Allergenic Pollen in Ambient Air in the Territory of the City of Pančevo for the Period from February 3, 2025, to November 2, 2025. Pančevo, Serbia, 2026. Available from: https://www.pancevo.rs/?wpfb_dl=5742 (accessed on March 2, 2026).

EcoTER'26
eco.tfbor.bg.ac.rs
32nd International Conference
Ecological Truth & Environmental Research
24–26 June 2026, Hotel Sunce,
Sokobanja, Serbia

Original Research

REMOVAL OF SYNTHETIC DYE FROM AQAEOUS SOLUTIONS USING *Qercus cerris* ACORN CUPS

DOI: 10.5937/EcoTER26250N

Milena Nikolić[1,a*], Aleksandar Zdravković[1,b], Dragana Marković Nikolić[1,c], Goran Petković[1,d], Tanja Nikolić[1,e]

[1]Academy of Applied Studies of Southern Serbia, Department of Higher Technology and Art School, Vilema Pušmana 17, 16000 Leskovac, SERBIA

[a] https://orcid.org/0000-0002-6631-936X
[b] https://orcid.org/0000-0001-9906-3543
[c] https://orcid.org/0000-0003-3171-9838
[d] https://orcid.org/0009-0001-4375-2857
[e] https://orcid.org/0009-0007-8932-6128

Abstract

The aim of this research was to examine the potential application of the biosorbent obtained from the oak acorn cups (lat. Quercus cerris) to remove the methylene blue from aqueous model solutions. The following parameters were optimized: pH values, biosorbent dose and initial concentrations of methylene blue. The highest sorption capacity of this sorbent towards methylene blue was achieved at following conditions: pH 8, initial concentration of methylene blue 25 mg/dm^3, biosorbent dose 9 g/dm^3. After linear fitting, the experimental kinetic data fitted pseudo-second order model.

Keywords: biosorbent, *Quercus cerris*, methylene blue, pseudo-second order kinetics.

INTRODUCTION

Quercus cerris occupies drier and moderately fertile habitats in lowland and hilly areas of Serbia, where large forests with other species of oak and hornbeam are formed.

Due to lower technological quality, different color of its core part and its tendency to crack, *Quercus cerris* wood is not adequate for industrial processing. It is used as firewood, because of the similar calorific value as hornbeam and beech. However, the main advantage is that it can be used in soil conservation, erosion suppression and reforestation of bare lands due to its strong and branched root system [1]. *Quercus cerris* is often planted in urban areas as an ornamental tree because of its attractive and well-shaped canopy. Furthermore, acorns represent a potential resource in the food industry. Gluten-free and nutritive-valuable flour obtained from acorns was found to be rich in essential unsaturated fatty acids (oleic and linoleic acid), minerals (K, Mg, P, Ca, Fe, Mn) and phenolic compounds with conspicuous antioxidative effect (gallic and syringic acids, catechin, flavanols) [2]. Due to its physicochemical characteristics, flour can be used for preparation of bread [3] and biscuits [4]. However, acorn caps cannot be used in human diet, therefore are discarded but suitable for investigation and discovering new ways of use.

* *milenai.chem@gmail.com*

Methylene blue is a cationic dye used for food and pharmaceutical industries but even more for wool, silk, temporary hair dyes, cotton and textile [5]. Wastewater produced from the textile industry often contains a mixture of several colors and may cause serious health and environmental problems [6]. Thermal and photostability of dye in the environment affects the absorption and reflection of sunlight, which reduces the intensity of photosynthesis in aquatic bodies and causes disturbances in the natural food chain. Therefore, the inevitable impact of these pollutants requires treatment before discharge into the mainstream and causes environmental degradation. Outpouring of colored wastewater into the ecosystem causes eutrophication, aesthetic pollution and disturbance of aquatic life [7]. Although antioxidant, cardio-protective, antimalarial and antidepressant properties have been demonstrated in therapeutic doses, long-term exposure to methylene blue can also cause health problems such as anemia, cancer, vomiting, eye irritation, nausea [8].

Based on the above facts, the aim of this research was to investigate the potential application of a biosorbent derived from *Quercus cerris* acorn caps (QC) for the removal of methylene blue from the aquatic environment. According to our knowledge, there are no available studies published regarding biosorption of pollutants onto this type of sorbent.

MATERIALS AND METHODS

Biosorbent preparation and characterization

Fully ripe acorns of the *Qercus cerris* were collected in the vicinity of Leskovac, in the Pusta Reka region. The caps were separated from the acorns for more efficient drying and left in a well-ventilated place for a month, then coarsely crushed in a porcelain mortar, ground in a laboratory blender and sieved on a laboratory sieve with 1 mm diameter. The QC biosorbent was then used in sorption experiments. Evaluation of QC biosorbent was performed according to iodine number method [9]. Point of zero charge (pH_{pzc}) was determined by mixing 0.05 g of QC biosorbent and 20 mL of 0.1 M KCl and varying the pH from 2 to 12 using HCl or NaOH. The pH values were measured by digital pH meter (HI-2209, Hanna, USA).

Sorption experiments

The sorption study was conducted in order to analyze the effect of pH, biosorbent dose and initial concentration of methylene blue. Deionized water was used for preparation of all solutions. The concentration of methylene blue was measured spectrophotometrically at 620 nm. The removal efficiency (%) was calculated according to the Equation 1:

$$\%=(c_0-c_t)/c_0*100 \quad (1)$$

RESULTS AND DISCUSSION

The material and reagents for measuring iodine number are not expensive, and the time required to perform the analysis is relatively short. The QC biosorbent was evaluated using the iodine number method, with the result yielding q_i = 195.4 mg/g. Since used in native condition, lower value of iodine number may indicate a low microporosity of the surface of the biosorbent, but this could undoubtedly be improved by chemical or thermal modification.

One of the most important factors affecting the efficiency of the sorption process is the pH value of the aquatic environment, due to the influence (protonation/deprotonation) on the

functional groups of the pollutants as well as the sorbent [10]. The pH_{pzc} for QC biosorbent was found to be 6.23 meaning its surface will be negatively charged at higher pH values. Since methylene blue is a cationic dye, it is expected for alkaline conditions to be favorable for its sorption onto QC biosorbent. The influence of pH on the removal of methylene blue from the water was examined in the range of pH values from 2 to 12 with other parameters as follows: initial concentration of methylene blue 25 mg/dm^3, QC biosorbent dose 5 g/dm^3. The greatest removal efficiency occurred at pH 8, and increased negligibly with further increase of pH, (Figure 1) therefore this value was chosen for further investigations. Higher sorption capacity of methylene blue in alkaline conditions was also reported for sorbents obtained from *Osmanthus fragrans* [11] and *Stipa tenacissima* plants [12].

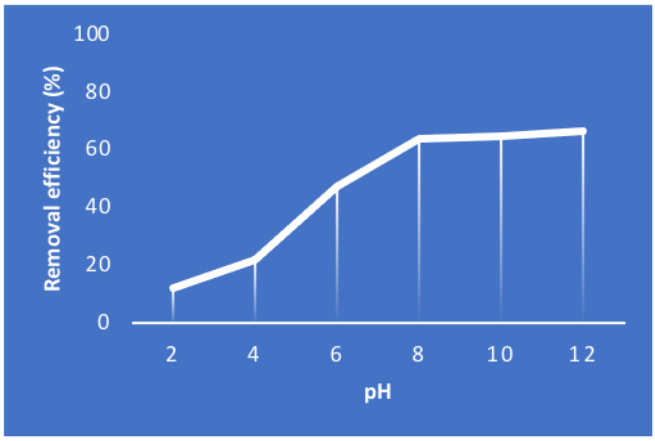

Figure 1 *The methylene blue removal efficiency as a function of pH*

The effect of biosorbent dose on removal efficiency of methylene blue was investigated at pH 8 and initial concentration of methylene blue 25 mg/dm^3 and is represented in Figure 2. As it can be seen, increase in biosorbent dose (up to 9 g/dm^3) led to greater removal efficiency (up to 83.6%) due to greater number of binding sites on the surface of the QC biosorbent.

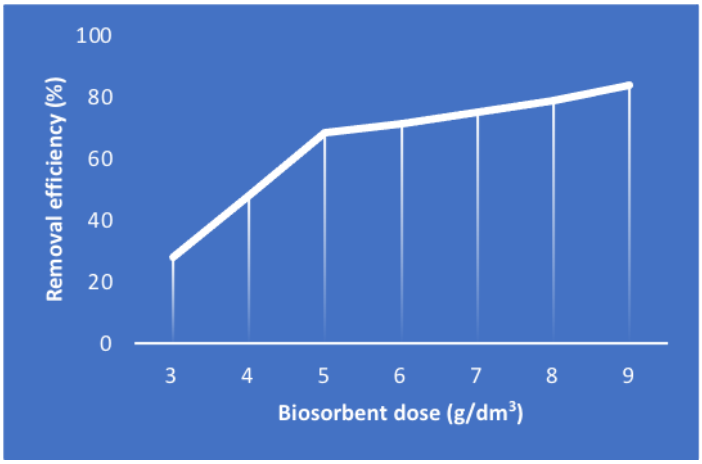

Figure 2 *Effect of biosorbent dose on removal efficiency of methylene blue*

The initial concentration is an important kinetic parameter for the process of binding the polluting substance to the binding spots of the biosorbent. The influence of the initial

concentration of methylene blue on its removal from an aqueous solution by QC biosorbent was investigated at initial concentrations of methylene blue from 5 to 65 mg/dm^3 at pH 8, and QC biosorbent dose 9.0 g/dm^3. The result is shown in Figure 3. At lower concentrations of methylene blue, sufficient number of binding spots on the surface of the QC biosorbent were available and the removal efficiency was 87.4%, 69.3% and 63.6% for 5, 15 and 25 mg/dm^3. As the concentration increased the binding sites were saturated, and the removal efficiency dropped significantly with a further increase in the initial concentration of methylene blue, yelding only 17% for 65 mg/dm^3.

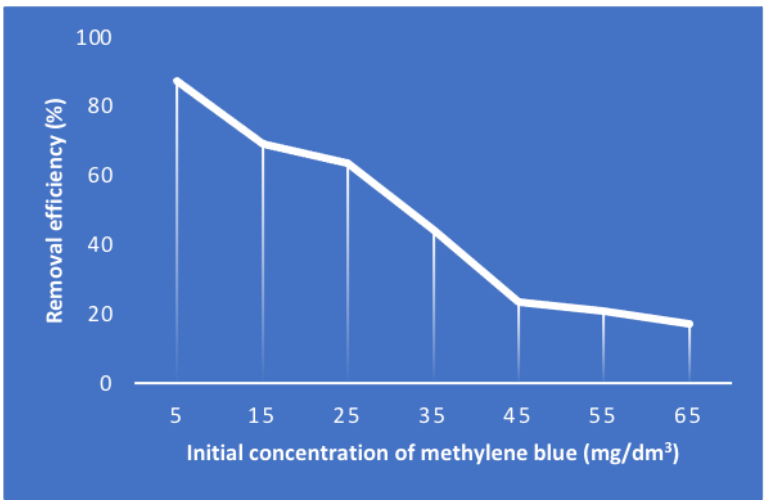

Figure 3 *Effect of initial concentration on removal efficiency of methylene blue*

The sorption capacity of QC biosorbent towards methylene blue over time, q_t (mg/g), was calculated according to the Equation 2:

$$q_t = \frac{(c_0 - c_t)V}{m} \tag{2}$$

where c_0 and c_t represent the initial concentration and concentration of the methylene blue solution in time t (mg/dm^3), respectively, V volume of the methylene blue solution (dm^3), and m the mass of the QC biosorbent (g).

A model suitable for describing the kinetics of the sorption process can be determined based on experimentally obtained sorption capacities. Pseudo-first order (Equation 3) and pseudo-second order (Equation 4) kinetic models are the most often used to determine the order of the reaction and the rate constant of the sorption process.

$$dq_t/dt = k_1(q_e - q_t) \tag{3}$$
$$dq_t/dt = k_2(q_e - q_t)^2 \tag{4}$$

where k_1 (1/min) is the pseudo-first-order rate constant, k_2 (g/mg min) is the pseudo-second-order rate constant, q_t (mg/g) is the sorbent capacity at time t, and q_e (mg/g) is the sorbent capacity in the equilibrium state.

According to Equation 3, the results were obtained for the pseudo-first order kinetics and presented in the Figure 4.

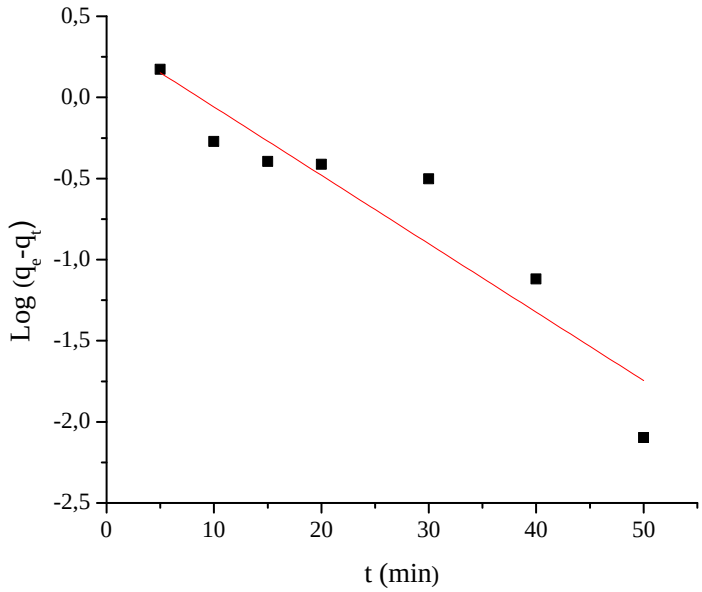

Figure 4 *Kinetic model of pseudo-first order*

According to Equation 4, the results were obtained for the pseudo-second order kinetics and presented in the Figure 5.

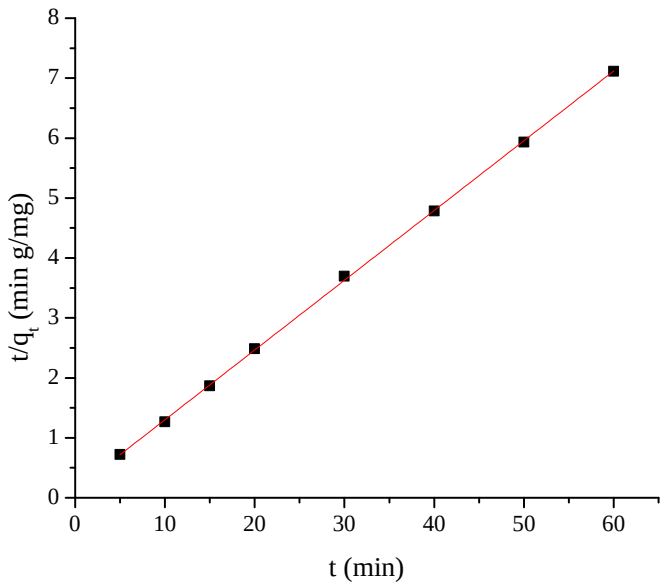

Figure 5 *Kinetic model of pseudo-second order*

The software package Origin Pro 8.0 (OriginLab Corporation, USA) was applied for linear fitting of experimental data and the kinetic parameter values are given in Table 1.

According to the linear curves in the Figures 4 and 5 and the correlation coefficients in Table 1, it is evident that the sorption of methylene blue onto QC biosorbent follows pseudo-second order kinetics. The correlation coefficient for the pseudo-second order model is higher than the correlation coefficient for the pseudo-first order model. The value of the

calculated sorption capacity according to the pseudo-second-order model ($q_{e,cal}$=8.594 mg/g) is significantly closer to the experimental sorption capacity ($q_{e,eks}$=8.436 mg/g), than the value of the calculated sorption capacity according to the pseudo-first order model ($q_{e,cal}$=2.308 mg/g).

Table 1 *Kinetic parameters of sorption models of methylene blue*

Kinetic model	Parameter	Methylene blue
Eksperimental	$q_{e,exp}$ (mg/g)	8.436
Pseudo-first order	$q_{e,cal}$ (mg/g)	2.308
	k_1 (1/min)	9.71
	R^2	0.8567
Pseudo-second order	$q_{e,cal}$ (mg/g)	8.594
	$k_2 \times 10^3$ (g/mg min)	9.87
	R^2	0.9997

CONCLUSION

Qurcus cerris acorn caps were used for biosorption of cationic dye methylene blue from aqueous media. Biosorbent was used in native condition. Sorption of methylene blue onto QC biosorbent followed pseudo-second order kinetics.

The point zero charge of biosorbent was at pH 6.23, thus alkaline conditions were favorable for sorption of methylene blue. Also, biosorption was notably influenced by biosorbent dose and initial concentration of methylene blue. Even though potential usage of QC biosorbent in native condition was estimated, the study highlighted its potential to be chemically or thermally modified in order to improve its sorption properties.

REFERENCES

[1] de Rigo D, Enescu CM, Houston Durrant T *et al*. Quercus cerris in Europe: distribution, habitat, usage and threats. In: San-Miguel-Ayanz J, de Rigo D, Caudullo, G, Houston Durrant, T, Mauri, A, editors. European Atlas of Forest Tree Species. Luxembourg, European Commission; 2016. p. 148.

[2] Martins, R.B., Gouvinhas, I., Nunes, M.C., *et al*. Curr. Res. Food Sci. 2022, 5, 2211–2218.

[3] Skendi, A., Mouselemidou, P., Papageorgiou, M., *et al.* Food Chem. 2018, 253, 119–126.

[4] Korus, A., Gumul, D., Krystyjan, M., *et al.* Eur. Food Res. Technol. 2017, 243 (8), 1429–1438.

[5] Khan, I., Saeed, K., Zekker, I., *et al.* Water. 2022, 14(2), 242.

[6] Wang, X., Jiang, J., Gao, W. Water Sci Technol. 2022, 85 (7), 2076–2096.

[7] Holkar, C.R., Jadhav, A.J., Pinjari, D.V., *et al.* J. Environ. Manage. 2016, 182, 351–366.

[8] Fito, J., Abewaa, M., Mengistu, A. Sci. Rep. 2023, 13, 5427.

[9] Du, C., Liu, B., Hu, J. *et al.* Mater. Lett. 2021, 285, 129–137.

[10] Banerjee, S., Chattopadhyaya, M.C. Arab J of Chem. 2017, 10, S1629–S1638

[11] Chai, B., Cheng, X., Ren Z,. *et al*. Desalin. Water Treat. 2016, 57, 18868–18878.

[12] Ladjali, S., Dahdouh, N., Amokrane, S., *et al*. APTEFF. 2021, 52, 33–44.

EcoTER'26
eco.tfbor.bg.ac.rs
32nd International Conference
Ecological Truth & Environmental Research
24–26 June 2026, Hotel Sunce,
Sokobanja, Serbia

Original Research

KINETIC AND THERMODYNAMIC ASPECTS OF PESTICIDE SORPTION ONTO HORSE CHESTNUT SEED SORBENT

DOI: 10.5937/EcoTER26256N

Milena Nikolić[1,a*], Aleksandar Zdravković[1,b], Dragana Marković Nikolić[1,c], Nebojša Ristić[1,d], Ivanka Ristić[1,e]

[1]Academy of Applied Studies of Southern Serbia, Department of Higher Technology and Art School, Vilema Pušmana 17, 16000 Leskovac, SERBIA

[a] https://orcid.org/0000-0002-6631-936X

[b] https://orcid.org/0000-0001-9906-3543

[c] https://orcid.org/0000-0003-3171-9838

[d] https://orcid.org/0009-0004-9941-471X

[e] https://orcid.org/0009-0003-2838-8713

Abstract

The sorbent obtained from horse chestnut acorn was tested for sorption capacity of acetamiprid in the aquatic media. Sorbent dose, contact time and temperature were varied. The kinetic data fitted best with a pseudo-first order model. Thermodynamic results indicate that the process of removing acetamiprid from the aquatic media was spontaneous at 25 °C. The maximum sorption capacity of the horse chestnut sorbent for acetamiprid (q_{max}=13,52 mg/g) was obtained with a sorbent dose 4 g/dm^3, at 25 °C, pH 7.43, and initial concentration of acetamiprid 100 mg/dm^3.

Keywords: biosorption, horse chestnut, *Aesculus hippocastanum*, acetamiprid.

INTRODUCTION

The intensive use of synthetic pesticides in modern agriculture has led to significant contamination of surface and groundwater systems, posing a severe threat to aquatic ecosystems and human health. Consequently, the development of efficient, low-cost, and sustainable remediation technologies is a global priority. Recent research has pivoted toward biosorption-utilizing waste biomass as a renewable alternative to expensive activated carbons [1]. Horse chestnut seed, a widely available but underutilized lignocellulosic byproduct, presents a promising matrix for this purpose. Its chemical composition, rich in starch, proteins, and polyphenols [2], provides a variety of functional groups that may serve as active sites for pesticide binding. This study aimed to investigate the feasibility of horse chestnut seed sorbent for removal of acetamiprid from aqueous solutions. In order to understand the underlying mechanisms governing this process, the analysis of kinetic models and thermodynamic parameters was performed to determine the rate limiting steps and to evaluate spontaneity and nature (physisorption, chemisorption or ion exchange) of the process.

* *milenai.chem@gmail.com*

MATERIALS AND METHODS

The horse chestnut seeds were separated from the caps and left in a well-ventilated place to dry. The seeds were then ground in a rotary mill (SR 300, Retsch, Germany) and sieved granulometrically on a vibro device (AS 200 basic, Retsch, Germany). The fraction of 1 mm diameter was used for the experiments. The sorbent was not chemically or thermally modified.

In order to examine the influence of the sorbent dose on the biosorption of acetamiprid, a series of experiments was performed using 0.5, 1, 2, 4 i 6 g/dm^3 of biosorbent. The initial concentration of 100 mg/dm^3 of acetamiprid and the stirring rate of 100 rpm were constant. The pH of aqueous model solution of acetamiprid was 7.43 and was not adjusted after in order to observe the sorption process in natural conditions.

For thermodynamic parameters, 4 g of biosorbent was mixed with 100 cm^3 of a 100 mg/dm^3 solution of acetamiprid, at temperatures of 25 ^{o}C, 35 ^{o}C and 45 ^{o}C. For kinetic parameters, the experiments were conducted using 4 g of biosorbent at 25 ^{o}C and samples were taken after 5, 10, 20, 30, 40, 50 and 60 min. The suspensions were then filtered through cellulose 0.45 µm filters (Econofilters, Agilent Technologies, Germany) and the concentration of acetamiprid was determined in the obtained solutions.

RESULTS AND DISCUSSION

The amount of adsorbed acetamiprid onto horse chestnut seed biosorbent was calculated according to the Equation 1:

$$q_t = \frac{(c_0 - c_t)V}{m} \tag{1}$$

where c_0 and c_t represent the initial concentration and concentration of acetamiprid solution in time t (mg/dm^3), respectively, V volume of acetamiprid solution (dm^3), and m the mass of the biosorbent (g).

The effect of sorbent dose on acetamiprid removal from aqueous solution has been illustrated in the Figure 1.

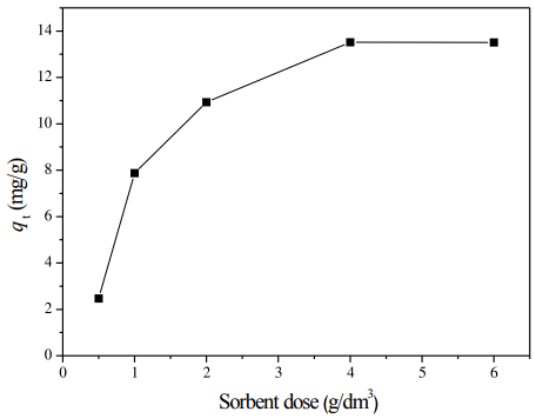

Figure 1 *Effect of sorbent dose on acetamiprid removal from aqueous solution (pH=7.43, initial concentration of acetamiprid 100 mg/dm^3, 25 ^{o}C, time 60 min)*

The sorption capacity increased as the sorbent dose increased from 0.5 to 4 g/dm^3, since larger number of binding sites was available for interaction with the molecules of acetamiprid. There was no significant increase in the sorption capacity when applying higher doses of sorbent. Therefore, the dose of 4 g/dm^3 was used for further experiments.

The basic thermodynamic quantities, Gibbs free energy change (ΔG°), enthalpy (ΔH°) and entropy (ΔS°), are used to determine the spontaneity of a process, the nature of the reaction and the type of sorption and were calculated by using Equations 2 and 3:

$$\Delta G^{\circ} = -RT \ln K_c \tag{2}$$

$$\ln K_c = \frac{\Delta S^{\circ}}{R} - \frac{\Delta H^{\circ}}{RT} \tag{3}$$

Via linear plot of ln K_c vs. $1/T$, the values $\Delta H°$ and $\Delta S°$ were calculated (Figure 2).

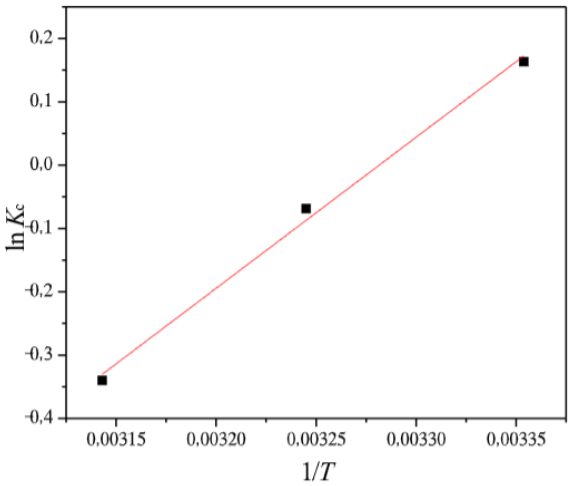

Figure 2 *Thermodynamic dependence ln Kc=f(1/T) for the biosorption of acetamiprid onto horse chestnut seeds sorbent*

According to results represented in the Table 1, the Gibbs free energy increases with an increase in temperature. The process is spontaneous at 25 ^{o}C (ΔG°<0), which is not the case at higher temperatures (ΔG°>0). The values of enthalpy and entropy show that biosorption of acetamiprid onto horse chestnut seed sorbent was exothermic, with the system becoming less disordered.

Table 1 *Thermodynamic parameters of acetamiprid biosorption onto horse chestnut seeds sorbent*

T (K)	Δ*G*° (kJ/mol)	Δ*H*° (kJ/mol)	Δ*S*° (kJ/mol K)	R^2
298.16	-0.406			
308.16	0.175	-19.829	-0.065	0.992
318.16	0.899			

Based on ΔH° the mechanism of interaction between the sorbent and sorbate can be determined. Enthalpy value in the range of 2–20 kJ/mol indicates physical sorption, in the range of 20–80 kJ/mol indicates ion exchange, and the ΔH°>80 kJ/mol indicates

chemisorption [3]. In this case, the most likely dominant mechanism of acetamiprid biosorption were physical interactions.

The sorption capacity increased up to 30 min of the sorption process, with no significant increase afterwards. Figure 3 shows the curves corresponding to the nonlinear forms of pseudo-first and pseudo-second order kinetic models. The kinetics of pollutant sorption from water to sorbents was described in the literature by pseudo-first and pseudo-second order models [4,5]. The nonlinear forms of the pseudo-first and pseudo-second order models are shown by equations 4 and 5:

$$q_t = q_e(1 - e^{k_1 t}) \tag{4}$$

$$q_t = \frac{q_e^2 k_2 t}{1 + q_e k_2 t} \tag{5}$$

where k_1 (1/min) is the pseudo-first order rate constant, k_2 (g/mg min) is the pseudo-second-order rate constant, q_t (mg/g) is the sorbent capacity at time t, and q_e (mg/g) is the sorbent capacity in the equilibrium state.

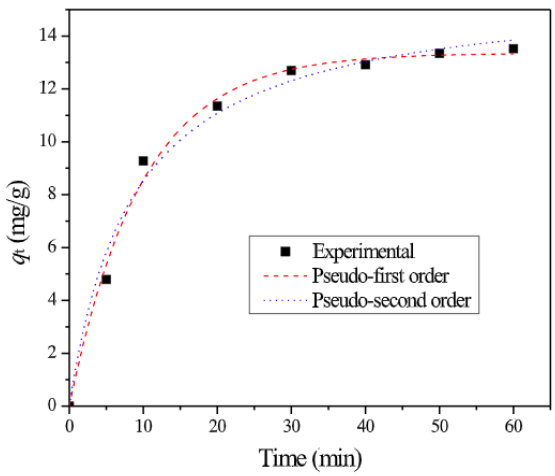

Figure 3 *Kinetic models of pseudo-first and pseudo-second order of acetamiprid biosorption*

Comparing the results of these two models, the pseudo-first order model is more adequate for describing the process of acetamiprid biosorption (Table 2).

Table 2 *Kinetic parameters of sorption models of acetamiprid*

Kinetic model	Parameter	Acetamiprid
Eksperimental	$q_{e,exp}$ (mg/g)	13.520
Pseudo-first order	$q_{e,cal}$ (mg/g)	13.354
	k_1 (1/min)	0.102
	R^2	0.993
Pseudo-second order	$q_{e,cal}$ (mg/g)	15.831
	$k_2 \times 10^3$ (g/mg min)	7.350
	R^2	0.986

The pseudo-first order model showed stronger correlation with the experimental data (R^2 = 0.993) compared to the pseudo-second order model (R^2 = 0.986). Also, the calculated value of sorption capacity according to the pseudo-first order model is closer to the experimental one.

CONCLUSION

According to obtained results, horse chestnut seeds could serve as effective and ecologically sustainable biosorbent for the removal of acetamiprid from polluted water. The kinetic analysis indicated that the data followed the pseudo-first order model more closely. Thermodynamic investigations confirmed the process to be exothermic ($\Delta H° < 0$), spontaneous at 25 ^{o}C ($\Delta G° < 0$) and characterized by decrease in randomness at the solid-solution interface.

REFERENCES

[1] Danish, M., Ahmad, T. Renew. Sustain. Energy Rev. 2018, 87, 1–21.

[2] Baraldi, C., Bodecchi, L., Cocchi, M., *et al.* Food Chem. 2007, 104(1), 229–236

[3] Liu, Y., Liu, Y. J. Sep. Purif. Technol. 2008, 61, 229–242.

[4] Lagergren, S., Handlingar, 1898, 24, 1–39.

[5] Ho, Y.S., McKay, G. Process Saf. Environ. Prot. 1998, 76(4), 332–340.

EcoTER'26
eco.tfbor.bg.ac.rs
32nd International Conference
Ecological Truth & Environmental Research
24–26 June 2026, Hotel Sunce,
Sokobanja, Serbia

Original Research

COMPARATIVE KINETIC ANALYSIS OF CATIONIC DYES ADSORPTION ONTO SUSTAINABLE LIGNOCELLULOSIC BIOSORBENTS

DOI: 10.5937/EcoTER26261P

Jovana Perendija[1,a*], Verica Ljubić [1,b], Dragana Milošević[1,c], Slobodan Cvetković[1,d], Mihal Đuriš [1,e], Željka Milovanović[1, f]

[1] University of Belgrade, Institute of Chemistry, Technology and Metallurgy, National Institute of the Republic of Serbia, Njegoševa 12, 11001 Belgrade, SERBIA

[a] https://orcid.org/0000-0002-6318-9053 [b] https://orcid.org/0000-0002-8648-6421
[c] https://orcid.org/0000-0003-3548-6832 [d] https://orcid.org/0000-0003-4417-4443
[e] https://orcid.org/0000-0002-1585-7707 [f] https://orcid.org/0000-0002-1998-5239

Abstract

This study evaluates the biosorption performance of sorghum-, hemp-, and hop-based biosorbents for the removal of methylene blue (MB) and malachite green (MG) from aqueous solutions. A rapid initial uptake of both dyes was observed due to the abundance of available active binding sites, followed by a gradual decrease in adsorption rate until equilibrium was reached. Kinetic analysis revealed that the pseudo-second-order (PSO) model best describes the adsorption process for both MB and MG on all investigated biosorbents (R^2 = 0.999), indicating that chemisorption is the dominant mechanism. The hemp-based biosorbent exhibited the highest rate constant k_2 and the fastest equilibrium time for MB removal (180 min), while sorghum and hop reached equilibrium after 360 min. For MG removal, hemp and sorghum achieved equilibrium after 180 min, whereas hop required 360 min. The intra-particle diffusion (IPD) model indicated a multi-stage adsorption process, where both film diffusion and intra-particle diffusion contribute, with boundary layer effects playing an important role. Overall, the results demonstrate that the investigated biosorbents are effective for MB and MG removal, with hemp showing the most favorable kinetic performance.

Keywords: biosorption, kinetic study, malachite green, methylene blue, waste biomass.

INTRODUCTION

Industrial activities and rapid population growth have significantly contributed to water pollution. Nowadays, substantial efforts are focused on controlling pollutant levels in water in order to mitigate their adverse effects on ecosystems, biodiversity, and, most importantly, human health [1]. Among various water contaminants, synthetic cationic dyes represent a serious environmental concern due to their ability to reduce light penetration and photosynthetic activity, thereby degrading aquatic ecosystems [2]. According to available reports, approximately 12% of the annual production of cationic dyes is discharged into industrial wastewater streams, contributing considerably to environmental pollution [3]. Widely used dyes such as malachite green and methylene blue may adversely affect reproductive and immune systems even at low exposure levels and have been reported to exhibit carcinogenic and mutagenic properties [4].

* *j.nikolic@ihtm.bg.ac.rs*

Among the numerous methods applied for the treatment of dye-contaminated wastewater, adsorption has emerged as one of the most effective and economically favourable approaches. In recent years, increasing attention has been directed toward the use of waste biomass materials as bio-based adsorbents due to their biodegradability, renewability, availability, and high adsorption efficiency [5]. The biomasses investigated in this work represents a widely available lignocellulosic material characterized by large number of different functional groups, a well-developed fibrous structure, and favourable surface properties that may enhance the removal of organic dyes from aqueous solutions. The sorghum, hemp, and hop biomasses used in this study contain cellulose, hemicellulose, and lignin, whose functional groups enable interactions with dye molecules through electrostatic interactions, hydrogen bonding, π–π interactions, etc.

Biosorption kinetics were investigated as an important aspect of understanding the mechanisms governing dye removal, with the aim of determining the biosorption rate and identifying the potential rate-controlling steps of the process. Therefore, the objective of this study was to evaluate and compare the biosorption kinetic parameters of malachite green and methylene blue onto biosorbents derived from sorghum, hemp, and hop in a batch system, as well as to assess differences in the efficiency of cationic dye removal from aqueous solutions.

MATERIALS AND METHODS

Material

Preparation of Biosorbent

The waste biomasses used in this study were obtained from the Institute of Field and Vegetable Crops, Backi Petrovac, Serbia. Waste stems of sorghum, hemp, and hop were chopped and washed with deionized water, air-dried under ambient conditions, and subsequently oven-dry at 65 °C for 24 h. The dried biomasses were ground into fine particles and sieved using a laboratory sieve. The biomass fraction with a particle size smaller than 0.519 mm was used in all biosorption experiments.

Biosorption experiments

Batch biosorption experiments were conducted to evaluate the performance of sorghum-, hemp-, and hop-based biosorbents for the removal of methylene blue (MB) and malachite green (MG) and from aqueous solutions. The experiments were carried out in 50 mL Erlenmeyer flasks by mixing the biosorbents with aqueous dye solutions containing MB or MG. The kinetic study was performed to investigate the effect of contact time on the biosorption capacity under the following conditions: contact time ranging from 5-960 min, biosorbent dose of 2.5 g L^{-1}, initial dye concentration of 30 mg L^{-1}, pH of 6.5, and temperature of 25 °C. After biosorption, the samples were filtered through a 0.22 μm nylon syringe filter, and the residual dye concentrations were determined using a UV–Vis spectrophotometer (Lambda 25/35/45, PerkinElmer). The biosorption capacity (q_e) (mg g^{-1}), as well as the parameters of the pseudo-first-order (PFO), pseudo-second-order (PSO), and intra-particle diffusion (IPD) models were calculated according to the equations reported by Perendija *et al*. [6].

RESULTS AND DISCUSSION

In this study, the effect of contact time on the biosorption of methylene blue (MB) and malachite green (MG) onto sorghum-, hemp-, and hop-based biosorbents was investigated in detail. In the initial stage of biosorption (5–30 min), a rapid uptake of both dyes was observed due to the abundance of available active binding sites on the biosorbent surfaces. This creates a strong driving force for mass transfer and enables rapid diffusion of dye molecules from the solution to the biosorbent surface. As contact time increases, the biosorption rate gradually decreases as these active sites become progressively occupied by MB and MG molecules, leading to a reduction in available binding capacity.

For MB biosorption (Figure 1a)), equilibrium was reached after 360 min using sorghum and hop, while hemp achieved equilibrium more rapidly, after 180 min. Beyond these time points, no significant changes in adsorption capacity were observed, confirming that equilibrium conditions had been established. These results suggest that the hemp-based biosorbent exhibits the fastest adsorption kinetics and the shortest time required to reach equilibrium for MB removal. In the case of MG biosorption (Figure 1b)), equilibrium was reached after 180 min using sorghum and hemp, whereas hop required 360 min to reach equilibrium, reflecting slower adsorption kinetics compared to the other two biosorbents. The adsorption capacity values obtained for both dyes using all three materials were very similar, with hop showing the highest adsorption capacity. Overall, these results indicate that all three biosorbents are comparably effective for dye removal under the applied conditions, differing primarily in the rate of equilibrium attainment.

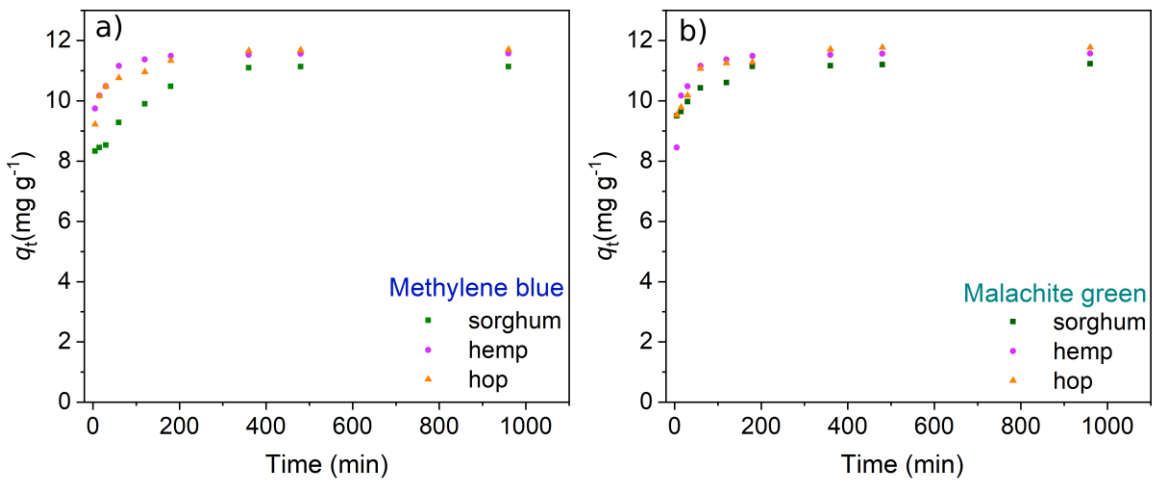

Figure 1 *Effect of contact time on the biosorption of a) MB; b) MG onto sorghum, hemp, and hop*

Kinetic PFO, PSO, and IPD models, were applied to describe the adsorption rate and process mechanism. According to results presented in Table 1 and Table 2, the PSO model provided the best fit for both MB and MG adsorption onto all investigated biosorbents, as evidenced by very high correlation coefficients (R^2 = 0.999) and close agreement between experimental and calculated q_e values. This demonstrates that chemisorption is the dominant mechanism controlling the biosorption process. The hemp-based biosorbent exhibited the highest pseudo-second-order rate constant (k_2) for MB removal, reflecting the fastest adsorption kinetics and the shortest equilibrium time among the investigated materials.

Table 1 *Kinetic parameters obtained by linear regression analyses of PFO,PSO, and IPD kinetic models applied to the experimental data for biosorption of MB onto sorghum, hemp, and hop biosorbents*

Model parameters	Sorghum	Hemp	Hop
Experimental $q_{e,\,exp}$ (mg g^{-1})	11.1	11.6	11.7
PFO			
$q_{e,\,cal}$ (mg g^{-1})	3.91	1.13	1.99
k_1 (min^{-1})	1.26x10^{-2}	1.02x10^{-2}	0.995x10^{-2}
R^2	0.957	0.918	0.982
PSO			
$q_{e,\,cal}$ (mg g^{-1})	11.2	11.6	11.7
k_2 (g mg^{-1}min^{-1})	1.02x10^{-2}	4.15x10^{-2}	1.98x10^{-2}
R^2	0.999	0.999	0.999
IPD			
I stage			
k_{dif} (mg g^{-1}min$^{-0.5}$)	0.191	0.193	0.179
C_1	7.74	9.42	9.23
R^2	0.925	0.929	0.735
II stage			
k_{dif} (mg g^{-1}min$^{-0.5}$)	0.032	0.004	0.018
C_2	10.3	11.4	11.2
R^2	0.317	0.742	0.405

Table 2 *Kinetic parameters obtained by linear regression analyses of PFO,PSO, and IPD kinetic models applied to the experimental data for biosorption of MG onto sorghum, hemp, and hop biosorbents*

Model parameters	Sorghum	Hemp	Hop
Experimental $q_{e,\,exp}$ (mg g^{-1})	11.2	11.6	11.8
PFO			
$q_{e,\,cal}$ (mg g^{-1})	1.42	1.28	1.99
k_1 (min^{-1})	8.66x10^{-3}	10.6x10^{-3}	9.63x10^{-3}
R^2	0.887	0.891	0.946
PSO			
$q_{e,\,cal}$ (mg g^{-1})	11.3	11.6	11.8
k_2 (g mg^{-1}min^{-1})	2.49x10^{-2}	3.84x10^{-2}	1.98x10^{-2}
R^2	0.999	0.999	0.999
IPD			
I stage			
k_{dif1} (mg g^{-1}min$^{-0.5}$)	0.137	0.299	0.217
C_1	9.20	8.51	9.05
R^2	0.931	0.707	0.908
II stage			
k_{dif2} (mg g^{-1}min$^{-0.5}$)	0.005	0.004	0.025
C_2	11.1	11.3	11.1
R^2	0.901	0.741	0.389

A similar trend was observed for MG adsorption, where hemp also showed the highest k_2 value, while sorghum displayed slightly slower kinetics. Nevertheless, both biosorbents reached equilibrium within the same time interval. In contrast to PSO, the PFO model showed a poorer fit, as reflected by lower correlation coefficients and significant deviations between experimental and calculated q_e values, suggesting that physisorption alone does not

adequately describe the systems. The results obtained from the IPD model revealed multi-linear plots with positive intercepts, confirming that intra-particle diffusion is not the sole rate-controlling step in the biosorption processes. The positive intercepts further indicate the contribution of boundary layer (film) diffusion, particularly during the initial stages of biosorption. Although intra-particle diffusion may contribute to the internal transport of dye molecules within the biosorbent particles, the results suggest that its contribution is secondary and does not govern the overall biosorption rate. This is further supported by the significant decrease in the correlation coefficient in the second stage of the IPD plots (MB removal by all biosobents and MG removal by hop), showing that the model does not adequately describe this stage of the process. Overall, the biosorption process appears to be primarily governed by chemisorption and surface adsorption, while film diffusion and intra-particle diffusion act as supporting mechanisms for all biosorbents used for MB and MG removal.

CONCLUSION

The investigated sorghum-, hemp-, and hop-based biosorbents showed similar potential for the removal of MB and MG from aqueous solutions. Biosorption was characterized by rapid initial uptake followed by a slower approach to equilibrium, with hemp exhibiting the fastest kinetics and the shortest equilibrium times. Kinetic modeling showed consistent trends for all three biosorbents, with the pseudo-second-order model providing the best fit for both dyes, indicating that chemisorption is the dominant mechanism. In contrast, the pseudo-first-order model showed a poorer fit to the experimental data. The intra-particle diffusion model suggested that biosorption proceeds through multiple stages and is not governed solely by intraparticle diffusion. Positive intercepts indicated the contribution of boundary layer diffusion, particularly at the early stages of biosorption. Overall, the process is controlled by a combination of surface biosorption and diffusion mechanisms.

ACKNOWLEDGEMENT

This research has been financially supported by the Ministry of Science, Technological Development and Innovation of Republic of Serbia (Contract No. 451-03-33/2026-03/200026).

REFERENCES

[1] Tkachenko O., Li H., Dobele G., *et al*., React. Funct. Polym. 2025, 213, 106275.
[2] Yadav S., Asthana A., Singh A.K., *et al*. J. Hazard. Mater. 2021,409, 124840.
[3] Salah Omer A., El Naeem G.A., Abd-Elhamid AI., *et al*. J. Mater. Res. Technol. 2022, 19, 3241–3254.
[4] Muinde, V.M., Onyari, J.M., Wamalwa, B., *et al*. Environ. Chem. Ecotoxicol. 2020, 2 115–125.
[5] Halysh, V., Sevastyanova, O., Pikus, S., *et al*. Cellulose. 2020, 27(14), 8181–8197.
[6] Perendija J., Milošević D., Popović M., *et al*. Hem. Ind. 2024, 78(3), 253–264.

EcoTER'26
eco.tfbor.bg.ac.rs
32nd International Conference
Ecological Truth & Environmental Research
24–26 June 2026, Hotel Sunce,
Sokobanja, Serbia

Review

MECHANISMS AND FACTORS INFLUENCING Ni(II) BIOSORPTION BY BACTERIAL EXOPOLYSACCHARIDES: A REVIEW

DOI: 10.5937/EcoTER26266L

Verica Ljubić[1,a*], Jovana Perendija[1,b], Dragana Milošević[1,c], Željka Milovanović[1,d], Slobodan Cvetković[1,e], Katarina Trivunac[2,f]

[1] Institute of Chemistry, Technology and Metallurgy, University of Belgrade, Njegoševa 12, 11000 Belgrade, SERBIA

[2] Faculty of Technology and Metallurgy, University of Belgrade, Karnegijeva 4, 11000 Belgrade, SERBIA

[a] https://orcid.org/0000-0002-8648-6421 [b] https://orcid.org/0000-0002-6318-9053

[c] https://orcid.org/0000-0003-3548-6832 [d] https://orcid.org/0000-0002-1998-5239

[e] https://orcid.org/0000-0003-4417-4443 [f] https://orcid.org/0000-0002-9251-744X

Abstract

This review paper analyses the biosorption of Ni^{2+} ion by using unmodified bacterial exopolysaccharides (EPS), based on data from available literature, while this system has been investigated less compared to other heavy metals. Nickel is important both as a potential pollutant and as essential microelement in the function of biocatalysts and nickel-enzymes. The focus of the paper is the influence of the chemical composition of EPS, its spatial organization, as well as the role of pH value and the hydration radius of Ni^{2+} ion in bonding process. The mechanisms of the biosorption for EPS of different composition were analyzed and proposed in relation to the structural and chemical characteristics of the system, and their interpretation is related to the Langmuir and Freundlich isotherm model. The review of the literature shows that bacterial EPS have a significant biosorption potential toward Ni^{2+} ion and that biosorption of Ni^{2+} ion with bacterial EPS is the result of several simultaneous mechanisms, where the composition and structure of EPS play a key role.

Keywords: bacterial EPS, heavy metals, nickel removal, biosorption.

INTRODUCTION

A significant environmental problem today is water pollution with heavy metals, due to their toxicity, persistence and accumulation in living organisms. Finding a solution for this problem is becoming one of the most attractive areas for researchers around the world. Due to the limitation of conventional methods for removal of heavy metal ions from aqueous solutions, biosorption has attracted increasing attention in recent years as an efficient, cost-effective and environmentally friendly approach for the water treatment [1].

Among the various biosorbents, bacterial EPS are recognized as particularly interesting biomaterials, as evidenced by the growing number of researches in this area [2]. EPS represents polysaccharide biopolymers of high molecular weight that microorganisms excrete

* *verica.ljubic@ihtm.bg.ac.rs*

into the external environment in order to survive in stressful external conditions, and they can be synthetized by both Gram-positive and Gram-negative bacteria, including non-pathogenic, pathogenic and probiotic bacterial strains [3]. The potential of EPS as a biosorbents is related to the presence of the functional groups, such as hydroxyl, carboxyl, phosphate and amino groups, which enable interaction with heavy metal ions [1,4]. Additional advantages of bacterial EPS are biocompatibility, relatively simple, environmentally friendly and economical isolation, as well as the possibility of application without chemical modification [5].

Although EPS have been studied in the biosorption of various heavy metal ions, including Pb^{2+}, Cd^{2+}, Zn^{2+}, etc., the biosorption of Ni^{2+} ions by bacterial EPS is still insufficiently researched [6]. Nickel has significant industrial importance and is frequently released into the environment, while at the same time it is an essential trace element involved in the function of certain nickel-enzymes. Therefore, the development of efficient biosorption systems for the removal of Ni^{2+} ions is of particular importance.

The aim of this review paper is to analyze and compare available research on Ni^{2+} ion biosorption using bacterial EPS, with a focus on removal efficiency (adsorption capacity), the influence of experimental conditions on biosorption, and possible mechanisms of EPS-Ni^{2+} ion interaction.

MATERIALS AND METHODS

Data used in this review paper were collected by searching scientific databases, such as Scopus, SpringerLink, Web of Science, ScienceDirect and PubMed. Relevant scientific papers and review articles related to the adsorption of nickel ions with unmodified bacterial EPS, adsorption capacities and adsorption mechanisms were analyzed. The literature search was performed by using key words related to ‘bacterial EPS’, ‘nickel adsorption’, ‘heavy metal removal’, ‘exopolysaccharides’ and ‘biosorption’. The comparative analysis includes 12 scientific papers published in period 2008-2024, while the remaining literature was used to interpret the results and discuss the mechanism.

RESULTS AND DISCUSSION

Comparative analysis of Ni^{2+} biosorption with bacterial EPS

A comparative overview of the biosorption properties of bacterial exopolysaccharides towards Ni^{2+} ions is presented in the Table 1. The table summarizes the available literature data on the biosorption of Ni^{2+} ions by chemically unmodified bacterial EPS, including EPS-producing bacterial strains and their Gram type, chemical characteristics of EPS and basic biosorption parameters. It is important to note that due to variations in experimental conditions across studies, the reported data are not directly comparable in a strict quantitative sense.

The influence of chemical composition of EPS

The differences in the values of maximum adsorption capacity (q_{max}) and efficiency of Ni^{2+} ion removal (R, %) between different EPS indicate that the chemical composition of EPS have a significant influence on their adsorption properties.

Table 1 *Comparative analysis of Ni^{2+} ion biosorption with bacterial EPS*

Bacterial source of EPS	Gram-type	Chemical characteristics/ functional groups	pH	q_{max}, mgg^{-1}	R, %	Isotherm	Reference
Alteromonas sp. JL2810	G-	Uronic acids Neutral sugars Groups C=O, C-O-C, OH	5,0	344,8	n.r.	Langmuir	[7]
Klebsiella oxytoca J7	G-	Neutral sugars Uronic acids Aminosugars	5,5	270,0	99,3	Langmuir	[8]
Lactobacillus reuteri B2	G+	Neutral sugars	8,0	161,0	93,0	Langmuir	[9]
Rhodococcus rhodochorus 202 DSM	G+	Neutral sugars Lipids, Proteins Groups C=O, -O-C=O, C-N, amino, amide	6,5	154,1	n.r.	Freundlich	[10]
Rhodococcus opacus 89 UMCS	G+	Neutral sugars Lipids, Proteins Groups C=O, -O-C=O, amino, amide	6,5	129,3	n.r.	Freundlich	[10]
Jeotgalicoccus huakuii	G+	Groups OH, COOH, Amino, amid, phosphate	5,0	81,0	91,0	Langmuir	[11]
Serratia plymuthica As3-5a	G-	Groups C=O, C=C, C-N, N-H	6,6	80,5	91,5	Freundlich	[12]
Ensifer meliloti MS-125	G-	Neutral sugars Uronic acids	6,0	54,0	85,0	Langmuir	[13]
Agrobacterium tumefaciens F2	G-	Neutral sugars Proteinaceous components Groups C=O, C-O-C	6,0	51,3	78,0	Langmuir	[14]
Serratia plymuthica SC3i	G-	Groups C=O, C=C, C-N, N-H	6,6	33,5	89,4	Freundlich	[12]
Pseudomonas aureginosa MTCC 1688	G-	Uronic acids Neutral sugars Proteins Groups C=O; amino/amide	6,0	26,7	9,0	n.r.	[15]
Paenibacillus jamilae	G+	Neutral sugars Uronic acids Acetic/pyruvic acids Aminosugar Proteins	5,5	17,7	n.r.	Freundlich	[16]
Mixed bacterial culture	G-	n.r.	n.r.	3,3	66,6	n.r.	[17]
Pseudomonas fluorescens	G-	Neutral sugars Uronic acids	n.r	1,45	29,5	Freundlich	[18]

Table compiled and organized by the author from data reported in the literature.

Higher values of capacities and removal efficiencies were generally observed for EPS of heterogeneous composition, mainly for those with a large proportion of anionic functional groups, such as carboxyl groups. Carboxyl groups mainly originate from uronic acids, which are more commonly present in EPS with certain Gram-negative bacteria [4]. This can be linked to the specific structure of their cell wall, whose certain parts (outer membrane)

contains lipopolysaccharides that are rich in phosphates and carboxyl groups, which may contribute to the synthesis of more negatively charged EPS [3]. The Gram-type of the EPS-producing bacterium does not appear to directly determine Ni^{2+} biosorption efficiency, although Gram-negative strains more frequently produce anionic EPS.

The best adsorption capacity for Ni^{2+} ions has EPS from a Gram-negative bacterial strain *Alteromonas* JL2810, which contains a high proportion of uronic acids [7]. The chemical composition of EPS depends on the bacterial strain, its genetic potential for polysaccharide synthesis, as well as on environmental conditions that can affect the expression of biosynthetic pathways and the structures of the produced EPS.

However, anionic functional groups are not the only factor determining the efficiency of Ni^{2+} ion adsorption on EPS. This is clearly observed in EPS from Gram-positive bacterial strain *L. reuteri* B2 composed predominantly of neutral sugars, which also had a high adsorption capacity [9]. These results suggest that, besides chemical composition, the structural organization of the EPS matrix significantly influences adsorption of Ni^{2+} ions. The spatial arrangement of EPS polysaccharide chains can form 3D networks with interchain pores and microcavities that enable physical entrapment of Ni^{2+} ions within the EPS matrix [3]. Such structural organization may increase the accessibility of binding sites, in addition to the abundance of charged functional groups on the EPS surface. Additionally, such interactions can be influenced by the high hydration energy of the Ni^{2+} ions [16] and the resulting stable hydration shell which contributes to their effective hydration radius and may affect their mobility and diffusion through the EPS matrix, thereby influencing the overall adsorption efficiency.

In addition to carboxyl groups originating from uronic acids, other functional groups such as amino, amide and phosphate groups can also significantly participate in Ni^{2+} ion adsorption [1,4]. The presence of these groups increases the number and diversity of potential active sites for Ni^{2+} ion binding through electrostatic interactions, complexation, or ion exchange, thereby contributing to the overall adsorption capacity [1,16]. This is especially important for systems where the proportion of anionic functional groups is limited. Amide groups are commonly associated with protein components present in EPS matrix. Protein and lipid components may additionally increase the heterogeneity of EPS and contribute to Ni^{2+} ions binding [3], providing oxygen- and nitrogen-containing donor groups. This is, according to the table, especially pronounced in two EPS from *Rhodococcus* strains (*R. opacus* and *R. rhodochorus*), which, although they predominantly contain neutral sugars in their composition, have a high adsorption capacity for Ni^{2+} ions due to the presence of protein and/or lipid components [10]. In addition, the presence of aminosugars in the EPS structure, as in EPS from *K. oxytoca* J7 strain [8], may also contribute to the increased adsorption capacity, because they introduce additional active sites (functional groups) capable of the interaction with Ni^{2+} ions. Abundantly present hydroxyl groups in the EPS can contribute to the formation of hydrogen bonds and stabilizations of 3D polysaccharide network, which indirectly affects the availability of binding sites. Therefore, the adsorption efficiency of EPS toward Ni^{2+} ions cannot be explained solely by the presence of uronic acids, but rather to the combined contribution of multiple functional groups and the overall structural organization of the EPS.

The influence of the pH on the Ni^{2+} ion biosorption with bacterial EPS

The presented results indicate that the adsorption capacity of EPS towards Ni^{2+} ions does not depend exclusively on the pH value, but on the interaction between the environment and the chemical composition and structure of the EPS. Adsorption experiments in all the above studies were performed at pH values of 5-8. At pH values above 8, hydrolysis of Ni^{2+} ions and formation of nickel hydroxide speciation occur, which may interfere with the interpretation of adsorption result, due to possible microprecipitation and precipitation phenomena. At pH below 5, protonation of EPS functional groups, carboxyl and amino groups, is dominant, which consequently leads to a decrease in the number of negatively charged active sites for Ni^{2+} ion binding [1,3]. At the same time, the concentration of H^+ is increased, which can lead to competition with Ni^{2+} ions for active sites on EPS.

The highest adsorption capacities were observed with EPS rich in uronic acids, or with uronic acids and aminosugars, EPSs from *Alteromonas sp*. JL2810 and *Klebsiella oxytoca* J7, which showed high efficiency of Ni^{2+} ion removal and high adsorption capacities at pH values 5,0-5,5. This can be associated with a favorable degree of deprotonation of carboxyl groups at this pH values, while the formation of hydroxide species is still limited.

EPS predominantly composed of neutral sugars (EPS from *Lactobacillus reuteri* B2) showed high adsorption capacity, which is expressed at pH 8,0 when a larger number of functional groups are in the deprotonated form. These results indicate that, in addition to the ionization of functional groups, the spatial organization of the EPS matrix is also significant, as it may increase the accessibility and exposure of active sites for Ni^{2+} ion binding and consequently enhance adsorption efficiency. In contrast, lower values of adsorption capacity were observed for EPS with a combination of neutral sugars and uronic acids at pH 6–7. These results suggest that adsorption efficiency cannot be explained solely by the ionization of carboxyl groups, since the spatial organization of EPS and accessibility of active sites within the EPS matrix may also significantly influence Ni^{2+} ion binding and adsorption efficiency

Proposed mechanisms of Ni^{2+} ion biosorption with bacterial EPS

In Figure 1, a schematic overview of the proposed Ni^{2+} ion biosorption mechanisms in relation to EPS composition and structure is presented.

The interaction of Ni^{2+} ions with EPS mostly includes several simultaneous mechanisms, in which the dominant role is played by electrostatic interaction, ion exchange and complexation of Ni^{2+} ions with functional groups of EPS [1,16]. Carboxyl (COO^-), phosphate (PO_4^{3-}) and pyruvyl groups (CH_3COCOO^-) contribute to the negative charge of the EPS surface and enable the binding of cations through electrostatic attraction and coordination interactions. Binding of Ni^{2+} ions to negatively charged functional groups can be also accompanied by the replacement of previously bound cations or protons from the EPS surface (ion exchange). Hydroxyl (OH^-), carbonyl (C=O), amino ($-NH_2$) and amide (-CONH-) groups can also participate in metal coordination via oxygen and nitrogen donor atoms [16].

In addition to the chemical composition, the spatial organizations, porosity and crosslinking degree of EPS matrix play an important role which affect the availability of active sites for ion binding and diffusion processes. Due to the strong hydration of Ni^{2+} ion,

its mobility through the dense and less porous parts of the EPS matrix can be limited, while the structure of the polysaccharide network can contribute to ions retention in the interchain spaces.

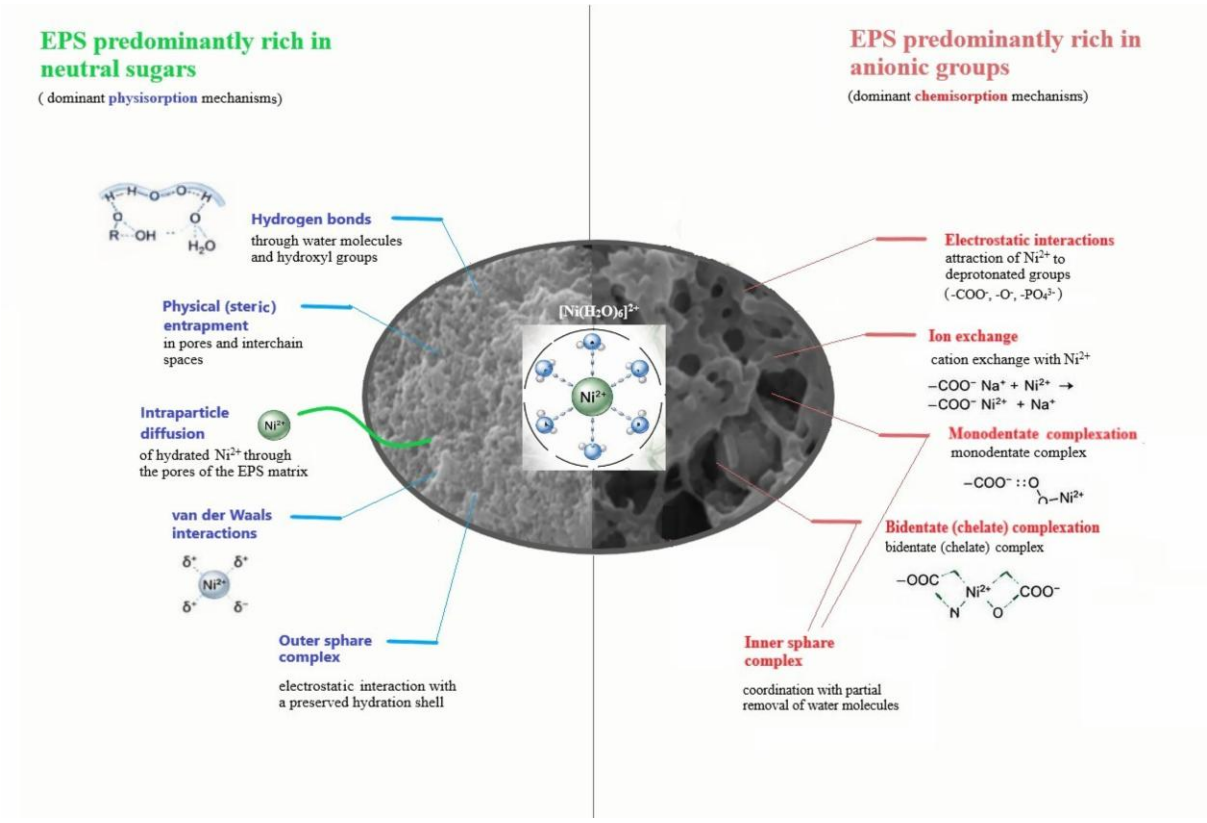

Figure 1 *Proposed mechanism of Ni^{2+} ion biosorption with bacterial EPS*

Although interparticle diffusion and physical trapping of Ni^{2+} ions may be more pronounced in EPS predominantly rich in neutral sugars, these mechanisms can also occur in anionic EPS, but are generally secondary in relation to binding via functional groups.

Although Langmuir's model frequently describes Ni^{2+} ion biosorption with EPS dominantly rich in neutral sugars, like from *L. reuteri* B2, the successful application of the model was also recorded in systems with more structurally complex EPS, with uronic acids, aminosugars and other components, like EPS from K. *oxytoca* J7, *Alteromonas sp*. JL2810 and *A. tumefaciens* F2. On the other hand, Freundlich's model better described biosorption with EPS which, in addition to the saccharide components, also contained other substituents such as proteinaceous and lipid components, acetyl and pyruvyl groups. This indicate that the chemical composition of EPS by itself is not sufficient for the prediction of the isothermal model, but rather the dominance and availability of certain type of binding sites and bonds that are realized with Ni^{2+} ions.

CONCLUSION

The biosorption of Ni^{2+} ions by bacterial EPS is a complex process governed by a combination of chemical composition, structural organization and environmental conditions.

Functional groups such as carboxyl, phosphate, hydroxyl, amino, carbonyl and amide groups play a central role in the binding of Ni^{2+} ions through electrostatic interactions, surface complexation and ion exchange. However, the adsorption behaviour is additionally influenced by the porosity of EPS, the degree of cross-linking, and the heterogeneity of the matrix, which determine the availability of active sites, diffusion processes and possible physical retention of hydrated Ni^{2+} ions within the EPS matrix. Differences in the composition of bacterial EPS, including the presence of proteins, lipids, uronic acids and pyruvic or acetyl substituents, contribute to differences in adsorption efficiency and agreement with isotherm models. Accordingly, the Langmuir and Freundlich models can reflect different degrees of homogeneity and heterogeneity of binding sites, while the chemical composition of EPS is not a reliable indicator of the type of adsorption behaviour. Overall, a better understanding of the relationship between the structure of bacterial EPS and the adsorption mechanisms represents an important step towards more efficient application of microbial EPS as sustainable biosorbents for the Ni^{2+} removal from water.

ACKNOWLEDGEMENT

This research has been financially supported by the Ministry of Science, Technological Development and Innovation of Republic of Serbia (Contract No. 451-03-33/2026-03/200026).

REFERENCES

[1] Wang, J., Chen, C. Biotechnol. Adv. 2009, 27(2), 195–226.

[2] Wang, W. Chem. Biol. Technol. Agri. 2023, 10(1), 137.

[3] Flemming, H.C., Wingender, J. Nat. Rev. Microbiol. 2010, 8(9), 623–633.

[4] Flemming, H.C., Wingender, J. Water Sci Technol. 2001, 43(6), 1–8.

[5] Pagliaccia, B. J. Hazard. Mater. 2022, 424(C), 126661.

[6] Gupta, P., Batul D. Biotechnol. Rep. 2017, 13, 58–71.

[7] Zhang, Z. Mar. Drugs. 2017, 15(6), 175.

[8] Ljubić, V. J. Polym. Environ. 2023, 32(3), 1105–1121.

[9] Ljubić, V. Biomass. Convers. Biorefin. 2022, 14(10), 11523–11538.

[10] Dobrowolski, R. Bioresour. Technol. 2017, 225, 113–120.

[11] Munir, A. Chemosphere. 2024, 351, 141170.

[12] Zanetti, R. Water. 2017, 14(21), 3410.

[13] Lakzian, A. Asian J. Chem. 2008, 20(8), 6075–6080.

[15] Chug, R. Biochem. Biophys. Rep. 2021, 26, 100972.

[16] Morillo Pérez, J.A. World J. Microbiol. Biotechnol. 2008, 24(11), 2699–2704.

[17] Gawali, A. Int. J. Life Sci. 2014, 2(4), 373–77.

[18] Nkoh, J. Colloids. Surf. B. 2019, 183.

EcoTER'26
eco.tfbor.bg.ac.rs
32nd International Conference
Ecological Truth & Environmental Research
24–26 June 2026, Hotel Sunce,
Sokobanja, Serbia

Original Research

ENZYMATIC DEGRADATION OF PHENOL VIA HRP PERIODATELY IMMOBILIZED ONTO GMA-CO-EGDMA MACROPOROUS CARRIERS

DOI: 10.5937/EcoTER26273B

Dunja Banđur[1,a*], Radivoje Prodanović[2,b], Milica Spasojević Savković[3,c], Mira Stanković[1,d], Dragana Bartolić[1,e], Olivera Prodanović[1,f], Nevena Surudžić[1,g]

[1] University of Belgrade, Institute for Multidisciplinary Research, National Institute of the Republic of Serbia, Kneza Višeslava 1, 11030 Belgrade, SERBIA

[2] University of Belgrade, Faculty of Chemistry, Studentski trg 12-16, 11000 Belgrade, SERBIA

[3] University of Belgrade, Innovative Centre of the Faculty of Chemistry, Studentski trg 12-16, 11000 Belgrade, SERBIA

[a] https://orcid.org/0009-0008-2782-7629 [b] https://orcid.org/0000-0003-4662-1825

[c] https://orcid.org/0000-0001-9134-6637 [d] https://orcid.org/0000-0003-0084-3158

[e] https://orcid.org/0000-0002-9337-9288 [f] https://orcid.org/0000-0003-4460-5485

[g] https://orcid.org/0000-0002-0544-6365

Abstract

Wastewater contamination remains a critical environmental challenge, prompting extensive research into the application of immoblized enzymes for remediation. Horseradish peroxidase (HRP), a widely utilized enzyme, exhibits enhanced stability and reusability when tethered to a solid support. In this study, macroporous poly(GMA-co-EGDMA) copolymers were synthesized via dispersion polymerization and functionalized with ethylenediamine. HRP was then immobilized through the periodate method and tested for the removal of phenol in a batch reactor. The resulting biocatalyst has maintained rellatively high activity during four cycles of repeated use.

Keywords: wastewater treatment, phenol, HRP, periodate, macroporous beads.

INTRODUCTION

As urban and industrial growth continues to strain the environment, water pollution has emerged as a critical global challenge. Daily, industrial effluents, agricultural runoff, and poor waste management discharge heavy metals, toxic compounds, and organic pollutants into water bodies. Among these contaminants, phenols and phenolic compounds are of particular interest due to their toxicity, persistence and resistance to natural degradation [1]. Therefore, the development of efficient methods for their removal from wastewater has become a critical area of environmental research.

A wide range of enzymes immobilized on different carriers is frequently used for these purposes. By attaching the enzyme to a solid support, enhanced stability and improved reusability can be observed [2]. Among numerous plant-derived enzymes, horseradish

* *dunja.bandjur@imsi.bg.ac.rs*

peroxidase (HRP) is particularly notable as one of the most frequently used peroxidases in these applications [3].

Numerous methods have been developed for the immobilization of HRP, which can be broadly classified into four major groups: adsorption, covalent binding, entrapment and cross-linking. By applying covalent binding, strong linkage between the enzyme and carrier is achieved, thus preventing the leakage and increasing stability and stereospecificity [4].

Carriers, including biopolymers, synthetic polymers and inorganic materials are used for the purpose of enzyme immobilization. There is a growing preference for the usage of synthetic polymers due to their well-defined chemical composition and superior purity. By selecting appropriate monomer units, synthetic polymers can be engineered to exhibit specific mechanical properties, stability and porosity required for a given application. Another advantage of these materials is that they contain different functional groups on the surface (carboxyl, hydroxyl, epoxy, amine etc.), which can be further subjected to the surface modification [5].

MATERIALS AND METHODS

Materials

For the copolymer synthesis, glycidyl methacrylate (GMA), ethylene glycol dimethacrylate (EGDMA), 1-dodecanol and cyclohexanol were purchased from Sigma Aldrich (St. Louise, Mo, USA). Horseradish peroxidase (150–250 U/mg), sodium periodate and pyrogallol were also obtained from Sigma Aldrich and used for enzyme immobilization. Ethylenediamine, used for the amination of copolymer samples, was sourced from Merck (Kenilworth, New Jersey, USA), while hydrogen peroxide was procured from AppliChem GmbH (Darmstadt, Germany).

Copolymer Preparation and Amination

To synthesize the copolymer, a contionous phase of 2.78 wt% PVP (Mw = 24 000 g/mol) in ethanol was heated to 70 °C. A mixture containing GMA/EGDMA monomers (5.0 g, 90/10 ratio), AIBN initiator (0.05 g) and inert porogens (2.25 g of 1-dodecanol and 2.25 g of cyclohexanol) was added and stirred for 6 hours. The resulting copolymer was rinsed five times with ethanol and air-dried. Copolymer was resuspended in toluene and further subjected to amination with ethylenediamine. The samples were washed with ethanol and water until reaching pH 6 and then oven-dried at 50 °C. Amino group concentrations were subsequently quantified via acid-base titration.

Copolymer Characterization

The pore size distribution of the poly(GMA-co-EGDMA) copolymers was determined using mercury porosimetry (Carlo Erba 2000, software Milestone 200). Surface morphology was further characterized via scanning electron microscope (Tescan FE-SEM Mira 3 XMU).

Horseradish Peroxidase Immobilization by Glutaraldehyde Method

To immobilize the enzyme, aminated copolymers were deaerated for 10 minutes, washed twice with 0.1 mol/L sodium phosphate buffer pH 7.0, and incubated in glutaraldehyde for 2 hours. Horseradish peroxidase was then added at concentration of 25 mg/g. Following

incubation, the samples were washed twice, resuspended in the same phosphate buffer, and stored at 4 °C.

Horseradish Peroxidase Immobilization by Periodate Method

To immobilize the enzyme via periodate oxidation, HRP was first oxidized with 50 mmol/L sodium periodate in sodium acetate buffer (pH 5.0) and dialyzed overnight. Aminated copolymer particles were deaerated, rinsed with 0.1 mol/L sodium phosphate buffer pH 7.0, and incubated with appropriate concentration of oxidized HRP (25 mg/g) for 48 hours. Following incubation, the samples were washed and stored in phosphate buffer at 4 °C.

Enzyme Activity Studies

Peroxidase activity was measured spectrophotometrically at 420 nm (Shimadzu Corporation UV-2501PC, Japan). For the soluble enzyme assay, 10 µL of sample and 10 µL of H_2O_2 were added to 1 mL of pyrogallol (13 mmol/L). The immobilized enzyme assay utilized 9 mg of copolymer-bound HRP, 30 µL of H_2O_2 and 3 mL of pyrogallol. Filltered aliquots were analyzed at 60-second intervals to determine activity.

Phenol removal

Phenol removal with immobilized HRP was conducted in a batch reactor by introducing appropriate amount of immobilizate into phenol solution (2 mmol/L in 50 mmol/L Tris-HCl buffer pH 7). For in situ delivery of hydrogen peroxide, glucose oxidase (0.187 U/mL) and glucose (3 mmol/L) were used. Aliquots were collected every 60 seconds, mixed with potassium hexacyanoferrate (III) and 4-aminoantipyrene. Following 10 minutes of color development, absorbance was measured at 510 nm. Phenol concentration was then quantified using a standard calibration curve.

RESULTS AND DISCUSSION

The diblock copolymers of glycidyl methacrylate and ethylene glycol dimethacrylate were synthesized by dispersion polymerization, which leads to the formation of spherical particles with pore size diameter of around 90 nm. SEM image of macroporous beads and chemical structure of copolymer are presented in Figure 1.

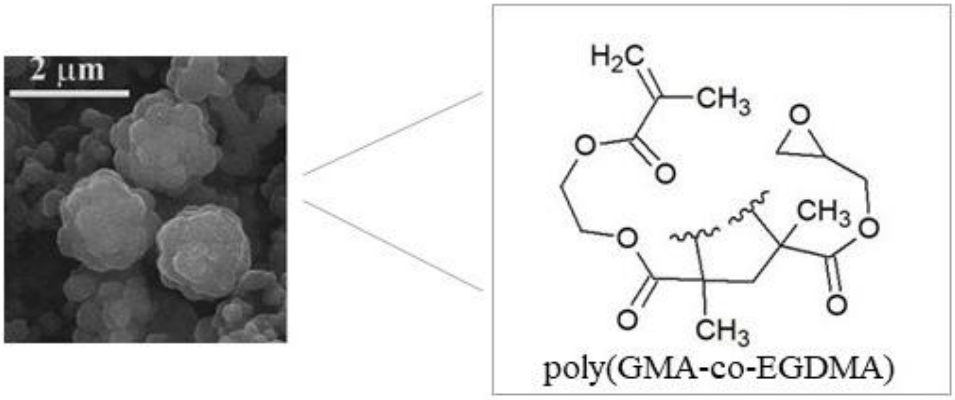

Figure 1 *SEM image and chemical structure of macroporous copolymers*

This study compares two methods for the immobilization of horseradish peroxidase (HRP) onto macroporous copolymers: the periodate method, which covalently bonds the enzyme's carbohydrate moiety to a copolymer surface, and the glutaraldehyde method, which attaches the enzyme to an activated carrier via its surface amino groups. An appropriate amount of HRP was added per gram of the copolymer (25 mg/g) and specific activity of immobilized enzyme was calculated (Table 1).

Table 1 *Specific activities of HRP immobilized by glutaraldehyde and periodate method*

	Glutaraldehyde method	Periodate method
Enzyme activity (U)	0.027	0.072
Specific activity (U/g)	2.96	7.36
Specific activity (50 mg of polymer)	148.05	367.87

Results presented in Table 1 show that higher specific activity was achieved by using periodate method (7.36 U/g) compared to the glutaraldehyde method (2.96 U/g). This biocatalyst was used for the removal of phenol in a batch reactor. As previously described in our research [6], higher phenol removal efficiency can be observed when using system composed of glucose oxidase (GOx) and glucose for the delivery of hydrogen peroxide into the reaction mixture for phenol removal. Oxidation reaction in the presence of glucose and GOx is presented in Figure 2. Hydrogen peroxide is essential for peroxidase-catalyzed reactions because it oxidizes the native enzyme. This activation enables the enzyme to accept and oxidize phenolic compounds at its active state.

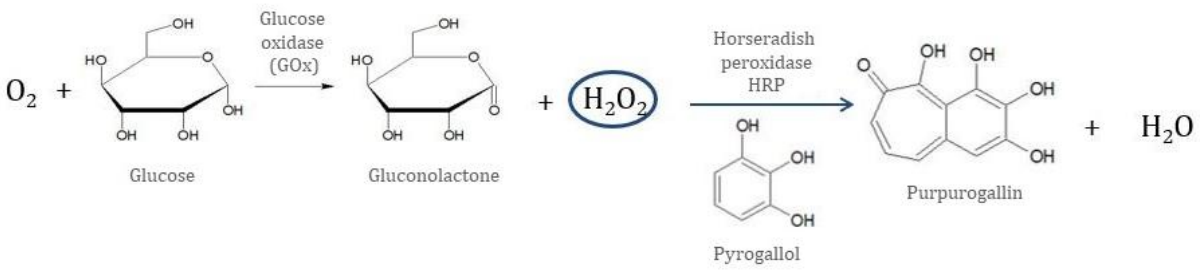

Figure 2 *Hydrogen peroxide oxidation in the presence of glucose and glucose oxidase*

Within five hours of repeated use of 25 mg/g HRP immobilized on macroporous beads in a batch reactor with the hydrogen peroxide delivery system composed of 0.187 U/mL of glucose oxidase and 3 mmol/L of glucose, efficiency of phenol removed in the solution was 35% (Figure 3).

To evaluate operational stability, immobilized HRP (25 mg/g) was tested over multiple phenol removal cycles. Results presented in Figure 4 indicate that enzyme could be reused for up to four cycles, with efficiency and activity monitored after each use. After four consecutive cycles, the immobilized enzyme retained 45% of its initial activity.

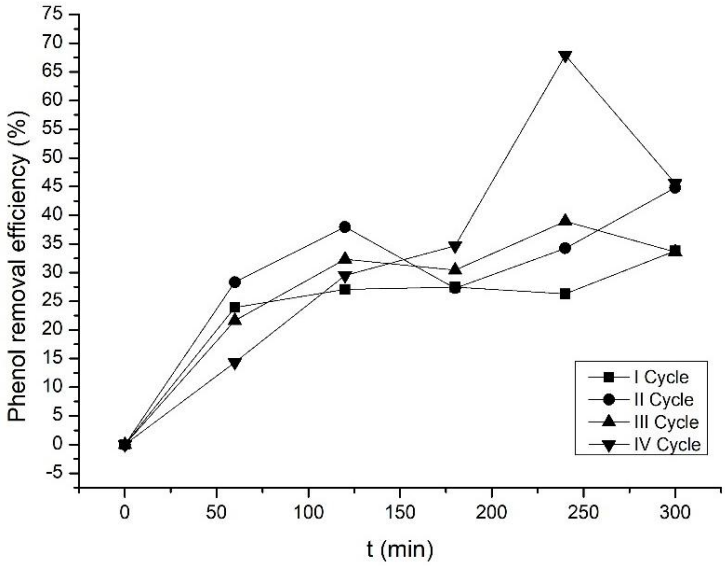

Figure 3 *Phenol removal in a batch reactor by periodate-immobilized HRP*

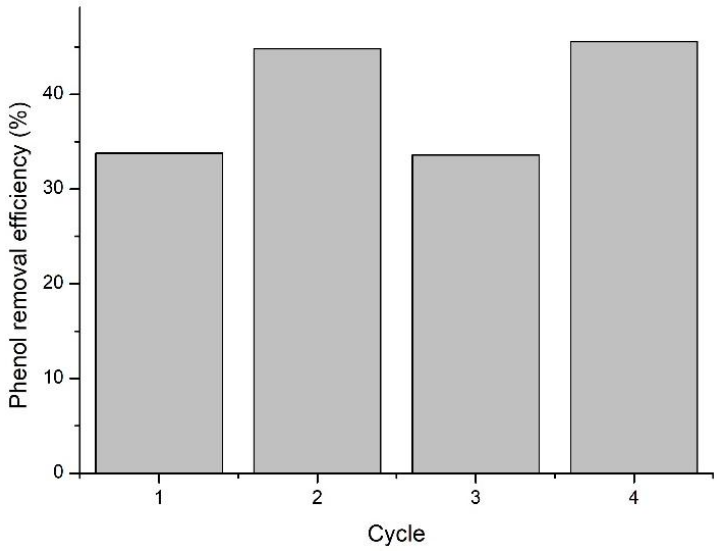

Figure 4 *Operational stability of immobilized HRP onto microporous beads*

CONCLUSION

Macroporous copolymers of glycidyl methacrylate and ethylene glycol dimethacrylate were synthesized by dispersion polymerization, resulting in 90 nm spherical particles. In comparing immobilization strategies for horseradish peroxidase, the periodate method yielded higher specific activity than the glutaraldehyde method. Periodate-immobilized HRP (25 mg/g) was tested for the removal of phenol in a batch reactor. Using glucose/glucose oxidase system for controlled hydrogen peroxide delivery, the residual phenol concentration reached 75.55 mmol/L after five hours of repeated use. The biocatalyst maintained 45% of its initial activity after four consecutive cycles.

ACKNOWLEDGEMENT

This work was supported by the Ministry of Science, Technological Development and Innovation of the Republic of Serbia (Grant No. 451-03-33/2026-03/200053, University of Belgrade, Institute for Multidisciplinary Research).

REFERENCES

[1] Bayramoglu, G., Arica, M.Y. J. Hazard. Mater. 2008, 156, 148–155.

[2] Magnin, D., Dumitriu, S., Chornet, E. J. Bioact. Compat. Polym. 2003, 18, 355–373.

[3] Alemzadeh, I., Nejati, S. J. Hazard. Mater. 2009, 166, 1082–1086.

[4] Fernández-Lorente, G., Terreni, M., Mateo, C., *et al*. Enzyme Microb. Technol. 2001, 28 (4–5), 389–396.

[5] Prodanović, R.M., Milosavić, N.B., Jovanović, S.M., *et al*. J. Serb. Chem. Soc. 2006, 71 (4), 339–347.

[6] Pantić, N., Spasojević, M., Stojanović, Ž., *et al*. J. Polym. Environ. 2022, 30 (7), 1–16.

EcoTER'26
eco.tfbor.bg.ac.rs
32nd International Conference
Ecological Truth & Environmental Research
24–26 June 2026, Hotel Sunce,
Sokobanja, Serbia

Original Research

SORPTION OF TEXTILE DYES ONTO BISMUTH-MODIFIED WOOD WASTE SORBENT: KINETIC AND EQUILIBRIUM ANALYSIS

DOI: 10.5937/EcoTER26279V

Nena Velinov Georgiev[1,a*], Miljana Radović Vučić[1,b], Milica Petrović[1,c], Miloš Kostić[1,d], Milan Momčilović[1,e], Jelena Mitrović[1,f], Aleksandar Bojić[1,g]

[1] University of Niš, Faculty of Science and Mathematics, Department of Chemistry, Višegradska 33, 18 000 Niš, SERBIA

[a] https://orcid.org/0000-0001-9043-8521 [b] https://orcid.org/0000-0001-6820-5844

[c] https://orcid.org/0000-0002-7537-0327 [d] https://orcid.org/0000-0001-6488-5184

[e] https://orcid.org/0000-0001-5370-0148 [f] https://orcid.org/0000-0001-9634-7727

[g] https://orcid.org/0000-0002-9853-2747

Abstract

Textile dye contamination in aquatic environments represents a major ecological issue due to its persistence, harmful effects on aquatic organisms, and possible risks to human health. In this work, wood waste modified with bismuth was evaluated as a low-cost sorbent for the removal of textile dyes Reactive orange 16 from water. Sorption behaviour was examined through kinetic and equilibrium analyses in order to better understand the interaction between the dye molecules and the sorbent surface. The obtained results were best described by the pseudo-second-order kinetic model and the Langmuir isotherm model ($r^2 \geq 0.99$), indicating predominantly monolayer sorption on homogeneous active sites. The prepared material exhibited a maximum sorption capacity of 415.22 mg/g, highlighting its potential application as an effective and sustainable sorbent for wastewater treatment.

Keywords: wood waste, modification, bismuth, sorption, textile dye.

INTRODUCTION

Water pollution represents one of the major environmental challenges due to its harmful effects on ecosystems and human health [1]. Among various pollutants, textile dyes are of particular concern because of their extensive industrial use, complex chemical structure, and resistance to natural degradation processes [2]. The discharge of untreated dye-containing wastewater into aquatic environments can reduce light penetration, disturb aquatic life, and introduce potentially toxic or mutagenic compounds into the ecosystem [3].

Conventional wastewater treatment methods are often insufficient for efficient dye removal, while advanced techniques may require high operational costs and complex infrastructure [4]. In recent years, sorption has gained attention as an efficient, economical, and environmentally friendly approach for wastewater treatment [5]. Waste-derived materials, such as wood waste, are especially promising sorbents due to their abundance, low cost, and presence of functional groups capable of binding pollutants.

* *nena.velinov@yahoo.com; nena.velinov@pmf.edu.rs*

Therefore, this study focused on the preparation of a bismuth-modified wood waste sorbent and the investigation of its potential for the removal of Reactive orange 16 dye through kinetic and equilibrium sorption analyses.

MATERIALS AND METHODS

Reagents

Reactive orange 16 was obtained from Sigma-Aldrich (USA) and used without any purification. $Bi(NO_3)_3x5H_2O$, HNO_3 and NaOH were of analytical grade and purchased from Merck (Germany).

Sorbent preparation

Wood waste used in this study was obtained from a furniture production facility located in Eastern Serbia. The collected sawdust was initially sieved, and particles within the 0.4–0.8 mm size range were selected and thoroughly rinsed several times with deionized water. The material was subsequently treated with 0.5 M NaOH solution for 90 min in order to modify the surface properties, followed by repeated washing with deionized water until the filtrate reached approximately neutral pH. For the chemical modification, 10 g of the pretreated sawdust was introduced into a solution containing 2.0 g of $Bi(NO_3)_3{\cdot}5H_2O$ dissolved in 30.0 cm³ of 2 M HNO_3. The suspension was stirred for 30 min, after which the solid phase was separated by filtration, rinsed four times with ultrapure water, and dried at 55.0 °C for 120 min.

Procedure

Fresh working solutions of the textile dye were prepared daily by dilution of the stock solution (1.00 g/dm^3). Sorption experiments were performed by contacting the dye solutions with the sorbent at a concentration of 2.0 g dm^{-3} under acidic conditions (pH 2.0). The pH of the mixtures was adjusted using NaOH and HNO_3 solutions. Samples of the dye solution were collected prior to sorption (0 min) and at predetermined time intervals of 1, 5, 10, 20, 40, 60, 90, 120, and 180 min. The residual dye concentration in the solutions was determined spectrophotometrically at 495 nm using a Shimadzu UV-1800 spectrophotometer. The amount of dye sorbed at time t, expressed as q_t (mg/g), was calculated according to the following equation:

$$q_t = \frac{(c_0 - c_t)\cdot V}{m} \tag{1}$$

where c_0 and c_t are the starting and final concentrations of the dye (mg/dm^3), respectively, V is volume of the solution (dm^3) and m is mass of the sorbent (g).

Sorption modelling

Kinetic and equilibrium experiments were performed using initial dye concentrations ranging from 10.0 to 500.0 mg/dm^3, while the sorbent dosage was maintained at 2.0 g/dm^3. To evaluate the sorption behavior of the prepared material, pseudo-first-order [7] and pseudo-second-order [8] kinetic models were employed for the analysis of sorption kinetics. Equilibrium data were further interpreted using the Langmuir [9], Freundlich [10], and Sips

[11] isotherm models. The nonlinear forms of the applied kinetic and isotherm equations (Table 1 and Table 2) were used for the calculation of sorption parameters, as nonlinear modeling provides a more accurate representation of the experimental data compared to linearized approaches.

RESULTS AND DISCUSSION

Kinetic study

The experimental results and calculated parameters obtained from the pseudo-first-order and pseudo-second-order kinetic models are shown in Table 1.

Table 1 *Kinetic parameters for dye sorption onto bismuth-modified wood waste*

Model	Equation	Parameter	Value			
Experimental		c_0 [a]	50.0	100.0	250.0	500.0
		$q_{e,\,exp}$ [b]	25.0	49.99	124.97	249.89
Pseudo-first order	$q_t = q_e(1 - e^{-k_1 t})$	$q_{e,\,cal}$ [c]	24.97	49.62	122.22	234.87
		k_1 [d]	2.67	1.06	0.64	0.15
		r^2	0.997	0.994	0.980	0.965
Pseudo-second order	$q_t = \frac{q_e^2 k_2 t}{1 + q_e k_2 t}$	$q_{e,\,cal}$	25.0	50.0	125.01	250.03
		k_2 [e]	4.08	1.96	1.05	0.27
		r^2	0.999	0.999	0.999	0.998

[a] c_0 – initial concentrations of the dye (mg/dm^3)
[b] $q_{e,\,exp}$ – experimental equilibrium sorption capacities (mg/g)
[c] $q_{e,\,cal}$ – calculated sorption capacities (mg/g)
[d] k_1 – pseudo-first order rate constants (1/min),
[e] k_2 – pseudo-first order rate constants (g/mg·min)

The equilibrium sorption capacities (q_e) predicted by both the pseudo-first-order and pseudo-second-order kinetic models were generally consistent with the experimentally determined values. However, the pseudo-second-order model provided q_e values that were in closer agreement with the experimental data and exhibited higher correlation coefficients (r^2 = 0.998–0.999) compared to the pseudo-first-order model (r^2 = 0.965–0.997). The pseudo-first-order model adequately described the sorption process at lower dye concentrations, where a large number of available active sites existed on the sorbent surface. In contrast, at higher concentrations, the applicability of this model decreased due to progressive occupation and saturation of the active sorption sites. The obtained results indicate that the pseudo-second-order kinetic model provides a better fit for the experimental data compared to the pseudo-first-order model in the case of dye sorption onto the bismuth-modified wood waste. This is supported by higher correlation coefficients and by the fact that the calculated q_e values are in closer agreement with the experimentally determined ones across all tested conditions.

Therefore, the pseudo-second-order model can be considered more appropriate for describing the investigated sorption system. These findings suggest that the sorption process depends on the concentration of dye in solution as well as on the amount accumulated on the sorbent surface at equilibrium. The rate-controlling step is likely associated with interactions involving electron sharing or exchange between the sorbent surface and dye molecules [12].

Equilibrium study

The calculated parameters obtained from the application of the Langmuir, Freundlich, and Sips isotherm models, together with the corresponding experimental results, are presented in Table 2.

Table 2 *Isotherm parameters for dye sorption onto bismuth-modified wood waste*

Model	Equation	Parameter	Value
Langmuir	$q_e = \frac{q_m K_L C_e}{1 + K_L C_e}$	q_m [c]	415.22
		K_L [d]	6.02
		r^2	0.999
Freundlich	$q_e = K_F c_e^{\frac{1}{n}}$	K_F [e]	225.21
		n_F [f]	6.58
		r^2	0.877
Sips	$q_e = \frac{q_m K_S C_e^{1/n}}{1 + K_S C_e^{1/n}}$	q_m	416.32
		K_S [g]	3.857
		n_S [h]	0.99
		r^2	0.998

[c] q_m – maximal sorbent capacity (mg/g), [d] K_L – Langmuir constant (dm^3/mg)
[e] K_F – Freundlich constant (dm^3/mg), [f] $1/n_F$ – Freundlich exponent
[g] K_S – Sips constant (dm^3/mg), [h] $1/n_S$ – Sips exponent

The Langmuir isotherm model showed the best agreement with the experimental data, with correlation coefficients exceeding 0.99, indicating that it describes dye sorption onto the bismuth-modified wood waste more accurately than the Freundlich model, which exhibited a lower r^2 value (0.877). This suggests that the sorption process predominantly occurs as monolayer coverage on a finite number of homogeneous active sites, with no further uptake once saturation is reached. The maximum sorption capacity estimated from the Langmuir model was 415.22 mg g^{-1} (Table 2).

In contrast, the Freundlich model did not adequately represent the experimental data due to its lower correlation coefficient, although the value of the Freundlich exponent (n_F = 6.58) indicates favourable sorption conditions, as it falls within the range of 1 to 10, suggesting a generally favourable interaction between sorbate and sorbent.

The Sips isotherm model also provided an excellent fit to the experimental data, with a high correlation coefficient (r^2 = 0.998) and a calculated equilibrium sorption capacity (416.32 mg g^{-1}) that closely matched the experimentally obtained value (Table 2). This confirms that the Sips model adequately describes dye sorption onto the bismuth-modified wood waste. As a hybrid model combining the Langmuir and Freundlich approaches, the Sips equation behaves like the Freundlich model at lower concentrations, while at higher concentrations it converges toward the Langmuir model, accounting for monolayer sorption on a finite number of active sites. The heterogeneity factor (n_S = 0.99) being close to unity indicates that the sorbent surface is nearly homogeneous. In practical terms, this suggests that the system behaviour approaches the Langmuir model, meaning that the equilibrium data can be effectively described by monolayer sorption assumptions [13].

CONCLUSION

A novel bismuth-modified wood waste sorbent was successfully synthesized and used for textile dye removal. The kinetic study revealed that dye sorption onto the prepared material follows the pseudo-second-order model, indicating that the process depends on both the concentration of dye in solution and the amount accumulated on the sorbent surface at equilibrium. Equilibrium data were best described by the Langmuir isotherm model, suggesting monolayer coverage on a homogeneous surface. The maximum sorption capacity of the bismuth-modified wood waste was determined to be 415.22 mg g^{-1}, demonstrating its potential applicability as an effective material for dye removal from aqueous solutions.

ACKNOWLEDGEMENT

The authors would like to acknowledge financial support from the Ministry of Science, Technological Development and Innovation of the Republic of Serbia (Agreement No 451-03-33/2026-03/200124 and 451-03-34/2026-03/200124).

REFERENCES

[1] Kaya, M., Wood. Sci. Technol. 2018, 52, 245–260.

[2] Leme, D.M., de Oliveira, G.A.R., Meireles, G., *et al*. Toxicol. Environ. Health. Part. A. 2015, 78, 287–300.

[3] Kadhom, M., Albayati, N., Alalwan, H., *et al*. Sustain. Chem. Pharm. 16 (2020) 100259.

[4] da Rocha Ferreira, G.L., Vendruscolo, F., Antoniosi Filho, N.R. Heliyon 2019, 5, e01450.

[5] Wang, J., Chen, N., Li, M., *et al.* J. Environ. Polym. Degrad. 2018, 26, 1559–1572.

[6] Adegoke, K.A., Adesina, O.O., Okon-Akan O.A., *et al.* Curr. Res. Green Sustain. Chem. 2022, 5, 100274.

[7] Lagergren, S., Kongl. Vetensk. Acad. Handl. 1898, 24, 1–39.

[8] Ho, Y.S., McKay, G. Process Saf. Environ. Prot. 1998, 76, 183–191.

[9] Langmuir, I. J. Am. Chem. Soc. 1918, 40, 1361–1403.

[10] Freundlich, H.Z. Phys. Chem. 1906, 57A, 385–470.

[11] Sips, R. J. Chem. Phys. 1948, 16, 490–495.

[12] Lahuri, A.H., Rahim, A.A., Nordin, N., *et al.* Catal. Today 2023, 418, 114111.

[13] Munagapati, V.S., Wen, H.-Y., Gollakota, A.R.K., *et al.* J. Mol. Liq. 2022, 368, 120657.

EcoTER'26
eco.tfbor.bg.ac.rs
32nd International Conference
Ecological Truth & Environmental Research
24–26 June 2026, Hotel Sunce,
Sokobanja, Serbia

Original Research

SELF-MADE PULSATING ATMOSPHERIC PRESSURE CORONA PLASMA REACTOR FOR DEGRADATION OF A TEXTILE DYE IN SYNTHETIC TEXTILE EFFLUENT

DOI: 10.5937/EcoTER26284R

Saša Rančev[1,a], Milica Petrović[2,b], Slobodan Najdanović[2,c], Nena Velinov Georgiev[2,d*], Jelena Mitrović[2,e], Miljana Radović Vučić[2,f], Aleksandar Bojić[2,g]

[1] University of Niš, Faculty of Science and Mathematics, Department of Physics, 33, Višegradska str., 18000 Niš, SERBIA

[2] University of Niš, Faculty of Science and Mathematics, Department of Chemistry, 33, Višegradska str., 18000 Niš, SERBIA

[a] https://orcid.org/0000-0001-6105-0034 [b] https://orcid.org/0000-0002-7537-0327
[c] https://orcid.org/0000-0001-9383-4394 [d] https://orcid.org/0000-0001-9043-8521
[e] https://orcid.org/0000-0001-9634-7727 [f] https://orcid.org/0000-0001-6820-5844
[g] https://orcid.org/0000-0002-9853-2747

Abstract

A self-made pulsating atmospheric-pressure corona plasma reactor was tested for the degradation of textile dye Reactive Blue 4. The reactor generated a corona-type discharge in air with low-intensity streamers, without sparks. The effect of the initial dye concentration, input reactor voltage, and pH was examined using model dye water solutions. A 50 mg dm^{-3} dye solution was completely decolorized at 18 kV and its native pH of 6.8 in less than 40 minutes. The chemical oxygen demand (COD) was reduced by 82% and 85% after 120 and 180 minutes of treatment, respectively. Decolorization rate and efficiency decreased with increasing initial dye concentration and with decreasing input voltage. Decolorization proceeded slightly faster in acid-neutral media than in alkaline media. The major degrading agent was determined to be the hydroxyl radical, generated by plasma. Textile effluent, containing 56 mg dm^{-3} RB 4, sulphates and carbonates, with pH 11.8, after removing the dyed fabric, was completely decolorized in 85 minutes, and the COD was reduced by about 76% and 78% after 120 and 180 minutes of treatment, respectively, which demonstrated the high potential of the reactor.

Keywords: corona discharge, textile effluent, RB 4, degradation.

INTRODUCTION

Textile dyeing effluents containing dyes and additives used in dyeing processes pose an environmental problem due to the high chemical stability of textile dyes and their resistance to conventional wastewater treatments. Advanced oxidation processes (AOPs) are based on the degradation of hazardous organic compounds by the highly reactive oxidative species, such as hydroxyl radical, ·OH, produced by powerful energy sources. AOPs showed high efficiency in dye degradation and mineralization, but many of them are expensive and difficult for large-scale work [1]. Plasma processes are based on electrical discharge at high voltage in air and/or water, which causes their ionization and the generation of oxidative

* *nena.velinov@yahoo.com; nena.velinov@pmf.edu.rs*

species that attack and degrade the dye molecule, often leading to its mineralization. There are several types of plasma sources [2–5]. Atmospheric-pressure corona plasma exhibited many advantages, such as high efficiency, low cost, simple equipment, and relatively low energy consumption [6], which made it a choice for the removal of Reactive Blue 4 (RB 4), a representative of a large group of reactive textile dyes. In this paper, RB 4 was removed from a synthetic textile dyeing effluent by the self-made pulsating atmospheric pressure corona plasma reactor. The degrading reactive species were identified, and the process was optimized using model solutions before applying it to the effluent.

MATERIALS AND METHODS

Self-made plasma reactor

Dye degradation was done using a self-made corona plasma reactor, consisting of a power supply, a DC pulse generator, a high-voltage output stage, and an open cell. The positive corona discharge was created in the air over the water phase, on the tips of the multipoint anode, made of Ti needles, while the cathode was the dye solution's surface. The reactor cell was a PVC cylinder. The electrical contact was centered at the bottom of the cell and connected to the ground potential. The discharge current was controlled by the electronic circuitry of a device, adjusting the voltage at the multipoint anode. Gases produced by the discharge were removed through the exhaust system. The current and voltage signals were recorded using a digital oscilloscope TDS 2024C. The working frequency was 40 kHz. Corona discharge was without sparks and with the appearance of low-intensity streamers. The experimental setup is shown in Figure 1.

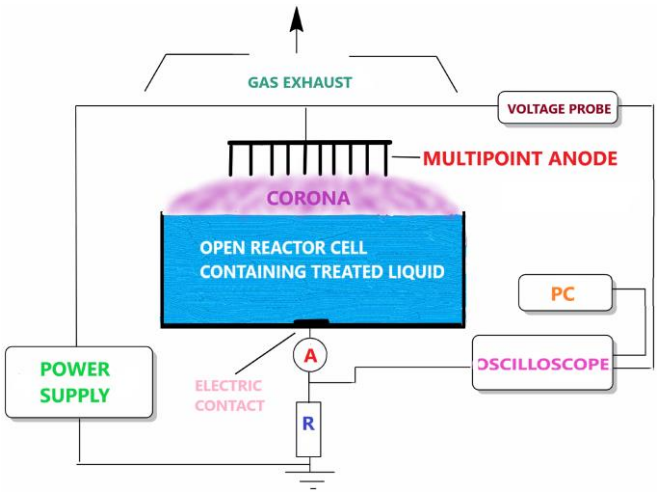

Figure 1 *Scheme of a self-made pulsating atmospheric-pressure corona plasma reactor*

Dye degradation experiments

RB 4 was purchased from Sigma Aldrich and used without purification. The working model dye solutions were prepared using deionized water by dissolving the required amount of dye in deionized water (stock solutions) and by diluting those solutions to the required concentrations. Solutions were then transferred to the plasma reactor cell and treated with cold plasma in open air at fixed time intervals. For the synthetic effluent experiment, a dyebath was prepared according to the references [7,8]. It contained 500 mg dm^{-3} RB 4,

50 g dm^{-3} Na_2CO_3, 100 g dm^{-3} Na_2SO_4, and 100 g dm^{-3} previously washed cotton fabric. Dying was performed at 40°C for 30 minutes. The dyed fabric was then removed, cooled to room temperature, and the effluent was treated using a self-made plasma reactor in the same way as the model solutions. Dye concentration was measured using a UV-VIS spectrophotometer Shimadzu UV-1650 PC (Japan) at 600 nm. Chemical oxygen demand (COD) was determined using the kit consisting of thermoreactor RD125, the Lovibond® COD Vario tube test, and the Lovibond® Multidirect photometer (Lovibond). The pH was measured using a SensIon3 pH meter (Hach, USA). The dye removal efficiency was presented as the percentage (%) of the dye removed at time *t*. The COD decrease was expressed as a percentage (%) of the initial COD removed at the treatment time *t*.

RESULTS AND DISCUSSION

Effect of initial dye concentration on decolorization

A radical scavenger test was performed to identify the oxidative species participating in the degradation. The addition of isopropanol (·OH scavenger) reduced the decolorization rate by more than 90%, while the other tested scavengers did not notably affect it. Thus, it was assumed that the ·OH radical was the major dye-degrading agent. It was produced by plasma decomposition of the plasma-generated H_2O_2 (which was also detected in the treated solutions) via a mechanism described elsewhere [9].

Decolorization rate and efficiency decreased with increasing initial dye concentration (C_0). (Figure 2a). Complete decolorization was achieved in less than 40 minutes for lower C_0 values, and it took significantly more time at higher C_0 values. As the initial dye concentration in the solution increased, the ratio between dye concentration and ·OH became less favorable, which reflected the decolorization rate. The effect was more pronounced at higher concentrations, where that ratio became more significant.

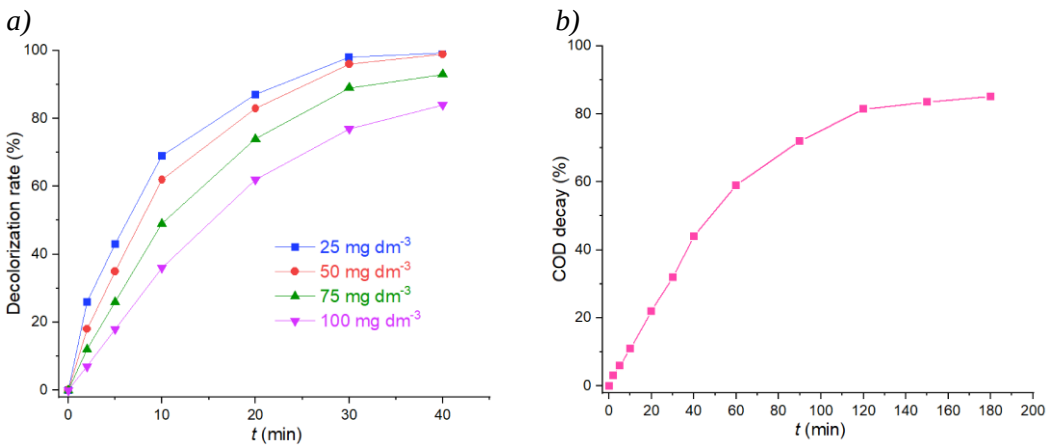

Figure 2 *a) Effect of initial dye concentration on decolorization rate; b) COD decay in the RB 4 plasma degradation process (50 mg dm^{-3} dye solution, 18 kV, native pH)*

Chemical oxygen demand (COD)

COD decay increased with the increase in electrolysis time, rapidly at shorter times, and slowly at longer times (Figure 2b). The increase was becoming less significant as the

electrolysis time was extended over 120 minutes. It reached about 82% after 120 minutes, and 85% after 180 minutes of the treatment, so it can be assumed that it approximately entered its equilibrium between 120th and 180th minutes of electrolysis. That value can be considered high.

Effect of operational parameters

Effect of input voltage

Decolorization rate and efficiency increased with increasing input discharge voltage (*U*) at a constant current density of 1.2 mA (Figure 3a). *U* is one of the most important factors affecting the plasma reaction rate because it is directly linked to the reactive species generation and acceleration. Higher input voltage provided more energy and intensified ionization and thus generation of dye-degrading radical oxidative species, which reflected the decolorization rate and efficiency. The input voltage was tested in the range 8V – 18V because the first value is the minimum U at which the ionization occurred in this case (the corona disappeared at lower values), and the second is the highest value of the stable corona and the selected discharge regime (Above that value sparks started to appear and the discharge became unstable).

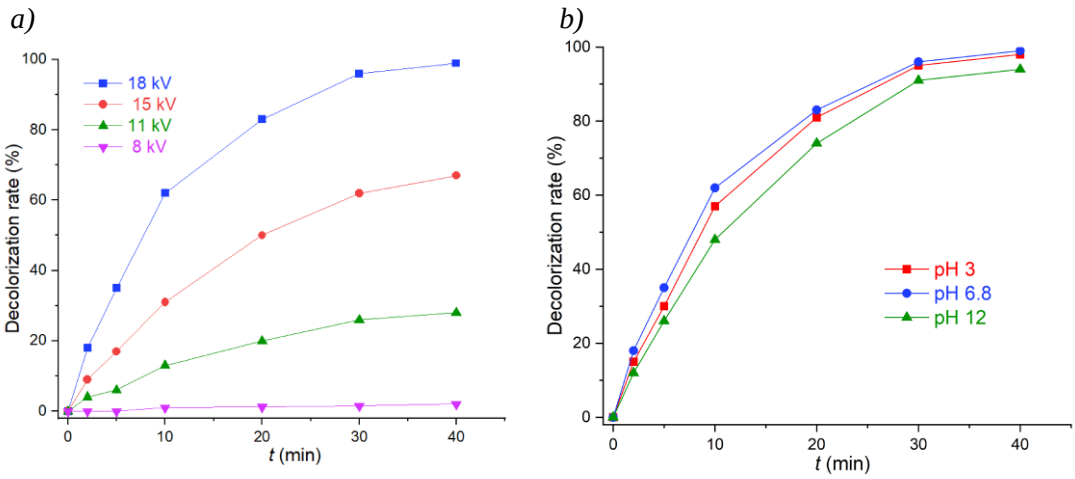

Figure 3 *a) Effect of reactor input voltage; b) initial pH on RB 4 decolorization in plasma degradation process (50 mg dm^{-3} dye solution)*

Effect of initial pH

The pH affects the decolorization rate because the present H^+ and OH^- ions can react with the plasma-generated oxidative species that degrade organics. In this case, pH had a relatively slight effect on the RB 4 decolorization rate and efficiency (Figure 3b). Decolorization was faster in acidic and neutral media (pH of 6.8 was the native pH of the treated model solution), with negligible differences, achieving complete decolorization in less than 40 minutes. In an alkaline medium, decolorization proceeded slightly slower, and its efficiency was slightly lower than in acidic/neutral media in the same treatment time. The reason was probably the reaction of hydroxyl radicals with hydroxyl ions, which had a quenching effect (due to the formation of a much weaker O·- radical), and thus reduced the quantity of hydroxyl radicals for dye oxidation [10]. However, the decolorization remained relatively fast and efficient in the entire examined pH range.

Plasma treatment of a textile effluent

The remaining dye concentration in the textile effluent after dyeing and removing the dyed fabric was 56 mg dm^{-3}, and its pH was 11.8. The effluent was treated with plasma at 18 kV without any previous treatment. Decolorization was completed in about 85 minutes (Figure 4).

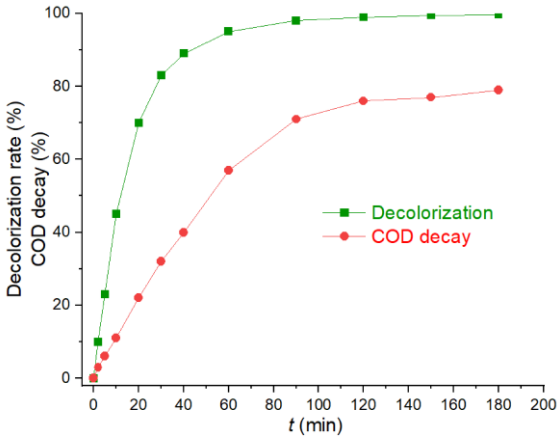

Figure 4 *Decolorization rate and COD decay in the plasma treatment of a dyeing effluent*

The COD removal reached its equilibrium value of 76% at about the 120th minute of the treatment and remained approximately the same in the next 60 minutes (it was 78% after 180 minutes of the treatment), and this can be considered its maximum value at given conditions, which is considered high for a typical dyebath. The decolorization process can be compared with the decolorization of the model solution containing 50 mg dm^{-3} RB 4 at pH 12. It proceeded somewhat more slowly because of the presence of SO_4^{2-} and CO_3^{2-} ions, which react with hydroxyl radicals, forming corresponding less active radicals and therefore making the decolorization process less efficient than it would be in the absence of sulphates and carbonates.

CONCLUSION

A self-made pulsating atmospheric-pressure corona plasma reactor exhibited high efficiency in the degradation of textile dye Reactive Blue 4. The corona operated with the streamers and without the sparks. It was found that the degradation proceeded mostly via plasma-generated hydroxyl radical ·OH. The effect of initial dye concentration and operational parameters on decolorization rate and efficiency was examined. Decolorization rate decreased with increasing initial dye concentration. It increased with increasing input reactor voltage due to more intensive ionization and the generation of oxidative species. It proceeded somewhat faster in the acidic-neutral media than in alkaline media because of the quenching effect of hydroxyl ions. Textile dyeing effluent, prepared according to a practical recipe, was decolorized in about 85 minutes without any previous treatment. The chemical oxygen demand decreased by about 85% for the tested model solution, and by about 78% for the textile dyeing effluent after 180 minutes of the treatment. The plasma generator showed notable potential for practical use.

ACKNOWLEDGEMENT

The authors would like to acknowledge financial support from the Ministry of Science, Technological Development, and Innovation of the Republic of Serbia (Agreement No 451-03-33/2026-03/200124 and 451-03-34/2026-03/200124).

REFERENCES

[1] Ma, D., Yi, H., Lai, C., *et al.* Chemosphere 2021, 275, 130104.
[2] Takeuchi, N., Yasuoka, K. Jpn. J. Appl. Phys. 2021, 60, SA0801.
[3] Aggelopoulos, C.A., Dolinski, O. Chemosphere 2024, 347, 140667.
[4] Hentit, H., Ghezzar, M.R., Womes, M., *et al*. J. Mol. Catal. A: Chem. 2014, 39, 37–44.
[5] García, M.C., Mora, M., Esquivel, D., *et al.* Chemosphere 2017, 180, 239–246.
[6] Kusumandari, K., Saraswati, T.E., Wulandari, S.W., *et al.* Indian J. Phys. 2022, 96, 1001–1008.
[7] Epolito, W.J., Lee, Y.H., Bottomley, L.A., *et al*. Dyes Pigm. 2005, 67, 35–46.
[8] Stef Francis/home/Procion MX Dyeing Instructions, Available from: https://www.stef-francis.co.uk/product-category/dyes-paints-instructions-and-wooden-stamps/procion-mx-dyeing-instructions/
[9] Petrović, M., Jovanović, T., Rančev, S. *et al*. J. Environ. Chem. Eng. 2022, 10, 107931.
[10] Jiang, B, Zheng, J, Liu, Q., *et al*. Chem. Eng. J. 2012, 204–206, 3–39.

EcoTER'26
eco.tfbor.bg.ac.rs
32nd International Conference
Ecological Truth & Environmental Research
24–26 June 2026, Hotel Sunce,
Sokobanja, Serbia

Original Research

THERMALLY ACTIVATED PEROXYDISULFATE DEGRADATION OF REACTIVE TEXTILE DYES

DOI: 10.5937/EcoTER26290M

Jelena Mitrović[1,a], Nena Velinov Georgiev[1,b*], Milan Momčilović[1,c], Milica Petrović[1,d], Miloš Kostić[1,e], Slobodan Najdanović[1,f], Aleksandar Bojić[1,g]

[1] University of Niš, Faculty of Natural Science and Mathematics, Višegradska 33, 18000 Niš, SERBIA

[a] https://orcid.org/0000-0001-9634-7727 [b] https://orcid.org/0000-0001-9043-8521

[c] https://orcid.org/0000-0001-5370-0148 [d] https://orcid.org/0000-0002-7537-0327

[e] https://orcid.org/0000-0001-6488-5184 [f] https://orcid.org/0000-0001-9383-4394

[g] https://orcid.org/0000-0002-9853-2747

Abstract

This study examines the potential degradation of the anthraquinone textile dye Reactive Blue 19 (RB 19) and the azo dye Reactive Orange 16 (RO 16) through the application of thermally activated peroxydisulfate. The influence of basic operating parameters, such as the initial pH value of the solution, initial peroxydisulfate concentration, and temperature, was investigated. The degradation reaction followed pseudo-first-order kinetics for both dyes under investigated conditions. The degradation rate constants for these dyes increased with a rise in the concentration of peroxydisulfate up to a certain threshold, as well as with an increase in temperature, and in an acidic environment. The findings offer significant insights into the implementation of advanced oxidation processes utilizing thermally activated persulfate for the remediation of textile dye contaminated wastewater.

Keywords: wastewater, advanced oxidation processes, sulfate radicals, decolorisation.

INTRODUCTION

In the context of rapid industrial development, the daily discharge of wastewater is increasing, and the composition of organic pollutants within this wastewater is becoming progressively more complex [1]. This trend poses a significant threat to human health and the environment. Organic contaminants, such as pharmaceuticals, pesticides, and textile dyes, cannot be completely degraded using conventional wastewater treatment; therefore, developing an effective treatment to eliminate these pollutants from aqueous media and preventing the formation of toxic byproducts is required.

Advanced oxidation processes (AOPs) rely on the *in-situ* production of reactive species which have a high redox potential and are non-selective; therefore, they can oxidize any organic contaminant [2]. In the initial stages of research on advanced oxidation processes, the emphasis was predominantly on the role of hydroxyl radicals and the utilization of hydrogen peroxide as an oxidant. However, there has been a growing interest in processes that involve

* *nena.velinov@yahoo.com; nena.velinov@pmf.edu.rs*

the activation of persulfates, such as peroxymonosulfate (PMS) or peroxydisulfate (PDS). Generally, persulfates without activation exhibit poor activity toward most organic pollutants. Persulfates achieve high oxidation capacity through two pathways: (a) radical oxidation via the generation of sulfate radicals ($SO_4^{\bullet-}$, 2.5–3.1 V) and hydroxyl radicals ($^{\bullet}OH$, 1.8 V) and (b) non-radical processes based on singlet oxygen ($_1O^2$) and electron-transfer pathways [3]. Various methods have been employed for persulfate activation in the past decades, involving UV light, heat, ultrasound, alkalis, and catalysts [1].

One of the first methods used to activate persulfates in situ was heating. The production of two sulfate radicals can be accomplished by cleavage of the peroxide bond when an appropriate amount of energy equal to the bond dissociation energy is applied into the persulfate anion (equation 1) [4].

$$S_2O_8^{2-} + \text{heat} \rightarrow 2SO_4^{\bullet-} \quad (1)$$

The activation energy for thermally activated persulfates decreased from 134 kJ/mol under neutral conditions to 116 kJ/mol and 129 kJ/mol under acidic and neutral conditions, respectively [5]. Practically, temperatures up to 30 °C resulted in negligible activation of the oxidant, with its half-life extending from days to month. Conversely, at temperatures ranging from 40 to 70 °C, the half-life is reduced to hours or even minutes.

While the heat-activated persulfate process is energy-intensive, it offers several advantages over alternative methods. Notably, it does not necessitate the use of rare or costly catalysts and is not constrained by size-scaling limitations associated with radiation-based techniques. Furthermore, the process requires minimal equipment and is relatively straightforward to manage. It presents a viable option for the industrial-scale application of heat or steam cogeneration. Additionally, integrating this process with renewable energy sources can mitigate its environmental and energy impacts.

In this study, the degradation of two textile dyes with different structures was examined using thermally activated peroxydisulfate. The investigation focused on the influence of varying initial peroxydisulfate concentrations, initial pH values, and reaction temperatures on the degradation characteristics. This research may offer an effective method for the removal of textile dyes in wastewater treatment processes.

MATERIALS AND METHODS

All used chemicals were reagent grade and were purchased from Sigma-Aldrich (USA). All solutions were prepared with ultrapure water from the Smart2Pure system with a conductivity of 0.055 μSm^{-1} (Thermo Scientific, USA).

All experiments were conducted using 100 cm^3 of working solution, which contained the specified initial oxidant ($S_2O_8^{2-}$) concentration, the textile dye RB 19 or RO 16, and at the corresponding pH values. The influence of each effect was examined by varying its value while keeping the other parameters constant. The degradation experiments were carried out in a thermostat in batch condition. Sampling of the dye solution was carried out at the beginning of the treatment and at time intervals of 5, 10, 15, 20 and 25 minutes, respectively. The absorbance of RB 19 dye was measured using a UV-Vis spectrophotometer UV-1800

(Shimadzu, Japan) at the wavelength of the maximum absorption of this dye of 592 nm, while the absorbance of RO 16 was measured at a wavelength of 494 nm.

The pseudo-first-order kinetic model, represented by equation (2), was employed to monitor the kinetics of each textile dye degradation [6]:

$$\ln \frac{c_t}{c_0} = -k_{app} t \tag{2}$$

where c_0 is the initial dye concentration, c_t is textile dye concentration at treatment time t, k_{app} is the apparent pseudo-first-rate constant, t is the treatment time. By plotting $\ln(c_t/c_0)$ against time, the k_{app} values were derived from the experimental data. The obtained values of the coefficient of determination r^2 for each investigated conditions were sufficiently high to confirm that the degradation kinetics of the textile dyes RB 19 and RO 16 by thermally activated peroxydisulfate followed pseudo-first-order reaction kinetics.

RESULTS AND DISCUSSION

Effect of initial pH

The results presented in Figure 1a show a decrease in the pseudo-first-order rate constant with an increase in the initial pH for thermally activated persulfate degradation of textile dye RB 19. The obtained pseudo-first-order rate constant was 0.117 min^{-1} (r^2 = 0.93) in acidic medium and decreased significantly in neutral medium to 0.072 min^{-1} (r^2 = 0.98). Further increases in pH led to a slight decrease in the pseudo-first-order rate constant, which was 0.061 min^{-1} (r^2 = 0.99) in an alkaline medium. The results presented in Figure 1b show that the pseudo-first-order rate constant for thermally activated persulfate degradation of textile dye RO 16 decreased with increasing initial pH values. The pseudo-first-order rate constant was 0.09 min^{-1} (r^2 = 0.93) in acidic medium and decreased significantly to 0.06 min^{-1} (r^2 = 0.88) in neutral medium. Further increases in pH led to a slight decrease in the pseudo-first-order rate constant, which reached value 0.052 min^{-1} (r^2 = 0.87) in an alkaline medium.

a) *b)*

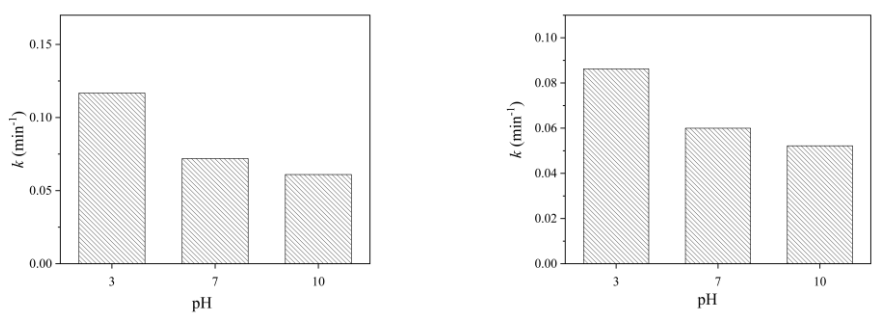

Figure 1 *Effect of initial pH value on pseudo-first-order rate constant for thermally activated peroxydisulfate degradation of textile dyes: a) RB 19; b) RO 16*

Generally, the initial pH of the solution can favor, hinder, or have no effect on organic pollutant elimination. The pH of aqueous solutions can affect the distribution and yield of

reactive species, which directly affects the rate of micropollutant degradation. Under neutral conditions, there is a contribution from both reactive species ($SO_4^{\bullet-}$ and $^{\bullet}OH$), whereas under acidic conditions, persulfate can undergo acid-catalyzed degradation with the formation of a larger amount of $SO_4^{\bullet-}$ according to the reaction (3) [7].

$$S_2O_8^{2-} + H^+ \rightarrow HS_2O_8^- + e^- \rightarrow SO_4^{\bullet-} + SO_4^{2-} + H^+ \quad (3)$$

Effect of initial peroxydisulfate concentration

The results presented in Figure 2a revealed that there is a significant increase in the pseudo-first-order reaction rate constant for thermally activated peroxydisulfate degradation of textile dye RB 19 from 0.032 min^{-1} (r^2 = 0.96) to 0.22 min^{-1} (r^2 = 0.99) with an increase in the initial peroxydisulfate concentration from 5 to 40 mmol dm^{-3}. Further increasing the initial peroxydisulfate concentration decreased the pseudo-first-order reaction rate constant, whose value was 0.14 min^{-1} (r^2 = 0.98) for an initial peroxydisulfate concentration of 80 mmol dm^{-3}. The results from Figure 2b revealed that there is a significant increase in the value of the pseudo-first-order reaction rate constant from 0.005 min^{-1} (r^2 = 0.9) to 0.113 min^{-1} (r^2 = 0.97) with an increase in the initial peroxydisulfate concentration from 5 to 40 mmol dm^{-3} in case of thermally activated peroxydisulfate degradation of textile dye RO 16. Further increasing the initial peroxydisulfate concentration led to a slight increase in the pseudo-first-order reaction rate constant, whose value was 0.12 min^{-1} (r^2 = 0.98) for an initial peroxydisulfate concentration of 80 mmol dm^{-3}.

a) *b)*

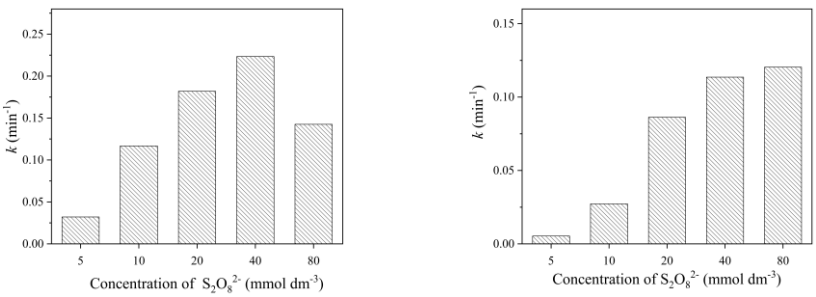

Figure 2 *Effect of initial peroxydisulfate concentration on pseudo-first-order rate constant for thermally activated peroxydisulfate degradation of textile dyes: a) RB 19; b) RO 16*

The increase in the removal efficiency of the investigated textile dyes RB 19 and RO 16 with an increase in the initial peroxydisulfate concentration may be due to an increase in the rate of formation of sulfate anion radicals, according to equation 1. An increase in the initial concentration of peroxydisulfate from 40 to 80 mmol dm^{-3} did not lead to a proportional increase in the removal efficiency of the investigated textile dyes. This trend is probably due to the reaction of the sulfate anion radical with the peroxydisulfate anion, as well as the sulfate anion radicals with each other, when the peroxydisulfate anion is present in excess, as shown by the reactions (5) and (6) [8].

$$SO_4^{\bullet-} + S_2O_8^{2-} \rightarrow SO_4^{2-} + S_2O_8^{\bullet-} \quad (5)$$

$$SO_4^{\bullet-} + SO_4^{\bullet-} \rightarrow S_2O_8^{2-} \quad (6)$$

Finally, the addition of large amounts of oxidants should be performed with caution. Although this usually increases the efficiency of the process, it also increases the cost of supplying the chemicals. Simultaneously, upon activation, each persulfate ion is converted into two sulfate ions, which present in high concentrations can be considered as pollutants.

Effect of temperature

The results from Figure 3a depict that the pseudo-first-order reaction rate constant increases slightly from 0.01 min^{-1} (r^2 = 0.98) to 0.03 min^{-1} (r^2 = 0.98) with an increase in temperature from 40 to 50 °C in case of thermally activated peroxydisulfate degradation of textile dye RB 19. Further increasing the temperature to 60 °C and 70 °C led to a significant increase in the pseudo-first-order reaction rate constant to 0.117 min^{-1} (r^2 = 0.93) and 0.132 min^{-1} (r^2 = 0.82), respectively. The results for thermally activated peroxydisulfate degradation of textile dye RO 16 (Figure 3b) revealed that the pseudo-first-order reaction rate constant increases slightly from 0.06 min^{-1} (r^2 = 0.89) to 0.008 min^{-1} (r^2 = 0.88) with an increase in temperature from 40 to 50 °C. Further increasing the temperature to 60 °C and 70 °C led to a significant increase in the pseudo-first-order reaction rate constant to 0.089 min^{-1} (r^2 = 0.93) and 0.162 min^{-1} (r^2 = 0.91), respectively.

a) *b)*

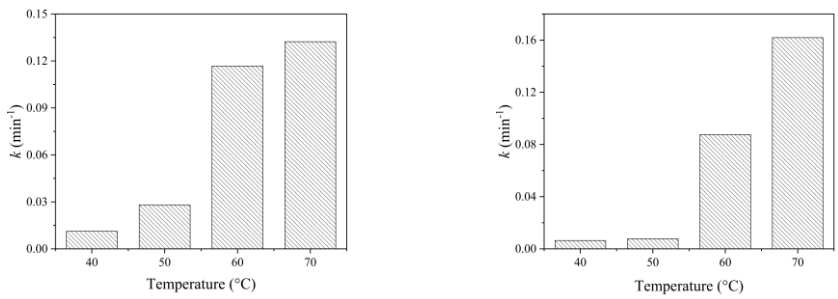

Figure 3 *Effect of temperature on pseudo-first-order rate constant for thermally activated peroxydisulfate degradation of textile dyes: a) RB 19; b) RO 16*

It can be assumed that the rate of pollutant degradation by thermally activated persulfate increases with increasing temperature, because the concentration of generated reactive species, such as $SO_4^{\bullet-}$, which are available for pollutant degradation increases (reaction 1). Although increased temperatures generally favor thermally activated persulfate processes owing to the increase in the concentration of generated radicals, the energy costs are high at very high temperatures. In addition, the rapid formation of radicals, specific to high-temperature processes, is accompanied by a faster rate of interaction of sulfate radicals, which can lead to unnecessary consumption of persulfate [9]. Dominguez et al. (2020) suggested that persulfate degradation consists of two simultaneous/parallel reactions: a) the production of sulfate radicals and b) non-productive persulfate degradation [10]. The activation energy of persulfate is between 128.48 and 140.16 kJ/mol, while the apparent activation energy of

organic pollutants ranges from 80 to 160 kJ/mol [11]. Therefore, for certain organic pollutants, increasing the temperature favors non-productive persulfate degradation rather than the oxidation of organic pollutants. Moreover, from an engineering point of view, the choice of process temperature requires a preliminary calculation of energy and chemical costs to achieve the required efficiency in a time frame that allows industrial application.

The temperature dependence of k_{app} can be estimated using the Arrhenius equation [4]. The apparent activation energy for each organic pollutant was calculated using a linear regression of the graphical dependence of $\ln k_{app}$ as a function of 1/T. In general, a higher activation energy of an organic pollutant indicates that it is more difficult to degrade using thermally activated persulfate. Based on the experimental results, the apparent activation energies of the textile dyes RB 19 and RO16 were 79 kJ/mol and 107.6 kJ/mol, respectively. The lower values of the apparent activation energy of the textile dye RB 19 by thermally activated peroxydisulfate indicate that the degradation of this dye is favored over the degradation of the textile dye RO 16. Based on data from the literature on the apparent activation energies of some organic pollutants, such as trimethoprim (177.8 kJ/mol), ketoprofen (169.74 kJ/mol), atrazine (141 kJ/mol), p-nitrophenol (127.8 kJ/mol), and bisphenol A (133.5 kJ/mol), it can be concluded that both tested textile dyes are more susceptible to degradation by thermally activated peroxydisulfate than the above-mentioned compounds [11].

CONCLUSION

It can be concluded that the thermally activated peroxydisulfate degradation of the textile dyes RB 19 and RO 16 was favored in acidic environments compared to neutral and alkaline environments. The pseudo-first-order rate constant of the tested textile dyes depended on the initial peroxydisulfate concentration and increased with increasing its concentration up to 40 mmol dm^{-3}. Further increases in the oxidant concentration led to a significant decrease in the pseudo-first-order rate constant of the textile dye RB 19, whereas the rate constant of the dye RO 16 changed slightly. An increase in the treatment temperature led to an increase in the degradation rate constants of the tested dyes. The apparent activation energies for the degradation of textile dye RB 19 and RO 16 were 79 and 107.6 kJ/mol, respectively, indicating that the degradation of RB 19 dye was favored over the degradation of textile dye RO 16 by thermally activated peroxydisulfate.

ACKNOWLEDGEMENT

The authors would like to acknowledge financial support from the Ministry of Science, Technological Development and Innovation of the Republic of Serbia (Agreement No 451-03-33/2026-03/200124 and 451-03-34/2026-03/200124).

REFERENCES

[1] Li, N., Wu S., Dai, H., *et al*. Chem. Eng. J. 2022, 450, 137976.

[2] Meng, S., Zhou, C., Sun Y., *et al*. Environ. Sci. Technol. 2026, 60, 11, 8303–8314.

[3] Yan, Y., Wei, Z., Duan, X., *et al*. J. Environ. Sci. Technol. 2023, 57, 33, 12153–12179.

[4] Sonawane, S., Rayaroth, P.M., Landge, V.K., *et al*. Curr. Opin. Chem. Eng. 2022, 37, 100839.

[5] Matzek, L.W., Carter, K.E., Chemosphere. 2016, 151, 178–188.

[6] Acero, J.L., Benítez, F.J., Real, F.J., *et al*. Sep. Purif. Technol. 2018, 201, 41–50.

[7] Lalas, K, Arvaniti, O.S., Zkeri E., *et al*. Sci. Total Environ. 2022, 846, 157378.

[8] Hsieh, S-C., Lai, W. W-P., Lin, A.Y-C., Environ. Sci. Pollut. Res. 2021, 28, 18021–18034.

[9] Arvaniti, O.S., Bairamis, F., Konstantinou, I., *et al*. Chem. Eng. J. 2020, 4, 100062.

[10] Dominguez, C.M., Romero, A., Lorenzo, D., *et al*. J. Environ. Manag. 2020, 261, 110240.

[11] Arvaniti, O.S., Ioannidi, A.A., Mantzavinos, D., *et al*. J. Environ. Manag. 2022, 318, 115568.

EcoTER'26
eco.tfbor.bg.ac.rs
32nd International Conference
Ecological Truth & Environmental Research
24–26 June 2026, Hotel Sunce,
Sokobanja, Serbia

Original Research

DIRECT INFUSION MS AS A PROMISING TOOL FOR PESTICIDES QUALITATIVE SCREENING IN APPLES

DOI: 10.5937/EcoTER26297A

Darko Anđelković [1,a], Milica Branković[2,b*]

[1] University of Niš, Faculty of Agriculture, Kosančićeva 4, 37000 Kruševac, SERBIA

[2] University of Niš, Faculty of Sciences and Mathematics, Department of Chemistry, Višegradska 33, 18000 Niš, SERBIA

[a] https://orcid.org/0000-0002-2526-6070

[b] https://orcid.org/0000-0002-8671-7066

Abstract

Frequent pesticide application, along with their health risk keep the need for continuous pesticides residue monitoring in food. Nowadays multiresidue pesticides analysis in complex matrices is mostly quantitative chromatography-based analysis. Methods that are primarily designed for qualitative analysis and exclude the usage of chromatography much less can be found in literature. Primary goal of this investigation was to launch a non-chromatography based direct infusion ESI/MS method designed for fast qualitative pesticides screening in fruit. The method was intended to be shorter and simpler than usual methods. As such, the method can be used in early stages in pesticides residues evaluation process, and the obtained results can decide whether to proceed evaluation with some quantitative method or do not.

Keywords: mass spectrometry, sample preparation, fungicides.

INTRODUCTION

The main contribution of vitamins and nutrients to the human diet originates from fruits and vegetables, among which apples are the most consumed. Around 80 million metric tons of this fruit is predicted to be globally produced in 2022/23, of which is about half a million to 13 million tons in EU only [1]. Apple production is highly dependent on pesticides since the usage of these chemicals ensures satisfactory crop yields. Frequent pesticide application, along with their health risk keep the need for continuous pesticides residue monitoring in food.

Nowadays multiresidue pesticides analysis in complex matrices is mostly quantitative chromatography-based analysis. Methods that are primarily designed for qualitative analysis and exclude the usage of chromatography much less can be found in literature.

Primary goal of this investigation was to launch a non-chromatography based direct infusion ESI/MS method designed for fast qualitative pesticides screening in fruit. The method was intended to be shorter and simpler than usually applied mostly quantitative

* *milica.brankovic1@pmf.edu.rs*

methods. As such, the method can be used in early stages in pesticides residues evaluation process, and the obtained results can decide whether to proceed evaluation with some quantitative method or do not.

Due to its cuticle structure and composition, apple peel was targeted for analysis. Peel is a natural barrier, thus can retain most of the applied pesticides. Peel retention capacity of several fruits (apple, grape, pear) was confirmed by some studies [2–4] that non-systemic pesticides were better localized than the systemic, since the latter express deeper penetration pattern [5,6].

The method was developed for five pesticides mostly used in apple production in Serbia - pyrimethanil, cyprodinil (fungicides, anilino-pyrimidines), boscalid (fungicide, pyridine-carboxamides), trifloxystrobin (fungicide, Strobilurin) and bifenthrin (insecticide, pyrethroids).

MATERIALS AND METHODS

Chemicals

High purity standards of pyrimethanil and cyprodinil were purchased from AccuStandard®, USA. Formic acid (98%) and high purity standards of boscalid, trifloxystrobin and bifenthrin were purchased from Sigma-Aldrich®, Germany. HPLC grade methanol was produced by J.T. Baker, USA; ammonium-formate (98%) and HPLC grade hexane, deionized water and ethanol were produced by Carlo Erba, Italy.

For high purity standards weighing procedures analytical balance Sartorius BP110S (Germany) was used.

In sample preparation procedure following appliances were used: peeler and slicer (China), balance (acc. ± 0.01 g) KB 2000-2N KERN (Germany), kitchen blender 0.9L BL142A TEFAL (France), centrifuge Jouan C4i Thermo Scientific (USA), evaporator TurboVap® LV Zymark (USA), hotplate Harry Gestigkeit GmbH (Germany), syringe microfilter Nylon Hydrophylic 0.22 µm, Membrane Solutions (USA) and 500 µL glass syringe, Unimetrics (USA). Apples of Golden Delicious variety were purchased in a local supermarket.

Instruments and instrumental configuration for screening analysis

Surveyor LC pump (Thermo Finnigan, USA) and LCQ Advantage mass spectrometer (Thermo Finnigan, USA) with 3D ion trap analyzer, were used. Data was acquired and analyzed by Xcalibur™ software, version 1.4 SR1.

LC pump and mass spectrometer were coupled via PEEK tubing system interconnected with LC union Tee (syringe - LC union Tee branch (30 cm) and LC union Tee - ESI source branch (10 cm)) (Figure 1). The configuration provides simultaneous inflow of mobile phase from the LC pump and sample from the syringe pump to the mass spectrometer. The mobile phase inflow (0.30 % FA + 0.01 % AMF water solution) can be delivered by LC pump or any other pump. The aim is to provide and maintain constant environment in the source during sequential analysis; optionally, it gives an opportunity to adjust parameters such as pH, salt presence etc.

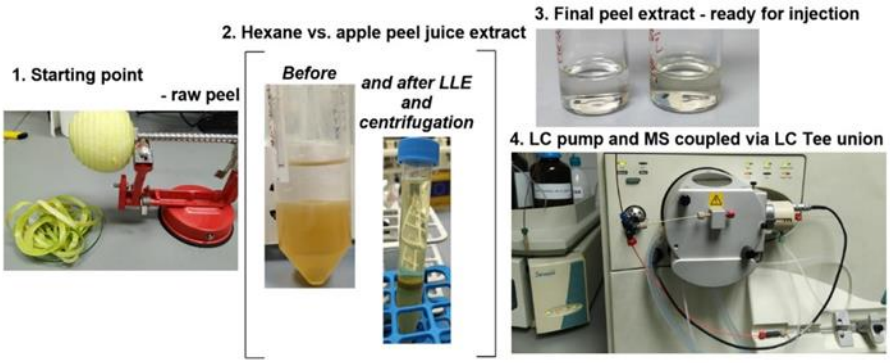

Figure 1 *An insight into screening analysis*

Sample preparation

Procedural blanks

Ten-gram peel portion was mixed with water (20 mL) and blended. The obtained mash was centrifugated (10 min/3500 rpm); filtrate (15 mL) was liquid-liquid extracted with hexane (10 mL); hexane extract (6 mL) was separated from aqueous phase by centrifugation (3 min/3500 rpm), evaporated to dryness, redissolved in 1.50 mL 0,05% AMF in methanol, filtered through 0.22 µm syringe filter and analyzed.

Procedural standards

Ten-gram peel portion was fortified with five-pesticides mixture as follows: calculated volume of pesticides stock solution was applied to the peel surface with a pipette, taking care all the solution was uniformly distributed. Upon solvent evaporation, peel was capped and refrigerated for 30 minutes. Fortified peel was then treated according to the procedural blanks' preparation procedure. Fortification levels were 0.05; 0.10; 0.20; 0.50 and 0.75 $mgkg^{-1}$ of peel.

Screening analysis steps

Extracts were injected into the source in purge syringe mode (25.00 $\mu Lmin^{-1}$); simultaneous mobile phase inflow rate was 50.00 $\mu Lmin^{-1}$. Screening analysis was performed in two steps. First step was the MS^1 analysis (full scan mode, scan range *m/z* 150-600). The second step was the subsequent MS^2 analysis (full scan mode) of selected pesticide-specific parent ions (Table 1). Total runtime was 12 min (2 min for MS^1 analysis and 2 min for MS^2 analysis of each pesticide).

Table 1 *Analytically significant ions (*m/z*) of investigated pesticides*

Pesticide	Pyrimethanil	Cyprodinil	Boscalid	Trifloxystrobin	Bifenthrin
Molecular weight, $gmol^{-1}$	199.25	225.29	343.2	408.4	422.9
m/z of $[M+H^+]$ (monoisotopic)	200.12	226.13	343.04	409.14	423.13
Base ion observed in the MS^1 spectra (parent ion for MS^2), *m/z*	200.4	226.4	342.9	408.7	439.6
Daughter ions in the MS^2 spectra, *m/z* (descending abundance)	107.1 183.4 159.2	210.2 185.1 144.1 159.0 108.1	307.3 140.0	186.1 206.1	181.1 166.1
Normalized collision energy, %	50 (55) [a]	55	35 (45) [a]	30 (40) [a]	23 (50) [a]

[a] At this value parent ions of pesticides are completely converted into daughter ions.

RESULTS AND DISCUSSION

Method development

Two possible outcomes of the screening are the confirmation of pesticides presence or absence. In first case, pesticides amount in apples can be assessed by methods approved by national or EU/USA regulations. In latter case, the analysis finishes at that point *i.e.*, there is no need to conduct any further analysis. The method itself excludes complex sample preparation or expensive chemicals consummation (sorbent packages, salts etc.), thus offering both time- and cost-effectiveness when analyzing large number of samples, which might not be the case with certified quantitative methods.

First step of the sample preparation was peel blending assisted with the addition of water. Since water is a non-aggressive medium, extraction can be performed in any type of blender; also, highly abundant waxes are not extracted. The second step was the liquid-liquid extraction of filtered water extract with hexane. Hexane does not extract salts from the initial extract, which is important, since larger quantity of non-volatile salts injected directly into the source in a short period of time can form deposits and cause clogging problems.

Dry residue amount in peel extracts was determined in a separate experiment. The amount originating from 50 g of peel after evaporation for 24 h at room temperature was around 1 mg (1.15 ± 0.12 mg).

Heating (30 min at 50 °C) decreased the amount to 0.2 mg and further heating (30 min at 100 °C) resulted in no measurable amounts, suggesting the deposition in the source is improbable, since the screening starts with 10 g of peel and the lowest capillary temperature in source is usually 200 °C, which surely provides complete evaporation of any dry residue.

Complete prevention of waxes occurrence in hexane extract is impossible since the final water extract is cloudy (Figure 1). Our previous study [7] showed the final sample preparation step - hexane to methanol exchange by evaporation - provides the complete removal of extracted waxes. The step also provides analyte concentration and, in this case, more appropriate analyte carrier when operating with ESI/MS systems.

Qualitative analysis

Ions originated from peel extracts are mainly observed at *m*/*z* values higher than 290 (Figure 2). Background spectrum (mobile phase only) and blank apple extracts spectra differ in 5 to 6 additional ions of higher abundance.

MS^2 analysis was performed on all fortified and non-fortified samples. Detected pesticides pseudo-molecular ions were fragmented at both lower and higher normalized collision energy; for MS^2 fragments quantification higher energy was used (the value is given in parenthesis in Table 1).

Pesticides' fragmentation patterns in the neat solution and in spiked procedural blank (5.00 μgmL^{-1}) (spectrum can be found in [8]) are similar i.e., there are no new-formed fragments. However, in spiked extract smaller number of pyrimethanil and cyprodinil fragments was observed; most characteristic fragments of each pesticide (first two fragments, Table 1) are among them. Boscalid, trifloxystrobin and bifenthrin fragmentation patterns do not differ.

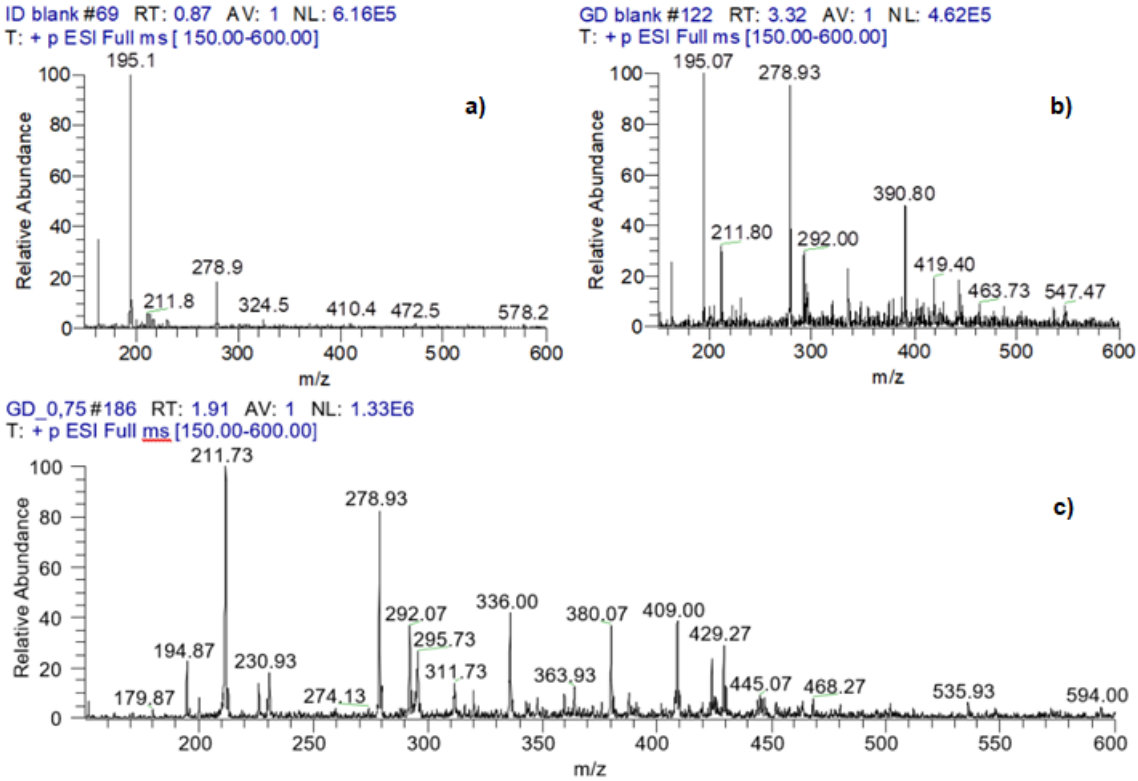

Figure 2 *Full scan MS[1] background spectra (mobile phase only) (a); full scan MS[1] spectra of non-fortified (b) and fortified Golden Delicious peel extract (0.75 mgkg^{-1}) (c)*

Comparison of pesticides fragmentation pattern in procedural standard (0.050 mgkg^{-1}, Figure 3) to the pattern in the non-procedural analogue (procedural blank spiked at 0.25 µgmL^{-1}, spectrum can be found in [8]) shows the following:

- Fragmentation of pyrimethanil (*m/z* 200) results in *m/z* 183, 173, 131 and 85 (Figure 3a) of which *m/z* 183 and perhaps *m/z* 173 can be related to the pesticide; *m/z* 107 is not observed. At higher collision energy (CID = 55) *m/z* 183 becomes dominant. In 0.75 mgkg^{-1} fortified peel (spectrum can be found in [8]) three pyrimethanil characteristic fragments are observed (*m/z* 107, 125 and 183) which clearly confirms the pesticide presence. At higher concentrations, the most abundant pyrimethanil fragment is *m/z* 107 (spectrum can be found in [8]). However, at lower concentrations *m/z* 183 becomes more reliable for pyrimethanil identification.
- Presence of cyprodinil can be reliably confirmed by observing at least four characteristic fragments i.e., *m/z* 210, 159, 133 and 108 (Figure 3b).
- Presence of boscalid, trifloxystrobin and bifenthrin can be also reliably confirmed by observing *m/z* 307 and 140 (Figure 3c), *m/z* 186 and 206 (Figure 3d) and *m/z* 181 and 166 (Figure 3e).

Qualification of boscalid, trifloxystrobin and bifenthrin in apple extracts is reliable since the fragmentation pattern is well preserved and mostly unchanged at different pesticides concentration in samples. Fragmentation patterns of cyprodinil and pyrimethanil are altered in terms of lower diversity of the fragments. This is more pronounced for pyrimethanil,

particularly at lower concentrations, and might cause the identification of this pesticide to be slightly challenging.

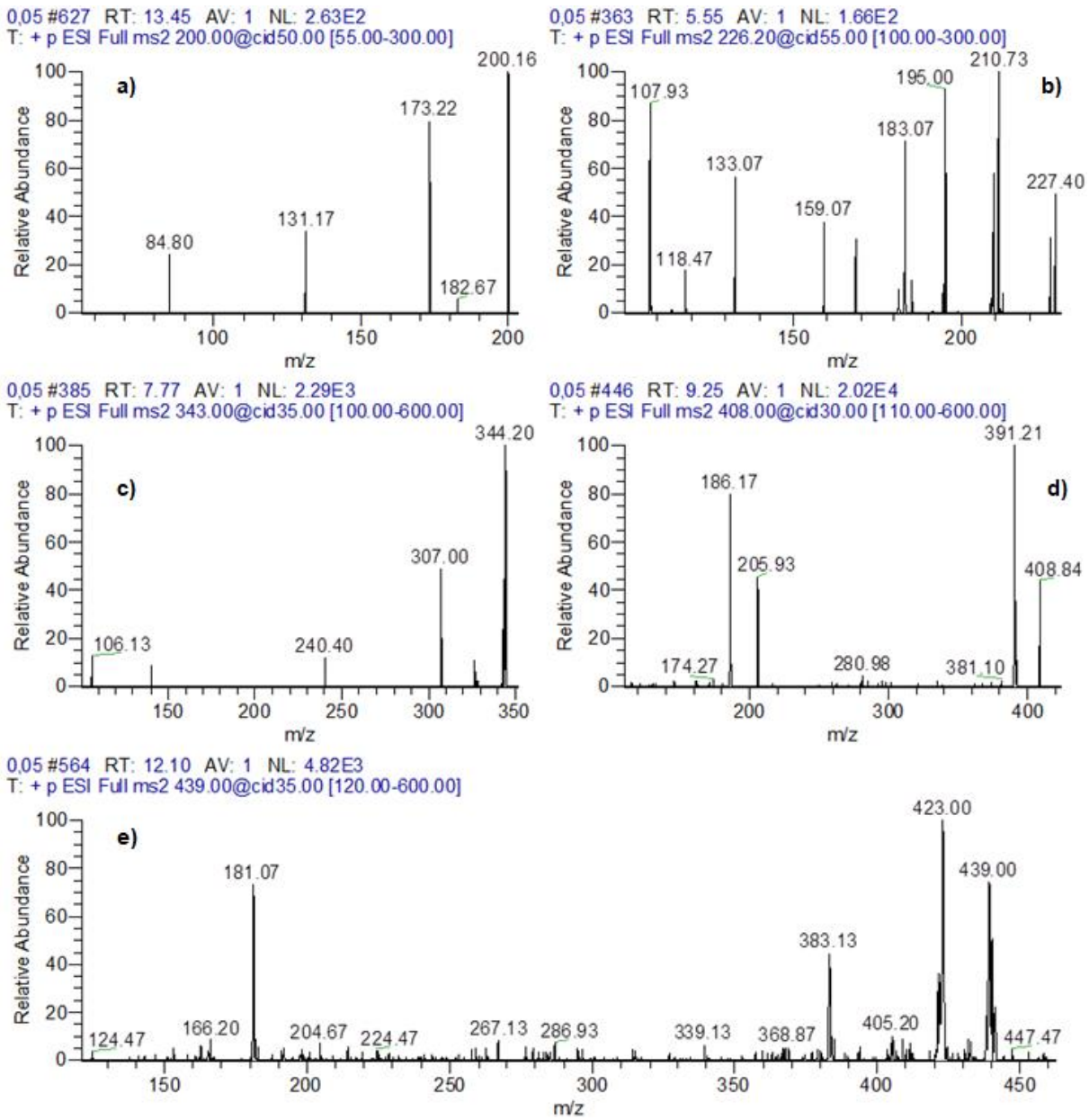

Figure 3 *Direct injection full scan MS^2 spectra after the fragmentation of protonated molecular ion of: a) pyrimethanil (m/z 200.4); b) cyprodinil (m/z 226.4); c) boscalid (m/z 343.0); d) trifloxystrobin (m/z 408.7); and e) bifenthrin (m/z 439.7) in extract of fortified Golden Delicious peel (0,050 mgkg^{-1})*

CONCLUSION

The developed method involved direct infusion ESI/MS analysis on 3D ion trap mass spectrometer. ESI behavior and fragmentation pattern of selected pesticides were first evaluated by MS^1 and MS^2 analysis of pesticides neat solutions, then same type of analysis was performed on a series of fortified Golden Delicious peel samples to assess method's qualification parameters.

Qualification criteria were the observation of MS^2 pesticide-characteristic fragments in samples spectra. Following the criteria, pesticides were detected in the lowest fortified sample (0.05 $mgkg^{-1}$ of peel or approx. 0.005 $mgkg^{-1}$ of fruit), meaning the method can qualify pesticides below MRL levels. Qualification of one of five investigated pesticides can be slightly challenging since the fragmentation in extracts leads to a smaller number of pesticide fragments when compared to that in the neat solution.

The developed method can be considered cost-effective and fast since the sample preparation itself does not include any expensive reagents and the chromatography was omitted.

ACKNOWLEDGEMENT

The authors are grateful to the Ministry of Science, Technological Development and Innovation of the Republic of Serbia for financial support according to the contract with registration No. 451-03-33/2026-03/200124 and 451-03-34/2026-03/200383.

REFERENCES

[1] USDA, Foreign Agricultural Service, Fresh Apples, Grapes, and Pears: World Markets and Trade Report, Washington D.C., WA, 2022

[2] Xu, X-M., Yu, S., Li, R., *et al*. Food Chem., 135, 2012, 161–169.

[3] Han, J-I., Fang, P., Xu, X-M., *et al*. Food Control, 54, 2015, 338–346.

[4] Hwang, J-I., Seok, D-R., Kim, J-E. Appl. Biol. Chem., 62, 2019, 34.

[5] Lozowicka, B., Kaczynski, P., Mojsak, *et al*. J. Food Comp. Anal., 90, 2020, 103494.

[6] Yang, T., Zhao, B., Hou, R., *et al*. J. Food Sci., 81, 2016 T2891–T2901.

[7] Andelkovic, D., Brankovic, M., Kocic, G., *et al*. Biomed. Chrom., 34 (1) 2020, e4720.

[8] Andjelkovic, D., Brankovic, M., *et al*. Food Control, 133, Part A, 2022, 108620.

EcoTER'26
eco.tfbor.bg.ac.rs
32nd International Conference
Ecological Truth & Environmental Research
24–26 June 2026, Hotel Sunce,
Sokobanja, Serbia

Original Research

CALIBRATION PERFORMANCES OF A MULTIRESIDUE PESTICIDES ANALYSIS IN LEMON AND LETTUCE ON QqQ AND ION TRAP MASS SPECTROMETERS

DOI: 10.5937/EcoTER26304A

Darko Anđelković[1,a], Milica Branković[2,b*]

[1] University of Niš, Faculty of Agriculture, Kosančićeva 4, 37000 Kruševac, SERBIA,

[2] University of Niš, Faculty of Sciences and Mathematics, Department of Chemistry, Višegradska 33, 18000 Niš, SERBIA

[a] https://orcid.org/0000-0002-2526-6070

[b] https://orcid.org/0000-0002-8671-7066

Abstract

As highly selective and sensitive, mass spectrometry currently stands for the most used analytical technique for both qualitative and quantitative analysis in many fields. One of the most significant factors in analytical calibration and quantification studies is sensitivity, which can be defined as the increment in measured signal per unit change in analyte concentration. Several factors such as the effective sample preparation, mobile phase composition, chromatographic column parameters and mass spectrometer features can affect analyte signal and result in various levels of sensitivity. The aim of this study was to evaluate calibration performances of the pesticides analysis in fruit and vegetable across the two instruments, by comparing the sensitivity on the two most exploited mass analyzers, that is on the linear ion trap and triple quadrupole mass analyzer. The comparison of sensitivity for solvent-based and QuEChERS treated lemon- and lettuce-based pesticides standards demonstrated triple quadrupole as a highly sensitive instrument.

Keywords: fruit, vegetables, mass spectrometry, QuEChERS.

INTRODUCTION

As highly selective and sensitive, mass spectrometry currently stands for the most used analytical technique for both qualitative and quantitative analysis in many fields such as life sciences, forensics, environmental and food safety.

One of the most significant factors in analytical calibration and quantification studies is sensitivity. Sensitivity is defined as the increment in measured signal per unit change in analyte concentration; it can be related to the detection limits, meaning the higher the sensitivity, the lower the detection limits. In practice, across the specified concentration range this parameter can be estimated via the slope of the calibration function.

The basics of sensitivity lay in the in-source ionization efficiency and subsequent transfer efficiency from the atmospheric pressure to the low-pressure region of the mass spectrometer. Several factors such as the effective sample preparation, mobile phase composition,

* *milica.chem@outlook.com; milica.brankovic1@pmf.edu.rs*

chromatographic column parameters and mass spectrometer features can enhance analyte signal when carefully chosen and optimized and can result in a highly sensitive method of analysis [1–3]. In addition to these factors, mass analysis and detection are significant factors in the sensitive analysis. Since the key point of difference between the mass spectrometers is mass analyzer, the improvement in its construction is a promising method for sensitivity enhancement.

Quadrupole tandem mass analyzer (triple quadrupole, QqQ) combines three transmission quadrupoles in a linear configuration, of which the first and the third quadrupole have the role of scanning or filtering device and the central one has the role of a collision cell. Stages of tandem mass analysis within this analyzer (parent ion isolation, parent ion fragmentation, daughter ions isolation and transmission towards the detector) are performed successively in space.

On the contrary, in the ion trap analyzer stages of tandem mass analysis are performed in the same space, successively in time. Since the ion trap works on the principle of filling and emptying the same space with ion packages, the main phenomenon that can affect sensitivity is the space charge effect which arises from the Coulomb interactions between the ions trapped in small space. This phenomenon is circumvented by the accumulation of a limited number of ions, determined in the instrument cycle called the pre-scan.

The aim of this study was to evaluate calibration performances of the analysis across the two instruments, by comparing the sensitivity on the two most exploited mass analyzers, that is on the linear ion trap and triple quadrupole mass analyzer. Performances were evaluated in the simplest MS mode, that is in the MS^1 full scan mode, primarily by the cross-analysis of solvent-based standards of 15 pesticides from different chemical classes. Then, the evaluation was broadened to pesticide standards in lettuce and lemon treated with the QuEChERS sample preparation procedure. These matrices are chosen due to the differences in their composition and appearance; lettuce is a leafy highly pigmented vegetable; lemon is fruit with high amount of water and acid.

MATERIALS AND METHODS

Chemicals

Formic acid (FA) (98%) and 15 high purity pesticide standards (acetamiprid, azoxystrobin, boscalid, buprofezin, cyprodinil, difenoconazole, fenhexamid, kresoxim-methyl, metsulfuron-methyl, propiconazole, pyraclostrobin, pyrimethanil, pyriproxyfen, tebuconazole and trifloxystrobin) were produced by Sigma-Aldrich®, Germany. Ammonium-formate (AMF) (98%), deionized water and HPLC grade ethanol were produced by Carlo Erba, Italy. HPLC grade methanol (MeOH) and acetonitrile (AcN) were produced by J.T. Baker, USA. Prepacked QuEChERS extraction pouches (1 g of NaCl, 4 g of $MgSO_4$, 1 g of trisodium citrate dihydrate and 0.5 g disodium hydrogen citrate) and dispersion kits (25 mg PSA and 150 mg $MgSO_4$) were produced by Hillium, USA. Syringe microfilters (Nylon Hydrophilic 0.22 µm) were produced by Membrane Solutions, USA. Fresh lettuce and lemons were purchased in a local supermarket.

Instruments and instrumental parameters

Samples were analyzed subsequently on two separate LC/MS systems. A sharing point between the systems were the very same chromatography column used for the analytes separation (Hypersil GOLD (C_{18}, 150mm×2.1mm, particle size 3 µm) and the same ionization type (ESI+). 10 µL of the sample was loaded on a column in a partial loop injection mode and eluted with a mixture of: eluent A (solution of 0.10 % of FA and 0.03 % of AMF in water) and eluent B (MeOH) following the gradient: 0–2 min (90 % A), 2–7 min (90-30 % A), 7–30 min (30 % A), 30–35 min (30–90 % A), 35–40 min (90 % A) with flow equal to 300 µL min^{-1}.

Procedures

Stocks preparation

Single-pesticide stock solutions (1 $mgmL^{-1}$ each) were prepared by dissolving high purity pesticide standards in ethanol. Multi-pesticide solutions were prepared by mixing and diluting single stocks in ethanol.

Sample preparation

One kilogram of fresh lettuce and lemon was cut and homogenized by blending for 5 min. Ten grams of the obtained homogenate of each matrix were extracted with 10 mL of acetonitrile, after which an extraction pouch was added. The mixture was immediately vortexed for one minute and centrifugated (10 min/3000 rpm). A supernatant aliquot was subjected to a dispersive extraction by the addition of one dispersion kit per mL of supernatant. The mixture was vortexed for one minute and centrifugated (10 min/3000 rpm). The supernatant was microfiltered prior to instrumental analysis.

Calibration standards preparation

Solvent-based standard series was prepared by spiking acetonitrile with a multi-pesticide standard solution. For each matrix, standard series with 7 calibration levels was prepared by spiking the obtained blank extracts with multi-pesticides standard solutions.

RESULTS AND DISCUSSION

Calibration performances assessed via pesticides analytical standards

Sensitivity, denoted as parameter a of the calibration function $y = ax + b$, for analysis of pesticide standards on a triple quadrupole is given in Table 1. The comparison of this parameter across analytes (solvent-based standards) revealed the highest sensitivity of the instrument towards buprofezin and cyprodinil (>200×10^6 arb. units per µgmL^{-1}). Mid-range sensitivity (10–60×10^6 arb. units per µgmL^{-1}) was achieved for 8 of 15 analytes; the instrument is the least responsive to boscalid, difenoconazole, fenhexamid, kresoxim methyl and metsulfuron methyl with the slopes ranging from approx. 1 to 5 ×10^6 arb. units per µg mL^{-1} (Table 1).

Almost the same trend could be observed on the linear ion trap instrument (Table 2). The highest instrumental sensitivity could be observed for buprofezin and cyprodinil, however, the differences between analytes in sensitivity were not as pronounced as on the QqQ instrument. Sensitivity for trifloxystrobin, pyriproxyfen and azoxystrobin was not much lesser than the

sensitivity for buprofezin and cyprodinil. On the QqQ instrument sensitivity for buprofezin and cyprodinil was about 4 times higher than the sensitivity for the following three pesticides, however, on the linear ion trap instrument it is higher by only about 1.5 times. Buprofezin on the QqQ instrument expressed about 3.7 times higher sensitivity than the pyrimethanil, but on the linear ion trap its sensitivity is only about 1.7 times higher than the sensitivity of pyrimethanil. Tebuconazole on the QqQ expressed about 3 times higher sensitivity than acetamiprid, however, on the linear ion trap sensitivity for these analytes are comparable (Tables 1 and 2).

When compared across the instruments, much higher sensitivity could be observed for the instrument with QqQ analyzer. Sensitivity enhancement ranged from 4.28 times for boscalid to 71.24 times for buprofezin. Since the separation parameters (column, flow, mobile phases composition) and the ionization type were the same, these differences can be attributed to the two main features that distinguish the instruments used within this study, that is the ion optics and mass analyzers features.

Table 1 *Linear regression parameters (y = ax + b, conc. range 0.01 – 15.00 µg mL^{-1}) for the analysis of solvent-based, lemon-based and lettuce-based pesticides standards on a triple quadrupole instrument*

	a ($\times10^6$)	b ($\times10^6$)	R^2	a ($\times10^6$)	b ($\times10^6$)	R^2	a ($\times10^6$)	b ($\times10^6$)	R^2
	Solvent			**Lemon**			**Lettuce**		
Acetamiprid	13.51	11.04	0.9924	11.17	9.04	0.9881	9.76	12.20	0.9648
Azoxystrobin	50.78	-3.57	0.9995	32.20	15.34	0.9931	17.76	16.43	0.9699
Boscalid	1.07	1.67	0.9977	0.89	0.22	0.9990	0.58	0.14	0.9985
Buprofezin	219.41	2.19	0.9999	69.23	48.51	0.9799	118.17	94.73	0.9748
Cyprodinil	213.60	15.60	0.9999	68.28	60.18	0.9790	97.04	90.62	0.9660
Difenoconazole	5.17	0.10	0.9985	17.40	3.97	0.9991	13.24	1.32	0.9958
Fenhexamid	5.05	-0.65	0.9992	6.19	22.7	0.9923	3.00	-0.16	0.9992
Kresoxim methyl	2.32	0.05	0.9999	3.18	0.23	0.9999	1.37	0.22	0.9958
Metsulfuron methyl	2.60	2.29	0.9981	1.34	2.32	0.9988	1.08	2.95	0.9721
Propiconazole	33.96	0.91	1.0000	23.76	3.84	0.9983	22.22	5.04	0.9979
Pyraclostrobin	22.80	-0.14	1.0000	16.61	2.55	0.9993	12.49	5.41	0.9905
Pyrimethanil	58.54	45.89	0.9907	31.86	49.00	0.9947	36.10	51.75	0.9943
Pyriproxyfen	40.34	-20.23	0.9410	24.84	-19.68	0.9702	36.70	-34.50	0.9570
Tebuconazole	38.83	-0.04	1.0000	22.70	3.57	0.9987	23.19	6.18	0.9965
Trifloxystrobin	46.46	4.43	0.9998	53.91	17.42	0.9970	32.00	18.97	0.9848

Calibration performances assessed via matrix-based pesticides standards

In QuEChERS treated lettuce analyzed on the QqQ instrument the highest sensitivity was achieved for buprofezin (118×10^6 arb. units per µgmL^{-1}); the sensitivity for the following cyprodinil was about 1.2 times lower (Table 1). A mid-range sensitivity ($9.8–36\times10^6$ arb. units per µg mL^{-1}) was achieved for 9 of 15 analytes, while the instrument had lower sensitivity ($0.5 – 3.0\times10^6$ arb. units per µgmL^{-1}) for 4 of 15 analytes (Table 1). The lowest sensitivity of 0.58×10^6 arb. units per µg mL^{-1} was achieved for boscalid.

The highest sensitivity in lettuce extracts analyzed on the linear ion trap instrument of 2.34×10^6 arb. units per µg mL^{-1} was achieved for cyprodinil (Table 2) and it was 41 times

lower than the corresponding one on the QqQ instrument. Almost equal sensitivity was achieved for azoxystrobin, buprofezin, pyriproxyfen and trifloxystrobin (Table 2). The lowest sensitivity of 0.02×10^6 arb. units per µg mL^{-1} was achieved for metsulfuron methyl and it was 54 times lower than the sensitivity for this pesticide on the QqQ instrument. In general, sensitivity on the QqQ was higher than the sensitivity on the linear trap from 5.27 times (boscalid) to 68 times (buprofezin).

In QuEChERS treated lemon analyzed on the QqQ instrument the highest sensitivity was achieved for buprofezin and cyprodinil ($\approx69\times10^6$ arb. units per µgmL^{-1}) (Table 1). A mid-range sensitivity ($11–54\times10^6$ arb. units per µgmL^{-1}) was achieved for 9 of 15 analytes. Lower sensitivity ($0.9–6.2\times10^6$ arb. units per µgmL^{-1}) was achieved for 4 of 15 analytes (Table 1). The lowest sensitivity of 0.89×10^6 arb. units per µg mL^{-1} was achieved for boscalid.

The highest sensitivity in lemon extracts analyzed on the linear ion trap instrument of 1.13×10^6 arb. units per µg mL^{-1} was achieved for cyprodinil (Table 2) and it was 60 times lower than the corresponding one on the QqQ instrument. On the linear trap, almost equal sensitivity was achieved for azoxystrobin, pyriproxyfen and trifloxystrobin, while on the QqQ sensitivity for these pesticides decreased as follows trifloxystrobin > azoxystrobin > pyriproxyfen. The lowest sensitivity of 0.01×10^6 arb. units per µg mL^{-1} was achieved for metsulfuron methyl and it was 134 times lower than the sensitivity for this pesticide on the QqQ instrument. In general, the sensitivity on the QqQ was higher than the sensitivity on the linear trap from 15 times (boscalid) to 138 times (pyraclostrobin).

Table 2 *Linear regression parameters (y = ax + b, conc. range 0.01 – 15.00 µg mL^{-1}) for the analysis of solvent-based, lemon-based and lettuce-based pesticides standards on a linear ion trap instrument*

	a ($\times10^6$)	b ($\times10^6$)	R^2	a ($\times10^6$)	b ($\times10^6$)	R^2	a ($\times10^6$)	b ($\times10^6$)	R^2
	Solvent			**Lemon**			**Lettuce**		
Acetamiprid	0.71	0.52	0.9816	0.20	0.17	0.9767	0.43	0.36	0.9698
Azoxystrobin	2.34	2.06	0.9803	0.62	0.60	0.9647	1.19	1.46	0.9528
Boscalid	0.25	0.65	0.9713	0.06	0.39	0.9997	0.11	0.61	0.9945
Buprofezin	3.08	2.27	0.9838	0.81	0.43	0.9876	1.73	1.36	0.9739
Cyprodinil	4.21	2.86	0.9909	1.13	0.98	0.9736	2.34	2.70	0.9748
Difenoconazole	1.13	-0.09	0.9986	0.30	0.04	0.9990	0.57	0.004	0.9945
Fenhexamid	0.55	0.10	0.9986	0.14	0.03	0.9991	0.27	0.10	0.9930
Kresoxim methyl	0.19	0.02	0.9979	0.05	0.01	0.9974	0.09	0.01	0.9944
Metsulfuron methyl	0.06	0.18	0.9638	0.01	0.09	0.9859	0.02	0.15	0.9726
Propiconazole	0.79	0.13	0.9991	0.21	0.07	0.9957	0.40	0.10	0.9965
Pyraclostrobin	0.63	0.36	0.9893	0.12	0.07	0.9930	0.28	0.14	0.9883
Pyrimethanil	1.82	1.14	0.9935	0.37	0.14	0.9961	0.90	0.54	0.9924
Pyriproxyfen	2.75	1.02	0.9944	0.68	0.29	0.9925	1.33	0.77	0.9882
Tebuconazole	0.75	0.05	0.9998	0.20	0.03	0.9991	0.36	0.09	0.9962
Trifloxystrobin	2.70	0.63	0.9980	0.70	0.29	0.9946	1.33	0.68	0.9908

On the QqQ instruments, in all tested matrices correlation coefficient (R^2) was close to 1; it ranged from 0.9410 to 1.000 (solvent-based standards), from 0.9702 to 0.9999 (lemon-based standards) and from 0.9570 to 0.9992 (lettuce-based standards). On the linear ion trap instrument the conclusions were similar. Correlation coefficient ranged from 0.9638 to 0.9998

(solvent-based standards), from 0.9647 to 0.9991 (lemon-based standards) and from 0.9528 to 0.9965 (lettuce-based standards). Deviation from the back-calculated concentration was in case of each linear regression for each analyte on both instruments less than 20%. Evaluation results for both calibration parameters suggest that, under the tested conditions, reliable analytes quantification could be performed.

CONCLUSION

Calibration performances of analysis on the linear ion trap and triple quadrupole mass analyzers was compared. A batch of solvent-based and QuEChERS treated lettuce- and lemon-based standards of 15 pesticides from 9 chemical classes was analyzed, with both analyzers operating in full scan MS^1 mode. Sensitivity, correlation coefficients and deviation from the back-calculated concentration were estimated from the calculated linear regression. A much higher sensitivity was observed in analysis on the triple quadrupole; the sensitivity for boscalid in solvent was about 4 times higher and for buprofezin 71 times higher on the triple quadrupole than on the linear trap. The same trend in sensitivity could be observed in fruit and vegetables extracts. Shifting from linear trap to triple quadrupole, sensitivity enhancement ranged from about 5 to even 138 times. The other two calibration parameters on both instruments were acceptable, demonstrating the potential for reliable analytes quantification in actual samples analysis.

In conclusion, triple quadrupole instrument has provided much higher sensitivity in multiresidue pesticides analysis. Such instruments should be implemented when highly sensitive analysis is required.

ACKNOWLEDGEMENT

The authors are grateful to the Ministry of Science, Technological Development and Innovation of the Republic of Serbia for financial support according to the contract with registration No. 451-03-33/2026-03/200124 and 451-03-34/2026-03/200383.

REFERENCES

[1] Gao, S., Zhang, Z-P., Karnes, HT. J. Chrom. B 2005, 825, 98–110.

[2] Churchwell, M.I., Twaddle, N.C., Meeker, L.R., *et al*. J. Chrom B 2005, 825, 134–143.

[3] Vatansever, B., Lahrichi, SL., Thiocone, A., *et al*. J. Sep. Sci. 2010, 33, 2478–2488.

EcoTER'26
eco.tfbor.bg.ac.rs
32nd International Conference
Ecological Truth & Environmental Research
24–26 June 2026, Hotel Sunce,
Sokobanja, Serbia

Original Research

THE NATURE OF THE MATRIX EFFECT IN GC/MS PESTICIDES ANALYSIS IN APPLES AND ITS RELATION TO EXTRACT DILUTION

DOI: 10.5937/EcoTER26310A

Darko Anđelković[1,a], Milica Branković[2,b*]

[1] University of Niš, Faculty of Agriculture, Kosančićeva 4, 37000 Kruševac, SERBIA,

[2] University of Niš, Faculty of Sciences and Mathematics, Department of Chemistry, Višegradska 33, 18000 Niš, SERBIA

[a] https://orcid.org/0000-0002-2526-6070

[b] https://orcid.org/0000-0002-8671-7066

Abstract

The alteration in pesticides instrumental signal in complex samples analysis is defined as the matrix effect. The effect is a result of analytes and matrix components interaction within the injector, detector, or chromatography column and its level depends upon several factors such as the type of extraction solvent, clean-up, analyte concentration and chemical class, type and concentration of the matrix etc. The aim of this investigation was to assess the nature of the matrix effect in different matrices, by analysing different apple varieties and separately the peel and the flesh of a variety. Additionally, the possibility of the matrix effect minimization by dilution of sample extracts was investigated. Varietal differences in composition, as well as differences in the composition of peel and flesh, reflected in distinctive matrix effect for these matrices. The dilution seems to be promising approach for the matrix effect minimization. However, how much dilution is allowed depends on the desirable sensitivity of analysis.

Keywords: apple peel, apple flesh, solvent extraction, mass spectrometry.

INTRODUCTION

In complex samples analysis, alteration in pesticides instrumental signal is expected, since sample extracts usually contain great quantity of co-extractives which can influence analyte ionization and detector response. The alteration is defined as the "matrix effect" and its nature can be twofold: the matrix enhancement effects testify to the analyte signal enhancement compared to that in organic solvent; the matrix weakening effects testify to the opposite, that is analyte signal is much more suppressed than that in organic solvent. The effect is a result of analytes and matrix components interaction within the injector, detector, or chromatography column [1]. The level of the effect depends upon several factors such as the type of extraction solvent, clean-up, analyte concentration and chemical class, type and concentration of the matrix, chromatographic separation column and moreover, the structure of inlet, regarding the number and type of the activity points [2,3].

* *milica.chem@outlook.com; milica.brankovic1@pmf.edu.rs*

Several procedures such as the modifications to sample clean-up [4], addition of internal labeled standards, calibration in the matrix or its combination [5], addition of analyte protectants [6] or sample dilution [7] are usually applied to minimize the matrix effect. To estimate the matrix effect two different procedures are usually applied. Single concentration level approach compares analyte signal in a certain matrix and in solvent, at individual concentration level. Multi-concentration level approach compares the slopes of calibration graphs for matrix matched standards against calibration standards in the solvent.

Apples are complex matrices consisting of many compounds including sugars (fructose, glucose, sucrose), organic acids, amino acids, phenolic compounds (chlorogenic acid, protocatechuic acid and hydroxycinnamic acids) and fatty acids from C_{18} family [8,9]. This matrix is quite different among apple varieties and between peel and flesh within a variety. Main differences are expressed in acidity, sugar and pigment content, composition and content of phenolic compounds [10,11].

The aim of this investigation was to evaluate GC/MS analysis of several pesticides in apples by investigating the aspect of the matrix effect. The aim was to assess the nature of the matrix effect in different matrices, by analyzing different apple varieties and separately the peel and the flesh of a variety. Additionally, the possibility of the matrix effect minimization by dilution of sample extracts was investigated. Four pesticides, of which 3 are fungicides and 1 is insecticide, regularly used in apple crops protection were implemented into evaluation.

MATERIALS AND METHODS

Chemicals

Analytical pesticides standards were purchased from AccuStandard® (pyrimethanil and cyprodinil) and from Sigma-Aldrich® (trifloxystrobin and bifenthrin). Dibutyl adipate (DBA) was obtained from Sigma-Aldrich (St Louis, MO, USA). HPLC grade hexane was purchased from Fisher Scientific (USA).

Procedures

Analytical standards preparation

Stock solutions of 100 μgmL^{-1} of individual standards were prepared in hexane and in methanol and were stored in a freezer. Stock standard mixtures of pesticides (working solutions) were prepared freshly each time in hexane by mixing appropriate quantities of the hexane stock solution and subsequent dilution, resulting in final pesticide concentrations: 1, 2.5, 5, 10, 25 and 50 μgmL^{-1}. Internal standard solution (ISTD) of 10 μgmL^{-1} was prepared by dissolving DBA with hexane.

Sample preparation

Granny Smith, Demi Rouge and Golden Delicious apples were randomly chosen at the open-air market (JP ‘Tržnica’, city of Niš, Serbia). Apple fruits were free of visible damage and pests. Two hundred grams of sample taken from five individual units of selected apple varieties were peeled. Peel and flesh were separately chopped and homogenized in food chopper. Analytical sub portions of 20 g were transferred to a glass container. Afterwards, an extraction with 20 mL of hexane was performed. Obtained extracts were transferred to glass

cone tubes and centrifuged (10 min at 3,800 rpm). The upper hexane layer was separated from the solids–water dispersion and used for further experiments.

Instrumental analysis

The gas chromatographic analysis was performed on Agilent 6890 gas chromatograph equipped with 5973 Mass Selective Detector and 7683 autosampler and SGE 25QC2/BPX5 0.25 capillary column (25 m×0.22 mm×0.25 mm, non-polar). The mass spectra were recorded under an electron impact ionization (EI) voltage of 70 eV. The gas chromatograph was operated in split less injection mode. The oven temperature was programed from 90 °C to 280 °C (4 min) at 20°C/min rate; post run: 300 °C (2 min). Helium was the carrier gas with constant flow rate of 1.0 $mLmin^{-1}$. The MSD was used in the single ion-monitoring mode (SIM) at following *m/z*: 198 (pyrimethanil), 224 (cyprodinil), 116, 207, 131 (trifloxystrobin), 181, 166, 165 (bifenthrin) and 185 (DBA).

Matrix effect evaluation

The matrix effect (ME) was calculated by using the Eq. $ME\ (\%) = {(S_1 - S_2)}/{s_2} \times 100$, where S_1 is the slope of the calibration curve obtained by diluting of standards in organic extracts and S_2 is the slope of the curve obtained in organic solvent. Depending on the value of this percentage, matrix effects can be classified into different categories: no matrix effect (from -20 to +20 %), a weak matrix effect (from ±20 to ±50 %) and a strong matrix effect (>±50 %). Four solution sets containing the four pesticides at concentrations 0.10, 0.25, 0.50, 1.00, 2.50 and 5.00 μgmL^{-1} each were prepared by mixing the reagents volumes as presented in Table 1.

Table 1 *Composition of solution sets prepared in fruit matrix with different dilution factors*

Set No.	ISTD vol., µL	Pesticide stock vol., µL	Apple extract vol. (AE_v), µL	Solvent vol., µL	Final vol. (F_v), µL	Dilution factor ($DF=F_v/AE_v$)
1	100	100	0	800	1000	/
2	100	100	800	0	1000	1.25
3	100	100	200	600	1000	5.00
4	100	100	100	700	1000	10.00

RESULTS AND DISCUSSION

Data acquisition for each apple variety was accomplished within one batch. The sequence of 42 injections was performed from lower to higher pesticides concentrations within single set, according to the following pattern: solvent-based, flesh-based and peel-based samples with decreasing dilution factor. Analytes responses were normalized to DBA as internal standard. ME was estimated in relation to the matrix type and matrix concentration.

The matrix effect *vs.* matrix type

The matrix effect was evaluated in six different matrices, that is, separately in peel and flesh of three apple varieties. As can be seen in figure 1 for most matrices there is no matrix effect, i.e., the matrix effect is in the range of ±20 %.

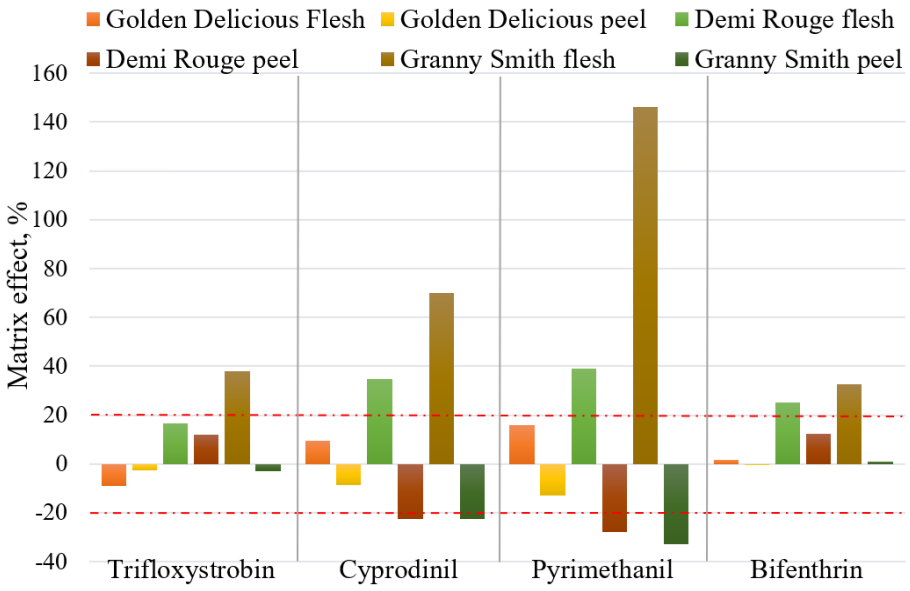

Figure 1 *Matrix effect in peel and flesh extracts (DF=1.25) of tested apple varieties: dotted lines indicate range considered as no matrix effect*

The matrix effect for all tested pesticides was mostly pronounced in Granny Smith extracts. This variety is known for much higher pigment content in both peel and flesh than other apple varieties such as Royal Gala, Golden Delicious [12] and much higher acid content. The positive matrix effect for all pesticides was observed in Granny Smith flesh extract, while in peel extract the effect was negative. Different nature of the ME in these matrices might be explained by the relative abundance of waxes present in these two. In chromatograms of peel extracts of tested varieties (not shown here), a peak of a compound eluting at 12.37 minutes can be observed. Mass spectra of the compounds contain mass fragments that suggest long-chain aliphatic structure, that is suggest the compound is from the group of waxes. This compound was most abundant in peel extract of Granny Smith, while in peel extracts of Golden Delicious and Demi Rouge variety was 5-times and 1.5-times less abundant, respectively. Comparison of chromatograms of peel and flesh extract of Granny Smith variety (not shown here) showed 42-times higher presence of this compound in peel that matches the fact that apple waxes prevail in peel.

The positive matrix effect observed in flesh extracts can be explained by phenomena called "matrix-induced chromatographic response enhancement effect". The phenomena indicate that the co-extractives "compete" with the analytes for the injector active sites, causing transfer of a larger amount of analyte to the column. The inversion of the matrix effect in peel extract (with exception of bifenthrin) was possibly due to the evaporation and re-condensation in the injector of much larger amounts of waxes, which fixate analytes in wax matrix and/or blocks entrance to the column and analyte loading.

The matrix effect *vs.* matrix concentration

The matrix concentration is the mass of the extracted test portion divided by the volume of the extraction solvent. Here, the concentration of obtained extract was 1 gmL^{-1} and after the dilution decreased to 0.80 (DF=1.25), 0.20 (DF=5) and 0.10 gmL^{-1} (DF=10).

Figure 2 shows the ME behaviour with dilution for tested pesticides in all matrices; additional discussion is made on dilution graphs for pesticides with the most pronounced ME (Figure 1).

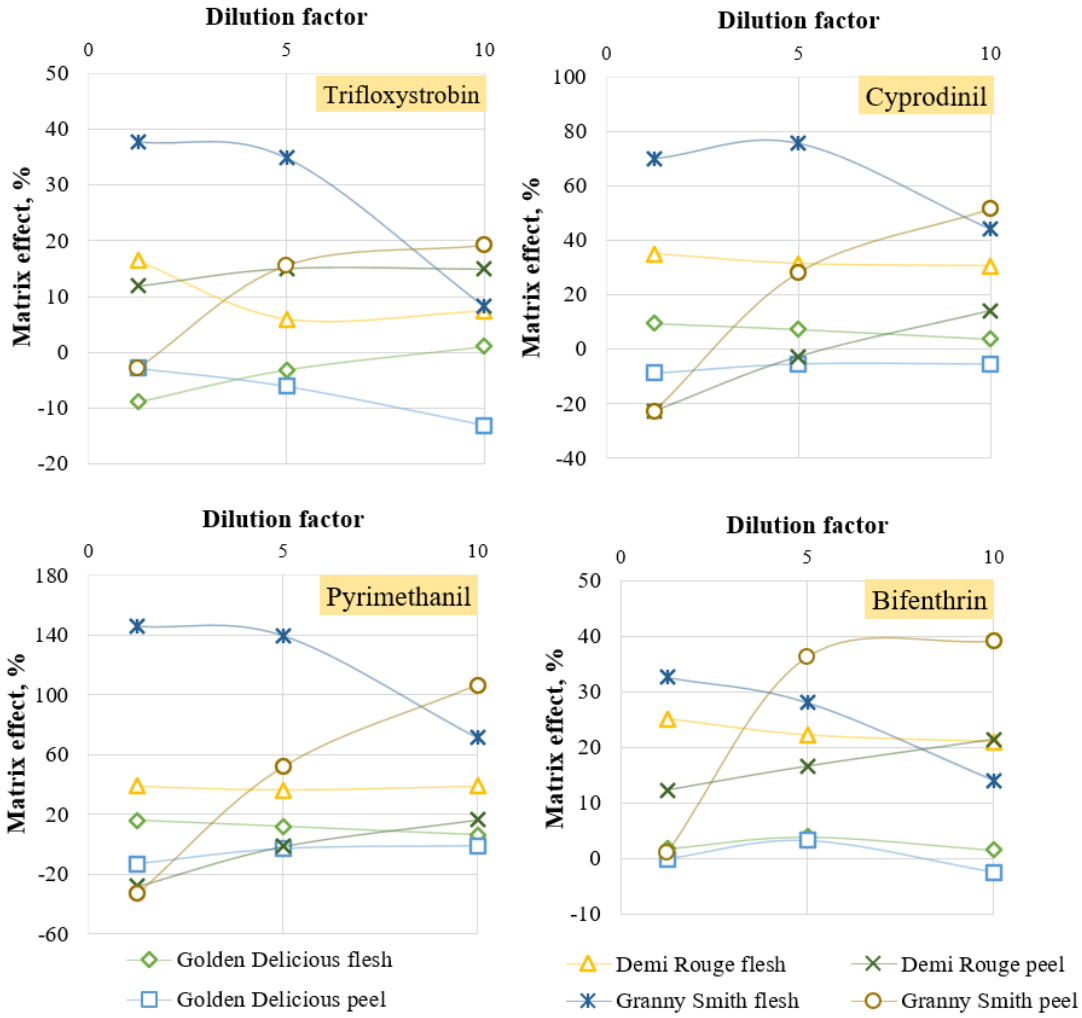

Figure 2 *The matrix effect* vs. *extract dilution factor*

The highest ME for trifloxystrobin (37.80 %) was observed in Granny Smith flesh extract and after 8-fold matrix dilution decreased to 8.20 % (4.6 times). For cyprodinil, the ME was most pronounced in Demi Rouge (34.90 %) and Granny Smith flesh extract (70.10 %). Final dilution resulted in 1.13- and 1.6-times lower ME, respectively. For pyrimethanil the ME in Demi Rouge flesh extract remained at about 40 % after the dilution, but in Golden Delicious peel and Granny Smith flesh extract decreased 14.3 and 2 times, respectively.

For the Granny Smith peel extract matrix effect – dilution graphs were different. The initial ME for all pesticides in this matrix, with exception of bifenthrin (0.98%), was negative, nevertheless with dilution moved towards positive values making an inversion. Inversion for trifloxystrobin ranged from -2.80 % (DF=1.25) to 19.20 % (DF=10). Increase in ME values from -22.50 to 51.50 % (cyprodinil) and from -33.00 to 106.40 % (pyrimethanil) made the inversion even higher. Negligible ME value for bifenthrin (0.98 %) increased with 8-fold matrix dilution up to 39.20 % (40 times). The manifestation of inversion with dilution is possibly related to reduction in the concentration of waxes.

CONCLUSION

In Golden Delicious variety, both in peel and flesh, the matrix effect for all tested analytes was negligible. Noticeable matrix effect for all analytes was observed for Demi Rouge and Granny Smith variety. The matrix effect in flesh matrices was positive. However, in peel matrices it was negative. In both cases, the matrix effect was more pronounced in Granny Smith variety.

Dilution of sample extracts in most cases led to minimization of the ME. In flesh matrices, the dilution resulted in less positive matrix effect values, in peel matrices it resulted in less negative values. However, in Granny Smith peel, the dilution resulted in inverted matrix effect. The highest difference was observed for pyrimethanil, where the matrix effect changed from – 33 % to 106 % after the dilution.

Matrix type has some influence on the expressed matrix effect. Varietal differences in composition, as well as differences in the composition of peel and flesh, reflected in distinctive matrix effect for these matrices. The dilution seems to be promising approach for the matrix effect minimization. However, how much dilution is allowed depends on the desirable sensitivity of analysis.

ACKNOWLEDGEMENT

The authors are grateful to the Ministry of Science, Technological Development and Innovation of the Republic of Serbia for financial support according to the contract with registration No. 451-03-33/2026-03/200124 and 451-03-34/2026-03/200383.

REFERENCES

[1] de Sousa, F.A., Costa, A.I.G., de Queiroz, M.E.L.R., *et al.*, Chromatographia 2013, 76, 67–73.

[2] Pang, G.F., Fan, C.L., Chang, Q.Y., Yang, F., Cao, Y.Z. In Analysis of Pesticide in Tea, Chromatography-Mass Spectrometry Methodology; Amsterdam: Elsevier, 2018. pp. 535–595.

[3] Silvestro, L., Tarcomnicu, I., Savu, S.R. In Tandem Mass Spectrometry – Molecular Characterization; Coelho, A.V., Ed.; IntechOpen: London, 2013. pp. 3–37.

[4] Kim, Y.A., El-Aty, A.M.A., Rahman, M.M., *et al.*, J. Chromatogr. B. 2018, 1076, 130–138.

[5] Tsuchiyama, T., Katsuhara, M., Nakajima, M., J. Chromatogr. A. 2017, 1524, 233–245.

[6] Li, Y., Chen, X., Fan, C., *et al.*J. Chromatogr. A. 2012, 1266, 131–142.

[7] Ferrer, C., Lozano, A., Aguera, A., Jimenez Giron, A., Fernandez-Alba, A.R., J. Chromatogr. A. 2011, 1218, 7634–7639.

[8] Wu, J., Gao, H., Zhao, L., *et al.*Food Chem. 2007, 103, 88–93.

[9] Persic, M., Mikulic-Petkovsek, M., Slatnar, A., *et al.*, LWT—Food Sci. Technol. 2017, 82, 23–31.

[10] Lata, B.;, Trampczynska, A., Paczesna, J., Sci. Hortic. 2009, 121, 176–181.

[11] Raudone, L., Raudonis, R., Liaudanskas, M., *et al.*, Sci. Hortic. 2017, 216, 186–192.

[12] Kalinowska, M., Bielawska, A., Lewandowska-Siwkiewicz, H., *et al.*, Plant Physiol. Biochem. 2014, 84, 169–188.

EcoTER'26
eco.tfbor.bg.ac.rs
32nd International Conference
Ecological Truth & Environmental Research
24–26 June 2026, Hotel Sunce,
Sokobanja, Serbia

Original Research

DEGRADATION OF PONCEAU S DYE BY ADVANCED OXIDATION PROCESSES: COMPARATIVE ANALYSIS AND TOXICITY OF TRANSFORMATION PRODUCTS

DOI: 10.5937/EcoTER26316S

Isidora Santrač[1,a*], Filip Sekereš[2,b], Marijana Živković[3,c], Jelena Korać Jačić[1,d], Milica Milenković[4,e], Jelena Danilović Luković[1,f]

[1] University of Belgrade, Institute for multidisciplinary research, National Institute of the Republic of Serbia, Kneza Višeslava 1, 11030 Belgrade, SERBIA

[2] University of Belgrade, Faculty of Physical Chemistry, Studentski trg 12–16, 11000 Belgrade, SERBIA

[3] University of Belgrade Institute of Chemistry, Technology and Metallurgy – National Institute of the Republic of Serbia, Studentski trg 12–16, 11000 Belgrade, SERBIA

[4] University of Belgrade, Faculty of Chemistry, Studentski trg 12–16, 11000 Belgrade, SERBIA

[a] https://orcid.org/0000-0001-8533-4250 [b] https://orcid.org/0009-0006-3691-7445

[c] https://orcid.org/0000-0002-1978-1308 [d] https://orcid.org/0000-0002-3802-6009

[e] https://orcid.org/0000-0003-2053-3704 [f] https://orcid.org/0000-0003-2411-5032

Abstract

This study investigates the degradation of Ponceau S (PS), a synthetic azo dye, using advanced oxidation processes (AOPs), including UV irradiation, UV/Fe(III), and UV/Fe(III)/H_2O_2 systems. The aim was to compare the decolorization efficiency and kinetics of these processes, and to assess the toxicity of the generated products on the extremophilic microalga Chlamydomonas acidophila PM01. UV irradiation alone showed no significant effect on PS degradation. In contrast, systems involving Fe(III) ions led to notable decolorization. This was further enhanced in the presence of H_2O_2 due to increased generation of hydroxyl radicals. The highest degradation efficiency was observed in the UVA/Fe(III)/H_2O_2 and UVB/Fe(III)/H_2O_2 systems. Toxicity assessment revealed that untreated PS did not significantly affect microalgal growth or viability. However, degradation products formed during AOPs treatment induced a decrease in cell viability, implying the emergence of reactive and potentially harmful intermediates. These findings highlight the importance of evaluating both degradation efficiency and ecotoxicological impact when applying AOPs for dye removal from wastewater.

Keywords: photodegradation, Ponceau S, AOPs, toxicity, *Chlamydomonas acidophila* PM01.

INTRODUCTION

Synthetic azo dyes are the most widely used classes of colorants in industries such as textiles, printing, cosmetics, food processing, and pharmaceuticals [1]. However, their presence in wastewater represents a significant environmental concern due to their high

*isantrac@imsi.bg.ac.rs

stability, resistance to biodegradation, and potential toxicity [2]. Also, the presence of aromatic rings and azo (–N=N–) bonds in their structures, makes their removal from aquatic environments by conventional wastewater treatment methods challenging [3,4]. Ponceau S (PS) is azo dye commonly used in dying industry of textile, leather and paper and as a staining reagent for proteins in biochemical analyses [5–7].

Advanced oxidation processes (AOPs) offer promising opportunities for degradation or even mineralization of synthetic dyes. Among AOPs, those involving hydrogen peroxide such as H_2O_2/UV, the Fenton process and the photo-Fenton process generate highly reactive and no selective hydroxyl radicals $^{\bullet}OH$. Hydroxyl radicals are also produced by photolysis of Fe(III) hydroxo complexes without addition of H_2O_2 [8,9].

The aim of this study is (a) to compare the decolorization rates of PS dye induced by UV irradiation, UV induced photolysis of Fe(III) hydroxo complexes, and UV induced photolysis of Fe(III) hydroxo complexes in the presence of H_2O_2, and (b) to evaluate toxicity of PS and its degradation products on extremophilic microalga *Chlamydomonas acidophila* PM01.

MATERIALS AND METHODS

Reagents

The PS was purchased from Serva GmbH. Hydrogen peroxide (H_2O_2, 30%) was obtained from Sigma-Aldrich, while $FeCl_3 \times 6H_2O$ was supplied by Centroprom. All experiments were carried out using bidistilled, deionized ultrapure water (18 MΩ). Stock solutions of PS (1 mM), $FeCl_3$ (1 mM), and H_2O_2 (10 mM) were prepared in deionized water. The pH of the solutions was adjusted to pH 5 using NaOH or HCl.

UV-Vis spectroscopy

The UV-visible (UV-Vis) spectra of samples were recorded from 200 to 800 nm using UV-Vis spectrophotometer Shimadzu UV-i1900 with a spectrometric quartz cell (1 cm path length). All samples were freshly prepared, and measurements were performed immediately after preparation. Scan time was 50 s.

Irradiation

Samples were prepared in deionized water pH 5 (sample volume 1 mL), placed in a quartz cuvette (1 cm × 1 cm × 5 cm), and exposed to UV radiation up to 10 minutes using a lamp equipped with a filter for visible light (Carl Roth GmbH, Karlsruhe, Germany, H469.1), and UV tubes (Sankyo Denki, Tokyo, Japan). Measurements were carried out immediately after sample preparation (for non-irradiated systems), or 30 s after the end of UV irradiation. The UV A and UV B lamps emitted maximum radiation at wavelengths of 312 nm and 352 nm, respectively. The irradiation took place in a temperature-controlled chamber, and the irradiance was set at 17 J $m^{-2}s^{-1}$ for UV A and 7.7 J $m^{-2}s^{-1}$ for UV B.

Algae culture and growth analysis

C. acidophila strain PM01 was isolated from acid mine drainage from Parys Mountain, Anglesey North Wales, UK. Microalgae were grown under photoautotrophic conditions in an optimal, nutrient sufficient modified MAM medium, with a composition prepared according to Olaveson and Stokes (1989) [10]. The initial pH of the medium was set to ~3. Microalgal

culture replicates were added to 50 mL of MAM medium in 100 mL Erlenmeyer flasks at the initial density of 5×10^5 cells/mL. Microalgae were grown at 22 °C on orbital shakers (120 rpm) in a growth cabinet with a continuous photon flux of 120 µmol m^{-2} s^{-1} (MST TL-D Reflex 36W840 1 SLV/25 tubes, Philips, Amsterdam, The Netherlands). The culture's growth was monitored on the three independent samples by optical density at 750 nm (OD_{750}) and 680 nm (OD_{680}), and the viability of the cell cultures, until the reaching of late stationary phase of growth (19 days). Cultures were treated using degradational products of PS in final concentrations 50 µM PS, 20 µM Fe^{3+} and 100 µM H_2O_2. After 24 h of treatment, both treated cultures and corresponding controls (untreated) were assessed for the biomass concentration (OD_{750}), an indirect indicator of chlorophyll a content (OD_{680}) [11]. Absorbance at 750 nm was used to correct for turbidity, and the OD_{680}/ OD_{750} ratio was taken as a relative chlorophyll a per unit biomass [12]. OD was estimated using a UV-Vis spectrophotometer (Jenway Genova Plus, Staffordshire, UK). For measurements, samples were diluted to maintain the OD values below 1. The effects of PS degradation products on cell viability were tested using the Evans Blue stain, commonly used measure of cell viability [13]. Non-viable cells have compromised or ruptured membranes with increased permeability, which enables the uptake and accumulation of Evans Blue dye. Cell viability is expressed as the percentage of Evans Blue negative cells. At least 100 cells were analyzed per sample.

RESULTS AND DISCUSSION

The effect of UV irradiation on the degradation of PS azo dye in aqueous solution at pH 5 was investigated using UV–Vis spectroscopy (Figure 1).

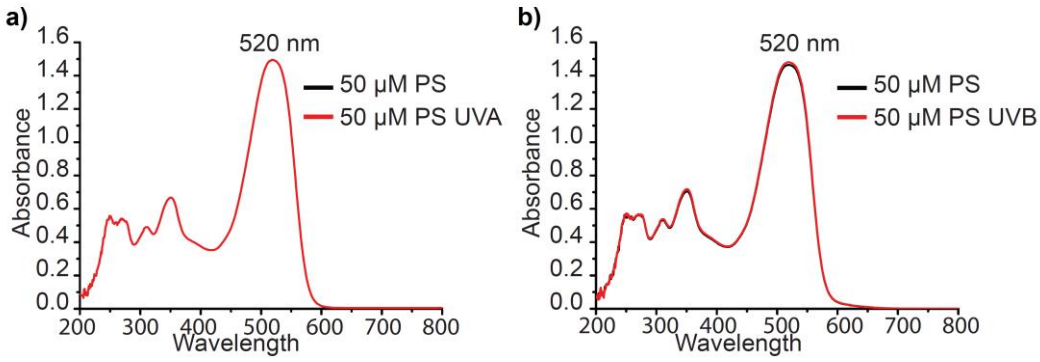

Figure 1 *Effect of UV irradiation on 50 µM PS in aqueous solution at pH 5 under: a) UVA irradiation; b) UVB irradiation*

The UV–Vis spectrum of PS exhibits four distinct absorption maxima in the 200–400 nm range, along with a prominent absorption band in the visible region at 520 nm, which can be attributed to n→π* transitions of the N=N chromophore [14]. After exposure of PS to UVA and UVB irradiation (Figure 1a,b), no changes in the absorption maxima or band positions were observed. These results indicate that UVA and UVB irradiation do not promote degradation of PS via photo induced reactions under the applied experimental conditions.

On the other hand, the effects $^{\bullet}OH$ radicals produced by UV induced photolysis of Fe(III) hydroxo complexes on the degradation of PS (50 μM) are shown in Figures 2a,b). A noticeable decrease in absorbance at 520 nm is observed upon UV irradiation of PS in the presence Fe^{3+} ions. Under UVA irradiation, the absorbance decreases progressively, as confirmed by the time-dependent plot (Figure 2a), where A_{520} drops significantly over 10 minutes. Similar results are observed under UVB irradiation (Figure 2b). Time-dependent measurements further demonstrate that the degradation process follows a gradual decline in absorbance intensity, indicating a continuous transformation or degradation of the absorbing species. Additionally, the reduction in absorbance at 520 nm is more pronounced in the UV irradiated system containing Fe^{3+} ions and H_2O_2, compared to Fe^{3+} alone (Figure 2c,d).

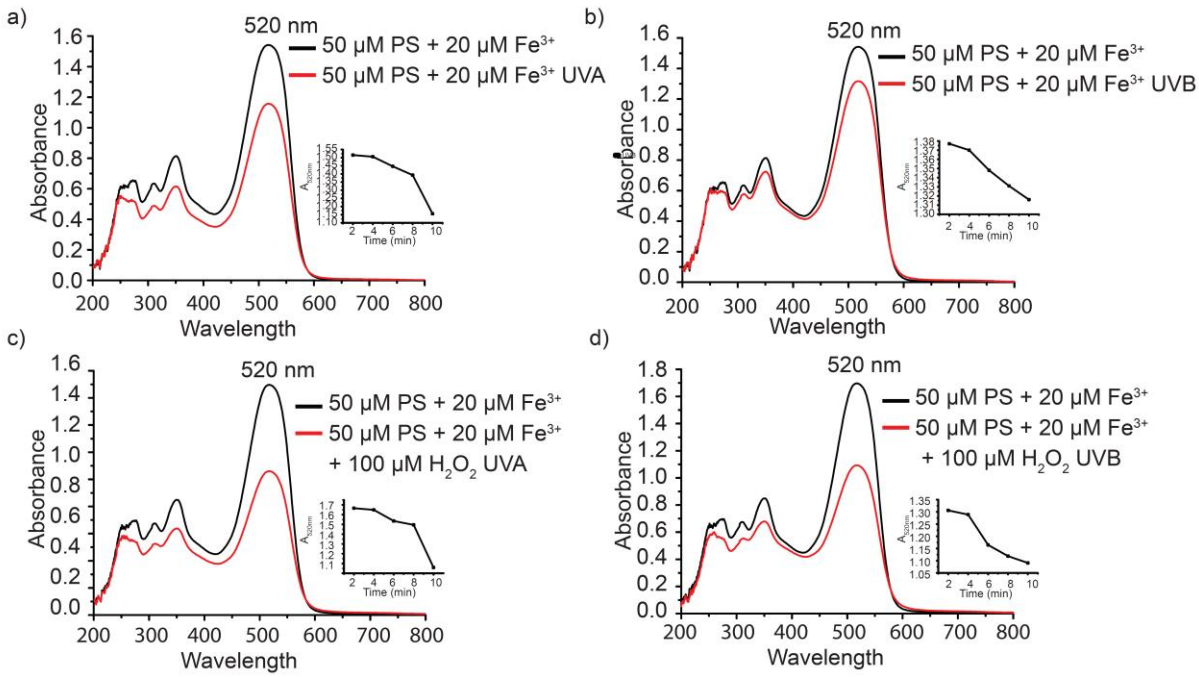

Figure 2 *Effect of UV irradiation on a 50 μM PS aqueous solution in the presence of 20μM Fe^{3+} at pH 5 under: a) UVA irradiation; b) UVB irradiation; as well as in the presence of 20 μM Fe^{3+} and 100 μM H_2O_2 under: c) UVA irradiation; d) UVB irradiation*

The efficiency of the UV/Fe^{3+} and UV/Fe^{3+}/H_2O_2 systems, as well as the reaction kinetics for these processes are presented at Figure 3. Under UVA irradiation (Figure 3a), the decolorization efficiency gradually increase with time for both systems. However, the UVA/Fe^{3+}/H_2O_2 system consistently showed higher removal efficiency than UVA/Fe^{3+} alone. After 10 minutes, the decolorization reached approximately 35% in the presence of H_2O_2, compared to about 24% without it. The rate constant for UVA/ Fe^{3+}/H_2O_2 ($k = 0.01983\ min^{-1}$) is higher than that of UVA/Fe^{3+} ($k = 0.01469\ min^{-1}$), confirming the positive role of H_2O_2 in decolorization process. This improvement can be attributed to the photo-Fenton-like reaction, where H_2O_2 reacts with Fe^{2+} to produce highly reactive $^{\bullet}OH$ radicals. Under UVB irradiation (Figure 3b), the decolorization efficiency was evidently higher for the UVB/Fe^{3+}/H_2O_2 system compared to the UVB/Fe^{3+} system. The UVB/Fe^{3+}/H_2O_2 system achieved approximately 35% removal within 10 minutes, whereas the UVB/Fe^{3+} system

reached only about 12%. This enhanced performance under UVB can be attributed to its higher photon energy, which facilitates more efficient photolysis of H_2O_2 and faster regeneration of Fe^{2+}, thereby accelerating hydroxyl radical production. The kinetic constants further support this observation: the rate constant for the UVB/Fe^{3+}/H_2O_2 system (k = 0.02506 min^{-1}) is significantly higher than that for the UVB/Fe^{3+} system (k = 0.00598 min^{-1}), indicating a substantially faster reaction rate when both UVB and H_2O_2 are present.

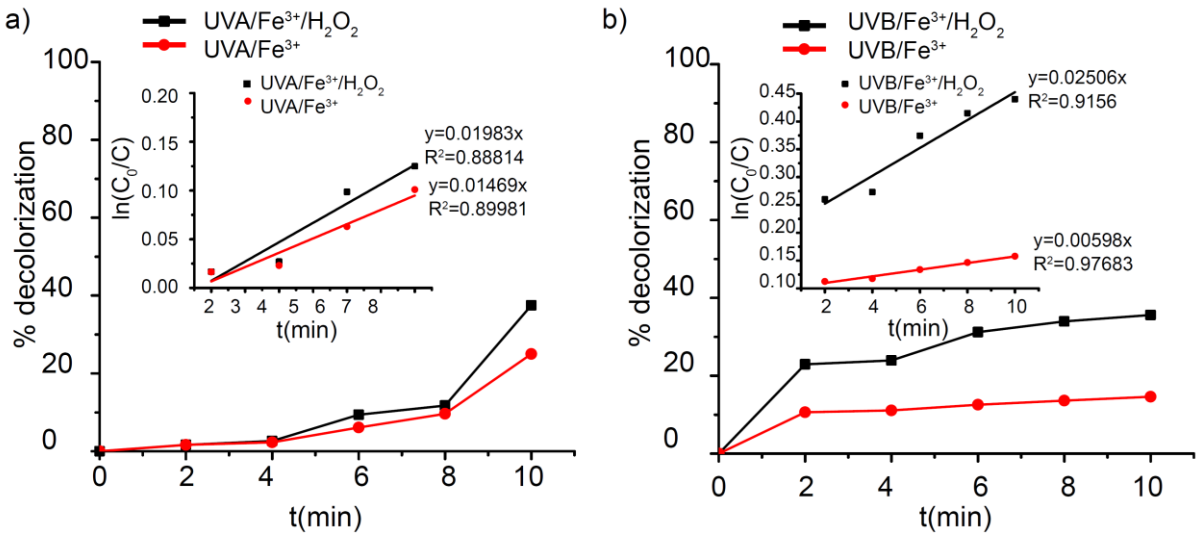

Figure 3 *Comparison of PS decolorization by UV/Fe^{3+} and UV/Fe^{3+}/H_2O_2 systems under: a) UVA; b) UVB irradiation. Experimental conditions: [PS] = 0.05 mM, [H_2O_2] = 1 mM, [Fe^{3+}] = 0.02 mM, pH 5. Inset: Kinetics of the decolorization processes*

Azo dyes and their degradation products have been widely reported to exert toxic effects on aquatic organisms, including microalgae, with impacts on growth and photosynthetic pigments as part of stress responses [15]. Regardless of the wavelength, OD values followed a similar trend (Figure 4a). Treatments with H_2O_2 led to an increase in OD, likely reflecting an oxidative stress response (Figure 4a). Low-dose exposure to H_2O_2 can trigger stress acclimation responses in microalgae, which may temporarily enhance metabolic activity without causing immediate damage [16] An increase in OD values was also observed in the case of PS exposed to UV irradiation (Figure 4a). Since we established that no significant photodegradation occurs under UV irradiation alone (Figure 1), this suggests that the effects are attributable to the parent azo dye [17]. On the other hand, treatment using pure PS exhibited similar OD values to the control (Figure 4a). Although, to the best of our knowledge, no data are available on the effects of PS on microalgae, other azo dyes, including typical monoazo compounds, have been reported to exert toxic effects on microalgae [18,19]. Therefore, rather than outright cytotoxicity, PS exposure may instead elicit transient metabolic responses that can include stress-induced changes in photosynthetic activity. Interestingly, the A_{680}/A_{750} ratios, which reflect chlorophyll content relative to biomass, were very similar across all treatments. This ratio is commonly used as an indicator of photosynthetic activity and the physiological state of microalgal cells [12] suggesting that

photosynthetic function was largely maintained in all treated groups. However, peaks were observed in the Fe treatment and in all combinations with UVA (Figure 4a).

A marked reduction in viability was observed in *C. acidophila* following 24 h treatment with H_2O_2 and Fenton reagents, and was likewise evident in samples treated with PS in combination with Fe^{3+} or H_2O_2 (Figure 4b). Hydrogen peroxide and Fenton-type reactions are well known to induce cytotoxicity through the generation of highly reactive hydroxyl radicals, leading to oxidative damage, lipid peroxidation, and cell death [20]. High impact on cell viability was observed following PS photodegradation under UVB irradiation (Figure 4b), where no changes in absorption maxima or band positions were detected (Figure 1b). This effect may be attributed to light screening and photophysical interference in the presence of the azo dye rather than to the degradation products themselves, as strongly absorbing dyes can attenuate incident radiation through absorption and inner filter effects [21]. Further, the trend in viability largely mirrored that observed during the decolorization process (Figures 3 and 4). Thus, PS in combination with Fe^{3+} and H_2O_2 and UVA induced a decrease in viability of more than 10% compared to the corresponding control (Figure 4b). A similar trend, although to a lesser extent, was also observed for treatments using photolysis products of PS under both types of irradiations (Figure 4b). However, this did not reflect the relationship observed in decolorization efficiency (Figure 3). Specifically, photolysis under UVA irradiation was approximately twice as effective, whereas the percentage of viable cells remained nearly the same for both treatments (Figure 4b). These results suggest that, under the applied AOPs for PS degradation, cytotoxic effects may arise due to the formation of reactive and potentially toxic transformation products [22].

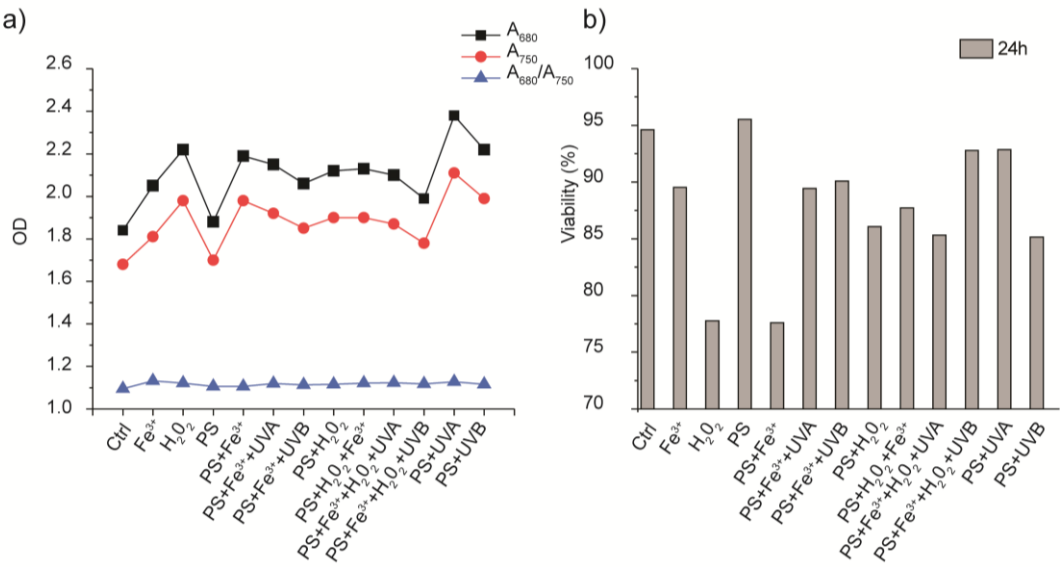

Figure 4 *a) Growth (optical density at 750 nm and 680 nm); and b) cell culture viability (Evans Blue staining) determined 24h after the exposure to PS and its degradation products*

CONCLUSION

The results of this study demonstrate that UV irradiation alone is not effective for the degradation of PS, confirming its photostability under the applied conditions. In contrast, the

inclusion of Fe(III) ions significantly enhances the decolorization process, while the addition of H_2O_2 further improves efficiency due to intensified hydroxyl radical production via photo-Fenton-like reactions. Among the tested systems, the UVA/Fe(III)/H_2O_2 and UVB/Fe(III)/H_2O_2 processes showed the highest degradation rate and overall efficiency.

Toxicity assessment revealed that the parent dye did not significantly affect the growth and viability of *Chlamydomonas acidophila* PM01. However, degradation products formed during AOPs treatment exhibited appreciable effects on cell viability, indicating the generation of reactive and potentially harmful intermediates. These findings emphasize that, in addition to removal efficiency, the formation and impact of transformation products must be carefully considered when applying AOPs for wastewater treatment.

ACKNOWLEDGEMENT

The authors are grateful to the Ministry of Science, Technological Development and Innovation of the Republic of Serbia for financial support according to the contract with registration No. 451-03-33/2026-03/ 200053, 451-03-33/2026-03/ 200168 and 451-03-33/2026-03/ 200026.

REFERENCES

[1] Slama, H.B., Chenari Bouket, A., Pourhassan, Z., *et al*. Appl. Sci. 2021, 11 (14), 6255.

[2] Parida, V.K., Singh, N., Priyadarshini, M., *et al*. J. Ind. Eng. Chem. 2025. 150, 247–264.

[3] Hassaan, M.A., El Nemr, A., Hassaan, A. Am. J. Environ. Sci. Eng. 2017, 1 (3), 64–67.

[4] Elmorsi, T.M., Riyad, Y.M., Mohamed, Z.H., *et al*. H.M. J. Hazard. Mater. 2010, 174 (1–3), 352–358.

[5] Meena, R.C., Pachwarya, R.B., Meena, V.K., *et al*. Am. J. Environ. Sci. 2009, 5 (3), 444–450.

[6] Chung, K.T. Mutat. Res./Rev. Genet. Toxicol. 1983, 114 (3), 269–281.

[7] Bannur, S.V., Kulgod, S.V., Metkar, S.S., *et al*. Anal. Biochem. 1999, 267 (2), 382–389.

[8] Komić, S.M., Pristov, J.B., Popović-Bijelić, A., *et al*. Appl. Catal., B 2016, 185, 174–180.

[9] Thomas, N., Dionysiou, D.D., Pillai, S.C. J. Hazard. Mater. 2021, 404, 124082.

[10] Olaueson, M.M., Stokes, P.M. J. Phycol. 1989, 25 (3), 529–539.

[11] Griffiths, M.J., Garcin, C., van Hille, R.P., *et al*. J. Microbiol. Methods 2011, 85 (2), 119–123.

[12] Sivakaminathan, S., Hankamer, B., Wolf, J. *et al*. Sci. Rep. 2018, 8 (1), 1–13.

[13] Zuppini, A., Andreoli, C., Baldan, B. Plant Cell Physiol. 2007, 48 (7), 1000–1009.

[14] Chatib, B., Laftani, Y., Khayar, M., *et al*. Iran. J. Chem. Chem. Eng. 2021, 40 (1), 111–121.

[15] Hernández-Zamora, M., Martínez-Jerónimo, F. Ecotoxicology. 2019. 28(8), 890–902.

[16] Barone, M.E., Parkes, R., Herbert, H., *et al*. Appl. Biochem. Biotechnol. 2021, 193 (12), 4052–4067.

[17] Akshaya Vidhya, T., Veena Gayathri, K., Senthil Kumar, P., *et al*. Int. J. Chem. Eng. 2022, 2022 (1), 7083772.

[18] Hernández-Zamora, M., Martínez-Jerónimo, F. Ecotoxicology 2019, 28 (8), 890–902.

[19] Liang, J., Zhang, C.M., Zhu, C.C. Chemosphere 2024, 349, 140947.

[21] Winterbourn, C.C. In: Proceedings of the International Congress of Toxicology – VII; July 2–6; Washington, USA. 1995. p. 969–974.

[22] Abrusci, C., Marquina, D., Santos, A., *et al*. J. Photochem. Photobiol., A 2007, 185 (2–3), 188–197.

EcoTER'26
eco.tfbor.bg.ac.rs
32nd International Conference
Ecological Truth & Environmental Research
24–26 June 2026, Hotel Sunce,
Sokobanja, Serbia

Original Research

BIOLOGICAL EFFECTS OF EVANS BLUE AND ITS DEGRADATION PRODUCTS ON GROWTH AND VIABILITY OF THE GREEN MICROALGA *Chlamydomonas acidophila* PM01

DOI: 10.5937/EcoTER26324S

Isidora Santrač[1,a*], Filip Sekereš[2, b], Marijana Živković[3,c], Jelena Korać Jačić[1,d], Milica Milenković[4,e] Jelena Danilović Luković[1,f]

[1] University of Belgrade, Institute for multidisciplinary research, National Institute of the Republic of Serbia, Kneza Višeslava 1, 11030 Belgrade, SERBIA

[2] University of Belgrade, Faculty of Physical Chemistry, Studentski trg 12–16, 11000 Belgrade, SERBIA

[3] University of Belgrade Institute of Chemistry, Technology and Metallurgy – National Institute of the Republic of Serbia, Studentski trg 12–16, 11000 Belgrade, SERBIA

[4] University of Belgrade, Faculty of Chemistry, Studentski trg 12–16, 11000 Belgrade, SERBIA

[a] https://orcid.org/0000-0001-8533-4250 [b] https://orcid.org/0009-0006-3691-7445

[c] https://orcid.org/0000-0002-1978-1308 [d] https://orcid.org/0000-0002-3802-6009

[e] https://orcid.org/0000-0003-2053-3704 [f] https://orcid.org/0000-0003-2411-5032

Abstract

This study investigates the degradation of Evans Blue (EB) under UV irradiation and oxidative conditions, as well as the impact of its transformation products on the growth and viability of Chlamydomonas acidophila PM01. UV–Vis analysis showed that EB is stable under direct UV exposure, while the presence of Fe^{3+} *and* H_2O_2 *significantly enhanced its degradation via photo-Fenton processes. Cellular response analysis showed that EB alone had no notable effect on algal growth. However, its degradation products containing EB,* Fe^{3+}*, and* H_2O_2 *caused reduced cell density and increased physiological stress, while products formed under UVB irradiation significantly decreased viability. These findings suggest that although EB itself is relatively stable and non-toxic, its degradation products may exert considerable ecological impact.*

Keywords: photodegradation, Evans Blue, toxicity, viability, *Chlamydomonas acidophila* PM01.

INTRODUCTION

The environmental fate and biological effects of dye degradation products remain insufficiently understood, particularly in aquatic systems where such compounds may interact with primary producers. While EB is widely used as a biological stain, its transformation under UV irradiation in oxidative conditions can lead to the formation of reactive intermediates with altered biological activity [1]. Green microalgae, such as *Chlamydomonas acidophila*, represent sensitive model organisms for assessing the impact of such compounds,

* *isantrac@imsi.bg.ac.rs*

as this extremophilic species exhibits high metabolic plasticity and tolerance to various environmental stressors, including heavy metals [2]. In this context, the present study investigates the effects of Evans Blue degradation products on the growth and cell viability of *C. acidophila* PM01.

MATERIALS AND METHODS

Reagents

The Evans Blue was purchased from Serva GmbH. Hydrogen peroxide (H_2O_2, 30%) was obtained from Sigma-Aldrich, while $FeCl_3 \times 6H_2O$ was supplied by Centroprom. All experiments were carried out using bidistilled, deionized ultrapure water (18 MΩ). Stock solutions of EB (1 mM), $FeCl_3$ (1 mM), and H_2O_2 (10 mM) were prepared in deionized water. The pH of the solutions was adjusted to pH 5 using NaOH or HCl.

UV-Vis spectroscopy

The UV-visible (UV-Vis) spectra of samples were recorded from 200 to 800 nm using UV-Vis spectrophotometer Shimadzu UV-i1900 with a spectrometric quartz cell (1 cm path length). Samples were prepared in deionized water pH 5 (sample volume 1 mL), placed in a quartz cuvette (1 cm × 1 cm × 5 cm), and exposed to UV radiation up to 60 minutes using a lamp equipped with a filter for visible light (Carl Roth GmbH, Karlsruhe, Germany, H469.1), and UV tubes (Sankyo Denki, Tokyo, Japan). Measurements were carried out immediately after sample preparation (for non-irradiated systems), or 30 s after the end of UV irradiation. The UV A and UV B lamps emitted maximum radiation at wavelengths of 312 nm and 352 nm, respectively. The irradiation took place at 25 ºC in a temperature-controlled chamber, and the irradiance was set at 17 J $m^{-2}s^{-1}$ for UV A and 7.7 J $m^{-2}s^{-1}$ for UV B.

Algal culture growth and viability assessment

The *Chlamydomonas acidophila* strain PM01 was originally isolated from acid mine drainage at Parys Mountain (Anglesey, North Wales, UK). Cultures were maintained under photoautotrophic conditions in modified MAM medium enriched with nutrients and prepared according to Olaveson and Stokes [3]. The medium was adjusted to an initial pH of approximately 3. For cultivation, microalgal inocula were transferred into 50 mL of MAM medium in 100 mL Erlenmeyer flasks at a starting density of 5×10^5 cells/mL. Cultures were incubated at 22 ºC on an orbital shaker (120 rpm) under continuous illumination (120 μmol m^{-2} s^{-1}; MST TL-D Reflex 36W840 1 SLV/25, Philips, Amsterdam, The Netherlands). Growth progression was followed by measuring optical density at 750 nm and 680 nm (OD_{750} and OD_{680}) until the early stationary phase was reached (15 days). Following cultivation, cultures were exposed for 24 h to degradation products of EB under defined conditions (10 μM EB, 20 μM Fe^{3+}, and 100 μM H_2O_2), alongside corresponding untreated controls. Biomass was estimated via OD_{750}, while OD_{680} served as a proxy for chlorophyll a content [4]. Turbidity correction was performed using OD_{750}, and the OD_{680}/OD_{750} ratio was used to estimate relative chlorophyll a content per biomass unit [5]. Absorbance measurements were carried out using a UV–Vis spectrophotometer (Jenway Genova Plus, Staffordshire, UK), with samples appropriately diluted to keep absorbance values below 1. Cell viability after exposure to EB degradation products was assessed using EB staining [6].

This assay identifies cells with compromised membranes, as non-viable cells accumulate the dye due to increased membrane permeability. Viability was expressed as the percentage of Evans Blue-negative cells, with at least 100 cells evaluated per sample.

RESULTS AND DISCUSSION

The UV-Vis spectra of EB exhibited characteristic absorption bands at 247, 311, 398, and 620 nm (Figure 1). These bands are associated with π→π* and n→π* electronic transitions of the aromatic rings, azo groups (–N=N–), and the extended conjugated chromophoric system [7]. The most intense band at 620 nm, located in the visible region, is responsible for the characteristic blue colour of the dye and serves as the main indicator of dye degradation during treatment.

Irradiation with UVA did not induce any changes in the UV–Vis spectrum of EB, while UVB irradiation caused only slight changes in absorbance intensity, indicating limited direct photolysis of Evans Blue under the applied conditions. These findings are in agreement with earlier studies demonstrating that azo dyes are generally resistant to degradation under UV irradiation [8].

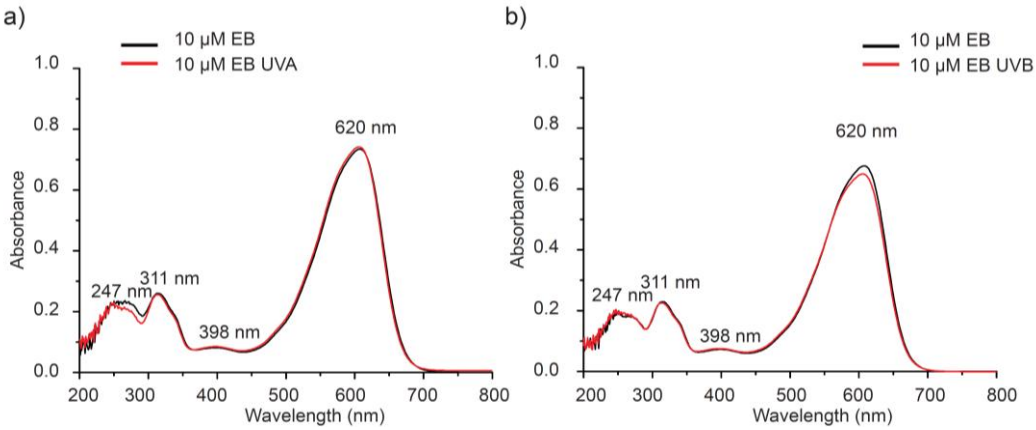

Figure 1 *Effect of UV irradiation (30 min) on 10 μM EB in aqueous solution at pH 5 a) UVA irradiation; b) UVB irradiation*

In the presence of Fe^{3+} ions, a gradual decrease in the absorbance at 620 nm was detected during both UVA and UVB treatment (20–60 min) confirming enhanced degradation compared with irradiation alone (Figure 2). This effect can be attributed to the formation of reactive oxygen species through iron-mediated photochemical reactions. Slightly higher efficiency under UVB irradiation was observed, likely due to its higher photon energy (Figure 2 b).

The highest degradation efficiency was achieved in the EB/Fe^{3+}/H_2O_2 systems under both UVA and UVB irradiation (Figure 2). A pronounced reduction of the 620 nm band with increasing treatment time indicated effective degradation of the azo chromophore. This behavior is associated with Fenton and photo-Fenton processes, where hydroxyl radicals are generated and rapidly react with the dye structure [8].

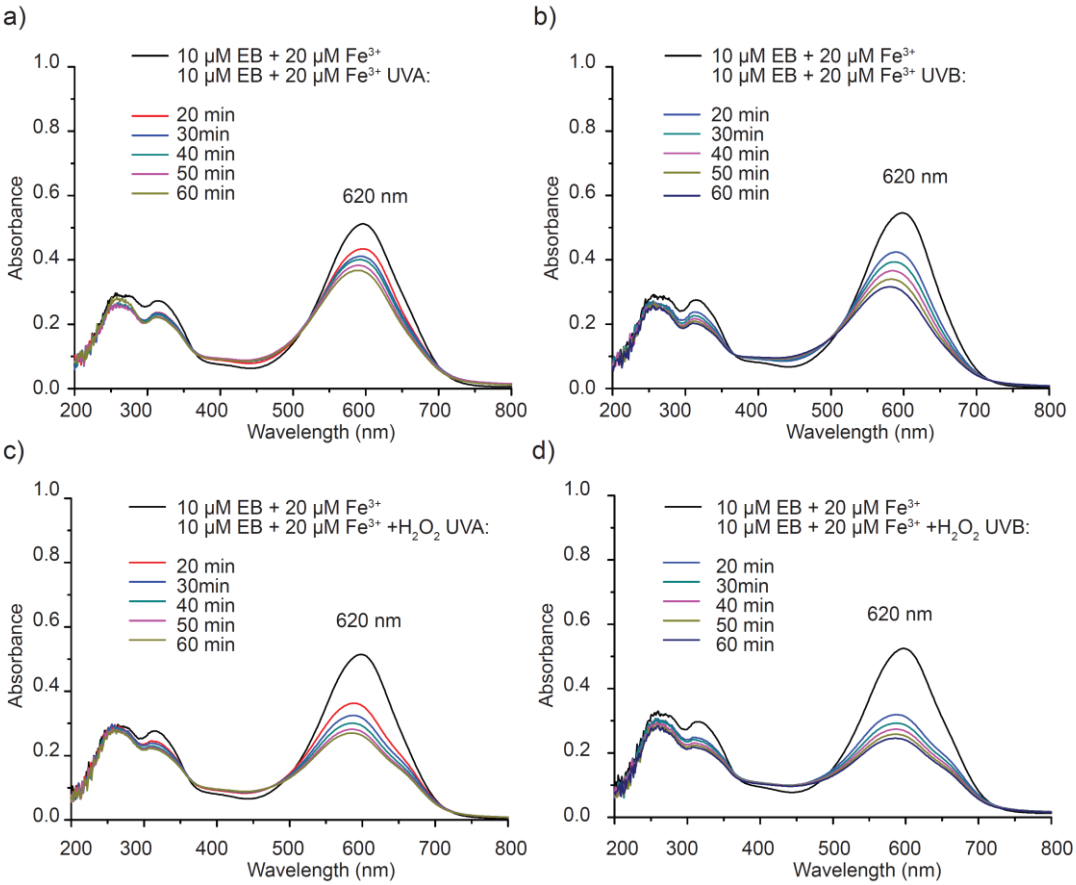

Figure 2 *Effect of UV irradiation on a 10 μM EB aqueous solution in the presence of 20 μM Fe^{3+} at pH 5 under: a) UVA irradiation; and b) UVB irradiation, as well as in the presence of 20 μM Fe^{3+} and 100 μM H_2O_2 under: c) UVA irradiation; and d) UVB irradiation*

Overall, the degradation efficiency followed the order:

$$UV < UV/Fe^{3+} < UV/Fe^{3+}/H_2O_2$$

These results demonstrate that UV-assisted Fenton-based processes significantly improve the removal of Evans Blue from aqueous solution compared with direct photolysis alone.

The effect of EB and its degradation products on the viability and growth of *Chlamydomonas acidophila* PM01 was further investigated. OD values displayed a consistent pattern independent of wavelength (Figure 3a). Although treatment with EB alone had no effect on OD, its degradation products did (Figure 4a). Fe^{3+} alone, as well as Fe^{3+} combined with EB and UVB or with EB, H_2O_2, and UVB, modestly increased both OD_{680} and OD_{750} in *Chlamydomonas acidophila* PM01 cultures. Since the OD_{680}/OD_{750} ratio remained comparable to the control, this indicates a proportional increase in biomass and chlorophyll content, rather than major changes in cellular physiology [9] (Figure 3a). On the other hand, treatment with EB in combination with Fe^{3+} and H_2O_2, in the absence of UV radiation, led to a sharp decrease in both OD values, accompanied by an increase in the OD_{680}/OD_{750} ratio (Figure 3a). This pattern suggests that this treatment primarily affected cell density rather than pigment integrity, resulting in a higher proportion of chlorophyll relative to biomass [5]. Iron availability and oxidative stress associated with H_2O_2 can influence pigment metabolism in microalgae, potentially inducing adaptive changes in chlorophyll and accessory pigment

content as part of stress acclimation responses [10,11]. Although OD_{680} and OD_{750} values in the Fe^{3+} or H_2O_2 treatment were similar to the control, the decreased OD_{680}/OD_{750} ratio indicates reduced chlorophyll content per unit biomass, suggesting impairment of the photosynthetic apparatus, likely due to oxidative stress associated with Fenton-type reactions, where Fe^{3+} is reduced to Fe^{2+}, enabling hydroxyl radical generation [12] (Figure 3a). Although the photosynthetic apparatus of *Chlamydomonas* species is generally resistant to the harmful effects of H_2O_2, the magnitude and direction of the response are highly species-dependent and require optimization for targeted metabolite production [13]. However, oxidative stress may also lead to reduced pigment yields [14]. A marked reduction in viability was observed in *C. acidophila* PM01 following 24 h treatment of product of EB photodegradation by UVB radiation (Figure 3b). The observed outcomes may be attributed to the formation of multiple aromatic intermediates, which can exhibit altered biological activity and enhanced cytotoxicity compared to the parent dye [1]. Further, likewise was evident in samples treated with EB in combination with Fe^{3+} and/or H_2O_2 (Figure 3b). This effect could be explained by elevated oxidative stress resulting from high concentrations of highly reactive hydroxyl radicals, which consequently lead to cell death [15].

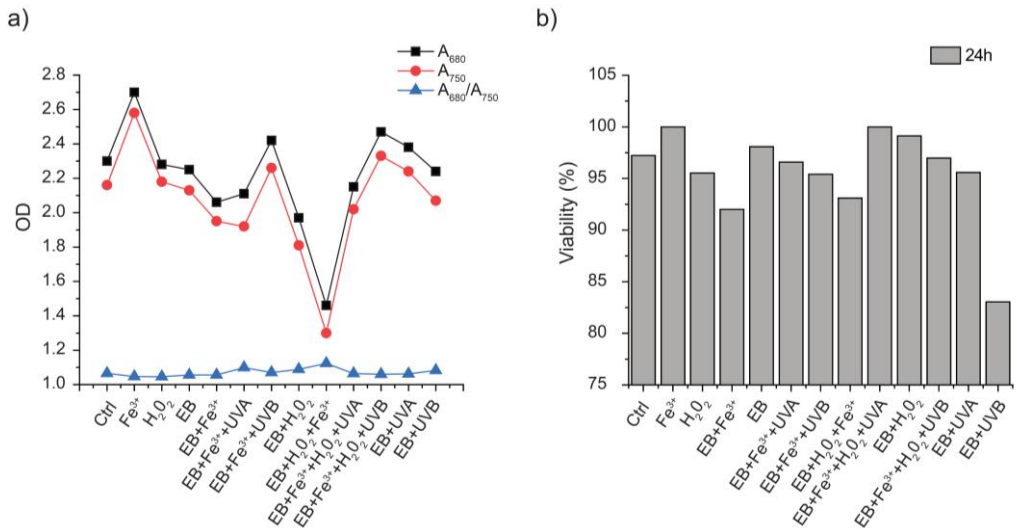

Figure 3 *a) Growth of algal cultures, monitored by optical density at 750 and 680 nm, and b) cell viability evaluated using Evans Blue staining, 24 h after treatment with EB and its degradation products*

CONCLUSION

The obtained results show EB stability in mildly acidic aqueous solutions under UVA irradiation, and its slight degradation under UV B irradiation. Additionally, EB/Fe^{3+}/H_2O_2 processes significantly improve the removal of EB from aqueous solution compared with direct photolysis alone.

In *Chlamydomonas acidophila* PM01, most treatments caused only minor, wavelength-independent changes in OD_{680} and OD_{750}, indicating largely proportional changes in biomass and chlorophyll content without major physiological alterations. In contrast, EB combined with Fe^{3+} and H_2O_2 (without UVB) reduced cell density while increasing the

OD_{680}/OD_{750} ratio, suggesting stress-induced shifts in pigment-to-biomass balance. These combinations also decreased viability, indicating that oxidative stress and reactive intermediates are the main drivers of cytotoxicity.

ACKNOWLEDGEMENT

The authors are grateful to the Ministry of Science, Technological Development and Innovation of the Republic of Serbia for financial support according to the contract with registration No. 451-03-33/2026-03/ 200053, 451-03-33/2026-03/ 200168 and 451-03-33/2026-03/ 200026.

REFERENCES

[1] Antonin, V.S., Garcia-Segura, S., Santos, M.C. *et al*. J. Electroanal. Chem. 2015, 747, 1–11.

[2] Spijkerman, E., Barua, D., Gerloff-Elias, A., *et al*. Extremophiles. 2007, 11 (4), 551–562.

[3] Olaueson, M.M., Stokes, P.M. J. Phycol. 1989, 25 (3), 529–539.

[4] Griffiths, M.J., Garcin, C., van Hille, R.P., *et al.* J. Microbiol. Methods 2011, 85 (2), 119–123.

[5] Sivakaminathan, S., Hankamer, B., Wolf, J., *et al*. J. Sci. Rep. 2018, 8 (1), 1–13.

[6] Zuppini, A., Andreoli, C., Baldan, B. Plant Cell Physiol. 2007, 48 (7), 1000–1009.

[7] Khanum, R., Ali, R.S., Rangaswamy, H.R., *et al.* Results Chem. 2023, 5, 100890.

[8] Kusic, H., Koprivanac, N., Srsan, L. J. Photochem. Photobiol. A Chem. 2006, 181 (2–3), 195–202.

[9] Kesisoglou, I., Tam, V.H., Tomaras, A.P., *et al*. Comput. Chem. Eng. 2022, 158, 107617.

[10] Jiang, Y., Sun, M., Zheng, M., *et al*. Chem. Eng. J. 2024, 485, 149872.

[11] Barros, M.P.D., Pedersén, M., Colepicolo, P., *et al*. Aquat. Microb. Ecol. 2003, 30, 275–282.

[12] Pignatello, J.J., Oliveros, E., MacKay, A. Crit. Rev. Environ. Sci. Technol. 2006, 36 (1), 1–84.

[13] Takeda, T., Yokota, A., Shigeoka, S. Plant Cell Physiol. 1995, 36 (6), 1089–1095.

[14] Barone, M.E., Parkes, R., Herbert, H., *et al*. Appl. Biochem. Biotechnol. 2021, 193 (12), 4052–4067.

[15] Winterbourn, C.C. In: Proceedings of the International Congress of Toxicology – VII; July 2-6; Washington, USA. 1995. p. 969–974.

EcoTER'26
eco.tfbor.bg.ac.rs
32nd International Conference
Ecological Truth & Environmental Research
24–26 June 2026, Hotel Sunce,
Sokobanja, Serbia

Original Research

ANNUAL EFFECTIVE DOSE DUE TO INGESTION OF HERBAL INFUSIONS FROM ASTERACEAE MEDICINAL PLANTS

DOI: 10.5937/EcoTER26330V

Irina Vasić[1,a*], Igor Čeliković[1,b], Aleksandra Samolov[1,c], Tamara Milanović[1,d], Aleksandar Kandić[1,e], Mirjana Đurašević[1,f]

[1] „Vinča" Institute of Nuclear Sciences, National Institute of Republic of Serbia, University of Belgrade, Mike Petrovića Alasa 12–14, 11000 Belgrade, Serbia

[a] https://orcid.org/0000-0002-9852-6742 [b] https://orcid.org/0000-0002-5642-4393

[c] https://orcid.org/0000-0002-6912-2407 [d] https://orcid.org/0000-0002-5948-851X

[e] https://orcid.org/0000-0002-7610-1663 [f] https://orcid.org/0000-0002-1557-7414

Abstract

Five medicinal herbs belonging to the Asteraceae family (chamomile, yarrow, marigold, dandelion, and elecampane) from Serbia purchased from a local health food store in Serbia were investigated to determine the activity concentrations of ^{137}Cs, ^{210}Pb, ^{226}Ra, ^{228}Ac, and ^{40}K and to assess the radiological risk associated with their consumption. The annual effective doses due to ingestion, assuming daily consumption of 200 mL of herbal infusion prepared from these plants, are estimated. The results showed that ^{40}K is the main contributor to the total radioactivity, ^{210}Pb and ^{226}Ra are moderate, although present across all samples. Among all radionuclides, ^{210}Pb and ^{40}K provided the highest contribution to the annual effective dose. The calculated annual effective doses for each sample were significantly below the recommended limit of 100 µSv/year.

Keywords: medicinal plants, radionuclides, radiological assessment, ingestion dose.

INTRODUCTION

Medicinal herbs are widely consumed throughout the world in the form of infusions, decoctions, and other traditional preparations, and are generally perceived as safe due to their natural origin. In Serbia, herbal infusions prepared from medicinal plants remain an important part of everyday dietary and therapeutic practice. However, like other plant-based food products, medicinal herbs can accumulate radionuclides (both natural and anthropogenic) from soil and atmospheric deposition, making their regular consumption a potential pathway of internal radiation exposure to humans [1]. Naturally occurring radionuclides such as ^{210}Pb, ^{226}Ra, ^{228}Ac, and ^{40}K are particularly relevant because of their environmental ubiquity and potential transfer into plant tissues, while ^{137}Cs is important as an anthropogenic radionuclide originating mainly from past nuclear fallout [2,3]. Species belonging to the Asteraceae family are of particular relevance in this context, as many are commonly used for the preparation of medicinal herbal infusions and may therefore contribute to radionuclide intake through ingestion. In addition, some representatives of the Asteraceae family have been reported to

*irina.kandic@vin.bg.ac.rs

accumulate environmental contaminants, including radionuclides and trace elements, through soil - plant transfer processes, which may contribute to their transfer into consumable plant material [2,4,5]. *Taraxacum officinale* (dandelion), in particular, has been shown to accumulate elevated levels of environmental contaminants, especially in polluted environments [6]. Given their frequent use in traditional and everyday consumption, the occurrence of radionuclides in these medicinal plants may represent a relevant pathway of internal exposure for consumers. In this context, the determination of radionuclide activity concentrations and the estimation of annual effective dose due to ingestion are essential for evaluating their radiological significance.

The aim of this study was to determine the activity concentrations of ^{137}Cs, ^{210}Pb, ^{226}Ra, ^{228}Ac, and ^{40}K in selected medicinal herbs from the Asteraceae family (chamomile, yarrow, marigold, dandelion and elecampane) from Serbia purchased from a local health food store, and to estimate the annual effective dose associated with their daily consumption of 200 mL herbal infusions.

MATERIALS AND METHODS

Five medicinal herb samples (chamomile, yarrow, marigold, dandelion, and elecampane) from Serbia were purchased from a local health food store. The corresponding common English and Latin names, botanical family, analyzed plant part, and recommended amount of dried material for the preparation of 200 mL of infusion are listed in Table 1. The samples, purchased in dried form, were ground and homogenized. The prepared material was then packed into standard cylindrical PVC containers (125 mL). Approximately 30 g of each sample was used, ensuring consistency with the working standard employed for detector calibration. The working standard was based on dried grass as a matrix of similar biological composition and was spiked with a radioactive solution containing a mixture of gamma-emitting radionuclides:^{210}Pb, ^{241}Am, ^{109}Cd, ^{139}Ce, ^{57}Co, ^{60}Co, ^{137}Cs, ^{113}Sn, ^{85}Sr, and ^{88}Y, supplied by the Czech Metrology Institute (CMI) [7].

Table 1 *Investigated medicinal herbs, their English and Latin names, family affiliation, plant part used, and recommended amount of dried material for preparation of 200 mL of herbal infusion.*

English name	Latin name	Familly	Plant part	Recommended amount [2,8,9]
Chamomile	*Matricaria chamomilla*	Asteracea	flower	2.5 g
Yarrow	*Achillea millefolium*	Asteracea	herb	2 g
Marigold	*Calendula officinalis*	Asteracea	flower	3 g
Dandelion	*Taraxacum officinale*	Asteracea	leaf	1.5 g
Elecampane	*Inula helenium*	Asteracea	root	1 g

The working standard was prepared at the Laboratory for nuclear and plasma physics, ‘‘Vinča” Institute of Nuclear Sciences, University of Belgrade [10,11]. All samples were measured in a close to detector geometry using a coaxial HPGe spectrometer (Canberra GX5019) with a relative efficiency of 55% and an energy resolution of 1.9 keV for ^{60}Coat

1332.5 keV. The gamma spectra of the medicinal herb samples were acquired and analyzed using Canberra Genie 2000 software. To ensure acceptable counting statistics, the samples were measured for up to 585,000 s. The activity concentrations of ^{137}Cs, ^{210}Pb, ^{226}Ra,^{228}Ac, and ^{40}K in the medicinal plants samples were determined from the corresponding full-energy gamma peaks at 661.66 keV, 46.54 keV, 186.21 keV, 911.20 keV, and 1460.82 keV respectively, after applying background corrections. In the case of ^{40}K, correction of the 1460.82 keV peak was also performed to eliminate the contribution of the adjacent ^{228}Ac line at 1459.13 keV. The combined measurement uncertainty was estimated by applying the general law of uncertainty propagation. The dominant sources of uncertainty were counting statistics and efficiency calibration (contributing 5%), whereas the effect of sample mass uncertainty was considered negligible.

The annual effective dose for ingestion in the case of daily consumption of 200 mL of herbal infusion prepared from medicinal herbs was calculated based on the obtained values of specific activities of radionuclides ^{137}Cs, ^{210}Pb, ^{226}Ra, ^{228}Ac, and ^{40}K, using the following formula [12] (1):

$$E_{ing} = A_s H C_d DF_{ing} \tag{1}$$

where A_s is the specific activity in [Bq/kg], H is the amount of medicinal plant consumed in [kg/year], C_d is the dissolution coefficient of the radionuclide during the infusion preparation, and DF_{ing} is the coefficient of effective ingestion dose [Sv/Bq].

Radionuclide solubility coefficients, C_d, for herbal infusion preparation are: 0.6 for ^{137}Cs [13], 0.5 for^{210}Pb [14], 0.2 for ^{226}Ra [15], 0.0005 for ^{228}Ac [16], and 0.9 for ^{40}K [17].

The effective dose coefficients, DF_{ing}, used in the calculations are:1.310^{-8} Sv/Bq for ^{137}Cs, 6.910^{-7} Sv/Bq for ^{210}Pb, 2.8 10^{-7} Sv/Bq for ^{226}Ra, 4.3 10 $^{-10}$Sv/Bq for ^{228}Ac, and 6.210^{-9}Sv/Bq for ^{40}K [16].

RESULTS AND DISCUSSION

The activity concentrations of ^{137}Cs, ^{210}Pb, ^{226}Ra, ^{228}Ac, and^{40}K in 5 selected medicinal plants collected from a local herbal store in Serbia, together with the associated measurement uncertainties at the 1σ confidence level, are presented in Table 2.

Table 2 *Activity concentration of radionuclides in Asteraceae medicinal plants*

Plant species	^{137}Cs	^{210}Pb	^{226}Ra	^{228}Ac	^{40}K
	[Bq/kg]				
Chamomile	< 0.3	9.4 ± 1.0	9.3 ± 1.7	4.7 ± 0.9	628 ± 33
Yarrow	< 0.3	13.3 ± 2.0	3.8 ± 0.3	< 2.1	450 ± 24
Marigold	< 0.3	12.0 ± 2.1	17.2 ± 1.6	< 2.1	753 ± 39
Dandelion	< 0.3	28.3 ± 3.9	3.2 ± 0.3	3.2 ± 0.4	874 ± 45
Elecampane	0.6 ± 0.2	7.3 ± 0.7	4.5 ± 0.4	3.0 ± 0.4	734 ± 38

The obtained results are in general agreement with the data reported in the available literature [2,18–20], indicating that the activity concentrations of the investigated

radionuclides fall within the expected ranges for medicinal plants. However, it should be emphasized that the amount of published data on ^{210}Pb in such materials is relatively limited [2,8,20].

Table 3 presents the estimated individual annual effective doses resulting from the ingestion of ^{137}Cs, ^{210}Pb, ^{226}Ra, ^{228}Ac, and ^{40}K, assuming a daily consumption of 200 mL of herbal infusion. Due to the extremely low solubility coefficient of ^{228}Ac, its contribution was considered negligible and therefore excluded from the estimation of the individual annual effective dose.

Table 3 *Estimated individual annual effective doses resulting from the ingestion of ^{137}Cs, ^{210}Pb, ^{226}Ra, ^{228}Ac, and ^{40}K in 200 mL of herbal infusion, including measurement uncertainties at the 1σ confidence level*

Plant species	**^{137}Cs**	**^{210}Pb**	**^{226}Ra**	**^{40}K**	**Total annual effective doses**
	[nSv/year]	**[μSv/year]**			
Chamomile	< 2.14	2.92 ± 0.31	0.48 ± 0.09	3.20 ± 0.17	6.60 ± 0.57
Yarrow	< 1.71	3.35 ± 0.50	0.16 ± 0.01	1.83 ± 0.10	5.34 ± 0.61
Marigold	< 2.56	4.53 ± 0.78	1.05 ± 0.10	4.60 ± 0.24	10.18 ± 1.12
Dandelion	< 1.28	5.35 ± 0.73	0.10 ± 0.01	2.67 ± 0.14	8.12 ± 0.88
Elecampane	1.71 ± 0.57	0.92 ± 0.09	0.09 ± 0.01	1.49 ± 0.08	2.50 ± 0.18

The individual annual effective dose due to ingestion of ^{137}Cs, ^{210}Pb, ^{226}Ra, and ^{40}K through the consumption of 200 mL of herbal infusion prepared from the investigated medicinal plants was found to be up to 1.71 nSv, 5.35 μSv, 1.05μSv, and 4.60 μSv, for ^{137}Cs, ^{210}Pb, ^{226}Ra, and ^{40}K, respectively. The highest total annual effective dose was observed in the marigold sample. Among all radionuclides, ^{210}Pb and ^{40}K provided the highest contribution to the annual effective dose. Notably, the contribution of ^{40}Kis relatively uniform and reflects its natural abundance in plant tissues. This can be explained by the essential biological role of potassium in plants. In contrast, ^{137}Cs exhibits a negligible contribution in all samples, likely due to low environmental levels or values below detection limits. Additionally, ^{228}Ac does not contribute to the total dose, due to its very low solubility.

The total annual effective doses obtained for all investigated herbal infusions are considerably lower than the recommended limit of 100 μSv/year prescribed by *Regulation on limits of radionuclide content in drinking water, foodstuffs, feeding stuff, drugs, items of general use, building materials, and other goods to be placed on the market* [21]. This indicates that these herbal infusions are radiologically safe for use.

CONCLUSION

Five medicinal herbs from the Asteraceae family were analyzed for the activity concentrations of ^{137}Cs, ^{210}Pb, ^{226}Ra, ^{228}Ac, and ^{40}K, and the corresponding annual effective doses due to ingestion were estimated for the daily consumption of 200 mL of herbal infusion. The calculated annual effective doses were significantly below the regulatory limit of

100 μSv/year, indicating that the investigated herbal infusions do not pose a significant radiological risk to consumers.

ACKNOWLEDGEMENT

The authors are grateful to the Ministry of Science, Technological Development and Innovation of the Republic of Serbia for financial support according to the contract with registration No.451-03-33/2026-03/ 200017, through the realization of the research themes 0642601 and 1702607.

REFERENCES

[1] Oprea, E., Pintilie, V., Bufnea, V., *et al*. Farmacia 2014, 62 (4), 658–663.

[2] Kandić, I., Kandić, A., Čeliković, I., *et al*. Sci. Total Environ. 2020, 701, 134554.

[3] Bal, S.Ş., Kurşat, M., Kuluöztürk, M.F., *et al*. J. Environ. Radioact. 2023, 257, 107089.

[4] Wierzchowska-Renke, K., Mysłek-Laurikainen, B., Głowniak, K., *et al*. Herba Pol. 2002, 48 (2), 82–88.

[5] Vural, A. Environ. Sci. Pollut. Res. 2024, 31 (11), 16667–16684.

[6] Respondek, Z., Isinkaralar, O., Świsłowski, P., *et al*. Plants 2024, 13 (13), 1805.

[7] CMI, Radioactive Standard, ER X, Cert. No 9031-Ol-427/12.Prague: Czech Metrology Institute; 2012.

[8] Đurašević MM, Čeliković IT, Samolov A, *et al*. In: Proceedings of the 32nd Symposium DZZSCG; 2023; p. 42–48.

[9] Institute for Medicinal Plant Research "Dr Josif Pančić". Available from: https://www.mocbilja.rs

[10] Vukanac, I., Đurašević, M., Kandić, A., *et al*. Appl. Radiat. Isotopes 2008, 66 (6–7), 792–795.

[11] Kandić, A., Vukanac, I., Đurašević, M., *et al*. Appl. Radiat. Isotopes 2012, 70 (9), 1860–1862.

[12] United Nations Scientific Committee on the Effects of Atomic Radiation (UNSCEAR). Sources, Effects and Risks of Ionizing Radiation. New York: United Nations; 2016.

[13] Balonov M, Barnett CL, Belli M, *et al*. Handbook of Parameter Values for the Prediction of Radionuclide Transfer in Terrestrial and Freshwater Environment. Vienna: IAEA; 2010.

[14] Kametani, K, Ikebuchi, H, Matsumura, T, *et al*. Radioisotopes 1981, 30 (12), 681–683.

[15] Silva, R.C., Lopes, J.M., Silva, L.F., *et al*. An. Acad. Bras. Ciênc. 2025, 97 (Suppl. 4), e20240854.

[16] Eckerman, K., Harrison, J., Menzel, H.G., *et al*. Compendium of Dose Coefficients Based on ICRP Publication 60. Ann. ICRP 2012, 41 (Suppl.).

[17] Samolińska, W., Kiczorowska, B., Kwiecień, M., *et al*. Biol. Trace Elem. Res. 2017, 175 (2), 495–502.

[18] Jevremović, M., Lazarević, N., Pavlović, S., *et al*. Isot. Environ. Health Stud. 2011, 47(1), 87–92.

[19] Mitrović, J., Ajtić, M., Lazić, M., *et al*. Environ. Pollut. 2016, 215, 273–279.

[20] Đurašević, M., Rajković, K., Milić, P., *et al*. Microchem. J. 2025, 116267.

[21] Official Gazette of the Republic of Serbia. Regulation on limits of radionuclide content in drinking water, foodstuffs, feeding stuffs, drugs, items of general use, building materials and other goods to be placed on the market; 2018; 36/2018-54.

EcoTER'26
eco.tfbor.bg.ac.rs
32nd International Conference
Ecological Truth & Environmental Research
24–26 June 2026, Hotel Sunce,
Sokobanja, Serbia

Original Research

CONCENTRATIONS OF METALS AND METALLOIDS IN MEAT OF THE COMMON CARP (*Cyprinus carpio*) FARMED USING FEED BASED ON INVERTEBRATE ANIMAL PROTEIN ORIGIN

DOI: 10.5937/EcoTER26336N

Dušan Nikolić[1,a*], Stefan Marjanović[2,b], Milena Dimitrijević[1,c], Zoran Marković[2,d], Aleksandra Dobričić[2,e], Marko Stanković[2,f], Božidar Rašković[2,g]

[1] University of Belgrade – Institute for Multidisciplinary Research, National Institute of the Republic of Serbia, Department of Biodiversity and Environmental Research, Kneza Višeslava 1, 11030 Belgrade, SERBIA

[2] University of Belgrade – Faculty of Agriculture, Institute of Animal Sciences, Nemanjina 6, 11080 Belgrade, SERBIA

[a] https://orcid.org/0000-0003-2004-1662 [b] https://orcid.org/0000-0002-5796-7023

[c] https://orcid.org/0000-0003-1659-5945 [d] https://orcid.org/0000-0003-3703-9921

[e] https://orcid.org/0009-0001-7867-7922 [f] https://orcid.org/0000-0002-0555-5297

[g] https://orcid.org/0000-0001-7190-5833

Abstract

The global shortage of fish meal (FM) presents a significant challenge to the sustainability of aquaculture and the aquafeed industry. Consequently, numerous studies have investigated alternative ingredients to replace FM in fish feed. However, the use of novel feed ingredients may pose risks not only to farmed fish but also to human consumers, particularly due to the potential accumulation of metals and metalloids in fish tissues. In this study, four experimental diets for common carp (Cyprinus carpio) were formulated using different animal protein sources: fish meal, earthworm meal, mealworm meal, and zooplankton meal. A 12-week feeding trial was conducted with juvenile (1+) carp under two rearing systems: (1) intensive (laboratory tanks), and (2) semi-intensive (earthen pond). The aim of the study was to determine the concentrations of harmful elements (Pb, As, Cr, Cu, Fe, Li, Zn, Ni, Mn, Cd, Co, Al, Sr) in carp fillets and to assess potential risks for consumers. Additionally, the study compares the effects of different protein sources and rearing systems on element accumulation.

Keywords: aquaculture, fish meal, mealworm meal, earthworm meal, zooplankton meal.

INTRODUCTION

Aquaculture and captive fisheries have been the fastest growing food production sector in the past thirty years [1]. However, this growth has come at a cost, with the most significant negative impact being the reduction in the number of pelagic fish in the oceans due to systematic overfishing. This has jeopardised the sustainability of feed production for aquatic organisms because of the limitation of two key resources: fish meal (FM) and fish oil [2]. In

* *dusan@imsi.rs*

recent decades, scientists have sought alternative ingredients to create balanced diets that meet the nutritional requirements and support optimal growth of farmed fish, without relying on FM. Alternative ingredients can be of plant or animal origin, with most studies focusing on plant sources for economic reasons. However, plants contain several anti-nutritional factors that reduce the growth and overall health of farmed fish [3]. In contrast, proteins of animal origin are better suited for inclusion in fish feed, and the most promising animals are insects [4]. Among these is the insect species at the centre of the present study – the yellow mealworm, *Tenebrio molitor* L., 1758 (TM). Two other invertebrate species, which are more common and frequently used as natural food for fish, are the earthworm *Eisenia fetida* (Savigny, 1826) (EF) and zooplankton (ZO), a mixture of different organisms from various taxa, mostly copepods, cladocerans and rotifers. Zooplankton from fish ponds has been used as a preferred food source, especially for nursing a fish larvae (and to a lesser extent for older fish), due to its high protein and lipid content [5].

Two nutritional assays were conducted using diets in which fish meal was replaced with the aforementioned invertebrate species. The focus species was the common carp (*Cyprinus carpio* L., 1758), one of the most important species in global aquaculture [6]. This fish is reared using all available systems, but in the present study, we used intensive (laboratory trial) and semi-intensive (pond trial) rearing systems.

The aim of this study was to determine the concentrations of 13 potentially toxic metals and metalloids (Pb, As, Cr, Cu, Fe, Li, Zn, Ni, Mn, Cd, Co, Al, and Sr) in fish meal (FM), earthworms (EF), mealworms (TM), and zooplankton (ZO), as well as in fish feeds containing these ingredients (CFM, CEF, CTM, and CZO), and in the fillets of common carp reared in intensive and semi-intensive systems. The main goal of the study was to determine whether some animal proteins pose a higher risk for fish nutrition and human consumption.

MATERIALS AND METHODS

Experimental diets

Four isoproteinaceous experimental diets were formulated to replace fish meal (FM) with different animal protein sources: earthworm meal (EM), mealworm meal (MM), and zooplankton meal (ZM) (Table 1). The origins of the alternative protein sources were as follows: (1) EM was produced from earthworms reared at the earthworm farm “Ranč Jablan” (Surdulica, Serbia) on a mixture of manure collected from local farmers and fruit and vegetable waste; (2) MM was produced from microwave-dried whole mealworms, purchased online from the “RANZ natural pet food” company (China); (3) ZO was collected from earthen ponds at two fish farms (“Kapetanski rit”, Kanjiža, Serbia, and the “Centre for Fishery and Applied Hydrobiology” (CEFAH), Faculty of Agriculture, University of Belgrade), from water abundant in zooplankton species, using a plankton net with a mesh size of 55 µm and a ring diameter of 55 cm.

Table 1 *List of ingredients (%) in experimental feeds for common carp*

Ingredients	Experimental diet			
	CFM	CEF	CTM	CZO
Fish meal	18.1	-	-	-
Earthworm meal	-	17.1	-	-
Mealworm meal	-	-	21.2	-
Zooplankton meal	-	-	-	24.1
Soybean seed, whole	25.0	25.0	25.0	25.0
Sunflower seed	20.0	20.0	20.0	20.0
Wheat	14.7	15.0	19.8	10.2
Maize	11.0	10.0	5.0	8.0
Corn starch	6.0	6.0	5.0	6.0
Soybean oil	2.9	2.9	-	2.6
Monocalcium phosphate	0,4	0.9	0.9	1.0
NaCl	0.2	0.2	0.2	0.2
$CaCO_3$	0.5	1.7	1.7	1.7
Lysine	0.2	0.2	0.0	0.2
Mineral and vitamin premix	1.0	1.0	1.0	1.0

Feeding trials

Two feeding trials were conducted with one- year-old juvenile common carp. The fish were hatched at CEFAH, reared in earthen ponds, and fed commercial compound feed (FM) prior to the start of the feeding trials. The fish were acclimatised to tanks/cages and new environmental conditions for 14 days. Both trials lasted 12 weeks; this duration was chosen to distinguish between the transfer of elements from feed to muscle under laboratory conditions and in earthen ponds. In earthen ponds, common carp also feed on benthic macroinvertebrates and zooplankton species, and are exposed to other sources of metals originating from the environment (water and sediment). In both studies, fish were provided with feed amounting to 2.5% of their total body mass. The calculated daily feed ration was distributed manually in two meals per day.

First experiment – laboratory trial

The first experiment was conducted in the Laboratory of Fish Nutrition (Faculty of Agriculture, University of Belgrade). A total of 120 common carp juveniles (12.4 ± 2.7 g) were transferred from CEFAH and randomly distributed into 12 indoor conical-bottomed tanks – T (four experimental groups in triplicate, 10 fish per replicate, totalling 30 fish per group), each with a volume of 120 L. During the acclimation period, the fish were fed FM feed *ad libitum*. Dechlorinated municipal tap water was used, and each tank had a separate flow-through system with an exchange rate of 0.36 L/min. A natural photoperiod was maintained (March–June).

Second experiment – field study in earthen ponds

Cage system K was established at CEFAH in one of the ponds. After an acclimation period, fish were measured and stocked into 12 cages (0.22 m^3; 0.6 × 0.6 × 0.6 m), with 10 individuals per cage (10.1 ± 1.0 g). The cages were arranged in two rows with a 40 cm walkway between them to allow monitoring, feeding, and handling. The distance between cages was approximately 30 cm, and they were suspended on a support cable with their upper

parts above the water surface for easier access. To prevent oxygen deficiency, each cage was connected to an air compressor via diffusers and tubing to ensure adequate aeration. The cages were covered with protective mesh to prevent fish escaping.

Element analysis

At the end of the experiment, muscle tissue was sampled from two individuals per cage (left dorsal side below the dorsal fin), and the samples from each cage/tank were pooled into a single bag. All samples were stored at −20 °C prior to analysis. The concentrations of 13 elements (μg g^{-1} dry weight, dw) were determined using inductively coupled plasma optical emission spectrometry (ICP-OES; Avio 200, PerkinElmer). Wavelength lines (λ, nm) of the measured elements were as follows: Pb (220.353), As (193.696), Cr (267.716), Cu (327.393), Fe (238.204), Li (670.784), Zn (206.200), Mn (257.610), Ni (231.604), Cd (228.802), Co (228.616), Al (396.153), and Sr (407.771). To evaluate potential contamination from the reagents used in this study, four analytical blanks (without tissue) were processed following the same procedure as the samples. Quality control of the analytical process was assessed using certified reference materials, including IAEA-336 Lichen (AQCS, International Atomic Energy Agency) and BCR-185R Bovine Liver (European Commission Joint Research Centre). For all analysed elements, the measured concentrations ranged between 90% and 115% of the certified values.

Element concentrations in muscle tissue were evaluated against the maximum allowed concentrations (MACs) established for fish meat under the national legislation of the Republic of Serbia [7] and the regulation of the European Commission [8]. These regulatory frameworks are aligned with regard to the MACs for Cd (0.05 μg/g) and Pb (0.3 μg/g). Furthermore, Serbian national legislation defines additional MACs for Cu (30 μg/g), Zn (100 μg/g), and As (2 μg/g).

Statistical analysis

All values are presented as mean ± standard deviation (SD). Normality was assessed using the Shapiro–Wilk test, and homogeneity of variances (homoscedasticity) was evaluated using Levene's test. As the data did not meet the assumption of normality, the non-parametric Kruskal–Wallis *H* test was applied, followed by the Mann–Whitney *U* test as a post hoc analysis. Statistical analyses were performed using Statistica 12.0 software (StatSoft Inc., USA). The level of statistical significance was set at $P < 0.05$.

RESULTS AND DISCUSSION

A number of studies have been published recently in which novel foods derived from invertebrate species are screened for the presence of metals and other elements, and the risk to humans is assessed [9–11]. Concentrations of elements usually do not exceed maximum allowable concentrations, but there are exceptions, and some elements have been found in elevated concentrations [9–11]. The concentration of elements depends on the environment in which invertebrates are reared and the food they consume, and these data are usually not known when these products are acquired. In contrast, fish are well known for their bioaccumulation properties for certain elements [12].

The concentrations of Pb, As, Cd, and Co were below the detection limits in all cases studied, and Ni (0.005 ± 0.001 µg/g) was detected only in CZO. Although variations in mean values were observed, no statistically significant differences were identified among the groups for the analysed elements, which is most likely attributable to the limited sample size included in the study (Table 2).

Table 2 *Element concentrations (µg/g) in fish feed and fillets of common carp reared in laboratory tanks and earthen ponds in a semi-intensive system. All values are presented as mean ± standard deviation (SD). ND indicates values below the detection limit: 0.005 µg/g for Cr and Cu, 0.002 µg/g for Li, 0.01 µg/g for Al, and 0.001 µg/g for Sr*

	Cr	Cu	Fe	Li	Zn	Mn	Al	Sr
FM	ND	0.005±0.002	0.182±0.006	ND	0.095±0.003	0.009±0.001	0.090±0.006	0.203±0.029
EF	ND	0.013±0.002	1.185±0.145	ND	0.123±0.007	0.071±0.013	1.371±0.220	0.016±0.002
TM	ND	0.023±0.006	0.049±0.023	ND	0.105±0.030	0.011±0.004	0.015±0.017	0.006±0.002
ZO	0.010±0.006	0.013±0.010	2.793±2.390	0.010±0.008	0.075±0.011	0.238±0.203	0.044±0.013	0.005±0.009
CFM	ND	0.041±0.043	0.175±0.037	ND	0.099±0.013	0.059±0.001	0.058±0.004	0.045±0.004
CEF	ND	0.015±0.002	0.366±0.043	ND	0.076±0.018	0.059±0.008	0.240±0.034	0.010±0.001
CTM	ND	0.021±0.002	0.189±0.044	ND	0.088±0.003	0.059±0.005	0.072±0.009	0.010±0.001
CZO	0.006±0.001	0.034±0.008	1.701±0.065	0.005±0.001	0.090±0.005	0.144±0.008	3.085±0.090	0.162±0.005
K_{CFM}	ND	ND	0.014±0.016	ND	0.050±0.030	0.001±0.001	0.011±0.011	0.007±0.004
K_{CEF}	ND	ND	0.015±0.018	ND	0.036±0.029	0.001±0.002	0.011±0.011	0.005±0.007
K_{CTM}	ND	0.003±0.002	0.083±0.090	ND	0.072±0.016	0.002±0.001	0.021±0.001	0.008±0.008
K_{CZOO}	ND	0.004±0.002	0.020±0.021	ND	0.058±0.036	0.002±0.001	0.013±0.014	0.005±0.003
T_{CFM}	0.008±0.009	0.011±0.015	0.026±0.029	0.008±0.011	0.053±0.056	0.003±0.002	0.009±0.003	0.001±0.001
T_{CEF}	ND	ND	0.007±0.003	ND	0.020±0.008	0.001±0.001	0.011±0.010	0.002±0.001
T_{CTM}	ND	ND	0.002±0.001	ND	0.021±0.005	0.001±0.001	ND	ND
T_{CZOO}	ND	ND	0.019±0.004	ND	0.026±0.001	0.001±0.001	0.023±0.003	0.004±0.004

In the present study, most metals and metalloids were found at lower concentrations in muscle tissue compared to raw ingredients or fish feed. In cyprinids, the bioaccumulation pattern in tissues is typical for most metals: the highest concentrations are found in the liver, the lowest in muscles, with other organs (such as gills) positioned in between [13]. The concentrations of six elements in muscle tissue were below the maximum allowed concentrations (MACs) established by both national legislation and European Commission regulations. Therefore, common carp meat can be considered safe for human consumption.

In a recent study, concentrations of three metals (Pb, Cd, and Ni) with adverse effects on animals were detected in various insect-based products available for purchase via e-commerce in the European Union [9]. Average concentrations ranged from 0.02 to 2.23 µg/g, which contrasts with the present study, as two of these three elements were below the detection limit. The highest detected concentration in feed was Al, found in zooplankton feed. This is expected, as invertebrates are known to contain high concentrations of Al [14-15]; however, it is questionable why Al concentrations in zooplankton were lower than those found in the

feed. A probable reason is the addition of other plant-based ingredients, which lowered the concentrations in zooplankton.

CONCLUSION

The significance of this preliminary study lies in assessing whether alternative feed sources for common carp (yellow mealworm, earthworm, and zooplankton) are safe for fish consumption and whether they influence fish meat quality in terms of the accumulation of potentially toxic elements. Although the observed differences were not statistically significant due to the small sample size, it was determined that common carp meat is safe for human consumption.

ACKNOWLEDGEMENT

The authors are grateful to the Ministry of Science, Technological Development and Innovation of the Republic of Serbia for financial support according to the contract with registration No. 451-03-33/2026-03/200053 and No. 451-03-34/2026-03/200116.

REFERENCES

[1] Bartley DM. World Aquaculture 2020–A brief overview. FAO Fisheries and Aquaculture Circular No. 1233. Rome: FAO; 2020. p. 46.

[2] Salin KR, Arun VV, Mohanakumaran Nair C, *et al*. Sustainable aquafeed. In: Hai F, Visvanathan C, Boopathy R., editors. Sustainable aquaculture. Springer International Publishing; 2018. p. 123–151.

[3] Kortner TM, Løkka G, Francis G, *et al*. Antinutritional factors and adventitious toxins. In: Kumar N, editor. Feed and Feeding for Fish and Shellfish. Academic Press; 2025. p. 153–172.

[4] Alfiko, Y., Xie, D., Astuti, R.T., *et al*. Aquac. Fish. 2022, 7 (2), 166–78.

[5] Anton-Pardo, M., Adámek, Z. J. Appl. Ichthyol. 2015, 31, 7–14.

[6] Verdegem, M., Buschmann, A.H., Latt, U.W., *et al.* J. World Aquac. Soc. 2023, 54 (2), 206–250.

[7] Official Gazette of the Republic of Serbia No. 22/2018 and No. 90/2018. Regulation on the maximum permitted residue levels of pesticides in food and animal feed and feed and animal feed for which maximum quantities of residues of pesticides are permitted. Annex 5 – Regulation on maximum allowed amounts of certain contaminants in food and feed for animals of plant and animal origin. 2018. Available from: www.pravno-informacioni-sistem.rs/SlGlasnikPortal/prilozi/5.html.

[8] EC. No. 1881/2006 of 19 December 2006 setting maximum levels for certain contaminants in foodstuffs (Text with EEA relevance). Official Journal of the European Union No. 1881/2006, 2006, 364. 5-24. Available from: https://eur-lex.europa.eu/eli/reg/2006/1881/oj

[9] Gori, A., Armani, A., Pedonese, F., *et al*. Food Control 2025, 1, 167, 110781.

[10] Sikora, D., Proch, J., Niedzielski, P., *et al*. J. Food Compos. Anal. 2023, 121, 105367.

[11] San Onofre, N., Vie, D., Soriano, J. M., *et al*. Toxics. 2024, 12(10), 741.

[12] Bosch, A.C., O'Neill, B., Sigge, G.O., *et al*. J. Sci. Food Agric. 2016, 15, 96 (1), 32–48.

[13] Jia, Y., Wang, L., Qu, Z., *et al*. Environ. Sci. Pollut. Res. Int. 2017, 24 (10), 9379–9386.

[14] Handy RD. Dietary exposure to toxic metals in fish. In: Taylor EW, editor. Toxicology of aquatic pollution. Cambridge University Press; 1996. p. 29–60.

[15] Dulić, Z., Živić, I., Pergal, M., *et al*. Ann. Limnol. - Int. J. Lim. 2018, 54, 4.

EcoTER'26
eco.tfbor.bg.ac.rs
32nd International Conference
Ecological Truth & Environmental Research
24–26 June 2026, Hotel Sunce,
Sokobanja, Serbia

Original Research

LABEL-FREE FLUORESCENCE-BASED OPTICAL BIOSENSOR FOR RAPID DETECTION OF FUNGAL PATHOGENS

DOI: 10.5937/EcoTER26343B

Dunja Banđur[1,a*], Dragana Bartolić[1,b], Mira Stanković[1,c], Miloš Prokopijević[1,d], Nevena Surudžić[1,e], Slavica Stanković[2,f], Miodrag Mićić[3,4,g]

[1] University of Belgrade, Institute for Multidisciplinary Research, National Institute of the Republic of Serbia, Kneza Višeslava 1, 11030 Belgrade, SERBIA

[2] Maize Research Institute "Zemun Polje", Slobodana Bajića 1, Belgrade, 11185, SERBIA

[3] Department of Engineering Design Technology, Cerritos College, 11110 Alondra Blvd, Norwalk, CA 90650, USA

[4] RotaPrep Incorporated, 2913 El Camino Real, #242, Tustin, CA 92782, USA

[a] https://orcid.org/0009-0008-2782-7629 [b] https://orcid.org/0000-0002-9337-9288

[c] https://orcid.org/0000-0003-0084-3158 [d] https://orcid.org/0000-0002-3768-9732

[e] https://orcid.org/0000-0002-0544-6365 [f] https://orcid.org/0000-0001-7901-1121

[g] https://orcid.org/0000-0001-8823-0879

Abstract

The aim of this study was to design a rapid, label-free method based on fluorescence spectroscopy for detection and identification of different fungal pathogens. Three species were investigated: Aspergillus flavus, Fusarium verticillioides, and Alternaria alternata. Fungal lysates were deposited onto a nitrocellulose membrane and analyzed under UV-A illumination, where differences in the intensity and morphology of fluorescent signals were observed. Additionally, fluorescence spectra revealed characteristic profiles with clearly distinct positions and intensities of emission maxima in the 410–460 nm range. A. alternata exhibited a maximum emission around 460 nm, while A. flavus and F. verticillioides showed peaks in the 410–430 nm range.

The obtained results confirm that the combination of a membrane-based platform and optical detection enables reliable spectral discrimination of fungal pathogens without the need for labels. The proposed method represents a simple, fast, and potentially portable solution for monitoring food contamination and developing optical biosensors.

Keywords: Fungal pathogens, fluorescenece spectroscopy, *Aspergillus flavus*, *Fusarium verticillioides*, *Alternaria alternata*.

INTRODUCTION

Fungal pathogenic cultures are a major source of food contamination due to crop infestation and production of hazardous toxins that pose a serious health threat to livestock and humans [1]. *Aspergillus flavus* (*A. flavus*) produces aflatoxins (AFs) that are considered

* *dunja.bandjur@imsi.bg.ac.rs*

as environmental carcinogens. Secondary metabolites of *Fusarium verticillioides* (*F. verticillioides*) include fumonisins, which cause severe animal and human diseases [2]. In addition to these genera, *Alternaria alternata (A. alternata)* is recognized as an important plant pathogen capable of producing a wide range of mycotoxins, including alternariol, tenuazonic acid, and altenuene, which have been associated with cytotoxic, mutagenic, and genotoxic effects [3,4]. These fungal species frequently contaminate cereals, fruits, vegetables, and stored agricultural products, leading not only to significant economic losses but also to reduced food quality and safety.

The occurrence of mycotoxigenic fungi is strongly influenced by environmental conditions such as temperature, humidity, and storage practices, which facilitate fungal growth and toxin biosynthesis. Due to the high stability of many mycotoxins during food processing, contamination remains a persistent global problem and represents a major challenge for the food and feed industry. Therefore, continuous monitoring and investigation of fungal growth characteristics and toxin production are essential for understanding contamination pathways and developing effective prevention strategies.

Early detection of plant pathogens is critical for global food security and minimizing crop losses. Traditional diagnostic methods, such as Polymerase Chain Reaction (PCR) and enzyme-linked immunosorbent assay (ELISA), offer high sensitivity and specificity, but are poorly suited for field deployment. They require complex sample preparation, expensive laboratory equipment, and trained personnel, which can result in significant delays between sampling and diagnosis [5]. While conventional lateral flow assays (LFAs) provide rapid on-site testing, they rely heavily on antibodies. These biological reagents are expensive, susceptible to thermal degradation under field conditions, and often require complex conjugation steps.

The objective of this research was to develop a rapid, label-free screening test based on fluorescence measurements using an optical fiber, and to detect three different fungal species (*A. flavus*, *F. verticillioides* and *A. alternata*) based on their corresponding emission peak maxima.

MATERIALS AND METHODS

Sample preparation

Three fungal species, *A. flavus*, *F. verticillioides*, and *A. alternata* were grown at 25 °C. Fungal mycelium for each culture was collected after 7 days. Zymo Research (ZR) BashingBeads (Zymo Research Corporation, Irvine, CA, USA) were used as a lysing matrix and added into standard lysing tubes with 100 mg of collected wet weight fungal mycelium. Fungal samples were homogenized for three 60-second cycles (180 seconds total) with a handheld lysing device, MonoLyser (RotaPrep Inc., Tustin, CA, USA) at 50% power. After each cycle, the samples were cooled on ice for 2 minutes. The obtained fungal lysate was applied onto a Fusion 5 membrane and observed under UV-A light. Unlike traditional nitrocellulose, which is a microporous polymer film that relies purely on surface adsorption to bind proteins, Fusion 5 is a proprietary structured material containing glass fibers that allows

a single layer to act simultaneously as a sample pad, conjugate release pad, and analytical membrane without requiring multi-component assembly [6].

Fluorescence spectroscopy

A specific volume of the fungal extract was deposited onto the membrane surface and allowed to dry at room temperature. The fluorescence spectra of the samples were captured via an optical fiber cable at an excitation wavelength of 287 nm. Both excitation and emission slits were fixed at 5 nm, and the emission wavelengths were scanned from 305 to 500 nm with a data increment of 1 nm. The baseline fluorescence spectrum of the pristine membrane was recorded under identical conditions and subtracted from the sample spectra to eliminate background interference. Fluorescence spectra were normalized to the maximum intensity to enable comparison between samples.

RESULTS AND DISCUSSION

The macro-morphological evaluation of the isolated strains (Figure 1) revealed distinct phenotypic variations in color, texture, and growth patterns that are characteristic of each genus. These visual features—including the dark melanin pigmentation of *A. alternata*, the aerial pinkish mycelium of *F. verticillioides*, and the granular yellow-green spores of *A. flavus* are in full agreement with diagnostic criteria for these phytopathogenic species.

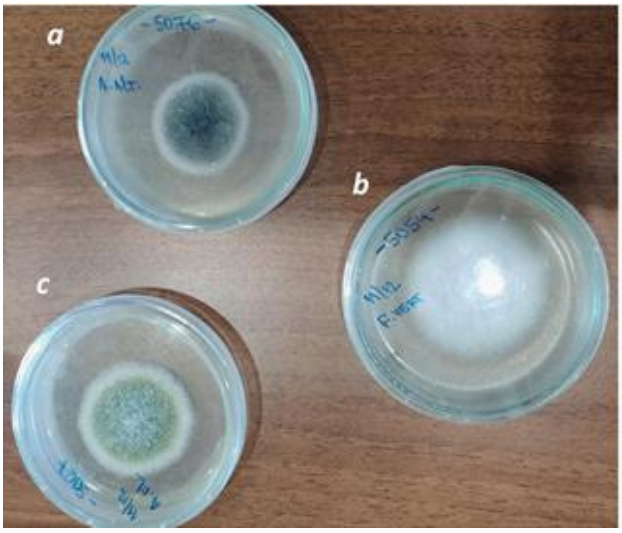

Figure 1 *Macrophotographs of fungal colonies in petri dishes: a) Alternaria alternata; b) Fusarium verticillioides; and c) Aspergillus flavus*

Figure 2a shows fungal lysates deposited on a nitrocellulose membrane under UV-A illumination, revealing clear differences in fluorescence intensity and spot morphology among the tested species. *Alternaria alternata* exhibited a more diffuse and broader fluorescent signal, while *A. flavus* and *F. verticillioides* formed more compact spots with lower signal spreading. Notably, *A. flavus* showed a darker central region within the fluorescent spot, possibly indicating uneven biomass distribution or local fluorescence quenching. Overall, these differences suggest species-specific variations in metabolite composition and optical properties, supporting label-free optical differentiation of fungal pathogens.

Figure 2b presents fluorescence emission spectra of fungal lysates under UV excitation, showing distinct spectral profiles for all three species. *A. alternata* displayed a broader emission and a red-shifted maximum around 460 nm with higher intensity in the 450–500 nm range. In contrast, *A. flavus* and *F. verticillioides* showed stronger peaks at 410–430 nm with a faster intensity decrease at higher wavelengths. These spectral differences reflect variations in fluorescent biomolecules and confirm that fluorescence spectroscopy can effectively distinguish fungal species based on their optical fingerprints, highlighting the potential of the label-free biosensor for rapid detection.

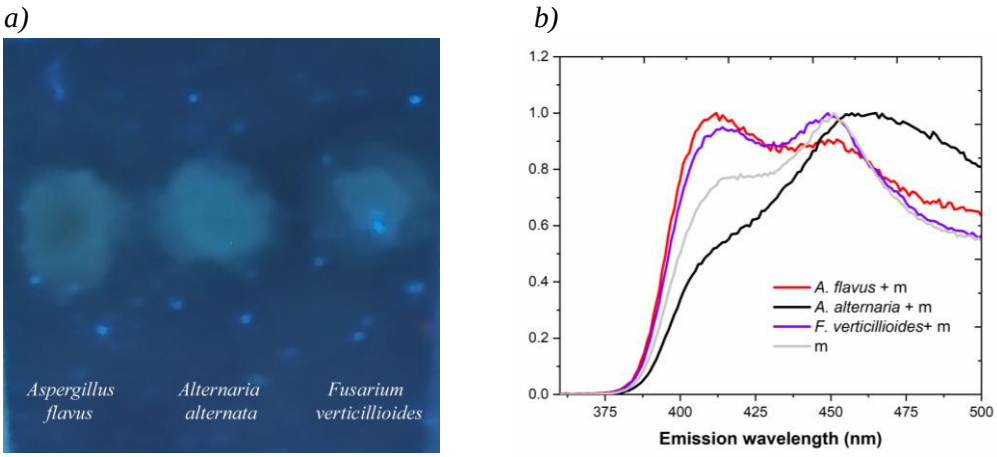

Figure 2 *a) Fungal lysate on membrane under UV-A light; b) fluorescence emission spectra*

CONCLUSION

This study shows that UV-A fluorescence imaging combined with optical spectroscopy enables fast, label-free differentiation of fungal pathogens. Distinct fluorescence patterns and emission spectra provide clear optical fingerprints for *A. alternata*, *A. flavus*, and *F. verticillioides*.

The results confirm species-specific spectral differences, particularly a red-shifted emission in *A. alternata* and lower-wavelength peaks in the other two species.

Overall, the method offers a simple and rapid approach with strong potential for portable biosensing and food safety applications.

ACKNOWLEDGEMENT

This research was funded by the Ministry of Science, Technological Development and Innovation of the Republic of Serbia according to the contract with registration No. 451-03-33/2026-03/200053 and 451-03-33/2026-03/200040, and the Science Fund of the Republic of Serbia, Program DIJASPORA, #GRANT No. 9029-YF-SAIGE, Rapid field-deployable lateral flow diagnostics for combating fungal pathogens in agriculture - COMBAT_AGRI).

REFERENCES

[1] Bartolić, D., Mojović, M., Prokopijević, M., *et al*. J. Sci. Food Agric. 2021, 102 (1), 2500–2505.

[2] Savić, I., Nikolić, M., Nikolić, A., *et al*. Genetika. 2021, 53 (2), 641–649.

[3] Ostry, V. World Mycotoxin J. 2008, 1(2), 175–188.

[4] Saleh, I., Zeidan, R., Abu-Dieyeh, M. Arch. Toxicol. 2024, 98, 1659–1683.

[5] Patel, R., Mitra, B., Vinchurkar, M., *et al*. Heliyon. 2022, 8 (11), e11855.

[6] Jones, K. FUSION 5: A New Platform For Lateral Flow Immunoassay Tests. In: Wong, R., Tse, H. Lateral Flow Immunoassay. Totowa, NJ: Humana Press; 2009. p. 1–15.

EcoTER'26
eco.tfbor.bg.ac.rs
32nd International Conference
Ecological Truth & Environmental Research
24–26 June 2026, Hotel Sunce,
Sokobanja, Serbia

Original Research

REDOX BIOMARKERS IN SEMINAL PLASMA OF CULTURED RAINBOW TROUT: TOS, TAS, AND OSI

DOI: 10.5937/EcoTER26348J

Katarina Jovičić[1,a], Vesna Đikanović[1,b*], Jelena S. Vranković[1,c]

[1] Department of Hydroecology and Water Protection, Institute for Biological Research "Siniša Stanković"—National Institute of the Republic of Serbia, University of Belgrade, Bulevar despota Stefana 142, 11108 Belgrade, SERBIA

[a] http://orcid.org/0000-0002-5105-1532

[b] https://orcid.org/0000-0002-3876-3420

[c] https://orcid.org/0000-0002-2060-8633

Abstract

This study aimed to evaluate seminal plasma levels of total oxidant status (TOS), total antioxidant status (TAS), and oxidative stress index (OSI) in cultured rainbow trout (Oncorhynchus mykiss) as biomarkers of potential oxidative stress. Seminal plasma redox status, determined by measuring TOS and TAS to calculate OSI, can indicate the fertility potential of fish semen more efficiently than assessing individual antioxidant enzymes and non-enzymatic antioxidants separately. Screening these three parameters provides a rapid and reliable test for evaluating the redox status and fertility of fish semen, which is particularly valuable for artificial insemination protocols.

Keywords: Rainbow trout, seminal plasma, redox status, fertility.

INTRODUCTION

Aquaculture plays an essential role in meeting the increasing global demand for high-quality animal protein, with freshwater fish contributing significantly to human nutrition [1]. Among cultured species, *Oncorhynchus mykiss* is one of the most economically important, valued for its rapid growth, adaptability, and nutritional quality. In intensive aquaculture systems, reproductive efficiency is a key factor influencing production success, particularly in artificial fertilization protocols [2]. In externally fertilizing fish, spermatozoa exhibit short-lived motility following activation, making them highly sensitive to environmental and physiological conditions. One of the major factors affecting sperm function is oxidative stress, which occurs when the production of reactive oxygen species (ROS) exceeds the antioxidant capacity of seminal plasma [3]. Elevated ROS levels can induce lipid peroxidation, reduce sperm motility, and impair DNA integrity, ultimately compromising fertilization success and early embryonic development [4,5].

Seminal plasma contains both enzymatic (e.g., superoxide dismutase, catalase, glutathione peroxidase) and non-enzymatic antioxidants that protect spermatozoa from oxidative damage [6]. In this context, total oxidant status (TOS) and total antioxidant status (TAS) are widely

* *djiki@ibiss.bg.ac.rs*

used to assess overall redox balance, while their ratio, the oxidative stress index (OSI), provides an integrative indicator of oxidative stress. Compared with individual antioxidant markers, these parameters offer a rapid and comprehensive assessment of oxidative status in biological systems [7–9].

Despite their potential relevance, the relationship between oxidative stress indicators and reproductive performance in rainbow trout remains insufficiently understood, particularly at the level of seminal plasma under aquaculture conditions.

Therefore, the aim of this study was to evaluate oxidative status in the seminal plasma of cultured rainbow trout using TOS, TAS, and OSI, and to provide baseline data for their potential application as indicators of seminal physiological condition.

MATERIALS AND METHODS

Rearing conditions

Rainbow trout *(Oncorhynchus mykiss*) were maintained at the "Little Danube" Centre for Fisheries and Applied Hydrobiology (University of Belgrade - Faculty of Agriculture, Serbia) in indoor recirculating aquaculture systems (RAS) optimized for commercial trout production. Water quality parameters, including temperature (T), pH, and dissolved oxygen (DO), were monitored daily using a Multi 340i multi-parameter meter (WTW, Weilheim, Germany), with electrodes submerged 0.05 m below the surface. Mean values (± SD) are presented in Table 1.

Table 1 *Some physicochemical parameters of rearing water*

Parameter	T (°C)	DO (mg/L)	pH
Mean ± SD	10.5 ± 1.00	9.07 ± 0.59	7.49 ± 0.04

Milt sampling

Milt was collected from five mature male rainbow trout via gentle abdominal massage, stripping directly into sterile 15 mL glass tubes to avoid contamination with urine, feces, or water (Figure 1). Samples were immediately transported to the laboratory in a portable cooler at 4°C and processed within 1 hour. Seminal plasma was isolated by centrifugation (Eppendorf centrifuge, 3000 × g, 10 min, 4°C), and the supernatant was aliquoted and stored at -80°C until analysis.

TOS, TAS, and OSI measurements

Total oxidant status and TAS were quantified using commercial colorimetric assay kits: TOS Colorimetric Assay Kit (Elabscience E-BC-K802-M) and TAS Colorimetric Assay Kit (Elabscience E-BC-K801-M), following manufacturer protocols. TOS and TAS absorbance were determined at 560 nm and 660 nm, respectively, using an ELISA microplate reader (BioTek Instruments, USA) in accordance with the assay instructions. TOS results were expressed as µmol H_2O_2 equivalents/L, and TAS as mmol Trolox equivalents/L.

The oxidative stress index (OSI) was calculated according to the formula:

OSI (arbitrary unit) = [TOS (µmol H_2O_2 eq/L) / TAS (mmol Trolox eq/L × 1000)]

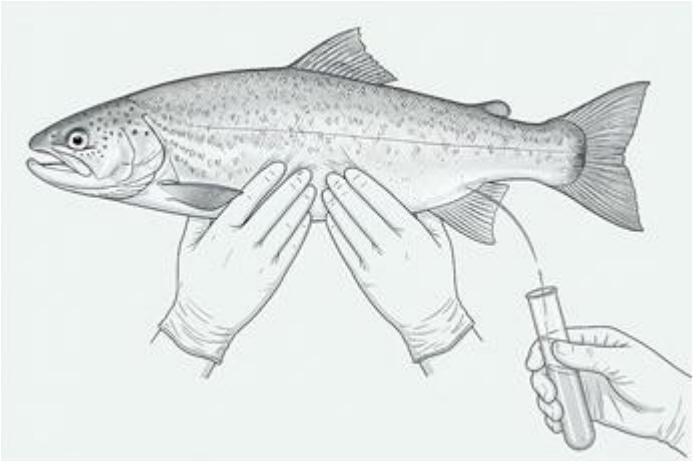

Figure 1 *Schematic representation of semen collection from male rainbow trout by gentle abdominal stripping*

RESULTS AND DISCUSSION

The present study demonstrated measurable variation in TOS, TAS, and OSI in the seminal plasma of cultured male rainbow trout, indicating inter-individual differences in seminal redox balance (Table 2). TOS values ranged from 65.58 to 121.89 µmol H_2O_2 eq/L, whereas TAS varied from 0.85 to 1.11 mmol Trolox eq/L, suggesting that although the seminal plasma of the examined males retained a considerable antioxidant capacity, the oxidant burden differed among individuals. The calculated OSI values point to a generally moderate oxidative state across samples, without pronounced outliers, which may reflect the combined influence of broodstock condition, rearing history, and individual physiological variability (Figure 2).

Table 2 *Total oxidant status (TOS) and total antioxidant status (TAS) in seminal plasma of cultured male rainbow trout (Oncorhynchus mykiss)*

Sample	TOS (µmol H_2O_2 eq/L)	TOS (µmol H_2O_2 eq/g ww*)	TAS (mmol Trolox eq/L)	TAS (mmol Trolox eq/g ww*)
1	78.21	469.26	1.11	6.63
2	65.58	393.47	0.85	5.10
3	76.11	456.63	1.10	6.61
4	121.89	731.37	0.91	5.47
5	84.25	603.23	0.93	5.62

‘ww = wet weight. Values represent individual male samples (n=5).

TAS represents an integrative measure of antioxidant capacity, reflecting the combined contribution of enzymatic and non-enzymatic components. Compared with single-parameter assays, it provides a broader estimate of the antioxidant defense system in seminal plasma and may better reflect the capacity of the sample to neutralize ROS [10]. This is particularly relevant in fish semen, where oxidative stability plays an important role in maintaining sperm functionality and fertilization potential [11].

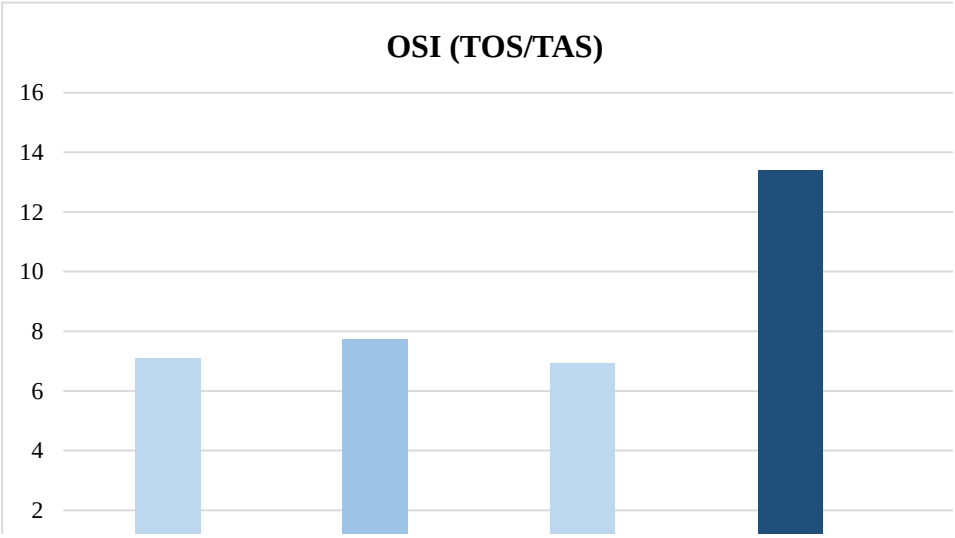

Figure 2 *Oxidative stress index (OSI) calculated as TOS/TAS × 10 ratio in seminal plasma samples from individual rainbow trout males*

In aquaculture of *Oncorhynchus mykiss*, TOS, TAS, and OSI have been reported as useful indicators of redox status under varying environmental and nutritional conditions. Previous studies suggest that these markers are sensitive to factors such as diet, rearing conditions, and exposure to stressors, indicating that they are context-dependent rather than fixed species-specific values [12]. Accordingly, the values obtained in the present study should be interpreted as indicative of the physiological status of the examined broodstock population rather than as universal reference ranges. The observed inter-individual variability may therefore be associated with differences in diet, metabolic status, age, or environmental conditions.

The OSI values obtained in this study are particularly informative, as they reflect the balance between oxidant load and antioxidant protection in a single parameter. Lower OSI values are generally associated with reduced oxidative stress and improved preservation of sperm structural integrity, especially under storage or cryopreservation conditions [13–15]. In the present study, the redox profile suggests the absence of pronounced oxidative imbalance in the analysed samples. However, since functional sperm parameters were not assessed, these findings should be interpreted with caution and cannot be directly linked to sperm performance.

Taken together, the results indicate that seminal plasma of cultured rainbow trout exhibits measurable but variable antioxidant capacity and oxidant load, and that OSI may serve as a useful indicator of seminal redox status. Future studies should integrate these parameters with sperm motility, membrane integrity, DNA stability, and fertilization success in order to better understand the functional significance of redox variation. Such an approach would strengthen the application of TAS, TOS, and OSI as biomarkers in reproductive management and broodstock assessment.

CONCLUSION

This study provides one of the first assessments of TOS, TAS, and OSI in the seminal plasma of cultured *Oncorhynchus mykiss*, establishing baseline redox values under controlled RAS conditions. The obtained results indicate moderate TOS and TAS levels, resulting in OSI values consistent with a balanced redox status in the analysed samples. These findings contribute to the understanding of seminal redox homeostasis in aquaculture and suggest that TOS, TAS, and OSI may serve as useful indicators of seminal physiological condition. However, given the absence of direct functional sperm parameters, these results should be interpreted with caution. Future research should aim to relate redox parameters to sperm motility, membrane integrity, and fertilization success, and to validate OSI thresholds across seasonal and genetic variability in order to refine their application in commercial hatchery management.

ACKNOWLEDGEMENT

The authors are grateful to the Ministry of Science, Technological Development and Innovation of the Republic of Serbia for financial support according to the contract with registration No.451-03-33/2026-03/200007. The content of this study is in line with following United Nations (UN) Sustainable Development Goals, under the frame of the UN Agenda for Sustainable Development (Transforming our World: The 2030 Agenda for Sustainable Development-UN, 2015): Goal 14.

REFERENCES

[1] Bakhsh, M., Ghazali, M.H., Yar M.K., *et al.* Univ. Sindh. J. Anim. Sci. 2023, 7(4), 23–35.
[2] Marković, Z., Poleksić, V. Aquac. Eur. 2013, 38, 32–37.
[3] Bucak, M.N., Ateşşahin, A., Varol, Ş., *et al.* Theriogenology 2008, 67(4), 671–678.
[4] Sandoval-Vargas, L., Silva Jiménez, M., Risopatrón González, J., *et al.* Rev. Aquacult. 2021, 13, 365–387.
[5] Wang, Y., Fu, X., Li, H. Front. Endocrinol. 2025, 16, 1520835.
[6] Tavilani, H., Goodarzi, M. T., Vaisi-raygani, A. *et al.* Int. Braz. J. Urol. 2008, 34(4), 485–491.
[7] Erel, O. Clin. Biochem. 2005, 38, 1103–1111.
[8] Erel, O. Clin. Biochem. 2004, 37, 112–119.
[9] Dastan, S.D., Gulhan, M.F., Selamoglu, Z. *et al.* Iran. J. Fish. Sci. 2017, 16(1), 326–340.
[10] Duran, U., Çenesiz, S. BMC Vet. Res. 2025, 21(1), 302.
[11] Xue, S.H., Xu, B.B., Yan, X.C. *et al.* Vet. Sci. 2025, 12(7), 658.
[12] Şahinöz, E., Aral, F., Doğu, Z. *et al.* Appl. Ecol. Environ. Res. 2019, 17(2), 3371–3385.
[13] Barranco, I., Rubio, C.P., Tvarijonaviciute, A. *et al.* Antioxidants 2021, 10(8), 1203.
[14] Qamar, A.Y., Naveed, M.I., Raza, S. *et al.* Anim. Biosci. 2023, 36(3), 385–403.
[15] Ünal, İ., Uysal, H. Anim. Reprod. Sci. 2024, 270, 107618.

EcoTER'26
eco.tfbor.bg.ac.rs
32nd International Conference
Ecological Truth & Environmental Research
24–26 June 2026, Hotel Sunce,
Sokobanja, Serbia

Original Research

UTILIZATION OF A PRODUCT FROM SULFURIC ACID PRODUCTION, POLLUTING THE ENVIRONMENT, WITH APPLICATION IN FERROUS METALLURGY

DOI: 10.5937/EcoTER26353P

Petar B. Petrov[1,a*]

[1] University of Chemical Technology and Metallurgy, Department of Ferrous Metals And Material Science, Saint Kliment Ohridski 8, 1756 Sofia, BULGARIA

[a] https://orcid.org/0009-0006-6957-0097

Abstract

In our country works considerable plants for sulphuric acid production, which generate considerable quantities of discarded vanadium catalyst which pollutes the environment. In that time, an ore deposit Obrochiste in Republic of Bulgaria contains a lot of reserves of carbonate manganese ore. The effective utilization on this ore defies a research interest for a long time. Processing of both materials in electrothermal furnace exact agglomeration to suitable sizes and decarbonatization of the ore. This creates an opportunity to utilize a polluting product. It is supposed that the most suitable method for common agglomeration is the sinter process. The aim of this development is to establish the main physical parameters of the process on laboratory sintering in laboratory sinter cup of carbonate manganese ore and waste vanadium catalyst. For preliminarily modeling of the process was used the specific calculation program. It was made qualitative and quantitative characteristic of received sinter from point of view for further thermal manufacturing.

Keywords: waste vanadium catalyst, carbonate manganese ore, sinter.

INTRODUCTION

The complex receiving of elements from carbonate manganese ore and waste vanadium catalyst with heat metallurgical method is not effective to direct manufacturing of raw materials. It is necessary to be joint agglomerated this materials. Attempt for joint agglomeration and sintering of starting raw materials is doing for the first try in department Metallurgy of ferrous metals by UCTM Sofia [1].

For modeling of joint agglomeration is using a modificated variant of calculated program Agloprice. Raw materials for the sinter are: coke breeze, manganese concentrate and waste catalyst [1]. A flux material was not use.

After the expert analysis of the receiving results from different variants and with view for the effective of the next heat metallurgical manufacturing of sinter, i. e. to introduce sufficiency quantity of Mn in alloy from maximum drawing out of V and optimal quantity of Si, Al, Ca and Fe. On this way are select compositions of raw materials for laboratory

* *pbpetrov@uctm.edu*

agglomeration. The most suitable for this experiment are starting materials with 80, 70 and 60 % manganese concentrate and 20, 30 and 40 % vanadium catalyst [1].

MATERIALS AND METHODS

Instalation for sinter

The laboratory agglomeration of manganese concentrate and vanadium catalyst is going on in laboratory sinter cup, Figure 1. The cup is a truncated pyramid which upper and lower radix have quadratic a vertical section. The lower radix is 150 mm and the upper size – 160 mm. The effective height of raw materials is 300 mm. The calculated effective worked volume of the sinter cup is 7,21 dm^3 [2].

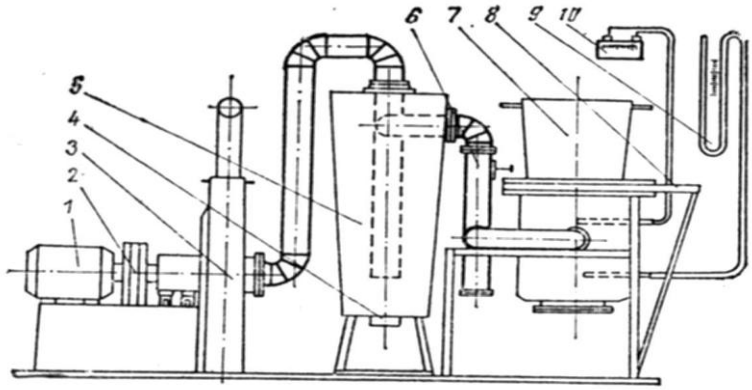

Figure 1 *Scheme of laboratory sinter installation: 1 – electrical motor; 2 – connector; 3 – vacuum system; 4 – outlet for cleaning of dust filter; 5 – dust filter; 6 – shutter; 7 – sinter cup; 8 – base; 9 – manometer; 10 – voltmeter*

Chemical composition

The chemical composition of the used raw materials is show to Table 1 [3–5].

Table 1 *Chemical composition of raw materials*

Chemical composition of waste vanadium catalyst, %						
V_2O_5	Fe_2O_3	SiO_2	K_2O	Na_2O	Al_2O_3	SO_3
4,12	3,40	57,12	6,71	3,93	0,82	23,88

Chemical composition of coke breeze for sintering, %									
FeO	SiO_2	Al_2O_3	CaO	MgO	S	FeS_2	C	volatiles	MnO
3,71	6,08	2,31	1,18	0,46	1,79	1,16	78,62	4,20	0,49

Chemical composition of manganese concentrate, %					
MnO	CO_2	FeS_2	Fe_2O_3	P_2O_5	SiO_2
44,56	19,33	2,25	1,79	0,31	12,40
MgO	CaO	Al_2O_3	K_2O+Na_2O	H_2O_h and others	loss at burning
2,00	3,90	2,10	1,15	1,20	8,97

Technological implementation

The manganese concentrate and coke breeze are with size which is over 30 mm. The vanadium catalyst is with size which is over 7 mm and they are not suitable for direct

agglomeration. It is necessary to accomplish of preliminary preparation of this materials – grinding and rolling. The grinding is going on in mechanical cylinder with working frequency of rotation – 25 rev/min. The continuance of grinding is 15 min to fraction (- 3 mm). The fraction (+ 3 mm) is going for new grinding [6-9]. The grinding materials there are following filling weights: Mn concentrate – 1,2 kg/dm^3, V catalyst – 0,56 kg/dm^3, coke breeze - 0,95 кg/dm^3.

The rolling is accomplish in disk rolling machine with working frequency of rotation – 20 rev/min and slope of the disk – 45 °. The duration of rolling is 4 – 5 min. From the raw materials, in rolling machine was add 30 % return sinter from previous agglomeration. The dampness in the raw materials is about 4 % (0,25 kg for one portion raw materials). For the best rolling is add about 0,30 – 0,35 kg water for one portion raw materials and on this way is reach dampness of the raw materials about 9 %, which is normal for the sinter practice. At the bottom of the sinter cup (Figure 1, p. 7) is the grid and over it there is 2 – 3 cm return sinter (about 0,50 kg), from previous sinter process, but it is more coarse from the raw materials. The rolling is accomplish with the aim the sinter engine making better contact with the fractions of the concentrate and the catalyst and for more effective permeability of the gases to the raw materials from sinter process [6–9].

The sinter cup is with working volume 7,21 dm^3. The data of the calculation program for raw materials are calculate from the volume of the sinter cup in the necessary kilograms for the three variants of sintering. First it is defy the volume of each raw material, which it fills in the working volume of the sinter cup, as take into account his filling weight. From the receiving volume with the help of filling weight is calculate the necessary weight of the respective raw component [1,10]. Because of the big heat loss from working with this size of the sinter cup in comparatively with sinter process from laboratory conditions, the volume of coke breeze is doubling [1].

At the first variant (80 % concentrate и 20 % catalyst), according to calculates of the program, are necessary 7,32 kg coke breeze and 135,68 kg mixture (concentrate and catalyst) for receiving to 100 kg sinter. The calculated data for the laboratory sinter cup for concentrate, catalyst and coke breeze are – 5,04 kg, 1,26 kg and 0,68 kg. The mixture for agglomeration at this variant is with weight 6,98 kg, as return sinter is 1,89 kg from this weight. The general weight of the mixture reply to volume about 7,19 dm^3, which is approximately equal to the volume of the sinter cup.

At the double variant (70 % concentrate и 30 % catalyst), according to calculates of the program, are necessary 6,82 kg coke breeze and 132,89 kg mixture (concentrate and catalyst) for receiving of 100 kg sinter. The calculated data for laboratory sinter cup for concentrate, catalyst and coke breeze are – 4,11 kg, 1,77 kg and 0,61 kg. The mixture for agglomeration at this variant is with weight 6,49 kg, as return sinter is 1,76 kg from this weight. The general weight of the mixture reply to volume about 7,22 dm^3, which inessential exceed the volume of the sinter cup.

At the three variant (60 % concentrate и 40 % catalyst), according to calculates of the program, are necessary 6,34 kg coke breeze and 130,21 kg mixture (concentrate and catalyst) for receiving of 100 kg sinter. The calculated data for laboratory sinter cup for concentrate, catalyst and coke breeze are – 3,30 kg, 2,19 kg and 0,52 kg. The mixture for agglomeration at

this variant is with weight 6,01 kg, as return sinter is 1,65 kg from this weight. The general weight of the mixture reply to volume about 7,21 dm^3, which is equal to the volume of the sinter cup.

The filling of raw materials is accomplished carefully to the walls of the sinter cup with the aim to avoid the congestion of the layer to the raw materials. The layer of the raw materials must to have optimal permeability of the gases. After the including of the vacuum installation is making a fire of upper layer to the raw materials with torch of gas. The time of the sinter process is about 25 min. Each minute is reading results for the temperature with thermocouple to voltmeter (Figure 1, p. 10) and the vacuum – with manometer (Figure 1, p. 9) [6].

RESULTS AND DISCUSSION

From the select three variants three sinters with 20, 30, and 40 % catalyst are received. Figure 2 show the parts of agglomerate with 70 % manganese concentrate and 30 % catalyst.

Figure 2 *Sinter with 70 % concentrate and 30 % catalyst*

The data from the measures of the temperature and the vacuum for these three processes of agglomeration are show in Figures 3 and 4.

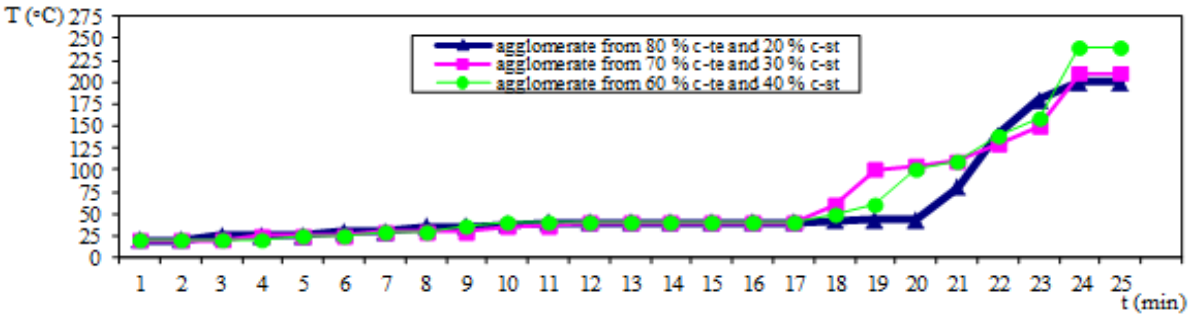

Figure 3 *Changing of the temperature for the three sinter process*

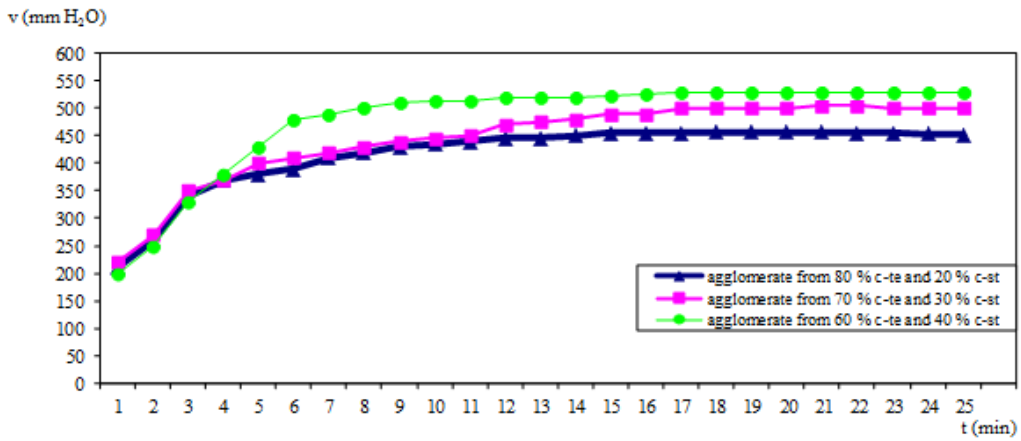

Figure 4 *Changing of the vacuum for the three sinter process*

According to the Figures 3 and 4 each of these three processes are with continuation about 25 minutes. The temperature of the process and necessary vacuum make increase with increase of quantity to the catalyst, because of more odds and ends, which is locate in the porous of the formation sinter. This follow to their occlusion especially in the variant with 40 % vanadium catalyst.

According to calculations making from a microscope drill the sinters there are following chemical composition, which is show in Table 2.

Table 2 *Chemical composition of receiving sinters*

oxide	sinter with 80 % c-te : 20 % c-st	sinter with 70 % c-te : 30 % c-st	sinter with 60 % c-te : 40 % c-st
MgO, %	6,11	5,80	5,40
FeO, %	3,77	3,68	3,59
SiO_2, %	18,30	23,61	18,51
Al_2O_3, %	4,87	4,64	4,41
MnO, %	60,59	53,67	47,03
CaO, %	6,09	5,48	4,89
V_2O_5, %	1,94	2,46	2,97

This chemical composition as independently definition can not explain chemical and structure characteristics of receiving sinters. For more entire picture of their complicated composition and fragmentariness has been making analysis with X-ray phases apparatus – TYR – M 62, with CoK_α ray and length of the wool of X-ray - λ = 0,178892 nm and computer record of receiving results. The data of analysis, accomplished with X-ray phases apparatus are show in Table 3.

In the diffraction picture of sinter with 100 % Mn concentrate are registered three basic crystal phases: MnO (manganosite), Mn_3O_4 (hausmanite) and $2MnO.SiO_2$. At Table 3 we can see that from complex agglomeration of Mn concentrate with V catalyst, the lines of clean manganese oxides are displaced in direction to form of the alloys with SiO_2. This is due to the higher content of SiO_2 in waste vanadium catalyst (Table 1) and specifically conditions to the sinter process (T ≈ 1200 °C).

Table 3 *Composition of phases to the receiving sinters*

sinter variant	80 % c-te : 20 % c-st	70 % c-te : 30 % c-st	60 % c-te : 40 % c-st
	$2MnO.SiO_2$	$Mn_2.SiO_4$	$Mn.Mn_6.SiO_2$
fixed	SiO_2(α quartz)	MnO	V_2O_4
crystal	SiO_2(α crystobalite)	V_3O_5	V_3O_5
phases	-	V_3O_7	SiO_2(α crystobalite)
	-	SiO_2(α crystobalite)	-

The analysis accomplished with X-ray phases apparatus show availability of V_3O_5, V_3O_7 and V_2O_4 and the quantity of vanadium versus oxygen increase with the increase to percentage of catalyst in the sinter. The phases composition of sinter with higher contents of vanadium catalyst (30 and 40 %) is optimum for the aim of the next receiving to complex alloy.

From this analysis were not discovered phases of Fe and Ca.

The three sinters are with normal porous and structure. Their division of fraction is show in Table 4.

Table 4 *Fraction composition of receiving sinters*

80 % c-te : 20 % c-st			70 % c-te : 30 % c-st			60 % c-te : 40 % c-st		
fr. (mm)	kg	%	fr. (mm)	kg	%	fr. (mm)	kg	%
+30	3,400	61,10	+30	3,700	75,82	+30	3,100	61,37
+20	0,165	2,95	+20	0,100	2,05	+20	0,060	1,19
+15	0,055	0,99	+15	0,060	1,23	+15	0,000	0,00
+12	0,245	4,40	+12	0,220	4,51	+12	0,150	2,97
+5	0,580	10,42	+5	0,300	6,15	+5	0,560	11,09
-5	1,120	20,13	-5	0,500	10,25	-5	1,180	23,37
generally	5,565	100,00	generally	4,880	100,00	generally	5,050	100,00
loss	1,435		loss	1,620		loss	0,950	

The bases technological parameters of receiving sinters are show in Table 5. These are: production of sinter – A; sintering rate – V; quantity of good sinter – K; density – ρ; macro porous – δ; hardness - σ.

Table 5 *Technological parameters of the sinters*

technolog. parameters	80 % c-te : 20 % c-st	70 % c-te : 30 % c-st	60 % c-te : 40 % c-st
A, %	71,07	66,58	74,16
V, m/min	0,012	0,012	0,011
K, %	69,45	83,61	65,55
ρ, g/sm^3	3,38	2,76	2,52
δ, %	33	40	43
σ, kgp/sm^3	28	13	8

At the calculated parameters follow that with 30 % catalyst the production of sinter is least, but the percentage of good sinter is most. Sintering rate is comparatively constant and if we use 40 % vanadium catalyst we can see a little decrease. Density and compressive decrease with the increase of quantity to catalyst in sinter, because of the catalyst is brittle material. At the same time the macro porous increase because the vanadium catalyst there is a high

temperature of melting and its fragments don't suffer partial melting, like the fragments of manganese concentrate. This predispose, around each catalyst fragment to stick from partial melting concentrate and on this way the porous in the sinter will be increase.

Of the sinters considered, the variant with 70% manganese concentrate and 30% vanadium catalyst is most suitable (because K = 83,61%) for subsequent high-temperature processing to an alloy containing vanadium. In this variant, a relatively high percentage of catalyst would be utilized.

CONCLUSION

It is elaborate a method for receiving of sinter from carbonate manganese concentrate and waste vanadium catalyst. For the first time is accomplish joint agglomeration of carbonate manganese concentrate and waste vanadium oxygen catalyst in laboratory sinter cup with correlation 80/20, 70/30 and 60/40.

Production of sinter, sintering rate and quantity of good sinter are normal. The hardness decrease with increase the quantity of catalyst. The sinters of this agglomeration processes there are a good porously and they are right for the next heat metallurgical manufacturing with carbon to complex alloy. The most suitable for this is the 70/30 sinter.

So far, the presented possibility for the utilization of a polluting product from the production of sulfuric acid is at the laboratory level. For processing the resulting sinter to an alloy with vanadium (which would find application in steelmaking as a deoxidizing and alloying alloy), it is necessary to carry out large-scale production of this sinter.

REFERENCES

[1] Marinov, *et. al.* J. Univ. Chem. Tech. Metall. 2006, 41 (2), 171–174.

[2] Avramov A, Ivanchev I, Tsanev T. Metallurgy of iron. Sofia: Technics; 1994. p. 105. (In Bulgarian).

[3] Ilarionov. Vanadium catalysts for contact production of sulfuric acid. Moskow: Chemical literature; 1963. p. 34. (In Russian).

[4] Problems and prospects in the enrichment of manganese ore from the Obrochishte deposit. 1991. Available from: https://digital.libsu.uni-sofia.bg/bg/v/51083.

[5] Gasik, Liakishev, Emlin. Theory and technology of ferroalloy production. Moskow: Metallurgy; 1988. p. 93–130. (In Russian)

[6] Drakalijski C, Metallurgy of cast iron. Sofia: Technics; 1994. p. 61–84. (In Bulgarian).

[7] Vegman. Blast furnace production. Ore preparation and blast furnace process. Moscow: Metallurgy; 1989, p. 496. (In Russian)

[8] Kolesanov, Khlaponin, Krivosheev, Chikurov, *et. al*. Improving sintering processes. Kiev: Technics; 1983. p. 110. (In Russian).

[9] Mischenko, *et. al.* Bulletin of scientific, technical and economic information, 2020, 76 (8), 790–802. (In Russian)

[10] Frolov, *et. al*. Bulletin of scientific, technical and economic information, 2012, 68 (10), 37–44. (In Russian)

EcoTER'26
eco.tfbor.bg.ac.rs
32nd International Conference
Ecological Truth & Environmental Research
24–26 June 2026, Hotel Sunce,
Sokobanja, Serbia

Original Research

VALORIZATION OF BREWERY SPENT GRAIN INTO BIOPLASTIC FILMS: INFLUENCE OF BIOMASS LOADING ON BARRIER AND ANTIOXIDANT PROPERTIES

DOI: 10.5937/EcoTER26360K

Despina Kostadinova Jankovski[1,a*], Milica Arizanova[1,b], Bozidar Ristovski[1,c], Elena Velickova[1,d], Donka Doneva-Shapcheska[1,e]

Faculty for Technology and Metallurgy, University of Ss. „Cyril and Methodius“, Ruđer Bošković 16, 1000 Skopje, NORTH MACEDONIA

[a] https://orcid.org/0000-0001-9999-9798

[b] https://orcid.org/0000-0003-0245-6901

[c] https://orcid.org/0000-0003-4493-2144

[d] https://orcid.org/0000-0003-3259-5726

[e] https://orcid.org/0000-0003-3618-9872

Abstract

Brewery spent grain (BSG), the major by-product of the brewing industry, represents a promising feedstock for the development of sustainable bioplastic materials. In this study, chitosan-based bioplastic films containing different BSG loadings were prepared using glycerol as a plasticizer to evaluate the influence of biomass incorporation on film properties. Prior to film preparation, BSG was subjected to mild acetic-acid hydrolysis to improve the release of bioactive compounds. The films were characterized in terms of thickness, water vapor permeability, and antioxidant activity using the DPPH radical scavenging assay. The incorporation of BSG influenced the structural and barrier properties of the films while enhancing their antioxidant potential due to the presence of phenolic compounds naturally associated with lignocellulosic biomass. Increased BSG loading resulted in higher radical scavenging activity, indicating the potential of these materials for active packaging applications. Overall, the results demonstrate the feasibility of valorizing brewery spent grain into functional bioplastic films, contributing to sustainable packaging development and circular bioeconomy strategies.

Keywords: brewery spent grains, chitosan, bioplastic films, antioxidant activity, active packaging.

INTRODUCTION

The global packaging industry is currently facing a significant challenge due to the environmental contamination caused by the widespread use of fossil-fuel-derived synthetic plastics [1,2]. Transitioning toward sustainable alternatives and a circular bioeconomy is now imperative to mitigate the environmental impact of plastic pollution [3,4]. In this context,

* *despina@tmf.ukim.edu.mk*

agricultural side streams and lignocellulosic residues have emerged as strategic renewable feedstocks to replace petroleum-based industrial components [2,5].

Brewer's spent grain (BSG) is one attractive agri-food wastes for the fabrication of bio-based materials [6]. It is the primary solid by-product of the brewing process, accounting for approximately 85% of the total brewery waste output. Annually, the brewing industry generates between 38 to 39 million tons of BSG worldwide [7]. Despite its potential, BSG is currently underutilized, often limited to low-value applications such as animal feed or disposed of in landfills [7,8]. Valorizing this waste stream into bioplastic films represents a promising strategy for reintegrating brewery residues into the production cycle [5].

The suitability of BSG for film formation stems from its rich chemical composition [6]. It is a lignocellulosic material composed of dietary fibers, including cellulose (12%–33%), hemicellulose (20%–42%), and lignin (10%–28%), as well as a significant protein fraction (19%–30%) [7,8]. Furthermore, BSG contains valuable phytonutrients, notably phenolic compounds such as ferulic and p-coumaric acids, which are concentrated in the barley grain's outer layers [7]. These compounds impart important functional characteristics, such as radical scavenging and antioxidant capacity, making BSG-based materials ideal for active food packaging designed to extend the shelf life of oxidative-prone products [2,9,10].

However, biopolymers derived from BSG often yield films that are inherently brittle [10]. To overcome this, glycerol is frequently employed as a plasticizer; it decreases the attractive forces between polymer chains, thereby enhancing film flexibility, handling, and bulk mechanical properties [11]. While several studies have explored films made from isolated BSG proteins or specific fractions like arabinoxylans [9,11], research into the direct use of whole BSG waste in varying loads for film fabrication remains a growing area of interest.

The objective of this study was to valorize brewery spent grain (BSG) by incorporating it into bioplastic films at different loading concentrations (5, 15, 25, and 50%) using glycerol as a plasticizer. The effect of BSG addition on the physical and barrier properties of the films, including water vapor permeability (WVP), was evaluated. Antioxidant activity was also determined using the 2,2-diphenyl-1-picrylhydrazyl (DPPH) radical scavenging assay to assess the potential of the films for packaging applications.

MATERIALS AND METHODS

Preparation of BSG and bioplastic films

Brewery spent grain (BSG) was obtained from a local brewery in Skopje, North Macedonia. The material was dried at 50 °C for 24 h, milled, and sieved to obtain a particle size below 150 µm. Mild hydrolysis was applied to partially disrupt the lignocellulosic structure of BSG and improve the extractability of bound antioxidant compounds. Briefly, BSG (5 wt%) was dispersed in 1 M acetic acid and continuously stirred at 40 °C for 24 h, according to the methodology described by Arizanova et al. (2026) [12]. Medium molecular weight chitosan (190,000–310,000 Da; degree of deacetylation >75%) was purchased from Merck (Italy). Glycerol, used as a plasticizer, was obtained from Fisher Scientific (USA). All chemicals and reagents used in the study were of analytical grade. Four film formulations

were prepared by mixing the chitosan and BSG solutions in different ratio, as presented in Table 1. Films' appearance is shown in Figure 1.

Table 1 *Formulations of the prepared bioplastic films*

Formulation	Chitosan:BSG ratio	Chitosan (g)	BSG (g)	Total Glycerol (g)
Ch	100:0	1	0	0.3
Ch-BSG-1	85:15	0.85	0.15	0.3
Ch-BSG-2	75:25	0.75	0.25	0.3
Ch-BSG-3	50:50	0.50	0.50	0.3
Ch-BSG-4	25:75	0.25	0.75	0.3

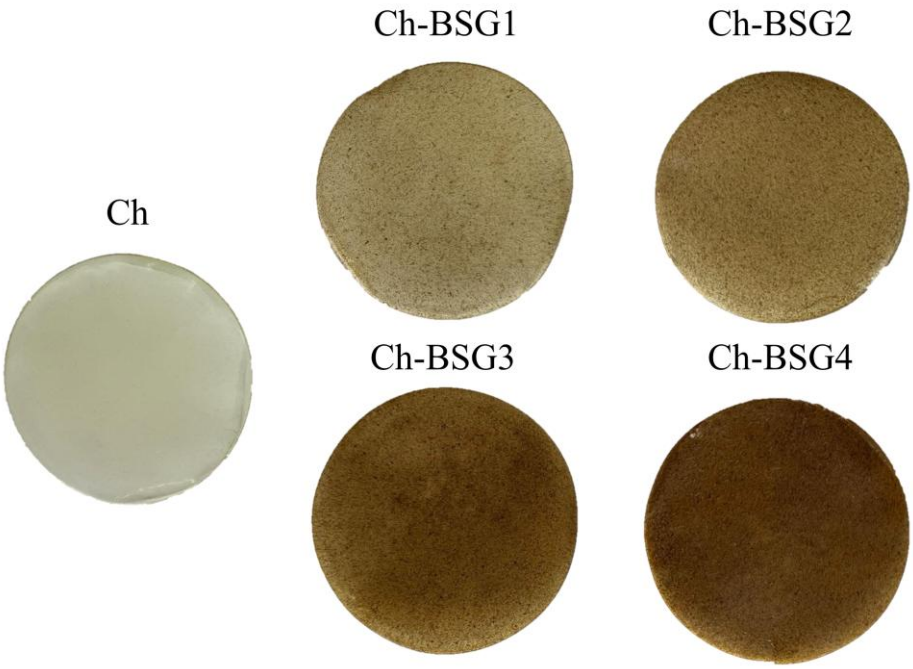

Figure 1 *Appearance of prepared bioplastic films*

Film thickness (δ)

The thickness of the prepared films was determined using a digital caliper (Extol, China) with a precision of ±0.02 mm. Measurements were taken at ten randomly selected locations across each film sample to account for possible heterogeneity. The final thickness values are expressed as the average ± standard deviation (SD).

Water vapor permeability

The water vapour permeability of the prepared films was evaluated using the gravimetric cup method based on the ASTM E96 (2015) standard, with slight modifications [13]. Permeability cells containing 3 mL of distilled water were sealed with the film samples and subsequently transferred to a desiccator maintained at low relative humidity using silica gel. The experiment was conducted at 25 °C, and the mass loss of the cups was monitored periodically over a 24 h period. The reduction in mass corresponded to the migration of water vapour through the film matrix from the high-humidity side (100 % RH inside the cup)

toward the lower-humidity environment (30 % RH outside the cup). The WVP values were determined according to the following equation:

$$WVP = \frac{WVTR * \delta}{P_{H_2O} * \Delta RH}$$

where δ represents the average thickness of the film, WVTR is the water vapor transmission rate, P_{H_2O} denotes the saturation vapor pressure of water at 25 °C, and ΔRH corresponds to the relative humidity gradient across the film.

Antioxidant properties

The antioxidant potential of the bioplastic films was assessed using the DPPH radical assay, based on a modified procedure described by Merino et al. (2023) [14]. Film samples weighing ~0.05 g were immersed in 4 mL of a 0.1 mM DPPH solution prepared in ethanol. The interaction between the films and the radical solution was monitored by measuring the reduction in absorbance at 517 nm over a period of 24 hours, using a Cary 6000i UV–Vis–NIR spectrophotometer (USA). The radical scavenging activity (RSA, %) was calculated according to the following equation:

$$RSA\ (\%) = \frac{A_0 - A_{1,t}}{A_0} \times 100$$

where A_0 represents the initial absorbance of the DPPH solution at 517 nm, and A_t corresponds to the absorbance of the solution in the presence of the film sample at a given time.

RESULTS AND DISCUSSION

Film thickness (δ)

The thickness of the prepared films is presented in Figure 2. The pure chitosan film (Ch) exhibited the lowest thickness (0.26 ± 0.03 mm), while the incorporation of brewer's spent grain (BSG) increased the thickness up to 0.37 ± 0.01 mm in Ch-BSG2. This increase is attributed to the lignocellulosic and predominantly insoluble nature of BSG particles, which are dispersed within the biopolymer matrix as a reinforcing biofiller and contribute to a bulkier structural organization [5,7]. Similar thickness ranges (0.25–0.38 mm) have been reported for thermoplastic starch composites reinforced with BSG fibers, confirming that the incorporation of lignocellulosic biomass typically increases the total volume and structural complexity of biopolymer films [7]. The initial rise in thickness is associated with the presence of bulky insoluble particles that partially disrupt the compact polymer network and restrict biopolymer chain mobility. Interestingly, further increases in BSG loading (Ch-BSG3 and Ch-BSG4) did not result in continuous thickening, with both films stabilizing at approximately 0.35 mm. This plateau likely reflects particle aggregation and more efficient packing at higher biomass concentrations, combined with a reduced proportion of continuous hydrated matrix surrounding the particles as the chitosan fraction decreases. Similar non-linear thickness trends have been observed in other BSG-derived composite systems, as well as for poly(vinyl alcohol) composite films [10,15].

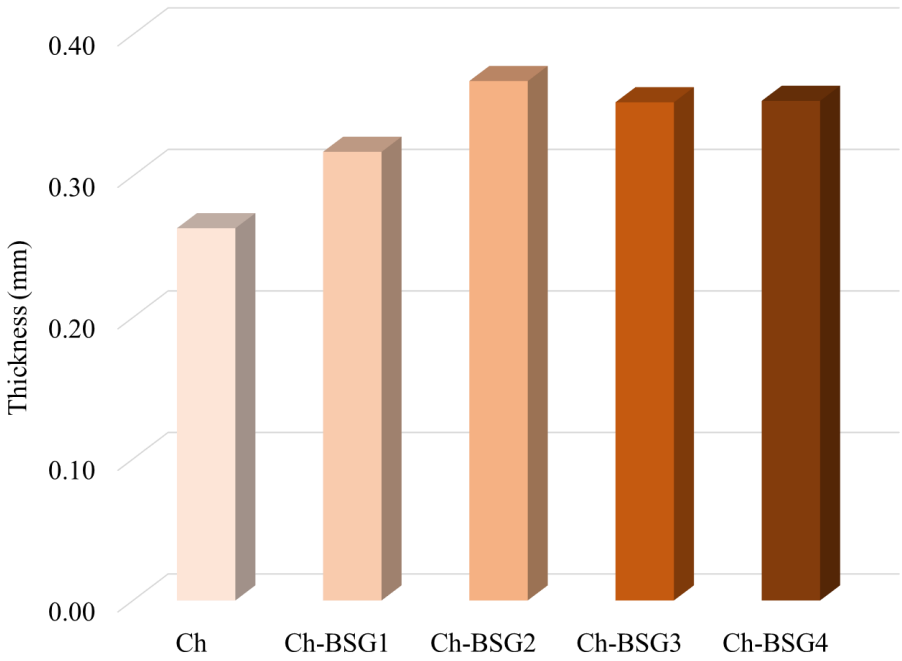

Figure 2 *Films' thickness*

Water vapour permeability

The water vapor permeability (WVP) values of the prepared films are presented in Figure 3. The incorporation of BSG resulted in a gradual increase in WVP, reaching approximately 4.1×10^{-10}, 4.8×10^{-10}, and 4.9×10^{-10} g/m·s·Pa for Ch-BSG1, Ch-BSG2, and Ch-BSG3, respectively, and increasing more markedly to 6.3×10^{-10} g/m·s·Pa for Ch-BSG4. This behaviour can be attributed to the hydrophilic nature of BSG constituents, including residual proteins, hemicelluloses, and cellulose, which contain polar functional groups (–OH, $–NH_2$, –COOH) capable of interacting with water molecules through hydrogen bonding [10]. As a result, water sorption and diffusion through the film matrix are facilitated. The obtained values are comparable to those reported for BSG protein-based films, which exhibited WVP values between 3.03 and 4.58×10^{-10} g/m·s·Pa and similarly showed increased permeability with higher biomass incorporation [11]. The increase in WVP further suggests that BSG particles partially disrupt the intermolecular interactions within the dense chitosan network, generating a less compact structure that promotes moisture transport [3]. Although lignocellulosic fillers may sometimes improve barrier performance by increasing diffusion tortuosity, the pronounced hydrophilic character of whole BSG appears to dominate in the present system, resulting in increased permeability.

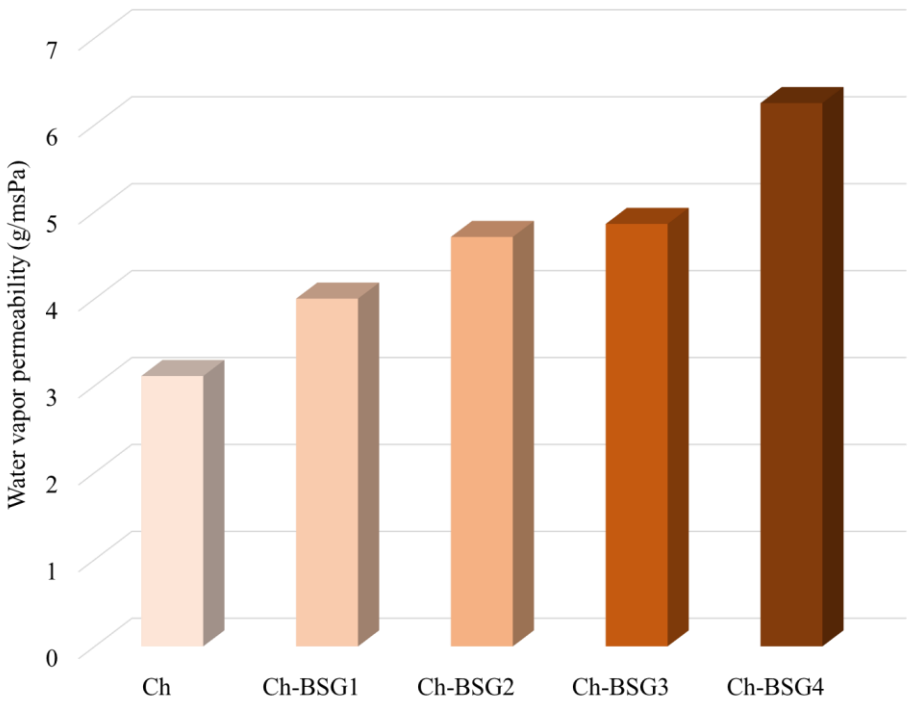

Figure 3 *WVP (x 10–10 g/msPa) of films*

Antioxidant properties

The addition of BSG enhanced the antioxidant activity of the composite films, with a marked increase observed at higher loadings: 32% for Ch-BSG2, 75% for Ch-BSG3, and nearly complete scavenging (99%) for Ch-BSG4. Notably, the antioxidant performance of Ch-BSG3 exceeded that previously reported for films based on isolated BSG proteins, which showed only 5.44% inhibition at a comparable polymer-to-BSG ratio [7]. This suggests that the utilization of whole BSG preserves a broader spectrum of bioactive constituents compared to isolated protein fractions. The observed behaviour is consistent with the presence of hydroxycinnamic acids in BSG, particularly ferulic and *p*-coumaric acids, which are recognized as the major antioxidant compounds in barley husk-derived materials [16,17]. In addition, the mild acetic-acid hydrolysis applied during film preparation likely promoted the release of bound phenolics through partial disruption of ester and ether linkages within the lignocellulosic matrix, thereby increasing their bioavailability and reactivity toward DPPH radicals [5,7]. The high scavenging activity observed at elevated BSG loadings was comparable to that reported for advanced active packaging systems, such as BSG-arabinoxylan films supplemented with ferulic acid [9]. Overall, these findings demonstrate the potential of whole BSG as a functional bioactive filler for the development of antioxidant bioplastic films.

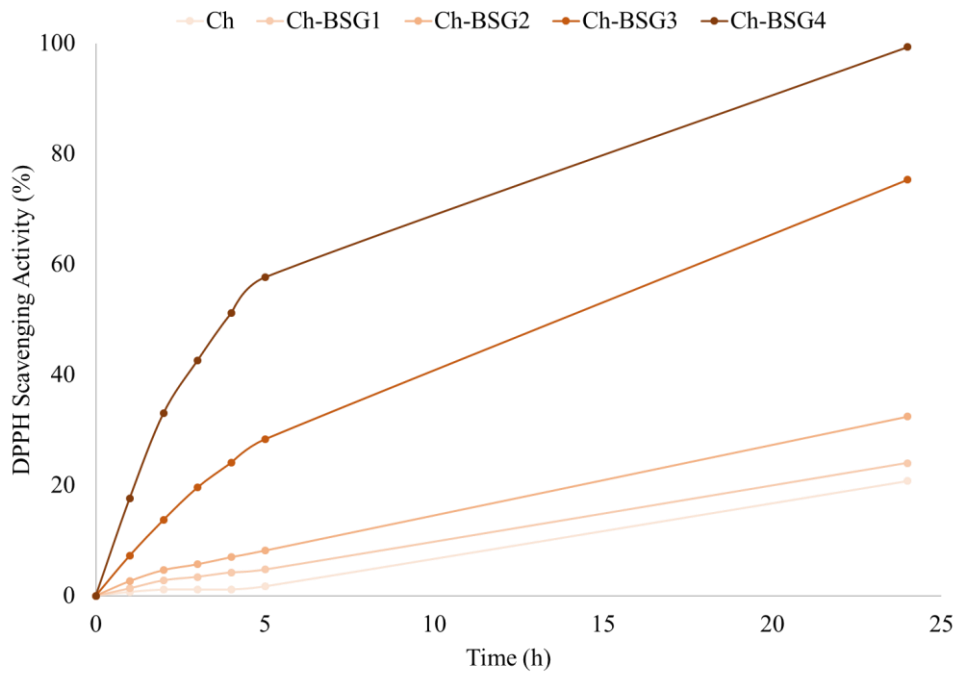

Figure 4 *DPPH scavenging activity of films (%) as a function of time (h)*

CONCLUSION

The present study demonstrated the successful incorporation of BSG into chitosan-based bioplastic films with improved functional properties. Increasing BSG loading enhanced the antioxidant activity of the films, while also affecting their barrier behavior through increased water vapor permeability. The highest BSG concentration resulted in nearly complete DPPH radical scavenging, confirming the contribution of phenolic compounds naturally present in BSG. These findings highlight the potential of brewery spent grain as a sustainable raw material for the development of active bioplastic packaging, contributing to waste valorization and circular bioeconomy approaches.

REFERENCES

[1] De Luca, S., Mueller, K., Tomei, L., *et al*. Adv. Polym. Technol. 2025, 2025, 5060184.

[2] Mujtaba, M., Fraceto, L.F., Fazeli, M., *et al*. J. Clean. Prod. 2023, 402, 136815.

[3] Pontillo, A.R.N., Chen, S., Ordóñez, D.F., *et al*. RSC Sustain. 2025, 3, 2301.

[4] Baiano, A., Fiore, A. Circular Economy 2025, 4, 100158.

[5] Kalak, T. Sustainability 2025, 17(20), 9288.

[6] Henkin, J.M., Mainali, K., Sharma, B.K., *et al*. Biomass 2025, 5(3), 42.

[7] Aradwad, P., Raut, S., Abdelfattah, A., *et al*. Compr. Rev. Food Sci. Food Saf. 2025, 24(1), e70150.

[8] Zeko-Pivač, A., Tišma, M., Žnidaršič-Plazl, P., *et al*. Front. Bioeng. Biotechnol. 2022, 10, 870744.

[9] Moreirinha, C., Vilela, C., Silva, N.H.C.S., *et al*. Food Hydrocoll. 2020, 108, 105836.

[10] Proaño, J.L., Salgado, P.R., Cian, R.E., *et al*. J. Sci. Food Agric. 2020, 100(15), 5458–5465.

[11] Shroti, G.K., Saini, C.S. Appl. Food Res. 2022, 2(1), 100043.

[12] Arizanova, M., Velickova, E., Dimitrovski, D., *et al*. ACS Mater. AU 2026, 6(1), 202–212.

[13] American Society for Testing and Materials E96. Standard Test Method for Water Vapor Transmission of Materials. West Conshohocken: ASTM International; 2015.

[14] Merino, D., Bellassi, P., Paul, U.C., *et al*. Food Hydrocoll. 2023, 139, 108580.

[15] Lin. L., Mirkin. S., Park. H.E. Processes 2023, 11(8), 2400.

[16] Moreira, M.M., Morais, S., Carvalho, D.O., *et al*. Food Res. Int. 2013, 54(1), 382–388.

[17] Meneses, N.G.T., Martins, S., Teixeira, J.A., *et al*. Sep. Purif. Technol. 2013, 108, 152–158.

EcoTER'26
eco.tfbor.bg.ac.rs
32nd International Conference
Ecological Truth & Environmental Research
24–26 June 2026, Hotel Sunce,
Sokobanja, Serbia

Original Research

SOUTHEASTERN EUROPEAN BLACKBIRD *Turdus merula aterrimus* (MADARÁSZ, 1903) IN THE BALKAN PENINSULA

DOI: 10.5937/EcoTER26368N

Boris Novaković[1,a*], Marko Raković[2,b]

[1] Serbian Environmental Protection Agency, Ministry of Environmental Protection of the Republic of Serbia, Žabljačka 10A, 11160 Belgrade, SERBIA

[2] Department of Biodiversity and Environmental Research, University of Belgrade-Institute for Multidisciplinary Research, Despota Stefana Blvd. 142, 11060 Belgrade, SERBIA

[a] https://orcid.org/0000-0003-4846-6371

[b] https://orcid.org/0000-0002-3658-3362

Abstract

The present study data on ecology and evolution of Eurasian Blackbird subspecies - Southeastern European Blackbird (Turdus merula aterrimus) in the Balkan Peninsula. As would be expected for a widespread passerine bird species in the world, a total of 16 geographical Common Blackbird subspecies are recognized within the Turdus merula species complex denoting a typical example where bird populations show signs of evolutionary differentiation and regional adaptation, but not enough isolation to form completely separate species. Southeastern European Blackbird breeds in Hungary, southeastern Europe to Crete, Rhodes, northern Turkey, Caucasus, Transcaucasia and northern Iran, and its distribution range overlaps with a nominal subspecies (Turdus merula merula), and most probably with another subspecies, T. merula syriacus (Greek islands and Mediterranean coast of southern Turkey). This study stated it is very difficult to distinguish the traits by field observations of nominal Eurasian Blackbird subspecies, Turdus merula merula, and Southeastern European Blackbird subspecies, Turdus merula aterrimus with confidence as well as in the Balkan Peninsula Eurasian Blackbird showed clinal variability and extensive intergradation rather than "clear" subspecies' distinction. Also for the studied Blackbird subspecies, the data on intraspecific variability, autecology and evolution are provided.

Keywords: Southeastern European Blackbird, subspecies, distribution, clinal variability, Balkan Peninsula.

INTRODUCTION

The Common Blackbird *Turdus merula* Linnaeus, 1758, is a species of true thrush (family Turdidae; order Passeriformes). It is also called Eurasian Blackbird (especially in North America, to distinguish it from the unrelated New World blackbirds), or simply Blackbird, where this does not lead to confusion with a similar-looking local species. It breeds in Europe, Asia, and North Africa, and has been introduced to Australia and New Zealand. Depending on latitude, the Common Blackbird may be resident, partially migratory or fully migratory. As

* *boris.novakovic@sepa.gov.rs*

would be expected for a widespread passerine bird species, 16 geographical subspecies are recognized within *Turdus merula* species complex [1]. The Blackbird species complex illustrates a typical example where bird populations show signs of evolutionary differentiation and regional adaptation, but not enough isolation to form completely separate species. In Europe and adjacent areas, a five Blackbird subspecies are distributed: *T. m. merula*, the nominal subspecies widely distributed throughout most of Europe; *T. m. aterrimus* (southeastern Europe to Crete, Rhodes, northern Turkey, Caucasus, Transcaucasia); *T. m. syriacus* (Mediterranean coast of southern Turkey); *T. m. azorensis* (endemic to the Azores archipelago) and *T. m. cabrerae* (Madeira archipelago, western and central Canary Islands). Also, three of previously known Asian Blackbird subspecies, are now identified as full species, such as Chinese Blackbird (*Turdus mandarinus*), Indian Blackbird (*Turdus simillimus*) and Tibetian Blackbird (*Turdus maximus)* [2].

Southeastern European Blackbird, *Turdus merula aterrimus* (Madarász, 1903) differs from the nominal subspecies *(Turdus merula merula)* in several morphological traits. It is generally smaller in body size and shows more subdued plumage coloration. Adult males of *T. m. aterrimus* typically have duller black plumage with reduced gloss compared to the deep, glossy black of *T. m. merula* males. Females are usually paler and browner, often with less pronounced dark mottling on the underparts. It breeds in Hungary, southeastern Europe to Crete, Rhodes, northern Turkey, Caucasus, Transcaucasia and northern Iran, and its distribution range overlaps with a nominal subspecies, and most probably with one more Blackbird subspecies, *T. m. syriacus*, distributed on the Mediterranean coast of southern Turkey south to Jordan, Israel and the northern Sinai [2].

The present study pointed out that the occurrence of three subspecies of Blackbird distributed in the same areas – range overlapping *(merula, aterrimus, syriacus)* revealed the possibility of the subspecies' hybridization and clinal variation, with some features gradient variation in the subspecies' traits, but on the other hand, the possibility of the species ecological vicariance due to habitat discontinuity (i.e. habitat fragmentation and deterioration).

MATERIALS AND METHODS

Based on literature data as well as newly data obtained in the field (2022–2025 period), Blackbirds were observed throughout Serbia. The birds have been visually (by using 10 and 12x binoculars magnification) and acoustically identified. Also, the bird censuses were carried out with main goal to record infrequent and discontinuous species singing in terms of subspecies' song variability evaluation and the Blackbird subspecies' distinction.

RESULTS AND DISCUSSION

Based on literature data [2], two Blackbird subspecies are distributed in Serbia, nominal *(Turdus merula merula)*, and the studied subspecies, Southeastern European Blackbird *(Turdus merula aterrimus).*

The data obtained from field surveys in Serbia (2022–2025 period) revealed both subspecies are very hard to distinct in the field based on visual observations as well as acoustical identification.

Our predictions are that Southeastern Blackbird *(T. merula aterrimus)* is widely distributed than it expected. Bearing in mind Serbia is also part of an important transition and intergradation area between western-central European *T. m. merula* populations and Southeastern Balkan *aterrimus* populations, it is more likely many blackbirds in northern and northwestern Serbia (particularly in the Pannonian Plain, Vojvodina) may show more *merula*-like characteristics or intermediate traits. These regions are biogeographically connected to the Carpathian Basin and Central Europe, where *merula* is predominantly distributed Blackbird subspecies.

Also, it is most probably typical *aterrimus* taxonomic characters tend to become stronger toward mountainous, southern, and southeastern regions of Serbia, while northern lowland (Pannonian Plain, Vojvodina) populations are most probably intermediate (this is possible "scenario"). Our predictions are the clinal variation in the Common Blackbird is expected due to its vast range involving differences in plumage, size and other features correlated with environmental gradients, such as, at the first place, humidity and understory coverage at site. Also, we suppose that the species' clinal variation is linked with latitudinal/altitudinal, predominantly forest and shrubland habitat typology, with regard to different terrestrial ecoregions distributed in the Balkan Peninsula.

In fact, the most Serbian blackbirds are most likely to be regarded as belonging to a clinal *merula–aterrimus* population continuum rather than representing completely "pure" subspecies, i.e. the subspecies transition showed continuous morphological and genetic shifts rather than "clear" subspecies separation based on diagnostic subspecies characters from the literature sources [1]. Due to the gene flow between populations is extensive, there is no sharp boundary between the two subspecies. Thus, Serbia represents part of a broad clinal transition zone where many individuals combine characteristics of both *merula* and *aterrimus*, including urban areas where "urban race" of Blackbird is determined, and it is characterized by shorter telomeres compared with birds occurred in natural habitats [3]. This makes telomere length a promising candidate for examining the effects of urbanization on the health status of individuals.

Why does the European Blackbird's dark coloration match the ground color of the less widespread of its breeding habitats, the riparian forest, although its main European population occurs in the pale-litter woodland? It is argued that crypsis of all the age stages was more necessary in riparian stands, as this habitat is more risky for the species owing to a high ground vegetation surrounding a foraging bird. Poorer crypsis of Blackbird plumage in pale-litter habitats may be a neutral feature, being compensated by easier scanning of the surroundings over the lower and sparser herb vegetation and by a tendency to remain in dark sites. The black plumage of the Blackbird male, perhaps reinforced by sexual selection in pristine forest conditions may also retain its cryptic function [4].

On the other hand, the Common Blackbird colouration could be explained partly in line with Gloger's rule because its dark feathers contain high amounts of melanin. In warmer and more humid environments, darker plumage may provide advantages such as stronger feather

durability, better resistance to feather-degrading bacteria, and improved crypsis in shaded forests and dense vegetation.

Also, environmental exposure to sulfur can affect intracellular thiol levels in organisms [5]. Pheomelanin synthesis in melanocytes is promoted by high thiol levels [6]. Accordingly, the results of study [7] showed that birds with phenotypes profusely pigmented by pheomelanin breeding in Iceland develop their plumage in sites with soils with higher sulfur contents than sites of birds with phenotypes produced by lower amounts of pheomelanin. This is observed considering both intraspecific and interspecific covariation between pheomelanin content of feathers and soil sulfur content, at least across the 13 species of birds included in this study suggesting that exposure to high sulfur soil levels in Iceland has favored the expression of pheomelanin-based plumage phenotypes, likely through an increase in thiol levels during development, which is supported by the results of this study [7], indicating that the plumage pigmentation phenotype of Icelandic birds is a phylogenetically conserved trait strongly favored by natural selection. The soil characteristics represent an additional environmental factor affecting the expression of melanin-based pigmentation in birds, likely by influencing exposure to sulfur and intracellular thiol levels, meaning that soil arises as a novel source of vertebrate phenotypic diversity [7]. Regarding the species from the present study, Common Blackbird is a ground-foraging and semi-arboreal songbird exposed to sulfur from soil.

The Common Blackbird is one of the principal avian hosts of Usutu virus (USUV) in Europe [10]. In the Balkans, the impact probably varies geographically depending on mosquito abundance, climate, habitat fragmentation, and urbanization. Potentially, southeastern and southern Blackbird populations (*aterrimus* and *syriacus* subspecies) have stronger viral exposure in warmer regions where mosquito vectors remain active longer. Urban populations could also be vulnerable due to high bird density and artificial water sources favor mosquito transmission. However, blackbirds reproduce efficiently and populations often recover after outbreaks through immigration and successful breeding. Consequently, Usutu virus probably could act as an additional ecological pressure affect the different subspecies' (*merula* and *aterrimus*) population density in the Balkan Peninsula.

Based on data related to molecular methods and DNA barcoding and the data obtained by using universal standard marker – region of mitochondrial COI (Cytochrome c oxidase subunit I) gene, there are no available DNA confirmation for the subspecies of Blackbird in genetic databases – BOLD [8] and NCBI [9], but only for a species level (*Turdus merula*).

In the Balkan Peninsula, the majority of blackbirds are probably best to be considered not as "pure" *merula* or *aterrimus*, but as part of a continuous clinal population with predominantly *aterrimus* characters toward the southeast and more *merula*-like tendency toward the north and northwest (this is possible "scenario"). Possibly, in the southeastern Balkans and especially in the East Thrace (European part of Turkey), the ranges of *aterrimus* and *syriacus* are overlapped.

CONCLUSION

As conclusion, it is very difficult to distinguish the characters of nominal Blackbird subspecies, *Turdus merula merula*, and Southeastern European Blackbird subspecies, *Turdus*

merula aterrimus with confidence, especially in the Balkans where the Eurasian Blackbird showed broad clinal variability and extensive intergradation, which is corroborated by the data provided in present study. The differences between these two subspecies are subtle rather than sharply diagnostic, involving slight variability in body size, plumage tone and glossiness.

Also, it is very difficult and often impossible to distinguish the nominate European blackbird (*Turdus merula merula*) from the Southeastern European subspecies (*T. m. aterrimus*) in the field based on visual observations. Distinguishing each subspecies required a bird in the hand and precise biometrics, and it is more likely that many local clines have "intermediate" characteristics. Due to both subspecies interbreed randomly in secondary contact zones, many birds display "intermediate" combinations of characters that do not fit precisely into either subspecies description. For example, a bird may show a *merula*-like body size, but *aterrimus*-like plumage tone, or *vice versa*.

Besides, based on bird vocalization and song patterns, it is very hard to differentiate *Turdus merula merula* from *Turdus merula aterrimus*. Consequently, subspecies (*merula* and *aterrimus*) could not be acoustically identified in the field during our surveys.

Apparently, it is more likely that the difference of two Blackbird subspecies, between nominal (*merula*) and Southeastern (*aterrimus)* to be gradual and somewhat artificial rather than discrete. In practice, assigning individual blackbirds to one subspecies or the other in southeastern Europe is often tentative unless the bird originates from a population near the "core" of one subspecies' range. However, because the region is a broad zone of intergradation, "pure" or typical *aterrimus* individuals are not easy to separate from *merula*-like birds.

Within the Common Blackbird complex, the relationship among nominal *Turdus merula merula*, *T. m. aterrimus* and *T. m. syriacus* could be interpreted as an example of weak or incomplete incipient speciation. These subspecies likely diverged during periods of geographic isolation in different Pleistocene refugia, where local adaptation and genetic drift produced gradual differences in plumage, body size, migration and species autecology in general. However, when populations re-expanded after glaciations, they came back into secondary contact and continued interbreeding extensively across the Balkans and eastern Mediterranean regions.

The genetic differences that do exist likely originated during Pleistocene isolation in separate glacial refugia. During these periods, populations in western Europe, the Balkans, and the eastern Mediterranean became partially isolated and accumulated small differences in mitochondrial DNA, allele frequencies, and locally adaptive genes through drift and natural selection. After postglacial expansion, secondary contact allowed extensive hybridization, which "blurred" many of these distinctions.

The results of our study revealed recent Blackbird populations in the Balkans usually form gradual genetic clines rather than sharply separated lineages.

Among the three Blackbird subspecies (*merula*, *aterrimus* and *syriacus*), *merula* and *aterrimus* are probably genetically very close because of continuous contact across Central Europe and the Balkans. *Syriacus* may show somewhat higher differentiation due its "core" distribution lies farther southeast in Anatolia and the Near East, where partial geographic and

ecological separation persisted longer. Even so, the species divergence is still shallow compared with true species-level splits. For all the three Blackbird subspecies (*merula, aterrimus, syriacus)* feature variability "scenario", a several interacting processes are expected: allopatric divergence in glacial refugia, secondary contact and hybridization, ecological vicariance and clinal adaptation along environmental gradients. Despite this variability, reproductive isolation between most populations remains weak or absent. Thus, all subspecies are still classified within a single species connected by varying degrees of gene flow.

In this sense, Common Blackbird represents a continuum between geographic variation and incipient speciation rather than fully discrete evolutionary population model. Some peripheral or isolated populations may eventually diverge further, but recently the species complex remains unified by extensive interbreeding across wide area of its range.

verall, the Balkan Peninsula act as a major biogeographic crossroad where Central European, Pontic, Mediterranean, and Middle East faunal influences intersect. This fact explains why Blackbird populations in the Balkans show broad clinal variability and complex intergradation rather than sharply separated subspecies boundaries.

REFERENCES

[1] Clement, P., Hathway, R. Thrushes. Helm identification guides. London: Christopher Helm; 2000. p. 46.

[2] Collar, N., Christie, D.A. Eurasian Blackbird (*Turdus merula*), version 1.0. In: del Hoyo, J., Elliott, A. Sargatal, J., Christie, D.A., de Juana, E. editors. Birds of the World. Cornell Lab of Ornithology; 2021. Ithaca, NY, USA.

[3] Ibáñez-Álamo, J.D., Pineda-Pampliega, J., Thomson, R.L. *et al.* Biol. Lett. 2018, 14(3), 20180083.

[4] Tomiałojć, L., Bursell, J. Int. J. Biodivers. 2007, 7, 127–132.

[5] Kuklińska, K., Wolska, L., Namieśnik, J., Cieszynska, M. Trends Anal. Chem. 2013, 48, 14–21.

[6] Ito, S., Wakamatsu, K. Photochem. Photobiol. 2008, 84(3), 582–592.

[7] Rodríguez-Martínez, S., Arnalds, Ó., Guðmundsson, J., *et al.* J. Ornithol. 2023, 164(3), 639–649.

[8] Ratnasingham, S., Hebert, P.D.N. Mol. Ecol. Notes. 2007, 7 (3), 355–364.

[9] National Center for Biotechnology Information (NCBI). Gene [Internet]. Bethesda (MD): National Library of Medicine (US); [2026] – [cited 2026 May 15]. Available from: https://www.ncbi.nlm.nih.gov/gene/

[10] Musto, C., Tamba, M., Calzolari, M., *et al.* Eur J Wildl Res. 2022, 68(2), 23.

EcoTER'26
eco.tfbor.bg.ac.rs
32nd International Conference
Ecological Truth & Environmental Research
24–26 June 2026, Hotel Sunce,
Sokobanja, Serbia

Original Research

PROPERTIES OF PLANT AND SOIL SHAPING FRUIT AND OIL TRAITS IN DIFFERENT CULTIVARS OF *Olea europaea* L.

DOI: 10.5937/EcoTER26374N

Pasquale Napoletano[1,a*†], Ermenegilda Vitale[2,b†], Anna De Marco[3,c¥], Carmen Arena[2,d¥]

[1] Department of Agriculture, Food, Environment and Forestry (DAGRI), University of Florence, 50144 Florence, ITALY

[2] Department of Biology, University of Naples Federico II, 80126 Naples, ITALY

[3] Department of Pharmacy, University of Naples Federico II, 80131 Naples, ITALY

[a] https://orcid.org/0000-0003-4647-516X

[b] https://orcid.org/0000-0002-2379-9754

[c] https://orcid.org/0000-0002-3774-5538

[d] https://orcid.org/0000-0002-9718-2941

Abstract

Geographical and climatic conditions influence plant–soil interactions, shaping fruit characteristics and olive oil quality, particularly within the Mediterranean basin. In Italy, Olea europaea cultivars exhibit different responses to local pedoclimatic conditions resulting in extra virgin olive oils (EVOO) with diverse properties. This study investigated five Italian cultivars grown in two contrasting regions: Pisciottana (PIS), Ravece (RAV), and Ortice (ORT) in Campania, and Frantoio (FRA) and Moraiolo (MOR) in Umbria. Soil properties analyzed included pH, cation exchange capacity (CEC), soil organic matter (SOM), nitrogen (N), C/N ratio, microbial carbon (Cmic), and endogenous mineralization coefficient (CEM). Plant traits assessed were specific leaf area (SLA) and maximum photochemical efficiency (Fv/Fm), while fruit and oil characteristics included dry matter (DM), free acidity, total polyphenol content (TPC), and peroxide value. Soils in Umbria were predominantly alkaline, with lower CEC and SOM, that promoted conservative plant strategies with reduced SLA. Campania soils showed higher nutrient availability, favoring more acquisitive strategies with increased SLA and vegetative growth. High N in PIS and RAV promoted vegetative growth over fruit biomass leading to TPC reduction. ORT cultivar showed high microbial activity but lower SLA and F_v/F_m*. Our results highlight how soil properties regulate plant performance and oil quality through fine soil–plant feedback mechanisms.*

Keywords: soil quality, soil nutrients, leaf traits, fruit and oil production, geographical and climatic conditions.

INTRODUCTION

The Mediterranean basin is the main olive-growing area in the world, with over 97%, and Italy ranks second among the olive-oil producers [1]. Here, *Olea europaea* L. is very rich in

* *pasqunapoletano@gmail.com*

† These authors contributed equally

¥ These authors contributed equally

variety due to both the environmental and geographic variability that substantially characterizes the entire Italian territory. Bartolini *et al.* [2] reported that the Italian olive germplasm includes 600 cultivars, corresponding to the half of the world total which is around 1200. The growth environment plays a key role in the development and characterization of the different varieties of *O. europaea*. Soil may affect the plant individual response, influencing with its physical-chemical and biological properties (including pH, organic matter quality, nutrients, water availability, and pedoclimatic characteristics) photosynthesis and thus primary productivity. The specific geographic and ecological peculiarities determine different fruit and oil characteristics generating ecotypes with distinct eco-physiological traits. Consequently, extra virgin olive oil (EVOO), a key component of the Mediterranean diet, shows variability in its composition depending on factors such as cultivar, climate, soil conditions, harvesting methods, and processing techniques. These variables shape oil chemical profile, particularly its fatty acid composition, phenolic compounds, and antioxidant content, thereby influencing taste, stability, and nutritional properties. Each cultivar is generally associated with specific soil physical, chemical, and biological properties, and presents distinct leaf functional traits that reflect its ability to utilize the available resources within the environment. Different cultivars may experience varying levels of stress in the proper habitats, showing different degrees of tolerance or sensitivity to environmental conditions and management practices during fruit development and ripening.

Environmental conditions significantly influence both yield and oil quality: however, the interactions between soil factors and productivity in olive trees are still not fully understood. This study aims to explore how soil properties drive plant response through leaf functional traits, and how these interactions shape fruit characteristics and ultimately oil quality. The analysis focuses on five Italian *Olea europaea* L. cultivars (Pisciottana, Ravece, Ortice, Frantoio, Moraiolo) cultivated across two contrasting regions of Italy.

MATERIALS AND METHODS

Study area

The experiment was carried out in five olive orchards composed each by a specific cultivar of *O. europaea* located in the Italian regions of Campania and Umbria. Campania region is in southern Italy where the summers are dry and winters are rainy. Three orchards were chosen: Pisciotta (P, Salerno Province, 40°7’0’’N, 15°14’0’’E) with cv. Pisciottana (PIS), Luogosano (Avellino Province, 40°59’18’’N, 14°59’30’’E) with cv. Ravece (RAV), Molinara (Benevento Province, 41°18’00’’N, 14°55’00’’E) with cv. Ortice (ORT). Umbria region is in central Italy, where climate is more continental. The Umbrian orchards were two, both located in Perugia (Perugia Province, 43°08’28’’N, 12°27’46’’E), one covered by cv. Frantoio (FRA), the other by cv. Moraiolo (MO), respectively. The cultivars were selected based on their specific production areas, while the study sites were chosen for their uniform conditions including weeds control practices, absence of pesticide use, long-term cultivation of the same cultivar, similar management regimes, and rainfed systems.

All the soils were classified as Cambisols for their early horizon differentiation in the subsoil, with medium and fine textured material derived from parent material [3].

The samplings of leaves and soils were conducted for two consecutive years, before the olive harvest simultaneously. Soil was collected in three subareas of each orchard, under at least five olive trees, at 0–40 cm of depth. For the assessment of leaf traits and chemical analyses, only healthy leaves were sampled around the canopy of trees, with no visible vegetative abnormalities or signs of viral infection. From each subarea, a standardized sampling procedure was carried out appropriately selecting ten fully expanded leaves around the entire canopy of the trees, at least 1.5 m from the soil. In addition, olives were harvested in the same subareas in different ways: hand picking, combing, gleaning, beating, and mechanical harvesting. Subsequently, oil was extracted in laboratory using an Abencor mill.

Soil analyses

Prior to measurements, the collected soil was sieved at <2 mm and two aliquots were obtained: one for chemical analysis, airdried at room temperature, while the other for biological features, stored immediately at 4°C and processed within one week since sampling. The following properties were measured: pH, cation exchange capacity (CEC), soil organic matter (SOM), total nitrogen (N), Carbon-to-Nitrogen ratio (C/N), microbial carbon (Cmic) and endogenous mineralization coefficient (CEM). Shortly, soil pH was measured potentiometrically, CEC via cation extraction with $BaCl_2$ at pH 8.2 and titration with EDTA [4]. Organic carbon (C) and N were obtained by CNS analyser (Thermo Finnigan, EA 112 series), in samples previously treated with HCl (10%) to remove carbonates, and C/N was calculated. SOM was derived multiplying C by 1.724 [5]. Cmic and CEM were measured according to Memoli *et al.* [6]. Briefly, Cmic was evaluated through the substrate-induced respiration method SIR after the addition of glucose (75 mM) as an easily mineralizable substrate. After the incubation of five days in the dark at 25°C, the CO_2 evolved was titrated with HCl 0.05 N and converted into C incorporated in the microbial biomass. CEM was obtained as ratio between the soil respiration monitored over ten days (determined similarly to Cmic but with the addition of distilled water, and monitored for ten days) and C.

Plant, olive and oil measurements

Specific leaf area (SLA) and maximal photochemical efficiency of PSII (F_v/F_m) were determined as eco-physiological markers. SLA was calculated as the ratio between leaf area and leaf dry mass. F_v/F_m was measured with a fluorometer FluorPen FP100 (Photon System Instrument spol. s.r.o., Drásov, Czech Republic) and calculated as: $(F_m-F_0)/F_m$, where F_0 represents the background fluorescence signal and F_m is the maximal fluorescence in the dark-adapted state (F_m). F_0 was induced by a weak measuring light of 0.5 µmol photons m^{-2} s^{-1} on 30 min dark-adapted leaves, while F_m was obtained by applying a 1 s saturating light pulse (3,000 µmol photons m^{-2} s^{-1}). For olives, dry matter (DM) and total polyphenol content (TPC) were assessed. Briefly, DM was obtained after olive drying at 75°C for 48 h in the oven whereas TPC was quantified with Folin-Ciocalteau and sodium carbonate, and the absorbance was measured after 90 min in the dark at 725 nm [7]. For oil, free acidity (FA), peroxide value (PV) and TPC were evaluated. FA was determined by mixing oil with ether and ethanol (1:1=v:v) and titration with KOH 0.1 M [8]. For PV, oil was mixed with acetic acid and chloroform (3:1=v:v), and potassium iodide, then titrated with sodium thiosulfate (Reg. CE 1989/03). Oil TPC was evaluated similarly to olive, but differed for absorbance measurement, occurring at 760 nm [9].

Statistical analysis

The statistical analysis was performed using OriginPro 2025 (OriginLab Corporation, Northampton, MA, USA) for soil, plant, olive and oil of the studied cultivars. The normality of the data distribution was assessed by the Shapiro-Wilk test and equal variance test was performed. Comparisons were tested by One-Way ANOVA followed by the Tukey test ($p < 0.05$). Spearman Rank Order Correlation was tested to evaluate the relationships between soil properties and plant traits ($p < 0.05$).

RESULTS AND DISCUSSION

The results for soil chemical and biological properties under different cultivars (PIS, RAV, ORT, FRA, MOR) of *O. europaea* are reported in the Table 1 and Figure 1, respectively.

Soils of the Umbria region, under FRA and MOR, were more alkaline than those from Campania (PIS, RAV, ORT), with pH values ranging from 8.4 to 8.5. FRA and MOR also showed lower CEC compared to others, as possibly related to the parent material, basically made of limestone, rich in carbonates. The high values of pH with low CEC could be related also to the scarce presence of clay particles and low SOM [10]. Indeed, in the Umbrian soils, SOM as well as N is less abundant compared to the other cultivars but, interestingly, MOR showed the highest C/N. The diverse ability of microorganisms in exploiting organic resources could be a possible reason [11]. Notably, CEM is the highest while Cmic is the lowest (Figure 1). In this context, the mineralization occurs rapidly due to low soil nutrients, potentially leaving a complex residue likely linked to a specific composition of the microbial community [12]. This explanation is also supported by the negative correlations between CEM and SOM and N (correlation coefficient: -0.620, $p < 0.001$ and -0.481, $p = 0.001$).

FRA also followed this trend as the similarity between the Umbrian soils is strictly related to similar lithology, edaphic properties and plant ecotypes. Conversely, among Campania cultivar, PIS and RAV were more similar to each other compared to ORT. In detail, this latter differed for SOM, N and CEM (Table 1). However, also ORT soils showed good CEC but a more intense activity of microorganisms, despite their quantity, indicating a better nutritional condition for olive plants and a faster organic matter turnover (Table 1, Figure 1).

Table 1 *Chemical properties of soils under different cultivars of O. europaea (Pisciottana-PIS, Ravece-RAV, Ortice-ORT, Frantoio-FRA, Moraiolo-MOR) displayed as mean ± standard error: pH, Cationic Exchange Capacity (CEC, $cmol_{+}kg^{-1}$), Soil Organic Matter (SOM, % dw), Nitrogen (N, % dw), Carbon-to-Nitrogen ratio (C/N). Different letters indicate statistically significant differences (One Way-ANOVA at p < 0.05)*

	pH	CEC	SOM	N	C/N
PIS	8.0 ± 0.1 B	13.9 ± 1.3 AB	7.00 ± 0.39 A	0.30 ± 0.01 A	10.50 ± 1.30 B
RAV	7.9 ± 0.1 B	19.1 ± 0.7 A	6.10 ± 0.30 A	0.32 ± 0.02 A	9.99 ± 0.78 AB
ORT	8.0 ± 0.1 B	13.3 ± 1.9 AB	3.31 ± 0.13 B	0.22 ± 0.02 B	14.92 ± 1.72 AB
FRA	8.4 ± 0.0 A	9.4 ± 1.4 B	3.48 ± 0.42 B	0.14 ± 0.02 B	18.20 ± 4.35 AB
MOR	8.5 ± 0.1 A	9.3 ± 0.8 B	3.91 ± 0.34 B	0.16 ± 0.01 B	27.29 ± 6.53 A

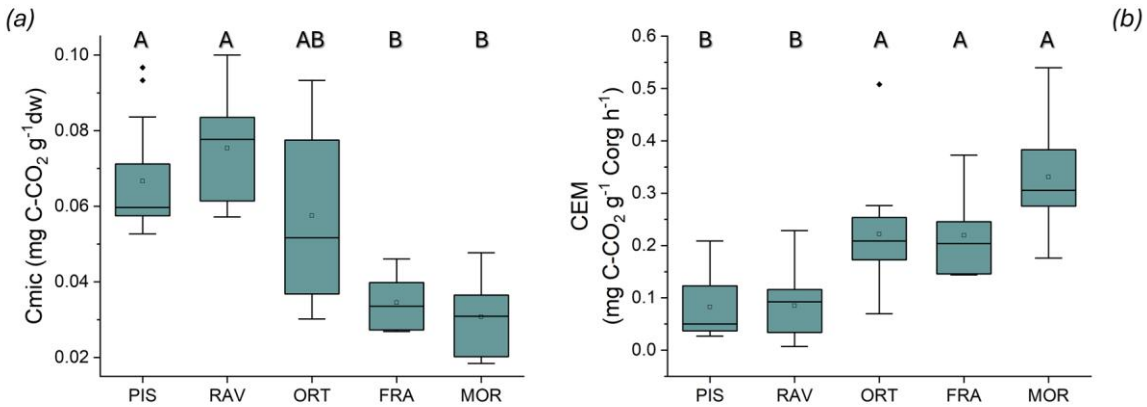

Figure 1 *Biological properties of soils under different cultivars of O. europaea (Pisciottana-PIS, Ravece-RAV, Ortice-ORT, Frantoio-FRA, Moraiolo-MOR) displayed as box plots representing the interquartile range (IQR) from the 25th to the 75th percentile. The horizontal line and the open square within each box represent the median and the mean, respectively. The whiskers extend to the maximum and minimum values within 1.5 times the IQR for: Microbial Carbon (Cmic, a) and Endogenous Mineralization Coefficient (CEM, b). Different letters indicate statistically significant differences (One Way-ANOVA at $p < 0.05$)*

However, among all the soil properties, only CEC is positively correlated with SLA (correlation coefficient: -0.329, p = 0.03), suggesting a balance between leaf resource acquisition and soil organic matter dynamics. As shown in Figure 2, SLA was highest in PIS and RAV and progressively decreased in FRA, MOR and ORT, where it reached the lowest value. This trend suggests that as the mineralization coefficient decreases, in absence of nutrient limitations, leaves tends to adopt a consume strategy. Conversely, in sites with higher mineralization rates but lower CEC and SOM, the soil capacity to retain nutrients may be limited. Under these conditions, plants tend to adopt a more conservative strategy, reflected in lower SLA.

Moreover, although none of the cultivars showed clear physiological stress signals, the F_v/F_m ratio significantly decreased in RAV and ORT compared to PIS and FRA cultivars. Lower values of SLA and F_v/F_m in the ORT cultivar support the relation between specific leaf area and the photosynthetic activity, reflecting the plant's capacity to acquire resources, affecting consequently its growth rate and potential biomass production [13,14].

As soils under PIS and RAV cultivars did not present limitation in the nutritional status, vegetative growth appears to predominate and an increase in fruit dry matter might be expected. However, the high soil N content may have driven the plants to invest more resources in vegetative growth than in fruit biomass accumulation, also reducing polyphenol content in both fruit and oil, which are characterized by more acidity. In fact, fruits of the RAV cultivar showed the lowest dry matter and polyphenol content. In concomitance, both PIS and RAV produced oils with the highest concentration of oleic acid and the lowest polyphenol content (Table 2).

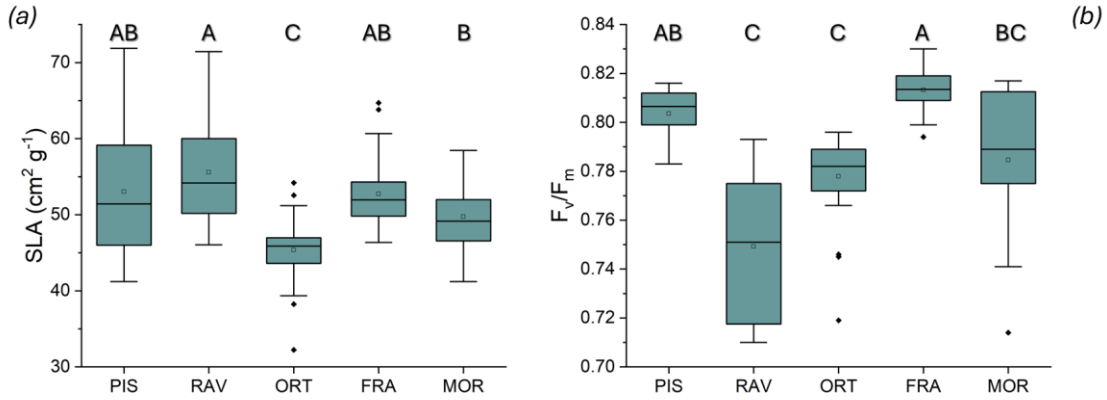

Figure 2 *Plant characteristics of different cultivars of O. europaea (Pisciottana-PIS, Ravece-RAV, Ortice-ORT, Frantoio-FRA, Moraiolo-MOR) displayed as box plots representing the interquartile range (IQR) from the 25th to the 75th percentile. The horizontal line and the open square within each box represent the median and the mean, respectively. The whiskers extend to the maximum and minimum values within 1.5 times the IQR for: Specific Leaf Area (SLA, a) and Maximum PSII Photochemical Efficiency (F_v/F_m, b). Different letters indicate statistically significant differences (One Way-ANOVA at $p < 0.05$)*

Table 2 *Chemical properties of fruits and soils of different cultivars of O. europaea (Pisciottana-PIS, Ravece-RAV, Ortice-ORT, Frantoio-FRA, Moraiolo-MOR) displayed as mean ± standard error: fruit Dry Matter (DM,% dw), Total Poliphenol Content (TPC, mg GAE 100 g^{-1} FW), oil Free Acidity (FA, % oleic acid), Peroxide Value (PV, meq O_2 kg^{-1} oil) and Total Poliphenols. Different letters indicate statistically significant differences (One Way-ANOVA at $p < 0.05$)*

	Fruit		Oil		
	DM	TPC	FA	PV	TPC
PIS	32.52 ± 0.07 AB	217.87 ± 6.94 A	0.66 ± 0.02 A	8.68 ± 0.09 B	154.96 ± 1.24 D
RAV	25.89 ± 5.14 B	151.13 ± 2.35 C	0.62 ± 0.03 A	7.50 ± 0.38 C	136.03 ± 1.20 E
ORT	37.75 ± 0.44 A	166.96 ± 3.11 B	0.42 ± 0.04 B	10.49 ± 0.35 A	176.65 ± 1.92 B
FRA	31.46 ± 0.84 B	165.25 ± 1.47 B	0.37 ± 0.02 B	9.20 ± 0.49 B	198.27 ± 1.42 A
MOR	34.68 ± 1.07 AB	218.33 ± 3.14 A	0.39 ± 0.02 B	7.24 ± 0.20 C	162.35 ± 1.64 C

CONCLUSION

Our results show a link between soil properties, leaf functional traits, and fruit and oil quality. Cation exchange capacity (CEC) was the only soil variable significantly associated with the specific leaf area (SLA), indicating the significant role of soil nutrient retention in affecting plant resource-use strategies.

Higher SLA and maximal photochemical efficiency of PSII (F_v/F_m) values in PIS and RAV likely indicate a growth strategy in response to favourable soil conditions. Conversely, lower values of these physiological indicators in FRA, MOR, and ORT reflect a transition toward more conservative traits. Despite the absence of visible stress, physiological differences among cultivars were evident.

At the productive level, higher soil nitrogen availability appears to promote vegetative growth despite of fruit production, leading to fruits characterized by lower dry matter and polyphenol content, but higher oleic acid and reduced antioxidants in oils. These results

highlight how soil properties influence both plant physiology and product quality, in terms of fruits and oil, through a close soil–plant interaction.

ACKNOWLEDGEMENT

The authors want to thank: Dr. Farinelli of University of Perugia, Dr. Barbarisi of University of Naples Federico II, Dr. Volpe of ISA-CNR, Avellino, National Park of Cilento and Vallo di Diano (SA), Gentilcore (BN) and La Molara (AV) farms.

REFERENCES

[1] Gagour, J., Ibourki, M., El Antari, A., *et al.* Eur. Food Res. Technol. 2024, 250, 1443–1456.

[2] Bartolini G, Prevost G, Messeri C, *et al.* Olive germplasm: cultivars and world-wide collections. Rome, 1999. p. 459.

[3] IUSS Working Group WRB: World Reference Base for Soil Resources 2014, Update 2015, World Soil Resources Report No. 106, FAO: Rome, Italy, 2015.

[4] Colombo C, Miano T, Metodi di analisi chimica del suolo. Ed. Pubblicità & Stampa, Bari, Italy, 2015.

[5] Pribyl, D.W., Geoderma 2010, 156, 75–83.

[6] Memoli, V., De Marco, A., Esposito, F., *et al.* Geoderma 2019, 337, 1–10.

[7] Hajimahmoodi, M., Sadeghi, N., Jannat, B., *et al.* J. Biol. Sci. 2008, 8, 779–783.

[8] European Commission. Commission Regulation (EC) No 1989/2003 of 6 November 2003. Official Journal of the European Union. 2003; L295:57–77.

[9] Del Caro, A., Vacca, V., Poiana, M., *et al.* Food Chem. 2006, 98, 311–316.

[10] Aprile, F., Lorandi, R., J. Agric. Sci. 2012, 4, 278–289.

[11] Rousk, J., Brookes, P.C., Baath, E. Soil Biol. Biochem. 2010, 42, 926–934.

[12] Garcia-Orenes, F., Cerdà, A., Mataiz-Solera, J., *et al.* Soil Till. Res. 2009, 106, 117–123.

[13] Hunt, R., Cornelissen, J.H.C. New Phytol. 1997, 395–417.

[14] Poorter, L., Bongers, F. Ecology 2006, 87, 1733–1743.

EcoTER'26
eco.tfbor.bg.ac.rs
32nd International Conference
Ecological Truth & Environmental Research
24–26 June 2026, Hotel Sunce,
Sokobanja, Serbia

Original Research

GERMINATION OF *Artemisia diffusa* Krasch. ex. Poljakov SEEDS ORIGINATED FROM RANGELAND SITES OF DIFFERENT GRAZING INTENSITIES

DOI: 10.5937/EcoTER26381R

Dragana Ranđelović[1,2,a*], Shuhrat Valiyev[2,b], Muhtor Nasirov[2,c], Jamshid Amirov[2]

[1]Institute for Tehcnology of Nuclear and Other Mineral Raw Materials, Boulevard Franchet d`Esperey 86, 11000 Belgrade, SERBIA

[2]Samarkand State University named after Sharof Rashidov, University Boulevard 15, 140104 Samarkand, UZBEKISTAN

[a] https://orcid.org/0000-0003-4976-7766

[b] https://orcid.org/0000-0003-1023-1622

[c] https://orcid.org/0000-0002-6557-6778

Abstract

Successful germination is key stage for population renewal, particularly important for insight into the regenerative capacity of the key species influenced by rangeland degradation. Germination responses of A. diffusa seeds collected from rangeland sites exposed to low, medium, and high grazing intensities under controlled laboratory conditions was accessed. Seeds originating from highly grazed sites exhibited significantly higher germination percentage, faster germination (lower mean germination time), and increased dry matter content compared to those from low grazing intensity sites, while seeds from medium grazing intensity sites showed intermediate responses. These results indicate improved early establishment capacity under increased grazing pressure. The observed patterns likely reflect maternal environmental effects and adaptive responses to grazing stress conditions. Further studies across a broader range of rangeland localities are needed to elucidate underlying mechanisms. The results may contribute to the improvement of seed sourcing strategies for rangeland restoration and management.

Keywords: rangeland, germination, grazing intensity, Karnabchul.

INTRODUCTION

Successful germination is a key stage in population renewal and is particularly important for understanding the regenerative capacity of key plant species affected by degradation processes. This is particularly important in the rangelands of Central Asia, where ecosystems are increasingly affected by grazing-induced degradation. *Artemisia diffusa* Krasch. ex. Poljakov is perennial chamaephyte shrub up to 50 cm tall. It is endemic species of Central Asia, often found in desert and semi-desert areas, including plain foothills and rangelands. More than 50 associations, which have so far been described in the territory of Uzbekistan, containing around 140 plant species [1]. Species is resistant to drought and serves as a valuable fodder food for livestock, especially during the autumn and winter time. Viable

* *d.randjelovic@itnms.ac.rs*

seeds are produced in November, characterized by B1–B3 dormancy [2]. Many habitats of *A. diffusa* in Uzbekistan are subjected to grazing of various intensity, where species projective cover was recognized as one of the indicators of rangeland degradation [3]. Species physiological traits, particularly photosynthesis and pigment content, but also biochemical traits such as content of carbohydrates and proteins, are adapted to varying grazing pressures, showing increased values under high grazing pressure [3]. On contrary, biochemical traits such as content of carbohydrates and proteins, showed decreased values under high intensity grazing stress [4]. Despite the recognized influence of grazing on plant physiological traits, its effects on seed quality and early establishment remain insufficiently understood.

Changes in environmental conditions, as well as maternal plant responses, are known to influence germination behaviour [5]. Successful germination represents a key stage for population renewal, so assessing germination traits of *A. diffusa* seeds originating from habitats with low, medium and high grazing intensities provides insight into the regenerative capacity of the species under rangeland degradation. Therefore, this study aims to access early germination responses of *A. diffusa* seeds collected from sites with different grazing pressures under laboratory conditions.

MATERIALS AND METHODS

Seeds were collected from the Karnabchul rangeland area in south-western Uzbekistan (39°51'32.2"N, 65°36'10.6"E) on gypseous soil sites with low, medium and high grazing intensities. Analysis of inorganic N and soil organic carbon content were conducted on composite soil samples from investigated sites. Inorganic nitrogen was presented as sum of ammonium nitrogen (determined by spectrophotometer method using Nesler reagent) and nitrate nitrogen (determined by Grandval-Lajoux colorimetric method). The soil organic carbon content was determined according to Kotzman's method.

Seed germination was tested in laboratory conditions by incubating seeds at constant temperature of 25 °C in thermostat chamber. Seeds were sterilized with 70% ethanol for 30 seconds prior to seeding and transferred into Petri dishes containing filter paper soaked in distilled water. Four replicates of 25 seeds were used for each level of degradation. Seeds were considered germinated when the length of radicle was >1 mm. Filter paper was saturated by moisture and kept constant during the experimental period that lasted 7 days. Cumulative number of germinated seeds was recorded daily. Fresh and dry weight of germinated seeds was measured after the experiment.

Germination percentage (GP, %) was calculated as ratio of total number of seeds germinated and number of seeds tested. Germination energy (GE, %) was calculated as number of germinated seeds after 3 days and total number of germinated seeds. Germination index (GI) was calculated as Σ Ni/Ti where Ni is number of germinated seeds during days of experiment, and Ti is number of days from the start. Mean germination time (MGT) is calculated as Σ (Ni x Ti)/Σ N_i where Ni is number of seed germinated on given day (Ti), and Σ Ni is total number of seeds germinated during the experiment. Seedling vigor index II (SVI-II) is calculated as the product of germination percentage and seedling dry weight. Dry matter content (DMC, %) was calculated as ratio between dry weight and fresh weight.

Data were tested for normality using the Shapiro–Wilk test and for homogeneity of variance using Levene's test. Germination percentage (GP), germination index (GI) and dry matter content (DMC) were transformed (by arcsine square-root transformation for GP and logarithmic transformation for GI and DMC) to meet the assumptions of parametric analysis. Additionally, differences among seeds from rangelands of different degradation levels were assessed using one-way analysis of variance (ANOVA), followed by Tukey's HSD test for multiple comparisons. As germination energy (GE) data did not meet assumptions of normality and homogeneity of variance even after transformation; Welch NOVA has been used to analyse the data. All statistical analyses were performed at a significance level of $p < 0.05$ in Statistica StatSoft 8.0 and Minitab 22 statistical software.

RESULTS AND DISCUSSION

Analysis of soil inorganic N (form of nitrogen immediately available to plants) and SOC showed increasing trend from low to high grazed sites (Figure 1), reflecting the difference between sites and available nutrition conditions for plants.

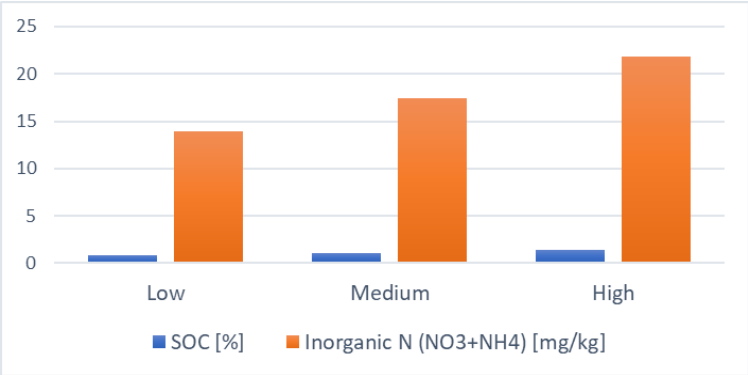

Figure 1 *Content of soil organic carbon (SOC) and inorganic N in Karnabchul soils under different levels of grazing*

Cumulative number of germinated seeds was presented in Figure 2, revealing highest number of germinated seeds from sites under high grazing pressure.

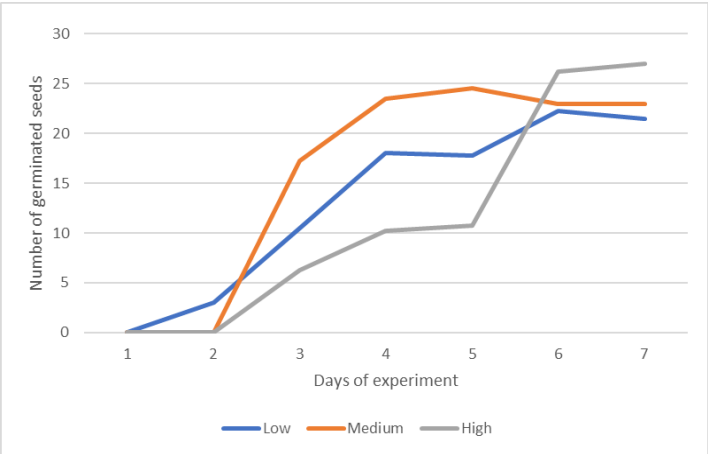

Figure 2 *Cumulative number of germinated A. diffusa seeds by day*

Results of analysis of variances on calculated germination indices and dry matter content are presented in Table 1. They revealed statistically significant differences between germination percentage, mean germination time and dry matter content among seeds originating from rangelands with different levels of degradation.

Table 1 *Analysis of variance (ANOVA) for germination indices of A. diffusa seeds from rangeland sites with low, medium and high grazing pressure, followed by post-hoc Tukey HSD test (statistically significant differences are marked with *)*

Germination indices	Low grazing intensity site	Medium grazing intensity site	High grazing intensity site	F-values	p-values
GP [%]	71.7 ± 3.33 [a]	76.67 ± 15.87[ab]	90 ± 2.72[b]	5.196	0.032*
GE 3 [%]	35.0 ± 39.0	57.5 ± 30.0	20.83 ± 4.19	2.730	0.176
GI	19.83 ± 8.01	23.64 ± 2.42	15.03 ± 1.37	3.889	0.061
MGT	22.43 ± 5.58[ab]	25.02 ± 2.53[a]	17.03 ± 0.82[b]	5.233	0.031*
SVI II	0.007 ± 0.0003	0.014 ± 0.0088	0.018 ± 0.0062	3.029	0.099
DMC [%]	0.536 ± 0.304[a]	1.469 ± 0.635[ab]	5.552 ± 3.224 [b]	12.897	0.002*

Germination percentage showed a significant increase with increasing grazing intensity, and it was in line with average laboratory seed germination ranges for *A. diffusa* of 46–94% reported by Gintzburger (2003). The highest GP was recorded in seeds originating from high grazing sites (90 ± 2.72%), which differed significantly from percentages obtained from seeds originating from low grazing rangelands (71.7 ± 3.33%), while seeds from medium grazed site showed intermediate values and did not differ significantly from either group. Seeds from highly grazed site exhibited the lowest mean germination time (17.03 ± 0.82), indicating faster germination compared to medium grazing sites (25.02 ± 2.53), whereas low grazing site showed intermediate values. Dry matter content was tenfold higher in seeds from high grazing environments (5.552 ± 3.224%) in comparison to seeds from low grazing sites (0.536 ± 0.304%), indicating enhanced resource provisioning. These sites were also characterized by higher levels of inorganic nitrogen and soil organic carbon content, suggesting more nutrients immediately available to plants. Dry matter content in seeds reflects stored reserves, including carbohydrates, proteins, and lipids, being important components for supporting early seedling growth. This is likely a characteristic for adaptive maternal response, where environmental conditions experienced by the mother plant regulate seed provisioning with essential nutrients, hormones, and proteins that further influence seed metabolism and influence germination processes under stress conditions. This is in line with previously reported physiological and biochemical adaptations of *A. difusa* plants on habitats with varying grazing intensities [3].

CONCLUSION

The present study revealed that seeds of *Artemisia diffusa* originating from rangeland sites of different grazing intensities showed differences in germination behaviour. Seeds collected from high grazing intensity sites exhibited significantly higher germination percentage, reduced mean germination time, and increased dry matter content in laboratory conditions, indicating enhanced seed quality and faster establishment potential under more intensively

grazed conditions. Observed differences are likely reflecting environmental maternal response and adaptation to the stress conditions. However, further research across a broader range of rangeland localities prone to grazing intensity gradients are necessary to determine whether the observed patterns are consistent for *A. diffusa* and to gain deeper insight into the ecological and physiological mechanisms responsible for the observed differences in germination behavior. Additionally, such results can be further utilized for rangeland restoration and management, particularly in terms of seed sourcing.

ACKNOWLEDGEMENT

The authors are grateful to the Ministry of Science, Technological Development and Innovation of the Republic of Serbia for financial support according to the contract with registration No. 451-03-33/2026-03/200023.

REFERENCES

[1] Kapustina, L.A. Torrell, M. Valles, J. Artemisia Communities in Arid Zones of Uzbekistan (Central Asia). In: McArthur, E. Durant Fairbanks, D. J., comps. Shrubland Ecosystem Genetics and Biodiversity: Proceedings; 2000 June 13–15; Provo, UT. Proc. RMRS-P-21. Ogden, UT: U.S. Department of Agriculture, Forest Service, Rocky Mountain Research Station. 2000. p. 104–112.

[2] Gintzburger, G. Toderich, K.N. Mardonov, B.K. *et al*. CIRAD; 2003. p. 426.

[3] Valiyev, S. Rajabov, T. Avutkhonov, B. *et al.*, Plant Sci. Today 2023, 10(3), 417–421.

[4] Valiyev, S.A. Urozov, T. Rajabov, T., Afr. J. Biol. Sci. 2024, 6(11), 1108–1116.

[5] Penfield, S., Curr. Biol. 2017, 27(17), R874–R878.

EcoTER'26
eco.tfbor.bg.ac.rs
32nd International Conference
Ecological Truth & Environmental Research
24–26 June 2026, Hotel Sunce,
Sokobanja, Serbia

Original Research

NEW FINDING SPECIES ABLEPHARUS KITAIBELII BIBRON & BORY, 1833 (REPTILIA: SQUAMATA: SCINCIDAE) IN BOSNIA AND HERZEGOVINA

DOI: 10.5937/EcoTER26386S

Mihajlo Stanković[1*], Natasa Beslac[2], Dragan Romčević[3]

[1] Pokret gorana, Svetog Save 19, 22000 Sremska Mitrovica, SERBIA

[2] Nacionalni park Kozara, Vuka Karadžića 43, 79101 Prijedor, BOSNIA AND HERZEGOVINA

[3] JP "Šume Republike Srpske, Šumsko gazdinstvo "Prijedor", Svetosavska bb, 79101 Prijedor, BOSNIA AND HERZEGOVINA

Abstract

On the territory of Bosnia and Herzegovina, 29 species of herpetofauna were recorded, of which 13 species are from the ordo Sauridae, while 15 species of reptiles live on Kozara mountain, of which 12 species and one intraspecies form are in the National Park. Ablepharus kitaibellii was recorded in 2012 at the Benkovac site within the NP Kozara*, with four specimens, in sunny weather, on a stony meadow, overgrown with rare herbaceous and shrubby plants. The size of the specimens ranged from 6 to 12 cm. The species is not endangered on a global level, but it is in Bosnia and Herzegovina, because we only have two pieces of data. The find at the Benkovac location is officially the second or third in the territory of Bosnia and Herzegovina, because we have one reliable piece of information from the vicinity of Ustikolina in the Federation of Bosnia and Herzegovina. At the national level, the species is not on the Red List of Flora and Fauna of either the Federation of Bosnia and Herzegovina or the Republic of Srpska. In order for this species to survive, species and habitat monitoring must be established and all research conducted will provide guidelines for active protection, e.g. "in situ" in their habitat or measures to improve conditions through active protection projects*.

Keywords: Reptiles, *Ablepharus kitaibelii*, NP. Kozara, Bosnia and Herzegovina.

INTRODUCTION

The genus Ablepharus belongs to the family Scincidae and subfamily Eugongylinae, which has 18 species in the world, and one species *Ablepharus kitaibelii* Bibron & Bory, 1833 is present in Europe [1]. According to Jablonski *et al*. [2], the total species diversity of the herpetofauna of Bosnia and Herzegovina is 29 species, of which the ordo *Testudines* has 3 species, and the ordo *Sauridae* and *Serpentes* have 13 species each. Jablonski *et al*. [2] lists the genera from the ordo Sauridae for the B&H area: *Algyroides, Anguis, Dalmatolacerta, Dinarolacerta, Hemidactylus, Lacerta, Podarcis, Pseudopus, Zootoca*, where we note that he does not mention the genus *Ablepharus*. The species *Ablepharus kitaibelii* Bibron & Bory, 1833 (Syn. *Ablepharus pannonicus* Fitzinger, 1824; *A. festae* Peracca, 1894; *Riopa rupellii* Gray, 1839) is the only representative of its genus in Europe, and the northernmost European species of *Scincidae* [3]. The very name of the genus *Ablepharus* originates from the Latin

* *trogloxen@gmail.com*

word ablepharia - the medical name for the lack of eyelids, which is also a characteristic of the genus *Ablepharus* [4]. The species *A. kitaibelii* is a small lizard with a slender cylindrical body up to 12 cm in length. It has a pyramid-shaped head and poorly developed legs. Its body is covered with smooth and shiny small scales, while the skin on the dorsal and ventral sides contains osteoderms. The eyelids are fused and immobile, and the lower eyelid is reduced to a transparent film that is fused with the upper eyelid. They have sexual dimorphism and the female is larger than the male. The dorsal side of the body is brown or bronze in color with usually four narrow double, mostly interrupted darker lines along the sides from the top of the head to the middle of the tail [5]. The ventral side of the body is metallic gray-bluish in color, which usually has orange tones during reproduction in males [6]. This is a polytypic species and we have four described and accepted subspecies in the range: *A. kitaibelii fitzingeri, A. kitaibelii stepaneki, A. kitaibelii fabichii* and *A. kitaibelii kitaibelii* [5]. The species is terrestrial, digs through the ground and belongs to the group of semifossorial organisms. During the day, there is a morning and afternoon peak of activity [7,8], and hibernation lasts from October to April. Its predators are snakes, lizards (genus *Lacerta*), birds and mammals [9,10]. It feeds on insects and larvae, spiders, centipedes and other invertebrates [11]. It is sexually mature in the second year, the species is oviparous, and mates from April to June, eggs are laid during May and June, and young lizards appear from the end of July to September [11]. It inhabits a wide range of dry habitats covered with low vegetation or leaves. It inhabits meadows, grassy slopes and forest edges [12]. It occurs most often on hilly, slightly inclined slopes of southern exposures covered with low vegetation and rare trees and bushes [8]. It inhabits different types of substrate (sedimentary or volcanic rocks) and the species is highly selective in its selection of microhabitats [13]. In the northern part of the area, it is found in steppe habitats, and going south with increasing altitude, the species is recorded along the edges of open oak forests [14]. According to Jablonski *et al*. [2] the species belongs to the East-Mediterranean element. In Europe, it is present in the south of Slovakia and Hungary, in most of Serbia, the southern and eastern parts of Romania, Bulgaria, Macedonia, Albania and Greece with the Aegean Sea, the Ionian Islands, and Turkey [12,15] and in Montenegro there is an isolated population near Berane [4]. According to Ljubisavljević and Džukić [5], the following threatening factors were identified for the species *A. kitaibelli*: habitat fragmentation, conversion to agricultural or forest land, construction of plantations and industrial zones, afforestation of oak habitats with conifer plantations, livestock grazing, urbanization, i.e. the spread of weekend settlements, picnic areas, peripheral parts of the city, and road infrastructure, the spread of non-native invasive species of plants by overgrowing the open habitats they need, chemical soil pollution with municipal or industrial waste and in agriculture with pesticides, etc. All of the above, with their presence and disturbance, has a direct negative impact on local populations, but also on the limited spread of the species and discontinuous distribution, especially in marginal populations in the area, which reduces the possibility of population renewal, and as a result, we may have their complete disappearance. During the 1990s, localities on the territory of Bosnia and Herzegovina were exposed to the effects of war, which certainly left a negative impact on the populations of both this and many other species. We must not forget natural phenomena such as fires, floods, succession of vegetation in the habitat, which affect the condition and survival of local populations. According to the IUCN classification and

Appendix 1- Red List status of Europe Reptilians (2009) its endangered status is the last concern (Lc) [16]. The species is on the list of the Habitats Directive in Annex IV, and on the list of the Berne Convention in Annex II [17,18].

The National Park has an area of 3,907.54 ha, declared in 1967, located on the edge of the Pannonian basin in the central part of the Kozare mountain. It is characterized by dense complexes of deciduous, coniferous and mixed forests, meadows, rocky fields, ponds-swamps, streams and rivers. Kozara is an island mountain formed by the uplift of the land by orogenic movements during the Alpine Orogeny, at the end of the Mesozoic and the beginning of the Tertiary, while the highest peaks rose from the Pannonian Sea in the middle of the Eocene. The geological composition is diverse, from Paleozoic and volcanic rocks to Mesozoic deposits of limestone, marl, dolomite, sandstone, etc. The hydrographic network is of the radial dendroid type, and consists mainly of permanent and periodic watercourses. Kozara has a moderate climate with a strong continental influence in the northeastern part and moderate-continental in the southwestern part of the park. The whole massif of Kozare vegetation belongs to the forest belt of the Illyrian region *Carpinion betuli illyrico-podolicum* [19]. In the montane zone and in the colder positions of the submontane zone, the *Abieti-Fagetum praepannonicum* community dominates and is widespread in most of the central and northern, colder part of the park, and the specificity of these habitats is that the fir here descends very low (up to 200 m.a.s.l.). On the exposed slopes and steep slopes of the southwestern part of the National Park, there is a forest of ass. *Festuco drymeiae-Quercetum petraeae*, while the southern side of Mrakovica is overgrown with *Quercum-Abietetum* forest, which is actually a vegetation transition between the *Abieti-Fagetum praepannonicum* and *Festuco drymeiae-Quercetum petraeae* communities and is also a specificity of Kozara. Forests of Kozara National Park occupy 90% of the area [19,20]. Such habitat conditions caused a diverse composition of the total fauna, especially the diversity of amphibians and reptiles of the Kozara National Park.

MATERIAL AND WORKING METHODS

Research and inventory of the diversity of the Kozara National Park was carried out in the period 2012–2024 when the inventory of the herpetofauna species diversity of the area was done. Specimens were caught with standard herpetological equipment on site for measurement and then released into nature. Their total body length was measured, they were examined in order to determine the presence of ticks and their overall state of health and condition was assessed on a scale of 1–5, where grade 1 is an individual with numerous visible injuries and scars, severely malnourished, slow and uncoordinated movement and grade 5 is an individual without visible injuries and scars, good overall health condition, good nutrition and movement coordination. The determination of the species in the field was carried out according to the literature [21–24].

Site description: The terrain where the species was found is a stony meadow (Figure 1) with a slope of 20–30%, directly exposed to the sun, overgrown with rare herbaceous vegetation with some low bushes. From the north, the area is bordered by degraded low forest

and from the south by a meadow that is occasionally mowed or used for livestock grazing, and was once a football field.

Figure 1 *Habitat of the species Ablepharus kitaibelii*

RESULTS AND DISCUSSION

The first official data for *A. kitaibelii* in Bosnia and Herzegovina was given by Sofradžija [25] for the locality "Ustikolina" [26]. The author collected 16 specimens and some of them are deposited in the natural history department of the National Museum of Bosnia and Herzegovina in Sarajevo (Figure 2). However, Ljubisavljević *et al*. [27] mention a possible second site for B&H near Bijeljina, citing the unpublished diploma thesis of Aleksić [28], but without any confirmatory photos or specimens. Those localities were not visited for a long time until the publication of the work by Zimić *et al*. [26], where the authors describe the "rediscovered" population mentioned by Sofradžija [25] at the Lozje locality (Cvilin, Ustikolina), with the fact that now a total of 21 individuals have been found, of which 13 were captured for further research and analysis, while the locality near Bijeljina was not the subject of field research. In addition to morphometric data for the species itself, the authors provide detailed data on the habitat (vegetation cover, other reptile species present, temperature and hydrological regime of the terrain and soil (air and soil humidity), etc.).

Figure 2 *Specimens of the species Ablepharus kitaibelii from the herpetological collection of the National Museum in Sarajevo (https://www.facebook.com/BHHUATRA)*

A total of 15 species of reptiles or 51.7% of the total diversity of B&H were recorded for the Kozara mountain area, of which 12 species (42.8%) and one intraspecies form are present in the Kozara National Park itself [29]. The lizard *Ablepharus kitaibellii* was recorded in 2012 at the Benkovac site (near the stadium) within the Kozara National Park, where four specimens were found [30]. The specimens were found on August 15, 2012~~.~~ between 10 a.m. and 12 p.m. in a clearing at the edge of a mixed oak forest (Figure 3). The weather was warm, sunny with a temperature of around 28–30°C. First, two specimens were observed on sunlit rocks. Later, two more specimens were found, one at the edge of the forest in fallen leaves, and the other specimen was walking over stones. Of the four specimens, three were in excellent condition, while one individual was generally weakly active, visibly malnourished, part of the tail with signs of regeneration was missing and small scars were present on the back. A complete overview of the measured values of total body length and health status is shown in Table 1.

Figure 3 *The species Ablepharus kitaibelii from the locality Benkovac (Photo: Stanković M.)*

Table 1 *Measured values of the total body length and estimated general health status and condition of Ablepharus kitaibelii in Kozara National Park on Benkovac, 2012*

Code	Body length (in cm)	Health and condition*
AK-1	8.6	4
AK-2	11.9	4
AK-3	10.4	5
AK-4	6.4	2

* scale 1 – 5; description is given in the section Materials and working methods

The body size of our specimens ranged from 6–12 cm, which coincides with the data from the Ustikolina site [26].

During a visit to the Benkovac site in 2014, the species was not recorded due to the extremely wet terrain when most of the meadow was under shallow water and the rocks on the slopes that make up the surrounding rock gardens were "soaked" by the water that flowed from them. Then in 2015, during a visit to the site, one specimen, 8.8 cm long, was found, but that year the beginning of the overgrowth of the rock garden-meadow by the nearby forest was observed and tall weedy vegetation. Since 2016, the species has not been recorded in the locality, and the terrain is overgrown with high vegetation with the spread of shrubby and

woody vegetation. The closest localities to ours are in the Papuk Nature Park (southwestern slope of the Turjak ridge) and in the city park in Ilok [31].

In Europe, the species has the status of endangered last concern (Lc) [16], while in Bosnia and Herzegovina *Ablepharus kitaibelii* should have the status of critically endangered species (CR), otherwise, at the national level, the species is not on the Red List of Flora and Fauna of the Federation of Bosnia and Herzegovina, nor on the Red List of Protected Species of Flora and Fauna of the Republic of Srpska, which should be changed in the next amendment or revision.

Endangering factors at the Benkovac site, in addition to the above-mentioned general endangering factors at the site, over the past ten years, the rocky meadow-meadow has been overgrown by high ruderal vegetation and the spread of forest (shrubby and woody) vegetation that was originally on the edge of the slope, and now the vegetation has almost completely overgrown and closed the sunny open parts of the rocky meadow with its structure.

Species protection measures in Bosnia and Herzegovina: According to the currently available data, this is one of the rarest reptile species in Bosnia and Herzegovina, and therefore legally, the species should be on the list of protected species in both entities of Bosnia and Herzegovina. Also, the habitats where the species is found must be officially legally protected, if they are not within an existing protected area such as the Benkovac site within the Kozara National Park, which could be set aside as a specially protected habitat within the park. Population and habitat condition monitoring should be established in all habitats. Work on education and raising the awareness of the population about the importance of protecting and preserving both the species itself and its habitat. We must bear in mind that this species has a cryptic way of life where there is a danger that its habitats will be completely destroyed or devastated before it is established that the species was there, which only indicates the need for further research of all potential habitats of the species in Bosnia and Herzegovina. In order to better protect the species, a detailed investigation of the state of the population and their habitats is necessary, especially those isolated populations exposed to stronger anthropogenic influence. All these population-ecological studies can indicate the need to undertake active protection such as "in situ" in their habitats [5]. Since there are specific cases of the species being the subject of illegal trade, such as the one recorded in 2014 in Bosnia and Herzegovina, when several specimens of *A. kitaibelii* were offered for sale as pets on the internet on the shopping portal (www.olx.ba) and when the ad was responded to and asked about the origin of the animals, the site administrator removed it from the web portal [26]. This example warns us that such situations must not happen in the future and that inspection authorities must monitor such sites and react to such situations. As a measure to protect the species and its habitat specifically at the Benkovac location, it is necessary to carry out remedial measures to clean and illuminate the terrain, which entails the removal of forest and part of the bushy vegetation that has since spread and conquered most of the area where the species was found.

CONCLUSION

The lizard *Ablepharus kitaibellii* was recorded at the Benkovac site (near the stadium) in the Kozara National Park, where four specimens were found in 2012, on a rocky slope at the edge of a mixed oak forest in warm, sunny weather. The species is not endangered on a global level, but it is in Bosnia and Herzegovina, because there are only two data so far. The finding of the species *A. kitaibelii* at the Benkovac locality is officially the second or third data for B&H, because for now we only have one reliable data from the vicinity of Ustikolina in the Federation of B&H, while the other literature data cites the unpublished diploma thesis that mentions another possible locality of this species for B&H, near Bijeljina without specific specimens or photographs. The species must be nationally listed on the Red List of Flora and Fauna of the Federation of Bosnia and Herzegovina, and on the Red List of Protected Species of Flora and Fauna of the Republic of Srpska. In order to preserve and survive this species, monitoring of species and habitats and the need to undertake active protection of their habitats or measures to improve habitat conditions through active protection projects must be established.

REFERENCES

[1] Uetz P, Freed P, Hošek J. Eugongylinae. The Reptile Database. Retrieved 10 October 2019.

[2] Jablonski, D., Jandzik, D., Gvoždík, V. North-West. J. Zool. 2012, 8 (2), 324–337.

[3] Herczeg, G, Tóth, T, Kovács, T, *et al*. Russ. J. Herpet. 2004, 11 (2), 99–105.

[4] Mićanović A, Muhović I. Vodič kroz svijet gmizavaca Crne Gore. Danilovgrad, Crna Gora: Crnogorsko društvo ekologa; 2023. p. 95.

[5] Ljubisavljević K, Džukić G. Kratkonogi gušter ((*Ablepharus kitaibelii* (Bibron & Bory, 1833)). In: Tomović Lj, Kalezić M, Džukić G, editors. Crvena knjiga faune Srbije II – Gmizavci. Beograd: Biološki fakultet Univerziteta u Beogradu, Zavod za zaštitu prirode Srbije, Alta nova; 2015.

[6] Ljubisavljević, K., Džukić, G., Kalezić, M.L. Herpetozoa 2002, 14 (3/4), 107–121.

[7] Pasuljević G. Glasnik Prirodnjačkog Muzeja u Beogradu, Serija B, 1965, 20, 311–314.

[8] Pasuljević G. (1966). Prilog poznavanju ekologije *Ablepharus kitaibelii* (Bibron et Bory). *Zbornik Filozofskog Fakulteta u Prištini*, *3*, 459-463.

[9] Gruber U. *Ablepharus kitaibelii* (Bibron und Bory 1833). Johannisechse. In: Böhme W, editor. Handbuch der Reptilien und Amphibien Europas. Wiesbaden: Akademische Verlag; 1981. pp. 297–302.

[10] Herczeg, G., Kovács, T., Korsós, Z., *et al*. Biol. 2007, 62 (4), 482–487.

[11] Pasuljević G., Morfološki varijabiliteti i biogeografsko-ekološki odnosi populacija *Ablepharus kitaibelii* (Reptilia: Squamata: Scincidae), (Bibron et Bory). Doktorska disertacija, PMF Univerziteta u Prištini, Priština, 1973.

[12] Speybroeck J, Beukema W, Bok B, *et al*. Field Guide to the Amphibians and Reptiles of Britain and Europe, London, UK: Bloomsbury Publishing Plc; 2016.

[13] Jelić D, Koller K. Nacionalni program za praćenje stanja očuvanosti vrsta u Hrvatskoj – Ivanjski rovaš (*Ablepharus kitaibelli*). Zagreb: Državni zavod za zaštitu prirode R. Hrvatske; 2014. pp. 3–11.

[14] Pasuljević, G. Acta Biol. Med. Exp. 1976, 1–2, 57–63.

[15] Szövényi, G, Jelić, D. North-West. J. Zool. 2011, 7 (1), 20–25.

[16] Cox NA, Temple HJ, European Red List of Reptiles, Luxembourg: Office for Official Publications of the European Communities; 2009.

[17] Bern Convention on the Conservation of European Wildlife and Natural Habitats.

[18] Council Directive 92/43/EEC of 21 May 1992 on the conservation of natural habitats and wild fauna and flora Anex IV - Animal and plant species of Community interest (i.e. endangered, vulnerable, rare or endemic in the European Community) in need of strict protection; Annex II- animal and plant species of community interest whose conservation requires the designation of special areas of conservation; Annex 5 - Animal and plant species of Community interest whose taking in the wild and exploitation may be subject to management measures.

[19] Bucalo V, Brujić J, Travar J, *et al*. Flora Nacionalnog parka Kozara. Milano, Banja Luka: Šumarski fakultet Univerziteta u Banja Luci i ERSAF Regionalni zavod za upravljanje šumama i agrokulturom Pokrajine Lombardija; 2007.

[20] Bucalo V, Brujić J, Travar J, *et al*. Šumarstvo, 2006, 4, 11–24.

[21] Arnold EN, Burton JA. A field guide to the Reptiles and Amphibians of Britain and Europe. London: Collins Grafton Street; 1985.

[22] Forey PA, Forey PE, Reptiles & Amphibians: Pocket reference guides. Brockhampton: Brockhampton press; 1997.

[23] Harry G, Borm L. Fauna Evrope – Priručnik za raspoznavanje životinjskih vrsta. Ljubljana: Mladinska knjiga; 1981.

[24] März R. Gewöll und Rupfungskunde. Berlin: Academie Verlag; 1987.

[25] Sofradžija A. Glasnik Zemaljskog Muzeja Bosne i Hercegovine 1978, 7, 37–38.

[26] Zimić A, Pećar D, Jelić D. North-West. J. Zool. 2018, 14 (1), 146–148.

[27] Ljubisavljević K, Tomović L, Simović A, *et al*. Ecol. Montenegrina 2015, 2, 247–254.

[28] Aleksić I. Biologija i ekologija panonskog guštera (*Ablepharus pannonicus*). BSc thesis. Biološka grupa, PMF, Beograd; 1954.

[29] Stanković M, Romčević D, Pjević Beslac N. In: 10. Simpozijum o zaštiti karsta, Akademski speleološko–alpinistički klub; Belgrade, Serbia. 2023. p. 81–85.

[30] Stanković M. Čovjek i krš 2013, 34, 47.

[31] Janev-Hutinec B, Kletečki E, Lazar B, *et al*. Crvena knjiga vodozemaca i gmazova Hrvatske. Zagreb: Ministarstvo, kulture R. Hrvatske i Državni zavod za zaštitu prirode. 2006.

EcoTER'26
eco.tfbor.bg.ac.rs
32nd International Conference
Ecological Truth & Environmental Research
24–26 June 2026, Hotel Sunce,
Sokobanja, Serbia

Original Research

CONTRIBUTION OF THE DISTRIBUTION OF THE SPECIES *Ricciocarpos natans* (L.) CORDA 1829 IN THE SNR ZASAVICA AND MACVI WITH THE ANALYSIS OF THE HABITAT

DOI: 10.5937/EcoTER26394S

Mihajlo Stanković[1*]

[1] Pokret gorana, Svetog Save 19, 22000 Sremska Mitrovica, SERBIA

Abstract

The species Ricciocarpos natans in Serbia was recorded in a small number of localities, mostly north of the Danube and Sava rivers. Through our research in Mačva, the species was found in a total of 38 localities, 20 of which are within the boundaries of the reserve and 18 outside the boundaries of the protected area, with a total of 63 findings within the boundaries of the protected area and outside it. The species is found in canals, swamps, lowland peatlands, mudflats, etc., most often in coastal vegetation Scirpo-Phragmitetum W. Koch 26 subass. typhaetosum (angustifoliae-latifoliae) Soó 73, or in floating Lemno-Salvinion natans Slavnić 56 and Lemno minoris-Spirodeletum polyrrhizae W. Koch 1954.

Keywords: *Ricciocarpos natans*, Mačva, Zasavica, habitat.

INTRODUCTION

Ricciocarpos natans (L.) Corda 1829 belongs to the genus *Ricciocarpos* Corda 1829, family *Ricciaceae* [1]. The species has a heart-shaped to kidney-shaped green thallus with fewer branches and its main character is the long purple sword-shaped scales that hang from the lower surface of the floating plants [2]. This is a rare swimming thalloid liverwort, which is found in shaded shallow warm nutrient-enriched waters and has a terrestrial form in mudflats when the water recedes. The species *Ricciocarpos natans* is a cosmopolitan, aquatic moss that inhabits eutrophic waters on most continents except the polar ones [2] and often forms dense, floating colonies [3]. It inhabits a variety of aquatic habitats with different water parameters and periods of occurrence and despite its wide ecological amplitude, the species is locally rare and of low diversity. The species is globally distributed, but it is rare in southern Europe. The population trend in Europe is considered stable and therefore the assessment is of least concern (Lc) [4], but many subpopulations at the national and regional level are threatened, *i.e.* declining or unstable and therefore listed as Critically Endangered (CR) (Slovenia), Endangered (EN) (Austria, Germany, Spain); vulnerable (VU) (eg Great Britain, Slovakia), etc. [5]. Occurs from sea level in the Mediterranean to 600 m.a.s.l. in Switzerland, or up to 1000 m.a.s.l. in France [4]. In Serbia, it was recorded in a small number of localities, mostly north of the Danube and Sava rivers [6], unfortunately new field visits to some known localities did not confirm its presence, and that is why the species is a candidate for the new

* *trogloxen@gmail.com*

Red List of bryophytes of Serbia. The dynamics of appearance is irregular over the years, due to the requirements of its habitat. In some parts of Europe, gametangia and sporophytes are rarely seen, and the spread is believed to be clonal [4]. Since this semi-aquatic moss in Serbia has been recorded in a small number of localities, mostly north of the Danube and Sava rivers, our data contribute to a better knowledge of its overall distribution in Serbia.

MATERIAL AND WORK METHODS

Floristic research involves the application of standard botanical methods of habitat survey. At the location, the number of specimens on the surface (if it is a small area) or the coverage of the surface (if it is a larger or large area) is determined, in addition to data on the species itself, data on other plants in the area, type of habitat, water depth, etc. are recorded. For each locality, GPS coordinates were determined using Google Earth Pro and the UTM field. We divided the sites into two groups. The first group consists of localities within the boundaries of SRP Zasavica, and the second group consists of localities outside the boundaries of the reserve, whose overview we now give:

✓ **Localities within the SNR Zasavica: Crna bara:** canal Jovača (44^{0}54´18.06"N-19^{0}25´03.61"E), CQ77; Ribnjača bara (44^{0}54´35.91"N-19^{0}24´30. 49"E), CQ77; **Radenković**: Batar (44^{0}55´39.15"N-19^{0}28´25.47"E), CQ77; Zelene bare (44^{0}54´ 47.78"N-19^{0}30´45.61"E), CQ87; Pačija bara (44^{0}56´22.26"N-19^{0}29´50.53"E), CQ87; Gajića ćuprija (44^{0}56´05.91"N-19^{0}29´02.65"E), CQ87; **Ravnje**: Čuturina kafana (44^{0}57´17.18"N-19^{0}27´38.96"E), CQ77; Batve (44^{0}56´02.63"N-19^{0}27´45.61"E), CQ77; Ravnjanska ćuprija downstream (44^{0}56´20.53"N-19^{0}25´57.22"E), CQ77; Ravnjanska ćuprija upstream (44^{0}56´16.03"N-19^{0}25´51.77"E), CQ77; Zovik (44^{0}56´31.46"N-19^{0}28´42.97"E), CQ77; **Prekopac** (44^{0}55´15.81"N-19^{0}25´20.43"E; 44^{0}55'39,40"N-19^{0}25'03,92"E), CQ77; **Banovo Polje**: Batar (44^{0}55´41.94"N-19^{0}28´27.75"E), CQ77; Ljubinkovića ćuprija (44^{0}55´09.81"N-19^{0}26´45.36"E), CQ77; Poljansko (44^{0}56´24.49"N-19^{0}26´03.30"E), CQ77; Ribnjača bara (44^{0}54´50. 97"N-19^{0}24´39.30"E), CQ77; **Zasavica II**: Valjevac flood zone, (44^{0}57´19.30"N-19^{0}31´33.88"E), CQ87; Valjevac canal (44^{0}57´15.77"N-19^{0}31´30.02"E), CQ87; Turske livade (44^{0}57´31.01"N-19^{0}31´40.28"E), CQ87, Vrbovac (44^{0}57´23.98"N-19^{0}27´49.96"E), CQ77.

✓ **Localities outside the boundaries of the protected area: Glušci:** Bitva (44^{0}54´01.29"N-19^{0}33´00.78"E), CQ87; Duga bara (44^{0}53´08.29"N-19^{0}30´30.66"E), CQ87; Kaluže (44^{0}52´25.91"N-19^{0}30´34.57"E), CQ87; Lanište (44^{0}54´03.47"N-19^{0}33´08.82"E), CQ87; Kupusina greda (44^{0}54´16.17"N-19^{0}37´07.90"E), CQ87; Crna bara (44^{0}53´53.10"N-19^{0}35´55.31"E), CQ87; Češljuška bara (44^{0}57´23.98"N-19^{0}27´49.96"E), CQ77; **Salaš Noćajski**: Skenovača (44^{0}55´50.24"N-19^{0}37´46.09"E), CQ97; **Noćaj**: Kojšanski kanal 1, (44^{0}57´31.85"N-19^{0}32´57.43" E), CQ87; Kojšanski kanal 2 (44^{0}57´27.25"N-19^{0}32´28.18"E), CQ87; **Metković**: Jabukovac (44^{0}52´05.41"N-19^{0}31´36.16"E), CQ86; Klenić (44^{0}51´06.08"N-19^{0}31´39.11"E), CQ86; **Šabac**: Veliki cerski kanal (confluence with the Sava River) (44^{0}44´37.35"N-19^{0}43´39.84"E), CQ95; Šabac (Major): Veliki cerski kanal (44^{0}44´37.35"N-19^{0}43´39.84"E), CQ95; **Lipolist**: Veliki cerski kanal (44^{0}43´08.69"N-19^{0}32´11.27"E), CQ85; **Bogatić**: Panjevine (44^{0}52´28.47"N-19^{0}29´38.21"E), CQ87; **Crna bara**: Šobatovac (44^{0}52´43.01"N-19^{0}26´06.12"E), CQ77; Neškovine (44^{0}53´24.13"N-19^{0}25´36.34"E), CQ77.

The type of vegetation was determined according to Kitnaes *et al*. [7] and Plavac *et al*. [8]. The determination of the gorse *Ricciocarpos natans* was made according to Pavletić [9], and the other plants present according to the relevant literature sources [10–12].

RESULTS WITH DISCUSSION

During the work on the flora of the reserve and northern Mačva, the presence of the rare aquatic moss *Ricciocarpos natans* was noted. The paper processed data for the period from 2004 to March 2026. Now we will give an overview of the localities where the species *Ricciocarpos natans* was found with accompanying data.

Localities within the boundaries of the protected area (SNR Zasavica): **Crna bara**: Jovača canal: 01.08.2004, P=1x3 m, Σ=17 individuals (indiv.); 28.04.2007, P=3x2 m, covered 20% of the surface; Ribnjača bara: 22.07.2010., forbidden ground, P=10x2 m, covered 40% of the surface; 04.08.2023, mudflat, P=10x4 m, covered 20% of the surface; **Radenković**: Batar: 10.12.2005, coastal part, P=2x10 m, covered 70% of the surface; 06.11.2014, coastal part, P=1x2 m, covered 20% of the surface; 30.03.2005, coastal part, P=3x7 m, covered 40% of the surface; Zelene bare: 08.06.2010, forbidden ground, P=1x1 m, Σ=20 indiv.; Pačija bara: 29.07.2010, peatland, P=50x10 m, covered 60% of the surface; 14.12.2011, peatland, P=20x7 m, covered 20% of the surface; 14.12.2014, peatland, P=4x7 m, covered 20% of the surface; 14.11.2014, peatland, P=50x10 m, covered 70% of the surface; 05.11.2014, peatland, P=8x5 m, covered 30% of the surface; 06.03.2016, peatland, P=5x1 m, Σ=9 indiv.; 06.08.2019, peatland, P=20x4 m, covered 30% of the surface; 22.04.2023, peatland, P=7x5 m, covered 40% of the surface; 16.03.2024, peatland, P=10x7 m, covered 50% of the surface; Gajica ćuprija: 31.01.2013, coastal part, P=1x1 m, Σ=7 indiv.; 05.02.2013, coastal part, P=2x3 m, Σ=2 indiv.; Vrbovac: 16.03.2024, coastal part, P=1x1 m, Σ=22 indiv.; **Banovo Polje**: Batar: 30.05.2005, coastal part, P=2x5 m, Σ=12 indiv.; 18.02.2026, coastal part, P=1x2 m, Σ=7 indiv.; 27.02.2026, coastal part, P=4x2 m, Σ=8 indiv.; Ljubinkovića ćuprija: 28.04.2007, coastal part, P=3x3 m, Σ=20 indiv.; 21.06.2018, coastal part, P=1x1 m, Σ= 13 indiv.; Poljansko: 05.02.2013, coastal part, P=3x1 m, Σ=15 indiv.; Ribnjača bara: 05.03.2016, forbidden ground, P=1x1 m, Σ=23 indiv.; 02.08.2016, forbidden ground, P=3x2 m, covered 20% of the surface; 09.08.2021, forbidden ground, P=30x5 m, covered 60% of the surface; 03.08.2022, forbidden ground, P=15x4 m, covered 20% of the surface; **Ravnje**: Čuturina kafana: 07.05.2006, coastal part, P=1x1 m, Σ=16 indiv.; Batve canal: 04.08.2010, P=20x2 m, covered 80% of the surface; 03.01.2022, P=10x2 m, covered 30% of the surface; Prekopac: 05.08.2010, mudflat, P=10x1 m, covered 20% of the surface; 09.09.2022, dry trough, P=30x20 m, covered 30% of the surface; Ravnjanska ćuprija: 17.04.2018, downstream 100 m, coastal part, P=100x2 m, covered 60% of the surface; 17.04.2018, upstream 200–300 m, coastal part, P=200x2 m, covered 30% of the surface; Zovik, canal: 02.08.2019, P=20x3 m, covered 80% of the surface; **Zasavica II**: Valjevac flood zone, 11.11.2019, dry mud flat, P=50x10 m, covered 30% of the surface; Valjevac canal, 16.11.2019, P=1x4 m, Σ=20 indiv.; Turske livade, canal, 19.03.2023, P=5x2 m, covered 30% of the surface.

Localities outside the boundaries of the protected area: Glušci: Bitva canal: 30.03.2005, P=3x4 m, covered 50% of the surface; 07.08.2021, P=2x1 m, Σ= 9 indiv.; 07.07.2023, P=3x5 m, covered 20% of the surface; Duga bara: canal, 07.09.2009, P=2x2 m,

Σ=22 indiv.; Kaluže: canal and spillway, 07.09.2009, P=10x4 m, covered 30% of the surface; Lanište: canal, 10.10.2009, P=2x3 m, covered 40% of the surface; Kupusina greda: forbidden ground, 25.07.2009, P=1x2 m, Σ= 28 indiv.; Crna bara: forbidden ground, 17.07.2014, P=1x1 m, Σ=11 indiv.; Češljuška bara: 05.08.2023, forbidden ground, P=2x7 m, covered 30% of the surface; 26.10.2023, forbidden ground, P=3x7 m, covered f 40% of the surface; **Salaš Noćajski**: Skenovača canal, 19.09.2006, P=1x1 m, Σ= 20 indiv.; **Noćaj**: Kojšanski canal 1, 15.06.2006, P=50x2 m, covered 60% of the surface; Kojšanski canal 2, 30.04.2006, P=100x2 m, covered 40% of the surface; **Metković:** Jabukovac canal, 15.11.2006, P=1x1 m, Σ=9 indiv.; Klenić, canal, 01.11.2015., P=1x1 m, Σ= 6 indiv.; **Šabac:** Veliki cerski canal (confluence with the Sava River), 29.09.2008, P=20x2 m, covered 40% of the surface; Šabac (Major): Veliki cerski canal, 28.10.2015, P=2x1 m, Σ=7 indiv.; **Lipolist**: Veliki cerski canal, 31.10.2009, P=1x1 m, Σ=18 indiv.; **Bogatić**: Panjevine, canal, 13.07.2009, P=3x2 m, covered 20% of the surface; **Crna bara**: Šobatovac, forbidden ground, 09.07.2010, P=2x1 m, Σ= 36 indiv.; Neškovine, riverbed Batar, 20.07.2011, P=5x2 m, covered 30% of the surface; **Radenković:** Virovlje, canal, 24.05.2020, P=1x1 m, Σ= 5 indiv.;

For the species *R. natans*, we have a total of 63 findings both within the SNR Zasavica and outside it in North Mačva, in a total of 38 localities, of which 20 are within the boundaries of the reserve and 18 within the protected area.

Analysis of localities within the boundaries of SNR Zasavica: Within the protected area, we have the largest number of finds (9) at the Pačija bara site, which represents a lowland peatland, followed by the Batar locality with 6 finds and the Ribnjača bar with 5 finds. At 15 locations, we counted individuals because it was about areas of a few square meters, and for areas larger than 10 m^2, an assessment of the coverage of the area was made and given in percentage (%). The most common surface coverage was 20–30%, in two cases we have coverage of 70–80% in the localities of Batar (2005), Batve (2010), Pačija bara (2014) and Zovik (2019). In 2018, we mention the site Ravnjanska ćuprija where 100 m upstream and about 200 m downstream from the bridge there was coverage of 60 and 30% in the shafts between the rushes. According to the type of habitat, the largest number of findings (15) is in the coastal zone of the watercourse, which is partially overgrown with vegetation. In six cases, the ephemeral type of terrain was forbidden, and in such habitats the species occurs only when the water is deeper than 30 cm, such is the case at Ribnjača pond, where this moss was recorded five times. In nine cases, the findings were in the lowland peatland at the Pačija bara site, while in two cases, the findings were in the mud (when the water recedes suddenly and quickly) or in the cracked mud itself after a slow withdrawal of water and percolation. Canals in the reserve are present in the protection zone and there were seven findings in the canals that are reclamation facilities. The emergent vegetation is *Scirpo-Phragmitetum* W. Koch 26 *subass. typhaetosum (angustifoliae-latifoliae*) Soó 73 developed along the canal banks and the species was found in water pockets between rushes. As the water depth increases in the canal, both floating and submerged plants appear, the most common vegetation being *Lemno-Salvinion natans* Slavnić 56, *Lemno minoris-Spirodeletum polyrrhizae* W. Koch 1954, *Ceratophylletum demersi* (Soó27) Hild.1956, *Lemnetum trisulcae* Knapp et Stoffers 1962, and *Ceratophyllo-Hydrocharidetum morsus-ranae*. Pop. 1962. In the reserve zone, the species *Ricciocarpos natans* occurs in the following priority Natura 2000

habitats: 7230, 3260 and 3150 [4]. Within the boundaries of the reserve, we have 15 localities where the species has been found. We will develop six localities where we will analyze the type of habitat and vegetation. **Pačija bara**: is a specific habitat that belongs to the type of lowland peatlands (Natura 2000 code 7230) [13]. It is a depression in GJ "Vrbovac" surrounded by 110 ha of arboriculture of hybrid poplar and willow on α/β-β clay soil. The total area is 1,07 ha. In the pond itself, there are single trees of *Salix alba* and bushy *Salix cinerea*, which in some parts create an almost impassable terrain. The community of *Thelyptero-Phragmitio-Salicetum cinereae* M. Jank. 1984 is sporadically developed, where in the herbaceous floor there are characteristic lumpy sods of species from the genus Carex (*Carex riparia, C. pseudocyperus, C. hirta, C. otrubae, C. vulpina*) that dominate the terrain. Pačija bara is a periodic water body, which in its deepest part has up to 0.7–0.8 m of water. *Thelypteris palustris* Schott and *Urtica kioviensis* Rogow. appear in the parts where the peat is more pronounced, and *Hottonia palustris* L. occasionally appears. In addition to species from the genus *Carex*, which dominate as the most common species, the following are present: *Mentha aquatica* L., *M. longifolia* (L.) Huds., *Sparganium erectum* L., *Lemna trisulca* L., *Spirodela polyrhiza* (L.) Schleid., *Riccia fluitans* L. **Bara Ribnjača** represents the rest of the wetlands in the inundation level of the rivers and dries up every year in the period from June to September. Vegetation consists of a wide emergent zone *Scirpo-Phragmitetum* V. Koch 26 *subass typhaetosum (angustifoliae-latifoliae*) Soo 73 and depending on the water level of the *Lemno-Salvinion natans* Slavnić 56, *Lemno minoris-Spirodeletum polyrrhizae* W. Koch 1954 and *Ceratophyllo-Hydrocharidetum morsus-ranae* Pop.1962, *Ceratophylletum demersi* (Soó 27) Hild.1956, *Lemnetum trisulcae* Knapp et Stoffers appear. 1962 and *Potameto-Ceratophylletum demersi* Jank.74. **Batar** is a tributary of Zasavica, 15 km long, rises near Sovljak. The protected part includes upstream from the mouth in a length of 5 km. Since the settlement of beavers in 2005, the habitat has changed drastically, siltiness has increased (mud depth over 1 m) and the water depth does not exceed 1 m. Coastal part of *Scirpo-Phragmitetum communities* W. Koch 26 *subass. typhaetosum (angustifoliae-latifoliae*) Soó 73, *Lemno-Salvinion natans* Slavnić 56, *Lemno minoris-Spirodeletum polyrrhizae* W. Koch 1954, *Ceratophyllo-Hydrocharidetum morsus-ranae* Pop. 1962 and *Ceratophylletum demersi* (Soó 27) Hild. 1956 appear in the riverbed (closer to the mouth) and *Lemnetum trisulcae* Knapp et Stoffers 1962 further upstream, depending on the water level [14]. The structure of the forest almost completely overlaps the watercourse, and part of the forest has entered the riverbed. The forest along the coast is a community of *Populeo-Salicetum* Raj. 1950. *subass. Ruboetosum* (Gajić 1954, Tóth 1958). em. Erdeši 1971. and further from the watercourse, depending on the configuration of the terrain and the level of groundwater, there are forests of *Genisto elatae-quercetum* Horv. 1938. *subass. Leucojo-fraxinetum* Glav. 1959, *Brachypodio silvaticae palustris-Quercetum* Erdeši. 1955 and *Genisto elatae-Quercetum* Horv. 1938. *subass.alno-carpinetosum* [15]. **Prekopac:** represents an ephemeral water area surrounded by forest. Until 2010, the water was in the trough all year round, after that the water appears in the spring and disappears in June. The bed of the Prekopac is overgrown with vegetation, *Scirpo-Phragmitetum* W. Koch 26 *subass typhaetosum (angustifoliae-latifoliae*) Soó73 or *subass. phragmitetosum* Schmalle 39. There is a narrow forest belt along the coast, and arable land continues to it. The forests belong ass. *Brachypodio silvaticae palustris-Quercetum* Erdeši. 1955 and *Genisto elatace-Quercetum* Horv.1938 *subass.alneto-carpinetosum betuli*

Vuk 1959. When the canal with water is over 0.5 m deep, the community *Ceratophyllo-Hydrocharidetum morsus-ranae* Pop. 1962 and *Hydrocharo-Nymphoidetum peltatae* Slavnić 56 appears, and when is water depth and up to 1.5 m there are communities of *Nymphaeetum albo-lutea* Nowinski 28 *subass.nupharetosum* (Timar) Kórpáti and *Potameto-Ceratophy-lletum demersi* Jank.74 [14]. **Kanal Jovača**: A narrow strip of occasionally flooded forests ass. *Genisto elatace-Quercetum* Horv 1938 *subbass. Leucoio-Fraxinetum angustifolia* Glav. 1959 appears in the canal bed itself. In the canal, when there is water, communities of *Lemno minoris-Spirodeletum polyrrhizae* W. Koch 1954 and *Lemnetum trisulcae* Knapp et Stoffers 1962 are developed, while the emersion zone consists of a community of *Scirpo-Phragmitetum* W. Koch 26 *subass. typhaetosum (angustifoliae-latifoliae*) Soó 73 and *subass. Schoenoplectetosum lacustris* Soó 73 [14]. The Valjevac pasture covers an area of 300 ha. The pedological base is characterized by mineral-marsh soil with a large influence of underground and flood waters, and the soil is characterized as scaly rite cherts. The terrain is slightly undulating, interspersed with beams and depressions. A semi-aquatic community *Scirpo-Phragmitetum* W. Koch 26 with three sub-associations was developed on the coast: *phragmitetosum* Schmalle 39, *subass. typhetosum (angustifoliae-latifoliae)* Soó 73 and *subass. Schoenoplectetosum lacustris* Soó 57, which occur in the form of larger or smaller areas and is dominated by the *subass. typhaetosum (angustifoliae-latifoliae)* [14]. This community is followed by the belt ass. *Acoro-Glyceretum maximae* and the presence of this association is conditioned by the high level of groundwater and frequent flooding, and as a special element of this community is the presence of the species *Utricularia australis* as an Atlantic-Mediterranean species whose presence indicates a mesophilic and weakly acidic type of water [16]. In that flood zone, the moss *Ricciocarpos natans* was found in the community of *Scirpo-Phragmitetum* W. Koch 26 and *Acoro-Glyceretum maximae*.

Analysis of localities outside the boundaries of the protected area: Outside the boundaries of the reserve, the species was found in a total of 16 localities with a total of 22 findings. We have the largest number of finds, three each, in two localities (Bitva and Veliki Cerski kanal), followed by Kojšanski canal 1 and 2 and Česljuška bar with two finds each. At 11 locations, individuals were counted on areas of a few square meters, while for areas larger than 10 m^2, an assessment of the surface coverage was made, and the values are given in percentages (%). The highest number of individuals counted was 36 in Šobatovac in 2010, followed by Kupusina greda with 28 and Duga bara with 22 individuals. In most cases the surface coverage was 30–40%, in two cases we had coverage over 50% and in one case the coverage was 60% at the Kojšanski canal 1 locality in 2006 and Bitva in 2005. Among the sites, the site Kojšanski kanal 1 and 2 stands out with the largest area covered by individuals on an area of 50–100 m long and 2 m wide, where the surface coverage was 40–60% and the species was in the shafts between the rushes. According to the type of habitat, the largest number of finds (16) is in canals, in five cases the terrain was a slightly sunken depression with water over 30 cm deep. In one case, the species was found in dry cracked mud covered by tall vegetation in the Neškovine locality. In the majority of cases, the canals are on average 2–3 m wide where the emergent vegetation of the community *Scirpo-Phragmitetum* W. Koch 26 subass *typhaetosum (angustifoliae-latifoliae)* Soó 73 is developed, which partly and completely covers the width of the canal and the individuals are found in water pockets

between the rush trees. The vegetation depends on the depth of the water and the most common species are *Lemno-Salvinion natans* Slavnić 56, *Lemno minoris-Spirodeletum polirrhizae* V. Koch 1954, *Ceratophilletum demersi* (Soo 27) et al. 1962., *Ceratophyllo-Hydrocharidetum morsus-ranae* Pop. 1962. and *Lemno-Utricularietum vulgaris* Soo 1928. Outside the boundaries of the reserve, we have 16 localities where this species has been found. We will single out five localities where we will analyze the type of habitat. **Bitva** is a river that rises near the village of Dublje near Bogatić, 31 km long and has a wide alluvial plain in the lower reaches. It flows north to Glušac, then turns east and flows into the Sava downstream from Mačvanska Mitrovica. The catchment area of Bitva is 85 km². Today, this area is criss-crossed by a network of canals whose sides are steep and deep, especially in the part between Bogatić, Radenković and Glušac, and is a key hydrotechnical facility for flood defense [17]. Most of the canal is under vegetation *Scirpo-Phragmitetum* W. Koch 26 *subass typhaetosum (angustifoliae-latifoliae*) Soó 73 or *subass. Phragmite-tosum* Schmalle 39. Depending on the water level, communities of *Lemno minoris-Spirodeletum polyrrhizae* W. Koch 1954, *Lemnetum trisulcae* Knapp et Stoffers 1962 and *Ceratophyllo-Hydrocharidetum morsus-ranae* Pop. 1962 occur in the canal. The canals partly pass through the forest belonging to the ass. *Brachypodio silvaticae palustris-Quercetum* Erdeši. 1955 and *Genisto elatace-Quercetum* Horv. 1938 *subass alno-carpinetosum betuli* Vuk 1959 [15]. **The Kojšan canal** partly goes through the forest or arable land. The canal is overgrown with *Scirpo-Phragmitetum* W. Koch 26 *subass typhaetosum (angustifoliae-latifoliae)* Soó 73, and *subass. phragmitetosum* Schmalle 39. The forests belong to the ass. *Brachypodio silvaticae palustris-Quercetum* Erdeši. 1955. In the period when there is a canal with water, the community *Ceratophyllo-Hydrocharidetum morsus-ranae* Pop. 1962 occurs, and when the canal is up to 1.5 m deep, the *Nymphaeto-Stratiotetum aloidi* Jank. 74 or *Hottonietum palustris* Tx. 37 occur [14]. **Veliki Cerski kanal** is the most important hydrotechnical, regulatory watercourse in the region. It includes drainage systems and surface flows. It stretches from the foot of Mount Cer to the Sava River where it flows into Šabac. The sides of the canal are very steep and deep, partly overgrown with thick bushy vegetation. In the largest part of the canal, a zone of emergent vegetation of *Scirpo-Phragmitetum* W. Koch 26 *subass typhaetosum (angustifoliae-latifoliae*) Soó 73, or *subass. Phragmitetosum* Schmalle 39. Depending on the water depth, communities of *Lemno minoris-Spirodeletum polyrrhizae* W. Koch 1954, *Lemnetum trisulcae* Knapp et Stoffers 1962, *Ceratophyllo-Hydrocharidetum morsus-ranae* Pop. 1962 occur in the canal. **Virovlje** the forbidden area is overgrown with *Scirpo-Phragmitetum* W. Koch 26 *subass typhaetosum* (*angustifoliae-latifoliae*) Soó 73, while communities of *Lemno minoris-Spirodeletum polyrrhizae* W. Koch 1954 and *Ceratophyllo-Hydrocharidetum morsus-ranae* Pop. 1962, *Ceratophylletum demersi* (Soó 27) Hild. 1956 or *Lemnetum trisulcae* Knapp et Stoffers 1962 appear in the bed, depending on the water level [14]. **Češljuška bara** is the rest of the pistevina in the inundation plane, which dries up in the summer. The vegetation consists of the emergent zone *Scirpo-Phragmitetum* V. Koch 26 *subass typhaetosum (angustifoliae-latifoliae)* Soo 73, and in the water *Lemno minoris-Spirodeletum polirrhizae* V. Koch de 19S. 27) Hild. 1956 L. and *Lemnetum trisulcae* Knapp et Stoffers 1962. It is generally noted that its appearance largely depends on the water level. The largest number of findings (6) were in 2009, 2010, and 2023, when it was a favorable hydrological year with high water all year round. However, we must single out the year 2014, when there was a hydrological maximum

in Serbia with large floods throughout the country when there were hundred-year waters. And even though the hydrological situation was good to excellent in those years, the surface coverage under the *R. natans* species ranged from 20–30%, except at the Pačija bara site, where 70% of the 50x10 m surface was covered. The species *R. natans*, together with the species *L. trisulca*, *R. fluitans*, *Utricularia vulgaris* and *Wolffia arrhizal*, belongs to the type of species limited to oligotrophic and mesotrophic waters, with the fact that species typical for mesotrophic and eutrophic spore and stagnant waters (*Salvinia natans* and *S. polyrhiza*) occur as sporadic specimens in the canals [18]. The species spreads primarily by vegetative propagation as the plants divide [19]. In addition to natural habitats such as ephemeral floodplains, low-lying peatlands and the shores of the Zasavice swamps, the species also inhabits semi-natural and anthropogenic habitats such as canals, excavations, etc. The species is also found in zones where the water recedes and muddy areas of varying density remain, and on dry parts of the coast with sods and cracks in the soil, where the moss was on the sides of the sods or in cracks. The most common plants that are present in the immediate vicinity of this moss are: *Berula erecta* (Hudson) Coville; *Lythrum salicaria* L.; *Mentha aquatica* L.; *M. longifolia* (L.) Hudson; *Polygonum amphibium* L.; *P.aviculare* L.; *P. hydropiper* L.; *P. mite* Schrank.; *Rumex hydrolapatum* Huds.; *Alisma plantago-aquatica* L.; *Scirpus lacstris* L.; *S. erectum* L.; *Juncus effusus* L.; *Lemna minor* L.; *L. trisulca* L., *U. vulgaris* L., *Ceratophyllum demesum* L. Threatening factors are habitat destruction, changes in natural seasonal water level fluctuations due to climate change and water quality problems. The species does not tolerate excessive competition from eutrophication and natural ecosystem succession [4].

CONCLUSION

The species *Ricciocarpos natans* in Serbia has been recorded in a very small number of localities, which are mostly related to terrain north of the Danube and Sava rivers. Through our research in Mačva, the species was found in a total of 38 localities, of which 20 are within the reserve and 18 belong to the Northern Mačva region, with a total of 63 findings both within the protected area and outside it in Northern Mačva. The species is most often found in coastal vegetation *Scirpo-Phragmitetum* W. Koch 26 *subass. typhaetosum (angustifoliae-latifoliae*) Soó 73, *Lemno-Salvinion natans* Slavnić 56 and *Lemno minoris-Spirodeletum polyrrhizae* W. Koch 1954. For conservation purposes species, we need confirmation of the occurrence and distribution of the species in all parts of its known range, and that is why our data contribute to a better knowledge of its overall distribution in Serbia.

REFERENCES

[1] Campbell DH. The Structure and Development of Mosses and Ferns (revised ed.). London: The Macmillan Co.; 1918. pp. 39–41.

[2] Schuster RM. The Hepaticae and Anthocerotae of North America. Vol. VI. Chicago: Field Museum of Natural History; 1992. pp. 413–421.

[3] Schofield WB. Introduction to Bryology. New York: Macmillan; 1985. p. 310.

[4] Sergio C, Porley RD. *Ricciocarpos natans* (Europe assessment). The IUCN Red List of Threatened Species. 2019. Available from: www.iucnredlist. org/species/168892/87730535

[5] Hodgetts NG, Lockhart N. Checklist and country status of European bryophytes –update 2020. Irish Wildlife Manuals. National Parks and Wildlife Service, Department of Culture, Heritage and the Gaeltacht, Dublin, Ireland. 2020.

[6] Pantović, J., Veljić, M., Grdović, S., *et al*. Cryptogamie, bryologie 2020, 41, 35–48.

[7] Kitnaes KS, Plavac I, Vukelić VP, *et al*. Sites Important for Biodiversity along the Sava River in the frame of the LIFE 3rd project: "Protection of biodiversity of the Sava River Basin floodplains". Project Report, 2010, 1–166.

[8] Plavac I, Vukelić VP, Baranović PR, *et al*. Habitat Interpretation Sheets - Natura 2000 habitat types occurring along the Sava River in the frame of the LIFE 3rd project: "Protection of biodiversity of the Sava River Basin floodplains". Technical Document, 2009, 1–129.

[9] Pavletić Z. Flora mahovina Jugoslavije. Botanical Institute, University of Zagreb; 1968.

[10] Gajić M, Karadžić D, Flora ravnog Srema sa posebnim osvrtom na Obedsku baru Šumarski fakultet Beograd i ŠG Sremska Mitrovica; 1991, pp. 77–357.

[11] Javorka S, Magyar flóra (Flora Hungarica), Studium Budapest; 1924–1925, pp. 1307.

[12] Josifović M, Flora SR Srbije I-X, SANU, odeljenje Prirodno-matematičkih nauka, Beograd; 1970–1986, pp. 197–198.

[13] Dobretić V, Delić J, Perić R, *et al*. In: Zbornik radova „Zasavica 2012", naučno-stručni skup sa međunarodnim učešćem o istraživanju biodiverziteta, Serbia. 2012. p. 17–57.

[14] Dobretić V, Stojšić V, Delić J, *et al*. Specijalni rezervat prirode Zasavica-Predlog za stavljanje pod zaštitu kao zaštićeno područje I kategorije; Novi Sad, Serbia. 2012, p. 1–259.

[15] Erdeši J, Janjatović G. In: Zbornik Naučnog skupa posvećenog istraživanjima vodenih ekosistema i plavnih zona; Sremska Mitrovica, Serbia. 2001. p. 57–64.

[16] Stanković M. In: Zbornik radova VIII naučno-stručni skup o prirodnim vrednostima i zaštiti životne sredine, Zaječar, Serbia. 2000.

[17] Marković JĐ. Enciklopedijski geografski leksikon Jugoslavije. Sarajevo: Svjetlos; 1990.

[18] Cvijanović, Lj.D., Lakušić, V.D., Živković, M.M., *et al*. Tuexenia 2018, 38 269–286.

[19] Allison KW, John C. The Liverworts of New Zealand. Dunedin: University of Otago Press; 1975. pp. 243–245.

EcoTER'26
eco.tfbor.bg.ac.rs
32nd International Conference
Ecological Truth & Environmental Research
24–26 June 2026, Hotel Sunce,
Sokobanja, Serbia

Original Research

PROCESS OPTIMIZATION OF ZnO–ASSISTED PHOTOCATALYTIC DEGRADATION OF METHYL ORANGE USING RESPONSE SURFACE METHODOLOGY

DOI: 10.5937/EcoTER26403S

Sonja Stanković[1,a*], Milan Radovanović[1,b], Ana Simonović[1,c], Žaklina Tasić[1,d], Aleksandar Cvetković[1,e], Vladan Nedelkovski[1,f], Dragana Medić[1,g]

[1] University of Belgrade, Technical Faculty in Bor, Vojske Jugoslavije 12, 19210 Bor, SERBIA

[a] https://orcid.org/0000-0003-0745-5422 [b] https://orcid.org/0000-0002-5175-6022

[c] https://orcid.org/0000-0003-2392-0048 [d] https://orcid.org/0000-0001-6544-1980

[e] https://orcid.org/0009-0003-5184-6874 [f] https://orcid.org/0000-0001-7724-1118

[g] https://orcid.org/0000-0001-9980-5949

Abstract

This study examines the photocatalytic degradation of methyl orange (MO) using ZnO nanoparticles, focusing on the effects of key operational parameters and process optimization through Response Surface Methodology (RSM). A Box–Behnken design was used to assess the impact of initial MO concentration, UV irradiation time, and catalyst dosage on degradation efficiency. Based on the experimental results, a quadratic regression model was developed and validated. The model showed a high coefficient of determination (R^2 = 0.9361), indicating good agreement between experimental and predicted values. Analysis of variance (ANOVA) identified the initial MO concentration as the most influential factor among the linear, interaction, and quadratic terms evaluated. Numerical optimization identified an initial MO concentration of 1 ppm, a UV irradiation time of 60 min, and a ZnO catalyst dosage of 0.2 g.

Keywords: ZnO, photocatalysis, methyl orange, optimization, RSM.

INTRODUCTION

Water pollution by organic pollutants is a significant environmental problem due to their adverse effects on aquatic ecosystems and human health. Synthetic azo dyes are particularly notable among these pollutants, as their widespread use in the textile, pharmaceutical, and other industries often leads to their presence in wastewater. Methyl orange (MO) is one of the most commonly used azo dyes. Because of its chemical stability and resistance to biodegradation, removing this compound by conventional methods can be difficult [1,2]. Therefore, photocatalysis is considered one of the most promising advanced oxidation processes for removing organic pollutants from water [1]. This process enables the decomposition of organic compounds under light in the presence of a semiconductor photocatalyst. Among various photocatalytic materials, ZnO has attracted considerable attention for its low cost, nontoxicity, chemical stability, and high exciton binding energy

* *sstankovic@tfbor.bg.ac.rs*

[3,4]. The efficiency of photocatalytic degradation depends on several process parameters, including the initial contaminant concentration, catalyst amount, and irradiation time [5].

This work aims to investigate the influence of process parameters (initial MO concentration, catalyst dosage, and UV irradiation time) on the efficiency of photocatalytic degradation of MO in the presence of ZnO as a catalyst, with particular emphasis on process optimization using response surface methodology (RSM).

MATERIALS AND METHODS

Synthesis of ZnO Nanoparticles

ZnO nanoparticles (ZnO NPs) were synthesized by a mechanochemical method using an agate mortar and subsequent calcination at 700°C. For the synthesis, zinc acetate dihydrate (NRK Inženjering, Belgrade, Serbia) and oxalic acid dihydrate (NRK Inženjering, Belgrade, Serbia) were used in analytical grade without further purification.

Photocatalytic measurements

Methyl orange was used to evaluate the photocatalytic activity of ZnO nanoparticles. The photocatalytic reaction was conducted in a homemade photoreactor under UV radiation (92 W). For laboratory tests, 30 mL of methyl orange solution was used. After the photocatalytic reaction, the solution was centrifuged and then analyzed with a UV–Vis spectrophotometer (Merck Spectroquant Pharo 300, Rahway, NJ, USA) at a wavelength of 502 nm.

Optimization process

Design–Expert software with the Box–Behnken design was used to examine the influence of process parameters on the efficiency of photocatalytic degradation of methyl orange and to optimize the process. The effects of three factors at three levels were studied: initial concentration of methyl orange (1, 50, and 100 ppm), UV irradiation time (30, 60, and 180 min), and catalyst dosage (0.05, 0.1, and 0.2 g). The Table 1 shows the range and levels of the three independent variables investigated.

Table 1 *Experimental factors and range levels in the experimental design*

Factors	Range level		
	-1	0	1
Initial concentration of methyl orange, C_0 (ppm)	1	50	100
Irridation time, t (min)	30	60	180
Catalyst dosage, m (g)	0.05	0.1	0.2

RESULTS AND DISCUSSION

Response Surface Methodology is a statistical and mathematical tool widely used to evaluate the relationship between process variables and the corresponding response. Unlike conventional optimization approaches, which vary one parameter while keeping all other conditions constant, RSM allows simultaneous examination of several independent variables. This approach enables more efficient interpretation of experimental results while significantly reducing the number of required experiments, experimental time, and reagent consumption. Among the various experimental designs used in RSM, the Box–Behnken design has received considerable attention in photocatalytic studies due to its efficient experimental arrangement,

satisfactory predictive capability, and good agreement between predicted and experimental values [6]. The effects of initial concentration of MO, UV irradiation time, and catalyst dosage on the efficiency of photocatalytic degradation of methyl orange were studied. Seventeen experiments were performed in random order. The center point was repeated several times to estimate errors. The Box–Behnken matrix with experimental and model–predicted methyl orange degradation efficiencies is shown in Table 2.

Table 2 *The Box–Behnken matrix with experimental and predicted degradation efficiencies of MO*

Run	Coded factor values			Actual factor values			E (%)	
	C_0	t	m	C_0	t	m	Experimental	Predicted
1	0	1	-1	50	180	0.05	63.67	56.5988
2	0	0	0	50	60	0.1	80.43	80.43
3	-1	1	0	1	180	0.1	100	100
4	1	-1	0	100	30	0.1	21.33	11.1613
5	1	0	-1	100	60	0.05	28.45	25.285
6	0	0	0	50	60	0.1	80.43	80.43
7	-1	0	-1	1	60	0.05	100	96.9025
8	0	1	1	50	180	0.2	94.64	81.3063
9	-1	-1	0	1	30	0.1	95.83	85.5937
10	0	0	0	50	60	0.1	80.43	80.43
11	1	0	1	100	60	0.2	35.11	38.2075
12	0	0	0	50	60	0.1	80.43	80.43
13	-1	0	1	1	60	0.2	100	100
14	0	-1	1	50	30	0.2	28.4	35.4712
15	0	-1	-1	50	30	0.05	27.66	40.9937
16	0	0	0	50	60	0.1	80.43	80.43
17	1	1	0	100	180	0.1	37.79	48.0262

Figure 1 shows a comparison of the experimentally obtained and model–predicted efficiency of photocatalytic decomposition of MO. All points are closely distributed around the regression line, indicating good agreement between the experimentally determined and model–predicted values [6,7].

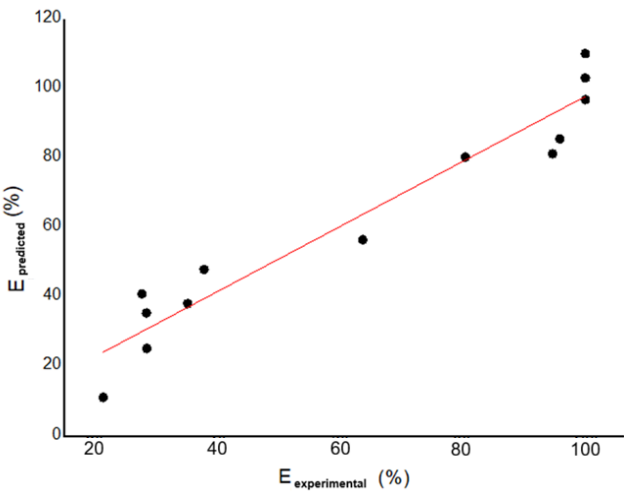

Figure 1 *Comparison of experimental and model–predicted methyl orange degradation efficiency*

To evaluate the adequacy and significance of the developed model, the experimental results were statistically analyzed using analysis of variance (ANOVA) [7]. The ANOVA results confirmed that the proposed quadratic model is statistically significant (Table 3).

Table 3 *Analysis of variance (ANOVA) for methyl orange removal with ZnO–NP*

Source	Sum of Squares	df	Mean Square	F–value	p–value	
Model	13342.59	9	1482.51	11.39	0.0021	significant
Co	9326.37	1	9326.37	71.65	< 0.0001	
t	1887.44	1	1887.44	14.50	0.0066	
m	184.03	1	184.03	1.41	0.2732	
$C_0 \cdot t$	37.76	1	37.76	0.2901	0.6069	
$C_0 \cdot m$	11.09	1	11.09	0.0852	0.7788	
$t \cdot m$	228.46	1	228.46	1.76	0.2268	
${C_0}^2$	20.33	1	20.33	0.1562	0.7044	
t^2	884.65	1	884.65	6.80	0.0351	
m^2	641.42	1	641.42	4.93	0.0619	
Residual	911.17	7	130.17			
Lack of Fit	911.17	3	303.72			
Pure Error	0.0000	4	0.0000			
Cor Total	14253.77	16				
$\mathbf{R^2}$	0.9361					
$\mathbf{R^2_{Adjusted}}$	0.8539					
Std. Dev.	11.41					
Adeq Precision	11.3146					

Based on the obtained F–values, the initial concentration of methyl orange had the strongest influence on photocatalytic degradation efficiency, followed by UV irradiation time and the quadratic effect of irradiation time. The interaction between the initial concentration of MO and catalyst dosage had the least impact on photocatalytic degradation efficiency. Additionally, probability values (p–values) lower than 0.05 for the investigated factors C_0, t, and t^2 indicate that these factors significantly influence MO degradation efficiency.

Model validation is an important step in assessing the ability to reliably predict responses from experimental data. The robustness of the developed model was evaluated by the experimentally determined coefficient of determination (R^2) and the adjusted coefficient of determination (R^2 adjusted) [8]. Both coefficients, with values greater than 0.80, indicate good agreement between the experimental and predicted values, confirming the model's satisfactory predictive ability and adequacy. Additionally, the adequate precision was 11.3146, well above the recommended value of 4. This result confirms an appropriate signal–to–noise ratio and indicates the reliability, applicability, and suitability of the model for predicting responses within the examined experimental domain [6].

Design Expert software was used to create 3D response surface plots (Figure 2), which show the influence of interactions among the investigated parameters on MO degradation efficiency. During the examination of the interaction of process parameters on the efficiency of photocatalytic decomposition of MO, one independent variable was kept constant while the

influence of the interaction between the other two independent variables on the efficiency of photocatalytic decomposition was examined.

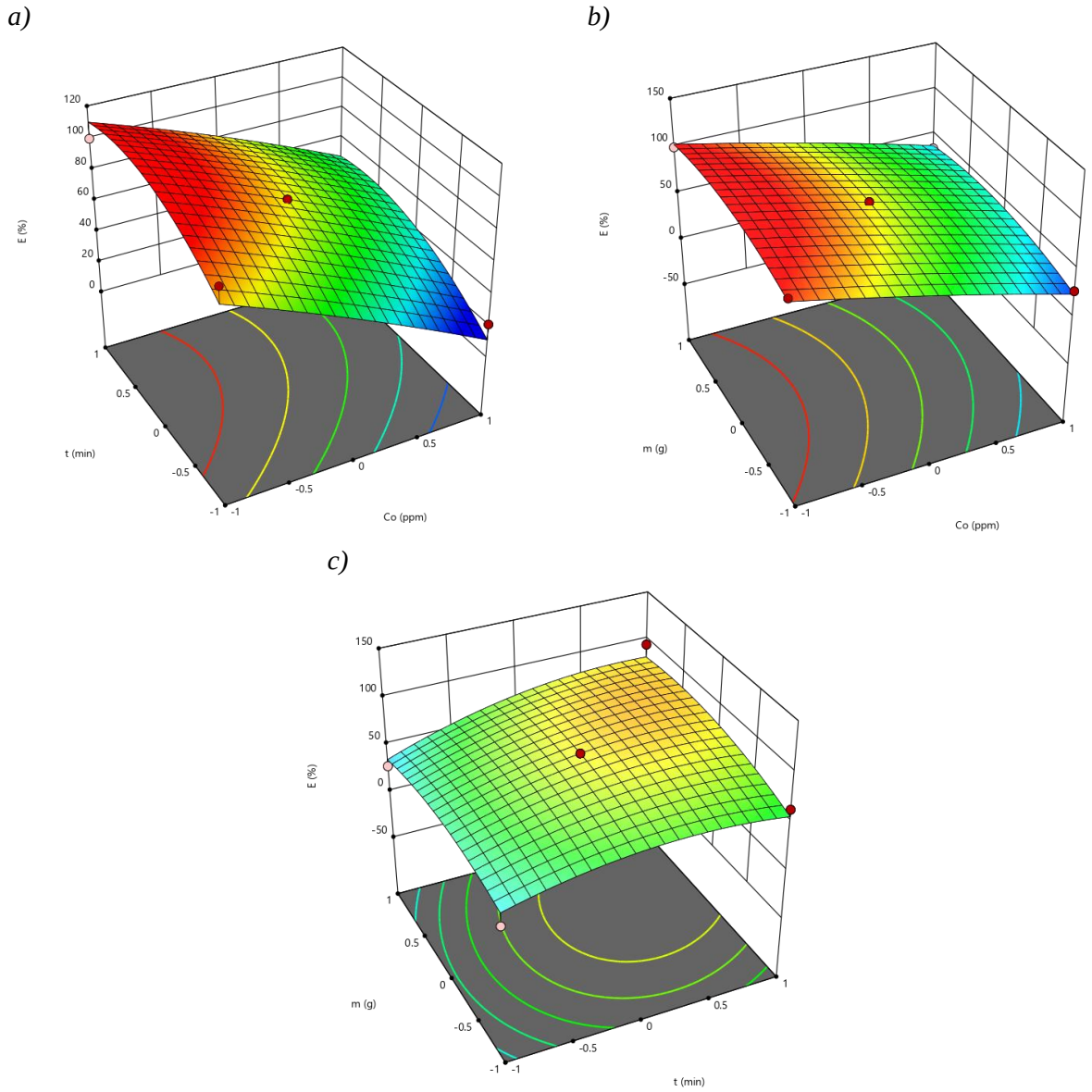

Figure 2 *3D response surface plots showing the effects of (a) initial MO concentration and UV irradiation time; (b) initial MO concentration and catalyst dosage;, and (c) catalyst dosage and UV irradiation time on the photocatalytic degradation efficiency of methyl orange*

The effect of the interaction between the initial concentration of MO and UV irradiation time on the efficiency of photocatalytic degradation at a constant catalyst dosage (0.1 g) is shown in Figure 2a. Increasing the UV irradiation time and decreasing the initial MO concentration both lead to higher degradation efficiency. This can be attributed to the greater availability of hydroxyl radicals (OH•) relative to the number of pollutant molecules, enabling more efficient degradation of MO. In contrast, at higher initial MO concentrations, more reactive species are required. However, with a constant catalyst dosage, the amount of generated OH• radicals is limited, resulting in lower degradation efficiency [9].

Figure 2b shows the effect of the initial concentration of MO and the catalyst dosage on the efficiency of MO photocatalytic degradation. Increasing the catalyst dosage while simultaneously decreasing the initial MO concentration leads to higher degradation efficiency. A larger catalyst dosage provides more active sites and excited charge carriers, promoting the formation of reactive radicals and enhancing the photocatalytic degradation process. Similar results were reported by Assimeddine et al. [10].

The effect of the interaction between catalyst dosage and UV irradiation time is shown in Figure 2c. The results indicate that increasing both factors positively affects MO degradation efficiency. Extending the irradiation time and increasing the catalyst dosage generate more OH• radicals, which accelerate the decomposition of methyl orange molecules and increase the efficiency of the photocatalytic process.

Numerical optimization determined the optimal process conditions: an initial MO concentration of 1 ppm, a UV irradiation time of 60 minutes, and a catalyst dosage of 0.2 g. Under these conditions, 100% photocatalytic degradation efficiency was achieved within the tested experimental range.

CONCLUSION

In this study, Response Surface Methodology was used to investigate the effects of initial MO concentration, UV irradiation time, and catalyst dosage on MO photocatalytic degradation efficiency and to determine the optimal operating conditions. The quadratic model showed good agreement with the experimental results, as indicated by high coefficients of determination and satisfactory adequacy of precision values, demonstrating its reliability for predicting photocatalytic degradation efficiency within the studied experimental domain. According to the ANOVA results, the initial MO concentration was the most influential factor affecting degradation efficiency. Numerical optimization identified the optimal conditions as an initial MO concentration of 1 ppm, a UV irradiation time of 60 min, and a ZnO catalyst dosage of 0.2 g. Under these conditions, 100% degradation of methyl orange was achieved, confirming the suitability of ZnO nanoparticles as an effective photocatalyst for dye removal.

ACKNOWLEDGEMENT

The authors are grateful to the Ministry of Science, Technological Development and Innovation of the Republic of Serbia for financial support according to the contract with registration No. 451–03–34/2026–03/200131.

REFERENCES

[1] Alhussain, H.,Ferjani, H., Ozewo, O.A., *et al*. Inorg. Chem. Commun. 2024, 162, 112272.

[2] Aldama–Huerta, O.A., Medellin–Castillo, N.A., Marin, F.C., *et al.* Appl. Sci. 2025, 15 (22) 12084.

[3] Shaba, E.Y., Jacob, J.O., Tijani, J.O., *et al.* Appl. Water Sci. 2021, 11, 48.

[4] Al–Rawashdeh, N.A.F., Allabadi, O., Aljarrah, M.T. *ACS Omega* 2020, *5*, 28046–82055.

[5] Tan, S.N., Zuen, M.L., Ramli, R.A., GAC 2025, 12, 100230.

[6] Stanković, S., Radovanović, M., Đorđievski, S. *et al.* Metals 2026, 16 (1) 71.

[7] Al, C., Zhou, D., Wang, Q., *et al.* Sol. Energy 2015, 13, 34–42.

[8] Moussa, S.B. J. Photochem. Photobiol. A. Chem. 2024, 447, 115284.

[9] Parida, K.M., Parija, S. Sol. Energy. 2006, 80, 1048–1054.

[10] Assimeddine, M., Farid, Z., Abdennouri, M., *et al.* Environ. Sci. Pollut. Res. 2023, 30, 62494–62507.

EcoTER'26
eco.tfbor.bg.ac.rs
32nd International Conference
Ecological Truth & Environmental Research
24–26 June 2026, Hotel Sunce,
Sokobanja, Serbia

Original Research

CHARACTERIZATION OF THE Sn78Bi22 ALLOY AS AN ENVIRONMENTALLY FRIENDLY LEAD-FREE SOLDER

DOI: 10.5937/EcoTER26410S

Uroš Stamenković[1,a*], Ivana Marković[1,b], Dragan Manasijević[1,c], Kristina Božinović[1,d], Milan Nedeljković[1,e], Avram Kovačević[1,f]

University of Belgrade, Technical Faculty in Bor, Vojske Jugoslavije 12, 19210 Bor, SERBIA

[a] https://orcid.org/0000-0002-7579-2159 [b] https://orcid.org/0000-0003-4431-9921

[c] https://orcid.org/0000-0002-7828-8994 [d] https://orcid.org/0000-0002-9834-448X

[e] https://orcid.org/0000-0002-7927-1334 [f] https://orcid.org/0000-0003-4009-4876

Abstract

The development of reliable lead-free solder alloys remains essential for applications in the electronics industry. This paper investigates the mechanical, electrical, and microstructural properties of a Sn78Bi22 solder alloy. The alloy was prepared by melting and casting, followed by a homogenization heat treatment. Tensile testing, Vickers microhardness measurements, electrical conductivity testing, and SEM/EDS microstructural analysis were performed at room temperature. The investigated alloy exhibited enhanced ultimate tensile strength (~93 MPa) and microhardness (45.5 HV0.05) compared with pure Sn, while electrical conductivity decreased to 5.4 MS/m. These changes were attributed to solid-solution strengthening, grain refinement, and the formation of a Bi-rich secondary phase, which also promoted brittle fracture during tensile testing. Microstructural observations revealed a Sn matrix with finely distributed Bi-rich phases, particularly along grain boundaries. The results contribute additional experimental data on the mechanical, electrical, and microstructural characteristics of non-eutectic Sn–Bi solder alloys.

Keywords: Sn78Bi22 alloy, mechanical properties, electrical conductivity, microstructure.

INTRODUCTION

Sn–Pb solders have been extensively used in the electronics industry for decades due to their excellent solderability, low melting temperature, low cost, and favourable mechanical properties. However, lead is unequivocally harmful to human health and the environment, necessitating the gradual elimination of lead-containing materials from electronic products. With the implementation of the Waste Electrical and Electronic Equipment (WEEE) and Restriction of Hazardous Substances (RoHS) directives, the European Union mandated the use of lead-free solder alloys in electronic assemblies [1,2].

In response to these regulations, numerous lead-free solder systems have been investigated over the past two decades, including Sn–Cu, Sn–In, Sn–Zn, Sn–Ag–Cu, and Sn–Bi alloys [2]. Among these candidates, the Sn–Bi system has attracted considerable attention due to its relatively low melting temperature and good wettability. In particular, the eutectic Sn58Bi

* *ustamenkovic@tfbor.bg.ac.rs*

alloy has been extensively studied and reported in the literature, as summarized by Kamaruzzaman *et al*. [3]. Despite its industrial applicability, the high bismuth content in eutectic Sn–Bi alloys leads to pronounced brittleness, which represents a significant drawback in terms of mechanical reliability and susceptibility to brittle fracture in solder joints.

To address these limitations, recent research efforts have increasingly focused on non-eutectic Sn–Bi alloys with lower bismuth contents (typically up to ~20 wt.% Bi), aiming to achieve a balance between mechanical strength, ductility, and functional properties. Shen investigated the mechanical strength and thermal behaviour of Sn–2.5Bi and Sn–5Bi alloys [4]. Yang *et al*. examined the effects of graphene nanosheets (GNS) on the microstructure and properties of Sn–20Bi solder alloys [2]. Lai *et al*. focused on non-eutectic Sn–Bi alloys, with particular emphasis on microstructural evolution and fracture behaviour [5].

Furthermore, Wang *et al*. reviewed recent progress in the development of low-temperature Sn–Bi solders and concluded that the intrinsic brittleness of bismuth remains a critical challenge, especially under mechanical shock loading in electronic devices. In addition, segregation of Bi-rich phases and excessive growth of the intermetallic compound (IMC) layer were identified as major reliability concerns that can compromise the long-term performance of solder joints [6].

Although substantial research has been devoted to the mechanical, microstructural, and physical properties of non-eutectic Sn–Bi solder alloys, further systematic investigations are still required to fully understand the structure–property relationships in this alloy system. In this context, the present study contributes additional experimental data and analysis to the existing body of knowledge on non-eutectic Sn–Bi solder alloys.

MATERIALS AND METHODS

Alloy preparation

Commercially pure tin (99.9 wt.%) and bismuth (99.9 wt.%) were used to prepare the Sn78Bi22 alloy. The metallic granules were placed in a graphite crucible and melted in a muffle furnace at 350 °C. During melting, the crucible was covered with a carbon piece to minimize oxidation. After complete melting, the alloy was mechanically stirred using a pure graphite stirrer to ensure chemical homogeneity.

The molten alloy was subsequently cast into a steel mold with a diameter of 13 mm. The as-cast samples were then homogenized in an electric furnace at 150 °C for 20 h to promote a more uniform distribution of Bi within the Sn matrix, followed by air cooling to room temperature.

After homogenization, the samples were sectioned for further characterization using a Struers Mesotom metallographic cutting machine.

Tensile strength measurements

To determine the tensile strength, a 5 mm diameter wire of the Sn78Bi22 alloy was prepared. The homogenized cast rod (initial diameter 13 mm) was gradually reduced to 5 mm using a calibrated Joliot rolling mill. The reduction process involved cold rolling with intermediate annealing steps to prevent excessive strain accumulation and cracking.

After reaching the final diameter, the wire was subjected to a final annealing treatment to eliminate residual deformation and ensure that the mechanical properties were representative of the homogenized state. Tensile testing was performed using a Mohr–Federhaff–Losenhausen universal testing machine.

Microhardness measurements

Microhardness measurements were carried out using a PMT-3 microhardness tester employing the Vickers method, in accordance with ASTM E384 [7]. A load of 0.5 N and a dwell time of 15 s were applied. Prior to testing, the sample surface was polished to a mirror finish. Five indentations were made at different locations on the sample surface, and the reported microhardness value represents the average of these measurements.

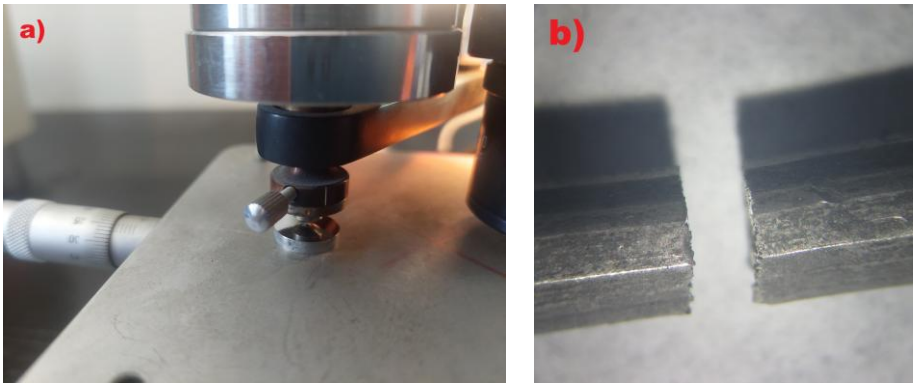

Figure 1 *Different measurements performed on the Sn78Bi22 alloy: (a) Vickers microhardness indentation on a polished surface; (b) fractured wire specimen after tensile testing, indicating brittle fracture behaviour*

Electrical conductivity measurements

Electrical conductivity was measured using a Foerster Sigmatest 2.063 conductivity tester. Three measurements were performed on each sample, and the average value was reported.

Microstructural characterization

Samples for microstructural analysis were prepared using standard metallographic procedures. Wet grinding was performed using SiC papers with grit sizes of #400, #600, #800, #1000, #2000, and #3000, followed by polishing with Al_2O_3 suspensions of 0.3 µm and 0.05 µm particle size.

The microstructure was revealed by chemical etching for 15 s using a solution composed of 2 ml HCl, 2 ml HNO_3, and 96 ml C_2H_5OH. Scanning electron microscopy (SEM) and energy-dispersive spectroscopy (EDS) analyses were conducted using a Tescan Vega 3 LMU scanning electron microscope equipped with an Oxford Instruments X-act EDS detector.

RESULTS AND DISCUSSION

Tensile strength is one of the most critical mechanical properties in solder materials, as it directly determines the ability of solder joints to withstand deformation and various types of mechanical loading during service. Figure 2 presents the engineering stress–strain curve of

the investigated Sn78Bi22 alloy. Pure β-tin is known to exhibit very low tensile strength at ambient conditions; reported ultimate tensile strength (UTS) values of approximately 16 MPa have been obtained from quasi-static tensile testing of bulk polycrystalline Sn, as reported by Zhou *et al*. [8].

The addition of bismuth leads to a pronounced improvement in tensile strength, as clearly evidenced in Figure 2. In the present study, the Sn78Bi22 alloy exhibited an ultimate tensile strength of approximately 93 MPa. This substantial increase in UTS is primarily attributed to the incorporation of 22 wt.% Bi, which promotes grain refinement of the Sn-rich matrix, solid-solution strengthening due to partial Bi solubility in Sn, and dispersion strengthening associated with the formation of finely distributed Bi-rich phases. These Bi-induced microstructural and compositional features act as effective obstacles to dislocation motion, thereby significantly enhancing the tensile strength of the alloy [5]. Similar trends have been reported in the literature: Yang *et al.* [2] observed slightly lower UTS values for Sn80Bi20 solder alloys, whereas Lai *et al.* [5] reported UTS values close to 95 MPa, which is in good agreement with the results obtained in the present work.

However, the supersaturation of the Sn matrix with the brittle Bi phase, while beneficial for strength enhancement, also promotes brittle fracture behaviour, as reported by Zhou *et al.* [9] and as observed on the fractured tensile specimen shown in Figure 1b.

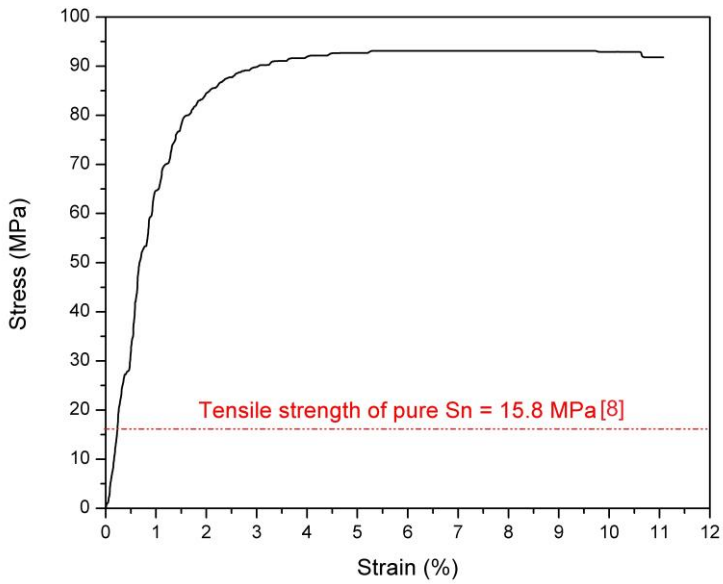

Figure 2 *Stress-strain curve of the investigated Sn78Bi22 alloy*

The microhardness results are consistent with the tensile strength measurements. Pure β-Sn exhibits very low hardness, with reported values in the range of 8–10 HV, as documented in the literature [4,10]. In the present study, the Sn78Bi22 alloy exhibited a significantly higher microhardness of 45.5 $HV_{0.05}$.

This pronounced increase in hardness is attributed to the same strengthening mechanisms identified in the tensile investigation, namely grain refinement, solid-solution strengthening, and dispersion strengthening induced by Bi addition. For comparison, Shen *et al.* [4] reported

a hardness of approximately 20 HV for Sn95Bi5, while Thongchai *et al*. [10] reported values of around 17 HV for Sn96Bi4 alloys. Considering both the literature data and the approximately sixfold increase in ultimate tensile strength relative to pure Sn (Figure 2), the observed rise in microhardness is in good agreement with the enhanced mechanical performance of the Sn78Bi22 alloy.

Electrical conductivity is a critical property in solder technology, as solder joints are required to efficiently transmit electrical power and signals between electronic components. Pure tin exhibits relatively low electrical conductivity compared to copper, with reported values of approximately 15–16% IACS, corresponding to ~8–9 MS/m at room temperature, depending on purity and microstructural condition. In contrast, bismuth possesses a significantly lower electrical conductivity, reported to be approximately 0.77 MS/m [11].

In the present study, the Sn78Bi22 alloy exhibited an electrical conductivity of 5.4 MS/m, which lies between the conductivity values of pure Sn and pure Bi. The observed reduction in electrical conductivity relative to pure Sn is expected and can be attributed to several alloying- and microstructure-related factors. First, the substantial atomic size mismatch between Sn and Bi introduces lattice distortion, which enhances electron scattering. Second, the addition of Bi leads to the formation of a supersaturated solid solution of Bi in the Sn matrix, further increasing scattering of conduction electrons. Third, the presence of Bi-rich phases within the microstructure introduces additional phase boundaries that act as electron scattering centres. Finally, Bi-induced grain refinement increases the total grain boundary area, which also contributes to increased resistivity.

Collectively, these effects result in an increase in electrical resistivity in accordance with Matthiessen's rule, whereby different scattering mechanisms contribute additively to the total resistivity of the alloy [12]. Similar reductions in electrical conductivity with increasing Bi content in Sn–Bi solder alloys have also been reported by other authors, confirming the trends observed in the present work [13,14].

Microstructural analysis further supports the previously discussed mechanical and electrical property trends. Figure 3 presents the SEM–EDS characterization of the Sn78Bi22 alloy. The microstructure consists of a supersaturated Sn–rich matrix with relatively fine grains, within which a Bi-rich phase is distributed throughout the structure, preferentially along grain boundaries. In backscattered electron (BSE) images, the Bi-rich phase appears brighter due to its higher atomic number and is identified by EDS spectra 1 and 3, whereas the β-Sn matrix corresponds to spectrum 2, as confirmed by the EDS analysis summarized in Table 1.

Such a microstructural configuration, characterized by a Sn-rich matrix reinforced by Bi-rich regions at grain boundaries and within the matrix, is consistent with observations reported in the literature for hypoeutectic Sn–Bi solder alloys [2,4,5,9,10].

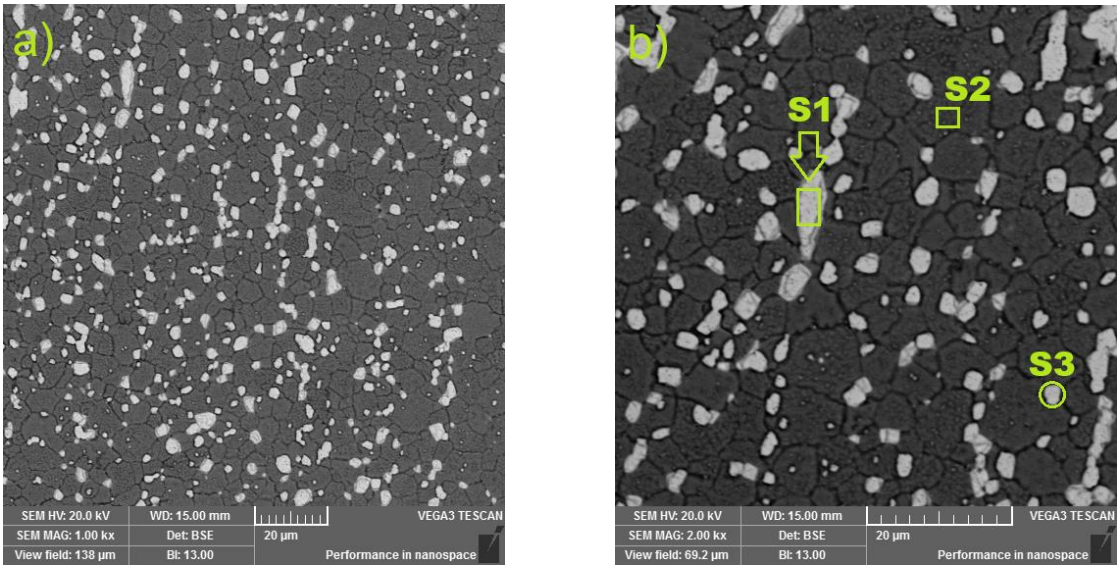

Figure 3 *SEM–EDS analysis of Sn78Bi22 alloy: a) x1000 magnification; b) x2000 magnification*

Table 1 *EDS analysis of the Sn78Bi22 sample*

Spectrum	*Bi*	*Sn*
Spectrum 1	95.31	4.69
Spectrum 2	2.95	97.05
Spectrum 3	84.6	15.4

CONCLUSIONS

In this study, the Sn78Bi22 solder alloy was systematically investigated with respect to its mechanical, electrical, and microstructural properties. The addition of bismuth resulted in a pronounced increase in ultimate tensile strength and microhardness, accompanied by a reduction in electrical conductivity when compared to pure tin. These changes in properties are attributed to several Bi-induced strengthening mechanisms, including solid-solution strengthening of the Sn-rich matrix, the formation of a Bi-rich secondary phase, and grain refinement effects.

Microstructural analysis confirmed the presence of a supersaturated Sn-rich matrix with Bi-rich phases distributed throughout the microstructure, particularly along grain boundaries, providing microstructural evidence that supports the observed mechanical strengthening and electrical conductivity trends.

ACKNOWLEDGEMENT

The authors are grateful to the Ministry of Science, Technological Development and Innovation of the Republic of Serbia for financial support according to the contract with registration No. 451-03-34/2026-03/ 200131.

REFERENCES

[1] Zhang, L., Tu, K.N. Mater. Sci. Eng. R Rep. 2014, 82, 1–32.

[2] Yang, W., Qin, W., Wu, J., *et al*. Materials. 2023, 16, 1550.

[3] Kamaruzzaman, L.S., Goh, Y. Solder. Surf. Mt. Technol. 2022, 34 (5), 300–318.

[4] Shen, Y.-A. JOM. 2023, 75 (11), 4922–4930.

[5] Lai, Z., Ye, D. J. Mater. Sci.: Mater. Electron. 2016, 27, 3182–3192.

[6] Wang, F., Chen, H., Huang, Y. *et al*. J. Mater. Sci.: Mater. Electron. 2019, 30, 3222–3243.

[7] ASTM E384–22. Standard Test Method for Microindentation Hardness of Materials. ASTM International, 2022. Accessed 23 January 2026. Available from: https://store.astm.org/e0384-22.html

[8] Zhou, J., Tan, X.F., McDonald, S.D. *et. al.* Materials. 2022, 15 (23), 8321.

[9] Zhou, S., Zhang, Y., Duan, J. *et al*. RSC Adv. 2023, 13, 35161–35171.

[10] Thongchai, C., Lohwongwatana, B., Puncreobutr, C. *et. al*. Eng. J. 2018, 22 (5), 171–183.

[11] Electrical Conductivity of the elements. Accessed 23 January 2026. Available from: https://periodictable.com/Properties/A/ElectricalConductivity.an.html

[12] Callister, Jr. W.D., Materials Science and Engineering: An Introduction, 3rd edn. New York: John Wiley & Sons, 1994.

[13] Lv, X., Pan, Z., Liu, Y. *et al*. Metals. 2025, 15, 157.

[14] Tan, X. F., Hao, Q., Zhou, J. *et al*. J. Electron. Mater. 2024, 53, 1183–1191.

EcoTER'26
eco.tfbor.bg.ac.rs
32nd International Conference
Ecological Truth & Environmental Research
24–26 June 2026, Hotel Sunce,
Sokobanja, Serbia

Original Research

CHANGE IN METAL REMOVAL DEGREE DURING COPPER ION BIOSORPTION ONTO RAW AND CALCINED CHICKEN EGGSHELLS

DOI: 10.5937/EcoTER26417M

Miljan Marković[1,a*], Milan Gorgievski[1,b], Vesna Grekulović[1,c], Nada Štrbac[1,d], Marina Marković[1,e], Kristina Božinović[1,f], Milica Zdravković[1,g]

[1] University of Belgrade, Technical Faculty in Bor, Vojske Jugoslavije 12, 19210 Bor, SERBIA

[a] https://orcid.org/0000-0002-4734-1481 [b] https://orcid.org/0000-0002-9899-719X

[c] https://orcid.org/0000-0001-6871-4016 [d] https://orcid.org/0000-0003-4836-1350

[e] https://orcid.org/0009-0007-7553-6423 [f] https://orcid.org/0000-0002-9834-448X

[g] https://orcid.org/0000-0001-9488-9151

Abstract

Copper ion biosorption using raw and calcined chicken eggshells as biosorbents was conducted. The change in metal removal degree over time was monitored. Biosorption experiments were carried out in batch conditions for 90 minutes, as this duration is considered sufficient to reach equilibrium between phases. The experiments were conducted at three temperatures: 25 °C, 30 °C, and 35 °C. The results showed that the Cu^{2+} removal degree increased with time for both raw and calcined chicken eggshells. The results also indicated that system temperature significantly affects the efficiency of the biosorption process. Copper ion biosorption onto raw eggshells was considerably faster and more efficient, with a higher copper removal degree at higher temperatures. Biosorption onto calcined eggshells was less dependent on temperature, with Cu^{2+} removal being slightly faster at 35 °C, but the overall efficiency remained the same at all temperatures.

Keywords: biosorption, metal removal degree, raw chicken eggshells, calcined chicken eggshells.

INTRODUCTION

Heavy metal water pollution is considered a serious problem due to its toxic effects on the environment. Many industries, including mining and metallurgy, generate significant amounts of wastewater and contribute to environmental pollution [1]. Various conventional methods are employed at the industrial level to treat wastewater, including adsorption, ion exchange, precipitation, cementation, and others. However, these methods have certain disadvantages, such as insufficient metal removal, toxic sludge generation, and high economic cost. In this context, adsorption of heavy metals using natural biosorbents, or biosorption, represents a potential method for wastewater treatment. Figure 1 shows the operational ranges of selected wastewater treatment technologies. It can be seen that biosorption is a potential alternative to conventional methods in the low concentration range, between 0.001 and 100 mg dm^{-3} [2–5].

* *mmarkovic@tfbor.bg.ac.rs*

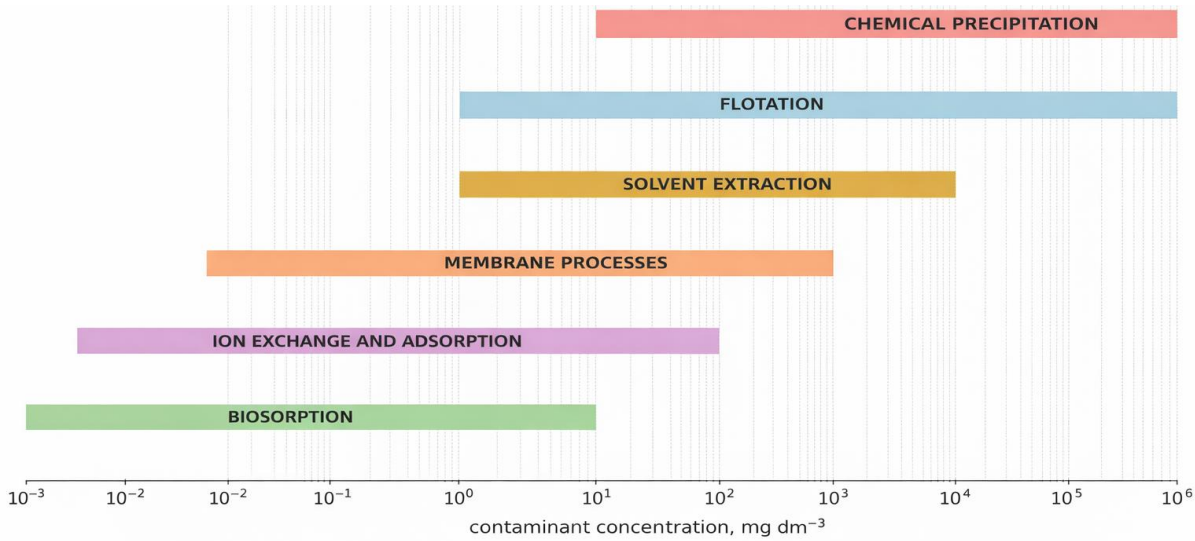

Figure 1 *Operational ranges of certain wastewater treatment methods [5]*

Biosorption is a physicochemical process for removing substances from a solution using biological materials as adsorbents. It relies on the ability of certain biomass to bind ions or molecules from aqueous solutions through various physicochemical and metabolic mechanisms [4,6].

The biosorption process offers several advantages over conventional wastewater treatment methods, including [7]:

- Low cost,
- Ability to remove heavy metals from wastewater at low concentrations,
- Ability to remove multiple heavy metals simultaneously,
- Capacity to treat large volumes of wastewater,
- No need to add chemicals,
- Functionality across a wide range of operational conditions, including process temperature, solution pH, and the presence of other metals,
- Low amounts of generated waste and toxic materials.

However, this process also has certain disadvantages, including [7]:

- Saturation of active sites within biosorbents,
- In some cases, reversible sorption of metal ions on the biomass.

MATERIALS AND METHODS

Chicken eggshells used for biosorbent preparation were collected from households in eastern Serbia. The collected raw chicken eggshells (RCE) were ground and sieved using laboratory sieves, and the (-1+0.4 mm) fraction was used for biosorption experiments. Calcined chicken eggshells (CCE) were prepared by calcining the raw chicken eggshells at 900 °C in a chamber furnace. Figures 2 and 3 show the raw and calcined chicken eggshell samples.

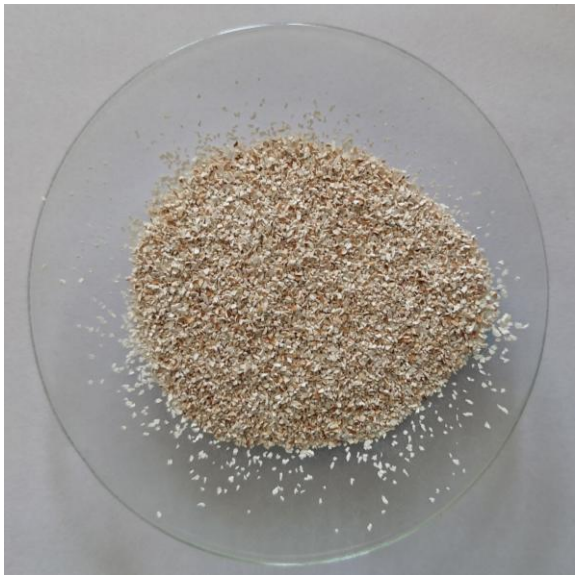

Figure 2 *Raw chicken eggshells (RCE)*

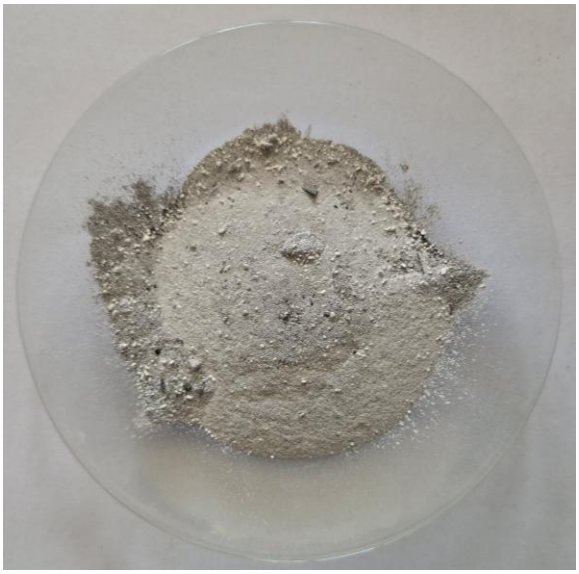

Figure 3 *Calcined chicken eggshells (CCE)*

Synthetic Cu^{2+} ion solutions were used for the biosorption experiments. The RCE and CCE samples were rinsed with distilled water before the biosorption experiments. Cu^{2+} concentrations in the solutions were determined using a Spectroquant Pharo 300 (Merck) spectrophotometer. The degree of copper removal was calculated based on the material balance using the following equation:

$$RD\ \% = \left(1 - \frac{C_{(t)}}{C_i}\right) \cdot 100 \qquad (1)$$

where: C_i and $C_{(t)}$ – are the initial and current copper ion concentrations, at time t (g dm^{-3});
RD % – is the metal removal degree (%).

RESULTS AND DISCUSSION

To determine the copper removal degree using RCE as a biosorbent, 0.05 dm^3 of the solution (initial concentration 0.5 g dm^{-3}) was brought into contact with 1 g of the biosorbent sample for various process times, ranging from 1 to 90 minutes. The biosorption experiments were conducted at three different temperatures: 25 °C, 30 °C, and 35 °C. After the biosorption experiments, the suspension was filtered, and the filtrate was analyzed for Cu^{2+} content. The Cu^{2+} removal degree was calculated using Equation (1). The results are shown in Figure 4.

The copper removal degree onto CCE was determined performing the same experiments, with the only different process parameter being the initial Cu^{2+} concentration of 5 g dm^{-3} in this case. The obtained results are shown on Figure 5.

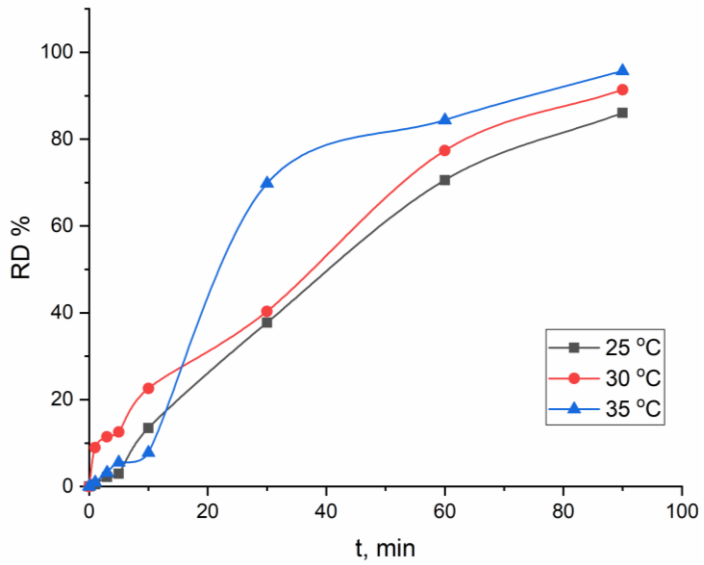

Figure 4 *Change in the removal degree with time during copper ions biosorption onto RCE, on different temperatures*

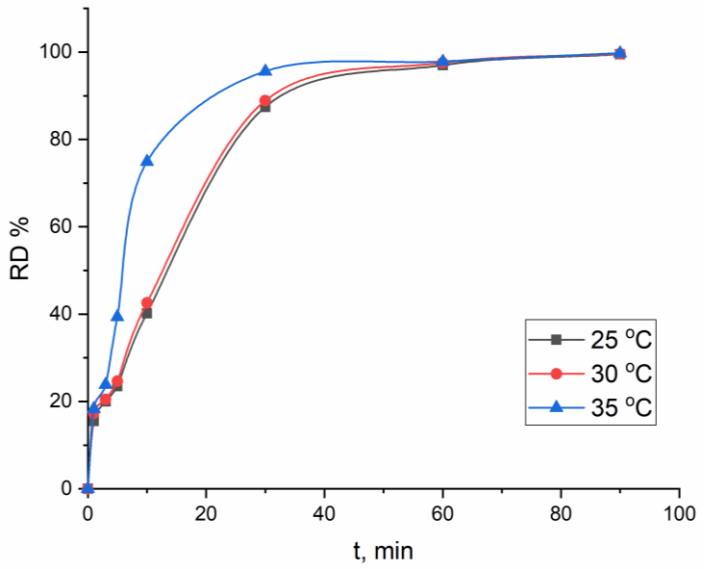

Figure 5 *Change in the removal degree with time during copper ions biosorption onto CCE, on different temperatures*

The obtained results show that the degree of metal removal increases with time during the biosorption of copper ions onto RCE (Figure 4) at all analyzed temperatures. It is also evident that system temperature is an important process parameter influencing the biosorption rate and efficiency. The degree of copper removal increased more rapidly at 35 °C, suggesting that the process is faster at higher temperatures. The recorded removal degree at 35 °C after 90 minutes was significantly higher (96%) than those at 30 °C (91%) and 25 °C (86%), indicating that system temperature plays a key role in biosorption efficiency in this case.

The results shown in Figure 5 indicate that the biosorption of Cu^{2+} ions onto CCE is less dependent on temperature. The degree of metal removal increases with time at all analyzed temperatures. The removal degree increased slightly faster at 35 °C compared to other

temperatures, with the final removal degree (after 90 minutes) reaching nearly 100% at all three temperatures.

CONCLUSION

Environmental protection is a crucial topic in the 21st century. Heavy metal wastewater pollution, including copper contamination, is a major environmental problem today. Recently, the scientific community has focused on investigating the use of various "living" and "non-living" biomass for removing pollutants from aqueous solutions and wastewater. This work demonstrates the potential of raw and calcined chicken eggshells for copper ion biosorption from aqueous solutions.

The results showed that both raw and calcined chicken eggshells are efficient biosorbents for copper ion removal, achieving high removal rates. In both cases, a metal removal rate of over 90% was recorded at all analyzed temperatures. However, the results also indicate that system temperature affects the process rate in both cases. Higher metal removal rates were observed at higher temperatures during the biosorption of copper ions onto raw chicken eggshells. Biosorption onto calcined chicken eggshells was shown to be less dependent on system temperature.

ACKNOWLEDGEMENT

The research presented in this paper was done with the financial support of the Ministry of Education, Science and Technological Development of the Republic of Serbia, within the funding of the scientific research work at the University of Belgrade, Technical Faculty in Bor, according to the contract with registration number 451-03-34/2026-03/200131.

REFERENCES

[1] Flores-Cano, J.V., Leyva-Ramos, R., Mendoza-Barron, J., *et al*. Appl. Surf. Sci. 2013, 276, 682–690.

[2] Zhao, J., Wen, X., Xu, H., *et al.* Environ. Technol. 2020.

[3] Garcia-Reyes, R.B., Rangel-Mendez, J.R., De la Torre, A.C. J. Hazard. Mater. 2009, 170, 845–854.

[4] Singh, S., Kumar, V., Dhanjal, D. S., *et al*. Bioremediat. Environ. Sustain. 2021, 219–233.

[5] Gorgievski, M., Adsorption of heavy metal ions from aqueous solution using wheat straw as an adsorbent, Doctoral dissertation, Bor, 2015.

[6] Gadd, G.M., J. Chem. Technol. Biotechnol. 2009, 84, 13–28.

[7] Shamim, S., Biosorption, Intech Open, London, 2018.

EcoTER'26
eco.tfbor.bg.ac.rs
32nd International Conference
Ecological Truth & Environmental Research
24–26 June 2026, Hotel Sunce,
Sokobanja, Serbia

Original Research

ENVIRONMENTAL ASPECTS AND EXPERIMENTAL INVESTIGATION OF SAC/GNS COMPOSITE LEAD-FREE SOLDER

DOI: 10.5937/EcoTER26422M

Ivana Marković[1,a*], Uroš Stamenković[1,b], Milan Nedeljković[1,c], Dragan Manasijević[1,d], Ljubiša Balanović[1,e]

[1] University of Belgrade, Technical Faculty in Bor, Vojske Jugoslavije 12, 19210 Bor, SERBIA

[a] https://orcid.org/0000-0003-4431-9921

[b] https://orcid.org/0000-0002-7579-2159

[c] https://orcid.org/0000-0002-7927-1334

[d] https://orcid.org/0000-0002-7828-8994

[e] https://orcid.org/0000-0002-3551-6731

Abstract

Ternary alloys of the Sn–Ag–Cu (SAC) system represent one of the most widely used lead-free solder materials due to their favorable mechanical properties and compliance with environmental regulations aimed at eliminating toxic lead from electronic components. Among these alloys, SAC338 (Sn–3.3Ag–0.8Cu) is recognized as one of the most promising alternatives to conventional Sn–Pb solders. Despite their ecological advantages, SAC alloys still exhibit challenges associated with the growth of intermetallic compounds and microstructural instability. The aim of this study was to investigate the influence of graphene nanosheet (GNS) additions on the microstructural properties of SAC composite. SAC composite containing up to 0.09 wt.% GNS were produced using powder metallurgy procedures. The results showed that the addition of GNS contributed to a more homogeneous microstructure and refinement of intermetallic phases such as Cu_6Sn_5 and Ag_3Sn. The addition of GNS improves the wettability of the composite solder by reducing the wetting angle, which enables better spreading of the molten solder and improves the quality of solder joints. From an environmental perspective, these improvements contribute to enhanced durability and longer service life of electronic components, leading to reduced material consumption, lower maintenance frequency, and decreased generation of electronic waste.

Keywords: SAC338, GNS, intermetallic phases, wettability.

INTRODUCTION

The rapid development of the electronics industry has resulted in increased consumption of electronic devices and a significant rise in electronic waste worldwide. Traditional Sn–Pb solder alloys, widely used for decades in electronic packaging, contain toxic lead that poses serious risks to human health and the environment. Due to the harmful effects of lead contamination, international environmental regulations such as the Restriction of Hazardous

* *imarkovic@tfbor.bg.ac.rs*

Substances (RoHS) Directive encouraged the replacement of lead-containing solders with environmentally acceptable alternatives [1–3].

Among the available lead-free materials, SAC alloys are considered the most promising candidates because of their favorable combination of mechanical strength, wettability, thermal stability, and soldering reliability. SAC338 alloy is especially important due to its eutectic composition and excellent performance in electronic packaging applications. Nevertheless, SAC alloys still exhibit several technological and ecological challenges. The formation of thick intermetallic compounds at the solder-substrate interface can reduce joint reliability and shorten service life. In addition, the relatively high silver content increases both production costs and environmental impact associated with mining and raw material extraction. Therefore, current research focuses on improving SAC alloys through reinforcement additions that can enhance performance while contributing to sustainability [4–6].

Nanomaterials such as GNS, carbon nanotubes, and ceramic particles have attracted considerable attention because they can refine the solder microstructure and suppress excessive intermetallic growth. These modifications may improve thermal stability and mechanical reliability, ultimately extending the operational lifetime of electronic devices and reducing electronic waste generation [7,8].

The aim of this paper was to investigate the effect of GNS content on the microstructural properties and wettability of SAC338–based composite materials. The obtained experimental results are expected to contribute to the further development of advanced composite solder materials with optimized properties for sustainable and environmentally responsible electronics manufacturing.

MATERIALS AND METHODS

SAC338 alloy and SAC338/GNS composite materials were produced using powder metallurgy techniques (PM). Environmentally, PM processing reduces material losses and energy consumption while allowing the production of advanced composite materials with enhanced functional properties. These factors support cleaner production technologies and more sustainable manufacturing practices in the electronics industry. Elemental powders of tin, silver, and copper were mechanically alloyed together with different concentrations of GNS (up to 0.09 wt.%) in the “Turbula T2F” mixer. Mechanical alloying was carried out for 5 h. The obtained powder mixture is then compacted under pressure of 150 MPa and subsequently sintered in the “Elektron ELP-08” furnace under an argon atmosphere at 190 °C for 2 h. The obtained samples were soldered onto copper substrates using flame soldering procedures.

Microstructural characterization was performed using scanning electron microscopy (SEM) “Tescan Vega 3LMU” coupled with energy dispersive spectroscopy (EDS) “Oxford Instruments X–act”. The investigations focused on the morphology of the solder matrix, distribution of GNS, and formation of intermetallic compounds at the solder-substrate interface. In order to determine the contact angle, the cross-sectional area of the solder joint was analyzed using micrographs and ImageJ software.

RESULTS AND DISCUSSION

Figure 1 shows the microstructures of the investigated samples after melting and solidification of the sintered specimens on a copper substrate, while Figure 2 presents the EDS analysis of the SAC/0.03GNS solder.

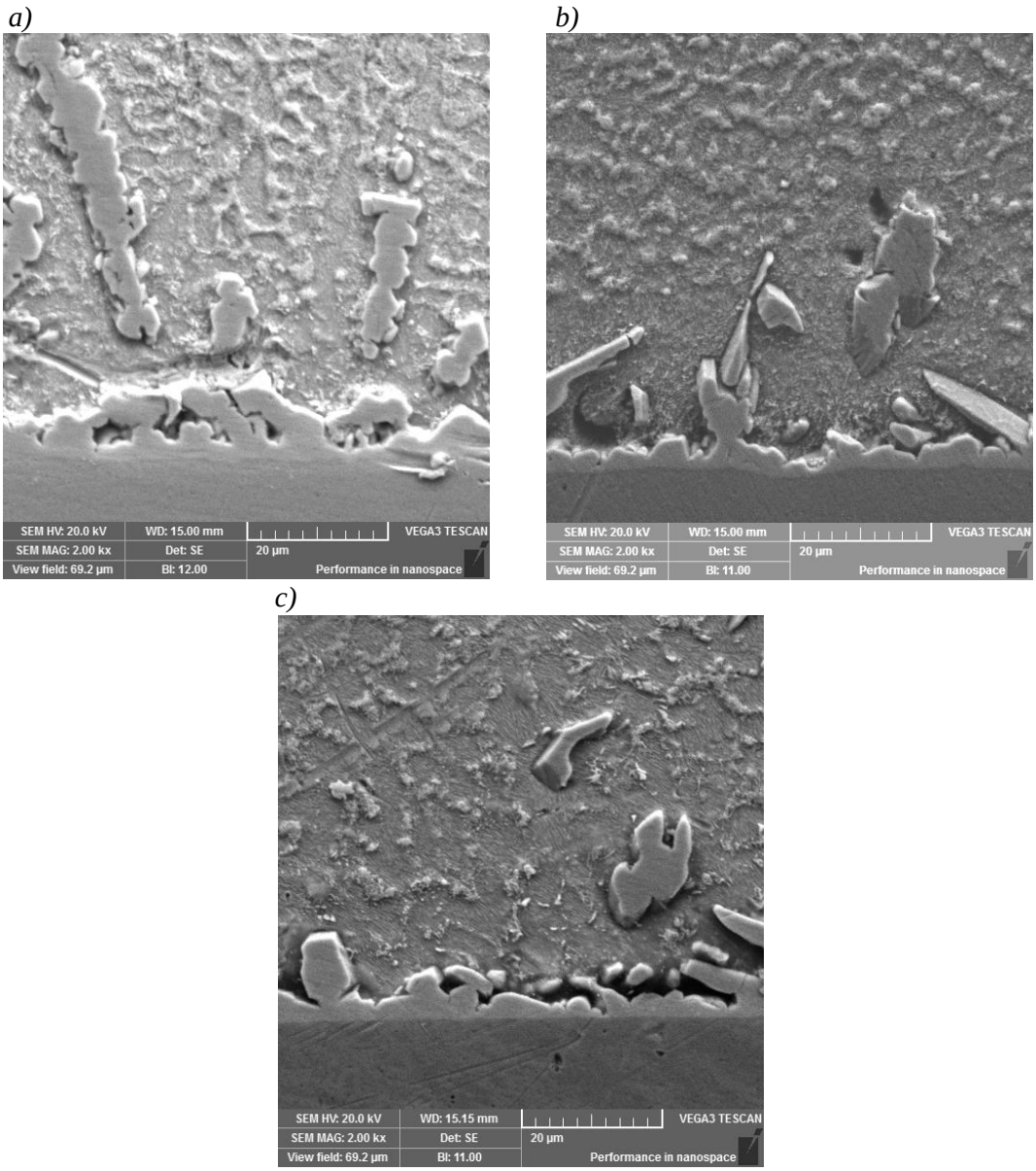

Figure 1 *SEM micrographs of the solders: a) SAC alloy; b) SAC/0.03GNS composite; c) SAC/0.09GNS composite*

All SEM micrographs of the solders reveal a relatively homogeneous matrix with clearly defined Sn–rich structures and needle-like Ag_3Sn phases forming a network within the β–Sn matrix. The primary Sn–rich dendritic phase represents the main solder structure, whereas the interdendritic regions consist of the β–Sn and Ag_3Sn eutectic mixture (Spectrum 5 in Figure 2).

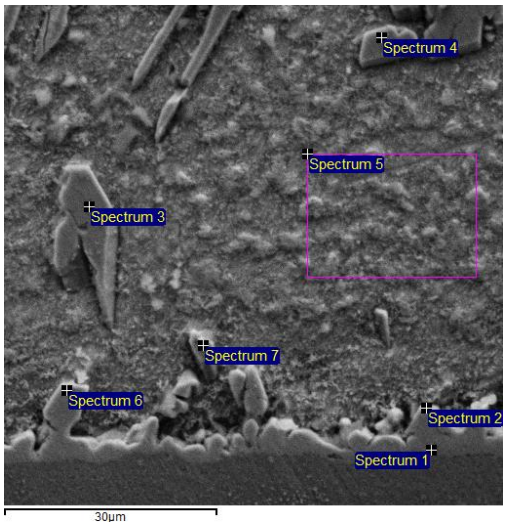

Spectrum	*Cu*	*Ag*	*Sn*
Spectrum 1	*54.12*		*45.88*
Spectrum 3	*52.63*		*47.37*
Spectrum 5		*12.09*	*87.91*

Figure 2 *EDS analysis of the SAC/0.03GNS composite solder*

With increasing GNS content, a higher degree of phase homogeneity was observed. The addition of GNS contributed to microstructural refinement and reduced phase segregation. Copper precipitated in the form of the Cu_6Sn_5 intermetallic phase (Spectrum 3 in Figure 2), whose content was higher near the copper substrate and gradually decreased with increasing distance from the interface. Furthermore, increasing GNS content resulted in a significant reduction in both the size and fraction of Cu_6Sn_5 particles [9,10].

At the interface between the solder and the copper substrate, the formation of an intermetallic compound (IMC) layer was observed (Spectrum 1 in Figure 2). During the melting process, copper atoms from the substrate diffused into the solder and reacted with tin, resulting in the growth of the intermetallic layer toward the solder interior. The thickness of the IMC layer plays an important role in determining the mechanical and electrical properties of the joint [11,12]. It was observed that increasing the GNS content in the solder reduced the thickness of the intermetallic layer.

a) *b)*

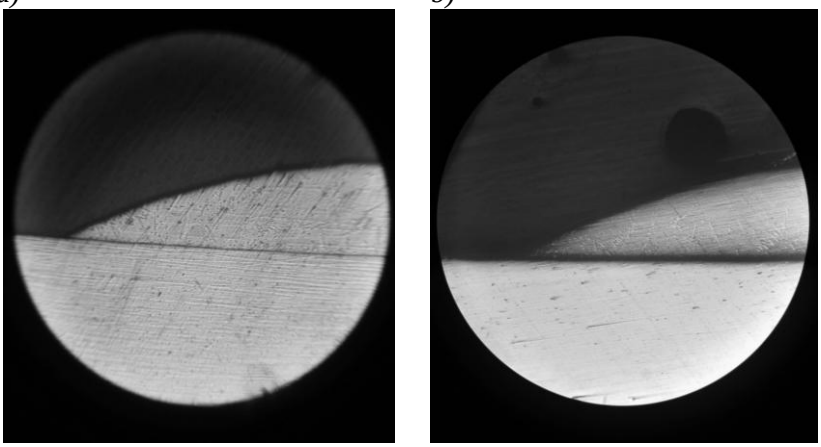

Figure 3 *Contact angles of (a) SAC338/0.03GNS; (b) SAC338/0.09GNS*

Contact angle analysis was performed for the SAC and SAC/GNS composite solders (Figure 3). The incorporation of GNS resulted in a reduction of the contact angle (from 85°

for SAC to 35° for SAC/0.09GNS) of the composite solders, indicating improved wetting behavior and enhanced spreading ability during the soldering process. Improved wettability promotes the formation of higher–quality and more reliable solder joints with fewer defects, such as pores and incomplete bonding [13]. From an environmental perspective, enhanced joint reliability contributes to longer service life of electronic components, reduced material losses during manufacturing and repair processes, and lower generation of electronic waste. Consequently, the addition of GNS supports the development of more sustainable and environmentally friendly lead-free solder materials for electronic applications.

CONCLUSION

The addition of reinforcement GNS improves the microstructural stability and reliability of SAC alloys by refining the microstructure and suppressing excessive intermetallic compound growth. These improvements extend the service life of electronic components and contribute to reducing electronic waste generation.

Powder metallurgy processing offers additional ecological advantages through lower material losses and improved manufacturing efficiency. Consequently, SAC composite reinforced with GNS constitute a promising direction for sustainable electronic materials and environmentally responsible electronic packaging technologies.

ACKNOWLEDGEMENT

The authors are grateful to the Ministry of Science, Technological Development and Innovation of the Republic of Serbia for financial support according to the contract with registration No. 451-03-34/2026-03/ 200131.

REFERENCES

[1] Cheng, S., Huang, C.M., Pecht, M. Microelectron. Reliab. 2017, 75, 77–95.

[2] Gharaibeh, A., Felhősi, I., Keresztes, Z., *et al.* Metals. 2020, 10(10), 1276.

[3] Anousheh, A., Soleimani, M. Mater. Des. 2025, 258, 114510.

[4] Xu, L., Wang, L., Jing, H., *et al*. J. Alloys Compd. 2015, 650, 475–481.

[5] da Rocha, G.S., Padua, G.F.R.C., do Nascimento, N.R. *et al.* J Mater Sci: Mater Electron, 2026, 37, 990.

[6] Mhd Noor, E.E., Singh, A. Solder. Surf. Mt. Technol. 2014, 26 (3), 147–161.

[7] Li, Y., Yu, S., Li, *et al.* Metals. 2023, 13(7), 1209.

[8] Ramli, M.I.I., Salleh, M.A.A.M., Abdullah, M.M.A.B. Materials. 2022, 15(4), 1451.

[9] Gain, A.K., Zhang, L. Mater. 2019, 5, 100234.

[10] Kumar Pal, M., Gergely, G., Koncz-Horváth, D., Gácsi, Z. Intermetallics, 2021, 128, 3–4.

[11] Kang, M.S., Kim, D.S., Shin, Y.E. Mater. 2019, 12(6), 936.

[12] Yang, M., Ji, H., Wang, S. *et al*. J. Alloys Compd. 2016, 679, 18–25.

[13] Yoon, J.W., Noh, B.I., Kim, B.K. *et al.* J. Alloys Compd. 2009, 486(1–2), 142–147.

EcoTER'26
eco.tfbor.bg.ac.rs
32nd International Conference
Ecological Truth & Environmental Research
24–26 June 2026, Hotel Sunce,
Sokobanja, Serbia

Original Research

THERMAL TRANSFORMATION OF NSAID-DERIVED MATERIALS: MORPHOLOGICAL AND COMPOSITIONAL INSIGHTS

DOI: 10.5937/EcoTER26427S

Katarina Stojanović[1,a*], Marija Simić[1,b], Danka Aćimović[1,c], Branislava Savić Rosić[1,d], Marija Ječmenica Dučić[1,e], Tanja Brdarić[1,f]

[1] University of Belgrade, Vinča Institute of Nuclear Sciences-National Institute of the Republic of Serbia, Mike Petrovića Alasa 12-14, 11000 Belgrade, SERBIA

[a] https://orcid.org/0009-0003-3467-9875 [b] https://orcid.org/0000-0001-9518-7709

[c] https://orcid.org/0000-0001-7506-9684 [d] https://orcid.org/0000-0002-4632-7960

[e] https://orcid.org/0000-0002-6437-519X [f] https://orcid.org/0000-0003-2547-7123

Abstract

The management and treatment of pharmaceutical waste has recently attracted increasing attention from the scientific and professional community. Residues derived from nonsteroidal anti-inflammatory drugs (NSAIDs) represent carbon-rich precursors suitable for thermal conversion into carbon materials with adaptable structural properties. Moreover, these materials show potential as functional materials due to their high surface area, porosity, and surface functional groups, enabling applications in adsorption and catalysis. The aim of this study was to investigate the influence of calcination temperature on morphological and compositional transformations of NSAID-derived materials. Samples were thermally treated at 400, 600, and 800 °C in air and characterized using scanning electron microscopy (SEM) and energy-dispersive X-ray spectroscopy (EDX). SEM analysis revealed pronounced temperature-dependent structural evolution from compact carbonaceous morphology at 400 °C to heterogeneous microstructures containing elongated and needle-like domains at 800 °C. EDX analysis confirmed progressive elemental redistribution with increasing temperature, indicating gradual decomposition of the organic matrix and enrichment of inorganic phases. The obtained results provide insight into the thermal transformation mechanisms of pharmaceutical-derived materials and demonstrate their potential as precursors for functional carbon-based materials.

Keywords: NSAID, calcination, SEM.

INTRODUCTION

The development of sustainable materials derived from waste resources has become an important research direction in modern materials science and environmental engineering, but also a promising source of secondary raw materials. In recent years, considerable attention has been devoted to converting organic waste into functional carbon-based materials through thermal processes such as pyrolysis and calcination, which produce carbon structures with

* *katarina.stojanovic@vin.bg.ac.rs*

tunable porosity, surface functionality, and morphological features [1,2]. These materials have attracted interest for a wide range of applications, including catalysis, adsorption, energy storage, and electrochemical environmental technologies.

Temperature plays a key role in determining the characteristics of thermally treated materials. Increasing calcination temperature promotes progressive decomposition of the organic matrix, release of volatile components, and formation of new inorganic phases, which can significantly affect the morphology and composition of the resulting materials [3]. Understanding these transformations is essential for evaluating the potential of such materials for further functional applications.

Pharmaceutical compounds represent an interesting, yet still insufficiently explored, precursor for thermally derived materials, as the increasing production of pharmaceuticals has generated significant amounts of pharmaceutical waste that pose a potential environmental risk [4]. Many pharmaceutical molecules contain aromatic rings and heteroatoms that can contribute to the formation of carbon materials with defined morphology during thermal treatment; however, systematic studies addressing the morphological and compositional evolution of pharmaceutical-derived materials during calcination remain limited.

In this study, NSAID-derived material was subjected to calcination at 400, 600, and 800 °C in order to investigate temperature-induced changes in morphology and elemental composition. Morphological characteristics were analyzed using scanning electron microscopy (SEM), while elemental composition was determined by energy-dispersive X-ray spectroscopy (EDX). The aim of this work was to provide insight into the thermal transformation behavior of pharmaceutical-derived materials and to evaluate the influence of calcination temperature on their morphological and compositional evolution.

MATERIALS AND METHODS

The NSAID tablets (2 g; diclofenac Duo, Brufen, and naproxen, Galenika), past their expiration date, were crushed into a powder and thermally treated in a cylindrical furnace in air. The samples were heated at a rate of 10 °C min^{-1} to 400, 600, or 800 °C, held at the target temperature for 60 min, and then cooled to room temperature under ambient conditions.

A FESEM-EDS system (FEI Scios 2) was used to examine surface morphology and elemental composition. Imaging was performed at an accelerating voltage of 5.0 kV, while EDS spectra were acquired with a collection time of 20 min. High-resolution SEM micrographs and corresponding EDS spectra were obtained from selected micro-areas at a chamber pressure of 2.8×10^{-4} Pa.

RESULTS AND DISCUSSION

SEM analysis revealed pronounced morphological transformations as a function of calcination temperature.

The sample calcined at 400 °C (Figure 1a) exhibits a relatively compact and agglomerated morphology dominated by large irregular particles. A prominent cauliflower-like aggregate can be observed in the central region, surrounded by smaller fragments and plate-like

particles. The surface appears relatively dense with limited visible porosity, suggesting that the organic precursor is only partially decomposed and that the material still retains a compact carbonaceous matrix.

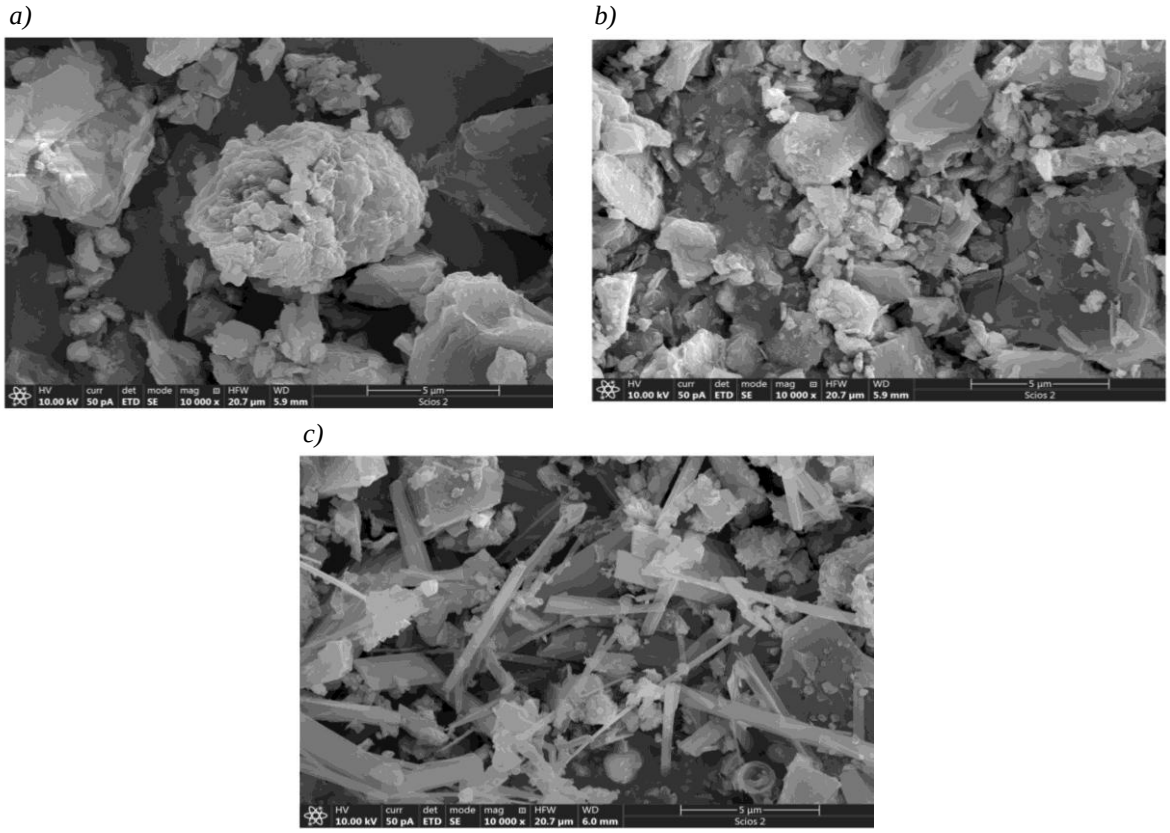

Figure 1 *SEM micrographs of NSAID-derived materials calcined at: a) 400 °C; b) 600 °C; and c) 800 °C*

A significant structural transformation occurs at 600 °C (Figure 1b). The morphology becomes more fragmented and heterogeneous, consisting of irregularly shaped particles with sharp edges and numerous smaller fragments distributed between larger grains. The structure appears more disordered compared to the 400 °C sample, indicating progressive decomposition of the precursor material and partial disintegration of the original particle aggregates. The increased number of smaller particles suggests release of volatile components and restructuring of the material during thermal treatment.

The material obtained at 800 °C (Figure 1c) shows a markedly different morphology characterized by the formation of elongated rod-like and needle-like structures distributed throughout the sample. These anisotropic microstructures coexist with smaller irregular fragments, resulting in a highly heterogeneous microstructure. The formation of such elongated domains suggests advanced structural reorganization and possible crystallization or growth of inorganic phases at elevated temperature. The presence of these structures significantly increases structural complexity and may contribute to enhanced surface accessibility of the material.

The observed morphological evolution demonstrates that increasing calcination temperature strongly influences the microstructure of NSAID-derived materials. Structural transformation from compact aggregates toward heterogeneous microstructures reflects progressive decomposition of the organic matrix and development of new structural features.

These results confirm that increasing calcination temperature promotes transformation from compact aggregates to heterogeneous microstructures with higher structural complexity.

Table 1 *Elemental composition of thermally treated samples (weight %)*

Temperature (^{o}C)	C (%)	O (%)	Na (%)	Mg (%)	Si (%)	Cl (%)	Ti (%)
400	43.792	29.776	8.578	5.061	8.797	2.487	1.509
600	11.025	13.915	21.499	14.894	33.527	4.755	0.384
800	35.744	25.951	18.979	1.7250	5.733	10.046	1.823

EDX analysis (Table 1) shows temperature-dependent variations in elemental composition. The 400 °C sample is dominated by carbon and oxygen, consistent with residual organic content. At 600 °C, the relative contribution of inorganic elements increases, indicating further decomposition of the organic matrix. Although the overall composition at 400 °C and 800 °C remains comparable in terms of major elements, the 800 °C sample exhibits higher apparent Na and Cl signals (Table 1). This is attributed to surface redistribution of inorganic species and increased detectability following extensive matrix decomposition, rather than bulk enrichment. At 800 °C, the coexistence of carbon with inorganic elements such as Na, Mg, and Si suggests the presence of multiple inorganic components, consistent with the observed morphological heterogeneity.

CONCLUSION

This study demonstrates that calcination temperature plays a key role in the structural evolution of NSAID-derived materials. Thermal treatment at 400–800 °C induces pronounced morphological and compositional changes. SEM analysis shows a transition from compact carbonaceous structures at lower temperatures to heterogeneous microstructures with elongated and needle-like features at higher temperatures. EDX results further indicate temperature-dependent redistribution of inorganic elements. These combined effects lead to increased structural complexity at elevated temperature, highlighting the importance of thermal treatment in tailoring the properties of pharmaceutical-derived carbon materials. The findings provide insight into their transformation behavior and support their potential use as precursors for functional carbon-based materials.

ACKNOWLEDGEMENT

The authors are grateful to the Ministry of Science, Technological Development and Innovation of the Republic of Serbia for financial support according to the contract with registration No. 451-03-33/2026-03/ 200017.

REFERENCES

[1] Yuan, X., Dissanayake, P.D., Gao, B., *et al.* J. Environ. Manage. 2021, 296, 113128.

[2] Ma, Q., Yu, Y., Sindoro, M., *et al.* Adv. Mater. 2017, 29, 1605361.

[3] Boakye, K., Khorami, M., Ganjian, E., *et al.* Int. J. Emerg. Technol. Innov. 2021, 2, 00016.

[4] Manole, F., Marian, P., Mekeres, G.M., *et al.* Pharmacophore 2023, 14(2) 106–110.

EcoTER'26
eco.tfbor.bg.ac.rs
32nd International Conference
Ecological Truth & Environmental Research
24–26 June 2026, Hotel Sunce,
Sokobanja, Serbia

Original Research

PRODUCTION COST ASSESSMENT OF SnO_2-MWCNT@SS ELECTRODE FOR WASTEWATER TREATMENT

DOI: 10.5937/EcoTER26432S

Katarina Stojanović[1,a*], Marija Simić[1,b], Danka Aćimović[1,c], Branislava Savić Rosić[1,d], Marija Ječmenica Dučić[1,e], Tanja Brdarić[1,f]

[1] University of Belgrade, Vinča Institute of Nuclear Sciences-National Institute of the Republic of Serbia, Mike Petrovića Alasa 12-14, 11000 Belgrade, SERBIA

[a] https://orcid.org/0009-0003-3467-9875 [b] https://orcid.org/0000-0001-9518-7709

[c] https://orcid.org/0000-0001-7506-9684 [d] https://orcid.org/0000-0002-4632-7960

[e] https://orcid.org/0000-0002-6437-519X [f] https://orcid.org/0000-0003-2547-7123

Abstract

The rising concern over environmental pollution has catalyzed advances in wastewater treatment technologies, particularly advanced oxidation processes (AOPs). These processes are effective for degrading harmful organic pollutants such as bisphenol A (BPA) through electrochemical systems, leveraging the unique properties of nanostructured electrodes like SnO_2-MWCNT@SS (tin dioxide-multiwall carbon nanotube at stainless steel substrate). However, the economic feasibility of producing such innovative materials is as crucial as their performance. This paper presents the cost analysis of producing SnO_2-MWCNT@SS electrodes, evaluating its competitiveness against other commercial materials and the economic implications of transitioning to industrial-scale production.

Keywords: advanced oxidation, nanostructured anodes, SnO_2-MWCNT, cost production.

INTRODUCTION

Advanced oxidation processes (AOPs) have gained significant attention as effective technologies for treating wastewater contaminated with organic pollutants [1,2]. These processes degrade organic molecules through oxidation, primarily utilizing hydroxyl radicals generated in electrochemical systems [3]. The generation and activity of these radicals are inherently linked to the properties of the anode material employed in the treatment process [4]. Recent studies have indicated that the degradation efficiency of various pollutants, such as bisphenol A (BPA), can be optimized through the careful selection of anode materials, which can include noble and transition metals, metal oxides [5], and carbon-based nanoparticles like carbon nanotubes (CNTs) and graphene oxide [6].

In line with recent trends, our research group investigated one particularly promising composite, the tin dioxide-multiwall carbon nanotube (SnO_2-MWCNT), which was synthesized with the intention of combining the high conductivity and surface area of MWCNTs with the catalytic properties of SnO_2 [7]. When deposited on a stainless steel

* *katarina.stojanovic@vin.bg.ac.rs*

substrate, nanostructured anode, termed SnO_2-MWCNT@SS, has been designed and utilized in degrading BPA, demonstrating robust performance in both classic electro-oxidation and the electro-Fenton process [7,8]. Results highlighted its effectiveness for organic pollutant degradation, comparable to the currently favored boron-doped diamond (BDD) electrodes.

Understanding the economic viability of the SnO_2-MWCNT@SS anode requires a close examination of the associated production costs. In this study, the costs associated with the preparation of SnO_2-MWCNT@SS were estimated to assess the economic feasibility of its production and its competitiveness with other commercially available electrodes. The cost calculations reflect laboratory-scale production based on current market prices for energy and materials. The comprehensive breakdown of production costs allows for a clear understanding of the financial investments required at the laboratory scale, which sets a foundation for assessing industrial viability.

MATERIALS AND METHODS

Following the procedure detailed in our previous study [7], the production of SnO_2-MWCNT@SS involves three primary phases: (i) functionalization of MWCNTs, (ii) synthesis of SnO_2 nanoparticles, and (iii) preparation of the SnO_2-MWCNT nano-composite and its deposition onto an SS substrate. The preparation process yielded approximately 10 cm² of SnO_2-MWCNT@SS electrode per production cycle.

Each phase's costs reflect both the energy consumption and the reagents utilized, with total costs calculated according to Equation 1. The total production cost was estimated as the sum of the expenditures on energy and reagents required to produce 1 cm² of SnO_2-MWCNT@SS under laboratory conditions.

$$\text{Total costs} = C_{fMWCNT} + C_{nano\text{-}SnO_2} + C_{SnO_2\text{-}MWCNT@SS} \quad (1)$$

The production costs of each phase, denoted as C_{fMWCNT}, $C_{nano\text{-}SnO_2}$, and $C_{SnO_2\text{-}MWCNT@SS}$, respectively, were estimated using Equation (2) [9]:

$$\text{Production costs (C)} = \sum\text{Energy costs} + \sum\text{Reagents costs} \quad (2)$$

The sources providing the prices of energy and reagents used in SnO_2-MWCNT@SS preparation are listed in Table 1.

Table 1 *Consumer prices of energy and reagents used in the cost analysis (Consumer price list)*

No	Consumer	Price
1	Electricity	0.1867 €/ kWh
2	MWCNT	17.32 €/ g
3	Nitric acid, 3 M	141.60 €/ L
4	Deionized water	18.60 €/ L
5	Hydrogen peroxide, 30 %	31.50 €/ L
6	Tin (II) chloride dehydrate	0.286 €/ g
7	Ammonia solution, 25 %	26.60 €/ L

Table 2 *continued*

8	Silver nitrate, 1 M	124.00 €/ L
9	Glacial acetic acid, 100 %	36.52 €/ L
10	Ethylene glycol	54.20 €/ L
11	Air	3.429 €/ m^3
12	Dimethylformamide	50.40 €/ L
13	Distilled water	1.00 €/ L
14	Acetone	39.00 €/ L
15	SS substrate	0.036 €/cm^2

RESULTS AND DISCUSSION

Cost of MWCNT functionalization

To initiate the production of SnO_2-MWCNT composite, MWCNTs must be effectively functionalized to enhance their interaction with metal oxides. Under laboratory conditions, approximately 20 g of functionalized MWCNT (fMWCNT) was prepared per production cycle. The cost for producing 1 mg of fMWCNT was estimated to be approximately 0.4 € (Table 2). The costs include the purchase of reagents such as nitric acid, hydrogen peroxide, and deionized water, along with energy consumption for mixing and drying processes, which collectively demonstrate that reagent costs dominate this phase. This high material cost underscores the importance of effective source management to optimize overall expenditure.

Table 3 *Cost breakdown for producing 1 mg of functionalized MWCNT*

STEP	Consumer	Consumption per cycle	Cost, €/ mg	No*
Mixing	MWCNT	25 mg	0.02165	2
Mixing	Nitric acid, 3 M	25 ml	0.177	3
Mixing	Stirrer (1.05 kW)	1.5 h at 70 °C	0.014702625	1
Washing 1	Deionized water	50 ml	0.0465	4
Dissolving	Hydrogen peroxide, 30 %	40 ml	0.063	5
Sonification	Ultrasonic bath (0.161 kW)	15 min at 25 °C	0.000375734	1
Washing 2	Deionized water	50 ml	0.0465	4
Drying	Oven (1.6 kW)	2 h at 75 °C	0.029872	1
TOTAL			**0.399600359**	

* No in Consumer price list (Table 1)

Cost of SnO_2 nanoparticles synthesis

The synthesis of SnO_2 nanoparticles was the second production phase, with an estimated cost of 3.96 € per gram of product (Table 3). The synthesis efficiency was approximately 80%, suggesting areas for cost reduction through improved methodologies or economies of scale. Therefore, similar to MWCNT functionalization, surpassing the financial limitations of raw materials and energy remains essential for a cost-efficient production model.

Table 4 *Cost breakdown for producing 1 g of SnO_2 nanoparticles*

STEP	Consumer	Consumption per cycle	Cost, €/ g	No*
Dissolving	Tin (II) chloride dehydrate	2.26 g	0.3575	6
Dissolving	Deionized water	20 ml	0.205752212	4
Dissolving	Ammonia solution, 25 %	2 ml	0.029424779	7
Washing	Ammonia solution, 25 %	2 ml	0.029424779	7
Washing	Silver nitrate, 1 M	1 ml	0.068584071	8
Mixing	Glacial acetic acid, 100%	2 ml	0.04039823	9
Mixing	Ethylene glycol	0.839 ml	0.025151438	10
Mixing	Stirrer (1.05 kW)	1 h at 70 °C	0.108426438	1
Drying	Oven (1.6 kW)	12 h at 120 °C	1.982654867	1
Annealing	Furnace (3.5 kW)	1 h (ramping)	0.36142146	1
Annealing	Furnace (3.5 kW)	2 h at 600 °C	0.72284292	1
Annealing	Air	3 h	0.010241482	11
Cooling	Air	3 h	0.010241482	11
TOTAL			**3.958891814**	

* No in Consumer price list (Table 1)

Cost of SnO_2-MWCNT@SS electrode preparation

The final preparation stage integrates the functionalized MWCNT and synthesized SnO_2 nanoparticles onto a stainless steel substrate. The total cost of producing 1 cm² of SnO_2-MWCNT@SS electrode is remarkably low, estimated at just 0.1579 €. The breakdown of costs for producing 1 cm² of SnO_2-MWCNT@SS electrode is presented in Table 4. The major costs are associated with reagents processing (Mixing step) and electrode preparation (other steps).

Table 5 *Cost breakdown for producing 1 cm² of the SnO_2-MWCNT@SS electrode*

STEP	Consumer	Consumption per cycle	Cost, €/ cm^2	No*
Mixing	nano-SnO_2	3.5 mg	0.001386	2
Mixing	fMWCNT	1 mg	0.04	3
Mixing	Dimethylformamide	1 ml	0.00504	12
Mixing	Ultrasonic bath (0.161 kW)	5 h	0.01502935	1
Washing	Distilled water	10 ml	0.001	13
Washing	Acetone	10 ml	0.039	14
Washing	Deionized water	10 ml	0.0186	4
Coating	SS substrate	10 cm^2	0.036	15
Drying	IC lamp (0.3 kW)	20 min	0.001867	1
TOTAL			**0.15792235**	

* No in Consumer price list (Table 1)

The cost distribution is illustrated in Figure 1(a), while the contributions of energy and reagents to the total cost are shown in Figure 1(b). A comparison of the estimated cost with the price of similar commercial materials is presented in Figure 1(c).

The calculated production costs of SnO_2-MWCNT@SS electrode with all required commodities reveal a significant potential for market competitiveness. Figure 1(a) indicates that reagents treatment for nanomaterial preparation accounts for over 60 % of total costs. The stainless steel substrate emerges as an essential cost driver, representing over 35 % (37. 32 %) of the electrode preparation costs. Interestingly, energy utilization accounts for only 14.25 %

of the total production cost (Figure 1 (b)), confirming that the process is energy efficient and primarily dependent on raw materials. This finding also emphasizes the importance of selecting low-cost yet high-performance materials to enhance overall production efficiency.

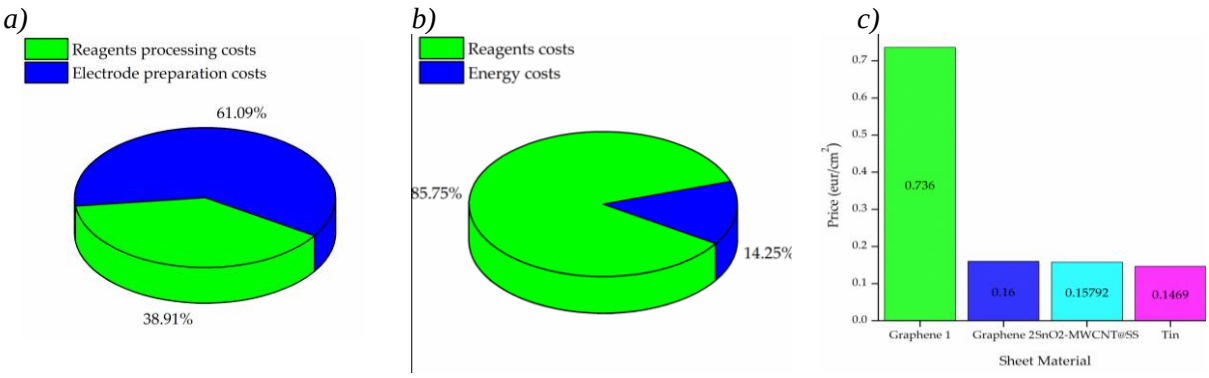

Figure 1 *Breakdown of total production costs for the SnO_2-MWCNT@SS electrode: a) comparison of rea-gent processing costs vs. electrode preparation costs; b) contribution of energy vs. reagent costs; c) cost comparison with similar commercial products*

As shown in Figure 1(c), when benchmarked against the price of similar carbon-based materials such as graphene sheets, SnO_2-MWCNT@SS exhibits costs that are approximately 1.30 – 78.54 % lower. The cost is also comparable to commercial tin sheets, with only a 7.50% price increase. Notably, SnO_2-MWCNT@SS is 94.28 % (or 17.5 times) cheaper than commercially available graphite plate electrodes for flow electrolysis cells. This comparative analysis not only validates the economic benefits of SnO_2-MWCNT@SS production but also signals a potential shift in industry practices, favoring the adoption of cost-effective nanostructured anodes over traditional materials.

CONCLUSION

When analyzing the input costs and following the methodology for lab-scale production, initial estimates suggest that the production and use of SnO_2-MWCNT@SS is economically feasible, especially when compared with BDD electrodes, which involve significantly higher production costs due to complex synthesis techniques and material expenses. The assessed production costs demonstrate strong potential for competing with existing commercial alternatives while maintaining advanced performance capabilities and enhancing the efficiency of organic pollutant degradation processes. Furthermore, the anticipated cost reductions achievable via larger-scale production with technical-grade reagents would increase the attractiveness of these electrodes, making them a viable solution for addressing environmental concerns. Finally, the production of SnO_2-MWCNT nano-composite and its use as a coating can also be economically beneficial in extending the lifetime of existing SS electrodes, solidifying the role of SnO_2-MWCNT@SS in sustainable wastewater treatment solutions.

In conclusion, the SnO_2-MWCNT@SS anode represents a significant development in the field of advanced oxidation processes for wastewater treatment. Its low production costs combined with demonstrated high efficacy in degrading BPA suggest that it possesses robust

potential in competing with existing electrode materials. As the field of electrochemical technologies continues to evolve, the economic viability and effectiveness of SnO_2-MWCNT@SS will likely make it a crucial in achieving effective wastewater treatment solutions in the near future.

ACKNOWLEDGEMENT

The authors are grateful to the Ministry of Science, Technological Development and Innovation of the Republic of Serbia for financial support according to the contract with registration No. 451-03-33/2026-03/ 200017.

REFERENCES

[1] Garcia-Segura, S., Ocon, J., Chong, M., *et al*. Process Saf. Environ. Prot. 2018, 113, 48–67.

[2] Qiao, J., Xiong, Y.J. Water Process Eng. 2021, 44, 102308.

[3] Xie, J., Zhang, C., Waite T. Water Res. 2022, 217, 118425.

[4] Panizza M. Importance of Electrode Material in the Electrochemical Treatment of Wastewater Containing Organic Pollutants. In: Comninellis C, Chen G, editors. Electrochemistry for the Environment. New York: Springer, 2010. p. 25–54.

[5] Zhang, Z., Li, Y., Dong, L., *et al*. Chin. Chem. Lett. 2023, 34, 107404.

[6] Baptista-Pires, L., Norra, G., Radjenovic, J. Water Res. 2021, 203, 117492.

[7] Simić, M., Savić, B., Ognjanović, M., *et al*. J. Water Process Eng. 2023, 51, 103416.

[8] Simić, M., Brdarić, T., Savić Rosić, B., *et al*. J. Environ. Chem. Eng. 2024, 12, 113369.

[9] Maroušek, J., Maroušková, A., Myšková, K., *et al*. Int. J. Environ. Sci. Technol. 2015, 12, 3385–3390.

Original Research

AMBROSIA-BASED BIOSORBENTS FOR REMOVAL OF RHODAMINE B FROM AQUATIC SOLUTION

DOI: 10.5937/EcoTER26438N

Natalija Nedić[1,a*], Sandra Bulatović[1,b], Tamara Tadić[1,c], Bojana Marković[1,d], Aleksandra Nastasović[1,e]

[1] University of Belgrade, Institute of Chemistry, Technology and Metallurgy (ICTM), Njegoševa 12, 11000 Belgrade, SERBIA

[a] https://orcid.org/0009-0002-5621-9223 [b]https://orcid.org/0000-0002-7861-4489
[c]https://orcid.org/0000-0003-4484-1568 [d]https://orcid.org/0000-0001-7608-8289
[e]https://orcid.org/0000-0002-8589-6437

Abstract

The utilization of different natural materials and their application as low-cost biosorbents in water treatments represents an efficient approach in environmental protection. In this study, the biosorption efficiency of Ambrosia-based biosorbents was analyzed before and after modification with magnetite. The biosorption process with both biosorbents was evaluated using the cationic dye Rhodamine B (RB). After 2h of contact time at an initial RB concentration of 25 ppm, the maximum removal efficiency for RB was 59.2% with non-magnetic, and 91.7% with magnetic biosorbent. Quantification of RB was performed using UV-Vis spectroscopy, while FTIR analysis confirmed the biosorption of RB onto both biosorbents. The results of this study demonstrated that Ambrosia-based biosorbents are economical and effective materials for the removal of RB from aqueous solution.

Keywords: biosorbents, Ambrosia, Rhodamine B.

INTRODUCTION

Clean and uncontaminated water has become a challenge for the global population. Preventive measures, such as water purification and recycling are crucial to ensure the availability of clean water and environmental protection. Industrial effluents, including contamination from agriculture, domestic, and clinical sources also contribute to the water pollution. Synthetic organic dyes in wastewaters are indestructible, carcinogenic, and resistant to environmental degradation [1]. Rhodamine B (RB) is a cationic, water-soluble synthetic organic dye, used in the manufacturing of dye lasers, stamp pads, fireworks, carbon sheets, etc. Because of its non-destructible nature and inherent structural stability, RB has been identified as a neurotoxic and carcinogenic compound [2]. Because of all of the above, it is very important to establish an environmentally acceptable approach that will enable the efficient and inexpensive removal of polluting compounds from wastewater so that they do not reach the environment.

* *natalija.nedic@ihtm.bg.ac.rs*

A weed species of concern in Europe is *Ambrosia artemisiifolia*, known as an alien plant responsible for significant health and economic impacts in the most affected areas including Hungary, Serbia, Croatia, Slovenia, Slovakia, Romania, France, and Italy. *A. artemisiifolia* is a highly invasive annual plant, with the ability to generate allergenic pollen [3]. The focus of this study was on the development and implementation of novel non-magnetic and magnetic biosorbents, derived from the *A. artemisiifolia* biomass, for the removal of the synthetic organic dye Rhodamine B (RB) from aqueous solution. The concentration of RB was determined using UV-Vis spectrophotometry. Magnetic vs. non-magnetic biosorbent offer several advantages for RB removal, particularly in simple and efficient separation from aqueous solution through the application of an external magnetic field. Also, the incorporation of magnetite enabled the functionalization of the biosorbent so that the newly created magnetic biosorbent exhibits greater sorption efficiency. These characteristics make magnetic biosorbent a cost-effective material with strong potential for future applications in wastewater treatment processes.

MATERIALS AND METHODS

Preparation of biosorbents

The *A. artemisiifolia* was collected from the peripheral of Belgrade, the capital of Serbia, by cutting the aboveground plant parts. The plant biomass was washed with tap water and dried at room temperature for one week. Dried biomass was chopped in an electric mill, and sieved to obtain biosorbent particles with a size smaller than 300 μm. The obtained non-magnetic biosorbent was washed with distilled water, and then dried overnight in an oven at 50 °C [4].

The preparation of the magnetic biosorbent was carried out using modified coprecipitation method, which involved dissolving of 3.9 g of $FeCl_3 \cdot H_2O$, and 1.7 g of $FeCl_2 \cdot H_2O$ in 190 cm^3 of deionized water, under a nitrogen (N_2) atmosphere at 80 °C, with stirring at 450 rpm for 20 minutes. Subsequently, 10 M NaOH was added, and the reaction mixture was stirred under the same conditions for an additional 30 minutes. Afterward, 0.2 g of the non-magnetic biosorbent was introduced into the reaction mixture, and stirring was continued under the same conditions for another 30 minutes. Finally, the prepared magnetic biosorbent was filtered, washed until neutral pH, and dried overnight in an oven at 50 °C [5].

Biosorption of RB

The biosorption process of RB was performed in a batch system. Both biosorbents (0.1 g) were added separately to the 10 ml of 25 ppm RB solution. The samples were shaken at 400 rpm at room temperature (25 °C), and a pH of 6.2. The RB concentration before and after biosorption in the water solution was determined spectrophotometrically at 554 nm (NOVEL-102S UV-Vis Double Beam Spectrophotometer, COLO Lab Experts, Slovenia). The removal efficiency of RB with Ambrosia-based biosorbents at equilibrium (*E (%)*) was determined using Equation (1) [4,5]:

$$E(\%) = \frac{C_0 - C}{C_0} \times 100 \quad (1)$$

where: C_0 (ppm) and C (ppm) are the concentrations of RB before and after biosorption process.

Fourier Transform Infrared Spectroscopy (FTIR)

FTIR spectra of Ambrosia-based biosorbents, before and after biosorption of RB, were taken in the range of 400–4000 cm^{-1}, in ATR mode using a Nicolet SUMMIT FTIR Spectrometer (Thermo Fisher Scientific, Waltham, MA, USA), in order to identify the functional groups of biosorbents that interact with dye molecules.

RESULTS AND DISCUSSION

The results obtained with UV-Vis spectroscopy showed efficient RB removal by both Ambrosia-based biosorbents. For non-magnetic biosorbent removal effiency of RB was 59.2%, while for magnetic it was 91.7% (Figure 1). The difference in the biosorption efficiency of magnetic compared to non-magnetic biosorbent can be attributed to magnetite.

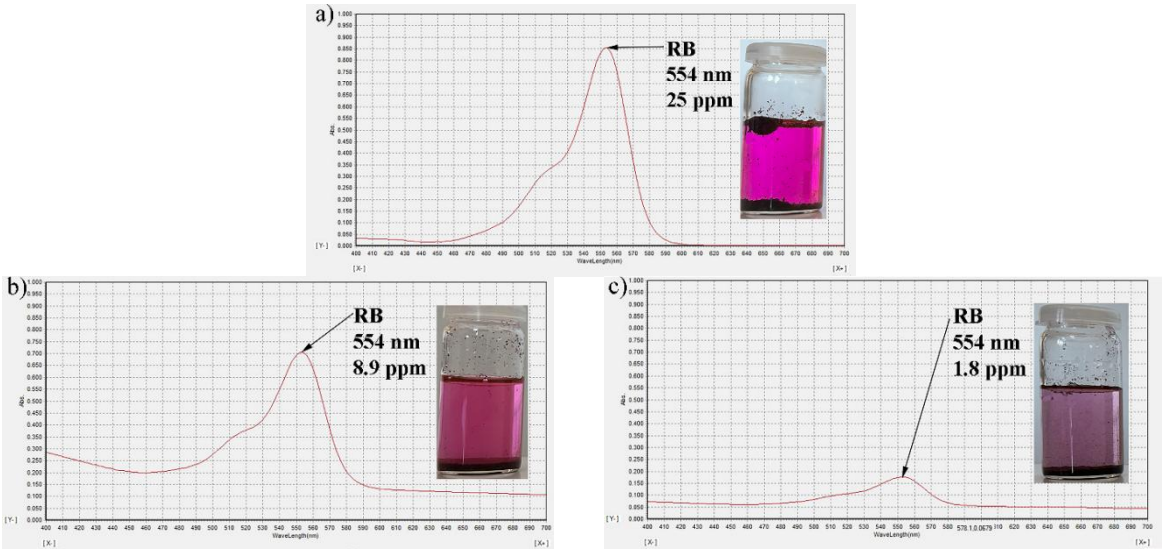

Figure 1 *UV–Vis spectrum: a) before biosorption of RB; b) after biosorption of RB with non-magnetic biosorbent; c) after biosorption of RB with magnetic biosorbent*

FTIR spectroscopy is a useful technique for identifying the characteristic functional groups present on the surface of biosorbents. A comparison of the FTIR spectra of the both biosorbents, before and after biosorption of RB, is presented in Figure 2. The FTIR spectra show broad bands around 3400 and 3300 cm^{-1}, which are attributed to the stretching vibrations of –OH and $–NH_2$ groups originating from cellulose, hemicellulose, and lignin [5]. The peaks observed at ~2920 and ~2850 cm^{-1} correspond to the stretching vibrations of $–CH_2$ and –CH groups of cellulose and hemicellulose [4]. Absorption bands at ~1600 cm^{-1} are associated with the stretching vibrations of aromatic structures [5]. The bands recorded at ~1420 and ~1418 cm^{-1} are due to C=C stretching vibrations [6]. Also, the absorption peaks at ~1600 and ~1420cm^{-1} indicate the presence of –COO of carboxyl, and C–O groups on the biosorbents surface [4]. The peaks at ~1330 and ~1030 cm^{-1} signifies the –OH and C–N bonds [7]. In addition, the peak observed at approximately 560 cm^{-1} corresponds to magnetite,

indicating a clear difference between the non-magnetic and magnetic biosorbent [4,5]. Based on the FTIR spectra, the functional groups that exhibit affinity for RB were –OH, $–NH_2$, and –COOH. Furthermore, several peaks shifted or disappeared after the biosorption process, which clearly indicates that the biosorption of RB onto the Ambrosia-based biosorbents occurred.

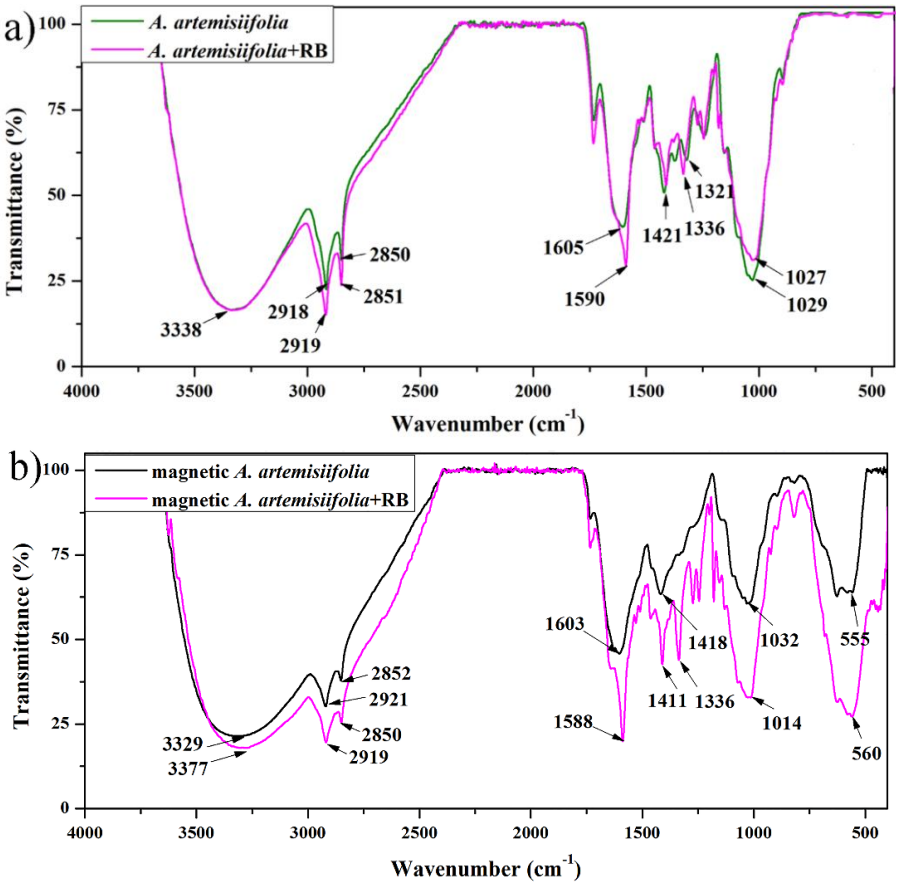

Figure 2 *FTIR spectra of: a) non-magnetic biosorbent; and b) magnetic biosorbent, before and after biosorption of RB*

CONCLUSION

Experimental results showed that both biosorbents, based on the biomass of *A. arthemisiifolia*, can be used for the removal of RB from aqueous solutions. Biosorption capacities obtained in batch experiments at 120 min and 6.2 pH were 1.3 and 2 mg/g for non-magnetic and magnetic biosorbent, respectively. Higher RB removal efficiency was obtained for the magnetic biosorbent, which, combined with its easy separation, gives the magnetic biosorbent a potential advantage for application in industrial wastewater treatment in the near future. FTIR analysis revealed shifts of characteristic biosorption bands, particularly 1605 to 1590 cm^{-1} and 1603 to 1588 cm^{-1}, together with changes in band intensities after biosorption, providing evidence of RB binding onto both biosorbents. This green approach has the potential to be implemented in the future, as a cost-effective method for the treatment of industrial wastewater, which will be the focus of future research.

ACKNOWLEDGEMENT

This research has been financially supported by the Ministry of Science, Technological Development and Innovation of Republic of Serbia (Contract No. 451-03-33/2026-03/200026). The research presented in this study aligns with Goal 6 (Ensure availability and sustainable management of water and sanitation for all) of the Agenda 2030 – United Nations Sustainable Development Goals (SDGs).

REFERENCES

[1] Şenol, Z.M., Messaoudi, N.E., Fernine, Y., *et al.* Biomass Convers. Biorefin. 2023, 14, 1–14.

[2] Oladoye, P.O., Kadhom, M., Khan, I., *et al*. GreenChE. 2024, 5, 440–460.

[3] Storkey, J., Stratonovitch, P., Chapman, D.S., *et al*. PLoS One. 2014, 9 (2), e88156.

[4] Nedić, N., Tadić, T., Marković, B., *et al*. J. Serb. Chem. Soc. 2025, 1–17.

[5] Nedić, N., Tadić, T., Marković, B., *et al*. Separations 2024, 11, 310.

[6] Saufi, H., Alouani, M.E., Aride, J., *et al*. Chem. Data Collect. 2020, 25, 100330.

[7] Swathilakshmi, A.V., Geethamala, G.V., Poonkothai, M., Biomass Convers. Biorefin. 2025, 15, 24083–24104.

EcoTER'26
eco.tfbor.bg.ac.rs
32nd International Conference
Ecological Truth & Environmental Research
24–26 June 2026, Hotel Sunce,
Sokobanja, Serbia

Original Research

EFFECT OF Ni AND Si ADDITIONS ON FUNCTIONAL PROPERTIES OF Cu-30Zn BRASS

DOI: 10.5937/EcoTER26443B

Ljubiša T. Balanović[1,a*], Uroš S. Stamenković[1,b], Ivana I. Marković[1,c], Kristina N. Božinović[1,d], Milan D. Gorgievski[1,e], Vesna J. Grekulović[1,f], Teodora S. Jogrić[1,g]

[1] University of Belgrade, Technical Faculty in Bor, Vojske Jugoslavije 12, 19210 Bor, SERBIA

[a] https://orcid.org/0000-0002-3551-6731 [b] https://orcid.org/0000-0002-7579-2159

[c] https://orcid.org/0000-0003-4431-9921 [d] https://orcid.org/0000-0002-9834-448X

[e] https://orcid.org/0000-0002-9899-719X [f] https://orcid.org/0000-0001-6871-4016

[g] https://orcid.org/0009-0009-6582-8160

Abstract

The present work investigates the effect of Ni and Si additions on functional properties of Cu-30Zn brass. One base alloy without Ni and Si additions and one alloy with Ni and Si additions were prepared by conventional casting from high-purity Cu, Zn, Ni and Si, followed by solution annealing at 900 °C for 2 h and water quenching, cold pressing, and subsequent ageing at 300 °C for 8 h. Building on earlier studies of Ni_2Si-strengthened Cu–Zn and Cu–Ni–Si alloys, this processing route was selected to promote the formation of fine Ni–Si-rich precipitates within an α-brass matrix and to combine solid-solution and precipitation strengthening with acceptable electrical and thermal conductivities. The heat-treated alloys were characterized by measurements of electrical conductivity, Vickers microhardness (HV0.15), Leeb hardness (HLD) and thermal conductivity. Increasing Ni and Si contents is expected to raise hardness through solid-solution and Ni_2Si-type precipitation strengthening, while moderately reducing conductivity due to enhanced electron scattering by solute atoms and nanoscale particles. The results of this study provide composition–property guidelines for designing lead-free, precipitation-strengthened brasses based on the Cu-30Zn system.

Keywords: Cu-30Zn brass, precipitation, microhardness, conductivity.

INTRODUCTION

Brass alloys are widely used in electrical and mechanical engineering due to their combination of good corrosion resistance, satisfactory strength and relatively high electrical and thermal conductivity [1,2]. Recent work on next-generation lead-free α + β brasses has further highlighted the need to maintain these properties while eliminating lead, especially for free-cutting and plumbing applications where human exposure and environmental release are critical concerns [3]. Systematic reviews of lead-free brass development for machining applications highlight the dual challenge of meeting increasingly strict environmental

* *ljbalanovic@tfbor.bg.ac.rs*

regulations while achieving machinability and performance comparable to conventional leaded brasses [4].

In recent years, special attention has been paid to Ni–Si-modified brasses, in which fine Ni_2Si precipitates provide significant precipitation strengthening while maintaining acceptable conductivity [1,2,5,6].

Chen *et al*. showed that the addition of 1.5–3 wt.% Ni and 0.34–0.68 wt.% Si to Cu–20Zn brass, followed by appropriate thermo-mechanical treatment, can almost double the tensile strength compared to conventional Cu–Zn alloys due to combined solid-solution and Ni_2Si precipitation strengthening [1], building on their earlier work on Ni–Si-modified Cu–10Zn and Cu–20Zn alloys [5]. In that previous study, the same authors examined Cu–10Zn and Cu–20Zn alloys with small Ni and Si additions in order to obtain high-strength brasses without a serious loss of ductility. They related the large increase in strength mainly to solid-solution and Ni_2Si-type precipitation strengthening and to the corresponding microstructural changes in the Cu–Zn matrix [5].

Systematic studies on Cu–Ni–Si alloys have demonstrated that an optimized Ni/Si mass ratio of about 4–5 leads to a dense distribution of nanoscale Ni_2Si precipitates and a favourable balance between hardness, strength and electrical conductivity [2].

Shan *et al*. used CALPHAD-aided design to develop complex Cu–Zn–Ni–Si brasses and to clarify how δ-Ni_2Si precipitates form and evolve as the main reinforcing phase in these alloys. By combining thermodynamic calculations with experimental verification, they optimised the alloy composition and heat-treatment parameters to promote a high volume fraction of finely dispersed δ-Ni_2Si particles, which provide strong precipitation strengthening while retaining acceptable toughness and castability [6].

Zhou and Su reported a novel Cu–Ni–Zn–Al alloy in which high strength is achieved primarily through a controlled precipitation-hardening treatment. In their study, they showed that suitable aging conditions lead to the formation of a fine, homogeneous distribution of strengthening precipitates in the Cu–Ni–Zn matrix, resulting in a marked increase in yield and tensile strength while maintaining reasonable ductility [7].

Rojas-Rodríguez *et al*. investigated how different precipitation-heat-treatment temperatures affect the microstructure, thermal properties and microhardness of an α-brass, showing a clear link between ageing conditions and property changes [8].

At the same time, there is growing interest in replacing traditional leaded brasses with environmentally friendly, precipitation-strengthened alloys that offer similar machinability and strength without toxic elements and with reduced environmental and health impacts of alloy production and recycling [1–3]. In this context, Ni–Si-strengthened Cu-based alloys are considered promising candidates for lead-free components in electrical and mechanical applications where a combination of high strength, good conductivity and improved environmental compatibility is required [1,2].

Previous work on Cu-30Zn brass has mainly focused on the effect of cold work and annealing on twin formation and anneal hardening, while systematic data on the influence of small Ni and Si additions on functional properties of Cu-30Zn-based alloys are still limited [1,9].

Therefore, the present study focuses on Cu-30Zn-based alloys with a small amount of Ni and Si, in order to clarify how these additions, in combination with solution treatment and ageing, influence conductivity and hardness.

MATERIALS AND METHODS

Experimental Procedures

Alloy preparation

Two Cu–30Zn–xNi–ySi alloys (L1–L2) were prepared from high-purity cathode copper, zinc, nickel and silicon. The charge for each composition was melted in an electric resistance furnace using a graphite crucible and a protective flux. After complete melting and initial homogenization, the alloy was remelted several times, with the crucible periodically inverted to enhance chemical homogeneity. In designing the alloy with additions, the Ni and Si contents were selected to maintain a Ni:Si mass ratio of 4.4:1, following previous CALPHAD-assisted studies on Ni–Si reinforced brass alloys [6], and experimental investigations of Ni_2Si-strengthened Cu–Zn brasses [1]. The nominal chemical compositions of the alloys are listed in Table 1.

Table 1 *Chemical composition of the alloys*

Sample	Ni (wt.%)	Si (wt.%)	Cu (wt.%)	Zn (wt.%)	Total (wt.%)
L1	0	0.00	70.00	30.00	100
L2	0.5	0.11	69.57	29.82	100

Solution treatment and ageing

The cast alloys were machined to remove surface defects. All samples were solution annealed at 900 °C for 2 h in air, followed by immediate quenching in water to obtain a supersaturated α-brass matrix. The heat-treatment schedule and deformation route were adopted from previous studies on Ni_2Si-strengthened Cu–Zn brasses [1], where specimens were hot-rolled by 80% and subsequently cold-rolled by 80%. In the present work, after solution annealing and quenching, the specimens were cold pressed in a hydraulic press under a load of 15 t in order to introduce a comparable level of plastic deformation prior to ageing. Ageing was carried out at 300 °C for 8 h in a resistance furnace, followed by air cooling to room temperature. All property measurements and investigations were performed on samples in this aged condition.

Property characterization

Electrical conductivity was measured at room temperature using a Sigmatest 2.063 eddy-current device on flat, ground specimens; for each alloy, at least five readings were taken and averaged. Microhardness was determined by the Vickers method (HV0.15) with a 0.15 kgf load and 10 s dwell time, and a minimum of five indents per condition were performed on polished cross-sections. Macroscopic hardness was evaluated using a portable Leeb hardness tester Time 5350, and the results are reported in HLD units. Thermal conductivity was determined indirectly from the measured thermal diffusivity and the specific

heat capacity of each alloy, using the approach originally proposed by Parker et al. [10,11], for homogeneous materials. Thermal diffusivity was measured by the light-flash method using a Discovery Xenon Flash (DXF 500 - TA Instruments) apparatus on disc-shaped samples with both faces finely polished, at 25, 50, 100, 200, 300, and 400 °C, and the thermal conductivity was then calculated for each composition and temperature using equation 1. In this method, once the thermal diffusivity and the specific heat capacity are known, the thermal conductivity can be calculated as the product of density, specific heat capacity and thermal diffusivity:

$$\lambda = \alpha \cdot \rho \cdot Cp \tag{1}$$

where: $\boldsymbol{\lambda}$ is the thermal conductivity (W/mK), $\boldsymbol{\alpha}$ is the thermal diffusivity (m^2/s), $\boldsymbol{\rho}$ is the density (kg/m^3) and $\boldsymbol{C_p}$ is the specific heat capacity (J/kgK).

The specific heat capacity of the investigated alloys was obtained by comparing the temperature rise of the sample with the temperature of a reference material of known specific heat under identical differential measurement conditions.

RESULTS AND DISCUSSION

Table 2 summarizes the basic geometrical characteristics and densities of the investigated samples L1 and L2, which were prepared as disc-shaped cylinders with a diameter of 12.7 mm.

Table 2 *Geometrical characteristics and densities of samples L1 and L2*

Sample	Mass (g)	Height (mm)	Height (cm)	Diameter (mm)	Diameter (cm)	Base area (cm^2)	Volume (cm^3)	Density (g/cm^3)	Density (kg/m^3)
L1	4.17	3.86	0.386	12.81	1.281	1.2882	0.4972	8.3865	8387
L2	4.02	3.72	0.372	12.82	1.282	1.2902	0.4799	8.3760	8376

Electrical conductivity measurements

Results of the electrical conductivity measurements are presented in Table 3, which lists the mean value of five measurements taken on each side of the sample and the corresponding overall average value for each alloy, while Table 4 compares these results with literature data for Cu–Zn brasses.

Table 3 *Electrical conductivity of Cu-30Zn–Ni–Si alloys*

Sample	Side I (MS/m)	Side II (MS/m)	Average (MS/m)
L1	12.9	14.3	**13.6**
L2	12.1	12.5	**12.3**

The base Cu–30Zn alloy from this work exhibits an electrical conductivity of 13.6 MS/m (23.45%IACS), which is lower than the nominal industrial value of about 16 MS/m (≈28%IACS). This reduction can be attributed to differences in thermomechanical processing

and cold pressing, as well as to microstructural defects and residual stresses associated with the specific melting and heat-treatment route used in this study.

Table 4 *Comparison of electrical conductivity of Cu–Zn brasses in this work and literature*

Sample	Electrical conductivity (MS/m)	Electrical conductivity (%IACS)	References
(L1)	**13.6**	**23.45**	**This work**
(L2)	**12.3**	**21.21**	**This work**
Cu–20Zn–1.5Ni–0.34Si	**12.9**	**22.3**	[1]
Cu–20Zn–3Ni–0.68Si	12.5	21.6	[1]
Cu–20Zn–15Ni	4.06	7	[12]
Cu–20Zn–10Ni–1.2Al	6.38	11	[7]

The addition of 0.5 wt.% Ni and 0.11 wt.% Si in Cu–30Zn leads to a moderate decrease in conductivity to 12.3 MS/m (21.21%IACS), consistent with the expected reduction due to solid-solution and precipitation strengthening. In contrast, alloys containing higher Ni contents, such as Cu–20Zn–15Ni [12] and Cu–20Zn–10Ni–1.2Al [7], show significantly lower conductivities (down to about 7%IACS, and 11%IACS), illustrating the strong detrimental effect of high Ni additions on electrical transport.

Vickers microhardness measurements (HV0.15)

Results of the Vickers microhardness measurements ($HV_{0.15}$) for samples L1 and L2 are presented in Table 5, showing individual indentations on both sides of each sample and the corresponding mean values.

Table 5 *Vickers microhardness ($HV_{0.15}$) of samples L1 and L2*

Sample	Side I			Mean (Side I)	Side II			Mean (Side II)
	I	II	III		I	II	III	
L1	131.48	124.57	122.92	126.30	121.31	109.48	115.17	115.30
L2	124.57	133.30	127.95	128.60	126.24	109.48	124.57	120.10

The measured microhardness values (about 115–129 HV0.15) fall within the range typically reported for thermomechanically treated Cu-30Zn brasses [1,5,9,13], with hardness values around 110–130 HV depending on the degree of cold work and alloying additions. The slightly higher mean hardness of L2 compared to L1 is consistent with reports in the literature that Ni and Ni_2Si-type precipitates contribute to additional strengthening of Cu–Zn brasses through solid-solution and precipitation hardening mechanisms [1,2,5,14].

Leeb hardness measurements (HLD)

Results of the Leeb hardness measurements (HLD) for samples L1 and L2 are presented in Table 6, showing individual impacts on both sides of each sample and the corresponding

mean values. The measured Leeb hardness values (about 350–422 HLD) correspond, according to standard hardness conversion charts [15], to Vickers hardness levels on the order of 110–130 HV, which is consistent with the microhardness results obtained for these alloys. Such hardness levels are in line with reported values for cold-worked or precipitation-strengthened CuZn30-based brasses [1,5], confirming that the applied thermomechanical treatment and Ni–Si additions provide a noticeable increase in hardness compared with annealed CuZn30 products described in datasheet literature [16].

Table 6 *Leeb hardness (HLD) of samples L1 and L2*

Sample	Side I			Mean (Side I)	Side II			Mean (Side II)
	I	II	III		I	II	III	
L1	343	247	461	350	376	379	338	364
L2	439	355	472	422	380	400	374	385

Thermal conductivity measurements

Thermal diffusivity, thermal conductivity and specific heat capacity were measured three times for each condition, and the values reported in Table 7 represent the corresponding mean values for samples L1 and L2.

Table 7 *Thermal diffusivity, thermal conductivity and specific heat capacity of samples L1 and L2*

Temperature (°C)	Thermal diffusivity (mm^2/s)		Thermal conductivity (W/mK)		Specific heat capacity (J/kgK)	
	L1	L2	L1	L2	L1	L2
25	35.42	30.90	131.49	112.02	421.25	411.53
50	36.30	32.52	135.09	114.43	432.10	420.12
100	38.73	34.65	138.13	124.77	425.35	422.23
200	41.37	37.42	152.06	137.29	438.25	438.05
300	43.22	39.41	161.59	147.00	445.78	445.37
400	44.71	41.79	172.83	162.89	460.87	465.37

The thermal diffusivity of L1 increased from 35.42 mm^2/s at 25 °C to 44.71 mm^2/s at 400 °C, whereas L2 increased from 30.90 mm^2/s to 41.79 mm^2/s over the same temperature range. In all cases, L1 exhibited higher diffusivity than L2, suggesting more efficient heat transport in the base alloy. The increase with temperature is typical for this type of material and can be related to changes in the thermal response of the matrix, as well as the temperature dependence of heat-carrier scattering.

The thermal conductivity of L1 rose from about 131.5 W/mK at 25 °C to 172.8 W/mK at 400 °C, while L2 increased from 112.0 W/mK to 162.9 W/mK. Again, L1 showed consistently higher values than L2 at all temperatures, which indicates that the Ni–Si additions reduced thermal transport in the alloy. This behaviour may be explained by increased scattering of heat carriers by solute atoms and possible second-phase particles,

together with the general temperature dependence of thermal properties in copper-based alloys.

The specific heat capacity of L1 was about 421 J/kgK at 25 °C and increased to around 461 J/kgK at 400 °C, while L2 changed from approximately 411 J/kgK to 465 J/kgK. Both alloys showed a gradual increase in C_p with temperature, which is expected because more vibrational modes become active as temperature rises. Small differences between L1 and L2 most likely reflect compositional differences and the effect of microstructure on heat storage.

Overall, the base Cu–30Zn alloy (L1) showed higher thermal diffusivity and thermal conductivity than the Ni–Si-containing alloy (L2) across the whole temperature range, indicating that the additions reduced thermal transport, while the effect on specific heat capacity was comparatively small.

Figures 1 show the temperature dependence of thermal diffusivity (a), specific heat capacity (b) and thermal conductivity (c) for alloys L1 and L2, together with literature data from [17], which reports our previously published results for a Cu–30Zn brass produced in the Sevojno Copper Rolling Mill.

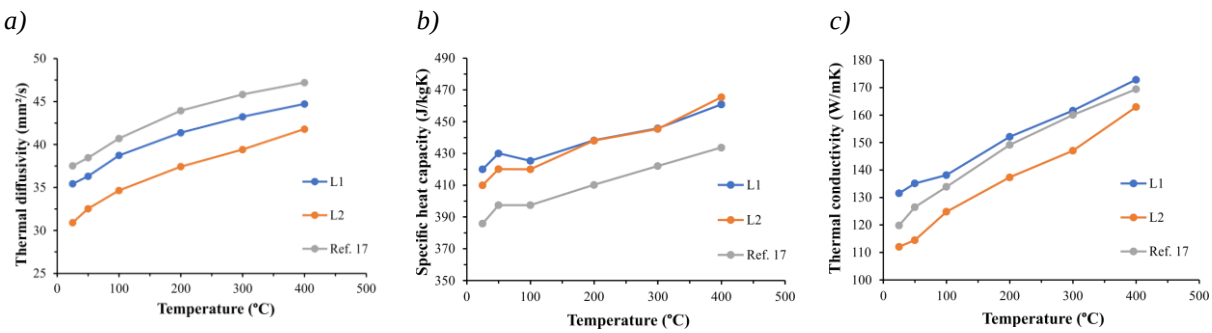

Figure 1 *Temperature dependence of (a) thermal diffusivity, (b) specific heat capacity and (c) thermal conductivity of investigated alloys L1 and L2, compared with literature data for Cu–30Zn brass [17]*

In our previous work [17], the examined sample was annealed at 540 °C for 4 h, had a composition of 70.1 wt.% Cu (balance Zn) with small amounts of impurities (0.001 wt.% Pb and 0.017 wt.% F), and was in a fully soft condition with an average grain size of about 0.035 mm. In this reference state, the material represents a well-annealed α-brass with relatively coarse grains, whereas in the present study, L1 and especially L2 were subjected to a different thermomechanical route (solution treatment, quenching, and cold pressing) and, in the case of L2, modified by Ni–Si additions. As a consequence, L1 generally exhibits slightly higher thermal transport properties than the annealed Cu–30Zn from [17], while L2 remains below both L1 and the reference curve, which is consistent with the combined influence of Ni–Si microalloying and the altered processing on thermal conductivity, thermal diffusivity and specific heat capacity.

CONCLUSION

The present study examined the effect of small Ni and Si additions on functional properties of Cu–30Zn brass processed by solution annealing, water quenching, cold pressing and

ageing. The results show that the Ni–Si-modified alloy L2 (0.5 wt.% Ni, 0.11 wt.% Si) achieves higher Vickers microhardness and Leeb hardness than the base Cu–30Zn alloy L1, confirming that the applied thermo-mechanical treatment promotes combined solid-solution and precipitation strengthening, most likely associated with the formation of fine Ni–Si-containing phases within the α-brass matrix.

At the same time, both electrical and thermal conductivities of L2 are moderately reduced compared with L1, but remain within the range reported for technologically relevant Cu–Zn brasses and previously studied Ni_2Si-strengthened alloys, thus preserving acceptable functional performance. Thermal diffusivity, thermal conductivity and specific heat capacity of both alloys increase with temperature, in agreement with literature data for α-brasses and Cu-based alloys, while L1 consistently exhibits higher thermal transport than L2 over the entire temperature range, reflecting the influence of Ni–Si additions and processing on heat-carrier scattering. The present results indicate that minor Ni–Si additions to Cu–30Zn brass, combined with an appropriate heat-treatment route, offer a viable strategy for designing lead-free, precipitation-strengthened brasses that achieve an improved strength–conductivity balance suitable for applications requiring both mechanical robustness and good thermal and electrical conductivity.

ACKNOWLEDGEMENT

The authors are grateful to the Ministry of Science, Technological Development and Innovation of the Republic of Serbia for financial support under contract No. 451-03-34/2026-03/200131.

REFERENCES

[1] Chen, W., You, K., Yin, J., *et al.* Met. Mater. Int, 2022, 28(10), 2555–2562.

[2] Li, J., Huang, G., Mi, X., *et al.* Materials 2019, 12(13), 2076.

[3] Oishi, K., Goto, H., Suzaki, K., *et al.* Mater. Trans. 2023,64(1), 191–195.

[4] Ribeiro, B.L., Monteiro, J., Truta, M., *et al.* 2026, 12(2), 971–993.

[5] Chen, W., Jia, Y., Yi, J., *et al.* J. Mater. Res., 2017, 32(16), 3137–3145.

[6] Shan, X., Peng, B., Li, G., *et al.* Mater. Sci. Eng. A, 2025, 923, 147759.

[7] Zhou, X.-Z., Su, Y.-C. Mater. Sci. Eng. A, 2010, 527(20), 5153–5156.

[8] Rojas-Rodríguez, I., Lara-Guevara, A., Salazar-Sicacha, M., *et al.* Mater. Sci. Appl. 2018, 9, 440–454.

[9] Birch, J., Jenkins, E., Vrettou, A., *et al.* Acta Mater. 2024, 278, 120277.

[10] Parker, W.J., Jenkins, R.J., Butler, C.P., *et al.* 1961, 32(9), 1679–1684.

[11] Gaal, P.S., Thermitus, M.A., Stroe, D.E., 2004, 78(1), 185–189.

[12] Zhou, X.Z., Su, Y.C., Sun, J.M. 2010, 45(11), 3080–3087.

[13] Xiao, Z., Yang, X., Wang, J., *et al.* 2017, 712, 268–276.

[14] Zheng, Z., Guo, P., Li, J., *et al.* J. Alloys Compd. 2020, 831, 154842.

[15] HardnessTest.co.uk, Hardness Conversion Chart. Available from: https://hardnesstest.co.uk/pages/hardness-conversion-chart, on: May 1, 2026.

[16] Aurubis, CuZn30 (C26000) – Technical datasheet, Aurubis AG, Hamburg, Germany.

[17] Balanović, L., Nikolajević, A., Manasijević, D., *et al.* Proceedings of the Metallurgical & Materials Engineering Congress of South-East Europe, June 4–7, Trebinje, Bosnia and Herzegovina, (2023).

Original Research

SYNERGISTIC INTERACTION BETWEEN Sb AND RARE-EARTH OXIDES IN SnO_2 ELECTROCATALYSTS

DOI: 10.5937/EcoTER26452S

Katarina Stojanović[1,a*], Marija Simić[1,b], Danka Aćimović[1,c], Branislava Savić Rosić[1,d], Marija Ječmenica Dučić[1,e], Danijela Maksin[1,f], Tanja Brdarić[1,g]

[1]University of Belgrade, Vinča Institute of Nuclear Sciences-National Institute of the Republic of Serbia, Mike Petrovića Alasa 12-14, 11000 Belgrade, SERBIA

[a] https://orcid.org/0009-0003-3467-9875 [b] https://orcid.org/0000-0001-9518-7709

[c] https://orcid.org/0000-0001-7506-9684 [d] https://orcid.org/0000-0002-4632-7960

[e] https://orcid.org/0000-0002-6437-519X [f] https://orcid.org/0000-0003-4842-1122

[g] https://orcid.org/0000-0003-2547-7123

Abstract

The synergistic interaction between Sb doping and rare-earth oxide modification of SnO_2 electrodes was investigated toward the oxygen evolution reaction (OER) using linear sweep voltammetry (LSV). Sb doping significantly improved electrode performance, increasing current density and reducing the onset potential to ~1.60 V vs SHE. The addition of rare-earth oxides further modulated the activity in a composition-dependent manner. Gd_2O_3 and Eu_2O_3 exhibited a positive synergistic effect, maintaining high conductivity while enhancing surface reactivity, whereas Sm_2O_3 showed a similar contribution. In contrast, Y_2O_3 disrupted the synergy, leading to electrode deactivation. The results demonstrate that optimal OER performance arises from the balance between bulk conductivity (Sb effect) and surface catalytic properties (rare-earth effect).

Keywords: SnO_2-Sb electrode, rare-earth oxides, LSV.

INTRODUCTION

Electrochemical oxidation processes, particularly the oxygen evolution reaction (OER), play a crucial role in environmental remediation and wastewater treatment. Tin dioxide (SnO_2)-based electrodes are widely studied due to their chemical stability and high oxygen overpotential [1]. However, their relatively low electrical conductivity limits their catalytic efficiency.

Doping with antimony (Sb) is a well-established strategy to enhance electrical conductivity and improve electrochemical performance. In recent years, additional surface modification using rare-earth oxides has attracted attention due to their ability to alter surface defect chemistry, oxygen mobility, and catalytic activity [2].

* *katarina.stojanovic@vin.bg.ac.rs*

A key challenge is achieving a balance between electrical conductivity and surface catalytic activity. Sb doping is known to improve the bulk conductivity of SnO_2, while rare-earth oxides can modify surface properties such as defect density and oxygen mobility.

However, the synergistic interaction between Sb doping and rare-earth oxide modification of SnO_2 electrodes toward to tne electrical conductivity and OER remains insufficiently understood. Therefore, this study systematically investigates the influence of Eu_2O_3, Gd_2O_3, Sm_2O_3, and Y_2O_3 on the electrochemical performance of Sb-doped SnO_2 electrodes, with particular emphasis on whether rare-earth oxide incorporation enhances or disrupts the overall electrocatalytic activity.

MATERIALS AND METHODS

SnO_2-based electrodes doped with Sb and modified with rare-earth oxides (Eu_2O_3, Gd_2O_3, Sm_2O_3, Y_2O_3) were synthesized according to procedures by Zhi [3] and Xin *et al*. [4]. Electrochemical measurements were performed using linear sweep voltammetry (LSV) in an Na_2SO_4 (0.1M, pH 4) as electrolyte.

The potential was scanned from −0.5 to 3.5 V vs Ag/AgCl at a constant scan rate (10mV/s). All potentials were converted to the standard hydrogen electrode (SHE) scale.

RESULTS AND DISCUSSION

The LSV curves (Figure 1a) clearly demonstrate that OER activity is governed by a synergistic interplay between Sb doping and rare-earth oxide modification.

The undoped SnO_2 electrode shows poor performance, confirming that both conductivity and catalytic activity are limited in the absence of modification. Introduction of Sb significantly enhances performance by improving charge transport, resulting in a lower onset potential (~1.60 V vs SHE) and a substantial increase in current density (Figure 1b).

The addition of rare-earth oxides further modulates this behavior, revealing distinct synergistic and antagonistic effects:

Gd_2O_3 and Eu_2O_3 preserve the high conductivity induced by Sb while enhancing surface catalytic properties, resulting in a positive synergistic effect. This is reflected in high current densities (~ 15 mA cm^{-2}) and relatively low OER onset potentials (Figure 1b, c).

Also, Sm_2O_3 exhibits a similar synergistic interaction, leading to moderate activity (~12 mA cm^{-2}), suggesting partial improvement of surface properties without fully optimizing the interface.

Y_2O_3, in contrast, disrupts the synergy between conductivity and catalytic activity. As shown in Figure 1, this sample exhibits negligible current response, indicating that Y_2O_3 likely blocks active sites or introduces an insulating effect that counteracts the benefits of Sb doping.

The overall trend (Figure 1): SnO_2–Sb > Gd_2O_3 > Eu_2O_3 ≈ Sm_2O_3 >> SnO_2 > Y_2O_3, confirms that the best performance is achieved when bulk conductivity (Sb effect) and surface reactivity (rare-earth effect) act in synergy.

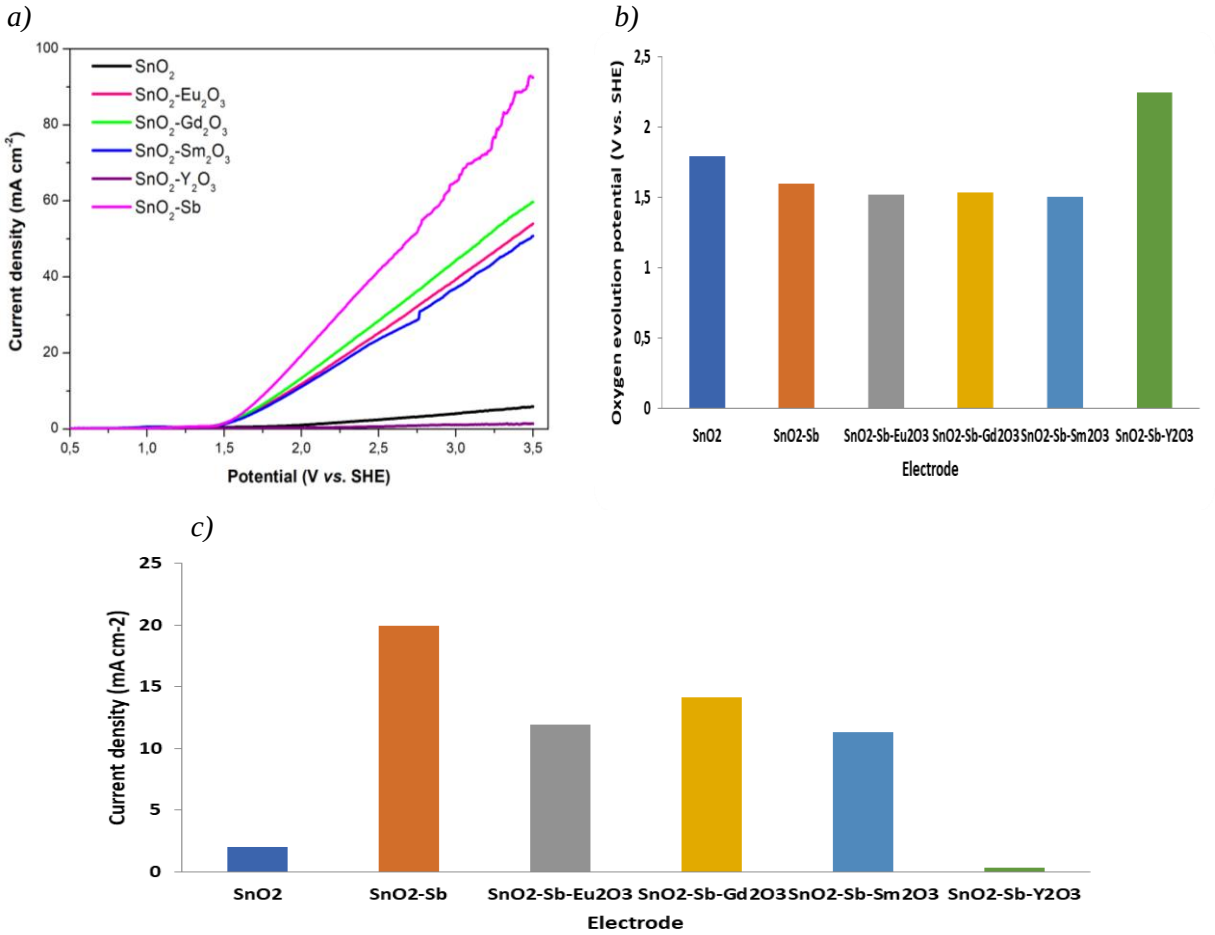

Figure 1 *a) LSV curves of SnO_2-based electrodes (SnO_2, SnO_2–Sb, and rare-earth modified electrodes) recorded in Na_2SO_4 (0.1M) electrolyte pH 4; b) OER potential bar chart; and c) current (at 2.0 V) bar chart. Potentials are presented vs SHE*

CONCLUSION

The results demonstrate that OER activity on SnO_2 electrodes is not determined by a single modification but by the synergy between Sb doping and rare-earth oxides. While Sb ensures efficient charge transport, rare-earth oxides tune surface catalytic properties. Gd_2O_3 , Eu_2O_3 and Sm_2O_3 exhibit a beneficial synergistic effect, whereas Y_2O_3 disrupts this balance, leading to deactivation. These findings highlight the importance of simultaneously optimizing bulk and surface properties in the design of efficient electrocatalysts.

ACKNOWLEDGEMENT

The authors are grateful to the Ministry of Science, Technological Development and Innovation of the Republic of Serbia for financial support according to the contract with registration No. 451-03-33/2026-03/ 200017.

REFERENCES

[1] Simić, M., Savić, B., Ognjanović, M., *et al*. J. Water Process Eng. 2023, 51, 103416.

[2] Brdarić, T., Aćimović, D., Stojanović, K., *et al*. Sustainability 2024, 16, 3982.

[3] Zhi, D., Qin, J., Zhou, H., *et al*. J. Appl. Electrochem. 2017, 47, 1313–1322.
[4] Xin, Y., Wang, Z., Qi, Y., *et al*. J. Alloys Compd. 2010, 507, 105–111.

EcoTER'26
eco.tfbor.bg.ac.rs
32nd International Conference
Ecological Truth & Environmental Research
24–26 June 2026, Hotel Sunce,
Sokobanja, Serbia

Original Research

QUANTITATIVE DETERMINATION OF ESSENTIAL AND TOXIC ELEMENTS CONTENT IN PEACH FRUITS BY ICP-OES METHOD

DOI: 10.5937/EcoTER26456D

Milan Đorđević[1,a*], Branka Stojanović[1,b], Aleksandar Zdravković[1,c], Danijela Stojadinović[1,d], Tanja Nikolić[1,e], Sandra Stojanović[1,f]

[1] Academy of Applied Studies Southern Serbia, Department of Higher Technology and Art School Leskovac, Vilema Pušmana 17, 16000 Leskovac, SERBIA

[a] https://orcid.org/0009-0004-4455-4651 [b] https://orcid.org/0009-0002-3748-6422
[c] https://orcid.org/0000-0001-9906-3543 [d] https://orcid.org/0000-0002-6335-8101
[e] https://orcid.org/0009-0007-8932-6128 [f] https://orcid.org/0000-0001-6354-7511

Abstract

This paper deals with the contents of macroelements (K, Ca, Mg, Na, and P), microelements (Fe, Cu, Mn, B, Co, Cr, and Ni), and selected toxic elements (Al, As, Pb, and Cd) which were determined in peach fruits of several cultivars grown in Southeastern Serbia. The elemental composition was analyzed using the inductively coupled plasma optical emission spectrometry (ICP-OES) method. As expected, potassium was the most abundant macroelement, with the highest concentration recorded in the cultivar Adria (5944 mg kg^{-1}). The remaining macroelements were present at lower concentrations, without pronounced differences among the samples. In contrast, some variability was observed among microelements, particularly for iron (5.5–11.1 mg kg^{-1}) and copper (0.831–1.598 mg kg^{-1}), while manganese exhibited more stable levels. Nickel and chromium were detected only in trace amounts. Toxic elements were present at low concentrations; cadmium was not detected in any sample, while lead ranged from 0.009 to 0.024 mg kg^{-1}, which is significantly below established regulatory limits. Overall, the results indicate that the analyzed fruits are safe for consumption. The observed differences in elemental composition are most likely associated with cultivar characteristics, given that all samples originated from the same cultivation area.

Keywords: peach, minerals, ICP-OES determination.

INTRODUCTION

Metals in fruits are present as salts of corresponding organic and inorganic acids or in the form of complex compounds, which is of great importance for their bioavailability. In addition to air, soil, and water, the metal content in fruits may be influenced by agricultural practices, industrial processing, the use of preservatives and additives, and other factors. Elevated levels of certain heavy and toxic metals represent an important parameter both in assessing potential adverse effects on human health and as indicators of environmental pollution. The presence of metals in the human body is primarily a consequence of dietary intake; therefore, monitoring metal content in commonly consumed foods in relation to recommended daily intakes is essential.

* *milan.djordjevic3093@gmail.com*

After gaseous toxins, metals rank second among the most significant causes of occupational diseases. Heavy metals are defined as metals with a density greater than 4 g cm^{-3} [1].

According to their biological function, metals are classified into:

1. Essential metals (Cu, Fe, Mn, Cr), which are indispensable for life. Their deficiency or insufficient intake may lead to severe physiological disorders or even death. They play crucial roles as structural components of enzymes and as enzymatic activators. These elements are present in very low concentrations and are therefore referred to as trace elements. They exert biological functions only within a narrow concentration range, while higher concentrations may result in toxicity.

2. Non-essential metals (Pb, Al, Cd, Hg, As), which have no known biological function and exhibit exclusively toxic effects [2]. The widespread occurrence of heavy metals in the environment represents a serious ecological and health concern due to their toxicity, non-biodegradability, long half-life in soil, and tendency to accumulate in living systems through the food chain. Heavy metals occur naturally in soils through weathering of parent rock but may also be introduced anthropogenically via industrial activities, fossil fuel combustion, agrochemical application, and atmospheric deposition, leading to long-term contamination of soil and water systems. In aquatic environments, metals can form poorly soluble carbonates, sulfates, and sulfites that accumulate in sediments. Plants absorb heavy metals from soil, water, fertilizers, and pesticides. Through plant consumption, these metals enter animal and human organisms, initiating processes such as bioaccumulation and biomagnification within the food chain.

Toxic metals are primarily associated with occupational and chronic poisoning resulting from exposure to metal vapors or particles during industrial processes. The main routes of exposure are the respiratory tract and skin for occupationally exposed individuals, and the respiratory and gastrointestinal tracts for the general population. Absorption of heavy metals from air occurs predominantly via inhalation, where aerosols or vapors enter the lungs, bind to plasma proteins, and are transported to target organs where toxic effects are exerted. Dermal absorption occurs through the epidermis, hair follicles, or sebaceous glands. Heavy metals are typically deposited in specific target organs; for example, cadmium accumulates in the kidneys with a biological half-life of 10–30 years, while lead accumulates in bones with a half-life of approximately 10 years. Metals are generally metabolically inert and do not undergo transformation in the body, except for metalloids (As, Sb, Se), whose organic and inorganic forms may be detected in urine [2]. Metal toxicity primarily arises from interactions with proteins, lipids, and nucleic acids, binding to functional groups such as amino, hydroxyl, carboxyl, and thiol groups, thereby inhibiting biological activity. Some metals promote the formation of free radicals, inducing oxidative stress. As protoplasmic toxins, they interact with intracellular structures, bind to sulfhydryl groups of proteins, and inactivate their function. Certain metals exhibit genotoxic and carcinogenic effects, while others may trigger hypersensitivity reactions [3].

MATERIALS AND METHODS

Sample collection and preparation

Healthy fruits of peach cultivars (Radmilovcanka, June Gold, Blake, Hale, Vesna, and Adria) were obtained directly from producers in Southeastern Serbia. The samples were harvested at full maturity during the 2025 growing season.

The accurately weighed samples (approximately 10 g) of previously homogenized fresh fruit material were transferred into porcelain crucibles and subjected to thermal treatment in an electric furnace. The furnace was programmed to increase the temperature from 50 °C to 450 °C over a period of 8 hours, followed by maintaining this temperature constant for an additional 12 hours. After the complete digestion the cooled dry residues were dissolved in 2.5 ml HNO_3 (1:1, v/v), filtered through Whatman No. 42 filter paper and transferred to a 50 ml volumetric flask with deionized water [4].

Instrumentation

Metal concentrations were determined by ICP-OES (iCAP 6000, Thermo Scientific, UK). Sample masses were measured using a Mettler Toledo (Switzerland) analytical balance, and high-purity water (0.05 µS cm^{-1}) was obtained using MicroMed high purity water system, Thermo Electron LED GmbH (Germany).

Measurements were conducted under optimized conditions (RF power 1150 W; pump rate 50 rpm; nebulizer gas flow 0.7 L min^{-1}; coolant gas flow 12 L min^{-1}; auxiliary gas flow 0.5 L min^{-1}). Emission lines were selected to minimize interferences and ensure optimal signal-to-background ratios.

An individual analytical method was developed through the selection of appropriate instrumental parameters. Calibration curves, expressing the dependence of relative emission intensity at a selected wavelength on analyte concentration, were constructed using a blank solution (deionized water) and two standard solutions of different concentrations were prepared by dilution of a primary reference standard. All measurements were performed in triplicate. The optimal (analytical) wavelength was selected based on the relative signal intensity as a measure of method sensitivity, the accuracy of the standard response, and the extent of spectral interferences arising from coexisting elements in this complex sample matrix. An inductively coupled plasma optical emission spectrometer (ICP-OES) was employed for the determination of metal ions in fruit samples. Owing to its high sensitivity (ppb level), wide linear dynamic range for numerous elements, low susceptibility to chemical interferences, and capability for simultaneous multielement analysis, ICP-OES represents a near-ideal technique for the determination of metal ions in fruit matrices. The analysis of mineral content in fruit is inherently challenging due to the complexity of the matrix. Minerals are typically present at very low concentrations and are associated with significant amounts of organic matter, necessitating careful and appropriate sample preparation. In this paper, a dry ashing procedure was applied. Dry ashing is an inexpensive, simple, and rapid digestion method most applied for the elemental analysis of organic and inorganic samples. This process converts a large amount of sample into a small quantity of ash composed of inorganic compounds (mainly oxides).

RESULTS AND DISCUSSION

In order to determine the mineral composition of peaches (*Prunus persica* L.), samples from six different cultivars were analysed. This selection aimed to evaluate whether differences in elemental composition are cultivar-dependent. Using optimized analytical conditions, the concentrations of selected elements were determined in the fruit samples. Tables 1, 2, and 3 present the mean values of elemental content obtained from three consecutive measurements ± standard deviation (SD), calculated on a wet weight basis (mg kg^{-1} ww).

Table 1 *The content of essential macroelements ±sd (mg kg^{-1}ww) in peach fruit*

Varieties	Ca	K	Mg	Na	P
Adria	166±2	5944±43	97.1±0.6	54.6±0.2	374±3
Vesna	100±1	5459±41	96.8±0.5	62.3±0.3	402±5
Hale	163±2	1639±24	92.5±0.5	174±1	313±2
Blake	163±2	4049±36	108±0.7	230±2	335±3
June Gold	122±1	3620±29	112±0,8	140±1	381±4
Radmilovcanka	152±2	4151±31	96.4±0.3	115±1	373±3

In contrast to the fact that all samples originated from the same locality, the content of macroelements (Ca, K, Mg, Na, and P) in the analyzed peach cultivars exhibited noticeable variations among different varieties. Potassium (K) was the predominant element in all samples, with the highest concentration observed in the Adria cultivar (5944 mg kg^{-1}) and the lowest in the Hale cultivar (1639 mg kg^{-1}). This finding is consistent with literature data indicating that potassium is the most abundant macroelement in fruit tissues [5]. The contents of calcium (Ca), magnesium (Mg), and phosphorus (P) showed more moderate variation, suggesting relatively stable regulation and well-defined physiological roles of these elements in plant metabolism. In contrast, sodium (Na) exhibited a wider range of variation, which may be attributed to differences in its availability in the soil, as well as cultivar-specific characteristics influencing its uptake and accumulation [6]. The results obtained in this study are in agreement with those reported by Basar *et al.* [7] for peaches cultivated in Turkey, as well as by Manzoor *et al.* [8] for peaches grown in Pakistan.

Sodium and potassium are key elements responsible for maintaining electrolyte balance in the human body and for regulating blood pressure. The recommended daily values for macrominerals, expressed as Daily Value percentages (% DV) for adults and children over four years of age, are as follows: Ca 60 mg kg^{-1} (6%), Mg 90 mg kg^{-1} (22.5%), P 200 mg kg^{-1} (20%), and K 1900 mg kg^{-1} (54.29%). These values, also referred to in the literature as Recommended Daily Intake (RDI), represent approximate intake levels of essential nutrients sufficient to meet the requirements of healthy individuals [9].

The results presented in this paper indicate a certain degree of variability in the content of the investigated microelements (B, Co, Cr, Cu, Fe, Mn and Ni) among the analysed peach cultivars, despite all samples originating from the same locality. Given the uniform environmental conditions, the observed differences can primarily be attributed to

cultivar-specific characteristics, particularly differences in metal uptake and accumulation capacity.

Table 2 *The content of essential microelements ±sd (mg kg^{-1}ww) in peach fruit*

Varieties	B	Co	Cr	Cu	Fe	Mn	Ni
Adria	7.5±0.3	0.004±0.000	0.075±0.003	0.831±0.033	6.1±0.1	0.52±0.03	0.091±0.003
Vesna	7.9±0.3	0.005±0.000	0.118±0.006	0.991±0.040	8.9±0.2	0.41±0.02	0.081±0.06
Hale	2.1±0.1	0.001±0.000	0.088±0.004	0.914±0.068	8.6±0.2	0.42±0.02	0.21±0.02
Blake	5.8±0.2	0.002±0.000	0.084±0.003	1.223±0.039	11.1±0.3	0.51±0.03	0.16±0.01
June Gold	5.6±0.2	0.009±0.001	0.079±0.003	1.598±0.053	9.7±0.2	0.66±0.03	0.57±0.03
Radmilovcanka	5.1±0.1	0.003±0.000	0.084±0.004	0.892±0.039	5.5±0.2	0.41±0.02	0.18±0.04

As far as iron is concerned, a relatively wide concentration range was observed, with the Blake cultivar exhibiting the highest Fe content (11.1 mg kg^{-1}), while the lowest concentration was found in the Radmilovcanka cultivar (5.5 mg kg^{-1}). Similar ranges have been reported in the literature for peaches and other fruits, indicating that the obtained values fall within typical limits [10]. Therefore, it can be assumed that the observed variations are not a consequence of external contamination but rather reflect intrinsic physiological differences among cultivars.

Copper content varied within a narrower range compared to iron. The June Gold cultivar showed the highest concentration (1.598 mg kg^{-1}), whereas the lowest value was recorded in the Adria cultivar (0.831 mg kg^{-1}). Overall, all measured values fall within ranges commonly reported for fruit [11]. Manganese (0.41–0.66 mg kg^{-1}) concentrations were relatively uniform across cultivars, suggesting tighter physiological regulation of these element in plant tissues. In contrast, boron exhibited somewhat greater variability, particularly between the Vesna and Hale cultivars. This finding is expected, as boron availability in plants is strongly influenced by soil physicochemical properties as well as cultivar-specific traits [12]. Manganese plays an important role in carbohydrate metabolism and acts as an antioxidant. Iron is a key component of erythrocytes and hemoglobin. Adequate intake contributes to reducing the toxic effects of cadmium, whereas excessive intake may inhibit the absorption of copper and iron. Copper is an essential microelement with a biocatalytic role, important for pigmentation, maintenance of central nervous system function, and prevention of anemia. However, excessive exposure may lead to adverse effects that are often underestimated. Nickel participates in iron metabolism, influences its absorption from food, and plays a significant role in erythropoiesis, as well as in the metabolism of carbohydrates, lipids, hormones, and cell membrane components.

Among the essential trace minerals present in the analysed samples, chromium and cobalt are of paramount importance. Chromium is well known for its role in maintaining normal blood glucose levels and is involved in the metabolism of carbohydrates, lipids, and proteins. Due to its relatively low absorption efficiency, higher dietary intake is required. The recommended daily intake of chromium [12] ranges from 0.2 µg for infants to 15 µg for children aged 4–8 years, 35 µg for adolescents and adult men, and 25 µg for adult women. Cobalt is a trace element that constitutes an integral part of vitamin B_{12}, which plays a crucial

role in protein synthesis, normal growth, maintenance of epithelial tissues, and erythrocyte formation. However, prolonged exposure to elevated cobalt levels may result in excessive erythrocyte production, cardiotoxic effects, and thyroid dysfunction. In the analysed samples, cobalt concentrations ranged from 0.001 to 0.009 mg/kg.

The recommended daily values for selected microelements, expressed as percentage of Daily Value (% DV), are as follows: Cu 0.68 mg kg^{-1} (34%), Fe 2.5 mg kg^{-1} (13.89%) and Mn 0.61 mg kg^{-1} (30.5%) [10]. These values represent approximate intake levels sufficient to meet the nutritional requirements of healthy individuals.

The content of toxic metal in the analysed peach samples is essential as a parameter for assessing their safety for human consumption. The concentrations of Al, Cd, Pb, and As were determined, and the obtained results are presented in Table 3.

Table 3 *The content of toxic elements ±sda (mg kg-1 ww) peach fruit*

Varieties	Al	As	Pb	Cd
Adria	6.8±0.2	0.041±0.002	0.009±0.000	nd
Vesna	3.2±0.1	0.034±0.002	0.009±0.000	nd
Hale	8.1±0.2	0.065±0.002	0.020±0.001	nd
Blake	5.8±0.1	0.058±0.002	0.024±0.002	nd
June Gold	6.2±0.2	0.061±0.003	0.015±0.001	nd
Radmilovcanka	3.2±0.1	0.044±0.003	0.013±0.001	nd

The results of the analysis of toxic elements (Al, As, Pb, and Cd) indicate that their concentrations are low in all examined samples. Cadmium (Cd) was not detected, while the lead (Pb) content ranged from 0.009 to 0.024 mg kg^{-1}, which is significantly below the maximum permissible level for fruit established by European Union regulations (0.10 mg kg^{-1}). Arsenic (As) and aluminium (Al) were present at low to moderate concentrations, without pronounced differences among cultivars. The obtained results are consistent with literature data, where toxic elements in fruits are typically detected at trace levels.

Although all samples were collected from the same locality, the observed differences in elemental composition indicate a significant influence of cultivar characteristics. On the other hand, the role of soil as the primary source of elements cannot be neglected, as its chemical properties and pH directly affect element bioavailability. Additionally, the potential influence of atmospheric deposition, particularly in areas near road traffic, may contribute to the presence of certain elements; however, in this study, no elevated concentrations were observed that would indicate significant anthropogenic impact.

CONCLUSION

The obtained results confirm that the analysed peach cultivars from Southeastern Serbia represent a valuable source of essential macro- and microelements, with potassium identified as the dominant macroelement (up to 5944 mg kg^{-1} in the Adria cultivar). Iron and copper

contents exhibited greater variability among cultivars, whereas manganese was relatively uniform, and nickel and chromium were present only in trace amounts.

Toxic elements were detected at low concentrations; cadmium was not found in any sample, while lead levels (0.009–0.024 mg kg^{-1}) were significantly below the maximum permissible limits, confirming the safety of the analysed samples for human consumption.

Given the uniform sampling location, the observed differences in elemental composition can primarily be attributed to cultivar-specific characteristics, in accordance with the aim of the study. These findings highlight the importance of cultivar selection in the context of nutritional quality, while future research should focus on the influence of soil properties and agricultural practices on element accumulation. Based on the analysed parameters, the investigated peach cultivars can be considered both nutritionally valuable and safe for consumption.

ACKNOWLEDGEMENT

The authors gratefully acknowledge the financial support provided by the Academy of Applied Studies Southern Serbia.

REFERENCES

[1] Duffus, J.H. Pure Appl Chem. 2002, 74 (5), 793–807.

[2] Majkić N. Medicinska biohemija. Beograd: 2006. Grafopan doo, p. 605.

[3] Bulat Z. Mehanizmi toksičnosti otrova. U: Toksikologija sa analitikom. Beograd; 2010/11.

[4] Radojević M, Bashkin V. Practical Environmental Analysis. Cambridge, UK: The Royal Society of Chemistry; 1999.

[5] FAO. Mineral composition of fruits and vegetables. FAO Report; 2018.

[6] Kabata-Pendias A. Trace Elements in Soils and Plants. 4th ed. Boca Raton: CRC Press; 2011.

[7] Basar, H. Elemental composition of various peach cultivars. Sci Hortic. 2006, 107, 259–263.

[8] Manzoor, M., Anwar, F., Mahmood, Z., *et al*. Molecules. 2012, 17, 6491–6506.

[9] U.S. Department of Agriculture, Agricultural Research Service. USDA Food Composition Databases: Peaches, raw (No. 09236). 2016.

[10] AlJuhaimi, F., Akçay Kulluk, D., Gökmen Yılmaz, F. Biol Trace Elem Res. 2025, 203, 1676–1684.

[11] Sardar, K., Ali, S., Hameed, S., *et al*. Greener J Environ Manage Public Saf. 2013, 2(4), 172–179.

[12] Institute of Medicine. Dietary Reference Intakes for Vitamin A, Vitamin K, Arsenic, Boron, Chromium, Copper, Iodine, Manganese, Molybdenum, Nickel, Silicon, Vanadium, and Zinc. Washington, DC: National Academy Press 2001:773 p.

EcoTER'26
eco.tfbor.bg.ac.rs
32nd International Conference
Ecological Truth & Environmental Research
24–26 June 2026, Hotel Sunce,
Sokobanja, Serbia

Original Research

ANTIOXIDANT ACTIVITY OF CLOVE ESSENTIAL OIL

Sofija Banković[1,a*], Maja Lj. Petrović[2,b], Ana Janković[1,c], Marica Rakin[2,d], Maja Vukašinović Sekulić[2,e]

DOI: 10.5937/EcoTER26463B

[1] Innovation Center of the Faculty of Technology and Metallurgy, University of Belgrade, Karnegijeva 4, 1100 Belgrade, SERBIA

[2] Faculty of Technology and Metallurgy, University of Belgrade, Karnegijeva 4, 11000 Belgrade, SERBIA

[a] https://orcid.org/0009-0002-9883-2296 [b] https://orcid.org/0000-0002-1053-7739
[c] https://orcid.org/0000-0002-5605-3297 [d] https://orcid.org/0000-0001-5791-942X
[e] https://orcid.org/0000-0001-5374-5020

Abstract

The aim of this study was to determine the antioxidant activity of two different samples of clove essential oils (CEO) and their main bioactive compound, eugenol, in relation to their potential application as natural antioxidants in food products. Radical scavenging activity was evaluated using DPPH and ABTS assays, whereas electron-donating capacity was assessed with the ferric reducing antioxidant power (FRAP) assay. Both analyzed CEO showed a high polyphenol content (TPC), which correlates well with the presence of eugenol as the main bioactive compound in these oils. The high phenolic content was consistent with the results for both radical scavenging activity and reducing power. In all tests, eugenol demonstrated the strongest antioxidant effect, confirming its role as the primary contributor to the antioxidant properties of CEO. Both CEO exhibited strong antioxidant power, with negligible differences likely due to variations in their chemical composition. The results of this study highlights the potential application of CEO and eugenol as natural antioxidants in food production, while further research will focus on their encapsulation to enhance stability and bioavailability.

Keywords: natural antioxidants, clove essential oil, eugenol, radical scavenging, polyphenols.

INTRODUCTION

The primary cause of food degradation is lipid auto-oxidation, particularly in products with a high content of unsaturated fatty acids. This process results in the deterioration of sensory characteristics and nutritional value, as well as changes in chemical composition that may pose a health risk [1,2]. Lipid auto-oxidation occurs when unsaturated fatty acids react with oxygen, producing free radicals, which further initiate oxidation reactions [2–4]. To inhibit this process in food products, antioxidants are used [1]. Antioxidants can act as radical scavengers or through mechanisms that do not involve direct scavenging of free radicals, such as chelating metal ions, inhibiting the decomposition of lipid hydroperoxides, scavenging reactive oxygen species, or regenerating oxidised radical scavengers [2–5]. Synthetic

* *sbankovic@tmf.bg.ac.rs*

antioxidants commonly used in the food industry are phenolic substances, such as butylated hydroxytoluene (BHT), butylated hydroxyanisole (BHA), *tert*-butylhydroquinone (TBHQ) and propyl gallate [5]. Due to safety concerns related to the use of synthetic antioxidants and the current demand for cleaner food and natural additives, various natural antioxidants have been investigated [6,7].

Essential oils are complex mixtures of volatile compounds derived from plants and represent a rich source of natural antioxidants [8, 9]. The antioxidant activity of essential oils is dependent on their chemical composition and is associated with the concentration of phenolic compounds. They can neutralize peroxyl radicals by donating a hydrogen atom from the phenolic hydroxyl group [9, 10]. Furthermore, the synergistic activity of various bioactive compounds present in essential oils contributes to a stronger antioxidant effect [2].

Clove (*Syzygium aromaticum*) is a significant source of phenolic compounds, including flavonoids, hydroxycinnamic acids, hydroxybenzoic acids, and hydroxyphenyl propenes [11]. Clove essential oil (CEO) is typically obtained from dried buds. The main bioactive compound in CEO is eugenol, with its content often exceeding 70% [11,12]. Both CEO and eugenol have been shown to exhibit strong antioxidant effects, due to the phenolic structure of eugenol and its ability to scavenge free radicals and reactive oxygen species [13,14]. Other bioactive compounds present in CEO, such as eugenol acetate and *β*-caryophyllene, also contribute to this effect [15]. In addition to antioxidant activity, CEO and eugenol possess strong antibacterial and antifungal properties and are both classified as "generally recognized as safe" by the United States Food and Drug Administration which makes them potential alternatives to conventional food preservatives [16,17].

The aim of this study was to evaluate the radical scavenging activity, ferric reducing antioxidant power (FRAP), and total polyphenol content (TPC) of two different CEO and eugenol, considering their potential application as natural antioxidants in food products.

MATERIALS AND METHODS

Chemicals

Clove essential oil (CEO_1) was obtained from the local market (*Probotanic, Serbia)*. Clove oil (CEO_2) and eugenol were purchased from *Sigma-Aldrich*. The other chemicals used in this study were Folin-Ciocalteu reagent (*Carlo Erba*), 96% ethanol (*Betahem*), gallic acid (*Merck*), 2,2-diphenyl-1-picrylhydrazyl (DPPH) (*Sigma-Aldrich*), 2,2'-azino-bis(3-ethylbenzothiazoline-6-sulfonic acid) diammonium salt (ABTS) (*Thermo Fisher Scientific*), disodium hydrogen phosphate (*Superlab*), potassium dihydrogen phosphate (*Merck*), potassium persulfate (*Riedel de Haën*), 2,4,6-tris(2-pyridyl)-s-triazine (TPTZ) (*Sigma-Aldrich*), iron(III) chloride hexahydrate (*Moss&Hemoss*). Sodium chloride, potassium chloride, sodium acetate, acetic acid, hydrochloric acid, and iron (II) sulfate heptahydrate were purchased from *Zorka Pharma*.

Antioxidant activity assays

Determination of total polyphenols

To determine the total polyphenol content (TPC), clove essential oils (CEO) and eugenol were diluted in ethanol at concentrations ranging from 0.0001% to 10%. In a 96-well

microplate, 20 µl of each sample dilution was mixed with 160 µl of distilled water and 10 µl of Folin-Ciocalteu reagent. After 1 minute, 20 µl of sodium carbonate solution (7.5% m/v) was added, and the mixture was incubated in the dark for 1 hour. Absorbance was measured at 750 nm using a microplate reader, against a blank containing 20 µl ethanol instead of the sample.

A calibration curve was prepared by mixing various concentrations of gallic acid (0.05–1.2 mg/ml) with the reagents described above. TPC was expressed as mg gallic acid equivalents (GAE) per 1 ml of undiluted CEO or eugenol.

DPPH radical scavenging activity

To determine DPPH (2,2-diphenyl-1-picrylhydrazyl) radical scavenging activity, a 200 µM DPPH solution was prepared in 96 % ethanol. In a 96-well microplate, 250 µl of DPPH solution was mixed with 50 µl of essential oil or eugenol samples diluted in ethanol at various concentrations (0.0001–10%). After incubation in the dark for 1 hour, absorbance was measured at 517 nm against a blank (96% ethanol).

Radical scavenging activity (RSA) for each sample concentration was expressed as the percentage reduction of the initial DPPH concentration, calculated using the following equation:

$$\mathrm{RSA}, \% = (\mathrm{A_C} - \mathrm{A_S})/\mathrm{A_C} \times 100\% \tag{1}$$

where A_c is the absorbance of the control, which contained 50 µl of 96% ethanol and 250 µl of 200 µM DPPH solution, and A_s is the absorbance of the sample. The concentration required to reduce the initial free radical concentration by 50% (IC_{50}) was calculated using logarithmic interpolation:

$$\mathrm{IC_{50\%}} = \mathrm{c_1} \times \left(\frac{\mathrm{c_2}}{\mathrm{c_1}}\right)^{\frac{\log^{50}/_{\mathrm{RSA_1}}}{\log^{\mathrm{RSA_2}}/_{\mathrm{RSA_1}}}} \tag{2}$$

where c_1 and c_2 are the sample concentrations, and RSA_1 and RSA_2 are their radical scavenging activities.

ABTS radical scavenging assay

First, the ABTS (2,2'-azino-bis(3-ethylbenzothiazoline-6-sulfonic acid)) radical cation was prepared by mixing 5 ml of 7 mM ABTS solution in phosphate-buffered saline (PBS, 5 mM, pH = 7.4) with 0.088 ml of 140 mM potassium persulfate aqueous solution. The mixture was stored in the dark at 4ºC for 24 hours prior to use. To prepare the working solution, the ABTS cation was diluted approximately 50-fold with PBS to achieve an absorbance of 0.750 ± 0.050 at 734 nm. In a 96-well microplate, 250 µl of the ABTS working solution was mixed with 30 µl of essential oil or eugenol samples diluted in ethanol at various concentrations (0.0001–10%). Absorbance was measured after 5 minutes at 734 nm against a blank (PBS).

RSA was expressed as the percentage reduction of the initial ABTS concentration, calculated using equation (1), while the IC_{50} value was determined using formula (2). The control sample was prepared by mixing 30 µl of PBS and 250 µl of ABTS working solution.

The ferric reducing antioxidant power (FRAP) assay

The FRAP reagent was prepared by mixing acetate buffer (pH = 3.6), a 10 mM 2,4,6 – tripyridyl-s-triazine (TPTZ) solution in 40 mM HCl, and a 20 mM $FeCl_3 \cdot 6H_2O$ solution in distilled water at a volume ratio of 10:1:1. In a 96-well microplate, 10 µl of the sample (diluted in ethanol at concentrations ranging from 0.0001% to 10%) was mixed with 290 µl of the FRAP reagent. After 5 minutes, the absorbance was measured at 593 nm. The blank consisted of ethanol and the FRAP reagent.

A standard curve was prepared using $FeSO_4 \cdot 7H_2O$ aqueous solutions at concentrations ranging from 0.1 mM to 2.5 mM. For calibration, 10 µl of each standard solution was mixed with 290 µl of the FRAP reagent. Absorbance was measured after 5 minutes at 593 nm against a blank (10 µl of distilled water and 290 µl of the FRAP reagent). Antioxidant capacity was expressed as mmol of Fe^{2+} equivalents per gram of CEO or eugenol.

RESULTS AND DISCUSSION

The antioxidant activity of clove essential oils (CEO) and eugenol was examined using methods based on different mechanisms, including radical scavenging activity (DPPH, ABTS) and reducing antioxidant power (FRAP). Since the antioxidant effect of essential oils is related to phenolic compounds, total polyphenol content (TPC) was evaluated using the Folin-Ciocalteu method.

The Folin-Ciocalteu method is based on the transfer of electrons from phenolic compounds and other reducing species to molybdenum, forming blue complexes that are measurable spectrophotometrically at 750 nm [18]. The TPC for each sample was calculated using a gallic acid standard curve (R^2=0.9988). Eugenol, as a pure phenolic compound, exhibited the highest TPC (585.11 ± 4.47 mg GAE/g). Both CEO showed notable polyphenol content, with CEO_1 displaying higher TPC (472.97 ± 2.90 mg GAE/g) than CEO_2 (442.77 ± 2.80 mg GAE/g). The examined essential oils displayed a greater TPC than that reported by Nada *et al.* (9.32 ± 0.35 mg GAE/g) [19]. Lower TPC values for CEO were also reported by Sarrami *et al.* (345.95 ± 7.85 mg GAE/g) [20], while Zengin *et al.* reported a higher polyphenol content (635.327 ± 11.71 mg GAE/ml) [21]. The variation in the phenol content of essential oils arises from differences in their chemical composition, which depends on the method and conditions of extraction, the biological properties and geographical origin of the plant, as well as the soil quality and climatic conditions where the plant was cultivated [20].

The DPPH radical scavenging activity assay is a colorimetric method that measures the ability of an antioxidant substance to reduce the free radical diphenyl-picrylhydrazyl to its non-radical form. During this reaction, the colour of the free radical changes from purple to yellow and is measured spectrophotometrically at 517 nm [8]. The free radical scavenging activity at various concentrations of the examined samples was calculated using equation (1). Results were expressed as IC_{50}, the concentration of the substance required to decrease the initial free radical concentration by 50%. IC_{50} values were calculated using equation (2). IC_{50} values decrease as antioxidant activity increases; therefore lower values indicate stronger antioxidant activity.

Table 1 *Antioxidant activity of clove essential oils and eugenol*

	$IC_{50\%}$, µg/ml		FRAP, mmol Fe^{2+}/g	TPC, mg GAE/g
	DPPH	ABTS		
CEO_1	75.78 ± 2.34	17.25 ± 0.02	12.85 ± 0.09	472.97 ± 2.90
CEO_2	96.80 ± 2.86	28.89 ± 0.87	10.71 ± 0.19	442.77 ± 2.80
Eugenol	66.24 ± 1.83	17.30 ± 0.75	16.69 ± 0.29	585.11 ± 4.47

The results of the DPPH assay are presented in Table 1. Eugenol exhibited stronger DPPH radical scavenging activity than both CEO, with the lowest IC_{50} value (66.24 ± 1.83 µg/ml). CEO_1 (75.78 ± 2.34 µg/ml) had a higher IC_{50} than eugenol, but displayed a stronger radical scavenging effect than CEO_2 (96.80 ± 2.86 µg/ml). The DPPH results were consistent with the TPC results. The correlation between the DPPH radical scavenging activity and the TPC is due to the ability of antioxidants to neutralize free radicals, such as DPPH, by donating a hydrogen atom from the phenolic hydroxyl group [9,10].

The ABTS radical scavenging activity assay measures the ability of antioxidant compounds to neutralize the intensely blue-coloured ABTS radical cation. The decrease in colour intensity depends on the antioxidant effect and can be monitored spectrophotometrically at 734 nm. Because the ABTS cation is soluble in both water and organic solvents, this method enables the determination of both lipophilic and hydrophilic compounds [22]. Radical scavenging activity was determined using equation (1) and used to calculate IC_{50} with formula (2). Results are shown in Table 1. CEO_2 displayed the lowest antioxidant activity, with the highest IC_{50} value (28.89 ± 0.87 µg/ml). Unlike the DPPH assay results, the IC_{50} values for eugenol (17.30 ± 0.75 µg/ml) and CEO_1 (17.25 ± 0.02 µg/ml) were very similar. This inconsistency between methods is due to the fact that ABTS radicals are more reactive than DPPH radicals. Reactions with ABTS radicals involve both hydrogen atom and electron transfer, whereas reactions with DPPH radicals involve only hydrogen atom transfer [5,17]. Therefore, complex mixtures such as essential oils are more sensitive to the ABTS assay than to DPPH. In addition, the ability of CEO to scavenge free radicals may be stronger than that of eugenol due to the synergistic effect of bioactive compounds, such as eugenol acetate and β-caryophyllene [2,15].

The results obtained for the ABTS and DPPH assays were consistent with previous reports on the radical scavenging activity of CEO. Depending on the extraction procedure and resulting chemical composition, reported IC_{50} values for DPPH ranged from 0.2 to 170.5 µg/ml for CEO and from 4.4 to 130.5 µg/ml for eugenol [23, 24]. Higher IC_{50} values for CEO in both assays were reported by Olszowy *et al.* (IC_{50} = 0.32 ± 0.02 mg/ml for DPPH and IC_{50} = 0.16 ± 0.01 mg/ml for ABTS) [25]. Thongmee *et al.* reported stronger radical scavenging activity for CEO in both assays (IC_{50} = 3.54 ± 0.2 µg/ml for ABTS and IC_{50} = 8.70 ± 2.26 µg/ml for DPPH) [26]. These differences can be attributed to varying reaction conditions and the chemical composition of the essential oils.

The FRAP assay relies on the ability of antioxidants to reduce the yellow Fe^{3+}-TPTZ complex to the blue Fe^{2+}-TPTZ complex through electron transfer. The reducing capacity of a compound is an important indicator of its antioxidant activity, as electron-donating properties enable the neutralization of free radicals [17]. The intensity of the blue-coloured complex was measured spectrophotometrically at 593 nm, and the antioxidant capacity was calculated

using a calibration curve (R^2 = 0.9994). The results, expressed as mmol Fe^{2+} equivalents per gram of undiluted sample, are presented in Table 1.

Eugenol showed the strongest reducing power (16.69 ± 0.29 mmol $Fe^{2+/}$g), followed by CEO_1 (12.85 ± 0.09 mmol $Fe^{2+/}$g), while CEO_2 (10.71 ± 0.19 mmol $Fe^{2+/}$g) displayed the lowest activity. These results indicate strong reducing capacity and are consistent with the DPPH radical scavenging activity and TPC. Costa *et al.* reported similar findings (at a sample concentration of 25 µg/ml, 285.62 µM Fe^{2+} for eugenol and 270.79 µM Fe^{2+} for CEO) [27]. However, the values in the present study are significantly higher than those reported by Olszowy *et al.* (62,273 ± 3,000 µmol Fe^{2+}/100 g essential oil) [25]. Olszowy *et al.* also documented higher IC_{50} values for both radical scavenging activity assays, indicating lower overall antioxidant activity. Similarly, Sarrami *et al.* reported lower FRAP values (112.37 ± 8.81 mM Fe^{2+}), higher IC_{50} values for the DPPH assay (0.83 mg/ml), and lower total polyphenol content (345.95 ± 7.85 mg GAE/g) [20]. The high variability in the results may be due to differences in the chemical composition of the examined essential oils and variations in reaction conditions, such as incubation time and sample-reagent volume ratio. Additionally, the use of an aqueous FRAP reagent presents a limitation for analysing hydrophobic essential oils, in contrast to the DPPH reagent, which is diluted in an organic solvent. Furthermore, overestimated FRAP values have been reported for different substances, indicating that there is no relationship between the Fe^{2+} equivalent value and the number of electrons an antioxidant can donate [18]. This may be caused by the formation of oxidation products that absorb at 593 nm, increasing the measured absorbance [28].

In all assays, except for ABTS, eugenol exhibited the strongest antioxidant activity, indicating its role as the primary contributor to the antioxidant activity of CEO. Both CEO demonstrated strong antioxidant activity, suggesting a high eugenol content. However, CEO_1 showed slightly higher antioxidant power across all assays. This is because the antioxidant activity of essential oils depends on their chemical composition, which is influenced by various factors, such as extraction methods, genetics, planting area, and the phenological stage of the clove tree [18,29].

CONCLUSION

The results of this study show that clove essential oil (CEO) and its major constituent, eugenol, have a high polyphenol content and the ability to scavenge free radicals and reduce ferric ions. Eugenol displayed the strongest DPPH radical scavenging activity and electron-donating properties, indicating its role as the primary contributor to the antioxidant activity of CEO. Both essential oils demonstrated strong ferric reducing and radical scavenging activities, suggesting a high eugenol content. The observed differences between the two CEO in this study confirm that the antioxidant activity of essential oils derived from the same plant species may vary, most likely as a result of differences in their chemical composition. For a more precise characterization of essential oils, gas chromatography - mass spectrometry (GC-MS) analysis should be employed. The results highlight the potential application of CEO and eugenol as natural antioxidants in food products. Due to their strong aroma and high volatility, further research should focus on encapsulation strategies.

ACKNOWLEDGMENTS

This work was supported by the Ministry of Science, Technological Development and Innovation of the Republic of Serbia (Contract No. 451-03-34/2026-03/ 200135 and 451-03-33/2026-03/200287).

REFERENCES

[1] Parveen, B., Rajinikanth, V., Narayanan, M. Discov. Appl. Sci. 2025, 7 (845), 1–29.

[2] Noshirvani, N.J. Food Quality 2024, 1, 1–18.

[3] Eze, C.N., Aduba, C.C., Ezema, B.O., *et al*. Cogent Food & Agriculture. 2025, 11(1), 1–22.

[4] Pokorny J., Antioxidants in Food Preservation. In: Rahman M. S., Handbook of food preservation. Boca Raton: CRC Press; 2007. p. 264.

[5] Gulcin, I. Arch. Toxicol. 2012, 86(3), 345–391.

[6] Ren, J., Li, Z., Li, X., *et al.* Foods. 2025, 14(7), 1–21.

[7] Novais, C., Molina, A.K., Abreu, R.M.V., *et al.* J. Agric. Food Chem. 2022, 70, 2789−2805.

[8] Martiniakova, S., Acsova, A., Hojerova, J., *et al.* Acta Chimica Slovaca. 2022, 15(1), 1–11.

[9] Ferrentino, G., Morozova, K., Horn, C., *et al.* Curr. Pharm. Des. 2020, 26, 519–541.

[10] Ricardo-Rodrigues, S., Rouxinol, M.I., Agulheiro-Santos, A.C., *et al.* Appl. Biosci. 2024, 3(1), 87–101.

[11] Hussain, S., Rahman, R., Mushtaq, A., *et al.* Int. J. Chem. Biochem Sci. 2017, 11, 129–133.

[12] Salnus, S. Hayyan Journal. 2025, 2(3), 51–70.

[13] Ulanowska, M., Olas, B. Int. J. Mol. Sci. 2021, 22 (7), 1–13.

[14] Valarezo, E., Ledesma-Monteros, G., Jaramillo-Fierro, X., *et al.* Plants 2025, 14(13), 1–43.

[15] Haro-Gonzales, J., Castillo-Herrera, G.A., Martínez-Velázquez, M., *et al*. Molecules 2021, 26(21), 1–25.

[16] Biernasiuk, A., Baj, T., Malm, A. Molecules 2023, 28(1), 1–22.

[17] Gulcin, I., Elmastas, M., Aboul-Enein, H.Y. Arab. J. Chem. 2012, 5, 489–499.

[18] Karadag, A., Ozcelik, B., Saner, S. Food Anal. Methods. 2009, 2, 41–60.

[19] Nada, H.G., Mohsen, R., Zaki, M.E., *et al.* J. Food Meas. Charact. 2022, 16, 673–686.

[20] Sarrami, S., Akrami Mohajeri, F., Sadeghizadeh-Yazdi, J. *et al.* J. Nutr. Food Secur.. 2023, 8(3), 343–352.

[21] Zengin, H., Baysal, A.H. J. Food Process. Preserv. 2015, 39, 1261–1271.

[22] Munteanu I.G., Apetrei, C. Int. J. Mol. Sci. 2021, 22(7), 1–30.

[23] Suttiarporn, P., Seangwattana, T., Srisurat, T., *et al.* Curr. Res. Green Sustain. Chem. 2024, 8, 1–11.

[24] Hassine D.B., El Euch, S.K., Rahmani, R., *et al.* BioMed Res. Int. 2021, 1–11.

[25] Olszowy, M., Dawidowicz, A.L. Montash Chem. 2016, 147, 2083–2091.

[26] Thongmee, A., Wanakhachornkrai, O, Chongsaet, W., *et al.* PLoS One 2025, 20(10), 1–12.

[27] Costa, E.P., Santos, M.M., Paula, R.A., *et al.* ACS Omega 2025, 10, 31033–31045.

[28] Magalhaes, L.M., Segundo, M.A., Reis, S., *et al*. Anal. Chimica Acta 2008, 613, 1–19.

[29] Alfikri, F.N., Pujiarti R., Wibinoso M.G., *et al.* Hindawi Scientifica 2020, 1–8.

EcoTER'26
eco.tfbor.bg.ac.rs
32nd International Conference
Ecological Truth & Environmental Research
24–26 June 2026, Hotel Sunce,
Sokobanja, Serbia

Original Research

GROWTH PARAMETERS RESPONSE OF *Ocimum basilicum* `Genovese` TO PHOSPHATE GLASS AS AN ALTERNATIVE FERTILIZER

DOI: 10.5937/EcoTER26471R

Dragana Randjelović[1,a*], Veljko Savić[1,b], Vladimir Topalović[1,c], Marija Koprivica[1,d], Jelena Nikolić[1,e]

[1] Institute for Technology of Nuclear and other Mineral Raw Materials, Franchet d`Esperey 86, 11000 Belgrade, SERBIA

[a] https://orcid.org/0000-0003-4976-7766

[b] https://orcid.org/0000-0002-8602-8260

[c] https://orcid.org/0000-0002-4177-4649

[d] https://orcid.org/0000-0002-1451-5959

[e] https://orcid.org/0000-0002-9624-8865

Abstract

The potential of phosphate glass as a fertilizer was evaluated through its effect on the growth of Ocimum basilicum `Genovese` under controlled greenhouse conditions. A pot experiment was conducted over eight weeks using a factorial design with two substrate types differing in nutrient availability (P—nutrient-poor and F—nutrient-rich) and three fertilizer application rates (0, 1, and 2 g/kg supstrate). Plant height and number of fully developed leaves were monitored as key growth parameters and expressed as relative values compared to the respective substrate controls. Results showed that plant response depended strongly on substrate type while the effects of fertilizer were limited reflecting the dominant influence of substrate type and opposing fertilization responses among substrates. In the nutrient-poor substrate, phosphate glass enhanced growth, increasing both height and leaf number, indicating that growth was initially nutrient-limited. In contrast, in the nutrient-rich substrate, fertilization reduced growth, suggesting adverse effects of excessive nutrient availability. Statistical analysis using the Kruskal–Wallis test confirmed significant differences among treatments. Overall, phosphate glass shows promise as a controlled-release fertilizer, particularly in nutrient-deficient systems, highlighting the importance of optimizing application rates in accordance with substrate conditions.

Keywords: phosphate glass, *O. basilicum* `Genovese`, fertilizer, nutrients.

INTRODUCTION

Sustainable agriculture represents one of the key challenges of modern society, given the need to ensure sufficient food production for a growing population while simultaneously preserving natural resources and the environment. The intensive use of conventional mineral fertilizers, although contributing to high yields, is often associated with negative environmental impacts such as eutrophication of water bodies, soil degradation, and

* *d.randjelovic@itnms.ac.rs*

greenhouse gas emissions. Consequently, increasing attention is being directed toward the development of alternative solutions that enable efficient nutrient supply to plants while minimizing environmental harm. In this context, particular emphasis is placed on fertilizers with controlled nutrient release, which reduce losses due to leaching and improve nutrient use efficiency [1,2].

Phosphate glass fertilizers represent a promising class of materials capable of meeting these requirements. Their structure enables gradual and controlled release of nutrients, which is directly related to the composition and structure of the glass network. In contrast to conventional fertilizers, which dissolve rapidly and may lead to nutrient losses, phosphate glasses provide a more prolonged and uniform nutrient supply. Furthermore, the ability to incorporate various macro– and micronutrients into the glass matrix allows precise tailoring of fertilizer composition to meet specific crop requirements. Another significant advantage of these materials lies in their reduced environmental impact, as controlled nutrient release lowers the risk of soil and water contamination. Owing to these characteristics, phosphate glass fertilizers represent an innovative approach in the development of sustainable agrochemical products and hold considerable potential for application in modern agriculture [3–7].

Phosphate glass fertilizers function through the controlled dissolution of a glass matrix in aqueous environments. When in contact with soil moisture, the glass undergoes hydration followed by ion exchange and gradual breakdown of P–O–P bonds, leading to the release of nutrient ions into the surrounding medium. The dissolution rate depends on the glass composition, particularly the degree of network connectivity and the presence of modifying cations, which regulate the mobility of ions and the stability of the structure [8,9].

An important feature of these materials is their responsiveness to plant demand. During periods of active growth, increased water uptake and root activity enhance local moisture and ion exchange processes, promoting faster dissolution and nutrient release. In contrast, as the growing season ends and plant activity decreases, the driving forces for glass dissolution—such as water flux and ion gradients—are reduced. As a result, nutrient release slows down, minimizing unnecessary losses and improving overall efficiency [10,11].

The aim of this research was to investigate the effect of phosphate glass as a fertilizer on the growth and development of *Ocimum basilicum* ‘Genovese’ under greenhouse conditions. The impact of different fertilizer doses was analyzed in two types of substrates differing in nutrient content. Plant growth was evaluated based on plant height and leaf number, supported by statistical analysis of the obtained results.

MATERIALS AND METHODS

In order to synthesize phosphate glass fertilizer, a batch was formulated using the following raw materials: $(NH_4)_2HPO_4$, K_2CO_3, $CaCO_3$, SiO_2, MgO, ZnO, and MnO_2. After prior drying, the components were homogenized in a mortar to obtain a uniform glass mixture. The prepared batch was subsequently melted in a Nabertherm G100/9 electric furnace at 1230 °C for 1 h. The molten mass was then cast onto a steel plate and allowed to cool under ambient conditions. The obtained phosphate glass was ground in an agate mortar

and stored in a desiccator until further use. The glass was physicochemically characterized, and its chemical durability was also examined in distilled water and in a 2% citric acid solution (commonly used under laboratory conditions to simulate the root environment). A detailed characterization and chemical durability of this glass have been presented in our previous studies [8,9]. The chemical composition of the glass was determined using gravimetric analysis for silicon (Si) and spectroscopic methods. Specifically, atomic absorption spectroscopy (AAS) with a PERKIN ELMER 703 instrument was used to analyze Ca, K, Mg, Cu, and Zn, while UV/VIS spectroscopy with a PHILIPS 8610 spectrophotometer was used for phosphorus determination.

To assess the effect of the phosphate glass fertilizers on *O. basilicum* `Genovese` performances in two different commercially available substrates, Plagron Pro Mix (labelled as poor in nutrients- P) and Florabella (labelled as rich in nutrients - F), a pot experiment was performed in the greenhouse conditions for 8 weeks. The Florabella substrate contains black and white sphagnum peat, clay, compost, wood fibers, and 1.5 kg/m³ of NPK fertilizer (12:12:17.2); pH = 5.5–6.5; electrical conductivity = 45 mS/m. Plagron Pro Mix is an organic blend of white and black peat and worm castings. Its composition is: 60% white peat, 30% black peat, and 10% worm castings; pH (H_2O) = 6.5–7.5; electrical conductivity: 0.5–0.8 mS/cm; dry matter content 37%, organic matter content: 75%. The experiment was conducted as a factorial design with two substrate types (P and F) and three fertilizer levels (0, 1, and 2 g/kg substrate). Each treatment consisted of 5 replications, resulting in a total of 30 pots. Each pot contained five plants.

O. basilicum `Genovese` seeds were obtained from commercial supplier „SemeSemena" d.o.o. and were soaked in 3% H_2O_2 for 10 minutes for disinfection and rinsed with distilled water prior to seeding. Ten seeds were sown per pot; upon emergence, seedlings were thinned to five individuals per pot, selecting those with the most uniform size and vigor for further treatment.

During experimental period temperature was set to 25/16 °C during a day/night cycle of 16/8 h. Relative air humidity was kept around 40%, and the artificial light was provided by multiply T5 fluorescent tubes with luminous flux of 2000 lm. Soil moisture was kept on 80% of field capacity during the experiment.

Plant height is measured from the soil surface to the highest apical meristem using digital caliper with 0.02 mm accuracy. Number of leaves is determined by counting fully expanded leaves. Plant growth parameters were expressed as relative values (%) with respect to the control of each substrate, which was set to 100%. Kruskal-Wallis test was applied for statistical analysis of variance and analyses were conducted in Statistica Statsoft 8.0 package.

RESULTS AND DISCUSSION

The chemical composition of the glass whose effect on *O. basilicum* `Genovese` plants was investigated in our present study is presented in Table 1.

Table 1 *The chemical composition of the phosphate glass*

	Oxides						
	P_2O_5	K_2O	CaO	MgO	ZnO	SiO_2	MnO
mol%	45.4	25.6	14.5	9.3	1.2	3.1	0.9
wt.%	62	23.2	7.8	3.6	1	1.8	0.6

Plant height and number of leaves recorded during the experiment are presented in Figures 1–4. Height of plants in treatments with P substrate was ranging 10.5–16.1 cm, while the height of basil in treatments with F substrate reached twofold values, ranging from 22.1 to 33.9 cm. Number of leaves in in treatments with P substrate ranged from 8–14, whereas number of leaves in treatments with F substrate ranged from 30–52. Slight increase in both plant height and number of leaves was observed in P1 and P2 in comparison to their control (PK), whereas opposite trend was observed in F1 and F2 treatments in comparison to their control (FK).

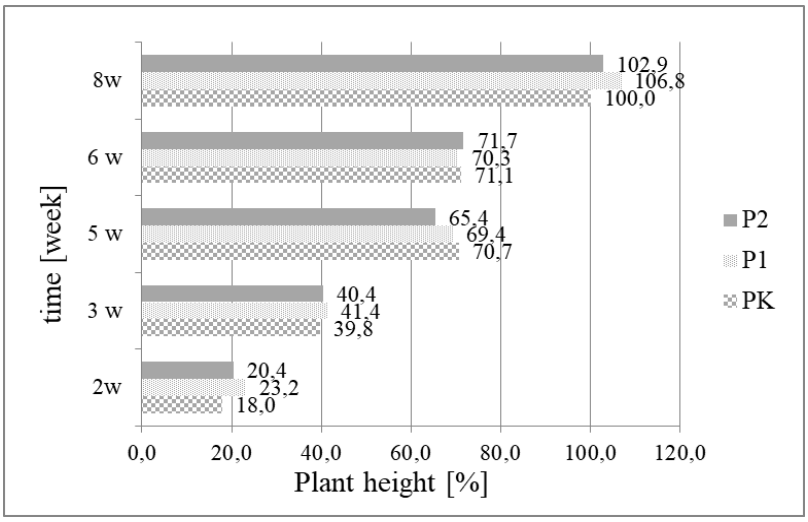

Figure 1 *Height of Ocimum basilicum `Genovese` reached during the experiment in substrate P (data are shown as relative percentages).*

For P treatment, plant height showed slight increase in fertilized treatments (Figure 1), particularly in later stage of the experiment (weeks 6 and 8) in comparison to the control (up to 106.8% for P1 treatment). Number of leaves developed at week 2 in P substrate was identical for all treatments, indicating uniform seed emerging (Figure 2). Up to week 6, control plants had the highest number of developed leaves in comparison to fertilized treatment, but by the end of experiment that trend changed favouring the development of leaves in both fertilized treatments, particularly P2 (109.5%).

In the F substrate, plant height shows slight responsiveness to fertilization (Figure 3), with the control performing better than both fertilized treatments in later stages of the experiment (week 6 and 8), indicating that nutrient availability was already sufficient for optimal growth. Particular reduction of growth height is notable in P1 treatment (93.8%). The differences were more pronounced in number of leaves (Figure 4), where at the later stages of the experiment control outperformed both treatments, particularly F2 (100% in FK in comparison to 74.2%).

This phenomenon indicates that nutrient availability is already sufficient in control pots and that additional fertilization could have detrimental effects to the vegetative growth.

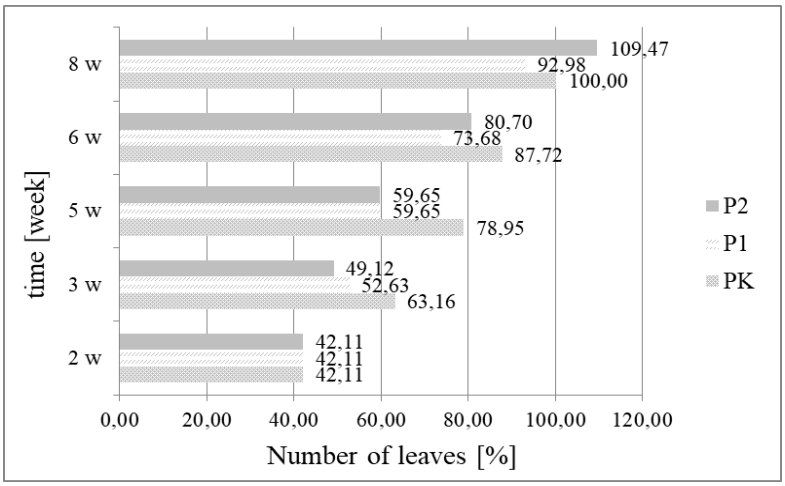

Figure 2 *Number of leaves of Ocimum basilicum `Genovese` reached during the experiment in substrate P (data are shown as relative percentages).*

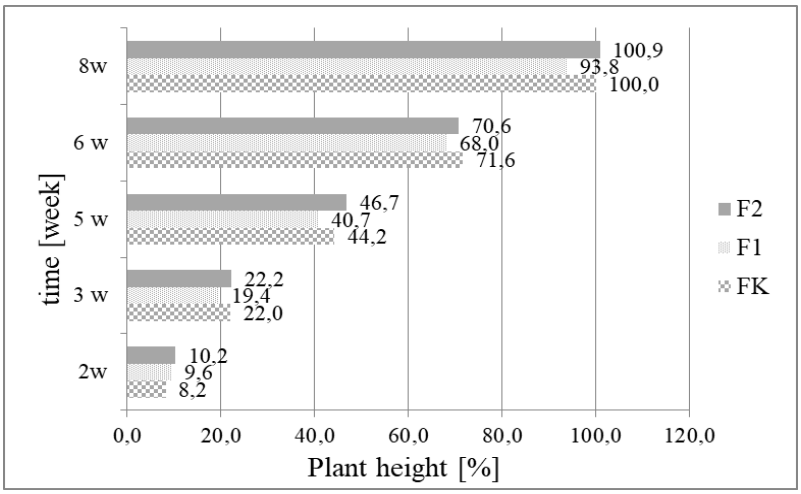

Figure 3 *Height of Ocimum basilicum `Genovese` reached during the experiment in substrate F (data are shown as relative percentages)*

Non-parametric Kruskal-Wallis test showed the significant differences among measured vegetative growth parameters (Table 2). During the early growth stages (week 2) differences among plant height and leaf numbers among treatments were not statistically significant, revealing that initial growth was predominantly supported by seed reserves. During later growth phases (weeks 3–8) significant differences between plant height and leaf number among the treatments were observed. However, analysis of plant height and number of leaves showed no statistically significant differences among fertilizer treatments ($F= 0.0134$, $p = 0.9867$ and $F = 0.3609$, $p = 0.6998$, respectively), which can be explained by dominant effect of substrate type and opposing responses to fertilization observed in different substrates.

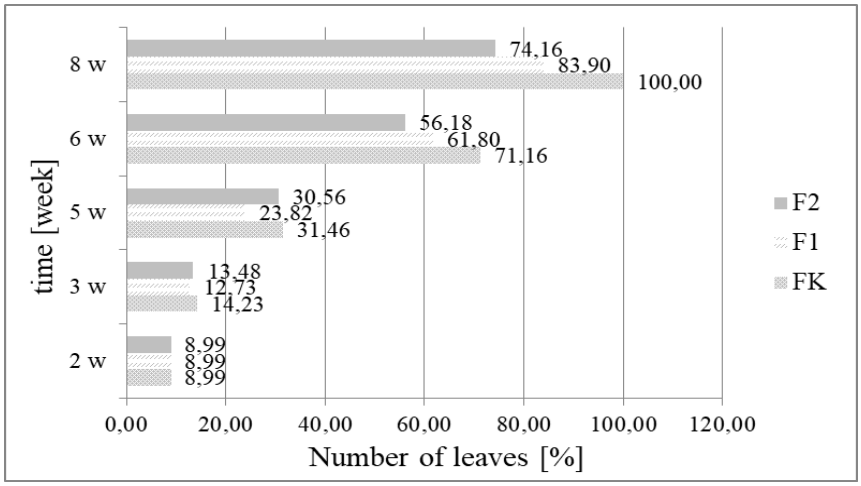

Figure 4 *Number of leaves of Ocimum basilicum `Genovese` reached during the experiment in substrate F (data are shown as relative percentages)*

Table 2 *Non-Parametric (Kruskal–Wallis) analysis of plant height and number of leaves in O.basilicum `Genovese` during the experimental period (statistically significant differences are marked with *)*

Experiment period [week]	Plant height		Number of leaves	
	KW-H F value	p-value	KW-H F value	p-value
2	15.958	0.007	0	-
3	18.850	0.002*	11.698	0.0392*
5	26.303	0.00008*	31.366	0.00001*
6	26.596	0.00007*	30.372	0.00001*
8	26.884	0.0006*	28.881	0.00002*

In the P substrate, the addition of phosphate glass fertilizer resulted in modest improvement in both plant height and leaf number, suggesting that vegetative growth was primarily limited by substrate conditions that initially had restricted nutrient availability. In contrast, in the F substrate, initially rich in nutrients, additional fertilization reduced vegetative growth. These findings highlight the need to optimize glass fertilizer dosage according to the initial substrate conditions during the *O. basilicum* `Genovese` cultivation process. Additional investigations are needed to provide deeper insight into soil-fertilizer-plant chemical interactions as well as to identify physiological processes underlying observed plant responses.

CONCLUSION

In this study, the effect of phosphate glass as a fertilizer on the growth and development of *Ocimum basilicum* `Genovese` under substrates with different initial nutrient status was investigated. The obtained results indicate that the effect of glass fertilizer application strongly depends on the nutrient availability of the substrate. In the nutrient-poor substrate, a slight improvement in vegetative growth was observed, reflected in increased plant height and leaf number, confirming the potential of phosphate glasses as a controlled-release nutrient

source. In contrast, in the nutrient-rich substrate, additional fertilization resulted in reduced plant growth, suggesting a possible negative effect of excessive nutrient availability and emphasizing the importance of proper dosage depending on cultivation conditions.

Statistical analysis showed that substrate type had a dominant influence on the observed growth parameters, while differences among fertilizer doses were not statistically significant, which can be explained by the opposing responses observed in different substrates. These findings confirm that the application of phosphate glass fertilizers requires careful adjustment to agroecological conditions in order to achieve optimal efficiency and avoid potential adverse effects.

The obtained results contribute to a better understanding of the application of glass fertilizers in sustainable agriculture, while also highlighting the need for further research. Future studies will focus on a more detailed investigation of the influence of glass composition, as well as the kinetics and mechanisms of its dissolution and nutrient uptake by plants, with the aim of optimizing their application and improving overall efficiency.

ACKNOWLEDGEMENT

The authors are grateful to the Ministry of Science, Technological Development and Innovation of the Republic of Serbia for financial support according to the contract with registration No. 451-03-33/2026-03/200023.

REFERENCES

[1] Shelef O, Fernández-Bayo JD, Sher Y. *et al.* Elucidating Local Food Production to Identify the Principles and Challenges of Sustainable Agriculture. In: Galanakis C. M, Sustainable Food Systems from Agriculture to Industry, Academic Press; 2018. p. 47–81.

[2] Ryo, M., Schiller, J., Stiller, S., *et al*., J. Sustain. Agric. Environ. 2023, 2(1), 40–44.

[3] Labbilta, T., Ait-El-Mokhtar, M., Harech, M.A., *et al.*, J. Non-Cryst. Solids 2024, 625, 122765.

[4] da Silva Soares, J.H., Boaventura, T.W., de Moura, A.C.A., *et al.* ACS Agric. Sci. Technol. 2025, 5, 142−157.

[5] Ersundu, M.C., Kuzu, B., Ersundu, A.E. J. Non-Cryst. Solids 2022, 576, 121239.

[6] Vujošević, A., Matijašević, S., Smiljanić, S., *et al.* Materials Protection 2019, 60(1), 96–104.

[7] Moharrami, F., Bolandnazar, S., Salteh, S.A., *et al.* Sci. Reports 2026, *article in press*.

[8] Nikolić J, Đošić J, Topalović M, *et al.* In: Proceedings of 6th Metallurgical & Materials Engineering Congress of South-East Europe, 4–7 June, Trebinje, Bosnia and Herzegovina, 2025, p. 134–140.

[9] Tošić, M.B., Nikolić, J.D., Grujić, S.R., *et al.* J. Non-Cryst. Solids 2013, 362(1), 185–194.

[10] Ouis, M.A., Abd-Eladi, M., Abou-Baker, N.H. Silicon 2018, 10(2), 293–299.

[11] Cacini, S., Rinaldi, S., Massa, D., *et al.*, Sci. Hortic. 2020, 274, 109660.

EcoTER'26
eco.tfbor.bg.ac.rs
32nd International Conference
Ecological Truth & Environmental Research
24–26 June 2026, Hotel Sunce,
Sokobanja, Serbia

Review

INTEGRATED HYBRID SYSTEMS FOR RESIDENTIAL ENERGY AUTONOMY: A LITERATURE REVIEW

DOI: 10.5937/EcoTER26478G

Milan Grozdanović[1,a*], Marko Mančić[2,b], Jelena Đoković[1,c], Dejan Tanikić[1,d], Ana Đorđević[2,e]

[1] University of Belgrade, Technical Faculty in Bor, Vojske Jugoslavije 12, 19210 Bor, SERBIA

[2] University of Niš, Faculty of Mechanical Engineering in Niš, Aleksandra Medvedeva 14, 18104 Niš, SERBIA

[a] https://orcid.org/0000-0002-5618-9274 [b] https://orcid.org/0000-0001-7078-9658
[c] https://orcid.org/0000-0001-5542-8088 [d] https://orcid.org/0000-0003-0702-5721
[e] https://orcid.org/0000-0001-6465-3471

Abstract

The global transition to sustainable energy systems requires innovative solutions for energy storage and the decarbonization of the energy sector. This paper presents a literature review and comparative analysis of literature in the field of hybrid energy systems integrating photovoltaic panels, a hydrogen system, and heat pumps for residential applications. While conventional battery-based systems address the issue of daily fluctuations, the analysis shows that the introduction of hydrogen enables the necessary seasonal autonomy, bridging the gap between summer energy production and winter consumption.

The key results of the review indicate that the thermal integration of components, a process known as micro-trigeneration, the overall system efficiency (thermal and electrical combined) can exceed 80% by utilizing waste heat from the electrolyzer and fuel cell for space heating and domestic hot water production. Such synergy enables a reduction in the required battery capacity by 60–75%, thereby significantly optimizing resource utilization and reducing the environmental footprint of the energy system. Additionally, the paper analyzes the impact of advanced control strategies, such as fuzzy logic, on system stability and the longevity of fuel cells. In conclusion, integrated hybrid systems represent a promising pathway for the development of net-zero energy buildings; however, further efforts to reduce capital investment costs are necessary for their broader commercialization.

Keywords: renewable energy sources, hydrogen, heat pump, trigeneration.

INTRODUCTION

The global energy transition from fossil fuels to zero-carbon energy systems has become an imperative within environmental strategies and the "Green Agenda" [1]. In this context, renewable energy sources (RES), particularly photovoltaic (PV) and PV thermal (PVT) systems, play a leading role in the decarbonization of the power sector. However, the primary challenge of PV systems remains their intermittency and seasonal variability, which requires the implementation of advanced energy storage (ES) solutions to ensure a reliable energy

* *mgrozdanovic@tfbor.bg.ac.rs.*

supply throughout the year [2,3]. While lithium-ion batteries (LIB) are widely used for short-term balancing of daily fluctuations, hydrogen (H_2) is emerging as a key energy vector for long-term, i.e., seasonal ES [1,4]. The integration of an electrolyzer, hydrogen storage tank, and fuel cell (FC) enables surplus solar energy generated during the summer months to be efficiently stored and utilized during the winter period, when PV production is minimal and the demand for thermal and electrical energy is at its peak [4,5]. In addition to the decarbonization of the power sector, the decarbonization of the heating sector represents one of the greatest challenges. Heat pumps (HP) are recognized as the most efficient technology for space heating and domestic hot water (DHW) production; however, their operation significantly increases grid load during winter [6]. The synergy between the hydrogen system (electrolyzer, storage tank, and FC) (HS) and HP offers an innovative solution in the form of "sector coupling". Of particular scientific interest is the possibility of utilizing waste heat (WH) generated as a byproduct in the electrolyzer and FC. Research indicates that this thermal integration can increase the overall efficiency of hybrid systems above 80%, thereby significantly improving the coefficient of performance (COP) of the HP and reducing total primary energy consumption [6,7].

Although there is extensive literature on individual components, there is a need for a comprehensive review that analyzes the interaction of these technologies within integrated residential systems. The importance of this review lies in the systematization of the latest trends in system configuration, energy management strategies, and the analysis of energy autonomy of zero-energy buildings [5,8]. The central research question is: To what extent can the synergistic integration of hydrogen storage and HP eliminate seasonal energy deficits in residential buildings while maintaining thermodynamic efficiency? To address this, the study evaluates how hydrogen-based hybrid systems can bridge the gap between summer production and winter consumption [2,4], while simultaneously increasing overall energy and exergy efficiency through the recovery of WH in trigeneration systems (CCHP) [6,7]. Furthermore, this review seeks to identify the economic and operational trade-offs that currently limit the mass adoption of these integrated solutions [9,10].

MATERIALS AND METHODS

The methodology of this paper is based on a literature review and a comparative analysis of scientific literature addressing integrated hybrid energy systems. The focus of the research is on the synergy between PV panels, battery storage, and the HS in combination with HP for residential applications.

Literature selection criteria and sources

This review is based on selected relevant scientific papers addressing hybrid systems (PV, H_2 and HP) and related hybrid energy configurations. Primary sources include papers indexed in databases such as Web of Science, Scopus, and IEEE Xplore. The selection criteria included:

- Studies analyzing hybrid systems with at least three key components: PV, storage, and HP [4,6].
- Research focused on the energy self-sufficiency of residential buildings and “zero-energy” complexes [5,8].

- Studies employing advanced simulation tools (e.g., MATLAB/Simulink, TRNSYS, HOMER) for modeling energy flows [3,11].

The literature was selected based on relevance to residential-scale hybrid renewable systems, explicit inclusion of hydrogen-based storage, and the presence of either HP integration, energy management optimization, or thermal recovery analysis. Papers dealing exclusively with transport applications, industrial-scale hydrogen production, or isolated component-level analyses without system integration were excluded.

Classification of analyzed systems

The methodological approach includes the classification of the analyzed systems into two main categories for easier comparison:

1. **Systems with separated energy flows:** where the hydrogen subsystem is used exclusively for the storage and regeneration of electrical energy.
2. **Integrated trigeneration systems:** where WH from the electrolysis process and FC operation is utilized to improve the performance of the HP [6,9].

Key performance indicators

For the purpose of objective evaluation of different solutions, the following key parameters are defined and analyzed:

- Energy autonomy rate: the ability of the system to meet the building's energy demand without relying on the electrical grid throughout the year [4].
- HP COP: analysis of the impact of thermal integration on heating efficiency, particularly at low outdoor temperatures [6,7].
- Overall system efficiency: comparison of energy losses across different conversion stages (electrolysis, storage, regeneration) [9,12].
- Energy management optimization**:** analysis of control algorithms, ranging from rule-based strategies to advanced fuzzy logic and Model Predictive Control (MPC), used to balance energy flows between the battery and hydrogen storage [3,11,13,14]. This indicator evaluates the system's ability to maintain power balance while reducing energy consumption by up to 17.9% compared to conventional methods [14].
- System stability and component longevity: A critical parameter that evaluates how control strategies impact the operational lifespan of the FC stack and electrolyzer membrane [5]. It focuses on the reduction of damaging start-stop cycles and the mitigation of efficiency degradation, which can otherwise lead to a 13.4% to 15.1% increase in fuel consumption over a 10-year period due to hardware aging [15].

This methodological structure enables a systematic insight into the current state of the art and the identification of critical factors for the future development of hybrid hydrogen systems in the residential sector.

RESULTS AND DISCUSSION

The analysis of the collected literature indicates that the integration of the HS with HP and PV systems addresses the critical shortcomings of conventional solutions based exclusively on battery storage.

Energy autonomy and the role of hydrogen in seasonal balancing

One of the most significant findings of the research is the advantage of hybrid storage configurations in achieving seasonal autonomy. While battery systems demonstrate high efficiency in charge–discharge cycles on a daily basis, they are not economically viable for long-term ES due to self-discharge and high capital costs per unit of capacity [2,3].

The synthesis of data shows that the introduction of a hydrogen storage tank enables bridging the gap between peak summer production and peak winter consumption [4,5]. Studies indicate that, in hybrid configurations, battery capacity can be drastically reduced (in some cases from 115 kWh to as little as 27 kWh), as hydrogen serves as a seasonal buffer. This approach not only increases the level of energy independence of the building, but also significantly reduces the environmental footprint associated with the production of LIB [6].

Thermal integration and efficiency improvement

A critical point of discussion in recent studies is the thermal coupling between hydrogen components and HP. In conventional systems, heat generated during electrolysis and FC operation is often considered a loss. However, modern trigeneration concepts utilize this "waste" heat for preheating fluids or directly for the heating system [6,7].

The key findings in this area include:

- Improvement of COP: The use of WH from the FC enables the HP to operate under more favorable temperature conditions, thereby directly increasing its COP, particularly at low outdoor temperatures [6,7].
- Overall system efficiency: While the electrical efficiency of individual components may be relatively low (e.g., around 40–50%), complete thermal integration enables the system to achieve an overall system efficiency of over 80% [1,6].
- Coverage of DHW demand**:** It has been established that WH can cover up to 80% of the annual DHW demand in the residential sector [6].

Advanced energy management strategies

The overall efficiency of the system largely depends on the applied control algorithm. The literature review identifies a transition from simple rule-based algorithms to advanced optimization methods.

Systems employing fuzzy logic or dynamic programming demonstrate significantly better performance in balancing energy flows between PV panels, the battery, and the electrolyzer [3,11]. These algorithms not only minimize operational costs but also extend the lifespan of FC by avoiding abrupt power fluctuations and frequent on/off cycling [3]. The results suggest that intelligent control can reduce component degradation, which is one of the main challenges for the commercialization of hydrogen technologies [11].

Comparison with traditional systems

Compared to conventional micro-cogeneration systems (e.g., those based on internal combustion engines), the integrated hybruid system offers the complete elimination of local greenhouse gas emissions and silent operation, which is crucial for urban residential environments [12]. Although initial investment costs remain higher, exergy analysis shows

that FC offer better efficiency under partial load compared to internal combustion engines, making them well suited for the variable energy demands of households [9,12].

Table 1 *Overview of key studies on integrated hybrid systems*

Authors	System configuration	Primary focus / Methodology	Key findings and results
Rutnik *et al.*	PV + Battery + H_2 loop	Seasonal autonomy of residential buildings	Enables bridging the winter energy deficit to achieve 100% energy autonomy
Cikatić Šanić & Barbir	PV + electrolyzer + FC + HP	Thermal integration and trigeneration	Overall system efficiency exceeds 80%, while WH recovery covers 78.42% of thermal demand
Zidane & Belaid	PV + H_2 subsystem / MPC	Control strategies and operational stability	Advanced management reduces energy consumption by 3.9% to 17.9% compared to base strategies
Patin *et al.*	H_2 multi-energy system	Multi-objective optimization	Optimized systems cover 63% of building demand and achieve a 23% reduction in total costs
Mobayen *et al.*	Integrated solar system	Dynamic analysis of zero-energy complexes	Annual generation of 29,145.8 kWh achieved with a thermal comfort index of only 6.8%.
Sun *et al.*	PVT + HP + PEM electrolyzer	Thermodynamic analysis of trigeneration	Synergy between PVT and HP maximizes COP and significantly improves exergy efficiency
Jafari & Malekjamshidi	Hybrid renewable system	2D dynamic programming	Real-time optimization enables 100% utilization of available surplus PV energy for hydrogen generation
Vivas *et al.*	Hybrid systems with H_2	Review of control strategies	Confirms hydrogen as a superior solution for long-term storage due to high energy density (33.3 kWh/kg)
Ceran *et al.*	PV system with hydrogen storage	Analysis of the effects of aging	Component degradation over 10 years lead to a 13.4% to 15.1% increase in fuel consumption
Jia *et al.*	CCHP system with biomass and SOFC	3E evaluation	System reaches 83% energy efficiency and approximately 41% exergetic efficiency
Kurses *et al.*	PV + HP + H_2	Economic and environmental analysis	Project payback periods range from 4.6 to 8.9 years, depending on local climatic conditions

This analysis reveals several clear trends in literature that directly address the central research question regarding seasonal energy autonomy and efficiency:

- Dominance of hybrid storage: The reviewed studies, particularly [2] and [4], confirm that while batteries are efficient for daily cycles, hydrogen is the only viable solution for seasonal balancing. This hybrid approach allows for a 60% to 75% reduction in required battery capacity, which is crucial for the physical and economic feasibility of zero-energy buildings.

- Thermodynamic synergy through sector coupling: The integration of HP with the HS significantly alters the efficiency landscape. Analysis shows that utilizing WH from electrolysis and FC operation for water preheating can elevate the overall system efficiency to above 80% [6], with some configurations reaching 83% energy and 41% exergy efficiency [9]. This confirms that trigeneration is not just an addition, but a necessity for maximizing the COP of HP in winter conditions [7].
- System intelligence and longevity: A critical finding is the shift toward advanced algorithms. While simple rule-based strategies suffice for basic operation, MPC and fuzzy logic are essential for mitigating the 13.4% to 15.1% efficiency degradation caused by component aging over a 10-year [15]. Furthermore, these intelligent systems can reduce overall energy consumption by up to 17.9% [14], directly answering the need for operational stability mentioned in this study's objectives.

CONCLUSION

The analysis conducted in this review paper confirms that the synergistic integration of PV panels, the HS, and HP effectively eliminates seasonal energy deficits in residential buildings while significantly enhancing thermodynamic efficiency.

The main conclusions of the study, which provide a comprehensive answer to the research questions, are summarized as follows:

1. Effective bridging of seasonal gaps: Hydrogen storage represents a superior solution for long-term energy autonomy compared to standalone battery systems. By converting summer surplus PV energy into H_2, buildings can achieve 100% energy independence during winter months, while simultaneously optimizing the system's environmental footprint through reduced reliance on lithium-ion storage.
2. Achievement of high-efficiency trigeneration: The integration of thermal and electrical flows is the key to surpassing the limitations of individual components. The recovery of WH for residential thermal demand enables the system to meet up to 78.42% of heating and hot water needs, maintaining a total efficiency level above 80%.
3. Critical role of intelligent management: To ensure the commercial viability and equipment longevity of these systems, advanced control strategies are indispensable. They not only maximize the utilization of surplus PV energy in real-time but also protect sensitive components from damaging start-stop cycles, thereby preserving efficiency over long operational horizons.
4. Economic and environmental feasibility: While capital costs remain a challenge, the analyzed systems show a promising payback period of 4.6 to 8.9 years under favorable conditions. This makes them a key pillar for achieving the "Green Agenda" goals and transitioning toward a truly net-zero residential sector.

In conclusion, integrated hybrid systems are not only technologically feasible but are currently the most robust answer to the challenge of year-round energy autonomy in sustainable architecture.

ACKNOWLEDGEMENT

This research was financially supported by the Ministry of Science, Technological Development and Innovation of the Republic of Serbia (Contract No. 451-03-34/2026-03/ 200131 and 451-03-33/2026-03/ 200109).

REFERENCES

[1] Guilbert, D., Vitale, G. Clean Technologies. 2021, 3, 881–907.

[2] Vivas, F.J, De las Heras, A., Segura, F., *et al*. Renew. Sustain. Energy Rev. 2018, 82(1), 126–155.

[3] Zidane, N., Belaid, S.L. J. Renew. Energ. 2024, 1(1), 107–115.

[4] Rutnik, M., Pregelj, B., Jovan, D.J., *et al*. Energy Convers. Manage. 2026, 355, 121244.

[5] Patin, M., Bégot, S., Gustin, F., *et al*. Int. J. Hydrogen Energy 2024, 67, 875–887.

[6] Cikatić Šanić, D., Barbir, F. Int. J. Hydrogen Energy 2022, 47(82), 35068–35080.

[7] Sun, X., Liu, L., Zhou, W., *et al*. Optimization and Thermodynamic Analysis of a Solar-driven Integrated PVT-Heat Pump-PEM Electrolyzer System for Trigeneration. 2026, Available from: https://ssrn.com/abstract=6471147.

[8] Mobayen, S., Assareh, E., Dezhdar, A., *et al*. Energy Convers. Manage. 2025, 341, 119924.

[9] Jia, J., Zang, G., Paul, M.C. Int. J. Energy Res. 2021, 45, 15182–15199.

[10] Kurses, M., Olympios, A.V., Harraz, A.A., *et al*. Appl. Energy 2025, 399, 126511.

[11] Jafari, M., Malekjamshidi, Z. Renew. Energy. 2020, 146, 254–266.

[12] Aliabadi, A.A., Thomson, M.J., Wallace, J.S. Energy Fuels 2010, 24(3), 1704–1710.

[13] Gerlach, L., Bocklisch, T. Energies 2021, 14(6), 1777.

[14] Holtwerth, A., Xhonneux, A., Müller, D. Energy Convers. Manag.: X. 2024, 22, 100561.

[15] Ceran, B., Mielcarek, A., Hassan, Q., *et al*. Appl. Energy. 2021, 297, 117161.

EcoTER'26
eco.tfbor.bg.ac.rs
32nd International Conference
Ecological Truth & Environmental Research
24–26 June 2026, Hotel Sunce,
Sokobanja, Serbia

Original Research

GREEN ENGINEERING APPROACH TO Sn-0.7Cu/xGNS COMPOSITES PRODUCED BY POWDER METALLURGY: MICROSTRUCTURAL AND MECHANICAL PROPERTIES FOR SUSTAINABLE ELECTRONICS

DOI: 10.5937/EcoTER26485N

Milan Nedeljković[1,a*], Srba Mladenović[1,b], Vladan Ćosović[2,c], Ivana Marković[1,d], Jasmina Petrović[1,e], Uroš Stamenković[1,f]

[1]University of Belgrade, Technical Faculty in Bor, Vojske Jugoslavije 12, 19210 Bor, SERBIA

[2]University of Belgrade - Institute of Chemistry, Technology and Metallurgy, 11001 Belgrade, SERBIA

[a] https://orcid.org/0000-0002-7927-1334 [b] https://orcid.org/0000-0002-3844-7399

[c] https://orcid.org/0000-0001-7644-4036 [d] https://orcid.org/0000-0003-4431-9921

[e] https://orcid.org/0000-0002-9131-339X [f] https://orcid.org/0000-0002-7579-2159

Abstract

The increasing demand for environmentally friendly electronic materials has encouraged the development of lead-free solder alloys and sustainable production technologies. Despite numerous alternatives, the eutectic Sn-0.7Cu alloy has been recognized as a promising candidate for lead-free solder applications due to its low cost, acceptable mechanical properties, and compliance with RoHS and WEEE regulations. This study investigates the effect of graphene nanoparticles, in the form of graphene nanosheets (GNS), on the microstructural and mechanical properties of Sn-0.7Cu matrix composites produced via powder metallurgy. GNS was incorporated into the matrix in small weight fractions (0, 0.02, 0.04, 0.06, 0.08, and 0.10 wt.%) to promote microstructural refinement and enhance the mechanical properties of the composites. Optical microscopy was used to characterize the microstructure of the sintered samples, while microhardness was measured using the Vickers method. The results indicate that increasing the graphene content significantly refines the grains, reducing the average grain size by approximately 54 % and increasing the microhardness by about 16 % compared to the base alloy.

Keywords: lead-free solder, graphene nanoparticles, powder metallurgy, composites.

INTRODUCTION

The electronics industry faces growing demands to develop materials that combine high performance with environmental sustainability. The replacement of toxic Sn-Pb solders with lead-free alternatives has been strongly encouraged by environmental regulations such as the RoHS and WEEE Directive [1]. Among lead-free systems, eutectic Sn-0.7Cu solder is widely used due to its ecological acceptability, relatively low cost, excellent wettability, and satisfactory soldering performance. However, its mechanical properties are lower than those of eutectic Sn-Pb and Sn-Ag-Cu solders, potentially affecting the reliability of soldered joints

* *mnedeljkovic@tfbor.bg.ac.rs*

[2]. The incorporation of reinforcement phases through composite technology provides an effective strategy for improving the performance of Sn–Cu solder.

Over the past decade, nanocomposite solders obtained by incorporating nanoparticles into conventional solders have been extensively investigated to improve the performance of solder joints under various service conditions [3]. Numerous studies have employed various types of nanoparticles to modify lead-free solders. However, to date, relatively few studies have focused on the incorporation of carbon-based nanomaterials, particularly graphene, which has attracted significant interest in advanced materials research due to its outstanding properties. [4]. Graphene, in the form of graphene nanosheets (GNS), is a two-dimensional carbon nanomaterial with exceptional mechanical strength, high thermal and electrical conductivity, and a large specific surface area, making it an ideal reinforcement phase for enhancing the properties of metal matrix composites [5].

Among the various techniques available for adding reinforcements to a solder matrix, powder metallurgy (PM) is the most frequently used. From a sustainability perspective, this technique offers an efficient processing route that minimizes material waste, enables near-net-shape production, and provides precise control over composition. Compared to conventional casting, PM can reduce energy consumption and lower environmental impact [6].

The main focus of this research is to investigate the effect of small amounts of GNS on the microstructure and microhardness of the Sn-0.7Cu based composites. The composites were synthesized using the PM technique, and the results were compared with those of the base alloy.

MATERIALS AND METHODS

Materials used in this study included atomized tin (Sn) and copper (Cu) powders, with particle sizes up to 75 μm, and GNS with an average diameter of 5-10 μm and a thickness of 3-5 nm. Six different compositions, Sn-0.7Cu/xGNS (x = 0, 0.02, 0.04, 0.06, 0.08, and 0.10 wt.%) were synthesized. For each composition, the corresponding powders were first mixed in a “Turbula T2F” three-axis mixer at 50 rpm for 30 hours to produce the Sn-0.7Cu matrix powder. The matrix powder and GNS were then mechanically alloyed in a high-energy planetary ball mill “FRITSCH Planetary Ball Mill P-7” at 100 rpm for 3 hours to ensure a uniform distribution of GNS within the matrix. The resulting powder mixture was cold compacted using a “Mohr-Federhaff-Losenhausen” hydraulic press under a uniaxial pressure of 300 MPa. Compacted samples were then sintered in a furnace at 185 °C for 3 hours in an argon atmosphere to obtain the final specimens.

The microstructural analysis of the sintered samples was performed using a “Reichert MeF2” optical microscope at a magnification of 1000x. After standard metallographic preparation by grinding and wet polishing, the samples were etched with a solution of (2 mL HCl + 98 mL of 95 % methanol).

The microhardness of the samples was measured in accordance with the ASTM E384 standard [7] using a PMT-3 Vickers microhardness tester. To ensure reliable results, the sample surfaces were carefully ground and polished. A pressing force of 0.05 N and a load

duration of 15 seconds were applied. Each measurement was repeated six times, and the average value was calculated.

RESULTS AND DISCUSSION

Figure 1 shows the optical microphotographs of the investigated sintered samples with different GNS contents. The microstructure of the Sn-0.7Cu base alloy is shown in Figure 1a, while Figures 1(b–f) illustrate the microstructures of the samples containing GNS. It can be observed that the addition of reinforcement particles significantly reduces the grain size, as confirmed by measurements of the average grain size using ImageJ software (Figure 2). The average grain size continuously decreased from 27.19 μm to 12.64 μm with increasing GNS content. The Sn-0.7Cu/0.10GNS composite exhibited the finest microstructure, with approximately 54 % lower grain size than the Sn-0.7Cu base alloy.

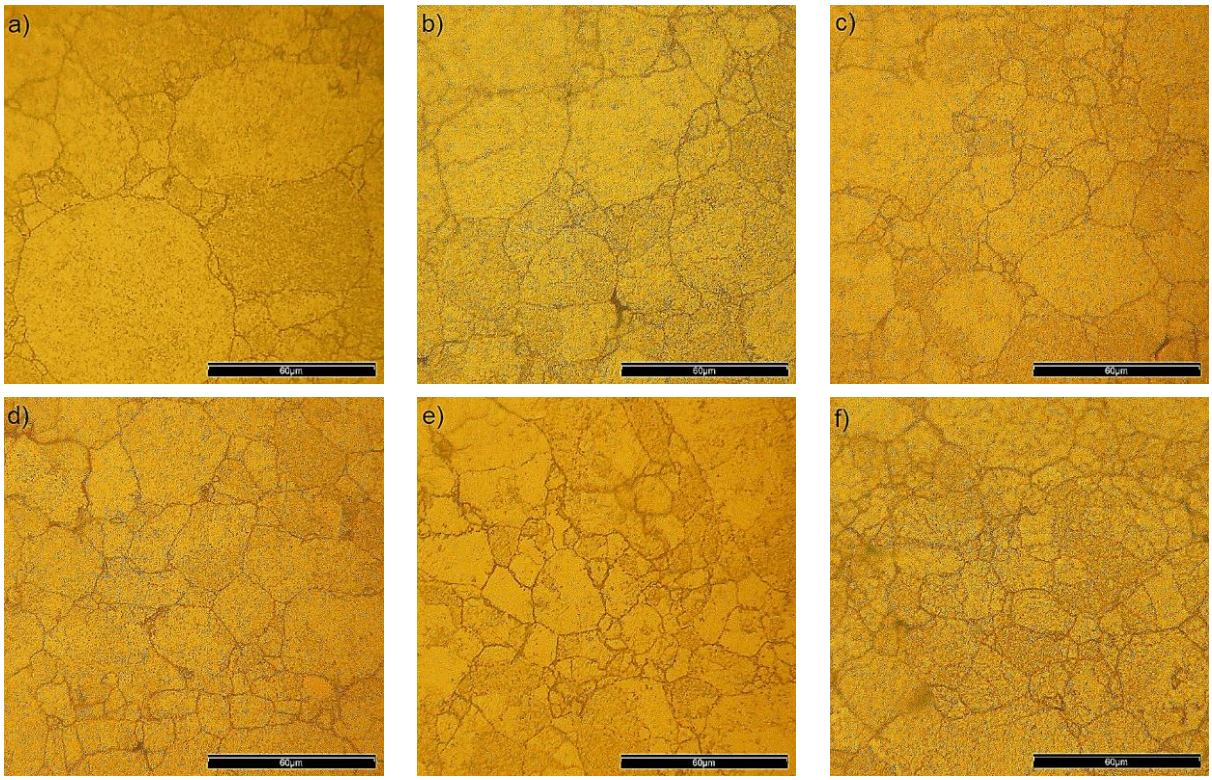

Figure 1 *Optical microphotographs of the sintered Sn-0.7Cu/xGNS samples: a) Sn-0.7Cu; b) Sn-0.7Cu/0.02GNS; c) Sn-0.7Cu/0.04GNS; d) Sn-0.7Cu/0.06GNS; e) Sn-0.7Cu/0.08GNS; f) Sn-0.7Cu/0.10GNS*

Microstructural analysis indicated that the addition of GNS affected the grain morphology of the composites. Optical micrographs showed that the grains are polygonal with well-defined boundaries. The microstructure is heterogeneous, showing variations in grain size, which may be attributed to the non-uniform distribution of GNS during the powder metallurgy process. Porosity is minimal, indicating good consolidation of the powder during the sintering process. At this magnification, GNS particles are not visible. GNS reinforced samples exhibited significant grain refinement and a more homogeneous microstructure

compared to the base alloy. The observed grain refinement can be attributed to the role of GNS as a barrier to grain growth during sintering. The presence of GNS at the grain boundaries may inhibit atomic diffusion, reducing grain boundary mobility and resulting in a finer microstructure. Similar findings were also reported by Yang *et al*. in their study [8].

Figure 3 illustrates the effect of different contents of GNS on the microhardness of the sintered Sn-0.7Cu/xGNS samples. The results indicate a linear trend of increasing microhardness with increasing GNS content. The Sn-0.7Cu base alloy exhibits a microhardness of 18.72 $HV_{0.05}$, while composite Sn-0.7Cu/0.10GNS has a microhardness of 21.65 $HV_{0.05}$ (15.65 % higher than the Sn-0.7Cu base alloy). This enhancement can be attributed to the grain refinement induced by GNS, as well as the restriction of dislocation movement at the grain boundaries, where GNS particles act as barriers during deformation. These findings are consistent with the observations by Yin *et al*. [9], confirming that even small additions of GNS significantly improve the mechanical properties of the composites.

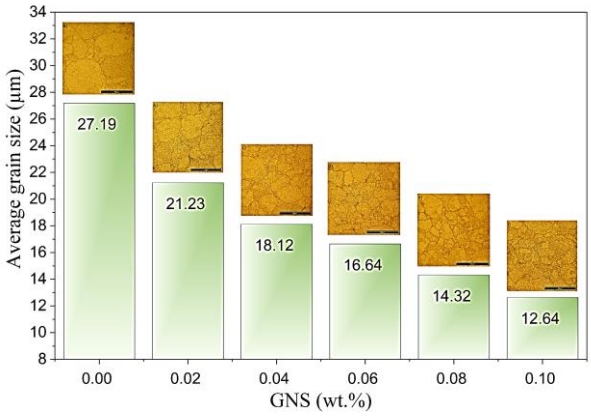

Figure 2 *Effect of GNS content on the average grain size*

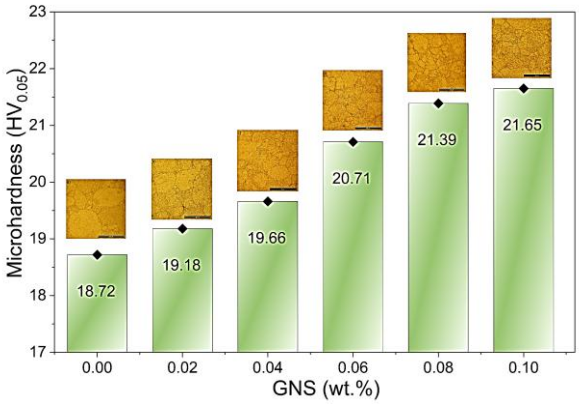

Figure 3 *Effect of GNS content on the microhardness*

CONCLUSION

In this study, Sn-0.7Cu based composites reinforced with GNS (0, 0.02, 0.04, 0.06, 0.08, and 0.10 wt.%) were successfully fabricated using the powder metallurgy technique. From a green engineering perspective, the PM process applied in this study offers several environmental advantages compared to conventional casting processes. Unlike traditional solder production, which requires complete melting of the alloy at temperatures typically above 250 °C, the PM process involves sintering at a significantly lower temperature of 185 °C. This reduced processing temperature directly lowers energy consumption during manufacturing and consequently decreases CO_2 emissions. Additionally, PM enables near-net-shape fabrication, which minimizes material waste and reduces oxidation losses commonly occurring during repeated melting operations. Material utilization efficiency in PM processing is typically above 95 %, contributing to improved resource efficiency.

Overall, the incorporation of very small amounts of GNS (≤ 0.10 wt.%) results in a significant increase in microhardness (≈16%) and considerable grain refinement (≈54%), enhancing the long-term reliability of solder joints. These improvements can extend the service life of electronic components and reduce e-waste. The combination of lower energy

demands, high material efficiency, and improved functional properties demonstrates that the developed Sn-0.7Cu/xGNS composites offer a sustainable solution for lead-free electronics applications.

ACKNOWLEDGEMENT

The research presented in this paper was done with the financial support of the Ministry of Science, Technological Development, and Innovation of the Republic of Serbia, with the funding of the scientific research work at the University of Belgrade, Technical Faculty in Bor, according to the contract with registration number 451-03-34/2026-03/ 200131.

REFERENCES

[1] Ma, H., Suhling, J.C., J. Mater. Sci. 2009, 44(5), 1141–1158.

[2] Zhong, X.L., Gupta, M.J. Phys. D: Appl. Phys. 2008, 41(9), 095403.

[3] Li, M.L., Zhang, L., Jiang, N., *et al*. Mater. Des. 2021, 197, 109224.

[4] Lv, Y., Yang, W., Mao, J., *et al*. J. Mater. Sci. Mater. Electron. 2020, 31(1), 202–211.

[5] Urade, A.R., Lahiri, I., Suresh, K.S. JOM 2023, 75(3), 614–630.

[6] Kruzhanov, V., Arnhold, V., Powder Metall. 2012, 55(1), 14–21.

[7] ASTM E384-10, Standard test method for Knoop and Vickers hardness of materials, ASTM International, West Conshohocken, PA, 2010.

[8] Yang, W., Lv, Y., Zhang, X., *et al*. Mater. Sci. Mater. Electron. 2020, 31(17), 14035–14046.

[9] Yin, L., Zhang, Z., Su, Z., *et al*. J. Electron. Mater. 2020, 49, 7394–7399.

EcoTER'26
eco.tfbor.bg.ac.rs
32nd International Conference
Ecological Truth & Environmental Research
24–26 June 2026, Hotel Sunce,
Sokobanja, Serbia

Review

TEXTILE WASTE MANAGEMENT IN THE CONTEXT OF THE CIRCULAR ECONOMY AND ITS SOCIOECONOMIC EFFECTS

DOI: 10.5937/EcoTER26490U

Snežana Urošević[1,a*], Milovan Vuković[1,b]

[1] University of Belgrade, Technical Faculty in Bor, Vojske Jugoslavije 12, 19210 Bor, SERBIA

[a] https://orcid.org/0000-0002-6647-0449

[b] https://orcid.org/0000-0003-1715-1078

Abstract

The textile industry, although it represents an important economic sector, simultaneously generates large amounts of waste and has a significant negative impact on the environment. The problem is further intensified by the emergence of fast fashion, which encourages the short-term use of products and their accelerated disposal, despite the fact that many of them are still functionally usable. This model of production and consumption leads to increased exploitation of resources, growth in the amount of waste and deepening of environmental consequences. The application of circular economy principles in the textile industry represents a key step towards sustainable resource management. It is based on reuse, repair, recycling and rational use of materials, which extends the life cycle of products and reduces the amount of waste that ends up in landfills. Textile waste management represents an increasingly significant challenge for modern societies in the context of sustainable development. Textile waste management through this concept not only contributes to environmental protection, but also has significant socioeconomic effects. This paper analyzes the socioeconomic effects of textile waste management, with a focus on employment opportunities and the circular economy

Keywords: textile waste, circular economy, environment, recycling, employment.

INTRODUCTION

The circular economy is a concept aimed at reducing negative impacts on the environment by extending the life of products [1]. Its practical application is based on the principles of sharing, borrowing, reusing, repairing and recycling existing materials and products, to the greatest extent possible. After the end of the use cycle, the materials from which the product is made are processed and used again, most often for the production of new products. This cyclical process of recycling and reuse aims to continuously reduce the amount of waste that is disposed of, as well as to preserve natural resources [2].

Unlike the traditional linear model, in which raw materials are exploited for the production of goods that are discarded and disposed of in landfills after use, the circular economy tends to close material flows and extend the life cycle of resources. The circular economy represents an important instrument for achieving the goals of sustainable development, as it implies

* *surosevic@tfbor.bg.ac.rs*

long-term investments in sustainable management of raw materials, improvement of energy efficiency, reduction of pollution, application of renewable energy sources, as well as development of models of sustainable production and consumption [3].

The textile industry is one of the sectors with a particularly high level of waste generation, which is why the application of circular economy principles in this area can achieve significant economic and environmental benefits. The UN Sustainable Development Agenda 2030 defines the key goals of the development of modern society, whereby the transition to a circular economy is recognized as one of the priority directions of action in the field of environmental protection and mitigation of climate change [4].

On the one hand, circular models enable the creation of new jobs in the sectors of collection, sorting, recycling and production of secondary products. On the other hand, reducing the consumption of resources and more efficient use of materials contributes to reducing production costs and increasing the economic viability of the sector. In addition, the application of the circular economy has the potential to influence consumer awareness and promote more responsible habits in the use of textile products, which in the long term contributes to reducing pressure on the environment and improving social sustainability. In this context, effective management of textile waste becomes a strategic goal that integrates environmental, economic and social aspects, thereby enabling the sustainable development of the sector and society as a whole.

TEXTILE WASTE MANAGEMENT AND TEXTILE RECYCLING

In European Union countries, less than half of end-of-life clothing is collected for reuse and recycling, with only 1% of used clothing being turned into new clothing [5]. The low percentage of recycling is largely due to the fact that the technologies for recycling clothing into fibers that can be reused to make new items are still in the early stages of development. Generating large amounts of textile waste, donating clothes to less developed countries and exporting them in the form of used products, create short-term solutions that reduce the amount of textile waste in developed countries and increase this problem in less wealthy countries, which take upon themselves the storage of clothes after their use [6].

Textile recycling means the reuse or processing of textile materials with the aim of reducing waste, preserving resources and reducing the negative impact on the environment. As such, textile recycling is an important part of sustainable waste management and has a major impact on environmental protection. In addition, clothing that cannot be reused can be converted into products such as recycled fabric or other materials for recycling.

Textile recycling includes the collection, sorting, processing and reuse of old or damaged textile products, such as clothing, bedding and other textile materials. Clothing recycling is a model for converting and processing textile waste or useless clothing into new fashion products when the original condition of the clothing is difficult to reuse [7]. Sources of textile waste, such as waste from textile and clothing production, commercial services and consumption, have raised concerns about the creation of innovative circular textile solutions worldwide. In recent years, the management and disposal of textile waste has become an increasingly urgent global problem [8–11].

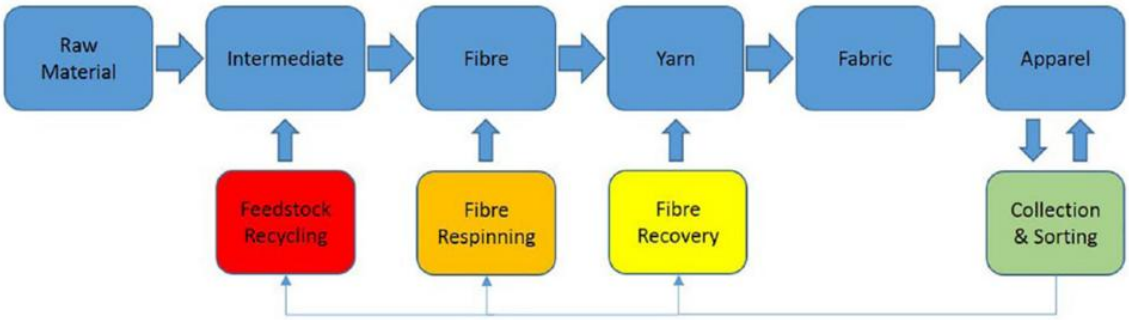

Figure 1 *Textile processing chain and recycling processes [10]*

Textile recycling offers the following advantages and benefits to society:

- Reduction of waste and reduction of landfills (a huge amount of textiles end up in landfills, where they decompose slowly);
- Resource saving (textile production consumes a lot of water, energy and chemicals);
- Less pollution (synthetic materials release microplastics and are more difficult to decompose);
- Reduction of CO_2 emissions (less textile production means less greenhouse gas emissions);
- Encourages the circular economy (increases the use of materials that have already been produced);
- Support for sustainable fashion (encourages responsible behavior in fashion and consumption).

Textile disposal is done in several ways depending on the type of textile, its condition and the local infrastructure for waste management. These are the main ways to dispose of textiles:

- Donation to humanitarian organizations (Red Cross, local NGOs);
- Sale or exchange (through second-hand stores, online platforms or flea markets);
- Household reuse (old clothes can be turned into wipes, pillowcases, bags, etc.);
- Boutiques that accept old clothes (e.g. H&M, Zara in some countries);
- Specialized bins/containers for textiles (often in larger markets and in urban areas there are containers for collecting textiles);
- Industrial recycling (textiles are mechanically or chemically processed into raw materials for new clothes, insulating materials, furniture filling, etc.);
- Recycling centers (local recycling centers), municipal points and waste;
- Landfilling (if there are no other options, textiles end up in landfills, where they degrade slowly and synthetic materials can pollute soil and water, and this is the least sustainable option to avoid whenever possible).

Textile recycling is an important step towards preserving our planet. Disposing of old clothes responsibly, repairing clothes that can still be worn and avoiding buying more than we need are steps that can mean a lot for our future.

The used clothing/textile industry is a resilient, adaptable business model with clearly defined costs [12]. Textile-to-textile recycling offers many long-term strategic advantages that reuse/resale does not:

a) no competition with the new fashion retail sector/employment,
b) a work-based strategy for separation from original material resources,
c) the possibility of training the existing workforce,
d) a large job creation is needed to meet the global demand for ecological fibres [13].

THEORETICAL FRAMEWORK: WASTE MANAGEMENT AND SOCIOECONOMIC IMPACTS

Effective waste management does not only mean its disposal, but also the transformation of waste into a resource. In the context of textiles, socioeconomic effects are reflected in:

- reducing raw material costs,
- generating jobs (especially for vulnerable groups),
- development of innovative business models.

The role of the state and the legislative framework is crucial, especially in the application of the principle of extended producer responsibility (EPR), which encourages the design of products for durability and recyclability.

According to the latest available data from the Statistical Yearbook of the Republic of Serbia for the year 2025, the number of employees in the textile industry sector (the number includes the production of textiles, clothing and leather) is 49,843 [14]. The given data refer only to the general category, and do not refer to the reuse and recycling of textiles. There is no exact statistical number exclusively for textile recycling employees in Serbia, but it is possible to get only a rough estimate. As the total number of employees in the recycling sector is around 5,000–6,000 people, but textile recycling makes up only a small part of that, probably around 500 employees, most often in private companies dealing with the collection and processing of secondary raw materials.

Germany currently collects up to 75% of its textile waste for reuse and recycling [15]. According to the European Environment Agency (EEA), the recycling and sustainable manufacturing sectors have created more than 4 million jobs, with textile recycling identified as a significant sub-sector for growth. A 2020 study by the European Clothing and Textile Confederation estimates that around 20 jobs can be created for every 1,000 metric tons of textiles collected.

The analysis of given data sources clearly shows the potential for creating new jobs in the transition of the circular economy [16]. This transition is gaining strength, as public concern puts the facts about textile waste, its disposal and complex production processes in the center of attention [17]. The industry is now on its way to viewing its waste stream as a strategic raw material, and the circular model as the best long-term solution for providing raw materials for textile production. Powering this reshaping of the unused value of textile waste is a revolutionary technology that is fast approaching. This is certainly a huge opportunity, along with the potential for huge growth. Once the production process is up and running, this renewed industry will require the creation of new jobs and the acquisition of skills related to the preparation of textiles for recycling.

On the other hand, the main drivers of the economy in the textile industry of Serbia are employees, who should have attitudes about an eco-oriented ethos [18]. In other words, it is

necessary that the employee has safe and healthy working conditions, regular payment of personal income, work relationship without overtime that is not conditioned by discrimination or forced labor, and that all legal conditions apply to their work relationship [15]. Opening new jobs means that employees can count on safe work, social and health benefits, and the workplace to be the center of everyday life, because in addition to salary, it also provides a wide range of social services (education, training, hot meals, health insurance, childcare, subsidized vacations, etc.) [19].

Understanding how employment can be applied to textile recycling in the future is crucial for creating new jobs through the circular economy [20]. The fact that 61,000 people are already employed in the textile sector in Serbia, which indicates that it is a powerful sector, it is necessary to single out the category of textile recycling/reuse, which can bring strong growth in the next business cycle [18]. As the textile recycling sector grows, more workers will be needed to collect, sort and process materials for recycling, including both „low-skilled" and „high-skilled" jobs [21].

The workforce should be multi-skilled and with a smaller number of workers. Workers should rotate around different projects, while managers should be able to lead projects, measure performance, drive innovation, manage talent and communicate effectively. This also presents new challenges for skill development and requires a fundamentally different skill set for managers and workers [15].

The most common jobs in the textile recycling sector:

- Operators for sorting and sorting textiles;
- Technicians for material separation (e.g. cotton, polyester, wool, etc.);
- Designers for "zero-waste" fashion;
- Engineers for sustainable fiber development;
- Experts in logistics and waste management.

The National Employment Service describes the textile sorter job as follows: „Textile sorters work along conveyor belts to manually separate unwanted textiles into specific material categories in plants. Qualifications: entry level/physically demanding". The reuse/resale market depends on intensive sorting in order to generate income. Every textile-to-textile recycling platform today incorporates manual sorting into its operations. Sorting is generally considered unskilled work at entry levels, with minimal compensation [22].

The disposal of textile waste is of key importance for the circular economy strategy and is linked to an increase in the number of jobs. The Environmental Protection Agency helps in collecting and diverting textile waste, and converting it into valuable raw materials. However, recruiting and retaining workers is perhaps the biggest challenge facing the labor market in the textile sector in Serbia.

Effective and profitable implementation of a new workforce is not a problem if the required workers cannot be recruited and retained. Retaining highly skilled workers, such as engineers and plant operators, is a challenge that can be solved through retraining and upskilling. The use of vocational training and education is a modern approach for „lifelong

training" while encouraging the acceptance of circular strategies [23]; which, if adopted, will strengthen the efforts of Serbia's textile/recycling industry to retain its workforce.

CONCLUSION

The textile recycling sector represents an important segment of the broader circular economy and has seen rapid growth in recent years, due to the increasing demand for sustainable fashion, strengthening of legal regulations that limit textile waste and growing consumer awareness of environmental problems. The increase in activity in this sector is accompanied by the growth of employment, especially in areas that combine digital tools, sustainable design and waste management, thus opening real chances for career development within the circular economy.

The long-term impact on job creation in the textile sector can be significantly improved through regulatory and economic policies. The introduction of legal frameworks, such as extended producer responsibility, contributes to increasing the recycling rate, intensifying the collection of textile waste and creating new jobs. The data show that there is significant potential for employment in the areas of collection, sorting, processing and recycling of textile waste.

The application of the circular economy model, in which waste is viewed as a strategic raw material, is one of the key ways to ensure the long-term provision of resources in the textile sector. Improving business models and harmonizing operations with the principles of the circular economy in the Republic of Serbia can contribute to increasing the competitiveness of national companies, while simultaneously solving social and economic challenges, especially in the textile sector.

Textile waste management has great potential for socioeconomic development, especially in countries like Serbia, which has a long tradition of textile production and a high unemployment rate in certain regions. By combining environmental and social goals, Serbia should develop a national plan for textile waste management in accordance with EU practices and increase consumer awareness of sustainable consumption.

ACKNOWLEDGEMENT

The authors are grateful to the Ministry of Science, Technological Development and Innovation of the Republic of Serbia for financial support according to the contract with registration No. 451-03-34/2026-03/200131.

REFERENCES

[1] Radev, R., Marinova, V. Textile waste in the context of the circular economy, E3S Web of Conferences-TransSiberia 2023, p. 402, 08048.

[2] European Parliament, The circular economy: what it is and why it matters, European Parliament, Strasbourg, 2015.

[3] Radukić S, Kostić Z. Ciljevi održivog razvoja u Republici Srbiji u svetlu Agende 2030, In D. Kostić, S. Vasilev Stattev (Eds.), Regionalni razvoj i prekogranična saradnja, 2019, p. 43–1440, Srpska akademija nauke i umetnosti-ogranak u Nišu, Niš.

[4] Radukić, S., Petrović-Ranđelović, M., Kostić, Z. J. Econ. Sustain. Dev., 7(1), 1–14.

[5] European Parliament, The impact of textile production and waste on the environment (infographics), European Parliament, Brussels. 2024. Available from: https://www.europarl.europa.eu/topics/en/article/20201208STO93327/the-impact-of-textile-production-and-waste-on-the-environment-infographics

[6] Roadrunner – The Environmental Crisis Caused by Textile Waste, 2021. Available from: https://www.roadrunnerwm.com/blog/textile-waste-environmental-crisis

[7] Park, H.J., Lin, L.M. J. Bus. Res. 2020, 117, 623–628.

[8] Baloyi, R.B., Gbadeyan, O.J., Sithole, B., *et al*. Text. Res. J. 2024, 94(3–4), 508–529.

[9] Candido RG, Recycling of textiles and its economic aspects. In Fundamentals of natural fibres and textiles, Woodhead Publishing, 2021, p. 599–624.

[10] Piribauer, B., Bartl, A. WM&R 2019, 37(2), 112–119.

[11] Pešević D. Upravljanje otpadom, Prirodno-matematički fakultet, Univerzitet u Banjoj Luci, 2022.

[12] Mishra, A., Dutta, P., Jayasankar, S., *et al*. BIJ, 2023, 30(3), 975–1020.

[13] Han, F., Lang, C., Qiu, Y. J. Clean. Prod. 2022, 370, 133509.

[14] Republički zavod za statistiku, Registrovana zaposlenost 2025. Available from: https://publikacije.stat.gov.rs/G2026/HtmlL/G20261025.html

[15] Piribauer, B., Bartl, A. WM&R 2019, 37(2), 112–119.

[16] Dissanayake, D.G.K., Weerasinghe, D. Circ. Econ. Sustain., 2022, 2(1), 25–45.

[17] Lövin, I., Baylan I. Circular economy – Strategy for the transition in Sweden, Elanders, 2020. Available from: https://faolex.fao.org/docs/pdf/swe208661.pdf

[18] Rani, S., Jamal, Z. Int. J. Home Sci., 2018, 4(1), 164–168.

[19] Dimitrijević D, Teze za nove strategije razvoja tekstilne i odevne industrije – deo 2. Tekstilna industrija, 2020, 68(4), 65–76.

[20] Muthu, S.S. (Ed.). Circular economy in textiles and apparel: Processing, manufacturing, and design. Woodhead publishing. 2018.

[21] Soeling, P.D., Aulia, M.I.I., Indriati, F.J. Southwest Jiaotong Univ., 2021, 568–580.

[22] Program upravljanja otpadom u Republici Srbiji za period 2022–2031. godine, Vlada Srbije, 2022. Available from: https://www.ekologija.gov.rs/sites/default/files/2022-02/program_upravljanja_otpadom_u_rs_za_period_2022-2031._god_0_2.pdf

[23] Queiroz, G.C., Abreu, M.C.S.D., Rebouças, S.M. D.P. RAE, 62(5) 1–22.

EcoTER'26
eco.tfbor.bg.ac.rs
32nd International Conference
Ecological Truth & Environmental Research
24–26 June 2026, Hotel Sunce,
Sokobanja, Serbia

Original Research

GREEN PURCHASING DETERMINANTS AMONG GENERATION Z: AN EXPLORATORY FACTOR ANALYSIS

DOI: 10.5937/EcoTER26497V

Danijela Voza[1,a*], Milica Veličković[1b], Marija Panić[1c], Aleksandra Fedajev[1d], Sanela Arsić[1e], Dušan Mladenović [2,f]

[1] University of Belgrade, Technical Faculty in Bor, Vojske Jugoslavije 12, 19210 Bor, SERBIA

[2] Masaryk University, Faculty of Economics and Administration, Brno, CZECH REPUBLIC

[a] https://orcid.org/0000-0003-0895-731X [b] https://orcid.org/0000-0002-4332-2216

[c] https://orcid.org/0000-0001-7287-758X [d] https://orcid.org/0000-0002-6974-6631

[e] https://orcid.org/0000-0002-1957-566X [f] https://orcid.org/0000-0001-5101-2181

Abstract

Growing environmental challenges and increasing awareness of sustainability issues have led consumers to show greater interest in environmentally friendly products and services. At the same time, Generation Z, as a generation raised in a digital environment, has increasingly become the focus of research on consumer behavior and environmentally responsible consumption. The aim of this study is to examine how members of Generation Z perceive and distinguish the constructs of environmental concern, perceived environmental knowledge, green purchase intention, and green purchasing behaviour, as well as to identify their latent structure. Exploratory Factor Analysis (EFA) was applied to analyze the data collected through a survey of 517 Generation Z respondents. The results showed that the data met the requirements for conducting factor analysis (KMO=0.956; χ^2=8014.026; $p<0.001$). Although the theoretical model included four constructs, three factors were extracted, explaining 60% of the total variance. The findings revealed that environmental concern and green purchase intention loaded onto the same dimension, indicating that respondents did not clearly distinguish between these constructs. In contrast, green purchasing behaviour and perceived environmental knowledge emerged as separate dimensions. The results suggest that, among Generation Z respondents, environmental concern and purchase intention may represent a broader dimension of environmental orientation.

Keywords: Generation Z, green products, environmental concern, environmental knowledge, green purchase intention.

INTRODUCTION

Environmental degradation and the increasing frequency of ecological problems have led to greater public awareness and concern about environmental protection. As a result, individuals are becoming more environmentally responsible and are increasingly trying to reduce their negative impact on the environment by turning to green products and services. In line with this trend, producers are also shifting their focus toward products and services that

* *dvoza@tfbor.bg.ac.rs*

meet the demands of environmentally oriented consumers. Green products satisfy consumer needs similarly to conventional products while reducing environmental impact throughout their life cycle and incorporating environmentally friendly characteristics. Their growing presence in the market reflects broader efforts toward sustainable production and consumption.

Previous research has yielded inconsistent findings regarding the relationship between environmental concern and green purchasing behavior. Joshi and Rahman (2015) identified environmental concern as an important determinant of green purchase behavior and suggested that consumers who are more concerned about environmental issues are generally more oriented toward environmentally responsible choices [1]. Previous studies have also indicated that environmental concern may strengthen purchase intentions, which can later be reflected in actual consumer behavior. However, findings by Braga Junior *et al*. (2015) showed no significant relationship between environmental concern and consumers' declared purchases of green products [2]. Such differences in findings suggest that environmental concern alone may not be sufficient to explain green purchasing behavior and that other factors may also play an important role.

Green product knowledge refers to consumers' subjective understanding and awareness of the environmental characteristics of green products, as well as their potential environmental impact [3]. It has been recognized as an important determinant of green purchase intention and consumer decision-making [4]. Empirical findings further indicate that environmental knowledge is positively and significantly associated with the intention to purchase green products [5]. Nevertheless, some studies suggest that knowledge does not always directly translate into actual behavior [6].

Generation Z includes individuals born approximately between the mid-1990s and early 2010s and is considered the first generation raised in a fully digital environment. Growing up with constant access to technology and social media has significantly shaped their attitudes, lifestyles, and consumption patterns. Members of this generation are often associated with greater awareness of social and environmental issues, including sustainability and responsible consumption [7]. Due to their increasing market influence and purchasing power, Generation Z has attracted considerable attention in research on consumer behavior and green purchasing practices.

The aim of this study is to examine the relationships between environmental concern, perceived environmental knowledge, purchase intention, and green purchasing behaviour among members of Generation Z. In addition, the study seeks to identify the latent structure of these constructs and to determine whether the theoretically defined dimensions are clearly distinguished in respondents' perceptions. Particular attention is given to understanding how Generation Z perceives environmental orientation and its connection with intentions and actual behaviour in the context of green products and services.

MATERIALS AND METHODS

Data collection

Data were collected in 2025 using an online survey administered to Generation Z respondents from the Czech Republic and Serbia. A total of 517 valid responses were obtained. The questionnaire included four groups of items corresponding to the constructs examined in this study: Environmental Concern (seven items), Perceived Environmental Knowledge (four items), Green Purchase Intention (five items), and Green Purchasing Behaviour (six items). All statements were measured using a seven-point Likert-type scale, where 1 indicated complete disagreement and 7 indicated complete agreement.

Data analysis

To examine the structure of the constructs used in the study, Exploratory Factor Analysis (EFA) was conducted. Before proceeding with factor extraction, the suitability of the data for factor analysis was assessed using the Kaiser–Meyer–Olkin (KMO) measure and Bartlett's Test of Sphericity.

RESULTS

Exploratory Factor Analysis

Prior to conducting factor analysis, the adequacy of the data was examined. The Kaiser–Meyer–Olkin measure of sampling adequacy was 0.956, indicating that the data were highly suitable for factor analysis. In addition, Bartlett's Test of Sphericity was statistically significant ($\chi^2(231)=8014.026$, $p<0.001$), confirming that sufficient correlations existed among the variables (Table 1).

Table 1 *Measures of sampling adequacy and sphericity test results*

Kaiser-Meyer-Olkin Measure of Sampling Adequacy.		**.956**
Bartlett's Test of Sphericity	Approx. Chi-Square	8014.026
	df	231
	Sig.	**.000**

Exploratory Factor Analysis was performed using Principal Axis Factoring with Oblimin rotation. Since the analyzed constructs were expected to be related, an oblique rotation method was considered more appropriate. Based on the eigenvalue criterion greater than one, three factors were extracted, accounting for 60.0% of the total variance (Table 2).

Although the initial framework included four constructs: Environmental Concern (EC), Perceived Environmental Knowledge (PEK), Green Purchase Intention (GPI), and Green Purchasing Behaviour (GPB), the analysis resulted in a three-factor structure.

The first factor (F1) explained the largest proportion of variance (49.38%) and consisted mainly of items related to environmental concern and green purchase intention. This result suggests that respondents did not clearly distinguish concern for environmental issues from intentions to purchase environmentally friendly products. These findings suggest that

environmental concern and purchase intention form a broader dimension of environmental orientation among Generation Z respondents.

Table 2 *Pattern matrix and explained variance of extracted factors*

Items	F1	F2	F3
EC_4	.730		
EC_3	.660		
EC_6	.658		
EC_1	.643		
EC_5	.594		
GPI_2	.580		
EC_7	.556		
GPI_4	.552		
GPI_1	.508		
EC_2	.418		
GPB_4		-.809	
GPB_1		-.772	
GPB_6		-.746	
GPB_3		-.640	
GPB_5		-.540	
GPI_5	.498	-.529	
GPB_2		-.479	
GPI_3	.433	-.455	
PEK_3			.859
PEK_2			.760
PEK_4			.678
PEK_1			.628
Eigenvalue	11.25	1.92	1.21
% Total variance	49.38	6.78	3.85
% Cumulative variance	49.38	56.16	60.00

* EC = Environmental Concern; GPI = Green Purchase Intention; GPB = Green Purchasing Behaviour; PEK = Perceived Environmental Knowledge. Extraction method: Principal Axis Factoring. Rotation method: Oblimin with Kaiser normalization. Only factor loadings above 0.40 are presented.

The second factor (F2) included items measuring green purchasing behaviour. High factor loadings across these items indicated a relatively clear and stable construct. The third factor (F3) represented perceived environmental knowledge. All items associated with this dimension demonstrated strong loadings and a consistent factor structure.

The Pattern Matrix also indicated overlap among two green purchase intention items. In particular, the statements "*I would be willing to influence others to purchase green products*" and "*I would pay a somewhat higher price for products and food free of chemical substances which damage the environment*" showed meaningful loadings on more than one factor.

DISCUSSION

The obtained results indicate that the proposed four-dimensional structure was not fully supported. Instead of four separate constructs, the analysis resulted in three extracted factors. The most notable result refers to Environmental Concern and Green Purchase Intention,

which loaded onto the same factor, indicating that Generation Z respondents did not clearly separate concern for environmental issues from intentions to purchase environmentally friendly products. One possible explanation for this finding is that Generation Z consumers may perceive environmental responsibility not only as an attitude but also as an expression of personal identity. Consequently, concern for environmental issues may directly translate into intentions to purchase green products. Similar findings have been reported in previous studies, which identified environmental concern as an important factor associated with green purchase behaviour suggesting that environmentally concerned consumers are generally more likely to make environmentally responsible choices [8].

At the same time, some Green Purchase Intention items showed loadings on more than one factor. In particular, statements related to willingness to influence others and willingness to pay higher prices for environmentally friendly products demonstrated overlap with other dimensions. This may indicate that such statements involve not only purchase intention but also elements of personal commitment or social influence.

Although environmental concern appeared to be closely related to purchase intention, green purchasing behaviour emerged as a separate factor. This suggests that positive attitudes and intentions do not always result in actual purchasing behaviour, which is consistent with previous findings in the field of green consumer research [9].

CONCLUSION

This study showed that environmental concern and green purchase intention were perceived as closely related dimensions among Generation Z respondents, while green purchasing behaviour and environmental knowledge emerged as separate constructs. These results contribute to a better understanding of green consumer behavior and suggest that environmental concern may play an important role in shaping purchasing intentions among younger consumers.

The limitation of this study is that data were collected through self-reported measures and focused only on respondents from Serbia and the Czech Republic. Future studies could include broader cross-cultural samples and apply confirmatory factor analysis to validate the obtained structure.

ACKNOWLEDGEMENT

This research was supported by the Science Fund of the Republic of Serbia, GRANT No 338. Project title: Enhancing Collaboration in Promoting Attitudes and Consumption Trends for green products and services (ECO-PACT).

REFERENCES

[1] Joshi, Y., Rahman, Z. Int. strateg. manag. rev. 2015, 3(1–2), 128–143.

[2] Braga Junior, SS, da Silva D, Gabriel Mlds, de Oliveira Braga. In: Proceedings of the Asian Conference on Environment-Behaviour Studies; Aug 25–27; Seoul, South Korea. 2015. p. 99–108.

[3] Wang, H., Ma, B., Bai, R. Sustainability. 2019, 11(4),1193.

[4] Yadav, R., Pathak G.S. Ecol Econ. 2017, 134, 114–122.

[5] Liu, M., Lyu, B., Suwandej, N. Sci Rep. 2026, 16, 15801.

[6] Bartiaux, F. J Clean Prod. 2008, 16, 1170–1180.

[7] Djafarova, E., Foots S. Young Consum. 2022, 23(3), 413–431.

[8] Balaskas, S., Panagiotarou, A., Rigou, M. Sustainability. 2023, 15, 13204.

[9] Hughner, R.S., McDonagh, P., Prothero, A., Shultz, C.J., Stanton, J. J Consum Behav. 2007, 6(2–3), 94–110.

EcoTER'26
eco.tfbor.bg.ac.rs
32nd International Conference
Ecological Truth & Environmental Research
24–26 June 2026, Hotel Sunce,
Sokobanja, Serbia

Original Research

GREEN METAKAOLIN GEOPOLYMERS: SYNTHESIS AND CHARACTERIZATION DURING AGEING

DOI: 10.5937/EcoTER26503I

Marija Ivanović[1,a*], Sanja Knežević[1,b], Ljiljana Kljajević[1,c], Nataša Mladenović Nikolić[1,d], Isidora Maksimović[2,e], Katarina Cmiljanović[3,f], Snežana Nenadović[1,g]

[1] Department of Materials, "VINČA" Institute of Nuclear Sciences, National Institute of the Republic of Serbia, University of Belgrade, Belgrade, SERBIA

[2] Department of Chemical engineering, Technological-metallurgical faculty, University of Belgrade, Belgrade, SERBIA

[3] Department of Chemistry, Chemical faculty, University of Belgrade, Belgrade, SERBIA

[a] https://orcid.org/0000-0002-1152-4171 [b] https://orcid.org/0000-0002-9371-4066
[c] https://orcid.org/0000-0003-4678-0420 [d] https://orcid.org/0000-0001-8814-0734
[e] https://orcid.org/0009-0009-9639-8351 [f] https://orcid.org/0009-0009-4681-349X
[g] https://orcid.org/0000-0003-4846-8801

Abstract

Metakaolin-based geopolymers represent a significant advancement in sustainable development and the green economy, particularly within the construction industry, by providing a high-performance alternative to traditional Ordinary Portland Cement (OPC). By using metakaolin, a highly reactive aluminosilicate material derived from thermal treatment of kaolin clay, these binders significantly reduce carbon emissions and enable the immobilization of industrial wastes. This paper outlines the production of geopolymer using a metakaolin as an environmentally friendly, energy saving, clean technology to conserve natural environment and resources. The paper examines the influence of NaOH concentration on the physico-chemical properties of geopolymers during the aging process. Two samples with different concentrations were synthesized. Analyzes were performed using XRF, XRD, FTIR and SEM methods.

Keywords: metakaoloin, geopolymer, green materials, ageing time, characterisation.

INTRODUCTION

In recent decades, there has been increased attention to environmental issues and the need to reduce CO_2 emissions in order to combat climate change. In addition to the high greenhouse gas emissions associated with the ordinary Portland cement (OPC) production process, the huge environmental impact of the cement industry is also associated with the massive consumption of raw materials (lime, aggregates, water) and the high demand for energy [1,2]. There is growing interest in developing new binders with a reduced carbon footprint, high performance and durability, which could be used as green alternatives to OPC [3,4]. Geopolymers are innovative class of ceramic materials that possess advanced technological features, such as low energy consumption of production for construction

* *marija@vin.bg.ac.rs*

purposes. Geopolymers are usually obtained through inexpensive and ecofriendly synthetic procedures with low waste gas emission [5,6], which is one of the reasons why they are called the green materials [7]. Geopolymers have attracted global attention as an environmentally friendly alternative to OPC for the production of mortar and concrete [8] synthesized by the reaction between an aluminosilicate precursor, which can be obtained from natural minerals and/or from industrial waste (metakaolin, ash, mining-furnace slag, etc.) and alkaline activators. Synthesis of geopolymers can be made by mixing a reactive aluminosilicate material as precusor with high alkaline solutions. NaOH or KOH are the most commonly used components of activator solutions. The concentration of hydroxide in the solution of activator plays an important role in the process of geopolymerization [9]. Most of the research and knowledge [10] concerning a mechanism of geopolymerization are based on the use of metakaolin as a precursor. Metakaolin is a good source of silicon and aluminum which are highly reactive and react with alkaline activator.

The presented study aims at analyzing the effect of different concentrations of sodium hydroxide (NaOH) on the structure of obtained inorganic polymer during the geopolymerization reaction. The physical and chemical properties from the starting material to the final geopolymers have been monitored to understand the geopolymerization mechanism.

MATERIALS AND METHODS

In this work, natural white clay (kaolin) was used as the starting material.Kaolin is a soft, earthy, natural mineral powder rich in the mineral kaolinite ($Al_2Si_2O_5(OH)_4$). Kaolin was obtained from Rudovci (Lazarevac Serbia). Further calcination of kaolin at 750 °C yielded metakaolin, which we used for the synthesis of geopolymer (GP).

For the synthesis of GP, in addition to MK, we also need an alkaline activator. The alkaline activator solution was prepared from a solution of Na_2SiO_3 and different molar concentrations of NaOH (2M and 8M). The geopolymer (GP) samples were formed from metakaolin and the different alkaline solutions, which were mixed for 10 min and then left at room temperature for one day. After that, the sample mixture was kept in a drying oven for 2 days at 60 °C. The curing and in the same time aging, of geopolymer samples has been followed for 7, 14, 21 and 28 days in covered molds at opened chamber and room relative humidity of 95. Based on different concentrations of NaOH, 2 samples were synthesized, namely GP2M and GP8M. The molar ratio of SiO_2/Na_2O and Al_2O_3/Na_2O of obtained geopolymer samples is shown in Table 1.

Table 1 *The molar ratio of SiO_2/Na_2O and Al_2O_3/Na_2O of GP2M and GP8M*

Samples	GP2M	GP8M
SiO_2/Na_2O	3.50	2.45
Al_2O_3/Na_2O	1.98	1.46

After the synthesis was completed, the physicochemical characteristics of the samples were examined and measured every 7 days during the aging process. The samples were characterized by X-ray diffractometry (XRD). FTIR (Fourier Transform Infrared

Spectroscopy) was used to identify and analyze the chemical composition of the materials. The samples were finely and homogeneously dispersed in anhydrous potassium bromide (KBr) pellets (1.5/150 mg KBr). Spectral data of the samples were collected in the region from 4000–400 cm^{-1}. The surface morphology of the samples was studied using field emission scanning electron microscopy (FESEM, Tescan MIRA 3 XMU) at 20 kV. The samples were sputtered with Au/Pd alloy before analysis.

RESULTS AND DISCUSSION

As previously mentioned, the structural changes that occur during geopolymerization of alkali-activated materials were monitored depending on the NaOH concentration (2M and 8M) and time (7, 14, 21 and 28 days) using FTIR and XRD methods.

Figure 1 shows the results of the XRD patterns of the synthesized geopolymer samples, GP2M (a) and GP8M (b). One way to monitor the changes in the crystal structure during the geopolymerization reaction is to monitor the changes in the XRD patterns of the samples cured at different times at room temperature. It is also important to compare the XRD patterns of the samples cured at room temperature and with different concentrations of NaOH. XRD analysis of almost all geopolymer samples revealed their amorphous structure with the position of the amorphous halo in the range of 18°–32° 2θ, indicating a short-range ordering of the reference sample with a crystalline addition of SiO_2 (α-quartz). The presence of muscovite was also observed. The lines characteristic of quartz (Q), muscovite (M), and zeolite (Z) are shown in Figure 1.

a) *b)*

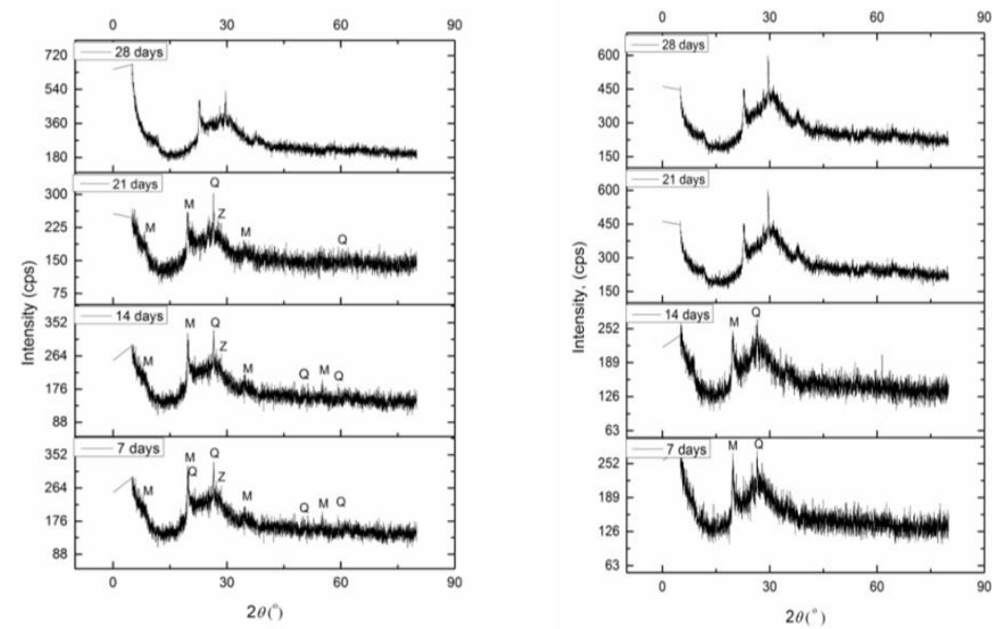

Figure 1 *X-ray diffractograms of a) GP2M sample; and b) GP8M sample every 7 days, up to 28th day*

When comparing the XRD patterns of GP2M and GP8M samples aged at room temperature for 7, 14, 21 and 28 days, it is observed that the intensity of the main peaks of quartz and muscovite decreases after 28 days. It is characteristic that the amorphous halo is somewhat narrow and shifted to a higher angle for GP8M aged 21 and 28 days. Zhang *et al*. [11] found that the proportion of the crystalline phase gradually increases with longer curing times.

FTIR spectra of geopolymers after aging time at room temperature are shown in Figure 2. Spectras show a broad band with a maximum at ~3450 cm^{-1} and a small band at 1635 cm^{-1}, which are attributed to stretching and deformation vibrations of physically adsorbed water molecules (O-H) on the surface, respectively. The FTIR absorption spectra of these samples were compared with known absorption lines in the literature.

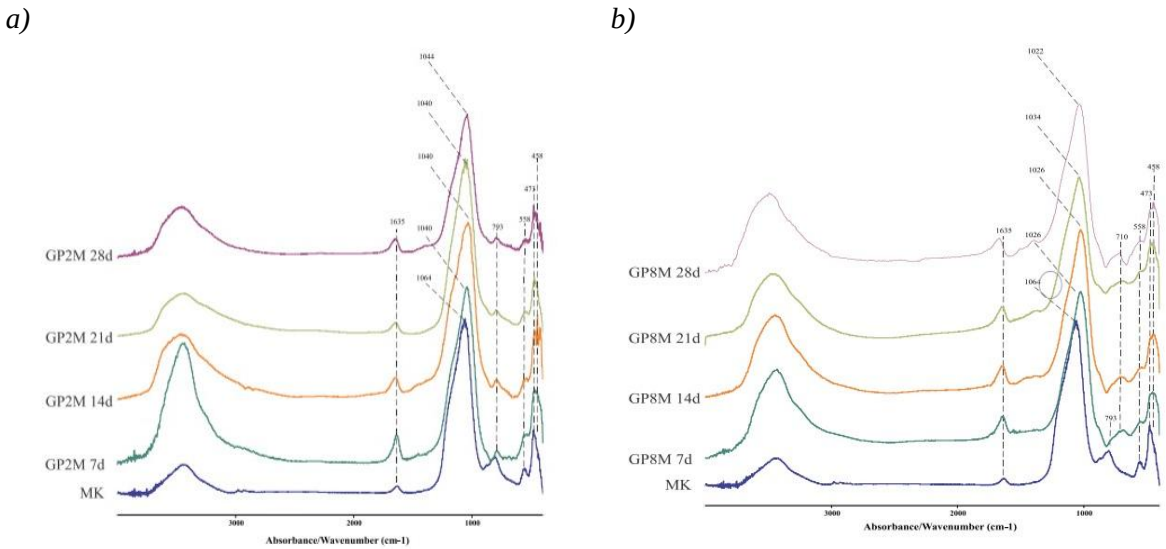

Figure 2 *FTIR of GP2M (a); and GP8M (b) samples after 7, 14, 21 and 28 days*

The FTIR spectra of the samples show a strong peak at ~1000 cm^{-1}, which is associated with the asymmetric Si-O-Si stretching vibrations and is an imprint of geopolymerization [12]. In the spectral range of 1200-1000 cm^{-1}, there are two broad bands, (Si-O-Si stretching vibration) and another (Si-O and Si(Al)-O stretching vibration) [13]. The influence of NaOH concentration on the changes in chemical structure that occur during geopolymerization can be seen by comparing the given spectra. The bands located at 1100 and 1000 cm^{-1}, which belong to the stretching of Si-O bonds [14], shift to the right, and the shape of these bands changes due to the structural rearrangements of the geopolymer during 7-28 days of aging, and due to the influence of different NaOH concentrations in the activator solutions. The broadening of these bands is more pronounced when using 8M NaOH concentration.

According to the literature [15], wide strip at 710 cm^{-1} could be attributed to asymmetric stretching Si-O-Al. On the other hand, the band of the Al-O bond at 793 cm^{-1} is also shifted to the right. The intensity of the Si-O-Al (Si) bond band at 710 cm^{-1} increases with concentration of NaOH. These shifts indicate that there are fine changes of the aluminosilicates structure as the geopolymer synthesis progresses. The intensity of the peaks at 558 cm^{-1} for the GP8M sample increases with the time. This type of addiction has not been observed to sample

GP2M. If we look at the end of the process, we can see clear influence of molarity. Peak that occurs on 1044 cm^{-1} for sample GP2M is moving on 1022 cm^{-1} for sample GP8M. It also shows a wide strip on 710 cm^{-1} for GP8M sample, while on GP2M sample is not noticed. With increasing molarity of NaOH, intensity of strip on 793 cm^{-1} is decreasing on the value of the strip on 710 cm^{-1}.

Both methods XRD and FTIR, revealed that the concentration of NaOH has higher effect on structural changes in geopolymer than aging time.

Various types of morphologies were formed during the geopolymerization process. The surfaces of geopolymers GP2M and GP8M aged for 28 days are shown in Figure 3. Figure 3a shows micrographs of GP2M. We can see the foam structure, probably the incomplete dissolution process of metakaolin and incomplete geopolymerization. The layered gel porous structure of GP8M is shown in Figure 3b. There are also a number of individual particles. The samples show a porous microstructure formed by unreacted micron-sized particles and the geopolymer matrix formed during polycondensation.

a) *b)*

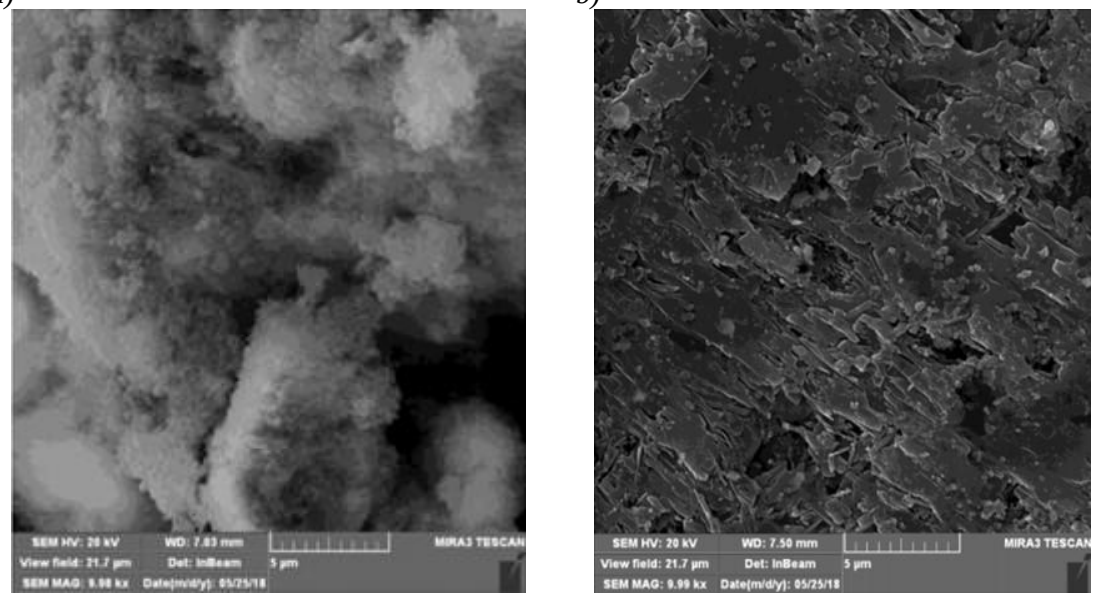

Figure 3 *SEM of GP2M (a); and GP8M (b)*

Based on the micrographs, it can be observed that increasing the NaOH concentration results in significant differences in the microstructure of the GP2M and GP8M samples. The surface morphology of the GP2M sample indicates an incomplete geopolymerization process, whereas the surface of the GP8M sample consists of dense plate-like formations generated through the geopolymerization of metakaolin, which most likely represent the strongest constituents of the newly formed geopolymeric material.

CONCLUSION

Metakaolin-based geopolymers represent a significant advancement in sustainable development and the green economy. Results presented in this paper reveal a diverse

influence that the concentration of NaOH and aging time have on a process of polymerization of a metakaolin. More compact structure of the geopolymer, which correlates to the degree of polymerization is obtained with increasing concentration of NaOH, but also with the time of aging. On the other hand, no significant changes in its crystallinity have been observed with the increase of NaOH concentration in the activation solution. The most important outcome of this study is that is possible to control the properties of a geopolymer, with respect to its application, by avoiding the investment of the energy and solely by the process that is completely eco-friendly.

REFERENCES

[1] Li, X., Ma, W., Li, S., *et al.* Construct. Build. Mater. 2024, 441, 137542.

[2] Oliveira, R.B.D., Leite, G., Possan, E., *et al*. Construct. Build. Mater. 2023, 397, 132382.

[3] Supriya, R., Chaudhury, U., Sharma, P.C, *et al*. J. Clean. Prod. 2023, 417, 137466.

[4] Manzi, S., Molari, L., Bignozzi, M.C., *et al.* Buildings 2024, 14(5), 1191.

[5] Duxson, P., Fernandez-Jimenez, A., Provis, L., *et al*. Mater. Sci., 2007, 42(9), 2917–2933.

[6] Habert, G., Lacaillerie, J.B., Roussel, N. J. Clean. Product. 2011, 19(11), 1229–1238.

[7] Wu, Y., Lu, B., Bai T., *et al.* Construct. Build. Mater. 2019, 224, 930–949.

[8] Kriven, W.M., Leonelli, C., Provis, J.L., *et al.* J. Am. Ceram. Soc. 2024, 107, 5159–5177.

[9] Wang, H., Li, H., Yan, F. A: Physicochem. Eng. Aspects 2005, 268, 1–6.

[10] De Silva, P., Sago-Crenstil, K., Sirivivatnanon, V. Cement Concrete Res. 2007, 37, 512–518.

[11] Zhang, B., MacKenzie, K.J.D., Brown, I.W.M. J Mater. Sci. 2009, 44, 4668–4676.

[12] Kljajević, Lj., Nenadović, S., Nenadović, M., *et al.* Ceram. Inter. 2017, 43(9), 6700–6708.

[13] Prud'homme, E., Michaud, P., Joussein E., *et al.* Sol–Gel Sci. Technol. 2012, 61, 436–448.

[14] Simonsen, M.E., Sonderby, C., Li Z., Sogaard, E.G. J. Mater. Sci. 2009, 44, 2079–2088.

[15] Allahverdi, A., Mehrpour, K., Kani, E.N. IUST Inter. J. Eng. Sci. 2008, 19(3), 1–5.

EcoTER'26
eco.tfbor.bg.ac.rs
32nd International Conference
Ecological Truth & Environmental Research
24–26 June 2026, Hotel Sunce,
Sokobanja, Serbia

Original Research

DIAGNOSING CRITICAL RAW MATERIALS SECTOR READINESS IN CANDIDATE COUNTRIES: A PESTLE-BASED ASSESSMENT OF NORTH MACEDONIA

DOI: 10.5937/EcoTER26509P

Dragi Peltechki[1,a*]

[1] Goce Delcev University of Shtip, Faculty of Natural and Technical Sciences, Krste Misirkov 10A, 2000 Shtip, N. MACEDONIA

[a] https://orcid.org/0009-0003-1375-1890

Abstract

The Critical Raw Materials Act (CRMA), adopted by the European Union in 2024, has reorganised the regulatory horizon facing suppliers of raw materials destined for European industrial value chains. Mineral-rich states located along the EU's enlargement frontier are now confronted with a dual obligation: aligning their domestic regulatory frameworks with the EU acquis as a precondition of accession, and demonstrating sufficient governance, environmental, and traceability performance to qualify as compliant upstream partners under the CRMA's strategic-supplier expectations. This paper offers a structured macro-environmental diagnostic of North Macedonia using the PESTLE framework as the analytical instrument. Results indicate that North Macedonia's mineral endowment and existing concentrate-export profile already articulate the country into European supply chains for lead, zinc, and copper, while ferro-nickel exports have undergone a contraction in recent periods. However, sectoral readiness for deeper integration is constrained by deficits in environmental enforcement capacity, by the absence of domestic intermediate processing capability, and by an extractive-waste inventory. The analysis identifies a feasible development trajectory built on two reinforcing pillars – ESG upgrading of operating concentrate streams, and pilot-scale secondary recovery integrated with mandated remediation at priority sites – while underlining that institutional credibility, rather than mineral prospectivity, is the rate-limiting determinant of progress.

Keywords: critical raw materials, PESTLE diagnostic, secondary raw materials, mining governance, North Macedonia.

INTRODUCTION

Three policy currents converge on the question of how candidate countries integrate into the European raw-materials economy. The first is the shift in industrial strategy that has accompanied the European Green Deal and the digital transition: meeting decarbonisation targets in transport, electricity generation, and energy storage requires materials whose supply is geographically concentrated and economically volatile [1]. The second is the consolidation of this strategic concern into binding regulation through the CRMA, Regulation (EU) 2024/1252, which lists 34 critical and 17 strategic raw materials and assigns 2030 benchmarks to the share of European demand to be satisfied by domestic extraction,

* *dragi.31345@student.ugd.edu.mk*

processing, and recycling, while simultaneously capping single-source third-country dependency [1]. The third is the reactivation of EU enlargement in the Western Balkans (WB), where the acquis-alignment process now intersects with the same raw-materials agenda through a layered set of strategic partnerships, accession-conditioned reform, and access to financing instruments oriented towards green and circular industries.

For N. Macedonia, these currents arrive at a sector whose trajectory has been shaped by the long arc of Balkan mineral exploitation. Polymetallic veins at Sasa, Toranica, and Zletovo, porphyry copper-gold systems at Bučim and Borov Dol, the legacy ferro-nickel platform at Kavadarci, and a constellation of feasibility-stage projects (Ilovica-Štuka, Plavica and Crn Vrv, Kazandol, Kadiica) together constitute a base from which European-facing supply commitments could in principle be expanded [2–4]. Yet the same heritage has bequeathed an extensive footprint of unremediated tailings, slag heaps, and contaminated dumps, several of which have been the subject of recent geochemical re-examination as potential secondary sources of EU-listed materials [5–8]. These two faces of the country's mineral profile – prospectivity and liability – occupy the same physical and institutional space, and any credible CRM development trajectory must address them in parallel.

The literature on WB mining has matured considerably over the last decade. Region-wide assessments compiled under the RESEERVE project produced a WB Mineral Register documenting both primary and secondary deposits in compliance with INSPIRE specifications [3,9]. Geochemical and mineralogical studies have characterised tailings in Serbia and N. Macedonia in support of European secondary-supply strategies [7,8]. Strategic policy commentary from the Adria region has analysed CRMA implications for candidate jurisdictions [2,10]. Resource-efficiency assessments across Eastern and South-Eastern Europe have benchmarked N. Macedonia against comparator economies [11]. What remains thinner in the literature is a country-level synthesis that combines this scientific evidence with the institutional and regulatory dimensions captured in EU accession monitoring, and that assesses readiness against the specific CRMA performance benchmarks now in force.

This paper aims to contribute that country-level synthesis. First, it operationalises the PESTLE framework as a structured diagnostic for sectoral readiness, rather than as a generic environmental-scanning device. Second, it organises the available evidence on N. Macedonia along six analytical dimensions, each evaluated against an explicit EU-anchored benchmark. Third, it derives a parsimonious set of evidence-grounded policy levers calibrated to the CRMA's strategic-supplier expectations and to the country's accession trajectory.

MATERIALS AND METHODS

The CRMA codifies an interventionist response to documented vulnerabilities in European raw-materials supply. Its substantive innovations include the formal designation of strategic and critical materials lists, the establishment of share-of-demand benchmarks for domestic capacity by 2030, the introduction of fast-tracked permitting for projects designated as strategic, the creation of due-diligence obligations along industrial value chains, and explicit provisions for the recovery of critical materials from extractive waste [1,12].

The PESTLE technique was developed in the strategic-management literature as a tool for cataloguing macro-environmental influences on the success or failure of an organisation, an industry, or a market, by sorting those influences into political, economic, social, technological, legal, and environmental categories [13]. The framework's adaptability to sector-level analysis has been demonstrated across diverse contexts, including the construction industry [13], distributed energy infrastructure in Mozambique [14], and low-grade copper-mining viability in Zambia [15].

The diagnostic follows a four-step procedure. First, evidence is extracted from a curated source base and assigned to one of the six PESTLE dimensions. Second, each dimension is summarised against an EU-derived benchmark drawn from CRMA articles, accession monitoring criteria, or relevant directives. Third, dimension-level findings are aggregated into a cross-cutting analytical narrative that traces compounding interactions between dimensions – conditions in which a deficiency in one register amplifies constraints in another. Fourth, the findings are translated into an evidence-anchored set of policy levers, each tied to an institutional actor and a measurable indicator.

To ensure that the diagnostic rests on traceable evidence, only four categories of sources are admitted: (i) peer-reviewed journal articles and conference papers; (ii) official EU regulatory and monitoring documents; (iii) intergovernmental statistics from established providers; and (iv) sectoral analyses produced by recognised research institutions. Press materials and unverified secondary aggregations are excluded. Within these categories, recency was prioritised wherever the underlying conditions are subject to rapid change – particularly in the political, economic, and legal dimensions.

The geochemical evidence base draws on Steiner et al.'s tailings characterisations [7], the regional secondary-raw-materials assessment of Šajn et al. [6], the Veles slag-deposit study [8], the long-standing Lojane investigation by Alderton and co-authors [16], and the Jugohrom hexavalent-chromium contamination study by Mihailovski *et al*. [17]. The legal-regulatory evidence is anchored in Regulation (EU) 2024/1252 [1] and the European Commission's 2025 enlargement monitoring report on N. Macedonia [18]. Production and trade statistics are taken from the Reichl and Schatz World Mining Data compilation [19], the European Training Foundation (ETF) review on critical-raw-materials skills [20], and the WB Mineral Register [9]. WB context and policy framing rely on Borojević Šoštarić [2,10], Giannakopoulou *et al*. [11], Pličanič *et al*. [21], Kursunoglu [5], and Righetti *et al*. [12].

RESULTS AND DISCUSSION

The diagnostic findings are summarised in Table 1, which juxtaposes the principal evidence available for N. Macedonia in each PESTLE dimension against the corresponding EU benchmark. The narrative below elaborates the entries and links each to the underlying source.

Three patterns emerge from the dimension-level findings.

The first concerns the relationship between political and legal conditions on the one hand and economic outcomes on the other. The country's existing concentrate exports demonstrate that European supply chains can absorb upstream output produced under current conditions:

the buyer side has accommodated, through pricing and contracting, the risks attaching to the WB as a sourcing region. What it has not absorbed – and is unlikely to absorb in the CRMA era – is investment exposure to the regulatory, environmental, and litigation risks that accompany upstream expansion or processing investment. The Kazandol arbitration and the Ilovica-Štuka procedural history both illustrate the cost of misaligned environmental and concession governance for project economics. CRMA due-diligence expectations will sharpen this distinction further. The credibility deficit identified in the political dimension therefore translates not into a failure of current trade flows but into a constraint on the deepening of those flows toward higher-value processing stages.

Table 1 *Macro-environmental diagnostic of the N. Macedonia's CRM sector against EU benchmarks*

Dimension	Evidence (North Macedonia)	EU benchmark	Diagnostic verdict
Political	Closer alignment with EU accession trajectory; persistent rule-of-law and anti-corruption concerns flagged in 2025 monitoring [18]; institutional reorganisation through a dedicated Ministry of Energy, Mining and Mineral Resources	Trusted-supplier governance under CRMA Article 8; rule-of-law conditionality under enlargement	Material gap in enforcement credibility
Economic	Lead, zinc, and copper concentrates exported at scale; mining and quarrying contributes a modest share of GDP; ferro-nickel exports show a sharp contraction in 2024 reporting [20]	CRMA 2030 benchmarks for extraction, processing, recycling; single-source cap [1]	Upstream participation present; intermediate processing absent
Social	Documented community opposition and concession termination at Kazandol (2018); pollution incident at Toranica (2025) with parliamentary scrutiny [18]; weak public participation in environmental decision-making	Acquis on public participation in EIA/SEA; CRMA ESG and community-consent expectations	Elevated social-licence risk
Technological	Active flotation and SX/EW capacity at Bučim; underground operations at Sasa with paste-backfill modernisation; characterised tailings inventory of approximately 175 megatonnes [7]; no domestic intermediate refining	CRMA recycling benchmark; BAT compliance for extractive industries	Secondary-resource potential not yet operationalised
Legal	2025 Mineral Resources Act introducing strategic-project designation and concession-fee revisions; EIA and SEA frameworks not fully aligned with the EU acquis [18]	EIA and SEA Directives; Environmental Liability Directive; CRMA due-diligence obligations	Partial alignment; environmental-law gaps require closure
Environmental	Hexavalent chromium concentrations at Jugohrom reported at 132.98 mg/L against a 0.01 mg/L maximum allowable level [17]; arsenic and antimony concentrations exceeding 10,000 ppm at Lojane [7,16]; structural shortfalls in inspection capacity [18]	Water Framework Directive; Mining Waste Directive; Habitats Directive; NATURA 2000	Documented non-compliance at legacy sites

The second pattern concerns the joint geochemical and environmental signature of the legacy tailings inventory. Sites characterised in the published literature as environmental hotspots – Lojane, Veles, Probištip, the broader Sasa complex – are the same sites characterised as containing materially relevant concentrations of CRM-listed or prospectively listed elements [6–8,16]. This co-location offers an opportunity to design integrated remediation–recovery interventions whose financial logic differs from greenfield primary mining. The capital intensity of secondary-resource recovery is in general lower than that of new mine development; the social-licence risk profile is different (the underlying sites are not pristine and remediation has independent public-interest justification); and the alignment with CRMA recycling and circularity provisions is direct. Whether this opportunity becomes operational depends on the establishment of three preconditions: a national inventory of secondary resources with risk-ranked prioritisation; environmental-monitoring capacity sufficient to ensure that recovery activities do not exacerbate existing contamination; and contracting structures – with downstream EU processors – through which the recovered material can be priced and traded under CRMA-compatible due-diligence regimes.

The third pattern concerns the function of EU accession as a meta-driver. Accession conditionality, the CRMA, the Reform and Growth Facility, the WB CRM cooperation track, the ETF's CRM-skills agenda, and the broader strategic-autonomy literature all push in the same direction with respect to the institutional reforms that the diagnostic identifies as constraining [18,20]. The historically novel feature of the present moment is the alignment of these external drivers with the commercial incentives of EU-side processors and battery-supply-chain participants seeking near-shore, traceable raw-materials inputs. This alignment is unlikely to persist indefinitely. The CRMA's 2030 benchmarks will catalyse capacity investment elsewhere – in Serbia, in the Iberian Peninsula, in Scandinavia, and outside Europe under strategic-partnership agreements – and the windows of opportunity for any specific candidate jurisdiction to be designated as a priority partner are correspondingly time-bound.

Two further observations should be recorded. First, the analysis here is conducted at a level of aggregation that may obscure differences across deposits and operators. Site-level techno-economic studies remain necessary for the design of any specific intervention, particularly at Lojane, where geochemical hazards constrain the operational envelope, and at Veles, where urban proximity raises additional planning and consent considerations. Second, the diagnostic does not address the wider regional political economy in which competition among WB jurisdictions for European preference operates: a comparative assessment across Serbia, Bosnia and Herzegovina, Albania, Montenegro, and Kosovo would supplement the country-level findings reported here.

CONCLUSION

This paper has presented a structured PESTLE diagnostic of the readiness of North Macedonia's critical raw materials sector for deeper integration into European supply architectures shaped by the CRMA. The diagnostic indicates that geological prospectivity and existing concentrate-export flows are not the rate-limiting determinants. The decisive factors are the credibility of environmental enforcement, the alignment of EIA and SEA frameworks

with the EU acquis, the transparency of concession governance, and the operational integrity of tailings-safety regimes – conditions whose present performance falls materially short of CRMA strategic-supplier expectations.

Six policy levers follow from the analysis, presented here without ranking and with explicit linkages to the diagnostic evidence.

First, a national strategy on critical and secondary raw materials, mapped explicitly to the CRMA's strategic and critical materials lists and to the 2030 benchmarks. Such a strategy should incorporate a standardised inventory and risk-ranking of tailings and extractive waste, building on the geochemical work of Steiner *et al.* [7] and Šajn *et al.* [6,8] and prioritising sites where commodity recovery is co-located with documented environmental hazard.

Second, comprehensive EIA and SEA acquis alignment, in line with the European Commission's 2025 recommendations [18]. This is the legal reform with the largest single effect on investment risk reduction and on the eligibility of any subsequent strategic-project designations under the Mineral Resources Act.

Third, an extractives-transparency standard covering concession agreements, beneficial ownership, environmental permits, inspection outcomes, and revenue flows, published as open and machine-readable datasets. Such transparency is a precondition both for CRMA due-diligence compliance and for the credibility of the anti-corruption agenda that EU monitoring identifies as unresolved [18].

Fourth, mandatory tailings-safety audits and emergency-response protocols across operating and inactive facilities, with independent monitoring and public reporting. The Toranica incident demonstrates that present arrangements are inadequate even at active mines [18], while the geochemical signatures at Lojane document the urgency of pre-emptive action at legacy sites [7,16].

Fifth, pilot-scale secondary-recovery initiatives at high-priority sites – Lojane, Probištip, Sasa, and the Veles slag landfill – designed in tandem with mandated remediation, governed by strict water and emissions controls, and conditional on community consent. Pilot results should be reported against CRMA recycling-benchmark progress and feed the national strategy referenced above.

Sixth, sustained investment in human capital and applied-research infrastructure, with priority on hydrometallurgy, geometallurgy, and environmental monitoring. Coordinated programming with the ETF's CRM skills agenda [20] and with regional research groups conducting Western Balkans tailings-geochemistry work [6,7] would shorten the lead time required to operationalise the recommendations above.

The shared feature of these levers is that they precede, rather than accompany, large-scale primary-mining expansion. The position taken here is that an upstream investment-led trajectory in advance of governance reform would compound rather than resolve the dimensions of risk identified by the diagnostic. The sequence matters: institutional credibility is the threshold condition under which both the CRMA's strategic-supplier expectations and the broader objectives of the EU accession process can be jointly met.

REFERENCES

[1] European Union. Regulation (EU) 2024/1252 of the European Parliament and of the Council of 11 April 2024, Official Journal of the European Union, L 216, 2024.

[2] Borojević Šoštarić, S., Giannakopoulou, S., Adam, K., *et al*. Geologia Croatica, 2022, 75, special issue.

[3] Rokavec, D., Draksler, M., Levstek, D., *et al.* Geologija 2021, 64(1), 95–105.

[4] Petrušev, E., Stolić, N., Šajn, R., *et al.* Geologica Macedonica, 2021, 35(1), 49–58.

[5] Kursunoglu, S. J. Sustain. Met. 2025, 11, 2023–2050.

[6] Šajn, R., Ristović, I., Čeplak, B. Minerals, 2022, 12(5), 547.

[7] Steiner, T.M.C., Bertrandsson Erlandsson, V., Šajn, R., *et al.* Geologia Croatica 2022, 75, 291–302, special issue.

[8] Šajn, R., Stafilov, T., Boev, B., *et al.* Geologica Macedonica, 2020, 34(2), 89–104.

[9] Hribernik, K, Šinigoj, J, Rokavec, D: In 21st International Multidisciplinary Scientific GeoConference SGEM, 2021.

[10] Borojević Šoštarić, S.: In 7th Croatian Geological Congress, Poreč, 2023.

[11] Giannakopoulou S, Chalkiopoulou F, Adam K. In Materials Proceedings, 5(83), 2021.

[12] Righetti E., Tekin D., Rizos V. How the EU can pursue strategic cooperation on secondary raw materials with the Western Balkans, CEPS Policy Brief, January 2026.

[13] Dalirazar, S., Sabzi, Z. Int. J. Constr. Manag. 2020.

[14] Soares, C.A., Shendrikova, D., Crevani, G., *et al.* Energy Strategy Rev. 2023, 45, 101040.

[15] Kangwa S, Mutambo V: In Society of Mining Professors 6th Regional Conference, Johannesburg, 2018.

[16] Alderton, D., Serafimovski, T., Burns, L., *et al.* Carpathian J. Earth Environ. Sci. 2014, 9(1), 43–56.

[17] Mihailovski S, Mircovski V, Ilijovski Z. Rudarsko-geološko-naftni zbornik, 2021.

[18] European Commission. 2025 Report on North Macedonia, COM (2025) 530 final, 2025.

[19] Reichl C, Schatz M. World Mining Data 2021, Federal Ministry of Agriculture, Regions and Tourism, Vienna, Austria, 2021.

[20] European Training Foundation. Skills for Critical Raw Materials, ETF, Turin, 2025.

[21] Pličanič, S., Mladenović, A., Mauko Pranjić, A., *et al.* Geologica Macedonica, 2020, 34(2), 149–156.

EcoTER'26
eco.tfbor.bg.ac.rs
32nd International Conference
Ecological Truth & Environmental Research
24–26 June 2026, Hotel Sunce,
Sokobanja, Serbia

Original Research

SUSTAINABLE TRANSPORT AND FIGHT AGAINST POLLUTION, CASE STUDY

DOI: 10.5937/EcoTER26516S

Marija Stojanoska[1,a*], Vaska Atanasova[1,b]

[1] University "St. Kliment Ohridski", Faculty of Technical Sciences, Bitola, MACEDONIA

[a] https://orcid.org/0009-0001-5733-543X

[b] https://orcid.org/0009-0000-6790-0845

Abstract

Environmental pollution represents one of the greatest contemporary environmental problems that has a significant impact on people's health and quality of life. One of the main sources of pollution is traffic, especially through the emission of harmful gases from motor vehicles, increased traffic congestion and the excessive use of fossil fuels. Therefore, the need for the introduction of sustainable transport systems is becoming more pronounced. This paper deals with the role of sustainable transport in reducing pollution, with particular emphasis on urban public transport and the application of electric vehicles. Through an analysis of public transport and the possibilities for implementing ecological transport solutions, the benefits of using sustainable transport systems are seen.

Keywords: pollution, line, electric, sustainable, public.

INTRODUCTION

According to research, especially in urban environments, the largest source of air pollution and noise comes from transportation. To reduce negative environmental effects, the implementation of sustainable transportation systems is proposed. Sustainable transportation refers to modes of transport that are sustainable in terms of their social and environmental impacts. The components for assessing sustainability include the specific vehicles used for road, water, or air transport; the energy source; and the infrastructure used to accommodate the transport.

Existing urban mobility habits are characterized by continuous urban expansion and a dependence on automobiles. Sustainable transportation arises in this context to reduce the negative impact associated with this increased urban mobility and to promote more environmentally friendly modes of transport.

The city of Bitola already has public city transportation; the vehicles run on diesel fuel, which further pollutes the environment. The public city transportation lines are not just urban; some of them also serve the nearby rural areas. This research focuses on route no. 14 from Scheherazade to the village of Kravari. Calculations have been made for the implementation

* *marija.stojanoska2@uklo.edu.mk*

of a new line with an electric vehicle. A comparative analysis has also been conducted between the current diesel-powered system and an electric one.

MATERIALS AND METHODS

Bitola is the largest urban center in the fertile and largest Macedonian plain, Pelagonia, and the second-largest city in the Republic of Macedonia, with an area of 320 km². The city of Bitola is located in the far southwestern part of the Republic of Macedonia.

The municipality comprises 65 villages, including the village of Kravari. Kravari is a rural village located southwest of the city of Bitola, about 5 km from the city center. The population is predominantly engaged in agricultural and livestock activities, while the rest of the residents are employed in services and industry in Bitola.

- Demographics: The population is age-diverse, but there is a noticeable trend of young people migrating to the city and abroad. Families average 3–5 members.
- Infrastructure: The village is connected by a paved regional road to Bitola. Public transportation is limited, with a few bus routes per day.
- Education and Healthcare: There is an elementary school in the village, but high school students travel to Bitola. Access to healthcare services is limited, so residents often use healthcare facilities in the city.

The rural area of Kravari is also served by public city transportation. Line 14 has 28 stops. It starts from Sheherezade, makes a full circle past the Faculty of Education, the Hospital, and the City Park, going first to the village of Bistrica, then to the village of Kravari where it stops at three stations, and then returns back past the train station stop, Karposh 4, to Bela Chesma.

The first public transport vehicle departs from the Sheherezade station at 6:00 AM, and the last departure is at 7:30 PM. The first public transport vehicle in the rural area of Kravi, at the Kravi 1 stop, is at 6:35 AM. The next one is at 7:35 AM, one hour later. At the same Kravari 1 station, the public transport vehicle stops at 6:35 and 7:35 AM, then the next service is from 11:35 AM to 3:00 PM. The vehicles run on one-hour intervals; at 3:00 PM, the vehicle does not appear at the station, nor does it at 6:00 and 7:00 PM. This analysis shows that the vehicles run at an irregular frequency, are late, or do not appear at the stop at all, which makes public transportation less attractive for the residents of Kravari. Figure 1 shows public city transport line number 14, along with the stops. The method used in this research is the household survey questionnaire.

The household survey questionnaire is a research method used to collect data from individuals or households in order to analyze behaviors, attitudes, opinions, or demographic information. This method is popular in sociological and economic research, as well as in marketing.

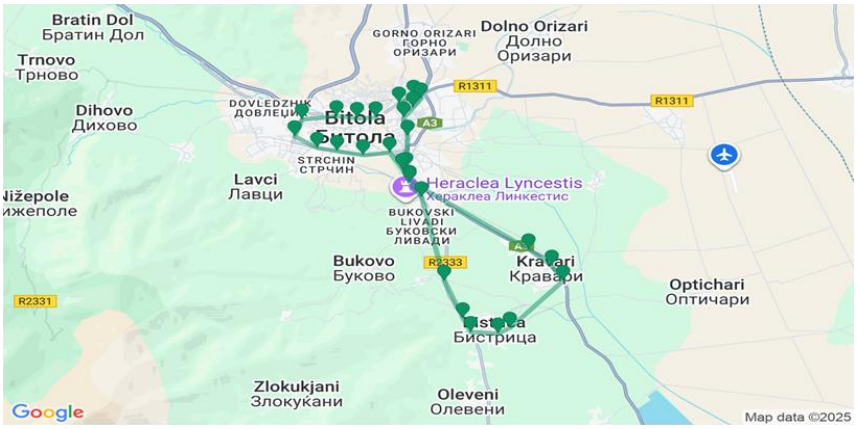

Figure 1 *Public city bus line No.14*

The survey was conducted on December 20, 2024. Although the residents of Kravari cite the regularity and frequency of public transportation as their priority, the analysis indicates that some of the problems can also be overcome through organizational and operational measures, such as introducing a full-day schedule, combining bus and minibus services, introducing a new fleet of vehicles that pollutes less and is quieter, and clearly defined protocols for replacing a vehicle in case of a breakdown. Such measures allow for an improvement in service quality without a significant increase in costs. Given that the biggest problem is the lack of a direct line to Kravari, the proposal is to introduce a new line, as shown in the image 2.

Figure 2 *Proposal for a new public city transit line*

RESULTS AND DISCUSSION

The distance of the analyzed Sheherazad–Kravari route is approximately 12 km one way, while the return route to the starting point is about 7.74 km. The total distance per round trip is approximately 20 km. With a turnaround time of 50 minutes, the resulting average operating speed is about 24 km/h, which is characteristic of rural public transport with stops in settlements.

The turnaround time for the analyzed route is determined based on the total distance and the actual operating speed characteristic of rural public transportation. For a distance of approximately 20 km and an average operating speed of around 24 km/h, the calculated

turnaround time is approximately 50 minutes, which is consistent with the field conditions and the existing traffic regime.

In reality, two vehicles can be used, one in each direction, for backup, service stability, or that vehicle can be operated as a minibus only during peak periods.

But what if we look at the revenues and costs for a single trip? In Bitola, the service is provided by standard buses, and the ticket price is 30 denars.

We know that these are rural areas with very few residents who use public city transportation. So from this, the following arises:

If we have standard vehicles that are 12 meters long, diesel fuel at a price of 64.5 denars/liter, an average number of 50 passengers per trip, and a line length of 20 kilometers per trip, and the price increases to 40 denars, we get the following calculations in Table 1.

Table 1 *Introduction of a new line with a diesel-powered vehicle*

Category	Per Turn	Daily (8 turns)
Fuel	516 denars/turns	4.128 denars/day
Driver	193 denars/turns	1.544 denars/day
Depreciation	260 denars/turns	2.080 denars/day
Maintenance	240 denars/turns	1.920 denars/day
Total	1.189 denars/turns	9.512 denars/day
Revenue	2.000 denars/turns	16.000 denars/day
Profit	811 denars/turns	6.488 denars/day

Given that we need to care for the environment, we should strive to implement sustainable transportation systems, including electric public city transit. The consumption of an electric 12-meter city bus is 1.15 kWh/km. The price of electricity in Macedonia during the analysis period was 23.629 denars/kWh. A new 12-meter electric city bus in the EU typically has a purchase price of around 300,000 to 600,000 euros, which is generally higher than that of a diesel bus. However, total cost of ownership (TCO) analyses often reveal that electric buses are comparable or even cheaper over their lifetime due to lower energy and maintenance costs.

Charging infrastructure: The additional costs for depot charging systems, which can add significant investment and range from 10,000 to 30,000 euros per vehicle.

Electric buses are typically charged once a day, usually overnight. However, high-demand or long-distance routes may require additional short top-ups during the day, known as opportunity charging. Modern electric buses can travel between 150 and 350 km on a single charge. The exact distance depends on the battery size, passenger load, terrain, and temperature. City buses with moderate battery sizes (around 300–400 kWh) typically complete their daily routes without recharging. But if routes include hills, heavy traffic, or cold weather, the range can be reduced. Bus manufacturers offer different battery options, so cities can choose the right balance between weight, cost, and range. Some electric buses also use regenerative braking to recapture energy during stop-and-go driving, extending the battery's lifespan throughout the day.

A standard electric bus has an overall lifespan of 12 to 15 years, with some manufacturers and studies suggesting they can last up to 20 years with proper maintenance and battery management. This is comparable to, or potentially longer than, the typical 10- to 15-year lifespan of a diesel bus. The battery is the most critical component, and its lifespan is usually 8 to 10 years in automotive applications before its capacity drops to about 80%. At this point, the battery can be replaced and repurposed for other uses, such as energy storage, while the bus chassis continues to operate.

Accordingly, calculations were made for the deployment of an electric bus, and the final results are presented in Table 2.

Table 2 *Introduction of a new line with a electric-powered vehicle*

Indicator	Value	Note
Energy consumption	1.15 kWh/km	Average cost for a 12 m electric bus
Electricity price	23.629 denars/kWh	Source: gorivo.mk
Cost per km	27.17 denars/km	1.15 × 23,629
Cost per trip	543 denars/cycle	20 km per trip
Driver cost per trip	193 denars/cycle	Salary 34,000 denars/month
Depreciation per trip	450 denars/cycle	Price 18,000,000 denars, 800,000 km
Maintenance cost per trip	160 denars/cycle	8 denars/km
Total cost per trip	1,346 denars/cycle	Total of all costs
Number of trips per day	8	Operating time ~8 hours
Total daily cost	10,768 denars/day	1,346 × 8
Revenue per trip	2,000 denars/cycle	50 passengers × 40 denars
Daily revenue	16,000 denars/day	8 trips
Daily financial result	+5,232 denars/day	Revenue − expenses

According to the analysis conducted, we can say that the diesel bus is currently more cost-effective, mainly due to lower depreciation. However, the electric bus has advantages in terms of maintenance and environmental protection, making it a better solution for sustainable urban transportation in the long run.

CONCLUSION

Public urban transportation is one of the most important segments of urban planning and the sustainable development of cities. In recent years, many cities have been transitioning from diesel buses to electric buses for environmental, economic, and technological reasons.

Electric public transportation represents a modern and sustainable solution for urban environments. Although the initial investment is higher, the long-term benefits for the environment, health, and operating costs are significant.

Diesel buses still have an advantage in terms of range and lower initial cost, but their negative impact on the environment is gradually making them a less attractive solution.

For this reason, a large number of cities around the world are gradually transitioning to electric public transportation as part of their sustainable development and pollution reduction strategies.

In rural areas and on longer routes where passenger numbers are lower but distances are greater, diesel buses can be simpler to implement, given the fuel infrastructure and the lower charging/infrastructure requirements.

Electric buses are best suited for routes with frequent charging, short distances, and higher environmental standards, such as the central city lines in Bitola. For rural areas, additional charging infrastructure is required for them to be efficient.

ACKNOWLEDGEMENT

The authors are grateful to the students of the Faculty of Technical Sciences in Bitola. They were third-year students (winter semester) who were taking the Traffic Planning course. They are also grateful to the residents of the rural village of Kravari who agreed to be interviewed.

REFERENCES

[1] Ministry of Environment and Physical Planning. Improving Air Quality: Strategies and Measures for Air Quality Plans. Skopje: MOEPP; Available from: https://ripz.moepp.gov.mk/Uploads/PDFFiles_Planovi/20.%20Improving%20Air%20Quality.%20Strategies%20and%20measures%20for%20air%20quality%20plans_MK.pdf

[2] Basuki, I. Int. J. Transp. Dev. Integr. 2025, 9(2), 449–460.

[3] Radio Free Europe. Air Pollution and Public Transport in Macedonia. 2018. Available from: https://www.slobodnaevropa.mk/a/29180749.html

[4] Zhang Y, Li X, Wang H, *et al*. Research on Driver Model of Public Transportation Energy Consumption System Based on Computer Cloud Computing Analysis. 2020.

[5] Bloomberg News. US Cities Are Paying Too Much for New Transit Buses. 2025. Available from: https://www.bloomberg.com/news/articles/2025-09-26/us-cities-are-paying-too-much-for-new-transit-buses

[6] Gorivo.mk. Fuel Prices in North Macedonia. 2025. Available from: https://gorivo.mk/

[7] Alibaba Group. Euro 6 Coach Bus Price. 2025. Available from: https://www.alibaba.com/showroom/euro-6-coach-bus-price.html

[8] City of Saskatoon. Electric Bus Operational Report. Saskatoon; 2023. Available from: https://pub-saskatoon.escribemeetings.com/filestream.ashx?DocumentId=175837

[9] Wang, J., Li, P., Chen, H., *et al*. World Electr. Veh. J. 2024, 15(1), 27.

[10] Stojanoska M. Planning of Public Transport in Small Cities Using PTV Vision VISUM Software. Master's Thesis. Bitola; 2023.

[11] Asia Pacific Gender. Demand Responsive Transport: What if You Could Call a Bus Taxi. 2024. Available from: https://www.asiapacificgender.org/blogs/demand-responsive-transport-what-if-you-could-call-bus-taxi

[12] Heinrich Böll Foundation. Public and intermodal transport for connecting rural and urban areas. 2024. Available from: https://eu.boell.org/en/public-and-intermodal-transport-unite-rural-and-urban-areas

[13] Krstanoski, N., Atanasova, V., Stojanoska, M. Int. J. Eng. Res. Sci. 2025, 11(12), 1–7.

[14] Atanasova, V., Stojanoska, M., Krstanoski, N. Am. J. Eng. Res. 2025, 14 (12), 87–92.

EcoTER'26
eco.tfbor.bg.ac.rs
32nd International Conference
Ecological Truth & Environmental Research
24–26 June 2026, Hotel Sunce,
Sokobanja, Serbia

Original Research

ADDITIONAL RECORDS ON BENTHIC DIATOM *Encyonema bonapartei* Heudre, C.E.Wetzel & Ector (Cymbellales, Bacillariophyceae) IN WATER BODIES OF THE UVAC SPECIAL NATURE RESERVE (SERBIA)

DOI: 10.5937/EcoTER26523G

Luka Grbović[1,a*], Olga Jakovljević[2,b], Jelena Krizmanić[2,c], Bojana Tubić[1,d], Margareta Kračun Kolarević[2,e], Stefan Anđus[1,f], Božica Vasiljević[1,g]

[1] University of Belgrade, Institute for Biological Research "Siniša Stanković" – National Institute of the Republic of Serbia, Bulevar despota Stefana 142, 11108 Belgrade, SERBIA

[2] University of Belgrade, Faculty of Biology, Takovska 43, 11000 Belgrade, SERBIA

[a] https://orcid.org/0009-0004-4298-8229 [b] https://orcid.org/0000-0002-3079-8602

[c] https://orcid.org/0000-0003-4020-7412 [d] https://orcid.org/0000-0003-2050-177X

[e] https://orcid.org/0000-0002-8885-2456 [f] https://orcid.org/0000-0002-1102-7984

[g] https://orcid.org/0000-0002-9856-5311

Abstract

With the rapid global decline of biodiversity in freshwater habitats, there is an increasing need to document rare taxa. The goal of this study is to report new findings on the distribution of Encyonema bonapartei, a rare diatom previously described only in France and Serbia. In 2024, we identified E. bonapartei at two additional sampling sites in the Uvac Special Nature Reserve, at reservoirs where it was not recorded in the earlier 2021 study. The values of physicochemical parameters and ecological status classes were consistent with previous research.

Keywords: diatoms, *Encyonema bonapartei*, Uvac, distribution, rare species.

INTRODUCTION

The geographical distribution of microscopic eukaryotes is a key research topic for understanding their role in the biosphere [1]. Since the early 20th century, the ubiquity hypothesis, commonly summarised as “everything is everywhere” [2], has strongly influenced research on the biogeography of microorganisms [3,4]. The hypothesis suggests that, due to their high dispersal ability, geography may play a lesser role in shaping distribution patterns than ecological factors. However, this postulate remains controversial [5]. In the case of diatoms, although they are generally considered ubiquitous, many taxa exhibit distinct biogeographical patterns [6–8]. Rare diatom taxa are of particular interest in this context, as their limited records may reflect either specific ecological requirements and restricted distribution patterns or insufficient data on their occurrence due to limited sampling effort [9,10].

* *luka.grbovic@ibiss.bg.ac.rs*

Microscopic observations of the unique morphological features of the diatom *Encyonema bonapartei* Heudre, C.E.Wetzel & Ector noted in 2021 in samples from the Uvac Special Nature Reserve, led to its first report in the algal flora of Serbia [11]. The species was initially observed in the canals of the Great East region of France in 2014 and described by Heudre *et al*. [12]. According to existing data, *E. bonapartei* has been documented only in France and Serbia. As a rare taxon, its ecological preferences and distribution remain insufficiently understood.

The aim of this study is to highlight the expansion of *E. bonapartei* distribution in Serbia, and to characterise the community structure, ecological status, and physicochemical conditions of the sampling sites where the taxon was recorded.

MATERIALS AND METHODS

Study area

The Uvac River is located in southwest Serbia, stretching for 119 km, with three reservoirs constructed along it (Zlatar, Radoinja, and Sjenica lakes) [13]. A significant part of the river, particularly the gorge and the reservoirs, is designated as the Special Nature Reserve "Uvac". The river uniquely meanders around ten times [14] as it flows from the Pešter plateau to its confluence with the Lim River near Priboj. The survey of the Special Nature Reserve was conducted in August and October 2024. The sampling sites at the rivers Uvac, Marić, Zlošnica, Tisovica, Kladnica, Veljušnica, and Vapa, as well as the reservoirs Lake Sjenica, Lake Zlatar, and Lake Radoinja, are mainly consistent with the 2021 study [11].

Samples collection and analysis

Phytobenthos sampling was carried out in accordance with standard protocols [15]. The surfaces of five stones from the euphotic zone were scrubbed, the material was rinsed into a sampling bottle and preserved with a 4% formaldehyde solution. In the laboratory, samples were cleaned of organic matter [16]. Cleaned frustules were then mounted in Naphrax mounting resin. Permanent slides were examined using a Carl Zeiss AxioImager.M1 microscope, with an AxioCam MRc5 camera. The relative abundance of identified taxa was attained based on 400 counted valves. The indicative ecological status of the sampling sites was determined according to national laws [17], based on values of the IPS and CEE indices [19] exported from OMNIDIA software [18]. In addition to phytobenthos sampling, physicochemical parameters: temperature (T, °C), dissolved oxygen (O_2, mg/L), oxygen saturation (O_2, %), electrical conductivity (EC, µS/cm) and pH were measured using YSI's ProDSS Multiparameter Handheld Meter. Measurements of ammonium (NH_4^+, mg/L), orthophosphate (PO_4^{3-}, mg/L), nitrite (NO_2^-, mg/L) and nitrate (NO_3^-, mg/L) were performed using a multiparameter photometer Lovibond® MD 600.

RESULTS

Community structure

Compared with the 2021 study [11], the presence of *E. bonapartei* was confirmed in the 2024 investigation in samples from the Marić River and Lake Zlatar, and newly recorded at sampling sites on Lake Radoinja and Lake Sjenica (Table 1).

Table 1 *Sampling sites where E. bonapartei was recorded in 2024 (+ present in sample, / absent from sample)*

Sampling site	Coordinates	Sampling month	
		August	October
Marić River	N 43.520074; E 19.801116	+	/
Lake Radoinja	N 43.521818; E 19.743199	+	+
Lake Zlatar	N 43.510045; E 19.811677	/	+
Lake Sjenica	N 43.417847; E 19.927749	+	+

In the August survey, 30 taxa were identified in the Lake Radoinja sample. The dominant taxa (with relative abundance ≥ 5%) were *Staurosirella pinnata* (Ehrenberg) Williams et Round (34.34%), *Achnanthidium minutissimum* (Kützing) Czarnecki (13.46%), *E. bonapartei* (12.06%), *Staurosira venter* (Ehrenberg) Grunow (7.66%) and *Pseudostaurosira brevistriata* (Grun.) Williams et Round (7.42%). Of the 26 taxa recorded in the Marić River sample, the dominant taxa were *A. minutissimum* (63.25%), *S. pinnata* (8.84%), and *Denticula tenuis* Kützing (7.63%). *E. bonapartei* was identified in low abundance (0.8%). In the Lake Sjenica sample, 61 taxa were identified, with *E. bonapartei* also found in low abundance (0.21%). High relative abundance was documented for taxa *Achnanthidium catenatum* (Bily et Marvan) Lange-Bertalot (39.12%), *A. gracillimum* (13.81%), *Fragilaria gracilis* Østrup (7.95%), *Nitzschia fonticola* Grunow (7.11%) and *Pantocsekiella costei* (Druart et F. Straub) K.T. Kiss et Ács (5.23%). In the October survey, 24 taxa were identified in the Lake Radoinja sample. The dominant taxa were *E. bonapartei* (38.24%), followed by *A. minutissimum* (30.77%), *Encyonopsis minuta* Krammer et Reichardt (9.45%) and *E. subminuta* (5.71%). A total of 71 taxa were identified in the Lake Zlatar sample. The most abundant taxa were *A. minutissimum* (16.48%), *E. bonapartei* (16.48%), *Amphora pediculus* (Kützing) Grunow (8.58%), *A. inariensis* (8.35%), *Diatoma ehrenbergii* Kützing (6.32%), and *Grunowia tabellaria* (Grunow) Rabenhorst (5.64%). In the October Lake Sjenica sample, 32 taxa were identified, with the dominant taxa being *Fragilaria crotonensis* Kitton (24.44%), *A. minutissimum* (17.94%), *A. catenatum* (11.21%), and *A. straubianum* (5.83%).

E. bonapartei was present in both seasons in Lake Radoinja samples, with a noticeable increase in relative abundance in October (38.24%) compared to August (12.06%). The Marić River sample contained the taxon in low abundance in August (0.8%), however it was not found in the October sample. In the Lake Sjenica August sample *E. bonapartei* was present with a low relative abundance (0.21%), which increased to 0.9% in October sample. In the Lake Zlatar sample, the species was present only in October, in high abundance (16.48%).

Physicochemical parameters

The water at the sampling sites was characterised by increased alkalinity, high conductivity and high dissolved oxygen, except at the Marić River in August, where the percentage of dissolved oxygen was significantly lower. The temperature was highest in August at Lake Sjenica and lowest in October at the Marić River. Lake Zlatar was surveyed only in October and showed similar physicochemical parameter values to the Marić River and Lake Radoinja, with slightly lower conductivity. Regarding nutrient concentrations, nitrite levels were very low across all sampling sites. Nitrate concentrations were also low, with the highest value measured in October at the Marić River. Ammonium concentration was elevated in August at Lake Sjenica, while showing low values at other sites. The highest concentrations of orthophosphates were measured in August at the Marić River, while the lowest were below the detection limit in October at Lake Radoinja (Table 2).

Table 2 *Physicochemical parameters measured in the Marić River and Radoinja, Sjenica and Zlatar lakes*

Sampling site	Marić River		Lake Radoinja		Lake Sjenica		Lake Zlatar	
Sampling month	August	October	August	October	August	October	August	October
T (°C)	/	10.0	20.9	13.0	23.3	14.6	/	14.1
O_2 (%)	50.6	108.3	105.5	107.7	104.3	79.8	/	101.4
O_2 (mg/L)	/	13.8	9.18	11.4	8.78	8.1	/	10.42
EC (µS/cm)	259.5	355	280	286	237.2	262	/	244.4
pH	7.75	8.32	8.42	8.29	8.64	8.37	/	8.73
NH_4^+ (mg/L)	0.03	0.03	0.02	0.03	0.82	0.04	/	0.02
PO_4^{3-} (mg/L)	0.9	0.22	0.27	<0.06	0.25	0.21	/	0.39
NO_2^- (mg/L)	<0.01	<0.01	<0.01	<0.01	<0.01	0.01	/	<0.01
NO_3^- (mg/L)	<0.08	0.54	0.11	0.39	<0.08	<0.08	/	0.17

Indicative ecological status assessment

In both the August and October surveys, the Marić River site showed an indicative ecological status of class I ("high"), while lakes Radoinja, Zlatar and Sjenica showed class II ("good") (Table 3).

Table 3 *Indicative ecological status based on the IPS and CEE diatom indices*

Sampling site	Marić River		Lake Radoinja		Lake Sjenica		Lake Zlatar
Sampling month	August	October	August	October	August	October	October
IPS	16.2	18.6	15.6	17.6	17.2	17.1	17.0
CEE	15.7	17.6	16.4	17.3	15.6	17.8	16.6

DISCUSSION

The first occurrence of *E. bonapartei* in Serbia was documented only in the Marić River and Lake Zlatar, in 2021 study [11]. The taxon was very abundant in the August sample from Lake Zlatar (24.22%) and was absent in the October sample. At the same sampling site in the 2024 investigation, it was abundant in the October sample (16.48%) and was not found in August. In the 2021 samples from the Marić River, *E. bonapartei* was recorded in low abundance (2.39%) only in October, whereas in 2024, it was numerous in the August sample

(5.71%). During 2024, this diatom species was recorded at new localities: in samples from Lake Radoinja (situated downstream of Lake Zlatar), it was among the most abundant taxa, and in Sjenica Lake (situated upstream of Lake Zlatar), it was found in low abundances.

The dominant taxa recorded at the sampling sites of concern for this study can be found in a wide range of environmental conditions. Taxa *A. gracillimum*, *F. gracilis* and *E. subminuta* prefer oligotrophic, circumneutral waters [20,21], while *N. fonticola*, *D. ehrenbergii*, *D. tenuis* and *P. costei* can inhabit alkaline, oligo- to β-mesosaprobic habitats [22–24]. Benthic diatoms *A. catenatum*, *P. brevistriata* and *A. straubianum* tolerate meso- to eutrophic conditions [23,25,26]. A high tolerance range to pollution is characteristic of *A. minutissimum*, *F. crotonensis* and *A. pediculus* [20,27,28], while *E. minuta* is pollution sensitive [20,21]. In alkaline waters *S. venter* and *S. pinnata* are frequently found together, with *S. venter* occurring in waters of moderate conductivity and nutrient content [29], while *S. pinnata* is an indicator of moderate environmental stress [30]. *G. tabellaria* is found in medium to high electrolyte rich-habitats, predominantly artificial still waters [22].

The physicochemical parameters were within the expected ranges. Compared to the previous study [11], significantly increased concentrations of orthophosphates and ammonium were measured in the August 2024 sample of the Marić River. When compared to Heudre *et al*. [12], our measurements showed that *E. bonapartei* is present in waters with both lower and higher temperatures, as well as lower conductivity. The ecological status values did not significantly change from earlier investigations [11,31].

CONCLUSION

Three years after the first record of the diatom *E. bonapartei* in Serbia, it was again identified in the Uvac Special Nature Reserve, at two additional sampling sites: at Lake Radoinja and Lake Sjenica. At these reservoirs, species was not recorded in the earlier 2021 study. Additionally, its presence was confirmed at the original sampling sites – the Marić River and Lake Zlatar. The other dominant taxa mainly belong to the genera *Achnanthidium*, *Fragilaria*, *Encyonema*, *Diatoma*, *Staurosira*, *Staurosirella* and *Pseudostaurosira*. The physicochemical parameters showed expected values for the sampling sites. The determined ecological status classes were consistent with previous findings.

ACKNOWLEDGEMENT

This study was supported by the Uvac Special Nature Reserve (No. 570/24 from 05.07.2024.), and Ministry of Science, Technological Development and Innovation of the Republic of Serbia (Nos. 451-03-33/2026-03/200007, 451-03-34/2026-03/200178 and 451-03-33/2026-03/200178). The content of this study is in line with following United Nations (UN) Sustainable Development Goals, under the frame of the UN Agenda for Sustainable Development (Transforming our World: The 2030 Agenda for Sustainable Development – UN, 2015): Goals 15.

REFERENCES

[1] Tarcz, S., Krenek, S., Berendonk, T.U., *et al*. J. Biogeogr. 2026, 53(4), e70206.

[2] Baas Becking, L.G.M. Diligentia Wetensch Serie 1934, 18(19), 263.

[3] Fontaneto D, Hortal J. At least some protist species are not ubiquitous. In: Biogeography of microscopic organisms. 2013.

[4] Taxbck, L., Linder, H.P., Cantonati, M. Water 2017, 9(12), 967.

[5] Fontaneto D, Brodie J. Why biogeography of microorganisms. In: Biogeography of microscopic organisms: Is everything small everywhere. 2011.

[6] Vyverman, W., Verleyen, E., Sabbe, K., *et al*. Ecology 2007, 88(8), 1924–1931.

[7] Astorga, A., Oksanen, J., Luoto, M., *et al*. Glob. Ecol. Biogeogr. 2012, 21(3), 365–375.

[8] Soininen, J. Int Rev Hydrobiol. 2004, 89(2), 139–150.

[9] Wang, N., Xiong, J., Wang, X.C., *et al*. Environ. Sci. Pollut. Res. 2018, 25(28), 28460–28470.

[10] Stenger-Kovács, C., Korponai, J., Abubaker, B., *et al*. Biodivers. Conserv. 2025, 34(6), 2095–2118.

[11] Vasiljević, B., Jakovljević, O., Krizmanić, J., *et al*. Oceanol. Hydrobiol. Stud. 2024, 53(3), 290–298.

[12] Heudre, D., Wetzel, C.E., Ector, L. Phytotaxa 2016, 284(4), 273–280.

[13] Veljić, M., Marin, P.D., Lakušić, D., *et al*. Arch. Biol. Sci. 2006, 58(3), 187–194.

[14] Božić, S., Tomić, N., Pavić, D. Acta Geoturistica 2014, 5(2), 18–30.

[15] Institute for Standardization of Serbia. Water quality–Guidance standard for the routine sampling and pre-treatment of benthic diatoms from rivers. Belgrade: SRPS EN 13946:2015.

[16] Taylor JC, Harding WR, Archibald CGM. A methods manual for the collection, preparation and analysis of diatom samples. Version 1. 2007, 60.

[17] Službeni glasnik Republike Srbije 33/2023. Plan upravljanja vodama na teritoriji Republike Srbije do 2027. godine (*in Serbian*).

[18] Lecointe, C., Coste, M., Prygiel, J. Hydrobiologia 1993, 269(1), 509–513.

[19] Coste M. Étude des méthodes biologiques d'appréciation quantitative de la qualité des eaux. Rapport Cemagref QE Lyon-AF Bassin Rhône Méditerranée Corse. 1982, 218.

[20] Bey M-Y, Ector L. Atlas des diatomées des cours d'eau de la région Rhône-Alpes. Tome 2: Araphidées, Brachyraphidées. Direction Régionale de l'Environnement, de l'Aménagement et du Logement Rhône-Alpes. 2013, 184–261.

[21] Juettner, I., Wetzel, C.E., Van de Vijver, B., *et al*. Fottea 2023, 23(1), 122–140.

[22] Bona, F., Falasco, E., Fassina, S., *et al*. Hydrobiologia 2007, 583(1), 265–274.

[23] Houk, V. Fottea 2010, 10, 1–498.

[24] Bahls LL. Diatoms of Montana and Western North America: catalog and atlas of species in the Montana Diatom collection. Academy of Natural Sciences of Philadelphia. 2023.

[25] Rudinskaya, A., Druzhinina, O. Biology 2025, 14 (9), 1226.

[26] Marquardt, G.C., Costa, L.F., Bicudo, D.C., *et al*. Plant Ecol. Evol. 2017, 150(3), 313–330.

[27] Levkov Z. Diatoms of Europe: diatoms of the European inland waters and comparable habitats. 5. Amphora sensu lato. Gantner. 2009.

[28] Potapova, M., Hamilton, P.B. J. Phycol. 2007, 43(3), 561–575.

[29] Bahls LL. Diatoms of Montana and Western North America: catalog and atlas of species in the Montana Diatom collection. Academy of Natural Sciences of Philadelphia. 2021.

[30] Reavie ED, Kireta AR. Centric, araphid and eunotioid diatoms of the coastal Laurentian Great Lakes. 2015.

[31] Čađo, S., Novaković, B., Đurković, A., *et al*. Voda i sanitarna tehnika 2020, 50(3–4), 19–40.

EcoTER'26
eco.tfbor.bg.ac.rs
32nd International Conference
Ecological Truth & Environmental Research
24–26 June 2026, Hotel Sunce,
Sokobanja, Serbia

Original Research

AQUATIC MACROINVERTEBRATE FAUNA AT SELECTED SAMPLING SITES IN THE GRADAC RIVER

DOI: 10.5937/EcoTER26530T

Bojana Tubić[1,a], Jelena Đuknić[1,b], Nikola Marinković[1,c], Nataša Popović[1,d], Luka Grbović[1,e*], Maja Raković[1,f], Momir Paunović[1,g]

[1] Department of Hydroecology and Water Protection, Institute for Biological Research "Siniša Stanković"—National Institute of the Republic of Serbia, University of Belgrade, Bulevar despota Stefana 142, 11108 Belgrade, SERBIA

[a] https://orcid.org/0000-0003-2050-177X [b] https://orcid.org/0000-0003-3635-5463
[c] https://orcid.org/0000-0002-0360-5393 [d] https://orcid.org/0000-0001-6136-7867
[e] https://orcid.org/0009-0004-4298-8229 [f] https://orcid.org/0000-0001-6899-6113
[g] https://orcid.org/0000-0002-6432-1191

Abstract

Aquatic macroinvertebrates from four sites along the Gradac River, a protected karst watercourse in western Serbia, were studied in June and October 2025 using the Kick and Sweep method. A total of 77 taxa from 14 groups were recorded, with insects (Diptera, Trichoptera, Ephemeroptera, and Coleoptera) dominating both in richness and abundance, comprising nearly 80% of the community, while gastropods accounted for about 11%. The most abundant species were Lepidostoma hirtum, Sericostoma personatum, and Holandriana holandrii, all recorded at the Sunčani vir site. At the Konjički klub site, the invasive snail Potamopyrgus antipodarum was recorded. The presence of Agriotypus armatus, an aquatic hymenopteran parasitoid of the caddisfly pupa Silo pallipes, at the Downstream Konjički klub site was noted. The high proportion of taxa sensitive to moderate organic pollution indicates low organic load and good ecological status. These results confirm the Gradac River as a near-natural, well-preserved watercourse and support its role as a reference site for biomonitoring and freshwater conservation in Serbia.

Keywords: aquatic macroinvertebrate, diversity, saprobic valence, Gradac River.

INTRODUCTION

Aquatic macroinvertebrates are organisms that, at least during a part of their life cycle, inhabit aquatic ecosystems (such as the bottom, detritus, macrophytes, or filamentous algae) and can be collected with a hand nets mesh size 200–500 µm [1].

Communities of aquatic macroinvertebrates are most commonly used in biomonitoring programs [1] because they possess features that make them reliable indicators of changes in ecological conditions in aquatic ecosystems. The low mobility of these organisms allows spatial analysis of environmental factors and stress impacts, while their relatively long life cycles enable examination of temporal changes caused by environmental shifts. The Gradac Gorge is recognized as a protected area due to its natural and ecological significance. Specifically, the river flows through a karst gorge designated as a nature reserve under state

* *luka.grbovic@ibiss.bg.ac.rs*

protection. This status helps preserve the Gradac as one of the few nearly natural and well-preserved watercourses in Serbia. The protected status ensures the conservation of the river's high ecological integrity, supporting diverse and sensitive aquatic communities, including aquatic macroinvertebrates, indicators of water quality and ecosystem health. This protection helps maintain the river's role as a reference site for freshwater biodiversity and ecological research in the region, safeguarding it from significant anthropogenic pollution and habitat destruction.

In Serbia, such protected areas are managed according to national conservation laws with the aim of sustaining long-term ecological values, habitat diversity, and associated ecosystem services. The inclusion of the Gradac River in this framework highlights its conservation importance beyond local scales, contributing to regional biodiversity conservation goals as well.

In this study we assess the aquatic macroinvertebrate fauna at selected sampling sites in the Gradac River to evaluate its biological diversity. The study aimed to (i) analyse the composition and diversity of macroinvertebrate communities, and (ii) identify organic pollution-sensitive taxa as indicators of good water quality. Through these analyses, the study seeks to provide insight into the degree of ecological integrity and preservation of the Gradac River ecosystem.

MATERIALS AND METHODS

Sampling of aquatic macroinvertebrates in the Gradac River was conducted in June and October 2025 at four selected sites: Sunčani vir, Peak of Degurić dam, Konjički klub, and Downstream Konjički klub (Figures 1).

Samples were collected using the Kick and Sweep (K&S) sampling method from all available microhabitat types, following established standards [2], with a benthic hand net FBA (25 × 25 cm, with the mesh sizes of 250 and 500 µm). Biological material was collected, transferred to 500 ml containers, and fixed with 96% ethanol in the field. This sampling procedure ensures a representative sample of aquatic macroinvertebrates from various microhabitats within the investigated sector. The samples are considered semi-quantitative because equal effort was applied at each site within a defined time interval. The K&S sampling method follows recognized standards [3] adapted to the specific habitat and research requirements.

Sorting and identification of aquatic macroinvertebrates were performed based on morphological characteristics, using binocular stereoscopic microscopes ZEISS Stemi 2000C (×50) and Nikon SMZ 800N (×120), and a ZEISS Axio Lab. A1 microscope (×630), supported by appropriate identification keys.

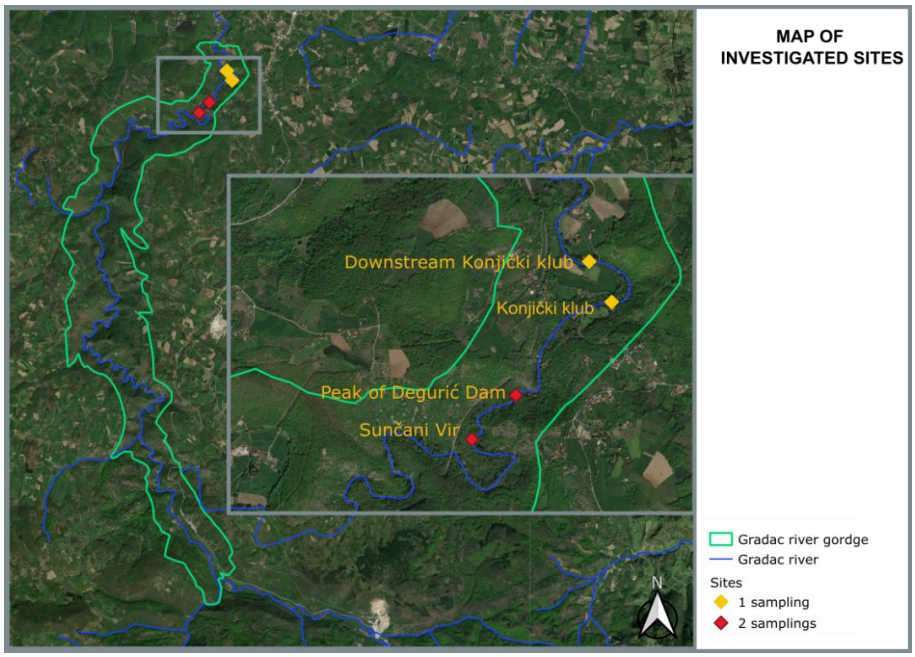

Figure 1 *Sampling sites of the Gradac River*

RESULTS AND DISCUSSION

A total of 77 taxa from 14 macroinvertebrate groups were recorded at four studied sites on the Gradac River.

The aquatic macroinvertebrate communities at the studied sites were most diverse in the insect groups. The group Diptera (26 taxa), Trichoptera (15 taxa), Ephemeroptera (10 taxa) and Coleoptera (8 taxa) were the most diverse in terms of the number of taxa. Also, among the insect groups, Odonata and Plecoptera were recorded with 2 taxa each, and Colembola with one taxon. The diversity of other macroinvertebrate groups was lower: Gastropoda was recorded with 5 taxa and groups Hirudinea and Crustacea were recorded with 2 taxa each, while Oligochaeta and Hidrachnidia with only one recorded taxa each.

The number of taxa per site was almost even during the sampling in June and October. Highest number of taxa (34) was recorded at site Sunčani vir both in June and in October, while the lowest number of taxa (19) was recorded at Peak of Degurić dam during both sampling campaigns (Figure 2).

Larvae of the aquatic insects were the most abundant groups in the studied community, accounting for almost 80% (Figure 3). The insect groups Trichoptera (37.84%), Diptera (20.74%), and Ephemeroptera (11.23%) had the highest percentage participation. Coleoptera (5.62%) and Plecoptera (2.13%) had lower percentage participation, while the other recorded insect groups each accounted for less than 1%. Gastropoda was also quite abundant group, with 11.02% participation in the total community. The rest of the community consisted of groups with percentage participation under 5%: Crustacea (4.58%), Turbellaria (4.57%), Hirudinea (0.68%) and Oligochaeta (0.16%).

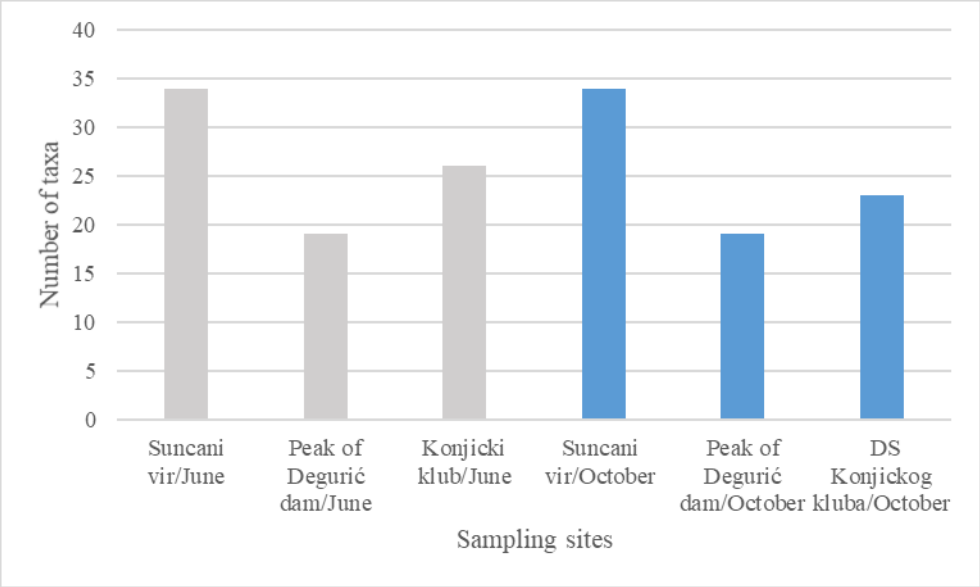

Figure 2 *Number of taxa per sampling sites in June and October on the Gradac River*

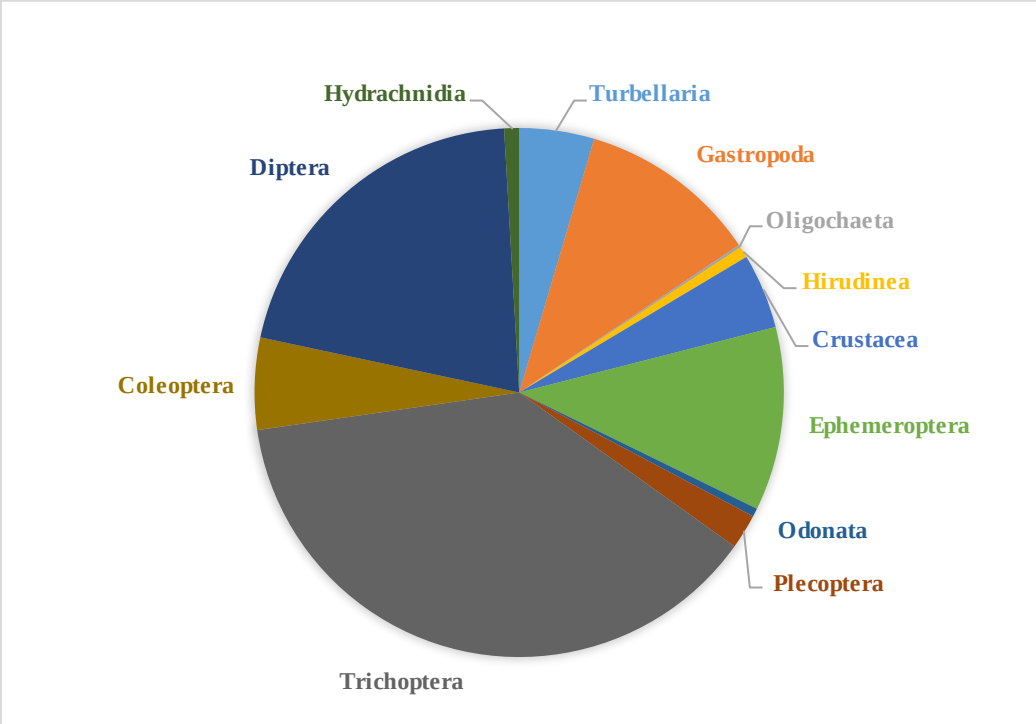

Figure 3 *Percentage participation of aquatic macroinvertebrate taxa in the total community of the Gradac River*

The most abundant species in the community were *Lepidostoma hirtum* (Fabricius, 1775) and *Sericostoma personatum* (Kirby & Spence, 1826) from the Trichoptera group, as well as *Holandriana holandrii* (C. Pfeiffer, 1828) from the Gastropoda group. All three species were recorded in significant numbers at investigated site Sunčani vir.

The site Konjički klub is hydromorphologically altered section of the Gradac River, affected by flow reduction, sediment deposition, and eutrophication. These conditions directly favor the establishment and persistence of invasive snail *Potamopyrgus antipodarum* (Gray,

1843), a species known for its high ecological tolerance, parthenogenetic reproduction, and ability to rapidly occupy disturbed and degraded habitats [4,5].

During sampling in October, the presence of the species *Agriotypus armatus* Curtis, 1832 was recorded at the sampling site Downstream Konjički klub. *A. armatus* is an aquatic parasitoid hymenopteran known to parasitize the pupae of the caddisfly *Silo pallipes* Fabricius, 1781. This parasitoid is unique because it lays its eggs underwater in the pupal cases of *S. pallipes*, an aquatic insect found in clean, well-oxygenated streams and rivers, such as hilly mountain rivers in Serbia, including the Gradac River. The presence of *A. armatus* indicates good water quality and a healthy aquatic ecosystem, as both the parasitoid and its host require relatively unpolluted habitats to thrive. Thus, *A. armatus* represents a fascinating example of aquatic parasitism within freshwater benthic insect communities in Serbian mountain rivers, highlighting complex biological interactions in these ecologically valuable habitats [6].

Most of the recorded taxa in the research area can be considered sensitive to moderate organic pollution, according to the ecological classification of taxa in relation to saprobic valence according to Moog [7]. A total of 41.28% of β-mesosaprobic organisms and 9.1% of α-mesosaprobic organisms were recorded. Among the identified taxa, 23.72% belong to the oligosaprobic group (taxa tolerant to a low degree of organic pollution), while 5.84% belong to the xenosaprobic group (taxa tolerant to a very low degree of organic pollution). Only a small percentage (0.61%) of the recorded taxa tolerate a high degree of organic pollution (polysaprobic taxa). For a quarter of the examined community (19.43%), there is no data on which to base their classification in terms of organic pollution tolerance.

CONCLUSION

The results show that the Gradac River supports a rich and diverse aquatic macroinvertebrate community, typical for small watercourses in hilly-mountainous watercourses, dominated by sensitive insect groups such as Trichoptera, Diptera, Ephemeroptera, and Coleoptera, with aquatic insects accounting for almost 80% of the total community. The presence of certain pollution-sensitive taxa, a high proportion of β-mesosaprobic and oligosaprobic organisms, and the occurrence of the aquatic parasitoid *Agriotypus armatus* indicate low organic pollution and good ecological status. However, the hydromorphologically altered section at Konjički klub displays signs of disturbance, reflected in habitat degradation and the presence of the invasive snail *Potamopyrgus antipodarum*. Overall, the protected status of the Gradac River has helped preserve its ecological integrity, making it a valuable reference site for biomonitoring and freshwater biodiversity studies in Serbia.

ACKNOWLEDGEMENT

This research was funded by the Ministry of Science, Technological Development and Innovation of the Republic of Serbia (Contract No. 451-03-33/2026-03/200007) and by the project "Natural Measures for Ecological Gradac"(Project No.: 00147066/00133820/2025/52), implemented within the initiative "EU for Green Agenda in Serbia", with financial support from Sweden and technical and financial support from the European Union, in partnership with the Ministry of Environmental Protection, and implemented by UNDP in cooperation with Sweden and the European Investment

Bank (EIB), with additional funding from the Governments of Sweden, Switzerland and Serbia. The content of this study is in line with following United Nations (UN) Sustainable Development Goals, under the frame of the UN Agenda for Sustainable Development (Transforming our World: The 2030 Agenda for Sustainable Development – UN, 2015): Goals 6, 13, and 15.

REFERENCES

[1] Rosenberg DM, Resh VH, Kerans BL. Freshwater biomonitoring and benthic macroinvertebrates. 1st ed. Springer New York, NY; 1993.

[2] Barbour MT, Gerritsen J, Snyder BD, *et al*. Rapid bioassessment protocols for use in streams and wadeable rivers: periphyton, benthic macroinvertebrates and fish. 1999.

[3] AQEM Consortium. Manual for the application of the AQEM system. A Compr Method to Assess Eur Streams Using Benthic Macroinvertebrates, Dev Purp Water Framew Dir Version 2002;1:2002.

[4] Marković, V., Gojšina, V., Novaković, B., *et al*. Zootaxa 2021, 5003, 1–64.

[5] Darden ST, Darden R. Nonindigenous Freshwater Organisms: Vectors, Biology, and Impacts; 2003.

[6] Bjelanović, K., Živić, I., Petrović, A., *et al*. Knowl. Manag. Aquat. Ecosyst. 2014, 5.

[7] Moog O. Fauna aquatica austriaca. Wasserwirtschaftskataster, Bundesministerium Für Land-Und Forstwirtschaft, Wien 1995.

EcoTER'26
eco.tfbor.bg.ac.rs
32nd International Conference
Ecological Truth & Environmental Research
24–26 June 2026, Hotel Sunce,
Sokobanja, Serbia

Original Research

DIATOM ASSEMBLAGES IN BIOFILMS OF FRUŠKA GORA WATERFALLS (SERBIA)

DOI: 10.5937/EcoTER26536J

Olga Jakovljević[1,a*], Aleksandar Božić[2,b], Slađana Popović[1,c]

[1] University of Belgrade, Faculty of Biology, Institute of Botany and Botanical Garden "Jevremovac", Department of Algology and Mycology, Takovska 43, 11000 Belgrade, SERBIA

[2] University of Belgrade, Faculty of Biology, Institute of Zoology, Studentski trg 16, 11158 Belgrade, SERBIA

[a] https://orcid.org/0000-0002-3079-8602

[b] https://orcid.org/0009-0000-1857-9055

[c] https://orcid.org/0000-0001-7112-5853

Abstract

The main aim of this study was to determine the diversity and composition of diatom species in the Dumbovački and Nadine kaskade waterfalls in Serbia. Diatoms are a group of microalgae that represent a dominant component of phytobenthos and play a fundamental ecological role in aquatic ecosystems. The measured physical and chemical parameters showed similar values at both study sites, i.e., the two waterfalls. A total of 33 diatom species were identified in the biofilms of the Dumbovački and Nadine kaskade waterfalls in June 2025. Amphora pediculus was the dominant diatom species in the biofilm of Nadine kaskade Waterfall, while it was subdominant in Dumbovački Waterfall, where Cocconeis euglypta was the dominant species.

Keywords: Dumbovački Waterfall, Nadine kaskade Waterfall, diatoms.

INTRODUCTION

Diatoms (Bacillariophyta) are among the most widespread groups of algae in freshwater ecosystems, inhabiting nearly all available habitats [1]. They represent a dominant component of phytobenthos and play a fundamental ecological role in aquatic ecosystems. The diversity and composition of diatom communities are strongly influenced by environmental variables such as temperature, light, moisture conditions, current velocity, salinity, pH, dissolved oxygen, and inorganic nutrient concentrations, as well as by anthropogenic factors including organic pollution, acidification, and eutrophication [1]. As primary producers, diatoms participate in the cycling of phosphorus, nitrogen, and silica [2]. In addition to aquatic environments, they colonize a wide variety of substrates outside water bodies, including soils, rocks, lichens, litter, vegetation, and bark. However, specific environmental conditions are required in these habitats, with light availability and moisture being particularly important factors [1]. Changes in the diversity and composition of diatom communities may reflect alterations in ecological conditions within a habitat and can therefore serve as indicators of changes in water quality [3]. Waterfalls typically contain a variety of microhabitats that

* *olga.jakovljevic@bio.bg.ac.rs*

provide favourable conditions for different groups of plants and microorganisms, including diatoms [4].

The aim of this study was to determine the diversity and composition of diatom species in the Dumbovački and Nadine kaskade waterfalls in Serbia. In addition, several physical and chemical parameters were measured.

MATERIALS AND METHODS

Study sites and water analysis

The Dumbovački Waterfall is situated in the forested area of the Fruška Gora National Park, located in the Vojvodina region of northern Serbia. Although the waterfall is not particularly rich in water, it is usually present during the summer months. The Dumbovački Waterfall is approximately 5 m high and is located on the Dumbovac Stream at an altitude of 275 m [5].

Nadine kaskade is a hidden and relatively lesser-known waterfall, also located within the forested area of Fruška Gora National Park. It is situated at the confluence of an unnamed tributary and the Srneći Stream, at an altitude of 302 m. The waterfall consists of several interconnected cascades formed along the steeper sections of the stream.

In the field, pH, water temperature (°C), electrical conductivity (µS/cm), total dissolved solids (ppt) and oxygen concentration (mg/l) and oxygen saturation (%) of the water samples were measured using Oakton® sensors (Eutech Instruments, Thermo Fisher Scientific, Waltham, MA, USA) and a YSI ProODO optical dissolved oxygen meter (YSI Inc., Yellow Springs, OH, USA).

Diatom sampling and laboratory work

Sampling was conducted in June in 2025 at two waterfalls (Figure 1). Biofilms were collected directly from the stone substrates (Figure 1), which were constantly moistened by water using scalpels, and were stored in Eppendorf tubes until transport to the laboratory. For detailed diatom analyses, the samples were treated using the $KMnO_4$ and HCl method [6], which removes organic material and enables observation of the silicified diatom cell walls that are essential for species identification. After that, permanent slides were prepared by air-drying the cleaned material onto coverslips and mounting them in the synthetic medium Naphrax®.

Figure 1 *Dumbovački (A) and Nadine kaskade (B) waterfalls and sampling sites (A1, B2)*

Diatom identification and microscopic analysis

A detailed qualitative analysis was performed, and all detected diatom taxa were identified using relevant taxonomic literature [7]. Permanent slides were examined using an AxioImager M1 light microscope equipped with an AxioCam MRc5 camera and AxioVision 4.9 software.

RESULTS AND DISCUSSION

The measured physicochemical parameters were similar at both locations, i.e., the waterfalls. The only notable difference was the higher oxygen concentration recorded at Dumbovački Waterfall (Table 1). In some Slovenian waterfalls, higher water temperature was associated with higher conductivity [3], which was not observed in our study. Previous studies have reported that conductivity increases by approximately 2–3% for every 1 °C rise in temperature [3].

Table 1 *Physicochemical water parameters measured at the sampling sites of the two waterfalls in June in 2025*

	Dumbovački Waterfall	Nadine kaskade Waterfall
pH	8.42	8.95
T (°C)	17.1	19
EC (µS/cm)	972	826
TDS (ppt)	0.6	0.5
O_2 (mg/l)	9.07	6.45
O_2 (%)	96.8	80

A total of 33 diatom species were identified in the biofilms of Dumbovački and Nadine Kaskade waterfalls in June 2025. At the individual site level, species richness differed slightly: 22 taxa were recorded at Dumbovački Waterfall and 19 at Nadine Kaskade Waterfall. All species belonged to 18 genera, with *Navicula*, *Amphora*, and *Gomphonema* representing the most species-rich genera (Figure 2). Compared with diatom diversity reported from several waterfalls in Slovenia (101 taxa), the diversity observed in this study can be considered relatively high [3].

Amphora pediculus (Kützing) Grunow was the dominant diatom species in the biofilm of Nadine Kaskade Waterfall, while it was subdominant at Dumbovački Waterfall, where *Cocconeis euglypta* Ehrenberg was dominant (Figure 3). This taxon has also been reported as one of the most frequently occurring diatom taxa in waterfalls of the Krka River [3]. Its tolerance range for nitrate is relatively wide; however, it is generally considered an indicator of mesotrophic conditions, although not a particularly reliable one [8]. The presence of some aerophytic species, such as *Humidophila contenta* (Grunow) R.L.Lowe, Kociolek, Johansen, Van de Vijver, Lange-Bertalot & Kopalová and *Aerophilia roeseana* (Rabenhorst) Danz, Van de Vijver & Kociolek, in Dumbovački Waterfall is noteworthy. Although waterfall biofilms often provide suitable habitats for aerophilic species, the sampled biofilm was continuously submerged. However, the hydrological conditions in the period prior to sampling are unknown and may have influenced species occurrence. The genus *Aerophilia* is typically aerophilous and is frequently found on wet rocks, in caves, in the splash zones of waterfalls, as well as on mosses and soils [9]. *A. roeseana* was originally described as *Melosira roeseana* from wet rocks in a waterfall in Germany in the 19th century [10].

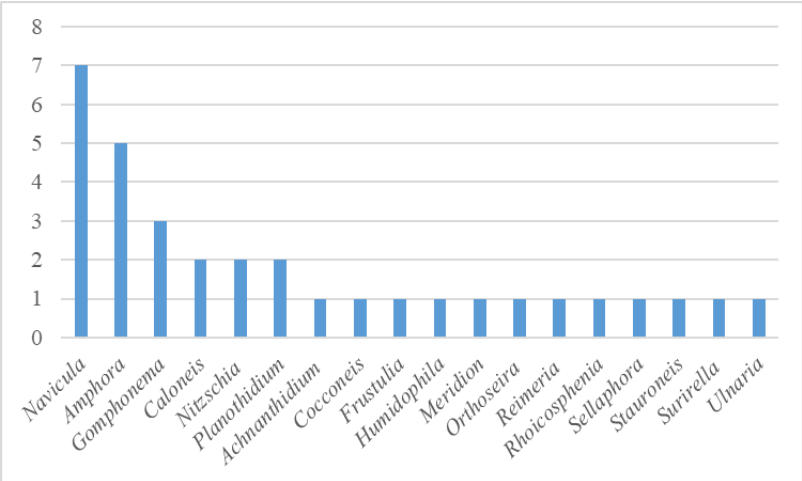

Figure 2 *Number of species within the identified diatom genera in the biofilms of two waterfalls in June 2025*

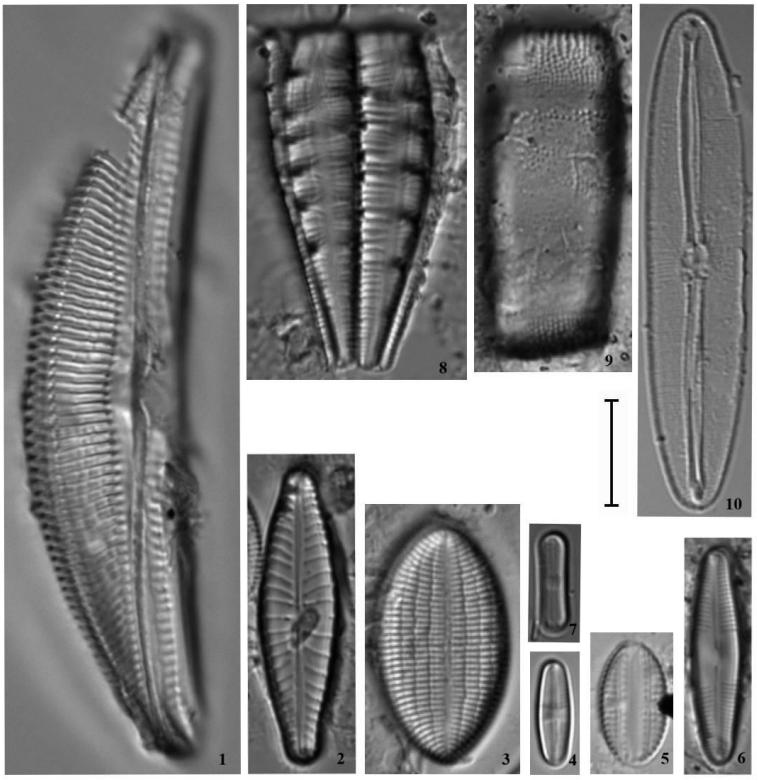

Figure 3 *LM micrographs of selected diatoms identified in biofilms from two waterfalls in June 2025. 1 – Amphora ovalis, 2 – Gomphonema micropus, 3 – Cocconeis euglypta, 4 – Sellaphora nigri, 5 – Amphora pediculus, 6 – Caloneis lancettula, 7 – Humidophila contenta, 8 – Meridion circulare, 9 – Aerophilia roeseana, 10 – Frustulia vulgaris. Scale bar 10 µm*

CONCLUSION

The diversity observed in this study can be considered relatively high for this type of aquatic ecosystem. *Navicula*, *Amphora*, and *Gomphonema* were the most species-rich genera. Investigating the diversity and composition of diatom communities, together with

measurements of physical and chemical parameters, represents an important first step in assessing potential anthropogenic impacts on these specific aquatic ecosystems.

ACKNOWLEDGEMENT

The authors are grateful to the Ministry of Science, Technological Development and Innovation of the Republic of Serbia for financial support according to the contract with registration No. 451-03-33/2026-03/200178.

REFERENCES

[1] Phister, L., Wetzel, C.E., Klaus, J. *et al*. WIREs Water 2017, 4(e1241), 1–13.

[2] Grudzinska I, Florentīne M. In: Proceedings of the 80th International Scientific Conference of the University of Latvia Innovative and applied research in Biology; Riga, Latvia. 2022. p. 9–22.

[3] Krivograd Klemenčić, A., Vrhovšek, D. Acta Mus. Nat. Pragae, Ser. B Hist. Nat. 2003, 59(3–4), 93–98.

[4] Noumssi, B., François, N.V., Théophile, F. *et al*. Asian J. Environ. Ecol. 2021, 14(2), 21–33.

[5] Available from: https://www.decijigrad.rs/atrakcije/dumbovacki-vodopad/

[6] Taylor JC, Harding WR, Archibald CGM. A Methods Manual for the Collection, Preparation and Analysis of Diatom Samples, Version 1.0. Pretoria: Water Research Commission; 2007. p. 49.

[7] Lange-Bertalot H, Hofmann G, Werum M. *et al*. Freshwater Benthic Diatoms of Central Europe: Over 800 Common Species Used in Ecological Assessment. Oberreifenberg: Koeltz Botanical Books; 2017. p. 942.

[8] Zoppi, M., Bona, F., Falasco, E. Ecol. Indic. 2026, 182(2026) 114493.

[9] Kochman-Kędziora, N, Van de Vijver, B. Pl. Ecol. Evol. 2024, 157(2), 113–124.

[10] Kochman-Kędziora, N., Kusber, W-H., Kociolek, J.P. *et al*. Notul. Algarum. 2023, 274, 1–10.

EcoTER'26
eco.tfbor.bg.ac.rs
32nd International Conference
Ecological Truth & Environmental Research
24–26 June 2026, Hotel Sunce,
Sokobanja, Serbia

Original Research

pH-DEPENDENT GROWTH RESPONSES OF *Chlorella* STRAINS IN BG11 MEDIUM

DOI: 10.5937/EcoTER26541P

Slađana Popović[1,a], Zorica Krantić[1], Olga Jakovljević[1,b*], Ana Anđelković[2,c], Ana Milićević[1,d]

[1] University of Belgrade, Faculty of Biology, Institute of Botany and Botanical Garden "Jevremovac", Department of Algology and Mycology, Takovska 43, 11000 Belgrade, SERBIA

[1] Institute for Plant Protection and Environment, Department of Weed Research, Teodora Drajzera 9, 11040 Belgrade, SERBIA

[a] https://orcid.org/0000-0001-7112-5853
[b] https://orcid.org/0000-0002-3079-8602
[c] https://orcid.org/0000-0001-6616-1710
[d] https://orcid.org/0009-0003-9029-0522

Abstract

Chlorella was among the first algae to be successfully cultured and remains one of the most well-known and extensively studied genera of microalgae. Several species are widely used as model organisms in environmental, industrial, and health-related research. Nevertheless, many strains remain unexplored and may possess valuable traits, both within described species and among novel isolates from extreme habitats such as caves. In this study, two Chlorella strains were examined: a commercially available strain and one isolated from lampenflora in Lazar Cave. Both showed notable resilience and the ability to grow across a range of initial pH conditions, with alkaline media proving most favourable for their growth.

Keywords: *Chlorella*, algal cultures, pH value, BG11 medium, lampenflora.

INTRODUCTION

Microalgae constitute a highly diverse and ubiquitous group of photosynthetic microorganisms with a global distribution, yet they also exhibit notable levels of endemism. They inhabit a wide range of aquatic and terrestrial environments, including many that are extreme, poorly explored, and understudied [1]. Despite their immense diversity, only a small fraction of microalgal species has been successfully isolated and maintained in culture collections worldwide. Of these, only a few hundred – mainly those of commercial relevance – have been thoroughly characterised in terms of genomic architecture, biochemical composition, and physiological traits [2].

Chlorella was the first alga to be successfully isolated in culture and played a pivotal role in early studies of photosynthesis and carbon dioxide assimilation in plants. It was also among the first microalgae investigated for mass cultivation and the earliest to be produced on a commercial scale. Intensive research on *Chlorella* began in the early 1950s, coinciding with

* *olga.jakovljevic@bio.bg.ac.rs*

the first large-scale cultivation efforts in the United States, while commercial production was established in 1961 [3,4].

Among *Chlorella* species, physiological and biochemical properties have been studied in considerable detail for *C. vulgaris* and *C. pyrenoidosa* [5]. In addition to these well-known taxa, other *Chlorella* strains have also been investigated and evaluated for various applications (e.g., Guccione *et al*. [5]). However, certain habitats remain underexplored as potential sources of novel representatives of the genus. Caves, in particular, represent such environments, where microalgae typically occur in entrance zones or in areas illuminated by artificial light in show caves, forming communities known as lampenflora.

This study focuses on two *Chlorella* strains, one commercial and one isolated from show cave lampenflora and examines their growth responses in culture media with varying initial pH values.

MATERIALS AND METHODS

Chlorella strains and cultivation

For the purposes of this study, two *Chlorella* strains were used: a commercial strain obtained from a culture collection and a strain isolated from the lampenflora of Lazar Cave in eastern Serbia [6,7].

BG11 medium, prepared according to Rippka *et al*. [8], was used for algal cultures. The lampenflora-derived *Chlorella* strain was initially isolated in test tubes with solid BG11 medium, then cultivated and subcultivated on Petri dishes [6], and subsequently maintained in liquid medium. The commercial strain was maintained exclusively in liquid BG11 medium. Both strains were grown in a controlled growth chamber at 19–22 °C under a 12 h light: 12 h dark photoperiod. Cultures were regularly monitored by light microscopy using a Zeiss Axio Imager M1 microscope equipped with a digital camera, and images were analysed with AxioVision 4.8 software.

Experimental design

Prior to the experiment, a small aliquot of each *Chlorella* culture was transferred into liquid BG11 medium (pH 7.4) and incubated in a growth chamber until high cell density was reached. Subsequently, BG11 media with initial pH values of 3, 5, 7, 9, and 11 were then prepared, dispensed into 100 mL Erlenmeyer flasks (each containing up to 50 mL of medium), and sterilised by autoclaving at 114 °C for 25 minutes.

In the first part of the experiment, both *Chlorella* strains were inoculated into the prepared media with varying initial pH, with three replicates per pH level for each strain. Cultures were grown for two weeks on an orbital shaker at room temperature under a 12 h light: 12 h dark photoperiod. Growth was monitored by measuring optical density (OD) at 680 nm using a spectrophotometer, starting at the beginning of the experiment and subsequently every 2–3 days (three times per week) to generate growth curves.

In the second part of the experiment, the lampenflora-derived *Chlorella* strain was inoculated into the prepared media with varying initial pH values and cultivated for one month in a growth chamber at 19–22 °C under a 12 h light: 12 h dark photoperiod. Biomass production was assessed at the end of the experiment by determining chlorophyll *a*

concentration (μg L^{-1}) using the standard spectrophotometric method (ISO 10260:1992(E)) [9].

RESULTS AND DISCUSSION

The experiment assessing the growth response of two *Chlorella* strains was conducted over a two-week period and included the exponential phase of algal growth. As shown in Figure 1, the lampenflora-derived *Chlorella* strain exhibited a slightly longer lag phase, with more pronounced growth beginning after the second measurement, whereas the commercial strain showed detectable growth from the first measurement. Despite this difference in initial adaptation, both strains displayed a broadly similar growth pattern across media with different initial pH values. No growth was observed in either strain at pH 3. Among the remaining pH treatments, the lowest optical density (OD) values were recorded at pH 5, while the highest values were observed at pH 11 for both strains. Although the overall growth trends were comparable, final OD values differed slightly between the strains, with the commercial strain (Figure 2b) consistently exhibiting higher values across all pH conditions.

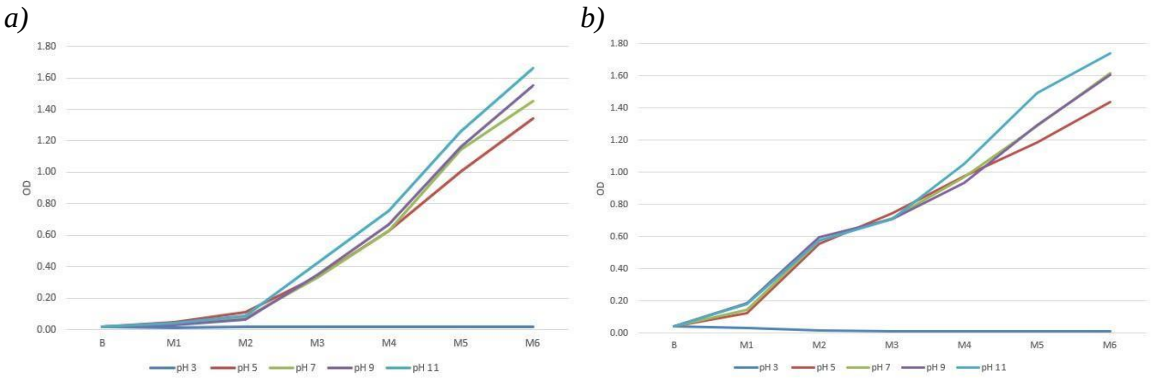

Figure 1 *Growth response of (a) the Chlorella strain isolated from lampenflora (left) and (b) the commercial Chlorella strain (right) after two weeks of cultivation. OD – optical density; B – initial measurement of OD at the beginning of the experiment; M1–M6 – subsequent OD measurements*

The second experiment involved cultivating the lampenflora-derived *Chlorella* strain in a growth chamber, with primary production assessed after one month. The results were consistent with those of the previous experiment: no growth was observed at pH 3, while among the remaining treatments, the lowest biomass production occurred at pH 5 and the highest at pH 11.

Many studies have identified pH as a critical parameter to optimise when aiming to increase biomass yield [10]. Reported optimal pH values for *Chlorella* growth vary among strains, indicating that species within this genus can tolerate a wide range of pH conditions. Gaysina [11] demonstrated that *C. vulgaris* exhibits high resistance to both acidic and alkaline environments. During cultivation, it maintained its basic morphological characteristics across a pH range of 4–11.5. At pH 3.5, approximately 30% of the cells lost their green pigmentation, while more pronounced discolouration was observed at pH 2–3 and pH 12. In contrast, El-Sheekh *et al*. [12] evaluated the growth of *C. vulgaris* at pH values of 6, 7, 9, 11, and 12, reporting the highest optical density at pH 12. Similarly, Gong *et al*. [10] observed a

favourable response of *C. vulgaris* to alkaline conditions, identifying a pH range of 10–10.5 as optimal compared to pH values of 7, 8, and 9. According to Gaysina [11], it is also recognised that algal strains capable of tolerating extreme pH conditions have considerable potential for biotechnological applications.

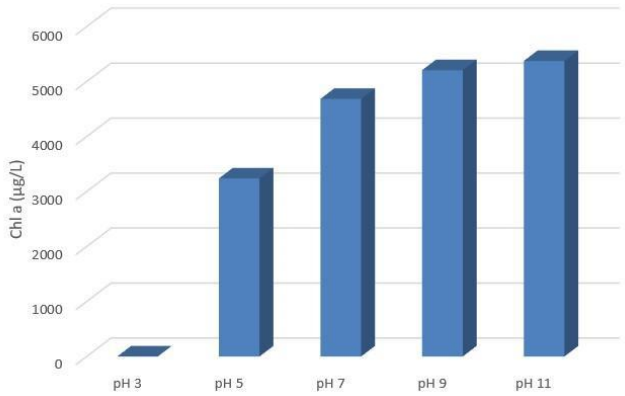

Figure 2 *Chlorophyll a content of Chlorella culture isolated from lampenflora after one month of cultivation*

CONCLUSION

Although *Chlorella* is one of the most extensively studied genera of microalgae, a considerable proportion of its species remain uncultured or insufficiently characterised. These unexplored or understudied strains may possess unique traits, such as tolerance to extreme environments or novel metabolic capabilities, with significant ecological and biotechnological potential. In this context, exploring extreme habitats, such as caves, is particularly valuable, as it can reveal previously unknown diversity and expand our understanding of the genus.

ACKNOWLEDGEMENT

The authors gratefully acknowledge the Ministry of Science, Technological Development and Innovation of the Republic of Serbia for financial support under Contract No. 451-03-33/2026-03/200178 and No. 451-03-33/2026-03/200010.

REFERENCES

[1] Khavari, F., Saidijam, M., Taheri, M., *et al.* Mol. Biol. Rep. 2021, 48(5), 4757–4765.
[2] Castro JC, Cobos M. Biochemical profiling, transcriptomic analysis, and biotechnological potential of native microalgae from the Peruvian Amazon. In: Ahmad, A., Banat, F., Taher, H., editors. Algal Biotechnology. Amsterdam: Elsevier; 2022. p. 305–321.
[3] Borowitzka MA. Biology of microalgae. In: Levine, I.A., Fleurence, J., editors. Microalgae in Health and Disease Prevention. London: Academic Press; 2018. p. 23–72.
[4] Ieviņa, B., Romagnoli, F. Environ. Clim. Technol. 2020, 24(2), 203–220.
[5] Guccione, A., Biondi, N., Sampietro, G., *et al.* Biotechnol. Biofuels. 2014, 7, 84.
[6] Nikolić, N., Subakov Simić, G., Golić, I., *et al.* Arch. Biol. Sci. 2021, 73(3), 341–351.
[7] Popović, S.S., Nikolić, N.V., Pećić, M.N., *et al.* Geoheritage. 2023, 15(1), 14.
[8] Rippka, R., Deruelles, J., Waterbury, J.B., *et al.* J. Gen. Microbiol. 1979, 111(1), 1–61.

[9] International Organization for Standardization. Water quality—measurement of biochemical parameters—spectrometric determination of the chlorophyll-a concentration. Geneva: ISO; 1992. p. 6.

[10] Gong, Q., Feng, Y., Kang, L., *et al.* In: Proceedings of the 6th International Conference on Applied Energy (ICAE2014); May 30–Jun 2, 2014; Taipei, Taiwan. 2014. p. 2012–2015.

[11] Gaysina, L.A. Plants. 2024, 13 (3), 357.

[12] El-Sheekh, M.M., El Sabagh, S., Abou-El-Souod, G., *et al.* Egypt. J. Exp. Biol. Bot. 2018, 14 (1), 121–131.

EcoTER'26
eco.tfbor.bg.ac.rs
32nd International Conference
Ecological Truth & Environmental Research
24–26 June 2026, Hotel Sunce,
Sokobanja, Serbia

Original Research

ASSESSMENT OF THE LENGTH–WEIGHT RELATIONSHIP AND RELATIVE CONDITION FACTOR OF SCADAR BLEAK IN THREE WESTERN BALKAN LAKES

DOI: 10.5937/EcoTER26546K

Nataša Kojadinović[1,a*], Simona Đuretanović[1,b] ,Milena Radenković[1,c] , Aleksandra Milošković[2,d], Tijana Veličković[1,3,e], Marija Jakovljević[1,f], Vladica Simić[1,g]

[1] University of Kragujevac, Faculty of Science, Department of Biology and Ecology, Radoja Domanovića 12, 34000 Kragujevac, SERBIA

[2] University of Kragujevac, Institute for Information Technologies Kragujevac, Jovana Cvijića bb, 34000 Kragujevac, SERBIA

[3] Department of Organisms and Ecosystems Research, National Institute of Biology, Večna pot 121, 1000 Ljubljana, SLOVENIA

[a] https://orcid.org/0000-0001-9847-3823 [b] https://orcid.org/0000-0003-4508-161X
[c] https://orcid.org/0000-0002-2052-4464 [d] https://orcid.org/0000-0003-2407-7099
[e] https://orcid.org/0000-0001-9152-056X [f] https://orcid.org/0000-0002-2168-7548
[g] https://orcid.org/0000-0001-6787-9783

Abstract

Length –weight relationship gives information on the condition and growth patterns of fish. This study presents the weight–length relationship and relative condition factor of Alburnus scoranza (Bonaparte, 1845) in Lake Ohrid, Lake Skadar, and the Vlasina Reservoir. The b value from the length–weight relationship indicates negative allometric growth, ranging from 2.572 to 2.660. The relative condition factor (Kn) varied from 0.656 to 1.792, indicating differences in the well-being of individuals across the studied populations. The results of this study will support fisheries researchers, environmentalists, and scientists in developing future monitoring and conservation strategies for this fish species.

Keywords: Scadar bleak, Allometric growth, Lake Ohrid, Lake Skadar, Vlasina Reservoir.

INTRODUCTION

Alburnus scoranza (Bonaparte, 1845) is one of the 20 species of bleaks recognized in European freshwater systems [1]. Contrary to the situation with *Alburnus alburnus* (Linnaeus, 1758) which has the widest distribution range, *A. scoranza* is endemic to the Southeaster Adriatic Ecoregion. According to Marić (1995) [2] the Scoranza bleak inhabits only Ohrid-Drim – Skadar system, but Simić et al. (2012) [3] confirmed the presence of this species in the Vlasina reservoir in southern Serbia. The occurrence of the *A. scoranza* population in the Vlasina reservoir represents an extension of this species' range from the Adriatic to the Black Sea basin.

* *natasa.kojadinovic@pmf.kg.ac.rs*

According to the IUCN, the Scadar bleak was classified as Least Concern (LC) in 2008. However, based on new analyses, its status was updated to Near Threatened (NT) in 2023. Over the last five decades, a statistically significant decline in the abundance of this species has been observed in Skadar Lake [4], but it is still very important for recreational and commercial fisheries. These data indicate the need for continuous monitoring of fish populations, especially those with small ranges and affected by multiple threats. Fish population studies are an essential element contributing to understanding the health of fish populations, which is also needed for sustainable management strategies [5].

The parameters length–weight ratio (LWR) and condition factor (CF) play a key role in biological studies of fish and fisheries [6]. These indices provide valuable insights into the growth patterns, general health, and well–being of fish populations, and can be used as indicators of environmental quality and anthropogenic impacts. Given the limited distribution and the recent decline in abundance of *A. scoranza*, it is essential to establish baseline data on these parameters for populations outside its core range.

The aim of the present study was to determine the size structure, length–weight ratio and relative condition factor of *A. scoranza* populations from Lake Sladar, Lake Ohrid and Vlasina Reservoir, thus providing the first data for this translocated population.

MATERIALS AND METHODS

Samples were collected from two natural lakes, Ohrid and Skadar, as well as from the artificial lake Vlasina. Lake Ohrid is oligotrophic, and of the 20 autochthonous fish species, 35% are endemic to the lake [7]. Lake Skadar is the largest lake on the Balkan Peninsula and, like Ohrid, also represents a biodiversity hotspot for many biotic groups. The Vlasina reservoir was formed on the upper reach of river Vlasina (belonging to the Danube basin), by flooding a large mountain peat bog [3]. Since its formation, it has been a place of active anthropogenic introduction of fish species with the purpose of increasing its fishing attractiveness. The geographical location (south Serbia) and ecological status (cold water oligotrophic accumulation) of the new reservoir probably contributed to the decision to perform the first and subsequent stockings with species from the teritory of Macedonia and Montenegro [8], namely the Ohrid–Drim–Skadar hydrosystem, belonging to the Adriatic basin.

The field research was conducted during the summer of 2014. Fishes were sampled using netting tools (gill nets with mesh size 0.5, 10–12 and 14–16 mm). In the laboratory sampled fish specimens were identified to species according to Kottelat and Freyhof (2007) [1] and Simonović (2001) [9], and measured to the nearest 1 mm (total length, L) with a sliding caliper, and weighed to the nearest 0.1 g (weight, W).

The length-weight relationship was calculated using the following Le Cren (1951) [10] equation:

$$W = a\,L^{b}$$

where W is the total weight (expressed in grams), L is the total length (expressed in centimetres), a is a coefficient related to body form and b is an exponent indicating isometric

growth when equal to 3. The parameters a and b were estimated by linear regression on the transformed equation:

$$log(W) = log(a) + b\ log(L)$$

The degree of correlation amoung the variables was evaluated using the determination coefficient r^2 [10]. If b = 3, growth is isometric, if b < 3, it is negative allometric and if b > 3, it is positive allometric [11,12].

RESULTS AND DISCUSSION

The length-weight relationships (LWR) are very useful tools in ecological studies. This parameter, associated with the condition factor, is considered an excellent indicator of animal welfare [13]. A total of 250 individuals from three distinct ecosystems were analyzed during the research (Table 1).

Table 1 *Descriptive statistics and estimated parameters of the length–weight relationship and condition factor for A. scoranza from the studied localities*

	N	TL range	W range	a	b	SE (b)	R^2	Kn
Ohrid	100	10.2–15.5	9.3–25.5	0.017	2.660	0.172	0.708	0.990
Skadar	100	12.1–16.1	17.5–33.9	0.035	2.617	0.132	0.769	0.656
Vlasina	50	11.9–14.3	11.1–20.2	0.011	2.572	0.230	0.759	1.792

The exponent of the length–weight relationship (*b*) indicates negative allometric growth in all three analyzed populations of *A. scoranza*, meaning that individuals grow faster in length than in weight. Our results are consistent with previously published studies conducted on this species in Lake Skadar and Lake Ohrid [14,15].

The highest *b* value was recorded in the population from Lake Ohrid (2.660), while the lowest value was observed in individuals from Lake Vlasina (2.572). Although the differences are relatively small, they may indicate certain environmental differences among the studied localities. The species *A. scoranza* was probably introduced into the Vlasina reservoir from Lake Ohrid in 1989, under the name used then, *A. albidus* (plašica), with the purpose of providing natural food for the Ohrid trout (*Salmo letnica*) introduced earlier. Simić et al. (2012) [3] based on the analysis of the units of roach captured during 2003 and 2011, confirmed the presence of the species *A. scoranca.* The presence of the *A. scoranza* population in the Vlasina reservoir in southern Serbia signifies an expansion of this species' range from the Adriatic to the Black Sea basin.

The most comprehensive analysis of the Scoranza bleaks in Skadar Lake was carried out by Marić in several studies [2,16,17]. His research also focuses on length-weight ratios and suggests that for the analysis age groups need to be analyzed separately because of different growth models. This is a very important recommendation that could be used in future research.

Body condition is a key indicator of health at the individual or population level since it is closely related to important fitness variables, such as growth, reproduction, behavior and survival [18] The highest mean condition factor (1.792) was recorded in the Vlasina

population, suggesting favorable environmental conditions and adequate food resources for this species in the reservoir ecosystem. In contrast, the lowest value was observed in Lake Skadar (0.656), while individuals from Lake Ohrid showed intermediate values (0.990). The condition factor value recorded for the Lake Ohrid population is in agreement with the findings of Trajchevski and Talevska (2020), who reported a similar value (0.95) for *A. scoranza* in Lake Ohrid. [19].

CONCLUSION

In conclusion, this study contributes to the knowledge of the biology and ecology of *A. scoranza* and provides baseline data useful for future conservation programs, fisheries management, and comparative studies of populations within and outside the species' native range.

ACKNOWLEDGEMENT

The research presented in this article is part of. Grant (Agreement No. 451-03-34/2026-03/ 200122 and 451-03-33/2026-03/200122) funded by the Serbian Ministry of Science, Technological Development and Innovation

REFERENCES

[1] Kottelat M, Freyhof J Handbook of European freshwater fishes. Berlin: Publications Kottelat, Cornol and Freyhof, 2007. p. 646.

[2] Marić, D. Biol. Conserv. 1995, 72, 187–194.

[3] Simić, V., Simić, S., Paunović, M. *et al*. Arch. Biol. Sci. 2012, 64(3), 981–990.

[4] Marić D, The Ichthyofauna of Lake Skadar/Shkodra: Diversity, Economic Significance, Condition, and Conservation Status. In: Pešić, V., Karaman, G. & Kostianoy, A. (Eds.) Lake Skadar/Shkodra Environment. The Handbook of Environmental Chemistry. 2018. p. 363–381.

[5] Froese, R., Branch, T., Proels, A. Fish. Fish. 2011, 12, 340–351.

[6] Oliviera, V., Loverde-Oliviera, S., Mateus, L. J. Appl. Ichthyol. 2014, 31(1), 225–227.

[7] Milošević, D., Talevski, T. Acta Zool. Bulg. 2016, 68(3), 391–394.

[8] Blaženčić J. Vlasinsko jezero – hidrobiološka studija. Beograd: Biološki fakultet; 1997. p. 244.

[9] Simonović P Uvod u ihtiologiju. Univerzitet u Beogradu, Biološki fakultet. Beograd (2010), p.316.

[10] Le Cren, E.D. J. Anim. Ecol. 1951, 20(2), 201–219.

[11] Ricker, W.E. Bull. - Fish. Res. Board Can. 1975, 191, 1–382.

[12] Froese, R. J. Appl. Ichthyol. 2006, 22, 241–253.

[13] Urbanski, B., Brambilla, E., Nogueira, M. Biota Neotr. 2023, 32(2).

[14] Milošević, D., Mrdak, D. J. Appl. Ichthyol. 2016, 32, 1331–1333.

[15] Milošević, D., Talevski, T. Acta zool. Bulg. 2016, 68(3), 391–399.

[16] Marić, D., Burzanović, K. Ecol. Mon. 2021, 40, 80–92.

[17] Burzanović, Marić D, In: 1st SouthEast European Ichtyological Conference; 27–29.09.; Sarajevo, Bosnia and Herzegovina. 2017.

[18] Gubiani, E., Rauro, R., Ribeiro, R., *et al*. Acta Limnol. Bras. 2020, 32.

[19] Trajchevski, B., Talevska, T. Acta Zool. Bulg. 2020, 185–188.

EcoTER'26
eco.tfbor.bg.ac.rs
32nd International Conference
Ecological Truth & Environmental Research
24–26 June 2026, Hotel Sunce,
Sokobanja, Serbia

Original Research

QUANTIFYING SAMPLING CONTRIBUTION TO MEASUREMENT UNCERTAINTY IN MICROBIOLOGICAL GROUNDWATER ANALYSIS

DOI: 10.5937/EcoTER26551O

Vesna Obradović[1,a], Marija Perović[1,b*], Tanja Vučković[1]

[1] Jaroslav Černi Water Institute, Jaroslava Černog 80, 11226 Belgrade, SERBIA

[a] https://orcid.org/0009-0008-2157-0615 [b] https://orcid.org/0000-0003-2045-001X

Abstract

Sampling is often an underestimated source of measurement uncertainty in microbiological water quality assessment. This study quantifies the contribution of groundwater sampling to overall measurement uncertainty using a balanced split-level design and statistical approaches recommended by ISO 29201 (Annex H) and EURACHEM (Annex D). Groundwater samples were collected during 2023–2024 across different seasons following the EN ISO 19458 sampling protocol. Ten duplicate samples were taken under reproducible field conditions by two operators at the same location within a short time interval. Each sample and its replica were analyzed in duplicate for aerobic mesophilic bacteria (CFU·mL^{-1}) using Standard Method 9215B. Data were processed using range statistics (split-level design), classical one-way ANOVA, and robust ANOVA (RANOVA) after logarithmic transformation. Results showed that the relative standard uncertainty of sampling (23.35–24.45%) was almost twice the analytical uncertainty (12.53%) and approached the total measurement uncertainty (26.50%). The expanded sampling uncertainty (k=2.95% confidence) reached 46.7%, demonstrating that sampling is a dominant contributor to uncertainty in microbiological groundwater assessment. Although EN ISO 19458 showed acceptable performance (RSD < 30%), the results reveal that sampling uncertainty is frequently underestimated and should be routinely included in ISO/IEC 17025 uncertainty evaluations for microbiological groundwater analysis.

Keywords: groundwater sampling, measurement uncertainty, microbiological analysis, sampling uncertainty.

INTRODUCTION

A reliable evaluation of microbiological groundwater quality depends not only on laboratory analysis but also on the representativeness of the collected sample. Microbiological assessment of groundwater quality relies on the assumption that collected samples accurately represent *in situ* conditions. While laboratories routinely evaluate analytical uncertainty in accordance with ISO/IEC 17025, [1] the uncertainty introduced during sampling is rarely quantified in practice, despite clear requirements in ISO 29201 to address it [2].

Variability associated with groundwater sampling may arise from field conditions, operator influence, seasonal changes, and the applied sampling technique. Although EN ISO 19458 [3] provides detailed procedural guidance for microbiological water sampling, its performance is

* *marija.perovic@jcerni.rs*

typically assumed rather than experimentally verified through estimation of sampling uncertainty under real field conditions.

The present study addresses this gap by experimentally evaluating the contribution of groundwater sampling to overall measurement uncertainty using a balanced split-level design and statistical approaches recommended by ISO 29201 and EURACHEM guidelines [2,4].

MATERIALS AND METHODS

Study design

A balanced split-level (duplicate) design recommended by ISO 29201 (Annex H) and EURACHEM guidelines was applied in this study [2,4]. Ten independent duplicate samples were collected by two operators at the same sampling location, within a short time interval and under identical field conditions. Each sample and its replica were transported to the laboratory and analyzed independently. The structure of this experimental design is presented in Figure 1.

In this approach, two independent field samples (A and B) were collected at the same location. Each sample was subsequently analyzed in duplicate in the laboratory (A1, A2 and B1, B2), enabling separation of analytical and sampling variability through statistical evaluation.

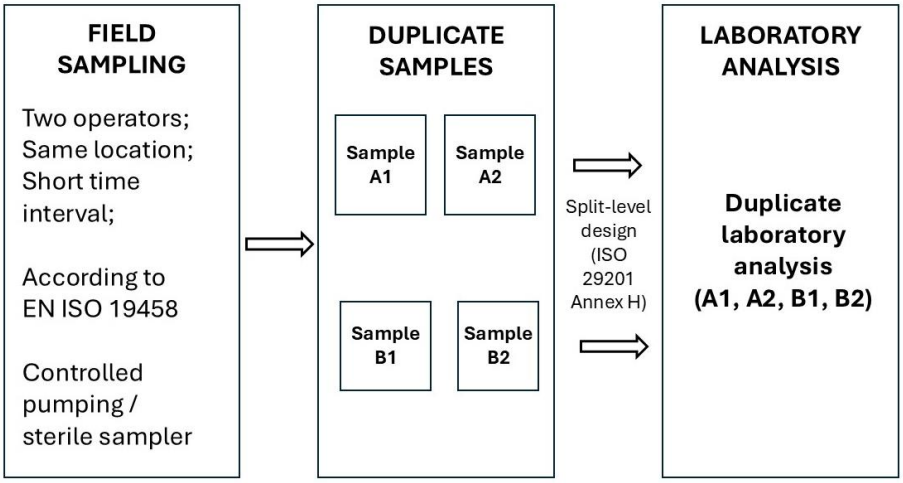

Figure 1 *Balanced split-level design for estimation of sampling and analytical uncertainty according to ISO 29201 Annex H*

Sampling procedure

Groundwater sampling was conducted in accordance with EN ISO 19458 [3]. Sterile 500 mL glass sampling bottles were used and protected from contamination until sampling. Depending on well conditions, sampling was performed either after controlled pumping through an installed outlet or using a sterile metal sampler for wells without permanent pumping systems. Extended pumping was applied when the objective was to characterize groundwater quality, ensuring stabilization of temperature and conductivity prior to sampling. Samples were transported to the laboratory in portable coolers for immediate analysis.

Microbiological analysis

Microbiological testing was performed using Standard Method 9215B for the determination of aerobic mesophilic bacteria (CFU·mL^{-1}) [5]. Each sample and its replica were analyzed in duplicate. Serial dilutions were prepared in phosphate dilution water and inoculated onto nutrient agar plates. Quality control of the method was ensured using reference strains (A. viridans ATCC 11563, B. spizizenii ATCC 6633, E. faecalis ATCC 29212, E. coli ATCC 25922, S. aureus ATCC 25923). Incubation was carried out under controlled conditions at 35 ± 0.5°C.

Verification approach for sampling uncertainty

Sampling uncertainty was verified using statistical approaches recommended by ISO 29201 Annex H and EURACHEM guidelines [2,4]. Data from duplicate sampling and duplicate laboratory analyses were processed after logarithmic transformation assuming lognormal distribution of microbiological counts.

Evaluation was performed using:

- range statistics within the split-level design,
- one-way ANOVA,
- robust ANOVA (RANOVA) using the Royal Society of Chemistry statistical tool [6].

Sampling standard deviation was derived using the split-level range statistics approach according to ISO 29201 Annex H [2] (Eq. 1):

$$S_{sampl}^2 = S_{meas}^2 - \left(\frac{S_{anal}}{\sqrt{2}}\right)^2 \quad (1)$$

Relative standard uncertainties (RSD, %) were calculated for analytical, sampling, and total measurement components. Expanded uncertainty was determined using a coverage factor k=2, corresponding to a 95% confidence level.

Control range charts (R-charts) were constructed during validation and internal quality control to monitor variability between duplicate results and to confirm the stability of the sampling process throughout the study, in accordance with ISO/IEC 17025 requirements [1]. Quality control included duplicate analyses performed under identical incubation conditions, using the same equipment and consumables to ensure reproducibility. R-charts were used to monitor variability between duplicate results in accordance with laboratory quality procedures and ISO/IEC 17025 requirements [1].

RESULTS AND DISCUSSION

The statistical evaluation of duplicate groundwater samples and their laboratory replicates enabled the separation of analytical, sampling, and total measurement uncertainty in microbiological analysis. Data were processed after logarithmic transformation using range statistics (split-level design), one-way ANOVA, and robust ANOVA (RANOVA), in accordance with ISO 29201 (Annex H) and EURACHEM recommendations [2,4].

The obtained relative standard uncertainties (RSD) showed clear differences between the analytical and sampling components, as summarized in Table 1. The relative analytical uncertainty was 12.53%, while the relative sampling uncertainty ranged between 23.35% and

24.45%, depending on the statistical approach applied. The relative standard uncertainty of the overall measurement was 26.50%.

These results demonstrate that the variability introduced during sampling is almost twice as large as the variability originating from laboratory analysis. Moreover, the sampling uncertainty approaches the total measurement uncertainty, indicating that sampling represents a dominant contributor to the variability of microbiological groundwater results.

The expanded sampling uncertainty (k=2.95% confidence level) reached 46.7%, as presented in Table 1, confirming that nearly half of the uncertainty associated with microbiological groundwater results originates from the sampling stage. This finding is particularly important in the context of ISO/IEC 17025 uncertainty evaluation, where laboratories often focus primarily on analytical sources of variability [1].

Comparison of classical ANOVA, robust ANOVA, and range statistics showed consistent results, confirming the reliability of the applied statistical model and the suitability of the balanced split-level design for evaluating sampling uncertainty under real field conditions [2,4,6]. The agreement between statistical approaches also validates the applicability of ISO 29201 Annex H for microbiological groundwater sampling [2].

The results further confirm that the application of the EN ISO 19458 sampling protocol under controlled conditions provides acceptable performance (RSD < 30%), in accordance with EURACHEM and NORDTEST recommendations for sampling quality [3,4,7]. However, despite proper adherence to the sampling standard, significant variability remains inherent to the sampling process due to field conditions, operator influence, and groundwater heterogeneity. These findings highlight that sampling cannot be considered a negligible step in microbiological groundwater assessment. Instead, it must be recognized as a major source of variability that should be experimentally quantified and routinely included in uncertainty evaluation [1,2].

Table 1 *Relative standard uncertainties of analytical, sampling and total measurement components in microbiological groundwater analysis*

Component	RSD (%)
Analytical uncertainty (Uanal)	12.53
Sampling uncertainty (Usampl)	23.35–24.45
Measurement uncertainty (Umeas)	26.50
Expanded sampling uncertainty (k=2)	46.7

CONCLUSION

This study demonstrates that sampling is a major contributor to overall uncertainty in microbiological groundwater analysis and cannot be treated as a minor or secondary step in the assessment process. By applying a balanced split-level design recommended by ISO 29201 Annex H, it was possible to experimentally separate analytical and sampling components of variability under real field conditions.

The results showed that sampling uncertainty was nearly twice as large as analytical uncertainty and approached the total measurement uncertainty, confirming that a significant

part of the variability in microbiological groundwater results originates from the sampling stage rather than from laboratory procedures.

Although the EN ISO 19458 protocol provided acceptable performance (RSD < 30%), the findings indicate that inherent field variability remains substantial even when the sampling procedure is properly implemented. These results emphasize the need to recognize sampling as a dominant source of uncertainty and to include experimentally determined sampling uncertainty in routine ISO/IEC 17025 uncertainty evaluations for microbiological groundwater analysis.

REFERENCES

[1] ISO/IEC 17025:2017. General requirements for the competence of testing and calibration laboratories. Geneva: ISO; 2017.

[2] ISO. (2012). *ISO 29201:2012 – Water quality — The variability of test results and the uncertainty of measurement of microbiological enumeration methods*. International Organization for Standardization.

[3] ISO. (2006). *EN ISO 19458:2006 – Water quality — Sampling for microbiological analysis*. International Organization for Standardization.

[4] Eurachem/CITAC. Accreditation for Microbiological Laboratories, Annex D. 3rd ed. Eurachem; 2023.

[5] APHA, AWWA, WEF. Standard Methods for the Examination of Water and Wastewater. 23rd ed. Washington DC: APHA; 2017. Method 9215B.

[6] Royal Society of Chemistry. Robust ANOVA calculator. 2024. Available from: https://www.rsc.org

[7] Nordtest. Handbook for Calculation of Measurement Uncertainty in Environmental Laboratories. NT TECHN REPORT 604. Espoo: Nordtest; 2007.

EcoTER'26
eco.tfbor.bg.ac.rs
32nd International Conference
Ecological Truth & Environmental Research
24–26 June 2026, Hotel Sunce,
Sokobanja, Serbia

Original Research

MEASUREMENT UNCERTAINTY OF WASTEWATER SAMPLING FOR MICROBIOLOGICAL ANALYSIS USING DUPLICATE SAMPLING AND ANOVA APPROACH

DOI: 10.5937/EcoTER26556O

Vesna Obradović[1,a], Marija Perović[1,b*], Jelena Lekić[1]

[1] Jaroslav Černi Water Institute, Jaroslava Černog 80, 11226 Belgrade, SERBIA

[a] https://orcid.org/0009-0008-2157-0615 [b] https://orcid.org/0000-0003-2045-001X

Abstract

Microbiological analysis of wastewater is strongly affected by sampling variability due to the heterogeneous distribution of microorganisms, turbulence, particulate association, and rapid biological changes within the matrix. For accredited laboratories operating under ISO/IEC 17025, it is therefore essential to quantify the contribution of sampling to overall measurement uncertainty. This study presents an ISO-compliant evaluation of wastewater sampling uncertainty for microbiological analysis based on duplicate sampling design, ANOVA statistics, and the component approach recommended by ISO 29201 Annex H. Sampling was conducted according to EN ISO 19458 using sterile techniques, with duplicate samples collected by two operators under identical conditions across different seasons (2021–2025). Each sample was analyzed in duplicate for fecal coliform bacteria using the MPN method. Measurement uncertainty components were estimated using range statistics, one-way ANOVA, and robust ANOVA approaches. The results showed relative standard uncertainties of 14.02% for analysis, 12.44–13.27% for sampling, and 15.30% for overall measurement, yielding an expanded sampling uncertainty of 26.54% (k = 2). These values are significantly lower than typical literature values for wastewater microbiology, demonstrating that strict implementation of standardized sampling protocols can effectively control variability. The presented approach provides a practical framework for ISO-compliant estimation of sampling uncertainty in microbiological wastewater monitoring.

Keywords: wastewater sampling, measurement uncertainty, microbiological analysis, ISO 19458, ANOVA.

INTRODUCTION

Microbiological examination of wastewater represents one of the most demanding tasks in water-quality monitoring due to the pronounced spatial and temporal variability of microorganisms within the wastewater matrix. Unlike physicochemical parameters, microbiological indicators are influenced by biological variability, uneven distribution, and frequent association with suspended particles. In addition, enumeration methods used for microbiological analysis are governed by counting statistics that are well described by Poisson distribution, where variability is inherent to the number of counted colonies rather than solely to analytical precision. These characteristics make the separation and

* *marija.perovic@jcerni.rs*

quantification of individual uncertainty components particularly challenging. For this reason, uncertainty estimation in microbiology typically relies on a top–down statistical approach based on repeated measurements of the same method rather than on individual component evaluation.

According to ISO/IEC 17025, accredited laboratories are required to evaluate and report measurement uncertainty, including the contribution arising from sampling. Standards such as EN ISO 19458 and ISO 29201 emphasize that, in microbiological analyses, the variability introduced during sampling may be comparable to or even greater than that introduced during laboratory analysis [1,2]. This is particularly relevant for wastewater, where matrix heterogeneity strongly affects the representativeness of the collected sample.

Wastewater represents a particularly complex matrix for microbiological analysis because microorganisms are unevenly distributed, frequently attached to suspended solids, and strongly influenced by hydraulic turbulence, flow variability, and environmental conditions within the sewer system. Additional variability arises from potential bacterial growth or die-off during transport and storage, as well as from differences in sampling technique, equipment cleanliness, sample handling, and operator experience. The type of sample collected (grab versus composite), the sampling location, and the degree of mixing at the sampling point further contribute to variability.

As a result, wastewater sampling introduces significantly greater uncertainty than sampling of groundwater or drinking water [3], and its contribution to overall measurement uncertainty cannot be neglected. The total measurement uncertainty can therefore be expressed as the combination of sampling and analytical components (Eq. 1):

$$u^2_{measurement} = u^2_{sampling} + u^2_{analytical} \quad (1)$$

where the variance introduced by sampling and the variance associated with laboratory analysis jointly determine the combined uncertainty of the reported result [4].

MATERIALS AND METHODS

Wastewater sampling for microbiological analysis was performed in accordance with EN ISO 19458 guidelines for microbiological water sampling [5], ensuring representativeness and prevention of secondary contamination. Samples were collected from municipal wastewater characterized by natural microbial contamination, without artificial spiking or pre-treatment.

Sterile 500 mL borosilicate glass bottles with leak-proof caps were used for sample collection. Prior to sampling, bottles were stored and handled under aseptic conditions. Grab samples were collected at a depth of 20–30 cm below the water surface using sterile samplers to avoid surface films and bottom sediments, which could bias bacterial counts. Care was taken to prevent disturbance of the surrounding matrix during sampling.

Immediately after collection, samples were placed in insulated containers with ice packs and transported to the accredited laboratory under controlled temperature conditions of (5 ± 3) °C. The time between sampling and analysis did not exceed the holding times prescribed by EN ISO 19458, thereby minimizing potential microbial growth or die-off during transport.

Sampling campaigns were conducted during different seasons between 2021 and 2025 in order to capture variability associated with temperature fluctuations, hydraulic load, and changes in wastewater composition.

Duplicate design and analytical procedure

A balanced duplicate (split-level) design was employed to quantify sampling and analytical variability separately. For each sampling event, two independent field samples were collected at the same location, under identical environmental and operational conditions, and within a short time interval of each sampling event. Duplicate sampling was performed by two trained operators to incorporate realistic field variability.

Each primary sample and its field duplicate were subsequently analyzed twice in the laboratory, resulting in full duplication at both the sampling and analytical levels. This hierarchical structure allows decomposition of total variability into:

- between-sample (sampling) variance, and
- within sample (analytical) variance.

At least ten complete duplicate sample sets were processed during the study period.

Microbiological analysis was performed using the Most Probable Number (MPN) method for fecal coliform bacteria according to internal procedure DMJČ008, based on the Colilert method. The method relies on defined substrate technology and selective enzymatic detection, with incubation under controlled conditions according to manufacturer and standard requirements. Quality control measures included reagent blanks, positive controls, and incubation temperature verification.

The balanced duplicate design applied in this study follows recommendations provided in ISO 29201 Annex H for estimation of measurement uncertainty in microbiological enumeration methods.

Statistical evaluation and uncertainty estimation

Measurement uncertainty was evaluated using range-based statistics derived from the duplicate design, supported by classical one-way ANOVA and robust ANOVA (RANOVA) approaches in accordance with ISO 29201 and EURACHEM/CITAC guidance [4].

Given that microbiological count data typically follows log-normal distribution, results were logarithmically transformed prior to statistical treatment. This transformation stabilizes variance and improves conformity with ANOVA assumptions. Calculations were performed using spreadsheet tools and the Royal Society of Chemistry uncertainty calculator.

The combined standard uncertainty was calculated as (Eq. 2):

$$u = \sqrt{u_a^2 + u_b^2} \tag{2}$$

and the expanded uncertainty at a 95% confidence level was obtained as (Eq. 3):

$$U = 2u \tag{3}$$

Sampling uncertainty was derived from the relationship between total measurement uncertainty and analytical uncertainty (Eq. 4):

$$S_{sampling} = \sqrt{S^2_{measurement} - \left(\frac{S_{analysis}}{\sqrt{2}}\right)^2} \quad (4)$$

RESULTS AND DISCUSSION

Application of ISO 29201 range statistics to the duplicate sampling data yielded a relative sampling uncertainty of 12.4% and a relative measurement uncertainty of 10.9%, with a relative standard deviation (RSD) of 11.78%. These results confirm the consistency and reproducibility of the balanced duplicate sampling design (Table 1).

To verify these findings, the same dataset was further evaluated using one-way ANOVA and robust ANOVA (RANOVA) approaches in accordance with EURACHEM guidance. The estimated relative standard uncertainties obtained by ANOVA indicated analytical variability of 14.02%, sampling variability in the range of 12.44–13.27%, and an overall measurement uncertainty of 15.30%. The calculated expanded sampling uncertainty was 26.54% (k = 2).

Although derived from different statistical approaches, both methods produced highly consistent estimates of sampling variability, confirming the reliability of the applied ISO 29201 duplicate design for uncertainty evaluation.

The obtained values are lower than those typically reported for microbiological analysis of wastewater, where substantial variability is commonly observed due to matrix heterogeneity and sampling conditions.

These results demonstrate that strict adherence to EN ISO 19458 sampling procedures, combined with a controlled duplicate sampling design, can substantially reduce variability introduced during sampling. Despite the inherent heterogeneity of wastewater, the applied protocol ensured reproducible sampling conditions, confirming that sampling uncertainty can be effectively managed. Under such controlled conditions, analytical variability remains the dominant contributor to the combined measurement uncertainty.

Table 1 *Comparison of uncertainty components obtained by ISO range statistics and ANOVA approaches*

Component	ISO 29201 Range Statistics (%)	ANOVA / RANOVA (%)
Analytical uncertainty	8.6	14.02
Sampling uncertainty	12.4	12.44–13.27
Measurement uncertainty	10.9	15.30
Expanded sampling uncertainty (k=2)	—	26.54
Relative standard deviation (RSD)	11.78	—

CONCLUSION

The results of this study confirm that the contribution of sampling to the overall measurement uncertainty in microbiological wastewater analysis can be quantitatively evaluated using ISO-recommended approaches based on duplicate sampling design and ANOVA statistics. The obtained sampling uncertainty, approximately 13%, was found to be comparable to the analytical uncertainty, demonstrating that sampling represents a significant and measurable component of total uncertainty that cannot be neglected.

The application of EN ISO 19458 procedures, together with strict control of sampling techniques, transport, and handling conditions, proved effective in reducing variability typically associated with wastewater matrices. Despite the inherent heterogeneity of wastewater, the implemented protocol enabled reproducible sampling conditions and reliable estimation of uncertainty components. These findings emphasize the importance of incorporating sampling uncertainty into laboratory quality management systems and accreditation frameworks, particularly in compliance with ISO/IEC 17025 requirements. A structured evaluation of sampling variability enhances the reliability of microbiological monitoring data and supports more robust decision-making in wastewater management and regulatory reporting.

REFERENCES

[1] International Organization for Standardization. ISO 29201:2017 Water quality—The variability of test results and the uncertainty of measurement of microbiological enumeration methods. Geneva: ISO; 2017.

[2] European Committee for Standardization. EN ISO 13843:2017 Water quality—Requirements for establishing performance characteristics of quantitative microbiological methods. Brussels: CEN; 2017.

[3] International Organization for Standardization. ISO/IEC 17025:2017 General requirements for the competence of testing and calibration laboratories. Geneva: ISO; 2017.

[4] Eurachem/CITAC. Guide: Accreditation for Microbiological Laboratories, Annex D. Teddington: Eurachem; 2023.

[5] International Organization for Standardization. EN ISO 19458:2006 Water quality—Sampling for microbiological analysis. Geneva: ISO; 2006.

EcoTER'26
eco.tfbor.bg.ac.rs
32nd International Conference
Ecological Truth & Environmental Research
24–26 June 2026, Hotel Sunce,
Sokobanja, Serbia

Review

PREPARATION AND APPLICATION OF MODIFIED ZEOLITE FROM INDUSTRIAL WASTE

DOI: 10.5937/EcoTER26561N

Maja Nujkić[1,a*], Žaklina Tasić[1,b], Tanja Kalinović[1,c], Dragana Medić[1,d], Ana Radojević[1,e], Jelena Kalinović[1,f], Jelena Jordanović[1,g], Stefan Đorđievski[2,h], Nataša Apostolov[1]

[1] University of Belgrade, Technical Faculty in Bor, Vojske Jugoslavije 12, 19210 Bor, SERBIA

[2] Mining and Metallurgy Institute Bor, Alberta Ajnštajna 1, 19210 Bor, SERBIA

[a] https://orcid.org/0000-0002-6110-5135 [b] https://orcid.org/0000-0001-6544-1980

[c] https://orcid.org/0000-0003-0161-0065 [d] https://orcid.org/0000-0001-9980-5949

[e] https://orcid.org/0000-0003-3138-154X [f] https://orcid.org/0000-0003-0088-2683

[g] https://orcid.org/0000-0002-8145-640X [h] https://orcid.org/0000-0003-1737-8766

Abstract

Organic compounds, heavy metals and other pollutants reach the soil, groundwater and surface water, then enter the human body through the food chain, representing a significant environmental and health problem. To develop sustainable and efficient methods for pollutant removal, increasing attention is being paid to the application of zeolites synthesised from industrial waste. Various industrial solid wastes are rich in silicates, crystalline and amorphous silicon, as well as aluminium, making them suitable raw materials for zeolite synthesis. Among the most commonly used waste materials are fly ash from coal, red mud, lithium and steel slag, coal tailings and other by-products of the metallurgical industry. This paper presents an overview of previous researches on the synthesis of zeolites from different types of industrial waste, with particular focus on the advantages and limitations of existing preparation procedures. The application of synthesised zeolites in gas purification, wastewater treatment and soil remediation is also analysed. The results of previous researches indicate the significant potential of these materials in environmental protection and the circular economy.

Keywords: zeolites, industrial solid waste, synthesis methods, environmental protection.

INTRODUCTION

Zeolites are porous, crystalline aluminosilicate materials with a three-dimensional skeletal structure. They occur naturally as a result of volcanic activity (natural zeolites) or are synthesised under controlled laboratory conditions (synthetic zeolites). Their structure is based on the spatial arrangement of TO_4 tetrahedra, where T represents atoms in tetrahedral coordination, most commonly silicon (Si) and aluminium (Al), but also other heteroatoms. The connection of these tetrahedra forms a three-dimensional network of channels and cavities, resulting in significant structural diversity among zeolites. The general structural

* *mnujkic@tfbor.bg.ac.rs*

formula of zeolite is $M_{x/n}[(AlO_2)_x(SiO_2)_y]\cdot\omega H_2O$, where M denotes compensating cations outside the aluminosilicate skeleton, n their valence, and x and y the numbers of aluminium and silicon tetrahedra in the structure. The parameter ω indicates the number of water molecules present in the pores of the crystal lattice [1]. Due to their large specific surface area, developed microporous structure, and ion exchange capacity, zeolites are widely used in various fields, including catalysis, adsorption, gas and liquid separation, filtration, and energy storage [2]. However, compared to synthetic zeolites, natural zeolites often show lower performance due to the complex conditions of their formation, variable chemical composition, and the presence of various impurities. These factors may limit their application in demanding industrial processes. Industrial solid wastes are often rich in silicates, as well as crystalline and amorphous silicon, and may contain various types of slag, including slag from the production of yellow phosphorus, iron and steel, and slag from the smelting of non-ferrous metals. The presence of silicon and aluminum in these materials makes them suitable raw materials for the synthesis of zeolite-type molecular sieves [3].

Current research shows recent scientific results about using of various types of industrial solid waste, such as coal fly ash, red mud, lithium slag, coal tailings, and steel slag, as low-cost alternative raw materials for synthesizing artificial zeolites [2]. This work summarizes and analyzes the advantages and disadvantages of different zeolite preparation methods, based on a literature review. It also presents the applications of various modified zeolites in gas purification, wastewater treatment, and soil remediation.

SYNTHESIS METHODS OF ZEOLITES

The zeolite crystallization process involves the dispersion, recombination, and polymerization of silicate and aluminate species. Industrial solid wastes are complex, heterogeneous systems containing a significant proportion of inert components, which affect the kinetics and mechanism of zeolite formation from these raw materials. Zeolite synthesis from solid waste typically proceeds through four consecutive stages [3].

In the first phase, chemical pretreatment of the raw material is performed, most often using an HCl solution, to remove impurities such as Fe_2O_3 and CaO. This step increases the reactivity of the precursor and homogenizes the system. The second phase involves alkaline decomposition or alkaline fusion, during which amorphous silicon and aluminium phases dissolve. Stable crystalline components, such as corundum, have significantly lower solubility. The presence of OH^- ions in alkaline solutions or melts is crucial for increasing the solubility of Si and Al species. In this phase, the aluminosilicate structure breaks down, and Si–O and Al–O tetrahedra dissociate and form in the alkaline medium.

The third phase involves restructuring the aluminosilicate gel, during which the TO_4 tetrahedra are reorganized to form short-range structures. When the concentration of these structural units reaches a critical value, nucleation and the formation of ordered nanocrystalline cores occur. This process initiates further polymerization and recombination of tetrahedra on the surface of the cores.

In the final stage, crystal growth occurs as TO_4 tetrahedra are incorporated onto the surface of the cores according to specific crystallographic rules. Continuous growth leads to the formation of a stable zeolite structure with defined porosity and morphology [4–6].

Conventional hydrothermal method

The conventional one-step hydrothermal method enables the direct conversion of pretreated raw materials into zeolites. First, the materials are dissolved in an alkaline solution (NaOH or KOH), which dissolves silicates and aluminates. Then, by mixing and controlled aging of the solution – with the possible addition of silicon and aluminium sources to adjust the molar ratio – a silicoaluminate gel forms. The gel is subjected to hydrothermal crystallization, typically at temperatures of 80–200 °C for 12–48 hours, resulting in zeolite crystals. The final product is obtained after drying or calcination [4].

In the study by Constantin *et al*. [7], zeolite was synthesized from fly ash using combined alkaline and hydrothermal methods. The resulting material had an adsorption capacity of approximately 17 mg/g for Cd^{2+} ions, with the adsorption process reaching equilibrium quickly and following the Langmuir model. The adsorbent could be reused for multiple cycles without significant loss of efficiency. These results indicate that hydrothermally synthesized zeolites from fly ash provide a sustainable and effective solution for removing heavy metals from aquatic environments.

Alkaline fusion hydrothermal method

A key aspect of the alkaline fusion method is the calcination of the raw material with a solid alkaline compound at high temperature. During this process, resistant components of crystalline aluminosilicates, such as mullite and quartz in the raw material, are activated and decomposed. This stage produces a reactive precursor for the subsequent synthesis steps. After cooling the calcined material, deionized water is added, and the mixture is stirred at room temperature to form an intermediate gel, rich in silicon and aluminum. The gel is crucial because it ensures proper distribution of the active components and forms the foundation for crystallization. The final zeolite is produced by hydrothermal crystallization, in which the gel is subjected to controlled temperature and environmental conditions, resulting in the formation of the desired crystal structure and porous material. This method combines efficient activation of raw materials with precise control of crystallization, enabling the production of zeolites with high purity and well-defined properties [8].

Buzukashvili *et al*. [9] synthesized zeolite from fly ash using a combination of fusion and hydrothermal methods, producing a material with strong adsorption properties for removing heavy metals from aqueous solutions. The maximum adsorption capacities were 495 mg/g for Pb^{2+}, 248 mg/g for Cu^{2+}, 177 mg/g for Zn^{2+}, and 130 mg/g for Ni^{2+} ions. The adsorption process followed the Langmuir isotherm model and pseudo-second-order kinetics. The developed magnetic zeolite also enables easy extraction of the adsorbent from the solution after treatment, further increasing its practical significance in water purification processes.

Ultrasonic assistance in the hydrothermal synthesis of zeolites

Ultrasonic assistance is an effective method for synthesizing zeolites from raw materials containing inert substances. First, the raw materials are mixed with an alkaline solution, and the mixture undergoes ultrasonic treatment. Ultrasonic waves deliver high energy to

molecules through cavitation and mechanical effects, increasing molecular movement, accelerating chemical reactions, and facilitating the dissolution of silico-alumina oxides from solid waste. Microbubbles generated by ultrasound further promote the formation of zeolite crystals. After ultrasonic treatment, zeolites are produced by hydrothermal crystallization [2]. In recent years, significant progress has been made in this area.

For example, applying ultrasound in the synthesis of zeolite RHO reduced the crystallization time from 7–8 days with the conventional method to about 2 days with ultrasound, while maintaining high crystallinity and characteristic crystal morphology. This demonstrates ultrasound's ability to accelerate nucleation and growth of the crystalline phase [10].

In another case, ultrasound-pretreated hydrothermal synthesis of zeolite CHA enabled the transformation of zeolite T into a less dense CHA phase without the need for an organic template or seeds, and with improved CO_2 adsorption capacity. This highlights the use of ultrasound in manipulating interfacial conversions and enhancing product properties [11].

These examples show that ultrasonic assistance not only accelerates crystallization kinetics and shortens synthesis time, but also improves control over the morphology and properties of zeolite materials. This creates opportunities for broader application of this method in industrial processes such as catalysis, adsorption, and separation, especially when using raw materials with a high content of inert substances.

Microwave- assisted synthesis method

The microwave-assisted synthesis method is among the most advanced techniques for accelerating the hydrothermal crystallization of zeolites, due to the direct interaction of microwave radiation with the reaction mixture. Over the past decade, this method has attracted considerable attention because it can drastically reduce synthesis time, improve control over nucleation and crystal growth, and produce materials with enhanced functional properties. Compared to conventional hydrothermal procedures, microwave heating enables rapid and uniform attainment of the target temperature throughout the entire system, which intensifies crystallization kinetics.

Recent research further confirms the potential of this method for valorizing industrial waste. For example, Zang *et al*. [12] work reported the microwave-assisted synthesis of Na-P1-type zeolites and sodalite from fly ash, with the resulting materials demonstrating high efficiency in removing Pb^{2+} and Cd^{2+} ions from aqueous solutions (adsorption capacities exceeding 100 mg/g, depending on synthesis conditions). Under optimized conditions, zeolite with high crystallinity (~51.7%) and significantly increased ion exchange capacity (CEC ≈ 2.58 meq/g) was obtained, which is more than 100 times higher than that of the starting ash. This approach not only supports the development of efficient adsorbents but also enables sustainable waste management by converting waste into high-value-added materials.

Table 1 presents representative results for the adsorption of various pollutants using zeolites derived from different waste raw materials, with particular reference to adsorption capacity, selectivity, and stability during cyclic use.

Table 1 *Representative results of pollutant adsorption by solid waste-based zeolites*

Type of pollutant	Synthetic material	Name of zeolite	Adsorption capacity/ Removal efficiency	Synthesis method	Ref.
Toluen	Coal fly ash	Plasma-modified iron-enriched zeolite	98%	Ultrasonic-assisted, double stage fusion-hydrothermal synthesis	[13]
CO_2	Waste coal fly ash	Na-Ca^{2+}	0.4–0.8 mmol/g	Hydrothermal treatment	[14]
Benzen	Fly ash, natural clinoptilolite (ZN-C) and diatomite	Na-P1	1.40 µmol/g	Alkali hydrothermal method	[15]
Toluen			10.52 µmol/g		
o-ksilen			26.22 µmol/g		
m-ksilen			25.96 µmol/g		
Benzen	Fly ash, natural clinoptilolite (ZN-C) and diatomite	Na-X	383.67 µmol/g	Alkali hydrothermal method	[15]
Toluen			525.03 µmol/g		
o-ksilen			545.26 µmol/g		
m-ksilen			563.82 µmol/g		
NH_3	Waste fly ash, with vermiculite and unburned coal	NaX–Ver	38.46 mg/g	Hydrothermal syntheses	[16]
		NaX–FA	40.00 mg/g		
		NaX–C	21.05 mg/g		
Hg^o	Fly ash, red mud and steel slag	M-8FA2SS	99%	Supercritical hydrothermal synthesis	[17]
		M-4FA4RM2SS	97%		
		M-8RM2SS	92%		
Ni	Hard kaolin and industrial solid waste red mud	MZA	80.71 mg/g	Ultrafast Joule Heating (UJH) combined with Hydrothermal method	[18]
Co			82.73 mg/g		
Mn			85.91 mg/g		
Cu			207.20 mg/g		

APPLICATION OF ZEOLITE FOR GAS PURIFICATION

The purification of volatile organic compounds (VOC_s) is among the most important and dynamic areas of zeolite application, especially given increasingly strict environmental regulations and the need to decarbonize industrial processes.

To address this persistent problem, metal-modified zeolite catalysts have demonstrated exceptional performance due to their high specific surface area, well-developed microporosity, adjustable acidity, and pronounced thermal and chemical stability. These properties enable efficient use in both adsorption and catalytic decomposition of VOC_s, making them key materials in modern emission control technologies.

The removal of VOCs using zeolite catalysts relies primarily on a combination of adsorption and catalytic oxidation processes. The classical mechanism involves three main steps: (*i*) adsorption of VOC molecules on acidic active sites of the zeolite, (*ii*) activation of molecular oxygen on metal centers (such as Pt, Pd, Cu, or Mn), and (*iii*) oxidation of adsorbed organic molecules to end products, mainly CO_2 and H_2O. This synergistic effect between the zeolite support and the active metal phase is essential for achieving high conversion at relatively low temperatures.

A significant trend is the increasing use of zeolites synthesized from solid waste for VOC purification, supporting the principles of the circular economy. These materials not only reduce production costs but also help address waste management challenges [19].

APPLICATION OF ZEOLITE IN WASTEWATER TREATMENT

Water pollution by heavy metals is a serious environmental problem that requires efficient and sustainable solutions. Zeolites have emerged as highly effective adsorbents (Table 1), primarily due to their well-developed porous structure, high ion exchange capacity, and strong electrostatic interactions, which are the main mechanisms for metal ion binding.

Recent research has focused on zeolites synthesized from municipal waste ash under low pH conditions. After appropriate chemical or thermal modification, these materials can exhibit improved stability in acidic media and increased selectivity for certain metal ions. For example, one study found that zeolites produced by alkaline activation of municipal waste ash and subsequent surface modification retain significant adsorption capacity even at pH values below 4. Under these conditions, despite increased competition from H^+ ions, efficient removal of ions such as Pb^{2+} and Cu^{2+} occurs, attributed to the stabilization of active centers and increased specific surface area of the material. These results suggest that properly engineered zeolites from secondary raw materials, such as municipal waste ash, can provide a sustainable and economical solution for treating acidic industrial wastewater, especially where conventional adsorbents are less efficient [20].

APPLICATION OF ZEOLITE IN POLLUTED SOIL TREATMENT

Zeolite adsorbents have exceptional ion exchange and adsorption capacities, making them highly effective for remediating polluted soils. Their stable crystal structure, long-term effectiveness, resistance to pH changes, good permeability, and environmental friendliness make zeolites an increasingly sustainable solution for soil protection without the risk of secondary pollution. Their use in soils contaminated with heavy metals relies primarily on ion exchange, surface adsorption, and chemisorption. These processes bind toxic ions (e.g., Pb^{2+}, Cu^{2+}, Cd^{2+}), reducing their mobility and bioavailability and preventing their accumulation in plants and entry into the food chain. For example, Zhang *et al*. [21] synthesized MnO_2-modified clinoptilolite, in which the zeolite surface is enriched with manganese oxide phases that have a strong affinity for heavy metals. Applying this material to soil contaminated with Cd^{2+} and Pb^{2+} ions significantly reduced their bioavailability and mobility, decreasing plant accumulation by 42–68%. Additionally, improvements in soil chemical properties were observed, including increased pH and cation exchange capacity, which further contribute to contaminant stabilization. These results confirm the effectiveness of MnO_2-modified zeolites as promising materials for remediating soils contaminated with heavy metals [21].

CONCLUSION

Previous research shows that zeolites synthesized from solid waste are highly promising green functional materials with broad potential for environmental protection. Their use has demonstrated significant potential in adsorption processes, water and gas purification, and soil remediation. However, despite encouraging results, several challenges still limit their wider industrial application. It is necessary to investigate more thoroughly the mechanisms of interaction between zeolites and soil, and to develop more efficient hydrophobic zeolites and materials for gas and water purification. Another issue is that current methods of zeolite

regeneration mainly rely on thermal treatments or chemical reagents, which increase process costs and may cause secondary pollution. Research on zeolites derived from solid waste is currently mostly limited to the laboratory, while industrial application remains underdeveloped. Therefore, further research is essential to improve their performance, reduce production and regeneration costs, and enable broader commercial and sustainable use of these materials in the future.

ACKNOWLEDGEMENT

The authors are grateful to the Ministry of Science, Technological Development and Innovation of the Republic of Serbia for financial support according to the contract with registration No. 451-03-34/2026-03/200131.

REFERENCES

[1] Lin, Y.-J., Chen, J.-C. J. Environ. Chem. Eng. 2021, 9.

[2] Han, C., Yang, J., Dong, S., *et al.* Sep. Purif. Technol. 2025, 354, 128957.

[3] Khan, A.H., Lopez-Maldonado, E.A., Khan, N.A., *et al.* Chemosphere 2022, 291, 133088.

[4] Ren, Z., Wang, L., Li, Y., *et al.* J. Clean. Prod. 2022, 349, 131441.

[5] Mallette, A.J., Shilpa, K., Rimer, J.D. Chem. Rev. 2024, 124, 3416–3493.

[6] Ke, G., Shen, H., Pengfei, Y. Materials 2019, 12, 3895.

[7] Constantin, M.A., Constantin, L.A., Constantinov, F.D., *et al.* Water 2025, 17, 593.

[8] Rios, C.A., Williams, C.D., Roberts, C.L., Fuel 2009, 88, 1403–1416.

[9] Buzukashvili, S., Sommerville, R., Hu, W., *et al.* Miner. Eng. 2024, 209, 108619.

[10] Ng, T.Y.S., Chew, T.L., Yeong, Y.F. *et al*. Sci. Rep. 2019, 9, 15062.

[11] Yin, X., Liu, N., Han, M., *et al.* Ultrason. Sonochem. 2023, 100, 106598.

[12] Zhou, Q., Jiang, X., Qiu, Q., *et al.* Sci. Total Environ. 2023, 855, 158741.

[13] Boycheva, S., Szegedi, Á., Lázár, K., *et al.* Catal. Today 2023, 418, 114109.

[14] Lee, K.M., Jo, Y.M. J Mater. Cycles Waste Manag. 2010, 12, 212–219.

[15] Bandura, L., Panek, R., Rotko, M. *et al.* Microporous Mesoporous Mater. 2016, 223, 1–9.

[16] Mokrzycki, J., Franus,W., Panek, R. Materials 2023, 16, 2142.

[17] Ma, L., Han, L., Chen, S., *et al.* Fuel Process. Technol. 2019, 189, 39–48.

[18] Fan, J., Huang, J., Chen, T., *et al*. Microporous Mesoporous Mater. 2026, 403, 114019.

[19] Lee, B.X.Y., Hadibarata, T., Yuniarto, A. Water Air Soil Pollut. 2020, 231.

[20] Qiu, Q., Jiang, X., Lv, G., *et al*. Powder Technol. 2018, 335, 156–163.

[21] Zhang, Y., Zhang, H., Wang, C., *et al*. J. Hazard. Mater. 2025, 494, 138597.

EcoTER'26
eco.tfbor.bg.ac.rs
32nd International Conference
Ecological Truth & Environmental Research
24–26 June 2026, Hotel Sunce,
Sokobanja, Serbia

Original Research

TRANSFORMATION OF WASTE FROM HAZARDOUS TO NON-HAZARDOUS: STABILIZATION OF SOLID RESIDUE OBTAINED AFTER TWO-STEP HYDROMETALLURGICAL TREATMENT OF EAF DUST

DOI: 10.5937/EcoTER26568T

Vanja Trifunović[1,a*], Snežana Milić[2,b], Ljiljana Avramović[1,c], Sanela Vasiljević[1,d], Dragana Medić[2,e], Vladan Nedelkovski[2,f], Dragana Božić[1,g]

[1]Mining and Metallurgy Institute Bor, Albert Ajnštajn 1, 19210 Bor, SERBIA

[2]University of Belgrade, Technical Faculty in Bor, Vojske Jugoslavije 12, 19210 Bor, SERBIA

[a] https://orcid.org/0000-0003-4839-8751 [b] https://orcid.org/0000-0002-5000-9156

[c] https://orcid.org/0000-0002-3747-1530 [d] https://orcid.org/0000-0001-6478-5335

[e] https://orcid.org/0000-0001-9980-5949 [f] https://orcid.org/0000-0001-7724-1118

[g] https://orcid.org/0000-0003-1055-8449

Abstract

The paper investigated the stabilization process of the solid residue obtained after the hydrometallurgical treatment of EAF dust, which, due to elevated concentrations of heavy metals, shows toxic properties and does not meet the requirements for safe disposal. Stabilization was carried out by adding lime (5–10 wt.%) with the aim of immobilizing heavy metals. The results of the LP and TCLP tests showed that the efficiency of the stabilization process depends on the pH value of the environment and the amount of added lime. Under optimal stabilization conditions, specifically with the addition of 6 wt.% lime, effective immobilization of metals was achieved and the waste was classified as non-hazardous, enabling its safe disposal in a non-hazardous waste landfill.

Keywords: EAF dust, stabilization, TCLP and LP tests.

INTRODUCTION

The melting of scrap iron in an electric arc furnace is one of the most commonly applied processes in steel production, during which a significant amount of intermediate product of the process – electric arc furnace dust (EAF dust) is generated [1–3]. Due to the high content of heavy metals such as zinc, lead, cadmium, and others, as well as their possibility of self-leaching, the electric arc furnace dust is classified as hazardous waste in many countries worldwide [4–6]. For this reason, EAF dust represents a serious environmental issue, but at the same time a potential secondary resource for the recovery of zinc and other valuable components, which makes it a subject of interest for a large number of researchers [7–10]. The application of hydrometallurgical processes for the treatment of EAF dust enables the recovery of high-purity metals. Compared to pyrometallurgical processes, hydrometallurgical processes often have lower emissions of gases and dust, which contributes to reducing the

* *vanja.trifunovic@irmbor.co.rs.*

negative impact of these processes on the environment [5,11–14]. However, after the application of hydrometallurgical treatment of EAF dust, a solid residue is obtained whose characteristics sometimes do not meet regulatory requirements for safe disposal (it may contain toxic components). Therefore, in order to meet the prescribed limit values, additional treatment of this solid residue is necessary [15–19].

In this paper, the possibility of stabilizing the solid residue obtained after the applied hydrometallurgical treatment of EAF dust was investigated. The treatment includes a two-step leaching process: EAF dust leaching with distilled water (pretreatment), followed by leaching of the obtained solid residue with a sulfuric acid solution. The stabilization process is aimed at reducing the mobility of the present heavy metals and transferring the solid residue from the category of hazardous to the category of non-hazardous waste, thus enabling its safe disposal. The investigation of the stabilization process in this paper was carried out in order to define the optimal amount of added lime required to ensure satisfactory characteristics of the stabilized material in terms of environmental acceptability. The efficiency of the stabilization process was evaluated using standard tests: the Leaching Procedure (LP test) and the Toxicity Characteristic Leaching Procedure (TCLP test), which are widely used for assessing the environmental and human health impact of waste after disposal, as well as for waste classification in accordance with current regulations.

MATERIALS AND METHODS

Characterization of the solid residue obtained after the applied two-step hydrometallurgical treatment of EAF dust

A physicochemical characterization of the solid residue obtained after the applied two-step hydrometallurgical treatment of EAF dust was carried out. As part of the physical characterization, the moisture content of the sample was determined. The pH value of the solid residue was measured according to method 9045D, which is used for measuring the pH value of soils and wastes. For the determination of the chemical composition of the solid residue, the following methods were used: Atomic Absorption Spectrophotometry (AAS), Inductively Coupled Plasma Atomic Emission Spectrometry (ICP-AES), Volumetry (V), Carbon and Sulfur Analyzer (CSA), Spectrophotometry (SF), and X-ray Fluorescence Spectrometry (XRF). To determine the concentration of fluoride ions, a ion-selective electrode (ISE) and a ion meter were used.

Environmental impact assessment and stabilization of the solid residue

The solid residue obtained after the applied two-step hydrometallurgical process, i.e., water leaching followed by acid leaching, was investigated in order to assess its potential impact on the environment and human health after disposal. For this purpose, Leaching Procedure (LP test) and the Toxicity Characteristic Leaching Procedure (TCLP test) were applied in accordance with the Regulation on Categories, Testing, and Classification of Waste (Official Gazette of RS 56/2010, 93/2019, 39/2021, 65/2024).

To ensure the safe disposal of the solid residue, an additional treatment of the investigated solid residue was carried out using a stabilization process. Stabilization is a physicochemical procedure in which contaminated solid material is transformed so that hazardous components

are converted into less mobile, less soluble, or less toxic forms. The process involves mixing the waste with binders (cement, fly ash, cement kiln dust, lime, etc.), where, in the presence of water, a hydrated matrix is formed, the pH value increases, and metal precipitation is promoted, resulting in their immobilization [20,21]. In this paper, quicklime (CaO) was chosen as the stabilization agent due to its affordability and high efficiency. Calcium from the lime acts as a flocculant and a source of alkalinity, reduces moisture content upon contact with water, disinfects the material through an exothermic reaction, prevents unpleasant odors, neutralizes acidity, and immobilizes metals such as Pb, Zn, Fe, Ni, and Cr into insoluble forms. Additionally, the reaction of calcium with silicon and aluminum oxides forms stable compounds that additionally encapsulate pollutants [20].

Since the solid residue obtained by the two-step leaching process was characterized as waste that cannot be disposed of in a landfill without additional treatment, experimental investigations of the stabilization process were conducted. These experiments involved mixing the wet solid residue (with a moisture content of 17%) with 5, 6, 7.5, and 10 wt.% lime. To assess the impact of the stabilized solid residue on the environment and human health, LP and TCLP tests were performed after each conducted experiment.

RESULTS AND DISCUSSION

Characterization of the solid residue obtained after the applied two-step hydrometallurgical treatment of EAF dust

As part of the physical characterization, the moisture content of the solid residue obtained after the applied hydrometallurgical treatment of EAF dust was determined to be 17.0%, while the measured pH value of the solid residue was 3.54. The results of the chemical characterization of the solid residue obtained after the applied hydrometallurgical treatment of EAF dust are presented in Table 1.

Table 1 *Chemical composition of the solid residue obtained after the applied two–step hydrometallurgical treatment of EAF dust*

Element	Content, %	Method	Element	Content, %	Method
Zn	8.01	V	Sn	0.0817	ICP-AES
Fe	38.90	AAS	Cd	0.0350	ICP-AES
Pb	3.80	ICP-AES	K	0.1623	ICP-AES
Na	0.15	ICP-AES	Cu	0.0950	ICP-AES
Ca	4.32	ICP-AES	Ni	0.0187	ICP-AES
Mn	2.24	ICP-AES	Cl	0.0075	SF
Si	0.96	XRF	F	0.0001	ISE
S	3.50	CSA	Cr	0.4917	ICP-AES
C	9.60	CSA	As	0.0048	ICP-AES

Considering the content of components in the solid residue, shown in Table 1, it can be further treated for the recovery of other valuable metals, such as lead [7,22–24]. In addition, the solid residue obtained after zinc recovery can be used in other industries [3,7,17,25,26].

However, if the utilization of the resulting solid residue is not foreseen in further planned activities, it may be disposed of in an appropriate landfill, following prior waste classification in accordance with applicable regulations.

Environmental impact assessment and solid residue stabilization

The results of the leachability test of the solid residue obtained after two-step leaching (Table 2) indicate elevated concentrations of cadmium, lead, zinc and sulfates in the LP eluate and lower pH value, which exceed the permitted limit values for disposal at non-hazardous and hazardous waste landfills. These findings confirm that additional treatment of solid residue is necessary prior to final disposal.

Table 2 *Leachability tests – LP tests of the solid residue before and after the stabilization process*

Parameter	Unit	Measured value					Reference value for inert waste[1)]	Reference value for non–hazardous waste[2)]	Reference value for hazardous waste[3)]
		Solid residue	Stabilized with 5 wt.% CaO	Stabilized with 6 wt.% CaO	Stabilized with 7.5 wt.% CaO	Stabilized with 10 wt.% CaO			
pH	**-**	**4.89**	8.07	10.22	10.98	11.67	-	**6–13[4)]**	-
Conductivity	µS/cm	3499	2482	2417	2821	3759	-	-	-
Antimony, Sb	mg/kg dm	0.07	0.07	<0.06	<0.06	<0.06	0.06	0.7	5
Arsenic, As	mg/kg dm	<0.20	<0.20	<0.20	<0.20	<0.20	0.5	2	25
Barium, Ba	mg/kg dm	0.28	1.9	1.4	1.90	0.44	20	100	300
Copper, Cu	mg/kg dm	12	<0.05	<0.05	<0.05	25	2	50	100
Cadmium, Cd	**mg/kg dm**	**11**	<0.04	0.04	<0.04	<0.04	**0.04**	**1**	**5**
Molybdenum, Mo	mg/kg dm	<0.07	1.1	1.5	1.9	3.5	0.5	10	30
Nickel, Ni	mg/kg dm	0.85	<0.07	<0.07	0.51	0.34	0.4	10	40
Lead, Pb	**mg/kg dm**	**118**	0.40	5.1	**41**	**100**	**0.5**	**10**	**50**
Selenium, Se	mg/kg dm	0.16	0.29	0.40	0.40	0.31	0.1	0.5	7
Chromium, Cr	mg/kg dm	0.13	<0.05	<0.05	0.05	0.14	0.5	10	70
Zinc, Zn	**mg/kg dm**	**5578**	7.8	22	2.8	21	**4**	**50**	**200**
Mercury, Hg	mg/kg dm	<0.0005	<0.005	<0.005	<0.005	<0.005	0.01	0.2	2
SO_4^{2-}	**mg/kg dm**	**28310**	16210	19686.8	14420	13970	**1000**	**20000**	50000
Cl^-	mg/kg dm	125.9	66.5	75.7	94.9	110.5	800	15000	25000
F^-	mg/kg dm	14	19	34	36	35	10	150	500

[1), 2), 3)]Annex 10 of the Regulation on Categories, Testing, and Classification of Waste (Official Gazette of RS 56/2010, 93/2019, 39/2021, 65/2024), Article 2, Parameters for testing waste and landfill leachates from inert[1)], non–hazardous[2)], and hazardous[3)] waste. Ambient temperature 21 °C, humidity 52%, pressure 970 hPa.
[4)]Reference value for pH according to the Regulation 56/2010, 93/2019, 39/2021, 65/2024, Annex 7, H15 – Waste that has the property to generate, by any means after disposal, another substance, e.g., leachate exhibiting any of the listed characteristics (H1–H14), ranges from 6 to 13.

The increased concentrations of cadmium, zinc and sulfates are likely a consequence of insufficient washing of the solid residue with water after the two–step leaching process, resulting in a portion of the pregnant leaching solution remaining trapped within the material. Additional washing could contribute to reducing their concentrations. Furthermore, the

measured pH value is below the prescribed limit values, which could also be corrected by additional washing of the solid residue with water. Based on the results of the TCLP test (Table 3), the solid residue after the second step of leaching – acid leaching, is classified as waste that cannot be disposed of, as it exhibits toxic properties due to elevated concentrations of cadmium and zinc in the eluate.

Considering the potentially harmful impact on the environment and human health, as confirmed by the results of both tests, it is clear that appropriate treatment of the solid residue is necessary prior to its final disposal in a landfill. To this end, in this paper, investigations of its chemical stabilization with the addition of lime (5–10 wt.%) were carried out.

The results of testing the toxic characteristics of the solid residue intended for disposal, before and after the implemented stabilization processes with the addition of lime at 5, 6, 7.5, and 10 wt.%, are presented in Table 3.

Table 3 *Toxic characteristics – TCLP tests of the solid residue before and after the stabilization process*

Element	Unit	Measured value					Reference value for waste toxicity[1)]
		Solid residue	Stabilized with 5 wt.% CaO	Stabilized with 6 wt.% CaO	Stabilized with 7.5 wt.% CaO	Stabilized with 10 wt.% CaO	
Antimony, Sb	mg/l	<0.006	0.038	<0.006	0.032	0.033	15
Arsenic, As	mg/l	<0.020	<0.020	<0.020	<0.020	<0.020	5
Barium, Ba	mg/l	0.018	0.16	0.068	0.095	0.098	100
Copper, Cu	mg/l	2.5	0.007	0.011	0.040	0.044	25
Cadmium, Cd	**mg/l**	**2.2**	0.79	0.40	0.16	0.050	**1**
Molybdenum, Mo	mg/l	<0.007	0.014	0.007	0.068	0.093	350
Nickel, Ni	mg/l	0.17	0.061	0.077	<0.007	<0.007	20
Lead, Pb	mg/l	2.4	2.2	0.76	1.4	0.40	5
Selenium, Se	mg/l	0.015	0.018	0.005	0.010	0.008	1
Chromium, Cr	mg/l	<0.005	<0.005	<0.005	0.008	0.010	5
Zinc, Zn	**mg/l**	**1141.7**	**306.1**	228.8	107.7	38.7	**250**
Mercury, Hg	mg/l	<0.0005	<0.0005	<0.0005	<0.0005	<0.0005	0.2
Vanadium, V	mg/l	<0.007	<0.007	<0.007	<0.007	<0.007	24
Silver, Ag	mg/l	<0.005	<0.005	0.005	<0.005	<0.005	5

[1)]Annex 10 of the Rulebook on Categories, Testing and Classification of Waste (Official Gazette RS 56/2010, 93/2019, 39/2021, 65/2024), Article 1, Parameters for testing the toxic characteristics of waste intended for disposal.

The results of the LP and TCLP tests indicate that the efficiency of the solid residue stabilization process significantly depends on the amount of added lime and the achieved pH value. With the addition of 5 wt.% lime, the LP test confirmed successful metal immobilization, as the concentrations of all elements were below the limit values for non–hazardous waste at a basic environment of pH≈8. However, the TCLP test revealed toxic characteristics due to an increased concentration of zinc, which can be explained by a

decrease in the pH value during the application of the extraction reagent and the subsequent dissolution of this metal.

With the addition of 7.5 wt.% lime, the TCLP test results did not indicate toxic characteristics of the stabilized solid residue, whereas the LP test results showed an increased concentration of lead above the permitted values for non–hazardous waste. The higher pH value (pH≈10.98) favored the formation of soluble lead compounds and its transfer to the eluate. A similar trend was observed with the addition of 10 wt.% lime, where the TCLP test again showed no toxicity, but the LP test recorded even greater lead leaching (pH≈11.67), even above the limits for hazardous waste disposal. These results confirm that a strongly basic environment increases the mobility of lead.

Remeteiová et al. [27] and Montentegro et al. [24] report in their studies that during the water leaching of EAF dust at pH values in the range of 6.5–11.0, approximately 53% of calcium is leached. The authors further note that at pH values above 11, leached calcium precipitates as hydroxide; however, under these conditions, the dissolution of lead compounds also occurs, resulting in the transition of lead into the solution. Considering that in this paper the LP tests were conducted using water as a reagent, and the use of lime for stabilization achieved a pH of the leaching solution of almost 11 (10.98 when stabilized with 7.5 wt.% lime) and above 11 (11.67 when stabilized with 10 wt.% lime), lead concentrations in the eluates exceeding the permissible limit for waste disposal can be attributed to those conditions.

The optimal results were achieved with the addition of 6 wt.% lime, where both the LP and TCLP tests showed that the concentrations of all elements were below the prescribed limit values, without showing any toxic characteristics. This confirms that the addition of 6 wt.% lime provides effective metal immobilization and enables safe disposal of the stabilized solid residue at the non–hazardous waste landfill.

CONCLUSION

Based on the results obtained in this paper, it can be concluded that the solid residue obtained after the two–step hydrometallurgical treatment of EAF dust, and due to elevated concentrations of heavy metals as determined by LP and TCLP tests, is classified as hazardous waste and does not meet the conditions for safe disposal, and therefore requires additional treatment.

The application of the stabilization process with the addition of lime proved to be an effective method for reduce the mobility and toxicity of metals from the investigated solid residue, where it was determined that the effectiveness of the process significantly depends on the amount of added stabilization agent and the pH value. At both lower and higher lime contents, undesirable effects were observed, such as the remobilization of certain metals (zinc at lower pH and lead at higher pH values).

According to the results of the LP and TCLP tests, the optimal stabilization conditions in the paper were achieved with the addition of 6 wt.% lime, when the concentrations of all analyzed elements in the eluate were below the prescribed limit values, without exhibiting any toxic characteristics. This allows for effective metal immobilization and the classification of

the waste as non–hazardous, thereby creating conditions for its safe disposal in a non–hazardous waste landfill. The obtained results indicate that the application of the stabilization process represents a reliable and economically acceptable solution for managing the solid residue obtained after the two–step hydrometallurgical treatment of EAF dust.

ACKNOWLEDGEMENT

The authors are grateful to the Ministry of Science, Technological Development and Innovation of the Republic of Serbia for financial support according to the contracts with registration No. 451-03-33/2026-03/200052 and 451-03-34/2026-03/200131.

REFERENCES

[1] Henriques, J. Sustainability 2023, 15, 15323.

[2] Li, Y.C.J. Cleaner Prod. 2020, 263, 121468.

[3] Silva, V.S.J. Mater. Res. Technol. 2019, 8(6), 5504–5514.

[4] Omran, M. Miner. Eng. 2025, 228, 109326.

[5] Wan, Y.J. Environ. Chem. Eng. 2024, 12, 113246.

[6] Wang, K. Met. 2025, 15, 437.

[7] Li, C. Sep. Purif. Technol. 2023, 312, 123355.

[8] Halli, P. Sep. Purif. Technol. 2020, 236, 116264.

[9] Rudnik, E. Hydromet. 2019, 188, 256–263.

[10] Halli, P. Miner. Eng. 2018, 124, 1–9.

[11] Gamutan, J.J. Environ. Chem. Eng, 2024, 12, 111789.

[12] Karahan, B.D. Mat. Chem. Phys. 2023, 302, 127734.

[13] Chen, Y. Sep. Purif. Technol. 2022, 281, 119936.

[14] Kaya, M. Hydromet. 2020, 195, 105362.

[15] Altarawneh, S. Chem. Eng. J. 2024, 493, 152873.

[16] Xue, Y. Mater. 2022, 15, 4127.

[17] Saeta, J.M.T. Met. 2021, 11, 1603.

[18] Schoeman, Y. Case Stud. Chem. Environ. Eng. 2021, 3, 100097.

[19] De Buzin, P.J.W.K. J. Mater. Res. Technol. 2017, 6(2), 194–202.

[20] Pinasseau A., Zerger B., Roth J., et al., Reference Document on Best Available Techniques (BAT) Reference Document for Waste Treatment, Industrial Emissions Directive 2010/75/EU (Integrated Pollution Prevention and Control), European Commission, 2018.

[21] Fernández, A.I., J. Environ. Eng. 2003, 129(3), 275–279.

[22] Hamann, C., J. Hazard. Mater. 2024, 465, 133421.

[23] Yang, J. Process Saf. Environ. Prot. 2023, 170, 960–970.

[24] Montenegro, V. Waste Biomass Valorization 2016, 7(6), 1531–1548.

[25] Yubonmhat, K. Heliyon. 2024, 10, e25792.

[26] Lozano-Lunar, A. J. Cleaner Prod. 2019, 211, 1375–1388.
[27] Remeteiová, D. Appl. Water Sci. 2023, 13, 138.

EcoTER'26
eco.tfbor.bg.ac.rs
32nd International Conference
Ecological Truth & Environmental Research
24–26 June 2026, Hotel Sunce,
Sokobanja, Serbia

Original Research

HOW STRUCTURAL MODIFICATIONS INFLUENCE ENVIRONMENTAL RISK: A CASE STUDY OF STEROIDAL DERIVATIVES

DOI: 10.5937/EcoTER26576S

Isidora Santrač[1,a*], Jelena Korać Jačić[1,b], Milica Milenković[2,c], Marijana Živković[3,d]

[1] University of Belgrade, Institute of Multidisciplinary Research – National Institute of the Republic of Serbia, Kneza Višeslava 1, 11030 Belgrade, SERBIA

[2] University of Belgrade, Faculty of Chemistry, Studentski trg 12–16, 11000 Belgrade, SERBIA

[3] Institute of Chemistry, Technology and Metallurgy – National Institute of the Republic of Serbia, Department of Chemistry, Studentski trg 12–16, 11000 Belgrade, SERBIA

[a] https://orcid.org/0000-0001-8533-4250

[b] https://orcid.org/0000-0002-3802-6009

[c] https://orcid.org/0000-0003-2053-3704

[d] https://orcid.org/0000-0002-1978-1308

Abstract

Steroid hormones are important endocrine-disrupting compounds due to their widespread use and continuous release into the environment via human and livestock excretion, veterinary applications, and pharmaceuticals. The environmental behavior of structurally modified steroidal hydrazones and derivatives remains largely unknown. We conducted an in silico assessment using EPI Suite to predict physicochemical properties, environmental fate, bioaccumulation, and aquatic toxicity. The analyzed derivatives exhibit higher lipophilicity (log Kow 3.27–5.60), increased molecular weight (344–530), and lower water solubility (<5 mg L^{-1}) than reference steroids, suggesting limited mobility and enhanced sorption. Predicted log Koc values (3–8) indicate strong soil and sediment adsorption, while BIOWIN3 suggests slow biodegradation. Bioaccumulation potential (log BCF/BAF) is elevated, with dietary uptake contributing for certain derivatives. Acute toxicity estimated via ECOSAR shows very high toxicity for fish (LC_{50} 0.06–0.42 mg L^{-1}) and high to very high toxicity for daphnids (0.05–1.69 mg L^{-1}). These in silico findings indicate that the studied steroidal derivatives may pose a significant environmental risk, warranting further experimental validation and careful consideration of their fate and effects in aquatic and terrestrial ecosystems.

Keywords: *in silico* assessment, environmental fate, bioaccumulation, aquatic toxicity, lipophilicity.

INTRODUCTION

Steroid hormones represent a major class of endocrine-disrupting compounds due to their extensive medical use and continuous release from both natural and anthropogenic sources [1–2]. They are introduced into the environment through various pathways, including human and livestock excretion, veterinary applications, agricultural runoff, and pharmaceutical

* *isantrac@imsi.bg.ac.rs*

residues. As active pharmaceutical agents, they are widely employed in the treatment of reproductive disorders, growth-related conditions, and cancers.

The environmental occurrence and adverse effects of steroidal compounds, particularly estrogens, androgens, and progestogens, have been widely documented, even at trace concentrations. Their persistence and high biological activity raise significant concerns regarding ecological imbalance and potential risks to human health. At the same time, the development of novel steroid-based therapeutics, including cytotoxic derivatives, necessitates a more comprehensive evaluation of their environmental impact. Integrating environmental considerations into early-stage drug design is therefore essential, alongside improvements in wastewater treatment, analytical detection, and regulatory control.

The selected reference compounds include estrogens (estradiol and ethinyl estradiol), an androgen (testosterone), and a corticosteroid (prednisolone), representing major classes of biologically active steroids (Figure 1). Their inclusion enables a comparative evaluation of the environmental behavior and toxicity of structurally modified androstenedione- and progesterone-based derivatives. In this context, the present study provides a systematic *in silico* assessment of the environmental properties of steroidal hydrazones and their derivatives, with a comparative analysis against selected reference steroid compounds recognized as environmental contaminants.

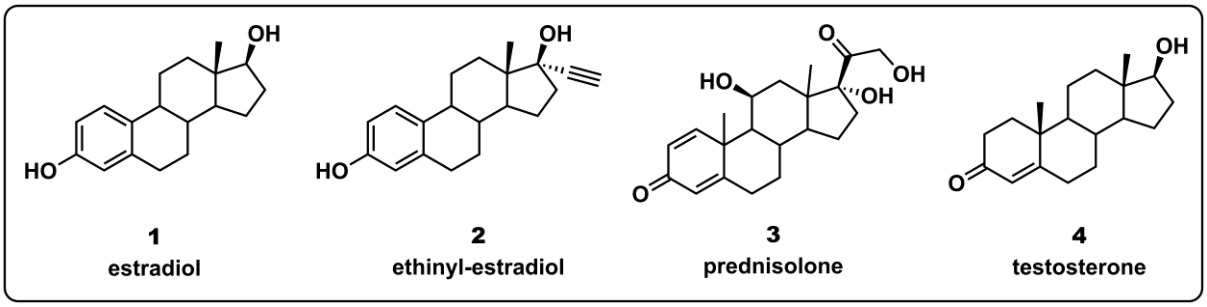

Figure 1 *Chemical structures of the selected reference steroidal compounds*

MATERIALS AND METHODS

Assessed compounds

The compounds analyzed in this study were previously synthesized and reported [3–5], whereas the quinoxaline derivatives were included based on data from our previous work [6].

In silico environmental assessment

Physicochemical properties (log Kow, water solubility), environmental fate (log Koc), biodegradability (BIOWIN3), bioaccumulation (log BCF/BAF), and aquatic toxicity (fish and daphnid LC_{50}) of the steroidal derivatives were predicted using the EPI Suite (https://episuite.dev/EpiWebSuite/#/). The calculations were performed using relevant modules, including KOWWIN, WSKOWWIN, KOCWIN, BIOWIN3, BCFBAF, and ECOSAR.

RESULTS AND DISCUSSION

Steroidal compounds chosen for the environmental assessment are presented in Figure 2.

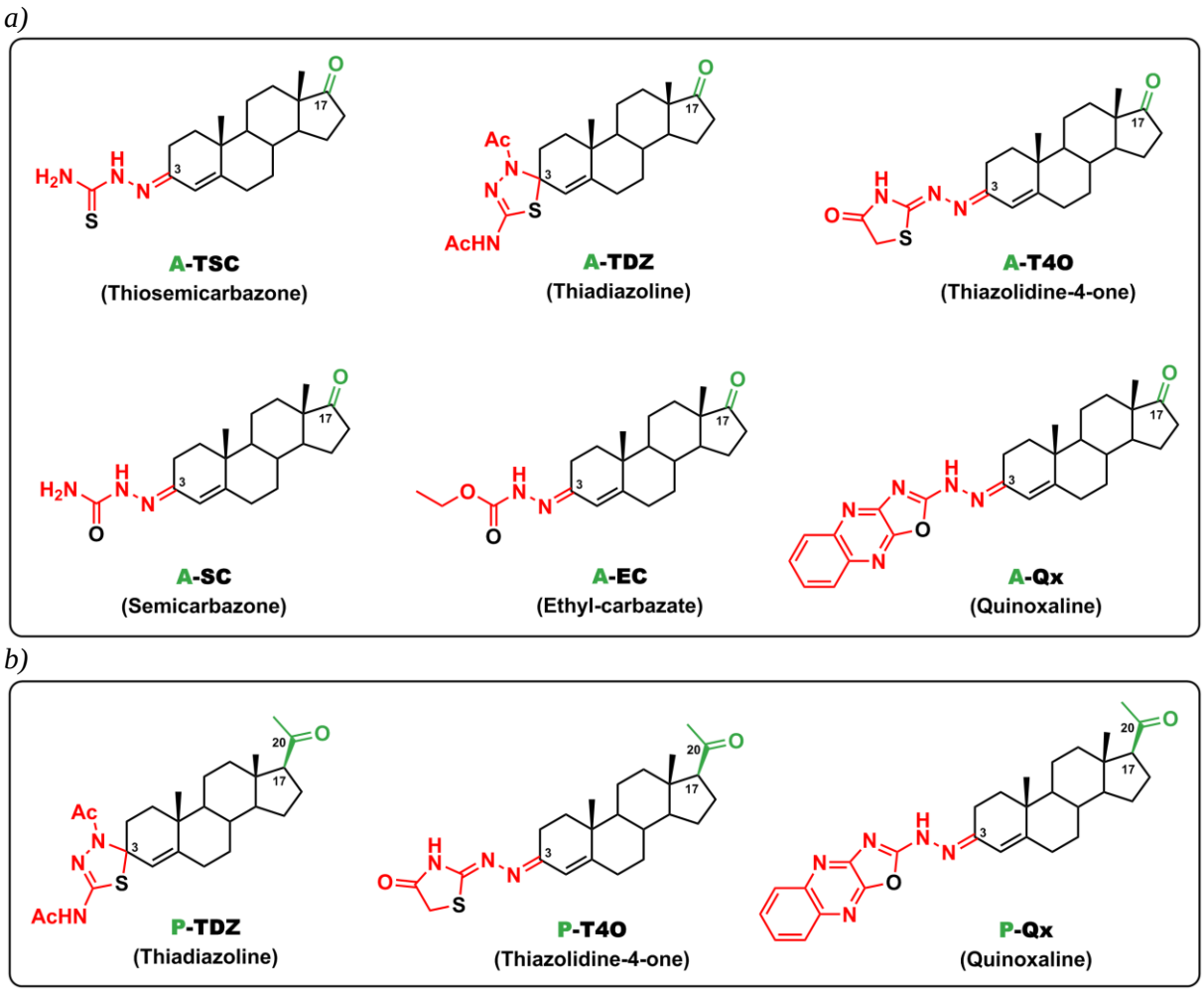

Figure 2 *Chemical structures of the analyzed steroidal derivatives: a) androstenedione derivatives, and b) progesterone derivatives*

To evaluate these aspects, predicted physicochemical, environmental fate, and ecotoxicity parameters of the analyzed steroidal derivatives are presented in Table 1, alongside selected reference steroid compounds for comparison (1–4).

Physicochemical parameters such as lipophilicity (log Kow), water solubility (Ws), and molecular weight (MW) are key determinants of environmental distribution and govern processes such as sorption, bioaccumulation, and biodegradation.

The predicted log Kow values of the reference compounds range from 1.40 to 4.12, with prednisolone showing the lowest and ethinyl estradiol the highest lipophilicity. In contrast, the analyzed steroidal derivatives exhibit higher log Kow values (3.27–5.60), indicating increased lipophilicity. The highest value was observed for the **P-Qx** derivative, while the lowest corresponds to the **A-TDZ** derivative. Overall, progesterone derivatives are more lipophilic than the corresponding androstane analogues, suggesting that structural modifications significantly influence hydrophobicity. Increased lipophilicity may reduce water solubility

and enhance sorption to organic matter, which can contribute to higher bioaccumulation potential and persistence in the environment. In line with these observations, the molecular weights of the analyzed steroidal derivatives (344–498) are higher than those of the reference compounds (272–360), reflecting increased structural complexity. In addition, the predicted water solubility of the modified compounds is significantly lower (< 5 mg L^{-1}) compared to the reference steroids (48–341 mg L^{-1}). This reduction in water solubility is consistent with the increased lipophilicity of the analyzed compounds and suggests limited mobility in aqueous environments. Instead, such compounds are more likely to associate with organic matter and accumulate in sediments. Furthermore, the combination of higher molecular weight and low solubility may contribute to reduced biodegradation rates and enhanced bioaccumulation potential.

Table 1 *Predicted physicochemical parameters, environmental fate, and ecotoxicity parameters of steroidal derivatives*

Compd.	log Kow	Ws (mg L^{-1})	MW	BIO3	log Koc	log BCF	log BAF	F-LC_{50} (mg L^{-1})	D-LC_{50} (mg L^{-1})
A-TSC	4.63	0.60	360	1.9	5.07	2.72	2.45	0.09	0.62
A-TDZ	3.27	2.61	444	1.5	4.59	1.83	2.15	0.42	1.69
A-T4O	4.34	0.60	400	1.8	5.22	2.53	2.34	0.14	0.81
A-SC	3.68	4.85	344	1.9	4.64	2.10	1.55	0.22	1.03
A-EC	4.67	0.46	373	1.9	5.23	2.75	3.17	0.09	0.51
A-Qx	4.69	0.009	470	1.7	7.70	2.76	2.67	0.11	0.77
P-TDZ	3.50	1.12	472	1.4	5.07	1.98	2.38	0.36	1.57
P-T4O	5.25	0.07	428	1.8	5.69	3.13	2.82	0.06	0.21
P-Qx	5.60	0.001	498	1.7	8.18	3.36	3.22	0.19	0.05
1	3.94	93.53	272	2.4	4.19	2.27	1.52	4.03	2.74
2	4.12	48.42	296	2.0	4.65	2.38	1.28	3.06	2.11
3	1.40	341	360	2.0	2.05	0.59	0.43	42.85	26.51
4	3.27	74.88	288	2.3	3.34	1.82	2.17	17.17	10.96

Compd. – compound.
log K_{OW} – octanol-water partition coefficient; indicator of compound lipophilicity.
Ws – water solubility; predicted solubility of the compound in water.
MW – molecular weight.
BIO3 – aerobic biodegradability (BIOWIN3 model).
log K_{OC} – organic carbon-water partition coefficient; indicator of adsorption to soil/sediment.
log BCF – bioconcentration factor; accumulation from water into organisms.
log BAF – bioaccumulation factor; accumulation from water and food.
F-LC_{50} – predicted lethal concentration for 50% of fish over 96 hours.
D-LC_{50} – predicted lethal concentration for 50% of *Daphnia spp.* over 48 hours.

The reduced water solubility and increased lipophilicity of the analyzed steroidal derivatives are expected to influence their adsorption to soils and sediments. This behavior is further reflected in the predicted log Koc values, with structural modifications leading to a wider range of soil adsorption compared to reference steroid contaminants (4.64–8.18 vs. 2.05–4.65), indicating increased variability in environmental mobility and potential accumulation in sediments. Among the reference compounds, prednisolone remains relatively mobile in the environment (log Koc < 3), whereas estradiol, ethinyl estradiol, and testosterone exhibit moderate adsorption to soil organic matter (log Koc = 3.34–4.65). In contrast, **A-TDZ** and **A-SC** derivatives show moderate adsorption (log Koc = 3–5), while the remaining

modified compounds display very high adsorption potential (log Koc > 5), suggesting strong binding to soil and sediment organic matter and a tendency for accumulation in sediments. This behavior is consistent with the increased lipophilicity of the modified steroidal derivatives.

Consistent with these properties, steroid-based derivatives exhibit relatively slow predicted biodegradation rates according to the BIOWIN3 model, reflecting the known environmental persistence of steroidal contaminants. The reference compounds, testosterone and estradiol, are predicted to degrade within weeks to months (BIOWIN3 = 2.3–2.4). In contrast, heterocyclic derivatives with higher molecular weights, including both TDZ and Qx classes, show slower degradation kinetics (BIOWIN3 = 1.3–1.7), suggesting extended persistence in the environment. The remaining compounds are predicted to degrade on a timescale of months (BIOWIN3 = 1.8–2.0), indicating limited biodegradation potential. These predictions should be interpreted with caution, as BIOWIN3 provides an estimate of primary biodegradation timeframe rather than complete mineralization.

As expected from their increased lipophilicity and sorption potential, the predicted log BCF values (1.83–3.36) indicate moderate to high bioaccumulation potential for the studied compounds, exceeding that of reference steroids (0.58–2.38). Similar trends were observed for log BAF values. Notably, **A-EC** and both TDZ derivatives exhibited higher BAF than BCF values, suggesting that dietary uptake contributes substantially to overall bioaccumulation for these compounds.

The environmental relevance of these compounds is further highlighted by their predicted acute aquatic toxicity. Toxicity was estimated using ECOSAR as LC_{50} (96 h) for fish and LC_{50} (48 h) for *Daphnia spp.*, with the most conservative (lowest) predicted value among applicable models selected for each endpoint.

The analyzed steroidal derivatives exhibit pronounced aquatic toxicity, with generally higher sensitivity observed in fish than in daphnids. The higher toxicity of the analyzed compounds relative to the reference steroids may be attributed to the presence of hydrazone functionality, suggesting its role in enhancing aquatic toxicity. The predicted LC_{50} values for fish (0.06–0.42 mg L^{-1}) indicate very high toxicity of the investigated compounds, whereas the reference compounds show considerably lower toxicity (3.06–42.85 mg L^{-1}). A similar trend is observed for daphnids, with the analyzed compounds classified as highly to very highly toxic (0.05–1.69 mg L^{-1}), in contrast to the reference compounds, which range from moderately to highly toxic (2.11–26.51 mg L^{-1}). Although direct comparison between fish and daphnid toxicity should be made with caution due to differences in exposure duration and test conditions, the results suggest that fish may represent the more sensitive trophic level for the majority of the investigated compounds. This may be associated with the higher lipophilicity of the compounds, which facilitates membrane permeation and potential bioaccumulation in aquatic organisms.

These findings highlight the potential environmental risk and underscore the need for further experimental validation and environmentally conscious design of steroid-based compounds.

CONCLUSION

In summary, the analyzed steroidal derivatives exhibit increased lipophilicity, higher molecular weight, and lower water solubility compared to reference steroids, resulting in stronger sorption to organic matter, slower predicted biodegradation, and higher bioaccumulation potential. Structural modifications, particularly the introduction of heterocyclic and hydrazone functionalities, contribute to these trends and are associated with pronounced aquatic toxicity, with fish generally representing the most sensitive trophic level. Taken together, these *in silico* predictions suggest that the studied compounds may pose a significant environmental risk, highlighting the need for further experimental validation and careful consideration of their fate and effects in aquatic and terrestrial ecosystems.

ACKNOWLEDGEMENT

The authors are grateful to the Ministry of Science, Technological Development and Innovation of the Republic of Serbia for financial support according to the contract with registration No. 451-03-33/2026-03/200026, 451-03-33/2026-03/200053 and 451-03-33/2026-03/200168.

REFERENCES

[1] Almazrouei, B., Islayem, D., Alskafi, F., *et al*. Emerg. Contam. 2023, 9, 100210.

[2] Xu, R., Liu, S., Pan, Y.F., *et al*. J. Hazard. Mater. 2024, 461, 132673.

[3] Živković, M.B., Matić I.Z., Rodić M.V., *et al*. RSC Adv. 2016, 6, 34312–34333.

[4] Živković, M.B., Matić, I.Z., Rodić, M.V., *et al*. J. Steroid Biochem. Mol. Biol. 2017, 174, 72–85.

[5] Živković, M.B., Novaković, I.T., Matić, I.Z., *et al*. Steroids 2019, 148, 36–46.

[6] Živković MB, Šegan S, Sladić DM. In: Proceedings of the 3rd International Conference on Chemo and Bioinformatics; September 25–26; Kragujevac, Serbia, 2025. p. 487–490.

EcoTER'26
eco.tfbor.bg.ac.rs
32nd International Conference
Ecological Truth & Environmental Research
24–26 June 2026, Hotel Sunce,
Sokobanja, Serbia

Original Research

IMPACT OF FOG DISPERSION ON AVIATION AND ENVIRONMENTAL SAFETY

DOI: 10.5937/EcoTER26582J

Jelena Janjić[1,a*], Mlađen Ćurić[2]

[1] Akademija strukovnih studija Politehnika, Katarine Ambrozić 3, Belgrade, SERBIA

[2] Independent researcher, Belgrade, SERBIA

[a] https://orcid.org/0009-0003-5820-3839

Abstract

Fog is one of the most hazardous meteorological phenomena, significantly impacting aviation safety and the continuity and regularity of aviation operations, particularly in general aviation. It also causes substantial economic losses due to frequent operational disruptions and temporary airport closures. Moreover, fog remains one of the most complex atmospheric phenomena to forecast and observe with high accuracy.

The Vojvodina region, the focus of this study, is characterized by frequent fog, particularly during the colder part of the year. It hosts several small airports and airfields, which, despite their limited infrastructure, are regularly used and often operate without certified low-visibility landing systems. Under such conditions, fog dispersion techniques could serve as a potential supplementary operational approach for enhancing operational aviation safety. To illustrate the described meteorological conditions and their potential impact on aviation operations, this study analyzes the synoptic situation on 14 November 2025, during which an aircraft accident occurred at Subotica Airport (LYSU), resulting in severe injuries to the passenger and the death of the pilot.

This study provides a critical assessment of the potential to improve aviation safety at small airports and airfields in the Vojvodina region by applying fog dispersion methods, with particular consideration of their environmental implications. The study focuses on scenarios where certified low-visibility landing systems are not operationally available.

Keywords: fog dispersion, aviation safety, low-visibility operations, environmental impact.

INTRODUCTION

According to the International Civil Aviation Organization (ICAO) and the World Meteorological Organization (WMO), fog is defined as "a suspension of very small water droplets (and sometimes minute ice particles) in the atmosphere, reducing the horizontal visibility at the Earth's surface to less than 1000 m." [1]. Due to the substantial reduction in horizontal visibility, fog represents one of the most hazardous meteorological phenomena affecting aviation operations, particularly during approach and landing phases.

The Vojvodina region, characterized by flat terrain, extensive grassland areas, numerous water bodies, and high near-surface humidity, is conducive to frequent fog occurrence, especially during the colder part of the year. The region hosts several small airports and

* *jjanjic@politehnika.edu.rs*

airfields with limited infrastructure and without certified low-visibility landing systems, primarily used for general aviation operations such as flight training, sport aviation, and private flying. Users of these small airports and airfields often lack access to locally relevant meteorological information and may rely on meteorological data and forecasts intended for larger airports or on observations from the nearest synoptic weather stations. These factors may adversely affect aviation safety at such locations.

In situations where landing operations under low-visibility conditions are not possible, it is relevant to consider methods for artificially improving visibility. One such approach is fog dispersion. According to the World Meteorological Organization, fog dispersion, or fog dispersal, is "a form of weather modification aimed at artificially improving visibility through the dissipation of fog."

The Serbian Center for Investigation of Accidents in Transport (CINS) initiated an official investigation into the accident at Subotica Airport (LYSU) on 14 November 2025. The final investigation report was not publicly available, and the probable cause of the accident is unknown at the time of writing [2]. However, multiple reports referenced poor visibility, fog occurrence, and difficulties in conducting the accident investigation due to unfavourable meteorological conditions.

MATERIALS AND METHODS

Fog dispersion methods and their effects

Fog dispersion methods depend primarily on the type of fog present [3,4]. Based on the temperature conditions under which fog forms, fog may be classified into three categories: warm fog, supercooled fog, and ice fog [3].

Warm fog (FG) consists of water droplets at temperatures above 0°C. This type of fog is highly stable, very common, and considered the most difficult to disperse artificially [5,6].

Supercooled fog or freezing fog (FZFG) forms at temperatures below 0°C but still consists partially or entirely of liquid water droplets due to the insufficient presence of ice-nucleating particles - INPs [5,6].

Finally, ice fog consists predominantly of ice crystals and most commonly occurs at temperatures below −30°C [5].

Based on the mathematical formulation of daytime visibility presented in [7], visibility can be most effectively improved by reducing the diameter of fog droplets. Additionally, considering the spatial scale required for effective fog modification at airports, the most practical and efficient approaches are air-mixing and air-replacement techniques, particularly evaporation-based and thermal fog dispersal methods, which have historically shown the greatest operational applicability in aviation fog dissipation [3,4].

The evaporation method consists of two main approaches: removing water vapor from the air and increasing the air's capacity to hold water vapor without condensation.

Freezing fog (FZFG) is considered one of the most hazardous fog types in aviation because it combines reduced visibility with icing conditions affecting aircraft, runways, and airport equipment [6,8]. Its greatest operational impact occurs during taxi, take-off, and

landing phases [9,10]. Fog dispersion can be achieved through two approaches: homogeneous nucleation by locally cooling the air with liquid propane or dry ice, and heterogeneous nucleation by introducing ice-nucleating particles (INPs) into the atmosphere [3,11–13].

Warm fog dissipation can be achieved through direct heating, hygroscopic seeding, and mixing with drier air. Direct heating for localized fog dissipation may be achieved using hydrocarbon fuels or laser energy [3]. Recent research suggests that UV-C photolysis technology may potentially contribute to fog dissipation not only through localized heating but also by reducing the efficiency of cloud condensation nuclei (CCN) by approximately 35–45%, thereby potentially limiting fog reformation [14].

Currently, no satisfactory operational methods for effective *ice fog* dispersion have been identified; therefore, mitigation efforts are mainly focused on preventing or limiting ice fog formation [3,15,16].

According to the WMO Statement on Weather Modification [15] and recently published studies [17,18], commonly used seeding agents have generally not demonstrated significant adverse impacts on human health or the environment under standard operational conditions. However, the use of large quantities of such materials should still be approached with caution and careful environmental consideration.

According to [15], further progress in weather modification research requires high-quality observations, numerical modelling, well-designed experiments, and international collaborative efforts. Furthermore, significant social, ethical, environmental, and legal challenges remain important challenges with weather modification practices [15].

RESULTS AND DISCUSSION

Overview of Meteorological Data and LYSU Characteristics

This study analyzes the synoptic situation on 14 November 2025, with additional focus on the resulting weather conditions at Subotica Airport (LYSU).

As previously discussed, the effectiveness of fog dispersion methods is highly dependent on the spatial extent of the area being influenced. The runways at Belgrade Nikola Tesla Airport measure approximately 3.5 km × 45 m [19], while the runway at Subotica Airport is considerably smaller, with dimensions estimated at approximately 800 m × 30 m [20]. Additionally, the runway surface at Subotica Airport is grass-covered, unlike the concrete surfaces at Belgrade Airport. Grass-covered surfaces tend to retain near-surface moisture more efficiently, which may enhance local fog formation processes. Lake Palić is located approximately 6 km in a straight line from Subotica Airport and may represent an additional local source of atmospheric moisture.

Surface synoptic observations (SYNOP reports) from nearby meteorological stations were used to reconstruct the synoptic and local meteorological conditions during the event. SYNOP reports use a standardized WMO coding format for reporting surface meteorological observations at fixed synoptic hours [21]. The data include air temperature, dew point temperature, atmospheric pressure, pressure tendency, wind direction and speed, horizontal visibility, cloud cover, cloud type, present and past weather phenomena, precipitation amount, and additional information on atmospheric and surface conditions.

These observations are reported according to internationally standardized procedures, and each station is assigned a unique WMO station identifier [22]. The nearby stations considered in this study were Sombor (13160), Palić (13067), Kikinda (14117), Novi Sad – Rimski Šančevi (13168), Beograd Surčin (13272), Beograd Košutnjak (13275), and Szeged (12982), Hungary (Figure 1). For the sake of brevity, only the most relevant observations associated with the analyzed meteorological situation and study area are discussed and presented in this study. Beograd Surčin is also known as Belgrade Nikola Tesla Airport, with ICAO code LYBE [23]. Additionally, METAR (Meteorological Aerodrome Report) and TAF (Terminal Aerodrome Forecast) aviation weather reports were used in the analysis. TAF and METAR are standardized aviation weather observation and forecasting formats defined by ICAO and WMO [8,24]. METAR and TAF for LYBE, Batajnica Military Air Base (LYBT), Osijek Airport (LDOS), Pécs–Pogány Airport (LHPP), Budapest Ferenc Liszt International Airport (LHBP), Kecskemét Air Base (LHKE), Arad International Airport (LRAR), and Timișoara Traian Vuia International Airport (LRTR) were used in the analysis. Meteorological observations from nearby airports, combined with satellite imagery (Figure 1), were used to assess the spatial extent of fog occurrence over the Pannonian Basin.

Figure 1 *Locations of SYNOP stations (red), airport meteorological observation and forecast stations (green), Subotica Airport – LYSU (purple), and radiosonde measurement sites (blue) within the Vojvodina region. Source: adapted from Windy.com*

The satellite analysis was performed using Meteosat geostationary satellite imagery distributed by EUMETSAT [25].

Synoptic surface and upper-level analysis charts provided by the Deutscher Wetterdienst (DWD) were used to analyze the large-scale atmospheric conditions during the event [26].

Upper-air conditions were analyzed using radiosonde (upper-air sounding) data. Radiosonde measurements provide vertical profiles of temperature, relative humidity, pressure, and wind in the atmosphere [27] (Figure 1).

Synoptic Situation Analysis

An analysis of the surface pressure field indicated the presence of an anticyclone, *i.e.*, a weak pressure-gradient field associated with a high-pressure system over the Balkan Peninsula. The analysis of upper-air charts further confirmed the influence of the high-pressure system through a pronounced anticyclonic ridge extending across parts of Central, Southern, and Southeastern Europe, with its axis positioned over Serbia and the Balkan Peninsula (Figure 2a, c, and d).

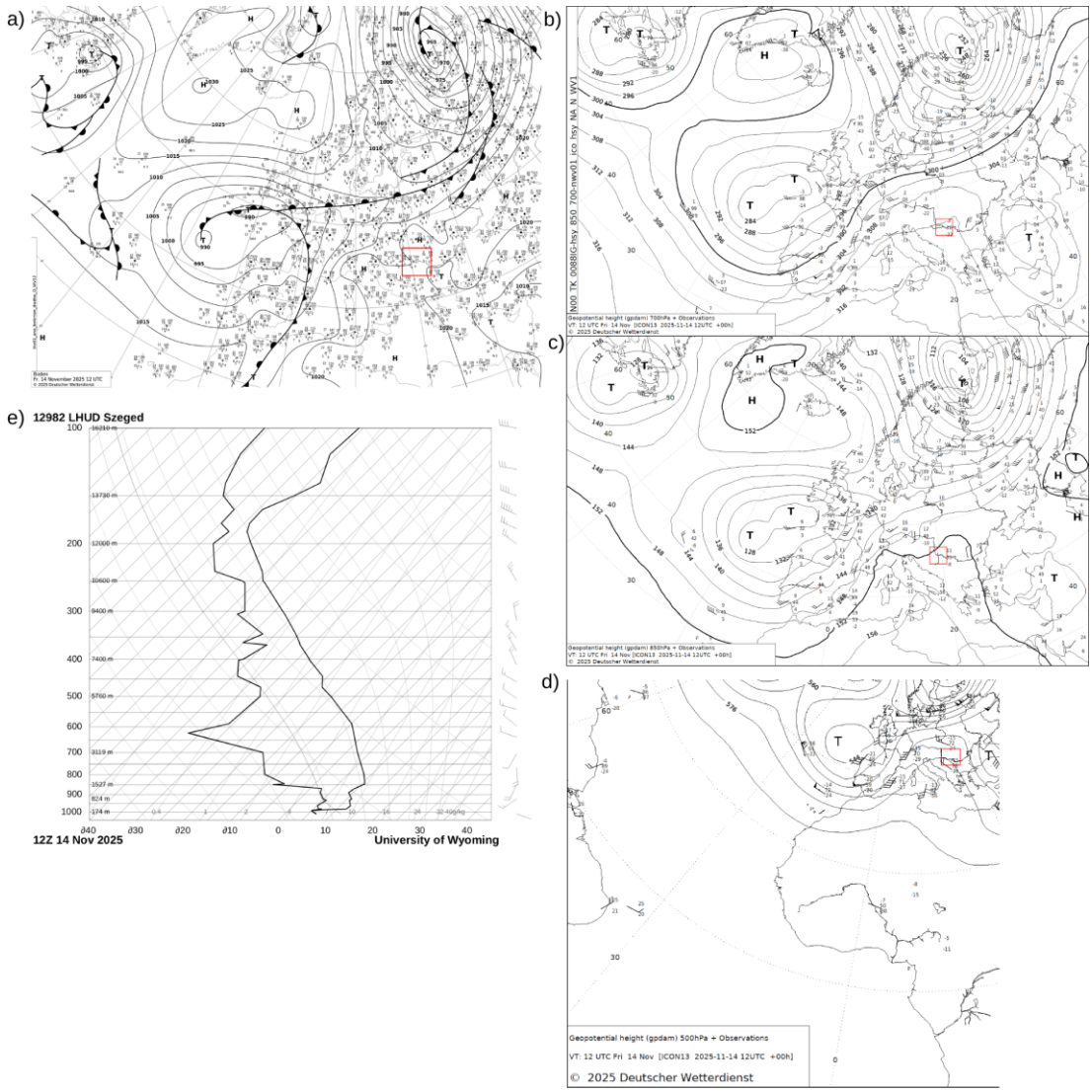

Figure 2 *Synoptic and upper-air meteorological conditions on 14 November 2025 at 12 UTC: (a) DWD surface synoptic analysis chart; (b–d) upper-level analysis charts at 700, 850, and 500 hPa; and (e) radiosonde (upper-air sounding) observations from Szeged. The red rectangle indicates the approximate location of Serbia within the analysis domain*

Radiosonde observations revealed a relatively warm and stable air mass for mid-November conditions, accompanied by a pronounced temperature inversion in the lower part of the vertical temperature profile. Surface observations also indicated weak near-surface winds, favoring nocturnal radiative cooling and fog formation (Figure 2b).

Satellite imagery revealed an extensive fog-covered area affecting most of the Vojvodina region during the night and early morning hours. Following sunrise (approximately 05:30 UTC), the spatial extent of the fog gradually decreased. By 09 UTC, the fog was primarily confined to areas north of Novi Sad. After 12 UTC, the fog remained largely limited to the northeastern part of Vojvodina.

As the dissipation process continued, around 13 UTC, a smaller fragmented portion of the fog field separated from the main area and persisted in the vicinity of the city of Subotica and Subotica Airport until approximately 14:30 UTC (Figure 3). The fragmented feature observed in satellite imagery may represent either residual fog or a transition toward low stratus cloudiness. After 14:30 UTC, the feature continued moving toward the northwest and had completely departed from the study area by 15 UTC according to available satellite observations.

Figure 3 *EUMETSAT satellite imagery showing fog distribution over the Vojvodina region at 14 UTC on 14 November 2025 [22]. The red rectangle indicates the approximate location of Subotica Airport (LYSU)*

SYNOP observations indicated that the Palić station reported fog-associated visibility reductions ranging from 0 to 600 m during the period from 06 to 18 UTC, when the station was operating in manual observation mode. Since air temperatures remained above 0 °C throughout the observed period, the event can be classified as warm fog.

Therefore, although satellite imagery indicated that the main fog-covered area had departed from the vicinity of Subotica by 15 UTC, surface observations continued to report reduced visibility conditions. This may indicate the persistence of a localized shallow fog layer or an area of restricted visibility that was not readily identifiable in the available satellite imagery.

According to the preliminary report issued by CINS, the accident occurred at approximately 15 LT (14 UTC). During this period, the fragmented feature identified in the satellite imagery was remained present within the study area.

From 13 UTC to 15 UTC, the main fog-affected area visible in satellite imagery extended northward toward Kecskemét Air Base (LHKE), where METAR observations reported reduced visibility due to fog, ranging from 200 to 350 m, accompanied by an overcast low stratus cloud layer with a cloud base at 200 ft (approximately 60 m).

CONCLUSION

It can therefore be concluded that the area of Subotica Airport was affected by fog or very low stratus cloudiness at the time of the accident. However, whether these meteorological conditions directly contributed to the accident remains to be determined by the official investigation. Due to its relatively small runway dimensions and localized fog occurrence, Subotica Airport may represent a suitable case study for the potential application of fog dispersion methods. Since the analyzed event was characterized by warm fog conditions, recently proposed warm fog dispersion techniques described by [14] may be applicable in similar operational environments.

The application of fog dispersion techniques at similar small airports and airfields could potentially provide significant benefits for aviation safety under low-visibility conditions. However, further investigations are necessary, particularly regarding the environmental, operational feasibility, and effectiveness under real atmospheric conditions.

REFERENCES

[1] World Meteorological Organization. International Cloud Atlas: Fog as seen from aircraft. 2017. Available from: https://cloudatlas.wmo.int/en/fog-as-seen-from-aircraft.html

[2] Center for Investigation of Accidents in Transport (CINS). Preliminary report on the accident involving Piper PA-38-112 Tomahawk YU-DPV near Subotica/Bikovo Airfield (LYSU), 14 November 2025. 2025. Available from: https://cins.gov.rs/wp-content/uploads/2025/11/03-25-1.pdf

[3] Ćurić M. Modifikacija vremena. Beograd: RHMZ; 2001. p. 236.

[4] Silverman BA. Fog and stratus dissipation technology. In: Hess WN, editor. Weather and climate modification. New York: John Wiley; 1986. p. 355–385.

[5] World Meteorological Organization. International cloud atlas: Manual on the observation of clouds and other meteors. 2017. Available from: https://cloudatlas.wmo.int/

[6] American Meteorological Society. Glossary of meteorology. Available from: https://glossary.ametsoc.org/

[7] Silverman BA, Weinstein AI. Fog. In: Hess WN, editor. Weather and climate modification. New York: John Wiley; 1974. p. 355–385.

[8] World Meteorological Organization. Manual on Codes: International Codes. Geneva: WMO; 2025. Available from: https://library.wmo.int/idurl/4/68695

[9] World Meteorological Organization. Aviation hazards related to winter weather. Geneva: WMO; 2021. Available from: https://wmo.int/

[10] Federal Aviation Administration. Aviation weather handbook (FAA-H-8083-28). Washington, DC: U.S. Department of Transportation; 2022. Available from: https://www.faa.gov/regulations_policies/handbooks_manuals/aviation/aviation_weather_handbook

[11] Dennis AS. Weather modification by cloud seeding. New York: Academic Press; 1980. p. 267.

[12] Kachurin LG. Fizicheskie osnovi vozdeistvija na atmosfernie procesi. Leningrad: Gidrometeoizdat; 1978. p. 364.

[13] Milošević D, *et al*. Experiment of supercooled fog dispersal at Sarajevo airport and skiing slopes of the 14th Winter Olympic Games. In: Proceedings of the 4th WMO Scientific Conference on Weather Modification; 1985 Aug 12–14; Honolulu, USA. 1985. p. 633–638.

[14] Khalid, S., Gupta, S.K., Chakkaravarthy, M., *et al*. Int J Aeronaut Space Sci. 2026, 27, 2423–2450.

[15] World Meteorological Organization. WMO statement on weather modification. 2025. Available from: https://public.wmo.int/content/wmo-statement-weather-modification

[16] Robinson, E., Thuman, W.C., Wiggins, E. Arctic. 1957, 10(2), 89–104.

[17] Yang, J., Li, J., Chen, M., *et al*. Atmos Chem Phys. 2024, 24, 13833–13848.

[18] Jung, S., J Wetl Res. 2026, 28(2), 72–81.

[19] Airport-data.com. Information about Belgrade Nikola Tesla International Airport (LYBE/BEG). Available from: https://airport-data.com/world-airports/LYBE-BEG/

[20] SMATSA. VFR Aeronautical Information Publication Serbia – Aerodrome LYSU Subotica. Available from: https://smatsa.rs/upload/vfraip/published/pdf/adr/VFR_LY_AD_2_LYSU_en.pdf.

[21] World Meteorological Organization. OSCAR/Surface Metadata Database. 2026. Available from: https://oscar.wmo.int/surface.

[22] World Meteorological Organization. WMO Publication No. 9, Volume A: Observing Stations. Geneva: WMO; 2026. Available from: https://community.wmo.int/site/knowledge-hub/programmes-and-initiatives/wmo-integrated-global-observing-system-wigos/pub9-vola-legacy-page.

[23] International Civil Aviation Organization. Location Indicators. 2025. Available from: https://store.icao.int/en/location-indicators-doc-7910

[24] International Civil Aviation Organization. Meteorological Service for International Air Navigation (Annex 3 to the Convention on International Civil Aviation). Montreal: ICAO; 2025.

[25] European Organisation for the Exploitation of Meteorological Satellites. Meteosat Series. Darmstadt: EUMETSAT; 2026. Available from: https://www.eumetsat.int/our-satellites/meteosat-series

[26] Deutscher Wetterdienst. General Information on Analysis and Short-Term Forecast Charts Europe. Offenbach: DWD; 2026. Available from: https://www.dwd.de/EN/specialusers/hobbymet/general_information_short_term_prognosis_europa.html

[27] World Meteorological Organization. Global Observing System (GOS). Geneva: WMO; 2026. Available from: https://wmo.int/activities/global-observing-system-gos/global-observing-system-gos

EcoTER'26
eco.tfbor.bg.ac.rs
32nd International Conference
Ecological Truth & Environmental Research
24–26 June 2026, Hotel Sunce,
Sokobanja, Serbia

Original Research

MICRO AND MESOPLASTIC PARTICLES IN WATER AND SEDIMENT IN SPECIAL NATURE RESERVE "OBEDSKA BARA"

DOI: 10.5937/EcoTER26590D

Vesna Djikanović[1,a*], Jelena S. Vranković[1,b], Katarina Jovičić[1,c]

[1] Department of Hydroecology and Water Protection, Institute for Biological Research "Siniša Stanković"—National Institute of the Republic of Serbia, University of Belgrade, Bulevar despota Stefana 142, 11108 Belgrade, SERBIA

[a] https://orcid.org/0000-0002-3876-3420

[b] https://orcid.org/0000-0002-2060-8633

[c] https://orcid.org/0000-0002-5105-1532

Abstract

Microplastic pollution is an emerging environmental issue affecting freshwater ecosystems, including protected areas. This study provides a preliminary assessment of microplastic occurrence in abiotic components (water and sediment) of the Special Nature Reserve "Obedska bara", a wetland of high ecological importance within the Danube River Basin. Samples were collected from two localities, followed by density separation and microscopic identification. Microplastics were detected in all water samples and in one sediment sample, with a total of nine particles identified. Fibres were dominant (eight particles), while one fragment was recorded. Particle lengths ranged from 0.5 to 16 mm, with white, red, and black fibres prevailing. The predominance of fibres suggests inputs from domestic wastewater, textile sources, and local anthropogenic activities. Although the detected abundance was low, the presence of microplastics in this protected ecosystem highlights their widespread distribution and potential ecological relevance. These findings represent a preliminary baseline and emphasize the need for further research involving increased sampling intensity, seasonal monitoring, and advanced analytical techniques to better understand microplastic dynamics in freshwater systems.

Keywords: freshwater, abiotic components, microplastic, fibres.

INTRODUCTION

There is increasing scientific and public concern over the presence of microplastics in the natural environment. Plastic pollution represents a complex transboundary environmental problem that requires coordinated cross-border initiatives and broad-based awareness-raising efforts among diverse stakeholders at local, national, and global levels. Microplastics have been detected in a wide range of aquatic environments, including freshwater systems such as rivers and lakes, transitional systems such as estuaries, and marine ecosystems [1].

Freshwater ecosystems are increasingly recognized as important pathways and sinks for microplastic pollution. Microplastics may negatively affect biodiversity, ecosystem

* *djiki@ibiss.bg.ac.rs*

functioning, food security, and potentially human health. Although marine systems have been extensively studied, research on freshwater microplastics has gained momentum only in recent years [1,2].

Microplastics are commonly defined as plastic particles smaller than 5 mm [3]. These particles vary widely in shape, size, and polymer type.

The Special Nature Reserve (SNR) “Obedska bara” (Ramsar site No. 136) is one of the oldest protected areas in Europe, having been under protection since 1874. It is characterised by high biodiversity and ecological importance within the Danube River Basin [4]. Despite its protected status, this ecosystem is exposed to various anthropogenic pressures.

The aim of this study was to detect and analyse the presence of microplastics in abiotic components (water and sediment) of the SNR “Obedska bara”, as a preliminary assessment of microplastic pollution in this protected freshwater ecosystem.

MATERIALS AND METHODS

Abiota samples were collected from two locations of the SNR "Obedska bara", Krstonošića okno (N 44.737054, E 20.044319), and Vok canal (N 44.735653, E 20.042796) (Figure 1).

Figure 1 *Map of the sampling locations, SNR "Obedska bara"*

Basic physico-chemical water parameters were measured at both sites. The parameter values are shown in Table 1.

Table 1 *Physico-chemical water quality parameters*

	Krstonošića okno	Vok canal
temperature (^{o}C)	19.8	22.5
O_2 (mg/l)	8.14	7.08
saturation (%)	92.8	84.3
conductivity (µS/cm)	422	436
pH	7.698	8.029
transparency (m)	1.5	2.8
NO_2^- (mg/l)	<0.01	0.02
NO_3^- (mg/l)	0.31	0.94

At each site, three water and three sediment samples were collected. Water samples were collected using a planktonic net (mesh size 200 µm) along a 30 m transect, while sediment samples were collected with a Van Veen grab (Figure 2). Water samples were filtered directly, while sediment samples were processed using density separation.

Figure 2 *Collecting of abiota samples*

Approximately 200 g of wet sediment was mixed with 500 mL of saturated NaCl solution in a glass container. The suspension was left to settle for 24 hours, after which the supernatant was filtered. Filtration was performed using cellulose membrane filters (pore size 8 µm; diameter 47 mm). Filters were examined under a stereomicroscope (Carl Zeiss Stemi 508), and suspected microplastic particles were identified based on visual characteristics such as colour, shape, and flexibility. Preventive measures were applied to minimize contamination, including the use of glassware and careful handling of samples.

RESULTS AND DISCUSSION

Microplastics were detected in all analysed water samples and in one sediment sample. A total of nine particles were identified, including eight fibres and one fragment. Although the total number of detected particles was relatively low, the results provide important preliminary insight into microplastic contamination in this area. Fibres were white (8), red (1), and black (1), with lengths ranging from 0.5 to 16 mm. The types and length ranges of plastic particles found in water and sediment are shown in Table 2.

Table 2 *Types and length ranges of plastic particles*

Water samples		Sediment samples	
type	length range (mm)	type	length range (mm)
white fibres	1 – 16	black fibres	0.5
red fibres	5		
red fragment	0.5		

The dominance of fibres among the detected particles is consistent with numerous studies conducted in freshwater environments, where fibres are frequently reported as the most abundant type of microplastics [3]. Fibres are commonly associated with domestic wastewater, synthetic textiles, fishing activities, and the degradation of larger plastic materials [5–7]. Their prevalence in this study may indicate the influence of nearby anthropogenic activities, including recreational use of the area and potential inputs from surrounding settlements.

The relatively low number of detected particles may be attributed to several factors, including limited sampling effort, small sample size, and methodological constraints related to visual identification. It is also possible that seasonal variation and hydrological conditions at the time of sampling influenced microplastic distribution and detectability. Therefore, the obtained results should be interpreted as a preliminary assessment rather than a comprehensive evaluation of microplastic pollution [8].

The presence of microplastics in water, contrasted with their limited occurrence in sediment, may be explained by particle characteristics and environmental conditions. Fibres, which dominated the samples, typically exhibit low density and high surface area, allowing them to remain suspended in the water column for extended periods [9]. Additionally, hydrodynamic conditions such as water flow, turbulence, and sediment composition may influence the deposition and accumulation of microplastics in sediments.

Furthermore, the ecological condition of the SNR “Obedska bara” has been affected by multiple anthropogenic pressures, including hydrological modifications, eutrophication, and sedimentation processes. These factors may indirectly contribute to the transport, redistribution, and retention of microplastics within the ecosystem. The detection of microplastics in such a protected area highlights the widespread nature of plastic pollution and its ability to reach even relatively preserved habitats [10]. In addition, anthropogenic pressures such as hydrological alterations, eutrophication, and land-use changes may contribute to the introduction and redistribution of microplastics within the reserve.

Although the abundance of microplastics was low, their presence raises concerns due to their potential ecological impacts. Microplastics can act as carriers of pollutants, facilitate the transport of invasive microorganisms, and be ingested by aquatic organisms, potentially leading to adverse biological effects. Therefore, even low concentrations of microplastics may be ecologically relevant, particularly in sensitive and protected ecosystems [11].

Future studies should aim to increase sampling intensity, include seasonal monitoring, and apply more advanced analytical techniques, such as spectroscopic identification, to confirm polymer types and improve the accuracy of microplastic detection. Integrating abiotic and biotic compartments would also provide a more comprehensive understanding of microplastic dynamics in freshwater ecosystems.

CONCLUSION

Microplastics were detected in water samples from the SNR “Obedska bara”, indicating that even protected freshwater ecosystems are not exempt from plastic pollution. The predominance of fibres suggests textile-related sources as a major contributor. Although the

detected abundance was low, this study provides a preliminary insight into the occurrence of microplastics in this ecologically important area. Further research with increased sampling effort and more advanced analytical techniques is needed to better understand the distribution, sources, and ecological implications of microplastics in freshwater protected areas.

ACKNOWLEDGEMENT

This research was supported by the Ministry of Science, Technological Development and Innovation of the Republic of Serbia, contract number 451-03-33/2026-03/200007, and the IPA-ADRION INTERREG programme of the European Union (ADRIPLAST00140). The content of this study aligns with the following United Nations Sustainable Development Goals, within the UN Agenda for Sustainable Development (Transforming our world: Agenda for Sustainable Development until 2030 – UN, 2015): Goals 6 and 14.

REFERENCES

[1] Wagner, M., Scherer, C., Alvarez-Muñoz, D. *et al.* Environ. Sci. Eur. 2014, 26(1), 1–9.

[2] Dris, R., Imhof, H., Sanchez, W. *et al.* Environ. Chem. 2015, 12, 539–550.

[3] Horton, A.A., Walton, A., Spurgeon, D.J. *et al.* Sci. Total Environ. 2017, 586, 127–141.

[4] Markićević, M. Bull. Fac. Geogr. 2002, 145–158.

[5] Mendoza L.M.R., Vargas, D.L., Balcer, M. Curr. Opin. Green Sustain. Chem. 2021, 32 100523.

[6] Ríos, J.M., Teixeira de Mello, F., De Feo, B. *et al.* Water 2022, 14(23).

[7] Napper, I.E., Thompson, R.C. Mar. Pollut. Bull. 2016, 112, 39–45.

[8] Prata, J.C., da Costa, J.P., Duarte, A.C. *et al.* TrAC Trends Anal. Chem. 2019, 110, 150–159.

[9] Enders, K., Käppler, A., Biniasch, O. *et al.* Sci Rep 9, 2019, 15207.

[10] Darwall WRT, Freyhof J, Lost fishes, who is counting? The extent of the threat to freshwater fish biodiversity. In Closs GP, Krkosek M, Olden JDE, editors. Conservation of Freshwater Fishes: Conservation Biology. Cambridge: Cambridge University Press; UK, 2015. p. 1–36.

[11] Wright, S.L., Thompson, R.C., Galloway, T.S. Environ. Pollut. 2013, 178, 483–492.

EcoTER'26
eco.tfbor.bg.ac.rs
32nd International Conference
Ecological Truth & Environmental Research
24–26 June 2026, Hotel Sunce,
Sokobanja, Serbia

Original Research

NUMERICAL ASSESSMENT OF THE IMPACT OF FLOATING PHOTOVOLTAIC SYSTEMS ON LAKE THERMAL REGIME

DOI: 10.5937/EcoTER26595P

Marko Pezdevšek[1], Andraž Roger[1], Matej Fike[1,a*], Klemen Sredenšek[1,b]

[1] University of Maribor, Faculty of Energy Technology, Hočevarjev trg 1, SI-8270 Krško, SLOVENIA

[a] https://orcid.org/0000-0001-6400-8798

[b] https://orcid.org/0000-0001-8301-6523

Abstract

This study examines the impact of floating photovoltaic (FPV) systems on lake thermal conditions using numerical modelling. A comparative analysis between a reference scenario without FPV coverage and a scenario with 50% surface coverage was performed using both one-dimensional (1D) and three-dimensional (3D) modelling approaches. The 1D model was applied to simulate vertical temperature profiles based on the assumption of dominant vertical heat transport and rapid horizontal mixing. It included key heat transfer processes such as shortwave and longwave radiation, latent and sensible heat fluxes, precipitation, and convective and conductive exchanges between the atmosphere and water column. In FPV scenarios, an additional greenhouse effect beneath photovoltaic modules was considered. The 3D modelling framework complemented the analysis by providing a spatially resolved representation of lake thermo-hydrodynamics. Computational domains were generated from bathymetric data and discretized using ICEM CFD, resulting in meshes of approximately 5 million elements per domain. Results indicate that FPV coverage modifies the lake's thermal balance by reducing solar radiation input and altering surface heat exchange processes. The strongest effects were observed in intermediate depths (5–20 m), where temperature reductions reached approximately 2 °C, particularly during peak summer conditions and late afternoon hours. In deeper layers (below 30 m), FPV influence was minimal. Overall, FPV systems significantly affect thermal stratification and vertical temperature distribution, primarily through reduced surface heating.

Keywords: floating photovoltaic, lake thermal regime, thermal stratification, numerical modelling, heat transfer.

INTRODUCTION

Lakes represent a fundamental component of the hydrosphere, acting as reservoirs and transport pathways for energy and matter between atmospheric, terrestrial, and aquatic systems. Due to their high thermal inertia and relatively long water residence times compared to other inland water bodies such as rivers and lagoons, lakes play an important role in regulating regional hydrological and climatic processes. In addition to their ecological significance, lakes provide essential ecosystem services, including freshwater supply, biodiversity support, recreation, and energy production. However, increasing anthropogenic

* *marko.pezdevsek@um.si*

pressures and climate-related changes continuously alter the physical and chemical characteristics of lake ecosystems, among which thermal conditions are particularly sensitive indicators of environmental change [1].

The thermal regime of a lake is governed by the balance between heat gains and losses, commonly expressed as the net heat flux exchanged between the lake and its surrounding environment. These processes are strongly influenced by meteorological conditions, solar radiation, wind-induced mixing, and hydrological inputs, resulting in temporal variability ranging from diurnal to seasonal and long-term climatic scales. Most heat exchange occurs at the air-water interface through shortwave and longwave radiation, sensible and latent heat fluxes, and evaporative cooling. Changes in these processes directly affect lake temperature profiles, thermal stratification, mixing dynamics, dissolved oxygen distribution, and overall ecosystem functioning [1].

In recent years, floating photovoltaic (FPV) systems have emerged as an increasingly attractive renewable energy solution due to their ability to generate electricity without occupying valuable terrestrial land resources. FPV installations are particularly suitable for artificial reservoirs and mining lakes, where large water surfaces can be utilized for solar energy production while potentially reducing evaporation losses. Nevertheless, the placement of FPV systems on lake surfaces modifies the radiative and turbulent heat exchange processes between water and atmosphere. By partially shading the water surface and altering local airflow conditions, FPV systems may influence water temperature, thermal stratification, and mixing processes, thereby affecting the ecological and physical dynamics of lakes.

To assess such impacts, various numerical modeling approaches have been developed for simulating lake thermal conditions. One-dimensional (1D) and three-dimensional (3D) hydrodynamic models are widely used to reproduce thermal stratification, vertical temperature profiles, and lake–atmosphere interactions. Wang *et al*. [2] applied a 1D model to simulate thermal stratification in Lake Qiandaohu using time-dependent light attenuation coefficients and turbulent diffusivity parameters. Similarly, Šarović *et al*. [3] developed a 1D model for warm monomictic lakes and demonstrated its applicability for both short-term and long-term thermal simulations. Gaillard *et al*. [4] evaluated a multi-column lake model for Lake Geneva as a computationally efficient alternative to fully 3D approaches, while Gu *et al*. [5] and Tasnim *et al*. [6] compared the performance of 1D and 3D models in simulating thermal and oxygen dynamics.

Alongside advances in lake thermal modeling, recent studies have increasingly focused on understanding the thermal impacts of FPV systems. Exley *et al*. [7], using the MyLake model, showed that FPV installations generally reduce surface water temperatures, shorten stratification periods, and increase mixing depth, with the magnitude of impacts depending on the extent of surface coverage and system configuration. Liu *et al*. [8] reported that FPV systems cool surface waters during daytime while retaining heat during nighttime, thereby reducing diurnal temperature variability and altering local microclimatic conditions. Field measurements by Ilgen *et al*. [9] confirmed that FPV systems can cool upper water layers by up to 2.8 °C during daytime conditions. Furthermore, Yang *et al*. [10] demonstrated that FPV installations reduce incoming shortwave radiation while enhancing longwave heat retention beneath photovoltaic modules, leading to modifications in the lake heat balance.

In this context, the present study investigates the potential influence of floating photovoltaic installations on the thermal regime of an artificial lake system. The primary objective is to quantitatively evaluate how different FPV coverage scenarios affect water temperature distributions, vertical thermal profiles, and seasonal thermal stratification. By applying established thermal modeling approaches and considering site-specific hydrological and meteorological conditions, the study aims to contribute to the broader understanding of FPV-lake interactions and to support the environmentally sustainable implementation of floating solar technologies.

1D MODEL

One-dimensional (1D) lake models are widely used for simulating thermal processes and vertical temperature dynamics in lakes. These models can be applied at the deepest part of a lake while accounting for the hypsographic curve, which describes the variation of lake surface area with depth, or they may rely on simplified geometric assumptions when detailed bathymetric data are unavailable. In such cases, the lake geometry is often approximated by an equivalent cylinder with a constant surface area equal to the lake surface area and an average depth. Alternatively, a simplified conical representation may be used when only the lake surface area and maximum depth are known.

Depending on the availability of observational data, 1D models can be calibrated either as whole-lake average models or as models representing individual measurement locations. This approach is particularly suitable for small and deep lakes, where vertical thermal variability dominates over lateral variability. The underlying assumption of 1D models is that horizontal mixing processes rapidly homogenize the water body, resulting in negligible horizontal density gradients and allowing the thermal structure to be described primarily along the vertical axis.

In this study, a 1D thermal model was applied to investigate the vertical temperature dynamics under scenarios without and with floating photovoltaic (FPV) coverage. The simulations incorporated the main heat transfer mechanisms governing lake thermal conditions, including shortwave and longwave radiation, latent and sensible heat fluxes, precipitation effects, and convective and conductive heat exchange between air and water layers. For scenarios involving FPV coverage, the additional greenhouse effect beneath the photovoltaic modules was also taken into account. The resulting vertical temperature distributions for the scenarios without and with FPV coverage are presented in Figures 1 and 2, respectively.

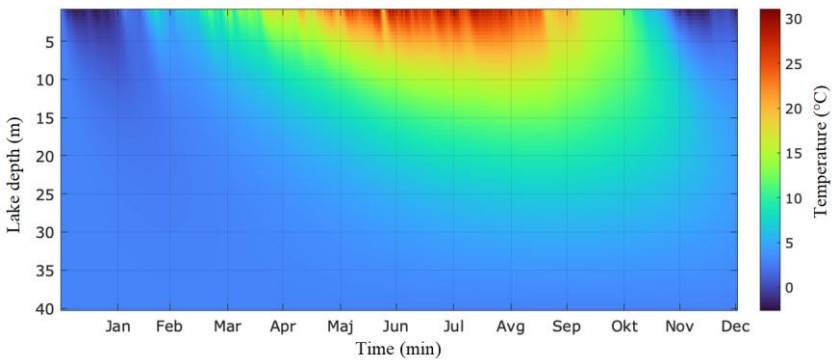

Figure 1 *The vertical temperature distributions for the scenarios without FPV*

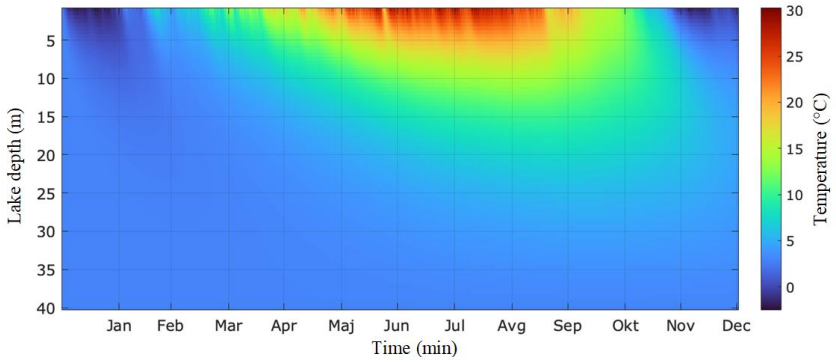

Figure 2 *The vertical temperature distributions for the scenarios with FPV*

3D MODEL

Three-dimensional (3D) models are used to simulate the complete thermo-hydrodynamic behavior of lakes, providing a realistic and detailed representation of the processes occurring within the water body. These models are particularly suitable for large water bodies or for simulations of specific processes where a high level of accuracy is required. In addition to temperature distribution, 3D models enable the simulation of flow fields and circulation patterns, allowing for a comprehensive understanding of lake dynamics.

The application of 3D models requires substantial computational resources as well as the availability of spatially distributed data for the specification of boundary conditions and model validation. Despite these requirements, 3D models provide valuable insight into complex physical processes in lakes and represent an important tool for both scientific research and water body management. For the present study, lake bathymetry was provided in LAS format and used to generate the computational geometry of the lake domain. Using the SolidWorks software package, two computational domains were created: the first representing the current lake conditions without floating photovoltaic (FPV) coverage, and the second representing a scenario with 50% surface coverage by FPV installations, as illustrated in Figure 3.

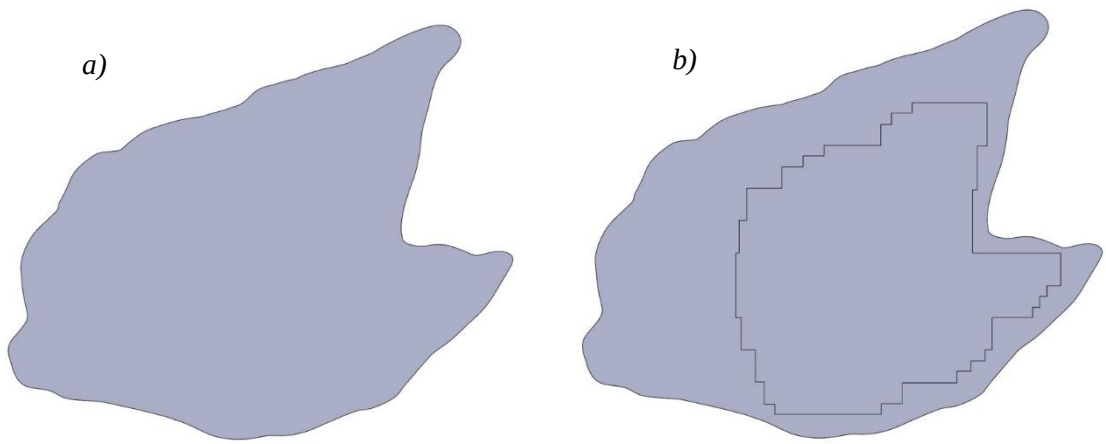

Figure 3 *a) Representsation of the current lake conditions without FPV coverage; b) a scenario with 50% surface coverage by FPV installations*

Computational meshes for both domains were generated using the ICEM CFD software package. Due to the geometric complexity of the lake bathymetry, the domains were discretized using tetrahedral elements. In the horizontal directions (x and y), the computational domain was meshed with an element size of 5 m, as shown in Figure 4.

In the vertical direction (z-direction, corresponding to depth), a prism-layer mesh was applied near the lake surface to improve the resolution of thermal stratification processes. For the upper 20 m of the water column, a vertical element height of 0.5 m was prescribed, while below 20 m depth the element height was gradually increased to 5 m. The final computational mesh consisted of approximately 5 million elements.

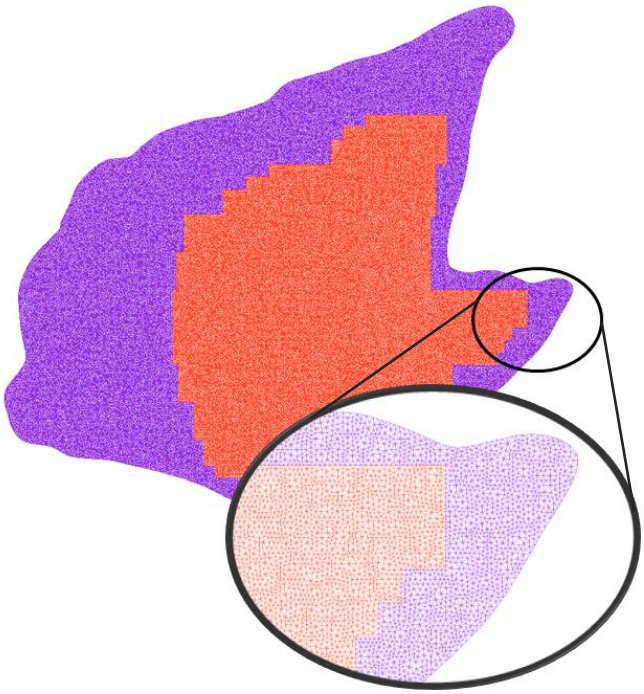

Figure 4 *Computational domain mesh*

The results of the 3D model analysis of vertical water temperature conditions under scenarios without and with floating photovoltaic (FPV) coverage are presented. The temperature calculations were based on governing equations which incorporate the main heat transfer mechanisms, including shortwave and longwave radiation, latent and sensible heat fluxes, precipitation effects, as well as convective and conductive heat exchange between air and water layers.

For both scenarios, transient simulations were performed using the Ansys CFX software package, which enables spatially resolved analysis of lake thermal conditions. The simulations were conducted for the warmest day of the year using a temporal resolution of 5 minutes. No-slip wall boundary conditions were prescribed at all solid domain surfaces, while a heat flux boundary condition was applied at the lake surface based on the equations used in the 1D model.

Table 1 demonstrates that FPV coverage influences lake water temperature differences (ΔT), with the magnitude of the effect depending on both time of day and water depth. At

06:00, the influence of FPV coverage is the smallest due to the low solar radiation intensity during the early morning hours. The smallest temperature difference was observed at a depth of 0.5 m (-0.44 °C), while the largest difference occurred between depths of 5 m and 10 m (-1.97 °C). At 12:00, when solar radiation intensity reaches its maximum, the temperature differences increase. The smallest temperature difference remained at 0.5 m depth (-0.52 °C), whereas the largest difference was again observed between 5 m and 10 m depth (-1.97 °C).

Table 1 *Average water temperature differences between scenarios with and without FPV coverage at different lake depths at 06:00, 12:00, and 18:00*

Depth/Time	**6:00**	**12:00**	**18:00**
0.5 m	- 0.44 °C	- 0.52 °C	- 0.97 °C
0.5 m – 2 m	- 1.01 °C	- 1.18 °C	- 1.38 °C
2 m – 5 m	- 1.73 °C	- 1.73 °C	- 1.73 °C
5 m – 10 m	- 1.97 °C	- 1.97 °C	- 1.97 °C
10 m – 20 m	-1.69 °C	-1.69 °C	-1.69 °C
20 m – 30 m	-0.85 °C	-0.85 °C	-0.85 °C
30 m – 40 m	- 0.22 °C	- 0.22 °C	- 0.22 °C

The greatest temperature differences occurred at 18:00, when the cumulative daytime heating effect in the scenario without FPV coverage reached its maximum. In the reference scenario without FPV, the lake surface was exposed to direct solar radiation throughout the day, resulting in higher water temperatures compared to the FPV-covered scenario, where the photovoltaic modules reduced incoming solar radiation. Consequently, the largest temperature differences between the two scenarios were observed during the evening hours, when the accumulated thermal effect was most pronounced. The smallest temperature difference at this time occurred between depths of 30 m and 40 m (-0.22 °C), while the largest difference remained between 5 m and 10 m depth (-1.97 °C).

Overall, the most significant temperature reductions were observed within the intermediate depth range between 5 m and 20 m, where temperature differences ranged from approximately -1.69 °C to -1.97 °C. These results confirm that FPV coverage substantially reduces water temperatures within these layers, whereas its influence becomes considerably weaker in deeper parts of the lake.

CONCLUSION

This study investigated the influence of floating photovoltaic (FPV) coverage on the thermal conditions of a lake system, with particular emphasis on seasonal temperature variability and the effects of partial surface coverage. Two scenarios were analyzed: a reference case without FPV coverage and a scenario with 50% surface coverage, enabling a comparative assessment of the impact of FPV installations on lake warming and cooling processes.

The analysis of the warmest day of the year, 20 June, demonstrated that the most pronounced temperature differences between the two scenarios occurred within the water layers between 5 m and 20 m depth, where reductions in water temperature ranged from approximately -1.69 °C to -1.97 °C. These results indicate that FPV coverage has the

strongest influence within the intermediate water layers, primarily due to the reduction of incoming solar radiation and the consequent limitation of daytime water heating beneath the photovoltaic modules. In deeper layers below 30 m depth, the impact of FPV coverage was considerably smaller, with temperature differences remaining below -0.22 °C, suggesting that reduced warming of the upper water layers has only a limited influence on deeper thermal conditions.

The largest temperature differences were observed during the late afternoon hours, when the cumulative daytime heating effect in the reference scenario without FPV coverage was most pronounced. The stronger solar energy absorption in the uncovered scenario resulted in significantly warmer water temperatures compared to the FPV-covered case. Consequently, the influence of FPV installations on the thermal regime was most evident within the upper and intermediate layers of the water column, while remaining negligible in deeper regions of the lake.

The obtained results confirm that FPV systems modify the thermal balance of lakes primarily through the reduction of incoming solar radiation and the suppression of surface water warming. The simulations indicate that FPV coverage can reduce water temperatures by approximately 2 °C within intermediate depth layers, which may have important implications for lake thermal stratification, mixing processes, and aquatic ecosystems.

Overall, the study provides a comprehensive assessment of the impact of floating photovoltaic installations on lake thermal conditions and contributes valuable information for future environmental evaluations and sustainable spatial planning of FPV systems.

REFERENCES

[1] Piccolroaz, S., Zhu, S., Ladwig, R., *et al*. Rev. Geophys. 2024, 62.

[2] Wang, X., Wang, W., He, Y., *et al*. J. Hydrol. 2023, 618, 129184.

[3] Šarović, K., Burić, M., Klaić, Z.B. Geosci. Model Dev. 2022, 15, 8349–8375.

[4] Gaillard, R., Perroud, M., Goyette, S., *et al*. Sci. Rep. 2022, 12, 353.

[5] Gu, H., Lu, B., Qi, C., *et al*. Water. 2021, 13, 913.

[6] Tasnim, B., Fang, X., Hayworth, J.S., Water. 2024, 16, 317.

[7] Exley, G., Armstrong, A., Page, T., *et al*. Sol. Energy. 2021, 219, 24–33.

[8] Liu, Z., Ma, C., Yang, Y., *et al*. J. Environ. Manage. 2024, 365, 121494.

[9] Ilgen, K., Schindler, D., Wieland, S., *et al*. Sci. Rep. 2023, 13, 7932.

[10] Yang, P., Chua, L.H.C., Irvine, K.N., *et al*. Water Res. 2021, 206, 117745.

EcoTER'26
eco.tfbor.bg.ac.rs
32nd International Conference
Ecological Truth & Environmental Research
24–26 June 2026, Hotel Sunce,
Sokobanja, Serbia

Original Research

SOURCE-ASSOCIATED HEALTH RISKS RELATED TO METALLIC AND CARBONACEOUS PM_{10} FRACTION AT TWO URBAN SITES IN SERBIA

DOI: 10.5937/EcoTER26602P

Bojana Petrović[1,a*], Maja Jovanović[1,b], Bojan Radović[2,c], Renata Kovačević[2,d], Milena Jovašević-Stojanović[1,e]

[1] University of Belgrade, Vinča Institute of Nuclear Sciences, The National Institute of the Republic of Serbia, Mike Petrovića Alasa 12-14, 11351, Vinča, Belgrade, SERBIA

[2] Mining and Metallurgy Institute Bor, Alberta Ajnštajna 1, 19210, Bor, SERBIA

[a] https://orcid.org/0009-0004-4089-4683

[b] https://orcid.org/0000-0002-0780-9801

[c] https://orcid.org/0000-0003-4884-1418

[d] https://orcid.org/0000-0003-4108-0855

[e] https://orcid.org/0000-0003-0765-6603

Abstract

Source apportionment studies and continuous monitoring of air pollutants are crucial for developing effective PM_{10} mitigation strategies. In addition to source identification and quantification, assessment of health risks posed by PM sources may contribute to more complete understanding of human exposure to this pollutant. Following the USEPA methodology, source-specific health risk assessment was performed in two urban background sites in Belgrade and Bor. For non-carcinogenic risk assessment included species were As, Cd, Pb, Ni, Sb, Se and EC, while for carcinogenic As, Cd, Pb, Ni, and EC were used. In Belgrade, non-carcinogenic risk was characterized as acceptable while smelter factor in Bor presented a hazard quotient (HQ) of 1.3, resulting in HI of 2.07, indicating unacceptable risk. The biggest contributor to total non-carcinogenic risk in Belgrade was traffic/industry and smelter in Bor. Carcinogenic risks (CR) for each source in both cities fell within the range of potential concern but total carcinogenic risk (TCR) was above 1×10^{-4} so the carcinogenic risk in both cities was classified as unacceptable. Results of one-year long WeBaSOOP campaign indicate that contributions of sources to PM_{10} mass concentration, as determined by positive matrix factorization, may differ from their contributions to health risks. Therefore, health risk assessment findings can provide valuable insights for policymakers when deriving PM_{10} mitigation measures.

Keywords: particulate matter, health risk, elemental carbon, heavy metals, source apportionment.

INTRODUCTION

Air pollution is a global challenge that affects both climate and human health. Although mitigations measures resulted in decease of air pollutants' levels in Europe (especially NOx

* *bojana.petrovic@vin.bg.ac.rs*

and SO_2) in the last decades [1], World Health Organization estimates that still 99% of the population lives in areas with unacceptable levels of pollutants, especially in areas like Northern Italy, Balkans and Eastern Europe [2,3]. In Serbia, the city of Bor, is known for its extensive copper deposits, which are among the largest in Europe. Therefore, the Mining-Metallurgical Complex Bor is considered as the primary source of environmental pollution in the region, due to emissions from the copper smelter, open pits, tailing ponds and associated industrial activities [4]. On the other hand, Belgrade, the capital of Serbia, with a population of approximately 1.7 million, and around 3 000 km^2 surface area, including inner city and surrounding settlements, due to its high-traffic arterial load, natural gas heating plants, proximity to an international airport, municipal landfill, coal thermal power plants, represents a complex urban environment with multiple sources of air pollution [5].

Among air pollutants, particulate matter (PM) represents the biggest health concern as it is classified as group 1 carcinogen, according to International Agency for Research on Cancer (IARC) [6]. IARC classified both outdoor polluted air and PM as carcinogenic based on the enough evidence that they may lead to development of lung cancer. PM represents heterogeneous mixture of chemicals which composition depends on the sources from which they originate [7]. Therefore, PM may consist of crustal elements (Al, Ti, Ca, Fe) if particles originate from mineral dust, trace elements (As, Cd, Pb, Ni, Cr, Cu, Sb, Sn, Se) if PM originates from industrial of traffic sources, as well as from wood or coal combustion [8]. Organic component includes presence of products of uncomplete combustion, like polycyclic aromatic hydrocarbons (PAHs) or products of fungal metabolism and growth like polyols [9]. These PM_{10} compounds exhibit varying toxic potentials, making both the size of the particles and their chemical composition critical predictors of PM toxicity [10].

According to the studies conducted so far, heavy metals (HMs) (e.g., As, Cd, Pb, Ni, Cr, Hg) are considered as important PM compounds from toxicological point of view [11,12]. WHO classified As, Cd, Pb and Hg among the chemicals of public concern while As, Cd, Ni and Cr are classified as carcinogenic to humans (group 1) by IARC. So, when evaluating health risk from PM_{10} exposure, it is important to take into consideration HMs even though they do not contribute substantially to the PM mass concentration. On the other hand, carbonaceous aerosols (organic carbon (OC) and elemental carbon (EC)) are often the largest component of PM. EC is emitted from the incomplete combustion of carbon-containing materials and is correlated with negative effects on both climate and health. However, health risk assessment studies that included EC are still limited [13]. Therefore, the aim of our study was to assess health risks from PM_{10} sources in relation to the presence of metallic and carbonaceous component, observed in Belgrade and Bor, Serbia.

MATERIALS AND METHODS

PM_{10} sampling, chemical characterization and PM_{10} source apportionment

PM_{10} sampling, chemical analysis of PM_{10}-bound HMs and EC and source apportionment of PM_{10} mass concentration during WeBaSOOP campaign in Belgrade (June 2023 – May 2024) and Bor (March 2023 – February 2024) were described in Petrovic *et al*. [14]. The source apportionment using positive matrix factorization (PMF) was used to identify independent factors that serve a proxy for PM_{10} emission sources. The PMF included 33

species (OC, EC, 4 ions, 27 elements, 10 organic tracers) in the model. For the source-specific health risk assessment, concentrations from the output that model assigned to each resolved factor were used in Eq. 1.

Source-related health risk assessment

To assess non-carcinogenic and carcinogenic health risk of specific factors apportioned by PMF in Bor and Belgrade during WeBaSOOP campaign, the Inhalation Dosimetry Methodology by USEPA was followed [15]. The risk analysis included only those species used in the PMF model that had available reference values for Inhalation Toxicity Reference Concentration (RfC) and Inhalation Unit Risk (IUR) in the Risk Integrated Information System (IRIS). HMs used for non-carcinogenic risk assessment in Belgrade were As, Cd, Ni, Pb and Sb while in Bor As, Cd, Ni, Pb, Sb and Se were considered. As more than 50% of Se values were below limit of detection, it was not included in non-carcinogenic risk assessment in Belgrade. In case of carcinogenic risk, As, Cd, Ni and Pb were included in both cities. To account for the influence of the carbonaceous fraction alongside the metallic fraction in the health risk, EC concentration values were incorporated. In case of EC, RfC and IUR values from IRIS database for diesel engine exhaust were used [13]. Inhalation exposure concentrations (IEC) for resident adult population in Belgrade and Bor were calculated following Eq. 1:

$$IEC = (CA \times ED \times EF \times ET)/ AT \quad (1)$$

Values of exposure parameters were taken from USEPA Exposure Factor Handbook [16]. CA represents HMs and EC concentration in the air (μg/m^3) obtained from PMF output where concentrations of HMs and EC were assigned to every factor. Exposure duration (ED) was 26 years, Exposure frequency (EF) 350 days per year (for residents), for Exposure time (ET) 24 hours per day were considered and Averaging time (AT) for non-carcinogenic risk was calculated as ED × 350 days/year × 24 hours/day while for carcinogenic risk, AT was 70 years × 350 days/year × 24 hours/day [15].

For non-carcinogenic risk, Hazard Quotients (HQ) for every HM and EC for each apportioned factor were calculated first (Eq. 2). The sum of HQs for each identified PM_{10} factor was Hazard Index (HI) (Eq. 3) which was used to classify the non-carcinogenic risk. It was considered acceptable when the HI value was below 1, and unacceptable when the HI value exceeded 1.

$$HQ = IEC/ (RfC \times 1000\ \mu g/mg) \quad (2)$$

$$HI = \sum HQs \quad (3)$$

Carcinogenic risk (CR) was calculated by multiplying IUR value for each HM and EC with IEC (Eq. 4) and total carcinogenic risk (TCR) (Eq. 5) was calculated as a sum of CRs for each factor in Belgrade and Bor. The acceptable TCR value is below 1×10^{-6}, TCR between

1×10^{-6} and 1×10^{-4} represent possible risk and values higher than 1×10^{-4} indicate unacceptable risk [17,18].

$$CR = IEC \times IUR \quad (4)$$

$$TCR = \sum CRs \quad (5)$$

RESULTS AND DISCUSSION

PM_{10} source apportionment

After the PMF analysis, seven factors were resolved in Belgrade and eight in Bor. In Belgrade, resolved factors were mineral dust (MD), biomass burning (BB), ammonium sulphate (SUL), primary biological aerosol particles (PBAP), biogenic secondary organic aerosol from isoprene ($BSOA_{Isoprene}$) and long-range transport and local NaCl mixed with combustion (NaCl/comb) [14]. In Bor, PMF resulted in 8 factors: $BSOA_{Isoprene,}$ Mixed combustion (MIXcomb), MD, secondary inorganic aerosol (SIA), Industrial dust (ID), PBAP, Smelter (SM) and BB [In preparation].

Source-related health risk assessment

Non-carcinogenic health risk assessment

Traditional health risk assessment methods do not differentiate risks from natural, anthropogenic, and secondary PM sources. Therefore, allocating health risks to the distinct sources identified by PMF is essential for better understanding source-specific health impacts. [13]. In Belgrade, obtained HQ values for every factor were below 1 and their sum resulted in HI value of 0.46 so non-carcinogenic risk from exposure to HMs and EC in the capital of Serbia was classified as acceptable (Table 1). The biggest HQ value was obtained for traffic/industry factor, then biomass burning and NaCl/comb factors, however, all values were below 1. In Bor, obtained HQ values were below 1 except for smelter factor (HQ = 1.3). The HI value for Bor was 2.07 so non-carcinogenic risk was characterized as unacceptable. After the smelter factor, biomass burning, and mixed combustion contributed the most to non-carcinogenic risk in Bor, but its values were negligible in comparison with $HQ_{smelter}$. The city of Bor is considered as a pollution “hot spot” at both the local and regional levels due to the nonferrous metallurgical industrial complex located in close proximity to the urban area, within sight and walking distance of residential zones. Until 2016, the outdated pyrometallurgy technology for copper production was applied [19] and since 2016, new technology for the melting copper concentrates in the smelter is used. However, according to our results, smelter activities still pose health risk for Bor inhabitants, mainly due to high As content in this factor. A study from 10 years ago, conducted by Jovanovic *et al.* [20] emphasised that Bor is more polluted by HMs, while Belgrade is more polluted by carbonaceous aerosols. EC, emitted from the combustion of fossil fuels such as diesel, coal, and biomass, was observed at higher levels in Belgrade during the heating season due to biomass burning, while elevated levels during spring and summer are likely associated with more pronounced traffic emissions in the city, compared to Bor [14].

The contributions of individual HMs and EC to the HQs varied among the PM_{10} factors. In Belgrade, the highest HQ values were obtained for EC in case of BB, TRA/IND and $BSOA_{Isoprene}$ factors. EC contributed around 50% to the HQs of SUL, NaCl/comb and PBAP factors also. Beside EC, Ni was the second dominant compound in risk contribution, with biggest contribution in NaCl/comb, MD, SUL and PBAP factors. The presence of EC in PBAP and $BSOA_{Isoprene}$ factors was less expected result. EC in these factors was observed in other PMF studies in Europe [9]. EC presence in factors from biological origin may be explained by the fact that, during OC/EC analysis, some types of PBAP char and evolve as EC [21]. In Bor, unlike in Belgrade, HQ values of HMs contributed the most to the HI (Table 2). HQ_{As} had the highest contribution to most of the apportioned factors – ID, SM, SIA, MD, BB and $BSOA_{Isoprene}$. Beside As, Ni contributed significantly to the health risk from MIXcomb, PBAP and ID, and, in case of Cd, SM and BB. The presence of Ni in the PBAP and BSOA isoprene factors in both Belgrade and Bor may result from atmospheric mixing processes, such as road dust resuspension, leading to the adsorption of elements onto particles of biological origin [22].

Table 1 *HQ values in Belgrade*

	MD	BB	SUL	PBAP	$BSOA_{Isoprene}$	TRA/IND	NaCl/comb	HI
As	3.6E-03	1.4E-02	9.1E-03	2.3E-03	2.9E-03	1.3E-02	6.5E-03	
Cd	3.2E-04	4.3E-03	1.9E-03	7.5E-04	3.0E-04	4.1E-03	1.4E-03	
Pb	2.2E-04	1.1E-03	3.2E-04	3.2E-04	4.8E-04	1.9E-03	7.8E-04	
Ni	3.2E-02	3.9E-03	1.7E-02	3.2E-02	2.1E-03	2.2E-02	3.1E-02	
Sb	2.1E-04	1.7E-04	3.2E-04	3.0E-05	1.8E-04	1.9E-03	4.0E-04	
EC	0	5.5E-02	2.0E-02	2.9E-02	1.0E-02	1.0E-01	3.3E-02	
HQ	3.6E-02	7.9E-02	4.9E-02	6.4E-02	1.6E-02	1.5E-01	7.3E-02	4.6E-01

MD – mineral dust, BB – biomass burning, SUL – ammonium sulphate, PBAP – primary biological aerosol particles, $BSOA_{Isoprene}$ – biogenic secondary organic aerosol from isoprene, TRA/IND – traffic/industry, NaCl/comb – long-range transport and road salt/local combustion.

Table 2 *HQ values in Bor*

	$BSOA_{Isoprene}$	MIXcomb	MD	SIA	ID	PBAP	SM	BB	HI
As	2.6E-02	5.4E-03	2.0E-02	3.2E-02	8.9E-02	2.1E-02	6.7E-01	4.9E-02	
Cd	9.3E-03	1.1E-03	0	1.1E-02	0	1.1E-02	4.5E-01	5.5E-02	
Pb	2.0E-03	1.3E-03	2.5E-03	4.8E-03	1.4E-02	2.8E-03	5.9E-02	2.4E-03	
Ni	1.5E-02	1.2E-01	0	9.8E-03	4.2E-02	4.1E-02	6.0E-02	2.9E-02	
Sb	7.1E-04	1.7E-04	1.6E-03	4.9E-04	5.2E-04	4.1E-04	1.4E-03	1.8E-04	
Se	4.3E-06	2.9E-06	8.8E-08	1.4E-05	4.3E-05	6.4E-06	1.7E-04	6.2E-06	
EC	1.3E-02	4.0E-02	1.3E-02	1.4E-03	3.0E-05	1.1E-02	5.8E-02	7.2E-02	
HQ	6.6E-02	1.7E-01	3.7E-02	5.9E-02	1.4E-01	8.7E-02	**1.3E+00**	2.1E-01	2.07

$BSOA_{Isoprene}$ – biogenic secondary organic aerosol from isoprene, MIXcomb – mixed combustion, MD – mineral dust, SIA – secondary inorganic aerosol, ID – industrial dust, PBAP – primary biological aerosol particles, SM – smelter, BB – wood burning. HI value higher than 1 is in bold.

Carcinogenic health risk assessment

In case of carcinogenic risk, independent CR values for factors in Belgrade and Bor were within the range of possible health risk (between 1×10^{-6} and 1×10^{-4}), except mineral dust in Belgrade, where CR value was in range of acceptable risk (Table 3). However, the total

carcinogenic risk in both Belgrade and Bor were above 1×10^{-4} so the carcinogenic tisk in Belgrade was classified as unacceptable and so does in Bor. Although having similar TCR values, factor that contributed the most to TCR in Belgrade was TRA/IND while SM contributed the most in Bor. EC was the dominant species contributing the most to CR in both Belgrade and Bor. Exceptions were the ID, SM, and SIA factors in Bor, where As contributed significantly to the CR values (Tables 3 and 4). The study of Li *et al.* [23] observed the highest total health risks, both carcinogenic and non-carcinogenic, from mining and smelting activities in region of Central China. According to WeBaSOOP campaign results smelting activities still represent the biggest health concern, in case of both non-carcinogenic and carcinogenic risk even though new technologies in smelting facility were applied in 2016 [19]. In the case of Belgrade, higher EC concentration and, consequently, the high contribution of the traffic factor to carcinogenic risk, may be attributed to the fact that passenger car fleet in Serbia primarily consist of imported, fossil-fuelled second-hand cars [24]. In concordance of our study were results of source-oriented health risk assessment where factor associated with road dust and petroleum volatilization contributed the most to the total cancer risk in Belgrade city centre [25].

Table 3 *CR values in Belgrade*

	MD	BB	SUL	PBAP	$BSOA_{Isoprene}$	TRA/IND	NaCl/comb	TCR
As	8.60E-08	3.45E-07	2.19E-07	5.47E-08	7.11E-08	3.05E-07	1.55E-07	
Cd	2.14E-09	2.85E-08	1.24E-08	4.99E-09	2.00E-09	2.77E-08	9.59E-09	
Pb	3.23E-09	1.64E-08	4.78E-09	4.80E-09	7.16E-09	2.83E-08	1.16E-08	
Ni	3.98E-08	4.89E-09	2.15E-08	3.97E-08	2.68E-09	2.73E-08	3.82E-08	
EC	0	3.06E-05	1.14E-05	1.61E-05	5.83E-06	5.76E-05	1.85E-05	
CR	1.31E-07	3.10E-05	1.17E-05	1.62E-05	5.91E-06	5.80E-05	1.87E-05	1.42E-04

MD – mineral dust, BB – biomass burning, SUL – ammonium sulphate, PBAP – primary biological aerosol particles, $BSOA_{Isoprene}$ – biogenic secondary organic aerosol from isoprene, TRA/IND – traffic/industry, NaCl/comb – long-range transport and road salt/local combustion.

Table 4 *CR values in Bor*

	$BSOA_{Isoprene}$	MIXcomb	MD	SIA	ID	PBAP	SM	BB	TCR
As	6.17E-07	1.30E-07	4.74E-07	7.58E-07	2.13E-06	5.03E-07	1.61E-05	1.18E-06	
Cd	6.19E-08	7.32E-09	0	7.50E-08	0	7.46E-08	3.02E-06	3.66E-07	
Pb	3.04E-08	1.94E-08	3.76E-08	7.18E-08	2.01E-07	4.09E-08	8.75E-07	3.58E-08	
Ni	1.88E-08	1.54E-07	0	1.22E-08	5.25E-08	5.16E-08	7.44E-08	3.61E-08	
EC	7.33E-06	2.22E-05	7.24E-06	7.68E-07	1.65E-08	5.92E-06	3.24E-05	4.01E-05	
CR	8.06E-06	2.25E-05	7.75E-06	1.68E-06	2.40E-06	6.59E-06	5.25E-05	4.18E-05	1.43E-04

$BSOA_{Isoprene}$ – biogenic secondary organic aerosol from isoprene, MIXcomb – mixed combustion, MD – mineral dust, SIA – secondary inorganic aerosol, ID – industrial dust, PBAP – primary biological aerosol particles, SM – smelter, BB – wood burning.

Comparing the contributions of the apportioned factors to total PM_{10} mass concentrations and to non-carcinogenic and carcinogenic risks, differences may be observed. In Belgrade, the main contributors to PM_{10} mass were BB, SUL, and MD, whereas TRA/IND, BB, and NaCl/comb were the dominant contributors for the assessed risks. Although SM contributed with small percent to PM_{10} mass in Bor, it was the dominant contributor to both HI and TCR.

This difference in contributions to PM_{10} mass and health risks supports the hypothesis that PM mass alone is insufficient when dealing with health risks posed by atmospheric particles.

CONCLUSION

Conducting source apportionment studies in order to identify and quantify main sources of PM_{10} is essential for targeted mitigation measures. The mass concentration of PM is not the most relevant metric when dealing with health impacts of airborne particles since major properties (chemistry, shape, size distribution, solubility, speciation) driving PM toxicity are not taken into account within this single mass metric. Therefore, to examine health risk from PM exposure, health risk assessment may be used as additional tool to identify sources that pose the biggest health concern regardless its contribution to the PM_{10} mass.

Results from non-carcinogenic health risk assessment showed unacceptable risk in Bor based on HI value of 1.3 for smelter factor. On the other hand, results for Belgrade showed acceptable risk. In case of carcinogenic risk, all values in both Belgrade and Bor were within range of possible risk. These findings may give additional information for policymakers when deriving PM_{10} mitigation strategies, to take into consideration source toxicity, beside solely its contribution to PM_{10} mass.

ACKNOWLEDGEMENT

This research was funded by the European Union's Horizon Europe Research and Innovation Program under GA 101060170 (WeBaSOOP project) and the Ministry of Science, Technological Development, and Innovation of the Republic of Serbia under GA 451-03-33/2026-03/ 200017.

REFERENCES

[1] Aas, W., Fagerli, H., Alastuey, A., *et al*. Aerosol Air Qual. Res. 2024, 24(4), 230237.

[2] World Health Organization. Ambient (outdoor) air pollution. 2024. Available from: https://www.who.int/news-room/fact-sheets/detail/ambient-(outdoor)-air-quality-and-health

[3] Belis, C.A., Matkovic, V., Ballocci, M., *et al*. Environ. Int. 2023, 182, 108347.

[4] Šerbula, S.M., Živković, D.T., Radojević, A.A., *et al*. Hem. Ind. 2015, 69(1), 51–58.

[5] Ćirović, Ž., Stojanović, D.B., Davidović, M., *et al*. Environments 2026, 13, 47.

[6] IARC. IARC monographs on the evaluation of carcinogenic risks to humans; volume 109. Lyon, France: International Agency for Research on Cancer, 2016.

[7] Fushimi, A., Nakajima, D., Furuyama, A., *et al*. Sci. Total Environ. 2021, 773, 145614.

[8] Zheng, L., Wu, D., Chen, X., *et al*. Sci. Data 2024, 11, 1206.

[9] Waked, A., Favez, O., Alleman, L.Y., *et al*. Atmos. Chem. Phys. 2014, 14, 3325–46.

[10] Weber, S., Uzu, G., Favez, O., *et al*. Atmos. Chem. Phys. 2021, 21, 11353–78.

[11] Tian, Y., Jia, B., Zhao, P., *et al*. Environ. Pollut. 2022, 312, 120004.

[12] Arregocés, H.A., Bonivento, G.J., Ladino, L.A., *et al*. Environ. Sci. Pollut. Res. Int. 2023, 30, 125915–30.

[13] Shi, JL, Zhu, CS, Qu, Y, et al. J. Hazard. Mater. 2025, 492, 138094.

[14] Petrović, B., Alastuey, A., Yttri, K.E., *et al*. Atmos. Chem. Phys. 2026.

[15] USEPA. Risk Assessment Guidance for Superfund Volume I: Human Health Evaluation Manual (Part F, Supplemental Guidance for Inhalation Risk Assessment). Washington D.C. 2009.

[16] USEPA. Exposure Factors Handbook: 2011 Edition. Washington D.C. 2011.

[17] Nahin, M.N.I., Islam, M.S., Moniruzzaman, M., *et al*. Next Sustain. 2026, 7.

[18] Vukelić, D., Petrović, B., Miljaković, E.A., *et al*. Environ. Toxicol. 2026, 1–11.

[19] Kovačević, R., Radović, B., Manojlović, D., *et al*. Atmosphere 2024, 15, 1498.

[20] Jovanović, M.V., Savić, J., Kovačević, R., *et al*. Sci. Total Environ. 2020, 708, 135209.

[21] Yttri, K.E., Canonaco, F., Eckhardt, S., *et al*. Atmos. Chem. Phys. 2020.

[22] Samaké, A., Jaffrezo, J.L., Favez, O., *et al*. Atmos. Chem. Phys. 2019, 19, 3357–74.

[23] Li, Y., Liu, S., Luo, Z., *et al*. Pedosphere 2026.

[24] Mijailović, R., Marković, N., Pešić, D., *et al*. Transp. Res. D. Transp. Environ. 2019, 73, 352–66.

[25] Obradović, J., Vesković, J., Jovašević-Stojanović, M., *et al*. Build. Environ. 2025, 279, 113050.

EcoTER'26
eco.tfbor.bg.ac.rs
32nd International Conference
Ecological Truth & Environmental Research
24–26 June 2026, Hotel Sunce,
Sokobanja, Serbia

Original Research

CLIMATE-INDUCED PROJECT SCOPE CREEP AND COST OVERRUNS IN LONG-HORIZON INFRASTRUCTURE PROJECTS: THE MEDIATING ROLE OF ADAPTIVE RISK RE-ASSESSMENT

DOI: 10.5937/EcoTER26610B

Usama Bin Moazzam[1,a*], Hassnain Nawab[1,b], Kainat Nasir[1], Iqra Batool[1]

[1] Shaheed Zulfikar Ali Bhutto Institute of Science and Technology (SZABIST), H-8/4, Islamabad, PAKISTAN

[a] https://orcid.org/0009-0004-7953-1310

[b] https://orcid.org/0009-0002-8975-0942

Abstract

Despite the many years of reform attempts, long term infrastructure projects have continued to show systematic problems with scope deviations, cost overruns, and delay. This study proposes a mediation model where adaptive risk reassessment is identified as the mediator through which climate disruptions affect project performance negatively. Building on megaprojects theory, contingency theory, and research on risk management effectiveness, the research posits that climate disruptions are not directly related to project outcomes; rather, the impact of climate disruptions is largely mediated by the number and effectiveness of risk review cycles carried out by the project team after each disruption event. Three hypotheses are generated from the model and framed in a way that allows for testing using survey or project archives data. The findings provide actionable insights for project managers and policymakers dealing with climate change risks in infrastructure development. Serbia is increasing its investment in infrastructure projects as part of the country's alignment with European Union policies, there is an urgent need for understanding the relationship between climate change and project performance with climate risk situation. The theoretical contribution of this study fills a significant void in the literature in treating climate change and contingencies.

Keywords: climate-induced disruptions, infrastructure projects, cost overruns, scope creep, adaptive risk re-assessment.

INTRODUCTION

Infrastructure projects consistently fail to deliver on time and within budget. Flyvbjerg et al. [1] surveyed 258 transport projects across 20 countries and found that nine out of ten experienced cost overruns, with rail projects averaging 44.7% above budget. A more recent study of 662 energy infrastructure projects across 83 countries, drawing on nearly nine decades of data, found that more than three-fifths exceeded their initial budgets, and that schedule overruns on renewable energy portfolios averaged between 15% and 25% [2]. These are not isolated failures. They point to something structural, a pattern that has persisted through decades of reform and institutional learning.

* *usamabmoazzam@gmail.com*

Scholarship has historically blamed cost overruns on optimism bias, strategic misrepresentation, and poor risk estimation [1,3]. Ika and Pinto [4] pushed back on the assumption that success and failure can be read off a single Iron Triangle of time, cost, and scope, arguing instead for contextually sensitive evaluations. Both lines of inquiry, however, treat the project's external environment as broadly stable. What has changed is that long-horizon projects, those taking four to twelve years to execute, now routinely encounter floods, heat episodes, and storms that simply were not in scope when the budget was set.

The IPCC Sixth Assessment Report [5] confirmed that even at 1.1°C of warming, extreme weather events affecting infrastructure are already more frequent and severe than historical baselines. Leal Filho *et al*. [6] reviewed infrastructure case studies across five continents and found that roads buckle in heat waves, bridges are undermined by flooding, and coastal assets are compromised by storm surge well ahead of their engineering design thresholds. At the macroeconomic level, the OECD [7] estimated that climate-induced failures are widening an already enormous global infrastructure investment gap.

Project management literature has been slow to respond. Most studies treat weather as one item in a checklist of risk factors rather than as a dynamic, escalating threat that compounds over a project's lifecycle [8]. This matters in practice: a project manager overseeing a dam in the Western Balkans or a highway in South Asia needs more than a generic risk register. They need a framework for translating a climate shock into a revised risk posture, a corrected scope baseline, and a defensible cost re-estimate.

This paper proposes a mediation model to address that gap. The relationship between climate-induced disruptions and project performance failure is not direct or inevitable. It passes through a mechanism: the quality and frequency of adaptive risk re-assessment during execution. Teams that treat risk re-assessment as an iterative, ongoing process rather than a one-time exercise at project initiation are better placed to absorb shocks before they cascade into overruns [9,10].

The paper makes three contributions. It brings climate science and project management literature into dialogue to theorize a clear causal chain from climate disruption to project failure. It builds a conceptual framework that researchers can take to survey or archival data. And it draws implications for practitioners and policy makers, with specific reference to Serbia's EU-alignment infrastructure agenda, where large transport and energy projects are now being planned and executed against a backdrop of rising climate volatility [11].

MATERIALS AND METHODS

Research design and approach

This paper is a conceptual study. It does not draw on primary survey data, field observations, or archival project records. Instead, it builds a theoretical model from systematic synthesis of published literature across three research domains. This design is appropriate when the goal is to identify and theorize a relationship that has not

previously been examined, and to produce testable hypotheses for future empirical work [31]. Conceptual research of this kind contributes by clarifying constructs, specifying causal pathways, and providing a framework that empirical researchers can then take to data [32]. The paper is a theory building exercise rather than a theory testing one.

The limitation this entails is clear: the three hypotheses developed here remain unconfirmed until a survey-based or archival study tests them against real project data. The justification for proceeding at the conceptual level is that no existing study has brought together climate disruption, adaptive risk management behavior, and project performance outcomes in a single integrated framework. The theoretical groundwork is a necessary first step before any data collection can be meaningfully designed.

Literature sources and search strategy

The review underpinning the model was conducted through systematic searches of Web of Science, Scopus, and Google Scholar. Three keyword clusters guided the search: (a) infrastructure project cost overruns, scope creep, and schedule delay; (b) climate change, extreme weather events, and infrastructure vulnerability; and (c) project risk management, adaptive risk assessment, and project success. Searches were restricted to peer-reviewed journal articles, conference proceedings, and authoritative institutional reports published between 2003 and 2025. This lower bound was relaxed only for foundational theoretical contributions with direct relevance to the model.

Sources were screened first by title and abstract for relevance to at least one keyword cluster, then by full text for theoretical or empirical content directly applicable to the proposed constructs. The final pool of 30 sources spans project management theory [1,4,9,10,18,19], climate and infrastructure research [5–8,24,27], and cost overrun and delay literature [2,3,12–17,22,25]. Institutional reports from the OECD [7], EBRD [21], and European Parliament [11] were included given their direct policy relevance to the Serbian infrastructure context examined in the discussion.

Theoretical foundations

Three theoretical traditions inform the model. The first is the megaproject management literature. Flyvbjerg *et al*. [1] established that cost overruns and scope deviation are systemic and statistically predictable rather than accidental, and subsequent work [2,3,12] has documented their distribution and root causes across industries and geographies. This tradition defines the dependent variable and justifies why infrastructure project failure is a phenomenon worth modelling.

The second tradition is contingency theory as applied to project management [4,19]. Contingency theory holds that the relationship between environmental uncertainty and organizational performance is not fixed. It is shaped by how the organization responds to that uncertainty. Applied to this paper, that means a climate shock does not automatically produce a cost overrun. This depends on the standard of

management's reaction, that is, if the project team conducts a systematic review of risk after the occurrence or views it as a standalone case.

The third tradition is risk management effectiveness research [9,18,20]. Zwikael and Ahn [9] provided the empirical foundation for treating risk management quality as a mechanism that stands between project risk exposure and project outcomes. Their multinational survey evidence showed that it is the quality of risk management practice, not merely the level of risk, that predicts project success. Baron and Kenny [31] provided the conceptual vocabulary for formalizing this mechanism as a mediator: a variable that transmits the effect of an independent variable to a dependent variable rather than simply moderating the size of that effect. That distinction is central to the theoretical contribution of this paper.

Together these three traditions lead to the same conclusion. Climate disruptions create project risk. But it is the adaptive risk management response not the disruption itself that primarily determines whether that risk materializes as project failure.

CONCEPTUAL FRAMEWORK AND HYPOTHESES

The structural context in which all three components operate is that of long-horizon infrastructure projects. Miller and Lessard [34] define these as large-scale engineering undertakings distinguished by irreversible capital commitments, multi-year execution timescales of typically four to twelve years, and sustained exposure to institutional and environmental uncertainty that accumulates throughout the delivery period. It is precisely this extended execution window that transforms episodic climate events into compounding threats to project performance, making the mediation mechanism theorized here both necessary and practically urgent.

The frequency and severity of climate-induced disruptions during project execution. Frequency is the count of distinct climate events, floods, heat episodes above engineering thresholds, and severe storms, at the project site during execution. Severity is the magnitude of each event relative to historical weather baselines [5,6]. Both dimensions are expected to independently increase the probability of scope deviation and cost overrun [15,16].

The adaptive risk re-assessment: how often it happens and how well. Hillson [35] defines risk management in projects as a structured and iterative process of identifying, analyzing, and responding to threats and opportunities throughout the project lifecycle, with the critical qualification that this process must be revisited dynamically as conditions evolve rather than treated as a one-time exercise at project initiation. Chapman and Ward [36] reinforce this view in the context of complex, uncertain environments, arguing that continuous re-appraisal of the risk picture what they term iterative risk assessment is a prerequisite for effective management under conditions of high environmental variability. Adaptive risk re-assessment, as operationalized in this paper, combines both formulations: it is the frequency and quality of post-disruption risk review cycles conducted by the project team. Protocol quality covers whether risk registers are updated after each disruption, whether

residual risk is re-priced, whether scope baselines are formally revised, and whether contingency allocations are adjusted dynamically. This construct builds directly on Zwikael and Ahn [9] and Chang *et al*. [20].

The project performance deviation, measured along three dimensions. Scope creep, defined by the Project Management Institute [37] as the uncontrolled expansion of project scope without corresponding adjustments to time, cost, and resources, is operationalized here as the scope deviation index the percentage of scope items added or modified after the approved baseline. Cost overrun, characterized by Flyvbjerg *et al*. [1] as a systemic and statistically predictable pattern in megaprojects in which final outturn costs consistently and substantially exceed the estimates on which project approval was based, and further quantified by Merrow [38] as a persistent structural feature of large industrial projects with average cost growth exceeding 25 percent against sanction estimates is measured as the percentage difference between final outturn cost and approved budget. Schedule delay, the ratio of actual to planned project duration, completes the Iron Triangle [1,4]. These three dimensions are operationalized in a way that allows the mediator to exert influence on each sub-dimension separately.

Three hypotheses follow from this structure:

H1: Greater frequency and severity of climate-induced disruptions during execution will increase project scope deviation, cost overrun, and schedule delay.

H2: Higher quality and frequency of adaptive risk re-assessment will reduce project scope deviation, cost overrun, and schedule delay.

H3: Adaptive risk re-assessment will mediate the relationship between climate disruptions and project performance failures, accounting for a significant share of the total effect.

RESULTS AND DISCUSSION

The framework draws on three bodies of literature that have, until now, developed in near-complete isolation from each other: megaproject cost overruns [1,2,12], climate impacts on infrastructure [5,6,7,8], and project risk management effectiveness [9,18–20]. Their intersection has become unavoidable. Climate disruptions are intensifying at precisely the moment when global infrastructure investment is accelerating, and the existing tools for managing project risk were not designed with a non-stationary climate in mind.

The standard policy response to climate-related infrastructure failures has been to invest in physical resilience: stronger materials, raised flood defenses, heat-tolerant pavements. These are worthwhile investments, but they are anticipatory and static. They protect against the specific scenarios that engineers modelled at the design stage. They offer little protection against unanticipated event combinations or climate trajectories that exceed design assumptions [8]. Adaptive risk re-assessment works differently. It does not require that every climate scenario be predicted in advance. It requires that the project organization has the reflexes to recalibrate when conditions deviate from assumptions.

This distinction matters in the Serbian context. The EBRD Country Strategy for Serbia 2023–2028 [21] identifies climate resilience as a priority across transport, municipal services, and energy infrastructure. The European Parliament [11] has called on Serbia to adopt a National Energy and Climate Plan and strengthen environmental impact assessment capacity. Neither document, however, addresses what should happen at the project execution level when a climate event disrupts a live construction program. That is the gap this paper fills. Adaptive risk re-assessment is the operationally actionable link between climate shock and project performance outcome. Investing in it through training, process design, and contractual provisions is likely to yield returns in reduced overruns.

Scope creep deserves particular attention. Farooqui *et al*. [13] and Rivera *et al*. [22] both found that scope creep in infrastructure projects is systematically underestimated in risk registers, partly because each individual scope change looks reasonable at the time it is approved. In a climate context, scope creep is harder to resist because it is physically imposed, not stakeholder-driven. A flood that damages completed sub-structure requires remediation that is both necessary and unbudgeted. Adaptive risk re-assessment does not prevent that damage, but it ensures that the cumulative scope impact is formally tracked, its cost implications are estimated, and the project sponsor has accurate information for decisions about continuation, redesign, or delay [9,14].

There is also a temporal dimension worth articulating. Climate disruption and project failure are not simultaneous. Between them lies a sequence of organizational decisions, taken in the days and weeks after an event. Whether to treat the event as an isolated incident or trigger a full risk review. Whether to update the risk register or leave it unchanged until the next scheduled review. Whether to revise the cost-to-complete estimate or hold the existing one. The quality of those decisions determines how much of the shock is absorbed and how much propagates into the final outturn. This is why the mediating effect is expected to be partial rather than total: some direct effect of climate severity on cost overrun will remain, but a meaningful share of variance in project outcomes should be explainable by the quality of the post-event response [18,19].

For empirical validation, a survey-based study of project managers on large infrastructure projects in climate-exposed regions is the most natural starting point. All three constructs, climate disruption experience, adaptive risk re-assessment quality, and project performance deviation, are measurable through project manager self-report and archival cross-validation. Structural equation modelling or path analysis can test the mediation hypotheses [9,16]. Qualitative case studies of projects that experienced major climate events, the 2021 floods in Germany and Belgium [6], or flood-affected dam construction in South Asia [16], could trace the specific decision pathways through which risk re-assessment either absorbed or failed to absorb the shock.

CONCLUSION

In long-horizon infrastructure projects, this study has suggested and theorized a mediation model whereby adaptive risk re-assessment is the link between climate-induced disturbances and project scope deviation, cost overruns, and schedule delays. The model combines three formerly separate bodies of work into a conceptual framework with three testable hypotheses.

The practical lesson is obvious. Though it is important, physical resilience engineering is not enough. The ability of the organization to repeatedly and methodically reevaluate risk following each weather event is what stops shocks from turning into disasters. Standardized post event review procedures, contractual clauses enabling dynamic scope re-baselining, and investment in project manager training all help to develop that capability. It is relatively inexpensive and has not received the policy and research attention that it deserves.

The governance consequence for Serbia and other EU applicant countries with ongoing infrastructure investment projects is plain. Project contracts and monitoring systems must go past risk registers submitted at the start of each project. Dynamic, event triggered risk management systems supported by project managers with the power and ability to change scope baselines in real time should become a requirement for EU infrastructure finance in the Western Balkans.

Future studies ought to concentrate on empirical validation. The most critical next phase is to operationalize the quality of the adaptive risk re-assessment process as a quantifiable metric [33]. A validated tool for this construct would allow survey-based testing of the mediation model across various infrastructure settings and would advance both the project management and climate adaptation fields.

ACKNOWLEDGEMENT

The authors are grateful to Shaheed Zulfikar Ali Bhutto Institute of Science and Technology (SZABIST), Islamabad, for institutional support during the preparation of this manuscript. No external funding was received for this study.

REFERENCES

[1] Flyvbjerg B, Bruzelius N, Rothengatter W. Megaprojects and Risk: An Anatomy of Ambition. Cambridge: Cambridge University Press; 2003. Available from: https://stopcrc.com/docs/Megaprojects-and-Risk.pdf

[2] Sovacool, B.K., Ryu, H. Renew Sustain Energy Rev. 2025, 123, 104057.

[3] Eliasson, J. Transp. Res. Part A. 2025, 198, 104532.

[4] Ika, L.A., Pinto, J.K. Int. J. Proj. Manag. 2022, 40(7), 835–848.

[5] IPCC. Climate Change 2022: Impacts, Adaptation and Vulnerability. Contribution of Working Group II to the Sixth Assessment Report. Cambridge: Cambridge University Press; 2022. Available from: https://www.ipcc.ch/report/ar6/wg2/downloads/

[6] Leal Filho, W., Abeldaño Zuñiga, R.A., Sierra, J., *et al*. Sci Rep. 2024, 14, 14147.

[7] OECD. Infrastructure for a Climate-Resilient Future. Paris: OECD Publishing; 2024. Available from: https://www.oecd.org/en/publications/2024/04/infrastructure-for-a-climate-resilient-future_c6c0dc64/full-report.html
[8] Buhl, M., Markolf, S. Sustain. Resilient Infrastruct. 2023, 8(sup1), 157–169.
[9] Zwikael, O., Ahn, M. Risk Anal. 2011, 31(1), 25–37.
[10] Pinto, J.K., Davis, K., Ika, L.A., *et al*. Int. J. Proj. Manag. 2022, 40(7), 831–834.
[11] European Parliament. Report on the 2023 and 2024 Commission Reports on Serbia (A10-0072/2025). Brussels: European Parliament; 2025. Available from: https://www.europarl.europa.eu/doceo/document/A-10-2025-0072_EN.html
[12] Durdyev, S., Hosseini, M.R. Int. J. Manag. Proj. Bus. 2020, 13(1), 20–46.
[13] Farooqui, R., Khan, I., Malik, F. Constr. Manag J. 2024, 36(4), 231–244.
[14] Rivera, A., Golpavar-Fard, M., El Asmar, M. J. Constr. Eng. Manag. 2020.
[15] Zagia, F., Kajewski, S., Omrani, S., *et al*. Int. J. Constr. Manag. 2026, 26(9), 1879–1904.
[16] Andrıć, J.M., Lin, S., Cheng, Y., *et al*. Sustainability. 2024, 16(24), 11159.
[17] Precious, D. Dev Eng. 2025, 6, 100188.
[18] Zwikael, O., Meredith, J. IEEE Trans Eng Manag. 2021, 68(6),1745–1757.
[19] Love, P.E.D., Pinto, J.K., Ika, L.A., *et al.* IEEE Trans Eng Manag. 2024, 71, 1940–1949.
[20] Chang, C.M Hossain, A. Infrastructures. 2024, 9(12), 226.
[21] European Bank for Reconstruction and Development. Serbia Country Strategy 2023–2028. London: EBRD. 2023. Available from: https://www.ebrd.com/content/dam/ebrd_dxp/assets/pdfs/country-strategies/serbia/EBRD-Latest-Serbia-Strategy.pdf
[22] Gomez-Cabrera A, Ponz-Tienda JL, Pellicer E, Sanz A. In: Proceedings of the XI Simpósio Brasileiro de Gestão e Economia da Construção and VIII Encuentro Latinoamericano de Gestión y Economía de la Construcción; 23-25 October; Londrina, Paraná, Brazil. 2019. p. 1–10.
[23] Li, Q., Punzo, G., Robson, C., *et al*. IEEE Syst. J. 2022, 18(1), 24–35.
[24] Dawson, R.J., Thompson, D., Johns, D., *et al*. Philos. Trans. R. Soc. A. 2018, 376, 20170298.
[25] Suvvari, SK. Innov Res Thoughts. 2022, 8(4), 360–371.
[26] Flyvbjerg B, Gardner D. How Big Things Get Done. New York: Currency; 2022.
[27] Zhao, Q., Gao, L., Meng, Q.Y., *et al*. Earth's futur. 2024, 12(12), e2024EF005179.
[28] Toljaga-Nikolić, D., Todorović, M., Dobrota, M., *et al*. Sustainability. 2020, 12(20), 8619.
[29] Albarracín-Rodríguez, A.V. Amorocho, A.J., Rincón-Guio, C.J., *et al*. Ind Integr Manag. 2023, 8, 1–23.
[30] Ochoa Pacheco, P., Coello-Montecel, D., Tello, M., *et al*. PLoS One. 2023, 18(12), e0295417.
[31] Baron, R.M. Kenny, D.A. J Pers Soc Psychol. 1986, 51 (6), 1173–1182.

[32] Jaakkola, E. AMS Rev. 2020, 10, 18–26.
[33] Krewski, D., Saunders-Hastings, P., Baan, R.A., *et al*. ALTEX. 2022, 39(4), 667–693.
[34] Miller R, Lessard D.R, The Strategic Management of Large Engineering Projects: Shaping Institutions, Risks, and Governance. Cambridge, MA: MIT Press; 2001.
[35] Hillson D, Managing Risk in Projects. Farnham: Gower Publishing; 2009.
[36] Chapman C, Ward S. Project Risk Management: Processes, Techniques and Insights. Chichester: John Wiley & Sons; 2003.
[37] Project Management Institute. A Guide to the Project Management Body of Knowledge (PMBOK Guide). Newton Square, PA: Project Management Institute; 2021.
[38] Merrow E.W, Industrial Megaprojects: Concepts, Strategies, and Practices for Success. Hoboken, NJ: John Wiley & Sons; 2011.

7th Student Section

Abstract

HEALTH IMPACTS AND PREVENTION STRATEGIES OF URBAN AIR POLLUTION

DOI: 10.5937/EcoTER26620K

Student: Dragana Kerkez[1]

Mentors: Svetlana Nešović[1*,a], Kristina Filipović[1,b], Jovana Krstić[1,c]

[1] University Business Academy Novi Sad, Faculty of Applied Sciences, Višegradska 47, 18000 Niš, SERBIA

[a] https://orcid.org/0000-0002-5927-9048

[b] https://orcid.org/0009-0004-2477-3769

[c] https://orcid.org/0000-0002-8269-0142

Abstract

Urban air pollution represents one of the most significant environmental health risks worldwide, particularly in rapidly developing urban areas. Epidemiological studies consistently link major air pollutants—including particulate matter (PM2.5 and PM10), nitrogen dioxide (NO_2), and sulfur dioxide (SO_2)—with a range of adverse health outcomes. This study analyzes the health impacts of urban air pollution, with a focus on respiratory and cardiovascular diseases, and evaluates current prevention and control strategies. The review synthesizes findings from 11 key peer-reviewed studies, including epidemiological analyses, systematic reviews, and policy evaluations, published between 1993 and 2024. The findings indicate that long-term exposure to PM2.5 is associated with a significant increase in the risk of chronic respiratory conditions, cardiovascular diseases, and premature mortality. Landmark cohort studies demonstrate a 6–15% increase in cardiovascular mortality per 10 μg/m³ rise in PM2.5 exposures. Vulnerable populations, including children and the elderly, are particularly susceptible to these effects. In addition, the synthesis of available evidence highlights that integrated prevention strategies—combining policy measures (e.g., emission standards), urban planning solutions (e.g., green infrastructure, traffic management), and technological innovations (e.g., clean energy, emission control systems)—have proven effective in reducing ambient pollutant levels and associated health burdens.

Keywords: urban air pollution, PM2.5, health impacts, respiratory diseases, prevention strategies

[*] *risticsvetlanaaa@gmail.com*

REFERENCES

1. Manisalidis, I., Stavropoulou, E., Stavropoulos, A., *et al*. E. Front. Public Health. 2020, 8(14), 1–10.
2. Jafari, A. J., Charkhloo, E., Pasalari, H. J. Environ. Health Sci. Eng. 2021, 19(2), 1911–1940.
3. Lin, D.-Y., Waller, S. T., Lin, M.-Y. Sustain. Cities Soc. 2024, 101, 104123.
4. Qin, Y. Environ. Dev. Sustain. 2023, 25, 12345–12360.
5. Millar, D. A., Howard, M. A., Naidoo, N., *et al*. Ann. Glob. Health. 2025, 90(1), 8.
6. Nasar-u-Minallah, M., Zainab, M., Jabbar, M. Environ. Sci. Pollut. Res. 2024, 31, 56789–56805.
7. Kura, B., Verma, S., Ajdari, E., *et al*. J. Environ. Prot. 2013, 4(8), 1–10.
8. Rukundo, S. K. Int. J. Environ. Res. Public Health. 2023, 20(5), 1–14.
9. Piracha, A., Chaudhary, M. T. Sustainability 2022, 14(15), 9234.
10. Dockery, D. W., Pope, C. A., Xu, X., *et al*. N. Engl. J. Med. 1993, 329(24), 1753–1759.
11. Markandya, A., Sampedro, J., Smith, S. J., *et al*. Environ. Res. Lett. 2018, 13 (8), 083001.

Abstract

ASSESSMENT OF THE IMPACT OF FINE SUSPENDED PARTICLES PM_{10} AND LEAD ABSORBED ONTO THEM IN AMBIENT AIR OF PANČEVO ON PUBLIC HEALTH

DOI: 10.5937/EcoTER26622Z

Student: Jelena Zec[1,a]

Mentors: Milena Rikalović[1*,b], Dubravka Nikolovski[2,c]

[1] Environment and sustainable development, University of Singidunum, Danijelova 32, 11010 Belgrade, SERBIA

[2] Institute of Public Health Pančevo, Miloša Obrenovića 2, 26000 Pančevo, SERBIA

[a] https://orcid.org/0009-0005-8960-0620

[b] https://orcid.org/0000-0002-1809-5461

[c] https://orcid.org/0000-0002-1602-095x

Abstract

This study presents a three-year air pollution monitoring (from 2022 to 2024) of fine particulate matters (PM_{10}) and lead (Pb) absorbed onto them in Pančevo. Two datasets were created for PM_{10} concentrations with average values from measurement points Strelište and Nova Misa: daily PM_{10} and a subset for days when lead was measured. *AirQ+* software was applied for health impact assessment – the evaluation of PM_{10} impact on total adult mortality (30+ years) applied for both datasets. Attributable risk was estimated for excess deaths from natural causes in adults. Lead concentration was analyzed relative to PM_{10} levels as its percentage in PM_{10} (for data subset, for corresponding days). The average annual concentration of PM_{10}, calculated as the mean from both monitoring sites, amounted to 34.15 (2022), 30.36 (2023) and 34.49 (2024) µg/m^3, or 33,00 µg/m^3 in three-year period, and for subset data – for days with lead measurements 37.38 (2022), 33.22 (2023) and 36.50 (2024) µg/m^3 , or 35.70 µg/m^3 in three-year period.

The average annual concentration of Pb, calculated as the mean from both monitoring sites, amounted to 0.0041 (2022), 0.0061 (2023) and 0.0021 (2024) µg/m^3 or 0.0040 µg/m^3 in three-year period. The estimated number of deaths from all natural causes among the adult population aged 30+ years attributable to air pollution by PM_{10} during reported period was 103 cases (95% CI: 78–150, AP 6.82%) - attributable cases per 100.000 population at risk was 126.92 (95%CI: 96.48–185.40, AP 6.82%) at an average three-year mean PM_{10} concentration on 33,00 µg/m^3; and for subset data was 117 cases (95% CI: 89–171, AP 7.80%) - attributable cases per 100.000 population at risk was 145,20 (95%CI: (110.51-211.57, AP 7,80%) at an average three-year mean PM_{10} concentration of 35.70 µg/m^3. There was no statistically significant difference between the main data set for

*mrikalovic@singidunum.ac.rs

PM_{10} and the subset of days when lead measurement were conducted was performed. The percentage of Pb present in fine particles, based on annual mean values, was 0.011% in 2022, 0.018% in 2023, and 0.005% in 2024.

The number of deaths from all causes among the adult population attributable to PM_{10} levels is significant. Although PM_{10} annual mean values are lower than those in Serbian national regulations, they remain above the limit values recommended by World Health Organization. Therefore, action plans for reducing particulate air pollution in Pančevo should continue to be developed. A simple conclusion that the share of lead is negligible in mortality from all natural causes cannot be drawn; further investigation of this impact (e.g., carcinogenic risk and other outcomes) is required. Additional research is also needed through epidemiological studies that have applied the *AirQ+* software, but for parameters not predefined by the software.

Keywords: PM_{10}, Pb, Impact Assessment, AirQ+, Air Pollution

ACKNOWLEDGEMENT

The authors would like to express their gratitude to the Institute of Public Health Pančevo for providing access to the data used in this study. Air quality measurements in Pančevo used for the preparation of this study were conducted on the basis of the Contract for additional air quality monitoring for the years 2022 and 2023, No. XI-13-404-233/2021 dated December 21, 2021, and the Contract for additional air quality monitoring for the years 2024 and 2025, No. XI-13-405-130/2023 dated December 28, 2023.

REFERENCES

1. WHO Regional Office for Europe, European Centre for Environment and Health, 2023. *AirQ: software tool for health risk assessment of air pollution*. Bonn, Germany: WHO Regional Office for Europe
2. Statistical Office of the Republic of Serbia.Available from: https://data.stat.gov.rs/
3. Institute of Public Health Pančevo. Annual Report on Ambient Air Measurements in the Area of the City of Pančevo for the year 2022. Pančevo, Serbia, 2023. Available online: https://www.pancevo.rs/?wpfb_dl=4912 (accessed on April 22, 2026).
4. Institute of Public Health Pančevo. Annual Report on Ambient Air Measurements in the Area of the City of Pančevo for the year 2023. Pančevo, Serbia, 2024.
5. Institute of Public Health Pančevo. Annual Report on Ambient Air Measurements in the Area of the City of Pančevo for the year 2024. Pančevo, Serbia, 2025. Available from: https://www.pancevo.rs/?wpfb_dl=5515 (accessed on April 22, 2026).

Abstract

PRESENCE AND INFLUENCE OF PHARMACEUTICAL POLLUTANTS IN THE ENVIRONMENT

DOI: 10.5937/EcoTER26624S

Student: Minja Stojadinović[1]

Mentor: Maja Nujkić[1*,a]

[1] University of Belgrade, Technical Faculty in Bor, Vojske Jugoslavije 12, 19210 Bor, SERBIA

[a] https://orcid.org/0000-0002-6110-5135

Abstract

Pharmaceutical substances constitute a significant group of modern environmental pollutants, with their presence in soil and air becoming more pronounced due to intensive production and widespread use of drugs in human and veterinary medicine, as well as in agriculture. Although they were originally developed to preserve human and animal health, their biological activity and chemical stability contribute to their persistence in various environmental components. In recent decades, pharmaceutical substances have been recognised as so-called emerging pollutants, whose effects on ecosystems and human health are increasingly being investigated within the framework of environmental protection.

The paper analyses the main sources and pathways by which pharmaceutical substances reach the soil and air. The pharmaceutical industry, healthcare institutions, households, and agricultural and veterinary activities are identified as significant sources. During the production, use, and disposal of medicines, these substances enter wastewater, from which, due to the insufficient efficiency of standard purification systems, they spread further into the environment. The role of improper disposal of unused medicines, as well as the use of veterinary antibiotics that reach the soil through manure, is particularly emphasised. Atmospheric deposition is also an important, but often neglected, route for the dissemination of pharmaceutical substances.

The paper provides an overview of the most frequently detected groups of pharmaceutical substances in the environment, including antibiotics, analgesics and non-steroidal anti-inflammatory drugs, hormones, and other biologically active substances. Special attention is given to antibiotics due to their link with the development of microorganism resistance, which represents one of the greatest global health and environmental challenges. Hormonal preparations are also analysed for their potential to cause endocrine disruption in animals and humans.

The paper examined the behaviour and fate of pharmaceutical substances in the environment, including processes such as adsorption in the soil, microbiological and chemical decomposition, air transport, and bioaccumulation in organisms. It was noted that

[*] *mnujkic@tfbor.bg.ac.rs*

long-term exposure to even low concentrations of these substances can disrupt the microbiological balance, reduce biodiversity, and pose potential risks to human health through the food chain.

Based on the analysed data, it was concluded that the problem of pharmaceutical pollutants is complex and requires an integrated approach within the framework of environmental protection. Improving wastewater treatment technologies, proper management of pharmaceutical waste, stricter regulation, and public education are key measures to reduce their negative impact. Continuous monitoring and further research are necessary to ensure effective management of these modern pollutants and to preserve the stability of the ecosystem.

Keywords: pharmaceutical substances, environmental pollutants, monitoring

ACKNOWLEDGEMENT

The research presented in this paper was done with the financial support of the Ministry of Education, Science and Technological Development of the Republic of Serbia, within the funding of the scientific research work at the University of Belgrade, Technical Faculty in Bor, according to the contract with registration number 451-03-34/2026-03/200131.

REFERENCES

1. Mosharaf, M.K., Gomes, R.L., Cook, S., *et al*. Chemosphere 2024, 364, 143055.
2. Eapen, J.V., Thomas, S., Antony, S. Explor. Drug Sci. 2024, 484–507.

Abstract

COPPER CORROSION INHIBITORS IN CHLORIDE ENVIRONMENTS

DOI: 10.5937/EcoTER26626J

Student: Nataša Janjić[1]

Mentor: Žaklina Tasić[1*,a]

[1] University of Belgrade, Technical Faculty in Bor, Vojske Jugoslavije 12, 19210 Bor, SERBIA

[a] https://orcid.org/0000-0001-6544-1980

Abstract

Due to the widespread use of copper, electrochemical investigation of copper in various environments is highly important. Although copper is resistant to atmospheric effects and many chemicals, it remains susceptible to corrosion in aggressive environments. Corrosion of copper in chloride-containing environments poses a significant problem in industry and material protection, as chloride ions destabilize the protective oxide layer and accelerate metal degradation. In solutions such as NaCl, electrochemical reactions occur involving the anodic oxidation of copper and the cathodic reduction of oxygen, with the presence of chloride ions significantly increasing the corrosion rate [1,2]. One of the most effective ways to protect copper is through the use of corrosion inhibitors. Inhibitors are substances added in small quantities and can be defined as chemical substances or combinations of substances that, when present in an appropriate concentration and form, prevent or reduce the corrosion process. The most commonly used inhibitors are organic compounds, especially azoles, imidazoles, and thiadiazoles. These substances contain heteroatoms such as nitrogen, sulfur, and oxygen, which enable their adsorption onto the copper surface and the formation of a stable protective film. Compared to other methods, inhibitors are easy to apply and can be used independently or in combination with protective coatings [3].

Green inhibitors are a group of compounds of animal or plant origin. In addition to being biodegradable, they do not contain heavy metals, making them environmentally friendly [1].

Aloe vera is a natural green corrosion inhibitor known for its wide range of applications. This spiny plant belongs to the cactus family and includes more than 500 species, most of which live in desert climates. It is used as an antibacterial and antifungal agent because it inhibits the activity of microorganisms. It also exhibits corrosion-resistant properties, as it affects the activity of microbial biofilms and leads to a lower rate of biocorrosion in corrosive environments. Aloe vera contains various active substances such as aromatic acids, polysaccharides, and certain minerals. The gelatinous substance found in its leaves is particularly effective in preventing copper corrosion. These components contribute to aloe vera's ability to form a protective layer on the metal surface, thereby preventing corrosion [2].

[*] *ztasic@tfbor.bg.ac.rs*

Keywords: copper, corrosion inhibitor, chloride environment, Aloe vera

ACKNOWLEDGEMENT

The research presented in this paper was done with the financial support of the Ministry of Science, Technological Development and Innovation of the Republic of Serbia, within the funding of the scientific research work at the University of Belgrade, Technical Faculty in Bor, according to the contract with registration number 451-03-134/2026-03/200131.

REFERENCES

1. Grekulović, V., Štrbac, N., Mitovski, A. Ecologica. 2021, 28(102), 309–314.
2. Mahmoud, G.A., Abdel-karim, A.M., Saleh, S.M., *et al*. J. Alloy Compd. 2025, 1010, 177540.
3. Petrović Mihajlović, M.B., Antonijević, M.M. Int. J. Electrochem. Sci. 2015, 10(2), 1027–1053.

Abstract

ADSORPTION ISOTHERMS FOR COPPER IONS BIOSORPTION ONTO GRAPE STALKS

DOI: 10.5937/EcoTER26628D

Student: Saška Dumitrašković[1]

Mentors: Milan Gorgievski[1*,a], Vesna Grekulović[1,b]

[1] University of Belgrade, Technical Faculty in Bor, Vojske Jugoslavije 12, 19210 Bor, SERBIA

[a] https://orcid.org/0000-0002-9899-719X

[b] https://orcid.org/0000-0001-6871-4016

Abstract

The removal of heavy metals from wastewater is environmentally important due to their toxicity, persistence, and tendency to accumulate in living organisms. In this context, biosorption has emerged as a promising, cost-effective, and sustainable alternative to conventional treatment methods. This study investigates the potential application of grape stalks waste (*Vitis vinifera* L.) as a low-cost biosorbent for the removal of Cu(II) ions from aqueous solutions. Batch equilibrium experiments were conducted, and the adsorption data were analysed using Langmuir, Freundlich, and Temkin isotherm models, which are commonly used to describe adsorption mechanisms, surface heterogeneity, and adsorbate–adsorbent interactions. The experimentally determined equilibrium adsorption capacity ($q_{e,exp}$) was 5.01 mg g^{-1}. The Langmuir isotherm model yielded a maximum monolayer adsorption capacity (q_m) of 9.02 mg g^{-1} and a Langmuir constant (K_L) of 2.966 dm^3 mg^{-1}, with a correlation coefficient of $R^2 = 0.98$. These results suggest partial monolayer adsorption on a relatively homogeneous surface with a finite number of active sites. The Freundlich model provided the best fit to the experimental data ($R^2 = 0.99$), with $K_F = 9.08$ and $1/n = 0.637$, indicating favourable adsorption on a heterogeneous surface with a non-uniform distribution of adsorption energies and the possibility of multilayer formation. The value of $1/n < 1$ confirms favourable adsorption and strong interaction between Cu(II) ions and the biosorbent surface. The Temkin isotherm model also adequately described the system ($R^2 = 0.96$), with $K_T = 41.22$ dm^3 g^{-1} and $B = 1.65$ J mol^{-1}, suggesting that the heat of adsorption decreases linearly with increasing surface coverage and indicating the involvement of both physical and chemical interactions. Overall, grape stalks waste demonstrated good efficiency for Cu(II) removal from aqueous solutions. The dominance of the Freundlich model indicates that adsorption is mainly governed by heterogeneous surface interactions, including ion exchange and complexation with functional groups present in lignocellulosic biomass.

Keywords: biosorption, copper ions, adsorption isotherms, grape stalks

[*] *mgorgievski@tfbor.bg.ac.rs*

ACKNOWLEDGEMENT

The research presented in this paper was done with the financial support of the Ministry of Education, Science and Technological Development of the Republic of Serbia, within the funding of the scientific research work at the University of Belgrade, Technical Faculty in Bor, according to the contract with registration number 451-03-34/2026-03/200131.

REFERENCES

1. Foo, K.Y., Hameed, B.H. Chem. Eng. J. 2010, 156, 2–10.
2. Ho, Y.S., McKay, G. Process Biochem. 1999, 34, 451–465.
3. Crini, G. Bioresour. Technol. 2006, 97, 1061–1085.
4. Langmuir, I. J. Am. Chem. Soc. 1918, 40, 1361–1403.
5. Demirbas, A. J. Hazard. Mater. 2008, 157, 220–229.

Abstract

THE IMPACT OF BIODEGRADABLE PLASTICS ON THE ENVIRONMENT

DOI: 10.5937/EcoTER26630J

Student: Veljko Jovanović[1]

Mentor: Maja Nujkić[1*,a]

[1] University of Belgrade, Technical Faculty in Bor, Vojske Jugoslavije 12, 19210 Bor, SERBIA

[a] https://orcid.org/0000-0002-6110-5135

Abstract

Plastic materials are among the most widespread products of modern society, but they also pose one of the greatest environmental problems due to their slow degradation and accumulation in the environment. Biodegradable plastic was developed as a potential solution to this issue, designed as a material that can be broken down by microorganisms into simpler, more environmentally friendly compounds. However, although it is often regarded as a more sustainable alternative to conventional plastics, its actual impact on the environment and ecosystems is still not fully understood. The aim of this paper is to analyse and review the impact of biodegradable plastics on various components of the environment, including soil, aquatic ecosystems, plants, animals, and potential effects on human health.

A review of previous research shows that biodegradable plastic can help reduce long-term pollution, as it breaks down into carbon dioxide, water, and mineral substances under certain conditions. However, numerous studies indicate that complete decomposition often occurs only in controlled industrial or laboratory settings, while in the natural environment decomposition may be incomplete, leading to the formation of microplastics. These tiny particles can persist in soil or water for long periods and potentially affect organisms and ecosystems.

Analysis of scientific papers shows that the most studied types of biodegradable plastics are polylactic acid (PLA), polybutylene adipate-co-terephthalate (PBAT), polybutylene succinate (PBS), and polyhydroxyalkanoates (PHA). Most research has been conducted under laboratory conditions and over a relatively short period, usually less than a few months, which limits the ability to observe long-term ecological effects.

The results of numerous studies indicate that biodegradable plastics can affect soil physicochemical properties, including changes in pH, soil structure, and nutrient availability. In some cases, there is a decrease in soil nitrogen content and changes in microbial communities, which can influence plant growth and development. Experiments have shown that the presence of biodegradable plastic can slow the growth of various plant species, including wheat, soybeans, maize, and lettuce, as well as reduce the content of chlorophyll and other important biochemical compounds.

[*] *mnujkic@tfbor.bg.ac.rs.*

The impact of biodegradable plastics has been observed in both terrestrial and aquatic organisms. In certain invertebrates, such as earthworms and insects, negative effects on growth, reproduction, and survival have been recorded, while in some organisms these effects were minimal or statistically insignificant. In aquatic ecosystems, plastics can cause metabolic disturbances, reduced growth, and organ damage in fish and other organisms, especially at higher concentrations and with longer exposure times.

In addition to environmental effects, potential risks to human health are also considered. Microplastics can enter the human body through food, water, and air, and some research indicates that biodegradable plastic can serve as a carrier of microorganisms and pollutants. During decomposition, small plastic particles can affect the balance of microorganisms in the digestive system and potentially cause inflammatory processes.

In conclusion, although biodegradable plastics represent a promising alternative to conventional plastic materials, their environmental effects depend on the type of plastic, concentration, duration of exposure, and environmental conditions. Previous research indicates that they can have both positive and negative impacts on ecosystems. Therefore, long-term research is needed to better understand their real effects and enable safe and sustainable use in the future.

Keywords: plastic materials, environmental, biodegradation

ACKNOWLEDGEMENT

The research presented in this paper was done with the financial support of the Ministry of Education, Science and Technological Development of the Republic of Serbia, within the funding of the scientific research work at the University of Belgrade, Technical Faculty in Bor, according to the contract with registration number 451-03-34/2026-03/200131.

REFERENCES

1. Zhou, D., Chen, J., Wu, J. Sustain. Mater. Technol. 2021, 28, e00251.
2. Li, M., Ma, Q., Su, T. J. Polym. Environ. 2024, 32 (3), 1039–1045.

Abstract

ELECTROCHEMICAL BEHAVIOR OF COPPER IN PRESENCE OF OAK BARK MACERATE

DOI: 10.5937/EcoTER26632K

Student: Marina Karabašević[1]

Mentors: Vesna Grekulović[1*,a], Milan Gorgievski[1,b]

[1] University of Belgrade, Technical Faculty in Bor, Vojske Jugoslavije 12, 19210 Bor, SERBIA

[a] https://orcid.org/0000-0001-6871-4016

[b] https://orcid.org/0000-0002-9899-719X

Abstract

Possibility for using oak bark macerate as an ecological inhibitor of copper corrosion in a chloride media was investigated in this paper. Electrochemical behavior of copper in 0.5 mol/dm^3 NaCl in the absence and in the presence of oak bark macerate in different concentrations was investigated by method of open circuit potential measurement and cyclic voltammetry method. Results of measuring the open circuit potential show that the values of the open circuit potential in the presence of oak bark macerate are more positive in relation to the value of the open circuit potential in the absence of oak bark macerate. Three current peaks appear on the anodic polarization curves, corresponding to the formation of copper chloride and copper oxide. Increasing oak bark macerate concentration leads to shifting of the current peaks potential to more positive values and current intensity value of current peaks decreases, which indicates the inhibitory effect of oak bark macerate.

Keywords: copper, electrochemical behavior, oak bark macerate

ACKNOWLEDGEMENT

The research presented in this paper was done with the financial support of the Ministry of Education, Science and Technological Development of the Republic of Serbia, within the funding of the scientific research work at the University of Belgrade, Technical Faculty in Bor, according to the contract with registration number 451-03-34/2026-03/200131.

REFERENCES

1. Abdullah, A. M., Al-Kharafi, F. M., Ateya, B. G. Scripta Mater. 2006, 54, 1673–1677.
2. Otmačić, H., Stupnišek-Lisac, E. Electrochim. Acta. 2003, 48, 985–991.
3. Pourbaix M, Atlas d'Equilibres Electrochimiques. Paris:Gauthier-Villars et Cie;1963.
4. Stević, Z., Rajčić-Vujasinović, M. Chem.Ind. 2007, 61, 1–6.

[*] *vgrekulovic@tfbor.bg.ac.rs*

5. Zdravković, M., Grekulović, V., Suljagić, J., *et al.* Prot.Met.Phys.Chem.Surf. 2024, 60, 544–553.
6. Zdravković, M., Vianello, R., Grekulović, V., *et al.* Results Eng. 2026, 29, 109812.
7. Zhang, D., Gao, L., Zhou, G. Appl.Surf.Sci. 2004, 225, 287–293.

Abstract

PHOTOCATALYTIC NANOMATERIAL FOR HEAVY METAL REMEDIATION

DOI: 10.5937/EcoTER26634N

Student: Snežana Nikolić[1]

Mentor: Maja Nujkić[1*,a]

[1] University of Belgrade, Technical Faculty in Bor, Vojske Jugoslavije 12, 19210 Bor, SERBIA

[a] https://orcid.org/0000-0002-6110-5135

Abstract

The paper presents an overview of modern methods for removing heavy metals and metalloids from wastewater, with a particular focus on the use of nanomaterials and their hybrid systems in combination with conventional treatment technologies. Heavy metals pose a serious environmental problem due to their toxicity, bioaccumulation, and long-term persistence. The study examines the main sources of pollution, including industrial activities, agriculture, and municipal wastewater, as well as their negative impacts on human health and ecosystems.

The paper gives special attention to conventional removal methods such as adsorption, membrane filtration, chemical precipitation, ion exchange, electrochemical processes, and advanced oxidation processes. It also discusses the application of nanomaterials such as TiO_2, ZnO, graphene-based materials, and magnetic nanomaterials. Due to their large specific surface area and high reactivity, these materials enable more efficient removal of metal ions.

For example, the use of Fe_3O_4 magnetic nanoparticles for arsenic removal from groundwater is described, achieving removal efficiencies greater than 90%, along with simple magnetic separation and adsorbent reusability. The factors influencing process efficiency are also analyzed, showing that increasing temperature enhances heavy metal removal by intensifying ion diffusion and improving interaction with the active sites of nanomaterials. It is also observed that lowering the initial pollutant concentration increases the removal percentage, as more active sites are available for metal ion adsorption.

The integration of nanomaterials with adsorption, membrane, electrochemical, and biological processes is emphasized to achieve a synergistic effect and improve treatment efficiency. Finally, the advantages, limitations, and future development directions of nanomaterials in environmental protection and wastewater treatment are discussed.

Keywords: pollutants, heavy metals, removal methods, nanomaterials, synergistic effect

[*] *mnujkic@tfbor.bg.ac.rs*

ACKNOWLEDGEMENT

The authors are grateful to the Ministry of Science, Technological Development and Innovation of the Republic of Serbia for financial support according to the contract with registration No. 451-03-34/2026-03/ 200131

REFERENCES

1. Sharma, S., *et al*. Mat. Sci. Semicond. Process. 2026, 204, 110269.
2. Wang, M., *et al*. Nano Mater. Sci. 2025.
3. Li, Jia-li., *et al*. J. Environ. Chem. Eng. 2025, 120586.
4. Rais, A., Imran, H. GSD, 2017, 5, 75-84.
5. Prateek, G., Swaroop, C., Superb, K.M. Environ. Nanotechnol. Monit. Manag. 2018, 10, 28–35.

Abstract

MECHANISMS AND CHALLENGES OF PHOTOCATALYTIC NANOMATERIALS IN HEAVY METAL REMOVAL

DOI: 10.5937/EcoTER26636A

Student: Nataša Apostolov[1]

Mentor: Maja Nujkić[1*,a]

[1] University of Belgrade, Technical Faculty in Bor, Vojske Jugoslavije 12, 19210 Bor, SERBIA

[a] https://orcid.org/0000-0002-6110-5135

Abstract

Water pollution by heavy metals and metalloids is a serious environmental and health issue due to their toxicity, persistence, and tendency to bioaccumulate. Conventional methods for removing these pollutants have limitations, including high costs and reduced efficiency at low concentrations. This paper provides an overview of the application of photocatalytic nanomaterials as a modern approach to removing heavy metals from wastewater. Various types of nanomaterials were analyzed, including carbon-based, metal oxide, graphitic carbon nitride, and zero-valent metal materials, as well as their mechanisms of action through adsorption, photocatalysis, and redox reactions. Graphitic carbon nitride was identified as the most economical, while solar-driven zero-valent metal systems demonstrated greater efficiency than those not exposed to radiation (the removal efficiency of Cr^{6+} ions with these systems was 78.5%). A synergistic removal effect was also observed by combining graphitic carbon nitride and nano zero-valent iron, achieving 98% Cr^{6+} removal within 60 minutes under visible light, significantly faster than with the individual nanomaterials. Special attention was given to integrating nanomaterials with conventional treatment methods to increase the efficiency and sustainability of the process.

Key factors affecting the performance of these systems were also considered, including pH, which critically affects the surface charge of the particles, catalyst dose, temperature, initial pollutant concentration, and potential nanotoxicity. It was observed that the adsorption capacity for heavy metal ions increases with the catalyst dose up to an optimal value, after which efficiency decreases due to light scattering.

The paper concludes that photocatalytic nanomaterials represent a promising solution for improving water purification technologies, but also addresses the challenges they face for broader practical application.

Keywords: heavy metals, photocatalytic nanomaterials, graphitic carbon nitride, conventional methods, synergistic effect

[*] *mnujkic@tfbor.bg.ac.rs*

ACKNOWLEDGEMENT

The authors are grateful to the Ministry of Science, Technological Development and Innovation of the Republic of Serbia for financial support according to the contract with registration No. 451-03-34/2026-03/ 200131.

REFERENCES

1. Sharma, S., Bassi, A., Hasan, I. Mat. Sci. Semicon. Process. 2026, 204, 110269.
2. Wang, M., Zheng, X., Oba, B.T., *et al.* Nano Mat. Sci. 2025 Aug 5.
3. Haghighizadeh, A., Rajabi, O., Nezarat, A., *et al*. Arab. J. Chem. 2024, 17(6), 105777.
4. Campillo-Cora, C., Rodríguez-Seijo, A., Pérez-Rodríguez, P., *et al.* Eur. J. Soil Biol. 2025, 124, 103706.
5. Salehpour, N., Mahdavi, P., Nojavan, S. Trends Environ. Anal. Chem. 2026, 23, e00299.

Abstract

BIODIESEL PRODUCTION FROM SUNFLOWER OIL USING CALCINED CIGARETTE ASH AS A WASTE-DERIVED CATALYST

DOI: 10.5937/EcoTER26638R

Students: Nebojša Radović[1,a], Aleksa Vizi[2,b], Željka Nikolić[3,c]

Mentors: Ivan Kojić[2,d], Ksenija Stojanović[1*,e]

[1] University of Belgrade – Faculty of Chemistry, Studentski trg 12-16, Belgrade, SERBIA

[2] Innovative Centre of the Faculty of Chemistry ltd., Studentski trg 12-16, Belgrade, SERBIA

[3] Institute of General and Physical Chemistry, Studentski trg 12-16, Belgrade, SERBIA

[a] https://orcid.org/0000-0002-7587-8569

[b] https://orcid.org/0009-0006-5253-7530

[c] https://orcid.org/0000-0002-2922-0256

[d] https://orcid.org/0000-0001-7737-1844

[e] https://orcid.org/0000-0002-5566-2648

Abstract

Biodiesel, a renewable fuel mainly composed of fatty acid methyl esters (FAMEs), is commonly produced by transesterification of triglyceride-rich feedstocks with short-chain alcohols, most often methanol [1,2]. Although homogeneous alkaline catalysts are widely used, heterogeneous catalysts are increasingly investigated because they can simplify product separation, reduce wastewater generation, and enable catalyst recovery and reuse [3]. In this context, ash-based catalysts obtained from waste materials are especially attractive, as they connect biodiesel production with waste valorization and green chemistry principles [3,4]. This work investigates the laboratory-scale production of biodiesel from sunflower oil using calcined cigarette ash as a low-cost waste-derived catalyst.

Cigarette ash was thermally treated at 800 °C to constant mass and stored under dry conditions before use. The catalytic transesterification reaction was carried out with 25.00 g of sunflower oil, 25.00 g of methanol, and 1.00 g of finely powdered calcined ash. The reaction mixture was magnetically stirred at 70 °C for 120 min. After cooling to room temperature, n-hexane and saturated sodium chloride solution were added to improve phase separation. The upper hexane layer, containing the formed methyl esters, was separated, filtered through filter paper to remove residual ash particles, diluted to a defined volume with n-hexane, and stored at low temperature prior to instrumental analysis.

The obtained biodiesel fraction was characterized by gas chromatography–mass spectrometry (GC-MS). The dominant products were identified by comparison of retention behavior and mass spectral data with the instrument database. GC-MS analysis confirmed the formation of

*ksenija@chem.bg.ac.rs

the methyl esters of palmitic, linoleic, oleic, and stearic acids, which are expected products of sunflower oil transesterification. Based on peak-area evaluation of these four major components, the relative composition of the obtained FAME fraction was 6.55% methyl palmitate, 55.25% methyl linoleate, 36.19% methyl oleate, and 2.00% methyl stearate. The predominance of methyl linoleate and methyl oleate is consistent with the fatty acid profile expected for sunflower oil, supporting the conclusion that the triglyceride feedstock was successfully converted into the corresponding methyl esters under the applied experimental conditions.

The results indicate that calcined cigarette ash may serve as a promising heterogeneous catalyst for biodiesel preparation from sunflower oil under simple laboratory conditions. The proposed procedure has both practical and environmental relevance because it combines renewable feedstock utilization, catalytic conversion, and valorization of an otherwise discarded waste material. However, the present results should be regarded as preliminary. Further work should include detailed catalyst characterization, optimization of the methanol-to-oil ratio and catalyst loading, determination of conversion and isolated yield, reusability testing, comparison with established heterogeneous catalysts, and evaluation of the final biodiesel according to relevant fuel-quality standards.

Keywords: biodiesel, sunflower oil, transesterification, cigarette ash, waste-derived catalyst

ACKNOWLEDGEMENT

The authors are grateful to the Ministry of Science, Technological Development and Innovation of the Republic of Serbia for financial support according to the contract with registration No. RS-MESTD-inst-2020-200168, RS-MESTD-inst-2020-200288, and RS-MESTD-inst-2020-200051.

REFERENCES

1. Ma, F., Hanna, M.A. Bioresour. Technol. 1999, 70 (1), 1–15.
2. Demirbas, A. Energy Convers. Manage. 2009, 50 (1), 14–34.
3. Tang, Z.E., Lim, S., Pang, Y. L., *et al.* Renewable Sustainable Energy Rev. 2018, 92, 235–53.
4. Miladinović, M.R., Zdujić, M.V., Veljović, D.N., *et al.* Renewable Energy. 2020, 147, 1033–43.

Abstract

IDENTIFICATION OF HEAVY METAL SOURCES IN RIVER SEDIMENT IN THE KRUPANJ AREA

DOI: 10.5937/EcoTER26640V

Student: Marija Vesković[1]

Mentor: Antonije Onjia[1*,a]

[1] University of Belgrade, Faculty of Technology and Metallurgy, Karnegijeva 4, 11120 Belgrade, SERBIA

[a] https://orcid.org/0000-0002-5694-7960

Abstract

Environmental pollution represents one of the major global challenges of the modern era. Rapid urbanization, industrialization, improper disposal of various types of waste, and increasing agricultural activities contribute significantly to environmental degradation and contamination. Heavy metal (HM) contamination in river systems is closely associated with anthropogenic activities and represents a significant environmental concern. Once introduced into aquatic ecosystems, heavy metals are deposited, adsorbed, and accumulated in the surface layers of sediments. These metals pose a serious environmental threat due to their toxicity to both aquatic and terrestrial organisms. In addition, they are highly persistent in the environment, difficult to eliminate and, their tendency to accumulate in water, sediments, plants, and living organisms may result in adverse effects on ecosystems and human health.

This study investigated sources of HMs in sediment samples along Jadar River in the vicinity of the city of Krupanj, Serbia. A total of twenty-five river sediment samples were collected and analyzed for ten HMs including: antimony (Sb), arsenic (As), cadmium (Cd), chromium (Cr), iron (Fe), manganese (Mn), nickel (Ni), lead (Pb), zinc (Zn), and mercury (Hg).

Principal component analysis (PCA) of metals in the sediment indicated that PC1 (57.0 %) and PC2 (26.3 %) collectively accounted for 83.3% of the total variance. On the first principal component As, Sb, Cd, Pb, Zn, and Hg exhibited strong positive loadings, all exceeding 0.75, indicating a common origin for these elements. Therefore, the first principal component may represent an anthropogenic influence, indicating intensive mining and agricultural activities. Previous studies have shown that the extraction of Sb is commonly associated with accompanying metals such as Pb, As, Zn, Cd, and Hg, while many of these metals may also originate from intensive agricultural practices. The Stolice Mine, located within the investigated area, is an antimony mine, which explains the elevated concentrations of this metal. Within the second principal component Cr, Fe, Mn, and Ni also showed positive loadings. A possible source of these metals in the investigated area may be related to geological processes. Rocks that have undergone sedimentation or metamorphic processes

[*] *onjia@tmf.bg.ac.rs*

can be enriched with metals such as Ni, Mn, Cr, and Fe which explains their presence in the investigated sediment. In addition, similar conclusions can also be drawn from the analysis of the dendrogram and the Pearson correlation matrix.

In this study, multivariate statistical analysis revealed the presence of two main factors influencing the distribution of heavy metals in the investigated area, with anthropogenic influence being the dominant one.

Keywords: pollution, anthropogenic influence, geological processes, multivariate statistics

ACKNOWLEDGEMENT

This work was financially supported by the Ministry of Science, Technological Development and Innovation of the Republic of Serbia (No. 451-03-34/2026-03/ 200135).

REFERENCES

1. Abdelaal, A., Ahmed, M., El-Alfy, M., *et al.* Mar. Pollut. Bull. 2024, 198, 115930.
2. Chen, Z., Zhao, Y., Liang, N., *et al.* Mar. Pollut. Bull. 2024, 205, 116621.
3. Jakovljević, K., Kostić, O., Nikolić, N., *et al.* Environ. Sci. Pollut. Res. 2020, 27(4), 4089–4103.
4. Levresse, G., Lopez, T., Tritlla, J., *et al.* Sci. Total Environ. 2012, 427–428, 115–125.
5. Magesh, N.S. Mar. Pollut. Bull. 2026, 229, 119722.
6. Vesković, J., Onjia, A. J. Hazard. Mater. 2025, 488, 137309.
7. Vesković, J., Stanković, S., Onjia, A., *et al.* Stoch. Environ. Res. Risk. Assess. 2024, 38 (4), 1597–1612.
8. Wang, L., Li, Y., Chen, P., *et al.* Environ. Monit. Assess. 2020, 192(12), 772.
9. Zou, H., Ren, B. Ecol Indic. 2023, 154, 110761.

Abstract

RECYCLING OF ERDITE AND $KFES_2$ FROM WASTE SLUDGE AS FUNCTIONAL MATERIALS FOR ENVIRONMENTAL PROTECTION

DOI: 10.5937/EcoTER26642J

Student: Aleksandra Jović[1]

Mentor: Maja Nujkić[1*,a]

[1]University of Belgrade, Technical Faculty in Bor, Vojske Jugoslavije 12, 19210 Bor, SERBIA

[a] https://orcid.org/0000-0002-6110-5135

Abstract

In the context of rapid urbanization and industrial development, sludge management has become a major environmental protection challenge. Traditional sludge disposal methods, such as landfilling and incineration, pose risks of secondary contamination to soil, water, and air, as well as the loss of potentially valuable resources contained in sludge. As a result, modern sludge management increasingly relies on the principles of sustainable development and the circular economy, which promote waste recycling and its conversion into useful products and energy.

This paper analyzes the composition of municipal and industrial sludge, with particular emphasis on iron-rich sludge generated during water treatment, electroplating, and metallurgical processes. Special attention is given to sludge purification and recycling methods, including calcination, hydrothermal treatment, Fenton oxidation, gasification, and anaerobic digestion. These methods enable waste reduction, energy recovery, and the production of functional materials with broad applications in environmental protection.

The main focus of the paper is the synthesis of erdite and $KFeS_2$ from iron-rich sludge. These Fe–S functional materials exhibit significant adsorption and catalytic properties due to their specific structure and large number of active surface groups. Hydrothermal synthesis enables the transformation of Fe oxides from sludge into nanostructured materials capable of efficiently removing organic pollutants, antibiotics, and heavy metals from wastewater. Research results indicate that the synthesized materials achieve high pollutant removal efficiency, transforming waste sludge into a valuable secondary raw material for the production of adsorbents and catalysts.

The paper also highlights the importance of modernizing wastewater treatment plants and implementing waste-to-energy technologies such as anaerobic digestion, incineration, and gasification. Integrating these technologies can reduce waste quantities, improve energy efficiency, and contribute to sustainable resource management. The paper concludes that recycling sludge into functional materials is an environmentally and economically justified solution that reduces pollution and advances circular economy principles.

[*]*mnujkic@tfbor.bg.ac.rs*

***Keywords**:* waste sludge, recycling, erdite, $KFeS_2$, functional materials, environmental protection, circular economy.

ACKNOWLEDGEMENT

The authors are grateful to the Ministry of Science, Technological Development and Innovation of the Republic of Serbia for financial support according to the contract with registration No. 451-03-34/2026-03/ 200131.

REFERENCES

1. Chen, X., Liu, Y., Wang, Z., *et al.* J Hazard. Mater. 2022, 430, 128412–128425.
2. Hu, Y., Zhang, L., Li, X., *et al*. J. Clean Prod. 2020, 258, 120715–120724.
3. Kiselev, A., Magaril, E., Rada, E.C., *et al*. Sustainability. 2020, 12(18), 7451–7465.
4. Olasupo, A.O., Ramphal, S.R., Maboeta, M.S., *et al*. Environ. Pollut. 2026, 345, 122345–122360.
5. Tyagi, V.K., Lo, S.L. Renew. Sustain. Energy Rev. 2013, 25, 708–728.

Abstract

INFLUENCE OF Ni AND Si ADDITIONS ON THE MICROSTRUCTURE, MECHANICAL PROPERTIES AND CONDUCTIVITY OF CuZn30 ALLOY

DOI: 10.5937/EcoTER26644J

Student: Teodora Jogrić[1]

Mentor: Ljubiša Balanović[1*,a]

[1] University of Belgrade, Technical Faculty in Bor, Vojske Jugoslavije 12, 19210 Bor, SERBIA

[a] https://orcid.org/0000-0002-3551-6731

Abstract

Growing demands for sustainable development and efficient material use encourage the design of copper alloys with longer service life and reduced environmental impact.

In this work, the CuZn30 alloy was modified with small additions of Ni (up to 3 mass%) and Si (up to 0.7 mass%) to investigate a simple approach to improving selected properties relevant to engineering applications. The concept is based on precipitation strengthening through the formation of the δ-Ni_2Si phase, which can enhance mechanical properties while moderately affecting electrical and thermal conductivity.

The experimental program included casting of selected alloy compositions, solution annealing at 900 °C for 2 h, water quenching, pressing, subsequent aging at 300 °C for 8 h, and characterization of electrical conductivity, microhardness, Leeb hardness, thermal conductivity, and microstructural analysis using SEM-EDS.

For the alloy containing 3 mass% Ni and 0.7 mass% Si, electrical conductivity decreased from 13.6 to 9.8 MS/m, while microhardness increased from 126.3 to 203.9 $HV_{0.15,}$ and Leeb hardness increased from 350 to 556 HDL compared with the base CuZn30 alloy. Thermal conductivity at 25 °C decreased from 131.49 to 90.62 W/mK, and at 400 °C from 172.83 to 141.19 W/mK for the same alloy. Microstructural analysis confirmed that fine δ-Ni_2Si precipitates were formed during the annealing process.

The results indicate that Ni and Si additions, combined with a simple heat-treatment route, can be an effective strategy to improve the properties of CuZn30 for environmentally eco-friendly engineering applications.

Keywords: brass, CuZn30 alloy, precipitation, microstructure, microhardness, conductivity

ACKNOWLEDGEMENT

The authors are grateful to the Ministry of Science, Technological Development and Innovation of the Republic of Serbia for financial support under contract No. 451-03-34/2026-03/200131.

[*] *ljbalanovic@tfbor.bg.ac.rs*

REFERENCES

1. Birch, J., Jenkins, E., Vrettou, A., *et al.* Acta Mater. 2024, 278, 120277.
2. Chen, W., You, K., Yin, J., *et al.* Met. Mater. Int. 2022, 28(10), 2555–2562.
3. Chen, W., Jia, Y., Yi, J., *et al.* J. Mater. Res. 2017, 32(16), 3137–3145.
4. Li, J., Huang, G., Mi X., *et al.* Materials. 2019, 12(13), 2076.
5. Rojas-Rodríguez, I., Lara-Guevara, A., Salazar-Sicacha, M., *et al.* Mater. Sci. Appl. 2018, 9, 440–454.
6. Zheng, Z., Guo, P., Li, J., *et al.* J. Alloys Compd. 2020, 831, 154842.
7. Zhou, X.-Z., Su, Y.-C. Mater. Sci. Eng. A. 2010, 527(20), 5153–5156.

Abstract

ENVIRONMENTAL IMPACT AND EMISSION CONTROL IN PYROMETALLURGICAL COPPER PRODUCTION

DOI: 10.5937/EcoTER26646L

Student: Jovana Levkić[1]

Mentors: Tanja Kalinović[1*,a], Jelena Kalinović[1,b]

[1] University of Belgrade, Technical Faculty in Bor, Vojske Jugoslavije 12, 19210 Bor, SERBIA

[a] https://orcid.org/0000-0003-0161-0065

[b] https://orcid.org/0000-0003-0088-2683

Abstract

Copper is one of the most important industrial metals due to its excellent electrical and thermal conductivity and its wide application in various industrial sectors. It is produced from primary and secondary raw materials using pyrometallurgical and hydrometallurgical processes. The main environmental problems in the refined copper production industry are air, water and soil pollution, as well as the generation of hazardous waste. However, copper production, particularly during roasting, smelting, converting, and refining operations, represents a significant source of air pollution. Given the growing environmental concerns and stricter regulatory requirements, it is essential to analyse copper production technologies and their contribution to atmospheric emissions, with a particular focus on particulate matter, metal-containing dust, and gaseous pollutants, as well as to evaluate the application of Best Available Techniques (BAT) for emission prevention and control. Best Available Techniques (BAT) for pyrometallurgical copper production include a combination of process optimization measures and advanced emission control technologies aimed at reducing atmospheric emissions, improving energy efficiency, and minimizing waste generation. This study was conducted as a literature review based on scientific publications, technical reports, and relevant regulatory documents related to copper production and environmental protection.

The review showed that pyrometallurgical processes for copper production are the dominant source of atmospheric pollution. Sulphur dioxide (SO_2) was identified as the main gaseous pollutant, while particulate matter may contain trace amounts of heavy metals and metalloids such as lead (Pb), cadmium (Cd), arsenic (As), mercury (Hg), and nickel (Ni). These pollutants can adversely affect air quality, ecosystems, and human health, particularly in areas surrounding smelting facilities. In addition to air emissions, copper production generates solid and liquid waste streams that require appropriate management to prevent secondary environmental contamination.

The analysed literature indicates that the implementation of BAT significantly reduces the environmental impact of copper production. Effective measures include the use of: enclosed

[*] *tkalinovic@tfbor.bg.ac.rs*

furnaces and sealed process systems to prevent fugitive emissions of dust and gases; efficient gas collection systems with centralized extraction from roasting, smelting, converting, and refining operations; application of high-efficiency dust removal technologies such as electrostatic precipitators (ESP), baghouse filters, and cyclones; wet gas cleaning systems for the removal of fine particulate matter and acid gases; recovery of sulphur dioxide (SO_2) through sulphuric acid production plants; optimization of process parameters, including temperature control and oxygen-enriched smelting, to improve process efficiency and reduce emissions; continuous monitoring and automatic control of emissions and process conditions; recycling and reuse of process dust, slag, and other by-products whenever technically feasible; use of energy-efficient technologies and heat recovery systems; proper treatment and management of wastewater and hazardous solid waste generated during the process. Modern emission control systems can achieve pollutant removal efficiencies exceeding 99%, contributing substantially to environmental protection.

In conclusion, understanding the technological stages of copper production and their associated emissions is essential for improving production efficiency and minimizing environmental impacts. The continuous application of BAT, environmental monitoring, and compliance with environmental standards are key factors in achieving sustainable copper production while meeting the increasing global demand for this strategically important metal.

Keywords: copper production, air pollution, sulphur dioxide, particulate matter, best available techniques

ACKNOWLEDGEMENT

The authors are grateful to the Ministry of Science, Technological Development and Innovation of the Republic of Serbia for financial support according to the contract with registration No. 451-03-34/2026-03/200131.

REFERENCES

1. Serbula, S.M., Milosavljevic, J.S., Kalinovic, J.V., *et al*. Sci. Total Environ. 2021, 777, 145981.
2. Zhou, H., Liu, G., Zhang, L., *et al*. Environ. Pollut. 2021, 270, 116203.
3. Li, X., Wang, X., Cai, B., *et al*. Process Saf. Environ. Prot. 2023, 174, 214–222.
4. Goodman, A.J., Ahabchane, H.E., Hayes, P.L. ACS ES&T Air. 2026, 3(2), 385–395.
5. Cusano, G., Gonzalo, R. M., Farrell, F., *et al*. Best Available Techniques (BAT) Reference Document for the Non-Ferrous Metals Industries. Industrial Emissions Directive 2010/75/EU (Integrated Pollution Prevention and Control). 2017. Available from: https://publications.jrc.ec.europa.eu/repository/handle/JRC107041
6. Orac, D., Laubertova, M., Piroskova, J. J. Min. Metall. Sect. B-Metall. 2020, 56(2), 221–228.

Abstract

IMPACT OF ARTIFICIAL INTELLIGENCE USE ON AIR POLLUTION

DOI: 10.5937/EcoTER26648R

Student: Mladen Radić[1]

Mentors: Jelena Kalinović[1*,a] Ana Radojević[1,b]

[1] University of Belgrade, Technical Faculty in Bor, Vojske Jugoslavije 12, 19210 Bor, SERBIA

[a] https://orcid.org/0000-0003-0088-2683

[b] https://orcid.org/0000-0003-3138-154X

Abstract

The rapid global advancement of Artificial Intelligence (AI) has positioned it as a critical driver of industrial progress. However, this digital transformation is accompanied by a significant environmental footprint that is often overlooked in mainstream discourse. The analysis examines the dual impact of AI on air pollution by employing a Life Cycle Assessment (LCA) methodology and a quantitative analysis of emission factors (EFi). Particular attention is given to the indirect environmental pressures generated by AI infrastructure, specifically data centers, which require massive amounts of electricity to power Graphics Processing Units (GPUs) during the training phases of deep learning models. In areas where the energy mix heavily relies on fossil fuels, these processes lead to significant emissions of sulfur dioxide (SO_2), nitrogen oxides (NO_x), particulate matter (PM), and carbon dioxide (CO_2).

A quantitative comparison between the energy systems of Serbia and the United States was conducted using specific emission factors. The results indicate that the environmental cost of training AI models is highly dependent on the sustainability of the local power grid. For instance, training a large language model such as Gemini requires approximately 1,600 MWh of energy. In Serbia, where coal-fired power plants dominate electricity generation, this process results in emissions exceeding 15 tons of SO_2 and 350 kg of particulate matter per model. In contrast, the same process in the United States generates approximately 260 kg of SO_2 and 14 kg of PM, corresponding to a more than 50-fold difference for certain pollutants. These findings highlight that the environmental impact of AI development is strongly influenced by the carbon and pollutant intensity of the underlying energy infrastructure.

The findings suggest that AI may act as a catalyst for the energy transition. AI systems can optimize smart grids, improve renewable energy forecasting, and enhance resource efficiency in industrial sectors. The concept of "Green AI" is proposed as an essential strategy, emphasizing algorithm optimization, hardware efficiency metrics such as Power Usage Effectiveness and Datacenter Infrastructure Efficiency (PUE/DCiE), and a systemic shift toward renewable energy sources. Sustainable AI development must be supported by

*jkalinovic@tfbor.bg.ac.rs

transparent regulatory frameworks and rigorous LCA applications to ensure that digital innovation does not compromise global air quality.

Keywords: artificial intelligence, air pollution, energy mix, life cycle assessment

ACKNOWLEDGEMENT

The authors are grateful to the Ministry of Education, Technological development, and Innovations of the Republic of Serbia for financial support, within the funding of the scientific research at the University of Belgrade – Technical Faculty in Bor (No. 451-03-34/2026-03/200131).

REFERENCES

1. Boubel, RW., Fox, DL., Turner, DB., *et al*. Fundamentals of Air Pollution. San Diego, Academic Press, 1994.
2. Slimani, S., Omri, A., Jabeur, S.B. Energy Economics. 2025, 148, 108643.
3. U.S. Environmental Protection Agency, USEPA, eGRID Summary Tables 2021: Emission Rates for Electricity Generation. Washington, (2023).
4. Electric Power Industry of Serbia (EPS). Environmental Status Report 2024. Belgrade, Serbia, 2024.
5. Bolón-Canedo, V., Morán-Fernández, L., Cancela, B., *et al*. Neurocomputing. 2024, 599, 128096.
6. Wang, W., Liu, Y., Dong, X. Economic Analysis and Policy. 2025, 88, 281–307.

Abstract

PLANTS AS BIOINDICATORS OF AIR POLLUTION

DOI: 10.5937/EcoTER26650D

Student: Nataša Đorđević[1]

Mentors: Jelena Kalinović[1*,a], Tanja Kalinović[1,b]

[1] University of Belgrade, Technical Faculty in Bor, Vojske Jugoslavije 12, 19210 Bor, SERBIA

[a] https://orcid.org/0000-0003-0088-2683

[b] https://orcid.org/0000-0003-0161-0065

Abstract

Air pollution represents one of the most critical environmental issues of the contemporary era. Air pollution is commonly defined as the presence of particulate matter and gaseous pollutants in the atmosphere at concentrations that pose risks to living organisms and ecosystem functionality. Some of the most significant atmospheric pollutants are particulate matter ($PM_{2.5}$ and PM_{10}), nitrogen oxides (NO_x), sulfur dioxide (SO_2), and tropospheric ozone (O_3). These substances contribute to environmental degradation and various health-related issues.

In recent years, considerable attention has been directed toward the use of plants as effective biomarkers and bioindicators of atmospheric pollution, owing to their inherent capacity to accumulate contaminants and exhibit measurable physiological and morphological responses. Plants are especially valuable in this context due to their ability to directly interact with atmospheric pollutants and respond through measurable physiological, biochemical, and morphological changes.

This paper provides a literature review of the applicability of selected plant species as biomarkers of air pollution, with particular emphasis on dandelion (*Taraxacum officinale*), pear (*Pyrus communis* L.), and horse chestnut (*Aesculus hippocastanum* L.). The obtained findings indicate species-specific responses including heavy metal accumulation and structural leaf alterations. *Taraxacum officinale* efficiently accumulates Pb, Cd, and Zn in its roots and leaves, making it a reliable indicator of urban environmental pollution. *Pyrus communis* L. was used to assess the impact of gaseous pollutants on plant physiological condition, and the results showed that exposure to NO_x and SO_2 leads to chlorosis, reduced photosynthetic activity, and increased accumulation of trace heavy metals in leaves. *Aesculus hippocastanum* L. was used for biomonitoring of urban air pollution, and the results showed that this species accumulates Pb, Cd, and Zn in leaf tissues, accompanied by necrosis, chlorotic spots, and premature leaf fall under elevated pollutant concentrations.

The analyzed species demonstrate complementary biomonitoring roles, where *Taraxacum officinale* primarily reflects heavy metal accumulation in soil and air, *Pyrus communis*

*jkalinovic@tfbor.bg.ac.rs

indicates physiological stress caused by gaseous pollutants, and *Aesculus hippocastanum* integrates both chemical accumulation and visible foliar damage, making them collectively effective indicators of urban air quality gradients.

Based on the obtained results, the authors concluded that plants could be suitable as a cost-effective and an environmentally friendly tool for air quality monitoring.

Keywords: air pollution, biomarkers, bioindicators, plants

ACKNOWLEDGEMENT

The authors are grateful to the Ministry of Education, Technological development, and Innovations of the Republic of Serbia for financial support, within the funding of the scientific research at the University of Belgrade – Technical Faculty in Bor (No. 451-03-34/2026-03/200131).

REFERENCES

1. World Health Organization (WHO). Air Quality Guidelines. 2005.
2. Markert, B., Breure, A.M., Zechmeister, H.G. Bioindicators and Biomonitoring Principles, Concepts and Applications. Amsterdam: Elsevier; 2003.
3. Gill, S.S., Tuteja, N. Plant Physiol. Biochem. 2010, 48, 909–930.
4. Vuković, G., Aničić Urošević, M., Škrivanj, S., *et al*. Sci. Total Environ. 2016, 542, 394–403.
5. Petrova, S., Yurukova, L., Velcheva, I. J. Bio. Sci. Biotech. 2012, 1(3), 241–247.

Author index

A
Aćimović, D. 427, 432, 452
Alagić, S. 51
Amirov, J. 381
Anđelković, A. 541
Anđelković, D. 297, 304, 310
Anđelković, T. 142, 222, 228
Anđus, S. 181, 523
Antonijević, M. 57, 233
Apostolov, N. 561, 636
Arena, C. 374
Arizanova, M. 360
Arsić, S. 497
Atanasova, V. 516
Atlagić, J.Č. 181
Avramović, Lj. 568

B
Bajić, B. 12
Balanović, Lj. 422, 443, 644
Banđur, D. 273, 343
Banković, S. 463
Bartolić, D. 273, 343
Batool, I. 610
Beslac, N. 386
Bezdan, A. 29
Bezdan, J. 29
Bin Moazzam, U. 610
Bogdanović, A. 57, 233
Bogdanović, D. 142, 222, 228
Bogdanović, G. 2
Bojić, A. 279, 284, 290
Božić, A. 536
Božić, D. 568
Božinović, K. 239, 410, 417, 443
Branković, M. 297, 304, 310
Brdarić, T. 427, 432, 452
Bulatović, S. 438
Budzakoska Gjoreska, B. 153

C
Cmiljanović, K. 503
Cocić, M. 146
Cvetković, A. 57, 233, 403
Cvetković, S. 261, 266

Č
Čeliković, I. 330
Čukanović, J. 83, 85, 93

Ć
Ćirović, Ž. 210
Ćosović, V. 485
Ćurić, M. 582

D
Damnjanović, Z. 146
Danilović Luković J. 316, 324
De Marco, A. 374
Dimitrijević, M. 336
Djikanović, V. 590
Dobričić, A. 336
Dodić, S. 12
Doneva-Shapcheska, D. 360
Drakulović, A. 46
Dudić, M. 222, 228
Dumitrašković, S. 628

Đ
Đikanović, V. 181, 348
Đoković, J. 478
Đorđević, A. 478
Đorđević, M. 112, 119, 456
Đorđević, N. 650
Đorđević, S. 83, 85, 93
Đorđievski, S. 561
Đuknić, J. 78, 530
Đurašević, M. 330
Đuretanović, S. 546
Đurić, S. 243
Đuriš, M. 261

F
Fedajev, A. 497
Fike, M. 595
Filipović, K. 620

G
Gajić, I.S. 22
Galečić, N. 83, 85, 93
Galjak, J. 135
Gorgievski, M. 239, 417, 443, 628, 632
Grbović, L. 523, 530
Grekulović, V. 239, 417, 443, 628, 632
Grozdanović, M. 478

I
Ivanović, M. 503

J
Jakovljević, M. 546
Jakovljević, O. 187, 523, 536, 541
Janković, A. 463
Janjić, J. 582
Janjić, N. 626
Ječmenica Dučić, M. 427, 432, 452
Jerinkić, D. 187
Jogrić, T. 443, 644
Jordanović, J. 561, 646
Jovanović, M. 602
Jovanović, V. 630
Jovanović, V.S. 51
Jovičić, K. 181, 348, 590
Jović, A. 642
Jovović, N. 46
Jovašević-Stojanović, M. 210, 602

K
Kalinović, J. 561, 646, 648, 650
Kalinović, T. 561, 646, 650
Kamenović, V. 146
Kandić, A. 330
Karabašević, M. 632
Kerkez, D. 620
Kleut, D. 210

Kljajević, Lj. 503
Knežević, S. 503
Kojadinović, N. 546
Kojić, I. 638
Kostić Kokić, I. 142, 222, 228
Korać Jačić, J. 316, 324, 576
Kolarov, R. 83, 85, 93
Koprivica, M. 471
Kostić, M. 279, 290
Kostadinova Jankovski, D. 360
Kovačević, A. 410
Kovačević, R. 146, 602
Kralj, K. 243
Kračun Kolarević, M. 523
Krantić, Z. 541
Krizmanić, J. 523
Krstić, J. 620
Krstić, M. 135

L

Lakušić, V. 71, 78
Lazić, Lj. 243
Lekić, J. 556
Levkić, J. 646
Lučić, M. 169

Lj

Ljubić, V. 261, 266

M

Maksimović, I. 503
Maksin, D. 452
Manasijević, D. 410, 422
Mančić, M. 478
Marić, A. 181
Marinković, N. 181, 530
Marjanović, S. 336
Marjanović, V. 63, 162
Marković, B. 438
Marković, I. 410, 422, 443, 485
Marković, Miljan 239, 417
Marković, Marina 239, 417
Marković, R. 162
Marković, Z. 336
Marković Nikolić, D. 100, 250, 256
Matić, B. 175
Medić, D. 51, 403, 561, 568
Meriluoto, J. 22
Mićić, D. 243
Mihalj Lubaščik, I. 22
Mićić, M. 343
Milanović, T. 330
Milenković, M. 316, 324, 576
Milentijević, G. 135
Milićević, A. 541
Milić, S. 51, 568
Milojević, S. 135
Milošević, D. 261, 266
Milošković, A. 546
Milovanović, Ž. 261, 266
Miltenović, Đ. 112
Mitić, T. 181
Mitrović, J. 279, 284, 290
Mladenović, D. 497
Mladenović Nikolić, N. 503
Mladenović, S. 485
Momčilović, M. 279, 290

N

Najdanović, S. 284, 290
Napoletano, P. 374
Nasirov, M. 381
Nasir, K. 610
Nastasović, A. 438
Nawab, H. 610
Nedelkovski, V. 403, 568
Nedeljković, M. 410, 422, 485
Nedić, N. 438
Nenadović, S. 503
Nešović, S. 620
Nikolić, D. 336
Nikolić, I. 46
Nikolić, Jelena S. 51
Nikolić, Jelena D. 471
Nikolić, M. 100, 119, 250, 256
Nikolić, S. 634
Nikolić, T. 100, 112, 119, 250, 456
Nikolić, Ž. 638
Nikolovski, D. 243, 622
Novaković, B. 71, 78, 368
Nujkić, M. 561, 624, 630, 634, 636, 642, 646

O

Obradović, V. 106, 551, 556
Ocokoljić, M. 83, 85, 93
Okolišan, A. 169
Onjia, A. 169, 640

P

Pajic, P. 194, 201
Palanački Malešević, T. 22
Panić, M. 497
Papludis, A. 51
Paskaš, N. 71, 78
Paunović, M. 530
Pavlović, S. 126
Pećić, M. 187
Peltechki, D. 509
Perendija, J. 261, 266
Perović, M. 106, 551, 556
Petković, G. 250
Petronijević, T. 222, 228
Petrović, B. 602
Petrović Mihajlović, M. 57, 233
Petrović, J. 485
Petrović, M. 279, 284, 290
Petrović, M.Lj. 463
Petrov, Dj. 83, 85, 93
Petrov, P. 353
Pezdevšek, M. 595
Popescu, F. 217
Popović, N. 530
Popović, S. 187, 536, 541
Prodanović, O. 273
Prodanović, R. 273
Prokopijević, M. 343

R

Radenković, M. 546

Radić, M. 648
Radmilović, V. 46
Radojević, A. 561, 646, 648
Radovanović, M. 57, 233, 403
Radović, B. 146, 602
Radović, N. 638
Radović Vučić, M. 279, 284
Radović, Ž. 40
Rakin, M. 463
Rakonjac, N. 194, 201
Raković, Marko 78, 368,
Raković, Maja 530
Rančev, S. 284
Randjelović, D. 471
Ranđelović, D. 381
Rašković, B. 336
Rikalović, M. 622
Ristić, I. 256
Ristić, N. 146, 256
Ristovski, B. 360
Roger, A. 595
Romčević, D. 386
Rudic, Ž. 194, 201

S

Samolov, A. 330
Santrač, I. 316, 324, 576
Savić, I. 22
Savić, V. 471
Savić Rosić, B. 427, 432, 452
Spasojević Savković, M. 273
Sekereš, F. 316, 324
Simić, M. 427, 432, 452
Simić, V. 546
Simonović, A. 18, 57, 233, 403
Skočajić, D. 83, 85, 93
Sredenšek, K. 595
Stajić, T. 243
Stamenković, U. 410, 422, 443, 485
Stanković, Mira 273, 343
Stanković, Marko 336
Stanković, Mihajlo 386,394
Stanković, N. 142, 222, 228
Stanković, Sonja 57, 403
Stanković, Slavica 343
Stojadinović, D. 100, 112, 119, 456
Stojadinović, Milutin 63
Stojadinović, Minja 624
Stojanoska, M. 516
Stojanović, B. 112, 119, 456
Stojanović, D. 210
Stojanović, G. 51
Stojanović, Katarina 427, 432, 452
Stojanović, Ksenija 638
Stojanović, S. 456
Stojanović, Z. 71
Stošić, D. 243
Surudžić, N. 273, 343
Svirčev, Z. 22
Svrkota, I. 63

Š

Štirbanović, Z. 162
Štrbac, N. 239, 417

T

Tadić, N. 40, 46
Tadić, T. 438
Tanikić, D. 478
Tasić, V. 146
Tasić, Ž. 57, 233, 403, 561, 626
Topalović, V. 471
Trajanovska, S. 153
Trajanovski, S. 153
Trajkovska, G. 243
Trifunović, V. 568
Trivunac, K. 266
Tubić, B. 523, 530

U

Urošević, S. 490

V

Valiyev, S. 381
Vasić, I. 330
Vasiljević, B. 523
Vasiljević, S. 568
Velinov Georgijev, N. 279, 284, 290
Velickova, E. 360
Veličković, M. 497
Veličković, T. 546
Vesković, J. 169
Vesković, M. 169, 640
Vilimonović, M. 169
Vitale, E. 374
Vizi, A. 638
Voza, D. 497
Vranković, J. 348, 590
Vukašinović Sekulić, M. 463
Vučković, T. 106, 551
Vučurović, D. 12
Vučurović, V. 5
Vukmanović, V. 175
Vuković, M. 490

W

Wadhawan, J. 1

Z

Zdravković, A. 100, 112, 119, 250, 256, 456
Zdravković, M. 239, 417
Zec, J. 243, 622
Zot, M. 217

Ž

Živić, I. 71, 78
Živković, M. 316, 324, 576
Živković Perišić, S. 175

Authors are responsible
for the content of their papers.

ISBN 978-86-6305-171-3

eco.tfbor.bg.ac.rs